THYROID HORMONE TRANSPORTERS: FROM MOLECULES TO PATIENTS

Stefan Groeneweg

Colofon

ISBN: 978-94-6375-719-5

Cover design by: Stefan Groeneweg and Ridderprint, www.ridderprint.nl

Printed by: Ridderprint, www.ridderprint.nl

The printing of this thesis has been financially supported by Rare Thyroid Therapeutics, Stockholm, Sweden

Thyroid Hormone Transporters: from Molecules to Patients

Schildklierhormoon transporters: van moleculen tot patiënten

Proefschrift

ter verkrijging van de graad van doctor aan de
Erasmus Universiteit Rotterdam
op gezag van de rector magnificus

Prof.dr. R.C.M.E. Engels

en volgens het besluit van het College voor Promoties.

De openbare verdediging zal plaatsvinden op

dinsdag 11 februari 2020 om 13.30 uur

door

Stefan Groeneweg

geboren te Rotterdam

Erasmus University Rotterdam

PROMOTIECOMMISSIE

Promotor:	Prof. dr. R.P. Peeters
Overige leden:	Prof. dr. H. Heuer
	Prof. dr. E. Fliers
	Prof. dr. A.T. van der Ploeg
Copromotor:	Dr. W.E. Visser

“How I wish, how I wish you were here”

- Roger Waters & David Gilmour -

In *memoriam* Prof. dr. Ir. Theo J. Visser

CONTENTS

Chapter

General introduction and aims of the thesis

1

Parts of this chapter are based on

Thyroid hormone transporters
Groeneweg S., van Geest F.S., Peeters R.P., Heuer H., Visser W.E. Endocrine Rev 2019 (accepted for publication)

Triiodothyroacetic acid in health and disease
Groeneweg S., Peeters R.P., Visser T.J., Visser W.E
J Endocrinol 2017

Therapeutic applications of thyroid hormone analogues
Groeneweg S., Peeters R.P., Visser T.J., Visser W.E
Mol Cell Endocrinol 2017

Disorders of thyroid hormone transport into the tissues
Groeneweg S., Visser W.E., Visser T.J.
Best Pract Res Clin Endocrinol Metab 2017

INTRODUCTION

Thyroid hormone is the common name for the prohormone 3,5,3',5'-tetraiodothyronine (T4, thyroxine) and the bioactive hormone 3,5,3'-triiodothyronine (T3). Thyroid hormone importantly governs development of many tissues and regulates metabolism throughout life. These functions of thyroid hormone are best illustrated by the symptoms of patients exposed to excessive thyroid hormone concentrations (hyperthyroidism) or diminished thyroid hormone concentrations (hypothyroidism). Hyperthyroidism, most frequently caused by auto-immune hyperthyroidism (Graves` disease), results in increased heart rate, weight loss, increased perspiration, restlessness and anxiety. Hypothyroidism, in adults most often caused by auto-immune thyroiditis (Hashimoto`s disease), on the other hand results in opposite symptoms including bradycardia, weight gain, cold intolerance, reduced cognitive function and depression. In addition, thyroid hormone is essential for normal development of tissues, particularly the brain as is illustrated by the detrimental effects of untreated prenatal and postnatal hypothyroidism (but also hyperthyroidism) on neurocognitive and motor development.

Thyroid hormone exerts its main effects through binding of the active hormone T3 to the nuclear T3 receptors (TRs) which modulates the expression of thyroid hormone responsive genes. Therefore, the intracellular T3 concentrations strongly determine the biological activity of thyroid hormone. Several processes are involved in the regulation of intracellular thyroid hormone concentrations, including the (free) T4 and T3 concentrations in serum, the activity of the intracellular deiodinating enzymes D1, D2, and D3 that can either activate or inactivate thyroid hormone, and the presence of transporter proteins at the cell membrane, facilitating the cellular uptake and efflux of T4 and T3 (**Figure 1**). Defects in either one of these processes can cause abnormal cellular thyroid hormone homeostasis and may result in clinical syndromes of resistance to thyroid hormone (RTH).

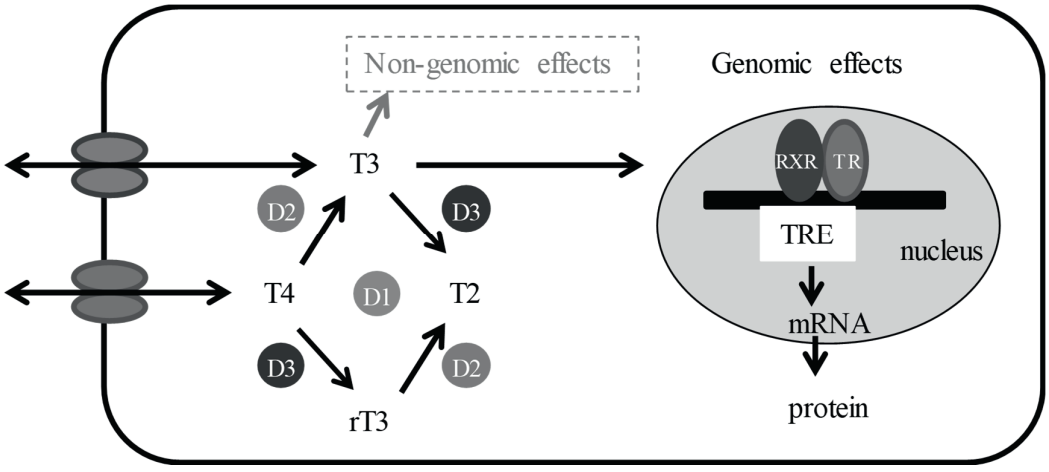

Figure 1 Transport, metabolism and action of thyroid hormone in a thyroid hormone target cell.

THYROID HORMONE SYNTHESIS AND THE HYPOTHALAMUS-PITUITARY-THYROID AXIS

Thyroid hormone is produced by the thyroid gland which is located in the neck, ventral to the trachea. The thyroid gland is composed of numerous follicles formed by the thyrocytes. Thyroid hormone is synthesized and stored in the colloid lumen of these follicles (1). Synthesis of thyroid hormone requires the trace element iodine (I^-) which is transported from the blood into the thyrocytes by the cell membrane tranporter protein Na^+/I^- symporter (NIS) (2, 3). Subsequently, another cell membrane transporter, pendrin (PDS), facilitates the release of I^- into the follicle lumen where it is oxidized by the enzyme thyroid peroxidase (TPO). The hydrogen peroxide that is required for this reaction is generated by the dual oxidase type 2 (DUOX2). The I^+ that is formed during this reaction rapidly reacts with specific tyrosyl residues of thyroglobulin (TG), a protein that is abundantly present in the colloid lumen, which ultimately results in the formation of mono-iodotyrosine (MIT) and diiodotyrosine (DIT). The coupling of two DIT molecules, again catalyzed by TPO, results in the formation of T4 and the coupling of a DIT and a MIT molecule results in the formation of T3. After internalization of the thyroid hormone containing TG molecules in the thyrocyte, the complexes are hydrolyzed in lysosomes which ultimately results in the release of T4 and T3 as well as non-coupled iodotyrosines. These non-coupled iodotyrosines are deiodinated by dehalogenase 1 (DEHAL1) (4). Finally, T4 and T3 are released into the blood stream. Mutations in several proteins involved in thyroid hormone synthesis have been reported to result in dyshormonogenesis leading to congenital hypothyroidism (4-7).

The thyroid gland predominantly secretes T4 and to a lesser extent T3, which amounts up to only ~ 20 percent of the daily hormone production in the thyroid. The majority of T4 and T3 molecules in the circulation are bound to proteins like thyroxine-binding globulin (TBG), transthyretin (TTR) and albumin. Only a small fraction (~0.02% of T4 and ~0.2% of T3) is present in an unbound state and can be measured as free T4 and free T3. The free fraction is available for transport into thyroid hormone target cells.

The production of thyroid hormones and their release into the blood stream is tightly regulated by the hypothalamus-pituitary-thyroid (HPT) axis. The production and secretion of thyroid hormone is stimulated by thyroid-stimulating hormone (TSH, thyrotropin). Binding of TSH to the TSH-receptor on the surface of thyrocytes results amongst others in the growth of thyrocytes, stimulates iodine uptake via NIS and triggers the release of T4 and T3 into the circulation. TSH is secreted by the anterior pituitary where its production and release is stimulated by thyrotropin releasing hormone (TRH) produced in the paraventricular nuclei (PVN) of the hypothalamus (8). Thyroid hormone negatively regulates the production of TSH and TRH, comprising a so-called negative feedback loop.

THYROID HORMONE ACTION

In 1952, it was recognized that T3 has greater biological potency than T4 (9-12). This fundamental discovery led to the concept that T4 functions as a prohormone, with T3 being the biologically active hormone. Thyroid hormone exerts its biological effects through genomic and non-genomic pathways.

Genomic actions of thyroid hormone are mediated through the nuclear thyroid hormone receptors (TRs), which function as ligand-dependent transcription factors. Three functional TR isoforms exist, namely TRα1, TRβ1, and TRβ2, which are highly homologous but differ in their tissue distribution and

substrate binding kinetics (13-15). TRs predominantly act as heterodimers with retinoid X receptors (RXRs) on thyroid hormone response elements (TREs) in the promoter region of T3-responsive genes (13, 16). Target genes can either by positively or negatively regulated by thyroid hormone. In case of positively regulated genes, TRs repress target gene transcription by recruitment of corepressors such as nuclear receptor corepressor 1 (NCoR1) in absence of ligand. Binding of T3 results in the dissociation of corepressors and allows the recruitment of coactivators, such as steroid receptor coactivator 1 (SRC1), resulting in activation of gene transcription (13, 17). The mechanism by which T3 negatively regulates gene expression is less well understood.

Heterozygous mutations or homozygous deletion of the genes encoding TRα (*THRA*) and TRβ (*THRB*) result in syndromes of resistance to thyroid hormone (RTH) α and β, respectively, with distinctive clinical phenotypes (18-25). Whereas the first patient with RTHβ has been reported decades ago (18), it was only recently that the first patients with mutations in TRα have been identified (21, 22). In both disorders, the mutant receptors exhibit a diminished T3 binding affinity and/or impaired interactions with one of the co-regulators involved in the mediation of T3 action and generally display a dominant negative effect over the wild-type receptor (23, 26-28). Biochemical hallmarks of RTHβ are elevated serum (free) T4, T3 and rT3 concentrations accompanied by non-suppressed or elevated TSH concentrations. The clinical features of RTHβ may comprise a combination of hypothyroid and thyrotoxic symptoms, resulting from the tissue-specific distribution of the TR isoforms. T3 action is reduced in tissues that predominantly express the (mutant) TRβ isoform, most importantly the pituitary and liver (29, 30). In contrast, tissues that predominantly express TRα, such as the heart and brain, are exposed to the high serum TH levels which may result in tachycardia, hyperactivity, anxiety and learning disabilities (29, 30). The reported phenotype of patients with RTHα is somewhat heterogenic and may include growth retardation, macrocephaly, constipation, intellectual disability and anemia (23, 24). These symptoms can be ascribed to reduced thyroid hormone action in tissues that mainly express TRα. Biochemical hallmarks of RTHα are high to high-normal (F)T3, low to low-normal (F)T4, low rT3 and normal TSH concentrations.

The non-genomic (or extranuclear) actions of thyroid hormone have only recently been recognized (31-35). Apart from T3 and T4, such non-genomic actions can be mediated through other iodothyronines and metabolites thereof, including the effects of 3,3’,5’-triiodothyronine (rT3) on cytoskeletal actin polymerization during brain development, the stimulatory effect of 3,5-diiodothyronine (T2) on mitochondrial energy metabolism and the rapid effects of thyronamines on the trace amine-associated receptor TAAR1 (33, 34, 36). In addition, T3 and T4, as well as several thyroid hormone metabolites have been reported to modulate αVβ3 integrin signaling (37, 38).

THYROID HORMONE METABOLISM

Thyroid hormone is subject to different (enzymatic) chemical modifications that regulate whole body and cellular thyroid hormone availability. In addition to deiodination (**Figure 2**), which comprises the removal of an iodine atom, alternate pathways of thyroid hormone metabolism exist (**Figure 3**).

Deiodination

The amount of T3 available for receptor action is importantly regulated by D1-3 which have distinct roles based on their differential tissue distribution, substrate preference and enzyme kinetics (summarized in **Table 1**). D1 and D2 predominantly have an activating function and are capable of converting T4 to T3 through outer-ring deiodination. In contrast, D3 converts T4 and T3 to the receptor-inactive metabolites rT3 and 3,3'-T2 through inner-ring deiodination (**Figure 2**).

Deiodinases are so-called selenoproteins as they contain the rare amino acid selenocysteine (Sec). Selenoproteins form a distinct group of 25 proteins in the human proteome. The incorporation of Sec in the catalytic domain of deiodinases is critical for proper enzyme activity and requires a sophisticated mechanism to translate an UGA codon that normally represents a stop sign in the messenger (m)RNA into a Sec. This process is governed by the presence of a selenocysteine insertion sequence (SECIS) element in the 3'-UTR of the mRNA. Specific proteins including Secis Binding Protein 2 (SBP2) are capable of recognizing the SECIS sequence and facilitate the recruitment of elongation factor, Sec transfer RNA ($tRNA^{[Ser]Sec}$) and other factors to insert Sec at the UGA codon.

Table 1 Characteristics of iodothyronine deiodinases.

	D1	**D2**	**D3**
Biochemical properties			
Molecular weight (kDa)	29	30.5	31.5
Preferred substrate	rT3	T4, rT3	T3,T4
Km (M)	10^{-7}	10^{-9}	10^{-9}
Half life	Hours	±20 min	Hours
Sub-cellular localization	Plasma membrane	ER	Plasma membrane
Susceptibility to PTU	High	Low	Low
Tissues with high activity	Liver, kidney	CNS, pituitary, BAT, placenta	CNS, placenta
Response to ↑T3 and T4			
Transcriptional	↑↑	↓	↑↑*
Translational	?	↓↓↓ (ubiquitination)	?
Physiological role	Clearance of rT3	Thermogenesis, development, provision of intracellular and plasma T3	Clearance of T3 and T4
Physiological regulation			
Induction	T3	Cold exposure, catecholamines	Tissue injury, T3
Repression	Fasting, illness	T3	Glucocorticoids

Abbreviations: ER, endoplasmic reticulum; CNS, central nervous system; BAT, brown adipose tissue. * In brain.
Adapted from Bianco and Kim, J Clin Invest. 2006

D1 is mainly expressed in the liver and kidney (39), where it is assumed to control whole body thyroid hormone metabolism and secure T3 availability for other peripheral organs. Indeed, the D1-blocking drug propylthiouracil (PTU) and genetic variation in *DIO1* both reduce serum T3 concentrations and increase serum FT4 and rT3 concentrations (40-42). This may point towards a decreased activation of T4 to T3 when D1 expression and/or activity are decreased. On the other hand, several other observations may argue against this assumption. First, mice deficient in D1 show normal serum T3

concentrations (43, 44), and second, the affinity of D1 for rT3 and sulfo-conjugated iodothyronines is much higher than its affinity for T4 (45). For this reason, it has been proposed that D1 may rather be responsible for the recycling of receptor-inactive iodothyronines. The expression of D1 is strongly positively regulated by thyroid hormone (46), and hence, D1 is currently regarded as the most sensitive marker for peripheral thyroid state.

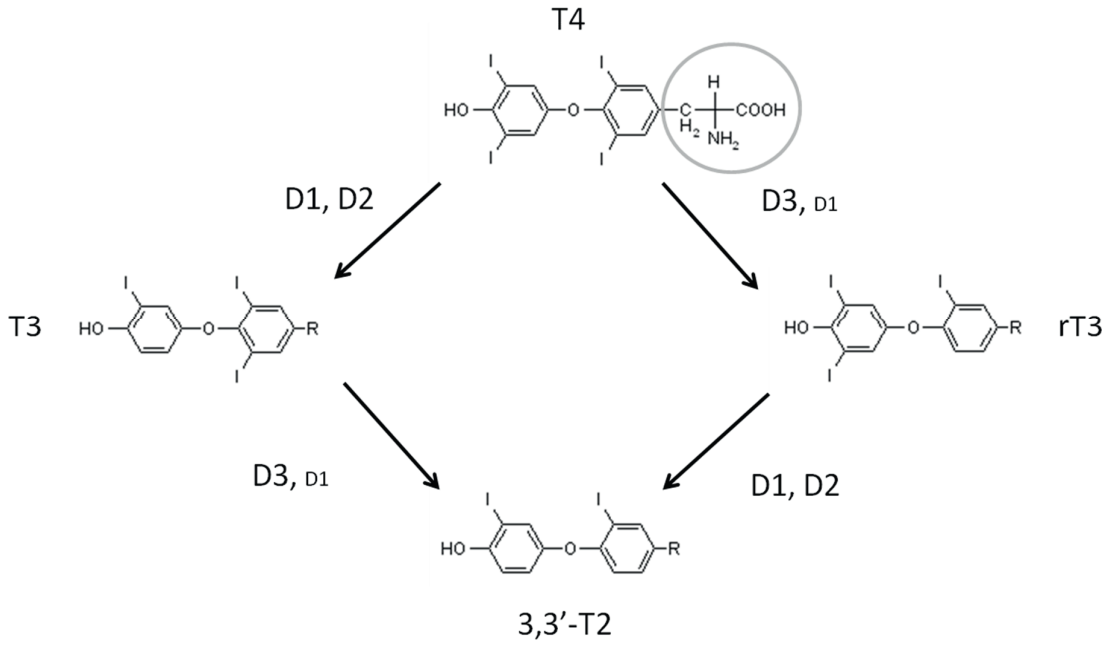

Figure 2 Structure of the iodothyronines and their activation or inactivation by the deiodinating enzymes D1-D3. The alanine side-chain of T4 is encircled and replaced by R in the other iodothyronines.

D2 essentially serves as a thyroid hormone activating enzyme and catalyzes the conversion of T4 to T3. D2 has been classically regarded to regulate local tissue thyroid hormone homeostasis, although D2 has also been implied to contribute to the production of the circulating T3 pool, more recently (47-49). D2 is most abundantly expressed in the central nervous system, pituitary and brown adipose tissue, where its presence governs intracellular T3 concentrations (50). Especially in brain, the expression of T3-responsive genes is highly dependent on local conversion of T4 to T3 in glial cells expressing D2 (51). It has been estimated that brain D2 is responsible for about 80% of cerebral T3 concentrations in rodents (52, 53). Nevertheless, inactivation of D2 in mice either globally or locally does not result in a pronounced neurological phenotype (54), suggesting that the brain exhibits sophisticated mechanisms to compensate for reduced D2 activity (48). D2 is inversely regulated by its substrates T4 and rT3 at posttranslational level through a ubiquitination-deubiquitination system that allows rapid adjustment of cellular thyroid hormone concentrations (49).

D3 is the main thyroid hormone inactivating enzyme and controls the availability of its preferential substrate T3 inside the cell. Based on its high expression levels in fetal tissues and pronouncedly increased mortality rate and growth retardation observed in D3 deficient mice, an important role in fetal development has been ascribed to D3 (55). In adult tissues, D3 is expressed in brain, particularly in neurons, pituitary and placenta. Moreover, D3 is induced during certain conditions including cell

injury, tumorogenesis, critical illness and hypoxia (48, 49, 56). The *DIO3* gene is subject to imprinting and preferentially the paternal allele is active.

No disease-causing mutations have been identified in either one of the deiodinating enzymes. However, several families with inactivating mutations in *SBP2* have been reported as well as one patient with defective $tRNA^{[ser]sec}$ (57, 58). Patients with mutations in SBP2 typically manifest elevated (F)T4 and rT3 concentration, while T3 concentrations are low or low-normal which may suggest impaired outer-ring deiodination. Similar, though less abundant, alteration have been documented in the patient with defective $tRNA^{[ser]sec}$.

Alternate pathways of thyroid hormone metabolism

Alternate pathways of thyroid hormone metabolism include conjugation of the phenolic hydroxyl group as well as decarboxylation or (oxidative) deamination of the alanine side-chain of iodothyronines (**Figure 3**). Although ether link cleavage is theoretically possible, it has been thought to represent a minor pathway of thyroid hormone metabolism. The different alternate pathways of thyroid hormone metabolism will be discussed here, with a particular focus on triiodothyroacetic acid (Triac, TA3).

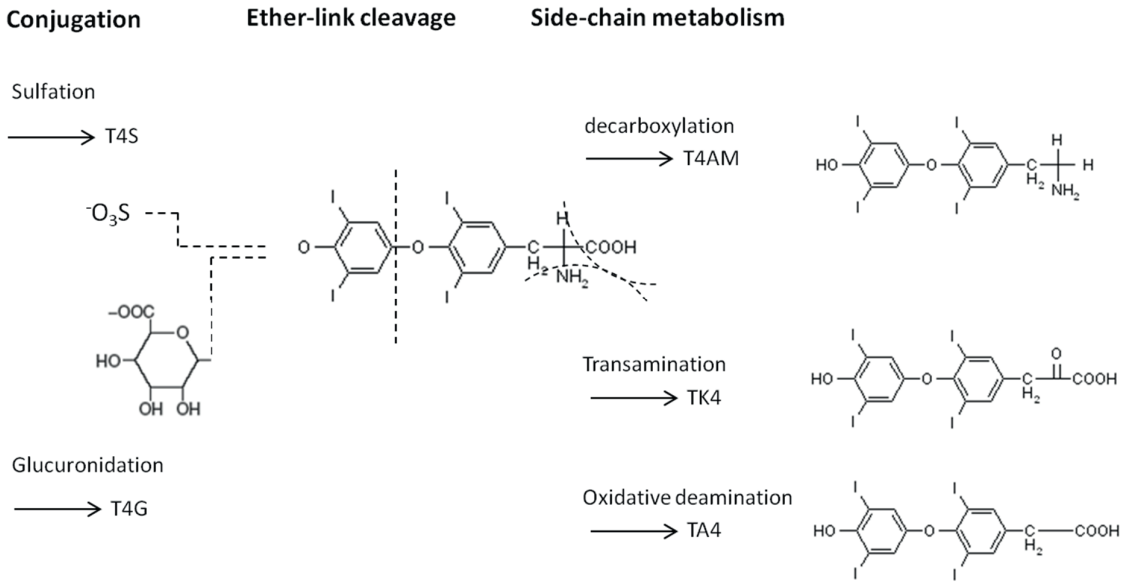

Figure 3 Schematic overview of the alternate pathways of thyroid hormone metabolism.

Conjugation of iodothyronines with glucuronic acid or sulfate is facilitated by UDP-glucuronyltransferases and cytosolic sulfotransferases, respectively, and increases their water-solubility. Glucuronidation of iodothyronines in the liver enhances their biliary excretion and comprises an important step in the entero-hepatic cycle of thyroid hormone. Part of the excreted T3G and T4G can be reabsorbed in the gastro-intestinal tract after hydrolysis to T3 and T4, respectively. Sulfation of iodothyronines greatly accelerates degradation by deiodination (59). In addition, bioactive T3 can be reconstituted from the pool of receptor-inactive sulfo-conjugated iodothyronines by tissue-specific sulfatases (60). This mechanism may be important during development, as serum sulfo-conjugated iodothyronine concentrations are greatly elevated during prenatal and neonatal stages as compared to the adult situation (61, 62).

In addition to the iodothyronines, potential biological actions have been ascribed to thyronamines and the iodothyroacetic acid derivatives Triac and 3,3',5,5'- tetraiodothyroacetic acid (Tetrac, TA4). In an attempt to identify the biological active thyroid hormone, Triac was first synthesized by Pitt-Rivers in the early 1950s (63). As it turned out that the biological effects of Triac were less potent than those of T3, Triac received little attention in the decades after. Following its potential application in treatment of patients with RTHβ, Triac regained attention in the 90s. Triac reportedly exerts potent TSH-suppressive effects in humans, while having relatively weak thyromimetic effects in peripheral organs compared to T3. Because of its thyromimetic properties, the use of Triac in the treatment of different thyroid diseases has been explored, including myxedema, TSH suppressive therapy in patient with differentiated thyroid cancer, goiter, and RTH syndromes (64-70). More recently, thyronamine (T0AM) and monoiodothyronamine (T1AM) were found to exert profound effects on the cardiovascular system and body temperature (36).

Although, the formation of the thyroacetic acid derivatives Triac and Tetrac has been demonstrated *in vivo* in rodents and human (71-78), the underlying mechanism has not been fully elucidated. Based on theoretical grounds and available experimental evidence, at least two plausible mechanisms may exist (**Figure 4**).

The first mechanism entails the decarboxylation and successive oxidative deamination of the alanine side chain of iodothyronines. Recently, purified human intestinal ornithine decarboxylase (ODC) was indeed demonstrated to facilitate the decarboxylation of 3,5-T2 to 3,5-diiodothyronamine (T2AM) and T4 to 3,3',5,5'-tetraiodothyronamine (T4AM) (79). It remains to be studied if other decarboxylases also possess this capacity. Although recent studies have demonstrated the presence of decarboxylated (iodo)thyronine metabolites 3-T1AM and T0AM in human serum (36), it remains to be studied if also other iodothyronamines exist *in vivo*. Studies using selective inhibitors indicated that monoamine oxidase (MAO) and/or semicarbazide-sensitive amine oxidase (SSAO) may convert 3-T1AM and T3AM to their aldehyde intermediates, which may be substrates for the abundantly expressed aldehyde dehydrogenase (ALDH), resulting in the formation of 3-iodothyroacetic acid (Monac, 3-TA1) and Triac, respectively (80). However, conversion of T4AM to Tetrac has not been demonstrated thus far. Although iodothyronamines are efficiently deiodinated, neither D1 nor D2 catalyze the conversion of T4AM to T3AM (81). This indicates that conversion of T4AM to T3AM is not an intermediate step in the conversion of T4 to Triac. Together, these studies support the hypothesis that at least some iodothyronines can be converted to their acetic acid metabolites via a thyronamine intermediate.

An alternative mechanism by which iodothyronines could be converted to iodothyroacetic acid derivatives may involve the conversion of the alanine side-chain to a pyruvic acid intermediate by aminotransferase(s), followed by decarboxylation to acetaldehyde and oxidation to acetic acid (82). However, the enzymes catalyzing these reactions remain to be identified.

Triac and Tetrac are metabolized through similar pathways as T3 and T4. The majority of Triac (and Tetrac) is inactivated through step-wise deiodination (83, 84), which is accelerated by sulfo-conjugation. In addition, glurunonidation enhances the biliary excretion of Triac and Tetrac. It is currently unknown which transporters facilitate the cellular uptake and efflux of Triac and Tetrac. Studies in rodents suggest that the Triac transporter(s) are widely expressed, given the increase in Triac concentration in many tissues after injection of Triac (75).

Triac mainly exerts its biological effects through binding to the nuclear TRs, with putatively a slight preference for the TRβ receptor (85-88). Importantly, Triac was found to transactivate at least certain mutant TRβ proteins more efficiently than equimolar concentrations T3, which led some to treat patients with RTHβ with Triac. In most patients that have reportedly been treated with Triac, TSH concentrations decreased with subsequent normalization of serum thyroid hormone concentrations and alleviation of (some) thyrotoxic symptoms.

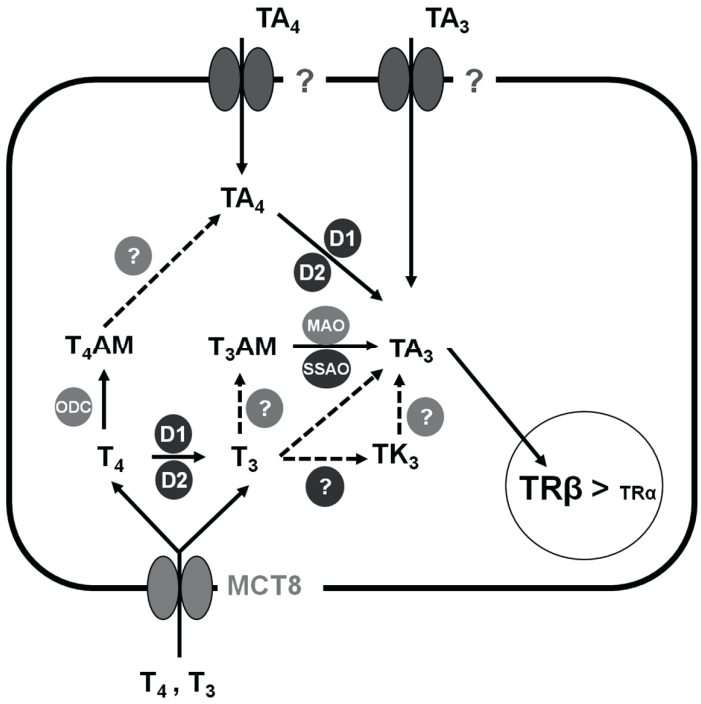

Figure 4 Schematic overview of cellular formation, metabolism and action of TA_3. Dashed lines represent processes for which the involved enzymes/transporters have not been identified but their existence may be assumed based on theoretical grounds or experimental data. D: deiodinase, MAO: monamine oxidase, SSAO: semicarbazide-sensitive amine oxidase, ODC: ornithine decarboxylase, TK_3: 3,3',5-triiodothyropyruvic acid.

THYROID HORMONE TRANPORTERS

Another level at which cellular thyroid hormone action is regulated comprises the transport of thyroid hormones across the cell membrane. It had been thought for many decades that thyroid hormones could enter their target cells through passive diffusion given the lipophilic nature of iodothyronines. However, accumulating evidence published from the 1970's onwards provided evidence that thyroid hormone transfer across the plasma membrane requires a carrier-mediated mechanism, and that the role of passive diffusion, if any, is limited (6, 7). These studies indicated that the transport of thyroid hormone into cells is a saturable process, may be inhibited by aromatic and/or aliphatic amino acids and may depend on Na^+ in some cell types. Yet, the identity of thyroid hormone transporter proteins started being elucidated in the late 90s. These early studies, providing the basis for a paradigm shift in

the field, are extensively summarized by Hennemann et al (89). The turn of the millennium marked the time of several discoveries that had a great impact on the field of thyroidology.

First, several transporters from different protein families were identified at the molecular level as thyroid hormone transporting proteins. This was a major breakthrough compared to the decades before when only the general characteristics of thyroid hormone transmembrane passage had been studied in non-transfected cells. The characterization of rat organic anion transporting polypeptide (Oatp) 1a1 as the first thyroid hormone transporter was rapidly followed by the identification of several human thyroid hormone transporters, of which monocarboxylate transporter (MCT)8 and OATP1C1 showed the highest specificity towards thyroid hormone (90-92).

A seminal discovery was the identification of a disorder associated with mutations in the thyroid hormone transporter MCT8. Mutations in MCT8 are associated with a severe form of intellectual disability accompanied by a specific thyroid hormone fingerprint in the blood (93, 94). These publications started a new era as it provided an ultimate proof for the physiological relevance of thyroid hormone transporters.

In addition, different models have been established to study the role of thyroid hormone transporters in health and disease. Particularly, various experimental models have enlarged the understanding on the (tissue-specific) contribution of various thyroid hormone transporters in the regulation of tissue thyroid hormone state. Novel global and tissue-specific transporter knock-out (ko) mouse models have been generated and characterized over the last years (95-105). In addition, zebrafish and chicken are emerging as complementary vertebrate models to study the role of thyroid hormone transporters. Finally, re-differentiated patient-derived induced pluripotent stem cells (iPSCs) have been employed as a human model to understand disease (106-110).

Finally, drug therapy development programs followed the identification of MCT8 deficiency. The abovementioned models largely facilitated testing potential therapeutic intervention for transporter defects. Such preclinical studies indicated that the use of thyroid hormone analogues may hold strong therapeutic potential in MCT8 deficiency, which formed the basis of one of the studies in this thesis (**chapter 5.2**).

As thyroid hormone transport is the major focus of this thesis, this section will briefly introduce several basic principles in thyroid hormone transport research and provide an overview of the functional characteristics and tissue distribution of the thyroid hormone transporters that have been identified to date, with a particular focus on the OATP1C1 and MCT8. For a more detailed overview, the reader is referred to the full review on thyroid hormone transporters (111).

General aspects of thyroid hormone transport

Thyroid hormone transporters govern the cellular uptake (transport from the extracellular compartment into the cell), the cellular efflux (transport from the cell into the extracellular compartment), or both. The currently known thyroid hormone transporters belong to four different protein families, which include the organic anion transporters (OATPs, and the SLC10 family), the L-type amino acid transporters (LATs) and the monocarboxylate transporters (MCTs).

Most thyroid hormone transporters have been identified through *in vitro* over-expression studies in cell lines or *Xenopus* oocytes, using [^{125}I]-radio-labeled iodothyronines to measure cellular thyroid hormone uptake. Such cellular expression systems are indispensable to ensure proper protein conformation and function. The substrate specificity of transporters is generally determined in direct uptake studies with the compounds of interest, or indirectly in (cis-)inhibition studies. It should be noted, that cellular thyroid hormone homeostasis in these systems not only depends on the over-expressed transporter of interest, but also on the set of endogenously expressed thyroid hormone transporters. These additional transporter proteins may importantly influence the transport direction (uptake or efflux), as well as the estimates of substrate affinity and transport rate of the transporter being studied. Therefore, reported Michaelis constants (Km values) merely reflect approximate measures for transporter affinity, rather than precise values as calculated in case for purified enzymes. It is important to highlight that some transporters may require specific conditions in order to function as thyroid hormone transporters. This particularly holds for the so-called secondary active transporters, which couple the uphill transport of thyroid hormone against its concentration or electrochemical gradient to the downhill transport of ions (e.g. Na^+ or H^+) along the electrochemical gradient. This is less relevant for transporters that rely on facilitated diffusion in which case thyroid hormones are transported along their concentration gradient across the cell membrane. Application of the appropriate and, moreover, physiologically relevant conditions is thus imperative to assess if a transporter accepts thyroid hormones as a substrate.

The Organic Anion Transporting Polypeptides (OATPs) family

Phylogenesis of the OATP superfamily

Organic anion transporting polypeptides (OATPs) form a gene superfamily with more than 300 members across at least 40 different species, together classified as the solute carrier family *SLCO* for gene classification and OATP for the corresponding protein nomenclature (112). The OATP superfamily represents a large group of homologous proteins that accept a wide range of substrates, including anionic, but also neutral and even cationic compounds. To date, up to ~40 different OATPs have been identified in humans, rats and mice, which form six major families (OATP1, OATP2, OATP3, OATP4, OATP5, and OATP6) that can be further categorized into several subfamilies (e.g. OATP1A, OATP1B and OATP1C) based upon their amino acid sequence identities (**Figure 5**) (112, 113). It should be noted that some of the members are not well conserved among species. In humans, 11 different OATPs have been identified of whom eight are capable of transporting iodothyronines *in vitro*. Four of these genes, encoding SLCO1A2, 1B1, 1B3 and 1C1, are clustered together with a related pseudogene on human chromosome 12p12.

Substrate specificity and transport direction

Rat OATP1A1 was the first member of the *SLCO* superfamily to be isolated (114) and proved to be a sodium-independent bile acid transporter (114-116). Soon afterwards, rat OATP1A1 was among the first transporters shown to transport iodothyronines (92). Following this observation, OATP1A2 was the first human OATP that was found to transport several iodothyronines (rT3, T3, and T4) (117, 118)

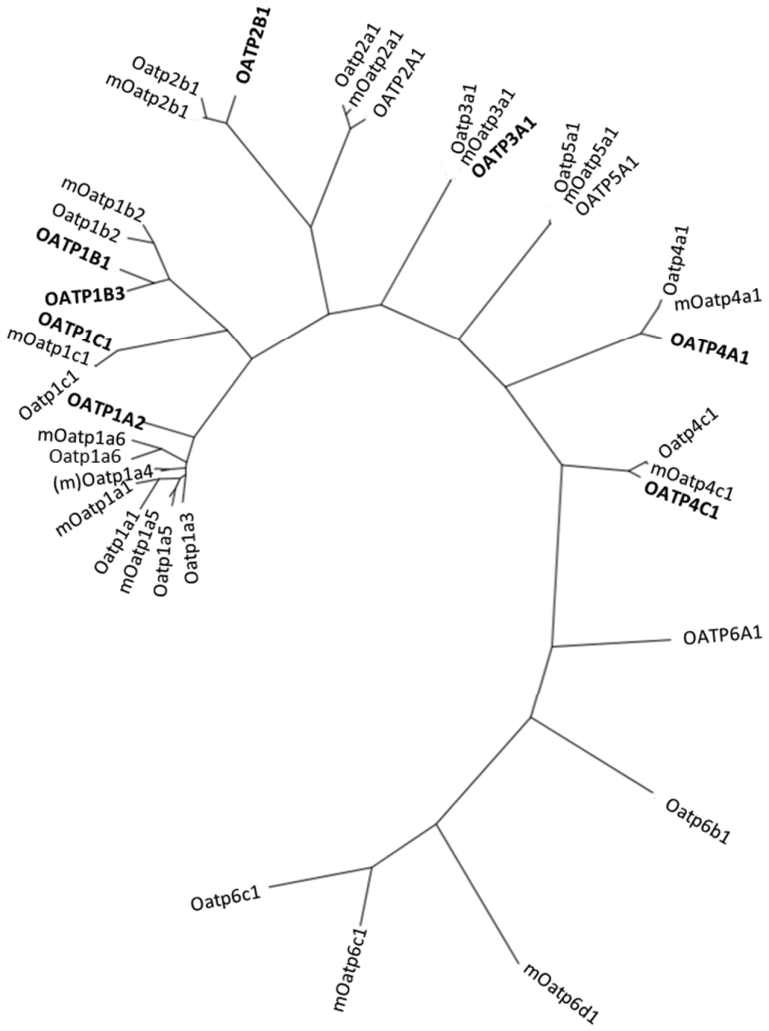

Figure 5 Phylogenetic trees of the OATP (SLCO) family, including the currently known members in rat, mouse and human. The phylogenetic tree has been generated using MUSCLE multiple sequence alignment of ENSEMBL reference protein sequences and PhyML algorithm through http://www.phylogeny.fr/alacarte.cgi. The thyroid hormone transporting (human) members are indicated in bold.

and their sulfo-conjugates (119), as well as a broad spectrum of other substrates, including conjugated and unconjugated bile acids, bromosulfophthalein (BSP) and dehydroepiandrosterone sulfate (DHEAS) (120, 121). In the subsequent years, additional OATPs have been cloned and functionally evaluated. These studies revealed that most human OATPs are multi-specific transporters that accept a broad range of substrates including several bile acids, steroid hormones and conjugates thereof, linear and cyclic peptides, prostaglandins and multiple drugs and other xenobiotics (reviewed in (111, 112, 122)). Several other members of the OATP family also facilitate the uptake of iodothyronines or metabolites thereof, including OATP1B1 (123-125), OATP1B3 (119, 126), OATP1C1 (91, 127), OATP2B1 (128), OATP3A1 (128, 129), OATP4A1 (117), OATP4C1 (112, 130, 131). Besides rat OATP1A1, rat OATP1A3 (124, 132), OATP1A4 (124), OATP1A5 (124), OATP1B1 (133), OATP1B2 (134), OATP1B3 (133), OATP1C1 (135), OATP4A1 (117), OATP4C1 (131), OATP6B1 (136), and OATP6C1 (136) also transport iodothyronines, each with their unique substrate preferences and affinities (summarized in (112, 130)).

Many of these OATPs show a relatively low affinity towards iodothyronines and transport a multitude of other substrates (111). For these reasons, it is currently unclear if all OATPs that were found to transport thyroid hormone *in vitro* also exert meaningful contributions to cellular thyroid hormone homeostasis *in vivo*.

Compared to other OATPs, OATP1C1 has the highest affinity for and greatest specificity towards iodothyronines, with apparent Km values of 90.4 nM for T4, and 127.7 nM for rT3, whereas its affinity for T3 seems considerably lower (91, 127). OATP1C1 also facilitates the uptake of sulfo-conjugated T4 (T4S) and enhances its intracellular metabolism by D1 (127). The uptake of T4 by OATP1C1 exhibits a biphasic kinetic profile, suggesting the presence of a low and a high affinity binding site (137). Moreover, rat OATP1C1 facilitates the efflux of T4 (135). Although the exact transport mechanism of OATPs is not fully understood, OATPs are known to act as organic anion exchangers (112, 138), and are therefore classified as secondary active transporters. The uptake by various OATPs is stimulated by a low extracellular pH, with the exception of OATP1C1 (128, 139).

Tissue distribution and regulation of expression

OATPs are expressed in virtually all tissues. Some members, such as OATP2B1, OATP3A1 and OATP4A1, are expressed ubiquitously, whereas the expression pattern of others, including OATP1B1, OATP1B3 and OATP1C1, is more restricted (140). Especially at mRNA level most OATPs are widely expressed, although the tissue expression profile has not always been confirmed at protein level due to lack of suitable antibodies. As OATP1C1 is subject of **chapter 6.4** of this thesis, its tissue distribution will be discussed in more detail here. For details on the other OATP members, the reader is referred to (111, 112).

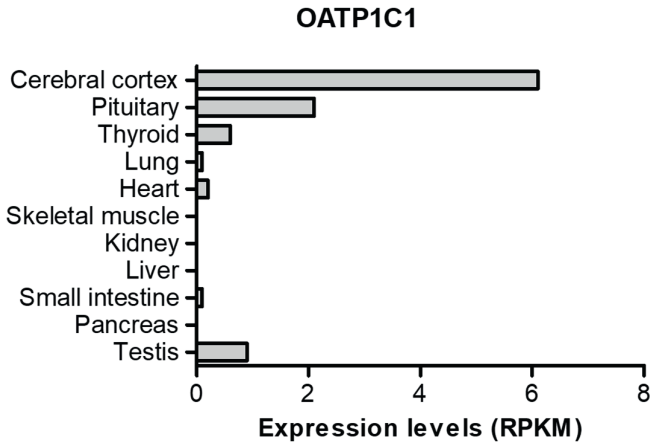

Figure 6 An overview of the tissue distribution of OATP1C1 at mRNA level in human based on the Genotype-tissue-expression (GTEx) RNA sequencing project, accessible through https://www.proteinatlas.org/.

OATP1C1 is considered as a brain-specific transporter, although a limited number of other tissues also express *OATP1C1* mRNA. In humans, these tissues include the Leydig cells of testes (91) and different structures of the eye (141, 142) (**Figure 6**). *OATP1C1* mRNA is widely abundant in human brain with highest expression in the cerebral cortex, amygdala, caudate nucleus, hippocampus and putamen, but not in the pons and cerebellum (91). OATP1C1 was also detected in the choroid plexus, but not at the blood-brain barrier (BBB) (143). In contrast to human and primates (144), OATP1C1 is highly abundant in the vascular endothelial cells of the BBB in adult rodent brain, where it is localized at the luminal

and abluminal side (96, 135, 145, 146). Similar to rodents, *oatp1c1* expression can be detected at mRNA level in vascular structures within the brain of zebrafish (107). The presence of OATP1C1 at the BBB thus importantly differs among species. In addition, OATP1C1 has also been detected in astrocytes and in the choroid plexus of rats (145), mice (143), and chickens (147).

Oatp1c1 transcript levels in rat capillary endothelial cells are affected by the thyroidal state as higher expression was found in hypothyroid animals and reduced expression in hyperthyroid animals (135, 148). Similarly, the expression levels of *Oatp1c1* increased in the fetal part of the placenta during maternal hypothyroidism in rat (149). A striking reduction in *Oatp1c1* expression has been observed in rodent brain capillary cells during inflammation (150). The exact molecular mechanisms involved in the transcriptional regulation of *OATP1C1* remain to be elucidated.

Na/taurocholate cotransporting polypeptide (NTCP; SLC10A1)

Phylogenesis of the SLC10 family

The SLC10 family comprises seven established members that are uptake transporters of bile acid, steroidal hormones, specific drugs, and a variety of other substrates (**Figure 7**) (151), of which only SLC10A1 (sodium/taurocholate co-transporting polypeptide, NTCP), also accepts thyroid hormones as substrates (152).

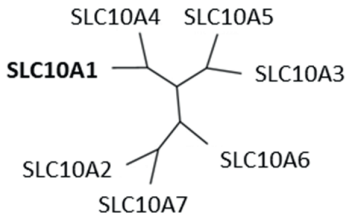

Figure 7 Phylogenetic trees of the human NTCP family. The thyroid hormone transporting (human) members are indicated in bold.

Substrate specificity and transport direction

Similar to its rat orthologue (153), human NTCP transports all physiological bile salts with affinities in the micromolar range (154, 155). In addition, NTCP transports sulfo-conjugated bile acids, sulfo-conjugated steroids such as estron-3-sulfate (E3S), and cholephilic compounds such as BSP with similar affinity; the latter two being frequently used as competitive (though non-selective) inhibitors of NTCP-mediated transport (155). Rat and human NTCP facilitate the uptake of T3 and T4, and, even more efficiently, of rT3 and the sulfo-conjugated iodothyronines T3S and T4S (92, 152). The uptake of T3S and T4S was largely inhibited in presence of 50 µM taurocholate, suggesting that transport of thyroid hormones by NTCP can be impeded if bile acid concentrations rise (e.g. after a meal) (152). NTCP does not facilitate the efflux of T3S or T4S (152).

Tissue distribution and regulation of expression

Similar to rodents (156-159), human NTCP is specifically expressed in liver (160). Expression levels are relatively low during fetal development, possibly contributing to the high T3S and T4S concentrations at that stage, and about 20-times higher in adult liver (161). The transcriptional regulation of NTCP is extensively reviewed elsewhere (162).

L-amino acid transporters

Phylogenesis of L-type amino acid transporters (LATs)

The system L, or L-type amino acid transporters (LAT) comprise a heterogenous group of proteins that transport neutral (branched chain and aromatic) amino acids in an Na^+-independent fashion (163-165). LAT1 and LAT2, are heterodimeric proteins composed of a common heavy chain (CD98; SLC3A2; 4F2hc) and different light chains (SLC7A5 and SLC7A8, respectively). SLC7A5 (LAT1) and SLC7A8 (LAT2) are the only members of the SLC7 family (**Figure 8**) involved in the transport of iodothyronines (166). Over the years, three additional proteins have been found to exhibit similar transporters characteristics as LAT1 and LAT2 and were termed LAT3-5 (SLC43A1-3) (167-171)). Although they were tested negative for thyroid hormone uptake, LAT3 and LAT4 may induce the cellular efflux of MIT, DIT and 3,3'-T2 (172).

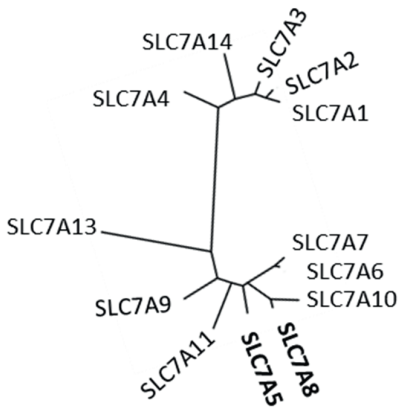

Figure 8 Phylogenetic trees of the human SLC7 family. The thyroid hormone transporting (human) members are indicated in bold.

Substrate specificity and transport direction

LAT1 and LAT2 are obligatory exchangers that transport (large) neutral amino acids, including L-leucine, L-isoleucine, L-tyrosine and L-tryptophan, typically in an energy and Na^+-independent fashion (165, 173, 174), with apparent affinities in the micromolar range (164, 165, 173, 175). LAT2 also accepts the small neutral amino acids glycine and alanine. Following observations that thyroid hormone uptake was inhibited by neutral amino acids in some cell-types (176-181), seminal studies of Ritchie et al. (182), and Friesema et al. (166) first showed direct thyroid hormone transport by human LAT1 and mouse LAT2, respectively.

LAT1 transports 3,3'-T2, rT3, T3 and T4 into the cell, whereas it only facilitates the efflux of 3,3'-T2 (166). Its apparent affinities for T4 (7.9 µM), T3 (0.8 µM), rT3 (12.5 µM), and 3,3'-T2 (7.9 µM) are considerably lower than for the various amino acids, but still greatly exceed the physiological thyroid

hormone concentrations in serum. The inhibition of L-leucine, L-tyrosine, and L-tryptophan uptake (at 10 μM) required supra-physiological concentrations of T3 (K_i 1.7 μM for L-leucine) or T4 (K_i 115 μM for L-leucine), while transport of T3 (at 0.1 μM) was almost completely blocked in presence of 100 μM L-leucine, L-tyrosine, L-tryptophan or L-phenylalanine, which is around the physiological concentrations of these amino acids in human serum (166, 183, 184).

LAT2 facilitates the uptake of 3,3'-T2 (apparent Km 18.6 μM) and to a lesser extent T3, but not rT3 or T4, whereas none of the iodothyronines seems to be a suitable substrate for LAT2-mediated efflux (172, 185, 186). In line, 10 μM T3 and T4 had no effect on LAT-2 mediated L-alanine uptake, and only minimal effects on L-leucine transport (183, 184). The uptake of 3,3'-T2 was inhibited by supra-physiological concentrations of L-leucine, L-isoleucine, L-methionine, and L-histidine (1 mM), and by various T1 and T2 derivatives, but not rT3 at a concentration of 10 μM (185). All LATs can be competitively inhibited by 2-aminobicyclo(2,2,1)-heptane-2-carboxylic acid (BCH) (187).

In seemingly contrast to the effects of excess amino acids on the extracellular side, the transport of iodothyronines by LAT1 and LAT2 can be greatly diminished by cellular amino acid depletion prior to uptake studies, suggesting that LAT1 and LAT2 may require a certain degree of amino acids at the intracellular side to create a suitable gradient for the transport of iodothyronines. Therefore, the amino acid gradient across the cell membrane may importantly determine the rate and direction by which LAT1 and LAT2 transport iodothyronines. At the same time, the relatively high concentrations of the various neutral amino acids inside and outside the cell may well limit the contribution of both transporters to iodothyronines transport *in vivo*.

Tissue distribution and regulation of expression

In humans and rodents, the CD98 heavy chain has a wide tissue distribution (175, 188). Therefore, the tissue distribution of LAT1 and LAT2 is mainly determined by the expression of the SLC7A5 and SLC7A8 light chains, respectively.

Lat1 light chain is predominantly expressed in placenta, brain, vascular endothelial cells, spleen, ovary, testis, retina, and to some extent in renal proximal tubuli at mRNA level in rodents (189-192). A similar tissue distribution was observed in humans, with abundant *LAT1* mRNA expression in brain, placenta and testis, as well as in bone, fetal liver and leukocytes (175). The presence of LAT1 protein has been confirmed in mouse and human brain microvasculature endothelial cells (BMEC) (97, 193, 194). LAT1 is also present in primary cultures of mouse neurons and astrocytes, although its contribution to T3 transport in astrocytes appears to be neglectably small (195).

LAT2 is highly expressed in kidney and to a lesser extent in placenta, skeletal muscle, liver, spleen and brain in rodents and human (165, 189, 190, 196-198). In rodents, LAT2 protein is highly abundant at the basolateral membrane of proximal tubuli in kidney (189, 190) and the basolateral membrane of small intestinal villi (190, 196). The expression of *LAT2* mRNA in the human small intestine is very low (198). In the developing and mature mouse brain, LAT2 is most prominently expressed in neurons of various brain regions and in choroid plexus structures (199, 200), whereas it is exclusively detected in microglia cells in the developing human brain (199).

Transcriptional regulation of *LAT1* and *LAT2* expression has not been studied in much detail, but seems not to be responsive to serum thyroid hormone status (195).

Monocarboxylate transporter (MCT) family

Phylogenesis of the monocarboxylate transporter (MCT) family

The *SLC16* gene family comprises 14 members and is also known as the monocarboxylate transporter (MCT) family (**Figure 9**) (201). The first members of this family to be identified were MCT1-4, which show strongest sequence conservation and facilitate the proton-linked transport of monocarboxylate metabolites involved in energy metabolism such as pyruvate, L-lactate and ketone bodies (201). More recently, MCT7 and MCT11 were found to facilitate the proton-linked transport of ketone bodies and pyruvate, respectively (202, 203). Recent studies identified substrates for MCT6 (bumetanide), MCT9 (carnitine) and MCT12 (creatine) (204, 205). Genetic mutations in these MCT transporters have been linked to various metabolic disorders (206-208).

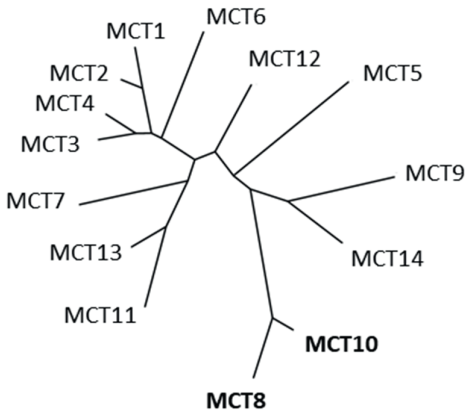

Figure 9 Phylogenetic trees of the human MCT family. The thyroid hormone transporting (human) members are indicated in bold.

The only members of the MCT family found to transport iodothyronines are MCT8 and MCT10 (90, 209). The gene encoding MCT8, *SLC16A2,* was first identified by Lafrenière et al. (210) and is located at the X-chromosome (Chr Xq13.2). The gene was originally called the X-linked PEST containing transporter (*XPTC*) due to the high abundance of Pro (P), Glu (E), Ser (S) and Thr (T) residues in the N-terminal domain of the predicted protein. It consists of 6 exons and 5 introns, of which the first intron is particularly large (~100 kb) (**Figure 10A**). The *SLC16A10* gene, encoding MCT10, has a very similar structural organization and is located on chr 6q21. Both genes are widely conserved across species and are likely to have arisen from a common ancestral gene through gene duplication.

MCT8 orthologues have been identified in mammals, rodents, birds, reptiles, amphibians, marsupials and fish, although only few of their gene products have been verified as thyroid hormone transporters (90, 211-213). Whereas *SLC16A10* only has one translational start site (TLS), two TLSs have been identified in *SLC16A2* of humans and some other mammals such as cow, elephant and seal. Most other species, including rat, mice, and zebrafish, have only one TLS corresponding to the most downstream TLS in human *SLC16A2*. Depending on which of the two TLSs is being used, the human MCT8 protein consists of 613 or 539 amino acids, classically referred to as “long” and “short” MCT8, respectively (**Figure 10A** and **B**). Since both isoforms exhibit similar transporter characteristics (see below) and the

homology among species is strongest starting from the second TLS, it nowadays commonly accepted that short MCT8 is the most relevant isoform. This conclusion recently led to a change in the MCT8 reference sequence and thus the amino acid residue numbering. Unfortunately, this re-numbering can cause confusion and ambiguity with regard to the nomenclature of variants and mutations in SLC16A2 that have been identified and reported over the last decades, which started counting from the first TLS. To avoid such confusion, the first TLS will be considered as the starting point of amino acid numbering throughout this thesis.

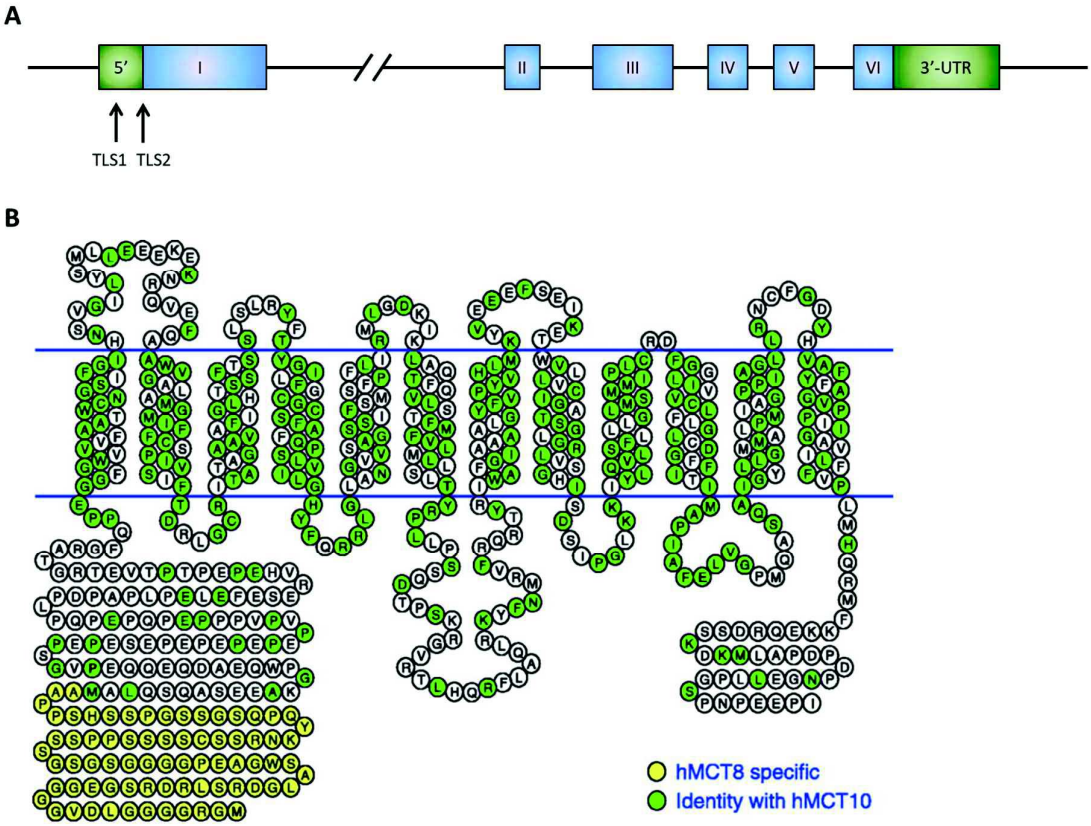

Figure 10 (A) Genomic structure of human *SLC16A2*. Arrows indicate the two possible translational start sites. **(B)** Putative transmembrane configuration of human MCT8 with 12 transmembrane domains and an intracellular N-terminus and C-terminus. The putative long variant of hMCT8 is indicated in yellow. The amino acid residues that are conserved between MCT8 and MCT10 are indicated in green. Figure adapted from (119).

Substrate specificity and transport direction

Early *in vitro* studies had suggested the involvement of a T-type amino acid transporter in the uptake of thyroid hormone into erythrocytes (214). Such a T-type amino acid transporter was identified and characterized by Kim et al. in the early 2000s and termed TAT1 (215, 216). TAT1 belongs to the MCT family (MCT10, *SLC16A10*) and was found to transport the aromatic amino acids phenylalanine, tryptophan and tyrosine very effectively, but seemingly not thyroid hormones (215, 216). Based on the high sequence homology, MCT8 (SLC16A2) was finally identified as the long-sought T-type amino acid transporter that was capable to transport T3 and T4 (90). These studies indicated highly effective transport of T4, T3, rT3 and 3,3'-T2 in oocytes expressing rat MCT8, with apparent Km values of 4.7

µM for T4, 4.0 µM for T3 and 2.2 µM for rT3 (**Table 1**). By contrast, overexpression of rat MCT8 did not induce the uptake of the aromatic amino acids, leucine, sulfo-conjugated iodothyronines or monocarboxylic acids such as lactate and pyruvate (90). Subsequent studies in transiently transfected mammalian cells indicated that also (the short isoform of) human MCT8 induces the intracellular accumulation of T4, T3, rT3 and 3,3'-T2, although the fold induction was less pronounced when compared to rat MCT8 in *Xenopus* oocytes (217). This apparent discrepancy was later explained by the observation that MCT8 does not only facilitate the cellular uptake, but also the cellular efflux of iodothyronines (209). Complementary studies indeed confirmed that upon co-transfection of MCT8 with the cytoplasmic high-affinity thyroid hormone-binding protein mu-crystallin (CRYM) the intracellular accumulation of T3 and T4 was strongly amplified by preventing MCT8-mediated thyroid hormone efflux (209). Expression of MCT8 greatly enhances the intracellular metabolism of iodothyronines, in particular by D3 (217, 218). These observations may indicate that under these overexpression conditions the bidirectional transport by MCT8 mainly increases T3 concentrations at the cell membrane where D3 is located. Using a similar approach, later studies demonstrated that MCT10 is an equally proficient T3 transporter as MCT8, but substantially less effective with T4 as a substrate (209). Based on the above mentioned studies, it was concluded that the transport of thyroid hormone by MCT8 and MCT10 likely concerns facilitated diffusion and is not sensitive to pH, or dependent on Na^+.

Detailed (cis-inhibition) studies on potential substrates and inhibitors for MCT8 suggested that MCT8 is specific for the L-enantiomers of thyroid hormone, and requires both the amino and the carboxy groups of the alanine side-chain of thyroid hormone as well as at least one iodine atom in each iodothyronine ring (219), although 3-iodothyronamine at high concentrations reduced MCT8-mediated thyroid hormone uptake (219, 220). In contrast to MCT8, T3 uptake by MCT10 was also effectively inhibited by 1 µM 3-T1, 3,-T1, and 3,5-T2, suggesting that the presence of an iodine in both rings might be a less stringent requirement for MCT10 (221). Moreover, rat MCT10-mediated uptake of tryptophan is inhibited by L-3,4-dihydroxyphenylalanine (L-dopa) and 3-O-methyl-dopa (215). Direct uptake studies confirmed that compounds lacking the αNH2 group of thyroid hormone (i.e. Triac and Tetrac) are no suitable substrates for MCT8 and MCT10, whereas its modification (i.e. N-bromoacetyl-iodothyronines) is tolerated (84, 222, 223). Similar studies confirmed that MCT10 directly transports 3,5-T2 and L-dopa (215, 216, 221). No substrates other than iodothyronines have been identified for MCT8 thus far, which appears remarkable given the large number of monocarboxylic acid-containing derivatives in relation to the limited number of identified monocarboxylate transporters.

MCT8-mediated thyroid hormone uptake is inhibited by the non-selective inhibitor BSP (219). The tri-cyclic antidepressant desipramine inhibits both MCT8 and MCT10 (224), whereas the flavonolignan silychristin appears to be a specific inhibitor of MCT8 (225). Moreover, several tyrosine kinase inhibitors have been found to interfere with MCT8 and MCT10 function through non-competitive inhibition (226-229). Although not as extensively studied as short MCT8, also the long isoform of human MCT8 efficiently transports iodothyronines (230, 231).

Expression and tissue distribution of MCT8 and MCT10

MCT8 mRNA levels are highest in liver and adrenal gland and somewhat lower in a variety of other tissues including brain, hypothalamus, vascular endothelial cells of the blood-brain-barrier, kidney, placenta, and thyroid (**Figure 11A**) (143, 232-236). Analysis of human fetal cerebral cortex at mid-

gestation revealed MCT8 immuno-positive signals in numerous neurons of the ventricular and subventricular zone, in choroid plexus structures and ependymal cells lining the ventricle as well as in the wall of microvessels (143, 199, 237). In the adult human central nervous system (CNS), MCT8 immuno-labeling was present in microvessels and choroid plexus structures, whereas neuronal MCT8 expression appeared to be weak (143, 199). Detailed studies of Alkemade et al. (2005) showed that MCT8 is present in neurons and astrocytes of the paraventricular and infundibular nuclei at the human blood-hypothalamus border (238). In choroid plexus epithelial cells, MCT8 was detected at both the basolateral and the apical membrane (233). Most of these studies presumably detected the short isoform of MCT8, as the protein size of human MCT8 reportedly was similar to that of its mouse orthologue (199). It is uncertain if the long isoform exists *in vivo* and in which tissues it is expressed.

In rodents, the MCT8 protein has been detected in the sinusoidal membrane of hepatocytes (90, 98), on the basolateral membrane of thyrocytes (97, 239, 240) and the proximal tubule cells in kidney (241, 242), retinal cells (243), placenta (244), and in different cell types in skeletal muscle (102). In mouse brain, MCT8 is localized in different neuronal populations of the cerebral and cerebellar cortex, hippocampus, striatum and hypothalamus, with highest expression during early postnatal stages. *MCT8* mRNA was also detected in oligodendrocytes and in astrocytes (143, 145, 199, 245-247). Similar to the human situation, mouse MCT8 protein is strongly expressed in capillary endothelial cells and in choroid plexus structures, indicating that MCT8 may facilitate the thyroid hormone transport across the BBB and the blood-cerebrospinal fluid barrier (BCSFB), respectively. Expression of MCT8 was also detected in mouse and human tanycytes, a specialized ependymal cell type lining the third ventricle and involved in the negative-feedback regulation within the HPT-axis (199, 238, 245, 248). In zebrafish, *Xenopus* and chicken, *mct8* is expressed in different areas of the brain, spinal cord and vascular system (107, 213, 249) (110, 147, 212, 250). Co-localization studies in zebrafish indicated that *mct8* is expressed in sensory and motor neurons, oligodendrocytes, but not astrocytes (107, 108, 251), which is reminiscent to the situation in mice. However, in all species, the cell-type specific expression pattern can vary depending on the brain region studied and the timing during development (200, 252).

In human, *MCT10* mRNA expression was predominantly detected in kidney, skeletal muscle, placenta, heart, and developing brain (**Figure 11B**) (216, 234, 236, 253). *MCT10* mRNA expression increased with gestational age in human placenta, and its expression levels were lower in fetus presenting intrauterine growth restriction (236). MCT10 protein has been detected at various stages and regions in the developing brain (253) and on the apical membrane of the choroid plexus (233). In the developing human hypothalamus, MCT10 expression was detected in different neuronal cell populations, including the PVN, supra-optic nucleus, lateral hypothalamus and infundibular nucleus, starting from the second trimester - although the expression levels and distribution pattern showed inter-individual variation and changed during development (233). In rodents, MCT10 is expressed in a great variety of tissues, including the thyroid, liver, kidney, chondrocytes, small intestine and skeletal muscle (97, 102, 254, 255). Of note, *Mct10* expression in the murine brain is low and appeared to be restricted to a subset of neurons, microglia cells and oligodendrocytes (195, 200), whereas *Mct10* is also highly enriched in mouse choroid plexus at embryonic stages (E15) (256). The tissue distribution of *mct10* in zebrafish has not been studied in much detail and appears to be restricted to the liver (107).

Little is known about the molecular mechanisms involved in the transcriptional regulation of *MCT8* and *MCT10*. Kogai et al. (2010) identified an enhancer element responsive to retinoic acid in F9 mouse teratocarcinoma cells (257). However, this element is not present at the corresponding location in the

human genome and, thus, it is currently unclear if the expression of the human *MCT8* gene is regulated by retinoic acid. Inspection of the *MCT8* proximal promoter sequence in different species suggests that *MCT8* lacks a classical TATA-box element and is thus regulated through other mechanisms (107, 257).

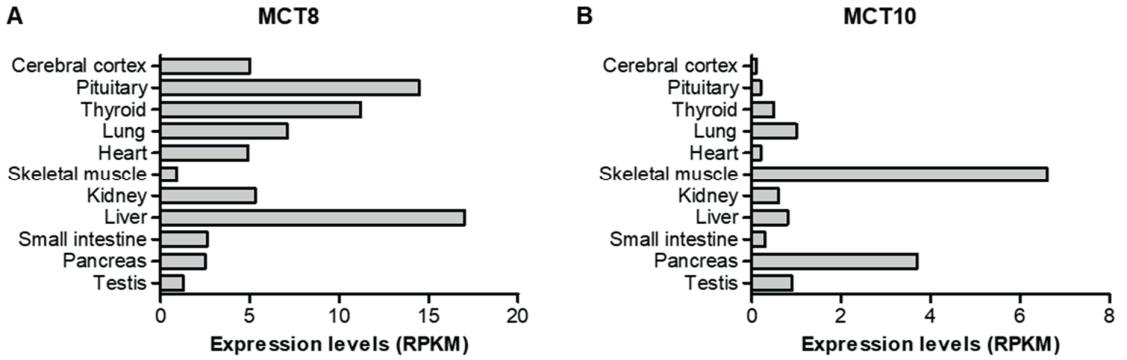

Figure 11 An overview of the tissue distribution of MCT8 (**A**) and MCT10 (**B**) at mRNA level in human based on the GTEx RNA sequencing project, accessible through https://www.proteinatlas.org/.

Although other specific factors and pathways that regulate *MCT8* (and *MCT10*) expression, especially in physiological relevant tissues, remain to be identified, several studies may provide some guidance for identifying such mechanisms. Recent studies in rodents indicated that expression of both *Mct8* and *Mct10* is responsive to feeding status and systemic inflammation since pronounced downregulation of hepatic and hypothalamic *Mct8* expression levels was found during fasting (258-260) and reduced *Mct8* expression in liver and brain vasculature during systemic inflammation (150, 258).

It still remains to be clarified to which extent *MCT8* expression is regulated by TH status. Whereas no significant changes in brain *Mct8* transcript levels were reported in congenital hypothyroid *Pax8* ko mice (245), *Mct8* expression was down-regulated in tanycytes of hypothyroid rats (261). Conversely, testicular *Mct8* expression was increased in hyperthyroid rats (262). In developing zebrafish, global *mct8* expression levels were reported to be thyroid hormone-responsive (148). Other studies may further support the link between the regulation of MCT8 expression and thyroid function. First, MCT8 expression levels were increased in thyroid tissue from patients with Graves' Disease and in the follicular thyroid cell line PCCL3 after stimulation with thyroid stimulating hormone (TSH), suggesting that *MCT8* expression in the thyroid may be TSH-responsive (263). Second, both thyroidal *Mct8* and *Mct10* mRNA expression levels were downregulated in thyrocyte-specific TRβ deficient mice (264). Finally, *Mct8* expression in the thyroid gland appears to respond to iodine status in rodents (265-268). These and other studies (e.g. (237, 247, 269-272)) may pave the way for future studies on the transcriptional regulation of *MCT8* and *MCT10*.

MOLECULAR MECHANISM OF THYROID HORMONE TRANSPORT

Most plasma membrane transporter proteins in humans belong to either the ATP-binding cassette (ABC) or to the SLC gene family. All currently known thyroid hormone transporters belong to the SLC family. The known thyroid hormone transporters have different polypeptide chain fold patterns, including the major facilitator superfamily (MFS) fold (MCTs and OATPs), the LeuT fold (LAT1 and LAT2),

and the NhaA fold (NTCP) (**Figure 12A-C**) (273). The MFS fold contains two nearly symmetrical bundles of six transmembrane domains (TMDs) that can exert a rotary movement against each other. The presence of the appropriate substrate induces a conformational change from the outside-open to the inside-open conformation (uptake) and *vice versa* (efflux) (274). The LeuT fold contains two inverted bundles of five TMDs followed by two TMDs that do not participate in this pseudo-symmetry. TMD1 and TMD6 are discontinuous and interrupted by a highly conserved non-alpha-helical segment involved in substrate binding (275). The NhaA fold comprises two inverted segments of five TMDs with TMD4 and 9 being unwound in the center to allow substrate interactions. Given the main focus of this thesis on MCT8, the reader is referred to the full review on thyroid hormone transporters for structural features of other transporters which will not be discussed here (111).

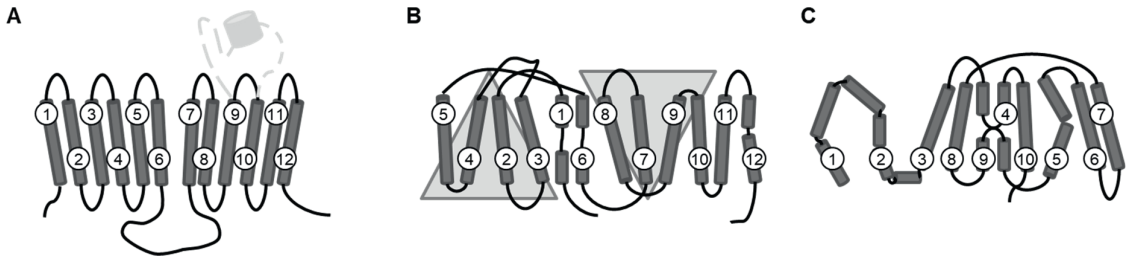

Figure 12 Schematic overview of the different protein folds of thyroid hormone transporter families. MCTs and OATPs are organized according the MFS-fold (**A**). Members of the OATP family contain a large extracellular loop between TMD9 and TMD10 with a KAZAL-like sequence motif (colored in grey). LAT1 (and LAT2) are organized according to a LeuT-fold (**B**) and NTCP according to the NhaA-fold (**C**).

Structure-function of MCT8 and MCT10

The MCT family is classified as a member of the MFS and shares a common topology with 12 TMDs and intracellular C- and N-termini (276) (**Figure 12**). No crystal structures are available for MCT8 or MCT10, or for any of the other MCTs. Therefore, structural information is mainly derived from analogies with (closely) related proteins through protein homology modeling and supported by *in vitro* studies that have evaluated the effects of amino acid substitutions on transport function, mostly focusing on MCT8. Several chapters in this thesis will describe studies onto the structure-function relation of MCT8. The available literature on this topic preceding these studies will be summarized here.

MCT8 and MCT10 presumably transport their substrates according to the rocker-switch model in which the presence of the appropriate substrate induces a conformational change from the outside-open to the inside-open conformation (uptake) and *vice versa* (efflux) (**Figure 13**) (274). The first three-dimensional MCT8 protein homology model was published by Kinne et al. (and was based on the crystal structure of the bacterial glycerol-3-phosphate transporter GlpT in the inward-open conformation (PDB#1pw4) (219, 277). The resulting model predicted a critical role for positively charged Arg445 (TMD8) and negatively charged Asp498 (TMD10) in T3 transport due to their location within the membrane plane. These residues were predicted to form a salt-bridge connecting TMD8 and TMD10. In analogy to the binding mode of T3 to the T3 receptors and the catalytic side of D3 (278, 279), it was postulated that MCT8 contains a so-called His-Arg clamp (280). Three of such His-Arg pairs were

identified in the inward-open model of MCT8, comprising residue pairs His192/Arg445, His192/Arg301 and His415/Arg301 (219, 280). Indeed, substitution of His192 or His415 by Phe or Ala affected transporter kinetics (281). In contrast, limited experimental evidence is available supporting a role of Arg301 in substrate binding. In fact, substitution of this residue by Ala greatly impaired protein stability, rather suggesting a role for this residue in the maintenance of protein stability (281).

For a long time, the generation of homology models in transporter conformations other than the inward-open conformation has been limited by the paucity of available crystal structure templates with sufficient homology to MCT8. Over the last years, additional templates became available, which allowed modeling the MCT8 structure in different conformations (see **chapter 2.4**).

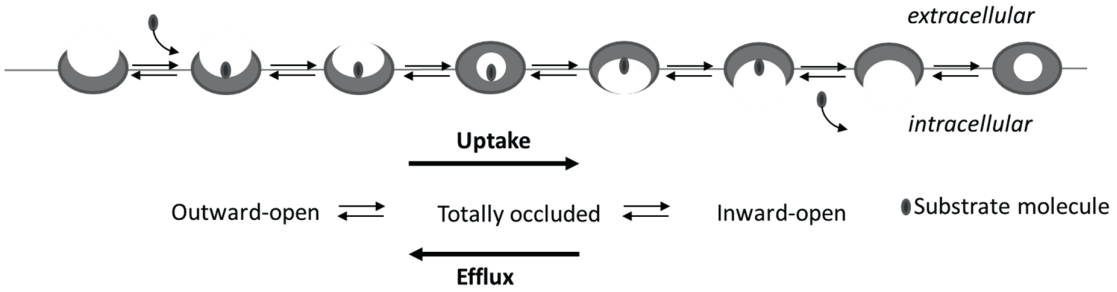

Figure 13 Schematic representation of the rocker-switch transport model.

Despite its 49% amino acid sequence identity to MCT8, predominantly concerning the 12 TMDs, MCT10 lacks sufficient homology to the available crystal structure templates. This poses a limitation for the generation of structural homology models of MCT10 and therefore progress of structure-function studies is hampered. Using a targeted mutational approach, Tyr184 was identified to limit the passage of T4 (221). Another mutational screen in MCT10, using the yeast Saccharomyces cerevisiae, suggested the involvement of Asn81 in the recognition of aromatic amino acid substrates (282). The impact of this and the other variants evaluated in this study on T3 transport was not tested. The available experimental evidence on the structure-function of MCT10 is thus limited.

The exact function of the extended N-terminal domain of MCT8, that is unique to the long isoform, is currently not fully elucidated. Recent studies suggested that the extension of the N-terminal Pro (P), Glu (E), Ser (S), Thr (T) rich region, known as the PEST domain (283), makes the MCT8 protein more susceptible to degradation through the ubiquitin-proteasome system (230). So far, there is no theoretical or experimental evidence that any of the MCT family members is being glycosylated (276). Some MCT proteins require ancillary proteins that govern proper plasma membrane translocation (284). It is currently unclear whether the two thyroid hormone transporting members, MCT8 and MCT10, require such ancillary proteins. If so, such factors differ from those required by MCT1-4 (285). Different experimental approaches have demonstrated the presence of MCT8 homo-dimers and multimers in cell lysates and living cells (285-287). The physiological relevance of these complexes and the domains involved in establishing these interactions are currently unknown.

MCT8 DEFICIENCY

Historical background of MCT8 deficiency

The relevance of thyroid hormone transporters became clear when the first patients with a genetic defect in MCT8 were identified. In 2004, Friesema et al. reported on patients with X-linked intellectual disability and abnormal thyroid function tests (low serum free (F)T4, high (F)T3, low rT3, and high-normal TSH concentrations) associated with genetic mutations in the *SLC16A2* gene (93). At the same time, Dumitrescu et al. reported on two other families with very similar abnormalities who also harbored genetic mutations in *SLC16A2* (94). Soon afterwards it was realized that the neurological features of MCT8 deficiency were reminiscent to those described by Allan, Herndon and Dudley in 1944 who published about a large family in which many male members were affected by intellectual disability (288). By reinvestigating this family over 50 years later, Stevenson and Schwartz provided a detailed description of the clinical phenotype of this disorder, originally termed the Allan-Herndon syndrome and later Allan-Herndon-Dudley syndrome (AHDS), and localized the affected gene to the X-chromosome (289, 290). Similarly, other families with this syndrome had been reported, in whom an X-linked mode of inheritance was suspected (e.g. (291-294)). Genetic sequencing and the presence of abnormal serum thyroid function tests in these families, confirmed that AHDS is caused by mutations in *SLC16A2* (295, 296). Following the trends in the nomenclature of inherited disorders, AHDS is nowadays preferentially termed after its disease-causing gene as MCT8 deficiency. At present, at least 320 affected individuals in 132 families have been reported in literature (OrphaNet, Allan-Herndon-Dudley syndrome, OMIM 300523) with a broad variety of underlying genetic mutations. These mutations range from large deletions, with loss of one or more exons, frameshift deletions, single amino acid deletions or insertions, to single amino acid substitutions. A comprehensive overview of these mutations and reports is provided in (111, 297, 298).

Clinical phenotype of MCT8 deficiency

Through case descriptions published over the last 15 years, it became increasingly clear that the clinical phenotype of MCT8 deficiency comprises two major entities: 1) a neurocognitive phenotype and 2) signs of thyrotoxicosis in peripheral tissues, also termed the peripheral phenotype. The main findings of these case reports and series are summarized in **Table 2**. In this introduction, a description of the clinical phenotype will be provided based on the available case reports and series preceding those described in this thesis (also reviewed in (111, 297)).

Pregnancies are uneventful and children during fetal or early postnatal life do not present with overt abnormalities. Affected children typically present developmental delay and feeding problems in the first year of life. Most children do not attain full head control due to global hypotonia and do not develop any speech. During development, hypotonia persists and is manifested by poor head control, drooling and swallowing problems. Affected children typically have an increased muscle tone in the limbs and neck and exhibit abnormal body posturing and signs of spasticity, including exaggerated tendon reflexes, contractures and pathological plantar reflexes. Based on the presence of these clinical features, patients have been classically described to exhibit spastic tetraplegia. Intellectual disability is present in all patients. Most patients are unable to sit independently and cannot walk, although some cases with a relatively less severe phenotype are able to walk, mostly with support, and have an ataxic gait (296, 299). Also the severity of the neurocognitive phenotype varies, with a minority having a

relatively less severe phenotype illustrated by the ability to talk in simple words and/or sentences. Only few cases with a seemingly less severe clinical phenotype have been described in detail so far. It is currently not established if the severity of the clinical phenotype is related to the functional impact of the underlying genetic mutation. Several dysmorphic features have been documented, of which an elongated face, abnormal anatomy of the ears (large, cupped/simple ears), chest malformations, and a myopathic facies are most frequently. Despite a normal head circumference at birth, some patients reportedly present microcephaly with advancing age. In addition, seizures can be present, although the exact prevalence is unknown. Evoked potentials are reportedly normal in some patients (300-303), but delayed in others (304-310).

The key hallmark on brain MRI is delayed myelination, which has been described in almost all affected children below five years of age (e.g. (310-312)). However, the progression of myelination to (near) normal in some older subjects may help to discriminate MCT8 deficiency from other white matter disorders such as leukodystrophies, cerebral palsy and Pelizaeus-Merzbacher disease with which MCT8 deficiency has been sometimes confused (305). Despite these notable improvements of myelination status on MRI, post-mortem investigation of a brain from an 11-year old patient with MCT8 deficiency has indicated that in this patient myelination was still considerably delayed compared to healthy controls (313). Other neuro-radiological features that have been frequently reported are the presence of widened ventricles and a thin corpus callosum. Although the neurocognitive features of MCT8 deficiency have been documented in many reported patients, most studies differ in terminology, applied testing methods, lack quantifiable parameters and have not been performed according to standardized protocols. Those limitations hampered proper inter-individual comparisons and the establishment of natural history data.

The neurological features are accompanied by abnormal thyroid function tests. In most patients total T4 and FT4 concentrations are below the reference range, whereas the T3 concentrations are elevated. Like T4, also rT3 concentrations are decreased in most patients. Therefore, T3/(F)T4 and T3/rT3 ratios are strongly elevated. In some patients, TRH-stimulation tests showed an inadequately low TSH response (307, 314). The elevated serum T3 concentrations may result in signs of hyperthyroidism in peripheral organs that rely on transporters other than MCT8. Although it is imperative to recognize and treat the chronic thyrotoxicosis in the peripheral tissues of these patients, only a minority of available studies have provided detailed descriptions of the peripheral phenotype. Instead, most studies rather focused on the pronounced neurocognitive phenotype.

Until recently, the lag in weight gain with advancing age and diminished muscle mass were the only features that had been widely reported, but in insufficient detail to allow compiling a natural history of body weight development. Both clinical features can possibly be attributed to the poor nutritional status due to difficulty swallowing on neurological basis, but also to the increased basal metabolism secondary to the hyperthyroid state in peripheral tissues (287, 307, 315, 316). Linear growth appears less affected than body weight, typically resulting in very low BMI scores. Despite being one of the most sensitive tissues for thyroid hormone, the cardiovascular system has not been widely studied in patients with MCT8 deficiency. Some patients reportedly exhibit cardiovascular signs of hyperthyroidism (300, 305, 315, 317, 318), whereas some others exhibited no obvious abnormalities (316, 319-322). Since the number of studies reporting on cardiovascular features is limited, the exact prevalence is currently unknown. The presence of low total cholesterol and prealbumin concentrations, and elevated sex hormone binding globulin (SHBG) concentrations described in some patients may indicate tissue hyperthyroidism in the liver (287, 300, 315-317, 319, 323-325), but the available data is very limit.

Table 3 Clinical features of MCT8 deficiency

Neurological phenotype	Peripheral phenotype
Clinical	**Clinical**
Severe intellectual disability	Progressive loss of body weight
Failure to achieve motor milestones	Muscle wasting
Hypotonia	(Increased perspiration)
Dystonia	(Tachycardia)
Dyskinetic movements	
Spasticity	
Brisk tendon reflexes	**Biochemical**
Contractures	Elevated serum (F)T3
Positive plantar extension reflex	Reduced serum (F)T4 and rT3
Feeding problems	(High) normal serum TSH
Scoliosis	(Elevated SHBG)
Dysmorphic features	
MRI	
Delayed myelination	
Thin corpus callosum	
Widened ventricles	

Symptoms that have been documented in only few patients are indicated between brackets. The content of this table is based on the available case reports preceding the studies described in this thesis.

Future studies are thus warranted to uniformly characterize the clinical phenotype of MCT8 deficiency in greater detail. Such studies should aim to identify common medical problems in patients with MCT8 deficiency and determine the type and frequency of systematic clinical assessments and the need for symptomatic treatment. Furthermore, such a study would offer a description of the natural history of MCT8 deficiency, which is currently lacking. In **chapter 4.1** we report on the in-depth phenotyping of a large international cohort of patients with MCT8 deficiency to satisfy these unmet needs.

Clinical phenotype of female carriers of mutations in the *SLC16A2* gene

Since the *SLC16A2* gene is located on the X-chromosome, mutations therein result in a clinical phenotype in males. Female carriers typically do not present with phenotypic characteristics of MCT8 deficiency because they have a second, unaffected, copy of the *SLC16A2* gene (326, 327). This results in the presence of functional MCT8 in at least a subset of cells. However, some female carriers reportedly have mild biochemical abnormalities that resemble those observed in affected male patients, and some of these carriers exhibited various degree of cognitive dysfunction (94, 296, 316, 328-330). This may be attributable to the presence of skewing in X-chromosome inactivation. Indeed, in one reported case, complete skewing of X-chromosome inactivation due an X-autosome translocation resulted in the exclusive expression of the mutant MCT8 allele and a clinical phenotype resembling male MCT8 deficiency (331). Since the clinical and biochemical characteristics of female carriers have not been systematically described, the penetrance of such manifestations is currently unknown.

PATHOPHYSIOLOGICAL MECHANISM OF MCT8 DEFICIENCY

The identification of the first patients with MCT8 deficiency provided ultimate proof for the physiological relevance of transport-mediated passage of thyroid hormone across cell membranes. This seminal discovery prompted the generation of different animal models to delineate the mechanism underlying the changes observed in patients with MCT8 deficiency. These studies have revealed important insights on the role of MCT8 in the HPT-axis and in the brain. A selection of these studies will be discussed in this section.

The role of MCT8 within the HPT axis and in peripheral tissues

Given the abundant presence of MCT8 in the PVN of the hypothalamus (238, 245, 248), pituitary (8) and thyroid gland (98, 239), it was not too surprising that a global lack of MCT8 in *Mct8* ko mice affects a proper function of the HPT axis on all levels (332). The high *Trh* mRNA expression levels in the hypothalamus are indicative for a pronounced thyroid hormone-deficient state in thyroid hormone-sensitive hypothalamic neurons and abnormal responses to TSH suppression tests indicate that also the pituitary does not properly sense the serum thyroid hormone concentrations (98, 99). By contrast, the thyroid hormone content of the thyroid gland was highly elevated pointing to tissue-specific thyroid hormone excess (98, 239, 240). As patients with MCT8 deficiency, *Mct8* ko mice exhibit elevated serum T3, low T4 and low rT3 concentrations while TSH concentrations are in the normal range or even slightly elevated (98, 99). Therefore, these animals are generally considered to pose a suitable model to determine the tissue-specific thyroidal state in the absence of MCT8.

A key problem which is still not completely resolved is the exact pathogenic mechanism that underlies the highly increased serum T3/T4 ratio. A disturbed thyroid hormone metabolism, in particular a rise in T4 to T3 conversion represents a likely explanation, and in fact, D1 and D2 activities were found to be altered in various tissues of *Mct8* ko mice (98, 99, 102). In order to pin-down the responsible deiodinase, Liao et al. generated *Mct8/Dio1* and *Mct8/Dio2* double mutant mice and could demonstrate by this elegant approach that D1 is primarily responsible for the odd abnormal T3/T4 ratio in *Mct8* ko mice (100). Still, it needs to be disclosed why D1 is elevated in MCT8 deficient mice and which tissue is critically involved in generating the high serum T3 concentrations. It is also unclear to which extent the thyroid itself may contribute to the increased T3/T4 ratio (239, 240).

Apart from the HPT axis, various organs show alterations in tissue-specific thyroid hormone status in the absence of MCT8. *Mct8* ko mice have an increased liver T3 content which is accompanied by increased D1 expression levels and activity, as well as reduced serum cholesterol concentrations (99). Similar to the liver, kidneys of *Mct8* ko mice were found to be in a hyperthyroid state as evidenced by a pronounced increased thyroid hormone content and a steep rise in D1 activity that even exceeded levels found in liver homogenates (242). *Mct8* ko mice also show enhanced energy expenditure and reduced fat mass (333). In addition, several lines of evidence indicate that the skeletal muscles and bone in adult *Mct8* ko mice are in a hyperthyroid state (102, 333, 334).

Role of MCT8 in the brain

The presence of severe intellectual and motor disability in patients with MCT8 deficiency and extensive neuropathological abnormalities in brains of a fetus and a child with MCT8 deficiency suggests that functional MCT8 is crucial for normal brain development (312, 313). Based on these and other studies,

it can be assumed that cortical and cerebellar development is delayed which is accompanied by diminished myelination, decreased expression of the calcium binding protein parvalbumin (PV) and impaired axonal maturation. These findings are all compatible with the diminished brain thyroid hormone content and suggest that brain abnormalities may be present during fetal development and involve both neurons and glia cells.

In contrast to these histo-morphological changes observed in patients with MCT8 deficiency, the brains of *Mct8* ko mice are surprisingly normal. This difference was attributed to the presence of alternative T4 transporters at critical sites in mice, that are absent in human (246). Indeed, Roberts et al demonstrated that the T4 transporter OATP1C1 is present in the brain microvessels of rodents, but not in those of human (143). The relevance of this transporter in mice was underscored by the *Mct8/Oatp1c1* double ko mice which showed highly reduced brain thyroid hormone content due to a strongly diminished blood to brain passage of both T4 and T3 (95). Unlike the single thyroid hormone transporter mutant mice, the *Mct8/Oatp1c1* dko animals showed similar histological abnormalities as seen in MCT8 deficient patients, including delayed cerebellar development, compromised maturation of cortical GABAergic interneurons and persistent hypo-myelination. These structural hallmarks are indicative for a widespread thyroid hormone deficiency in the CNS that was confirmed by assessing gene expression of well-established thyroid hormone regulated target genes. Moreover, *Mct8/Oatp1c1* dko mice exhibit pronounced locomotor impairments, learning disabilities, reduced muscle strength and gait abnormalities. In light of these findings, *Mct8/Oatp1c1* dko mice have been suggested as a more adequate mouse model for MCT8 deficiency in the human brain compared to the single *Mct8* ko mouse with its rather normal brain development.

Numerous studies have been carried out to delineate in which cell-types MCT8 is physiologically important in the CNS. The lack of any overt neuronal damage in *Mct8* ko mice, as well as the normal T3 uptake in MCT8 deficient cerebellar Purkinje cells *in vitro* suggested that MCT8 has no pivotal role in the transport of T3 into neurons in mouse brain (98, 199). It is unclear if this also applies to human neurons. The severely impaired passage of T3 from blood to brain in *Mct8* ko mice supports a critical function of MCT8 at the BBB and/or the BCSFB. In human as well as rodent brain, immuno-histochemical and RNAseq studies clearly demonstrated the presence of MCT8 in capillary endothelial cells of the BBB (143, 335, 336), choroid plexus structures and ependymal cells in rodents and human (143, 253), which may indeed be compatible with a critical role for MCT8 at these barriers. It is however not clear to what extent transfer of thyroid hormone in choroid plexus cells contributes to brain thyroid hormone supply (337) and how MCT8 exactly contributes to this process (338). Localization of MCT8 in glia cells is less well investigated. Though RNAseq data confirmed the presence of *Mct8* transcripts in FACS-sorted mouse astrocytes (335), ISH studies failed to detect any co-expression of *Mct8* and *Gfap*, an astrocytic marker, in the hippocampus of 21-day-old mice (245). Most likely, *Mct8* expression is only present in a subset of astrocytes. In humans, RNAseq analysis of cortical astrocytes derived from fetal (17-20 gestational weeks) or mature (8-63 year) brain samples and purified by immune-panning revealed *MCT8* expression in both cell populations (339). The contribution of MCT8 to thyroid hormone transport in these cells remains to be determined. It is also unclear if MCT8 is involved in the transport of thyroid hormone in oligodendrocytes.

Figure 14 Schematic representation of the pathophysiology of MCT8 deficiency. The current paradigm of MCT8 deficiency holds that tissues that largely rely on MCT8 for cellular thyroid hormone uptake, including the brain, are in a hypothyroid state; whereas tissues that rely on transporters other than MCT8 reside in a hyperthyroid state due to exposure to the elevated serum T3 concentrations.

In addition to mice, zebrafish represents another species in which brain function of Mct8 has been extensively studied (109, 110). Induction of *mct8* knock-down by morpholino injection resulted in larvae exhibiting a reduced brain size, a curved body axis with a deformed spinal cord and impaired mobility (111-113), whereas *mct8* ko zebrafish displayed reduced locomotor activity accompanied by neurological and behavioral deficiencies, hypo-myelination and a reduced number of oligodendrocytes, disturbed axonal branching of sensory neurons as well as reduced synaptic density of motor neurons (114, 115). Based on these profound alterations, Mct8 deficient zebrafish can be considered as a model system for MCT8 deficiency as well.

In summary, the current paradigm of MCT8 deficiency holds that tissues that importantly rely on functional MCT8 for their cellular thyroid hormone supply, especially the brain, reside in a hypothyroid state, whereas tissues that mostly rely on transporter other than MCT8 are exposed to the elevated serum T3 concentrations which results in symptoms of tissue thyrotoxicosis (**Figure 14**). Thus, the impact of MCT8 deletion on cellular thyroid hormone homeostasis is ultimately determined by the presence of redundant thyroid hormone transporters. Importantly, differences in tissue distribution and cell-specific function of thyroid hormone transporters among species may determine the cell-specific vulnerability towards thyroid hormone transporter defects.

THERAPEUTIC APPROACHES IN MCT8 DEFICIENCY

Classical (anti-)thyroid drugs

Based on the low serum FT4 concentrations and modestly increased TSH concentrations, a subset of patients have been suspected for mild (central) hypothyroidism and have been treated with L-T4 without any notable effects on neurocognitive development. Rather, in at least some cases serum T3 concentrations clearly further increased by L-T4 administration, which aggravated the hyperthyroid state in peripheral tissues. In an attempt to avoid inducing peripheral thyrotoxicosis, some patients

have been reportedly treated with antithyroid drugs, alone or in combination with L-T4 (315, 324, 340-342). Administration of methimazol had no effects on the serum thyroid function tests (342). Alternatively, the administration of PTU, which not only blocks thyroid hormone production but also inhibits the T4 to T3 conversion by D1, combined with L-T4 restored the abnormal TFTs and improved some clinical parameters in several patients (315, 324, 342). Yet, no positive effects on neurocognitive development were noted in these patients and the occurrence of severe side-effects limited its long-term applicability.

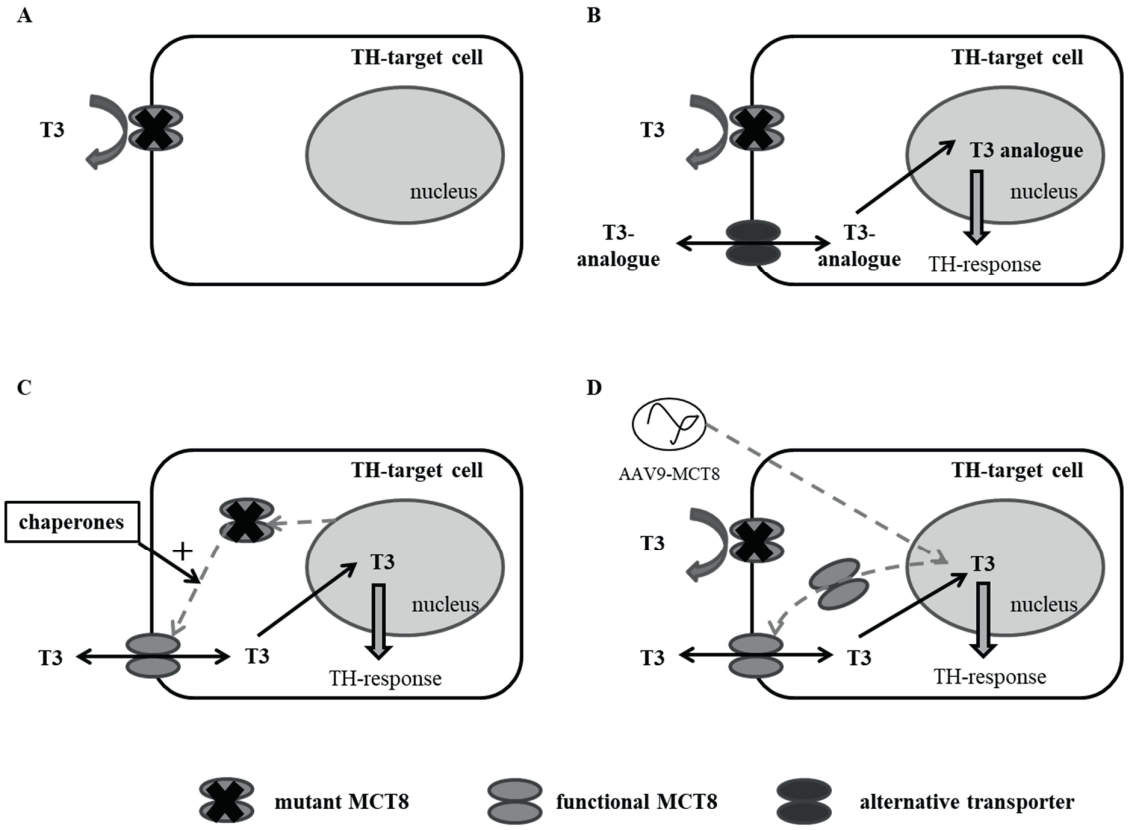

Figure 15 Overview of putative therapeutic approaches for MCT8 deficiency. (A) Schematic representation of an MCT8-dependent thyroid hormone target cell in which thyroid hormone (including exogenously administrated L-T4) uptake is diminished. (B) T3-analogue therapy involves molecules that bypass MCT8 for their cellular entry, but once inside the cell bind to the nuclear thyroid hormone receptor. Examples are Triac and DITPA. (C) Gene therapy aims to supply MCT8 deficient cells with wild-type MCT8 protein through viral vectors that contain wild-type MCT8 coding sequence. Through selection of specific viral vectors and promoter sequences, specific cell-types can be targeted. (D) Treatment with chemical (or molecular) chaperones aims to potentiate surface translocation of mutant MCT8 proteins that retained intrinsic transport activity.

The absence of beneficial effects of L-T4 treatment on the neurocognitive features prompted studies to alternative treatment strategies. Effective therapy for MCT8 deficiency entails 1) restoring thyroid hormone signaling in the brain and 2) alleviating the thyrotoxic state in peripheral tissues. Over the last decade, several therapeutic approaches have been investigated, including thyroid hormone analogues, and more recently gene therapy and chemical chaperones (**Figure 15A-D**) (reviewed in (70, 297, 298)), of which thyroid hormone analogues have been applied in patients (see **chapter 5.2**). This section will summarize the pre-clinical studies preceding these clinical studies.

Thyroid hormone analogues

The lack of beneficial effects of L-T4 treatment on neurodevelopment is likely attributable to the impaired transport of thyroid hormone across the BBB or into its target cells (**Figure 16A**). This led some groups to investigate the application of thyroid hormone analogues. Such analogues should enter the target cells independent from MCT8, but once inside cell exert similar effects as T3 (**Figure 16B**). The general hypothesis underlying the potential therapeutic mechanism of these analogues consist of the simultaneous inhibition of TSH secretion and hence endogenous thyroid hormone production, while providing adequate thyromimetic effects in all body tissues, including the brain (70).

The first thyroid hormone analogue that has been studied in the context of MCT8 deficiency was 3,5-diiodothyropropionic acid (DITPA) (343). DITPA is a ligand for TRα and TRβ, although its affinity is 300-times lower compared to T3, and hence high dosages are required to achieve similar effects as for L-T4 (344). Administration of DITPA to *Mct8* ko and control mice resulted in similar tissue availability of DITPA in the liver and brain, suggesting that DITPA enters these tissues independent from MCT8 (343). DITPA lowered serum TSH concentrations effectively in *Mct8* ko and wild-type control mice, which was followed by a reduction in serum T4, T3 and rT3 concentrations (343, 345). Consequently, DITPA was found to, at least partially, restore expression levels of several thyroid hormone target genes and deiodinase activity in the liver and brain of *Mct8* ko mice (343). Especially the reduction in D1 and D2 activity following DITPA administration may importantly contribute to the reduction of elevated serum T3 concentrations. Although administration of a low dose DITPA (0.3 mg/100 gram body weight per day) effectively restored the hypermetabolic state and abnormal serum thyroid function tests in *Mct8 ko* mice, it had only minor effects on thyroid hormone markers in the brain (345). Obviously the interpretation of these studies is complicated by the lack of neurological derangements in this mouse model. DITPA is able to cross the placenta and regulate thyroid hormone-dependent genes in the fetal mouse cerebral cortex, which would offer the possibility of early treatment initiation (346).

Another analogue that has been studied is Triac, which also acts through the T3 receptors, but enters the cell independent from MCT8 (85-87, 223). Importantly, daily administration of Triac between postnatal day 1-12 (200-400 ng/gram body weight per day) largely prevented the abnormal brain development in the a-thyroid *Pax-8* ko mice and *Mct8/Oatp1c1* dko mice (223), evidenced by normal cerebellar Purkinje cell dendritogenesis as well as cortical myelination which are all known to be TH-dependent processes (223). Administration of its precursor tetraiodothyroacetic acid (Tetrac), which has a longer half-life time than Triac, exhibited similar effects on brain development in *Pax8 ko* and *Pax8/Mct8* dko mice (84). Triac and Tetrac also ameliorated the neurodevelopmental abnormalities in zebrafish models for MCT8 deficiency (108, 109, 148, 251) and improves cerebellar Purkinje cell development in Mct8 deficient chicken (110). In addition to these neuro-developmental effects, low doses of Triac applied via the drinking water lowered T3 concentrations in serum of *Mct8* ko mice, suggesting that Triac has the potential to alleviate the peripheral phenotype in MCT8 deficiency (347). These studies have led to the initiation of a clinical trial in which the effects of Triac were studied in patients with MCT8 deficiency, the results of which are presented in **chapter 5.2** of this thesis.

Other possible therapeutic approaches

For a subset of mutations the application of chemical or pharmacological chaperones could restore MCT8 function. This approach is based on the concept that certain mutations result in misfolding of the MCT8 protein which is in turn rapidly degraded and prevented from reaching the plasma

membrane. Chaperones may improve the folding of such mutant proteins and potentiate their trafficking to the plasma membrane and hence (partially) restore their function (**Figure 16C**). Several chemical chaperones have been successfully applied in pre-clinical studies of several genetic disorders, including cystic fibrosis (348). Studies in stably transfected MDCK-1 cells suggested that the function of the p.F501del mutation, which is associated with a relatively less severe clinical phenotype, can be enhanced by with phenylbutyrate or dimethylsulfoxide, and to a lesser extent with genistein (349, 350). However, it remains to be studied if chaperones also restore the function of these and other mutant MCT8 proteins in other disease models, including patient-derived fibroblasts (see **chapter 5.1)**. Since MCT8 deficiency is a monogenetic disorder, gene therapy theoretically poses another attractive therapeutic approach to restore MCT8 function in tissues where it is of most physiological relevance (**Figure 16D**).

OBJECTIVES AND OUTLINE OF THE THESIS

The first part of the work presented in this thesis aimed to further elucidate the transport mechanism by which MCT8 transports iodothyronines and how this is affected by mutations encountered in patients with MCT8 deficiency. These studies focused on the identification of accessible and functionally relevant residues in MCT8. This knowledge was used to guide the generation of protein homology models for MCT8. The ultimate goal of these studies was to delineate the structure-function relationship in MCT8, which may help to assess tolerable variability and predict the impact of mutations encountered in patients. **Chapter 2** of this thesis contains several studies that identified important structural properties of MCT8, including functional studies that support the localization of Cys497 (**chapter 2.1**) and His192 (**chapter 2.2**) residues in the substrate binding pore and the presence of a salt-bridge between Arg445 (TMD8) and Asp498 (TMD10) (**chapter 2.3**). In **chapter 2.4** we show that Arg445 is a target for chemical modification by phenylglyoxal by combining mutational screens and chemical modification studies and constructed an MCT8 homology model in outward-open conformation. Based on this model, we predicted a differential role of Asn193 (TMD1) in the recognition and transport of T3 *versus* T4 and provided evidence for the formation of halogen bonds between this residue and iodine groups of the substrate molecule (**chapter 2.5**). In **chapter 2.6**, we have compared the functional characteristics of human MCT8 to its mouse and zebrafish orthologues, which comprise the most frequently used animal models to study human MCT8 deficiency. These studies revealed that both orthologues efficiently transported T3 and T4, further supporting the eligibility of these species as model for human MCT8 deficiency. The non-conserved regions between human and zebrafish MCT8 helped to define elements in human MCT8 that are critical for MCT8 function. In **chapter 2.7** we delineated the mechanism of MCT8 oligomerization and employed several strategies to study its physiological role. By using a metabolomic approach in transfected *Xenopus* oocytes, we identified MIT and DIT as novel substrates for MCT8 (**chapter 2.8**).

The second part aimed to delineate the clinical phenotype of MCT8 in greater detail taking advantage of a large international cohort of patients with MCT8 deficiency we established over the last decade. In **chapter 3** we have identified several families with novel mutations in MCT8 and described the clinical characteristics of the affected patients as well as the functional characteristics of these novel mutations. In **chapter 3.1** we describe two patients with different mutations affecting the same Gly564 residue associated with a different grade of severity of the clinical phenotype. In line with the

functional studies, the patient harboring the G564E mutation exhibited a relatively less severe phenotype, whereas the patient harboring the G564R exhibited a severe clinical phenotype of MCT8 deficiency. Although the majority of patients with MCT8 deficiency manifest severe developmental delay and intellectual disability, a small subset is able to walk and talk in simple sentences. In **chapter 3.2** we described two of such patients and demonstrate significant residual function of both mutant proteins in transfected cells and patient-derived skin fibroblasts. In **chapter 3.3** we described a series of patients with mutations in the C-terminal end of the MCT8 protein. These studies revealed that mutations beyond the predicted TMD12 had no or relatively mild effects on MCT8 function *in vitro* and were associated with relatively less severe phenotypes. In fact, the absence of any functional alterations in our *in vitro* and *ex vivo* experiments resulted in reconsideration of the diagnoses MCT8 deficiency in one of the patients and fueled additional diagnostic procedures. This study illustrates that functional evaluation of novel mutations in MCT8 is imperative to establish the correct diagnosis. In **chapter 3.4** we describe the endocrine and clinical phenotype of three female cases with heterozygous mutations in MCT8 and unfavorable skewing of X-chromosome inactivation.

Since the clinical phenotype of MCT8 has only been described in case reports and small case series, a uniform description of the clinical phenotype of MCT8 deficiency as well as its natural progression over time is lacking. **Chapter 4** focuses on establishing a better description of the phenotype associated with mutations in MCT8 deficiency. By conducting in-depth phenotyping studies in a large international cohort of patients with MCT8 deficiency, we have identified several novel features of MCT8 deficiency, including a broad spectrum of cardiovascular features, and establish natural history data for key parameters that can be used as a reference in the assessment of efficacy of future therapeutic interventions. In addition, we identified the primary causes of death in MCT8 deficiency and revealed that attaining head control is an important determinant in overall survival.

The third part aimed to explore therapeutic options for patients with MCT8 deficiency for which no effective therapy had been available. **Chapter 5** focuses on the therapeutic strategies for patients with MCT8 deficiency. In **chapter 5.1** we have assessed the effects of the chemical chaperone phenylbutyrate in *in vitro* overexpression systems complemented with *ex vivo* studies in patient-derived fibroblasts. **Chapter 5.2** describes the results of an international multicenter phase II clinical trial in which we have assessed the effectiveness of the thyroid hormone analogue Triac in alleviating the peripheral thyrotoxicosis in patient with MCT8 deficiency.

In order to identify novel key players in the regulation of thyroid hormone homeostasis, we performed a large meta-analysis of genome-wide association studies in which we studied the association between genetic variants and serum free T4 and TSH concentrations. These studies resulted in the identification of the novel thyroid hormone transporter SLC17A4 and the novel thyroid hormone metabolizing enzyme AADAT (**chapter 6.1**). The functional properties of human SLC17A4 have been characterized in more detail in **chapter 6.2**, which allows positioning this novel transporter among the other known thyroid hormone transporters. As a first step towards *in vivo* studies to the physiological role of SLC17A4, we thoroughly compared the functional properties of human and mouse SLC17A4 in **chapter 6.3** and also studied if other members of the SLC17 family are capable of transporting thyroid hormones. Finally, we have described the first patient with a homozygous inactivating mutation in the T4 transporter OATP1C1 which was associated with a profound neurodegenerative phenotype (**chapter 6.4**).

A general discussion of the findings described in this thesis as well as their implication on the field of thyroidology is presented in **chapter 7**.

REFERENCES

1. Vassart G, Dumont JE. The thyrotropin receptor and the regulation of thyrocyte function and growth. Endocr Rev. 1992;13(3):596-611.
2. Bizhanova A, Kopp P. Minireview: The sodium-iodide symporter NIS and pendrin in iodide homeostasis of the thyroid. Endocrinology. 2009;150(3):1084-90.
3. St Germain DL, Galton VA, Hernandez A. Minireview: Defining the roles of the iodothyronine deiodinases: current concepts and challenges. Endocrinology. 2009;150(3):1097-107.
4. Moreno JC, Klootwijk W, van Toor H, Pinto G, D'Alessandro M, Leger A, et al. Mutations in the iodotyrosine deiodinase gene and hypothyroidism. N Engl J Med. 2008;358(17):1811-8.
5. Zamproni I, Grasberger H, Cortinovis F, Vigone MC, Chiumello G, Mora S, et al. Biallelic inactivation of the dual oxidase maturation factor 2 (DUOXA2) gene as a novel cause of congenital hypothyroidism. J Clin Endocrinol Metab. 2008;93(2):605-10.
6. Moreno JC, Visser TJ. Genetics and phenomics of hypothyroidism and goiter due to iodotyrosine deiodinase (DEHAL1) gene mutations. Mol Cell Endocrinol. 2010;322(1-2):91-8.
7. Moreno JC, Visser TJ. New phenotypes in thyroid dyshormonogenesis: hypothyroidism due to DUOX2 mutations. Endocrine development. 2007;10:99-117.
8. Fliers E, Unmehopa UA, Alkemade A. Functional neuroanatomy of thyroid hormone feedback in the human hypothalamus and pituitary gland. Mol Cell Endocrinol. 2006;251(1-2):1-8.
9. Gross J, Pitt-Rivers R. Physiological activity of 3:5:3'-L-triiodothyronine. Lancet. 1952;1(6708):593-4.
10. Pitt-Rivers R. Metabolic effects of compounds structurally related to thyroxine in vivo: thyroxine derivatives. J Clin Endocrinol Metab. 1954;14(11):1444-50.
11. Mussett MV, Pitt-Rivers R. The thyroid-like activity of triiodothyronine analogues. Lancet. 1954;267(6850):1212-3.
12. Lerman J. The contribution of triiodothyronine to thyroid physiology. J Clin Endocrinol Metab. 1954;14(6):690-3.
13. Cheng SY, Leonard JL, Davis PJ. Molecular aspects of thyroid hormone actions. Endocr Rev. 2010;31(2):139-70.
14. Singh BK, Yen PM. A clinician's guide to understanding resistance to thyroid hormone due to receptor mutations in the TRalpha and TRbeta isoforms. Clin Diabetes Endocrinol. 2017;3:8.
15. Lazar MA. Thyroid hormone receptors: multiple forms, multiple possibilities. Endocr Rev. 1993;14(2):184-93.
16. Flamant F, Cheng SY, Hollenberg AN, Moeller LC, Samarut J, Wondisford FE, et al. Thyroid Hormone Signaling Pathways: Time for a More Precise Nomenclature. Endocrinology. 2017;158(7):2052-7.
17. Astapova I. Role of co-regulators in metabolic and transcriptional actions of thyroid hormone. J Mol Endocrinol. 2016;56(3):73-97.
18. Refetoff S, DeWind LT, DeGroot LJ. Familial syndrome combining deaf-mutism, stuppled epiphyses, goiter and abnormally high PBI: possible target organ refractoriness to thyroid hormone. J Clin Endocrinol Metab. 1967;27(2):279-94.
19. Sakurai A, Takeda K, Ain K, Ceccarelli P, Nakai A, Seino S, et al. Generalized resistance to thyroid hormone associated with a mutation in the ligand-binding domain of the human thyroid hormone receptor beta. Proc Natl Acad Sci U S A. 1989;86(22):8977-81.
20. Dumitrescu AM, Refetoff S. The syndromes of reduced sensitivity to thyroid hormone. Biochim Biophys Acta. 2013;1830(7):3987-4003.
21. Bochukova E, Schoenmakers N, Agostini M, Schoenmakers E, Rajanayagam O, Keogh JM, et al. A mutation in the thyroid hormone receptor alpha gene. N Engl J Med. 2012;366(3):243-9.
22. van Mullem A, van Heerebeek R, Chrysis D, Visser E, Medici M, Andrikoula M, et al. Clinical phenotype and mutant TRalpha1. N Engl J Med. 2012;366(15):1451-3.
23. van Gucht ALM, Moran C, Meima ME, Visser WE, Chatterjee K, Visser TJ, et al. Resistance to Thyroid Hormone due to Heterozygous Mutations in Thyroid Hormone Receptor Alpha. Curr Top Dev Biol. 2017;125:337-55.
24. Moran C, Chatterjee K. Resistance to Thyroid Hormone alpha-Emerging Definition of a Disorder of Thyroid Hormone Action. J Clin Endocrinol Metab. 2016;101(7):2636-9.
25. Weiss RED, A.M.; Refetoff, S. . Syndromes of impaired sensitivity to thyroid hormone in: Genetic diagnosis of endocrine disorders. 2016;second editon, Elsevier Inc(edited by Weiss RE and Refetoff S).

26. Hayashi Y, Weiss RE, Sarne DH, Yen PM, Sunthornthepvarakul T, Marcocci C, et al. Do clinical manifestations of resistance to thyroid hormone correlate with the functional alteration of the corresponding mutant thyroid hormone-beta receptors? J Clin Endocrinol Metab. 1995;80(11):3246-56.
27. Yoh SM, Chatterjee VK, Privalsky ML. Thyroid hormone resistance syndrome manifests as an aberrant interaction between mutant T3 receptors and transcriptional corepressors. Mol Endocrinol. 1997;11(4):470-80.
28. Liu Y, Takeshita A, Misiti S, Chin WW, Yen PM. Lack of coactivator interaction can be a mechanism for dominant negative activity by mutant thyroid hormone receptors. Endocrinology. 1998;139(10):4197-204.
29. Refetoff S, Weiss RE, Usala SJ. The syndromes of resistance to thyroid hormone. Endocr Rev. 1993;14(3):348-99.
30. Forrest D, Hanebuth E, Smeyne RJ, Everds N, Stewart CL, Wehner JM, et al. Recessive resistance to thyroid hormone in mice lacking thyroid hormone receptor beta: evidence for tissue-specific modulation of receptor function. EMBO J. 1996;15(12):3006-15.
31. Farwell AP, Dubord-Tomasetti SA, Pietrzykowski AZ, Leonard JL. Dynamic nongenomic actions of thyroid hormone in the developing rat brain. Endocrinology. 2006;147(5):2567-74.
32. Safran M, Farwell AP, Rokos H, Leonard JL. Structural requirements of iodothyronines for the rapid inactivation and internalization of type II iodothyronine 5'-deiodinase in glial cells. J Biol Chem. 1993;268(19):14224-9.
33. Moreno M, de Lange P, Lombardi A, Silvestri E, Lanni A, Goglia F. Metabolic effects of thyroid hormone derivatives. Thyroid. 2008;18(2):239-53.
34. Davis PJ, Leonard JL, Davis FB. Mechanisms of nongenomic actions of thyroid hormone. Frontiers in neuroendocrinology. 2008;29(2):211-8.
35. Cody V, Davis PJ, Davis FB. Molecular modeling of the thyroid hormone interactions with alpha v beta 3 integrin. Steroids. 2007;72(2):165-70.
36. Scanlan TS, Suchland KL, Hart ME, Chiellini G, Huang Y, Kruzich PJ, et al. 3-Iodothyronamine is an endogenous and rapid-acting derivative of thyroid hormone. Nature medicine. 2004;10(6):638-42.
37. Bergh JJ, Lin HY, Lansing L, Mohamed SN, Davis FB, Mousa S, et al. Integrin alphaVbeta3 contains a cell surface receptor site for thyroid hormone that is linked to activation of mitogen-activated protein kinase and induction of angiogenesis. Endocrinology. 2005;146(7):2864-71.
38. Moeller LC, Dumitrescu AM, Refetoff S. Cytosolic action of thyroid hormone leads to induction of hypoxia-inducible factor-1alpha and glycolytic genes. Mol Endocrinol. 2005;19(12):2955-63.
39. Berry MJ, Banu L, Larsen PR. Type I iodothyronine deiodinase is a selenocysteine-containing enzyme. Nature. 1991;349(6308):438-40.
40. Geffner DL, Azukizawa M, Hershman JM. Propylthiouracil blocks extrathyroidal conversion of thyroxine to triiodothyronine and augments thyrotropin secretion in man. J Clin Invest. 1975;55(2):224-9.
41. de Jong FJ, Peeters RP, den Heijer T, van der Deure WM, Hofman A, Uitterlinden AG, et al. The association of polymorphisms in the type 1 and 2 deiodinase genes with circulating thyroid hormone parameters and atrophy of the medial temporal lobe. J Clin Endocrinol Metab. 2007;92(2):636-40.
42. Peeters RP, van Toor H, Klootwijk W, de Rijke YB, Kuiper GG, Uitterlinden AG, et al. Polymorphisms in thyroid hormone pathway genes are associated with plasma TSH and iodothyronine levels in healthy subjects. J Clin Endocrinol Metab. 2003;88(6):2880-8.
43. Berry MJ, Grieco D, Taylor BA, Maia AL, Kieffer JD, Beamer W, et al. Physiological and genetic analyses of inbred mouse strains with a type I iodothyronine 5' deiodinase deficiency. J Clin Invest. 1993;92(3):1517-28.
44. Schneider MJ, Fiering SN, Thai B, Wu SY, St Germain E, Parlow AF, et al. Targeted disruption of the type 1 selenodeiodinase gene (Dio1) results in marked changes in thyroid hormone economy in mice. Endocrinology. 2006;147(1):580-9.
45. Bianco AC, Kim BW. Deiodinases: implications of the local control of thyroid hormone action. J Clin Invest. 2006;116(10):2571-9.
46. Zavacki AM, Ying H, Christoffolete MA, Aerts G, So E, Harney JW, et al. Type 1 iodothyronine deiodinase is a sensitive marker of peripheral thyroid status in the mouse. Endocrinology. 2005;146(3):1568-75.
47. Skarulis MC, Celi FS, Mueller E, Zemskova M, Malek R, Hugendubler L, et al. Thyroid hormone induced brown adipose tissue and amelioration of diabetes in a patient with extreme insulin resistance. J Clin Endocrinol Metab. 2010;95(1):256-62.
48. Bianco AC, Dumitrescu A, Gereben B, Ribeiro MO, Fonseca TL, Fernandes GW, et al. Paradigms of Dynamic Control of Thyroid Hormone Signaling. Endocr Rev. 2019.
49. Gereben B, Zavacki AM, Ribich S, Kim BW, Huang SA, Simonides WS, et al. Cellular and molecular basis of deiodinase-regulated thyroid hormone signaling. Endocr Rev. 2008;29(7):898-938.

50. Bianco AC, Silva JE. Nuclear 3,5,3'-triiodothyronine (T3) in brown adipose tissue: receptor occupancy and sources of T3 as determined by in vivo techniques. Endocrinology. 1987;120(1):55-62.
51. Freitas BC, Gereben B, Castillo M, Kallo I, Zeold A, Egri P, et al. Paracrine signaling by glial cell-derived triiodothyronine activates neuronal gene expression in the rodent brain and human cells. J Clin Invest. 2010;120(6):2206-17.
52. Crantz FR, Silva JE, Larsen PR. An analysis of the sources and quantity of 3,5,3'-triiodothyronine specifically bound to nuclear receptors in rat cerebral cortex and cerebellum. Endocrinology. 1982;110(2):367-75.
53. Bianco AC, Salvatore D, Gereben B, Berry MJ, Larsen PR. Biochemistry, cellular and molecular biology, and physiological roles of the iodothyronine selenodeiodinases. Endocr Rev. 2002;23(1):38-89.
54. Galton VA, Wood ET, St Germain EA, Withrow CA, Aldrich G, St Germain GM, et al. Thyroid hormone homeostasis and action in the type 2 deiodinase-deficient rodent brain during development. Endocrinology. 2007;148(7):3080-8.
55. Hernandez A, Martinez ME, Fiering S, Galton VA, St Germain D. Type 3 deiodinase is critical for the maturation and function of the thyroid axis. J Clin Invest. 2006;116(2):476-84.
56. Huang SA, Bianco AC. Reawakened interest in type III iodothyronine deiodinase in critical illness and injury. Nat Clin Pract Endocrinol Metab. 2008;4(3):148-55.
57. Dumitrescu AM, Liao XH, Abdullah MS, Lado-Abeal J, Majed FA, Moeller LC, et al. Mutations in SECISBP2 result in abnormal thyroid hormone metabolism. Nat Genet. 2005;37(11):1247-52.
58. Schoenmakers E, Carlson B, Agostini M, Moran C, Rajanayagam O, Bochukova E, et al. Mutation in human selenocysteine transfer RNA selectively disrupts selenoprotein synthesis. J Clin Invest. 2016;126(3):992-6.
59. Otten MH, Mol JA, Visser TJ. Sulfation preceding deiodination of iodothyronines in rat hepatocytes. Science. 1983;221(4605):81-3.
60. Wu SY, Green WL, Huang WS, Hays MT, Chopra IJ. Alternate pathways of thyroid hormone metabolism. Thyroid. 2005;15(8):943-58.
61. Chopra IJ, Wu SY, Teco GN, Santini F. A radioimmunoassay for measurement of 3,5,3'-triiodothyronine sulfate: studies in thyroidal and nonthyroidal diseases, pregnancy, and neonatal life. J Clin Endocrinol Metab. 1992;75(1):189-94.
62. Santini F, Cortelazzi D, Baggiani AM, Marconi AM, Beck-Peccoz P, Chopra IJ. A study of the serum 3,5,3'-triiodothyronine sulfate concentration in normal and hypothyroid fetuses at various gestational stages. J Clin Endocrinol Metab. 1993;76(6):1583-7.
63. Pitt-Rivers R. Physiological activity of the acetic-acid analogues of some iodinated thyronines. Lancet. 1953;265(6779):234-5.
64. Lerman J, Pitt-Rivers R. Physiologic activity of triiodo-and tetraiodo-thyroacetic acid in human myxedema. J Clin Endocrinol Metab. 1956;16(11):1470-9.
65. Trotter WR. Effect of triiodothyroacetic acid on blood-cholesterol levels. Lancet. 1956;270(6928):885-9.
66. Sherman SI, Ringel MD, Smith MJ, Kopelen HA, Zoghbi WA, Ladenson PW. Augmented hepatic and skeletal thyromimetic effects of tiratricol in comparison with levothyroxine. J Clin Endocrinol Metab. 1997;82(7):2153-8.
67. Sherman SI, Ladenson PW. Organ-specific effects of tiratricol: a thyroid hormone analog with hepatic, not pituitary, superagonist effects. J Clin Endocrinol Metab. 1992;75(3):901-5.
68. Mechelany C, Schlumberger M, Challeton C, Comoy E, Parmentier C. TRIAC (3,5,3'-triiodothyroacetic acid) has parallel effects at the pituitary and peripheral tissue levels in thyroid cancer patients treated with L-thyroxine. Clin Endocrinol (Oxf). 1991;35(2):123-8.
69. Brenta G, Schnitman M, Fretes O, Facco E, Gurfinkel M, Damilano S, et al. Comparative efficacy and side effects of the treatment of euthyroid goiter with levo-thyroxine or triiodothyroacetic acid. J Clin Endocrinol Metab. 2003;88(11):5287-92.
70. Groeneweg S, Peeters RP, Visser TJ, Visser WE. Therapeutic applications of thyroid hormone analogues in resistance to thyroid hormone (RTH) syndromes. Mol Cell Endocrinol. 2017;458:82-90.
71. Jouan P, Michel R, Roche J, Wolf W. The recovery of 3:5:3' -triiodothyroacetic acid and 3:3' -diiodothyronine from rat kidney after injection of 3:5:3' triiodothyronine. Endocrinology. 1956;59(4):425-32.
72. Albright EC, Lardy HA, Larson FC, Tomita K. Enzymatic conversion of thyroxine and triiodothyronine to the corresponding acetic acid analogues. Endocrinology. 1956;59(2):252-4.
73. Albright EC, Lardy HA, Larson FC, Tomita K. Enzymatic conversion of thyroxine to tetraiodothyroacetic acid and of triiodothyronine to triiodothyroacetic acid. J Biol Chem. 1957;224(1):387-97.

74. Rall JE, Rawson RW, Tata JR. Metabolism of L-thyroxine and L-3:5:3'-triiodothyronine by brain tissue preparations. Endocrinology. 1957;60(1):83-98.
75. Medina-Gomez G, Calvo RM, Obregon MJ. Thermogenic effect of triiodothyroacetic acid at low doses in rat adipose tissue without adverse side effects in the thyroid axis. Am J Physiol Endocrinol Metab. 2008;294(4):E688-97.
76. Braverman LE, Ingbar SH, Sterling K. Conversion of thyroxine (T4) to triiodothyronine (T3) in athyreotic human subjects. J Clin Invest. 1970;49(5):855-64.
77. Burger AG, Engler D, Sakoloff C, Staeheli V. The effects of tetraiodothyroacetic and triiodothyroacetic acids on thyroid function in euthyroid and hyperthyroid subjects. Acta Endocrinol (Copenh). 1979;92(3):455-67.
78. Burger AG. Nondeiodinative pathways of thyroid hormone metabolism. In Thyroid Hormone and Metabolism. 1986; chap. 8. Ed G Hennemann.:New York, NY, USA: Dekker Marcel.
79. Hoefig CS, Wuensch T, Rijntjes E, Lehmphul I, Daniel H, Schweizer U, et al. Biosynthesis of 3-Iodothyronamine From T4 in Murine Intestinal Tissue. Endocrinology. 2015;156(11):4356-64.
80. Wood WJ, Geraci T, Nilsen A, DeBarber AE, Scanlan TS. Iodothyronamines are oxidatively deaminated to iodothyroacetic acids in vivo. Chembiochem : a European journal of chemical biology. 2009;10(2):361-5.
81. Piehl S, Heberer T, Balizs G, Scanlan TS, Smits R, Koksch B, et al. Thyronamines are isozyme-specific substrates of deiodinases. Endocrinology. 2008;149(6):3037-45.
82. Wilkinson JH. Recent work on thyroid hormones. Postgraduate medical journal. 1957;33(381):333-7.
83. Rutgers M, Heusdens FA, Visser TJ. Metabolism of triiodothyroacetic acid (TA3) in rat liver. I. Deiodination of TA3 and TA3 sulfate by microsomes. Endocrinology. 1989;125(1):424-32.
84. Horn S, Kersseboom S, Mayerl S, Muller J, Groba C, Trajkovic-Arsic M, et al. Tetrac can replace thyroid hormone during brain development in mouse mutants deficient in the thyroid hormone transporter mct8. Endocrinology. 2013;154(2):968-79.
85. Martinez L, Nascimento AS, Nunes FM, Phillips K, Aparicio R, Dias SM, et al. Gaining ligand selectivity in thyroid hormone receptors via entropy. Proc Natl Acad Sci U S A. 2009;106(49):20717-22.
86. Takeda T, Suzuki S, Liu RT, DeGroot LJ. Triiodothyroacetic acid has unique potential for therapy of resistance to thyroid hormone. J Clin Endocrinol Metab. 1995;80(7):2033-40.
87. Messier N, Laflamme L, Hamann G, Langlois MF. In vitro effect of Triac on resistance to thyroid hormone receptor mutants: potential basis for therapy. Mol Cell Endocrinol. 2001;174(1-2):59-69.
88. Wagner RL, Huber BR, Shiau AK, Kelly A, Cunha Lima ST, Scanlan TS, et al. Hormone selectivity in thyroid hormone receptors. Mol Endocrinol. 2001;15(3):398-410.
89. Hennemann G, Docter R, Friesema EC, de Jong M, Krenning EP, Visser TJ. Plasma membrane transport of thyroid hormones and its role in thyroid hormone metabolism and bioavailability. Endocr Rev. 2001;22(4):451-76.
90. Friesema EC, Ganguly S, Abdalla A, Manning Fox JE, Halestrap AP, Visser TJ. Identification of monocarboxylate transporter 8 as a specific thyroid hormone transporter. J Biol Chem. 2003;278(41):40128-35.
91. Pizzagalli F, Hagenbuch B, Stieger B, Klenk U, Folkers G, Meier PJ. Identification of a novel human organic anion transporting polypeptide as a high affinity thyroxine transporter. Mol Endocrinol. 2002;16(10):2283-96.
92. Friesema EC, Docter R, Moerings EP, Stieger B, Hagenbuch B, Meier PJ, et al. Identification of thyroid hormone transporters. Biochem Biophys Res Commun. 1999;254(2):497-501.
93. Friesema EC, Grueters A, Biebermann H, Krude H, von Moers A, Reeser M, et al. Association between mutations in a thyroid hormone transporter and severe X-linked psychomotor retardation. Lancet. 2004;364(9443):1435-7.
94. Dumitrescu AM, Liao XH, Best TB, Brockmann K, Refetoff S. A novel syndrome combining thyroid and neurological abnormalities is associated with mutations in a monocarboxylate transporter gene. Am J Hum Genet. 2004;74(1):168-75.
95. Mayerl S, Muller J, Bauer R, Richert S, Kassmann CM, Darras VM, et al. Transporters MCT8 and OATP1C1 maintain murine brain thyroid hormone homeostasis. J Clin Invest. 2014;124(5):1987-99.
96. Mayerl S, Visser TJ, Darras VM, Horn S, Heuer H. Impact of Oatp1c1 deficiency on thyroid hormone metabolism and action in the mouse brain. Endocrinology. 2012;153(3):1528-37.
97. Muller J, Mayerl S, Visser TJ, Darras VM, Boelen A, Frappart L, et al. Tissue-specific alterations in thyroid hormone homeostasis in combined Mct10 and Mct8 deficiency. Endocrinology. 2014;155(1):315-25.
98. Trajkovic M, Visser TJ, Mittag J, Horn S, Lukas J, Darras VM, et al. Abnormal thyroid hormone metabolism in mice lacking the monocarboxylate transporter 8. J Clin Invest. 2007;117(3):627-35.
99. Dumitrescu AM, Liao XH, Weiss RE, Millen K, Refetoff S. Tissue-specific thyroid hormone deprivation and excess in monocarboxylate transporter (mct) 8-deficient mice. Endocrinology. 2006;147(9):4036-43.

100. Liao XH, Di Cosmo C, Dumitrescu AM, Hernandez A, Van Sande J, St Germain DL, et al. Distinct roles of deiodinases on the phenotype of Mct8 defect: a comparison of eight different mouse genotypes. Endocrinology. 2011;152(3):1180-91.
101. Mariotta L, Ramadan T, Singer D, Guetg A, Herzog B, Stoeger C, et al. T-type amino acid transporter TAT1 (Slc16a10) is essential for extracellular aromatic amino acid homeostasis control. J Physiol. 2012;590(24):6413-24.
102. Mayerl S, Schmidt M, Doycheva D, Darras VM, Huttner SS, Boelen A, et al. Thyroid Hormone Transporters MCT8 and OATP1C1 Control Skeletal Muscle Regeneration. Stem Cell Reports. 2018;10(6):1959-74.
103. Braun D, Wirth EK, Wohlgemuth F, Reix N, Klein MO, Gruters A, et al. Aminoaciduria, but normal thyroid hormone levels and signalling, in mice lacking the amino acid and thyroid hormone transporter Slc7a8. Biochem J. 2011;439(2):249-55.
104. Nunez B, Martinez de Mena R, Obregon MJ, Font-Llitjos M, Nunes V, Palacin M, et al. Cerebral cortex hyperthyroidism of newborn mct8-deficient mice transiently suppressed by lat2 inactivation. PLoS One. 2014;9(5):e96915.
105. Stohn JP, Martinez ME, Matoin K, Morte B, Bernal J, Galton VA, et al. MCT8 Deficiency in Male Mice Mitigates the Phenotypic Abnormalities Associated With the Absence of a Functional Type 3 Deiodinase. Endocrinology. 2016;157(8):3266-77.
106. Vatine GD, Al-Ahmad A, Barriga BK, Svendsen S, Salim A, Garcia L, et al. Modeling Psychomotor Retardation using iPSCs from MCT8-Deficient Patients Indicates a Prominent Role for the Blood-Brain Barrier. Cell Stem Cell. 2017;20(6):831-43 e5.
107. Vatine GD, Zada D, Lerer-Goldshtein T, Tovin A, Malkinson G, Yaniv K, et al. Zebrafish as a model for monocarboxyl transporter 8-deficiency. J Biol Chem. 2013;288(1):169-80.
108. Zada D, Tovin A, Lerer-Goldshtein T, Appelbaum L. Pharmacological treatment and BBB-targeted genetic therapy for MCT8-dependent hypomyelination in zebrafish. Dis Model Mech. 2016;9(11):1339-48.
109. de Vrieze E, van de Wiel SM, Zethof J, Flik G, Klaren PH, Arjona FJ. Knockdown of monocarboxylate transporter 8 (mct8) disturbs brain development and locomotion in zebrafish. Endocrinology. 2014;155(6):2320-30.
110. Delbaere J, Vancamp P, Van Herck SL, Bourgeois NM, Green MJ, Wingate RJ, et al. MCT8 deficiency in Purkinje cells disrupts embryonic chicken cerebellar development. J Endocrinol. 2017;232(2):259-72.
111. Groeneweg SvG, F.S.; Peeters, R.P.; Heuer, H.;Visser, W.E. Thyroid hormone transporters. Endocr Rev. 2019;(accepted for publication).
112. Hagenbuch B, Stieger B. The SLCO (former SLC21) superfamily of transporters. Molecular aspects of medicine. 2013;34(2-3):396-412.
113. Hagenbuch B, Meier PJ. Organic anion transporting polypeptides of the OATP/ SLC21 family: phylogenetic classification as OATP/ SLCO superfamily, new nomenclature and molecular/functional properties. Pflugers Arch. 2004;447(5):653-65.
114. Jacquemin E, Hagenbuch B, Stieger B, Wolkoff AW, Meier PJ. Expression cloning of a rat liver Na(+)-independent organic anion transporter. Proc Natl Acad Sci U S A. 1994;91(1):133-7.
115. Eckhardt U, Schroeder A, Stieger B, Hochli M, Landmann L, Tynes R, et al. Polyspecific substrate uptake by the hepatic organic anion transporter Oatp1 in stably transfected CHO cells. The American journal of physiology. 1999;276(4 Pt 1):G1037-42.
116. Meier PJ, Eckhardt U, Schroeder A, Hagenbuch B, Stieger B. Substrate specificity of sinusoidal bile acid and organic anion uptake systems in rat and human liver. Hepatology. 1997;26(6):1667-77.
117. Fujiwara K, Adachi H, Nishio T, Unno M, Tokui T, Okabe M, et al. Identification of thyroid hormone transporters in humans: different molecules are involved in a tissue-specific manner. Endocrinology. 2001;142(5):2005-12.
118. Kullak-Ublick GA, Ismair MG, Stieger B, Landmann L, Huber R, Pizzagalli F, et al. Organic anion-transporting polypeptide B (OATP-B) and its functional comparison with three other OATPs of human liver. Gastroenterology. 2001;120(2):525-33.
119. van der Deure WM, Peeters RP, Visser TJ. Molecular aspects of thyroid hormone transporters, including MCT8, MCT10, and OATPs, and the effects of genetic variation in these transporters. J Mol Endocrinol. 2010;44(1):1-11.
120. Kullak-Ublick GA, Hagenbuch B, Stieger B, Schteingart CD, Hofmann AF, Wolkoff AW, et al. Molecular and functional characterization of an organic anion transporting polypeptide cloned from human liver. Gastroenterology. 1995;109(4):1274-82.
121. Kullak-Ublick GA, Fisch T, Oswald M, Hagenbuch B, Meier PJ, Beuers U, et al. Dehydroepiandrosterone sulfate (DHEAS): identification of a carrier protein in human liver and brain. FEBS Lett. 1998;424(3):173-6.

122. Konig J, Seithel A, Gradhand U, Fromm MF. Pharmacogenomics of human OATP transporters. Naunyn Schmiedebergs Arch Pharmacol. 2006;372(6):432-43.
123. Konig J, Cui Y, Nies AT, Keppler D. A novel human organic anion transporting polypeptide localized to the basolateral hepatocyte membrane. American journal of physiology Gastrointestinal and liver physiology. 2000;278(1):G156-64.
124. Abe T, Kakyo M, Tokui T, Nakagomi R, Nishio T, Nakai D, et al. Identification of a novel gene family encoding human liver-specific organic anion transporter LST-1. J Biol Chem. 1999;274(24):17159-63.
125. van der Deure WM, Friesema EC, de Jong FJ, de Rijke YB, de Jong FH, Uitterlinden AG, et al. Organic anion transporter 1B1: an important factor in hepatic thyroid hormone and estrogen transport and metabolism. Endocrinology. 2008;149(9):4695-701.
126. Abe T, Unno M, Onogawa T, Tokui T, Kondo TN, Nakagomi R, et al. LST-2, a human liver-specific organic anion transporter, determines methotrexate sensitivity in gastrointestinal cancers. Gastroenterology. 2001;120(7):1689-99.
127. van der Deure WM, Hansen PS, Peeters RP, Kyvik KO, Friesema EC, Hegedus L, et al. Thyroid hormone transport and metabolism by organic anion transporter 1C1 and consequences of genetic variation. Endocrinology. 2008;149(10):5307-14.
128. Leuthold S, Hagenbuch B, Mohebbi N, Wagner CA, Meier PJ, Stieger B. Mechanisms of pH-gradient driven transport mediated by organic anion polypeptide transporters. American journal of physiology Cell physiology. 2009;296(3):C570-82.
129. Huber RD, Gao B, Sidler Pfandler MA, Zhang-Fu W, Leuthold S, Hagenbuch B, et al. Characterization of two splice variants of human organic anion transporting polypeptide 3A1 isolated from human brain. American journal of physiology Cell physiology. 2007;292(2):C795-806.
130. Hagenbuch B. Cellular entry of thyroid hormones by organic anion transporting polypeptides. Best Pract Res Clin Endocrinol Metab. 2007;21(2):209-21.
131. Mikkaichi T, Suzuki T, Onogawa T, Tanemoto M, Mizutamari H, Okada M, et al. Isolation and characterization of a digoxin transporter and its rat homologue expressed in the kidney. Proc Natl Acad Sci U S A. 2004;101(10):3569-74.
132. Takeuchi A, Masuda S, Saito H, Abe T, Inui K. Multispecific substrate recognition of kidney-specific organic anion transporters OAT-K1 and OAT-K2. The Journal of pharmacology and experimental therapeutics. 2001;299(1):261-7.
133. Abe T, Kakyo M, Sakagami H, Tokui T, Nishio T, Tanemoto M, et al. Molecular characterization and tissue distribution of a new organic anion transporter subtype (oatp3) that transports thyroid hormones and taurocholate and comparison with oatp2. J Biol Chem. 1998;273(35):22395-401.
134. Cattori V, Hagenbuch B, Hagenbuch N, Stieger B, Ha R, Winterhalter KE, et al. Identification of organic anion transporting polypeptide 4 (Oatp4) as a major full-length isoform of the liver-specific transporter-1 (rlst-1) in rat liver. FEBS Lett. 2000;474(2-3):242-5.
135. Sugiyama D, Kusuhara H, Taniguchi H, Ishikawa S, Nozaki Y, Aburatani H, et al. Functional characterization of rat brain-specific organic anion transporter (Oatp14) at the blood-brain barrier: high affinity transporter for thyroxine. J Biol Chem. 2003;278(44):43489-95.
136. Suzuki T, Onogawa T, Asano N, Mizutamari H, Mikkaichi T, Tanemoto M, et al. Identification and characterization of novel rat and human gonad-specific organic anion transporters. Mol Endocrinol. 2003;17(7):1203-15.
137. Westholm DE, Salo DR, Viken KJ, Rumbley JN, Anderson GW. The blood-brain barrier thyroxine transporter organic anion-transporting polypeptide 1c1 displays atypical transport kinetics. Endocrinology. 2009;150(11):5153-62.
138. Hagenbuch B, Gui C. Xenobiotic transporters of the human organic anion transporting polypeptides (OATP) family. Xenobiotica; the fate of foreign compounds in biological systems. 2008;38(7-8):778-801.
139. Kobayashi D, Nozawa T, Imai K, Nezu J, Tsuji A, Tamai I. Involvement of human organic anion transporting polypeptide OATP-B (SLC21A9) in pH-dependent transport across intestinal apical membrane. The Journal of pharmacology and experimental therapeutics. 2003;306(2):703-8.
140. Roth M, Obaidat A, Hagenbuch B. OATPs, OATs and OCTs: the organic anion and cation transporters of the SLCO and SLC22A gene superfamilies. British journal of pharmacology. 2012;165(5):1260-87.
141. Gao B, Huber RD, Wenzel A, Vavricka SR, Ismair MG, Reme C, et al. Localization of organic anion transporting polypeptides in the rat and human ciliary body epithelium. Experimental eye research. 2005;80(1):61-72.

142. Akanuma S, Hirose S, Tachikawa M, Hosoya K. Localization of organic anion transporting polypeptide (Oatp) 1a4 and Oatp1c1 at the rat blood-retinal barrier. Fluids Barriers CNS. 2013;10(1):29.
143. Roberts LM, Woodford K, Zhou M, Black DS, Haggerty JE, Tate EH, et al. Expression of the thyroid hormone transporters monocarboxylate transporter-8 (SLC16A2) and organic ion transporter-14 (SLCO1C1) at the blood-brain barrier. Endocrinology. 2008;149(12):6251-61.
144. Ito K, Uchida Y, Ohtsuki S, Aizawa S, Kawakami H, Katsukura Y, et al. Quantitative membrane protein expression at the blood-brain barrier of adult and younger cynomolgus monkeys. J Pharm Sci. 2011;100(9):3939-50.
145. Grijota-Martinez C, Diez D, Morreale de Escobar G, Bernal J, Morte B. Lack of action of exogenously administered T3 on the fetal rat brain despite expression of the monocarboxylate transporter 8. Endocrinology. 2011;152(4):1713-21.
146. Tohyama K, Kusuhara H, Sugiyama Y. Involvement of multispecific organic anion transporter, Oatp14 (Slc21a14), in the transport of thyroxine across the blood-brain barrier. Endocrinology. 2004;145(9):4384-91.
147. Van Herck SL, Geysens S, Delbaere J, Tylzanowski P, Darras VM. Expression profile and thyroid hormone responsiveness of transporters and deiodinases in early embryonic chicken brain development. Mol Cell Endocrinol. 2012;349(2):289-97.
148. Walter KM, Miller GW, Chen X, Yaghoobi B, Puschner B, Lein PJ. Effects of thyroid hormone disruption on the ontogenetic expression of thyroid hormone signaling genes in developing zebrafish (Danio rerio). Gen Comp Endocrinol. 2019;272:20-32.
149. Sun YN, Liu YJ, Zhang L, Ye Y, Lin LX, Li YM, et al. Expression of organic anion transporting polypeptide 1c1 and monocarboxylate transporter 8 in the rat placental barrier and the compensatory response to thyroid dysfunction. PLoS One. 2014;9(4):e96047.
150. Wittmann G, Szabon J, Mohacsik P, Nouriel SS, Gereben B, Fekete C, et al. Parallel regulation of thyroid hormone transporters OATP1c1 and MCT8 during and after endotoxemia at the blood-brain barrier of male rodents. Endocrinology. 2015;156(4):1552-64.
151. Claro da Silva T, Polli JE, Swaan PW. The solute carrier family 10 (SLC10): beyond bile acid transport. Molecular aspects of medicine. 2013;34(2-3):252-69.
152. Visser WE, Wong WS, van Mullem AA, Friesema EC, Geyer J, Visser TJ. Study of the transport of thyroid hormone by transporters of the SLC10 family. Mol Cell Endocrinol. 2010;315(1-2):138-45.
153. Hagenbuch B, Meier PJ. Sinusoidal (basolateral) bile salt uptake systems of hepatocytes. Seminars in liver disease. 1996;16(2):129-36.
154. Trauner M, Boyer JL. Bile salt transporters: molecular characterization, function, and regulation. Physiol Rev. 2003;83(2):633-71.
155. Geyer J, Wilke T, Petzinger E. The solute carrier family SLC10: more than a family of bile acid transporters regarding function and phylogenetic relationships. Naunyn Schmiedebergs Arch Pharmacol. 2006;372(6):413-31.
156. Boyer JL, Hagenbuch B, Ananthanarayanan M, Suchy F, Stieger B, Meier PJ. Phylogenic and ontogenic expression of hepatocellular bile acid transport. Proc Natl Acad Sci U S A. 1993;90(2):435-8.
157. Ananthanarayanan M, Ng OC, Boyer JL, Suchy FJ. Characterization of cloned rat liver Na(+)-bile acid cotransporter using peptide and fusion protein antibodies. The American journal of physiology. 1994;267(4 Pt 1):G637-43.
158. Stieger B, Hagenbuch B, Landmann L, Hochli M, Schroeder A, Meier PJ. In situ localization of the hepatocytic Na+/Taurocholate cotransporting polypeptide in rat liver. Gastroenterology. 1994;107(6):1781-7.
159. Cheng X, Buckley D, Klaassen CD. Regulation of hepatic bile acid transporters Ntcp and Bsep expression. Biochem Pharmacol. 2007;74(11):1665-76.
160. Kullak-Ublick GA, Glasa J, Boker C, Oswald M, Grutzner U, Hagenbuch B, et al. Chlorambucil-taurocholate is transported by bile acid carriers expressed in human hepatocellular carcinomas. Gastroenterology. 1997;113(4):1295-305.
161. Chen HL, Chen HL, Liu YJ, Feng CH, Wu CY, Shyu MK, et al. Developmental expression of canalicular transporter genes in human liver. Journal of hepatology. 2005;43(3):472-7.
162. Baghdasaryan A, Chiba P, Trauner M. Clinical application of transcriptional activators of bile salt transporters. Molecular aspects of medicine. 2014;37:57-76.
163. Palacin M. A new family of proteins (rBAT and 4F2hc) involved in cationic and zwitterionic amino acid transport: a tale of two proteins in search of a transport function. J Exp Biol. 1994;196:123-37.
164. Mastroberardino L, Spindler B, Pfeiffer R, Skelly PJ, Loffing J, Shoemaker CB, et al. Amino-acid transport by heterodimers of 4F2hc/CD98 and members of a permease family. Nature. 1998;395(6699):288-91.

165. Segawa H, Fukasawa Y, Miyamoto K, Takeda E, Endou H, Kanai Y. Identification and functional characterization of a Na+-independent neutral amino acid transporter with broad substrate selectivity. J Biol Chem. 1999;274(28):19745-51.
166. Friesema EC, Docter R, Moerings EP, Verrey F, Krenning EP, Hennemann G, et al. Thyroid hormone transport by the heterodimeric human system L amino acid transporter. Endocrinology. 2001;142(10):4339-48.
167. Babu E, Kanai Y, Chairoungdua A, Kim DK, Iribe Y, Tangtrongsup S, et al. Identification of a novel system L amino acid transporter structurally distinct from heterodimeric amino acid transporters. J Biol Chem. 2003;278(44):43838-45.
168. Cleal JK, Glazier JD, Ntani G, Crozier SR, Day PE, Harvey NC, et al. Facilitated transporters mediate net efflux of amino acids to the fetus across the basal membrane of the placental syncytiotrophoblast. J Physiol. 2011;589(Pt 4):987-97.
169. Bodoy S, Martin L, Zorzano A, Palacin M, Estevez R, Bertran J. Identification of LAT4, a novel amino acid transporter with system L activity. J Biol Chem. 2005;280(12):12002-11.
170. Stuart RO, Pavlova A, Beier D, Li Z, Krijanovski Y, Nigam SK. EEG1, a putative transporter expressed during epithelial organogenesis: comparison with embryonic transporter expression during nephrogenesis. Am J Physiol Renal Physiol. 2001;281(6):F1148-56.
171. Bodoy S, Fotiadis D, Stoeger C, Kanai Y, Palacin M. The small SLC43 family: facilitator system l amino acid transporters and the orphan EEG1. Molecular aspects of medicine. 2013;34(2-3):638-45.
172. Zevenbergen C, Meima ME, Lima de Souza EC, Peeters RP, Kinne A, Krause G, et al. Transport of Iodothyronines by Human L-Type Amino Acid Transporters. Endocrinology. 2015;156(11):4345-55.
173. Meier C, Ristic Z, Klauser S, Verrey F. Activation of system L heterodimeric amino acid exchangers by intracellular substrates. EMBO J. 2002;21(4):580-9.
174. Kanai Y, Segawa H, Miyamoto K, Uchino H, Takeda E, Endou H. Expression cloning and characterization of a transporter for large neutral amino acids activated by the heavy chain of 4F2 antigen (CD98). J Biol Chem. 1998;273(37):23629-32.
175. Yanagida O, Kanai Y, Chairoungdua A, Kim DK, Segawa H, Nii T, et al. Human L-type amino acid transporter 1 (LAT1): characterization of function and expression in tumor cell lines. Biochim Biophys Acta. 2001;1514(2):291-302.
176. Yan Z, Hinkle PM. Saturable, stereospecific transport of 3,5,3'-triiodo-L-thyronine and L-thyroxine into GH4C1 pituitary cells. J Biol Chem. 1993;268(27):20179-84.
177. Zhou Y, Samson M, Francon J, Blondeau JP. Thyroid hormone concentrative uptake in rat erythrocytes. Involvement of the tryptophan transport system T in countertransport of tri-iodothyronine and aromatic amino acids. Biochem J. 1992;281 (Pt 1):81-6.
178. Everts ME, Verhoeven FA, Bezstarosti K, Moerings EP, Hennemann G, Visser TJ, et al. Uptake of thyroid hormones in neonatal rat cardiac myocytes. Endocrinology. 1996;137(10):4235-42.
179. Blondeau JP, Beslin A, Chantoux F, Francon J. Triiodothyronine is a high-affinity inhibitor of amino acid transport system L1 in cultured astrocytes. J Neurochem. 1993;60(4):1407-13.
180. Lakshmanan M, Goncalves E, Lessly G, Foti D, Robbins J. The transport of thyroxine into mouse neuroblastoma cells, NB41A3: the effect of L-system amino acids. Endocrinology. 1990;126(6):3245-50.
181. Centanni M, Canettieri G, Viceconti N, Sibilla R, Bei A, Andreoli M. Effect of tryptophan on the early tri-iodothyronine uptake in mouse thymocytes. Eur J Endocrinol. 2000;143(1):119-23.
182. Ritchie JW, Peter GJ, Shi YB, Taylor PM. Thyroid hormone transport by 4F2hc-IU12 heterodimers expressed in Xenopus oocytes. J Endocrinol. 1999;163(2):R5-9.
183. Morimoto E, Kanai Y, Kim DK, Chairoungdua A, Choi HW, Wempe MF, et al. Establishment and characterization of mammalian cell lines stably expressing human L-type amino acid transporters. J Pharmacol Sci. 2008;108(4):505-16.
184. Khunweeraphong N, Nagamori S, Wiriyasermkul P, Nishinaka Y, Wongthai P, Ohgaki R, et al. Establishment of stable cell lines with high expression of heterodimers of human 4F2hc and human amino acid transporter LAT1 or LAT2 and delineation of their differential interaction with alpha-alkyl moieties. J Pharmacol Sci. 2012;119(4):368-80.
185. Kinne A, Wittner M, Wirth EK, Hinz KM, Schulein R, Kohrle J, et al. Involvement of the L-Type Amino Acid Transporter Lat2 in the Transport of 3,3'-Diiodothyronine across the Plasma Membrane. Eur Thyroid J. 2015;4(Suppl 1):42-50.
186. Hinz KM, Neef D, Rutz C, Furkert J, Kohrle J, Schulein R, et al. Molecular features of the L-type amino acid transporter 2 determine different import and export profiles for thyroid hormones and amino acids. Mol Cell Endocrinol. 2017;443:163-74.

187. Christensen HN. Role of amino acid transport and countertransport in nutrition and metabolism. Physiol Rev. 1990;70(1):43-77.
188. Nakamura E, Sato M, Yang H, Miyagawa F, Harasaki M, Tomita K, et al. 4F2 (CD98) heavy chain is associated covalently with an amino acid transporter and controls intracellular trafficking and membrane topology of 4F2 heterodimer. J Biol Chem. 1999;274(5):3009-16.
189. Pinho MJ, Serrao MP, Gomes P, Hopfer U, Jose PA, Soares-da-Silva P. Over-expression of renal LAT1 and LAT2 and enhanced L-DOPA uptake in SHR immortalized renal proximal tubular cells. Kidney Int. 2004;66(1):216-26.
190. Rossier G, Meier C, Bauch C, Summa V, Sordat B, Verrey F, et al. LAT2, a new basolateral 4F2hc/CD98-associated amino acid transporter of kidney and intestine. J Biol Chem. 1999;274(49):34948-54.
191. Tomi M, Mori M, Tachikawa M, Katayama K, Terasaki T, Hosoya K. L-type amino acid transporter 1-mediated L-leucine transport at the inner blood-retinal barrier. Invest Ophthalmol Vis Sci. 2005;46(7):2522-30.
192. Okamoto Y, Sakata M, Ogura K, Yamamoto T, Yamaguchi M, Tasaka K, et al. Expression and regulation of 4F2hc and hLAT1 in human trophoblasts. American journal of physiology Cell physiology. 2002;282(1):C196-204.
193. Kageyama T, Nakamura M, Matsuo A, Yamasaki Y, Takakura Y, Hashida M, et al. The 4F2hc/LAT1 complex transports L-DOPA across the blood-brain barrier. Brain Res. 2000;879(1-2):115-21.
194. Umeki N, Fukasawa Y, Ohtsuki S, Hori S, Watanabe Y, Kohno Y, et al. mRNA expression and amino acid transport characteristics of cultured human brain microvascular endothelial cells (hBME). Drug Metab Pharmacokinet. 2002;17(4):367-73.
195. Braun D, Kinne A, Brauer AU, Sapin R, Klein MO, Kohrle J, et al. Developmental and cell type-specific expression of thyroid hormone transporters in the mouse brain and in primary brain cells. Glia. 2011;59(3):463-71.
196. Kobayashi Y. Localization of the System L Amino Acid Transporters LAT1 and LAT2 in Rat Gastrointestinal Tract. . Journal of the Kyorin Medical Society. 2007;38:75–84.
197. Bassi MT, Sperandeo MP, Incerti B, Bulfone A, Pepe A, Surace EM, et al. SLC7A8, a gene mapping within the lysinuric protein intolerance critical region, encodes a new member of the glycoprotein-associated amino acid transporter family. Genomics. 1999;62(2):297-303.
198. Pineda M, Fernandez E, Torrents D, Estevez R, Lopez C, Camps M, et al. Identification of a membrane protein, LAT-2, that Co-expresses with 4F2 heavy chain, an L-type amino acid transport activity with broad specificity for small and large zwitterionic amino acids. J Biol Chem. 1999;274(28):19738-44.
199. Wirth EK, Roth S, Blechschmidt C, Holter SM, Becker L, Racz I, et al. Neuronal 3',3,5-triiodothyronine (T3) uptake and behavioral phenotype of mice deficient in Mct8, the neuronal T3 transporter mutated in Allan-Herndon-Dudley syndrome. J Neurosci. 2009;29(30):9439-49.
200. Muller J, Heuer H. Expression pattern of thyroid hormone transporters in the postnatal mouse brain. Front Endocrinol (Lausanne). 2014;5:92.
201. Halestrap AP, Meredith D. The SLC16 gene family-from monocarboxylate transporters (MCTs) to aromatic amino acid transporters and beyond. Pflugers Arch. 2004;447(5):619-28.
202. Rusu V, Hoch E, Mercader JM, Tenen DE, Gymrek M, Hartigan CR, et al. Type 2 Diabetes Variants Disrupt Function of SLC16A11 through Two Distinct Mechanisms. Cell. 2017;170(1):199-212 e20.
203. Hugo SE, Cruz-Garcia L, Karanth S, Anderson RM, Stainier DY, Schlegel A. A monocarboxylate transporter required for hepatocyte secretion of ketone bodies during fasting. Genes Dev. 2012;26(3):282-93.
204. Abplanalp J, Laczko E, Philp NJ, Neidhardt J, Zuercher J, Braun P, et al. The cataract and glucosuria associated monocarboxylate transporter MCT12 is a new creatine transporter. Hum Mol Genet. 2013;22(16):3218-26.
205. Murakami Y, Kohyama N, Kobayashi Y, Ohbayashi M, Ohtani H, Sawada Y, et al. Functional characterization of human monocarboxylate transporter 6 (SLC16A5). Drug Metab Dispos. 2005;33(12):1845-51.
206. van Hasselt PM, Ferdinandusse S, Monroe GR, Ruiter JP, Turkenburg M, Geerlings MJ, et al. Monocarboxylate transporter 1 deficiency and ketone utilization. N Engl J Med. 2014;371(20):1900-7.
207. Lara-Riegos JC, Ortiz-Lopez MG, Pena-Espinoza BI, Montufar-Robles I, Pena-Rico MA, Sanchez-Pozos K, et al. Diabetes susceptibility in Mayas: Evidence for the involvement of polymorphisms in HHEX, HNF4alpha, KCNJ11, PPARgamma, CDKN2A/2B, SLC30A8, CDC123/CAMK1D, TCF7L2, ABCA1 and SLC16A11 genes. Gene. 2015;565(1):68-75.
208. Kloeckener-Gruissem B, Vandekerckhove K, Nurnberg G, Neidhardt J, Zeitz C, Nurnberg P, et al. Mutation of solute carrier SLC16A12 associates with a syndrome combining juvenile cataract with microcornea and renal glucosuria. Am J Hum Genet. 2008;82(3):772-9.

209. Friesema EC, Jansen J, Jachtenberg JW, Visser WE, Kester MH, Visser TJ. Effective cellular uptake and efflux of thyroid hormone by human monocarboxylate transporter 10. Mol Endocrinol. 2008;22(6):1357-69.
210. Lafreniere RG, Carrel L, Willard HF. A novel transmembrane transporter encoded by the XPCT gene in Xq13.2. Hum Mol Genet. 1994;3(7):1133-9.
211. Bourgeois NM, Van Herck SL, Vancamp P, Delbaere J, Zevenbergen C, Kersseboom S, et al. Characterization of Chicken Thyroid Hormone Transporters. Endocrinology. 2016;157(6):2560-74.
212. Mughal BB, Leemans M, Lima de Souza EC, le Mevel S, Spirhanzlova P, Visser TJ, et al. Functional Characterization of Xenopus Thyroid Hormone Transporters mct8 and oatp1c1. Endocrinology. 2017;158(8):2694-705.
213. Arjona FJ, de Vrieze E, Visser TJ, Flik G, Klaren PH. Identification and functional characterization of zebrafish solute carrier Slc16a2 (Mct8) as a thyroid hormone membrane transporter. Endocrinology. 2011;152(12):5065-73.
214. Zhou Y, Samson M, Osty J, Francon J, Blondeau JP. Evidence for a close link between the thyroid hormone transport system and the aromatic amino acid transport system T in erythrocytes. J Biol Chem. 1990;265(28):17000-4.
215. Kim DK, Kanai Y, Chairoungdua A, Matsuo H, Cha SH, Endou H. Expression cloning of a Na+-independent aromatic amino acid transporter with structural similarity to H+/monocarboxylate transporters. J Biol Chem. 2001;276(20):17221-8.
216. Kim DK, Kanai Y, Matsuo H, Kim JY, Chairoungdua A, Kobayashi Y, et al. The human T-type amino acid transporter-1: characterization, gene organization, and chromosomal location. Genomics. 2002;79(1):95-103.
217. Friesema EC, Kuiper GG, Jansen J, Visser TJ, Kester MH. Thyroid hormone transport by the human monocarboxylate transporter 8 and its rate-limiting role in intracellular metabolism. Mol Endocrinol. 2006;20(11):2761-72.
218. van Mullem AA, van Gucht AL, Visser WE, Meima ME, Peeters RP, Visser TJ. Effects of thyroid hormone transporters MCT8 and MCT10 on nuclear activity of T3. Mol Cell Endocrinol. 2016;437:252-60.
219. Kinne A, Kleinau G, Hoefig CS, Gruters A, Kohrle J, Krause G, et al. Essential molecular determinants for thyroid hormone transport and first structural implications for monocarboxylate transporter 8. J Biol Chem. 2010;285(36):28054-63.
220. Ianculescu AG, Friesema EC, Visser TJ, Giacomini KM, Scanlan TS. Transport of thyroid hormones is selectively inhibited by 3-iodothyronamine. Mol Biosyst. 2010;6(8):1403-10.
221. Johannes J, Braun D, Kinne A, Rathmann D, Kohrle J, Schweizer U. Few Amino Acid Exchanges Expand the Substrate Spectrum of Monocarboxylate Transporter 10. Mol Endocrinol. 2016;30(7):796-808.
222. Visser WE, van Mullem AA, Jansen J, Visser TJ. The thyroid hormone transporters MCT8 and MCT10 transport the affinity-label N-bromoacetyl-[(125)I]T3 but are not modified by it. Mol Cell Endocrinol. 2011;337(1-2):96-100.
223. Kersseboom S, Horn S, Visser WE, Chen J, Friesema EC, Vaurs-Barriere C, et al. In vitro and mouse studies supporting therapeutic utility of triiodothyroacetic acid in MCT8 deficiency. Mol Endocrinol. 2014;28(12):1961-70.
224. Roth S, Kinne A, Schweizer U. The tricyclic antidepressant desipramine inhibits T3 import into primary neurons. Neurosci Lett. 2010;478(1):5-8.
225. Johannes J, Jayarama-Naidu R, Meyer F, Wirth EK, Schweizer U, Schomburg L, et al. Silychristin, a Flavonolignan Derived From the Milk Thistle, Is a Potent Inhibitor of the Thyroid Hormone Transporter MCT8. Endocrinology. 2016;157(4):1694-701.
226. Braun D, Kim TD, le Coutre P, Kohrle J, Hershman JM, Schweizer U. Tyrosine kinase inhibitors noncompetitively inhibit MCT8-mediated iodothyronine transport. J Clin Endocrinol Metab. 2012;97(1):E100-5.
227. Illouz F, Braun D, Briet C, Schweizer U, Rodien P. Endocrine side-effects of anti-cancer drugs: thyroid effects of tyrosine kinase inhibitors. Eur J Endocrinol. 2014;171(3):R91-9.
228. Braun D, Schweizer U. Authentic bosutinib inhibits triiodothyronine transport by monocarboxylate transporter 8. Thyroid. 2014;24(5):926-7.
229. Beukhof CM, van Doorn L, Visser TJ, Bins S, Visser WE, van Heerebeek R, et al. Sorafenib-Induced Changes in Thyroid Hormone Levels in Patients Treated for Hepatocellular Carcinoma. J Clin Endocrinol Metab. 2017;102(8):2922-9.
230. Zwanziger D, Schmidt M, Fischer J, Kleinau G, Braun D, Schweizer U, et al. The long N-terminus of the human monocarboxylate transporter 8 is a target of ubiquitin-dependent proteasomal degradation which regulates protein expression and oligomerization capacity. Mol Cell Endocrinol. 2016;434:278-87.

231. Kinne A, Roth S, Biebermann H, Kohrle J, Gruters A, Schweizer U. Surface translocation and tri-iodothyronine uptake of mutant MCT8 proteins are cell type-dependent. J Mol Endocrinol. 2009;43(6):263-71.
232. Nishimura M, Naito S. Tissue-specific mRNA expression profiles of human solute carrier transporter superfamilies. Drug Metab Pharmacokinet. 2008;23(1):22-44.
233. Friesema EC, Visser TJ, Borgers AJ, Kalsbeek A, Swaab DF, Fliers E, et al. Thyroid hormone transporters and deiodinases in the developing human hypothalamus. Eur J Endocrinol. 2012;167(3):379-86.
234. Loubiere LS, Vasilopoulou E, Glazier JD, Taylor PM, Franklyn JA, Kilby MD, et al. Expression and function of thyroid hormone transporters in the microvillous plasma membrane of human term placental syncytiotrophoblast. Endocrinology. 2012;153(12):6126-35.
235. Price NT, Jackson VN, Halestrap AP. Cloning and sequencing of four new mammalian monocarboxylate transporter (MCT) homologues confirms the existence of a transporter family with an ancient past. Biochem J. 1998;329 (Pt 2):321-8.
236. Loubiere LS, Vasilopoulou E, Bulmer JN, Taylor PM, Stieger B, Verrey F, et al. Expression of thyroid hormone transporters in the human placenta and changes associated with intrauterine growth restriction. Placenta. 2010;31(4):295-304.
237. Chan SY, Hancox LA, Martin-Santos A, Loubiere LS, Walter MN, Gonzalez AM, et al. MCT8 expression in human fetal cerebral cortex is reduced in severe intrauterine growth restriction. J Endocrinol. 2014;220(2):85-95.
238. Alkemade A, Friesema EC, Unmehopa UA, Fabriek BO, Kuiper GG, Leonard JL, et al. Neuroanatomical pathways for thyroid hormone feedback in the human hypothalamus. J Clin Endocrinol Metab. 2005;90(7):4322-34.
239. Di Cosmo C, Liao XH, Dumitrescu AM, Philp NJ, Weiss RE, Refetoff S. Mice deficient in MCT8 reveal a mechanism regulating thyroid hormone secretion. J Clin Invest. 2010;120(9):3377-88.
240. Trajkovic-Arsic M, Muller J, Darras VM, Groba C, Lee S, Weih D, et al. Impact of monocarboxylate transporter-8 deficiency on the hypothalamus-pituitary-thyroid axis in mice. Endocrinology. 2010;151(10):5053-62.
241. Becker HM, Mohebbi N, Perna A, Ganapathy V, Capasso G, Wagner CA. Localization of members of MCT monocarboxylate transporter family Slc16 in the kidney and regulation during metabolic acidosis. Am J Physiol Renal Physiol. 2010;299(1):F141-54.
242. Trajkovic-Arsic M, Visser TJ, Darras VM, Friesema EC, Schlott B, Mittag J, et al. Consequences of monocarboxylate transporter 8 deficiency for renal transport and metabolism of thyroid hormones in mice. Endocrinology. 2010;151(2):802-9.
243. Henning Y, Szafranski K. Age-Dependent Changes of Monocarboxylate Transporter 8 Availability in the Postnatal Murine Retina. Front Cell Neurosci. 2016;10:205.
244. Vasilopoulou E, Loubiere LS, Heuer H, Trajkovic-Arsic M, Darras VM, Visser TJ, et al. Monocarboxylate transporter 8 modulates the viability and invasive capacity of human placental cells and fetoplacental growth in mice. PLoS One. 2013;8(6):e65402.
245. Heuer H, Maier MK, Iden S, Mittag J, Friesema EC, Visser TJ, et al. The monocarboxylate transporter 8 linked to human psychomotor retardation is highly expressed in thyroid hormone-sensitive neuron populations. Endocrinology. 2005;146(4):1701-6.
246. Ceballos A, Belinchon MM, Sanchez-Mendoza E, Grijota-Martinez C, Dumitrescu AM, Refetoff S, et al. Importance of monocarboxylate transporter 8 for the blood-brain barrier-dependent availability of 3,5,3'-triiodo-L-thyronine. Endocrinology. 2009;150(5):2491-6.
247. Morte B, Gil-Ibanez P, Bernal J. Regulation of Gene Expression by Thyroid Hormone in Primary Astrocytes: Factors Influencing the Genomic Response. Endocrinology. 2018;159(5):2083-92.
248. Kallo I, Mohacsik P, Vida B, Zeold A, Bardoczi Z, Zavacki AM, et al. A novel pathway regulates thyroid hormone availability in rat and human hypothalamic neurosecretory neurons. PLoS One. 2012;7(6):e37860.
249. Campinho MA, Saraiva J, Florindo C, Power DM. Maternal thyroid hormones are essential for neural development in zebrafish. Mol Endocrinol. 2014;28(7):1136-49.
250. Van Herck SL, Delbaere J, Bourgeois NM, McAllan BM, Richardson SJ, Darras VM. Expression of thyroid hormone transporters and deiodinases at the brain barriers in the embryonic chicken: Insights into the regulation of thyroid hormone availability during neurodevelopment. Gen Comp Endocrinol. 2015;214:30-9.
251. Zada D, Tovin A, Lerer-Goldshtein T, Vatine GD, Appelbaum L. Altered behavioral performance and live imaging of circuit-specific neural deficiencies in a zebrafish model for psychomotor retardation. PLoS Genet. 2014;10(9):e1004615.
252. Zada D, Blitz E, Appelbaum L. Zebrafish - An emerging model to explore thyroid hormone transporters and psychomotor retardation. Mol Cell Endocrinol. 2017;459:53-8.

253. Chan SY, Martin-Santos A, Loubiere LS, Gonzalez AM, Stieger B, Logan A, et al. The expression of thyroid hormone transporters in the human fetal cerebral cortex during early development and in N-Tera-2 neurodifferentiation. J Physiol. 2011;589(Pt 11):2827-45.
254. Abe S, Namba N, Abe M, Fujiwara M, Aikawa T, Kogo M, et al. Monocarboxylate transporter 10 functions as a thyroid hormone transporter in chondrocytes. Endocrinology. 2012;153(8):4049-58.
255. Ramadan T, Camargo SM, Summa V, Hunziker P, Chesnov S, Pos KM, et al. Basolateral aromatic amino acid transporter TAT1 (Slc16a10) functions as an efflux pathway. J Cell Physiol. 2006;206(3):771-9.
256. Liddelow SA, Temple S, Mollgard K, Gehwolf R, Wagner A, Bauer H, et al. Molecular characterisation of transport mechanisms at the developing mouse blood-CSF interface: a transcriptome approach. PLoS One. 2012;7(3):e33554.
257. Kogai T, Liu YY, Richter LL, Mody K, Kagechika H, Brent GA. Retinoic acid induces expression of the thyroid hormone transporter, monocarboxylate transporter 8 (Mct8). J Biol Chem. 2010;285(35):27279-88.
258. Fontes KN, Cabanelas A, Bloise FF, de Andrade CBV, Souza LL, Wilieman M, et al. Differential Regulation of Thyroid Hormone Metabolism Target Genes during Non-thyoidal Illness Syndrome Triggered by Fasting or Sepsis in Adult Mice. Front Physiol. 2017;8:828.
259. Alvarez-Salas E, Mengod G, Garcia-Luna C, Soberanes-Chavez P, Matamoros-Trejo G, de Gortari P. Mct8 and trh co-expression throughout the hypothalamic paraventricular nucleus is modified by dehydration-induced anorexia in rats. Neuropeptides. 2016;56:33-40.
260. Schutkowski A, Wege N, Stangl GI, Konig B. Tissue-specific expression of monocarboxylate transporters during fasting in mice. PLoS One. 2014;9(11):e112118.
261. Herwig A, Campbell G, Mayer CD, Boelen A, Anderson RA, Ross AW, et al. A thyroid hormone challenge in hypothyroid rats identifies T3 regulated genes in the hypothalamus and in models with altered energy balance and glucose homeostasis. Thyroid. 2014;24(11):1575-93.
262. Romano RM, Gomes SN, Cardoso NC, Schiessl L, Romano MA, Oliveira CA. New insights for male infertility revealed by alterations in spermatic function and differential testicular expression of thyroid-related genes. Endocrine. 2017;55(2):607-17.
263. Badziong J, Ting S, Synoracki S, Tiedje V, Brix K, Brabant G, et al. Differential regulation of monocarboxylate transporter 8 expression in thyroid cancer and hyperthyroidism. Eur J Endocrinol. 2017;177(3):243-50.
264. Selmi-Ruby S, Bouazza L, Obregon MJ, Conscience A, Flamant F, Samarut J, et al. The targeted inactivation of TRbeta gene in thyroid follicular cells suggests a new mechanism of regulation of thyroid hormone production. Endocrinology. 2014;155(2):635-46.
265. de Souza EC, Dias GR, Cardoso RC, Lima LP, Fortunato RS, Visser TJ, et al. MCT8 is Downregulated by Short Time Iodine Overload in the Thyroid Gland of Rats. Horm Metab Res. 2015;47(12):910-5.
266. Hu Z, Zhuo X, Shi Y, Liu X, Yuan J, Li L, et al. Iodine deficiency up-regulates monocarboxylate transporter 8 expression of mouse thyroid gland. Chin Med J (Engl). 2014;127(23):4071-6.
267. Lebsir D, Manens L, Grison S, Lestaevel P, Ebrahimian T, Suhard D, et al. Effects of repeated potassium iodide administration on genes involved in synthesis and secretion of thyroid hormone in adult male rat. Mol Cell Endocrinol. 2018;474:119-26.
268. Serrano-Nascimento C, Salgueiro RB, Pantaleao T, Correa da Costa VM, Nunes MT. Maternal Exposure to Iodine Excess Throughout Pregnancy and Lactation Induces Hypothyroidism in Adult Male Rat Offspring. Sci Rep. 2017;7(1):15591.
269. Mebis L, Paletta D, Debaveye Y, Ellger B, Langouche L, D'Hoore A, et al. Expression of thyroid hormone transporters during critical illness. Eur J Endocrinol. 2009;161(2):243-50.
270. Cubuk C, Markowsky H, Herwig A. Hypothalamic control systems show differential gene expression during spontaneous daily torpor and fasting-induced torpor in the Djungarian hamster (Phodopus sungorus). PLoS One. 2017;12(10):e0186299.
271. Li J, Donangelo I, Abe K, Scremin O, Ke S, Li F, et al. Thyroid hormone treatment activates protective pathways in both in vivo and in vitro models of neuronal injury. Mol Cell Endocrinol. 2017;452:120-30.
272. Engels K, Rakov H, Zwanziger D, Moeller LC, Homuth G, Kohrle J, et al. Differences in Mouse Hepatic Thyroid Hormone Transporter Expression with Age and Hyperthyroidism. Eur Thyroid J. 2015;4(Suppl 1):81-6.
273. Schweizer U, Johannes J, Bayer D, Braun D. Structure and function of thyroid hormone plasma membrane transporters. Eur Thyroid J. 2014;3(3):143-53.
274. Forrest LR, Kramer R, Ziegler C. The structural basis of secondary active transport mechanisms. Biochim Biophys Acta. 2011;1807(2):167-88.

275. Gao X, Zhou L, Jiao X, Lu F, Yan C, Zeng X, et al. Mechanism of substrate recognition and transport by an amino acid antiporter. Nature. 2010;463(7282):828-32.
276. Poole RC, Sansom CE, Halestrap AP. Studies of the membrane topology of the rat erythrocyte H+/lactate cotransporter (MCT1). Biochem J. 1996;320 (Pt 3):817-24.
277. Huang Y, Lemieux MJ, Song J, Auer M, Wang DN. Structure and mechanism of the glycerol-3-phosphate transporter from Escherichia coli. Science. 2003;301(5633):616-20.
278. Nascimento AS, Dias SM, Nunes FM, Aparicio R, Ambrosio AL, Bleicher L, et al. Structural rearrangements in the thyroid hormone receptor hinge domain and their putative role in the receptor function. Journal of molecular biology. 2006;360(3):586-98.
279. Schweizer U, Schlicker C, Braun D, Kohrle J, Steegborn C. Crystal structure of mammalian selenocysteine-dependent iodothyronine deiodinase suggests a peroxiredoxin-like catalytic mechanism. Proc Natl Acad Sci U S A. 2014;111(29):10526-31.
280. Kleinau G, Schweizer U, Kinne A, Kohrle J, Gruters A, Krude H, et al. Insights into molecular properties of the human monocarboxylate transporter 8 by combining functional with structural information. Thyroid Res. 2011;4 Suppl 1:S4.
281. Braun D, Lelios I, Krause G, Schweizer U. Histidines in potential substrate recognition sites affect thyroid hormone transport by monocarboxylate transporter 8 (MCT8). Endocrinology. 2013;154(7):2553-61.
282. Uemura S, Mochizuki T, Kurosaka G, Hashimoto T, Masukawa Y, Abe F. Functional analysis of human aromatic amino acid transporter MCT10/TAT1 using the yeast Saccharomyces cerevisiae. Biochim Biophys Acta Biomembr. 2017;1859(10):2076-85.
283. Rechsteiner M, Rogers SW. PEST sequences and regulation by proteolysis. Trends Biochem Sci. 1996;21(7):267-71.
284. Kirk P, Wilson MC, Heddle C, Brown MH, Barclay AN, Halestrap AP. CD147 is tightly associated with lactate transporters MCT1 and MCT4 and facilitates their cell surface expression. EMBO J. 2000;19(15):3896-904.
285. Visser WE, Philp NJ, van Dijk TB, Klootwijk W, Friesema EC, Jansen J, et al. Evidence for a homodimeric structure of human monocarboxylate transporter 8. Endocrinology. 2009;150(11):5163-70.
286. Fischer J, Kleinau G, Muller A, Kuhnen P, Zwanziger D, Kinne A, et al. Modulation of monocarboxylate transporter 8 oligomerization by specific pathogenic mutations. J Mol Endocrinol. 2015;54(1):39-50.
287. Biebermann H, Ambrugger P, Tarnow P, von Moers A, Schweizer U, Grueters A. Extended clinical phenotype, endocrine investigations and functional studies of a loss-of-function mutation A150V in the thyroid hormone specific transporter MCT8. Eur J Endocrinol. 2005;153(3):359-66.
288. Allan W, Herndon CN, Dudley FC. Some examples of the inheritance of mental deficiency: apparently sex-linked idiocy and microcephaly. Am J Ment Defic. 1944;48:325-34.
289. Schwartz CE, Ulmer J, Brown A, Pancoast I, Goodman HO, Stevenson RE. Allan-Herndon syndrome. II. Linkage to DNA markers in Xq21. Am J Hum Genet. 1990;47(3):454-8.
290. Stevenson RE, Goodman HO, Schwartz CE, Simensen RJ, McLean WT, Jr., Herndon CN. Allan-Herndon syndrome. I. Clinical studies. Am J Hum Genet. 1990;47(3):446-53.
291. Passos-Bueno MR, Byth BC, Rosenberg S, Takata RI, Bakker E, Beggs AH, et al. Severe nonspecific X-linked mental retardation caused by a proximally Xp located gene: intragenic heterogeneity or a new form of X-linked mental retardation? Am J Med Genet. 1993;46(2):172-5.
292. Davis JGS, G.; Williams, M. K.; Spiro, A.; Shapiro, L. R. A new X-linked recessive mental retardation syndrome with progressive spastic quadriparesis. Am J Hum Genet. 1981:75A.
293. Zorick TS, Kleimann S, Sertie A, Zatz M, Rosenberg S, Passos-Bueno MR. Fine mapping and clinical reevaluation of a Brazilian pedigree with a severe form of X-linked mental retardation associated with other neurological dysfunction. Am J Med Genet A. 2004;127A(3):321-3.
294. Bialer MG, Lawrence L, Stevenson RE, Silverberg G, Williams MK, Arena JF, et al. Allan-Herndon-Dudley syndrome: clinical and linkage studies on a second family. Am J Med Genet. 1992;43(1-2):491-7.
295. Maranduba CM, Friesema EC, Kok F, Kester MH, Jansen J, Sertie AL, et al. Decreased cellular uptake and metabolism in Allan-Herndon-Dudley syndrome (AHDS) due to a novel mutation in the MCT8 thyroid hormone transporter. J Med Genet. 2006;43(5):457-60.
296. Schwartz CE, May MM, Carpenter NJ, Rogers RC, Martin J, Bialer MG, et al. Allan-Herndon-Dudley syndrome and the monocarboxylate transporter 8 (MCT8) gene. Am J Hum Genet. 2005;77(1):41-53.
297. Groeneweg S, Visser WE, Visser TJ. Disorder of thyroid hormone transport into the tissues. Best Pract Res Clin Endocrinol Metab. 2017;31(2):241-53.
298. Braun D, Schweizer U. Thyroid Hormone Transport and Transporters. Vitam Horm. 2018;106:19-44.
299. Visser WE, Jansen J, Friesema EC, Kester MH, Mancilla E, Lundgren J, et al. Novel pathogenic mechanism suggested by ex vivo analysis of MCT8 (SLC16A2) mutations. Hum Mutat. 2009;30(1):29-38.

300. Zung A, Visser TJ, Uitterlinden AG, Rivadeneira F, Friesema EC. A child with a deletion in the monocarboxylate transporter 8 gene: 7-year follow-up and effects of thyroid hormone treatment. Eur J Endocrinol. 2011;165(5):823-30.
301. Crushell E, Reardon W. Elevated TSH levels in a mentally retarded boy. Eur J Pediatr. 2010;169(5):573-5.
302. Armour CM, Kersseboom S, Yoon G, Visser TJ. Further Insights into the Allan-Herndon-Dudley Syndrome: Clinical and Functional Characterization of a Novel MCT8 Mutation. PLoS One. 2015;10(10):e0139343.
303. Yamamoto T, Shimojima K, Umemura A, Uematsu M, Nakayama T, Inoue K. SLC16A2 mutations in two Japanese patients with Allan–Herndon–Dudley syndrome. Human Genome Variation. 2014;1.
304. Gagliardi L, Nataren N, Feng J, Schreiber AW, Hahn CN, Conwell LS, et al. Allan-Herndon-Dudley syndrome with unusual profound sensorineural hearing loss. Am J Med Genet A. 2015;167(8):1872-6.
305. Vaurs-Barriere C, Deville M, Sarret C, Giraud G, Des Portes V, Prats-Vinas JM, et al. Pelizaeus-Merzbacher-Like disease presentation of MCT8 mutated male subjects. Ann Neurol. 2009;65(1):114-8.
306. Capri Y, Friesema EC, Kersseboom S, Touraine R, Monnier A, Eymard-Pierre E, et al. Relevance of different cellular models in determining the effects of mutations on SLC16A2/MCT8 thyroid hormone transporter function and genotype-phenotype correlation. Hum Mutat. 2013;34(7):1018-25.
307. Boccone L, Mariotti S, Dessi V, Pruna D, Meloni A, Loudianos G. Allan-Herndon-Dudley syndrome (AHDS) caused by a novel SLC16A2 gene mutation showing severe neurologic features and unexpectedly low TRH-stimulated serum TSH. Eur J Med Genet. 2010;53(6):392-5.
308. Tsurusaki Y, Osaka H, Hamanoue H, Shimbo H, Tsuji M, Doi H, et al. Rapid detection of a mutation causing X-linked leucoencephalopathy by exome sequencing. J Med Genet. 2011;48(9):606-9.
309. Rodrigues F, Grenha J, Ortez C, Nascimento A, Morte B, M MB, et al. Hypotonic male infant and MCT8 deficiency - a diagnosis to think about. BMC Pediatr. 2014;14:252.
310. Tonduti D, Vanderver A, Berardinelli A, Schmidt JL, Collins CD, Novara F, et al. MCT8 deficiency: extrapyramidal symptoms and delayed myelination as prominent features. J Child Neurol. 2013;28(6):795-800.
311. Sijens PE, Rodiger LA, Meiners LC, Lunsing RJ. 1H magnetic resonance spectroscopy in monocarboxylate transporter 8 gene deficiency. J Clin Endocrinol Metab. 2008;93(5):1854-9.
312. Matheus MG, Lehman RK, Bonilha L, Holden KR. Redefining the Pediatric Phenotype of X-Linked Monocarboxylate Transporter 8 (MCT8) Deficiency: Implications for Diagnosis and Therapies. J Child Neurol. 2015.
313. Lopez-Espindola D, Morales-Bastos C, Grijota-Martinez C, Liao XH, Lev D, Sugo E, et al. Mutations of the thyroid hormone transporter MCT8 cause prenatal brain damage and persistent hypomyelination. J Clin Endocrinol Metab. 2014;99(12):E2799-804.
314. Ono E, Ariga M, Oshima S, Hayakawa M, Imai M, Ochiai Y, et al. Three novel mutations of the MCT8 (SLC16A2) gene: individual and temporal variations of endocrinological and radiological features. Clin Pediatr Endocrinol. 2016;25(2):23-35.
315. Wemeau JL, Pigeyre M, Proust-Lemoine E, d'Herbomez M, Gottrand F, Jansen J, et al. Beneficial effects of propylthiouracil plus L-thyroxine treatment in a patient with a mutation in MCT8. J Clin Endocrinol Metab. 2008;93(6):2084-8.
316. Herzovich V, Vaiani E, Marino R, Dratler G, Lazzati JM, Tilitzky S, et al. Unexpected peripheral markers of thyroid function in a patient with a novel mutation of the MCT8 thyroid hormone transporter gene. Horm Res. 2007;67(1):1-6.
317. Rego T, Lado CG, Rodriguez PC, Santos FS, Angueira FB, Castro-Feijoo L, et al. Severe neurological abnormalities in a young boy with impaired thyroid hormone sensitivity due to a novel mutation in the MCT8 gene. Hormones (Athens). 2017;16(2):194-9.
318. Wang J, Zhang Q, Bao X, Chen Y, Yu S. [Clinical and genetic features of five patients with Allan-Herndon-Dudley syndrome]. Zhonghua yi xue yi chuan xue za zhi = Zhonghua yixue yichuanxue zazhi = Chinese journal of medical genetics. 2018;35(4):484-8.
319. Boccone L, Dessi V, Meloni A, Loudianos G. Allan-Herndon-Dudley syndrome (AHDS) in two consecutive generations caused by a missense MCT8 gene mutation. Phenotypic variability with the presence of normal serum T3 levels. Eur J Med Genet. 2013;56(4):207-10.
320. Papadimitriou A, Dumitrescu AM, Papavasiliou A, Fretzayas A, Nicolaidou P, Refetoff S. A novel monocarboxylate transporter 8 gene mutation as a cause of severe neonatal hypotonia and developmental delay. Pediatrics. 2008;121(1):e199-202.

321. Namba N, Etani Y, Kitaoka T, Nakamoto Y, Nakacho M, Bessho K, et al. Clinical phenotype and endocrinological investigations in a patient with a mutation in the MCT8 thyroid hormone transporter. Eur J Pediatr. 2008;167(7):785-91.
322. Islam MS, Namba N, Ohata Y, Fujiwara M, Nakano C, Takeyari S, et al. Functional analysis of monocarboxylate transporter 8 mutations in Japanese Allan-Herndon-Dudley syndrome patients. Endocrine journal. 2019;66(1):19-29.
323. Faruk Aydin O, Kara C, Jones J, Wood TC, May MM, Friez MJ, et al. Allan-Herndon-Dudley syndrome caused by a novel MCT8/SLC16A2 mutation in a Turkish family. Horm Res. 2013;80(Suppl 1):352-3.
324. Verge CF, Konrad D, Cohen M, Di Cosmo C, Dumitrescu AM, Marcinkowski T, et al. Diiodothyropropionic acid (DITPA) in the treatment of MCT8 deficiency. J Clin Endocrinol Metab. 2012;97(12):4515-23.
325. Anik A, Kersseboom S, Demir K, Catli G, Yis U, Bober E, et al. Psychomotor retardation caused by a defective thyroid hormone transporter: report of two families with different MCT8 mutations. Horm Res Paediatr. 2014;82(4):261-71.
326. Friesema EC, Jansen J, Heuer H, Trajkovic M, Bauer K, Visser TJ. Mechanisms of disease: psychomotor retardation and high T3 levels caused by mutations in monocarboxylate transporter 8. Nat Clin Pract Endocrinol Metab. 2006;2(9):512-23.
327. Schwartz CE, Stevenson RE. The MCT8 thyroid hormone transporter and Allan-Herndon-Dudley syndrome. Best Pract Res Clin Endocrinol Metab. 2007;21(2):307-21.
328. Ramos HE, Morandini M, Carre A, Tron E, Floch C, Mandelbrot L, et al. Pregnancy in women heterozygous for MCT8 mutations: risk of maternal hypothyroxinemia and fetal care. Eur J Endocrinol. 2011;164(2):309-14.
329. Dateki S, Haraguchi K, Sato T, Nakatomi A, Fujiwara M, Sakurai M, et al. A novel MCT8 mutation in a Japanese patient with Allan-Herndon-Dudley syndrome. Horm Res. 2013;80(Suppl 1):360.
330. Novara F, Groeneweg S, Freri E, Estienne M, Reho P, Matricardi S, et al. Clinical and Molecular Characteristics of SLC16A2 (MCT8) Mutations in Three Families with the Allan-Herndon-Dudley Syndrome. Hum Mutat. 2017;38(3):260-4.
331. Frints SG, Lenzner S, Bauters M, Jensen LR, Van Esch H, des Portes V, et al. MCT8 mutation analysis and identification of the first female with Allan-Herndon-Dudley syndrome due to loss of MCT8 expression. Eur J Hum Genet. 2008;16(9):1029-37.
332. Muller J, Heuer H. Understanding the hypothalamus-pituitary-thyroid axis in mct8 deficiency. Eur Thyroid J. 2012;1(2):72-9.
333. Di Cosmo C, Liao XH, Ye H, Ferrara AM, Weiss RE, Refetoff S, et al. Mct8-deficient mice have increased energy expenditure and reduced fat mass that is abrogated by normalization of serum T3 levels. Endocrinology. 2013;154(12):4885-95.
334. Leitch VD, Di Cosmo C, Liao XH, O'Boy S, Galliford TM, Evans H, et al. An Essential Physiological Role for MCT8 in Bone in Male Mice. Endocrinology. 2017;158(9):3055-66.
335. Zhang Y, Chen K, Sloan SA, Bennett ML, Scholze AR, O'Keeffe S, et al. An RNA-sequencing transcriptome and splicing database of glia, neurons, and vascular cells of the cerebral cortex. J Neurosci. 2014;34(36):11929-47.
336. Bernal J, Guadano-Ferraz A, Morte B. Thyroid hormone transporters--functions and clinical implications. Nat Rev Endocrinol. 2015;11(7):406-17.
337. Dratman MB, Crutchfield FL, Schoenhoff MB. Transport of iodothyronines from bloodstream to brain: contributions by blood:brain and choroid plexus:cerebrospinal fluid barriers. Brain Res. 1991;554(1-2):229-36.
338. Kakinuma H, Itoh M, Takahashi H. A novel mutation in the monocarboxylate transporter 8 gene in a boy with putamen lesions and low free T4 levels in cerebrospinal fluid. J Pediatr. 2005;147(4):552-4.
339. Zhang Y, Sloan SA, Clarke LE, Caneda C, Plaza CA, Blumenthal PD, et al. Purification and Characterization of Progenitor and Mature Human Astrocytes Reveals Transcriptional and Functional Differences with Mouse. Neuron. 2016;89(1):37-53.
340. Fu J, Refetoff S, Dumitrescu AM. Inherited defects of thyroid hormone-cell-membrane transport: review of recent findings. Curr Opin Endocrinol Diabetes Obes. 2013;20(5):434-40.
341. Gika AD, Siddiqui A, Hulse AJ, Edward S, Fallon P, McEntagart ME, et al. White matter abnormalities and dystonic motor disorder associated with mutations in the SLC16A2 gene. Dev Med Child Neurol. 2010;52(5):475-82.
342. Visser WE, Vrijmoeth P, Visser FE, Arts WF, van Toor H, Visser TJ. Identification, functional analysis, prevalence and treatment of monocarboxylate transporter 8 (MCT8) mutations in a cohort of adult patients with mental retardation. Clin Endocrinol (Oxf). 2013;78(2):310-5.
343. Di Cosmo C, Liao XH, Dumitrescu AM, Weiss RE, Refetoff S. A thyroid hormone analog with reduced dependence on the monocarboxylate transporter 8 for tissue transport. Endocrinology. 2009;150(9):4450-8.

344. Pennock GD, Raya TE, Bahl JJ, Goldman S, Morkin E. Cardiac effects of 3,5-diiodothyropropionic acid, a thyroid hormone analog with inotropic selectivity. The Journal of pharmacology and experimental therapeutics. 1992;263(1):163-9.
345. Ferrara AM, Liao XH, Ye H, Weiss RE, Dumitrescu AM, Refetoff S. The Thyroid Hormone Analog DITPA Ameliorates Metabolic Parameters of Male Mice With Mct8 Deficiency. Endocrinology. 2015;156(11):3889-94.
346. Ferrara AM, Liao XH, Gil-Ibanez P, Bernal J, Weiss RE, Dumitrescu AM, et al. Placenta passage of the thyroid hormone analog DITPA to male wild-type and Mct8-deficient mice. Endocrinology. 2014;155(10):4088-93.
347. Barez-Lopez S, Obregon MJ, Martinez-de-Mena R, Bernal J, Guadano-Ferraz A, Morte B. Effect of Triiodothyroacetic Acid Treatment in Mct8 Deficiency: A Word of Caution. Thyroid. 2016;26(5):618-26.
348. Wainwright CE, Elborn JS, Ramsey BW, Marigowda G, Huang X, Cipolli M, et al. Lumacaftor-Ivacaftor in Patients with Cystic Fibrosis Homozygous for Phe508del CFTR. N Engl J Med. 2015;373(3):220-31.
349. Braun D, Schweizer U. The Chemical Chaperone Phenylbutyrate Rescues MCT8 Mutations Associated With Milder Phenotypes in Patients With Allan-Herndon-Dudley Syndrome. Endocrinology. 2017;158(3):678-91.
350. Braun D, Schweizer U. Efficient Activation of Pathogenic DeltaPhe501 Mutation in Monocarboxylate Transporter 8 by Chemical and Pharmacological Chaperones. Endocrinology. 2015;156(12):4720-30.

Chapter 2

Molecular characterization of monocarboxylate transporter (MCT)8

Chapter

2.1

IMPORTANCE OF CYSTEINE RESIDUES IN THE THYROID HORMONE TRANSPORTER MCT8

Elaine C. Lima de Souza, **Stefan Groeneweg**, W. Edward Visser, Robin P. Peeters, Theo J. Visser

Endocrinology. 2013 May;154(5):1948-55.

ABSTRACT

The thyroid hormone (TH) transporter monocarboxylate transporter 8 (MCT8) is crucial for brain development as demonstrated by the severe psychomotor retardation in patients with MCT8 mutations. MCT8 contains 10 residues of the reactive amino acid cysteine (Cys) whose functional roles were studied using the Cys-specific reagent p-chloromercurybenzenesulfonate (pCMBS) and by site-directed mutagenesis. Pretreatment of JEG3 cells with pCMBS resulted in a dose- and time-dependent decrease of subsequent T3 uptake. Pretreatment with dithiothreitol did not affect TH transport or its inhibition by pCMBS. However, pCMBS inhibition of MCT8 was reversed by dithiothreitol. Inhibition of MCT8 by pCMBS was prevented in the presence of T3. The single and double mutation of C481A and C497A did not affect T3 transport, but the single mutants were less sensitive and the double mutant was completely insensitive to pCMBS. Similar effects on MCT8 were obtained using $HgCl_2$ instead of pCMBS. In conclusion, we have identified Cys481 and Cys497 in MCT8 as the residues modified by pCMBS or $HgCl_2$. These residues are probably located at or near the substrate-recognition site in MCT8. It remains to be investigated whether MCT8 function is regulated by modification of these Cys residues under pathophysiological conditions.

INTRODUCTION

Monocarboxylate transporter 8 (MCT8) is a thyroid hormone (TH) transporter, and its function is essential for normal development and function of different tissues, in particular brain (1, 2). Mutations in MCT8 lead to the Alan-Herndon-Dudley syndrome (AHDS), a severe X-linked psychomotor retardation accompanied by abnormal serum TH levels (3, 4). Like other members of the MCT family, MCT8 has 12 helical transmembrane domains (TMDs), with the amino- and carboxyl-terminal domains and a large loop region between TMDs 6 and 7 facing the cytoplasm. The MCT8 protein contains 539 or 613 amino acids, depending on which of the 2 translation start sites is used (2).

Ten of the amino acids in MCT8 are cysteine (Cys) residues, most which are located in putative TMDs (Cys184, Cys231, Cys281, Cys283, Cys436, Cys481, Cys491, and Cys497), one in the second intracellular loop (Cys244), and one in the last extracellular loop (Cys546) (5). Cys is a reactive amino acid due to the free thiol (SH) group in its side chain that in the thiolate (S^-) form is a potent nucleophile. Cys residues are prone to reversible and irreversible oxidation by reactive oxygen species, and they undergo nitrosylation by nitric oxide (NO) (6). Moreover, they have metal-binding properties; Cys interacts with numerous metal ions that play an important role to maintain specific structures or are part of the active site of certain enzymes (6). Cys residues are also involved in the formation of intramolecular or intermolecular disulfide (S-S) bonds, which are important for protein stability. All these modifications participate in a variety of biological processes such as protein folding, protein activity, cellular redox balance, antioxidant defense, and cell recognition, signaling, and trafficking.

Disulfide bonds are assembled during the oxidative folding process, and this process takes place in the endoplasmic reticulum (7). The formation and rearrangement of S-S bonds is catalyzed by a series of endoplasmic reticulum enzymes such as Ero1, PDI, and Erv2 (6). Disulfide bonds can exist only in oxidative compartments, thus between cysteines located in the extracellular domain of both membrane and secreted proteins, but not in the largely reductive environment of the cytoplasm. Under pathological conditions, unwanted intramolecular or intermolecular disulfide bond formation can take place (8).

The SH group in Cys may undergo oxidation reactions to form sulfenic (SOH), sulfinic (SO_2H), and sulfonic (SO_3H) derivatives. Moreover, the free SH group may also modulate the protein activity and participate in signaling events (9). Site-directed mutagenesis and specific SH-targeted reagents can be used to determine the role of Cys residues in the function of the proteins (10).

So far, most structural information about human MCT8 (hMCT8) is based on the mutations found in patients with AHDS (2, 11, 12). Thus, more information about the structure of MCT8 would help to understand the molecular mechanisms of its function and substrate interaction. Here, we used site-directed mutagenesis and the Cys-specific reagents p-chloromercurybenzenesulfonate (pCMBS) and mercury chloride ($HgCl_2$) to identify functionally important Cys residues.

Recently, our group has published about the mutation of all single Cys residues in MCT8 to Ala (5), showing that none of these mutations resulted in significant changes in TH uptake in transfected COS1 cells. We decided to carry out the present study in JEG3 cells because it has become clear that many mutations identified in AHDS patients have markedly larger effects in JEG3 cells than in COS1 cells, the reason of which is still unclear.

Our data demonstrate that pCMBS inhibits hMCT8 activity via the modification of the SH groups of Cys481 and Cys497. This inhibitory effect was prevented by addition of T_3 during the preincubation, suggesting that pCMBS and TH compete for binding to the substrate-recognition site in MCT8. Our results indicate that functionally important Cys residues contain free SH groups, rather than that they participate in the formation of S-S bonds.

MATERIALS AND METHODS

Materials

Nonradioactive iodothyronines were obtained from Henning (Berlin, Germany). [^{125}I]T_3 (1500–2000 mCi/μmol) was prepared in our laboratory as previously described (13). X-tremeGENE9 transfection reagent was obtained from Roche (Almere, The Netherlands). pCMBS, $HgCl_2$, and Na_2SeO_3 were obtained from Sigma (St Louis, Missouri).

Plasmids

pcDNA3_hMCT8 plasmid was obtained as described previously (2). Cys residues in hMCT8 were substituted with Ala by site-directed mutagenesis using the QuickChange site-directed mutagenesis kit (Stratagene, La Jolla, California) and pcDNA3_hMCT8 as the template as previously described (5). For the double mutant C481A+C497A, we used the C497A construct as a template to introduce the C481A mutation. The integrity of the mutant constructs was verified by sequencing of the entire inserts.

Cell culture and transfection

JEG3 choriocarcinoma cells were obtained and cultured in 6-well plates using DMEM/Ham's F12 medium, containing 9% heat-inactivated fetal bovine serum, penicillin-streptomycin, and 100nM Na_2SeO_3 as described previously (5). At 50% to 70% confluence, cells were transfected in duplicate with 250 ng pcDNA3_hMCT8 or empty pcDNA3 using X-TremeGENE 9 transfection reagent according to the manufacturer's guidelines. All studies were performed 48 hours after transfection when the highest transfection efficiency was observed.

Pretreatment of cells with pCMBS

JEG3 cells were washed once with PBS (pH 7.4) and incubated for 3 to 20 minutes at room temperature (RT) with 50μM to 300μM pCMBS or 1μM to 10μM $HgCl_2$ in 1.5 ml PBS in the absence or presence of 10μM T_3. Then, the cells were washed at RT once with PBS and once with PBS plus 0.1% BSA plus 0.1% glucose before the uptake experiments. After preincubation with T_3, cells were washed twice for 1 minute with PBS plus 0.1% BSA plus 0.1% glucose to ensure removal of unlabeled T_3 before the uptake assay with radioactive [^{125}I]T_3. To demonstrate reversal of inhibition, pCMBS- or $HgCl_2$-treated cells were subjected to a second preincubation for 15 minutes at RT with 1mM dithiothreitol (DTT). To demonstrate effects of the reduction of possible S-S bonds in MCT8 on pCMBS inhibition, cells were treated initially with 1mM DTT and subsequently with pCMBS before the uptake assay, with intermittent washing as indicated above.

TH uptake assay

After preincubation and washing, cells were incubated for 10 minutes at 37°C in 1.5 ml PBS containing 0.1% BSA, 0.1% glucose, and 1nM (1×10^5 cpm) ^{125}I-labeled T_3 and lysed with 0.1M NaOH. The amount of radioactivity was measured in a γ-counter. TH uptake by MCT8-transfected cells was corrected for uptake by control cells transfected with empty vector (pcDNA3).

Western blot analysis

Cells were washed with PBS and collected in 0.1 ml lysis buffer (10mM phosphate, [pH 7.2], 2mM EDTA, and protease inhibitors). The extracts were sonicated on ice, aliquoted, and stored at −80°C. Protein lysates (35 µg) were separated on 10% SDS-PAGE precast gels, blotted on nitrocellulose membranes, and probed with rabbit polyclonal antibody 3353 against hMCT8 amino acids 75 to 155 (Sigma-Aldrich, Zwijndrecht, The Netherlands) diluted 1:20 000 and with mouse monoclonal antihuman glyceraldehyde-3-phosphate dehydrogenase antibody MAB374 Chemicon International (Amsterdam, The Netherlands) 1:20 000 as a loading control. IRDye680 goat antirabbit and IRDye800 goat antimouse antibodies 1:20 000 (LI-COR Biosciences, Lincoln, Nebraska) were used as secondary antibody. Antibodies were detected with the Odyssey infrared detection system (LI-COR).

Statistical analysis

Data are presented as means ± SEM. Statistical analysis were performed using the GraphPad Prism version 5 software for ANOVA tests. Where appropriate, we used one-way ANOVA followed by Dunnett's or Bonferroni's multiple-comparison test or two-way ANOVA followed by Bonferroni's posttests.

RESULTS

MCT8 function is inhibited by pCMBS in a concentration- and time-dependent manner

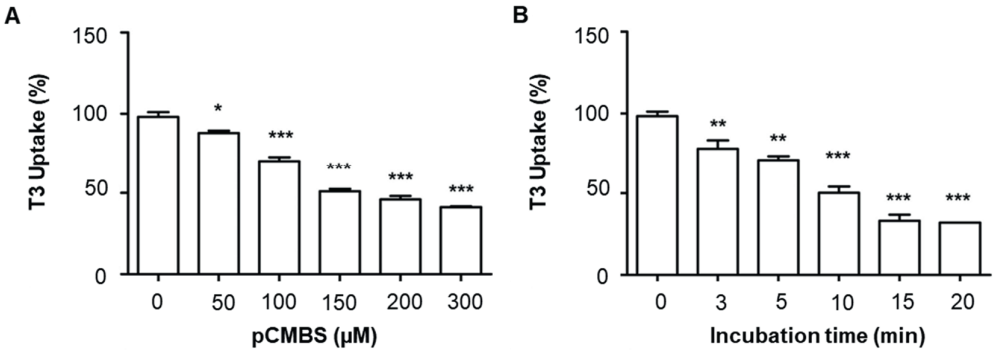

Figure 1. Effect of pCMBS on the T_3 uptake function of MCT8-expressing JEG3 cells. Data are corrected for uptake by JEG3 cells transfected with empty vector. A, Concentration-dependent effect of pCMBS during 5 minutes at RT, shown as mean ± SEM (n = 3). ***P < .001; *P < .05 vs PBS (0) (one-way ANOVA and Dunnett's multiple-comparison test). B, Time-dependent effect of pCMBS (100µM), shown as mean ± SEM (n = 3). ***P < .001; **P < .01 vs PBS (0) (one-way ANOVA and Dunnett's multiple-comparison test).

To examine whether free SH groups participate in the modulation of MCT8 function, MCT8-transfected JEG3 cells were pretreated for 3 to 20 minutes at RT with 50µM to 300µM pCMBS before analysis of T_3 uptake. As shown in **Figure 1, A** and **B**, T_3 uptake was significantly reduced in a concentration- and time-dependent manner.

The effect of pCMBS persisted after repeated washing, suggesting a covalent interaction between Cys residues and the SH-reactive compound. All additional experiments were done using 100µM pCMBS and an incubation time of 15 minutes. Under these conditions, cell viability was not affected as determined with an 3-[4,5-dimethylthiazol-2-yl]-2,5-diphenyltetrazolium bromide (MTT) viability assay (data not shown).

Reversibility of the pCMBS effect by DTT

pCMBS induces the covalent modification of Cys residues, but free SH groups may be regenerated by the reaction with DTT. We investigated whether this is also the case after inhibition of MCT8 by pCMBS. First we tested the effects of varying concentrations (1mM–100mM) of DTT on MCT8, but no change in transporter function was observed (data not shown). Next we examined whether DTT disrupts the binding of pCMBS to MCT8. This was done by successive incubations of MCT8-expressing cells for 15 minutes at RT with 100µM pCMBS and for 15 minutes at RT with 1mM DTT. After intermittent washings, cells were analyzed for T_3 uptake. As shown in **Figure 2**, treatment with DTT alone has no effect, whereas treatment with pCMBS alone induces about 50% reduction in T_3 uptake by MCT8. When cells were subsequently treated with DTT, the inhibitory effect of pCMBS was avoided. We also tested whether pretreatment with DTT increases the susceptibility of MCT8 to inhibition by pCMBS by liberating free SH groups from possible S-S bonds. However, pretreatment with DTT led to a less effective inhibition of MCT8 by pCMBS, which may result from reaction of pCMBS with some DTT left from the preincubation and, thus, to a decrease in pCMBS available for reaction with MCT8.

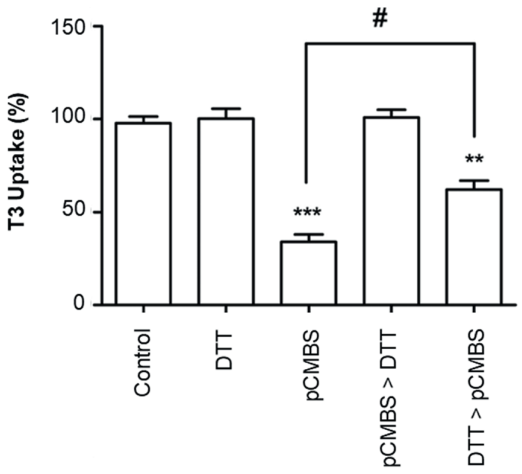

Figure 2. Reversibility of pCMBS effect on MCT8-mediated T_3 uptake by DTT. Cells were pretreated for 15 minutes at room temperature with PBS, 1mM DTT, or 100µM pCMBS, with pCMBS followed by DTT (pCMBS > DTT), or with DTT followed pCMBS (DTT > pCMBS). Results are shown as mean ±SEM (n = 3). ***P < .001; **P < .01 vs control; #P < .05 pCMBS vs DTT > pCMBS (one-way ANOVA and Bonferroni's multiple-comparison test).

Effect of the single Cys to Ala mutations in T_3 uptake in JEG3 cells

We intended to transfect cells with a limiting amount of MCT8 plasmid, providing proportional TH uptake rates. From the analysis of TH uptake versus the amount of pcDNA3_hMCT8 (**Supplemental Figure 1**), we chose 250 ng as the optimal amount of plasmid for the current experiments. We evaluated whether some of the Cys residues are important for the function of MCT8 in these conditions. As shown in **Figure 3A**, most single Cys to Ala mutations have little or no effect on T_3 uptake by MCT8, being significant only for the modest increase in T_3 uptake by the C281A mutant. Western blot analyses were performed with these mutants, and as shown in **Figure 3B**, all single Cys mutants were expressed at similar levels as monomers and homodimers, showing little effect of these mutations on the dimerization of MCT8 in keeping with our previous results (5).

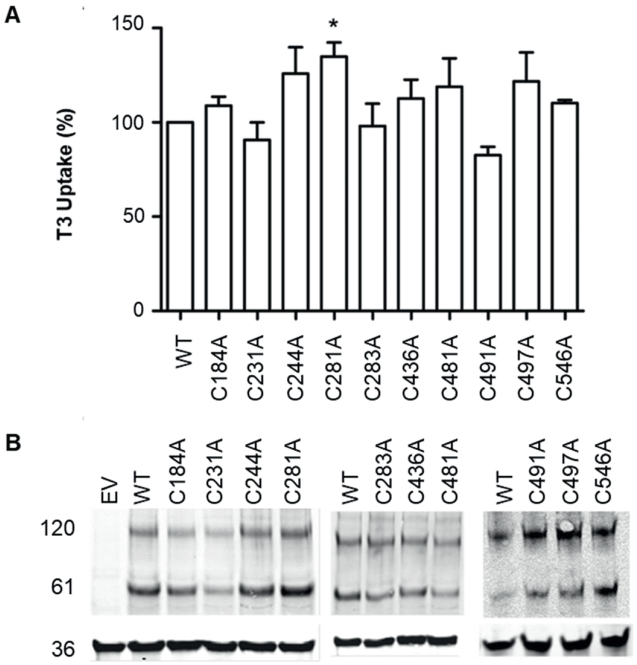

Figure 3. Function and expression of the single Cys to Ala mutants of MCT8 in transfected JEG3 cells. **A**, T_3 uptake of all single Cys to Ala mutants, shown as mean ± SEM (n = 3). *P < .05 vs WT (one-way ANOVA and Dunnett's multiple-comparison test). **B**, Expression of the MCT8 Cys to Ala mutants. Western blot analysis of total lysates from JEG3 cells transiently expressing WT or the Cys to Ala mutants. Cells were lysed, sonicated, and applied (35 µg protein) to 10% SDS-PAGE. The MCT8 dimer is 120 kDa, the MCT8 monomer is 60 kDa, and the glyceraldehyde-3-phosphate dehydrogenase is 36 kDa. Abbreviation: EV, empty vector.

pCMBS inhibits MCT8 by modification of Cys481 and Cys497

We further examined which Cys residues are involved in the inhibition of MCT8 by pCMBS. This was studied by pretreatment of the single Cys to Ala mutants with pCMBS, followed by analysis of T_3 uptake. As shown in **Figure 4A**, almost all Cys mutants are sensitive to pCMBS. However, the C481A and C497A mutants showed a significantly lower sensitivity to pCMBS than wild type (WT) MCT8 and the other mutants. To demonstrate that inhibition of MCT8 by pCMBS is entirely explained by modification of Cys481 and Cys497, we designed the C481A+C497A double mutant and tested it for T_3 transport and pCMBS inhibition. **Figure 4B** shows that the double mutant facilitates T_3 uptake

equally well as WT MCT8 but is completely insensitive to pCMBS. We analyzed the expression of the double mutant by immunoblotting, and the results indicate that protein levels are similar to WT MCT8, such as the presence of homodimers and monomers (**Figure 4C**). These results suggest that Cys481 and Cys497 are modified by pCMBS, resulting in the inhibition of MCT8 function.

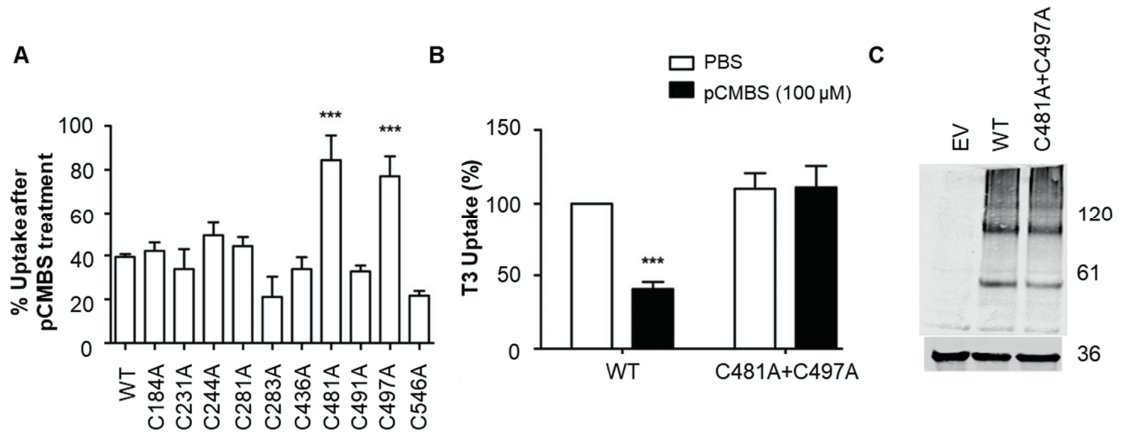

Figure 4. Cys481 and Cys497 in MCT8 are targets for pCMBS. **A**, T_3 uptake remaining after pCMBS pretreatment of WT and the Cys to Ala mutants expressed as percentage of uptake without pCMBS treatment, shown as mean ± SEM (n = 3). ***P < .001 vs WT (one-way ANOVA and Dunnett's multiple-comparison test). **B**, T_3 uptake by WT MCT8 and the C481A+C491A double mutant without or with pCMBS pretreatment, shown as mean ± SEM (n = 5). ***P < .001, PBS vs pCMBS (two-way ANOVA and Bonferroni posttests). **C**, Western blot analysis of total lysates from JEG3 cells transiently expressing WT or the C481A+C497A mutant. Cells were lysed, sonicated, and applied (35 µg of protein) to 10% SDS-PAGE. Abbreviation: EV, empty vector.

The Cys residues targeted by pCMBS are located at or near the substrate-recognition site

To test whether the Cys residues modified by pCMBS are located at or near the substrate-recognition site, we tested whether the effect of pCMBS on MCT8 function was alleviated in the presence of substrate. **Figure 5A** shows that 10µM T_3 decreases the inhibition of MCT8 by pCMBS. This may indeed indicate that binding of T_3 to MCT8 directly interferes with the access of pCMBS to its target Cys residues at positions 481 and 497. However, it could also be explained by a conformational change in the structure of MCT8 induced by substrate that makes these Cys residues inaccessible to pCMBS. To test these hypotheses, we preincubated MCT8 with pCMBS at 4°C instead of RT, which will strongly decrease the flexibility of MCT8 to undergo conformational changes (14). We found that T_3 uptake by MCT8 is markedly decreased if cells are incubated at 4°C instead of 37°C (**Supplemental Figure 2**). Thus, we tested whether the inhibition of MCT8 by pCMBS is still prevented by coincubation with T_3 at 4°C. **Figure 5B** shows that this is indeed the case. These results suggest that T_3 competitively prevents the interaction of pCMBS with Cys481 and Cys497. Conversely, modification of these residues by pCMBS blocks TH passage through MCT8. Therefore, the Cys481 and Cys497 residues are probably located at or near the substrate-recognition site.

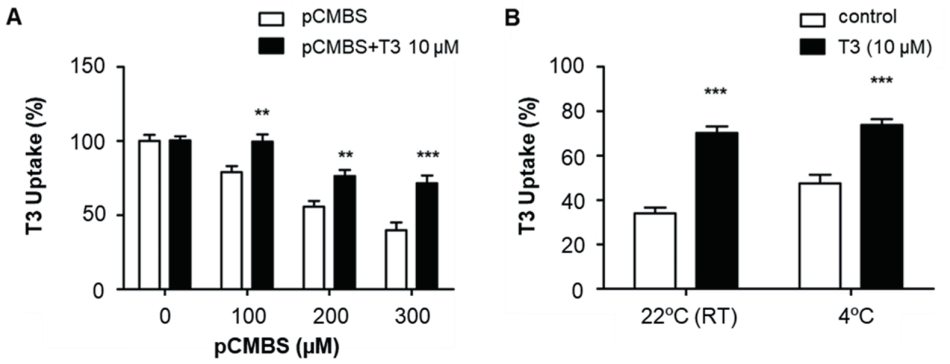

Figure 5. Protective effect of T_3 on the inactivation of MCT8 by pCMBS. **A**, MCT8-mediated T_3 uptake in transfected JEG3 cells pretreated for 5 minutes with 100µM to 300µM pCMBS in the absence or presence of 10µM T_3, shown as mean ± SEM (n = 6). **P < .01; ***P < .001, pCMBS vs pCMBS plus T_3 (two-way ANOVA and Bonferroni posttests). **B**, MCT8-mediated T_3 uptake after preincubation with 300µM pCMBS without or with 10µM T_3 at 4°C or 22°C (room temperature), shown as mean ± SEM (n = 3). ***P < .001, control vs T_3 (two-way ANOVA and Bonferroni posttests).

$HgCl_2$ also decreases T_3 uptake by MCT8

Mercury chloride is also reactive toward free SH groups and may even form cross-links between two nearby Cys residues (15). We have tested whether MCT8 is also sensitive to inhibition by $HgCl_2$, which was tested at 1µM and 10µM. Addition of 100µM $HgCl_2$ results in a marked loss in cell viability as substantiated by 3-[4,5-dimethylthiazol-2-yl]-2,5-diphenyltetrazolium bromide (MTT) assay (data not shown). As shown in **Figure 6A**, MCT8 is inhibited by $HgCl_2$ in a concentration-dependent manner. Subsequent treatment with DTT completely reverses the inhibition of the transporter by $HgCl_2$ as was also shown for the inhibition of MCT8 by pCMBS (**Figure 6B**).

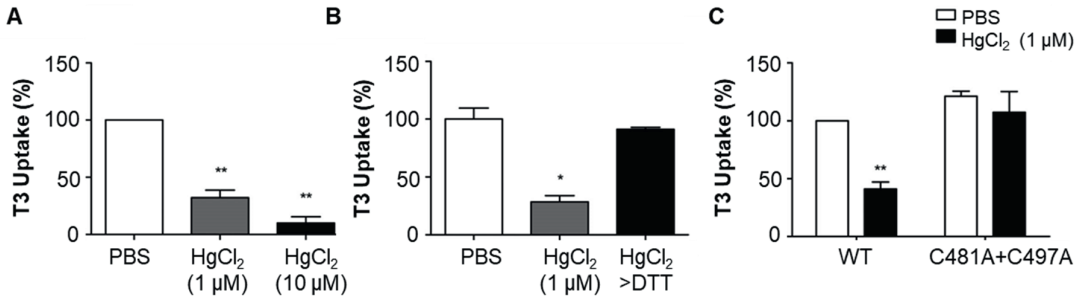

Figure 6. Inactivation of MCT8 by $HgCl_2$ and its reversibility by DTT. **A**, Effect of pretreatment with 1µM and 10µM $HgCl_2$on MCT8-mediated uptake of T_3, shown as mean ± SEM (n = 2). **P < .01 vs PBS (one-way ANOVA and Dunnett's multiple-comparison test). **B**, Reversibility of $HgCl_2$ effect on MCT8-mediated T_3 uptake by DTT. Cells were treated for successive periods of 15 minutes with $HgCl_2$ and DTT (or with PBS as control). Results are shown as mean ± SEM (n = 2). *P < .05 vs PBS (one-way ANOVA and Dunnett's multiple-comparison test). **C**, Effects of $HgCl_2$ on the uptake of T_3 by WT MCT8 or the C481A+C491A double mutant, shown as mean ± SEM (n = 3). **P < .01, PBS vs $HgCl_2$ (two-way ANOVA and Bonferroni posttests).

We further evaluated whether the same Cys residues responsible for the inhibition of MCT8 by pCMBS are also involved in the decrease in T_3 uptake induced by $HgCl_2$. Therefore, we pretreated the C481A+C497A double mutant for 15 minutes with 1µM $HgCl_2$. The double mutant is completely insensitive to $HgCl_2$ (**Figure 6C**).

DISCUSSION

In the present report, we demonstrate that the Cys-modifying reagent pCMBS inhibits MCT8. pCMBS is a membrane-impermeable reagent that binds covalently to the SH group of Cys residues through its mercury atom; this binding is reversed by thiol compounds such as DTT. pCMBS has been shown to modulate a wide variety of transporters (9, 15-17).

The predicted MCT8 structure shows 8 of the 10 Cys residues in TMDs, although one of these (Cys481) may be exposed on the extracellular surface. Cys244 is located in an intracellular loop and Cys546 in an extracellular loop. The character of Cys residues in TMDs will depend on whether their side chains face the lipids or the aqueous transport path. In the former case, the side chains will largely exist in the form of nondissociated thiol groups, and in the latter case, they may also be present as dissociated thiolate anions. Also, the lipid-facing Cys residues will not be accessible to pCMBS in contrast to the water-facing more superficially located Cys residues in the TMDs. Apparently, this is especially the case for Cys481 and Cys497.

It is likely that pCMBS binds covalently to these residues because inhibition of MCT8 function persists after washing but is reversed by treatment with DTT. Apparently, binding of pCMBS to Cys481 and Cys497 interferes with the passage of T_3 through the transporter. Because the presence of T_3 also prevents the modification of MCT8 by pCMBS, Cys481, and Cys497 may be located at or near the substrate-recognition site of the transporter. However, it cannot be excluded entirely that T_3-induced changes in MCT8 structure make Cys481 and Cys497 inaccessible to extracellular pCMBS. We have attempted to rule out this possibility by incubating MCT8-expressing cells at 4°C with pCMBS in the absence or presence of T_3, assuming that conformational changes in MCT8 are prevented at this low temperature. At 4°C, T_3 still protected MCT8 from inactivation by pCMBS, suggesting direct competition between T_3 and pCMBS for interaction with Cys481 and Cys497. However, MCT8 showed significant transport activity even at 4°C, indicating that conformational changes in MCT8 still can occur at this temperature.

Formation of disulfide bonds depends on the proximity of 2 Cys residues in the 3-dimensional MCT8 structure and their exposure to oxidative conditions. Therefore, disulfides would be formed especially in the oxidative environment of the endoplasmic reticulum and the extracellular milieu, but oxidative stress may also lead to formation of intracellular disulfide bonds (18). Treatment of MCT8-expressing cells with DTT does not affect MCT8 function, indicating that MCT8 does not contain S-S bonds accessible to extracellular DTT or that they are not important for MCT8 structure and transport activity.

MCT8 is also expressed in the thyroid, where it appears to play an important role in TH secretion (19). The thyroid gland produces H_2O_2 during the process of TH biosynthesis, and the redox state of the thyroid cells could thus affect Cys residues in MCT8. We tested whether H_2O_2 could modulate MCT8 function, but no effect was observed (data not shown). In addition, it is not clear whether the oxidative conditions on the luminal side of the apical membrane of thyroid cells have a bearing on the possible oxidation of Cys residues in MCT8 located in the basolateral membrane. Therefore, it is unlikely that the function of MCT8 in the thyroid cell is affected by the oxidative conditions required for TH synthesis.

Our previous study with Cys>Ala mutants of MCT8 was done by transfection of COS1 cells with an excessive amount of MCT8 plasmid, resulting in maximum TH uptake rates (5). Here we used a limited

amount of plasmid to increase the sensitivity to detect small changes in MCT8 function. Furthermore, as mentioned above, we also used JEG3 cells, which allow more sensitive detection of a decrease in MCT8 function by mutations identified in AHDS patients than COS1 cells. However, with this new approach, the different Cys>Ala mutants still showed little change in function compared with WT MCT8. The only significant difference was a modest increase in TH transport produced by the C281A mutation.

We showed that exposure to $HgCl_2$ also inhibits T_3 transport by MCT8. This has also been observed with other transporters. For instance, $HgCl_2$ inhibits glutamate transport by 2 glutamate transporter subtypes (20, 21). As in our study, the inhibition by $HgCl_2$ was reversed by DTT, indicating again the covalent modification of the free SH groups of Cys residues by $HgCl_2$. The same Cys residues in MCT8 targeted by pCMBS are also modified by $HgCl_2$ as revealed by studies with the double C481A+C497A mutant that is completely insensitive to $HgCl_2$. However, $HgCl_2$ is a more potent MCT8 inhibitor than pCMBS, because 1µM $HgCl_2$ produced the same inhibition as 100µM pCMBS.

Important differences between these two SH modifying reagents are their size and permeability. Although both pCMBS and $HgCl_2$ are membrane impermeable, they may be taken up by cells via transporters. This has been demonstrated for $HgCl_2$, which is taken up by cells that express the organic anion transporter 1 (OAT1) (22). We do not know whether JEG3 cells express this transporter. However, toxic effects of $HgCl_2$ are observed only at very high levels (100µM), suggesting minimal cellular uptake of mercury. The same holds true for pCMBS. Furthermore, the Cys residues modified by pCMBS and $HgCl_2$ are also accessible to DTT. Cell viability is also not affected by DTT concentrations up to 100mM, suggesting minimal cellular uptake of DTT. Therefore, Cys481 and Cys497 are likely to be exposed to the extracellular environment. Another characteristic of $HgCl_2$ is that it may cross-link 2 Cys residues. According to the model of MCT8 structure published recently (11), the distance between Cys481 and Cys497 appears too large (more than 20 Å) to allow cross-linking by Hg^{2+}.

It is interesting to note that the 2 Cys residues whose modification affects MCT8 function are located relatively close together, with Cys481 located in the outer parts of TMD9 and Cys497 located deeper in TMD10, but our results show that both must be in contact with the extracellular milieu. It has been suggested that especially mutations in TMD9 through TMD12 lead to MCT8 misfolding (11). Mutations of these 2 Cys residues have not been identified in patients, but other mutations associated with AHDS occur relatively frequently in TMD10, including L492P and F501del (23, 24). It should be pointed out that the C481A and C497A mutations by themselves do not affect MCT8 function, indicating that these Cys residues are not truly necessary for MCT8 function. However, the inhibition of MCT8 by their modification with pCMBS suggests that mutations of Cys481 and Cys497 to more bulky amino acids will also impair MCT8 function. It is remarkable that Cys497 is modified by pCMBS because this residue is located relatively deep in TMD10, based on the secondary structure (11, 12). Our findings of the protective effect of T_3 against the inactivation of MCT8 by pCMBS suggest that Cys497, like Cys481, are equally accessible to both substrate and inhibitor.

In conclusion, our data obtained by combining amino-acid–specific chemical modification and site-direct mutagenesis may contribute to a better understanding of the structure-function relationship of the MCT8 transporter. This is the first study to identify Cys residues that play a role in MCT8 function, of which Cys481 and Cys497 appear to be located in the substrate-recognition site. It remains to be determined whether MCT8 is also inactivated in vivo by modification of these Cys residues by

exogenous compounds, such as the environmental pollutant methylmercury, which has a negative effect on neurological development (25).

Acknowledgements

This work was supported by CNPq (Conselho Nacional de Desenvolvimento Científico e Tecnológico) Brazil.

Disclosure Summary: The authors have nothing to declare.

SUPPLEMENTAL FIGURES

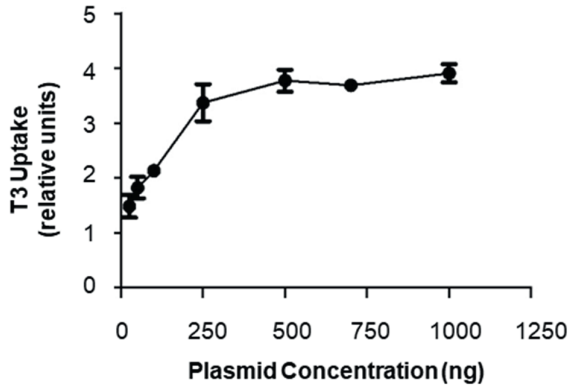

Supplemental Figure 1 Effect of the amount of hMCT8-pcDNA3 plasmid on MCT8-mediated T3 uptake. JEG3 cells were transiently transfected with 0-1000 ng hMCT8-pcDNA3, complemented with empty pcDNA3 to a total amount of 1000 ng DNA, and analyzed for T3 uptake.

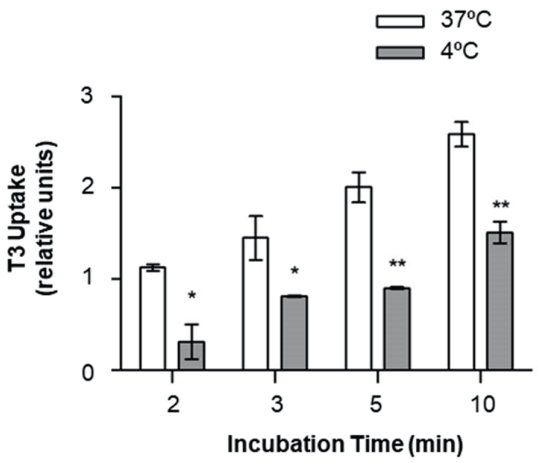

Supplemental Figure 2 Effects of incubation temperature on MCT8-mediated uptake of T3. Transfected cells were incubated for 2-10 min at 37˚C or 4˚C with [125I]T3. *p<0.05, **p<0.01 4˚C vs. 37˚C (two-way ANOVA Bonferroni posttests).

REFERENCES

1. Friesema EC, Ganguly S, Abdalla A, Manning Fox JE, Halestrap AP, Visser TJ. Identification of monocarboxylate transporter 8 as a specific thyroid hormone transporter. J Biol Chem. 2003;278(41):40128-35.
2. Friesema EC, Visser WE, Visser TJ. Genetics and phenomics of thyroid hormone transport by MCT8. Mol Cell Endocrinol. 2010;322(1-2):107-13.
3. Dumitrescu AM, Liao XH, Best TB, Brockmann K, Refetoff S. A novel syndrome combining thyroid and neurological abnormalities is associated with mutations in a monocarboxylate transporter gene. Am J Hum Genet. 2004;74(1):168-75.
4. Friesema EC, Grueters A, Biebermann H, Krude H, von Moers A, Reeser M, et al. Association between mutations in a thyroid hormone transporter and severe X-linked psychomotor retardation. Lancet. 2004;364(9443):1435-7.
5. Visser WE, Philp NJ, van Dijk TB, Klootwijk W, Friesema EC, Jansen J, et al. Evidence for a homodimeric structure of human monocarboxylate transporter 8. Endocrinology. 2009;150(11):5163-70.
6. Giron P, Dayon L, Sanchez JC. Cysteine tagging for MS-based proteomics. Mass spectrometry reviews. 2011;30(3):366-95.
7. Gruber CW, Cemazar M, Heras B, Martin JL, Craik DJ. Protein disulfide isomerase: the structure of oxidative folding. Trends Biochem Sci. 2006;31(8):455-64.
8. Trivedi MV, Laurence JS, Siahaan TJ. The role of thiols and disulfides on protein stability. Current protein & peptide science. 2009;10(6):614-25.
9. Lipton SA, Choi YB, Takahashi H, Zhang D, Li W, Godzik A, et al. Cysteine regulation of protein function--as exemplified by NMDA-receptor modulation. Trends in neurosciences. 2002;25(9):474-80.
10. Wilson MC, Meredith D, Fox JE, Manoharan C, Davies AJ, Halestrap AP. Basigin (CD147) is the target for organomercurial inhibition of monocarboxylate transporter isoforms 1 and 4: the ancillary protein for the insensitive MCT2 is EMBIGIN (gp70). J Biol Chem. 2005;280(29):27213-21.
11. Kinne A, Kleinau G, Hoefig CS, Gruters A, Kohrle J, Krause G, et al. Essential molecular determinants for thyroid hormone transport and first structural implications for monocarboxylate transporter 8. J Biol Chem. 2010;285(36):28054-63.
12. Kleinau G, Schweizer U, Kinne A, Kohrle J, Gruters A, Krude H, et al. Insights into molecular properties of the human monocarboxylate transporter 8 by combining functional with structural information. Thyroid Res. 2011;4 Suppl 1:S4.
13. Friesema EC, Kuiper GG, Jansen J, Visser TJ, Kester MH. Thyroid hormone transport by the human monocarboxylate transporter 8 and its rate-limiting role in intracellular metabolism. Mol Endocrinol. 2006;20(11):2761-72.
14. Lopez-Corcuera B, Nunez E, Martinez-Maza R, Geerlings A, Aragon C. Substrate-induced conformational changes of extracellular loop 1 in the glycine transporter GLYT2. J Biol Chem. 2001;276(46):43463-70.
15. Hastrup H, Sen N, Javitch JA. The human dopamine transporter forms a tetramer in the plasma membrane: cross-linking of a cysteine in the fourth transmembrane segment is sensitive to cocaine analogs. J Biol Chem. 2003;278(46):45045-8.
16. Oppedisano F, Galluccio M, Indiveri C. Inactivation by Hg2+ and methylmercury of the glutamine/amino acid transporter (ASCT2) reconstituted in liposomes: Prediction of the involvement of a CXXC motif by homology modelling. Biochem Pharmacol. 2010;80(8):1266-73.
17. Park JS, Hammond JR. Cysteine residues in the transmembrane (TM) 9 to TM11 region of the human equilibrative nucleoside transporter subtype 1 play an important role in inhibitor binding and translocation function. Mol Pharmacol. 2012;82(5):784-94.
18. Zha XM, Wang R, Collier DM, Snyder PM, Wemmie JA, Welsh MJ. Oxidant regulated inter-subunit disulfide bond formation between ASIC1a subunits. Proc Natl Acad Sci U S A. 2009;106(9):3573-8.
19. Di Cosmo C, Liao XH, Dumitrescu AM, Philp NJ, Weiss RE, Refetoff S. Mice deficient in MCT8 reveal a mechanism regulating thyroid hormone secretion. J Clin Invest. 2010;120(9):3377-88.
20. Toimela TA, Tahti H. Effects of mercuric chloride exposure on the glutamate uptake by cultured retinal pigment epithelial cells. Toxicol In Vitro. 2001;15(1):7-12.
21. Mutkus L, Aschner JL, Syversen T, Shanker G, Sonnewald U, Aschner M. Mercuric chloride inhibits the in vitro uptake of glutamate in GLAST- and GLT-1-transfected mutant CHO-K1 cells. Biological trace element research. 2006;109(3):267-80.
22. Torres AM, Dnyanmote AV, Bush KT, Wu W, Nigam SK. Deletion of multispecific organic anion transporter Oat1/Slc22a6 protects against mercury-induced kidney injury. J Biol Chem. 2011;286(30):26391-5.

23. Visser WE, Vrijmoeth P, Visser FE, Arts WF, van Toor H, Visser TJ. Identification, functional analysis, prevalence and treatment of monocarboxylate transporter 8 (MCT8) mutations in a cohort of adult patients with mental retardation. Clin Endocrinol (Oxf). 2013;78(2):310-5.
24. Visser WE, Jansen J, Friesema EC, Kester MH, Mancilla E, Lundgren J, et al. Novel pathogenic mechanism suggested by ex vivo analysis of MCT8 (SLC16A2) mutations. Hum Mutat. 2009;30(1):29-38.
25. Falluel-Morel A, Sokolowski K, Sisti HM, Zhou X, Shors TJ, Dicicco-Bloom E. Developmental mercury exposure elicits acute hippocampal cell death, reductions in neurogenesis, and severe learning deficits during puberty. J Neurochem. 2007;103(5):1968-81.

Chapter

Importance of His192 in the Human Thyroid Hormone Transporter MCT8 for Substrate Recognition

2.2

Stefan Groeneweg, Elaine C. Lima de Souza, W. Edward Visser, Robin P. Peeters, Theo J. Visser

Endocrinology. 2013 July;154(7):2525-32.

ABSTRACT

Monocarboxylate transporter 8 (MCT8) facilitates cellular uptake and efflux of thyroid hormone (TH). So far, functional domains within MCT8 are not well defined. Mutations in MCT8 result in severe psychomotor retardation due to impaired neuronal differentiation. One such mutation concerns His192 (H192R), located at the border of transmembrane domain (TMD) 1 and extracellular loop (ECL) 1, suggesting that this His residue is important for efficient TH transport. Here, we studied the role of different His residues, predicted within TMDs or ECLs of MCT8, in substrate recognition and translocation. Therefore, we analyzed the effects of the His-modifying reagent diethylpyrocarbonate (DEPC) and of site-directed mutagenesis of several His residues on TH transport by MCT8. Reaction of MCT8 with DEPC inhibited subsequent uptake of T3 and T4, whereas T3 and T4 efflux were not inhibited. The inhibitory effect of DEPC on TH uptake was prevented in the presence of T3 or T4, suggesting that TH blocks access to DEPC-sensitive residues. Three putative DEPC target His residues were replaced by Ala: H192A, H260A, and H450A. The H260A and H450A mutants showed similar TH transport and DEPC sensitivity as wild-type MCT8. However, the H192A mutant showed a significant reduction in TH uptake and was insensitive to DEPC. Taken together, these results indicate that His192 is sensitive to modification by DEPC and may be located close to a putative substrate recognition site within the MCT8 protein, important for efficient TH uptake.

INTRODUCTION

Thyroid hormones (THs) require transmembrane transport proteins to mediate their translocation across the cell membrane (1, 2). Once inside the cell, TH can regulate gene expression upon binding to one of the TH receptors (3). Monocarboxylate transporter 8 (MCT8, SLC16A2) facilitates the uptake and efflux of TH in different cell types (4-7). The importance of MCT8 is underlined by the impaired neuronal differentiation and consequent severe neurological phenotype, known as the Alan-Herndon-Dudley syndrome (AHDS), observed in patients harboring mutations in MCT8 (8, 9). The high serum T3 levels, combined with low serum T4 levels and normal levels of TSH are characteristic for AHDS patients (10).

Many mutations in MCT8 have been reported thus far (10). However, most of these studies have focused on the impact of mutations on TH transport function, whereas the pathological mechanism of the mutations at the molecular level has been scarcely studied (10-15). Currently, important functional domains within the MCT8 protein, such as the amino acid residues involved in substrate recognition and translocation have not been characterized yet, although recent structural models of MCT8 suggest important roles for charged amino acids (11).

For many transporter proteins, it has been shown that besides the charged Lys, Arg, Asp, and Glu residues, His residues may be involved in substrate recognition and translocation (16-22). Here, we studied the role of His residues, located within the predicted transmembrane domains (TMDs) or extracellular loops (ECLs) of MCT8 in substrate recognition and translocation. Previously, an H192R mutation in MCT8 was identified in an AHDS patient, supporting the hypothesis that this His residue may be important for MCT8 function (10, 11).

To study the role of His residues in TH transport by MCT8, we analyzed the effects of diethylpyrocarbonate (DEPC), a reagent that reacts with His to yield the N-carbethoxy derivative (23, 24), and of mutations of different His residues to Ala (H192A, H260A, and H450A) on MCT8-mediated TH transport. In some of the experiments, expression of the intracellular TH-binding protein μ-crystallin (CRYM) was used to reduce the efflux of TH, thereby increasing the net cellular TH uptake (25). Our results show that DEPC modifies H192, leading to a partial inhibition of TH transport. Interestingly, the effect of DEPC is prevented in the presence of the MCT8 substrates T3 and T4, suggesting that MCT8 indeed contains a His residue at or near the substrate-recognition site.

MATERIALS AND METHODS

Materials

Nonradioactive iodothyronines were obtained from Henning (Berlin, Germany). [3'-125I]T3 and [3',5'-125I]T4 (1500–2000 mCi/μmol) were prepared in our laboratory as previously described (26). X-tremeGENE9 transfection reagent was obtained from Roche Diagnostics (Almere, The Netherlands). DEPC was obtained from Sigma (Zwijndrecht, The Netherlands).

Plasmids

Cloning of hMCT8 in pcDNA3, and of the human cytosolic TH-binding protein CRYM in pSG5 has been described previously (25, 27). Expression of hCRYM reduces TH efflux, greatly increasing net cellular TH uptake. We introduced the following mutations into the pcDNA3_hMCT8 plasmid using

QuikChange site-directed mutagenesis (Stratagene, Amsterdam, The Netherlands) according to the manufacturer's protocol: H192A, H260A, and H450 (primers are listed in **Supplemental Table 1**). DNA sequencing confirmed the presence of the introduced mutations and the absence of unintended mutations.

Cell culture and transfection

JEG3 cells were cultured in 6- or 24-well dishes (Corning, Schiphol, The Netherlands) in DMEM/F12 medium (Invitrogen, Breda, The Netherlands), containing 9% heat-inactivated fetal bovine serum (Invitrogen), 2% penicillin/streptomycin (Roche, Woerden, The Netherlands), and 100nM sodium selenite (Sigma). Cells were transfected at 70% confluency, and all experiments were carried out 48 hours after transfection. For TH transport studies, cells were seeded in 24-well dishes and cotransfected in duplicate with 100 ng pcDNA3_hMCT8 (wild-type [WT] or mutant) and either 100 ng pSG5_hCRYM or pcDNA3 empty vector. For immunoblotting, cells were seeded in 6-well dishes and transfected with 500 ng pcDNA3_hMCT8 (WT or mutant) or empty pcDNA3. X-tremeGENE9 was used as the transfection agent according to manufacturer's protocol. We previously described the absence of significant differences in transfection efficiency between MCT8 mutants (14).

Immunoblotting

Cells were rinsed with PBS and collected in 100 µl 0.1M phosphate buffer (pH 7.2) and 2mM EDTA (P100E2). The cells were sonicated on ice and stored at −80°C until use. Homogenates (30 µg protein) were separated on 12% SDS-PAGE, blotted on nitrocellulose membranes, and probed with rabbit polyclonal antibody 3353 against hMCT8 amino acids 75 to 155 (Sigma, Stockholm, Sweden) diluted 1:20 000 and with mouse monoclonal glyceraldehyde-3-phosphate dehydrogenase antibody (Mab 374; Millipore, Amsterdam, The Netherlands) 1:20 000 as a loading control. IRDye680 goat antirabbit and IRDye800 goat antimouse antibodies 1:20 000 (LI-COR, Leusden, The Netherlands) were used as secondary antibody. Antibodies were detected with Odyssey Infrared Detection System (LI-COR).

TH uptake and efflux

Cells were washed with Dulbecco's PBS (D-PBS) medium and preincubated for 10 minutes at 37°C in D-PBS (pH 7.0, unless indicated differently) in the absence or presence of 1µM to 1mM DEPC and/or 1µM unlabeled T3 or T4. This incubation step was performed in the absence of BSA to prevent loss of DEPC reagent by reaction with BSA with possible additional consequences for TH binding to BSA. Thereafter, cells were washed twice with D-PBS plus 0.1% BSA and incubated for 15 or 30 minutes at 37°C with 1nM (5 × 104 cpm) [125I]T4 or [125I]T3 in 375 µl D-PBS plus 0.1% BSA. Finally, cells were washed once with D-PBS plus 0.1% BSA and lysed with 0.1M NaOH. The amount of radioactivity in the lysates was measured with a γ-counter.

For efflux studies, JEG3 cells were loaded for 30 minutes at 37°C with 1nM (5 × 104 cpm) [125I]T4 or [125I]T3 in D-PBS, briefly washed, and subsequently incubated for 3 minutes at 37°C with 0.5 ml fresh D-PBS plus 1% BSA. After incubation, medium and cells were collected without further washing and radioactivity was measured in both fractions with a γ-counter.

RESULTS

The structural elements responsible for the substrate selectivity of MCT8 toward TH are largely unknown. Because many charged amino acids are localized at the predicted extracellular part of the MCT8 protein, these residues could be plausible determinants for substrate selection and translocation (13). To study the role of His residues within a protein, the His-reactive reagent DEPC is often used (16-22). Because DEPC is membrane impermeable, it can chemically modify only His residues located in the accessible parts of TMDs or ECLs of membrane-bound proteins (23).

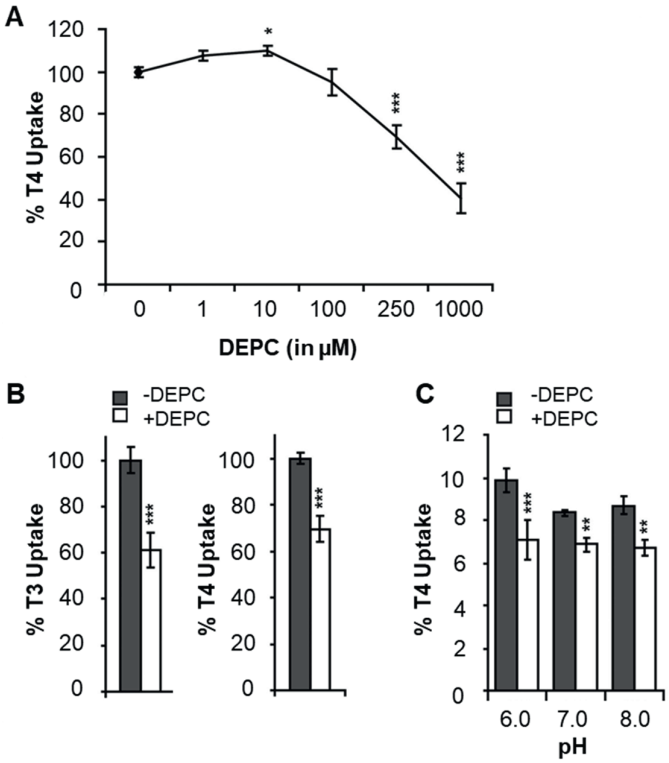

Figure 1 **A**, T_4 uptake by JEG3 cells transfected with hMCT8 and hCRYM cDNA in 30 minutes at 37°C after pre-incubation with indicated concentrations of DEPC for 10 minutes at room temperature. **B**, T_3 and T_4 uptake by JEG3 cells transfected with hMCT8 and hCRYM in 30 minutes at 37°C, after pre-incubation for 10 minutes at room temperature in the presence (+ DEPC), or absence (– DEPC) of 250µM DEPC. **C**, T_4 uptake by JEG3 cells transfected with hMCT8 and hCRYM in 30 minutes at 37°C after pre-incubation for 10 minutes in the presence of 250µM DEPC at indicated pH levels. All values are corrected for background TH uptake levels observed in JEG3 cells transfected with pcDNA3 empty vector, pre-incubated under the identical condition. TH uptake levels are expressed relative to MCT8-mediated TH uptake levels after pre-incubation in D-PBS without DEPC (0 or –DEPC). Results are presented as means ± SD (n = 2–4). Statistical significance was tested using 1-way ANOVA followed by Dunnett's multiple-comparison test in A, 2-tailed paired Student's *t* test in B, and 2-way ANOVA followed by Bonferroni's post-tests in C: *, $P < .05$; **, $P < .01$; ***, $P < .001$.

To study the role of His residues within MCT8, we incubated JEG3 cells expressing WT MCT8 and CRYM with increasing concentrations of DEPC in PBS and subsequently tested the cells for T4 uptake. Incubation with increasing DEPC concentrations resulted in a progressive decrease in T4 uptake by MCT8 (**Figure 1A**). Pre-incubation with 250µM DEPC resulted in a similar decrease in T3 and T4 uptake by MCT8 (**Figure 1B**). To exclude that this decrease in T4 and T3 uptake was due to an increased cell

death, we analyzed the toxicity of DEPC by a trypan blue exclusion assay. Concentrations up to 250µM DEPC did not result in an increased cell death. Only the highest concentration of 1mM DEPC resulted in a significant 25% to 30% increase in cell death over cells incubated without DEPC (data not shown). Therefore, all additional experiments were done using 250µM DEPC.

The imidazole ring of His typically has a pKa value around 6.0 to 6.5, which may be greatly influenced by surrounding residues. Because DEPC modifies only unprotonated imidazole rings, we pre-incubated JEG3 cells with 250µM DEPC at different pH levels before T4 uptake assays. The DEPC-mediated inhibition of T4 uptake by MCT8 decreased slightly when pH was increased from 6.0 to 7.3 and remained constant by the further increase of pH to 8.3 (**Figure 1C**). Increasing pH levels induce dissociation of His residues, leading to an increased susceptibility to DEPC modification. On the other hand, at higher pH levels, the stability of DEPC increases, and it may also modify Tyr, Lys, and Cys residues (23). These results show that the inhibiting effect of DEPC is already maximal within the pH range in which almost exclusively His residues are sensitive to DEPC modification.

To study whether the residues modified by DEPC may also be involved in substrate interactions, JEG3 cells transfected with WT MCT8 were pre-incubated with 250µM DEPC in the absence or presence of 1µM unlabeled T4 or T3 before [125I]T4 and [125I]T3 uptake assays. The intracellular TH-binding protein CRYM was not used in these experiments because this protein is saturated by 1µM T4 or T3. Also in the absence of CRYM, MCT8-mediated T3 and T4 uptake were reduced after pre-incubation with 250µM DEPC. This inhibitory effect was completely abolished when DEPC was co-incubated with 1µM T3 or T4 (**Figure 2, A** and **B**), resulting in TH uptake levels similar to cells not treated with DEPC. These results suggest that T3 and T4 protect susceptible residues from modification by DEPC.

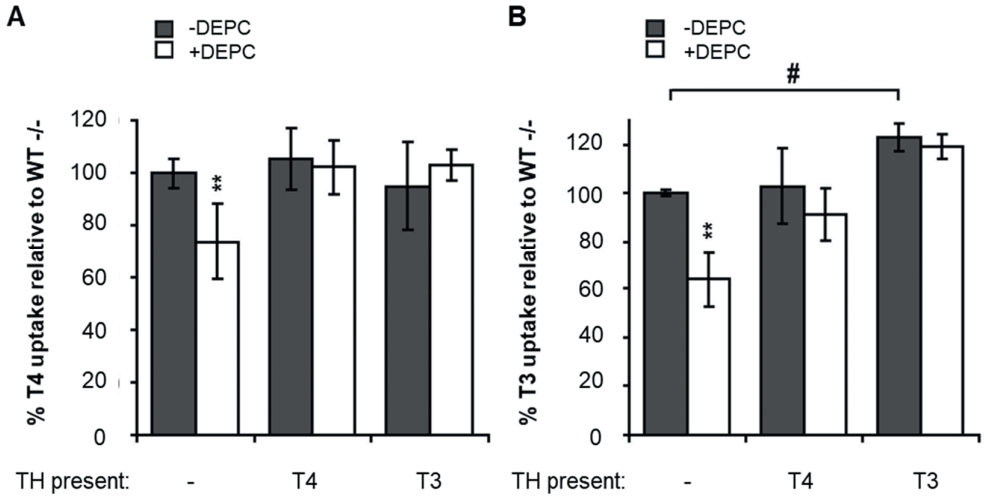

Figure 2. T4 (**A**) and T3 (**B**) uptake by JEG3 cells transfected with hMCT8 in 15 minutes at 37°C after pre-incubation for 10 minutes at room temperature in the presence (+ DEPC), or absence (− DEPC) of 250µM DEPC and in the absence (−) or presence of 1µM T4 or 1µM T3. All values are corrected for background TH uptake levels observed in JEG3 cells transfected with empty vector, pre-incubated under the identical condition. TH uptake levels are expressed relative to MCT8-mediated TH uptake levels after pre-incubation in D-PBS without DEPC or TH (−/−DEPC). Results are presented as means ± SD (n = 3–4). Two-way ANOVA followed by Bonferroni's post-test was used for statistical analysis of the effect of DEPC (**, $P < .01$), and 1-way ANOVA was followed by Dunnett's multiple comparison for the effect of the pre-incubation with T3 or T4 (##, $P < .01$).

Although DEPC may also modify other residues, we focused on conserved histidines within the predicted TMDs or ECLs of MCT8 as target residues for DEPC (13). To identify the target His residues, we introduced the following mutations: H192A, H260A, and H450A. Only the H450A showed a slight decrease in protein expression level compared with WT MCT8, whereas the expression levels of H192A and H260A were similar to WT (**Figure 3A**). Moreover, dimerization was still intact in all mutants (**Figure 3A**). Consequently, these MCT8 mutants were tested for T3 and T4 uptake and DEPC sensitivity.

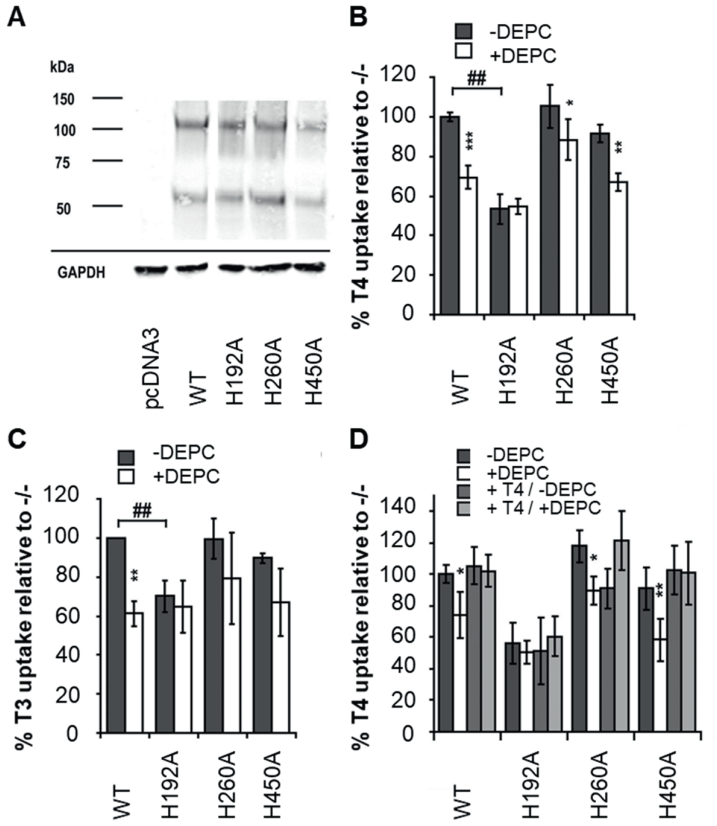

Figure 3 A, Western blot of lysates from JEG3 cells transfected with pcDNA3 empty vector or WT, H192A, H260A, and H450A mutant MCT8. MCT8 detection was performed with the N-terminal hMCT8 antibody (3353) visualized with IRDye680 goat antirabbit secondary antibody. Glyceraldehyde-3-phosphate dehydrogenase was used as loading control. A band of approximately 55 kDa, representing the hMCT8 monomer and a second band around 110 kDa representing the hMCT8 homodimer were observed in cells transfected with WT or mutant MCT8 constructs. **B** and **C**, T4 (**B**) and T3 (**C**) uptake by JEG3 cells transfected with hMCT8 WT, H192A, H260A, or H450A and hCRYM in 30 minutes at 37°C after preincubation for 10 minutes at room temperature in the presence (+ DEPC), or absence (− DEPC) of 250µM DEPC. **D**, T4 uptake by JEG3 cells transfected with hMCT8WT or mutant in 15 minutes at 37°C after preincubation for 10 minutes at room temperature in the presence (+ DEPC), or absence (− DEPC) of 250µM DEPC and in the absence or presence of 1µM T4 (+ T4). All values are corrected for background TH uptake levels observed in JEG3 cells transfected with empty vector, preincubated under the identical condition. TH uptake levels are expressed relative to WT MCT8-mediated TH uptake levels after preincubation in D-PBS without DEPC (0 or −DEPC). Results are presented as means ± SD (n = 3–4). Two-way ANOVA followed by Bonferroni's post-test was used for statistical analysis of the effect of DEPC (*, P < .05; **, P < .01; ***, P < .001), and 1-way ANOVA was followed by Dunnett's multiple comparison for the difference between WT and mutant MCT8 (##, P < .01) in B and C. Two-way ANOVA followed by Bonferroni's post-tests was used in D (*, P < .05; **, P < .01).

After co-transfection with CRYM, the H192A mutant showed 30% to 50% lower T4 uptake than WT MCT8, whereas T4 uptake of the H260A and H450A mutants was not affected (**Figure 3B**). T3 uptake was decreased by only 20% to 30% by the H192A mutation but was not affected by the H260A and H450A mutations (**Figure 3C**). In contrast to WT MCT8, pre-incubation with 250µM DEPC did not inhibit TH uptake by the H192A mutant. The H260A and H450A mutants showed similar sensitivity to DEPC as WT MCT8 (**Figure 3, B** and **C**). Co-incubation with 1µM T3 or T4 provided the same protection against DEPC inactivation of the H260A and H450A mutants as observed with WT MCT8 (**Figure 3D** and data not shown). These findings suggest that T3 and T4 are able to protect His192 from modification by DEPC.

We also investigated the effects the DEPC on TH efflux by WT MCT8 and the H192A, H260A, and H450A mutants. Because BSA strongly binds TH, efflux medium contained 1% BSA to prevent reuptake of released TH. WT MCT8 effectively facilitates T3 efflux, because almost 60% of T3 taken up by MCT8 in 30 minutes was released within 3 minutes (**Figure 4A**). The efficiency of T4 efflux was lower than T3 efflux, because only 35% of the preloaded T4 was released by MCT8 within 3 minutes (**Figure 4A**). However, no significant decrease of MCT8-mediated TH efflux was observed after preincubation with DEPC (**Figure 4A**). The H192A mutant showed a relatively small but significant decrease in TH efflux compared with WT MCT8, whereas TH efflux was not affected by the H260A and H450A mutations (**Figure 4B**). These data suggest that His192 might be of less importance for TH efflux than for TH uptake by MCT8.

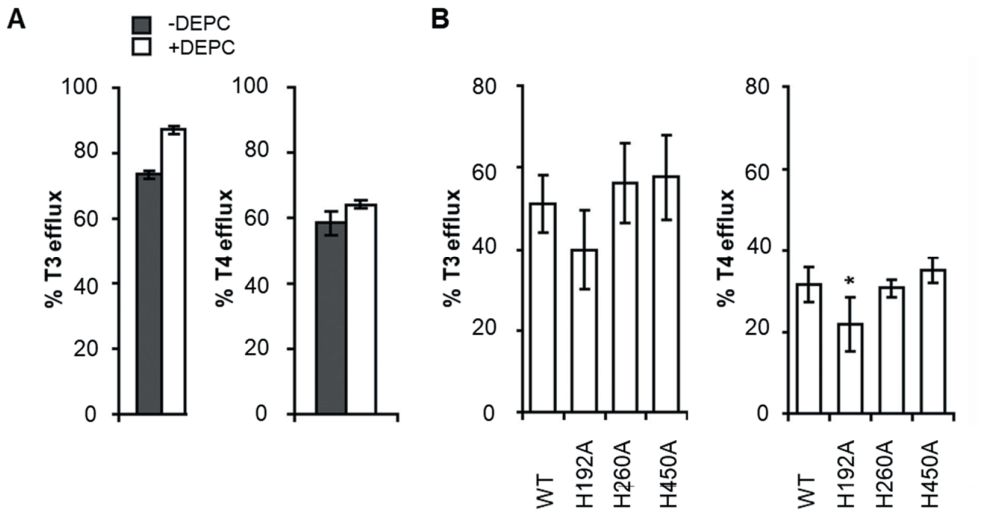

Figure 4 A, MCT8-mediated efflux of T3 and T4 from JEG3 cells transfected with WT MCT8 in the absence of hCRYM for 3 minutes in the presence of 1% BSA. Cells were first pre-incubated in the presence (+) or absence (−) of DEPC for 10 minutes at room temperature, followed by 30 minutes preloading in the presence of [125I]T3 or [125I]T4. **B**, MCT8-mediated efflux of T3 and T4 from JEG3 cells transfected with WT or mutant MCT8 in the absence of hCRYM. Transfected cells were incubated for 30 minutes in the presence of [125I]T3 or [125I]T4, briefly washed, and sequentially incubated for 3 minutes in D-PBS containing 1% BSA. The amount of radioactivity was measured in the supernatant and in the cell lysate, together representing the total cellular TH content after preloading. The efflux is expressed as percentage of total TH content that is present in the supernatant after 3 minutes incubation in the presence of 1% BSA, corrected for background. Results are presented as means ± SD (n = 2–4). Statistical analysis was done using 2-tailed paired Student's t test in A and 1-way ANOVA followed by Dunnett's multiple-comparison tests in B (*, $P < 0.05$; **, $P < 0.01$).

DISCUSSION

In this study, we described the inhibitory effect of the His-modifying reagent DEPC on MCT8-mediated TH transport. The inhibitory effect of DEPC was prevented in the presence of T3 and T4, suggesting that T3 and T4 are able to protect susceptible residues from DEPC modification. By site-directed mutagenesis of 3 putative target His residues, we observed that the H192A mutation resulted in a significant reduction in TH transport, whereas the H260A and H450A mutations had little effect. Moreover, the H192A mutant was insensitive to DEPC, suggesting that the inhibiting effect of DEPC is only mediated via His192 modification. This His192 residue is probably located at or near the substrate recognition site of MCT8.

To study the importance of His residues for MCT8 function, we combined chemical modification of MCT8 by DEPC and site-directed mutagenesis with functional TH transport assays. A concentration-dependent inhibition of MCT8-mediated TH transport was observed after preincubation with DEPC, with an EC50 value of ∼500μM. These results suggest that His residues within MCT8 are involved in TH transport. Unfortunately, incubation with DEPC at concentrations higher than 250μM resulted in an increase in cell death, thereby limiting the use of DEPC to concentrations up to 250μM. However, preincubation of transfected JEG3 cells with 250μM DEPC still reduced MCT8-mediated TH uptake with 30% to 40% irrespective of the expression of CRYM.

Similar effects of DEPC were observed on TH uptake by MCT8 in the absence or presence of the intracellular TH-binding protein CRYM. Because TH efflux is largely inhibited by expression of CRYM, these results suggest a predominant effect of DEPC modification on TH uptake. Indeed, there were no significant effects of DEPC modification on MCT8-mediated TH efflux.

Although DEPC is considered to be a rather specific His-modifying reagent, it may also react with Lys, Tyr, and Cys residues (23). However, DEPC has been shown to be more specific for His residues at pH 6 or below (23). Indeed, we already observed maximum inhibition of T4 transport after preincubation with DEPC at pH 6.0. The half-life time of DEPC tends to be shorter at pH values above 7.0, which could explain the relative decrease of the inhibitory effect of DEPC at higher pH. Furthermore, a mutation of an extracellular His residue (H192R) has been identified in an AHDS patient, suggesting that modification of extracellular histidines inhibits TH transport by MCT8 (10). Taken together, the inhibitory effect of DEPC is likely to be mediated by modification of 1 or more His residues.

Because DEPC is a membrane-impermeable reagent, we focused on the His residues located within the predicted TMDs or ECLs of MCT8. Therefore, we initially replaced His192, His260 or His450 with the inert neutral amino acid Ala. The H260A and H450A mutants showed similar T3 and T4 uptake and efflux rates as WT MCT8, whereas T3 and T4 uptake rates were significantly reduced (40%–45%) by the H192A mutation. However, TH efflux was less affected by the H192A mutation than TH uptake.

Moreover, the H192A mutant was completely insensitive to inhibition by DEPC, whereas the H260A and H450A mutants showed similar DEPC sensitivity as WT MCT8. These results suggest that the modification of His192 is responsible for the inhibition of MCT8 by DEPC. Lack of an inhibiting effect of DEPC on TH efflux seems in contradiction with the small reduction of TH efflux by the H192A mutation. However, modification of His192 by DEPC is only partial in contrast to complete replacement by Ala in H192A.

There are several possible mechanisms that could contribute to the reduced transport activity of the H192A mutant. Because the H192A mutant showed considerable residual TH uptake, whereas TH efflux was relatively mildly affected, it is reasonable to assume proper membrane localization of this mutant protein. Moreover, protein expression levels were comparable to WT MCT8, which makes it unlikely that the mutant protein is subject to enhanced degradation due to protein misfolding. Finally, the H192A mutation could decrease the affinity of the transporter for its substrates, resulting in less efficient substrate recruitment and ultimately a decrease in TH uptake rates. This is supported by the finding that DEPC modification of His192 is prevented by coincubation with T3 or T4, suggesting that T3 and T4 block the access of DEPC to His192, which in this case is located at or near the site involved in substrate selection.

Interestingly, preincubation of JEG3 cells with T4 seems to enhance subsequent TH uptake. This effect was less apparent after preincubation with T3. It has been previously shown that MCT8-mediated T4 efflux is less efficient than efflux of T3 (28). Hence, preincubation with excess unlabeled T4 may result in sufficiently high intracellular TH concentrations to competitively inhibit the efflux of radioactive T4 taken up during the subsequent incubation.

His residues have often been implicated in the transport mechanisms of both proton-coupled transporters and proton-independent transporters. His322 of the Escherichia coli lactose permease was suggested to be important for substrate recognition and translocation (28, 29). In addition, substrate protection experiments have shown that His65 in the plant proton-sucrose symporter is located at or near the substrate-binding site (16). In human oligopeptide transporter 1, a crucial His residue has also been shown to be located at the substrate-binding site. DEPC modification of this His residue was prevented by the human oligopeptide transporter 1 substrate glycylsarcosine (17). The mouse kidney organic anion transporter has been shown to be sensitive to DEPC modification, which could be prevented by an excess of its substrate p-aminohippurate, suggesting the location of His residues within the substrate-binding domain (18). Chemical modification with DEPC of the anion transporter band 3 (AE1) leads to near-complete inhibition of anion binding and transport (19-21). Modification of His residues of the H+/organic cation antiporter multidrug and toxin extrusion 1 (MATE1) results in a decrease in transport capacity, which is not prevented by the addition of substrate, showing that DEPC-sensitive histidines are not always located at substrate-binding sites (22).

T3 and T4 could block the access of DEPC to His192 via two different mechanisms: 1) the substrates interact with MCT8 at or near this residue, or 2) the substrates alter the conformation of MCT8 such that His192 becomes inaccessible to DEPC. The first mechanism implies a competitive interaction of DEPC and substrates with MCT8, whereas the second mechanism implies a noncompetitive interaction. In principle, these 2 mechanisms could have been distinguished by analysis of the effects of combinations of varying concentrations of DEPC and substrate. However, these studies were hampered by the cytotoxic effects of DEPC in concentrations higher than 250µM.

It therefore remains to be demonstrated whether TH directly interacts with His192 or whether modification or replacement of His192 disturbs the structure of the substrate-recognition site, thereby reducing the efficiency of substrate selection by other residues. However, based on our results, it is less likely that T3 and T4 directly bind to His192, because the H192A mutant shows considerable residual TH transport. Alternatively, modification or replacement of His192 could alter the local conformation of the MCT8 protein and thereby disrupt the interactions between TH and other amino

acid residues, necessary for proper substrate selection and translocation. Vice versa, substrate may induce a conformational change in the MCT8 structure, preventing the modification of His192 by DEPC.

Mutations in residues located in close linear proximity of His192 have been identified in AHDS patients. We have previously described the S194F mutation, which completely inactivates the MCT8 protein (15). The insertion of an Ile at position 189 (189insI) also results in a complete inactivation of MCT8-mediated TH transport (15). This insertion is likely to alter the helical structure of the distal end of TMD1, including the position of His192. In addition, according to the MCT8 homology model, His192 is also located within close spatial proximity of Arg445 and Asp498, which have been predicted to be crucial for substrate recognition and substrate transport across the putative substrate channel (11). Modification of Arg445 or Asp498 to Ala have been shown to drastically impair MCT8 function (11).

Moreover, the model predicts a channel-facing configuration of the side chain of His192, which is confirmed by our findings that His192 is sensitive to DEPC modification. Replacement of the His residue by Arg (H192R) as observed in an AHDS patient involves the introduction of a larger and positively charged side chain, resulting in a complete loss of function (10, 30, 31). Based on the results presented in this paper, it is mainly the positive charge and/or increased length of the Arg side chain that hampers MCT8 function rather than loss of the His residue itself. Taken together, our findings imply that we are exploring a true ligand channel. However, additional studies have to reveal which amino acid residues directly interact with TH.

Detailed characterization of interactions between TH and amino acid residues within MCT8 may be helpful to identify other TH transporters. Furthermore, His residues may also be localized in intracellular substrate recognition sites in MCT8, involved in the substrate selection and recruitment for MCT8-mediated efflux. Finally, insights in the substrate selection process may result in the development of new TH analogs targeted specifically to MCT8-expressing tissues.

In conclusion, we have demonstrated that His192 in MCT8 is sensitive to DEPC modification, which is prevented in the presence of T3 or T4 and by mutation to Ala (H192A). These results suggest that His192 is located at or near the site within the MCT8 protein involved in T3 and T4 recognition and recruitment before their translocation across the cell membrane.

Acknowledgements

Disclosure Summary: All authors have nothing to declare.

SUPPLEMENTARY DATA

Supplemental table 1 Primer list for mutagenesis reactions

name	**primer sequence**
H192A Fw	5'-GCTCCATCTTCGGCATCGCTAACTCTGTCGGGATCC-3'
H192A Rev	5'-GGATCCCGACAGAGTTAGCGATGCCGAAGATGGAGC-3
H260A Fw	5'-GGTGCTTTCATTGGCCTCGCTACCAGCTCCTTCACCAG-3'
H260A Rev	5'-CTGGTGAAGGAGCTGGTAGCGAGGCCAATGAAAGCACC-3'
H450A Fw	5'-GCGTCTTGTGTCAGGCGCCATCAGTGACTCCATC-3'
H450A Rev	5'-GATGGAGTCACTGATGGCGCCTGACACAAGACGC-3'

REFERENCES

1. Hennemann G, Docter R, Friesema EC, de Jong M, Krenning EP, Visser TJ. Plasma membrane transport of thyroid hormones and its role in thyroid hormone metabolism and bioavailability. Endocr Rev. 2001;22(4):451-76.
2. Visser WE, Friesema EC, Jansen J, Visser TJ. Thyroid hormone transport in and out of cells. Trends Endocrinol Metab. 2008;19(2):50-6.
3. Yen PM, Ando S, Feng X, Liu Y, Maruvada P, Xia X. Thyroid hormone action at the cellular, genomic and target gene levels. Mol Cell Endocrinol. 2006;246(1-2):121-7.
4. Price NT, Jackson VN, Halestrap AP. Cloning and sequencing of four new mammalian monocarboxylate transporter (MCT) homologues confirms the existence of a transporter family with an ancient past. Biochem J. 1998;329 (Pt 2):321-8.
5. Chan SY, Franklyn JA, Pemberton HN, Bulmer JN, Visser TJ, McCabe CJ, et al. Monocarboxylate transporter 8 expression in the human placenta: the effects of severe intrauterine growth restriction. J Endocrinol. 2006;189(3):465-71.
6. Alkemade A, Friesema EC, Unmehopa UA, Fabriek BO, Kuiper GG, Leonard JL, et al. Neuroanatomical pathways for thyroid hormone feedback in the human hypothalamus. J Clin Endocrinol Metab. 2005;90(7):4322-34.
7. Alkemade A, Friesema EC, Kuiper GG, Wiersinga WM, Swaab DF, Visser TJ, et al. Novel neuroanatomical pathways for thyroid hormone action in the human anterior pituitary. Eur J Endocrinol. 2006;154(3):491-500.
8. Friesema EC, Grueters A, Biebermann H, Krude H, von Moers A, Reeser M, et al. Association between mutations in a thyroid hormone transporter and severe X-linked psychomotor retardation. Lancet. 2004;364(9443):1435-7.
9. Dumitrescu AM, Liao XH, Best TB, Brockmann K, Refetoff S. A novel syndrome combining thyroid and neurological abnormalities is associated with mutations in a monocarboxylate transporter gene. Am J Hum Genet. 2004;74(1):168-75.
10. Friesema EC, Visser WE, Visser TJ. Genetics and phenomics of thyroid hormone transport by MCT8. Mol Cell Endocrinol. 2010;322(1-2):107-13.
11. Kinne A, Kleinau G, Hoefig CS, Gruters A, Kohrle J, Krause G, et al. Essential molecular determinants for thyroid hormone transport and first structural implications for monocarboxylate transporter 8. J Biol Chem. 2010;285(36):28054-63.
12. Kinne A, Roth S, Biebermann H, Kohrle J, Gruters A, Schweizer U. Surface translocation and tri-iodothyronine uptake of mutant MCT8 proteins are cell type-dependent. J Mol Endocrinol. 2009;43(6):263-71.
13. Friesema EC, Jansen J, Heuer H, Trajkovic M, Bauer K, Visser TJ. Mechanisms of disease: psychomotor retardation and high T3 levels caused by mutations in monocarboxylate transporter 8. Nat Clin Pract Endocrinol Metab. 2006;2(9):512-23.
14. Jansen J, Friesema EC, Kester MH, Milici C, Reeser M, Gruters A, et al. Functional analysis of monocarboxylate transporter 8 mutations identified in patients with X-linked psychomotor retardation and elevated serum triiodothyronine. J Clin Endocrinol Metab. 2007;92(6):2378-81.
15. Jansen J, Friesema EC, Kester MH, Schwartz CE, Visser TJ. Genotype-phenotype relationship in patients with mutations in thyroid hormone transporter MCT8. Endocrinology. 2008;149(5):2184-90.
16. Lu JM, Bush DR. His-65 in the proton-sucrose symporter is an essential amino acid whose modification with site-directed mutagenesis increases transport activity. Proc Natl Acad Sci U S A. 1998;95(15):9025-30.
17. Fujisawa Y, Tateoka R, Nara T, Kamo N, Taira T, Miyauchi S. The extracellular pH dependency of transport activity by human oligopeptide transporter 1 (hPEPT1) expressed stably in Chinese hamster ovary (CHO) cells: a reason for the bell-shaped activity versus pH. Biol Pharm Bull. 2006;29(5):997-1005.
18. Kuze K, Graves P, Leahy A, Wilson P, Stuhlmann H, You G. Heterologous expression and functional characterization of a mouse renal organic anion transporter in mammalian cells. J Biol Chem. 1999;274(3):1519-24.
19. Izuhara K, Okubo K, Hamasaki N. Conformational change of band 3 protein induced by diethyl pyrocarbonate modification in human erythrocyte ghosts. Biochemistry. 1989;28(11):4725-8.
20. Hamasaki N, Izuhara K, Okubo K, Kanazawa Y, Omachi A, Kleps RA. Inhibition of chloride binding to the anion transport site by diethylpyrocarbonate modification of Band 3. J Membr Biol. 1990;116(1):87-91.
21. Takazaki S, Abe Y, Yamaguchi T, Yagi M, Ueda T, Kang D, et al. Mutation of His 834 in human anion exchanger 1 affects substrate binding. Biochim Biophys Acta. 2010;1798(5):903-8.
22. Asaka J, Terada T, Tsuda M, Katsura T, Inui K. Identification of essential histidine and cysteine residues of the H+/organic cation antiporter multidrug and toxin extrusion (MATE). Mol Pharmacol. 2007;71(6):1487-93.

23. Miles EW. Modification of histidyl residues in proteins by diethylpyrocarbonate. Methods Enzymol. 1977;47:431-42.
24. Cheng KC, Nowak T. A histidine residue at the active site of avian liver phosphoenolpyruvate carboxykinase. J Biol Chem. 1989;264(33):19666-76.
25. Friesema EC, Kuiper GG, Jansen J, Visser TJ, Kester MH. Thyroid hormone transport by the human monocarboxylate transporter 8 and its rate-limiting role in intracellular metabolism. Mol Endocrinol. 2006;20(11):2761-72.
26. Mol JA, Visser TJ. Synthesis and some properties of sulfate esters and sulfamates of iodothyronines. Endocrinology. 1985;117(1):1-7.
27. Friesema EC, Jansen J, Jachtenberg JW, Visser WE, Kester MH, Visser TJ. Effective cellular uptake and efflux of thyroid hormone by human monocarboxylate transporter 10. Mol Endocrinol. 2008;22(6):1357-69.
28. Kaback HR. Use of site-directed mutagenesis to study the mechanism of a membrane transport protein. Biochemistry. 1987;26(8):2071-6.
29. Poolman B, Royer TJ, Mainzer SE, Schmidt BF. Lactose transport system of Streptococcus thermophilus: a hybrid protein with homology to the melibiose carrier and enzyme III of phosphoenolpyruvate-dependent phosphotransferase systems. J Bacteriol. 1989;171(1):244-53.
30. Vaurs-Barriere C, Deville M, Sarret C, Giraud G, Des Portes V, Prats-Vinas JM, et al. Pelizaeus-Merzbacher-Like disease presentation of MCT8 mutated male subjects. Ann Neurol. 2009;65(1):114-8.
31. Capri Y, Friesema EC, Kersseboom S, Touraine R, Monnier A, Eymard-Pierre E, et al. Relevance of different cellular models in determining the effects of mutations on SLC16A2/MCT8 thyroid hormone transporter function and genotype-phenotype correlation. Hum Mutat. 2013;34(7):1018-25.

Chapter

The Role of Arg445 and Asp498 in the Human Thyroid Hormone Transporter MCT8

2.3

Stefan Groeneweg, Edith C. H. Friesema, Simone Kersseboom, Wim Klootwijk, W. Edward Visser, Robin P. Peeters, Theo J. Visser

Endocrinology. 2014 Februari;155(2):618-626.

ABSTRACT

Monocarboxylate transporter 8 (MCT8) facilitates cellular influx and efflux of the thyroid hormones (THs) T4 and T3. Mutations in MCT8 lead to severe psychomotor retardation. Here, we studied the importance of 2 highly conserved residues (Arg445 in transmembrane domain 8 and Asp498 in transmembrane domain 10) for substrate recognition and helix interactions. We introduced single and double mutations (R445A, R445C, R445D, R445K, D498A, D498E, D498N, D498R, R445A+D498A, R445D+D498R, and R445K+D498E) in human MCT8 cDNA and studied the effects on MCT8-mediated TH uptake and metabolism in transfected cells. The impact of these mutations on MCT8 protein expression, dimerization capacity, and subcellular localization was studied by Western blotting and confocal microscopy. We found that mutations in Arg445 or Asp498 that alter the local charge resulted in a near-complete loss of TH uptake capacity, whereas the expression, stability, and subcellular localization of these mutant proteins was similar to those for wild-type MCT8. Given the impaired TH uptake, TH efflux could not be adequately studied. The importance of opposite charges at Arg445 and Asp498 was studied by exchanging these residues (R445D+D498R). In particular, T4 uptake was less severely reduced by the exchange mutation than by the single mutations. Mutations of Arg445 and Asp498 to equally charged residues (R445K and/or D498E) resulted in TH uptake levels similar to wild-type MCT8. The presence of 2 oppositely charged residues at positions Arg445 and Asp498 that are predicted in close structural proximity is crucial for efficient TH uptake, which may indicate the presence of an, at least transient, charge pair between these residues.

INTRODUCTION

Thyroid hormone (TH) is essential for normal brain development. Two forms of TH exist; the prohormone T4 is the main product secreted by the thyroid gland, whereas the active hormone T3 is largely produced in peripheral tissues by deiodination of T4. Because TH receptors and deiodinating enzymes are located intracellularly, transmembrane transporters are required to facilitate TH action and metabolism (1-3). One of the transmembrane transporters involved in this process is the monocarboxylate transporter 8 (MCT8, SLC16A2) (4). Mutations in the MCT8 gene lead to severe psychomotor retardation known as the Allan-Herndon-Dudley syndrome (AHDS). Characteristically, patients with AHDS have high serum T3 levels combined with low T4 levels and somewhat increased TSH levels (5, 6).

So far, only limited data are available regarding the structure of the MCT8 protein. More detailed insights into the structure of the MCT8 protein are necessary for the identification of specific functional domains involved in substrate recognition, protein stability, subcellular localization, and protein-protein interactions. Studies on these aspects will provide a better understanding of the variation in clinical phenotype and residual transport function caused by MCT8 mutations in patients with AHDS (7, 8).

The MCT8 protein has been predicted to have 12 transmembrane domains (TMDs) and an intracellular N terminus and C terminus (9). The strong conservation of Arg445 in TMD8 among all MCT members and the very specific conservation of Asp498 in TMD10 of MCT8 and MCT10 indicate an important function for both residues. Using different TMD prediction programs, Arg445 and Asp498 in MCT8 are consistently predicted within TMD8 and TMD10, respectively. These are remarkable locations for these charged amino acids, which are preferably located outside TMDs.

Furthermore, the homology model of the human (h) MCT8 protein, based on the crystal structure of the Escherichia coli glycerol-3-phosphate transporter (GlpT), suggests an important role for Arg445 in TMD8 and Asp498 in TMD10 in substrate recognition and translocation (9). Both residues are predicted to be located in close structural proximity within the putative substrate channel (9). The importance of Arg445 and D498 is illustrated by the fact that mutations in both residues (R445C and D498N) have been identified in patients with AHDS (10, 11).

Recently, His415 and Arg301 have been suggested to form an Arg-His clamp that orients substrates when entering or leaving the substrate channel of MCT8 from the intracellular side (12). In addition, His192 may participate in the formation of a second substrate-binding site together with Arg445 or Lys416 at the extracellular aspect of the protein (12, 13).

Here, we demonstrate that mutations in Arg445 or Asp498 that alter the local charge resulted in a near-complete loss of TH uptake capacity, whereas exchanging Arg445 and Asp498 has a less dramatic effect on TH uptake. Furthermore, we show that the residual TH uptake capacity depends not only on the presence of the correct charge at position 445 and 498 but also on the distance between these charged residues, suggesting the presence of an, at least transient, interaction between Arg445 and Asp498, important for MCT8 function.

MATERIALS AND METHODS

Materials

Unlabeled iodothyronine derivatives were obtained from Sigma-Aldrich (Zwijndrecht, The Netherlands). [125I]T3, [125I]T4, [125I]T3 sulfate (T3S), [125I]triiodothyroacetic acid (Triac), and [125I]tetraiodothyroacetic acid (Tetrac) were synthesized as described previously (14). Oligonucleotides were obtained from Integrated DNA Technologies, QuikChange XL-II Site-Directed Mutagenesis Kits were from Stratagene, transfection reagent X-tremeGENE 9 was from Roche, culture dishes were from Corning, SDS gels were from Thermo Fisher, nitrocellulose membrane was from GE Healthcare, BSA, D-glucose, MG132, and Na2SeO3 were from Sigma-Aldrich, and DMEM/F12 + GlutaMAX medium, fetal bovine serum, and penicillin/streptomycin were from Invitrogen.

Plasmids and site directed mutagenesis

pcDNA3-hMCT8, pCIneo-hD3, and pSG5-hCRYM plasmids were obtained as described previously (15, 16). hCRYM (μ-crystallin) is a cytoplasmic TH-binding protein, which greatly reduces the efflux of TH, thereby increasing the net cellular TH uptake.

We introduced the / Arg445 and Asp498 mutations in wild-type (WT) hMCT8 cDNA using the QuikChange protocol: R445A, R445C, R445D, R445K, D498A, D498E, D498N, and D498R. We also generated 3 double MCT8 mutants (R445A+D498A, R445D+D498R, and R445K+D498E) by introducing a second mutation in the single mutant construct. Primer information is provided in **Supplemental Table 1**. DNA sequencing was performed to confirm the presence of the mutations introduced.

Cell culture and transfection

JEG3 cells and COS1 cells were cultured in DMEM/F12 + GlutaMAX medium containing 9% heat-inactivated fetal bovine serum, 2% penicillin/streptomycin, and 100 nM Na2SeO3. For TH transport studies, cells were cultured in 6-well plates and co-transfected in duplicate at 75% confluence with 500 ng of WT or mutant pcDNA3-hMCT8 and 500 ng of pSG5-hCRYM. For metabolism studies, COS1 and JEG3 cells were cultured in 24-well plates and co-transfected in duplicate with 100 ng of WT or mutant pcDNA3-hMCT8 and 100 ng of pCIneo-hD3. Empty pcDNA3 vector was used as a control, and X-tremeGENE 9 was used as a transfection agent according to the manufacturer's protocol.

TH transport experiments

At 48 hours after transfection, cells were washed with 2 mL of incubation medium (Dulbecco's PBS containing 0.1% D-glucose and 0.1% BSA) and incubated for 30 minutes (unless indicated otherwise) at 37°C with 1 nM (1 × 105 cpm) [125I]T3, [125I]T4, [125I]T3S, [125I]Triac, or [125I]Tetrac in 1.5 mL of incubation medium. After incubation, cells were washed with incubation medium and lysed with 1 mL of 0.1 M NaOH. Radioactivity in the lysates was measured in a gamma counter.

TH metabolism assay

At 48 hours after transfection, cells were washed with 0.5 mL of incubation medium, and incubated for 4 hours at 37°C with 1 nM (5 × 105 cpm) [125I]T3 or for 8 hours with 1 nM (5 × 105 cpm) [125I]T4 in 0.25 mL of incubation medium. For analysis of TH metabolites, 100 μL of medium was mixed with 100 μL of ethanol and incubated for 30 minutes on ice. After centrifugation, 100 μL of supernatant was

added to 100 µL of 0.02 M ammonium acetate (pH 4.0), and 100 µL of the mixture was analyzed by HPLC as described previously (15).

Western blotting

Cells cultured in 6-well plates were transfected with 500 ng of WT or mutant pcDNA3-hMCT8 or pcDNA3 empty vector. If indicated, we added 1 µmol of MG132 to the incubation medium 24 hours after transfection to inhibit proteasomal degradation. At 48 hours after transfection, cells were rinsed with PBS and collected in 100 µL of 0.1 M phosphate buffer (pH 7.2) and 2 mM EDTA (P100E2). The cells were sonicated on ice and stored at −80°C until use. Total protein concentrations were determined with the Bradford assay, using the manufacturer's protocol (Bio-Rad Laboratories). After heating for 10 minutes at 80°C in the presence of 40 mM dithiothreitol, 25 µg of protein was separated on 12% SDS-PAGE gels, blotted onto nitrocellulose membranes, washed for 2 hours at 37°C in PBS containing 0.1% Tween 20 and 5% milk, and probed overnight at 4°C with rabbit polyclonal antibody 3353 against hMCT8 amino acids 75 to 155 (1:20 000; Sigma-Aldrich) or with mouse monoclonal GAPDH antibody (Mab 374, 1:20 000; Millipore), as a loading control. Next, the blots were incubated for 1.5 hours at room temperature with IRDye680 goat anti-rabbit and IRDye800 goat anti-mouse antibodies (1:20 000; LI-COR). Antibodies were detected with the Odyssey infrared detection system (LI-COR).

Immunocytochemistry

JEG3 and COS1 cells were cultured in 6-well dishes on 20-mm glass coverslips coated with poly-D-lysine (Sigma-Aldrich) and transfected with 500 ng of WT or mutant pcDNA3-hMCT8. After 24 hours, cells were fixed for 20 minutes at 37°C with 4% paraformaldehyde in PBS and permeabilized for 5 minutes at room temperature with 0.2% Triton X-100 in PBS. Samples were washed for 1 hour at room temperature in PBS containing 2% BSA and incubated overnight at 4°C with MCT8 antibody 3353 (1:1000), and mouse monoclonal ZO-1 antibody (1:50; Invitrogen). After being stained with goat anti-rabbit Alexa Fluor 488 and goat anti-mouse Alexa 633 (1:1000; Invitrogen), coverslips were mounted with Vectashield H-1200 containing 4’,6-diamidino-2-phenylindole (Brunschwig). Samples were examined on a Zeiss Meta 510 microscope using Zeiss LSM software (Carl Zeiss). A Plan Neofluar 40× 1.3 oil objective and lasers with 405, 488, and 633 nm wavelengths were used.

Statistical analysis

All uptake and metabolism results are expressed as means ± SD of at least 2 to 4 separate experiments in duplicate. Statistical significance was determined as indicated in the legends of the corresponding figures.

RESULTS

MCT8 protein is predicted to have 12 TMDs and an intracellular N terminus and C terminus (9). Here, we focused on the Arg445 (TMD8) and Asp498 (TMD10) residues of the MCT8 protein, which are highly conserved among different species (**Supplemental Table 2**). Furthermore, Arg445 is conserved in all members of the MCT family, whereas D498 is only present in MCT8 and MCT10, the only MCT family members known to transport TH.

We generated the following MCT8 mutants: R445A and D498A (charged residues substituted by neutral residues), R445C and D498N (as identified in patients with AHDS) (10, 11), R445D and D498R (substitution by oppositely charged residues), and 2 double mutants (R445A+D498A and R445D+D498R). In the latter, the Arg and Asp residues have been exchanged. To evaluate the effect of these mutations on MCT8-mediated TH transport, we performed TH uptake assays in transiently transfected COS1 cells. Transfection with WT MCT8 resulted in a 5- to 7-fold induction of T3 and T4 uptake over that in cells transfected with empty vector (data not shown). After correction for background TH uptake by endogenous transporters, no TH uptake was observed in COS1 cells expressing the D498A, D498N, D498R, or R445A+D498A mutants (**Figure 1A**). In contrast, the R445A, R445C, and R445D+D498R mutants showed significant T4 and T3 uptake, whereas only T3 uptake was significant in the R445D mutant. Interestingly, the exchange of Arg445 and Asp498 in the R445D+D498R double mutant has a less dramatic effect on TH uptake, in particular that of T4, than the D498R single mutation.

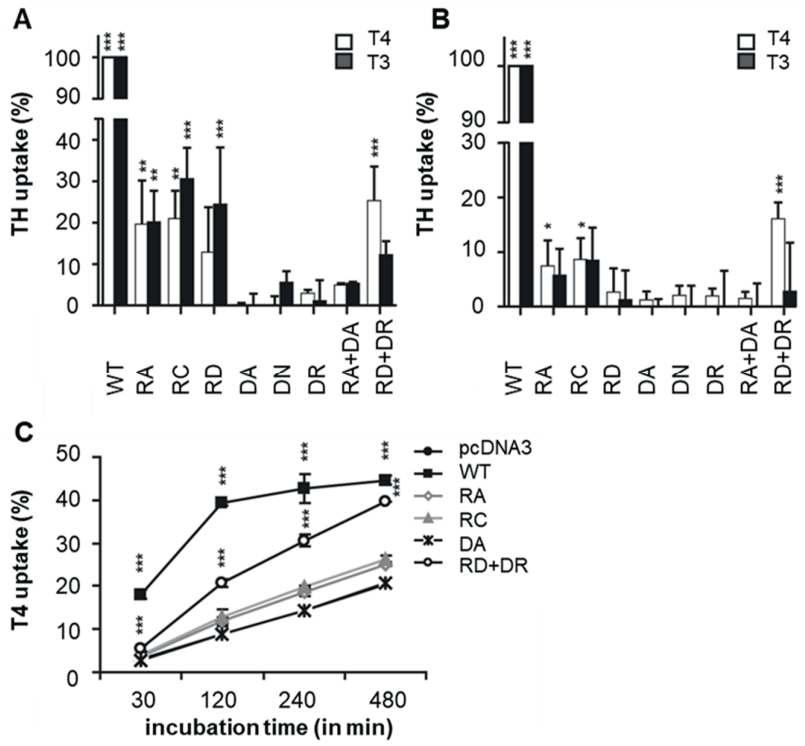

Figure 1 T3 and T4 uptake by COS1 (**A**) and JEG3 (**B**) cells cotransfected with WT or mutant hMCT8 and hCRYM cDNA after incubation for 30 minutes at 37°C. All values are corrected for background TH uptake levels observed in COS1 and JEG3 cells transfected with pcDNA3 empty vector (EV). TH uptake by MCT8 mutants is expressed relative to WT MCT8-mediated TH uptake. **C**, T4 uptake in JEG3 cells transfected with WT or mutant hMCT8 and hCRYM cDNA after incubation for the indicated times at 37°C. T4 uptake is expressed relative to the amount of T4 added to the cells at the start of the incubation. All results are presented as means ± SD (n = 3–4). *, P < .05; **, P < .01; ***, P < .001 compared with background using a one-way ANOVA analysis with a Dunnett posttest. RA, R445A; RC, R445; RD, R445D; DA, D498A; DN, D498N; DR, D498R; RA+DA, R445A+D498A; RD+DR, R445D+D498R.

Because endogenous MCT8 expression in COS1 cells may interfere with the function of transfected MCT8 constructs, we also tested TH uptake by WT and mutant MCT8 constructs in JEG3 cells that lack endogenous MCT8 expression (15). Transfection of JEG3 cells with WT MCT8 resulted in a 5-fold

increase in T4 and T3 uptake (data not shown). Once more, a complete loss of MCT8-mediated TH uptake was observed for the D498A, D498N, D498R, and R445A+D498A mutants (**Figure 1B**). TH uptake by the R445A and R445C mutants was further decreased in JEG3 cells and became insignificant for the R445D mutant. Appreciable T4 uptake by the R445D+D498R double mutant was still observed in JEG3 cells, but T3 uptake became undetectable.

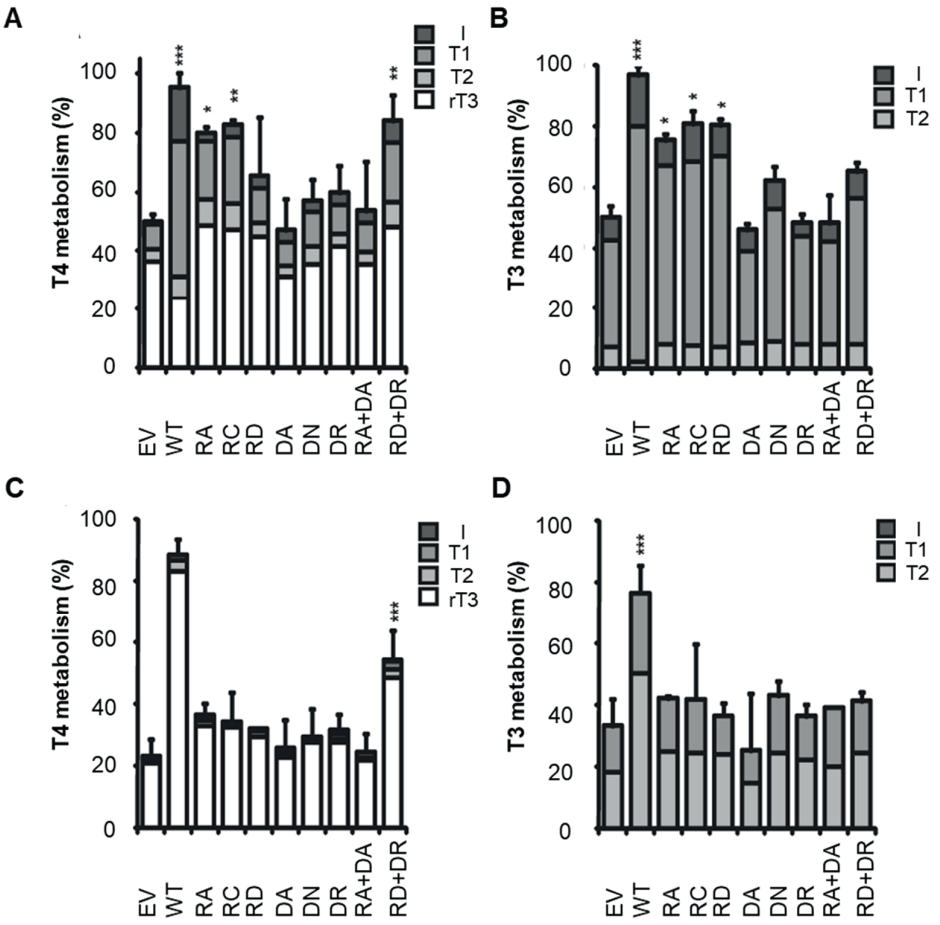

Figure 2 Metabolism of T4 and T3 in COS1 (**A** and **B**) and JEG3 cells (**C** and **D**) cotransfected with hD3 and pcDNA3 empty vector (EV), WT, or mutant MCT8 and incubated for 4 hours with 1 nM [125I]T3 or for 8 hours with [125I]T4 at 37°C. Metabolism is shown as a percentage of the different metabolites relative to the total amount of T3 or T4 added to the cells at the start of the incubation. Results are the means of at least 3 independent experiments performed in duplicate. Metabolism in cells expressing WT or mutant MCT8 was compared with that of cells transfected with EV using a one-way ANOVA analysis with a Dunnett posttest: *, $P < .05$; **, $P < .01$; ***, $P < .001$.

To analyze the dynamics of T4 uptake, we tested the effects of increasing incubation times on T4 uptake by JEG3 cells expressing WT MCT8 and different mutants in comparison with control cells transfected with empty vector. WT MCT8 showed a large induction of T4 uptake in the first 2 hours with no further increase after 4 hours (**Figure 1C**). T4 uptake by the R445D+D498R double mutant was only 20% of that of the WT after 30 minutes of incubation, whereas it approximated WT levels with prolonged incubation. This was not observed for the R445A and R445C single mutants, which showed

only minor increases in T4 uptake at all time-points. The D498A mutant was completely inactive at all time-points (**Figure 1C**).

The intracellular metabolism of TH is highly dependent on the rate of TH transport across the cell membrane (15). To study the capacity of the Arg445 and Asp498 mutants to increase intracellular TH availability, we studied TH metabolism in COS1 (**Figure 2, A** and **B**) and JEG3 (**Figure 2, C** and **D**) cells co-transfected with type 3 deiodinase (D3) and WT or mutant MCT8. In agreement with previous work, we observed a highly significant increase in T3 and T4 metabolism in both cell lines upon co-transfection of D3 with WT MCT8 (**Figure 2, A–D**). Because COS-1 cells express type 1 deiodinase endogenously, outer ring deiodination (of the reverse T3 and 3,3'-T2 metabolites) was also observed (15). In COS1 cells, the R445A, R445C, and R445D+D498R mutants increased T4 metabolism over background, whereas the R445A, R445C, and R445D mutants increased T3 metabolism (**Figure 2, A** and **B**). No other mutants significantly enhanced TH metabolism over background. However, in JEG3 cells, only the R445D+D498R double mutant increased T4 metabolism (**Figure 2C**), whereas none of the mutants induced T3 metabolism (**Figure 2D**).

To further study the importance of a positive charge at position 445 and a negative charge at position 498, we substituted Arg445 by an equally charged Lys residue (R445K) and Asp498 by an equally charged Glu residue (D498E), and we also generated a double mutant containing both substitutions (R445K+D498E). In JEG3 cells, the R445K mutant showed 30% lower T3 and T4 uptakes than WT MCT8. The D498E mutant and the R445K+D498E double mutant showed only insignificant differences compared with WT MCT8 (**Figure 3A**). Moreover, all 3 mutants facilitated T3 and T4 metabolism by D3 to extents similar to that of as WT MCT8 (**Figure 3, B** and **C**). Similar results were obtained in COS1 cells (**Supplemental Fig. 1, A–C**).

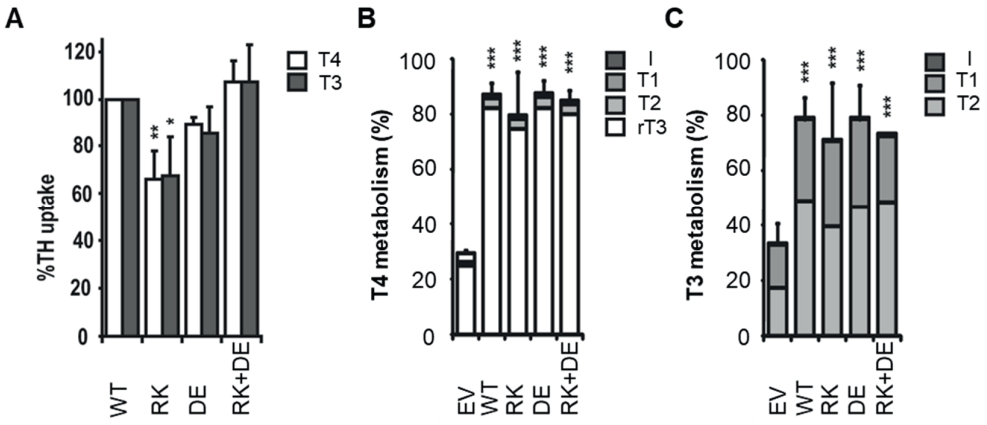

Figure 3 A, T3 and T4 uptake by JEG3 cells transfected with WT or mutant hMCT8 and hCRYM cDNA after incubation for 30 minutes at 37°C. All values are corrected for background TH uptake levels observed in JEG3 cells transfected with pcDNA3 empty vector (EV). TH uptake by MCT8 mutants is expressed relative to WT MCT8-mediated TH uptake. Results are presented as means ± SD (n = 2–4). *, P < .05; **, P < .01 compared with WT using a one-way ANOVA analysis with a Dunnett posttest. B and C, T4 (**B**) and T3 (**C**) metabolism in JEG3 cells cotransfected with hD3 and pcDNA3 EV, WT, or mutant hMCT8 and incubated for 4 hours with 1 nM [125I]T3 or for 8 hours with [125I]T4 at 37°C. Metabolism is shown as the percentage of T3 and T4 added to the cells at the start of the incubation. Results are the means of at least 3 independent experiments in duplicate. Metabolism in cells expressing WT or mutant MCT8 was compared with that of cells transfected with EV using a one-way ANOVA analysis with a Dunnett posttest: ***, P < .001. RK, R445K; DE, D498E; RK+DE, R445K+D498E.

Western blotting of total cell lysates of JEG3 and COS1 cells expressing WT or mutant MCT8 revealed bands around 55 and 110 kDa, corresponding to the predicted masses of the MCT8 monomer and homodimer, respectively (**Figure 4** and **Supplemental Fig. 2A**). Some differences in protein expression levels and monomer to dimer ratios between WT and mutant MCT8 were observed. In particular, expression of the R445D mutant was strongly decreased compared with that of WT MCT8 in both cell lines. This decrease could not be prevented by addition of MG132, a potent inhibitor of proteasomal protein degradation (**Supplemental Fig. 2B**). Remarkably, MCT8 protein expression levels were lower in JEG3 cells than in COS1 cells despite similar MCT8-induced TH transport rates in these cell lines.

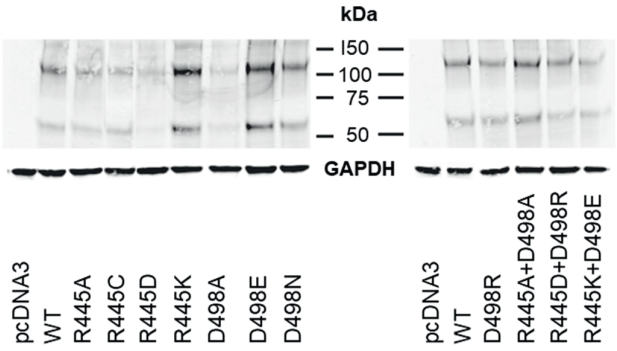

Figure 4 Representative Western blot of total lysates from JEG3 cells transfected with pcDNA3 empty vector, WT, or mutant hMCT8. MCT8 detection was performed with the N-terminal hMCT8 antibody (3353), which was visualized with IRDye680 goat anti-rabbit secondary antibody. GAPDH was used as loading control. A band of approximately 55 kDa, representing the hMCT8 monomer and a second band around 110 kDa representing the hMCT8 homodimer were observed in cells transfected with WT or mutant hMCT8 constructs (n = 3).

Given their predicted channel-facing side chains, Arg445 and Asp498 may partially determine the substrate selectivity of MCT8. Because most mutations in Arg445 and Asp498 resulted in functionally inactive MCT8 proteins, we were not able to determine adequate Km values for T3 and T4 transport by these mutants. Instead, we studied whether Arg445 and Asp498 may be involved in the exclusion of the TH metabolites Triac, Tetrac, and T3S as substrates for MCT8. Similar to WT MCT8, none of the tested mutants showed significant uptake of these substrates in COS1 cells (**Supplemental Fig. 3, A** and **B**).

Finally, we analyzed whether mutations of Arg445 and Asp498 impair MCT8 trafficking to the plasma membrane in transiently transfected JEG3 cells by confocal microscopy. All mutants tested showed a distribution pattern similar to that of WT MCT8, which, at least partially, followed the same distribution pattern as the plasma membrane marker ZO-1, suggesting proper plasma membrane localization (**Figure 5**). Similar distribution was observed in COS1 cells (data not shown).

DISCUSSION

Here, we showed that the charged residues Arg445 and Asp498 within MCT8 are crucial for efficient TH transport. Mutations of these residues, ie, R445C and D498N, have previously been reported in patients with AHDS (10, 11). Mutations of Arg445 and Asp498 that alter the local charge resulted in a (near) complete loss of TH uptake capacity of MCT8. The exchange of Arg445 and Asp498 or their

substitution by equally charged residues had less dramatic effects on the functionality of the resultant mutant proteins. We demonstrated that not only charge but also distance between these 2 charged groups is essential for proper MCT8 function. Moreover, protein expression levels of the Arg445 or Asp498 mutants were grossly similar to those of the WT, and all mutant proteins were expressed at the plasma membrane. Taken together, these findings support the presence of an, at least transient, interaction between Arg445 and Asp498, important for MCT8 function.

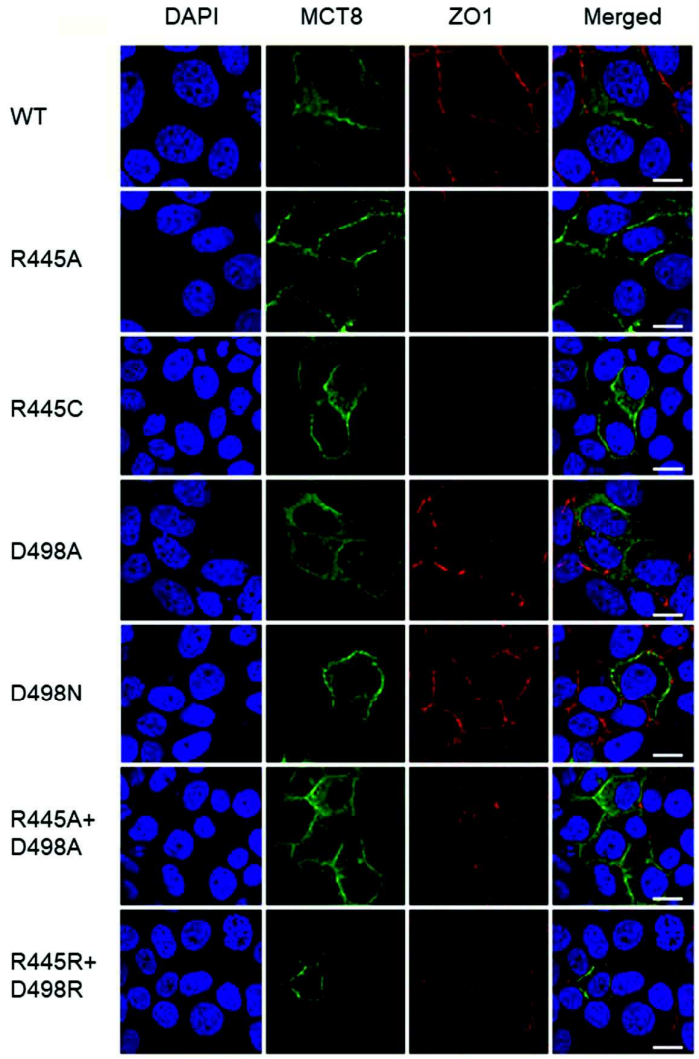

Figure 5 Cellular distribution of WT and mutant hMCT8 in JEG3 cells. Nuclear staining with 4',6-diamidino-2-phenylindole is presented in the first panel in blue, staining of MCT8 with Alexa 488 in the second panel in green, and staining of the cell membrane marker ZO-1 with Alexa 633 in the third panel in red. The fourth panel shows the merged image of all stainings. Scale bars correspond to 4 µm.

MCT8 and MCT1 are assumed to have a high degree of structural homology. A homology model of MCT1 based on the crystal structure of E. coli GlpT, and results of subsequent studies suggest important roles for Asp302 and Arg306 in TMD8 and Phe360 in TMD10, which are predicted to be located in close structural proximity (17, 18). Moreover, it has been shown that a charge pair between Asp302 and Arg306 plays an important role in protein folding and substrate translocation and

selectivity of MCT1 (19). Although the Arg residue in TMD8 has been conserved in MCT8 (Arg445), MCT8 lacks an Asp residue in TMD8. However, MCT8 contains an Asp at the position corresponding to Phe360 of MCT1 (Asp498). Assuming structural homology between MCT1 and MCT8, Arg445 and Asp498 are likely to be located within close structural proximity and have channel-facing side chains. This hypothesis was further supported by a recently published MCT8 homology model, also based on E. coli GlpT (9).

Our results strongly suggest that a balanced positive and negative charge at positions 445 and 498 is a prerequisite for efficient TH transport by MCT8, because transport is strongly reduced if this balance is disrupted. Interestingly, significant TH uptake is preserved if the balance is maintained by exchanging residues Arg445 and Asp498 (R445D+D498R). Although initial T4 uptake by the R445D+D498R mutant after up to 60 minutes of incubation is markedly decreased, accumulation of cellular T4 after prolonged incubation approximates that obtained with WT MCT8. The significance of this finding depends on whether MCT8 is crucial for the maintenance of steady-state intracellular TH levels or for more acute adaptations in local TH concentrations. This is an important question that needs to be addressed in future studies. However, except for the mild R445K and D498E mutations, the exchange mutation (R445D+D498R) is less severe than all the other R445 and D498 mutations. TH metabolism experiments confirmed the TH uptake results, because only the R445K, D498E, R445K+D498E, and R445D+D498R mutants increased the intracellular availability of T4 for D3-mediated metabolism to extents similar to that with WT MCT8. Although the R445A and R445C mutants showed low levels of TH uptake in JEG3 cells, no increase in TH metabolism was observed over background. These findings suggest that both mutations have less impact on TH efflux than TH uptake, resulting in a small increase in the intracellular TH levels available for metabolism by D3. However, given the impact of these mutations on TH uptake, intracellular TH levels were insufficient to adequately study TH efflux as described previously (15).

Interestingly, the R445K mutant showed a 30% reduction in TH uptake compared with that for WT MCT8, whereas the R445K+D498E mutant was as active as WT MCT8. These results may be explained by the shorter side chain of Lys compared with Arg. Although the ϵ-ammonium group of Lys forms better hydrogen bridges than the δ-guanidinium group of Arg with the side chain carboxylate groups of Asp and Glu, the larger distance between the charged groups of Lys445 and Asp498 may weaken their interaction. This interaction may be improved by the simultaneous D498E mutation because the longer side chain of Glu may compensate for the shorter side chain of Lys. Taken together, our findings suggest a crucial, at least transient, interaction between Arg445 and Asp498 which may be involved in the conformational changes in MCT8 required for TH transport. Furthermore, these results support the close spatial distance between Arg445 and Asp498 as predicted by the MCT8 homology model of Kinne et al (9). Evidence supporting a similar mechanism in MCT1 and GlpT has already been published (19, 20). Interactions between charged residues have also been shown, for instance, in the TSH receptor, where a salt bridge between Lys183 and Glu157 is crucial for receptor function (21). Here also, exchange of these residues results in a mutant protein with substantial TSH receptor activity.

The exact geometry of the charged residues at positions 445 and 498 in MCT8 appears to be more crucial for T3 uptake than for T4 uptake. None of the mutants in which the local charge at these positions was changed was able to facilitate T3 uptake, even though some of these mutants showed residual T4 uptake. This discrepancy between residual T3 and T4 uptake may have important clinical implications, because some mutations may lead to a complete block in T3 and T4 transport, whereas others still allow significant residual T3 or T4 uptake. It has been shown that T4 uptake by mouse

Oatp1C1 in the brain of Mct8 knockout mice prevents the severe neurological impairments observed in human patients with AHDS (22-26). Hence, a patient with AHDS with mutations in MCT8 that allow some residual T4 uptake may present with a less severe neurological phenotype. However, because the R445C and D498N mutations are the only mutations in these residues that have been identified in patients, we are not able to support this hypothesis with strong clinical evidence. It is also possible that other mutations have a greater inhibitory effect on T4 than on T3 transport, although again such mutations have not been identified yet in patients with AHDS.

Besides a possible role during substrate transition, the putative interaction between Arg445 and Asp498 might also be important for substrate recognition. Because most mutations of Arg445 and Asp498 result in a near-complete inactivation of MCT8, it was not possible to study their impact on the apparent Km values for T3 and T4. These values could have indicated whether the substrates directly interact with Arg445 or Asp498. However, modification of Cys497 by p-chloromercurybenzenesulfonate (pCMBS) has been shown to result in decreased TH transport, whereas the C497A mutation itself has no effect on TH transport. Moreover, the effect of pCMBS is prevented in the presence of T3 (27). Taken together, these findings suggest that modification of Cys497 with pCMBS interferes with the interaction of substrate with important residues in the MCT8 transport cavity. Given the close structural proximity of Asp498 and Cys497, Asp498 is clearly one of the candidate residues that play an important role in substrate interaction and selection.

Mutation of the Phe360 residue in MCT1 allows MCT1 to transport larger substrates (18). Therefore, we analyzed the effect of mutations in R445 or D498 on the exclusion of the TH analogs Triac and Tetrac and the TH metabolite T3S as substrates for MCT8. It has been shown previously that cellular uptake of these substrates is not mediated by WT MCT8 (9). Our data indicate that the charged side chains of R445 and D498 are at least not crucial in the exclusion of these substrates for transport by MCT8.

Many proteins require interactions with ancillary proteins for proper cellular localization and trafficking. It has been shown previously that the ancillary proteins embigin and basigin facilitate membrane localization of MCT1, MCT2, MCT3, and MCT4 (19, 28-30). These interactions are likely to be mediated via charged amino acids within the TMDs of these MCTs, because mutations in these residues resulted in impaired plasma membrane expression (19). However, there is no evidence for a role of embigin and basigin in plasma membrane localization of MCT8 (31). In addition to their role in interactions with ancillary proteins, charged residues in TMDs might also be important for protein dimerization or proper protein folding. It has been shown that misfolding of integral membrane proteins such as cystic fibrosis transmembrane conductance regulator (CFTR) could result in impaired cellular trafficking and increased degradation due to protein instability (32, 33).

Although the Western blot and immunofluorescence data do not allow exact comparative quantification, all mutants were at least clearly expressed at the protein level and translocated to the plasma membrane. Furthermore, all Arg445 and Asp498 mutant proteins showed homodimerization. In general, only small variations in protein expression levels were observed, except for R445D, levels of which were strongly reduced in both COS1 and JEG3 cells, and D498A, expression of which was only reduced in JEG3 cells. The positioning of 2 negatively charged amino acids in close proximity in the R445D mutant protein may destabilize the MCT8 protein and enhance its degradation. However, we were unable to increase R445D expression by inhibition of proteasomal degradation with MG132.

Taken together, the impact of mutations in Arg445 and Asp498 on TH uptake is unlikely to be caused by impaired protein expression, protein trafficking, homodimerization, or interactions with crucial ancillary proteins. However, mutations in Arg445 and Asp498 might still have subtle effects on protein folding, protein stability, and the regulation of MCT8 expression at the plasma membrane in the presence and absence of substrates. More sensitive methods to study the effect of mutations in Arg445 and Asp498 on protein stability, such as thermal stability assays, require purification of the MCT8 protein. However, successful purification of proteins with 12 TMDs has been rarely reported. Moreover, in our cell models we were not able to study the effects of these mutations on the polarization of MCT8 expression, which may be disturbed due to loss of interactions with putative ancillary proteins (34).

Our results further support the hypothesis that an extension of the classic rocker-switch model of substrate transport might indeed apply to MCT8 (12). According to this model, the MCT8 protein is able to alternate between an outward-facing and an inward-facing conformation, allowing substrate binding from the extracellular and intracellular sides of the transporter. A recent article by Braun et al (12) suggested the participation of an Arg301-His415 clamp in the inward-facing conformation for proper orientation of the substrate in the transporter channel at the intracellular side of the transporter. A second substrate interaction site might be present between His192 and Arg445 or Lys418 at the extracellular side of the protein. Modification or mutation of His192 has indeed been shown to strongly decrease TH uptake (12, 13). According to the MCT8 homology model published by Kinne et al (9), Arg445 is predicted to be located in close structural proximity to Asp498, which would theoretically allow salt-bridge formation. Our experimental data strongly support the existence of such a salt bridge. The integrity of this salt bridge has been suggested to play an important role in the maintenance of the inward-facing conformation in the absence of substrate at the extracellular side of the channel (12). Interactions of substrate with His192 and Arg445 or Lys418 might weaken this internal salt bridge, resulting in a conformational transition and the translocation of substrate.

In conclusion, our results support the presence of an, at least transient, charge pair between Arg445 and Asp498, important for MCT8 function. This charge pair is likely to be involved in substrate recognition or substrate-induced conformational changes, rather than the maintenance of a stable tertiary protein structure or interactions with other proteins

Acknowledgements

The authors received no special funding for this work.

Disclosure Summary: The authors have nothing to disclose.

SUPPLEMENTARY DATA

See next page.

Supplemental tables

Supplemental table S1 Primer list for mutagenesis reactions		
Mutant	**Primer**	**Sequence**
R445A	Forward	5'-GCTACCTCAGGCCTTGGG**GC**TCTTGTGTCAGGCC-3'
	Reverse	5'-GGCCTGACACAAGA**GC**CCCAAGGCCTGAGGTAGC-3'
R445C	Forward	5'-CCTCAGGCCTTGGG**T**GTCTTGTGTCAGGC-3'
	Reverse	5'- GCCTGACACAAGAC**A**CCCAAGGCCTGAGG-3'
R445D	Forward	5'-GCTACCTCAGGCCTTGGG**GA**TCTTGTGTCAGGCC-3'
	Reverse	5'-GGCCTGACACAAGA**TC**CCCAAGGCCTGAGGTAGC-3'
R445K	Forward	5'-GCTACCTCAGGCCTTGGG**A**A**G**CTTGTGTCAGGCCACATC-3'
	Reverse	5'-GATGTGGCCTGACACAAG**C**T**T**CCCAAGGCCTGAGGTAGC-3'
D498A	Forward	5'-CCTGGGCCTTTGCG**C**TGGCTTCTTCATCACC-3'
	Reverse	5'-GGTGATGAAGAAGCCA**G**CGCAAAGGCCCAGG-3'
D498E	Forward	5'-CTTTTCCTGGGCCTTTGC**G**A**G**GGCTTCTTCATCA-3'
	Reverse	5'-TGATGAAGAAGCC**C**T**C**GCAAAGGCCCAGGAAAAG-3'
D498N	Forward	5'-CCTGGGCCTTTGC**A**ATGGCTTCTTCATCACC-3'
	Reverse	5'-GGTGATGAAGAAGCCAT**T**GCAAAGGCCCAGG-3'
D498R	Forward	5'-CTTTTCTTGGGCCTTTGC**CG**TGGCTTCTTCATCACCATC-3'
	Reverse	5'-GATGGTGATGAAGAAGCCA**CG**GCAAAGGCCCAGGAAAAG-3'
Sequences of all used mutagenesis primers. Mutated nucleotides are underlined.		

Supplemental table S2 Conservation map of TMD8 and TMD10 in MCT8 among different species		
Species	**Predicted TMD8**	**Predicted TMD10**
Human	TWVLLVCIGATSGLG**R**LVSGHI	DFGGLIVVCLFLGLC**D**GFFITIMAP
Mouse	TWVLLVCIGATSGLG**R**LVSGHI	DFGGLIVVCLFLGLC**D**GFFITIMAP
Dog	TWVLLVCIGATSGLG**R**LVSGRV	GFGGLIVVCLFLGLC**D**GFFITIMAP
Elephant	TWVLLVCIGATSGLG**R**LVSGRI	GFGGLIVVCLFLGLC**D**GFFITIMAP
Chicken	DWILPVCLGGMSGLG**R**LISGRT	GFEGVIVICLFLGLC**D**GCFTTIMAP
Opossum	TWVLLVCIGATSGIG**R**LVSGRI	GFGGLIVVCLFLGLC**D**GFFTTIMAP
Zebrafish	E-VLLACIGITSGVG**R**LIFGRV	VFGGLIAVCLLMGLF**D**GCFICIMAP
Xenopus	EWVLLVCIGATSGIG**R**LASGRI	FESVIVV-CLFLGLC**D**GFLISMMSP
Alignment of the amino acid sequences of TMD8 and TMD10 of MCT8 in various species, showing high conservation of the R445 and D498 residues (bold, underlined). The multiple alignment tool of the UCSC browser was used to align the amino acid sequence of the loci of interest from different species.		

Supplemental figures

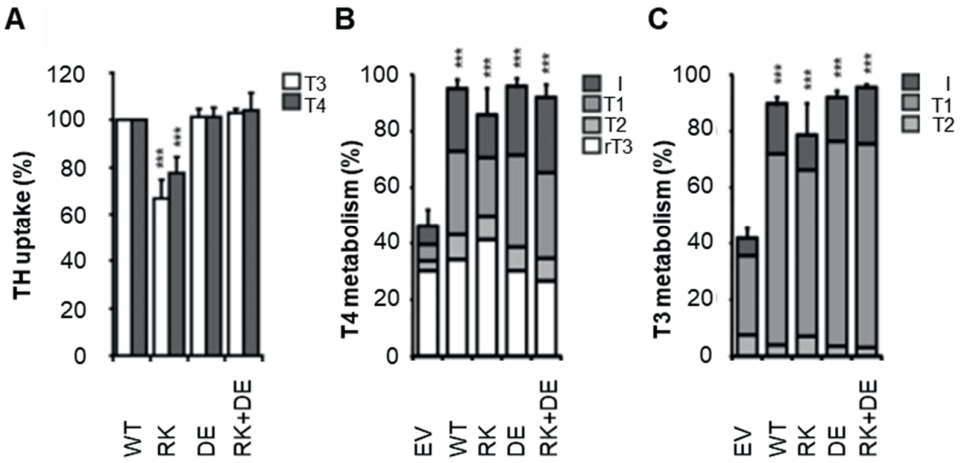

Supplemental Figure S1 (A) T3 and T4 uptake by COS1 cells co-transfected with WT or mutant hMCT8 and hCRYM cDNA after incubation for 30 min at 37 C. All values are corrected for background TH uptake observed in COS1 cells transfected with pcDNA3 EV. TH uptake by MCT8 mutants is expressed relatively to WT MCT8-mediated TH uptake. Results are presented as means ± SD (n = 2–4). *** P<0.001 compared to WT using a 1-way ANOVA analysis with Dunnett post-test. T4 (**B**) and T3 (**C**) metabolism in COS1 cells co-transfected with hD3 and pcDNA3 EV, WT or mutant hMCT8 and incubated for 4 h with 1 nM [125I]T3 or for 8 h with [125I]T4 at 37 C. Metabolism is shown as percentage of T3 and T4 added to the cells at the start of the incubation. Results are the means of at least 3 independent experiments in duplicate. Metabolism in cells expressing WT or mutant MCT8 was compared with cells transfected with EV using a 1-way ANOVA analysis with Dunnett post-test: *** P<0.001.

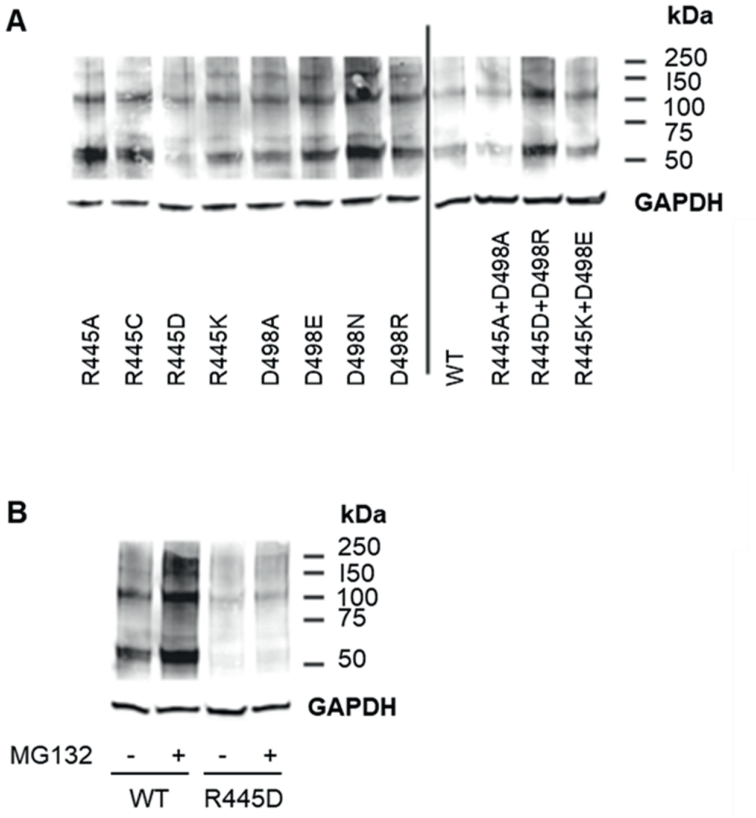

Supplemental Figure S2 (A) Western blot of total lysates from COS1 cells transfected with pcDNA3 EV, WT, or mutant hMCT8. (**B**) Western blot of lysates from COS1 cells transfected with WT or the R445D mutant hMCT8 cultured in the presence (+) or absence (-) of MG132 for 24 h. MCT8 detection was performed with the N-terminal hMCT8 antibody (3353) which was visualized with IRDye680 goat anti-rabbit secondary antibody. GAPDH was used as loading control. A band of approximately 55 kDa, representing the hMCT8 monomer and a second band around 110 kDa representing the hMCT8 homo-dimer were observed in cells transfected with WT or mutant hMCT8 constructs.

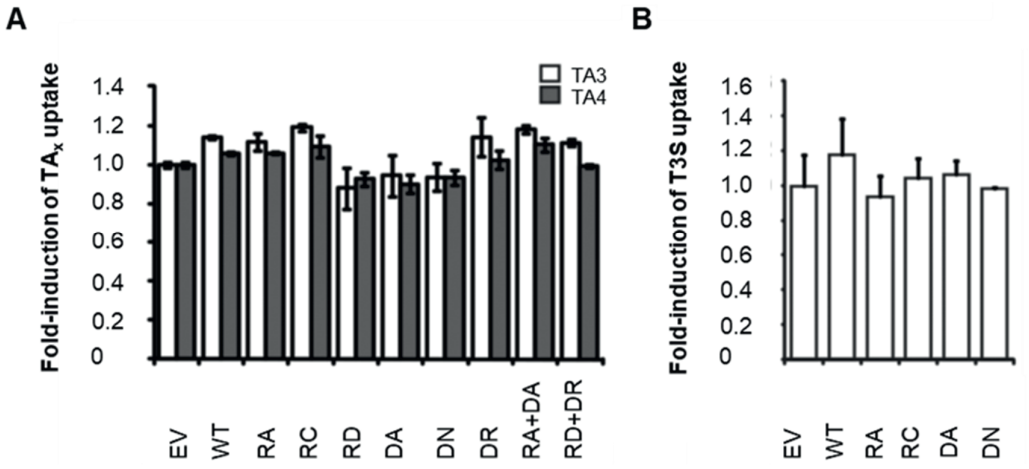

Supplemental Figure S3 (A) TA3 and TA4 and (**B**) T3S uptake by COS1 cells co-transfected with WT or mutant hMCT8, or pcDNA3 EV and hCRYM cDNA after incubation for 30 min at 37 C. Values are expressed as fold induction relative to pcDNA3 EV. Results are presented as means ± SD (n = 2-3). *** P<0.001 compared to pcDNA3 EV using a 1-way ANOVA analysis with Dunnett post-test.

REFERENCES

1. Bianco AC, Kim BW. Deiodinases: implications of the local control of thyroid hormone action. J Clin Invest. 2006;116(10):2571-9.
2. Yen PM, Ando S, Feng X, Liu Y, Maruvada P, Xia X. Thyroid hormone action at the cellular, genomic and target gene levels. Mol Cell Endocrinol. 2006;246(1-2):121-7.
3. Hennemann G, Docter R, Friesema EC, de Jong M, Krenning EP, Visser TJ. Plasma membrane transport of thyroid hormones and its role in thyroid hormone metabolism and bioavailability. Endocr Rev. 2001;22(4):451-76.
4. Friesema EC, Ganguly S, Abdalla A, Manning Fox JE, Halestrap AP, Visser TJ. Identification of monocarboxylate transporter 8 as a specific thyroid hormone transporter. J Biol Chem. 2003;278(41):40128-35.
5. Friesema EC, Grueters A, Biebermann H, Krude H, von Moers A, Reeser M, et al. Association between mutations in a thyroid hormone transporter and severe X-linked psychomotor retardation. Lancet. 2004;364(9443):1435-7.
6. Dumitrescu AM, Liao XH, Best TB, Brockmann K, Refetoff S. A novel syndrome combining thyroid and neurological abnormalities is associated with mutations in a monocarboxylate transporter gene. Am J Hum Genet. 2004;74(1):168-75.
7. Friesema EC, Visser WE, Visser TJ. Genetics and phenomics of thyroid hormone transport by MCT8. Mol Cell Endocrinol. 2010;322(1-2):107-13.
8. Jansen J, Friesema EC, Kester MH, Schwartz CE, Visser TJ. Genotype-phenotype relationship in patients with mutations in thyroid hormone transporter MCT8. Endocrinology. 2008;149(5):2184-90.
9. Kinne A, Kleinau G, Hoefig CS, Gruters A, Kohrle J, Krause G, et al. Essential molecular determinants for thyroid hormone transport and first structural implications for monocarboxylate transporter 8. J Biol Chem. 2010;285(36):28054-63.
10. Vaurs-Barriere C, Deville M, Sarret C, Giraud G, Des Portes V, Prats-Vinas JM, et al. Pelizaeus-Merzbacher-Like disease presentation of MCT8 mutated male subjects. Ann Neurol. 2009;65(1):114-8.
11. Ugrasbul F, H.H. A. A patient presenting with central hypothyroidism, developmental delay and poor head control. Should we be checking T3 levels? Horm Res. 2009;72(Suppl 1):458-9.
12. Braun D, Lelios I, Krause G, Schweizer U. Histidines in potential substrate recognition sites affect thyroid hormone transport by monocarboxylate transporter 8 (MCT8). Endocrinology. 2013;154(7):2553-61.
13. Groeneweg S, Lima de Souza EC, Visser WE, Peeters RP, Visser TJ. Importance of His192 in the human thyroid hormone transporter MCT8 for substrate recognition. Endocrinology. 2013;154(7):2525-32.
14. Mol JA, Visser TJ. Synthesis and some properties of sulfate esters and sulfamates of iodothyronines. Endocrinology. 1985;117(1):1-7.
15. Friesema EC, Kuiper GG, Jansen J, Visser TJ, Kester MH. Thyroid hormone transport by the human monocarboxylate transporter 8 and its rate-limiting role in intracellular metabolism. Mol Endocrinol. 2006;20(11):2761-72.
16. Friesema EC, Jansen J, Jachtenberg JW, Visser WE, Kester MH, Visser TJ. Effective cellular uptake and efflux of thyroid hormone by human monocarboxylate transporter 10. Mol Endocrinol. 2008;22(6):1357-69.
17. Wilson MC, Meredith D, Bunnun C, Sessions RB, Halestrap AP. Studies on the DIDS-binding site of monocarboxylate transporter 1 suggest a homology model of the open conformation and a plausible translocation cycle. J Biol Chem. 2009;284(30):20011-21.
18. Rahman B, Schneider HP, Broer A, Deitmer JW, Broer S. Helix 8 and helix 10 are involved in substrate recognition in the rat monocarboxylate transporter MCT1. Biochemistry. 1999;38(35):11577-84.
19. Manoharan C, Wilson MC, Sessions RB, Halestrap AP. The role of charged residues in the transmembrane helices of monocarboxylate transporter 1 and its ancillary protein basigin in determining plasma membrane expression and catalytic activity. Mol Membr Biol. 2006;23(6):486-98.
20. Law CJ, Almqvist J, Bernstein A, Goetz RM, Huang Y, Soudant C, et al. Salt-bridge dynamics control substrate-induced conformational change in the membrane transporter GlpT. Journal of molecular biology. 2008;378(4):828-39.
21. Smits G, Govaerts C, Nubourgh I, Pardo L, Vassart G, Costagliola S. Lysine 183 and glutamic acid 157 of the TSH receptor: two interacting residues with a key role in determining specificity toward TSH and human CG. Mol Endocrinol. 2002;16(4):722-35.
22. Dumitrescu AM, Liao XH, Weiss RE, Millen K, Refetoff S. Tissue-specific thyroid hormone deprivation and excess in monocarboxylate transporter (mct) 8-deficient mice. Endocrinology. 2006;147(9):4036-43.
23. Trajkovic M, Visser TJ, Mittag J, Horn S, Lukas J, Darras VM, et al. Abnormal thyroid hormone metabolism in mice lacking the monocarboxylate transporter 8. J Clin Invest. 2007;117(3):627-35.

24. Wirth EK, Roth S, Blechschmidt C, Holter SM, Becker L, Racz I, et al. Neuronal 3',3,5-triiodothyronine (T3) uptake and behavioral phenotype of mice deficient in Mct8, the neuronal T3 transporter mutated in Allan-Herndon-Dudley syndrome. J Neurosci. 2009;29(30):9439-49.
25. Wirth EK, Sheu SY, Chiu-Ugalde J, Sapin R, Klein MO, Mossbrugger I, et al. Monocarboxylate transporter 8 deficiency: altered thyroid morphology and persistent high triiodothyronine/thyroxine ratio after thyroidectomy. Eur J Endocrinol. 2011;165(4):555-61.
26. Mayerl S, Visser TJ, Darras VM, Horn S, Heuer H. Impact of Oatp1c1 deficiency on thyroid hormone metabolism and action in the mouse brain. Endocrinology. 2012;153(3):1528-37.
27. Lima de Souza EC, Groeneweg S, Visser WE, Peeters RP, Visser TJ. Importance of cysteine residues in the thyroid hormone transporter MCT8. Endocrinology. 2013;154(5):1948-55.
28. Kirk P, Wilson MC, Heddle C, Brown MH, Barclay AN, Halestrap AP. CD147 is tightly associated with lactate transporters MCT1 and MCT4 and facilitates their cell surface expression. EMBO J. 2000;19(15):3896-904.
29. Philp NJ, Ochrietor JD, Rudoy C, Muramatsu T, Linser PJ. Loss of MCT1, MCT3, and MCT4 expression in the retinal pigment epithelium and neural retina of the 5A11/basigin-null mouse. Invest Ophthalmol Vis Sci. 2003;44(3):1305-11.
30. Wilson MC, Meredith D, Fox JE, Manoharan C, Davies AJ, Halestrap AP. Basigin (CD147) is the target for organomercurial inhibition of monocarboxylate transporter isoforms 1 and 4: the ancillary protein for the insensitive MCT2 is EMBIGIN (gp70). J Biol Chem. 2005;280(29):27213-21.
31. Visser WE, Philp NJ, van Dijk TB, Klootwijk W, Friesema EC, Jansen J, et al. Evidence for a homodimeric structure of human monocarboxylate transporter 8. Endocrinology. 2009;150(11):5163-70.
32. Lewis HA, Zhao X, Wang C, Sauder JM, Rooney I, Noland BW, et al. Impact of the deltaF508 mutation in first nucleotide-binding domain of human cystic fibrosis transmembrane conductance regulator on domain folding and structure. J Biol Chem. 2005;280(2):1346-53.
33. Sharma M, Pampinella F, Nemes C, Benharouga M, So J, Du K, et al. Misfolding diverts CFTR from recycling to degradation: quality control at early endosomes. J Cell Biol. 2004;164(6):923-33.
34. Moyer BD, Denton J, Karlson KH, Reynolds D, Wang S, Mickle JE, et al. A PDZ-interacting domain in CFTR is an apical membrane polarization signal. J Clin Invest. 1999;104(10):1353-61.

Chapter

2.4

Outward-Open Model of Thyroid Hormone Transporter Monocarboxylate Transporter 8 Provides Novel Structural and Functional Insights

Stefan Groeneweg, Elaine C. Lima de Souza, Marcel E. Meima, Robin P. Peeters, W. Edward Visser, Theo J. Visser

Endocrinology. 2017 October;158(10):3292-3306.

ABSTRACT

Monocarboxylate transporter 8 (MCT8) facilitates cellular uptake and efflux of thyroid hormone (TH). Mutations in MCT8 result in severe intellectual and motor disability known as the Allan-Herndon-Dudley syndrome (AHDS). Previous studies have provided valuable insights into the putative mechanism of substrate binding in the inward-open conformation, required for TH efflux. The current study aims to delineate the mechanism of substrate binding in the outward-open conformation, required for TH uptake. Extensive chemical modification and site-directed mutagenesis studies were used to guide protein homology modeling of MCT8 in the outward-open conformation. Arg271 and Arg445 were modified by phenylglyoxal, which was partially prevented in the presence of substrate. Substrate docking in our outward-open model suggested an important role for His192 and Arg445 in substrate binding. Interestingly, mutations affecting these residues have been identified in patients who have AHDS. In addition, our outward-open model predicted the location of Phe189, Met227, Phe279, Gly282, Phe287, and Phe501 at the substrate-binding center, and their Ala substitution differentially affected the apparent Vmax and Km of T3 transport, with F189A, F279A, and F287A showing the highest impact. Thus, here we present an MCT8 homology model in the outward-open conformation, which supports the important role of His192 and Arg445 in substrate docking and identifies critical residues at the putative substrate-binding center. Our findings provide insights into MCT8 structure and function, which add to our understanding of the pathogenic mechanism of mutations found in patients who have AHDS and can be used to screen for novel substrates and inhibitors.

INTRODUCTION

Thyroid hormone (TH) requires TH transporter proteins to allow its cellular entry, action, and metabolism (1, 2). Monocarboxylate transporter 8 (MCT8) is the most specific TH transporter known to date and facilitates the transport of 3,3',5,5'-tetraiodo-L-thyronine (T4), 3,3',5-triiodo-L-thyronine (T3), and to a lesser extent 3,3',5'-triiodo-L-thyronine and 3,3'-diiodo-L-thyronine (3, 4). Entry of TH into the brain appears highly MCT8 dependent, indicating an important physiological role of MCT8 in TH homeostasis in the brain (5, 6). Mutations in the MCT8 (SLC16A2) gene result in the Allan-Herndon-Dudley syndrome (AHDS), which is characterized by severe intellectual and motor disability and peripheral thyrotoxicosis (7, 8). Different types of MCT8 mutations have been identified in patients who have AHDS (7, 8). Although most mutations result in a (near-) complete inactivation of TH transport capacity, the molecular pathogenic mechanism varies (7, 8). Several mutations have been found to interfere with protein expression and subcellular localization (truncating mutations, insertions/deletions, and missense mutations affecting Pro and Gly residues), whereas others specifically interfere with substrate translocation (mostly missense mutations) (9-14). Because protein structure and function are intimately related, detailed insights into the MCT8 structure are required to better understand its physiological substrate translocation mechanism and the impact of different mutations. However, crystal or nuclear magnetic resonance structures of MCT8 are currently lacking.

Because crystallization of integrated membrane proteins is cumbersome, protein homology modeling is an effective alternative if a suitable template structure is available. MCT8 belongs to the major facilitator superfamily (MFS), which have been suggested to share a common structural organization, even in the absence of apparent sequence similarity (15). Furthermore, all MFS proteins seem to use a similar substrate translocation mechanism according to the rocker-switch model, in which the binding of a substrate molecule to a substrate-binding center initiates the transition from the outward-open to the inward-open conformation (uptake) or vice versa (efflux) (15). Therefore, crystal structures of other MFS members could serve as suitable templates for MCT8 modeling.

Indeed, an MCT8 homology model in the inward-open conformation based on the Escherichia coli glycerol-3-phosphate transporter [GlpT; Protein Data Bank (PDB) no. 1PW4] has been previously reported (4). This model complies to several important in vitro studies that suggested a close structural proximity of Arg445, located in transmembrane domain (TMD) 8, and Asp498, located in TMD10, allowing the formation of a hydrogen bond between these residues, and a channel-facing orientation of His192 (TMD1) (4, 10, 11). Based on these findings, it was postulated that His192 and Arg445 form a His-Arg clamp, facilitating the docking of TH at the substrate-binding center in the inward-open conformation (4, 10). Moreover, it predicted most missense mutations, identified in patients who have AHDS, within TMDs or at helix-loop transitions, but not in extracellular loops (ECLs) or intracellular loops (ICLs) (4, 16). However, this model did not accommodate the accessible position of Cys497 as suggested by in vitro chemical modification studies with p-chloromercuribenzene sulfonate (pCMBS) (17). Moreover, the homology model in inward-open conformation mainly provides insights into substrate recruitment and docking from the intracellular side during TH efflux. For a better understanding of the full transport cycle, additional MCT8 models in other conformations are thus required. Specifically, a homology model in the outward-open conformation is warranted for a more detailed understanding into transporter structure and substrate docking from the extracellular side during TH uptake.

Therefore, we used chemical modification and site-directed mutagenesis studies, to guide protein homology modeling of MCT8 in the outward-open conformation. In addition to our previous chemical modification and mutational studies, we here present in vitro evidence supporting the localization of Arg445 at the substrate-binding center. Subsequent substrate docking and molecular dynamic simulation studies of our structure model indeed support the presence of a direct interaction of His192 and Arg445 with TH at the substrate-binding center. Finally, our findings suggest that other residues predicted at the substrate-binding center may be of differential importance for substrate docking and translocation, depending on their position and orientation toward the substrate. Our findings provide insights into MCT8 structure and function and contribute to a better understanding of the MCT8 substrate translocation cycle and the impact of pathogenic mutations found in patients who have AHDS. Moreover, our model can be used to screen for novel MCT8 substrates and inhibitors.

EXPERIMENTAL PROCEDURES

Materials

Unlabeled iodothyronine derivatives, bovine serum albumin (BSA), D-glucose, 2-hydroxy-5-nitrobenzyl bromide (HNBB), N-acetyl-imidazole (NAI), phenylglyoxal (PG), and phenylmethanesulfonyl fluoride (PMSF) were obtained from Sigma-Aldrich (Zwijndrecht, The Netherlands). [125I]T3 and [125I]T4 were synthesized as described previously (18). Transfection reagent X-tremeGENE 9 from Roche (Almere, The Netherlands), sodium dodecyl sulfate (SDS)-polyacrylamide gel electrophoresis gels from Thermo Fisher (Breda, The Netherlands), nitrocellulose membrane from GE Healthcare (Eindhoven, The Netherlands). Antibody information is summarized in **Supplemental Table 1**. Vectashield H-1200 containing 4',6-diamidino-2-phenylindole was obtained from Brunschwig (Amsterdam, The Netherlands).

Plasmids

Cloning of human MCT8 in pcDNA3, and of the human cytosolic TH-binding protein mu-crystallin (CRYM) in pSG5, has been described previously (19, 20). We introduced the following mutations into the pcDNA3.MCT8 plasmid using QuikChange site-directed mutagenesis (Stratagene, Amsterdam, The Netherlands) according to the manufacturer's protocol: W175F, W175A, W183F, W183A, W219F, W219A, W398F, W398A, W431F, W431A, R271K, R271A, R325K, R325A, R445K, R445A, R482K, R482A, R544K, R544A, F189A, M227A, F279A, G282A, F287A, F501A (primer sequences are listed in **Supplemental Table 2**). The position of the mutations is indicated using the NM_006517.3 reference sequence and uses +1 as the A of the ATG translation initiation codon of the long MCT8 isoform, with the initiation codon as codon 1. DNA sequencing confirmed the presence of the introduced mutations and the absence of unintended mutations.

Cell culture and transfection

COS-1 and JEG-3 cells were cultured in 6- or 24-well dishes (Corning, Schiphol, The Netherlands) in Dulbecco's modified Eagle medium/F12 medium (Invitrogen, Breda, The Netherlands), containing 9% heat-inactivated fetal bovine serum (Invitrogen), 2% penicillin/streptomycin (Roche, Woerden, The Netherlands), and 100 nM sodium selenite (Sigma-Aldrich). Cells were transfected at 70% confluency, and all experiments were carried out 48 hours after transfection. For TH uptake experiments, cells were seeded in 24-well dishes and transiently cotransfected in duplicate with 50 ng wild-type (WT) or

mutant MCT8, 50 ng pcDNA3 empty vector (EV), and either 100 ng pSG5.CRYM or pcDNA3 EV. For Western blotting, cells were seeded in six-well dishes and transiently transfected with 500 ng WT or mutant MCT8 or pcDNA3 EV. For immunocytochemistry, JEG-3 cells were cultured in 24-well dishes on 10-mm glass coverslips coated with poly-D-lysine (Sigma-Aldrich) and transiently transfected with 250 ng of WT or mutant pcDNA3-hMCT8. We previously described the absence of significant differences in transfection efficiency between MCT8 WT and mutants (21).

TH uptake

TH uptake experiments were performed according to previously described methods (11). If mentioned, cells were first preincubated for 15 minutes at room temperature (RT) in incubation medium [Dulbecco phosphate-buffered saline (D-PBS) and 0.1% D-Glucose] containing the indicated chemical modifier or vehicle without or with 10 µM T3, washed twice for 1 minute in incubation medium containing 1% BSA, and once for 1 minute in incubation medium without BSA, prior to the uptake assay. Uptake studies were performed for the indicated times at 37°C using incubation medium containing 0.1% BSA, 1 nM unlabeled T3 or T4, and 5 × 104 cpm [125I]T3 or [125I]T4. Kinetic studies were performed in the absence of CRYM. Cells were incubated for 10 minutes in incubation medium containing 5 × 104 cpm [125I]T3 and the indicated concentrations of unlabeled T3. All solutions of the chemical modifiers and their dilutions in incubation medium were prepared immediately before the experiments.

Cell viability assay and measurement of protein content

To exclude toxic effects of chemical modification reagents, cells were cultured in 96-well plates (cell viability) or 24 well-plates (protein measurement). After 72 hours, cells were incubated for 10 minutes with different concentrations of the chemical modification reagents as described above, washed once with phosphate-buffered saline (PBS) containing 0.1% BSA, and twice with PBS without BSA. The cells cultured in the 24-well plates were lysed in 0.1 M NaOH to measure total protein levels using the Bradford assay (BIO-RAD, Veenendaal, The Netherlands). The cells cultured in the 96-well plates were incubated for 3 hours at 37°C with 0.5 mg/mL 3-(4,5-dimethylthiazol-2-yl)-2,5-diphenyltetrazolium bromide in Dulbecco's modified Eagle medium-F12. After aspiration of the medium, cells were solubilized in dimethyl sulfoxide, and the absorbance of converted dye was measured at a 560 nm using a Victor 2 multilabel plate reader (Perkin Elmer, Rotterdam, The Netherlands).

Cell surface biotinylation

For cell surface biotinylation assays, COS-1 cells were cultured on 10-cm dishes and transiently transfected with 1500 ng WT or mutant MCT8 at 60% confluence. After 48 hours, cells were washed three times with ice-cold D-PBS containing 1 mM MgCl2 and 0.1 mM CaCl2 [Dulbecco phosphate-buffered saline containing 2 mM MgCl2 and 0.1 mM CaCl2 (D-PBS-CM)]. Surface proteins were subsequently labeled for 30 minutes at 4°C with 1 mg/mL EZ-Link Sulfo-NHS-Biotin (Thermo Fisher) in D-PBS-CM with gentle agitation. Free biotin was quenched by washing cells once with quenching buffer (D-PBS-CM, 100 mM glycine, pH 7.4) and an additional incubation with quenching buffer for 15 minutes at 4°C with gentle agitation. Cells were subsequently washed twice with ice-cold D-PBS-CM and lysed with immunoprecipitation buffer (50 mM Tris-HCl, 150 mM NaCl, 10 mM EDTA, 1% Triton X-100) containing protease inhibitor cocktail (Roche). Lysates were briefly sonicated and then clarified by centrifugation (5 minutes at 10,000g and 4°C). An aliquot of the clarified sample was stored as input control (5% of total volume). Biotin-labeled surface proteins were then isolated by incubating lysates

overnight at 4°C with 50 µL prewashed NeutrAvidin agarose beads (Thermo Fisher) under gentle rotation. Subsequently, beads were washed three times with immunoprecipitation buffer–containing protease inhibitors, and bound proteins were eluted by incubating the beads for 10 minutes at 70°C with 20 µL 4× SDS sample buffer. The eluate was analyzed by Western blotting as described later.

Western blotting

Western blots were carried out as previously described, with some modifications (11). After a brief wash with PBS, cells were harvested in lysis buffer containing 100 mM Na-phosphate and 2 mM EDTA and protease inhibitor cocktail (Roche), and sonicated for 10 seconds. After 10 minutes' incubation at 70°C in sample loading buffer containing SDS and dithiothreitol, samples were loaded on a 10% precast SDS–polyacrylamide gel electrophoresis gel (Thermo Fisher). After blotting, membranes were blocked for 2 hours in PBS containing 0.1% Tween and 5% milk and probed with MCT8 and glyceraldehyde-3-phosphate dehydrogenase (GAPDH) antibodies (as a loading control) overnight at 4°C (see **Supplemental Table 1** for details). MCT8 and GAPDH were visualized by Odyssey using IRDye680 goat anti-rabbit and IRDye800 goat anti-mouse (LI-COR, Leusden, The Netherlands) secondary antibodies, respectively.

Immunocytochemistry

Two days after transfection, cells were fixed for 20 minutes at 37°C with 4% paraformaldehyde in D-PBS and permeabilized for 5 minutes at RT with 0.2% Triton X-100 in PBS. Samples were washed for 1 hour at RT in D-PBS containing 1% BSA and incubated overnight at 4°C with MCT8 and ZO-1 antibodies (**Supplemental Table 1**). Primary antibodies were visualized with goat anti-rabbit Alexa Fluor 488 and goat anti-mouse Alexa 633 (**Supplemental Table 1**), respectively. Coverslips were mounted on glass slides using Vectashield H-1200 containing 4',6-diamidino-2-phenylindole (Brunschwig). Samples were examined on a Zeiss Meta 510 microscope using Zeiss LSM software (Zeiss NL, Sliedrecht, The Netherlands). A Plan Neofluar 40×1.3 oil objective and lasers of 405, 488, and 633 nm wavelength were used. Images were prepared using ImageJ software.

Protein homology modeling

The automatic homology modeling algorithm implemented in YASARA Structure Software (YASARA Biosciences GmbH, Vienna, Austria) was used to construct different MCT8 homology models in the outward-open conformation (22, 23). In summary, the sequence of MCT8 was PSI-BLASTed (24) with three iterations against the UniRef90 database to build a position-specific scoring matrix (PSSM) with related sequences. These included the MCT8 and MCT10 sequences from different species. The PSSM was used to search the PDB database for potential modeling templates. The putative templates were automatically ranked based on the alignment score and their structural quality according to WHAT_CHECK (25) obtained from the PDBFinder2 database (26). For the top five most suitable templates, five putative alignments with the MCT8 target sequence were generated per template using a secondary structure prediction and PSSM of the MCT8 target sequence (24, 27-29) and the sequence profile of the templates, derived from YASARA's Profiles from Sequence- and Structurally Related Proteins database and additional UniRef90 sequences, yielding a multiple sequence alignment that is anchored on an accurate structural alignment (28, 30). Next, for each alignment an initial rotamer solution was generated. If templates contain ligands, these molecules were considered in the homology modeling procedure. Loops were modeled by scanning a nonredundant subset of the PDB

database (>10,000 structures) for fragments with matching anchor points, a minimal number of bumps, and maximum sequence similarity. Side chains were added with YASARA's implementation of Side Chains With Rotamer Library (23, 31), side-chain rotamers were fine-tuned, and the hydrogen-bonding network was optimized. Finally, each model was subjected to a short energy minimization step with the YASARA2 force field as described previously (23). Because this is only a minimization, the water molecules mainly serve to screen for electrostatic interactions and it therefore does not matter that the MCT8 protein is normally not fully solvated.

In total 25 models were generated, based on five different template PDBs (**Supplemental Table 3**). All models were manually inspected and challenged by the obtained in vitro data as summarized in **Supplemental Table 4**. Based on the conformational state (outward-open), model quality and compatibility with as many as possible in vitro findings, the E. coliL-fucose-proton symporter, (FucP; PDB no. 3O7P) in the outward-open conformation was selected as the most suitable template (Psi-BLAST alignment score 77, coverage 67%, resolution 3.2 Å, z score crystal structure: 0.425). The alignment was slightly adapted at TMD10 to render Cys497 accessible for pCMBS modification. Furthermore, the secondary structure of ECL3 was slightly adjusted to allow a better fit with the presumed α-helical structure of TMD5 (32). The final alignment is provided in Supplemental Fig. 1. The final model was minimized without further constraints using the YASARA 2 force field. The final model was validated with WHAT_CHECK (25) and yielded an average quality z score of −1.29 (range: < −5, terrible to > 0, optimal), which is a satisfactory quality level.

Substrate docking and molecular dynamic simulations

After visualization of the molecular surface, a T3 molecule was manually introduced into the substrate pore in proximity of the proposed substrate-binding center in the outward-open conformation. Optimization of the protein structure and, if indicated, substrate position was performed using molecular dynamic simulations. For this purpose, the MCT8 protein model was first introduced into a membrane environment while keeping the substrate pore solvated with water (described in detail in **Supplemental Materials and Methods**). After an initial equilibration step of 250 ps, further molecular dynamic simulations were carried out in an AMBER 14 force field with periodic boundaries (23, 33). Snapshots of the substrate-binding pore were taken after 2 and 4 ns. Next, several residues with side-chains within 5 Å of the T3 molecule were selected for mutagenesis studies and further functional evaluation. All images were created using YASARA Structure and Pov-Ray v3.6 software (www.povray.org).

Statistical analysis

All uptake results are expressed as means ± standard error of the mean of at least two to six separate experiments in duplicate. P values <0.05 were regarded as statistically significant. Statistical significance was determined as indicated in the legends of the corresponding figures. Km and Vmax values were calculated using Michaelis-Menten equation implemented in GraphPad Prism, version 6 (GraphPad, La Jolla, CA). Linear regression was used to generate an Eadie-Hofstee plot from the kinetic data.

RESULTS

To identify accessible residues within MCT8 that are putatively important for MCT8 transport function, we first studied the effect of selective amino acid modifying reagents on MCT8-mediated T3 transport. We have previously shown that preincubation with His-reactive diethylpyrocarbonate (DEPC) and Cys-reactive pCMBS resulted in an inhibition of subsequent MCT8-mediated TH transport (11, 17). We now preincubated COS-1 cells coexpressing WT MCT8 and the intracellular TH binding protein CRYM with increasing concentrations of NAI, which targets accessible Tyr residues, PMSF, which targets accessible Ser residues, HNBB, which targets accessible Trp residues, and PG, which targets accessible Arg residues. Preincubation with increasing concentrations of NAI or PMSF did not result in significant impairment of MCT8-mediated T3 uptake (**Figure 1(a)** and **1(b)**), suggesting that no Ser or Tyr residues are modified, or that modification of potentially available Tyr or Ser residues does not interfere with substrate translocation. In contrast, preincubation with increasing concentrations of HNBB and PG resulted in a dose-dependent decrease in MCT8-mediated T3 uptake (**Figure 1(c)** and **1(d)**). No significant toxic effects were observed for the concentrations of HNBB and PG used, and the highest concentrations of PG and HNBB used in these studies did not affect MCT8 protein expression levels, or cell surface translocation (**Supplemental Fig. 2(a–c)**). Similar results were obtained in JEG-3 cells (data not shown).

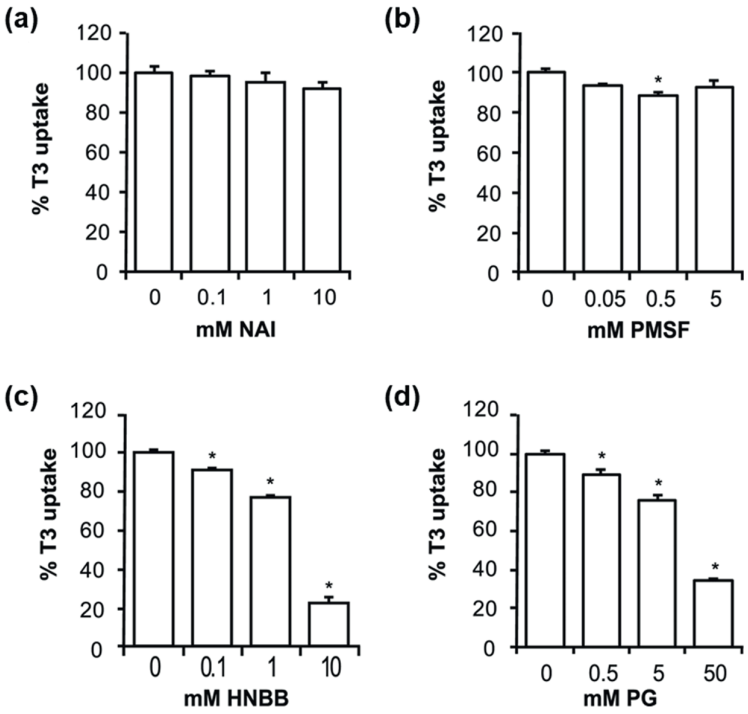

Figure 1 T3 uptake in 5 minutes by COS-1 cells cotransfected with MCT8 and CRYM cDNA, after 10 minutes' preincubation in the presence of increasing concentrations of (**a**) NAI, (**b**) PMSF, (**c**) HNBB, or (**d**) PG. All values are corrected for background T3 uptake levels observed in COS-1 cells transfected with pcDNA3 EV, preincubated under the identical conditions. T3 uptake levels are expressed relative to MCT8-mediated T3 uptake levels after preincubation in D-PBS without the indicated chemical modifier. Results are presented as means ± standard error of the mean (n = 3). Statistical significance was tested using one-way analysis of variance followed by Dunnett multiple-comparison test. Statistically significant differences are indicated with an asterisk (*).

To exclude that the observed inhibitory effect of HNBB was mediated by modification of CRYM, we confirmed these effects of HNBB on MCT8-mediated T3 uptake in the absence of CRYM (**Figure 2(a)**). To identify putative target residues for HNBB modification, a mutational screen of Trp residues located in the predicted ECLs and TMDs was performed. Trp175, Trp183, Trp219, Trp398, or Trp431 were substituted with Phe, maintaining the large aromatic group and hydrophobic properties of the side-chain, or with Ala, reducing the side-chain size. **Supplemental Table 5** summarizes the predicted locations within the protein and conservation of these Trp residues across species and MCT family members. Upon expression in COS-1 cells, the W175A, W219F, and W219A mutants showed a small but significant reduction of MCT8-mediated T3 uptake compared with WT (**Figure 2(b)**). Similar results were observed for T4 uptake (**Supplemental Figure 3(a)**). All mutants were detected as monomer and homo-dimer (**Supplemental Figure 3(b)**). None of the Trp-mutants displayed reduced HNBB sensitivity (**Figure 2(b)**). Indeed, when HNBB was tested at pH 6, where HNBB has the highest specificity for Trp residues, the inhibitory effects largely disappeared (**Figure 2(a)**). Taken together, these findings suggest that the main inhibitory effect of HNBB results from off-target modifications (34).

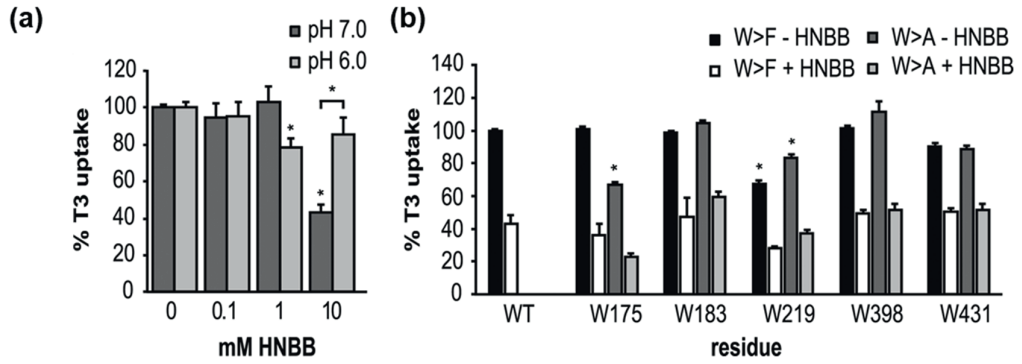

Figure 2 (a) T3 uptake by COS-1 cells transfected with MCT8 in the absence of CRYM in 5 minutes at 37°C after preincubation for 10 minutes in the presence of 10 mM HNBB at indicated pH level, and (**b**) T3 uptake by COS-1 cells coexpressing WT or mutant MCT8 and CRYM after preincubation in the presence or absence of 10 mM HNBB for 10 minutes. All values are corrected for background T3 uptake levels observed in COS-1 cells transfected with pcDNA3 EV, preincubated under identical conditions. T3 uptake levels are expressed relative to MCT8-mediated T3 uptake levels after preincubation in D-PBS without HNBB. Results are presented as means ± standard error of the mean (n = 3). Statistical significance was tested using two-way analysis of variance followed by Bonferroni posttests. Statistically significant differences are indicated with an asterisk (*).

To exclude that the observed inhibitory effect of PG was mediated by modification of CRYM, we first confirmed that these effects of PG on MCT8-mediated T3 uptake also occurred in the absence of CRYM (**Figure 3(a)**). To identify the putative target(s) for PG modification, we substituted Arg271, Arg325, Arg445, Arg482, or Arg544, all predicted to be located within ECLs or TMDs, with either Lys, maintaining the positive charge, or with Ala, resulting in a loss of positive charge and reduction of side-chain size. **Supplemental Table 5** summarizes the predicted locations within the protein and conservation of these Arg residues across species and the MCT family. The T3 uptake by the R271A,

R445K, R445A, and R544K mutants was significantly reduced (**Figure 3(b)**). Similar results were observed for T4 uptake (**Supplemental Figure 3(c)**). All mutants were detected as monomer and homo-dimer (**Supplemental Figure 3(d)**). All mutants showed a significant reduction in T3 and T4 uptake capacity after preincubation with 50 mM PG, except for the R445A mutant (**Figure 3(b); Supplemental Figure 3(c)**). Although the R271A mutant was still sensitive to PG modification, the degree of inhibition of subsequent T3 uptake was significantly lower compared with WT MCT8. None of the Arg to Lys mutants showed a reduction in PG sensitivity, which could be the result of lysine modification by PG (34). Taken together, these findings suggest that Arg445 and Arg271 are targets for PG modification. Next, we studied whether the inhibiting effect of PG could be prevented in the presence of 10 µM T3. Preincubation with T3 alone reduced subsequent [125I]T3 uptake by about 20% [Fig. 3(c)]. Preincubation with 50 mM PG resulted in a 50% reduction of subsequent T3 uptake compared with control cells. This effect was partially prevented in the presence of T3 (**Figure 3(c)**). These findings suggest that the presence of substrate partially protects against modification of Arg445 and/or Arg271 by PG, which may indicate that the side-chain of at least one of these residues faces the substrate channel.

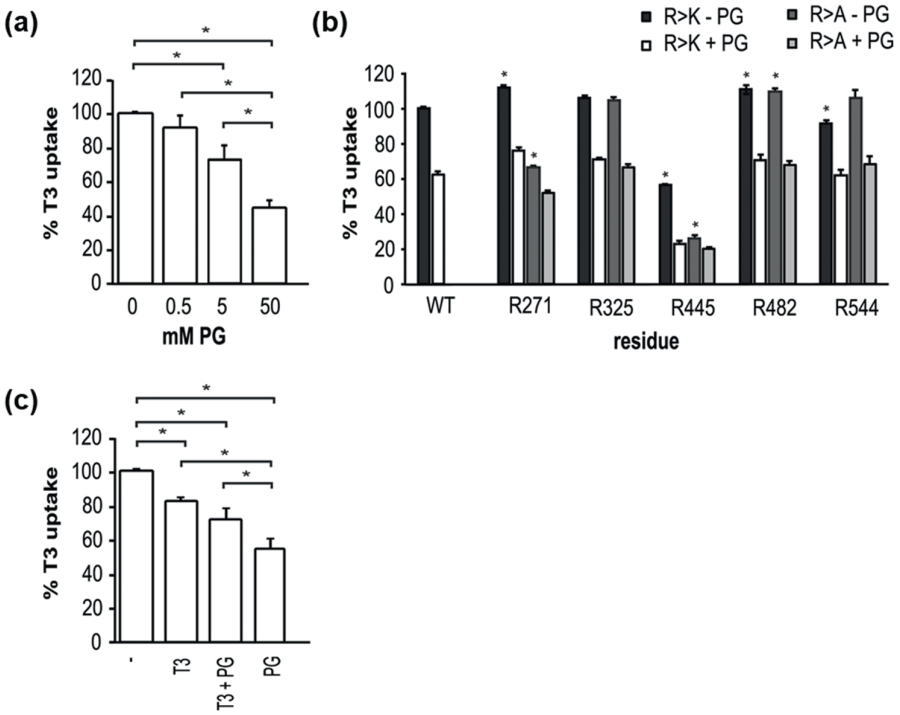

Figure 3(a) T3 uptake by COS-1 cells transfected with MCT8 in the absence of CRYM in 5 minutes at 37°C after preincubation for 5 minutes in the presence of indicated concentrations of PG, and (**b**) T3 uptake by COS-1 cells coexpressing WT or mutant MCT8 and CRYM after preincubation in the presence or absence of 50 mM PG for 10 minutes. (**c**) T3 uptake in 5 minutes in COS-1 cells expressing WT MCT8 and CRYM after preincubation in the presence of either vehicle, 50 mM PG, 10 µM unlabeled T3 alone, or 10 µM unlabeled T3 in combination with 50 mM PG. All uptake values are corrected for background T3 uptake levels observed in COS-1 cells transfected with pcDNA3 EV, preincubated under the identical condition. T3 uptake levels are expressed relative to MCT8-mediated T3 uptake levels after preincubation in D-PBS with vehicle. Results are presented as means ± standard error of the mean (n = 3 to 4). Statistical significance was tested using one-way analysis of variance (ANOVA) followed by (**a**) Dunnett multiple-comparison test and (**b, c**) a two-way ANOVA followed by Bonferroni posttests. Statistically significant differences are indicated with an asterisk (*).

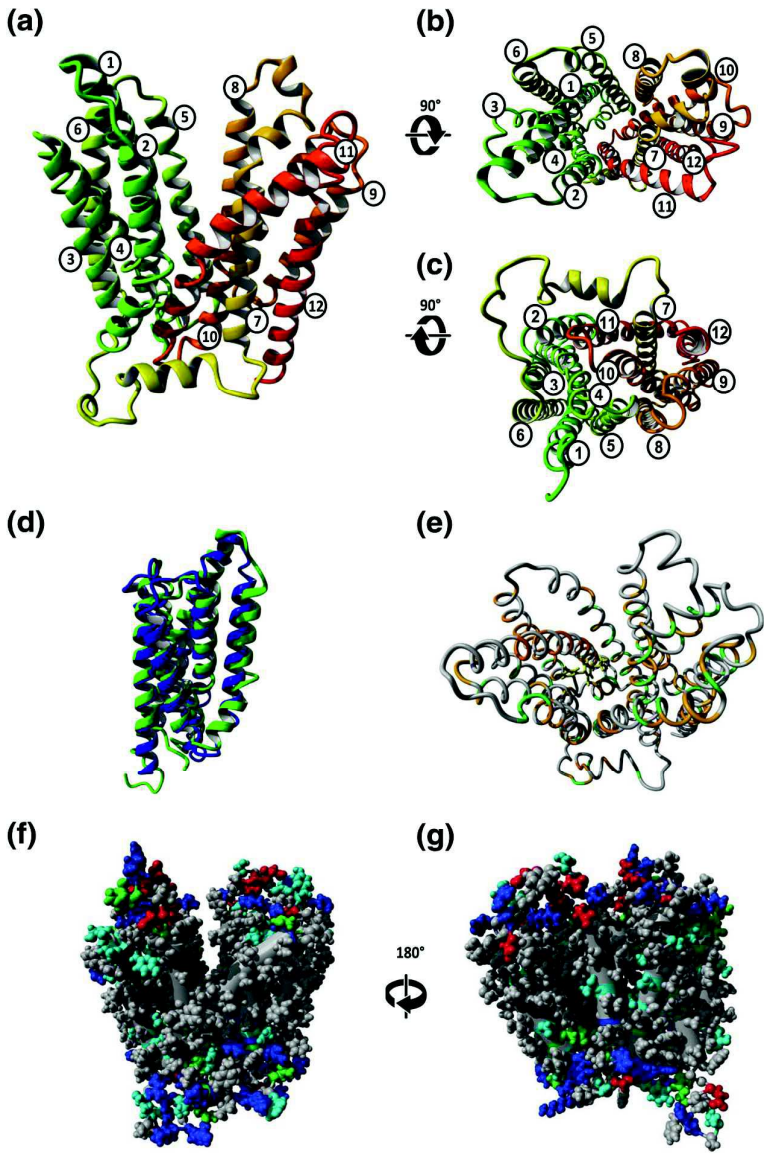

Figure 4 (a) Frontal, (**b**) extracellular, and (**c**) intracellular view of the overall structure of MCT8 homology model in the outward-open conformation in gradient color (N-terminus: green; C-terminus: red). Due to low structural and sequence homology with the template, the large intracellular N-terminus and part of the C-terminus are lacking. The MCT8 protein consists of two near symmetrical parts, each consisting of six transmembrane helices, interconnected by a large ICL between TMD6 and 7. The predicted TMD spans are as follows TMD1: Gln167-Glu204, TMD2: Phe215-Phe238, TMD3: Ile246-Phe264, TMD4: Leu270-His296, TMD5: Arg301-Gly328, TMD6: Phe337-Thr353, TMD7: Met387-Leu416, TMD8 Lys428-Pro456, TMD9: Leu458-Met477, TMD10: Asp483-Phe510, TMD11: Met516-Asn545, and TMD12: Val552-Asp585. The predicted TMD spans show high coincidence with previously reported predictions of MCT8 TMDs (4, 35). The secondary structure of the loops connecting the TMDs is difficult to predict with great certainty, but mostly consists of random coiled coils or turns, which allow greater flexibility. (**d**) The N-terminal half of the protein (residues 162-359: green) shows great structural similarities to the C-terminal half of the protein (residues 387-582: blue) and can almost be superimposed. Identical (green) and similar (orange) residues between MCT8 and the modeling template FucP are depicted in (**e**). Amino acid properties are depicted in (**f**) from the front side and (**g**) from the back side. In blue: positively charged residues (Arg, Lys, His), in red: negatively charged residues (Asp, Glu), in gray: hydrophobic residues, in light blue: polar residues containing a hydroxyl group (Ser, Thr, Tyr), and in green: the polar amides (Asn, Gln).

Next, different MCT8 homology models in the outward-open conformation were generated based on the crystal structure of the FucP (PDB no.3O7P and 3O7Q) (35) using the homology modeling tool of YASARA Structure (see Methods and **Supplemental Materials** and Methods sections and **Supplemental Table 3** for details). The model that best accommodated the current and previously reported in vitro data (**Supplemental Table 4**) was selected (template: PDB #3O7P) and further optimized (see **Supplemental Figure 1** for the final alignment).

The resulting outward-open model consists of a near symmetrical N-terminal half (TMD 1-6) and C-terminal half (TMD 7-12), connected by a large ICL (**Figure 4(a–d)**). The putative TMDs are indicated in the legend of **Figure 4(a)** and are mostly similar to previous reports (4, 36). All TMDs have a predominant α-helical organization, whereas the loops mostly consist of random coils or turns. The α-helical structure at the end of the large ICL3 linking TMD6 and TMD7 is an exception to this observation, a well-described phenomenon in MFS proteins including GlpT and FucP (35, 37). In line with most crystallized MFS transporters, TMD4 shows a less rigid α-helical structure, allowing greater helical flexibility to maximize substrate interactions (15). Of note, also the MFS signature sequence (DRXXXR) defining the two ends of ICL1 is present in MCT8 (DRLGCR) and properly located in our model (**Supplemental Figure 1**). Sequence identity (13.2%) and similarity (29.5%) to the FucP template (PDB no. 3O7P) are depicted in **Figure 4(e)**, and residue properties in **Figure 4(f)** and **4(g)**. Importantly, no charged and only few polar residues were found to face the lipid bilayer. Together, these observations re-enforce the accuracy of our model.

After embedding the MCT8 protein model in a lipid bilayer (see **Supplemental Materials and Methods**) and subsequent molecular dynamic simulations for 4 ns, all side-chains of residues that have been assessed in the present and previously reported chemical modification studies were localized in the model (**Figure 5(a); Supplemental Figure 4**). In line with these studies, Cys481 (ECL5), Cys497 (TMD10), Arg271 (ECL2), Arg445 (TMD8), and His192 (TMD1) are indeed predicted at accessible locations, allowing chemical modification (**Figure 5(a); Supplemental Figure 4**). The localization of Cys497, Arg445, and His192 at the substrate pore is in line with the observed protective effect of substrate on these modifications (10, 11). Moreover, the Asp498 residue is located in close proximity of Arg445, allowing interactions (10). Importantly, all other Cys, Arg, His, and Trp residues were found at positions that are inaccessible for chemical modification (in TMDs but not facing the substrate pore or in ICLs) or at positions where chemical modification is not likely to interfere with TH transport (*e.g.,* in ECLs).

Next, we located residues that are affected by missense mutations in patients who have AHDS of which also the Ala substitutions have been shown to be detrimental for MCT8 function (His192, Arg445, Asp498) in **Figure 5(b)** (10, 11). Indeed, the side-chains of these residues are all oriented toward the substrate pore. We have previously found that Ala substitution of Ser290, found to be mutated to Phe in a patient with AHDS, did not affect TH transport capacity, suggesting a less important role of the native Ser residue (14). Our model suggests that the side-chain of this residue is orientated toward TMDs 1, 3, and 6, compatible with the less important functional role of Ser290 itself. In this case, the introduction of the much larger Phe residue is more likely to be pathogenic caused by steric interference with residues located in the surrounding TMDs (**Figure 5(b)**).

Finally, we focused on the characterization of the substrate-binding center. By modeling of the molecular surface of the MCT8 protein, a central substrate pore was observed (**Figure 6(a)**).

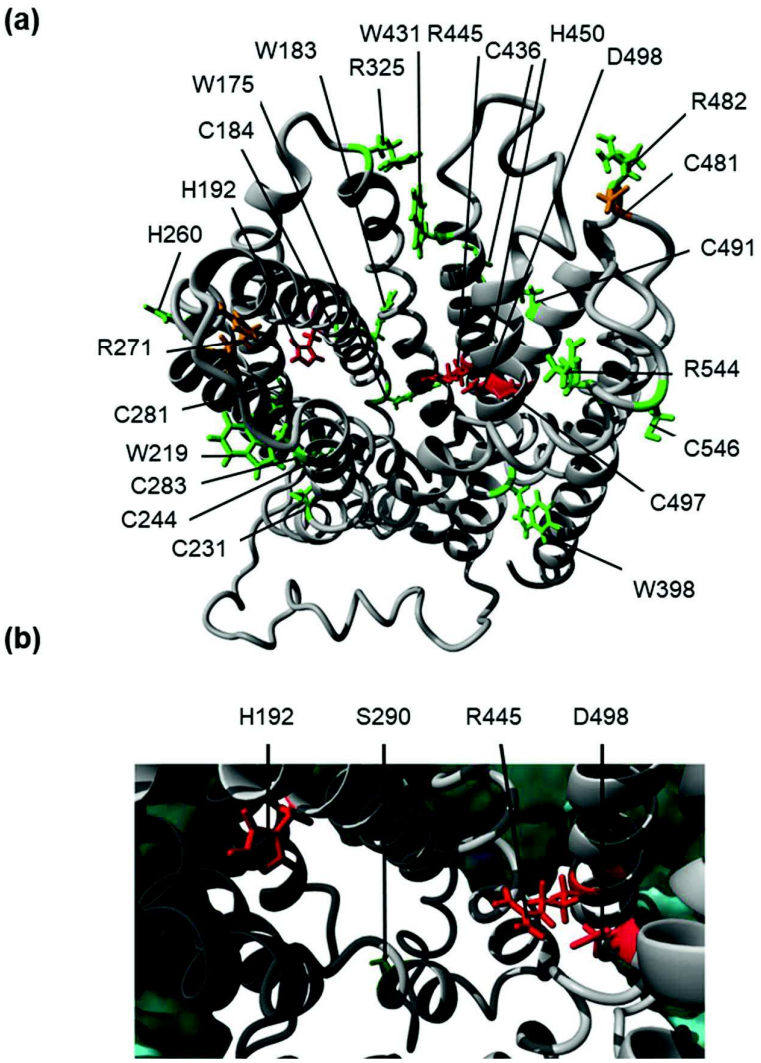

Figure 5 (a) Overview of the locations of all His, Cys, Trp, and Arg residues in MCT8 tested in the present and previously reported chemical modification studies, as well as the Asp498 residue. Residues that are not modified by any of the chemical modifiers are colored green, targets that are located outside the substrate pore are colored orange, and targets that are located within close vicinity of the predicted substrate-binding center are colored red, as well as the Asp498. For clarity reasons, the lipid bilayer is not depicted in this figure, but can be found in Supplemental Fig. 3. Images are generated using YASARA and PovRay imaging software. (**b**) Residues that have been found to be mutated in patients who have AHDS of which both the patient mutation and its Ala substitution have been tested. In red, both patient and Ala substitution strongly reduced MCT8-mediated TH transport; and in green, Ala substation was fully functional.

Hydrophobic residues in the middle and polar/charged residues at the bottom primarily flank this substrate pore (**Figure 6(a)**). Two basic residues (His192, Arg445) and one acidic residue (Asp498) were located at the bottom end, which is presumed to be the substrate-binding center. The distance between His192 and Arg445 is about 15 Å, which fits with the size of a TH molecule. We next modeled a T3 molecule at the substrate-binding center and highlighted the molecular surface of residue side-chains that are located within 5 Å (**Figure 6(b)**).

Indeed, the T3 molecule exactly fits between His192 and Arg445, which is in agreement with the current and previous in vitro data (**Fig. 6(b)** and **6(c)**) (4, 10, 11). During molecular dynamic simulations, a hydrogen bond between His192 and the phenolic hydroxyl group of T3 was observed, as well as an alternating hydrogen bond between the ω-amino groups of Arg445 and the carboxyl group of T3 (**Figure 6(c); Supplemental Figure 5**). Furthermore, a (transient) hydrogen bond between the δ-NH group of Arg445 and γ-COOH group of Asp498 was observed (**Supplemental Figure 5(a)**), whereas in the absence of substrate, the γ-COOH group of Asp498 could also interact with a ω-NH2 group of Arg445 (**Supplemental Figure 5(b)**). Although molecular dynamic simulations have limitations when performed on homology models, these predictions are consistent with the hypothesis that the presence of substrate can modify interhelical interactions between Arg445 (TMD8) and Asp498 (TMD10).

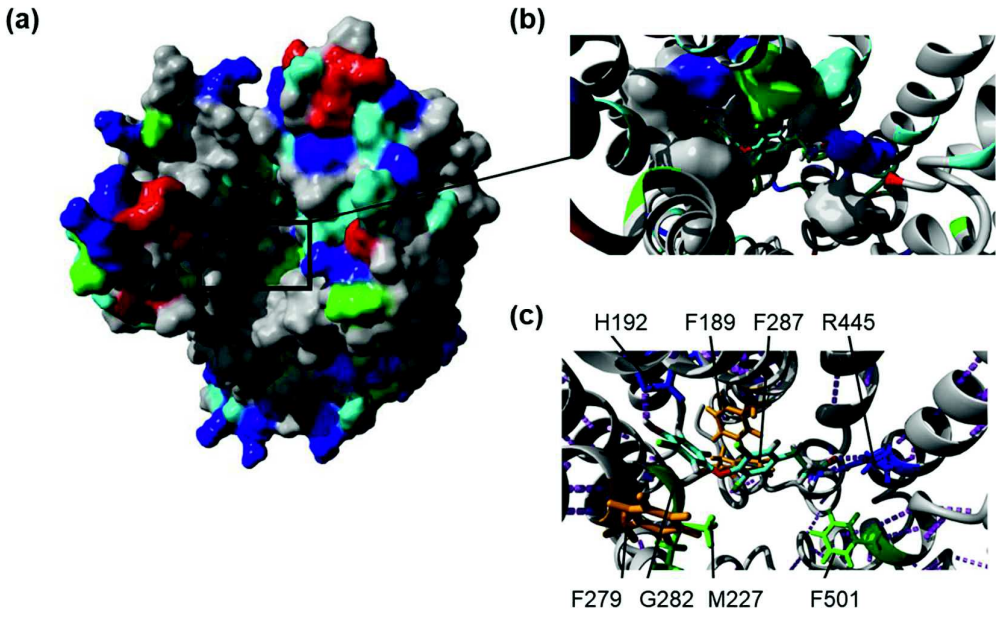

Figure 6 (a) Molecular surface of MCT8 colored similarly as in Figure 4(f) and 4(g). Note the accumulation of charged residues at the extracellular and intracellular termini, whereas the central substrate pore is predominantly formed by hydrophobic residues and polar/charged residues at the bottom. (**b**) A magnification from (**a**): the molecular surface of the presumed substrate-binding pocket, with a T3 molecule docked into the central cavity. (**c)** The presumed substrate-binding center, after a 2-ns Molecular Dynamic Simulation in an AMBER14 force field, depicted as carbon backbones with visible side-chains for the indicated residues, all located within 5 Å proximity of the T3 molecule. Dashed purple lines represent H-bonds involving carbon backbones or the depicted residues. Note the H-bond between His192 and the outer-ring hydroxyl group of T3, and between Arg445 and carboxyl group of T3. Images are generated using YASARA and PovRay imaging software.

Subsequently, we sought to test the accuracy of our homology model by predicting relevant residues in the substrate-binding center with subsequent functional assays. The following six residues were located within 5 Å distance from the T3 molecule: Phe189 (TMD1), Met227 (TMD2), Phe279 (TMD4), Gly282 (TMD4), Phe287 (TMD4), and Phe501 (TMD10) (**Figure 6(c)**). The aromatic side chain of Phe279 parallels that of His192, together forming a cavity in which the phenolic ring of TH perfectly fits. Both Phe189 and Gly282 form the bottom of this cavity. Phe287 forms the bottom of the substrate-binding center and faces the β-methylene group and tyrosyl ring of the T3 molecule. The side-chains of Met227 and Phe501 predominantly point toward the tyrosyl ring and β-methylene group of T3, respectively. To explore the importance of these relatively bulky Phe and Met side-chains in substrate translocation, we substituted these residues with the smaller Ala residue. Moreover, Gly282 was substituted with Ala to increase the size of the side-chain. Interestingly, we have previously described the inactivating effect of the G282C mutation, which was identified in a patient with AHDS (13).

In COS-1 cells, the F279A and F287A mutants showed the strongest decrease in TH uptake in the presence of CRYM (**Figure 7(d)**). Interestingly, T4 uptake was even more affected by the F287A mutation than T3 uptake. The F189A mutation also significantly reduced T3 uptake, whereas T4 uptake was less affected. The M227A mutant showed slightly higher T3 and T4 accumulation compared with WT (**Figure 7(d)**). The G282A and F501A mutations did not affect TH uptake at these low (1 nM) substrate concentrations. Although a similar pattern was observed in JEG-3 cells (**Figure 7(e)**), all mutations had a somewhat greater effect compared with COS-1 cells, in particular the F279A and G282A mutants. This discrepancy is a common observation (12, 38), and may be related to the lower protein expression levels in transiently transfected JEG-3 cells, perhaps reflecting a limited capacity to process overexpressed proteins. Hence, mutations that (also) affect protein stability or trafficking often display stronger impact on MCT8 transport function in JEG-3 cells.

Finally, we evaluated the impact of all mutations on T3 transport kinetics. All mutations resulted in a decrease of apparent Vmax of T3 transport, most predominantly for the F189A, F279A, and F287A substitutions (**Figure 8(a)** and **8(b)**; **Supplemental Table 6**). Moreover, the M227A, F279A, F287A, and F501A substitutions resulted in a significant reduction of apparent Km, which may be consistent with an altered mode of substrate binding (**Figure 8(b); Supplemental Table 6**). Upon normalization for cell surface protein expression levels, the Vmax of the F279A and G282A mutant did not significantly differ from WT, suggesting that the decrease in Vmax of these substituents may be predominantly driven by a reduction of cell surface expression levels (**Supplemental Table 6**). Interestingly, after correction for cell surface expression levels, the transport efficiency (as indicated by the Vmax/Km ratio) of the F279A and G282A mutants significantly increased over WT, which suggests that although both mutations interfere with cell membrane expression they may increase the intrinsic transport activity of MCT8. In contrast, the F189A and F287A mutants significantly reduced transport efficiency as indicated by the reduction in the Vmax/Km ratio (**Fig. 8(b); Supplemental Table 6**).

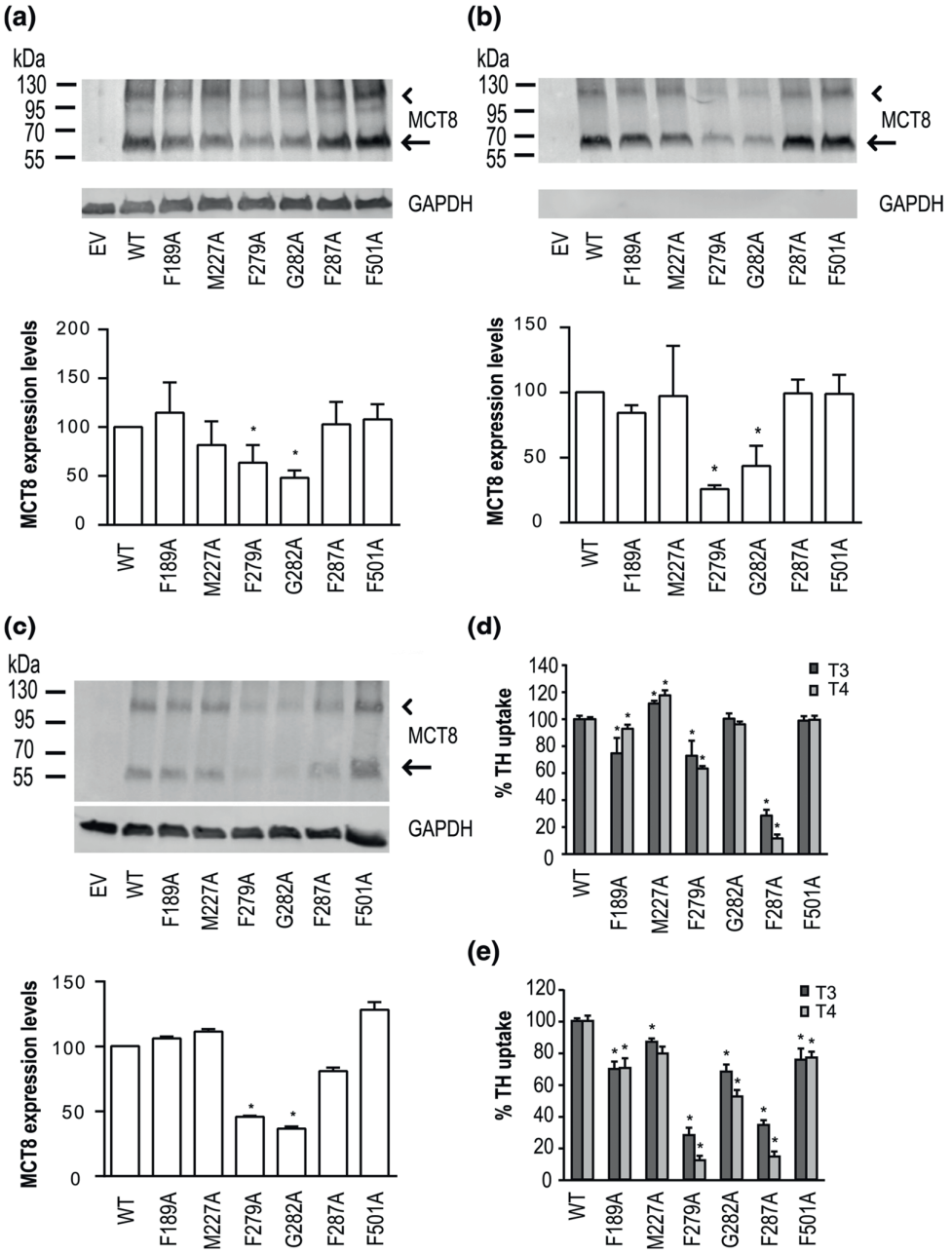

Figure 7 Representative Western blot analyses on (**a**) total lysates and (**b**) the cell surface fraction derived from COS-1 cells or (**c**) on total lysates derived from JEG-3 cells transfected with pcDNA3 EV, WT, or indicated mutant MCT8. (**a**) The total lysates in COS-1 cells comprise the 5% input sample of the cell surface biotinylation assay of which the biotinylated fraction is presented in (**b**). MCT8 detection was performed with the N-terminal MCT8 antibody (3353) and visualized with IRDye680 goat anti-rabbit secondary antibody. GAPDH was used as loading control. Bands of approximately 55 kDa, representing the MCT8 monomer (arrow), and a second band around 110 kDa, representing the MCT8 homodimer (arrowhead), were observed in cells transfected with WT or mutant MCT8 constructs. MCT8 and GADPH expression levels were quantified by densitometry using ImageJ. (**a** and **c**) For total lysates WT and mutant MCT8 expression levels are expressed as MCT8/GADPH ratio relative to WT MCT8 (100%) and presented as mean ± standard error of the mean (SEM) of two to three independent experiments. WT and mutant MCT8 cell surface expression levels in COS-1 cells are expressed as MCT8 (surface)/GADPH (input) ratio relative to WT MCT8 (100%) and presented as mean ± SEM of two independent

experiments. T3 (dark gray) and T4 (light gray) uptake by COS-1 (**d**) and JEG-3 (**e**) cells transiently cotransfected with WT or indicated mutant MCT8 and CRYM in 5 minutes at 37°C. All uptake values are corrected for background TH uptake levels observed in COS-1 or JEG-3 cells transfected with pcDNA3 EV. Results are presented as means ± SEM (n = 4 to 6). Statistical significance was tested using one-way analysis of variance followed by Dunnett multiple-comparison test. Statistically significant differences are indicated with an asterisk (*).

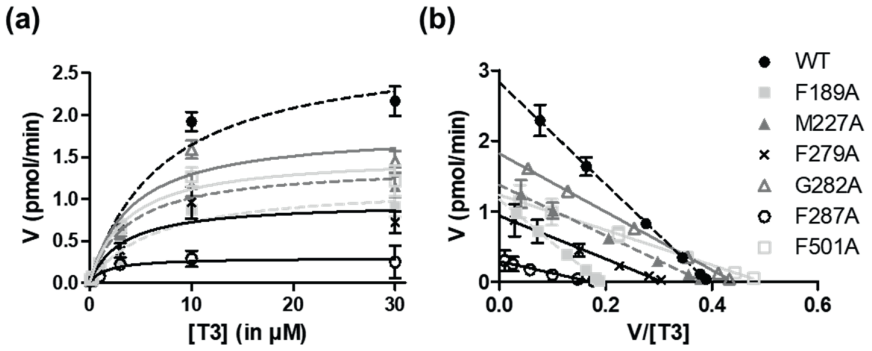

Figure 8 (a) Michaelis-Menten Plot showing kinetic properties of WT and mutant MCT8 transiently expressed in COS-1 cells in the absence of CRYM. The uptake in cells transfected with pcDNA3 EV was subtracted as background. Incubations were performed for 10 minutes at 37°C with increasing concentrations of T3. Data are expressed as means of three independent experiments performed in duplo ± standard error of the mean (SEM). (**b**) Eadie-Hofstee plot of the data depicted in (**a**), shown as mean values ± SEM. Km and Vmax values, uncorrected and corrected for protein expression levels, can be found in **Supplemental Table 6**.

DISCUSSION

In the current study, we provide insights into the protein structure and substrate docking mechanism of MCT8 in the outward-open conformation. Our current studies identified Arg271 and Arg445 as accessible residues. These and previously published in vitro findings (10, 11, 17) were used to guide the construction of an MCT8 homology model in outward-open conformation. In line with these studies, our model suggested that Arg445 (TMD8) and His192 (TMD1) directly interact with T3 at the substrate-binding center of MCT8 in the outward-open conformation. Moreover, we here demonstrated that other residues predicted at the substrate-binding center have varying importance for substrate translocation, depending on their relative orientation toward the substrate.

Extensive in vitro analyses were done to gather structural information to guide the homology modeling procedure. In addition to the previously identified accessible residues Cys481, Cys497, and His192, we here identified Arg271 and Arg445 as accessible targets for PG modification. Given the partial protective effect of substrate, at least one of these residues should be exposed at the substrate pore. Indeed, our outward-open model predicts Arg445 at the substrate-binding center and molecular dynamic simulations even suggested a direct interaction with the carboxyl group of T3. Although the importance of the Arg445 residue has been previously illustrated by the deleterious effects of the R445C mutation, found in a patient with AHDS, and the experimental R445A mutation (10, 39), we here provided in vitro evidence that may support the involvement of Arg445 in direct substrate interactions. Interestingly, iodothyronamines, which lack the carboxyl group, are not substrates for MCT8 (4). Together, this suggests that the interaction between the negatively charged carboxyl group of TH and the positively charged guanidine-group of Arg445 is an important determinant in substrate recognition. Of interest, Arg601 at the substrate-binding center of the T4 transporter Organic Anion

Transporter Protein 1C1 is also crucial for interaction with the carboxyl group of T4, suggesting that TH transporters may share common features in their substrate interaction mechanism (40).

Moreover, our model provides insights into how this interaction may induce conformational changes of the MCT8 protein upon substrate binding. Although molecular dynamic simulations should be interpreted with caution if performed on protein structure models, a hydrogen bond or electrostatic interaction between Arg445 (TMD8) and Asp498 (TMD10) is observed, in line with our previous in vitro data (10). Alterations of this interaction in the presence of substrate change the orientation of the Asp498 side-chain and hence TMD10, which may contribute to the substrate-induced conformational changes. The negatively charged carboxyl group of TH may thus compete with Asp498 for hydrogen bond formation with Arg445. The importance of the negatively charged Asp498 residue is illustrated by the deleterious effect of the D498N patient mutation and the artificial D498A mutation, whereas the artificial D498E mutant retains full activity (10, 41). Although we have previously shown that the charge exchange double mutant R445D+D498R retained partial transporter activity, this is strongly reduced compared with WT MCT8 (10). Despite the preservation of the putative salt-bridge in this double mutant that may partly account for its higher residual transporter activity compared with the corresponding single mutants, the charge distribution and hence the structure of the binding pocket is likely to be altered. We speculate that due to the incorrect orientation of the charged side-chains, the efficiency by which the salt-bridge is disturbed by the substrate molecule is reduced, resulting in the observed decreased transporter activity.

The other PG target, Arg271, is predicted at the extracellular end of TMD4, permitting PG modification from the extracellular environment. Although a direct interaction with substrate is not likely regarding its position, alterations in the local structure may be detrimental for MCT8 function, as is illustrated by the identification of the R271H mutation in a patient with AHDS (42). Given the mild effect of the Ala substitution, the positive charge of Arg271 is not likely to be crucial for the maintenance of structural integrity. Indeed, a Leu is located at the corresponding position in MCT10, an efficient T3 transporter (20).

In line with previous in vitro studies, His192 was found to interact with the phenolic hydroxyl group of TH at the putative substrate-binding center (11). Of note, also the corresponding residue in GlpT (Arg45) is suggested to directly interact with substrate (43, 44), whereas the corresponding residue in FucP (Asn45) is clearly accessible from the substrate pore (35). Interestingly, the neighboring Asp46 in FucP residue has been suggested to directly interact with substrate and its substitution by an Asn or Ala completely abrogated transport function (35). Based on the MCT8 homology model in the inward-open conformation, it was postulated that His192 and Arg445 could form a His-Arg clamp to dock TH at the substrate-binding center (4, 10). Also in the outward-open conformation, a TH molecule could be docked between both residues, suggesting a similar substrate docking mechanism in both conformations, which is not uncommon for MFS transporters (43). Interestingly, despite its clear susceptibility for DEPC, the substitution of His192 by Ala has only minor effects on TH transport (11, 45), which suggests an important role for other residues in substrate docking. In addition, it should be noted that FucP contains a proline-kink in TMD1 one turn above the Asp46 residue resulting in an irregular α-helical backbone pattern. Because this Pro is not preserved in MCT8, prediction of the exact orientation of amino acid side-chains in TMD1 may be less accurate.

Although the inward-open model predicted a second His-Arg clamp involving His415 and Arg301, this is not observed in our current outward-open model in which His415 (extracellular end of TMD7) and Arg301 (intracellular end of TMD5) are located at distant sites (45). Especially the location of His415 differs from previous studies where it was predicted to be positioned close to the substrate-binding center in the middle of TMD7. However, the abundance of charged residues in close proximity of His415 (Lys418-Glu429), which are preferably located outside the cell membrane, pull His415 toward the extracellular end of TMD7 in our current structural alignment. Importantly, this localization is supported by our previous studies suggesting that the inhibitory effect of the His-specific reagent DEPC is solely mediated through modification of His192 (11). This implies that all other His residues (including His415) are located at inaccessible positions, or at positions where modification by DEPC does not interfere with substrate passage. Nevertheless, in vitro studies have suggested that different His415 substitutions affect substrate interactions (45). Further studies are required to elucidate the exact functional role of His415 during substrate translocation.

In addition, we showed that the Ala substitutions of Phe189, Met227, Phe279, Gly282, Phe287, and Phe501, all found within 5 Å from the substrate molecule at the substrate-binding center, results in varying reductions in apparent Vmax. Moreover, M227A, F279A, F287A, and F501A induce a decrease in apparent Km, suggesting an altered mode of substrate binding. These findings strengthen the current localization of these residues in our model. We speculate that the impact of their Ala substitution on T3 transport kinetics is related to the predicted orientation of the side-chains of these residues toward the substrate molecule.

The bulky side-chain of Phe287 forms the bottom of the putative substrate-binding center, and predominantly faces the β-methylene group of the iodothyronine substrate. We speculate that shortening of the Phe287 side chain may result in narrowing of the substrate-binding center, limiting the space for the substrate molecule. This could explain the greater impact of the F287A substitution on the transport of the larger substrate molecule T4, compared with T3. Alternatively, shortening of its side-chain may have unfavorable effects on the orientation of the carboxyl group of the substrate toward the Arg445 residue. Interestingly, recent studies suggested that substitution of the corresponding residue in MCT10 (Tyr184) with Phe allows T4 transport by MCT10, supporting our hypothesis that the amino acid side-chain at this position is important for substrate docking and selection (46).

The aromatic side chain of Phe279 parallels the side chain of His192, which together with Gly282 and Phe189 form a cavity in which the phenolic ring of TH perfectly fits. We speculate that Phe279 and His192 prevent the rotation of the iodothyronine phenolic ring in the substrate pore. Shortening of the Phe279 side-chain to an Ala may increase substrate mobility and thereby alter transporter kinetics. Importantly, the F279A mutation clearly decreased cell surface expression, which indicates that a bulky side-chain at this position may be important for protein integrity. Although Phe189 and Gly282 both form the bottom of the cavity, Phe189 also faces part of the iodothyronine tyrosyl ring and likely modulates the angle between the two aromatic rings in TH. In addition to the larger change in side-chain volume in case of a Phe to Ala substitution, this may partly explain the greater impact of F189A compared with G282A. The observed reduction in Vmax of the G282A substituent appeared to be predominantly caused by a reduction in total MCT8 protein and cell surface expression levels, rather than interference with substrate translocation. Although it would have been of interest to study the impact of the introduction of larger residues at this position, further side-chain elongation to a Cys

already severely affects protein stability and subcellular localization, hampering the assessment of its impact on substrate translocation efficiency (13). Of note, Tyr34 in MCT1, corresponding to Phe189 in MCT8, was recently suggested to directly interact with its inhibitor AR-C155858, supporting our current findings (47).

The M227A and F501A mutants only moderately affect T3 transport kinetics, suggesting that these residues do not interact importantly with the substrate. Met227 is predicted to face the ether bond and one of the iodine substituents in the tyrosyl ring of the T3 molecule. Both 3,3',5'-triiodo-L-thyronine (rT3) and 3,3'-diiodo-L-thyronine, which have only one iodine substituent in this ring, are suitable substrates for MCT8. This indicates that double substitution of the inner ring is not required for iodothyronine transport by MCT8. Phe501 predominantly faces the β-methylene group of the alanine side-chain of T3 from the side. Because the carboxyl group already firmly interacts with the Arg445, located in close structural proximity, the relative contribution of Phe501 may be less important. It is not excluded that the bulky side-chains of the Met227 and Phe501 residues have a role in determining substrate specificity by excluding larger substrates.

The strength of our model is that it accommodates all currently available in vitro results from chemical modification studies. Moreover, any alternative alignment of especially TMD1, TMD4, TMD8, and TMD10, together constituting the major part of the substrate-binding center, would conflict with these in vitro findings, re-enforcing the accuracy of our current outward-open model. In contrast, strong structural clues for several other TMDs (e.g., TMDs 3, 6, 9, and 12) are currently lacking. Given their expected structural organization, these domains are likely to be inaccessible for chemical modification, warranting different experimental approaches to validate their structural organization. Characterization of missense mutations encountered in patients who have AHDS and the substitution of the affected residue by an Ala or a residue that shares specific functional or structural characteristics with the original residue could help to define which functional and structural properties of the native residue are required for optimal MCT8 function. This may help to further validate and optimize the predicted structure of these inaccessible domains. Although our current model explains many of the available in vitro data, this may also be the case for other models based on different templates or target-template alignments. In the end, discrepancies between the existing models (e.g., the position of His415) will be resolved only when crystal structures of MCT8 or one of its MCT family members have been elucidated. Additionally, the crystallization of other MFS members with higher sequence similarity to MCT8 than FucP (29.5%) would offer more suitable templates for structural modeling. We also emphasize that details on amino acid side-chain orientation should be considered with some reservation, especially in those parts of the model at which the predicted secondary structure of MCT8 differs from that of the template (e.g., TMD1). In this respect, it should also be noted that the relatively low resolution of the FucP template crystal (3.2 Å) may already hamper correct prediction of amino acid side-chains due to uncertainties in the template structure itself.

Taken together, we here report a structural model of MCT8 in outward-open conformation, providing insights into MCT8 structure and function. Our model improves our understanding of the recognition and binding of extracellular substrate. We demonstrate that our model can be used as a complementary tool in the analysis of the pathogenic mechanism of several previously reported missense mutations, identified in patients who have AHDS. Further refinement will also allow its use for in silico prediction of the pathogenicity of newly identified mutations and screens for putative novel MCT8 substrates and inhibitors.

Acknowledgements

We thank R. E. van Heerebeek and S. Leeuwenburg for their technical assistance and the Optical Imaging Center (Erasmus MC Rotterdam) for the technical support regarding the confocal imaging studies. After we submitted our original manuscript, another study addressing the MCT8 structure-function relationship was published online (48).

Financial Support: This work was supported by a grant from the Netherlands Organisation for Health Research and Development (project no. 113303005) (to W.E.V.) and from the Sherman Foundation (to W.E.V.).

Disclosure Summary: The authors have nothing to disclose.

SUPPLEMENTAL DATA

Supplemental Materials and Methods

Molecular dynamic simulations

Prior to molecular dynamic simulations, a T3 molecule was manually introduced into the substrate pore in proximity of the proposed substrate binding center at the bottom of the substrate pore. To mimic the natural environment of the MCT8 protein, all molecular dynamic simulations in the presence and absence of substrate were carried out in a membrane environment as described below.

Firstly, (fixed) water molecules were introduced in the substrate pore to keep the pore solvated during the equilibration step of the simulations. Next, a membrane structure consisting of phosphatidyl-ethanolamine molecules was set up automatically using the md_runmembrane macro of YASARA Structure. Briefly, the protein was scanned for exposed transmembrane helices (i.e. helices longer than 16 residues, with more than seven hydrophobic residues of which more than three had an accessible side-chain surface area >30% of the maximum). The major axis vectors of these helices (i.e. the direction vectors of the least-squares lines through the Cα atoms) were summed up to obtain the major axis of the protein, which was then oriented along the Y-axis, normally with respect to the plane of the membrane and the XZ-plane. The best shift of the membrane along this major axis was obtained by scanning the protein for the region with the largest number of exposed hydrophobic residues (see definition above) and a width of 28 Å (corresponding to the membrane core). Having placed an equilibrated membrane structure at this location named 'MemCenterY', the system was enclosed in a simulation cell of size [87.31*92.46*89.53] Å.

Next, the MCT8 protein was temporarily scaled by a factor 0.9 along the XZ-axes and strongly clashing membrane lipids were deleted (lipids with an atom closer than 0.75 Å to a protein atom). The temporary protein scaling, which was needed to avoid the deletion of too many lipids around the protein, was then slowly removed during a short simulation at 298 K in vacuo: the MCT8 protein (with all atoms kept fixed) was scaled by 1.02 along the XZ-axes every 200 femtoseconds, while the membrane was allowed to move, but restrained to ideal geometry (by pulling lipid residues with an atom further than 21.5 Å away from MemCenterY back into the membrane, and by pushing phosphorus atoms closer than 14 Å to MemCenterY back outwards). The force field was AMBER14,

with GAFF/AM1BCC parameters for non-standard residues. As soon as the MCT8 protein had reached its original size again, the protein side-chain pKa's were predicted (49), protonation states assigned according to pH 7.4, and the simulation cell was filled with water, 0.9% NaCl and counter ions (50). The main simulation was then run with the Particle Mesh Ewald algorithm and 8.0 Å cutoff for non-bonded real space forces, a 4 femtosecond time-step, constrained hydrogen atoms, and at constant pressure and temperature (NPT ensemble), as described in detail previously (51). During the initial 250 picoseconds, the membrane was restrained to avoid distortions while the simulation cell adapted to the pressure exerted by the membrane and additionally water molecules that became closer than 14 Å to MemCenterY were pushed outside the membrane, except for the water molecules inside the substrate pore which were released again during this step of the simulation to allow free movement. The source code of this simulation protocol and visualizations of the individual steps can be found at www.yasara.org/membranemd. After this equilibration step, further molecular dynamic simulations were carried out in an AMBER14 force field with periodic boundaries for a period of 4 nanoseconds. Snapshots of the substrate binding pore were taken after 2 and 4 nanosecond. All images were created using YASARA Structure and Pov-Ray v3.6 software (www.povray.org).

Supplemental tables

Supplemental Table 1 Antibody Table

Target protein/ antigen	Antigen Sequence (if known)	Name of Antibody	Species Raised (polyclonal or monoclonal)	Manufacturer (and catalog number)	Dilution used for WB	Dilution used for ICH
hMCT8	AA 52-155	MCT8	Rabbit (p)	ATLAS (HPA003353)	1:20000	1:1000
GAPDH		GAPDH	Mouse (m)	Millipore (Mab 374)	1:20000	
ZO1		ZO1	Mouse (m)	Invitrogen (61-7300)		1:1000
Rabbit IgG		IRDye680	Goat	LI-COR	1:20000	
Mouse IgG		IRDye800	Goat	LI-COR	1:20000	
Rabbit IgG		Alexa 488	Goat	Invitrogen		1:1000
Mouse IgG		Alexa 633	Goat	Invitrogen		1:1000

GAPDH: glyceraldehyde-3-phosphate dehydrogenase; ZO-1: zona occludens 1;P: polyclonal antibody; M: monoclonal anitbodyWB: Western Blot ; ICH: immunohistochemistry

Supplemental Table 2 Overview of primers

Name	sequence from 5' to 3'
W175F_Rev	cagcgaacaccaccacaaagccgaagccaccttc
W175F_Fw	gaaggtggcttcggctttgtggtggtgttcgctg
W175A_Fw	aaggtggcttcggcgcggtggtggtgttcg
W175A_Rev	cgaacaccaccaccgcgccgaagccacctt
W183F_Rev	tggagccgttgcaaaaggtggcagcgaacacc
W183F_Fw	ggtgttcgctgccacctttttgcaacggctcca
W183A_Rev	ggagccgttgcacgcggtggcagcgaac
W183A_Fw	gttcgctgccaccgcgtgcaacggctcc
W219F_Rev	gagggctccgacaaatgctgcttggaactccacttg
W219F_Fw	caagtggagttccaagcagcatttgtcggagccctc
W219A_Rev	gagggctccgaccgctgctgcttggaactc
W219A_Fw	gagttccaagcagcagcggtcggagccctc
W398F_Rev	aattccgaaggcaaagatgcggtaagtgcgttggcgg
W398F_Fw	ccgccaacgcacttaccgcatctttgccttcggaatt
W398A_Rev	cgcacttaccgcatcgcggccttcggaattgc
W398A_Fw	gcaattccgaaggccgcgatgcggtaagtgcg
W431F_Rev	ccaatacacaccaagagcacaaaggtctccttgatttctgag
W431F_Fw	ctcagaaatcaaggagacctttgtgctcttggtgtgtattgg
W431A_Rev	aatacacaccaagagcaccgcggtctccttgatttctgag
W431A_Fw	ctcagaaatcaaggagaccgcggtgctcttggtgtgtatt
R271K_Fw	caccagctccctaagcctgaaatacttcacctacgggattc
R271K_Rev	gaatcccgtaggtgaagtatttcaggcttagggagctggtg
R271A_Fw	agctccctaagcctggcctacttcacctacgg
R271A_Rev	ccgtaggtgaagtaggccaggcttagggagct
R325K_Fw	cttccccttcctcatcaaaatgctgggggataaga
R325K_Rev	tcttatcccccagcattttgatgaggaaggggaag
R325A_Fw	ccttccccttcctcatcgcaatgctgggggataaga
R325A_Rev	tcttatcccccagcattgcgatgaggaaggggaagg
R482K_Fw	tgattcccctgtgcaaggacttcgggggcc
R482K_Rev	ggcccccgaagtccttgcacaggggaatca
R482A_Fw	gcccccgaagtccgcgcacaggggaatc
R482A_Rev	gattcccctgtgcgcggacttcgggggc
R544K_Fw	ccccattgcaggcctactcaaaaactgttttggggactacc
R544K_Rev	ggtagtccccaaaacagtttttgagtaggcctgcaatgggg
R544A_Fw	cattgcaggcctactcgccaactgttttggggac
R544A_Rev	gtccccaaaacagttggcgagtaggcctgcaatg
F189A_FW	ggtgcaacggctccatcgccggcatccataactctg

Overview of primers continued	
Name	**sequence from 5' to 3'**
F189A_Rev	cagagttatggatgccggcgatggagccgttgcacc
M227A_Fw	gagccctcgcgatgggtgcgatcttcttctgttctcc
M227A_Rev	ggagaacagaagaagatcgcacccatcgcgagggctc
F279A_Fw	cttcacctacgggattctcgctggttgtggctgttccttc
F279A_Rev	gaaggaacagccacaaccagcgagaatcccgtaggtgaag
G282A_Fw	gattctctttggttgtgcctgttccttcgcctttc
G282A_Rev	gaaaggcgaaggaacaggcacaaccaaagagaatc
F287A_Fw	ggctgttccttcgccgctcagccatccctcgt
F287A_Rev	acgagggatggctgagcggcgaaggaacagcc
F502A_Fw	gcctttgcgatggcttcgccatcaccatcatggccc
F502A_Rev	gggccatgatggtgatggcgaagccatcgcaaaggc

Supplemental Table 3 Overview of top 5 templates for homology modeling

Name PDB	**Name**	**Psi-BLAST Alignment score**	**Coverage (in %)**	**Resolution (in A)**	**Quality score (crystal)**	**Conformation**
3O7Q	FucP	84	70	3.14	0.473	Outward-open
3O7P	FucP	77	69	3.20	0.425	Outward-open
4XNJ	PEPT-2	54	40	2.30	0.568	Inward-open
4D2D	PEPT-St	56	39	2.52	0.545	Inward-open
1PW4	GlpT	42	75	3.30	0.264	Inward-open

An overview of the characteristics of the top 5 most suitable crystal structures which were used to model different rotamer solutions of MCT8. FucP: *E. Coli* Fucose/Proton Symporter; PEPT-2: *E. Coli* peptide transporter *2;* GlpT: *E. Coli* Glycerol-3-Phosphate Transporter. The Psi-BLAST alignment score indicates the quality of the alignment of MCT8 to the indicated template (higher scores, indicate a better structural alignment). The percentage coverage indicates the amount of residues in MCT8 that were successfully aligned to the indicated template. The quality score reflects the quality of the PDB of the original crystal structure of the indicated template derived from the PDBFinder2 database ranging from 0.000 (terrible) to 1.000 (perfect).

Supplemental Table 4 Overview of structural hints derived from *in vitro* experiments

Res./mutation	Structural information	ref	Conclusion orientation/position
His192	Strong effect DEPC modification, part of substrate interaction site	11	Channel facing, substrate binding center
His260	No effect DEPC	11	ECL/ICL/hidden/lipid bilayer facing
His450	No effect DEPC	11	ECL/ICL/hidden/lipid bilayer facing
Trp175	No effect HNB	present	ECL/ICL/hidden/lipid bilayer facing
Trp183	No effect HNB	Present	ECL/ICL/hidden/lipid bilayer facing
Trp219	No effect HNB	Present	ECL/ICL/hidden/lipid bilayer facing
Trp398	No effect HNB	Present	ECL/ICL/hidden/lipid bilayer facing
Trp431	Marginal effect HNB modification	Present	Channel facing/ECL
Arg271	Target of PG, partial protective effect substrate, positive charge required,	Present	Channel facing/ECL, Arg271 or Arg445 at substrate binding center
Arg325	No effect PG	Present	ECL/ICL/hidden/lipid bilayer facing
Arg445	Target of PG, partial protective effect substrate, positive charge required, in structural proximity of Asp498	Present	Channel facing/ECL, Arg271 or Arg445 at substrate binding center, nearby Asp498 (H-bond)
Arg482	No effect PG	Present	ECL/ICL/hidden/lipid bilayer facing
Arg544	No effect PG	Present	ECL/ICL/hidden/lipid bilayer facing
Cys184	No effect PCMBS, or HgCl	17	ECL/ICL/hidden/lipid bilayer facing
Cys231	No effect PCMBS, or HgCl	17	ECL/ICL/hidden/lipid bilayer facing
Cys244	No effect PCMBS, or HgCl	17	ECL/ICL/hidden/lipid bilayer facing
Cys281	No effect PCMBS, or HgCl	17	ECL/ICL/hidden/lipid bilayer facing
Cys283	No effect PCMBS, or HgCl	17	ECL/ICL/hidden/lipid bilayer facing
Cys436	No effect PCMBS, or HgCl	17	ECL/ICL/hidden/lipid bilayer facing
Cys481	Target of PCMBS, partial protective effect substrate	17	Channel facing/ECL, Cys481 or Cys497 at substrate binding center
Cys491	No effect PCMBS, or HgCl	17	ECL/ICL/hidden/lipid bilayer facing
Cys497	Target of PCMBS, partial protective effect substrate	17	Channel facing/ECL, Cys481 or Cys497 at substrate binding center
Cys546	No effect PCMBS, or HgCl	17	ECL/ICL/hidden/lipid bilayer facing
Asp498	Close structural proximity of Arg445, negative charge required	10	Nearby Arg445 (H-bond)

Overview of the effects of different chemical modification studies and the conclusions that can be drawn from these studies regarding the orientation and position of the involved residues/ residue side-chains. All generated homology models were challenged by these structural hints and the most suitable model was selected for further loop optimization.

Supplemental Table 5 Conservation of Trp and Arg residues across species and other MCT family members

		Conservation	
Residue	***Predicted location***	***Species***	***Other MCTs***
Trp175	*TMD1*	All	All
Trp183	*TMD1*	All	MCT8 and MCT10
Trp219	*TMD2*	All	All
Trp398	*TMD7*	All	MCT8 and MCT10
Trp431	*TMD8*	All	MCT8
Arg271	*TMD4*	All	MCT8
Arg325	*ECL3*	Not (replaced by K)	MCT6,8,9,10
Arg445	*TMD8*	All	most
Arg482	*ECL5*	All	MCT3 and 8
Arg544	*ECL6*	All	MCT8,10,11,13

Overview of the conservation of indicated Trp and Arg residues among different MCT8 orthologs and other members of the MCT family. The predicted location is derived from previously described transmembrane predictions (4).

Supplemental Table 6 T3 transport kinetics by WT and mutant MCT8 proteins

		Non-normalized		*Cell surface expression levels*	*Normalized for cell surface protein expression levels*	
Construct	***Km (in µM)***	***Vmax (in pmol/min)***	***Vmax/Km***	***% relative to WT***	***Vmax (in pmol/min)***	***Vmax/Km***
WT	7.5 (± 1.4)	2.9 (±0.4)	0.39 (±0.04)	100	2.9 (±0.2)	0.39 (±0.04)
F189A	6.4 (± 1.0)	1.2 (±0.0) *	0.19 (±0.02) *	84.2 (±5.8)	1.4 (±0.1) *	0.23 (±0.03) *
M227A	3.9 (± 1.1)*	1.4 (± 0.3) *	0.38 (±0.05)	97.1 (±38.6)	1.4 (±0.3) *	0.40 (±0.06)
F279A	3.6 (±1.1) *	1.0 (± 0.3) *	0.31 (±0.10)	25.7 (±3.0) *	3.7 (±0.6)	1.23 (±0.38) *
G282A	4.4 (±0.8)	1.8 (±0.1) *	0.44 (±0.06)	43.4 (±15.5) *	4.18 (±0.2)	1.02 (±0.15) *
F287A	2.2 (±1.4) *	0.3 (±0.2) *	0.20 (±0.05) *	99.3 (±10.5)	0.3 (±0.2) *	0.20 (±0.05) *
F501A	2.4 (±0.4) *	1.2 (±0.3) *	0.49 (±0.04)	98.9 (±14.6)	1.3 (±0.2) *	0.50 (±0.04)

Overview of kinetic properties of T3 transport by WT or mutant MCT8. Kinetic analyses were performed in COS-1 cells transiently expressing WT or mutant MCT8 in the absence of CRYM. Data are present as means of 3 independent experiments performed in duplo +/- SEM. The Vmax and Vmax/Km ratios are presented as non-normalized values and presented as values normalized for cell surface protein expression levels using the cell surface expression levels of WT MCT8 as a reference. Cell surface expression levels were determined by surface biotinylation assays, of which a representative experiment is shown in Figure 7A. Cell surface expression levels were quantified by densitometry using ImageJ and presented as mean ± SEM of two independent experiments. One-way ANOVAs with Dunnet`s post-hoc tests for multiple comparison have been used to test for statistically significant differences. Significant differences are indicated by an *.

Supplemental figures

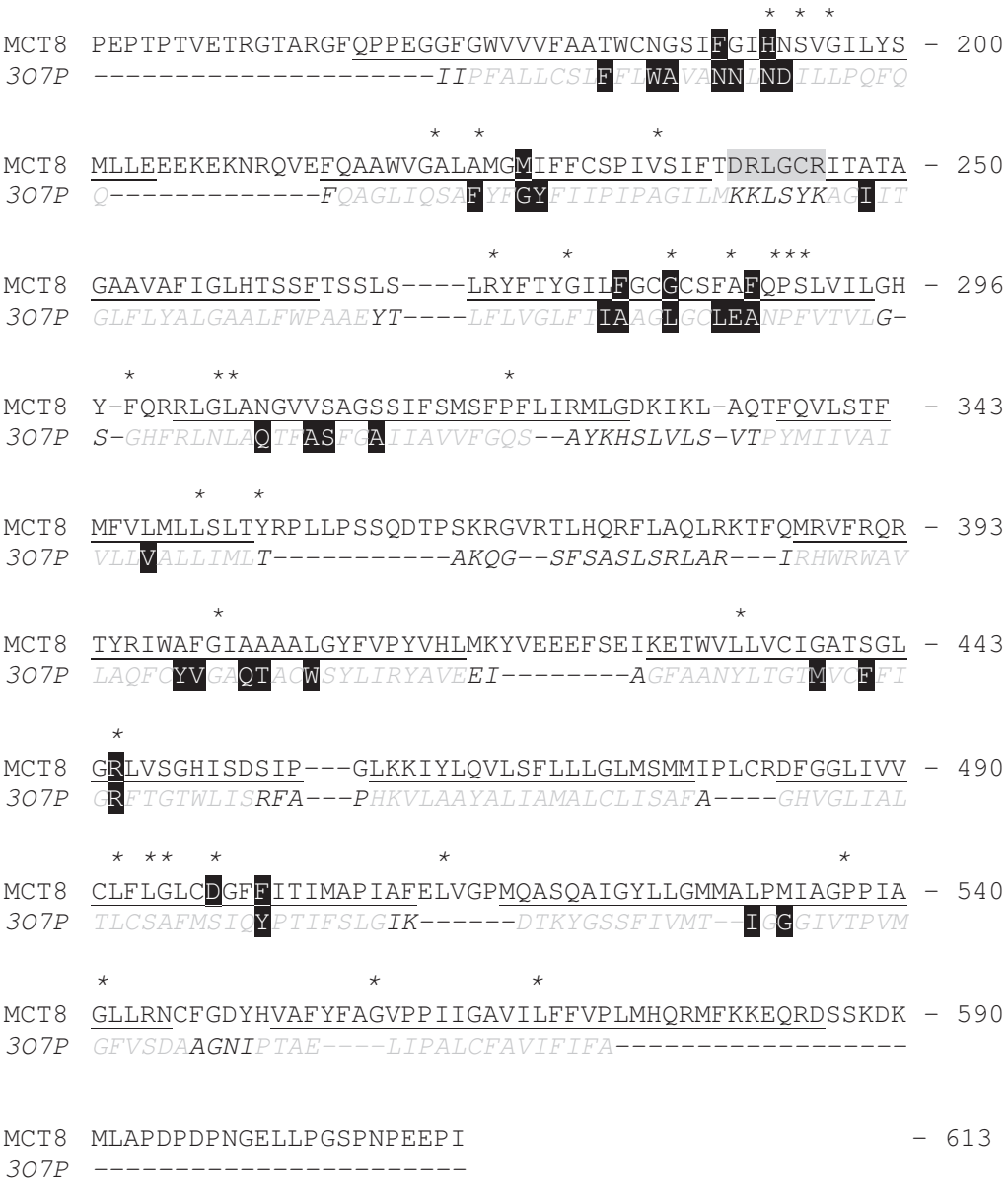

Supplemental Figure 1 Final alignment between MCT8 and FucP (3O7P) using multiple sequence alignments and position-specific scoring matrices (PSSM) implemented in YASARA Structure, as described in the methodology section. Here, the sequences of MCT8 (target) and FucP (template) are shown. Only template residues that keep their position in the model are displayed. All other residues (gaps in the template) are assumed to occupy a different position in the target model and are thus placed via loop modeling. (Helical) TMD parts are underlined (in MCT8) and grey (in FucP). Residues that have been found to be located at the predicted substrate binding center in MCT8 within 5 Å of the docked substrate molecule are highlighted in black. Residues that have accessible side-chains in FucP aligning the substrate pore are also highlighted in black and locations of single residue missense mutation found in AHDS patients are indicated with an *. When only taking into account the aligned residues, sequence similarity between target and template was found to be 29% (similarity was defined by a BLOSUM62 score>0, calculated by YASARA Structure).

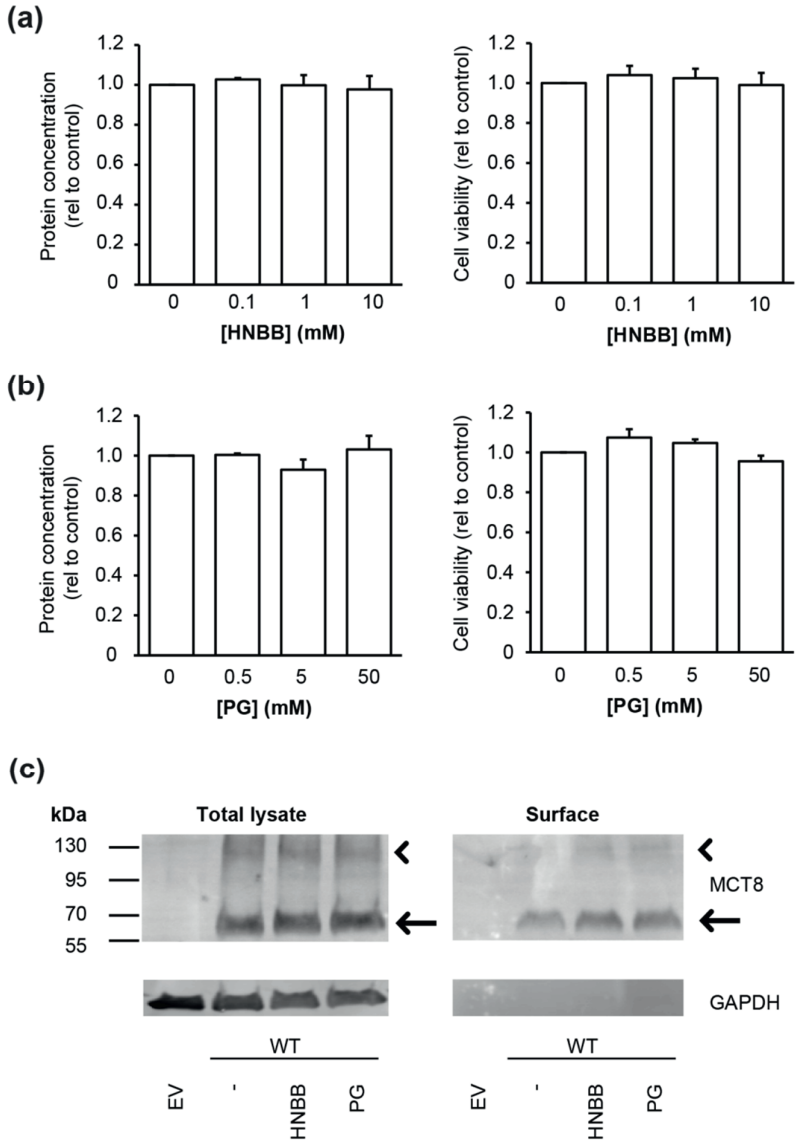

Supplemental Figure 2 Total protein concentration and cell viability of COS-1 cells pre-incubated for 10 minutes in the presence of increasing concentrations of 2-hydroxy-5-nitrobenzyl-bromide (HNBB) (**a**), or phenylglyoxal (PG) (**b**), demonstrating that these pre-incubation conditions do not induce cytotoxicity. (**c**) Representative Western blots showing the expression levels of WT MCT8 in the total lysate (left) and the cell surface fraction (right) of COS-1 cells pre-incubated with 10 mM HNBB or 50 mM PG prior to surface biotinylation assays. The total lysate (left) comprises a 5% input sample of the cell surface biotinylation assay by which the presented cell surface fraction (right) was isolated. MCT8 detection was performed with the N-terminal MCT8 antibody (3353) and visualized with IRDye680 goat anti-rabbit secondary antibody. Glyceraldehyde-3-phosphate dehydrogenase (GAPDH) was used as loading control. Bands of approximately 55 kDa, representing the MCT8 monomer (arrow), and a second band around 110 kDa, representing the MCT8 homodimer (arrowhead), were observed.

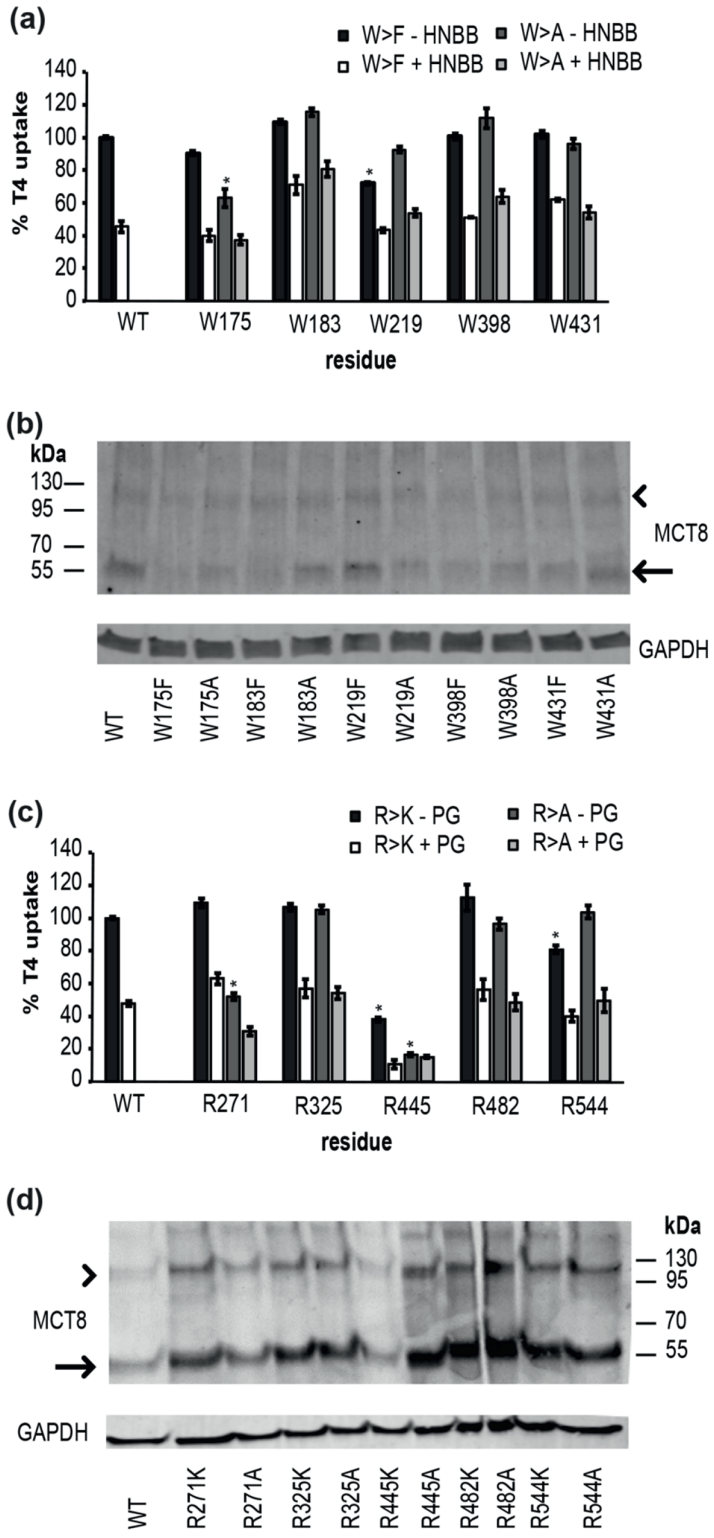

Supplemental Figure 3 Panel **(a)** and **(c)** show the T4 uptake by COS-1 cells co-expressing WT or mutant MCT8 and CRYM after pre-incubation in the presence or absence of 10 mM HNBB for 10 minutes. All values are corrected for background T3 uptake levels observed in COS-1 cells transfected with pcDNA3 empty vector (EV), pre-incubated under identical conditions. T3 uptake levels are expressed relative to MCT8-mediated T3 uptake

levels after pre-incubation in D-PBS without HNBB. Results are presented as means ± SEM (n = 3). Statistical significance was tested using 2-way ANOVA followed by Bonferroni's post-tests. *, P <0.05; **, P <0.01; ***, P <0.001. **(b)** and **(d)** Western blot of lysates from COS-1 cells transfected with WT or indicated mutant hMCT8. MCT8 detection was performed with the N-terminal MCT8 antibody (3353) and visualized with IRDye680 goat anti-rabbit secondary antibody. Glyceraldehyde-3-phosphate dehydrogenase (GAPDH) was used as loading control. The reactivity of the used antibodies with control cells transfected with the pcDNA3 EV can be found in **Figure 7A**. Bands of approximately 55 kDa, representing the MCT8 monomer (arrow), and a second band around 110 kDa, representing the MCT8 homodimer (arrowhead), were observed in cells transfected with WT or mutant MCT8 constructs.

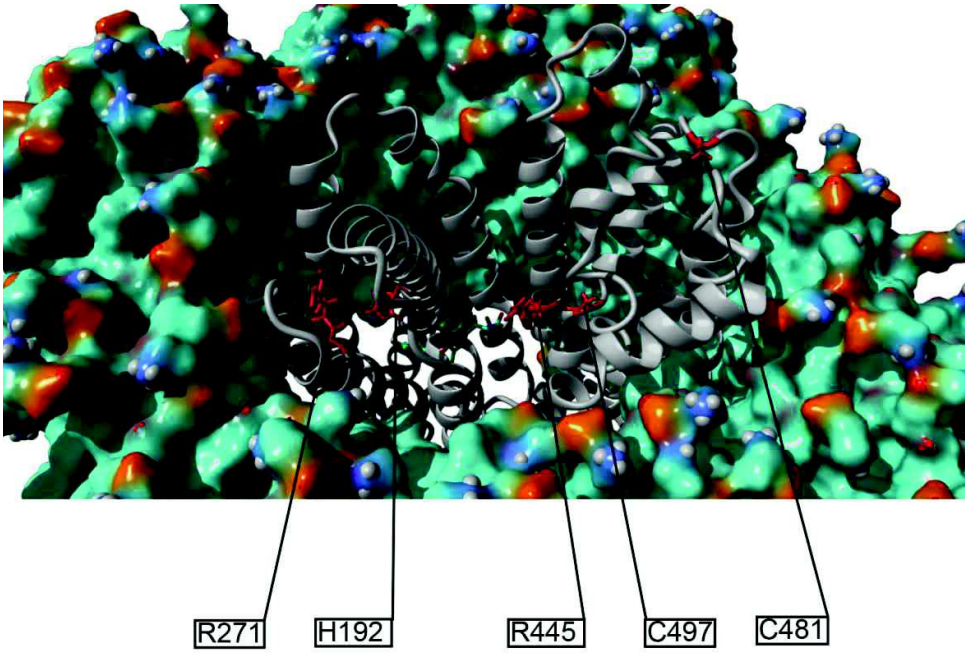

Supplemental Figure 4 MCT8 homology model in outward-open conformation integrated in a lipid bilayer. The residues that have been identified as targets for modifying reagents (His192, Arg271, Arg445, Cys481, and Cys497) are highlighted in red. The molecular surface of the lipid bilayer, consisting of phosphatidyl-ethanolamine molecules, is depicted. Note that Arg271 and Cys481 are not directly flanking the substrate pore. Image is generated using YASARA and PovRay imaging software.

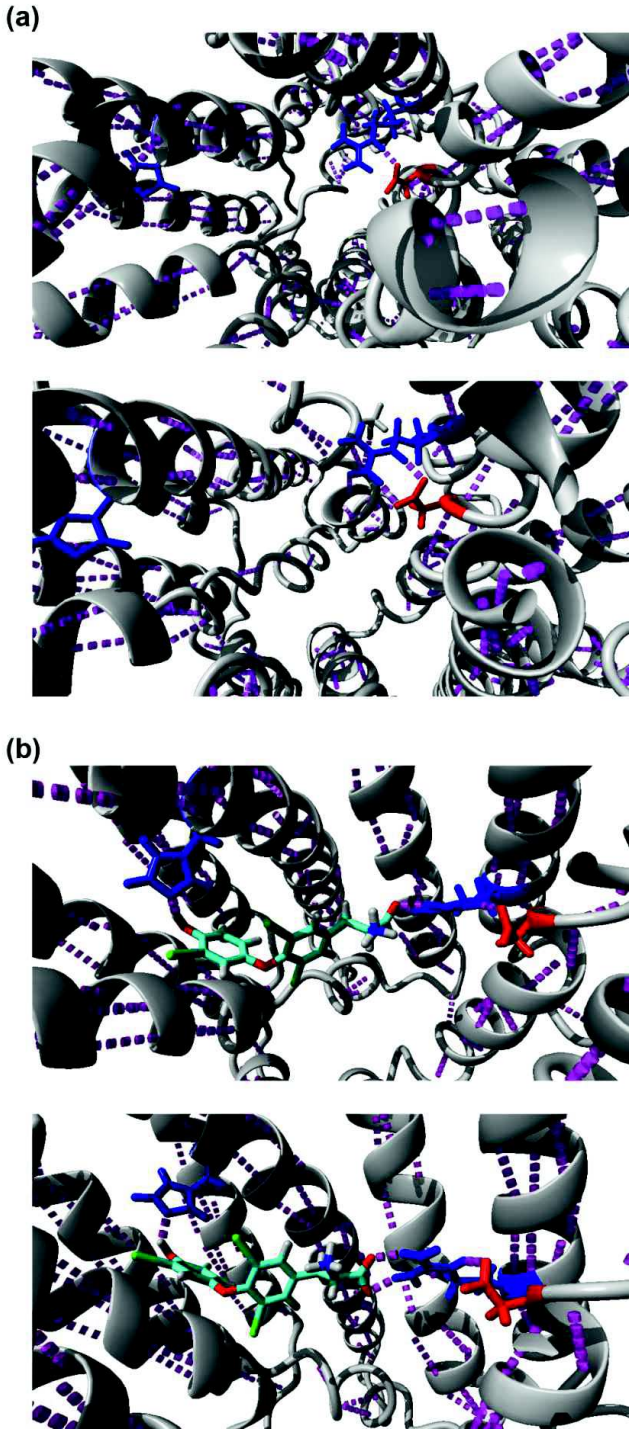

Supplemental Figure 5 Molecular dynamic simulations of the substrate pore of MCT8 in the absence **(a)** and presence **(b)** of a T3 molecule. Snapshots taken after 2 nanoseconds (upper panels of **A and B**) and 4 nanoseconds (lower panels of **A and B**), illustrating the dynamics of the H-bond formation. Note that in the absence of substrate Asp498 forms an alternating H-bond with the ω'-H2N and δ-NH group of Arg445, while in the presence of substrate H-bond formation is restricted to the δ-NH group of Arg445.

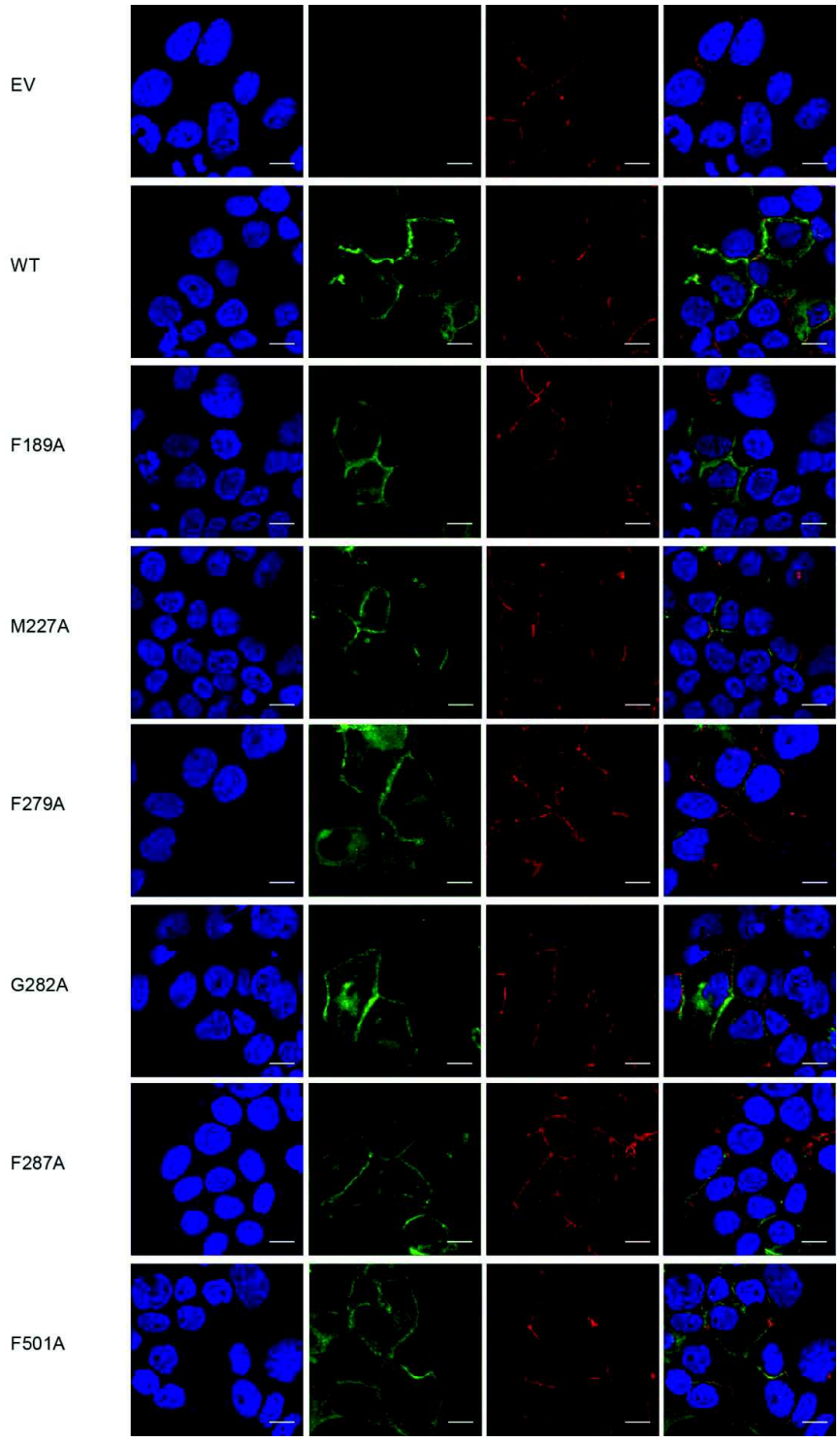

Supplemental Figure 6 Subcellular localization of WT and mutant MCT8 in transiently transfected JEG-3 cells assessed by confocal microscopy. The first panel shows the nuclear staining with DAPI (blue), the second panel MCT8 using goat-anti-rabbit Alexa488 (green), the third panel shows ZO-1 staining as a cell membrane marker using goat-anti-mouse Alexa633 (red) and the fourth panel shows the merged image. All mutants showed intact localization at the cell membrane. All images were generated using ImageJ software. The scale bar represents 4 µm.

REFERENCES

1. Yen PM. Physiological and molecular basis of thyroid hormone action. Physiol Rev. 2001;81(3):1097-142.
2. Hennemann G, Docter R, Friesema EC, de Jong M, Krenning EP, Visser TJ. Plasma membrane transport of thyroid hormones and its role in thyroid hormone metabolism and bioavailability. Endocr Rev. 2001;22(4):451-76.
3. Friesema EC, Ganguly S, Abdalla A, Manning Fox JE, Halestrap AP, Visser TJ. Identification of monocarboxylate transporter 8 as a specific thyroid hormone transporter. J Biol Chem. 2003;278(41):40128-35.
4. Kinne A, Kleinau G, Hoefig CS, Gruters A, Kohrle J, Krause G, et al. Essential molecular determinants for thyroid hormone transport and first structural implications for monocarboxylate transporter 8. J Biol Chem. 2010;285(36):28054-63.
5. Ceballos A, Belinchon MM, Sanchez-Mendoza E, Grijota-Martinez C, Dumitrescu AM, Refetoff S, et al. Importance of monocarboxylate transporter 8 for the blood-brain barrier-dependent availability of 3,5,3'-triiodo-L-thyronine. Endocrinology. 2009;150(5):2491-6.
6. Heuer H, Visser TJ. Minireview: Pathophysiological importance of thyroid hormone transporters. Endocrinology. 2009;150(3):1078-83.
7. Friesema EC, Grueters A, Biebermann H, Krude H, von Moers A, Reeser M, et al. Association between mutations in a thyroid hormone transporter and severe X-linked psychomotor retardation. Lancet. 2004;364(9443):1435-7.
8. Dumitrescu AM, Liao XH, Best TB, Brockmann K, Refetoff S. A novel syndrome combining thyroid and neurological abnormalities is associated with mutations in a monocarboxylate transporter gene. Am J Hum Genet. 2004;74(1):168-75.
9. Friesema EC, Visser WE, Visser TJ. Genetics and phenomics of thyroid hormone transport by MCT8. Mol Cell Endocrinol. 2010;322(1-2):107-13.
10. Groeneweg S, Friesema EC, Kersseboom S, Klootwijk W, Visser WE, Peeters RP, et al. The role of Arg445 and Asp498 in the human thyroid hormone transporter MCT8. Endocrinology. 2014;155(2):618-26.
11. Groeneweg S, Lima de Souza EC, Visser WE, Peeters RP, Visser TJ. Importance of His192 in the human thyroid hormone transporter MCT8 for substrate recognition. Endocrinology. 2013;154(7):2525-32.
12. Kinne A, Roth S, Biebermann H, Kohrle J, Gruters A, Schweizer U. Surface translocation and tri-iodothyronine uptake of mutant MCT8 proteins are cell type-dependent. J Mol Endocrinol. 2009;43(6):263-71.
13. Kersseboom S, Kremers GJ, Friesema EC, Visser WE, Klootwijk W, Peeters RP, et al. Mutations in MCT8 in patients with Allan-Herndon-Dudley-syndrome affecting its cellular distribution. Mol Endocrinol. 2013;27(5):801-13.
14. Armour CM, Kersseboom S, Yoon G, Visser TJ. Further Insights into the Allan-Herndon-Dudley Syndrome: Clinical and Functional Characterization of a Novel MCT8 Mutation. PLoS One. 2015;10(10):e0139343.
15. Forrest LR, Kramer R, Ziegler C. The structural basis of secondary active transport mechanisms. Biochim Biophys Acta. 2011;1807(2):167-88.
16. Kleinau G, Schweizer U, Kinne A, Kohrle J, Gruters A, Krude H, et al. Insights into molecular properties of the human monocarboxylate transporter 8 by combining functional with structural information. Thyroid Res. 2011;4 Suppl 1:S4.
17. Lima de Souza EC, Groeneweg S, Visser WE, Peeters RP, Visser TJ. Importance of cysteine residues in the thyroid hormone transporter MCT8. Endocrinology. 2013;154(5):1948-55.
18. Mol JA, Visser TJ. Synthesis and some properties of sulfate esters and sulfamates of iodothyronines. Endocrinology. 1985;117(1):1-7.
19. Friesema EC, Kuiper GG, Jansen J, Visser TJ, Kester MH. Thyroid hormone transport by the human monocarboxylate transporter 8 and its rate-limiting role in intracellular metabolism. Mol Endocrinol. 2006;20(11):2761-72.
20. Friesema EC, Jansen J, Jachtenberg JW, Visser WE, Kester MH, Visser TJ. Effective cellular uptake and efflux of thyroid hormone by human monocarboxylate transporter 10. Mol Endocrinol. 2008;22(6):1357-69.
21. Jansen J, Friesema EC, Kester MH, Milici C, Reeser M, Gruters A, et al. Functional analysis of monocarboxylate transporter 8 mutations identified in patients with X-linked psychomotor retardation and elevated serum triiodothyronine. J Clin Endocrinol Metab. 2007;92(6):2378-81.
22. Krieger E, Vriend G. YASARA View - molecular graphics for all devices - from smartphones to workstations. Bioinformatics. 2014;30(20):2981-2.
23. Krieger E, Joo K, Lee J, Lee J, Raman S, Thompson J, et al. Improving physical realism, stereochemistry, and side-chain accuracy in homology modeling: Four approaches that performed well in CASP8. Proteins. 2009;77 Suppl 9:114-22.

24. Altschul SF, Madden TL, Schaffer AA, Zhang J, Zhang Z, Miller W, et al. Gapped BLAST and PSI-BLAST: a new generation of protein database search programs. Nucleic Acids Res. 1997;25(17):3389-402.
25. Hooft RW, Vriend G, Sander C, Abola EE. Errors in protein structures. Nature. 1996;381(6580):272.
26. Hooft RW, Sander C, Scharf M, Vriend G. The PDBFINDER database: a summary of PDB, DSSP and HSSP information with added value. Comput Appl Biosci. 1996;12(6):525-9.
27. McGuffin LJ, Bryson K, Jones DT. The PSIPRED protein structure prediction server. Bioinformatics. 2000;16(4):404-5.
28. King RD, Sternberg MJ. Identification and application of the concepts important for accurate and reliable protein secondary structure prediction. Protein science : a publication of the Protein Society. 1996;5(11):2298-310.
29. Smith TF, Waterman MS. Identification of common molecular subsequences. Journal of molecular biology. 1981;147(1):195-7.
30. Qiu J, Elber R. SSALN: an alignment algorithm using structure-dependent substitution matrices and gap penalties learned from structurally aligned protein pairs. Proteins. 2006;62(4):881-91.
31. Canutescu AA, Shelenkov AA, Dunbrack RL, Jr. A graph-theory algorithm for rapid protein side-chain prediction. Protein science : a publication of the Protein Society. 2003;12(9):2001-14.
32. Canutescu AA, Dunbrack RL, Jr. Cyclic coordinate descent: A robotics algorithm for protein loop closure. Protein science : a publication of the Protein Society. 2003;12(5):963-72.
33. Duan Y, Wu C, Chowdhury S, Lee MC, Xiong G, Zhang W, et al. A point-charge force field for molecular mechanics simulations of proteins based on condensed-phase quantum mechanical calculations. J Comput Chem. 2003;24(16):1999-2012.
34. Lundblad RLM, F. Handbook of Biochemistry and Molecular Biology. 4th ed Boca Raton, FL: CRC Press; 2010. 2010.
35. Dang S, Sun L, Huang Y, Lu F, Liu Y, Gong H, et al. Structure of a fucose transporter in an outward-open conformation. Nature. 2010;467(7316):734-8.
36. van der Deure WM, Peeters RP, Visser TJ. Molecular aspects of thyroid hormone transporters, including MCT8, MCT10, and OATPs, and the effects of genetic variation in these transporters. J Mol Endocrinol. 2010;44(1):1-11.
37. Huang Y, Lemieux MJ, Song J, Auer M, Wang DN. Structure and mechanism of the glycerol-3-phosphate transporter from Escherichia coli. Science. 2003;301(5633):616-20.
38. Anik A, Kersseboom S, Demir K, Catli G, Yis U, Bober E, et al. Psychomotor retardation caused by a defective thyroid hormone transporter: report of two families with different MCT8 mutations. Horm Res Paediatr. 2014;82(4):261-71.
39. Vaurs-Barriere C, Deville M, Sarret C, Giraud G, Des Portes V, Prats-Vinas JM, et al. Pelizaeus-Merzbacher-Like disease presentation of MCT8 mutated male subjects. Ann Neurol. 2009;65(1):114-8.
40. Westholm DE, Marold JD, Viken KJ, Duerst AH, Anderson GW, Rumbley JN. Evidence of evolutionary conservation of function between the thyroxine transporter Oatp1c1 and major facilitator superfamily members. Endocrinology. 2010;151(12):5941-51.
41. Ugrasbul F, H.H. A. A patient presenting with central hypothyroidism, developmental delay and poor head control. Should we be checking T3 levels? Horm Res. 2009;72(Suppl 1):458-9.
42. Fuchs O, Pfarr N, Pohlenz J, Schmidt H. Elevated serum triiodothyronine and intellectual and motor disability with paroxysmal dyskinesia caused by a monocarboxylate transporter 8 gene mutation. Dev Med Child Neurol. 2009;51(3):240-4.
43. Moradi M, Enkavi G, Tajkhorshid E. Atomic-level characterization of transport cycle thermodynamics in the glycerol-3-phosphate:phosphate antiporter. Nat Commun. 2015;6:8393.
44. Law CJ, Almqvist J, Bernstein A, Goetz RM, Huang Y, Soudant C, et al. Salt-bridge dynamics control substrate-induced conformational change in the membrane transporter GlpT. Journal of molecular biology. 2008;378(4):828-39.
45. Braun D, Lelios I, Krause G, Schweizer U. Histidines in potential substrate recognition sites affect thyroid hormone transport by monocarboxylate transporter 8 (MCT8). Endocrinology. 2013;154(7):2553-61.
46. Johannes J, Braun D, Kinne A, Rathmann D, Kohrle J, Schweizer U. Few Amino Acid Exchanges Expand the Substrate Spectrum of Monocarboxylate Transporter 10. Mol Endocrinol. 2016;30(7):796-808.
47. Nancolas B, Sessions RB, Halestrap AP. Identification of key binding site residues of MCT1 for AR-C155858 reveals the molecular basis of its isoform selectivity. Biochem J. 2015;466(1):177-88.
48. Protze J, Braun D, Hinz KM, Bayer-Kusch D, Schweizer U, Krause G. Membrane-traversing mechanism of thyroid hormone transport by monocarboxylate transporter 8. Cell Mol Life Sci. 2017;74(12):2299-318.

49. Krieger E, Nielsen JE, Spronk CA, Vriend G. Fast empirical pKa prediction by Ewald summation. J Mol Graph Model. 2006;25(4):481-6.
50. Krieger E, Darden T, Nabuurs SB, Finkelstein A, Vriend G. Making optimal use of empirical energy functions: force-field parameterization in crystal space. Proteins. 2004;57(4):678-83.
51. Krieger E, Vriend G. New ways to boost molecular dynamics simulations. J Comput Chem. 2015;36(13):996-1007.

Chapter

Discriminative role of Asn193 in the transport of T3 and T4 by Monocarboxylate transporter 8

2.5

Stefan Groeneweg, Anna Dolcetta-Capuzzo, Robin P. Peeters, Marcel E. Meima, W. Edward Visser

Manuscript in preparation (intended as brief report)

ABSTRACT

Monocarboxylate transporter 8 (MCT8) is a highly efficient transporter of triiodothyronine (T3) and thyroxine (T4). By using protein homology modeling and site-directed mutagenesis, we here identified Asn193 in transmembrane domain 1 as a critical residue in substrate recognition by establishing halogen-bonds with the C5- and C5'-iodines in iodothyronines. Substitution of the Asn193 by Ala predominantly affected T4 transport and had only little effect on T3 transport. This indicates that in particular the interaction with the C5' iodine moiety is important for proper orientation of the outer ring of T4 while traversing the substrate channel. Together, these findings indicate that Ans193 has a discriminative role in the transport of T3 and T4.

INTRODUCTION

Thyroid hormones (TH) require transporter proteins to facilitate their transport across the cell membrane. Monocarboxylate transporter (MCT)8 is the most specific TH transporter identified to date, with 3,3',5-triiodothyronine (T3) and thyroxine (T4) being its preferred substrates (1). Mutations in MCT8 cause Allan-Herndon-Dudley syndrome (AHDS, or MCT8 deficiency), characterized by severe intellectual and motor disability and abnormal thyroid function tests (2). Although recent studies investigating the transport mechanism of MCT8 identified several substrate-interacting residues (3, 4), the presence of interactions with the iodine-moieties (i.e. halogen bonds (5)) has not been considered thus far. As such, it remains unclear if the structural requirements for the transport of T4 versus T3 differ, in order to accommodate the C5'-iodine. Here, we identified Asn193 as a key substrate-interacting residue that is of differential importance for the transport of T3 and T4.

RESULTS

Based on its orientation towards the substrate pore and its chemical properties, we postulated that the amide side-chain of Asn193 in transmembrane domain 1 may form halogen bonds with the iodine(s) of TH. To explore this hypothesis, we generated expression constructs in which Asn193 was substituted by Ala (loss of the amide side-chain and smaller size) or Ile (loss of amide and similar size). In transiently transfected COS-1 cells, the N193I and N193A mutations severely reduced MCT8-mediated T4 uptake in presence of the intracellular TH-binding protein CRYM, whereas T3 uptake was clearly less affected (**Figure 1A**). Similar results were obtained in JEG-3 cells (data not shown). Both mutations had minimal effects on the total and cell membrane expression levels of MCT8 (**Figure 1B**). In line, immunocytochemistry indicated intact cell membrane localization for both mutants (**Figure 1C**). These results suggested that substitution of Asn193 affects intrinsic transport properties. Indeed, both Asn193 mutants reduced the apparent affinity for T3, indicated by 2-3-times higher Km values than WT (**Figure 1D**). In case of N193A, this was accompanied by a 2-times increase in Vmax over WT, suggesting that the reduced affinity of this mutant has a favorable effect on the (maximum) transport rate of T3. By contrast, the increased apparent Km for T4 was accompanied by a decrease in apparent Vmax for both mutations. The lower affinity of both mutants for T4 may thus have unfavorable effects on T4 transport rate (**Figure 1D**). We next aimed to unravel the cause of these substrate-specific effects. By combining substrate docking and molecular morphing we constructed the trajectory of T4 through the substrate pore. Just before entering the substrate binding center, the distance and angle between the side-chain oxygen of Asn193 and C5-iodine of T4 allows the formation of a transient halogen bond (**Figure 1E and F**). Simultaneously, the distance and orientation of the C5'-iodine allows the formation of second halogen bond to the side-chain nitrogen of Asn193, which appears particularly important in fine-tuning the orientation of the large outer ring of T4 (**Figure 1F**). To further support that loss of Asn193 has the greatest impact on the transport of substrates with a fully saturated outer ring, we also studied the direct uptake of 3,3',5'-triiodothyronine (rT3) and 3,3'-diodothyronine (T2) (**Figure 1D**). Indeed, the effect of the N193A mutation on 3,3'-T2 uptake was smaller than that on T4 uptake, whereas an intermediate effect was observed for

rT3 (**Figure 1G**). Complementary (cis-) inhibition studies showed that inhibition of T3 uptake by 30 µM 3,3'-T2, rT3, and T3 was not significantly different between WT and N193A, whereas 30 µM T4 clearly less potently inhibited N193A than WT (**Figure 1H**).

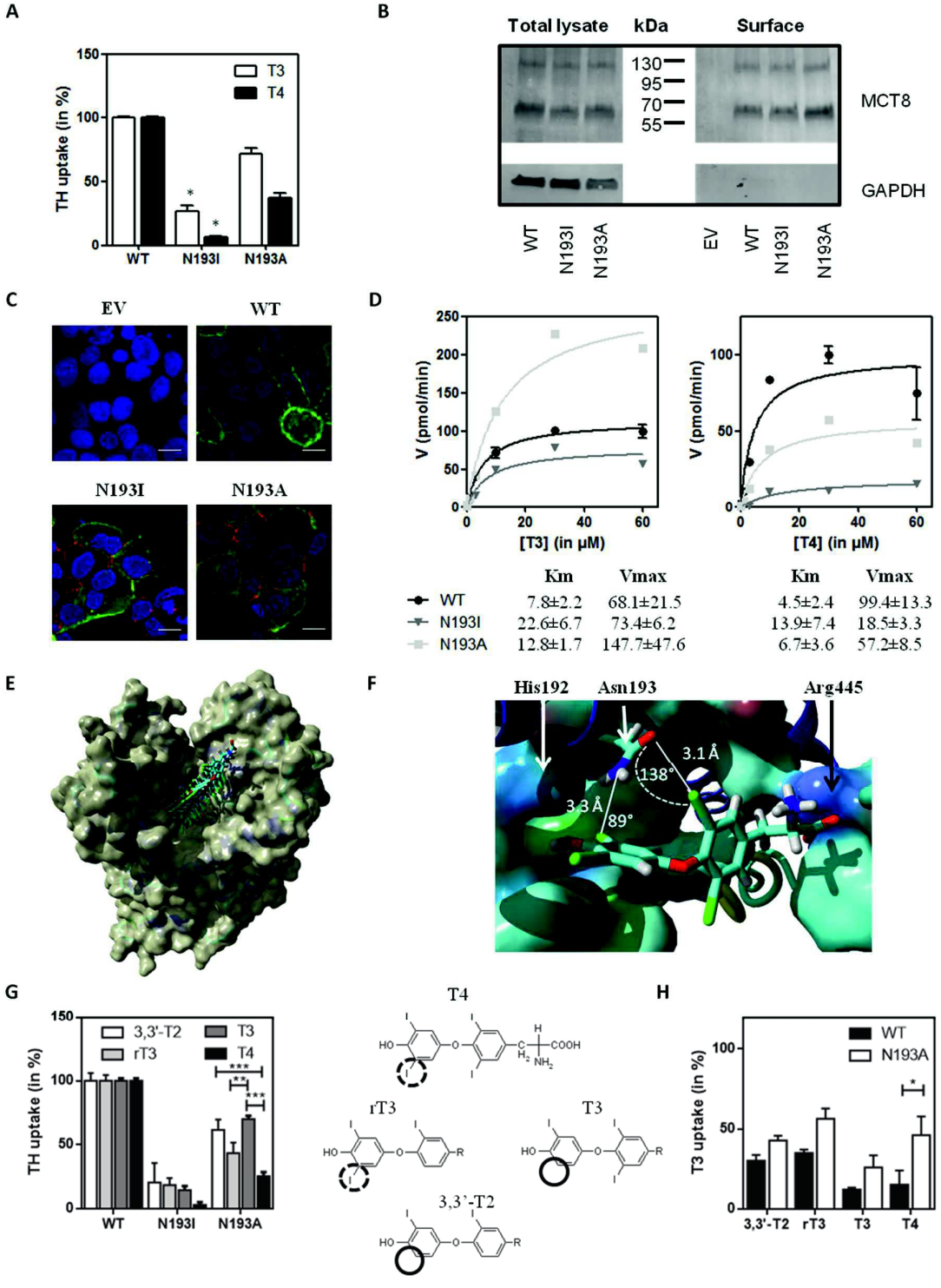

Figure 1 (**A**) T3 and T4 uptake in the presence of CRYM in COS-1 cells transiently transfected with WT MCT8 or indicated mutant (30 min at 37°C). Values are expressed relative to WT and corrected for background TH uptake by pcDNA3 empty vector transfected cells (N=3). Statistical significance was tested using two-way analysis of variance followed by Bonferroni posttests. Significant differences ($p<0.05$) to WT are indicated with an *. (**B**) Immunoblot of total lysates (left) and cell surface biotinylated fraction of COS-1 cells transiently transfected with WT or indicated mutant MCT8. GAPDH was used as a loading and purity control. (**C**) Immunocytochemistry in JEG-3 cells showing co-localization of MCT8 (green) and the membrane marker Zona Occludens (ZO)-1 (red) for WT and both mutant MCT8 proteins. Nuclei were stained with DAPI (blue). (**D**) Representative Michaelis-Menten plot derived from kinetic analyses (n=2-4) of T3 and T4 uptake in the absence of CRYM in COS-1 cells transfected with WT or indicated mutant MCT8. The apparent Km (in µM) and Vmax (in pmol/min) for T3 and T4 transport by WT and mutant MCT8 is provided at the bottom of the respective graphs. (**E**) The predicted trajectory of a T4 molecule from the outside of the substrate pore to the substrate binding center in our previously published MCT8 homology model {Groeneweg, 2017 #46}, using dynamic simulations and molecular morphing implemented in YASARA Structure. (**F**) Just before arriving at the substrate binding center, the C5-iodine and the side-chain oxygen of Asn193 are in close structural proximity (~3.1 Å) with overlapping Van der Waals radii and an σ-hole angle of 130-150°, which is optimal for the formation of a halogen bond between an iodobenzene and the side-chain oxygen of Asn {Zimmermann, 2016 #221}. Simultaneously, the σ-hole of the C5'-iodine is perpendicular to the side-chain nitrogen of Asn193 at a distance of 3.3Å, allowing the formation of a second halogen-bond that appears particularly important to fine-tune the orientation of the large outer ring of T4. (**G**) Uptake of indicated iodothyronines by COS-1 cells transfected with WT or mutant MCT8 and CRYM in 10 min at 37°C. For all substrates, values are expressed relative to WT uptake levels and corrected for background uptake in pcDNA3 empty vector transfected cells (N=3). Although both mutations resulted in a decrease of intracellular accumulation of all tested substrates, the impact was greater on the uptake of rT3 and T4 (saturated outer ring) than of 3,3'-T2 and T3 (non-saturated outer ring) (**H**) T3 uptake in COS-1 cells transfected with WT or mutant MCT8 (without CRYM) in the presence of 30 µM of indicated iodothyronines showing that especially cis-inhibition by T4 is clearly less effective in the N193A mutant than in WT. All values are corrected for background and expressed relative to the T3 uptake levels observed in cells expressing WT MCT8 or the N193A mutant in the presence of 1 nM T3 (N=2).

DISCUSSION

Here, we identified Asn193 in MCT8 as a key player in substrate recognition through formation of halogen bonds with the C5- and C5'-iodines in iodothyronines. Loss of the halogen bond with the C5'-iodine of T4 (and rT3) seemingly interferes with correct orientation of the outer ring at the substrate binding center and reduces transport efficacy. Loss of its interaction with the C5-iodine, common to T3 and T4, may instead favor the dissociation of substrates that lack the C5'-iodine (i.e. T3) from the transporter and thereby increase maximum transport rate.

The importance of halogen bonds in ligand specificity and design of protein-specific inhibitors is increasingly acknowledged. Furthermore, iodination of compounds is increasingly used to enhance delivery to target tissues. Although the iodines of TH yield strong potential to form halogen bonds (5), this type of interaction is only rarely considered in the field. Therefore, our present work adds to the existing literature on TH transport and stresses the need for further studies into this fundamental, but largely unexplored aspect of TH recognition by TH transporting proteins.

Acknowledgements

This work was supported by a grant from the Netherlands Organisation for Health Research and Development (project number 113303005) (to WEV) and from the Sherman Foundation (to WEV).

REFERENCES

1. Friesema EC, Ganguly S, Abdalla A, Manning Fox JE, Halestrap AP, Visser TJ. Identification of monocarboxylate transporter 8 as a specific thyroid hormone transporter. J Biol Chem. 2003;278(41):40128-35.
2. Friesema EC, Grueters A, Biebermann H, Krude H, von Moers A, Reeser M, et al. Association between mutations in a thyroid hormone transporter and severe X-linked psychomotor retardation. Lancet. 2004;364(9443):1435-7.
3. Protze J, Braun D, Hinz KM, Bayer-Kusch D, Schweizer U, Krause G. Membrane-traversing mechanism of thyroid hormone transport by monocarboxylate transporter 8. Cell Mol Life Sci. 2017;74(12):2299-318.
4. Groeneweg S, Lima de Souza EC, Meima ME, Peeters RP, Visser WE, Visser TJ. Outward-Open Model of Thyroid Hormone Transporter Monocarboxylate Transporter 8 Provides Novel Structural and Functional Insights. Endocrinology. 2017;158(10):3292-306.
5. Zimmermann MO, Lange A, Zahn S, Exner TE, Boeckler FM. Using Surface Scans for the Evaluation of Halogen Bonds toward the Side Chains of Aspartate, Asparagine, Glutamate, and Glutamine. Journal of chemical information and modeling. 2016;56(7):1373-83.

Chapter

In Vitro Characterization of Human, Mouse, and Zebrafish MCT8 Orthologues

2.6

Stefan Groeneweg*, Simone Kersseboom*, Amanda van den Berge, Anna Dolcetta-Capuzzo, Ferdy S. van Geest, Ramona E.A. van Heerebeek, Francisco J. Arjona, Marcel E. Meima, Robin P. Peeters, W. Edward Visser, Theo J. Visser

Thyroid. 2019;29(10):1499-1510.

ABSTRACT

Background - Mutations in the thyroid hormone (TH) transporter MCT8 cause MCT8 deficiency, characterized by severe intellectual and motor disability and abnormal serum thyroid function tests. Various Mct8 knock-out mouse models as well as mct8 knock-out and knockdown zebrafish models are used as a disease model for MCT8 deficiency. Although important for model eligibility, little is known about the functional characteristics of the MCT8 orthologues in these species. Therefore, we here compared the functional characteristics of mouse (mm) MCT8 and zebrafish (dr) Mct8 to human (hs) MCT8.

Methods – We performed extensive transport studies in COS-1 and JEG-3 cells transiently transfected with hsMCT8, drMct8 and mmMCT8. Protein expression levels and subcellular localization were assessed by immunoblotting, surface biotinylation and immunocytochemistry. Sequence alignment and structural modelling were used to interpret functional differences between the orthologues.

Results – hsMCT8, drMct8 and mmMCT8 all facilitated the uptake and efflux of 3,3'-T2, rT3, T3, and T4, although the initial uptake rates of drMct8 were 1.5-4.0-fold higher than for hsMCT8 and mmMCT8. drMct8 exhibited 3-50-fold lower apparent IC50 values than hsMCT8 and mmMCT8 for all tested substrates, and substrate preference of drMct8 (3,3'-T2, T3>T4>rT3) differed from hsMCT8 and mmMCT8 (T3>T4>rT3, 3,3'-T2). Compared to hsMCT8 and mmMCT8, cis-inhibition studies showed that T3 uptake by drMct8 was inhibited at a lower concentration and by a broader spectrum of TH metabolites. Total and cell surface expression levels of drMct8 and hsMCT8 were equal and both significantly exceeded those of mmMCT8. Structural modeling located most non-conserved residues outside the substrate pore, except for H192 in hsMCT8 which is replaced by a glutamine in drMct8. However, a H192Q substituent of hsMCT8 did not alter its transporter characteristics.

Conclusion - Our studies substantiate the eligibility of mice and zebrafish models for human MCT8 deficiency. However, differences in the intrinsic transporter properties of MCT8 orthologues may exist, which should be realized when comparing MCT8 deficiency in different in vivo models. Moreover, our findings may indicate that the protein domains outside the substrate channel may play a role in substrate selection and protein stability.

INTRODUCTION

Thyroid hormone (TH) importantly regulates growth, development and energy metabolism (1). These effects are largely mediated through binding of the active hormone 3,3',5-triiodothyronine (T3) to its nuclear receptors (2). Intracellular T3 concentrations are importantly regulated by deiodinating enzymes (3) and membrane transporter proteins (4). The most specific TH transporter identified to date is monocarboxylate transporter 8 (MCT8) which facilitates the cellular uptake and efflux of thyroxine (T4), T3, and to a lesser extent 3,3',5'-triiodothyronine (rT3) and 3,3'-diiodothyronine (3,3'-T2) (5). Mutations in MCT8 have been associated with MCT8 deficiency, also known as Allan-Herndon-Dudley syndrome (AHDS), which is characterized by severe intellectual and motor disability and abnormal serum thyroid function tests (TFTs; high T3, low T4 and high-normal TSH concentrations) (6, 7).

Over the last decade, different disease models have emerged to study the physiological role of MCT8 and the effects of its inactivation. These models include cell-based models and various *Mct8* knock-out (ko) and knock-down (kd) animal models, each with their own strengths and limitations (reviewed (8, 9)). *Mct8* ko mice replicate the abnormal serum TFTs observed in human patients, but surprisingly lack any neurological phenotype (10). This was later attributed to the presence of the T4 transporter organic anion transporting polypeptide (OATP)1C1 in the blood-brain-barrier of mice, but not of humans, which compensates the functional loss of MCT8 in mice (11, 12). Recently, models for MCT8 deficiency in non-mammalian vertebrates, including zebrafish, chicken and *Xenopus* (reviewed in (9)), have replicated various aspects of MCT8 deficiency in human.

Although the various animal models have advanced our understanding of MCT8 deficiency, several phenotypic characteristics importantly differ across species and, moreover, diverge from the phenotype observed in human (reviewed in (9)). Species-specific tissue distribution of MCT8 expression and the presence of alternative TH transporters at sites where MCT8 is expressed may importantly determine the relevance of animal models for human MCT8 deficiency. In this context, variation across species in transporter characteristics such as substrate preference, affinity and specificity, should also be considered (e.g. (13)). Detailed functional characterization of MCT8 orthologues is therefore imperative for the interpretation of findings from animal studies and their relevance for the human situation. Although the chicken and *Xenopus* mct8 orthologues have been recently shown to behave very reminiscent to human (hs) MCT8 (14, 15), such a detailed comparison is currently lacking for the MCT8 orthologues in mouse and zebrafish, despite their frequent use as a model for MCT8 deficiency.

Therefore, we functionally characterized the mouse and zebrafish orthologues of MCT8 and made a direct comparison with hsMCT8 in transiently transfected mammalian cell lines. Similar to hsMCT8, we found that both orthologues efficiently transported T3 and T4, which supports the eligibility to use both species as a model for human MCT8 deficiency and, moreover, provides insights into the tolerable variation in the non-conserved regions of MCT8. Nevertheless, we also observed differences in substrate affinity, uptake rate, and specificity of hsMCT8 and mmMCT8 *vs.* drMct8. Such differences should be considered when comparing MCT8 deficiency in different disease models.

MATERIALS AND METHODS

Materials

X-tremeGENE9 transfection reagent was obtained from Roche Diagnostics (Woerden, The Netherlands [NL]). Nonradioactive iodothyronines, bovine serum albumin (BSA), and D-glucose were obtained from Sigma Aldrich (Zwijndrecht, NL). [3'-125I]T3, [3',5'-125I]rT3, [3',5'-125I]T4, and [3'-125I]3,3',5-triiodothyroacetic acid (Triac; TA3) were produced as previously described (16, 17). [3'-125I]3,3'-T2 was generated accordingly using 3-T1. An overview of the antibodies is provided in **Supplemental Table 1**. All cell culture flasks and plates were obtained from Corning (Schiphol, NL).

Constructs

The generation of pcDNA3.1-drMct8 (accession number, CBK52149) (18), pcDNA3-hsMCT8 (accession number, NP_006508.2) (19) and pSG5-hsCRYM (20) has been previously described. Of note, the human *MCT8* gene contains two translational start sites (TLSs), of which the most upstream TLS is absent in most other species, including the mouse and zebrafish (**Supplemental Figure 1**). The physiological relevance of this additional TLS in human is yet unclear, since currently available studies were only able to detect the short isoform at protein level in human tissues. Therefore, the short hsMCT8 isoform was used in the current studies. A pCMVSPORT6.1- mmMCT8 (IMAGE:6313495, accession number NP_033223.2) cloning vector was obtained from Fermentas/ Thermo Scientific (Leon-Rot, Germany). The mmMCT8 coding sequence was sub-cloned into pcDNA3.1 using EcoR1 and BamH1 sites using standard cloning procedures. C-terminally V5-tagged constructs of hsMCT8, drMct8 and mmMCT8 were generated by PCR amplification of the cDNA (primers available upon request) and ligation of the amplicons into a pcDNA3 expression vector. The H192Q substitution in hsMCT8 was introduced by site-directed mutagenesis as previously described (21). The position of the mutation is determined using the NM_006517.3 reference sequence and using +1 as the A of the ATG translation initiation codon of the long MCT8 translational isoform, with the initiation codon as codon 1. All cDNA constructs were sequenced to confirm their correctness and presence of the introduced mutation.

Cell culture and transfection

COS-1 (African green monkey kidney fibroblasts) and JEG-3 (human choriocarcinoma) cells were cultured in DMEM/F-12 medium (Life Technologies, Bleiswijk, NL) supplemented with 9% heat-inactivated fetal calf serum (FCS; Invitrogen, Breda, NL) and 2% penicillin/streptomycin (Pen/Strep; Roche Diagnostics). For T3 uptake and efflux assays, COS-1 or JEG-3 cells were cultured in 24-well plates, and transiently transfected at 70% confluence with 100 ng pcDNA3 empty vector (EV), or expression constructs encoding hsMCT8, mmMCT8, or drMct8 in the presence or absence of 50 ng hCRYM according to manufacturer`s protocol. For immunoblotting and surface biotinylation studies, cells were seeded in 6-well plates (immunoblotting) or 10 cm dishes (surface biotinylation), and transiently transfected with 500 ng or 1500 ng pcDNA3 EV, hsMCT8-V5, mmMCT8-V5, or drMct8-V5 respectively. For immunocytochemistry, JEG3 cells were cultured in 24-well dishes on 10-mm glass coverslips coated with poly-D-lysine (Sigma-Aldrich) and transiently transfected with 250 ng pcDNA3 EV, or any of the V5-tagged MCT8 orthologues.

Uptake studies

TH uptake and kinetic studies were essentially carried out as previously described (21). Briefly, two days after transfection, cells were washed with incubation medium (D-PBS+Ca^{2+}/Mg^{2+} with 0.1% glucose and 0.1% BSA), and incubated in incubation medium containing 1 nM (50,000 cpm) [125I]3,3'-T2, [125I]T3, [125I]rT3, [125I]T4 or [125I]triiodothyroacetic acid (TA3) for indicated incubation times at 37°C, briefly washed with incubation medium and lysed with 0.1 M NaOH. The amount of radioactivity in the cell lysate was measured using a γ-counter (PerkinElmer). Since TA3 strongly binds to BSA, incubation medium without BSA was used during the initial wash and subsequent incubation. During cis-inhibition studies, 1-100 µM of unlabeled iodothyronine derivate or analogue was added to the incubation medium. All cis-inhibition studies were carried out in incubation medium without BSA.

Efflux assays

Efflux studies were essentially carried out as previously described (20). Cells were pre-loaded with 1 nM (50,000 cpm) [125I]3,3'-T2, [125I]T3, [125I]rT3 or [125I]T4 for 30 minutes. After a brief wash with incubation medium, cells were incubated in efflux medium (incubation medium containing 1% BSA) for indicated incubation times at 37 °C. Next, efflux medium was removed and cells were briefly washed in incubation medium and lysed in 0.1 M NaOH. The amount of radioactivity was measured in cell lysates.

Surface biotinylation and immunoblotting

Cell surface biotinylation assays were performed as previously described (21, 22). In short, after labeling of cell surface proteins with EZ-link Sulfo-NHS-biotin (Thermo Fisher Scientific, Bleiswijk, NL), cells were lysed with IP buffer (50 mM Tris-HCl, 150 mM NaCl, 10 mM EDTA, 1% Triton X-100), containing protease inhibitor cocktail (Roche), briefly sonicated and clarified from nuclear debris by centrifugation (15 000 rcf for 10 minutes). An aliquot (5% of the total volume) of the clarified lysate was saved as an input control. The biotinylated cell surface proteins were isolated using Neutravidin agarose beads (Thermo Fisher Scientific) and eluted with NuPAGE 1x lithium dodecyl sulfate (LDS) loading buffer (Thermo Fisher Scientific) by incubating the beads for 10 minutes at 70 °C prior to immunoblot analyses. Immunoblotting on total lysates and cell surface biotinylated fractions was carried as described in (22). V5-tagged proteins were probed with rabbit-anti-V5 antibody (1:1000 dilution; see **Supplemental Table 1** for details). Glyceraldehyde-3-phosphate dehydrogenase (GAPDH) was used as loading control. V5-tagged proteins and GAPDH were visualized using Odyssey detection methods (19). MCT8 and GADPH expression levels were quantified by densitometry using ImageJ. The expression levels of mmMCT8 and drMct8 in the input samples and total lysates are expressed as MCT8/GADPH ratio relative to hsMCT8 (100%) and the cell surface expression levels are expressed as MCT8 (surface)/GADPH (input) ratio relative to hsMCT8 (100%).

Immunocytochemistry

Immunocytochemistry was carried out according to previously established protocols (23) using rabbit anti-V5 antibody for the detection of V5-tagged constructs and mouse anti-zona occludens (ZO)-1 as a membrane marker.

Structural modeling

The presented structural model of hsMCT8 has been recently reported (21) and was used without further modification to indicate the location of residues in hsMCT8 that are not conserved in mmMCT8 or drMCT8. All images were created using YASARA Structure (24) and Pov-Ray v3.6 software (www.povray.org).

Statistical analysis

Results are shown as mean ± SEM of at least 3 experiments carried out in duplicate. GraphPad Prism version 6 (GraphPad Software, San Diego California, USA) was used for statistical analysis as indicated in the legend to the figures. The indications for statistically significant differences ($P<0.05$) as well as the applied statistical tests are explained in the corresponding figure legends.

RESULTS

To compare the functional characteristics, COS-1 cells were transiently transfected with pcDNA3 empty vector (EV), or expression constructs encoding hsMCT8, mmMCT8, or drMct8. In line with previous studies (19), cells expressing hsMCT8 showed significant ($P<0.05$) induction of intracellular 3,3'-T2, rT3, T3 and T4 accumulation at all tested incubation times, except for 3,3'-T2 accumulation after 30 and 60 minutes and T3 accumulation after 60 minutes (**Figure 1A-D**). Similar characteristics were found for mmMCT8 (**Figure 1A-D**). At all tested time-points, cells expressing drMct8 showed significantly higher intracellular accumulation of all tested substrates than cells expressing hsMCT8 or mmMCT8 (**Figure 1A-D**). The initial rates of uptake of all tested substrates were 1.5-4.0-fold higher in cells transfected with drMct8 than in cells transfected with hsMCT8 (**Figure 1E**). The initial rates of rT3, T3, and T4 uptake were slightly, but significantly, lower in cells transfected with mmMCT8 than in cells transfected with hsMCT8 (**Figure 1E**). A similar pattern was observed in JEG-3 cells, although the differences were less pronounced (**Supplemental Figure 2A-C**). Differences in the cell-membrane expression levels among the orthologues may contribute to this observation. Alternatively, the higher substrate accumulation in cells expressing drMct8 may suggest that drMct8 facilitates TH uptake at a higher rate and/or efflux at a lower rate than its mammalian counterparts.

Therefore, we first evaluated the protein expression levels of the different MCT8 orthologues in transiently transfected COS-1 and JEG-3 cells. Given the marked differences in the N-terminal and C-terminal amino acid sequence of hsMCT8 and mmMCT8 *versus* drMct8, the drMct8 protein was not detected with the available MCT8 antibodies or antisera (data not shown). Therefore, C-terminally V5-tagged constructs of all three MCT8 orthologues were generated, which allowed the detection of all constructs using the same antibody. Upon transient transfection of COS-1 and JEG-3 cells with these V5-tagged constructs, time courses for T3 and T4 uptake were similar to those obtained with the un-tagged constructs (**Supplemental Figure 3A and 3B**, and data not shown). Immunoblotting of total lysates and the surface biotinylated fraction of COS-1 cells expressing the V5-tagged orthologues showed similar total protein levels for all orthologues (**Figure 2A** and **C**). Cell surface expression levels were similar for hsMCT8 and drMct8, whereas those of mmMCT8 were significantly lower than hsMCT8 (**Figure 2B, C,** and **D**). Also in JEG-3 cells, the total protein levels of hsMCT8 and drMct8 exceeded those of mmMCT8 (**Supplemental Figure S4A**). All orthologues were detected at the plasma membrane in JEG-3 cells (**Supplemental Figure S4B**).

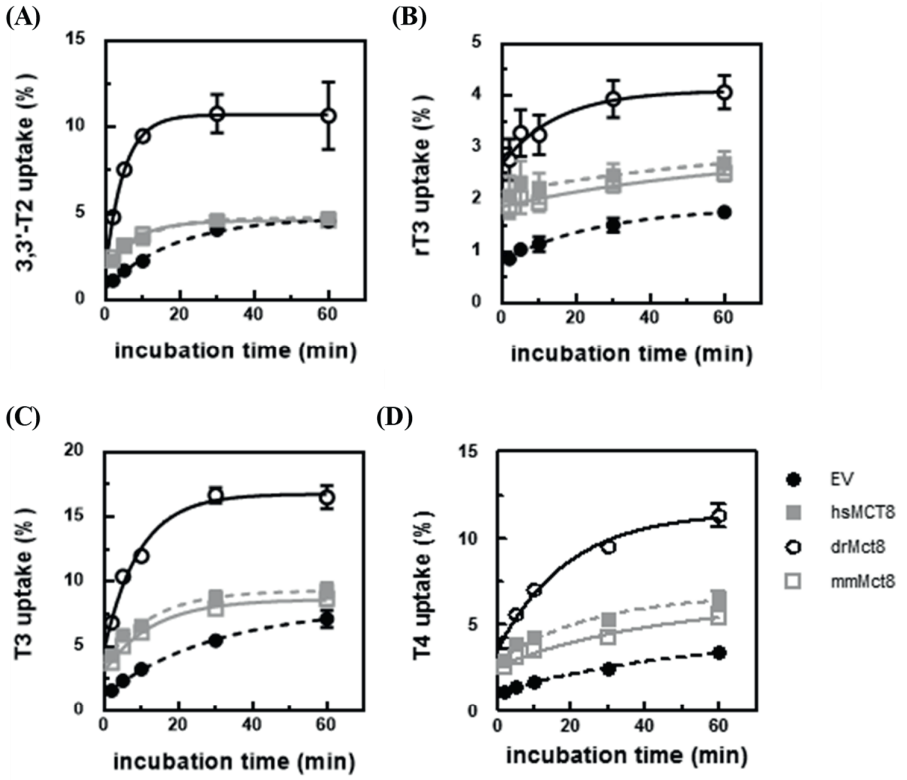

(E)

Initial rates of uptake (mean ± SD in %/min)

	3,3'-T2	rT3	T3	T4
hsMCT8	0.30±0.06	0.35±0.08	0.70±0.07	0.48±0.01
drMct8	1.17±0.05 *	0.55±0.09*	1.60±0.05*	0.83±0.03*
mmMCT8	0.29±0.06	0.26±0.04*	0.53±0.04*	0.34±0.00*

Figure 1 Uptake of 3,3'-T2 (**A**), rT3 (**B**), T3 (**C**) and T4 (**D**), by COS-1 cells transiently transfected with empty vector (EV), human (hs), mouse (mm) or zebrafish (dr) MCT8 after 2-60 minutes at 37°C. All uptake levels are expressed relative to the amount of radio-labeled hormone added to the cells at the start of the incubation and presented as means ± SEM (n=3). For each time-point, one-way ANOVA with a Bonferroni corrected post-hoc tests were conducted to assess for statically significant differences ($p<0.05$) in TH uptake between cells transfected with EV or any of the orthologues. The intracellular accumulation of all tested iodothyronines was higher in cells transfected with hsMCT8, drMct8, or mmMCT8 than in cells transfected with EV, except for 3,3'-T2 accumulation after 30 and 60 minutes and T3 accumulation after 60 minutes by cells transfected with hsMCT8 or mmMCT8. At all tested time-points, cells expressing drMct8 showed significantly higher intracellular accumulation of all tested substrates than cells expressing hsMCT8 or mmMCT8. (**E**) The initial rates of uptake for the tested substrates, presented as mean ± SD percentage uptake per minute during the first 5 minutes of incubation, the timeframe in which the intracellular accumulation of substrate still increased linearly. The percentage uptake denotes the percentage of radio-labeled hormone that has accumulated intracellularly relative to the amount of radio-labeled hormone added to the cells at the start of the incubation (1 nM (50000 cpm)) after correction for uptake levels observed in cells transfected with EV. Initial rates of uptake that significantly ($P<0.05$) differed from hsMCT8 are indicated with an * (One-Way ANOVA with Bonferroni post-hoc tests).

Taken together, this shows that higher substrate accumulation in cells expressing drMct8 cannot be explained by differential cell membrane expression levels, but rather is a consequence of differences in uptake and/or efflux efficiency. In turn, the slightly lower substrate accumulation in cells expressing mmMCT8 than in those expressing hsMCT8 may be related to the lower cell membrane expression levels of mmMCT8.

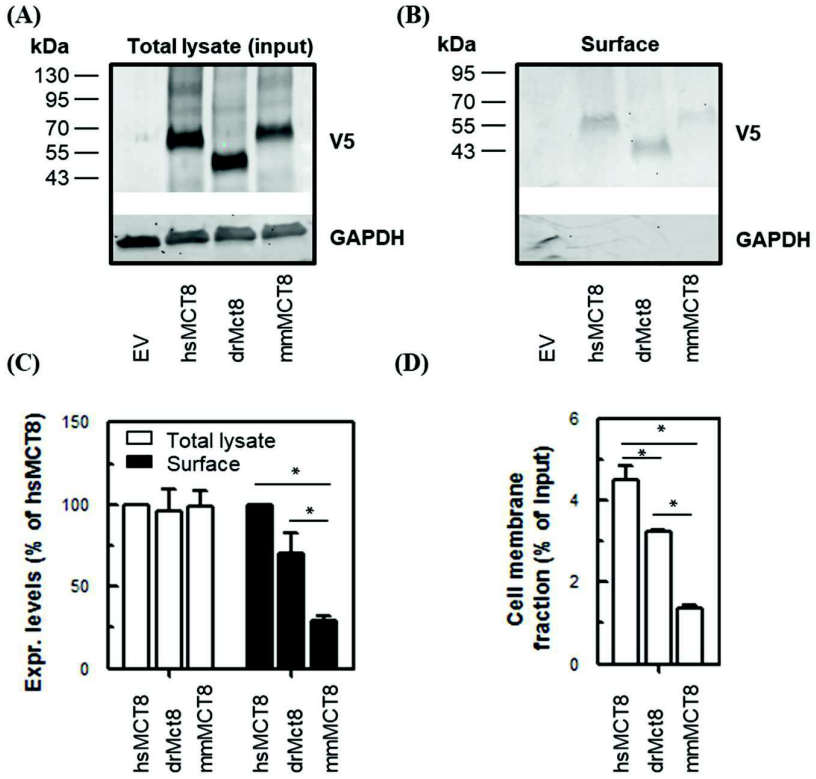

Figure 2 Representative immunoblot analyses on total lysates (**A**) and the surface biotinylated fraction (**B**) derived from COS-1 cells transfected with 1500 ng pcDNA3 EV, or indicated V5-tagged MCT8 orthologues. The total lysates comprise a 5% input sample of the clarified lysate from which the presented surface fraction was derived. Glyceraldehyde-3-phosphate dehydrogenase (GAPDH) was used as loading control. Expression levels are quantified and presented as mean ± SEM of 3 independent experiments (**C**). Statistical significance was tested using Two-way ANOVA followed by a Bonferroni multiple-comparison test and statistically significant differences ($p<0.05$) are indicated with an *. The cell fraction of total protein translocated to the cell membrane (surface / 5% input x 20) was calculated for each orthologue (**D**). Statistical significance was tested using One-way ANOVA followed by a Bonferroni multiple-comparison test and statistically significant differences ($p<0.05$) are indicated with an *.

Next, we specifically evaluated the uptake function of the three orthologues in the presence of the intracellular TH binding protein CRYM, which largely prevents TH efflux. As expected, intracellular accumulation of 3,3'-T2, rT3, T3 and T4 by any of the orthologues was higher in the presence than in the absence of CRYM (**Figure 3A-D**, **Supplemental Figure S5A-D**). Although relative differences in uptake of the iodothyronines decreased in the presence of CRYM, uptake of cells transfected with drMct8 was still significantly higher for all tested substrates. Similar results were obtained in JEG-3 cells and in COS-1 cells expressing the V5-tagged orthologues (data not shown). These results suggest that the uptake rate of drMct8 may by higher than that of hsMCT8 and mmMCT8.

To further explore the uptake efficiency of the orthologues, we performed saturation curves for 3,3'-T2, rT3, T3 and T4 transport in COS-1 cells. In line with previous studies, hsMCT8 showed considerably lower IC_{50} values for T3 and T4 than for rT3 and 3,3'-T2 (**Figure 4A-D** and **Table 1**). Similar IC_{50} values for all substrates were found for mmMCT8 (**Figure 4A-D** and **Table 1**). In contrast, drMct8 showed significantly lower IC_{50} values than hsMCT8 and mmMCT8 for all tested substrates, in particular for 3,3'-T2 (**Figure 4A-D** and **Table 1**). Interestingly, the transport of 3,3'-T2 and rT3 by drMct8 showed a biphasic character. Together, these results suggest that drMct8 has a greater affinity for the tested iodothyronines than its mammalian counterparts.

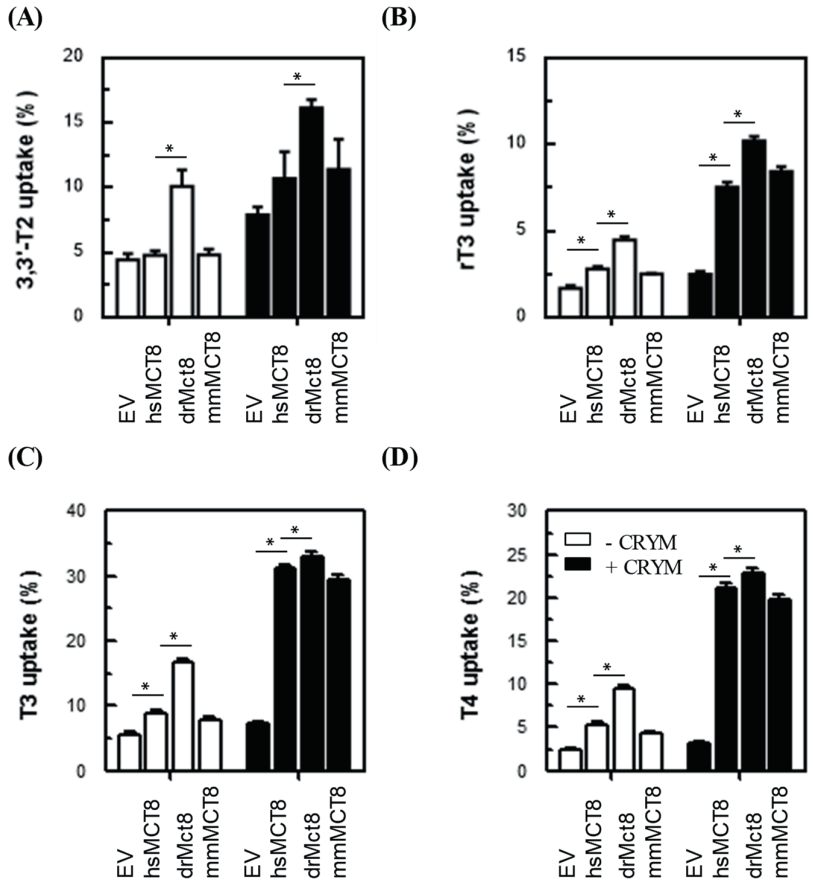

Figure 3 3,3'-T2 (**A**), rT3 (**B**), T3 (**C**) and T4 (**D**) uptake by EV, hsMCT8, drMct8 or mmMCT8 in transiently transfected COS-1 cells in the absence (white bars) or presence (black bars) of CRYM after 30 minutes incubation at 37°C. The amount of internalized substrate is expressed as a percentage of the amount of radioactivity added to the cells at the start of the incubation (1nM 50.000 cpm [125I]- labeled iodothyronines). Results are shown as means +/- SEM of at least 3 independent experiments in duplo. A two-way ANOVA with Bonferroni post-hoc tests was carried out to asses for significant differences between hsMCT8 vs. EV, drMct8 and mmMct8 under both conditions. Significant differences compared to hsMCT8 ($p<0.05$) are indicated with an *.

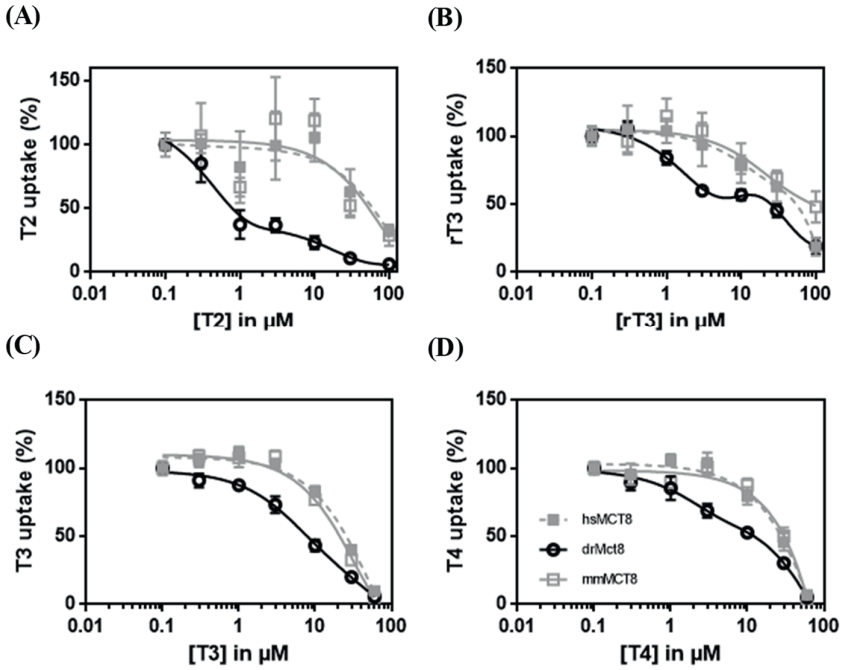

Figure 4 3,3'-T2 (**A**), rT3 (**B**), T3 (**C**) and T4 (**D**) saturation curves in COS-1 cells transiently transfected with EV, hsMCT8, drMct8, or mmMCT8 in the absence of CRYM after 10 minutes incubation at 37°C. All data points are corrected for background iodothyronine uptake in EV-transfected control cells and presented relatively to the amount of internalized iodothyronine in the presence of the lowest substrate concentration (0.01 µM). Apparent IC50 values are displayed in Table 1 and were determined as described in the footnote of Table 1, which also indicates statistically significant differences in IC50 values between hsMCT8 vs drMct8 and mmMCT8.

Table 1 IC_{50} values for the transport of different iodothyronines by hsMCT8, drMct8, or mmMct8.

	3,3'-T2	***rT3***	***T3***	***T4***
hsMCT8	61.0 [22.8-163.4]	39.0 [21.1-72.0]	23.8 [16.5-34.2]	23.5 [15.2-36.4]
drMct8	1.2 [0.8-2.0]*	13.5 [8.9-20.6]*	7.3 [6.0-9.0]*	8.9 [6.6-12.0]*
mmMCT8	58.0 [18.3-183.8]	76.8 [42.6-138.5]	19.9 [13.3-29.6]	24.9 [15.7-39.6]

Overview of the IC_{50} values in µM derived from the saturation curves presented in **Figure 4** presented in means [95% confidence interval]. IC_{50} were calculated after log-transformation of the X-axis (substrate concentration) followed by non-linear regression using the log[inhibitor] vs. normalized response tool of GraphPad Prism version 6. IC_{50} values that significantly differed from hsMCT8 are indicated with an * (One-Way ANOVA with Bonferroni post-hoc tests).

Since the net intracellular accumulation of TH is determined by cellular uptake and efflux, we subsequently studied the efflux of 3,3'-T2, rT3, T3 and T4. In general, iodothyronine efflux was markedly faster from cells transfected with either of the MCT8 orthologues than from cells transfected with empty vector, without significant differences between any of the orthologues (**Figure 5A-D**). This was also observed in JEG-3 cells (data not shown). Therefore, differences in transport efficiency among the orthologues appear to be restricted to the uptake of the tested substrates.

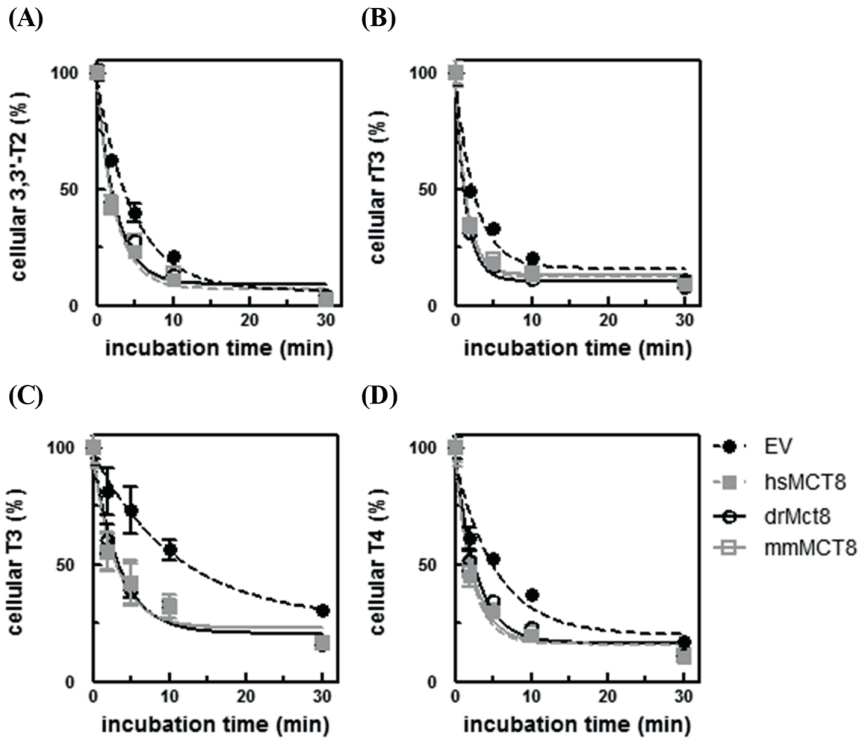

Figure 5 3,3'-T2 (**A**), rT3 (**B**), T3 (**C**) and T4 (**D**) efflux by EV, hsMCT8, drMct8, or mmMCT8 in transiently transfected COS-1 cells in 2-10 minutes in the absence of CRYM. Cells were incubated for 30 minutes with 1 nM (50000 cpm) of the indicated substrates (pre-loading), before efflux was measured. The amount of radio-activity that remained in the cell after 2-10 minutes incubation in efflux medium was measured and displayed relatively to the amount of radio-activity present after pre-loading (t=0). All results are presented as means ± SEM (n=3). For all tested substrates, the amount of radio-labeled hormone inside the cell after 2, 5, and 10 minutes incubation was lower in cells expressing any of the orthologues than in control cells (one-way ANOVA with a Bonferroni corrected post hoc test, $p<0.05$), with no significant differences among the orthologues. There were no significant differences in intracellular TH content between EV-transfected control cells and cells transfected with any of the orthologues after 30 minutes incubation in efflux medium.

To study substrate specificity of the MCT8 orthologues in more detail, we used *cis*-inhibition studies in which the T3 uptake capacity of the orthologues was studied in the presence of various potential unlabeled competitors, including iodothyronines, iodothyropropionic and –acetic acids, iodotyrosines, and the synthetic thyromimetic eprotirome (25). In line with the kinetic analyses, T3 uptake by hsMCT8 and mmMCT8 was reduced by about 50% in presence of 10 µM rT3, T3 or T4, whereas drMct8-mediated T3 uptake was already reduced by about 50% at the 1 µM concentration (**Figure 6A-C**).

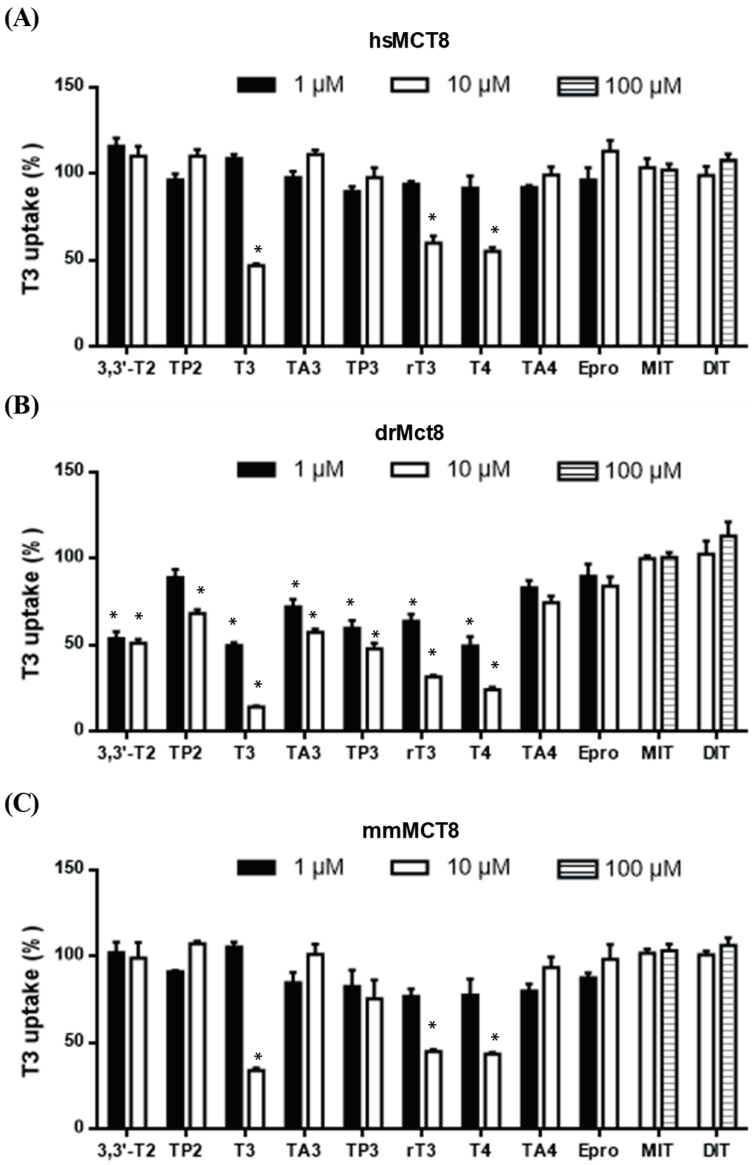

Figure 6 T3 uptake in COS-1 cells transiently transfected with hsMCT8 (**A**), drMct8 (**B**), or mmMct8 (**C**) and CRYM in the presence of indicated concentrations of unlabeled competitors. All uptake levels are corrected for background T3 uptake in EV-transfected control cells incubated in the presence of the same competitor. T3 uptake levels are displayed relative to the amount of intracellular [125I]-T3 in cells incubated in the absence of any competitors (100%) and presented as means ± SEM (n=3). A two-way ANOVA with Bonferroni post-hoc tests was carried out to asses for significant differences between the T3 uptake levels in the absence or presence of the tested competitors. Significant differences ($p<0.05$) from cells incubated in the absence of any competitor (100%) are indicated with an *. Abbreviations: TP2, diiodothyropropionic acid; TA3, triiodothyroacetic acid; TP3, triiodothyropropionic acid; TA4, tetraiodothyroacetic acid; Epro, eprotirome; MIT, monoiodotyrosine; DIT, diiodotyrosine.

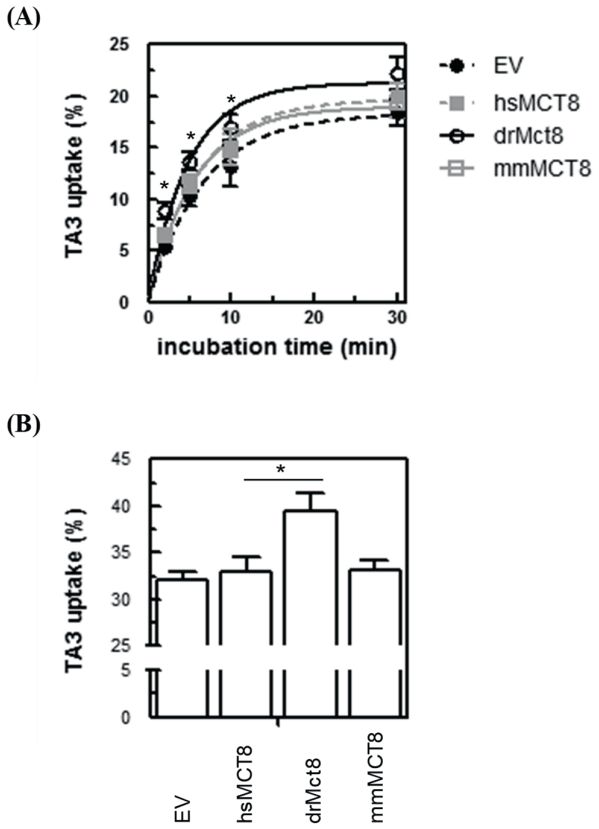

Figure 7 (**A**) Uptake of TA3 by EV, hsMCT8, mmMCT8, drMct8 in transiently transfected COS-1 cells in the absence of CRYM after 2-30 minutes at 37ºC. All uptake levels are expressed relative to the amount of radio-labeled hormone added to the cells at the start of the incubation (1 nM (50000 cpm) [125I]-TA3). All results are presented as means ± SEM (n=3). The cellular accumulation of Triac was significantly higher in drMct8-transfected cells than in EV, hsMCT8 and mmMct8-transfected cells at all incubation times, except 30 minutes (one-way ANOVA with a Bonferroni corrected post hoc test, *, P<0.05). (**B**) TA3 uptake in COS-1 cells transfected with the indicated constructs in the presence of CRYM after 30 minutes incubation at 37ºC. All uptake levels are expressed relative to the amount of radio-labeled hormone added to the cells at the start of the incubation (1 nM (50000 cpm) [125I]-TA3). All results are presented as means ± SEM (n=3). Significant differences are indicated with an * (one-way ANOVA with a Bonferroni corrected post hoc test, p<0.05).

In contrast to hsMCT8 and mmMCT8, T3 uptake by drMct8 was also markedly reduced by 1 and 10 µM 3,3'-T2. None of the other compounds reduced hsMCT8 or mmMCT8-mediated T3 uptake (**Figure 6A** and **C**). However, a significant dose-dependent reduction of drMct8-mediated T3 uptake was observed in presence of the acetic acid metabolite triiodothyroacetic acid (Triac, TA3), and the proprionic acid metabolites diiodothyropropionic acid (DITPA, TP2) and triiodothyropropionic acid (TP3) (**Figure 6B**). These findings suggest that TA3, TP2 and TP3 may be suitable substrates for drMct8, but not for hsMCT8 and mmMCT8. Indeed, cells transfected with drMct8 showed significantly higher intracellular accumulation of TA3 than cells transfected with EV, hsMCT8 or mmMCT8, both in absence (**Figure 7A**) and presence (**Figure 7B**) of CRYM. Taken together, these data indicate that drMct8 has a broader substrate specificity than hsMCT8 and mmMCT8.

Finally, we used multiple sequence alignments and homology modeling to identify the non-conserved residue(s) that may underlie the increase in substrate affinity and broader substrate specificity of

drMct8. Multiple sequence alignment showed an amino acid sequence identity of 94% and 57% and a sequence similarity of 97% and 77% between hsMCT8 and its mouse and zebrafish orthologue, respectively (**Supplemental Figure S1**). Most of the variation among the orthologues is present within the predicted intracellular N-terminal and C-terminal part of the protein and in the intracellular and extracellular loops, whereas the transmembrane domains (TMDs) are relatively well conserved. This is also the case for the recently characterized *Xenopus laevis* and chicken orthologues of MCT8 (**Supplemental Figure S1**), which are evolutionary more closely related to human than zebrafish (**Supplemental Figure S6**). Upon highlighting the amino acid residues that are not conserved between hsMCT8 and drMct8 in our structural model of hsMCT8 (19), we found that most of the non-conserved amino acids map to the intracellular and extracellular loops (**Figure 8A**). The few non-conserved amino acids located within the transmembrane domains predominantly have side-chains that point towards the lipid bilayer.

Most residues that flank the substrate pore, and as such likely determine substrate affinity and establish substrate interactions, are highly conserved, with the exception of H192 which is replaced by a glutamine in drMct8 (**Figure 8B**). Importantly, H192 has been suggested previously to form a direct substrate interaction (21, 26-28). In order to study if the differences in substrate affinity between hsMCT8 and drMct8 can be (partly) attributed to the non-conserved H192 residue, we next generated the H192Q substituent in hsMCT8. However, kinetic analyses of 3,3'-T2, rT3, and T3 transport by wild-type (WT) and H192Q mutant hsMCT8 showed identical curves without a bi-phasic character (**Figure 8C-E**), strongly suggesting that the lack of conservation at this position does not alter the affinity or binding mode for these substrates. In contrast, the H192Q mutant_hsMCT8 slightly shifted the T4 saturation curve to the left, suggesting that the affinity for T4 is somewhat higher in the H192Q mutant hsMCT8 (mean [95% CI], 14.6 [9.5-22.5] µM) than in WT hsMCT8 (26.9 [17.34-41.8]) (**Figure 8F**).

DISCUSSION

Over the last decade various mouse and zebrafish models have emerged to study the physiological role of MCT8 and the consequences of its inactivation. However, the intrinsic transporter properties of the mouse and zebrafish orthologues have not been compared to human MCT8 in detail thus far. Here, we demonstrated that the mouse and zebrafish orthologues efficiently transport T3 and T4, although remarkable differences between hsMCT8 and drMct8 were observed in substrate affinity, uptake rate and specificity. These findings support the eligibility of both animals to model human MCT8 deficiency, and moreover provided insights into the structural requirements and tolerable variation for efficient TH transport by MCT8. Nevertheless, our findings in mammalian overexpressing cell-lines also stress that differences in the intrinsic transporter properties of MCT8 orthologues may exist, which should be realized when comparing MCT8 deficiency in different *in vivo* models.

The eligibility of animal models for human MCT8 deficiency is importantly determined by three major factors: first, the species-specific tissue distribution of MCT8 expression; second, the presence of redundant transporters at sites where MCT8 is expressed; and third, the intrinsic transporter properties (e.g. substrate affinity and specificity) of the involved MCT8 orthologues. The relevance of tissue-specific distribution of various TH transporters is strengthened by the normal neurological phenotype observed in *Mct8 ko* mice. This observation can be largely attributed to the presence of Oatp1c1 at the BBB, which is absent in human (29), although differences in the basic functional characteristics of mouse and human MCT8 have not been excluded.

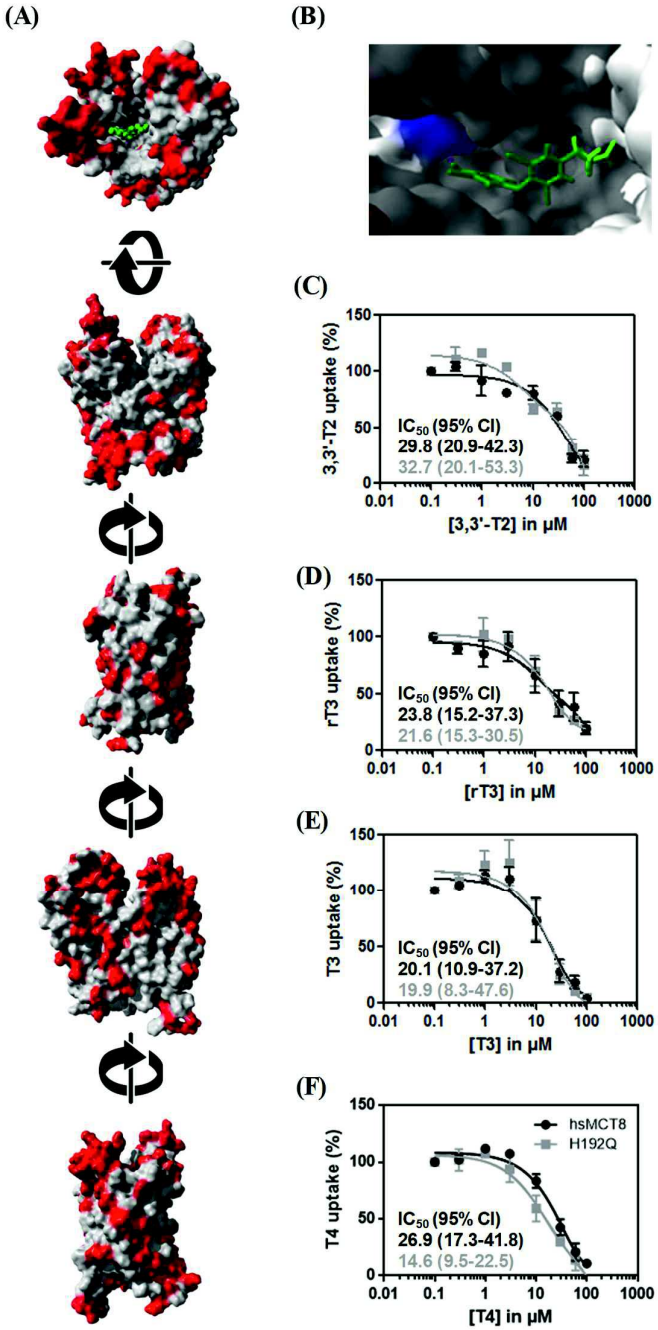

Figure 8 (**A**) structural model of hsMCT8 (described in 19) in which the residues that are not conserved between hsMCT8 and drMct8 are highlighted in black, displayed from different orientations. A T3 substrate molecule (green) is visible at the substrate binding center. (**B**) A magnification of the substrate channel, showing that His192 (in black) is the only non-conserved residue that flanks the substrate binding center. 3,3'-T2 (**C**), rT3 (**D**), T3 (**E**) and T4 (**F**) saturation curves in COS-1 cells transiently transfected with EV, WT hsMCT8 or the H192Q mutant in the absence of CRYM after 10 minutes incubation at 37 ºC. All data points are corrected for background iodothyronine uptake in EV-transfected control cells and presented relatively to the amount of internalized iodothyronines in the presence of the lowest substrate concentration (0.01 µM). Apparent IC50 values for hsMCT8 WT (black) and H192Q mutant (grey) are displayed in the left bottom of each graph and were determined as described in the footnote of **Table 1**, (La Jolla, USA).

Our current data show that the molecular characteristics of the mouse orthologue are largely similar to hsMCT8, which is in agreement with their high amino acid sequence identity and the mapping of non-conserved residues to domains outside the substrate pore which usually tolerate more structural variation. Thus, the differences in neurological phenotypes between patients with MCT8 deficiency and the *Mct8 ko* mouse model can be unequivocally attributed to the presence of compensatory thyroid hormone transporters (Oatp1c1) in the mouse BBB.

Interestingly, cell-surface expression levels of mmMCT8 were significantly lower than those of hsMCT8, which likely explains the slightly lower initial uptake rates of mmMCT8. We postulate that differences in the less well-conserved intracellular N-terminus and C-terminus may account for the reduced cell-surface expression levels. Indeed, many membrane proteins, including other members of the MCT family, require ancillary proteins for proper cell membrane targeting (30), some of which specifically bind to the C-terminus of their binding partner (31). Up to now, ancillary proteins have not been identified for MCT8. Since our experiments were conducted in transiently transfected mammalian cell-lines, it is possible that these cells lack important chaperone/ancillary proteins for the tested orthologues. Therefore, it is yet unclear if membrane targeting of mmMCT8 is also less efficient *in vivo* once the appropriate putative ancillary proteins are present.

Zebrafish are evolutionary more distant to human than mouse. Nevertheless, *mct8 kd* and *ko* zebrafish replicate several, though not all, important abnormalities in brain development that are observed in human patients with MCT8 deficiency, suggesting a similar biological function of Mct8 in zebrafish (32-34). Indeed, previous studies have demonstrated that drMct8 effectively transports T3 and to a lesser extent T4 (14, 18), and uptake levels were found to exceed those of its human (and chicken) orthologue in over-expressing JEG-3 cells, which is in agreement with our observations (14). Here, we extend on these studies and demonstrated that drMct8 exhibits 3-5-fold higher initial uptake rates for 3,3'-T2, rT3, T3, and T4 than its human and mouse counterpart, which is likely attributable to the higher apparent substrate affinity of drMct8 for these substrates. Previous studies had already indicated that drMct8 has a ~10-fold higher affinity for T3 than its human orthologue (18). Moreover, the substrate preference of drMct8 (3,3'-T2, T3>T4>rT3) differs from hsMCT8 and mmMCT8 (T3>T4>rT3, 3,3'-T2). Interestingly, the transport of especially 3,3'-T2, rT3 and to a lesser extent T3 showed clear biphasic kinetics, suggesting the presence of more than one mode of substrate docking. In contrast to hsMCT8, the T3 transport by drMct8 was inhibited by several other substrates including those containing a modified alanine side-chain. This was not the case for mmMCT8 (current study) and chicken MCT8 (14), which showed similar characteristics to hsMCT8. Unfortunately, no detailed kinetic and cis-inhibition studies are available for *Xenopus* MCT8. Future studies may reveal if the distinct properties of drMct8 are maintained in amphibians, and will elucidate an insightful evolutionary link between fish, mammals, rodents and birds.

Of interest, we here showed that drMct8 is able to modestly induce the transport of the thyroid hormone metabolite Triac, whereas various *in vitro* and *ex vivo* studies have demonstrated that neither hsMCT8 nor mmMCT8 facilitate the cellular transport of Triac (e.g. (23, 35)). Providing its profound thyromimetic actions and its MCT8-independent cellular entry in mouse and human models (36), the therapeutic potency of Triac is currently being explored in MCT8 deficiency. So far, promising results have been reported in the mouse, chicken, and zebrafish models (33, 35, 37). Although drMct8 transports Triac, treatment of *mct8 ko* zebrafish with Triac still resulted in restoration of myelination (29), suggesting the presence of additional Triac transporters at the BBB and neuronal cells in zebrafish.

Nonetheless, based on our observation, it should be realized that the contribution of MCT8 to the transport of TH metabolites and thyromimetic compounds may vary across species.

The broader substrate specificity of drMct8 and its capacity to transport Triac may substantiate recent studies demonstrating that Triac may have an important biological role in evolutionary more distant species. For example, in amphioxus Triac and not T3 was found to be the main receptor-active TH metabolite (38). In addition, a deiodinating enzyme was identified in amphioxus that exclusively metabolized iodothyroacetic acid derivatives instead of iodothyronines (17). An MCT8 orthologue in amphioxus has not been characterized yet. However, the induction of Triac transport by drMct8 may suggest that evolutionary more distant species could also possess an Mct8 orthologue capable of transporting iodothyroacetic acid derivatives such as Triac.

We sought to identify the origin of the functional differences of drMct8 *versus* hsMCT8. The H192Q substitution in hsMCT8, which changes the only non-conserved residue at the substrate pore into its corresponding residue in drMct8, did not recapitulate the differential transporter characteristics of drMct8. Since predominantly the uptake efficiency differs between hsMCT8 and drMct8, we therefore speculate that the non-conserved residues within the extra-cellular loops account for the functional differences between both orthologues. The extracellular loops of drMct8 are smaller than those of hsMCT8 which may pose fewer constraints for substrate molecules to enter the substrate pore. This may explain the higher initial uptake rates, the broader substrate specificity of drMct8, and the presence of multiple substrate binding modes as suggested by its biphasic kinetic profiles. Alternatively, variation in these loops may influence transporter efficiency by affecting the organization and dynamics of the helical bundles and hence the exact orientations of residue side-chains that flank the substrate channel. Nevertheless, it is important to stress that albeit extensive inter-species variation in these regions, drMct8 does efficiently transport T3 and T4. This suggests that naturally occurring variants in these non-conserved regions may also be tolerated in human. Indeed, so far no pathogenic mutations have been described in the predicted loop regions of MCT8 (8), with the exception of L512P in the predicted intracellular loop 5 (7).

Although our data in transiently transfected COS-1 and JEG-3 cells thus suggest that the transporter characteristics of drMct8 differ from hsMCT8, it should be emphasized that these differences may be cell type dependent, and may thus differ from the *in vivo* situation. Also in the current work, differences between drMct8 and hsMCT8 were more pronounced in COS-1 cells than in JEG-3 cells, which may be related to several factors. First, as for naturally occurring MCT8 mutations (i.e. (39)), COS-1 cells may better tolerate variation in the MCT8 sequence in terms of protein stability and subcellular trafficking than JEG-3 cells. Therefore, the increase in transport efficacy of drMct8, may be counterbalanced by unfavorable effects on drMct8 availability at the cell membrane in JEG-3 cells. Second, factors that influence MCT8 function (i.e. interacting proteins, post-translational modification) may differ among tissues. Third, the role of MCT8 in cellular TH homeostasis and its contribution to cellular TH uptake and efflux likely depends on the presence of other transporters and may, as such, differ between cell-types. Replication of our findings in vascular endothelial or neuronal cell lines would have been of great interest, being the cell types in which MCT8 is of most physiological relevance. However, such experiments are limited by the poor transfection efficacy of these cell lines (data not shown). Nevertheless, previous studies in transiently transfected COS-1 and JEG-3 cells have indicated that the residual activity of mutant MCT8 proteins in these cell lines reflects the degree of intellectual disability in patients with MCT8 deficiency (39-41). As such, these models apparently

represent MCT8 function at critical sites in the human body (i.e. the vascular endothelial cells of the BBB and neuronal cells).

Taken together, we demonstrated that the human, mouse and zebrafish orthologues of MCT8 overall have very similar transporter properties, although the non-conserved residues in drMct8 increased its affinity for iodothyronines and allowed the acceptance of a broader set of substrates that potentially include iodothyroacetic acid derivatives such as Triac. Therefore, our studies indicate that fundamental properties of MCT8 have been preserved during evolution, whereas the ability to accept alternative thyromimetic metabolites has been gradually declined. These molecular differences should be considered when comparing data between different species.

Acknowledgements

We thank Selmar Leeuwenburgh for the technical assistance, the Optical Imaging Center (Erasmus Medical Center Rotterdam) for technical support regarding the confocal imaging studies

Grants and funding

This work was supported by a grant from the Netherlands Organisation for Health Research and Development (project number 113303005) (to WEV), from the Sherman Foundation (to SK and WEV), and from the Smile Foundation (SK).

Author disclosure statement: Erasmus MC receives royalties from Rare Thyroid Therapeutics.

SUPPLEMENTAL MATERIALS

See next page.

Supplemental Tables

Supplemental Table S1 Antibody Table

Target protein/ antigen	Antigen sequence (if known)	Name of AB	Species raised (P or M)	Manufacturer (and catalog number)	Dilution used for WB	Dilution used for ICH	RRID
hsMCT8	AA 52-155	MCT8	Rabbit (P)	ATLAS (HPA003353)	1:20000	1:1000	AB_1079343
GAPDH		GAPDH	Mouse (M)	Millipore (Mab 374)	1:20000		AB_2107445
ZO1		ZO1	Mouse (M)	Thermo Fisher (33-9100)		1:1000	AB_2533147
V5-tag		V5	Rabbit (M)	Cell signaling mAB #13202	1:1000	1:1000	AB_2687461
Rabbit IgG		IRDye800	Goat	LI-COR (926-32211)	1:20000		AB_621843
Mouse IgG		IRDye680	Goat	LI-COR (926-68020)	1:20000		AB_10706161
Rabbit IgG		Alexa 488	Goat	Thermo Fisher (A11008)		1:1000	AB_143165
Mouse IgG		Alexa 633	Goat	Thermo Fisher (A21050)		1:1000	AB_2535718

AB: antibody; GAPDH: glyceraldehyde-3-phosphate dehydrogenase; ZO-1: zona occludens 1;P: polyclonal antibody; M: monoclonal antibody; WB: Western Blot ; ICH: immunohistochemistry

Supplemental Figures

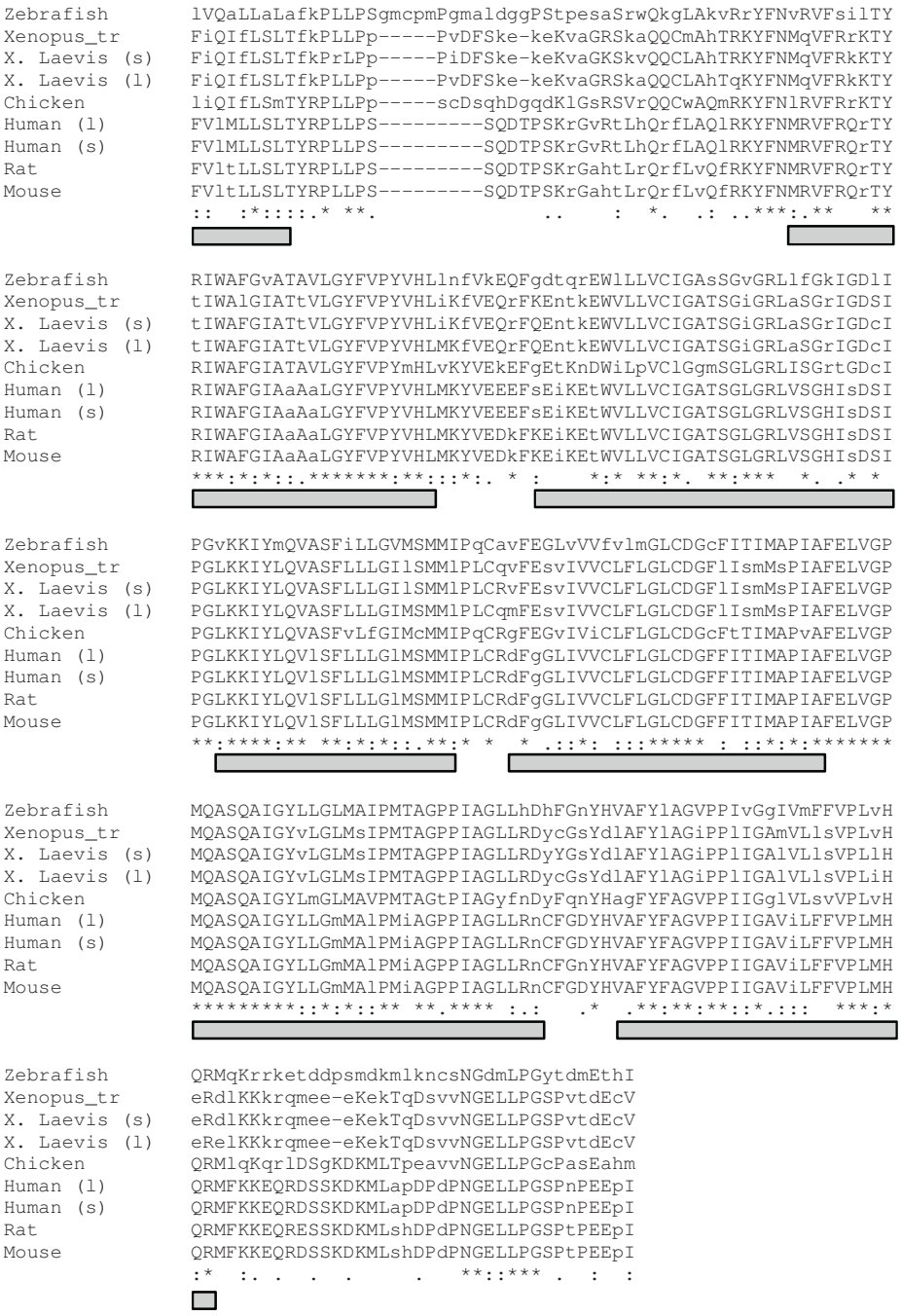

Supplemental Figure 1 Multiple sequence alignment of the short (s) and long (l) human, zebrafish and mouse MCT8 amino acid sequences. For comparison the sequences of *Xenopus Tropicalis* (Xenopus tr), the short (s) and long (l) isoforms of *Xenopus laevis* (X. Laevis), chicken, and rat MCT8 have been added. Identical amino acids in all species are indicated with an *. Conservation between amino acids with strongly similar properties (equivalent to scoring > 0.5 in the Gonnet PAM 250 matrix) is indicated with an :, whereas conservation between amino acids with weakly similar properties (equivalent to scoring 0< score <0.5 in the Gonnet PAM 250 matrix) are indicated with a . . The human-specific part of the intracellular N-terminus is colored in light grey. Predicted transmembrane domains of hsMCT8 are indicated by the light grey bars below the alignment. Multiple sequence alignments were generated using Clustal Omega, with some manual adjustments in the weakly conserved N-terminus to reduce gaps.

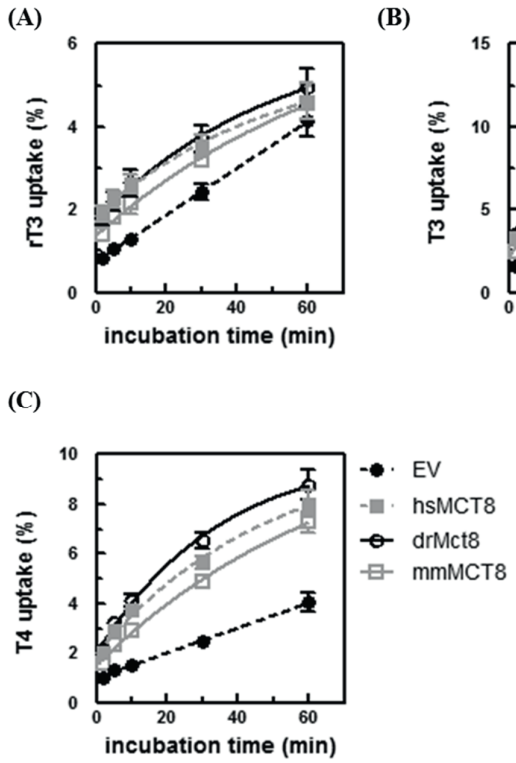

Supplemental Figure 2 Cellular accumulation of rT3 (**A**), T3 (**B**) and T4 (**C**) in JEG-3 cells, transiently transfected with empty vector (EV), human (hs), mouse (mm) or zebrafish (dr) MCT8 after indicated incubation times at 37ºC. All uptake levels are expressed relative to the amount of radio-labeled hormone added to the cells at the start of the incubation (1 nM (50000 cpm) of the respective [^{125}I]-labeled iodothyronines). All results are presented as means ± SEM (n=3). The cellular accumulation levels were higher in cells transfected with any of the MCT8 orthologues than in cells transfected with EV at all time-points, except for the 60 minute incubations with rT3 and T3 (one-way ANOVA with a Bonferroni corrected post hoc test, $P<0.05$). The intracellular accumulation of all tested substrates was not significantly different between cells expressing drMct8 and cells expressing hsMCT8 or mmMCT8.

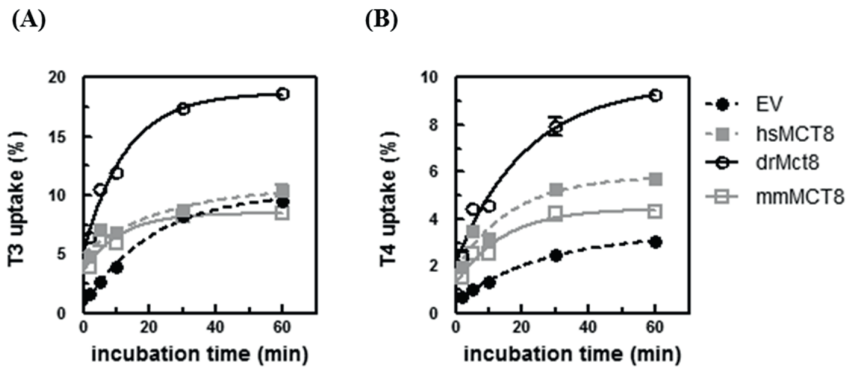

Supplemental Figure 3 Cellular accumulation of T3 (**A**) and T4 (**B**) in COS-1 cells, transiently transfected with empty vector (EV), or the V5-tagged hsMCT8, mmMCT8 or drMct8 after indicated incubation times at 37ºC. All uptake levels are expressed relative to the amount of radio-labeled hormone added to the cells at the start of the incubation (1 nM (50000 cpm) [^{125}I]-T3 or T4). All results are presented as means ± SEM (n=3). The cellular accumulation levels were higher in cells transfected with any of the V5-tagged MCT8 orthologues than in cells transfected with EV at all time-points, except for V5-hsMCT8 and V5-mmMCT8 at the 30 and 60 minute incubations with T3 (one-way ANOVA with a Bonferroni corrected post hoc test, $P<0.05$). The intracellular accumulation of all tested substrates was significantly higher in cells expressing V5-drMct8 than in cells expressing V5-hsMCT8 or V5-mmMCT8.

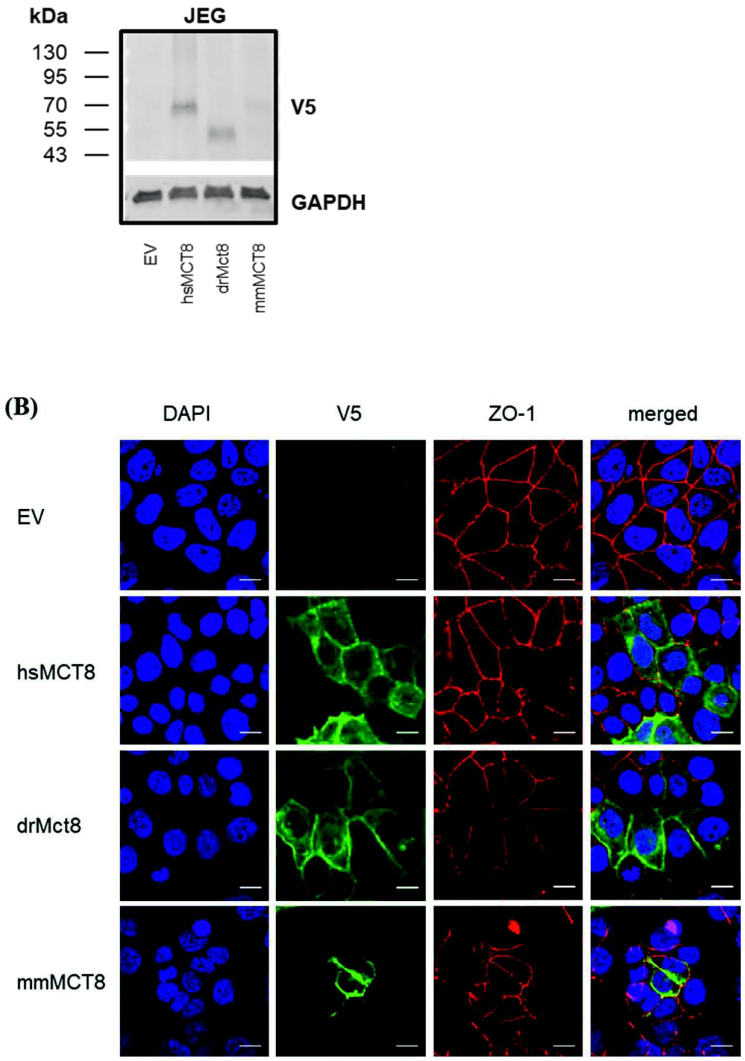

Supplemental Figure 4 (**A**) Representative immunoblot on total lysates derived from JEG-3 cells transfected with 500 ng of pcDNA3 EV or the indicated V5-tagged MCT8 orthologues. MCT8 detection was performed with the V5-tag antibody and visualized with IRDye800 goat anti-rabbit secondary antibody. Glyceraldehyde-3-phosphate dehydrogenase (GAPDH) was used as loading control. MCT8 and GADPH expression levels were quantified by densitometry using ImageJ. **(B)** Subcellular localization of the MCT8 orthologues in transiently transfected JEG-3 cells assessed by confocal microscopy. Fixated cells were stained for the cell membrane marker ZO-1 (red) and for the MCT8 orthologues by using V5-antibodies (green). DAPI was used as a nuclear staining (blue). In addition, a composite image is shown.

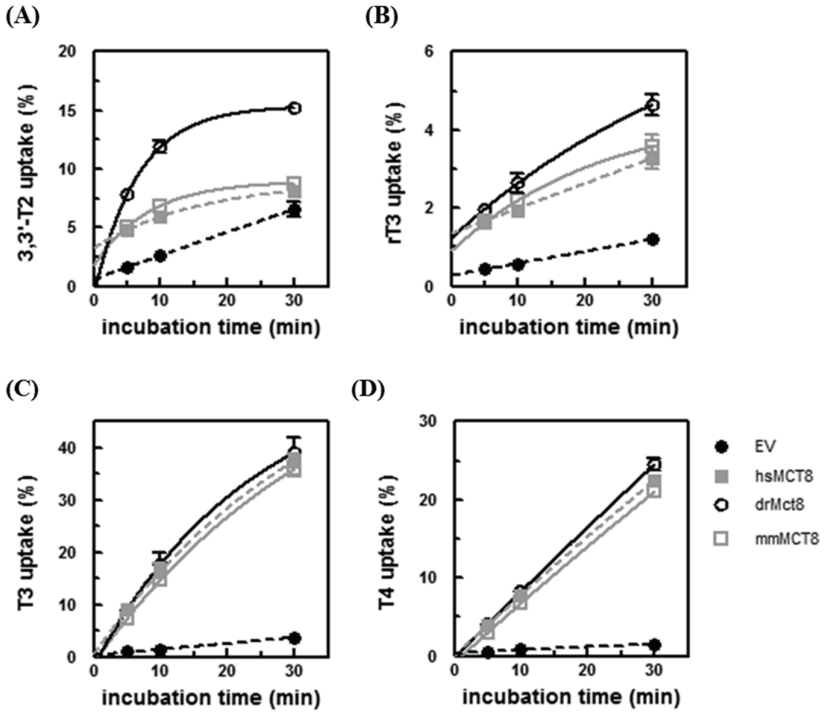

Supplemental Figure 5 Cellular accumulation of 3,3'-T2 (**A**), rT3 (**B**), T3 (**C**) and T4 (**D**) in COS-1 cells, transiently transfected with empty vector (EV), human (hs), mouse (mm) or zebrafish (dr) MCT8 and the intracellular TH-binding protein CRYM, after indicated incubation times at 37ºC. All uptake levels are expressed relative to the amount of radio-labeled hormone added to the cells at the start of the incubation (1 nM (50000 cpm) of the respective [^{125}I]-labeled iodothyronines). All results are presented as means ± SEM (n=3). The cellular accumulation levels were higher in cells transfected with any of the MCT8 orthologues than in cells transfected with EV at all time-points (one-way ANOVA with a Bonferroni corrected post hoc test, $P<0.05$). The intracellular accumulation of T3 and T4 was not significantly different between cells expressing drMct8 and cells expressing hsMCT8 or mmMCT8, whereas the intracellular accumulation of 3,3'-T2 (at all time-points) and rT3 (after 30 minutes) was significantly higher in cells transfected with drMct8, compared to cells transfected with hsMCT8 or mmMCT8 and CRYM ($P< 0.05$).

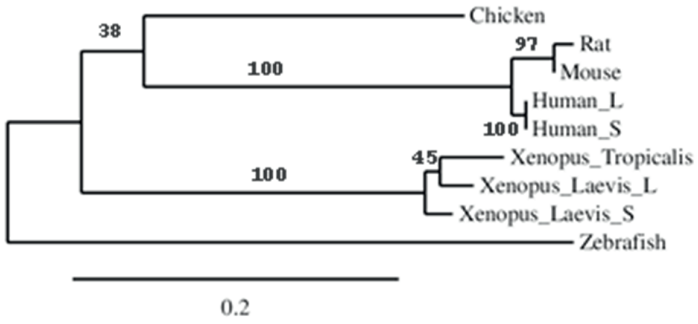

Supplemental Figure 6 Phylogenetic tree incorporating the (previously) studied MCT8 orthologues using maximum likelihood. Bootstrap test of phylogeny was performed with 500 replications. The numbers at the branches indicated the confidence level. Phylogenetic tree was constructed through www.phylogeny.fr.

REFERENCES

1. Yen PM. Physiological and molecular basis of thyroid hormone action. Physiol Rev. 2001;81(3):1097-142.
2. Yen PM, Ando S, Feng X, Liu Y, Maruvada P, Xia X. Thyroid hormone action at the cellular, genomic and target gene levels. Mol Cell Endocrinol. 2006;246(1-2):121-7.
3. Gereben B, Zavacki AM, Ribich S, Kim BW, Huang SA, Simonides WS, et al. Cellular and molecular basis of deiodinase-regulated thyroid hormone signaling. Endocr Rev. 2008;29(7):898-938.
4. Hennemann G, Docter R, Friesema EC, de Jong M, Krenning EP, Visser TJ. Plasma membrane transport of thyroid hormones and its role in thyroid hormone metabolism and bioavailability. Endocr Rev. 2001;22(4):451-76.
5. Friesema EC, Ganguly S, Abdalla A, Manning Fox JE, Halestrap AP, Visser TJ. Identification of monocarboxylate transporter 8 as a specific thyroid hormone transporter. J Biol Chem. 2003;278(41):40128-35.
6. Friesema EC, Grueters A, Biebermann H, Krude H, von Moers A, Reeser M, et al. Association between mutations in a thyroid hormone transporter and severe X-linked psychomotor retardation. Lancet. 2004;364(9443):1435-7.
7. Dumitrescu AM, Liao XH, Best TB, Brockmann K, Refetoff S. A novel syndrome combining thyroid and neurological abnormalities is associated with mutations in a monocarboxylate transporter gene. Am J Hum Genet. 2004;74(1):168-75.
8. Groeneweg S, Visser WE, Visser TJ. Disorder of thyroid hormone transport into the tissues. Best Pract Res Clin Endocrinol Metab. 2017;31(2):241-53.
9. Vancamp P, Darras VM. From zebrafish to human: A comparative approach to elucidate the role of the thyroid hormone transporter MCT8 during brain development. Gen Comp Endocrinol. 2018;265:219-29.
10. Trajkovic M, Visser TJ, Mittag J, Horn S, Lukas J, Darras VM, et al. Abnormal thyroid hormone metabolism in mice lacking the monocarboxylate transporter 8. J Clin Invest. 2007;117(3):627-35.
11. Mayerl S, Muller J, Bauer R, Richert S, Kassmann CM, Darras VM, et al. Transporters MCT8 and OATP1C1 maintain murine brain thyroid hormone homeostasis. J Clin Invest. 2014;124(5):1987-99.
12. Mayerl S, Visser TJ, Darras VM, Horn S, Heuer H. Impact of Oatp1c1 deficiency on thyroid hormone metabolism and action in the mouse brain. Endocrinology. 2012;153(3):1528-37.
13. Nakao N, Takagi T, Iigo M, Tsukamoto T, Yasuo S, Masuda T, et al. Possible involvement of organic anion transporting polypeptide 1c1 in the photoperiodic response of gonads in birds. Endocrinology. 2006;147(3):1067-73.
14. Bourgeois NM, Van Herck SL, Vancamp P, Delbaere J, Zevenbergen C, Kersseboom S, et al. Characterization of Chicken Thyroid Hormone Transporters. Endocrinology. 2016;157(6):2560-74.
15. Mughal BB, Leemans M, Lima de Souza EC, le Mevel S, Spirhanzlova P, Visser TJ, et al. Functional Characterization of Xenopus Thyroid Hormone Transporters mct8 and oatp1c1. Endocrinology. 2017;158(8):2694-705.
16. Mol JA, Visser TJ. Synthesis and some properties of sulfate esters and sulfamates of iodothyronines. Endocrinology. 1985;117(1):1-7.
17. Klootwijk W, Friesema EC, Visser TJ. A nonselenoprotein from amphioxus deiodinates triac but not T3: is triac the primordial bioactive thyroid hormone? Endocrinology. 2011;152(8):3259-67.
18. Arjona FJ, de Vrieze E, Visser TJ, Flik G, Klaren PH. Identification and functional characterization of zebrafish solute carrier Slc16a2 (Mct8) as a thyroid hormone membrane transporter. Endocrinology. 2011;152(12):5065-73.
19. Friesema EC, Kuiper GG, Jansen J, Visser TJ, Kester MH. Thyroid hormone transport by the human monocarboxylate transporter 8 and its rate-limiting role in intracellular metabolism. Mol Endocrinol. 2006;20(11):2761-72.
20. Friesema EC, Jansen J, Jachtenberg JW, Visser WE, Kester MH, Visser TJ. Effective cellular uptake and efflux of thyroid hormone by human monocarboxylate transporter 10. Mol Endocrinol. 2008;22(6):1357-69.
21. Groeneweg S, Lima de Souza EC, Meima ME, Peeters RP, Visser WE, Visser TJ. Outward-Open Model of Thyroid Hormone Transporter Monocarboxylate Transporter 8 Provides Novel Structural and Functional Insights. Endocrinology. 2017;158(10):3292-306.
22. Groeneweg S, van den Berge A, Meima ME, Peeters RP, Visser TJ, Visser WE. Effects of Chemical Chaperones on Thyroid Hormone Transport by MCT8 Mutants in Patient-Derived Fibroblasts. Endocrinology. 2018;159(3):1290-302.
23. Groeneweg S, Friesema EC, Kersseboom S, Klootwijk W, Visser WE, Peeters RP, et al. The role of Arg445 and Asp498 in the human thyroid hormone transporter MCT8. Endocrinology. 2014;155(2):618-26.

24. Krieger E, Vriend G. YASARA View - molecular graphics for all devices - from smartphones to workstations. Bioinformatics. 2014;30(20):2981-2.
25. Berkenstam A, Kristensen J, Mellstrom K, Carlsson B, Malm J, Rehnmark S, et al. The thyroid hormone mimetic compound KB2115 lowers plasma LDL cholesterol and stimulates bile acid synthesis without cardiac effects in humans. Proc Natl Acad Sci U S A. 2008;105(2):663-7.
26. Kinne A, Kleinau G, Hoefig CS, Gruters A, Kohrle J, Krause G, et al. Essential molecular determinants for thyroid hormone transport and first structural implications for monocarboxylate transporter 8. J Biol Chem. 2010;285(36):28054-63.
27. Braun D, Lelios I, Krause G, Schweizer U. Histidines in potential substrate recognition sites affect thyroid hormone transport by monocarboxylate transporter 8 (MCT8). Endocrinology. 2013;154(7):2553-61.
28. Groeneweg S, Lima de Souza EC, Visser WE, Peeters RP, Visser TJ. Importance of His192 in the human thyroid hormone transporter MCT8 for substrate recognition. Endocrinology. 2013;154(7):2525-32.
29. Roberts LM, Woodford K, Zhou M, Black DS, Haggerty JE, Tate EH, et al. Expression of the thyroid hormone transporters monocarboxylate transporter-8 (SLC16A2) and organic ion transporter-14 (SLCO1C1) at the blood-brain barrier. Endocrinology. 2008;149(12):6251-61.
30. Kirk P, Wilson MC, Heddle C, Brown MH, Barclay AN, Halestrap AP. CD147 is tightly associated with lactate transporters MCT1 and MCT4 and facilitates their cell surface expression. EMBO J. 2000;19(15):3896-904.
31. Lee HJ, Zheng JJ. PDZ domains and their binding partners: structure, specificity, and modification. Cell Commun Signal. 2010;8:8.
32. Vatine GD, Zada D, Lerer-Goldshtein T, Tovin A, Malkinson G, Yaniv K, et al. Zebrafish as a model for monocarboxyl transporter 8-deficiency. J Biol Chem. 2013;288(1):169-80.
33. Zada D, Tovin A, Lerer-Goldshtein T, Appelbaum L. Pharmacological treatment and BBB-targeted genetic therapy for MCT8-dependent hypomyelination in zebrafish. Dis Model Mech. 2016;9(11):1339-48.
34. Zada D, Tovin A, Lerer-Goldshtein T, Vatine GD, Appelbaum L. Altered behavioral performance and live imaging of circuit-specific neural deficiencies in a zebrafish model for psychomotor retardation. PLoS Genet. 2014;10(9):e1004615.
35. Kersseboom S, Horn S, Visser WE, Chen J, Friesema EC, Vaurs-Barriere C, et al. In vitro and mouse studies supporting therapeutic utility of triiodothyroacetic acid in MCT8 deficiency. Mol Endocrinol. 2014;28(12):1961-70.
36. Groeneweg S, Peeters RP, Visser TJ, Visser WE. Triiodothyroacetic acid in health and disease. J Endocrinol. 2017;234(2):R99-R121.
37. Delbaere J, Vancamp P, Van Herck SL, Bourgeois NM, Green MJ, Wingate RJ, et al. MCT8 deficiency in Purkinje cells disrupts embryonic chicken cerebellar development. J Endocrinol. 2017;232(2):259-72.
38. Paris M, Escriva H, Schubert M, Brunet F, Brtko J, Ciesielski F, et al. Amphioxus postembryonic development reveals the homology of chordate metamorphosis. Curr Biol. 2008;18(11):825-30.
39. Novara F, Groeneweg S, Freri E, Estienne M, Reho P, Matricardi S, et al. Clinical and Molecular Characteristics of SLC16A2 (MCT8) Mutations in Three Families with the Allan-Herndon-Dudley Syndrome. Hum Mutat. 2017;38(3):260-4.
40. Jansen J, Friesema EC, Kester MH, Schwartz CE, Visser TJ. Genotype-phenotype relationship in patients with mutations in thyroid hormone transporter MCT8. Endocrinology. 2008;149(5):2184-90.
41. Capri Y, Friesema EC, Kersseboom S, Touraine R, Monnier A, Eymard-Pierre E, et al. Relevance of different cellular models in determining the effects of mutations on SLC16A2/MCT8 thyroid hormone transporter function and genotype-phenotype correlation. Hum Mutat. 2013;34(7):1018-25.

Chapter

2.7

Insights into the mechanism of MCT8 oligomerization

Stefan Groeneweg, Amanda van den Berge, Elaine C. Lima de Souza, Marcel E. Meima, Robin P. Peeters, W. Edward Visser

Submitted

ABSTRACT

Mutations in the thyroid hormone transporter MCT8 result in the Allan-Herndon-Dudley syndrome (AHDS) characterized by severe intellectual and motor disability. The MCT8 protein is predicted to have 12 transmembrane domains (TMDs) and is expressed as monomers, homo-dimers and homo-oligomers. This study aimed to delineate the mechanism of MCT8 oligomerization. Co-immunoprecipitation studies demonstrated that lithium dodecyl sulfate effectively disrupts MCT8 protein complexes, indicating the involvement of non-covalent interactions. Successive C-terminal truncations of the MCT8 protein only altered the oligomerization pattern if introduced in the N-terminal half of the protein (TMD1-6). The truncation at extracellular loop 1 (E206X) still allowed homo-dimerization, but completely abrogated homo-oligomerization, while both were preserved by the C231X mutant (at TMD2), suggesting that the minimally required oligomerization sites are located proximal of Cys231. However, mutant constructs lacking the intracellular N-terminus or TMD1 and 2 were still capable to form homo-oligomers. Therefore, other domains distal of Cys231 are also likely to be involved in the formation of extensive multi-domain interactions. This hypothesis was supported by structural modelling. Despite multiple approaches, MCT8 oligomerization could not be fully abrogated unless a substantial part of the protein was removed, precluding detailed studies into its functional role. Together, our findings suggest that MCT8 oligomerization involves extensive non-covalent interactions between the N-terminal halves of MCT8 proteins. Most mutations identified in AHDS patients have only minor effects on MCT8 oligomerization and, thus, impaired oligomerization does not appear an important pathogenic mechanism.

INTRODUCTION

Normal brain development is highly dependent on adequate intra-cerebral thyroid hormone (TH) concentrations. Monocarboxylate transporter 8 (MCT8) plays a crucial role in the maintenance of TH homeostasis in the brain (1). Mutations in the SLC16A2 gene, encoding MCT8, result in MCT8 deficiency, also known as Allan-Herndon-Dudley Syndrome (AHDS), characterized by severe intellectual and motor disability, and abnormal thyroid function tests (2, 3). Many inactivating mutations have been reported to date, with different underlying pathogenic mechanisms (4).

The MCT8 protein is predicted to consist of two nearly symmetrical parts composed of 6 transmembrane domains (TMDs), interconnected by a large intracellular loop. Both, the C-terminus and N-terminus are predicted to be located intracellularly (5, 6). The MCT8 protein is expressed as a monomer, homo-dimer and possibly also as a homo-oligomer, in transient and stable overexpression systems (7, 8). Recently, it has been shown that MCT8 dimers are present in a cellular context and it was suggested that missense mutations in MCT8 differentially affect the oligomerization potency (9). Modulation of the MCT8 molecular surface by these mutations has been proposed as the mechanism accounting for this finding. Nevertheless, none of these mutations completely abrogated MCT8 oligomerization (9). Different protein oligomerization mechanisms have been described, including the formation of covalent (e.g. disulfide bonds), electrostatic (e.g. ionic bonds and hydrogen bonds) or hydrophobic interactions, or mediation of monomer-monomer contacts through ions (Ca^{2+} or Mg^{2+}) or small molecules (e.g. (10-16)). Conventional immunoblot studies have shown that MCT8 oligomers are, at least partially, resistant to the denaturing effects of the chaotropic agent sodium dodecyl sulfate (SDS) and the reducing effects of dithiothreitol (DTT), suggesting that MCT8 oligomerization is not solely mediated by (weak) non-covalent interactions or disulfide bonds (7). Indeed, all Cys residues within MCT8 can be substituted by Ala without affecting its oligomerization (7, 17).

Despite these studies, the exact mechanism involved in MCT8 oligomerization and the domain(s) of the MCT8 protein involved in this process remain to be characterized. It is furthermore unknown if the monomers (and dimers) detected on conventional immunoblots arise from the disruption of oligomeric complexes or solely reflect the quaternary protein organization inside the cell. Lack of this knowledge precludes further studies onto the relevance of MCT8 oligomerization for transporter function. It is also unclear if specific naturally occurring mutations in MCT8 may abrogate MCT8 oligomerization and to what extent this contributes to the pathogenicity of such mutations.

Here, we aimed to further delineate the MCT8 oligomerization mechanism and identify the domains involved in this process. Since MCT8 is able to form homo-oligomers, we postulated that each MCT8 protein should be able to interact with at least two other MCT8 proteins and should therefore contain at least two distinct domains that are involved in the formation of monomer-monomer contacts. Our findings indeed support that MCT8 oligomerization is mediated through extensive hydrophobic and electrostatic interactions between distinct domains within the N-terminal half of the protein, composed of multiple TMDs and putative loops. Despite multiple approaches, MCT8 oligomerization could not be fully abrogated unless a substantial part of the protein was removed, preventing studies into its functional role. Thus, our studies provide novel insights on the quaternary structural organization of MCT8.

MATERIALS AND METHODS

Materials

Unlabeled iodothyronines, DTT and EDTA were obtained from Sigma (Zwijndrecht, The Netherlands [NL]). [125I]T3 and [125I]T4 were synthesized as previously described (18). X-tremeGENE 9 transfection reagent was obtained from Roche Diagnostics (Almere, NL). An overview of all commercially available primary and secondary antibodies (AB) is provided in **Supplemental Table 1**. Purified polyclonal rabbit antisera against the C-terminus of hMCT8 (designated 1306), and hMCT10 (designated 1758) have been described previously (19, 20).

Plasmids

Cloning of wild-type human MCT8 (WT MCT8) cDNA into pcDNA3, human WT MCT10 cDNA into pcDNA3, and human μ-crystallin (CRYM) into pSG5 has been described previously (19, 20). CRYM is a cytosolic TH-binding protein, which greatly reduces the efflux of TH, thereby increasing the net cellular TH accumulation. The WT MCT8 construct used in the current studies contains the coding sequence for the short MCT8 isoform, starting at the second translational start site ($MCT8_{75\text{-}613}$). The N-terminally Flag-tagged hMCT8 (Flag-MCT8) construct was cloned into pcDNA3 after PCR amplification of WT MCT8 cDNA using forward primers containing the Flag-tag sequence (**Supplemental Table 2**). The cloning of N-terminally Myc-tagged MCT8 has been described previously (21). We introduced the following mutations into the non-tagged WT MCT8 construct using QuikChange site-directed mutagenesis (Stratagene, Amsterdam, NL) according to the manufacturer's protocol: E206X, C231X, R245X, F256X, Q335X, S448X, Q520X, and C546X. The location of these mutations are indicated in **Figure 2A** and **Supplemental Figure 1**. N-terminally truncated MCT8 constructs were generated by substituting the native translational start site by an Ala (resulting construct will be referred to as MCT8M75A). Next, downstream translational start sites were re-introduced, resulting in the N-terminally truncated constructs $MCT8_{97\text{-}613}$ and $MCT8_{147\text{-}613}$. All used primer pairs are enlisted in **Supplemental Table 2**. Sanger sequencing was performed to confirm the presence of the introduced mutations.

To generate a construct lacking TMD1 and 2 (referred to as $MCT8_{\Delta 170\text{-}234}$), amino acids 170-234 were removed from the WT MCT8 cDNA construct using a unique EcoNI restriction site located at nucleotide position 503-513 and a second EcoNI site which was introduced by site-directed mutagenesis at position 697-707 (primers in **Supplemental Table 2**). After EcoNI digestion and gel purification, (QIAquick Gel Extraction Kit; Qiagen, Venlo, NL) the linear cDNA lacking nucleotides 507-701 was re-ligated using T4 ligase (Roche). The deletion of C507-T701 was confirmed by DNA sequencing (Baseclear, Leiden, NL). A Flag-tagged variant of this construct was generated as described above.

A MCT1/8 chimera was generated by amplification of the cDNA sequence encoding the 5`UTR, translational start-site and the first 9 amino acids (covering the small intracellular N-terminal domain) of MCT1 from the pCMV-Sport6_MCT1 construct (Open Biosystems, St. Leon-Rot, Germany). Hind III and Nhe I restriction sites were added at the 5' and 3' end respectively, using primers listed in **Supplemental Table 2**. A fragment of 164 base pairs ranging from C502 to C666 was next amplified from the WT MCT8 construct and a Nhe I site was added at the 5' end (primers in **Supplemental Table 2**). A Bam HI restriction site was already present within the amplified fragment. Both PCR products were first digested with Nhe I, purified and ligated, resulting in a chimeric MCT1/8 fragment. This

fragment was further digested with Hind III and Bam HI, gel purified and ligated into a Hind III/Bam HI digested WT MCT8 cDNA construct. The chimeric construct was sequenced to confirm proper ligation.

Cell culture and transfection

COS1 and JEG3 cells were cultured in 6 or 24-well plates (Corning, Schiphol, NL) in DMEM/F12 medium (Invitrogen), containing 9% heat-inactivated fetal bovine serum (Invitrogen), 2% Pen/Strep (Roche) and 100 nM sodium selenite (Sigma). All transient transfections were done using X-tremeGENE 9, according to the manufacturer's protocol (Roche). We have previously shown the absence of differences in transfection efficiency between WT and mutant MCT8 constructs (22).

TH uptake experiments

For TH uptake studies, COS-1 or JEG-3 cells were seeded in 6 well plates, and co-transfected in duplicate at 75% confluence with indicated amount of pcDNA3 empty vector (EV control), or indicated amount of WT or mutant MCT8 and 500 ng CRYM or pcDNA3 empty vector. Two days after transfection, cells were washed with incubation buffer (Dulbecco`s PBS [D-PBS] containing 0.1% D-glucose and 0,1% BSA) and subsequently incubated for 30 minutes at 37 ˚C in incubation buffer containing 1 nM unlabeled T3 or T4 and 5x105 cpm [125I]T3 or [125I]T4, respectively. After incubation, cells were briefly washed with incubation buffer and lysed with 0.1 M sodium hydroxide. The amount of radioactivity in the lysates was measured with a gamma counter.

Co-immunoprecipitation studies

COS-1 cells cultured in 6 well plates were transfected with 500 ng of indicated constructs. Lysates were prepared 48 h after transfection in immunoprecipitation (IP) buffer (50 mM Tris-HCl, 150 mM NaCl, 10 mM EDTA, 1% Triton-X-100), containing protease inhibitor cocktail (Roche) and incubated on ice for 30 minutes. Lysates of 4 wells per condition were pooled, sonicated on ice and centrifuged at 16.100 g for 20 minutes to remove nuclear debris. A fraction of the supernatant was saved as input sample, whereas the remaining fraction was incubated overnight at 4 C with pre-equilibrated mouse monoclonal M2 anti-Flag beads. After 3 washes with IP buffer, Flag-MCT8 protein complexes were eluted using the M2 Flag peptide (Sigma) in IP buffer according to manufacturers' protocol. IP eluate and input lysate (20 µl each) were subjected to immunoblotting as described below.

Immunoblotting

For immunoblots on total cell lysates, JEG-3 and COS-1 cells were cultured in 6-well plates and transfected with 500 ng WT or mutant MCT8 (unless indicated otherwise). Two days after transfection cells were rinsed once with D-PBS, collected in a 100 mM sodium phosphate buffer containing 2 mM EDTA (P100E2, pH 7.2) and sonicated on ice. Protein levels were measured using a Bradford assay (BIO-RAD, Veenendaal, NL). After heating for 10 min at 70 ˚C in the presence of NuPAGE 1x lithium dodecyl sulfate (LDS) loading buffer (Thermo Scientific) and 10 mM DTT (unless otherwise indicated), 25 µg protein was separated on a 10% or 4-15% gradient mini-PROTEAN TGX Precast Protein Gel (BIO-RAD), blotted to polyvinylidene difluoride (PVDF) membranes, and probed as indicated in the figure legends with rabbit anti-MCT8 antiserum (directed against the C-terminus) (19), mouse M2 anti-Flag antibody, rabbit anti-Myc antibody, rabbit anti-MCT8 antibody (directed against the N-terminus) or MCT10 antiserum (20) (**Supplemental Table 1**). Mouse anti-GADPH and/or mouse anti-ZO1 antibody were

used as controls in co-immunoprecipitation (co-IP) studies. IRDye680 goat anti-rabbit and IRDye800 goat anti-mouse antibodies 1:20,000 (LI-COR, Leusden, NL) were used as secondary antibody. Antibodies were detected with OdysseyTM Infrared Detection System (LI-COR).

Native PAGE

For native PAGE, cells were cultured as described for conventional immunoblotting. Lysates were prepared in P100E2 buffer and sonicated for 10 seconds on ice, and after addition of native sample loading buffer (final concentrations: 31.25 mM Tris-HCl (pH 6.8), 12.5% glycerol, 0.5% bromophenol blue), 25 µg was separated on a 4-15% precast mini-PROTEAN TGX gradient gel (BIO-RAD) under native conditions (1xPAGE buffer: 25 mM Tris-base, 192 mM glycine, ~ pH 8.3), and further processed as described for conventional immunoblots.

Surface biotinylation assays

For surface biotinylation assays, cells were cultured on 10 cm dishes and transfected with 2000 ng of the indicated constructs at 75% confluence. Two days after transfection, surface proteins were labelled with sulfo-NHS-biotin (Thermo Scientific) and isolated according to previously described methods (6).

Immunocytochemistry

JEG3 cells were cultured on 10 mm glass coverslips coated with poly-D-lysine (Sigma) and transfected with 250 ng WT or mutant MCT8. After 24 hours, cells were fixed with 4% paraformaldehyde for 20 minutes at 37 ˚C, permeabilized with 0.2% triton X-100 (Sigma) in PBS for 5 minutes at room temperature (RT). Samples were blocked for 1 hour at RT in PBS containing 2% BSA, and incubated overnight with N-terminal MCT8 antibody 3353 (1:1000, Sigma), or C-terminal MCT8 antiserum (1:500) and mouse monoclonal ZO-1 antibody (1:500, Invitrogen) at 4 ˚C (**Supplemental Table 1**). After secondary staining with goat anti-rabbit Alexa Fluor 488 and goat anti-mouse Alexa 633 (Invitrogen), cover slips were mounted on glass slides with Prolong Gold containing DAPI (Invitrogen). Samples were examined on a Zeiss Meta 510 microscope using Zeiss LSM software (Carl Zeiss B.V., Sliedrecht, NL).

Homology modeling

YASARA Structure was used for molecular homology modelling of a putative homodimeric MCT8 complex using our previously published MCT8 homology model in outward-open conformation (6, 23-25). Two MCT8 monomers were manually juxta-positioned in a way that accommodates our in vitro findings. Molecular dynamic simulations were performed in an AMBER 14 force field with periodic boundaries for 4 ns to establish and optimize the interactions between the two monomers, as previously described (6). All images were created using YASARA Structure and Pov-Ray v3.6 software (www.povray.org).

Statistical analysis

All uptake and metabolism results are expressed as means ± SEM of at least 3 separate experiments in duplicate. Statistical significance was determined using indicated statistical tests carried out in GraphPad Prism, version 6.

RESULTS

In line with previous studies, MCT8 monomers (55 kDa), homo-dimers (110 kDa) and putative homo-oligomers (multiples of 55 kDa) were detected on a conventional immunoblot in total lysates of COS-1 cells transiently expressing wild-type (WT) MCT8, after pre-incubation with LDS sample buffer, containing 10 mM DTT (**Supplemental Figure 2A**). To study if Mg^{2+} and Ca^{2+} mediate these monomer-monomer interactions, lysates were incubated in the presence of increasing concentrations of the Mg^{2+}/Ca^{2+} chelator EDTA prior to immunoblot analysis. However, no reduction in oligomerization was observed (**Supplemental Figure 2A**). Moreover, lysates incubated in the presence of increasing concentrations DTT showed similar levels of oligomerization as those incubated in the absence of DTT, suggesting that disulphide bonds do not play a major role (**Supplemental Figure 2B**). In addition, bands corresponding to the size of WT MCT8 homo-dimeric complexes were detected in skin fibroblasts, which endogenously express MCT8 (**Supplemental Figure 2C**).

Importantly, from conventional immunoblots it cannot be concluded whether monomers result from the disruption of multimeric complexes during the experimental procedure. Moreover, it remains unclear whether the MCT8 dimers and oligomers as detected on conventional immunoblots, are formed in a cellular context, or during sample preparation due to random protein aggregation. To address these questions, we performed anti-Flag co-IP experiments on lysates of COS-1 cells co-expressing WT Flag-MCT8 and Myc-MCT8 or a mixture of lysates derived from COS-1 cells that separately expressed Flag-MCT8 or Myc-MCT8. Myc-MCT8 was co-precipitated when expressed together with Flag-MCT8, but not in mixed lysates from cells separately expressing Myc-MCT8 or Flag-MCT8 (**Figure 1A**). This strongly suggests that a cellular context is indeed required for the formation of monomer-monomer interactions. Interestingly, upon co-expression of both constructs, the Myc-MCT8 protein is predominantly present as a monomer in the IP sample, indicating that Flag-MCT8/Myc-MCT8 complexes are, at least partially, disrupted after pre-incubation in the presence of LDS sample buffer. Importantly, upon co-expression of Flag-MCT8 and MCT10, another T3 transporter with 49% amino acid sequence identity with MCT8, MCT10 was not detected in the IP fraction (**Supplemental Figure 3**). This illustrates the specificity of the MCT8 monomer-monomer interactions. To further validate that MCT8 monomer-monomer interactions may be mediated by non-covalent interactions, we next separated lysates of COS-1 cells transfected with MCT8 expression construct under native conditions. In the absence of LDS in the loading buffer, a pronounced band that poorly migrated through the gel was observed, whereas in the presence of LDS in the loading buffer, multiple bands were visible (**Figure 1B**). These findings confirm that MCT8 dimers/oligomers can be disrupted with LDS.

In order to identify the domains within MCT8 that are involved in oligomerization, we performed an extensive domain screen by introducing the following premature stop mutations in WT MCT8: R245X, Q335X, S448X and Q520X (AHDS patient mutations), and E206X, C231X, F256X, C546X (artificial mutations) (**Figure 2A**). These constructs are referred to as: $MCT8_{75\text{-}244}$, $MCT8_{75\text{-}334}$, $MCT8_{75\text{-}447}$, $MCT8_{75\text{-}519}$, $MCT8_{75\text{-}205}$, $MCT8_{75\text{-}230}$, $MCT8_{75\text{-}255}$, $MCT8_{75\text{-}545}$, respectively. Upon expression in COS-1 cells, all C-terminal-truncated mutants showed a complete loss of MCT8-mediated TH uptake (**Figure 2B**). Similar results were found in JEG-3 cells (data not shown). None of the truncated constructs were expressed at the cell membrane as assessed by confocal microscopy in transiently transfected JEG-3 cells (**Figure 2C**). As expected, the monomers of all premature stop mutants were expressed at a molecular weight below 55 kDa (**Figure 2D**). The $MCT8_{75\text{-}334}$, $MCT8_{75\text{-}447}$, $MCT8_{75\text{-}519}$, and $MCT8_{75\text{-}545}$ mutant proteins showed a similar degree of homo-dimerization as WT MCT8 (**Figure 2E**).

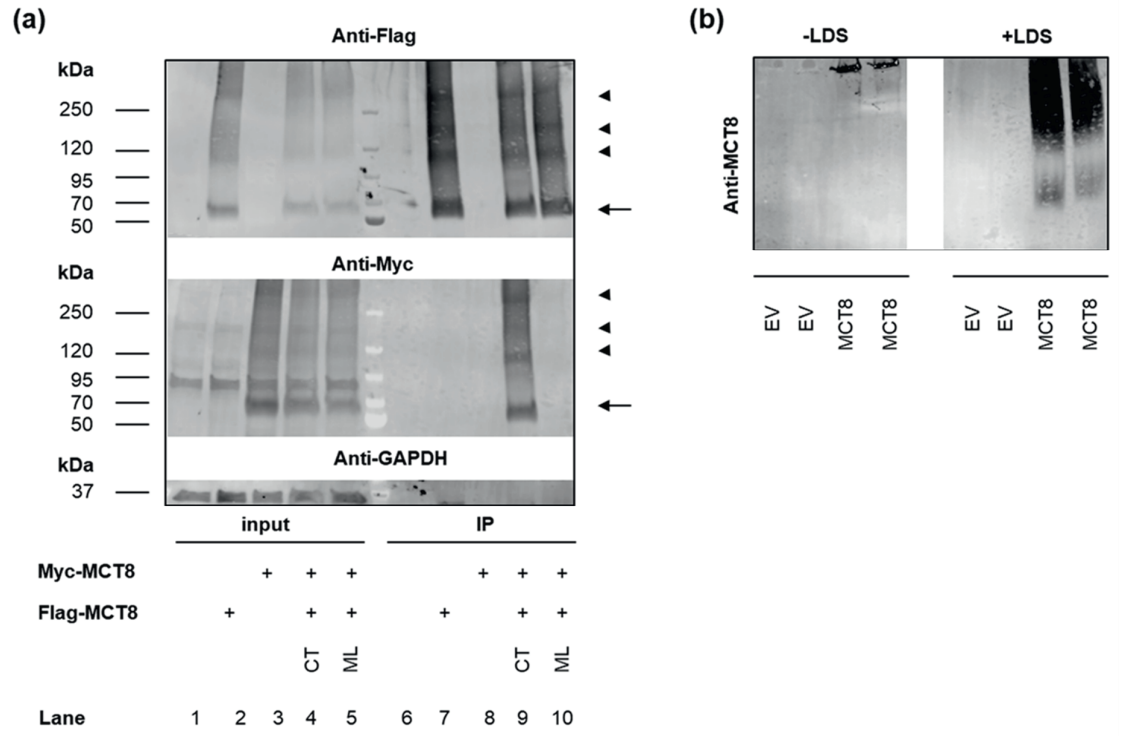

Figure 1 (**A**) Co-immunoprecipitation studies on lysates derived from COS-1 cells transiently expressing Flag-MCT8 (lane 2 and 7), Myc-MCT8 (lane 3 and 8) or both tagged constructs (lane 4 and 9). To exclude that the homo-dimerization results from an assay artefact, sonicated lysates derived from cells separately expressing Flag-MCT8 or Myc-MCT8 were mixed and incubated for 30 minutes on ice, prior to the immuno-precipitation step (lane 5 and 10). COS-1 cells transfected with pcDNA3 empty vector (EV) were taken along as a negative control (lane 1 and 6). The mouse monoclonal M2 Flag antibody was used for Flag-MCT8 detection, rabbit monoclonal anti-Myc for Myc-MCT8 detection. GAPDH was used to demonstrate the absence of nonspecific proteins in the IP sample. Note that Myc-MCT8 was only detected in the IP sample when co-expressed with Flag-MCT8 (lane 9). MCT8 monomer is indicated with an arrow and MCT8 dimer and oligomers with an arrow-head. (**B**) Native PAGE on lysates of COS-1 cells transiently transfected with pcDNA3 empty vector (EV) or WT MCT8. Twenty-five µg of total lysate was either incubated in presence of LDS-containing NuPAGE sample loading buffer at 70°C for 10 minutes (+LDS), or kept at room temperature in native sample loading buffer (final concentrations: 31.25 mM Tris-HCl (pH 6.8), 12.5% glycerol, 0.5% bromophenol blue) in the absence of LDS (-LDS, native conditions) prior to separation under native conditions (1xPAGE buffer). MCT8 detection was performed with the N-terminal MCT8 antibody (3353) and visualized with IRDye680 goat anti-rabbit secondary antibody. Abbreviations: CT, co-transfected; ML, mixed lysates.

Similar to WT MCT8, bands at multiples of the molecular weight of the monomer were observed for these mutants, which provides further evidence for the formation of homo-oligomeric complexes. Together, these findings indicate that the C-terminal half of the protein is not required for the stabilization of monomer-monomer interactions. Although the $MCT8_{75\text{-}230}$, $MCT8_{75\text{-}244}$, and $MCT8_{75\text{-}255}$ mutant proteins were still able to form homo-dimers and homo-oligomers, a relative increase in the monomer fraction was observed (**Figure 2D,E**). This implies on the one hand that TMD3-6 may contribute to the stabilization of monomer-monomer interactions and on the other hand that a sufficient part of both interaction sites in each monomer is still preserved in the $MCT8_{75\text{-}230}$ mutant protein.

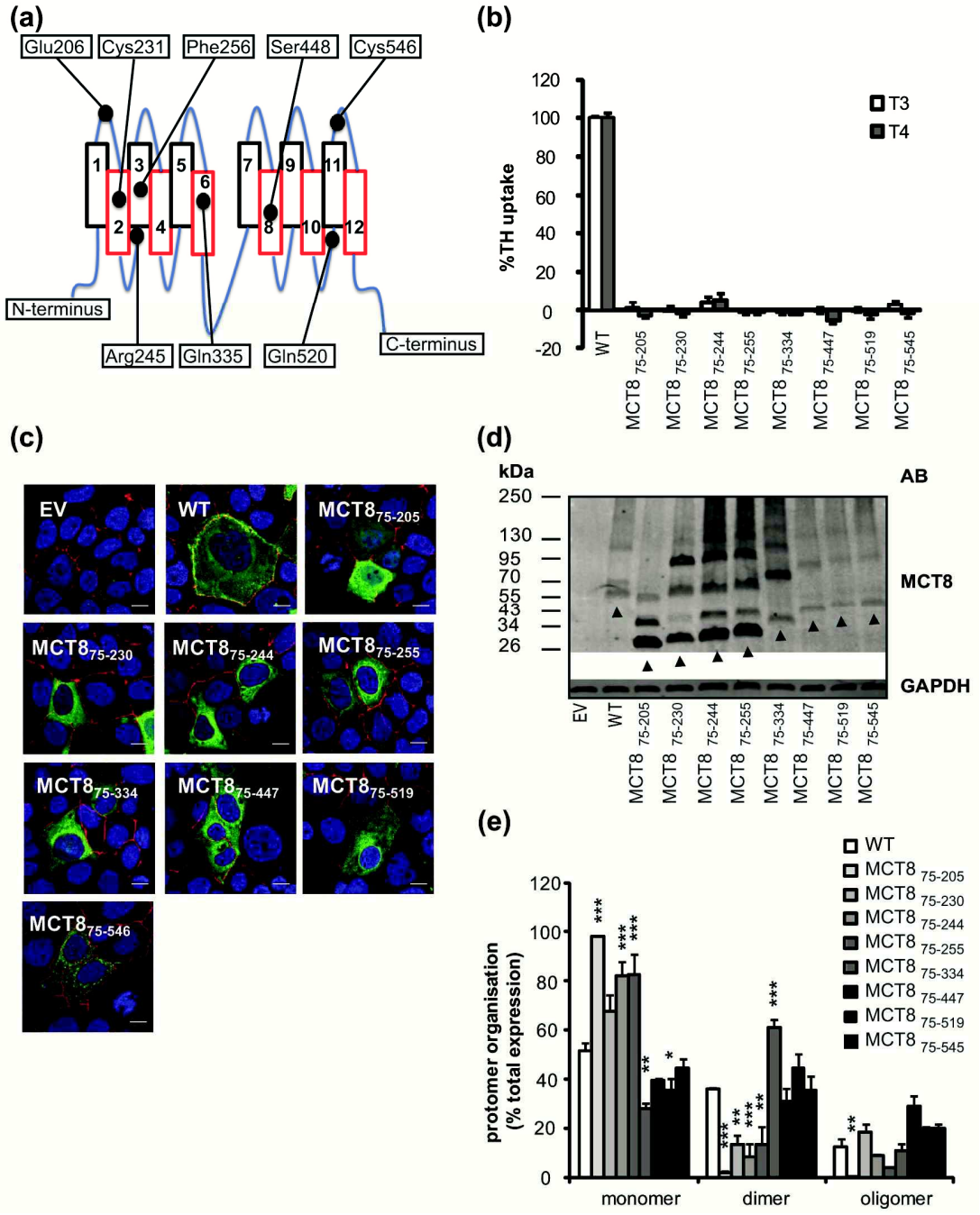

Figure 2 (**A**) Schematic representation of the MCT8 protein structure, in which the locations of the C-terminally truncating mutations are indicated. The E206X, C231X, R245X, F256X, Q335X, S448X, Q520X, and C546X mutant proteins will be further referred to as MCT8$_{75\text{-}205}$, MCT8$_{75\text{-}230}$, MCT8$_{75\text{-}244}$, MCT8$_{75\text{-}255}$, MCT8$_{75\text{-}334}$, MCT8$_{75\text{-}447}$, MCT8$_{75\text{-}519}$, MCT8$_{75\text{-}545}$, respectively. (**B**) Uptake of T3 (white bars) and T4 (grey bars) in COS-1 cells transiently transfected with WT MCT8 or the indicated mutant (500 ng) in the presence of CRYM (250 ng) in 30 minutes at 37°C. Uptake values are corrected for background TH uptake levels observed in COS-1 cells transfected with pcDNA3 empty vector. Results are presented as means ± SEM (n=3). Statistical significance was tested using 1-way ANOVA followed by Dunnett's multiple-comparison test. TH uptake levels for all mutants were significantly lower than WT (P<0.001). (**C**) Subcellular localization of WT and mutant MCT8 in transiently transfected JEG-3 cells assessed by confocal microscopy. Depicted is the merged image of the nuclear staining with DAPI (blue),

MCT8 staining with goat-anti-rabbit Alexa488 (green) and ZO-1 staining as a cell membrane marker using goat-anti-mouse Alexa633 (red). None of the mutants was expressed at the cell membrane. All images were generated using ImageJ software. The scale bar represents 4 µm. (**D**) Representative immunoblot of lysates from COS-1 cells transfected with WT or mutant MCT8 (N=3). MCT8 detection was performed with the N-terminal MCT8 antibody (3353) and visualized with IRDye680 goat anti-rabbit secondary antibody. Glyceraldehyde-3-phosphate dehydrogenase (GAPDH) was used as loading control. Monomers of WT and mutant MCT8 are indicated with arrow heads. (**E**) Quantification of the band intensities for monomer, homo-dimeric and oligomeric WT or mutant MCT8 as shown in (**D**) by densitometry using ImageJ. The order of the various mutant constructs as listed in the in-figure legend correspondent to the order of the bars. Results are presented as means ± SEM (n=3). Statistical differences were assessed using a 2-way ANOVA analysis followed by Dunnett's post-hoc tests; * P<0.05; ** P<0.01; *** P<0.001.

Further truncation of the protein completely abrogates homo-oligomerization and severely reduces the stability of homo-dimeric complexes, as is illustrated by the $MCT8_{75-205}$ mutant (**Figure 2D** and **2E**). We therefore postulate that the Glu206-Cys231 region (covering part of ECL1 and TMD2) constitutes at least a part of one interaction site, whereas the intracellular N-terminus and/or TMD1 comprise (part of) the second interaction site.

To further explore the role of the intracellular N-terminus in MCT8 oligomerization, a construct lacking all TMDs was generated. Unfortunately, this construct could not be detected at protein level (data not shown). Previous attempts to remove the entire intracellular N-terminal domain (ΔPest) also had detrimental effects on protein expression levels (7). Therefore, we substituted the intracellular N-terminus of MCT8 by the intracellular N-terminus of MCT1, resulting in an MCT1/8 chimera. As far as we know, the short intracellular N-terminus of MCT1 (9 amino acids long) is not involved in monomer-monomer interactions or interactions with other proteins (26-28). In addition, N-terminally truncated MCT8 constructs were generated through inactivation of the original translational start site (M75A) and subsequent introduction of two downstream alternative start sites (Q97M ($MCT8_{97-613}$) and R147M ($MCT8_{147-613}$) ; **Figure 3A**). Upon transient transfection in COS-1 cells, $MCT8_{97-613}$ showed near-normal TH uptake, while TH transport by $MCT8_{147-613}$ amounted to 55% of WT (**Figure 3B**). The MCT1/8 chimera did not induce TH uptake over background. Similar results were obtained in JEG-3 cells (data not shown).

$MCT8_{97-613}$ and $MCT8_{147-613}$ were still expressed at the cell membrane, whereas the MCT1/8 chimera showed a predominant intracellular distribution in JEG-3 cells (**Figure 3C**). Using anti-serum against the C-terminus of MCT8, $MCT8_{97-613}$ and $MCT8_{147-613}$ showed similar expression levels as WT upon transient expression in COS-1 (**Figure 3D**) and JEG-3 cells (data not shown), whereas the expression level of the MCT1/8 chimera was much lower in both cell lines. Nevertheless, all constructs were detected as monomer and homodimer and low levels of homo-oligomers were detected for WT MCT8, $MCT8_{147-613}$, and the MCT1/8 chimera (**Figure 3D**). These findings indicate that the intracellular N-terminus is not strictly required for oligomer formation, although a stabilizing role cannot be excluded.

Interestingly, the M75A construct showed 20% residual TH uptake (**Figure 3B**). Several bands were detected for the M75A mutant with the C-terminal anti-serum (**Figure 3D**), but not using the N-terminal MCT8 antibody (**Supplemental Figure 4**). This suggests the presence of in-frame alternative start-sites (AUG or non-AUG) downstream of residue 155, the end of the recognition sequence of the N-terminal MCT8 antibody. However, upon re-introduction of an optimal start site in case of the $MCT8_{97-613}$ or $MCT8_{147-613}$ constructs, these bands completely disappeared.

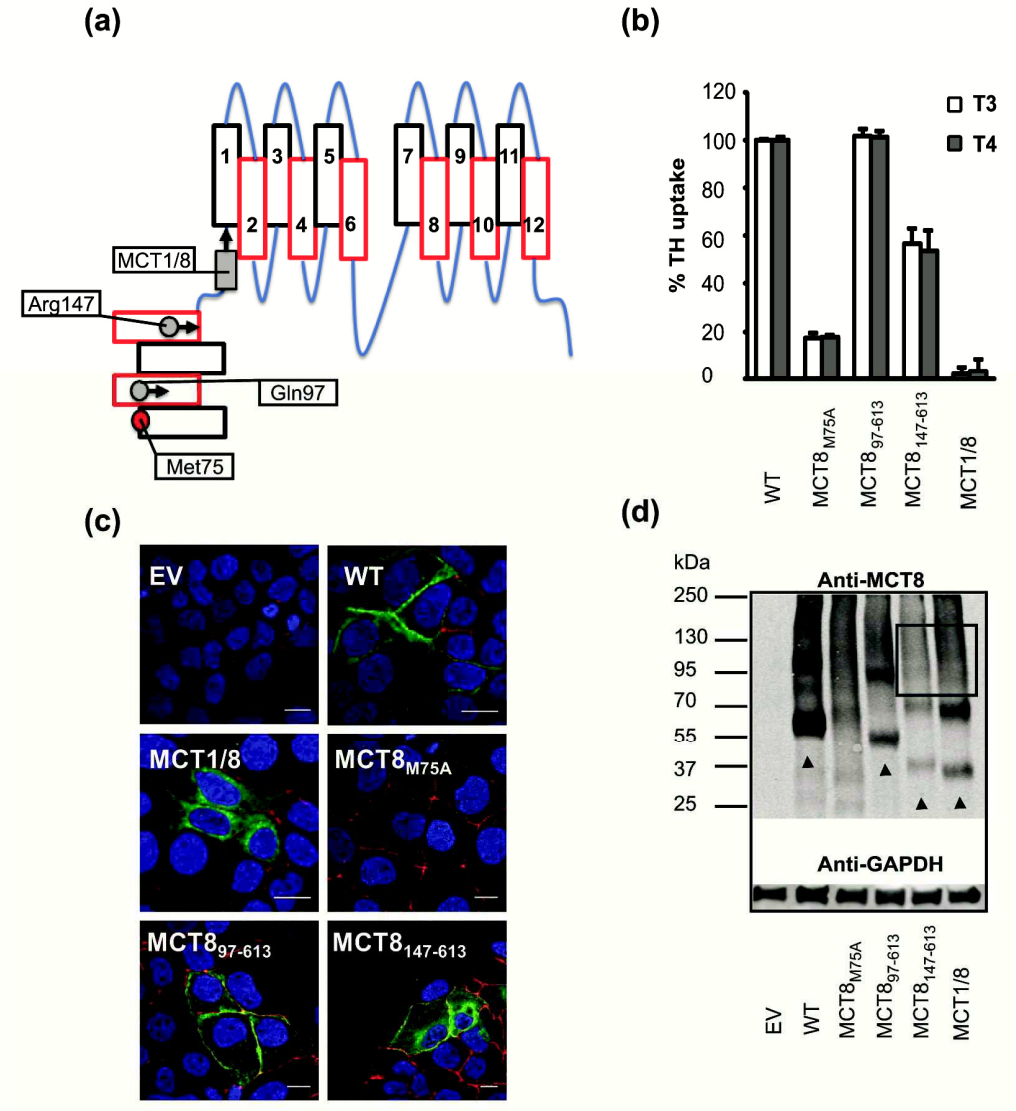

Figure 3 (**A**) Schematic representation of the MCT8 protein structure, in which the locations of the N-terminally truncating mutations are indicated. The inactivated original start (Met75) is indicated with a red circle and the introduced translation start sites with grey circles. The grey square represents the short intracellular N-terminus of MCT1 that directly precedes TMD1 in the MCT1/8 chimera. (**B**) T3 (white) and T4 (grey) uptake in COS-1 cells transiently transfected with 500 ng WT or mutant MCT8 and 250 ng CRYM in 30 minutes at 37 C. Uptake values are corrected for background TH uptake levels observed in COS-1 cells transfected with pcDNA3 empty vector. Results are presented as means ± SEM (n=3). Statistical significance was tested using 1-way ANOVA followed by Dunnett's multiple-comparison test. * P<0.05; ** P<0.01; *** P<0.001. (**C**) Subcellular localization of WT and mutant MCT8 in transiently transfected JEG-3 cells assessed by confocal microscopy depicted as described in **Figure 2C**. (**D**) Representative immunoblot of lysates from COS-1 cells transfected with WT or indicated mutant MCT8 (n=3). MCT8 detection was performed with the rabbit anti-MCT8 antiserum (1306, directed against the C-terminus of MCT8) and visualized with IRDye680 goat anti-rabbit secondary antibody. GAPDH was used as loading control. Monomers of WT and mutant MCT8 are indicated with arrow heads. The black box indicates the bands representing oligomers of $MCT8_{147-613}$ and MCT1/8 chimera.

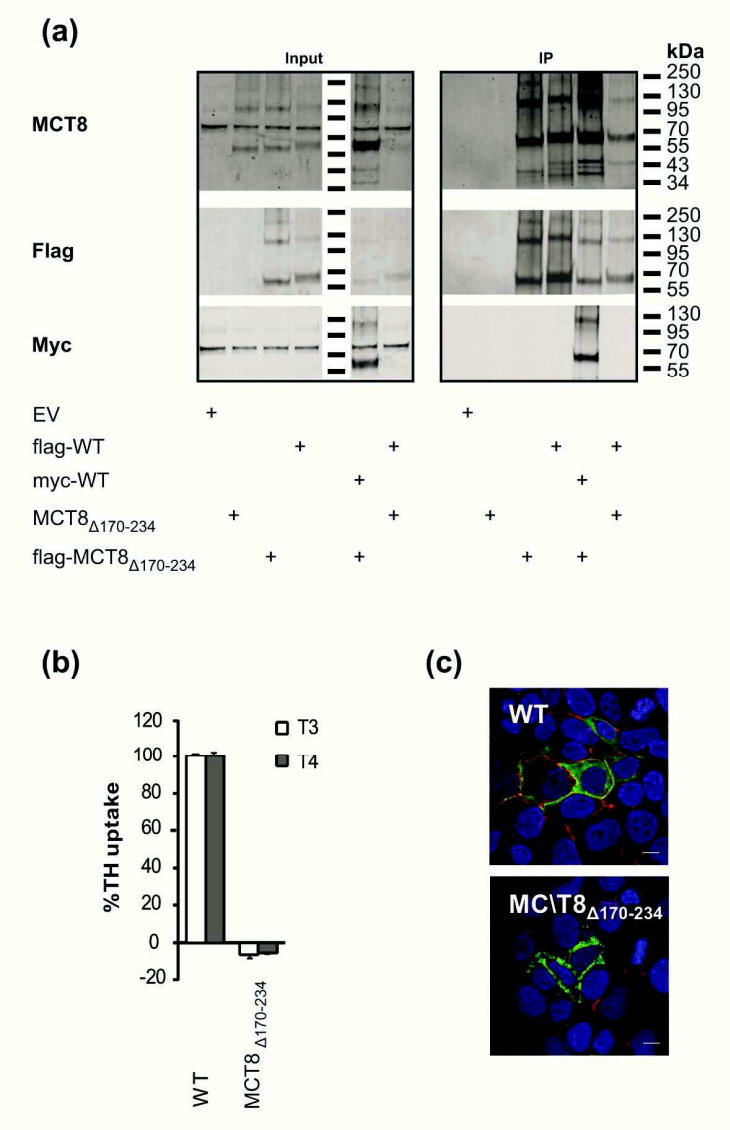

Figure 4 (**A**) Co-immunoprecipitation studies in COS-1 cells (co-)expressing WT MCT8 or MCT8$_{\Delta 170\text{-}234}$ mutant constructs containing indicated tags (representative blot of 2 repetitive experiments). Membranes have been stained with the mouse monoclonal M2 anti-Flag antibody and rabbit monoclonal anti-Myc, stripped, and subsequently stained with rabbit anti-MCT8 3353 antibody. Upon co-expression of flag-MCT8Δ170-234 and myc-MCT8WT, myc-MCT8WT was detected in the precipitated fraction after flag-based coIPs, indicating that flag-MCT8Δ170-234 and myc-MCT8WT form hetero-dimers. (**B**) T3 (white) and T4 (grey) uptake in COS-1 cells transiently transfected with 500 ng WT MCT8 or the MCT8$_{\Delta 170\text{-}234}$ mutant and 250 ng CRYM in 30 minutes at 37°C. Uptake values are corrected for background TH uptake levels observed in COS-1 cells transfected with pcDNA3 empty vector. Results are presented as means ± SEM (n=3). Statistical significance was tested using 1-way ANOVA followed by Dunnett's multiple-comparison test and revealed that both T3 and T4 uptake were significantly reduced in the MCT8Δ170-234 mutant (P <0.001). (**C**) Subcellular localization of WT and mutant MCT8 in transiently transfected JEG-3 cells assessed by confocal microscopy, depicted as described in Fig. 2C.

Taken together, these results suggest that both monomer-monomer interaction sites are located within the N-terminal half of the protein. Since the MCT8$_{75\text{-}230}$ mutant protein retained oligomerization potency and the intracellular N-terminus is not essential for oligomer formation, we postulate that one

interaction site at least includes TMD1 (Arg147-Glu206) and, the other site at least part of ECL1 and TMD2 (Glu206-Cys231). In addition, other domains within the N-terminal half of the protein may also be of importance in stabilization of monomer interactions, which is indeed supported by the observation that the MCT8 construct lacking TMD1 and TMD2 ($MCT8_{\Delta 170-234}$) is still able to form homo-dimers, homo-oligomers and hetero-dimeric complexes with WT Flag-MCT8 (**Figure 4A**). As expected, the $MCT8_{\Delta 170-234}$ protein is functionally inactive (**Figure 4B**) and not expressed at the cell membrane (**Figure 4C**).

Next, we aimed to incorporate these in vitro findings into a structural model of the MCT8 dimer, using our recently published MCT8 homology model in outward-open conformation (6). Indeed, TMD1 and TMD2 form part of the external surface of the protein and could thus be involved in the formation of monomer-monomer interactions (**Figure 5A,** and **B**). The N-terminal halves of two MCT8 monomers were juxta-positioned in an orientation that at least allowed the formation of interactions between TMD1 of one monomer and TMD2 of the other (**Figure 5C**). Upon molecular dynamic simulations, extensive contacts were observed between TMD1, 5 and 6 of one monomer, and TMD2 and 4 of the other (**Figure 5C**). In line with our in vitro findings, most of the residues involved in these contacts are hydrophobic or charged (**Figure 5D**). Although the predictability of the exact structural orientation of intra- and extracellular loops as well as the C- and N-terminal ends, is generally low in homology models, it is not excluded that also these domains contribute to the formation of monomer-monomer contacts. Importantly, in the current configuration, movement of the C-terminal half of the MCT8 protein is not influenced by MCT8 monomer-monomer interactions. Assuming a rocker switch model for substrate translocation (29), the current structural organization would therefore allow each MCT8 protein to change its conformational status independently of the interacting MCT8 protein(s).

To further confirm this hypothesis, we next aimed to interfere with the formation of MCT8 oligomeric complexes. Given the extensive nature of the interactions between MCT8 monomers, we were unable to generate an MCT8 construct lacking oligomerization potency without directly affecting its function as a TH transporter. Alternatively, we therefore explored to what extent hetero-dimerization between WT and functionally inactive truncated mutant MCT8 proteins could abrogate MCT8 function. For this reason we first studied whether the truncated and full-length MCT8 proteins were able to form hetero-dimers. Co-IP experiments were performed on COS-1 lysates co-expressing WT Flag-MCT8 and either the $MCT8_{75-519}$ (the largest truncated protein encountered in an AHDS patient), $MCT8_{75-205}$ (impaired oligomerization and reduced homo-dimerization), $MCT8_{75-230}$ or $MCT8_{75-244}$ (intact homo-dimerization and oligomerization) mutant proteins. All truncated mutants, including $MCT8_{75-205}$, were only detected in the IP fraction if co-expressed with WT Flag-MCT8, (**Figure 6**). In addition, bands representing the intact hetero-dimers of WT MCT8 and the $MCT8_{75-230}$ and $MCT8_{75-244}$ mutants were detected. These findings support the presence of a common dimerization mechanism and moreover suggest that the formation of interactions between WT and mutant MCT8 proteins already takes place before the trafficking to the cell membrane, since none of the truncated mutants is expressed at the cell membrane if expressed individually (**Figure 2C**).

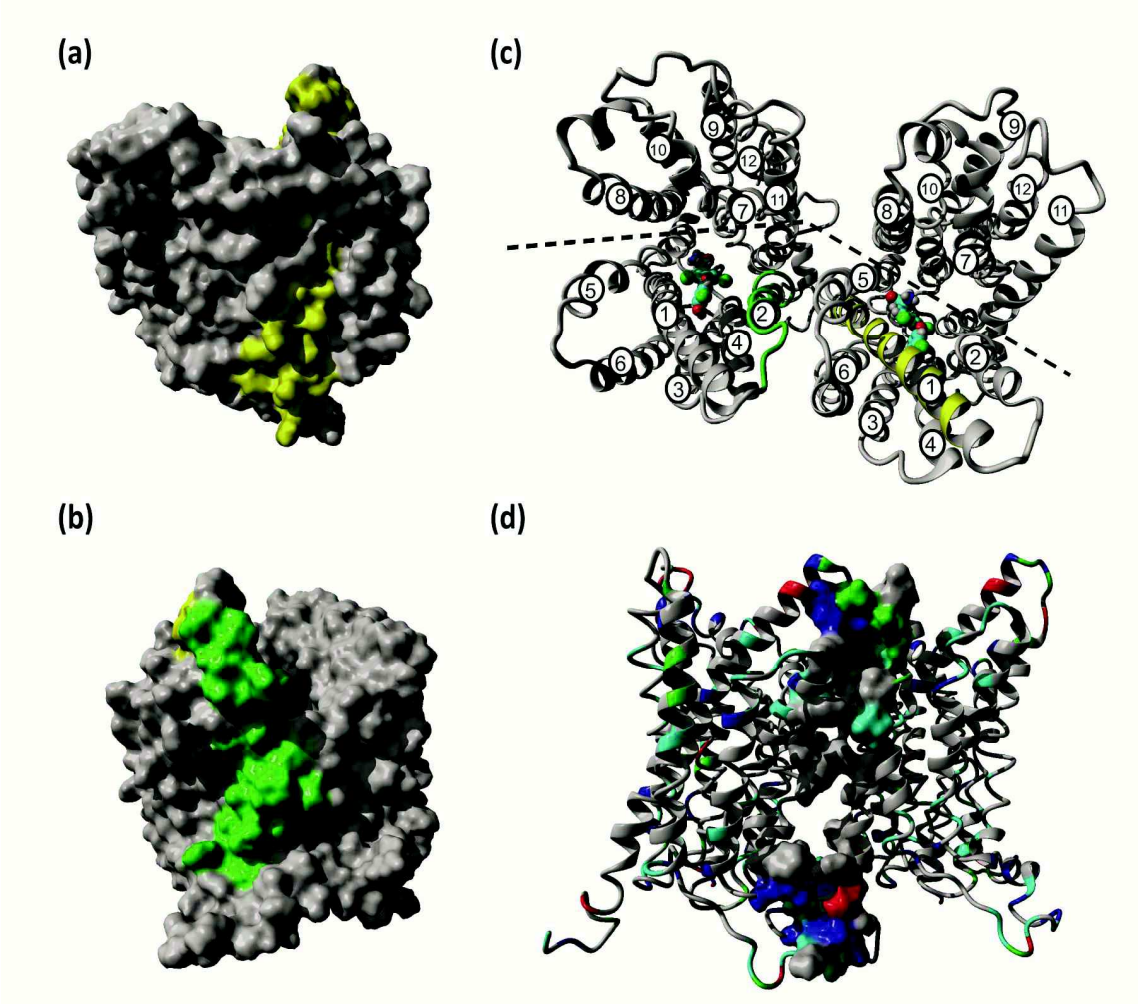

Figure 5 Structural homology model of the MCT8 monomer in which TMD1 (**A**) and TMD2 (**B**) are highlighted in yellow and green respectively. Parts of both TMDs compose the outer surface of the MCT8 protein (**C**) A putative organization of an MCT8 homodimeric complex, allowing the interaction of 2 distinct parts of the N-terminal half of two MCT8 proteins. This structural organization allows the formation of oligomeric complexes in which all monomers are interacting via a similar mechanism. Of note, in this orientation the movement of the C-terminal half of the MCT8 protein is not influenced by MCT8 monomer-monomer interactions. Assuming a rocker switch model for substrate translocation, each monomer can change its conformational status independently of the interacting monomer(s). (**D**) Frontal view of (**C**) in which the molecular surface is shown of the residues located within 5 Ångstrom from the other MCT8 protein, which theoretically allows interactions. Residues are colored according to residue type: in blue, positively charged residues (Arg, Lys, His); in red, negatively charged residues (Asp, Glu); in grey, hydrophobic residues; in light blue, polar residues containing a hydroxyl group (Ser, Thr, Tyr) and Cys residues; and in green, polar residues with an amide group (Asn, Gln). Note that the majority of MCT8 protein-protein interactions have a hydrophobic or electrostatic nature, which is in line with our in vitro experiments. Moreover, it is not excluded that the intracellular loops (ICLs) and extracellular loops (ECLs), including the large ICL3 that links TMD6 and TMD7, contribute to the formation of monomer-monomer interactions.

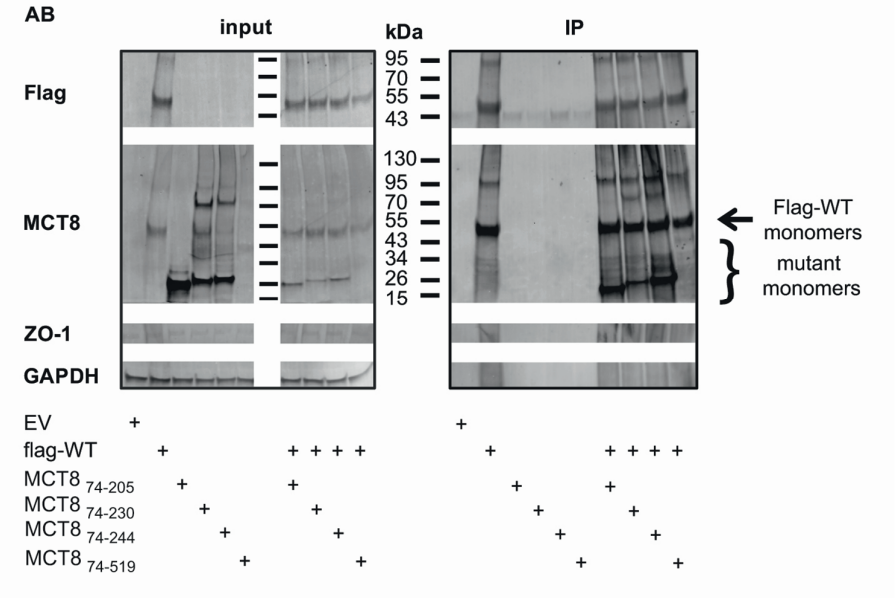

Figure 6 Co-IP studies on lysates derived from COS-1 cells transiently expressing either Flag-MCT8 or indicated mutant MCT8 or a combination of Flag-MCT8 and indicated mutant MCT8 constructs. Input and IP samples were run on separate gels (boxed). Blots were stained with rabbit anti-MCT8 antibody and mouse M2 anti-Flag antibody, stripped and stained for mouse anti-ZO-1 (a membrane marker to exclude impurities in the Co-IP procedure) and mouse anti-GAPDH as loading control. Note the presence of all truncated mutants (bracket) in the IP samples upon co-expression with WT Flag-MCT8 (arrow), indicating the presence of hetero-dimers.

Finally, we studied to what extent increasing concentrations of the $MCT8_{75-230}$ mutant could interfere with WT MCT8 TH transport function by competitive interference with WT MCT8 homo-dimerization/oligomerization. First, we confirmed the absence of the $MCT8_{75-230}$ protein at the plasma membrane in COS-1 cells using surface biotinylation assays (**Supplemental Figure 5**). Next, we performed Flag-tagged mediated co-immunoprecipitation on total lysates of COS-1 cells co-expressing Flag-MCT8 and Myc-MCT8 and increasing amounts of the $MCT8_{75-230}$ mutant. This resulted in a modest reduction of the amount of Myc-MCT8 detected in the IP samples, indicating that $MCT8_{75-230}$ is able to competitively interfere with the formation of WT Flag-MCT8 and Myc-MCT8 interactions (**Figure 7A,** and **B**). Nevertheless, even in presence of the highest concentration of the $MCT8_{75-230}$ mutant, Myc-MCT8 was still detected in the IP fraction, indicating incomplete disruption of the WT homo-dimers/oligomers. Parallel uptake assays showed no reduction in T3 uptake levels under these conditions (**Figure 7C**). These findings suggest that the observed reduction in homo-dimer formation does not result in a decrease in TH transport.

DISCUSSION

The present study provides novel insights into the mechanism of MCT8 oligomerization. Our findings suggest that MCT8 monomer-monomer interactions are formed through extensive non-covalent interactions between the N-terminal halves of MCT8 monomers, which are likely to be formed early in the trafficking process. Given the extensive nature of these interactions, monomer-monomer interactions could not completely be abolished by targeted mutations, including large deletions, preventing detailed studies into the physiological function of homo-dimerization and oligomerization.

Although homo-dimeric and homo-oligomeric organization of MCT8 has been described in many studies, it has long been unknown whether these complexes are formed inside the cell (e.g. (7, 8)). Recent bimolecular fluorescent complementation studies have demonstrated for the first time that at least MCT8 homo-dimers are likely to be formed in a cellular context (9). These findings are further substantiated by our current co-IP data, showing that the formation of MCT8 dimers and oligomers as detected on immunoblots is not an assay artefact but requires a cellular context.

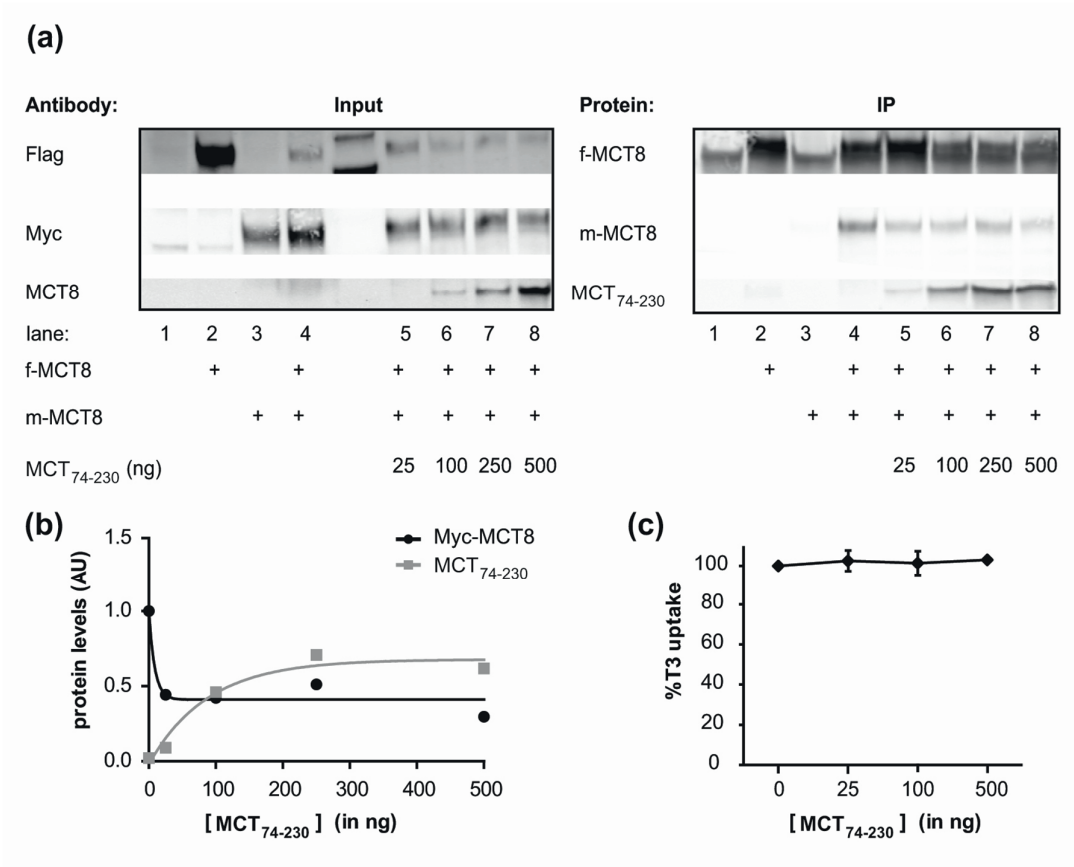

Figure 7 (**A**) Representative blots (N=2) of co-IP studies on lysates derived from COS-1 cells transiently expressing Flag-MCT8 (75 ng cDNA, lane 2), Myc-MCT8 (75 ng cDNA, lane 3) alone, or combined (lane 4), and COS-1 cells co-expressing Flag-MCT8 and Myc-MCT8 and increasing amounts of the $MCT8_{75-230}$ mutant construct (lane 5-8). Blots were subsequently stained with mouse M2 anti-Flag antibody and rabbit anti-Myc antibody, stripped and stained with rabbit anti-MCT8 antibody. Input and IP samples were run on separate gels (boxed). Note that increasing concentrations of $MCT8_{75-230}$ reduced the amount of Myc-MCT8 detected in the IP samples, indicating that $MCT8_{75-230}$ may compete with the formation of WT Flag-MCT8/Myc-MCT8 interactions. Please note the decrease in Flag-MCT8 signal on the input blot with increasing concentrations of $MCT8_{75-230}$ (**B**) Quantification by densitometry (using ImageJ) of the Myc-MCT8 and $MCT8_{75-230}$ protein levels in the IP samples shown in (**A**), expressed relative to the intensity of the Flag-MCT8 band in the same IP sample. (**C**) Parallel T3 uptake studies (30 minutes at 37 C) in COS-1 cells co-expressing equal amounts of WT Flag-MCT8 and Myc-MCT8 as in (**A**), increasing amounts of the $MCT8_{75-230}$ mutant, and a fixed amount of CRYM (250 ng). Results are presented as means ± SEM (n=3). There are no statistically significant differences as analyzed with a 1-way ANOVA followed by Dunnett's multiple-comparison test. Abbreviations: AU, arbitrary units.

In an attempt to elucidate the functional role of MCT8 oligomerization, we first aimed to identify the type of interaction(s) that underlie MCT8 oligomerization and the involved domains. Previous studies excluded that disulfide bonding mediates MCT8 oligomerization, as each Cys residue in MCT8 can be substituted by an Ala without affecting its oligomerization (17). Moreover, MCT8 oligomerization was barely enhanced by the Cys cross-linker HgCl2 (7). Here, we extended on these studies by showing that the addition of increasing concentrations DTT did not affect oligomerization. We also excluded the presence of Ca^{2+} and Mg^{2+} mediated oligomerization. Although previous conventional immunoblot studies suggested that MCT8 monomer-monomer interactions could not be completely abrogated by heat and SDS (7), our current co-IP experiments show that a substantial part of the MCT8 dimers are disrupted using LDS sample buffer, even in the absence of DTT. These findings were further substantiated by native PAGE experiments which showed that the addition of LDS is critical to disrupt the MCT8 complexes. Together, these observations have several important implications. Firstly, MCT8 is likely to be predominantly present as a complex under native conditions. Secondly, disruption of MCT8-MCT8 interactions by LDS suggests that non-covalent interactions (hydrophobic and electrostatic) are involved in MCT8 oligomerization. Finally, at least part of the monomers (and dimers) observed on immunoblots of total lysates are the result of the disruption of MCT8 oligomers during the procedure and thus do not necessarily reflect the amount of monomer inside the cell. It has been previously demonstrated for other proteins that strong hydrophobic interactions can be relatively heat and SDS (and LDS) resistant, which may explain why earlier studies concluded that MCT8 dimerization was SDS-resistant (30).

Our successive C-terminal and N-terminal truncation experiments mapped the monomer-monomer interaction sites to the N-terminal half of the MCT8 protein. This part contains 6 TMDs, typically strongly hydrophobic, flanked by charged residues in the ECLs and ICLs that allow electrostatic interactions. Although we showed that TMD1 and TMD2 are minimally required to form oligomeric complexes, as demonstrated by the $MCT8_{75\text{-}230}$ mutant, specific deletion of these TMDs resulted in a mutant protein that retained its oligomerization capacity. This suggests the presence of extensive monomer-monomer contacts involving other domains beyond TMD1 and 2. This was indeed further illustrated by structural modelling of a putative homo-dimeric conformation of MCT8, which not only suggested the involvement of multiple TMDs, but possibly also loop regions, including the large intracellular loop between TMD6 and 7. Of note, removal of a substantial part of the N-terminal PEST-domain (residues 75-147) resulted in a mutant MCT8 protein with substantial residual TH transport capacity, implying that naturally occurring variations in this region are likely to be well-tolerated.

In light of our current findings, it is not surprising that although the effects of many missense mutations have been studied, none of these mutations have been found to completely abrogate MCT8 protein-protein interactions (8, 9, 17, 21). Nevertheless, a subset of MCT8 missense mutations has been recently described to reduce MCT8 dimerization (S194F, A224T, L434W, and R445C), whereas others were found to enhance dimerization (del230F, V235M, and ins236V) (9). Since the affected residues in the first group are predicted to be located within the substrate pore, the authors speculated that oligomerization was affected through the effects of these mutations on the overall protein structure and thus protein surface. Interestingly, the mutations that were found to enhance MCT8 dimerization all affect TMD2, which may well be consistent with a direct contribution of TMD2 in stabilization of the interaction between MCT8 monomers as is suggested by our current data. However, in the current and previously reported studies we found that even large truncations and domain specific deletions are

not sufficient to completely abrogate MCT8 oligomerization (7). Therefore, we were unable to generate a mutant MCT8 protein that completely lacks homo-dimerization and oligomerization capacity, while retaining residual transport function. As an alternative, we explored whether co-expression of the truncated and functionally inactive $MCT8_{75-230}$ mutant interferes with WT MCT8 oligomerization. Although this approach resulted in an apparent reduction of interactions between WT MCT8 proteins, they were not completely abrogated. Moreover, no alterations in MCT8-mediated T3 uptake were observed under these conditions. This could mean that, at least in an overexpression system, a substantial alteration in the monomer:oligomer ratio has very little impact on MCT8 function. However, it is not excluded that the $MCT8_{75-230}$ mutant is mainly competing with WT homo-oligomerization inside the cell and not at the cell membrane given its impaired plasma membrane trafficking, which would result in the exclusive presence of the fully functional WT oligomers at the plasma membrane. The question if MCT8 oligomerization is required to achieve (optimal) transporter function thus remains unaddressed. It should however be noted that from a structural perspective, an MCT8 monomer should at least be sufficient to form a transporter channel and function as a transporter (e.g. (5)).

Although the effects of truncating mutations on the structure of the remaining MCT8 protein are generally unpredictable, we observed that all truncated proteins were still able to form heterodimers with WT MCT8. This finding at least suggests that the interacting domains in the resulting mutants are still being recognized by the WT protein, which may indicate at least some degree of structural preservation. Since none of the C-terminally truncated proteins reach the plasma membrane if expressed individually (**Figure 2C**), the presence of WT-mutant interactions, as assessed by co-IP, may suggest that the formation of MCT8 oligomers is likely to be an early event in the maturation and trafficking of the MCT8 protein. These observations further support recent studies of Fischer et al, showing the presence of MCT8 homo-dimerization in ER-like structures (9).

Given the important role of MCT8 in the blood-brain-barrier and neuronal cells (31), it would have been of interest to study MCT8 oligomerization in vascular endothelial or neuronal cell lines, as the presence of cell-type specific factors may importantly influence the type and extent of MCT8 protein-protein interactions. However, such experiments were limited by the poor transfection efficacy of these cell lines (data not shown). Nevertheless, we speculate that the domains involved in homo-oligomerization are not likely to differ between cell lines, since this is largely determined by the intrinsic properties of the MCT8 protein.

Taken together, our data show that MCT8 oligomerization is mediated through extensive non-covalent interactions involving TMDs and putative loops within the N-terminal half of the protein. Given the extensive nature of these interactions, we speculate that most mutations encountered in AHDS patients will only have minor effects on the oligomeric organization of MCT8. This is important to the field, since the property to form dimeric/oligomeric complexes has been specifically studied in many reports on the impact of mutations identified in patient with MCT8 deficiency.

Acknowledgements

We would like to dedicate this manuscript to the memory of Theo Visser, who suddenly passed away during finalization of this manuscript. He was deeply involved in the design of these studies and interpretation of the results.

We thank Ramona E. van Heerebeek and Selmar Leeuwenburgh for their technical assistance and the Optical Imaging Center (Erasmus MC Rotterdam) for the technical support regarding the confocal imaging studies.

Disclosure Summary: The authors have nothing to declare.

SUPPLEMENTAL MATERIALS

Supplemental Tables

Supplemental Table 1 Antibody Table

Target protein/ antigen	Antigen Sequence (if known)	Name of Antibody	Species Raised (polyclonal or monoclonal)	Manufacturer (and catalog number)	Dilution used for WB	Dilution used for ICH	RRID
hMCT8	AA 52-155 N-terminus	MCT8 (3353)	Rabbit (p)	ATLAS (HPA003353)	1:20000	1:1000	AB_1079343
hMCT8	AA 527–539 C-terminus	MCT8 (1306)	Rabbit (p)	Personal AB (19)	1:1000	1:500	AB_2661880
hMCT10	AA 473–487 and 503–515	MCT10 (1758)	Rabbit (p)	Personal AB (19)	1:1000		AB_2661879
GAPDH		GAPDH	Mouse (m)	Millipore (Mab 374)	1:20000		AB_2107445
ZO1		ZO1	Mouse (m)	Thermo Fisher (33-9100)	1:1000	1:1000	AB_2533147
Flag	Flag epitope	Flag-M2	Mouse (m)	Sigma (C3956)	1:1000		AB_439680
Myc	Myc epitope	Myc	Rabbit (m)	Sigma (F1804)	1:1000		AB_262044
Mouse IgG		IRDye680	Goat	LI-COR (926-68020)	1:20000		AB_10706161
Rabbit IgG		IRDye800	Goat	LI-COR (926-32211)	1:20000		AB_621843
Rabbit IgG		Alexa 488	Goat	Thermo Fisher (A11008)		1:1000	AB_143165
Mouse IgG		Alexa 633	Goat	Thermo Fisher (A21050)		1:1000	AB_2535718

GAPDH: glyceraldehyde-3-phosphate dehydrogenase; ZO-1: zona occludens 1; P: polyclonal antibody; M: monoclonal anitbody; WB: Western Blot; ICH: immunohistochemistry; AB, antibody.

Supplemental Table 2 Overview of primers

Name	sequence from 5' to 3'
E206X_Fw	CTCCATGCTGCTAGAGGAG**TAA**AAGGAAAAAAATCGC
E206X_Rev	GCGATTTTTTTCCTTTTACTCCTCTAGCAGCATGGAG
C231X_Fw	GATGGGTATGATCTTCTTC**TGA**TCTCCCATTGTGAGTATATTC
C231X_Rev	GAATATACTCACAATGGGAGATCAGAAGAAGATCATACCCATC
R245X_Fw	GACCGTTTGGGCTGC**TGA**ATCACAGCAACCG
R245X_Rev	CGGTTGCTGTGATTCAGCAGCCCAAACGGTC
F256X_Fw	GGGCTGCCGTTGCT**TAA**ATTGGCCTCCATACCAG
F256X_Rev	CTGGTATGGAGGCCAATTTAAGCAACGGCAGCCC
Q335X_Fw	ATAAGATCAAGCTGGCC**TAA**ACCTTCCAGGTGCTG
Q335X_Rev	CAGCACCTGGAAGGTTTAGGCCAGCTTGATCTTAT
S448X_Fw	GGCCTTGGGCGTCTTGTG**TAA**GGCCACATC
S448X_Rev	GATGTGGCCTTACACAAGACGCCCAAGGCC
Q520X_Fw	GGGCCCAATGCAGGCCTCA**TAG**GCCATTGG
Q520X_Rev	CCAATGGCCTATGAGGCCTGCATTGGGCCC
C546X_Fw	GCCTACTCCGCAAC**TGA**TTTGGGGACTACCATG
C546X_Rev	CATGGTAGTCCCCAAATCAGTTGCGGAGTAGGC
M74A_Fw	CAGTCCCCCCGCCGCG**GCTT**CGCTGCAAAGCCAGGC
M74A_Rev	GCCTGGCTTTGCAGCGAAGCCGCGGCGGGGGGACTG
Q97M_Fw	CTGGCAGGAGGCAGACCAGGAA**GCGATGGCG**CCGGTGGGTAG
Q97M_Rev	CTACCCACCGGCGCCATCGCTTCCTGGTCTGCCTCCTGCCAG
R147M_Fw	GAGTTCGAGTCCGAG**ATGGCG**CACGAACCCGAGCC
R147M_Rev	GGCTCGGGTTCGTGCGCCATCTCGGACTCGAACTC
MCT8 Eco NI_Fw	GGGTATGATCTTCTTCTGTTCTCCTATCGTAGGTATATTCACTGACCGTTTGGGCT
MCT8 Eco NI_Rev	AGCCCAAACGGTCAGTGAATATACCTACGATAGGAGAACAGAAGAAGATCATACCC
MCT1_Fw	CGTATTAAGCTTACTGGTCGGTCCTGTAGGTG
MCT1_Rev	GTATAAGCTAGCGGTGTATCCCACTGGCC
MCT8_Fw	CATATTGCTAGCCCTCCCGAAGGTGGCTTC
MCT8_Rev	GCTCCGACCCATGCTGCTTGG
Flag_MCT8_Fw	GATAAGCTTCAGAAATGGACTACAAAGACGATGACGACAAGGCGCTGCAAAGCCAGG
Flag_MCT8_Rev	ATCTCTAGATTAGATTGGTTCCTCAGGGTTGGG
Myc_MCT8_Fw	GATAAGCTTCAGAAATGGAACAAAAACTCATCTCAGAAGAGGATCTGGCGCTGCAAAGCCAGG
Myc_MCT8_Rev	ATCTCTAGATTAGATTGGTTCCTCAGGGTTGGG

Restriction sites within the primers are underlined; the locations of introduced mutations are depicted in bold.

Supplemental figures

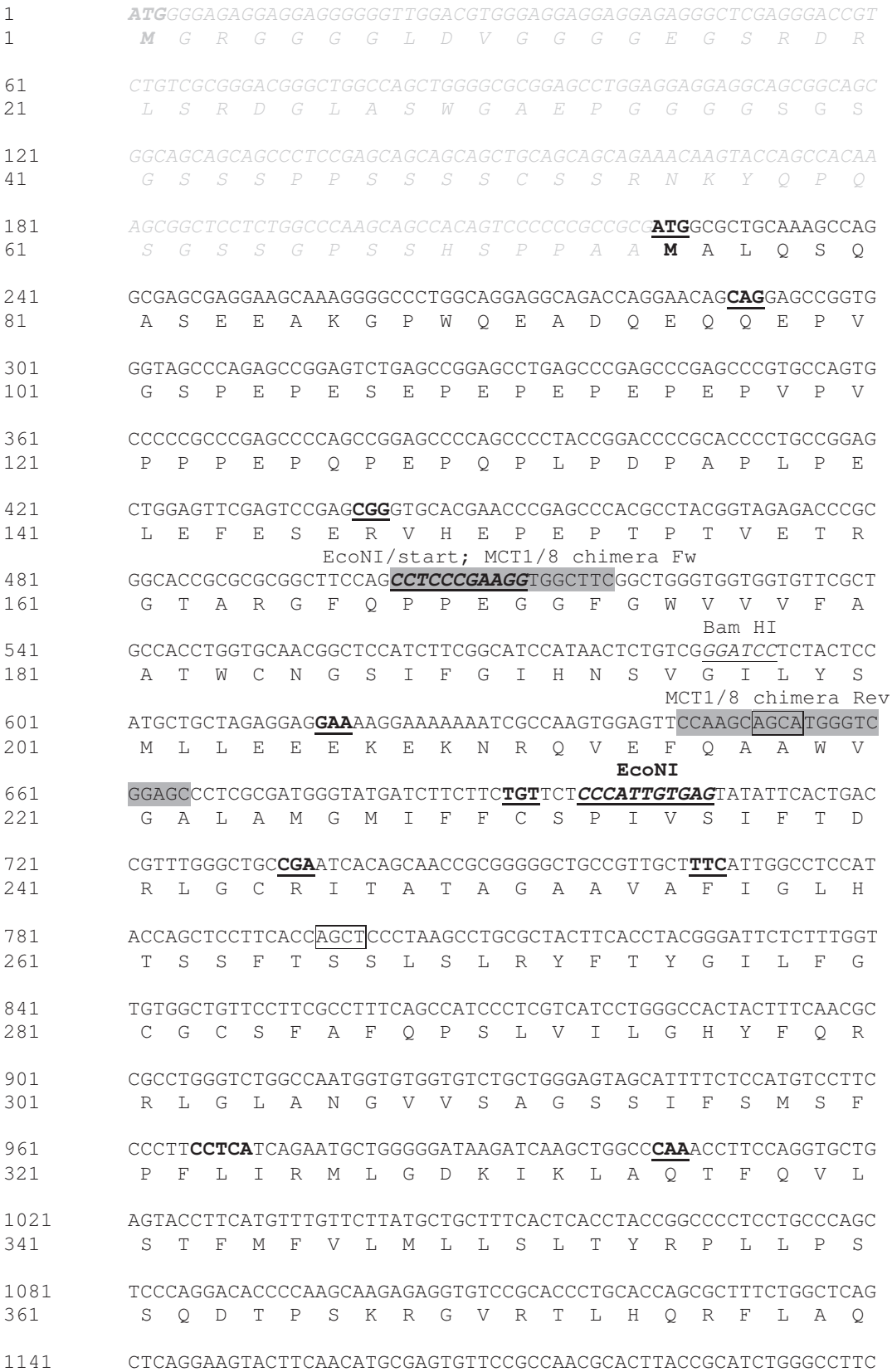

```
381          L  R  K  Y  F  N  M  R  V  F  R  Q  R  T  Y  R  I  W  A  F
1201      GGAATTGCTGCTGCTGCCCTTGGCTACTTTGTTCCCTATGTACACCTGATGAAGTATGTG
401          G  I  A  A  A  A  L  G  Y  F  V  P  Y  V  H  L  M  K  Y  V

1261      GAGGAGGAGTTCTCAGAAATCAAGGAGACCTGGGTGCTCTTGGTGTGTATTGGGGCTACC
421          E  E  E  F  S  E  I  K  E  T  W  V  L  L  V  C  I  G  A  T

1321      TCAGGCCTTGGGCGTCTTGTGTCAGGCCACATCAGTGACTCCATCCCTGGACTTAAGAAG
441          S  G  L  G  R  L  V  S  G  H  I  S  D  S  I  P  G  L  K  K

1381      ATCTACTTGCAGGTCCTTTCCTTCCTGCTCCTGGGCCTGATGTCCATGATGATTCCCCTG
461          I  Y  L  Q  V  L  S  F  L  L  L  G  L  M  S  M  M  I  P  L

1441      TGCCGGGACTTCGGGGGCCTTATCGTCGTCTGTCTTTTCCTGGGCCTTTGCGATGGCTTC
481          C  R  D  F  G  G  L  I  V  V  C  L  F  L  G  L  C  D  G  F

1501      TTCATCACCATCATGGCCCCCATTGCATTTGAGCTGGTGGGCCCAATGCAGGCCTCACAG
501          F  I  T  I  M  A  P  I  A  F  E  L  V  G  P  M  Q  A  S  Q

1561      GCCATTGGCTACCTCCTGGGCATGATGGCCCTGCCAATGATTGCTGGGCCCCCCATTGCA
521          A  I  G  Y  L  L  G  M  M  A  L  P  M  I  A  G  P  P  I  A

1621      GGCCTACTCCGCAACTGTTTGGGGACTACCATGTGGCCTTCTACTTTGCCGGTGTGCCC
541          G  L  L  R  N  C  F  G  D  Y  H  V  A  F  Y  F  A  G  V  P

1681      CCCATCATCGGGGCTGTAATCCTCTTCTTCGTCCCTCTGATGCATCAAAGGATGTTCAAG
561          P  I  I  G  A  V  I  L  F  F  V  P  L  M  H  Q  R  M  F  K

1741      AAAGAGCAGAGAGATTCCAGCAAGGATAAGATGTTGGCCCCTGACCCAGACCCCAATGGG
581          K  E  Q  R  D  S  S  K  D  K  M  L  A  P  D  P  D  P  N  G

1801      GAGCTACTGCCGGGCTCCCCCAACCCTGAGGAACCAATCTAA
601          E  L  L  P  G  S  P  N  P  E  E  P  I  *
```

Supplemental Figure 1 cDNA sequence of coding region of the hMCT8 construct that was used for the generation of all described mutant and tagged MCT8 constructs. This construct only contains the coding sequence of the short MCT8 isoform starting at Met75. The sequence encoding the unique part of the long MCT8 isoform is depicted in *light grey* and is shown to clarify the amino acid numbering. Locations of the introduced mutations are in bold, underlined. The Bam HI and Eco NI restriction sites are indicated and displayed in italic and underlined font, the locations of the forward and reverse primer used in the generation of the MCT1/8 chimera are highlighted in grey and the splice sites are boxed.

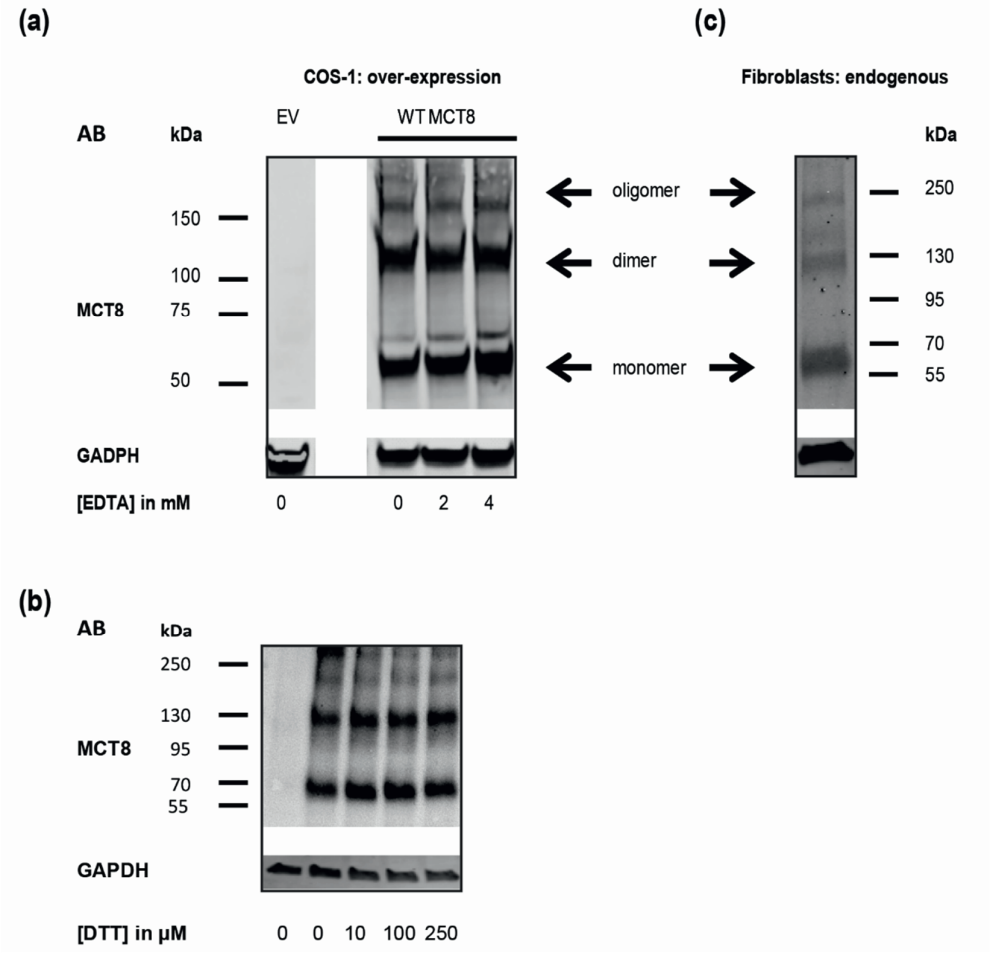

Supplemental Figure 2 (A) Immunoblot of total cell lysates derived from COS-1 cells transiently expressing WT MCT8 incubated with increasing concentrations of the Ca^{2+} / Mg^{2+} chelator EDTA for 30 minutes before the addition of LDS loading buffer, containing 10 mM DTT. Note that MCT8 is expressed as monomer (~55 kDa), homo-dimer (~110 kDa) and homo-oligomer (~170 kDa). Increasing concentrations of EDTA did not affect MCT8 oligomerization. MCT8 was detected using the N-terminal MCT8 antibody (3353) and GAPDH was used as a loading control. **(B)** Immunoblot on total lysates of COS-1 cells transiently expressing WT MCT8 incubated with increasing concentrations DTT in LDS for 10 minutes at 70°C prior to separation. Increasing concentrations of DTT did not affect MCT8 oligomerization. MCT8 was detected using the N-terminal MCT8 antibody (3353) and GAPDH was used as a loading control. **(C)** Immublot on total lysates derived from skin fibroblasts obtained from a healthy subject, using the N-terminal MCT8 antibody (3353) and GAPDH as a loading control. Note that endogenously expressed MCT8 is also detected as a monomer, homo-dimer and putative homo-oligomer. Abbreviations: EDTA, Ethylenediaminetetraacetic acid; EV, empty vector.

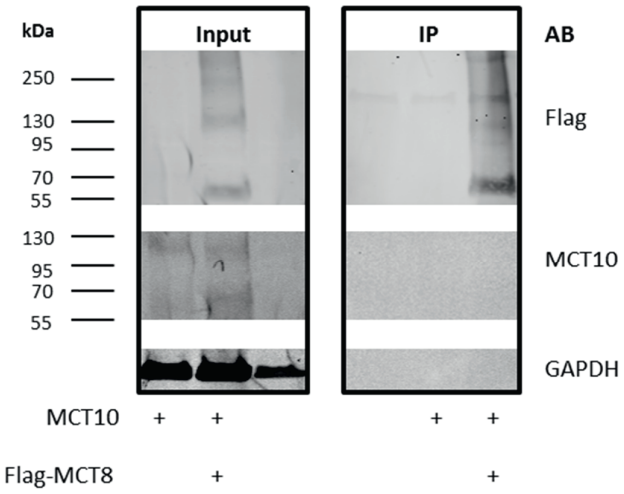

Supplemental Figure 3 Representative blots (N=3) of co-IP studies on lysates derived from COS-1 cells transiently expressing MCT10 alone (lane 2), or in combination with Flag-MCT8 (lane3). Blots were simultaneously stained with mouse M2 anti-Flag and rabbit anti-MCT10 antiserum (designated 1758). MCT10 could not be enriched by Flag-MCT8 mediated IPs. Abbreviations: AB, antibody; IP, immunoprecipitation.

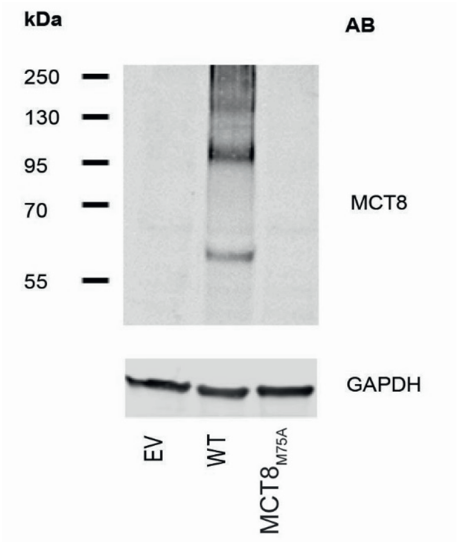

Supplemental Figure 4 Representative immunoblot of lysates from COS-1 cells transfected with WT MCT8 or the $MCT8_{M75A}$ mutant (N=2), performed as described in Fig. 2D. Note, that no signal was obtained upon inactivation of the natural translation start site (Met75) using antibodies directed against the N-terminus of MCT8. Abbreviations: AB, antibody; EV, empty vector.

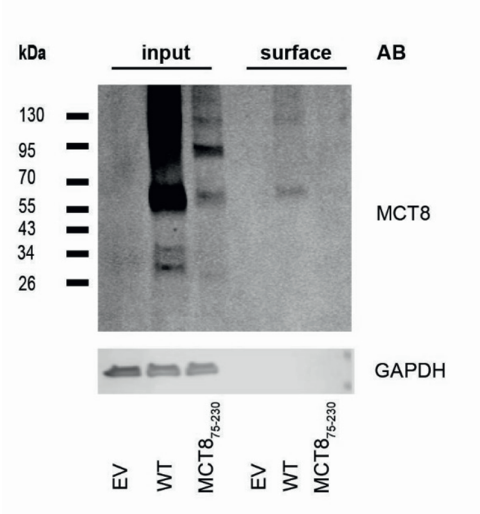

Supplemental Figure 5 Representative Western Blot analyses on total lysates and the cell surface fraction derived from COS-1 cells transfected with pcDNA3 EV, WT MCT8 or the $MCT8_{74-230}$ mutant. The input sample comprises 5% of the clarified lysate from which the presented surface fraction was derived. MCT8 detection was performed with the N-terminal MCT8 antibody (3353) and visualized with IRDye680 goat anti-rabbit secondary antibody. Glyceraldehyde-3-phosphate dehydrogenase (GAPDH) was used as loading control. Note the absence of GAPDH in the cell surface samples, demonstrating the purity of the cell surface fraction. Whereas bands corresponding to WT monomer and dimer were detected in the surface fraction, no bands corresponding to the $MCT8_{74-230}$ mutant MCT8 were observed, confirming the confocal data presented in **Figure 2C**. Abbreviations: AB, antibody; EV, empty vector; WT, wild-type.

REFERENCES

1. Friesema EC, Ganguly S, Abdalla A, Manning Fox JE, Halestrap AP, Visser TJ. Identification of monocarboxylate transporter 8 as a specific thyroid hormone transporter. J Biol Chem. 2003;278(41):40128-35.
2. Friesema EC, Grueters A, Biebermann H, Krude H, von Moers A, Reeser M, et al. Association between mutations in a thyroid hormone transporter and severe X-linked psychomotor retardation. Lancet. 2004;364(9443):1435-7.
3. Dumitrescu AM, Liao XH, Best TB, Brockmann K, Refetoff S. A novel syndrome combining thyroid and neurological abnormalities is associated with mutations in a monocarboxylate transporter gene. Am J Hum Genet. 2004;74(1):168-75.
4. Groeneweg S, Visser WE, Visser TJ. Disorder of thyroid hormone transport into the tissues. Best Pract Res Clin Endocrinol Metab. 2017;31(2):241-53.
5. Kinne A, Kleinau G, Hoefig CS, Gruters A, Kohrle J, Krause G, et al. Essential molecular determinants for thyroid hormone transport and first structural implications for monocarboxylate transporter 8. J Biol Chem. 2010;285(36):28054-63.
6. Groeneweg S, Lima de Souza EC, Meima ME, Peeters RP, Visser WE, Visser TJ. Outward-Open Model of Thyroid Hormone Transporter Monocarboxylate Transporter 8 Provides Novel Structural and Functional Insights. Endocrinology. 2017;158(10):3292-306.
7. Visser WE, Philp NJ, van Dijk TB, Klootwijk W, Friesema EC, Jansen J, et al. Evidence for a homodimeric structure of human monocarboxylate transporter 8. Endocrinology. 2009;150(11):5163-70.
8. Biebermann H, Ambrugger P, Tarnow P, von Moers A, Schweizer U, Grueters A. Extended clinical phenotype, endocrine investigations and functional studies of a loss-of-function mutation A150V in the thyroid hormone specific transporter MCT8. Eur J Endocrinol. 2005;153(3):359-66.
9. Fischer J, Kleinau G, Muller A, Kuhnen P, Zwanziger D, Kinne A, et al. Modulation of monocarboxylate transporter 8 oligomerization by specific pathogenic mutations. J Mol Endocrinol. 2015;54(1):39-50.
10. Yang Y, Mo W, Zhang JT. Role of transmembrane segment 5 and extracellular loop 3 in the homodimerization of human ABCC1. Biochemistry. 2010;49(51):10854-61.
11. Wei P, Liu X, Hu MH, Zuo LM, Kai M, Wang R, et al. The dimerization interface of the glycoprotein Ibbeta transmembrane domain corresponds to polar residues within a leucine zipper motif. Protein science : a publication of the Protein Society. 2011;20(11):1814-23.
12. Salazar G, Falcon-Perez JM, Harrison R, Faundez V. SLC30A3 (ZnT3) oligomerization by dityrosine bonds regulates its subcellular localization and metal transport capacity. PLoS One. 2009;4(6):e5896.
13. Wei W, Lampe L, Park S, Vangara BS, Waldo GS, Cabantous S, et al. Disulfide bonds within the C2 domain of RAGE play key roles in its dimerization and biogenesis. PLoS One. 2012;7(12):e50736.
14. Pace AJ, Gama L, Breitwieser GE. Dimerization of the calcium-sensing receptor occurs within the extracellular domain and is eliminated by Cys --> Ser mutations at Cys101 and Cys236. J Biol Chem. 1999;274(17):11629-34.
15. Boyson JE, Erskine R, Whitman MC, Chiu M, Lau JM, Koopman LA, et al. Disulfide bond-mediated dimerization of HLA-G on the cell surface. Proc Natl Acad Sci U S A. 2002;99(25):16180-5.
16. Dai Y, Walker SA, de Vet E, Cook S, Welch HC, Lockyer PJ. Ca2+-dependent monomer and dimer formation switches CAPRI Protein between Ras GTPase-activating protein (GAP) and RapGAP activities. J Biol Chem. 2011;286(22):19905-16.
17. Lima de Souza EC, Groeneweg S, Visser WE, Peeters RP, Visser TJ. Importance of cysteine residues in the thyroid hormone transporter MCT8. Endocrinology. 2013;154(5):1948-55.
18. Mol JA, Visser TJ. Synthesis and some properties of sulfate esters and sulfamates of iodothyronines. Endocrinology. 1985;117(1):1-7.
19. Friesema EC, Kuiper GG, Jansen J, Visser TJ, Kester MH. Thyroid hormone transport by the human monocarboxylate transporter 8 and its rate-limiting role in intracellular metabolism. Mol Endocrinol. 2006;20(11):2761-72.
20. Friesema EC, Jansen J, Jachtenberg JW, Visser WE, Kester MH, Visser TJ. Effective cellular uptake and efflux of thyroid hormone by human monocarboxylate transporter 10. Mol Endocrinol. 2008;22(6):1357-69.
21. Novara F, Groeneweg S, Freri E, Estienne M, Reho P, Matricardi S, et al. Clinical and Molecular Characteristics of SLC16A2 (MCT8) Mutations in Three Families with the Allan-Herndon-Dudley Syndrome. Hum Mutat. 2017;38(3):260-4.
22. Jansen J, Friesema EC, Kester MH, Milici C, Reeser M, Gruters A, et al. Functional analysis of monocarboxylate transporter 8 mutations identified in patients with X-linked psychomotor retardation and elevated serum triiodothyronine. J Clin Endocrinol Metab. 2007;92(6):2378-81.

23. Krieger E, Vriend G. YASARA View - molecular graphics for all devices - from smartphones to workstations. Bioinformatics. 2014;30(20):2981-2.
24. Krieger E, Joo K, Lee J, Lee J, Raman S, Thompson J, et al. Improving physical realism, stereochemistry, and side-chain accuracy in homology modeling: Four approaches that performed well in CASP8. Proteins. 2009;77 Suppl 9:114-22.
25. Duan Y, Wu C, Chowdhury S, Lee MC, Xiong G, Zhang W, et al. A point-charge force field for molecular mechanics simulations of proteins based on condensed-phase quantum mechanical calculations. J Comput Chem. 2003;24(16):1999-2012.
26. Kirk P, Wilson MC, Heddle C, Brown MH, Barclay AN, Halestrap AP. CD147 is tightly associated with lactate transporters MCT1 and MCT4 and facilitates their cell surface expression. EMBO J. 2000;19(15):3896-904.
27. Deora AA, Philp N, Hu J, Bok D, Rodriguez-Boulan E. Mechanisms regulating tissue-specific polarity of monocarboxylate transporters and their chaperone CD147 in kidney and retinal epithelia. Proc Natl Acad Sci U S A. 2005;102(45):16245-50.
28. Wilson MC, Meredith D, Halestrap AP. Fluorescence resonance energy transfer studies on the interaction between the lactate transporter MCT1 and CD147 provide information on the topology and stoichiometry of the complex in situ. J Biol Chem. 2002;277(5):3666-72.
29. Forrest LR, Kramer R, Ziegler C. The structural basis of secondary active transport mechanisms. Biochim Biophys Acta. 2011;1807(2):167-88.
30. Arumugam M, Ajitkumar P. Heat and SDS insensitive NDK dimers are largely stabilised by hydrophobic interaction to form functional hexamer in Mycobacterium smegmatis. Acta Biochim Pol. 2013;60(2):199-207.
31. Vatine GD, Al-Ahmad A, Barriga BK, Svendsen S, Salim A, Garcia L, et al. Modeling Psychomotor Retardation using iPSCs from MCT8-Deficient Patients Indicates a Prominent Role for the Blood-Brain Barrier. Cell Stem Cell. 2017;20(6):831-43 e5.

Chapter

Identification of iodotyrosines as novel substrates for the thyroid hormone transporter MCT8

2.8

Stefan Groeneweg*, Chantal Zevenbergen*, Elaine C. Lima de Souza*, Ferdy S. van Geest, Barbara Kloeckener-Gruissem, Endre Laczko, François Verrey, Simone M.R. Camargo, Marcel E. Meima, Robin P. Peeters, W. Edward Visser

Manuscript in preparation

ABSTRACT

Monocarboxylate transporter 8 (MCT8) is the most specific thyroid hormone transporter identified to date, deficiency of which has been associated with severe intellectual and motor disability and abnormal serum thyroid function tests. However, it is currently unknown if MCT8, like other TH transporters, also accepts alternative substrates, and if disruption of their transport may contribute to the observed phenotype.

In this study we aimed to identify such substrates by applying LC-MS-based metabolome analysis in lysates of control and MCT8-overexpressing *Xenopus* oocytes. A subset of identified candidate substrates was validated by direct transport studies in transiently transfected COS-1 cells and human fibroblasts which endogenously express MCT8. Moreover, transport characteristics were determined, including transport saturation and cis-inhibition potency of thyroid hormone transport.

Metabolome analysis identified 21 m/z scores, corresponding to 87 candidate metabolites, with a 2.0-times differential abundance in MCT8-injected oocytes compared to controls. These metabolites included 3,5-diiodotyrosine (DIT) and several amino acids, including glutamate and glutamine. In line with the metabolome studies, over-expression of MCT8 reduced the intracellular accumulation of [^{125}I]-DIT by ~60% in COS-1 cells. This effect was largely blocked in presence of T3 (IC_{50}: 2.5±xx µM) or T4 (IC_{50}: 5.8±xx µM). Conversely, increasing concentrations of DIT enhanced the uptake of T3 and T4. The MCT8-specific inhibitor silychristin increased the intracellular accumulation of DIT in human fibroblasts. COS-1 cells expressing MCT8 also exhibited a 50%-reduction in intracellular accumulation of [^{125}I]-3-monoiodotyrosine (MIT). In contrast, over-expression of MCT8 did not alter the intracellular accumulation of [^{3}H]-glutamate or [^{3}H]-glutamine in COS-1 cells. However, studies in human fibroblasts showed a ~2-times higher glutamate uptake in control fibroblasts compared to fibroblasts derived from patients with MCT8 deficiency, which was not affected in presence of silychristin.

Taken together, our results suggest that the iodotyrosines DIT and MIT can be exported by MCT8. MIT and DIT may interfere with MCT8-mediated transport of thyroid hormone *in vitro*, and *vice versa*. Future studies should elucidate if MCT8, being highly expressed in thyroidal follicular cells, also transports iodotyrosines *in vivo*.

INTRODUCTION

Thyroid hormone is crucial for the growth and development of virtually all tissues, especially the brain. Its main effects are exerted through binding of the active hormone 3,3',5-triiodothyroine (T3) to the nuclear T3 receptors (1). The amount of T3 available for receptor action is importantly controlled by the deiodinating enzymes (2). Since both, thyroid hormone action and metabolism, occur intracellularly, it needs to cross the cell membrane for which it requires TH transporter proteins (3). The most specific TH transporter identified to date is monocarboxylate transporter (MCT)8 which facilitates the cellular uptake and efflux of thyroxine (T4), T3, and to a lesser extent 3,3',5'-triiodothyronine (rT3) and 3,3'-diiodothyronine (3,3'-T2) (4-6). Mutations in MCT8 have been associated with MCT8 deficiency, characterized by severe intellectual disability and abnormal serum thyroid function tests (7, 8). The neuro-developmental features observed in MCT8 deficiency have been attributed to the hypothyroid state of the brain, whereas the etiology of the abnormal serum thyroid function tests has not been fully unraveled (Groeneweg et al, endo rev 2019). Although the clinical hallmarks of MCT8 deficiency likely originate from defective cellular transport of TH, it is not clear if defective transport of other, yet unknown, substrates may contribute to these features.

At present, it is unknown if MCT8 accepts other substrates than iodothyronines. The few available studies on the substrate specificity of MCT8 have only evaluated the direct transport of a limited number of potential substrates in MCT8-overexpressing *Xenopus* oocytes or mammalian cell lines, or applied cis-inhibition approaches which provide no definitive prove for direct transport (4-6, 9). These studies showed that MCT8 does not transport aromatic amino acids, whereas MCT8-mediated T3 transport was found to be reduced with a variable extent by different other iodothyronines. As an alternative for these targeted approaches, library screening or metabolome studies allow screening of a larger number of substrates and have been proven successful in identifying substrates for orphan transporters, such as creatine for MCT12 (10). Detailing the substrate specificity of MCT8 would provide essential information to unravel the pathogenesis of MCT8 deficiency and to guide development of therapeutic approaches.

Therefore, we performed metabolome analyses in control and MCT8-overexpressing *Xenopus laevis* oocytes and complementary studies in transfected COS-1 cells as well as in human fibroblasts from healthy controls or patients with MCT8 deficiency. With this approach, we identified diiodotyrosine (DIT) and mono-iodotyrosine (MIT) as the first substrates for MCT8-mediated efflux other than iodothyronines.

MATERIALS AND METHODS

Materials

X-tremeGENE9 transfection reagent was obtained from Roche Diagnostics (Woerden, The Netherlands [NL]). Nonradioactive iodothyronines were obtained from Henning (Berlin, Germany) and all non-radioactive amino acids, MIT and DIT from Sigma Aldrich, (Zwijndrecht, NL). The purity of MIT and DIT was >96% and >98%, respectively, with MIT containing up to 4% tyrosine. [^{125}I]-T_3, [^{125}I]-T_4, [^{125}I]-MIT and [^{125}I]-DIT were prepared as previously described (11, 12). [^{3}H]-labeled amino acids were obtained from GE Healthcare (Eindhoven, NL). Cell culture flasks and plates were obtained from Corning (Schiphol, NL).

Plasmids

The cloning of MCT1, MCT8, flag-tagged LAT1 and LAT2 into the pcDNA3 expression vector has been previously described (4, 9, 13, 14). The generation of the S194F, S290F, R445C, D498N, T239P and L543P mutant MCT8 expression constructs has been described previously (15-18). The mouse CD98-pcDNA3 expression construct was kindly provided by Dr. Gerd Krause (Leibniz-Forschungsinstitut für Molekulare Pharmakologie, Berlin, Germany).

Metabolomics in Xenopus laevis oocytes

Oocytes were surgically removed from *Xenopus laevis* and handled as previously described (19). A Nanoject II microinjector (Drummond) was used to inject 20 ng of MCT8 cRNA in a total volume of 50 nl. Oocytes were incubated for 2 days in ND96 medium (Hartmann Analytic, Brunswick, Germany) and subsequently for 1 h or 48 h in rich medium (n=20) (see (10) for composition) which was supplemented with metabolites mimicking human plasma (20) and Kao and Michayluk vitamin mix (Sigma Aldrich) (21). Both incubation media did not contain iodothyronines. Oocytes were lysed in ND96 supplemented with protease inhibitors (Sigma Aldrich). Samples were centrifuged (4°C; 25,000 rcf; 5 min). The supernatant was subjected to repeated (2×) centrifugation and concentrated to a final volume of 100 µl. For LC-MS analysis, three aliquots of 20 µl of the oocyte lysates were diluted (1:5) with 50 mM ammonium acetate in acetonitrile/methanol/water/saturated aqueous ammonium hydroxide (900:90:9:1,v/v, pH 9) and analyzed by LC-MS as described before (10). The resulting MS data were processed by Marker Lynx XS 4.1 (Waters, Manchester, UK) and analyzed as previously described (10). Briefly, the primary list of $[M-H]^-$ ions detected in any of the samples was queried in a Marker Lynx database containing 14,720 exact mass values, metabolite IDs, molecular formulas and pathway information of all KEGG listed metabolites (http://www.genome.jp/kegg/) and imported in R statistics for descriptive statistics, as well as univariate and multivariate data analyses. Between group analysis (BGA) was used to identify metabolites affected by the experimental conditions, i.e. potentially transported across the oocyte membrane by MCT8 (R library made4, (22)). The intensity data for the top candidates detected by BGA were additionally analyzed by one-way as well as two-way ANOVA (as appropriate).

Uptake and efflux experiments in Xenopus laevis oocytes

Oocytes were injected with either MCT8 or control cRNA (n=5 oocytes for each experimental condition) as described above. After injection, oocytes were kept at 18°C in ND96 medium supplemented with 5 mg/l doxycycline and gentamycin. Three days after injection, oocytes were washed with ND96 for 2 minutes at 25°C and incubated in ND96 medium containing 10 nM [125I]-T3 for 10 minutes at 25°C. After 10 minutes, incubation medium was removed and oocytes were washed with ND96. Oocytes were then lysed and internalized radio-activity was measured with a gamma counter.

Cell culture and transfection of COS-1 cells and human fibroblasts

COS-1 cells were cultured in DMEM/F-12 medium (Life Technologies, Bleiswijk, NL) supplemented with 9% heat-inactivated fetal bovine serum (Sigma Aldrich, Zwijndrecht, NL), and 1% penicillin-streptomycin (Roche Diagnostics, Almere, NL). For transport studies, COS1 cells were seeded in 24-well plates and transiently transfected in duplicate with 50 ng pcDNA3 empty vector or wild-type

MCT8. If indicated, cells were transfected with 50 ng MCT1, or 50 ng LAT1/2 and 50 ng CD98, or co-transfected with 50 ng MCT8 and 50 ng LAT1/2 as well as 50 ng CD98 plasmid, supplemented with pcDNA3 empty vector up to a total amount of 200 ng plasmid per well. All transfections were carried out at 70% confluence and X-treme GENE 9 (Roche Diagnostics) was used as a transfection reagent according to the manufacturer's protocol.

Fibroblasts of patients with MCT8 deficiency and healthy controls were derived from skin biopsies performed in the context of clinical care. For uptake studies, fibroblasts were seeded on 6-well plates and cultured in DMEM/F-12 medium with with 9% heat-inactivated fetal bovine serum and 1% penicillin-streptomycin until >95% confluence.

Uptake experiments COS-1 cells and human fibroblasts

Uptake studies were performed two days after transfection (COS-1 cells), or at >95% confluence (human fibroblasts) according to well-established protocols (4, 23). Briefly, cells were washed with incubation medium (Dulbecco's phosphate-buffered saline (DPBS)+ Ca^{2+}/Mg^{2+} + 0.1% D-glucose + 0.1% BSA) and incubated in incubation medium containing 10 nM (50,000 cpm) [^{125}I]-T4 or [^{125}I]-T3, or 10 µM (100,000 cpm) [^{125}I]-MIT, [^{125}I]-DIT, [^{3}H]-tryptophan, [^{3}H]-phenylalanine, [^{3}H]-tyrosine, [^{3}H]-leucine, [^{3}H]-alanine, [^{3}H]-glutamine or [^{3}H]-glutamate for indicated incubation times at 37°C. After incubation, cells were briefly washed with incubation medium and lysed with 0.1 M NaOH. The amount of internalized radio-activity was measured with a gamma-counter in case of [^{125}I]-radio-labeled compounds and with a beta-counter in case of [^{3}H] radio-labeled compounds. For inhibition studies, increasing concentrations of unlabeled DIT, MIT, T3 or T4 (1-100 µM), 1mM of the indicated amino acids or 1 mM of the selective LAT inhibitor 2-aminobicyclo-(2,2,1)-heptane-2-carboxylic acid (BCH) were added during incubation. Uptake levels in fibroblasts were adjusted for total protein levels measured by Bradford assay according to manufacturer's guideline (Bio-Rad, Veenendaal, NL).

Immunoblotting

The expression level of MCT8 protein in total lysates of non-injected (NI) oocytes and oocytes injected with MCT8 cRNA was analyzed using conventional immunoblotting techniques (e.g. (13)). Immuno-detection of MCT8 was carried out as previously described using rabbit polyclonal antibody HPA003353 against human MCT8 amino acids 75 to 155 from Sigma Aldrich (Manufacturer: Atlas Antibodies, Stockholm; RRID AB_1079343) (13).

RNA extraction and RT-qPCR of LAT transporters in COS1 cells

Total RNA was extracted from COS1 cells using High Pure RNA Isolation kit (Roche Diagnostics), according to the manufacturer's instructions. RNA (1 µg) was reversely transcribed using Transcriptor High Fidelity cDNA Synthesis kit (Roche Diagnostics). Quantitative real-time PCR was performed using qPCR Core kit for SYBR® Green (Eurogentec, Maastricht, NL). GAPDH was used as housekeeping gene for normalization of mRNA expression. PCR primers are listed in **Supplemental Table S1**.

Statistical analysis

Statistical analysis was performed using the GraphPad Prism software (Version 5, Graphpad Software Inc., San Diego, USA). Apparent IC_{50} values were calculated based on the log(inhibitor) *vs.* normalized response function in GraphPad Prism. All results are presented as the means ± SEM of at least 3

independent experiments performed in duplicate. Where appropriate, one-way or two-way ANOVA was applied followed by the Bonferroni's posttest.

RESULTS

Identification of di-iodotyrosine as substrate for MCT8 using metabolomics

Injection of Xenopus oocytes with MCT8 cRNA increased MCT8 protein expression levels and resulted in a ~10-times induction of T3 uptake (**Supplemental Figure S1**). To identify potential novel substrates for MCT8, oocytes injected with MCT8 or control cRNA were incubated in rich medium for 1 or 48h. Extracts of these oocytes were subjected to metabolome analyses, which yielded a dataset with unique mass / charge (m/z) scores (ratio of ion mass (m) and charge (z)). After exclusion of analytical and chemical noise, restriction to known metabolites in human, and application of a 2.0-times differential abundance threshold, we identified 4 m/z scores (corresponding to fragments of 14 candidate metabolites) to be less, and 10 m/z scores (corresponding to fragments of 42 candidate metabolites) to be more abundant in oocytes expressing MCT8 than in control oocytes after 1 h incubation (**Table 1**). In addition, we identified 5 m/z scores (corresponding to fragments of 11 metabolites) to be less, and 9 m/z scores (corresponding to fragments of 50 metabolites) to be more abundant in oocytes expressing MCT8 than in control oocytes after 48 h incubation, of which 7 m/z scores (corresponding to fragments of 30 metabolites) were overlapping between both time points (**Table 1**, for a full list of metabolites see **Supplemental Table S2**). Among the strongest hits we identified a fragment with an m/z score of 431.86, corresponding to the characteristics of 3,5-diiodotyrosine (DIT), which showed a 7.1-times higher accumulation in control oocytes over those injected with MCT8 cRNA. Moreover, being one of the precursor molecules of iodothyronines, DIT has important structural resemblances to known MCT8 substrates.

Transport of diiodotyrosine by MCT8

To validate if DIT is transported by MCT8, we next studied the intracellular accumulation of DIT in COS-1 cells transiently transfected with MCT8 or empty vector. The intracellular accumulation of DIT was ~2-times less in cells transfected with MCT8 than in cells transfected with the empty vector control (**Figure 1A**). To exclude that the observed reduction was due to cellular stress responses related to the over-expression of a membrane transporter, we also measured DIT accumulation in cells transfected with MCT1, a transporter from the same family that does not facilitate the transport of iodothyronines. In these cells, intracellular accumulation of DIT was similar to that observed in empty vector transfected control cells (**Supplemental Figure S2**). The difference in intracellular DIT accumulation between empty vector and MCT8-transfected cells increased over time during the first 30 minutes of incubation and remained stable thereafter (**Figure 1B**). The intracellular accumulation of DIT could not be potentiated by co-transfection with the intracellular TH-binding protein CRYM, precluding studies to elucidate if MCT8 also facilitate the uptake of DIT (data not shown). The MCT8-mediated efflux of DIT was diminished in presence of 100 µM unlabeled DIT, although at these concentrations also the cellular uptake in empty vector transfected cells was greatly reduced (**Figure 1C**). Apparent IC50 values for MCT8-mediated DIT efflux amounted up to ~18.8 (95% CI 13.0-27.3) µM (**Figure 1D**). MCT8-mediated DIT efflux was inhibited at lower concentrations of T3 (apparent IC50: ~2.5 µM (95% CI 1.0-6.4) µM) or T4 (apparent IC50: ~5.8 µM (95% CI 3.0-11.1) µM) (**Figure 1E** and **F**, respectively).

Table 1 Overview of identified m/z ratios and their corresponding putative metabolites

m/z	1h incubation MCT8/EV	P value	48h incubation MCT8/EV	P value	Number of candidate metabolites	Exemplary metabolites
109,04	8,73	<0,001	2,73	0,011	2	Dihydrothymine
118,05			2,98	0,038	7	L-Threonine, Aminoacetone
128,03	2,25	<0,001			15	L-Glutamic acid, N-Methyl-D-aspartic acid
145,06	2,20	<0,001	2,03	<0,001	4	L-Glutamine
171,00	0,04	0,043			6	Glycerol 3-phosphate, Phenylglyoxylic acid
173.00			0.43	0.0291	*2*	*S-Methyl benzenecarbothioate*
173,05	2,85	<0,001	4,73	0,0032	2	2-Aminoacrylic acid
179,05			2,02	0,0002	18	D-Fructose, D-glucose, D-galactose, myoinositol
207,03	2,06	<0,001			1	1,2-Dihydroxy-3-keto-5-methylthiopentene
230,96			*0,32*	*0,0024*	*1*	*3,5-Dichloro-4-hydroxy-2-methoxy-6-methylbenzoic acid*
272,08	*2,78*	<0,001			*1*	*7-Aminonitrazepam*
275,02	*2,92*	*0,015*	*2,69*	*0,011*	*1*	*Bis(2,5-dimethyl-3-furanyl) disulfide*
302,10	0,44	0,0098	0,40	0,014	6	N6-Methyladenosine
313,11	4,99	<0,001	3,39	0,0001	14	7,8-Dihydropteroic acid, Hydroxyenterolactones
331.01	0.35	0.020			*1*	*Diflubenzuron*
357.07	6.51	<0,001	3.98	<0,001	1	*Naphthoherniarin*
431,86			0,14	0,0030	1	3,5-Diiodo-L-tyrosine
510.39	<0.01	<0,001			*1*	*Rocuronium*
558,06			4,08	<0,001	1	Adenosine diphosphate ribose
605.00	8.95	0.030			1	*Cefodizime*
662.09			0.43	0.0003	1	*Fenugreekine*

Overview of candidate metabolites for MCT8 mediated transport based on the m/z ratios identified by metabolomic analyses in *Xenopus* oocytes (see methods for selection criteria). Exemplary metabolites considered as drugs, or specific to plants, herbs or spices are presented in italics. See **Supplemental Table S2** for a full list of candidate metabolites.

Increasing concentrations of DIT progressively enhanced MCT8-mediated uptake of T3 and in particular T4 in the absence of CRYM with strongest effects observed in presence of 100 µM DIT (**Figure 1G** and **H**, respectively). Together, these observations suggest that MCT8 primarily facilitates the cellular efflux of DIT which may compete with MCT8-mediated efflux of T3 and T4, and vice versa. The cellular uptake of DIT appears to be facilitated by transporters other than MCT8.

To enable modulation of the DIT concentration gradient across the cell membrane, we next sought to identify endogenous DIT transporters in COS-1 cells. To this purpose we measured the mRNA expression levels of the L-type amino acid transporters LAT1 and LAT2 in COS-1 cells, both of which have been previously shown to effectively facilitate the cellular uptake of MIT and DIT (24). Quantitative PCR showed high levels of LAT1, but not LAT2 expression in COS-1 cells (**Figure 2A**). Indeed, the cellular uptake of DIT was reduced by about 60% in presence of the LAT-inhibitor BCH indicating that LAT(1) importantly contributes to the cellular uptake of DIT in COS-1 cells, although additional transporters are likely involved (**Figure 2B**). Overexpression of LAT1 in COS-1 cells resulted in a further increase of cellular DIT uptake (**Figure 2C**) and potentiated MCT8-mediated cellular efflux of DIT (**Figure 2D**). Conversely, MCT8-mediated DIT efflux was diminished upon blocking endogenously expressed LATs with BCH (**Figure 2B**). Thus, MCT8-mediated DIT efflux rate likely depends on the concentration gradient of DIT across the cell membrane. Even in presence of a concentration gradient that would favor the cellular uptake of DIT, MCT8 does not facilitate the uptake of DIT.

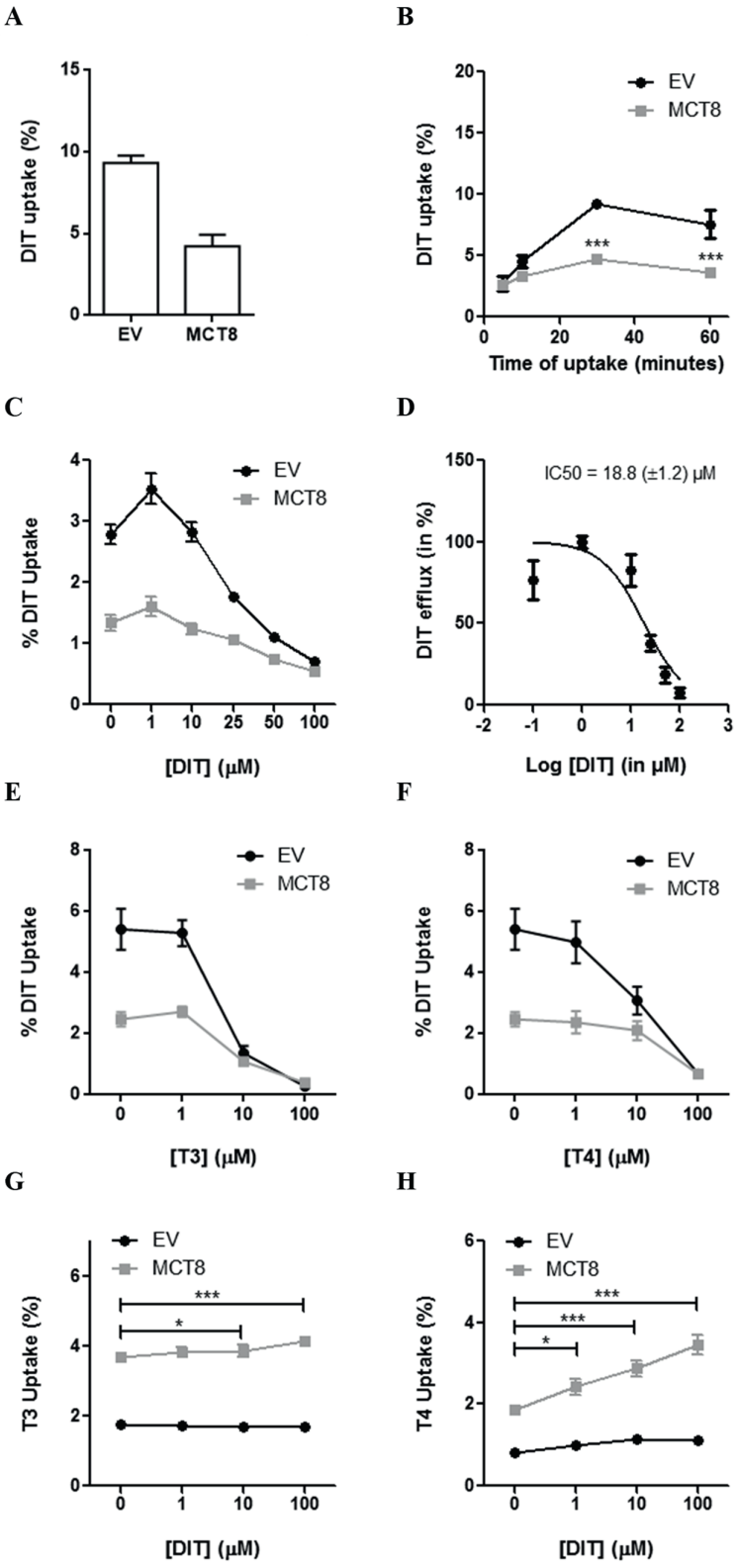
A
DIT uptake (%)
EV
MCT8
B
EV
MCT8
DIT uptake (%)
Time of uptake (minutes)
***
***
C
EV
MCT8
% DIT Uptake
[DIT] (µM)
D
IC50 = 18.8 (±1.2) µM
DIT efflux (in %)
Log [DIT] (in µM)
E
EV
MCT8
% DIT Uptake
[T3] (µM)
F
EV
MCT8
% DIT Uptake
[T4] (µM)
G
EV
MCT8
***
*
T3 Uptake (%)
[DIT] (µM)
H
EV
MCT8
***
***
*
T4 Uptake (%)
[DIT] (µM)

Figure 1 (A) Intracellular accumulation of DIT in COS-1 cells transiently transfected with pcDNA3 empty vector (EV) or MCT8 after 30 minutes incubation at 37 °C, expressed relative to the amount of [125I]-DIT added to the cells at the start of incubation. **(B)** Intracellular accumulation of DIT in EV or MCT8-transfected COS-1 cells after indicated incubation times. **(C)** Intracellular accumulation of DIT in EV or MCT8-transfected COS-1 cells in presence of indicated concentrations of cold DIT after 10 minutes incubation. **(D)** Saturation curve of MCT8-mediated DIT efflux derived from the data expressed in **(C)**. Intracellular accumulation of DIT in presence of increasing concentrations of T3 **(E)** and T4 **(F)**, respectively. Intracellular accumulation of T3 **(G)** and T4 **(H)** in presence of indicated concentrations of DIT in COS-1 cells transiently transfected with EV or MCT8 in the absence of the intracellular TH-binding protein CRYM after 10 minutes incubation at 37 °C. The MCT8-mediated T3 and T4 uptake (calculated by subtracting levels observed in EV-transfected cells from those in MCT8-transfected cells) in presence of indicated concentrations of DIT was compared to levels observed in the absence of DIT using paired ANOVA with Dunnet posttests. Statistically significant differences are indicated as follows: *, $p<0.05$, **, $p<0.01$, ***, $p<0.001$. Data are presented as means ± SEM of at least three independent experiments.

The transport of DIT is impaired in MCT8 mutants

To study if MCT8-mediated DIT transport is altered by mutations that have been identified in patients with MCT8 deficiency, we selected several well-characterized MCT8 mutations (15-18, 25, 26) with variable reduced MCT8-mediated T3 transport (**Figure 3A**). Accordingly, these mutations reduced MCT8-mediated efflux of DIT (**Figure 3B**). The impact of mutations on MCT8-mediated T3 uptake and MCT8-mediated DIT efflux strongly correlated ($R^2 = 0.88$, $p<0.01$), further supporting that the reduced cellular accumulation of DIT in presence of MCT8 is caused by direct MCT8-mediated DIT efflux (**Figure 3C**).

We then evaluated the intracellular DIT accumulation in fibroblast cultures derived from healthy controls and three patients with MCT8 deficiency harboring a mutation with a relatively less severe (T239P and L543P) or severe (splice site mutation resulting in a p.S267-S360del, further referred to as splice site mutant) impact on MCT8 function (18, 27). In line with previous studies (e.g. (18, 23)), cellular T3 uptake was lower in the patient-derived fibroblasts compared to controls. Moreover, T3 uptake levels in control fibroblasts decreased by ~70% in presence of the MCT8-specific inhibitor silychristin (28), whereas no reduction was observed in the splice site mutant fibroblasts, confirming the complete loss of MCT8 function in these cells (**Figure 3D**). T3 uptake was reduced by ~30 % and ~60 % in the T239P and L543P fibroblasts, respectively. Compared to the COS-1 cell line, the absolute intracellular accumulation of DIT was 10-times lower in human control fibroblasts (**Supplemental Figure S3**). The accumulation of DIT in control fibroblasts exceeded the levels observed in any of the patient fibroblast lines (**Figure 3E**). To dissect if this observation is caused by a differential role of MCT8 in the cellular transport of DIT in fibroblasts or by indirect effects of MCT8 deficiency on redundant DIT transporters, DIT transport was studied in absence and presence of silychristin. In presence of silychristin, intracellular DIT accumulation significantly increased in control fibroblasts, whereas no significant changes were observed in fibroblasts derived from MCT8 deficient patients, suggesting that MCT8 also primarily facilitates the efflux of DIT in this system (**Figure 3F**).

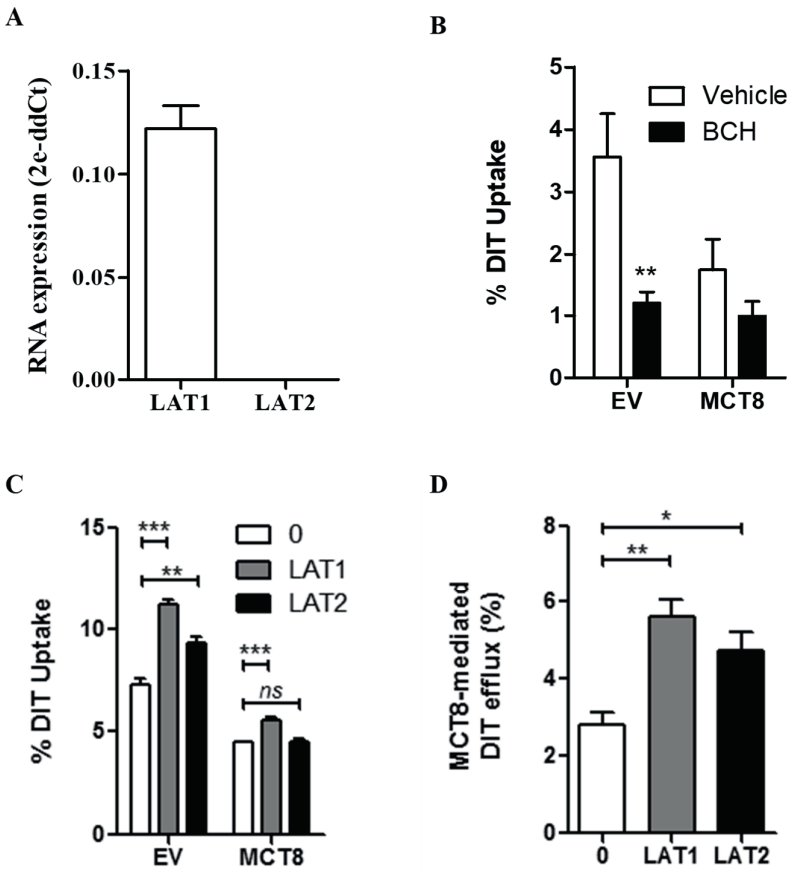

Figure 2 (A) LAT1 and LAT2 mRNA levels in non-transfected COS-1 cells. GAPDH (glyceraldehyde-3-phosphate dehydrogenase) was used as internal control. Results are presented as 2e-ddCt. **(B)** Intracellular DIT accumulation in empty vector (EV) or MCT8-transfected COS-1 cells after 30 minutes incubation at 37 °C in the presence or absence of 1 mM of the LAT-inhibitor BCH. Data are expressed relative to the amount of [125I]-DIT added to the cells at the start of the experiment and presented as mean ± SEM of at least three independent experiments. Significant within-group differences (Two-way ANOVA with Bonferroni posttests) between control and BCH-treated cells are indicated (*, $p<0.05$). **(C)** Intracellular accumulation of DIT in COS-1 cells co-expressing MCT8 and LAT1 or LAT2 as well as CD98 after 30 minutes incubation at 37 °C. Two-way ANOVA with Bonferroni posttests was used to analyze the differences between EV or MCT8-transfected cells in the absence or presence of either LAT1 or LAT2 (***, $p<0.001$, **, $p<0.01$). **(D)** Effect of co-transfection with LAT1 and LAT2 on MCT8-mediated DIT efflux. Data derived from **(C)** by subtracting levels observed in MCT8-transfected cells from those in EV-transfected cells. One-way ANOVA was used with Dunnet`s posttests to assess for statistically significant differences between control (0), LAT1, and LAT-2 co-transfected cells (**, $p<0.01$, *, $p<0.05$). All data are presented as the mean ± SEM of at least three independent experiments.

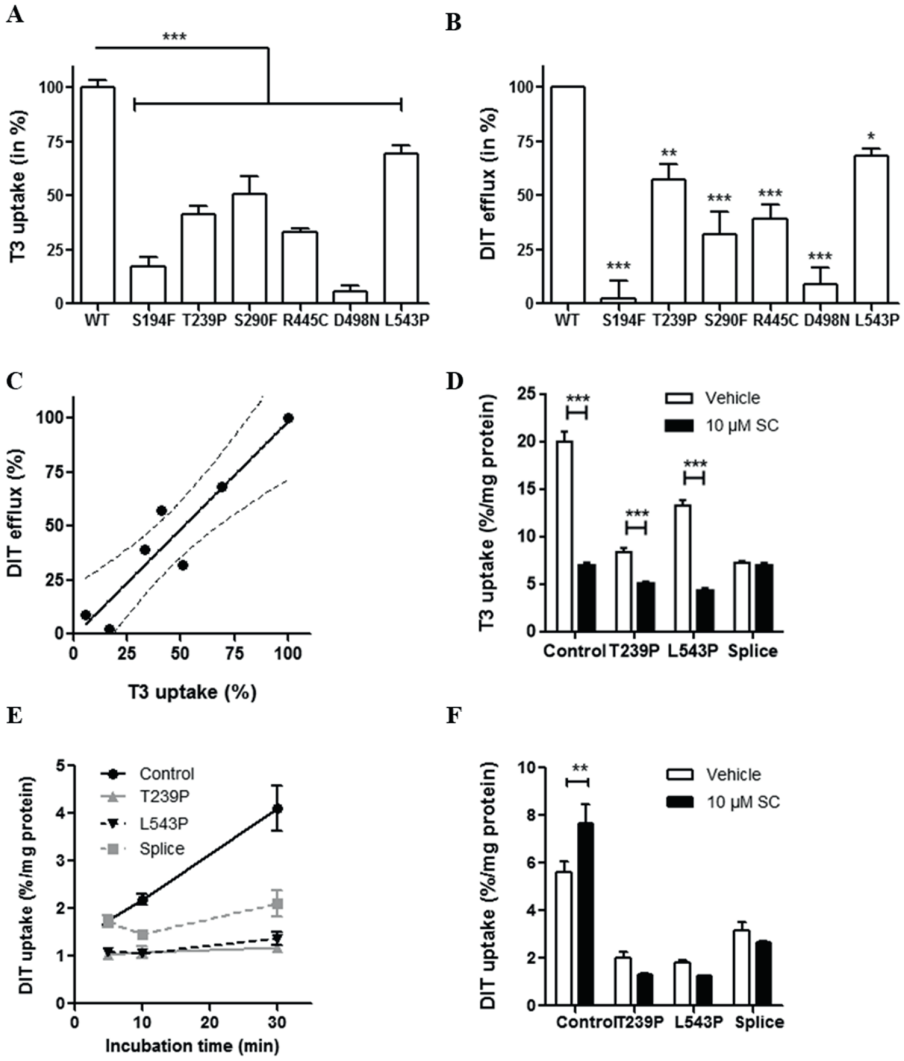

Figure 3 (A) Cellular T3 uptake in COS-1 cells transiently co-transfected with wild-type (WT) or indicated mutant MCT8 and CRYM after 30 minutes incubation at 37 °C. Uptake levels were corrected for those observed in empty vector transfected cells and expressed relative to WT (100%). One-way ANOVA with Bonferroni posttests were used and statistically significant differences to WT are indicated as follows p<0.001, ***. **(B)** Similarly, MCT8-mediated DIT efflux in transiently transfected COS-1 cells. **(C)** Correlation plot of MCT8-mediated T3 uptake and DIT efflux. Each dot represents the residual T3 uptake and DIT efflux of WT or one of the mutant MCT8 proteins presented in **(A)** or **(B)**. A Pearson correlation analysis was used to examine the association (r = 0.88, p = 0.001). **(D)** T3 uptake in patient and control fibroblasts in the absence (-) or presence (+) of 10µM silychristin (SC). **(E)** Intracellular accumulation of DIT in patient and control fibroblasts after indicated incubation times at 37°C. Data are presented as means ± SEM percentages internalized DIT per milligram protein. DIT uptake in fibroblasts of all three MCT8 deficient patients was significantly lower than in those obtained from healthy controls (mean of 2 different control cell lines) at 10 and 30 minutes (Two-way ANOVA with Bonferroni posttests: p<0.05 after 10 and p<0.001 after 30 minutes incubation, not indicated in graph). **(F)** Intracellular DIT accumulation in patient and control fibroblasts in the absence (-) or presence (+) of 10µM silychristin (SC). Two-way ANOVA with Bonferroni posttests were used to assess for differences in DIT or T3 uptake in presence and absence of SC (p<0.01, **; p<0.001, ***). All data are presented as means ± SEM of at least 3 independent experiments.

Transport of monoiodotyrosine by MCT8

Given its close structural and chemical resembles to DIT, we also studied if MCT8 facilitates the efflux of MIT. Indeed, the intracellular accumulation of MIT was ~35% lower in cells transfected with MCT8 than in empty vector transfected control cells after 30 minutes incubation (**Figure 4A**), with the largest reduction in intracellular MIT accumulation after 10 minutes incubation (**Figure 4B**). MCT8-mediated efflux of MIT was largely diminished in presence of 10 µM T3 and T4, with respective apparent IC50 values for T3 of 6.7 (95% CI, 3.0-15.0) µM and T4 of 6.4 (95% CI, 3.0-14.0) µM (**Figure 4C** and **4D**). MCT8-mediated uptake of T3 and T4 in the absence of CRYM was slightly, but significantly, increased in presence of 10 and 100 µM MIT, whereas no effects were observed at the 1 µM concentrations (**Figure 4E** and **4F**). The uptake of MIT in empty vector transfected control cells was strongly reduced by BCH, suggesting that LAT1 may represent an important transporter that facilitates the uptake of MIT in COS-1 cells (data not shown).

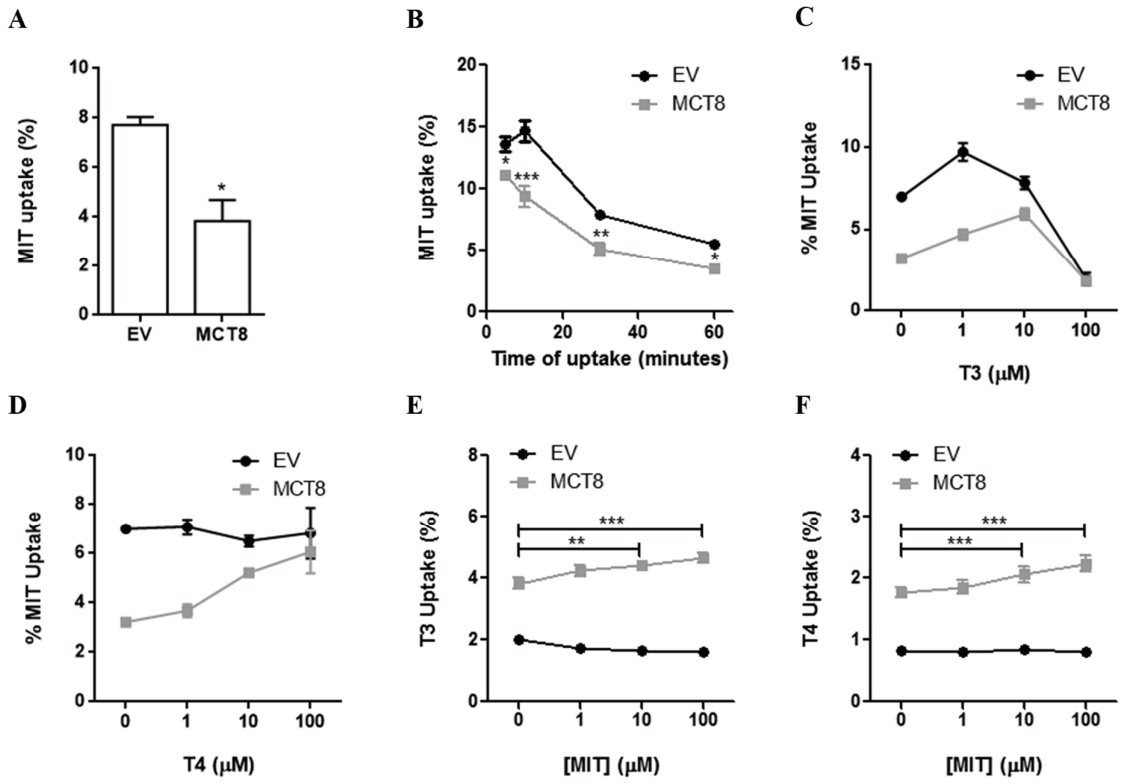

Figure 4 (A) Intracellular accumulation of MIT in COS-1 cells transiently transfected with pcDNA3 empty vector (EV) or MCT8 after 30 minutes incubation at 37 °C, expressed relative to the amount of MIT added to the cells at the start of incubation. **(B)** Intracellular accumulation of MIT in EV or MCT8-transfected COS-1 cells after indicated incubation times. **(C)** and **(D)** Intracellular accumulation of MIT in EV or MCT8-transfected COS-1 cells in presence of indicated concentrations T3 **(C)** or T4 **(D)** after 30 minutes incubation. Intracellular accumulation of T3 **(E)** and T4 **(F)** in presence of indicated concentrations of MIT in COS-1 cells transiently transfected with EV or MCT8 in the absence of the intracellular TH-binding protein CRYM after 10 minutes incubation at 37 °C. The MCT8-mediated T3 and T4 uptake (calculated by subtracting levels observed in EV-transfected cells from those in MCT8-transfected cells) in presence of indicated concentrations of MIT was compared to levels observed in the absence of MIT using paired ANOVA with Dunnet posttests ($p<0.01$, **; $p<0.001$, ***). Data are presented as means ± SEM of at least three independent experiments.

MCT8 does not directly transport amino acids

Some of the other m/z scores identified in the metabolome analysis corresponded to fragments of amino acids or closely related derivatives thereof, most notably threonine, glutamate and glutamine as well as products of aspartic acid, proline and arginine metabolism (**Table 1**). As several other TH transporters are known to transport amino acids, including MCT10, LAT1 and LAT2, we studied the effects of different amino acids on MCT8-mediated T3 and T4 transport in transiently transfected COS-1 cells. At a concentration of 1 mM, which is well-above their physiological concentrations in human serum, none of the tested amino acids significantly reduced MCT8-mediated T3 uptake (**Figure 5A**), whereas a slight, but significant, increase in cellular T4 uptake was observed in presence of 1 mM aspartic acid (**Figure 5B**).

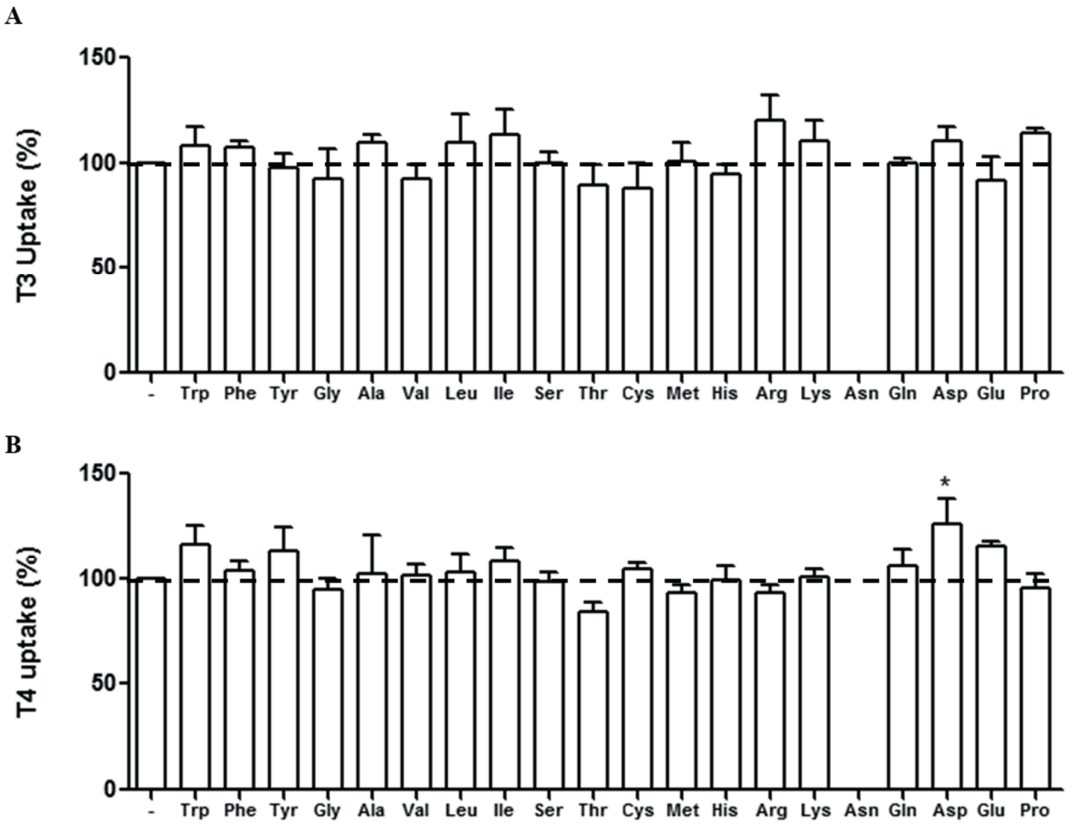

Figure 5 Cellular uptake of T3 **(A)** and T4 **(B)** in COS-1 cells transiently transfected with empty vector or MCT8 in the presence of 1 mM of indicated amino acids. Experiments were performed in the absence of CRYM. Uptake levels were corrected for those observed in empty vector transfected control cells incubated under the same conditions and expressed to MCT8-mediated T3 **(A)** or T4 **(B)** levels observed in the absence of competitive amino acids (-). One-way ANOVA was used with Dunnet`s posttests to assess for significant effects of indicated amino acids on MCT8-mediated T3 or T4 transport. Data are presented as means of 2-5 independent experiments.

We also studied the direct uptake of glutamate and glutamine, selected based on the availability of their [^{3}H]-radio-labeled isotopes and previous studies that showed alterations in these metabolites in brains of Mct8 knock-out mice (29). However, the intracellular accumulation of both amino acids did not differ between MCT8-transfected and control COS-1 cells (**Figure 6A** and **6B**). In line with the metabolome studies in Xenopus oocytes, MCT8 did not facilitate the transport of [3H]-tyrosine,

phenylalanine or tryptophan (substrates for MCT10), nor [5H]-alanine or leucine (substrates for LAT) (**Supplemental Figure S4A-E**). Although these results indicate that MCT8 does not directly transport glutamate or glutamine, MCT8 may modulate cellular factors involved in the transport or metabolism of these amino acids and therewith indirectly affects intracellular glutamate and glutamine concentrations. To substantiate this hypothesis, we measured glutamate accumulation in human fibroblasts derived from control subjects and patients with MCT8 deficiency. In line with the observations in Xenopus oocytes, we observed that glutamate uptake in control fibroblasts significantly exceeded levels observed in fibroblasts derived from MCT8 patients (**Figure 6C**). Despite these differences, glutamate uptake was not inhibited by silychristin, again supporting that MCT8 not directly transports glutamate (**Figure 6D**).

DISCUSSION

It is currently unknown if MCT8, like other TH transporters, also transports biological substances in addition to iodothyronines. Here, we addressed this knowledge gap by applying metabolome analyses in MCT8-overexpressing *Xenopus* oocytes. These studies demonstrated that MCT8 facilitates the cellular efflux of DIT, a process which modulates MCT8-mediated transport of T3 and T4 *in vitro*, and *vice versa*. Although metabolome analyses indicated that MCT8 also affects the intracellular concentrations of several amino acids or metabolites thereof, subsequent *in vitro* and *ex vivo* studies showed that MCT8 does not directly facilitate amino acid transport. Together, these findings illustrate that MCT8 not only regulates the intracellular concentrations of its direct substrates but also of metabolites that are not directly transported by MCT8 itself.

By comparing the metabolome of control and MCT8-expressing *Xenopus* oocytes, cultured in presence of rich medium, we here identified 21 differentially abundant m/z scores yielding in total 87 candidate substrates for MCT8. One of the metabolites that showed a lower abundance in MCT8-overexpressing oocytes than in controls was identified as DIT. The presence of MCT8 also reduced the intracellular accumulation of DIT in transfected COS-1 cells, which was in line with previous studies showing that the presence of MCT8 decreased intracellular DIT accumulation (30). Moreover, an increase in intracellular DIT accumulation was observed in human fibroblasts in presence of the MCT8-specific inhibitor silychristin. Together, these results strongly indicate that MCT8 facilitates the cellular efflux of DIT.

The transport mechanism of MCT8 entails facilitated diffusion and, hence, its transport rate is greatly determined by the concentrations of substrate in the intra- and extracellular compartment. Indeed, MCT8-mediated DIT efflux in COS-1 cells increased upon over-expression of LAT1 and LAT2, which both facilitate the cellular uptake of DIT (13), whereas blocking endogenous LATs with BCH had the opposite effect. Also in human fibroblasts, which lack potent endogenous DIT transporters, inhibition of MCT8 with silychristin increased the intracellular DIT accumulation. Thus, even in the presence of a concentration gradient that would favor the cellular accumulation of DIT, the uptake of DIT is not facilitated by MCT8. In contrast to these observations and to the effects of MCT8 mutations observed in transfected COS-1 cells, the cellular accumulation of DIT was reduced in fibroblasts derived from patients with MCT8 deficiency. Although the exact mechanism(s) remain to be elucidated, we speculate that this reduction is independent from the direct effects of these mutations on MCT8-mediated DIT transport.

Since MCT8 specifically facilitates the cellular efflux of DIT, the substrate criteria for recognition by MCT8 differ between the intracellular and extracellular side of the transporter. Whereas the absence of the outer-ring does not seem to exclude DIT as a substrate for cellular efflux, its presence appears obligatory for cellular uptake. Over-expression of MCT8 in COS-1 cells also reduced the intracellular accumulation of MIT, the chemical and structural properties of which resemble those of DIT except for the lack of the 5-iodine moiety. In contrast, MCT8 did not facilitate the uptake or efflux of tyrosine which lacks both iodine moieties. Therefore, the presence of at least one iodine-moiety on the (inner) phenolic ring appears to be critical for substrate recognition during the efflux cycle.

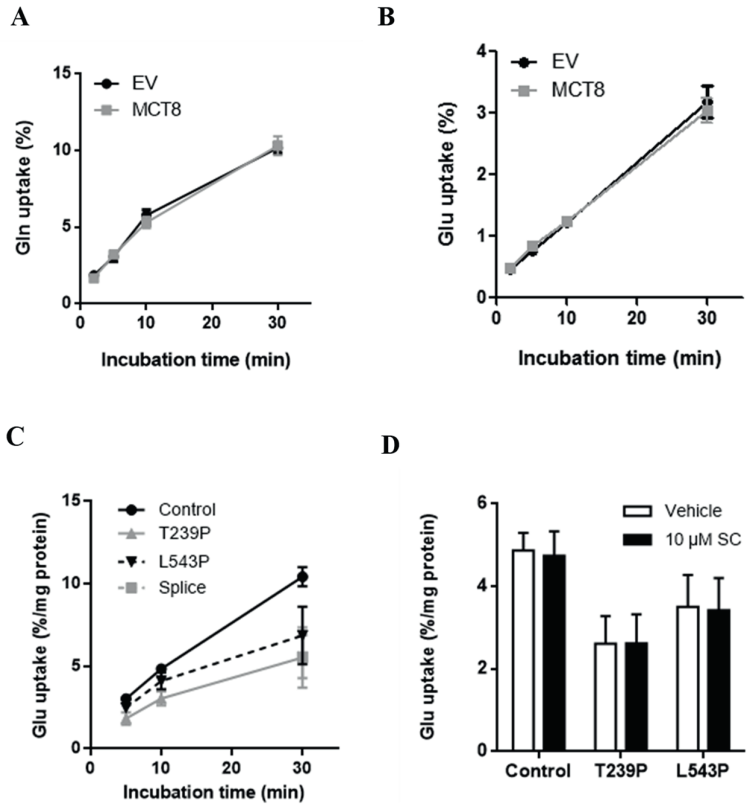

Figure 6 Intracellular accumulation of glutamine **(A)** or glutamate **(B)** in COS-1 cells transiently transfected with EV or MCT8, after incubation for 2, 5, 10 and 30 minutes at 37 °C. Differences between EV and MCT8-transfected cells were assessed for statistical significance by two way ANOVA with Bonferroni posttests. Data are expressed relative to the amount of [^{3}H]-labeled amino acid that was added to the cells at the start of the incubation and presented as the mean ± SEM of at least three independent experiments. **(C)** Intracellular accumulation of [^{3}H]-glutamate in patient and control fibroblasts after indicated incubation times at 37°C. Data are presented as mean ± SEM percentages internalized glutamate per milligram protein to correct for differences in cell density between different fibroblast lines. Glutamate uptake in fibroblasts of patients with MCT8 deficiency was significantly lower than in those of healthy controls (mean of 2 different control cell lines) after 30 minutes incubation (One-way ANOVA with Bonferroni posttests: $p<0.05$, not indicated in graph). **(D)** Glutamate uptake in patient and control fibroblasts in the absence (-) or presence (+) of 10µM silychristin (SC). Two-way ANOVA with Bonferroni posttests was used to assess for differences in glutamate uptake in presence and absence of SC. All data are presented as means ± SEM of at least 3 independent experiments.

Should MCT8 transport DIT and MIT *in vivo*, the physiological relevance is unclear. MIT and DIT are intermediates formed in the thyroid gland during the biosynthesis of TH (31). As DIT and MIT are released from the thyroid into the bloodstream (32-34), given its high expression in the thyroid gland, MCT8 might be a good candidate to facilitate their efflux (35, 36). In this context, it might be of interest to measure circulating DIT and MIT concentrations in patients with MCT8 deficiency.

Increasing concentrations of DIT and MIT preferentially inhibited the efflux of T4 over T3. It is unclear if this can have consequences on circulating T3 and T4 concentrations under certain conditions. During TSH-receptor stimulation, it has been reported that circulating DIT and MIT concentrations increase (37). Should the increased intrathyroidal DIT and MIT content under these conditions result in a relative inhibition of T4 over T3 export, this might represent an additional explanation for the elevated T3:T4 ratio in serum in patients with Graves' disease. In this context, it should be noted that the apparent IC50 values of MCT8-mediated DIT efflux for T3 and T4 are considerably lower than that of DIT (~18.8 µM), suggesting that T3 and T4 are the preferred substrates for MCT8-mediated efflux, although the comparison of these IC50 values might be complicated by the differential effects of these compounds on endogenously expressed DIT transporters.

Although metabolome analyses successfully identified DIT as a novel substrate, we found that MCT8 did not directly transport several other candidate substrates, which may have several reasons. First, other candidate substrates that were not further studied and yield the same fragmentation as those selected for the validation studies might be the actual substrates for MCT8. However, we were unable to validate most of these alternative candidate substrates *in vitro* due to the lack of radio-labeled compounds or appropriate LC-MS detection systems. Second, MCT8 may transport metabolites upstream or downstream in the pathway of the identified candidate metabolites, with the identified candidate substrates accumulating at the final or rate limiting step of the pathway. Finally, MCT8-expressing oocytes and controls may have been exposed to different TH concentrations during routine culture in presence of fetal bovine serum directly preceding the metabolome studies. With respect to the identified candidate substrates, in particular the expression and activity of factors involved in glutamate/glutamine transport and metabolism have been shown to be responsive to thyroid state, with lower cellular glutamate uptake and utilization documented during hypothyroidism (38, 39). In support of this mechanism, we observed higher glutamate accumulation in human fibroblasts derived from healthy controls compared to those derived from patients with MCT8 deficiency, providing an independent *ex vivo* model that confirmed our findings in *Xenopus* oocytes. Since our *in vitro* and *ex vivo* studies focused on individual cell types, it is challenging to extrapolate these observations to the *in vivo* situation in which intermediate metabolism is regulated through a complex interplay of different organs. This is illustrated by previous nuclear magnetic resonance spectroscopy studies in *Mct8* knock-out mice revealing an increase in fractional enrichment of glutamate and glutamine in brain after infusion of 1-13C glucose, which is possibly the consequence of the hyperthyroid state in the peripheral organs, rather than the hypothyroid state in the brains of these animals (29). Future studies on the metabolome of patients with MCT8 deficiency may help to elucidate the role and importance of MCT8 in the regulation of intermediate metabolism *in vivo*.

It is not excluded that potential MCT8 substrates have been missed with our approach. For instance, certain metabolites that occur *in vivo* might have been absent in the incubation medium, or might not have been formed in oocytes due to the lack of appropriate enzymes. Moreover, we used a 2-times differential abundance threshold in the metabolome analysis for selection of candidate substrates,

which may exclude potential substrates that are transported with low efficacy, or bi-directionally. In light of the 10-times induction of T3 uptake in oocytes expressing MCT8, we reasoned that this threshold would allow discriminating relevant substrates from analytical noise. In addition, synthetic and pharmacological substances were not deliberately added to the incubation medium and can therefore not be excluded as substrates for MCT8. Nevertheless, several drugs such as rocuronium and cefodizime, likely originating from procedures preceding the experiment (i.e. culture medium, anesthetics), were detected as being differentially present in oocytes expressing MCT8 *versus* controls. Finally, some substrates may require specific conditions in order to be transported by MCT8 which were not met in the current experiment, such as a favorable concentration gradient, a specific pH or the presence of co-factors.

Since none of the naturally occurring metabolites that were identified in the metabolome analyses exhibit a 10-times difference between control and MCT8-overexpressing oocytes as was observed for T3, our studies support the current concept that the primary function of MCT8 is the cellular transport of T3 and T4. Therefore, it is reasonable to assume that therapeutic interventions should primarily focus on restoring thyroid hormone signaling. Indeed, compensation of defective thyroid hormone transport by T3 analogues that bypass MCT8, such as tri-iodothyroacetic acid (Triac), fully rescued the neuro-developmental signs in various animal models for human MCT8 deficiency (40-42). Although a recent clinical trial showed that Triac alleviates the signs of peripheral thyrotoxicosis in patients with MCT8 deficiency (43), a further trial is needed to reveal if Triac may also rescue neuro-development in human once treatment is installed early in life.

Taken together, our studies identified DIT and MIT as novel substrates for MCT8 and thereby expand the substrate specificity of MCT8. Furthermore, deficiency of MCT8 may affect important pathways involved in intermediate metabolism, the implications of which need to be further studied. Nevertheless, in line with the current paradigm, our studies support that the iodothyronines T3 and T4 are the major substrates of MCT8.

Acknowledgements

The authors are grateful for the technical assistance of Ramona EA van Heerebeek.

W.E.Visser is supported by an Erasmus University Fellowship.

E.C. Lima de Souza is supported by a grant from the Sherman Group, Sydney, Australia.

SUPPLEMENTAL MATERIALS

See next page.

Supplemental Tables

Supplemental Table S1 Overview of qPCR primers in 5’ to 3’ direction	
GAPDH_Fw	AATGACCCCTTTATTGAC
GAPDH_Rev	TCCACGACGTACTCAGCGC
LAT1_Fw	GAAGGGTGATGTGTCCAATCT
LAT_Rev	GCAAAGAGGCCGCTGTATAA
LAT2_Fw	CATCGTAGGGAACATCATCGG
LAT2_Rev	GAGTTCAGCATAGCAGAGGG

Supplemental Table S2 Overview of identified m/z ratios and their corresponding putative metabolites

	m/z	1h incubation MCT8/EV	P value	48h incubation MCT8/EV	P value	Metabolite	pathway
1	109,04	8,73	<0,001	2,73	0,011	Dihydrothymine	Intermediate thymine catabolism (pyrimidine metabolism)
						L-Cyclo(alanylglycyl)	*Present in plants (e.g. cocoa bean)*
2	118,05			2,98	0,038	L-Threonine	Amino acid
						L-Allothreonine	Stereo-isomer of L-threonine
						Aminoacetone	Alpha-amino ketone produced through threonine dehydrogenase-mediated oxydation of threonine during starvation
						Ammonioacetone	Result from protonation of aminoacetone
						L-Homoserine	Intermediate of methionine, threonine and isoleucine formation from L-aspartate in bacteria (not in mammals)
						3-Aminopropionaldehyde	Beta-alanine metabolism, product of polyamine and pyrimidine catabolism
						Hydroxyethyl glycine	*Antibiotic*
3	128,03	2,25	<0,001			L-Glutamic acid	Amino acid
						D-Glutamic acid	Amino acid (isomer)
						DL-Glutamate	D-glutamine and D-glutamate metabolism
						Pyroglutamic acid	Cyclized derivative of L-glutamate (glutamate - glutathione cycle)
						5-Oxoprolinate	Cyclized derivative of L-glutamate (glutamate - glutathione cycle)
						Pyrrolidonecarboxylic acid	Cyclized derivative of L-glutamate (glutamate - glutathione cycle)
						N-Methyl-D-aspartic acid (NMDA)	Produced from D-aspartate metabolism by NMDA synthase
						N-Acetylserine	Produced through N-acetylation of serine in eukaryotes
						N-Acryloylglycine	An acyl glycine, minor products in fatty acid metabolism
						L-4-Hydroxyglutamate semialdehyde	Intermediate in arginine and proline metabolism
						Pyrroline hydroxycarboxylic acid	Intermediate of arginine and proline metabolism
						1-Pyrroline-4-hydroxy-2-carboxylate	Intermediate of arginine and proline metabolism
						3-(Carboxymethylamino)propanoic acid	*Plants and pulsus*
						dimethadione	*Anticonvulsive drug*
						O-Acetylserine	*Intermediate in the biosynthesis of cysteine in bacteria and plants.*
4	145,06	2,20	<0,001	2,03	<0,001	L-Glutamine	Amino acid
						D-Glutamine	Amino acid (isomer)
						Alanylglycine	Di-peptide, product of protein breakdown
						Ureidoisobutyric acid	Intermediate thymine catabolism (pyrimidine metabolism)
5	171,00	0,04	0,043			Glycerol 3-phosphate	Glycerophospholipide metabolism, intermediate of glycolysis
						Beta-Glycerophosphoric acid	Glycerolipid metabolism
						Phenylglyoxylic acid	Phenylalanine metabolism and intermediate in xylene, styrene and ethylbenzene degradation
						Ethylphosphate	*Product of metabolism of organophosphorus pesticides via diethylphosphate*
						(E)-8-Hydroxy-2-octene-4,6-diynoic acid	*Present in mushrooms*
						4-Hydroxyphthalide	*Present in cereals*
6	*173,00*			*0,43*	*0,029*	*S-Methyl benzenecarbothioate*	*Flavouring agent (food additive)*
7	*173,003*			*0,43*	*0,029*	*(Z)-5-[(5-Methyl-2-thienyl)methylene]-2(5H)-furanone*	*Component of herbs and spices*
8	173,05	2,85	<0,001	4,73	0,0032	2-Aminoacrylic acid	By-product of thyroglobulin-liothyronine (T3) production
						Serinyl-Serine	Di-peptide, product of protein breakdown

Supplemental Table S2 (Continued)

9	179,05			2,02	0,0002	D-Fructose	Monosaccharide metabolism
						D-Glucose	Monosaccharide metabolism
						Allose	Monosaccharide metabolism
						D-Mannose	Monosaccharide metabolism
						D-Galactose	Monosaccharide metabolism
						D-Tagatose	Monosaccharide metabolism
						Beta-D-Galactose	Monosaccharide metabolism
						L-Galactose	Monosaccharide metabolism
						L-Sorbose	Monosaccharide metabolism
						Beta-D-Glucose	Monosaccharide metabolism
						L-Gulose	Monosaccharide metabolism
						Alpha-D-Glucose	Monosaccharide metabolism
						Dihydroxyacetone (dimer)	Monosaccharide metabolism, food additive
						3-Deoxyarabinohexonic acid	Medium-chain hydroxy acid
						Myoinositol	Inositol phosphate metabolism
						Scyllitol	Inositol phosphate metabolism
						Levoinositol	Inositol phosphate metabolism
						12-Tridecene-4,6,8,10-tetraynal	*Plant*
						Methionine sulfoximine	*Present in flour treated with NCl3*
10	207,03	2,06	<0,001			1,2-Dihydroxy-3-keto-5-methylthiopentene	Cysteine and methionine metabolism
11	*230,96*			*0,32*	*0,0024*	*3,5-Dichloro-4-hydroxy-2-methoxy-6-methylbenzoic acid*	*Food additive and present orthomycin antibiotics*
12	*272,08*	*2,78*	<0,001			*7-Aminonitrazepam*	*Benzodiazepine*
13	*275,02*	*2,92*	*0,015*	*2,69*	*0,011*	*Bis(2,5-dimethyl-3-furanyl) disulfide*	*Synthetic flavouring agent*
14	302,10	0,44	0,0098	0,40	0,014	N6-Methyladenosine	Methylation of adenine, nucleoside product of tRNA degradation
						3'-O-Methyladenosine	Methylation of adenine
						1-Methyladenosine	Methylation of adenine
						2'-O-Methyladenosine	Methylation of adenine
						5-Methylcytidine	Modification of tRNA
						Glycerophosphocholine	Choline derivative, part of the glycerophospholipide metabolism
15	313,11	4,99	<0,001	3,39	0,0001	7,8-Dihydropteroic acid	Dihydrofolate biosynthesis
						2-Hydroxyenterolactone	Polyphenol
						6'-Hydroxyenterolactone	Polyphenol
						4-Hydroxyenterolactone	Polyphenol
						4'-Hydroxyenterolactone	Polyphenol
						5-Hydroxyenterolactone	Polyphenol
						2'-Hydroxyenterolactone	Polyphenol
						7-Hydroxyenterolactone	Polyphenol
						6-Hydroxyenterolactone	Polyphenol
						(-)-3,4,9-Trimethoxypterocarpan	*Isoflavonoid derivative (present in herbs and spices)*
						2,3,9-Trimethoxypterocarpan	*Isoflavonoid derivative (present in peas)*
						2'-Hydroxy-4,4',6'-trimethoxychalcone	*Present in plants*
						5,8-Dimethoxychalepensin	*Present in plants*
						beta,2-Dihydroxy-4,6-dimethoxy-3-methylchalcone	*Present in tea*
						p-Hydroxyphenethyl trans-ferulate	*Present in plants*
16	*331,01*	*0,35*	*0,020*			*Diflubenzuron*	*Insecticide*
17	357,07	6,51	<0,001	3,98	<0,001	Naphthoherniarin	Naphthoquinones (present in herbs and spices)
18	431,86			0,14	0,0030	3,5-Diiodo-L-tyrosine	Thyroid hormone synthesis
19	*510,39*	*<0,01*	<0,001			*Rocuronium*	*Anaesthetic*
20	558,06			4,08	<0,001	Adenosine diphosphate ribose	Purine metabolism, intermediate in NAD metabolism
21	*605,00*	*8,95*	*0,030*			*Cefodizime*	*Antibacterial drug*
22	662,09			0,43	<0,001	Fenugreekine	Purine nucleotide sugar

Overview of candidate metabolites for MCT8 mediated transport based on the m/z ratios identified by metabolomic analyses in *Xenopus* oocytes (see (ref) and method section for selection criteria). Metabolites that are considered drugs, or specific to plants, herbs or spices are presented in italics.

Supplemental Figures

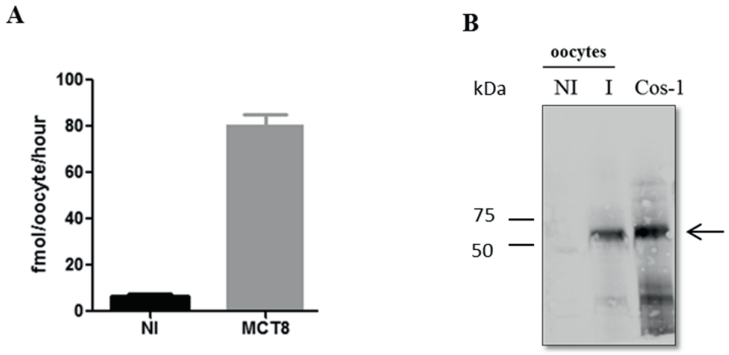

Supplemental Figure S1 (A) Uptake of T3 (10 nM) for 10 minutes in oocytes injected with MCT8 cRNA and non-injected (NI) oocytes. **(B)** Representative immunoblot on total lysates of control (NI) oocytes as well as oocytes injected with MCT8 cRNA. Total lysates of COS-1 cells transfected with MCT8 (COS-1) were taken along as a control. The band corresponding to the expected size of MCT8 monomers is indicated with an arrow.

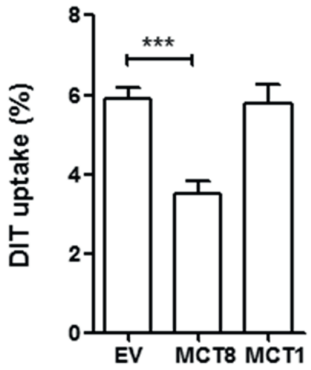

Supplemental Figure S2 Intracellular accumulation of DIT in COS-1 cells transiently transfected with pcDNA3 empty vector (EV), MCT8, or MCT1 after 30 minutes incubation at 37 °C, expressed relative to the amount of [125I]-DIT added to the cells at the start of incubation. Data are presented as the mean ± SEM of at least three independent experiments.

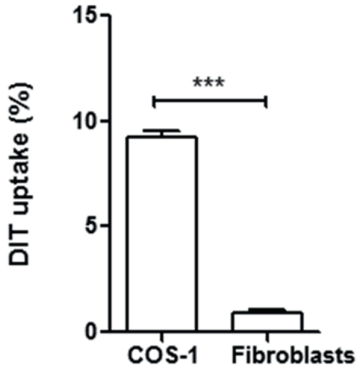

Supplemental Figure S3 Intracellular accumulation of DIT in COS-1 cells and human fibroblasts derived from healthy controls, after 30 minutes incubation at 37 °C. Data are expressed relative to the amount of [125I]-DIT that was added to the cells at the start of the incubation and presented as the mean ± SEM of three independent experiments. A paired T-test was used to assess for statistically significant differences (***, p<0.001).

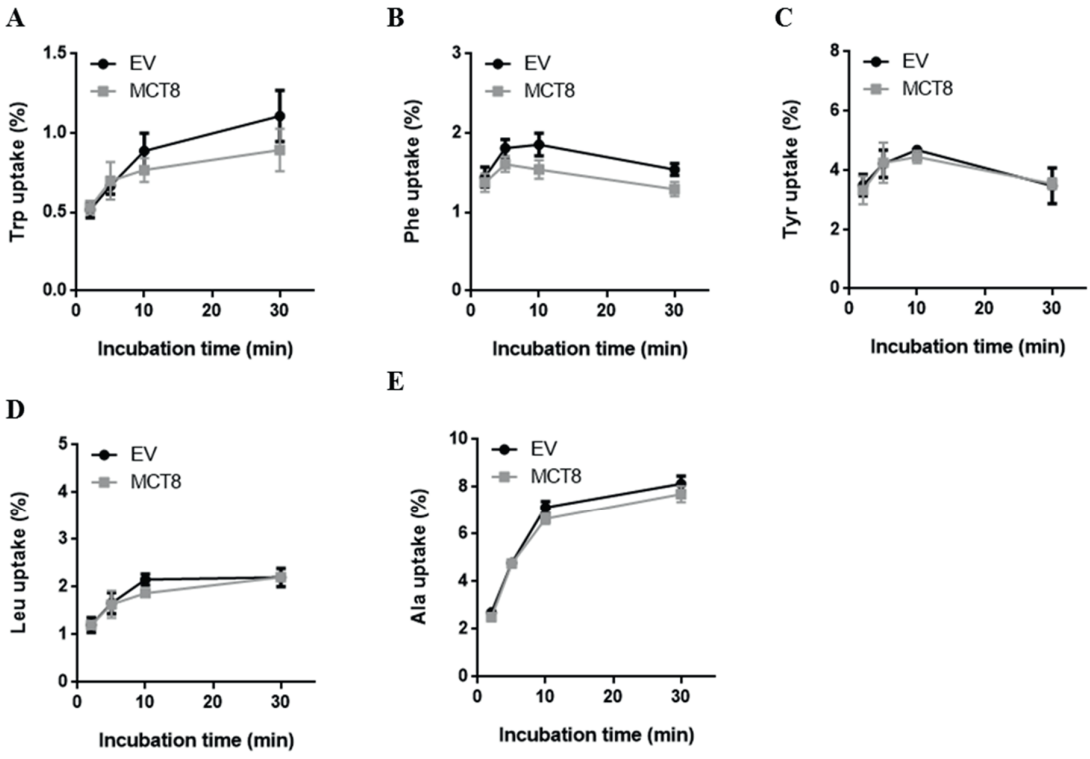

Supplemental Figure S4 Intracellular accumulation of indicated [3H]-labelled amino acids (**A-E**) at 10 µM concentrations in COS-1 cells transiently transfected with EV or MCT8, after incubation for 2, 5, 10 and 30 minutes at 37 °C. Differences between EV and MCT8-transfected cells were assessed for statistical significance by two way ANOVA with Bonferroni posttests. Data are expressed relative to the amount of [3H]-labelled amino acid that was added to the cells at the start of the incubation and presented as the mean ± SEM of at least three independent experiments.

REFERENCES

1. Yen PM, Ando S, Feng X, Liu Y, Maruvada P, Xia X. Thyroid hormone action at the cellular, genomic and target gene levels. Mol Cell Endocrinol. 2006;246(1-2):121-7.
2. Bianco AC, Dumitrescu A, Gereben B, Ribeiro MO, Fonseca TL, Fernandes GW, et al. Paradigms of Dynamic Control of Thyroid Hormone Signaling. Endocr Rev. 2019.
3. Hennemann G, Docter R, Friesema EC, de Jong M, Krenning EP, Visser TJ. Plasma membrane transport of thyroid hormones and its role in thyroid hormone metabolism and bioavailability. Endocr Rev. 2001;22(4):451-76.
4. Friesema EC, Ganguly S, Abdalla A, Manning Fox JE, Halestrap AP, Visser TJ. Identification of monocarboxylate transporter 8 as a specific thyroid hormone transporter. J Biol Chem. 2003;278(41):40128-35.
5. Kinne A, Kleinau G, Hoefig CS, Gruters A, Kohrle J, Krause G, et al. Essential molecular determinants for thyroid hormone transport and first structural implications for monocarboxylate transporter 8. J Biol Chem. 2010;285(36):28054-63.
6. Friesema EC, Kuiper GG, Jansen J, Visser TJ, Kester MH. Thyroid hormone transport by the human monocarboxylate transporter 8 and its rate-limiting role in intracellular metabolism. Mol Endocrinol. 2006;20(11):2761-72.
7. Friesema EC, Grueters A, Biebermann H, Krude H, von Moers A, Reeser M, et al. Association between mutations in a thyroid hormone transporter and severe X-linked psychomotor retardation. Lancet. 2004;364(9443):1435-7.
8. Dumitrescu AM, Liao XH, Best TB, Brockmann K, Refetoff S. A novel syndrome combining thyroid and neurological abnormalities is associated with mutations in a monocarboxylate transporter gene. Am J Hum Genet. 2004;74(1):168-75.
9. Friesema EC, Jansen J, Jachtenberg JW, Visser WE, Kester MH, Visser TJ. Effective cellular uptake and efflux of thyroid hormone by human monocarboxylate transporter 10. Mol Endocrinol. 2008;22(6):1357-69.
10. Abplanalp J, Laczko E, Philp NJ, Neidhardt J, Zuercher J, Braun P, et al. The cataract and glucosuria associated monocarboxylate transporter MCT12 is a new creatine transporter. Hum Mol Genet. 2013;22(16):3218-26.
11. Mol JA, Visser TJ. Synthesis and some properties of sulfate esters and sulfamates of iodothyronines. Endocrinology. 1985;117(1):1-7.
12. Moreno JC, Klootwijk W, van Toor H, Pinto G, D'Alessandro M, Leger A, et al. Mutations in the iodotyrosine deiodinase gene and hypothyroidism. N Engl J Med. 2008;358(17):1811-8.
13. Zevenbergen C, Meima ME, Lima de Souza EC, Peeters RP, Kinne A, Krause G, et al. Transport of Iodothyronines by Human L-Type Amino Acid Transporters. Endocrinology. 2015;156(11):4345-55.
14. Jackson VN, Price NT, Halestrap AP. cDNA cloning of MCT1, a monocarboxylate transporter from rat skeletal muscle. Biochim Biophys Acta. 1995;1238(2):193-6.
15. Groeneweg S, Friesema EC, Kersseboom S, Klootwijk W, Visser WE, Peeters RP, et al. The role of Arg445 and Asp498 in the human thyroid hormone transporter MCT8. Endocrinology. 2014;155(2):618-26.
16. Armour CM, Kersseboom S, Yoon G, Visser TJ. Further Insights into the Allan-Herndon-Dudley Syndrome: Clinical and Functional Characterization of a Novel MCT8 Mutation. PLoS One. 2015;10(10):e0139343.
17. Jansen J, Friesema EC, Kester MH, Schwartz CE, Visser TJ. Genotype-phenotype relationship in patients with mutations in thyroid hormone transporter MCT8. Endocrinology. 2008;149(5):2184-90.
18. Masnada S, Groenweg S, Saletti V, Chiapparini L, Castellotti B, Salsano E, et al. Novel mutations in SLC16A2 associated with a less severe phenotype of MCT8 deficiency. Metab Brain Dis. 2019.
19. Ramadan T, Camargo SM, Summa V, Hunziker P, Chesnov S, Pos KM, et al. Basolateral aromatic amino acid transporter TAT1 (Slc16a10) functions as an efflux pathway. J Cell Physiol. 2006;206(3):771-9.
20. Samuelsson M, Vainikka L, Ollinger K. Glutathione in the blood and cerebrospinal fluid: a study in healthy male volunteers. Neuropeptides. 2011;45(4):287-92.
21. Davey MR, Anthony P, Power JB, Lowe KC. Isolation, culture, and plant regeneration from leaf protoplasts of Passiflora. Methods Mol Biol. 2006;318:201-10.
22. Culhane AC, Perriere G, Considine EC, Cotter TG, Higgins DG. Between-group analysis of microarray data. Bioinformatics. 2002;18(12):1600-8.
23. Groeneweg S, van den Berge A, Meima ME, Peeters RP, Visser TJ, Visser WE. Effects of Chemical Chaperones on Thyroid Hormone Transport by MCT8 Mutants in Patient-Derived Fibroblasts. Endocrinology. 2018;159(3):1290-302.
24. Zevenbergen C, Meima ME, Lima de Souza EC, Peeters RP, Kinne A, Krause G, et al. Transport of Iodothyronines by Human L-Type Amino Acid Transporters. Endocrinology. 2015:en20151140.

25. Schwartz CE, May MM, Carpenter NJ, Rogers RC, Martin J, Bialer MG, et al. Allan-Herndon-Dudley syndrome and the monocarboxylate transporter 8 (MCT8) gene. Am J Hum Genet. 2005;77(1):41-53.
26. Capri Y, Friesema EC, Kersseboom S, Touraine R, Monnier A, Eymard-Pierre E, et al. Relevance of different cellular models in determining the effects of mutations on SLC16A2/MCT8 thyroid hormone transporter function and genotype-phenotype correlation. Hum Mutat. 2013;34(7):1018-25.
27. Visser WE, Jansen J, Friesema EC, Kester MH, Mancilla E, Lundgren J, et al. Novel pathogenic mechanism suggested by ex vivo analysis of MCT8 (SLC16A2) mutations. Hum Mutat. 2009;30(1):29-38.
28. Johannes J, Jayarama-Naidu R, Meyer F, Wirth EK, Schweizer U, Schomburg L, et al. Silychristin, a Flavonolignan Derived From the Milk Thistle, Is a Potent Inhibitor of the Thyroid Hormone Transporter MCT8. Endocrinology. 2016;157(4):1694-701.
29. Rodrigues TB, Ceballos A, Grijota-Martinez C, Nunez B, Refetoff S, Cerdan S, et al. Increased oxidative metabolism and neurotransmitter cycling in the brain of mice lacking the thyroid hormone transporter SLC16A2 (MCT8). PLoS One. 2013;8(10):e74621.
30. Mughal BB, Leemans M, Lima de Souza EC, le Mevel S, Spirhanzlova P, Visser TJ, et al. Functional Characterization of Xenopus Thyroid Hormone Transporters mct8 and oatp1c1. Endocrinology. 2017;158(8):2694-705.
31. Tietze F, Kohn LD, Kohn AD, Bernardini I, Andersson HC, Adamson MD, et al. Carrier-mediated transport of monoiodotyrosine out of thyroid cell lysosomes. The Journal of biological chemistry. 1989;264(9):4762-5.
32. Meinhold H, Beckert A, Wenzel KW. Circulating diiodotyrosine: studies of its serum concentration, source, and turnover using radioimmunoassay after immunoextraction. J Clin Endocrinol Metab. 1981;53(6):1171-8.
33. Faber J, Kirkegaard C, Meinhold H, Bregengaard C. Metabolic clearance and production of diiodotyrosine in healthy man. Scand J Clin Lab Invest. 1988;48(8):747-50.
34. Tan SA, Lewis JE, Berk LS, Wilcox RB. Extrathyroidal physiology of monoiodotyrosine in humans. Clin Physiol Biochem. 1990;8(3):109-15.
35. Dumitrescu AM, Liao XH, Weiss RE, Millen K, Refetoff S. Tissue-specific thyroid hormone deprivation and excess in monocarboxylate transporter (mct) 8-deficient mice. Endocrinology. 2006;147(9):4036-43.
36. Trajkovic M, Visser TJ, Mittag J, Horn S, Lukas J, Darras VM, et al. Abnormal thyroid hormone metabolism in mice lacking the monocarboxylate transporter 8. J Clin Invest. 2007;117(3):627-35.
37. Wellby ML, Hetzel BS. Demonstration of iodotyrosines in human plasma in response to thyroid stimulation. Nature. 1962;193:752-4.
38. Mendes-de-Aguiar CB, Alchini R, Decker H, Alvarez-Silva M, Tasca CI, Trentin AG. Thyroid hormone increases astrocytic glutamate uptake and protects astrocytes and neurons against glutamate toxicity. J Neurosci Res. 2008;86(14):3117-25.
39. Ardawi MS, Jalalah SM. Effects of hypothyroidism on glucose and glutamine metabolism by the gut of the rat. Clin Sci (Lond). 1991;81(3):347-55.
40. Kersseboom S, Horn S, Visser WE, Chen J, Friesema EC, Vaurs-Barriere C, et al. In vitro and mouse studies supporting therapeutic utility of triiodothyroacetic acid in MCT8 deficiency. Mol Endocrinol. 2014;28(12):1961-70.
41. Zada D, Tovin A, Lerer-Goldshtein T, Appelbaum L. Pharmacological treatment and BBB-targeted genetic therapy for MCT8-dependent hypomyelination in zebrafish. Dis Model Mech. 2016;9(11):1339-48.
42. Zada D, Tovin A, Lerer-Goldshtein T, Vatine GD, Appelbaum L. Altered behavioral performance and live imaging of circuit-specific neural deficiencies in a zebrafish model for psychomotor retardation. PLoS Genet. 2014;10(9):e1004615.
43. Groeneweg SP, R.P.; Moran, C.; Stoupa, A.; Auriol, F.; Tonduti, D.; Dica, A.; Paone, L.; Rozenkova, K.; Malikova, J.; van der Walt, A.; de Coo, IFM; McGowan, A.; Lyons, G.; Aarsen, F.K.; Barca, D.; van Beynum, I.M.; van der Knoop, M.M.; Jansen, J.; Manshande, M.; Lunsing, R.J.; Nowak, S.; den Uil, A.; Zillikens, M.C.; Visser, F.E.; Ambegaonkar, G.; Singh, Y.; de Rijke, Y.B.; Medici, M.; Bertini, E.S.; Depoorter, S.; Lebl, J.; Cappa, M.; de Meirleir, L.; Krude, H.; Craiu, D.; Zibordi, F.; Oliver Petit, I.; Polak, M.; Chatterjee, K.; Visser, T.J.; Visser, W.E. Effectiveness and safety of Triac in children and adults with MCT8 deficiency: an international, multicentre, single group, open-label, phase 2 trial. Lancet Diabetes Endocrinol. 2019;accepted.

Chapter 3

Identification of novel patients with MCT8 deficiency

Chapter

3.1

Clinical and Molecular Characteristics of SLC16A2 (MCT8) Mutations in Three Families with the Allan–Herndon–Dudley Syndrome

Francesca Novara*, **Stefan Groeneweg***, Elena Freri, Margherita Estienne, Paolo Reho, Sara Matricardi, Barbara Castellotti, W. Edward Visser, Orseta Zuffardi, Theo J Visser.

Human Mutat. 2017 Mar;38(3):260-264.

ABSTRACT

Mutations in the thyroid hormone transporter SLC16A2 (MCT8) cause the Allan–Herndon–Dudley Syndrome (AHDS), characterized by severe psychomotor retardation and peripheral thyrotoxicosis. Here, we report three newly identified AHDS patients. Previously documented mutations were identified in probands 1 (p.R271H) and 2 (p.G564R), resulting in a severe clinical phenotype. A novel mutation (p.G564E) was identified in proband 3, affecting the same Gly564 residue, but resulting in a relatively mild clinical phenotype. Functional analysis in transiently transfected COS-1 and JEG-3 cells showed a near-complete inactivation of TH transport for p.G564R, whereas considerable cell-type-dependent residual transport activity was observed for p.G564E. Both mutants showed a strong decrease in protein expression levels, but differentially affected V_{max} and K_m values of T3 transport. Our findings illustrate that different mutations affecting the same residue may have a differential impact on SLC16A2 transporter function, which translates into differences in severity of the clinical phenotype.

BRIEF REPORT

Thyroid hormone (TH) is critical for normal brain development. Since the metabolism and action of TH occurs intracellularly, transporter proteins are required to facilitate the transport of TH across the cell membrane (1). SLC16A2 (monocarboxylate transporter 8; MCT8; MIM# 300095) is the most specific TH transporter identified to date and is crucial for TH transport across the blood–brain barrier and into neuronal cells (2-6). Mutations in the *SLC16A2* gene result in the Allan–Herndon–Dudley syndrome (AHDS; MIM# 300523), characterized by a severe neurocognitive phenotype and abnormal serum TFTs (high T3, low rT3, low (F)T4, and borderline-high TSH) (7, 8). The neurocognitive phenotype comprises moderate–severe intellectual disability, axial hypotonia, dystonia, and progressive spasticity, leading to poor head control, inability to sit, stand, or walk independently, and an impaired or absent speech development (7, 8). Delayed myelination of central white matter is a key finding on brain MRI (9). Although intellectual and motor disabilities are often severe, mildly affected cases have been reported (10).

So far, over 100 mutations in *SLC16A2* have been associated with AHDS (11). Most of the clinically relevant missense mutations affect residues that are predicted to be located within transmembrane domains (TMDs) (6). Some mutations likely disturb substrate translocation (e.g., p.R445C and p.D498N), whereas others affect protein trafficking and stability (e.g., p.G282C and p.G558D) (12-14). Recent in vitro studies have shown that different substitutions of the same amino acid may differentially affect transporter function (15, 16). Here, we present three newly identified male AHDS patients with different mutations in SLC16A2: p.R271H, p.G564R, previously described by (10, 17), and the novel p.G564E mutation. Although the latter two mutations affect the same Gly564 residue, a striking difference in severity of the clinical phenotype was observed, which corresponded to the residual transport activities of these mutants determined in vitro.

This study was approved by the institutional review board of Foundation I.R.C.C.S. Neurological Institute “C. Besta”, Milan, Italy and written informed consent was obtained from all parents to use the medical information of their child for research purposes. A detailed patient description is provided in the **Supplemental Information**, pedigrees in **Supplemental Figure S1A** and historical TFTs of probands and family members in **Supplemental Table S1**.

In brief, proband 1 initially showed sustained poor head control and axial hypotonia, while distal hypertonia developed over the first year of life. At first presentation (2 years, 4 months), he showed a low body weight, muscular wasting, axial hypotonia, spastic dystonic tetraparesis (lower>upper limbs), and severe intellectual and motor disability (**Table 1**). Some vocalization was present. Brain MRI at the age of 2 years showed dilated ventricular and subarachnoid spaces, mild cerebellar vermis hypoplasia, thin corpus callosum, delayed myelination, and a mega cisterna magna (**Supplemental Figure S1B**). Although seizure-like episodes were reported since the age of 16 months, EEG showed, beside a poor organization of background activity, no epileptiform abnormalities. TFTs showed the “classical” AHDS pattern (**Table 1**). TFTs of mother were mildly abnormal (**Supplemental Table S1**).

Proband 2 showed growth and developmental delay from the first months of life with sustained axial hypotonia. Distal hypertonia became pronounced after 1 year. At first presentation (2 years of age), he had a low body weight (<P10), acquired microcephaly, severe axial hypotonia, spastic dystonic tetraparesis, and a severe intellectual and motor disability (**Table 1**). Verbal language and vocalization

were completely absent. Brain MRI showed a moderate delay in myelination and a thin corpus callosum at the age of 2 years (**Supplemental Figure S1B**). Although seizure-like episodes have been observed, these have never been detected on EEG. TFTs showed the classical AHDS pattern (**Table 1**), which was in retrospect already the case at the age of 7 months (**Supplemental Table S1**), prompting LT4 treatment until the age of 20 months without any improvement of symptoms. Also two maternal uncles have spastic tetraparesis, epilepsy, intellectual disability, and abnormal TFTs, and a similar phenotype was reported for two cousins of the mother (**Supplemental Table S1** and **Supplemental Figure S1**).

Proband 3 showed the mildest phenotype. Although a delay in psychomotor development was evident from the first months of life, head control was reached at 6 months and he was able to sit without support at 12 months and walk independently at 5 years. Records mention cyanosis at birth, but documented Apgar scores were 10/10. He first presented, at the age of 9 years, with peripheral dystonia, mild spastic features, extrapyramidal symptoms, and moderate to severe cognitive impairment (Griffiths scale: General Quotient 30; mental age 2 years and 8 months at chronological age 9 years and 3 months). He had a normal body weight (32 kg, P50) and no evident muscle wasting (**Table 1**). Language was limited to simple sentences. Brain MRI and EEG were normal. TFTs showed the classical AHDS pattern, even under LT4 treatment, initiated at the age of 20 months because of suspected central hypothyroidism (**Table 1** and **Supplemental Table S1**). TFTs of mother were mildly abnormal and her brothers were reported to have intellectual and motor disability and elevated serum FT3 levels (**Supplemental Table S1**).

Sequence analysis of the *SLC16A2* (NM_006517.3) gene revealed three different missense mutations: c.812G>A, p.R271H in proband 1; c.1690G>A, p.G564R in proband 2; and c.1691G>A, p.G564E in proband 3. In all cases, the mutation was inherited from the mother. Moreover, in family 2, the mutation was also present in the sister and both brothers of the mother. The p.R271H and the p.G564R mutations have been previously reported (10, 17), whereas the p.G564E is novel. Because of the striking difference in clinical phenotype associated with the mutations in the same G564 residue in probands 2 and 3, our functional analyses focused on these mutations (see **Supplemental Methods** for experimental details).

In addition to the patient mutations, we also studied the p.G564A mutation to determine if the Gly residue is critical for SLC16A2 function. These mutations were introduced in N-myc tagged wild-type (WT) SLC16A2 (further referred to as WT SLC16A2). The addition of the myc-tag did not interfere with SLC16A2 transport function (**Supplemental Figure S2**). Next, their impact on SLC16A2-mediated [^{125}I]T3 and [^{125}I]T4 transport was studied in transiently transfected COS-1 and JEG-3 cells. The p.G564A mutant showed a similar time-dependent increase in intracellular TH accumulation as WT SLC16A2 in both cell types, whereas the p.G564E mutant showed only 40%–60% of WT activity in COS-1 and 10%–15% in JEG-3 cells, depending on the incubation time (**Figure 1A–D**). In line with (10), the p.G564R mutant did not increase TH accumulation levels over background in both cell types.

Cellular TH accumulation is the resultant of TH uptake and efflux. To specifically study the effect on TH uptake capacity, cells were transiently co-transfected with WT or mutant SLC16A2 and the intracellular TH binding protein CRYM to reduce TH efflux. The p.G564A mutant showed similar TH uptake activity as WT in both cell lines, whereas residual TH uptake activity of the p.G564E mutant amounted to 40%–

50% of WT levels in COS-1 and 5%–10% in JEG-3 cells (**Figure 1E** and **F**). The p.G564R mutant did not increase TH uptake levels over background in both cell lines.

Table 1. Clinical findings at first presentation

	Proband 1	**Proband 2**	**Proband 3**
Age at first presentation	2 years, 4 months	2 years	9 years
Weight in kg (P)	12 (P10)	10 (<P10)	32 (P50)
Length in cm (P)	89 (P75)	81.5 (P25)	142 (P75)
Head circumference in cm (P)	49.5 (P50)	46.5 (P3)	53.5 (P75)
Acquired microcephaly	-	+	-
Failure to gain weight	+	+	-
Muscle wasting	progressive	nd	-
Axial hypotonia	+	+	+
Spastic features (hyperreflexia,	+	+	+
Peripheral and oromandibular dystonia	+	+	+
Pyramidal signs	+	+	+
Head balance	-	-	+
Ability to sit	-	-	+
Ability to walk	-	-	+
Speech development	some vocalization	-	vocalization
Cognitive < motor impairment	+	+	+
Serum FT3 in pg/ml (normal range)	7.51 (2.0-6.0)	8.7 (2.6-4.4)	6.6 (2.6-4.4) *
Serum FT4 in pg/ml (normal range)	5.8 (9.3-17.0)	5.1 (7.1-19.0)	7.4 (7.1-19.0) *
Serum TSH in mU/l (normal range)	2.66 (0.3-4.2)	2.9 (0.5-3.5)	2.5 (0.5-5.0) *
Seizures (on EEG)	-	-	-
Myelination on MRI (age performed)	delayed (2 years)	moderate delay (2 years)	normal (8 years)
Current treatment	physio-kinesiotherapy	physio-kinesiotherapy	LT4 mono therapy

Overview of clinical characteristics of the 3 index probands at time of first presentation. +: present, -: absent, nd: not determined, * indicates TFTs determined under LT4 treatment.

Immunoblotting revealed similar protein expression levels of WT SLC16A2 and the p.G564A mutant, whereas p.G564E and p.G564R protein levels were strongly reduced in both COS-1 and JEG-3 cells (**Figure 1G** and **H**). In COS-1 cells, all mutants were expressed as monomer and homo-oligomer. All constructs showed considerably lower expression levels in JEG-3 cells and the p.G564R and p.G564E proteins were nearly undetectable.

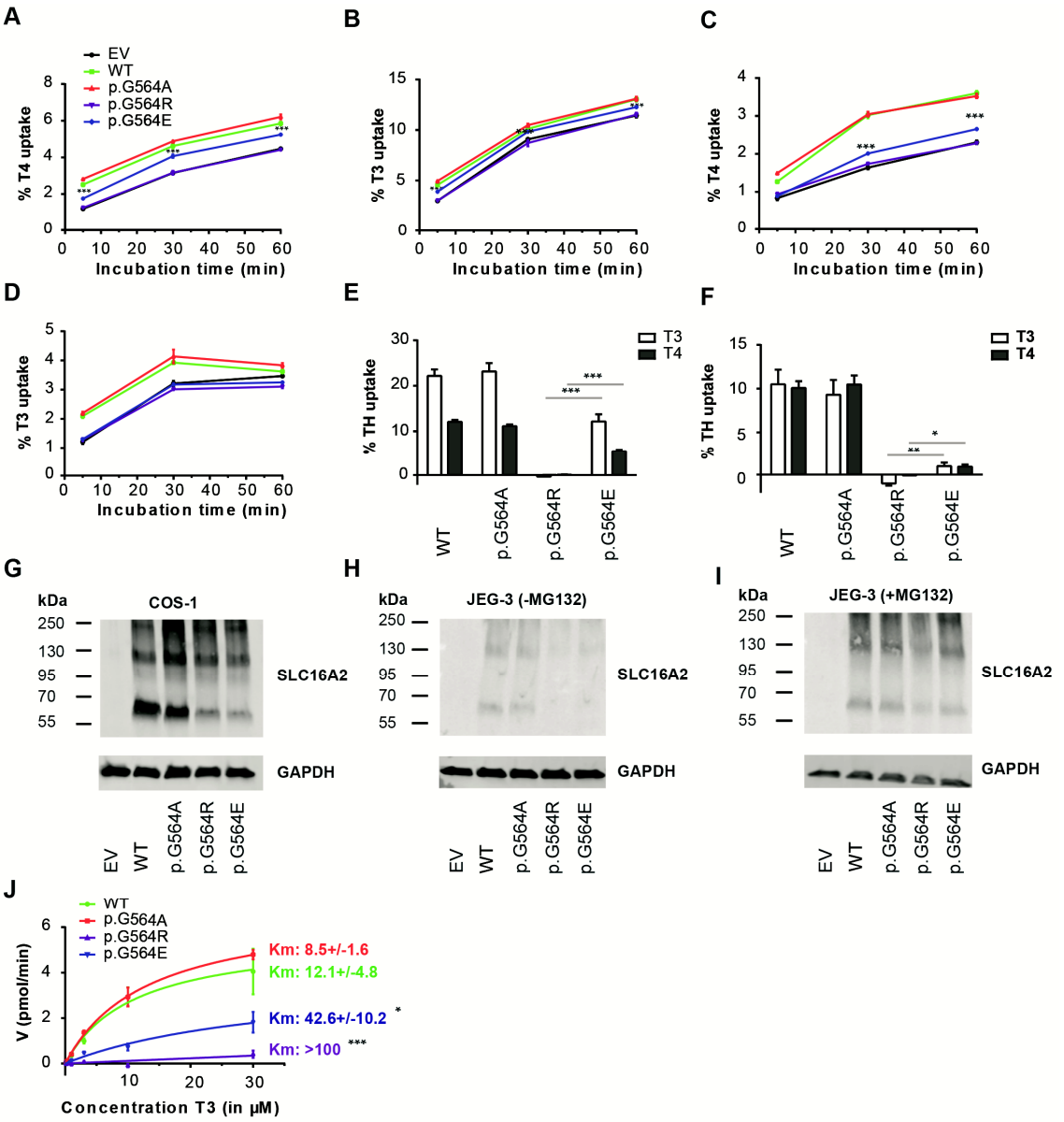

Figure 1 TH accumulation by COS-1 (**A, B**) and JEG-3 (**C, D**) cells, transiently transfected with pcDNA3 empty vector (EV), WT or mutant SLC16A2 after indicated incubation times at 37°C. TH uptake levels in COS-1 (**E**) and JEG-3 (**F**) cells transiently co-transfected with WT or mutant SLC16A2 and the intracellular TH binding protein hCRYM after incubation for 30 min at 37°C, corrected for background TH uptake levels observed in pcDNA3 EV transfected cells. All uptake levels are expressed relative to the amount of labeled TH added to the cells at the start of the incubation. All results are presented as means ± SEM (n = 2–4). Horizontal bars indicate group comparison with significant differences: *, $P < 0.05$; **, $P < 0.01$; ***, $P < 0.001$ using a one-way ANOVA analysis with a Bonferroni posttest. TH accumulation (**A–D**) and the TH uptake levels (**E** and **F**) of WT and p.G564A mutant SLC16A2 were not significantly different and significantly exceeded EV and p.G564R and p.G564E mutant SLC16A2 ($P < 0.001$; level of significance not shown in graph). Representative Western blots, performed in parallel, on total lysates of COS-1 (**G**) and JEG-3 cells (**H, I**) transfected with pcDNA3 EV, WT or mutant SLC16A2. JEG-3 cells were cultured in the absence (**H**) or presence (**I**) of the proteasomal inhibitor MG132 for 24 hr prior to lysate preparation. The N-terminal SLC16A2 antibody (3353) was used for SLC16A2 detection and GAPDH served as loading control. Bands at ~55 kDa and ~110 kDa represent SLC16A2 monomer and homodimer (n = 2–4). (**J**) Kinetic analysis of SLC16A2-mediated T3 transport in COS-1 cells in the absence of CRYM.

In the presence of the proteasomal inhibitor MG132 (24 hr), expression of the p.G564R and p.G564E proteins almost returned to WT levels (**Figure 1I**), suggesting an enhanced degradation rate. Subcellular localization in JEG-3 cells by confocal microscopy showed prominent cell membrane expression of WT and p.G564A mutant SLC16A2. Although the p.G564R and p.G564E showed some cell membrane localization, a large fraction was localized intracellularly (**Supplemental Figure S3**).

Finally, the impact on T3 transport kinetics was studied in transiently transfected COS-1 cells in the absence of CRYM. WT and p.G564A mutant SLC16A2 showed similar apparent K_m and V_{max} values (**Figure 1J**). The estimated K_m of the p.G564E mutant was threefold higher compared to WT, while the apparent V_{max} was clearly reduced. Estimated K_m values of the p.G564R mutant were even higher compared to p.G564E, whereas V_{max} was severely reduced (**Figure 1J**).

Here, we described three newly diagnosed AHDS patients with different underlying SLC16A2 mutations of which two affect the same Gly564 residue: p.G564R (proband 2) and p.G564E (proband 3). Interestingly, the p.G564E mutation resulted in a milder clinical phenotype, which corresponded to the residual transport activities of these mutants determined in vitro. Our data suggest that the replacement of the small neutral Gly564 residue by larger charged residues (Arg, Glu) not only reduces the stability of SLC16A2 but also has differential effects on its transport function.

Probands 2 shows the classical AHDS phenotype with severe intellectual and motor disability, whereas proband 3 is relatively mildly affected. Moderate–severe delay in myelination of central white matter was present in proband 2 at the age of 2 years, whereas myelination appeared normal in proband 3 at 8 years. Whether this accounts for the observed phenotypical differences is uncertain. Gradual normalization of myelination on brain MRI has been observed (18), whereas persistent hypo-myelination was found by post-mortem brain analyses (19). Both probands show extrapyramidal symptoms, most importantly dystonic features, once more underlining that the movement disorder comprises an important clinical component of AHDS (9).

Interestingly, also TFTs of proband 3 (without LT4 treatment) appear less abnormal than for proband 2, although age and assay-dependent differences cannot be excluded. Nevertheless, mutations such as p.G546E with a relatively low impact on SLC16A2 function may result in less T4 accumulation in the thyroid and less pronounced upregulation of D1 activity in peripheral tissues, both suggested to account for the abnormal TFT pattern in AHDS (20, 21). The presence of a normal body weight (P50) may indeed be indicative for a milder peripheral phenotype in proband 3, as a low body weight has been classically regarded as an important and objective consequence of abnormal thyroid function in AHDS.

Although, the residual transport activity of the p.G564E mutant greatly differed between COS-1 (40%–50%) and JEG-3 cells (5%–10%), the p.G564R mutant was functionally inactive in both (**Figure 1**). Previous studies have attributed this cell-type-dependent impact to differences in the effect of mutations on protein expression levels and subcellular localization (12, 22). Although the p.G564R and p.G564E mutations reduced SLC16A2 protein expression in both cell lines, mutant protein levels were very low in JEG-3 cells, which may, at least partially, explain the observed cell-type-dependent impact of the p.G564E mutation on transport activity.

Nevertheless, the effects of the p.G564E and p.G564R mutations on protein abundance and trafficking appear to be similar and thus do not provide an explanation for the observed differences in severity of

the clinical phenotype. This may suggest that these mutations differentially affect substrate translocation. Indeed, kinetic analysis confirmed that both mutations had a differential impact on T3 transport, with considerably lower apparent V_{max} and higher K_m values for the p.G564R mutant. Although the reduction in protein expression levels may account for the reduction in apparent V_{max} of both mutants, it is not expected to affect the apparent K_m value.

In view of the different effects of SLC16A2 mutations in JEG-3 and COS-1 cells, we speculate that these mutations also have differential effects on TH transport in different tissues in vivo. Although milder than the clinical phenotype associated with the p.G564R mutation, patients with the p.G564E mutation still display a profound AHDS phenotype. Our in vitro studies suggest that JEG-3 cells more so than COS-1 cells represent the preferable system to determine clinically relevant consequences of SLC16A2 mutations.

Interestingly, the p.G564A mutant showed normal protein expression levels, subcellular localization and TH transport activity. This is in line with the strong conservation of a small neutral residue at this position in all MCTs (Ala in SLC16A4, 5 and7, Ser in SLC16A1, and Gly in all other SLC16 family members) (6), suggesting that a small uncharged residue at this position is required for optimal protein structure and function. Although SLC16A2 has not been crystallized, an SLC16A2 protein homology model predicts TMD12 at the outside of the protein, predominantly facing the lipid bilayer or other TMDs (6). Substitution of Gly564 by a larger, charged residue is therefore not likely to directly interfere with substrate interactions, but rather cause unfavorable interactions with the lipid bilayer or surrounding residues. In line with our observations, this may destabilize protein structure. In turn, this may also affect the orientation of substrate interacting residues, explaining the increase in K_m values of both mutants. The importance of TMD12 is further illustrated by the inactivating effects of the p.G558D and p.L568P mutations, which also strongly reduce SLC16A2 protein levels (12). Interestingly, the apparent K_m value of the p.L568P mutant was found to be similar to WT SLC16A2 (12); the apparent K_m value of the p.G558D mutant has not been determined.

Although the abnormal TFT pattern is characteristic for AHDS, recognition of AHDS based on clinical symptoms is still challenging, as growth and developmental delay are general signs of neurological pathology in children. As for our probands, this often results in a delayed diagnosis, hampering adequate genetic counseling and initiation of therapeutic interventions. Importantly, previous reports have shown that the abnormal TFTs and hence the peripheral thyrotoxicosis can be restored by combination therapy with propylthiouracil (PTU) and LT4 (23). However, beneficial effects on the neurological symptoms were not observed. Mono-therapy with LT4 is strongly discouraged, since it worsens thyrotoxic symptoms. Beneficial effects on TFTs have also been observed in AHDS patients treated with the T3 analogue DITPA (24). Therapeutic effects of the even more potent T3 analogue Triac are currently under investigation. Since these compounds have T3-like effects, but do not rely on SLC16A2 for cellular transport, early treatment initiation may have beneficial effects on neurological outcomes. We therefore stress the importance of measurement of TFTs, most importantly including (F)T3, in all male patients presenting with intellectual and motor disabilities.

In summary, we have identified three AHDS patients with different mutations in the *SLC16A2* gene, two of which affected the same residue (Gly564). The p.G564E mutation is a novel mutation, with considerable residual TH transport activity in comparison with the p.G564R mutant, which is in line with the striking difference in severity of the clinical phenotype of both patients.

SUPPORTING INFORMATION

Supplemental methods

Serum analyses

FT3, FT4 and TSH levels were determined by electrochemiluminescence immunoassay (ECLIA) using ECLusys FT3, FT4 and TSH (Roche Diagnostics GmbH, Milan, Italy) and confirmed with the chemiluminescence immunoassay on ARCHITECT ci16200 Integrated System (Abbott Diagnostics, Abbott Park, Illinois, U.S.A.).

Mutational analysis

EDTA blood was obtained from the patients after informed consent of the parents. Genomic DNA was isolated using QIAamp DNA Blood Mini Kit (Qiagen, Milan, Italy) according to the manufacturer's protocol. All six *SLC16A2* coding exons and exon/intron boundaries were amplified by PCR using Go Taq(R) Flexi DNA Polymerase (Promega, Milan, Italy). Sequence primers and experimental conditions are available on request. Positions of the mutations are determined using the NM_006517.3 reference sequence and uses +1 as the A of the ATG translation initiation codon of the long SLC16A2 translational isoform, with the initiation codon as codon 1. Identified mutations have been submitted to Leiden Open Variation Database (LOVD), http://databases.lovd.nl/shared/transcripts/00019120.

Materials

[^{125}I]T_3 and [^{125}I]T_4 were synthesized as described previously (25). Unlabeled iodothyronines, BSA, D-glucose and Na_2SeO_3 were obtained from Sigma-Aldrich (Zwijndrecht, The Netherlands [NL]); culture dishes from Corning (Schiphol, NL); culture medium from Invitrogen (Bleiswijk, NL); transfection reagent X-tremeGENE 9 from Roche Diagnostics (Almere, NL); SDS gels from Thermo Fisher (Landsmeer,NL); nitrocellulose membrane from GE Healthcare (Eindhoven, NL); restriction enzymes from New England Biolabs (Ipswich, MA); rabbit polyclonal antibody 3353 against human SLC16A2 amino acids 75 to 155 from Sigma Aldrich (Manufacturer: Atlas Antibodies, Stockholm); mouse monoclonal glyceraldehyde-3-phosphate dehydrogenase antibody Mab 374 from Merck Millipore (Amsterdam, NL); IRDye680-labeled goat anti-rabbit IgG and IRDye800-labeled goat anti-mouse IgG antibodies from LI-COR (Leusden, NL); Alexa Fluor 488-labeled goat anti-rabbit IgG and Alexa Fluor 633-labeled goat anti-mouse IgG antibodies from Invitrogen; Vectashield H-1200 containing DAPI from Brunschwig (Amsterdam, NL).

Plasmids

Cloning of human SLC16A2 in pcDNA3, and of the human cytosolic TH-binding protein CRYM in pSG5 has been described previously (26, 27). A myc tag was introduced at the N-terminal end of SLC16A2 using standard PCR with primers mycMCT8fwd and mycMCT8rev (**Supplemental Table S2**). The PCR product was cloned into the pcDNA3 vector using HindIII and XbaI restriction enzymes. Myc-SLC16A2 is also referred to as wild-type (WT) SLC16A2. We introduced the p.G564R, p.G564E and p.G564A mutations into myc-SLC16A2 using the QuickChange XL-II Site-Directed Mutagenesis kit (Stratagene, Amstelveen, NL) according to the manufacturer's protocol; primers are listed in **Supplemental Table S2**. DNA sequencing confirmed the presence of the myc tag and introduced mutations, and the absence of unintended mutations.

Cell culture and transfection

COS1 and JEG3 cells were cultured in 6- or 24-well dishes in DMEM/F12 medium, containing 9% heat-inactivated fetal bovine serum, 2% penicillin/streptomycin, and 100 nM Na_2SeO_3. Cells were transfected at 70% confluence, and all experiments were carried out 48 hours after transfection. For TH uptake-experiments, cells were seeded in 24-well dishes and co-transfected in duplicate with 20 ng WT or mutant SLC16A2 and/or 100 ng pSG5-CRYM. The total amount of plasmid was adjusted to 200 ng using pcDNA3 empty vector (EV). For Western blotting, cells were seeded in 6-well dishes and transfected with 500 ng WT or mutant SLC16A2 or EV. X-tremeGENE9 was used as the transfection agent according to manufacturer's protocol. We previously described the absence of significant differences in transfection efficiency between WT SLC16A2 and mutants (17).

TH uptake

TH uptake-experiments were performed as previously described [Groeneweg et al., 2013]. Briefly, cells were washed with incubation medium (Dulbecco's PBS [D-PBS] plus 0.1% BSA and 0.1% D-glucose) and incubated for the indicated times with 1 nM (5×10^4 cpm) [^{125}I]T_4 or [^{125}I]T_3 in 375 µl incubation medium at 37 C. Finally, cells were washed once with incubation medium and lysed with 0.1 M NaOH. Radioactivity in the lysates was measured with a γ-counter. For kinetic analysis, indicated concentration of unlabelled T3 was added to the incubation mix.

Western blotting

Western blots were carried out as previously described (14). JEG3 and COS1 cells cultured in 6-well plates were transfected with 500 ng WT or mutant SLC16A2. Two days after transfection, cells were rinsed with D-PBS, collected in 100 mM sodium phosphate, 2 mM EDTA, pH 7.2 (P100E2), and sonicated on ice. SDS loading buffer containing 40 mM DTT was added to 25 µg protein and incubated for 10 minutes at 80 C. Samples were separated on a 10% SDS-PAGE gels (precast gels; Thermo Scientific, Etten-Leur, NL), blotted to nitrocellulose membranes, and probed with N-terminal SLC16A2 antibody. A GADPH antibody was used as a loading control. IRDye680 goat anti-rabbit and IRDye800 goat anti-mouse antibodies 1:20,000 (LI-COR, Bad Homburg, Germany) were used as secondary antibody. Antibodies were detected with Odyssey™ Infrared Detection System (LI-COR).

Immunocytochemistry

Immunocytochemistry was carried out as previously described (14). JEG-3 cells were cultured on 20 mm glass coverslips coated with poly-D-lysine (Sigma) and transfected with 500 ng WT or mutant SLC16A2. After 24 hours, cells were fixed for 20 minutes at 37 C with 4% paraformaldehyde, permeabilized for 5 minutes at room temperature (RT) with 0.2% triton X-100 in PBS. Samples were blocked for 1 hour at RT in PBS containing 2% BSA and incubated overnight with N-terminal SLC16A2 antibody 3353 (1:1000, Sigma) and mouse monoclonal ZO-1 antibody (1:500, Invitrogen) at 4 C. After secondary staining with goat anti-rabbit Alexa Fluor 488 and goat anti-mouse Alexa 633 (Invitrogen), cover slips were mounted with Prolong Gold containing DAPI (Invitrogen). Samples were examined on a Zeiss Meta 510 using Zeiss LSM software (Carl Zeiss B.V., Sliedrecht, NL).

Statistical analysis

All uptake and efflux results are expressed as means ± SE of at least 2 to 4 separate experiments performed in duplicate. Statistical significance was determined as indicated in the figure legends. Apparent Km and Vmax values were determined by Michaelis-Menten analysis using the GraphPad 6 program.

Detailed patient description

Family 1 – (pedigree)

Proband 1 is the unique child of healthy and non-consanguineous parents with a negative family history for neurological diseases, born at 41 weeks of gestation by caesarean section because of macrosomia (Supp. Fig. S1A). Birth weight was 4570 grams (P97), birth height as 53 centimeters (P50-P75) and head circumference was 38.5 centimeters (P98) and Apgar scores were 9/10. Historical data mentioned poor head control at the age of 4 months and dilatation of cerebral ventricles was noted on brain ultrasound. At the age of 8 months, generalized hypotonia with tetraparesis became evident and neurological examination revealed bilateral alternating esophoria, mild muscular wasting at all limbs, marked axial hypotonia combined with distal hypertonia (more evident to lower limbs), asymmetric motility, and forearm dystonia with hyperreflexia. At the age of 16 months, the first seizure was reported during sleep which protracted for 30 minutes with slow recovery. At the age of 19 months, brain MRI showed dilated ventricular and subarachnoid spaces of the frontotemporal region, mildly dilated 4th ventricle, mild cerebellar vermis hypoplasia, thin corpus callosum, delayed myelination and mega cisterna magna (not shown).

He came to our attention at the age of 2 years and 4 months with a relatively low body weight (12 kg: P10), normal head circumference (49.5 cm: P50) and length (89 cm: P75) and progressive muscular wasting and failure to gain weight were reported. Neurological examination revealed mild bilateral alternating esophoria and mild horizontal nystagmus, oromandibular dystonia with mild drooling, spastic and dystonic tetraparesis, more pronounced in lower limbs and on the right side, mild articular retractions of the lower limbs (popliteal, ischiocrural and ankle), and pyramidal signs (**Table 1**). He had no head control due to severe axial hypotonia and was unable to sit without support. In contrast to the severe motor disability, some vocalization and a good attention and interest for objects were present.

Blood tests including gas analysis were normal except for elevated glutamic acid transaminase (54 U/L). ECG and fundus oculi were normal. EEG showed a poor organization of background activity without epileptiform abnormalities, while spontaneous or auditory stimulus-evoked jerks (sursaut-like) were detected during sleep. Brain MRI was unchanged compared with that obtained at 19 months of age, and myelination was clearly delayed (**Supplemental Figure S1B**). These findings were not compatible with the diagnosis of cerebral palsy or other progressive encephalopathies. At the age of 3 years, abnormal TFTs were suggestive for AHDS (**Table 1** and **Supplemental Table S1**). TFTs of the healthy mother were mildly abnormal (**Supplemental Table S1**). The patient was treated with physio-kinesiotherapy.

Family 2 - (pedigree)

Proband 2 is the 3rd child of healthy and non-consanguineous parents and has 2 healthy sisters (Supp. Figure S1A). He was born at term by cesarean section (as his 2 older sisters) with a birth weight of 2,840 g (P10), height of 48 cm (P3-P10) and a head circumference of 35 cm (P50). Apgar scores were 10/10. Patient was referred to our center at the age of 2 years because of growth and developmental delay, already evident from the first months onwards, acquired microcephaly, hypotonia and progressive spastic tetraparesis starting at one year of age. In addition, blood tests at the age of 7 months showed abnormal TFTs (**Supplemental Table S1**). Previous ECG recordings were normal, while EEG recordings during wake and sleep had shown slow background delta activity of high amplitude and rare slow waves on the left occipital region. Brain MRI showed a thin corpus callosum and a moderately delayed myelination.

At first presentation (2 years of age) we found a low body weight (10 kg; <P10), normal length (81.5 cm; P25), and small head circumference (46.5 cm; P3). Neurological examination showed alternating esophoria, oromandibular dystonia, spastic dystonic tetraparesis, more pronounced on the right side, and pyramidal signs (**Table 1**). Marked postural impairment and absence of head control were evident due to axial hypotonia. During passive mobilization a "sursaut" reaction and sudden protracted hyperextension of 4 limbs, without consciousness impairment, were observed. Fundus oculi was normal. The child was quiet, with a good gaze contact, friendly and smiling. Verbal language or vocalization were absent. Both cognitive and motor development were severely impaired. The patient was treated until the age of 20 months of age with levothyroxine (LT4), without any change in clinical features. The treatment was then withdrawn and physio-kinesiotherapy was started. At 2 years of age, blood examination, including gas analysis, were normal except for abnormal serum TFTs, which were again characteristic for AHDS (**Table 1** and **Supplemental Table S1**). Brain MRI confirmed mild white matter maturation delay (moderate delay in myelination) and a thin corpus callosum (**Supplemental Figure S2**).

At the age of 3 years, parents had noticed frequent paroxysmal non-epileptic episodes characterized by global hypertonia protracted up to 30 seconds, sometimes serially, with mild tremor of upper limbs, without other symptomatology or detectable abnormalities on the EEG. At the age of six years, he was still not able to walk.

Two maternal uncles were affected by spastic tetraparesis, epilepsy and intellectual disability and the maternal aunt suffers from depression and anxiety disorder. TFTs of the two maternal uncles are shown in **Supplemental Table S1**. Two male cousins of the mother, presenting with spastic tetraparesis and intellectual disability, died at the age of 6 years. TFTs are unavailable for these family members.

Family 3 (pedigree)

Proband 3 was the first child of healthy and non-consanguineous parents (**Supplemental Figure S1A**). He was born at term with a birth weight of 3,600 g (P50) and birth length of 52 cm (P50). Although cyanosis was reported at birth, Apgar scores of 10/10 were documented. A delay in psychomotor development was evident from the first months of life, but head control was reached after 6 months and he was able to sit without support after 12 months. In the first months of his life, he slept much and was considered "a very quiet child". At 16 months of age, he was suspected to have central hypothyroidism and was treated with LT4 (**Supplemental Table S1**). Even though he was treated with

LT4, TFTs were still characteristic for AHDS at the age of 20 months (**Supplemental Table S1**). He started to walk independently at the age of 5 years. Moderate to severe cognitive impairment was reported at this age. Language delay was also present. When he was 8 years old, brain MRI showed no abnormalities.

He came to our attention at the age of 9 years and presented with a relatively normal body weight (32 kg, P50), length (142 cm, P75) and normal head circumference (53.5 cm, P75) and no evident muscle wasting. He showed spastic tetraparesis, extrapyramidal symptoms (hypomimia, open mouth with drooling, slowness of movement, difficulty of walking and impaired postural reactions) and moderate to severe cognitive impairment (Griffiths scale: General Quotient 30; mental age 2 years and 8 months at chronological age 9 years and 3 months) (**Table 1**). Language was limited to simple sentences. Brain MRI, EEG, fundus oculi, and evoked visual potentials were normal at that time. During hospitalization, TFTs were again abnormal, even though he was treated with 25 µg LT4/day (Supp. Table S1). Neurological and cognitive condition have been stable over time.

Two maternal uncles (current age 45 and 43 years) also suffer from spastic tetraparesis and cognitive delay and showed elevated serum FT3 levels (**Supplemental Table S1**). The other TFTs are not available. Both uncles have never been genetically tested for mutations in SLC16A2 nor evaluated in our hospital. Clinical characteristics and genetic tests are therefore unfortunately not available.

Supplemental Tables

Supp. Table S1. Overview of historical serum TFTs in probands and family members

	Age	FT4 (pg/mL)	FT3 (pg/mL)	TSH (mU/L)
Family 1				
Proband (II 1)	3 years	5.8 (9.3-17.0)	7.51 (2.0-6.0)	2.66 (0.3-4.2)
Mother (I 1)		8.0 (9.3-17.0)	4.07 (2.0-4.4)	3.79 (0.3-4.2)
Family 2				
Proband (III 1) *	7 months	5.2 (8.0-19.0)*	8.0 (1.8-4.2)*	2.5 (0.4-4.0)*
	2 years	5.1 (7.1-19.0)	8.7 (2.6-4.4)	2.9 (0.5-3.5)
Mother (II 4)		6.4 (7-14.8)	2.65 (1.71-3.71)	1.48 (0.45-3.5)
Uncle 1 (II 1)		5.2 (7-14.8)	3.79 (1.71-3.71)	1.34 (0.45-3.5)
Uncle 2 (II 2)		4.5 (7-14.8)	2.92 (1.71-3.71)	3.06 (0.45-3.5)
Family 3				
Proband (III 1)	16 months	7.1 (8.0-19.0)	4.9 (1.8-4.2)	4.1 (0.4-4.0)
	20 months	7.0 (8.0-19.0)*	4.9 (1.8-4.2)*	4.1 (0.4-4.0)*
	9 years	7.4 (7.1-19.0)*	6.6 (2.6-4.4)*	2.5 (0.5-5.0)*
Mother (II 4)		8.0 (8.0-19.0)	5.7 (1.4-4.2)	3.6 (0.4-6)
Uncle 2 (II 2)			5.4 (2.3-4.2)	
Uncle 3 (II 3)			6.7 (2.3-4.2)	

*) Determined under LT4 supplementation therapy.

Supp. Table S2. Overview of primers used for generation of myc- SLC16A2 and mutants

Primer name	Primer sequence (5`to 3`)
G564R_Fwd	TGCCCCCCATCATCAGGGCTGTAATCCTC
G564R_Rev	GAGGATTACAGCCCTGATGATGGGGGGCA
G564E_Fwd	GCCCCCCATCATCGAGGCTGTAATCCTCT
G564E_Rev	AGAGGATTACAGCCTCGATGATGGGGGGC
G564A_Fwd	CCCCCCATCATCGCGGCTGTAATCCTC
G564A_Rev	GAGGATTACAGCCGCGATGATGGGGGG
mycMCT8_Fw	GATAAGCTTCAGAAATGGAACAAAAACTCATCTCAGAAGAGGATCTGGCGCTGCAAAGC
mycMCT8_Re	ATCTCTAGATTAGATTGGTTCCTCAGGGTTGGG

Supplemental Figures

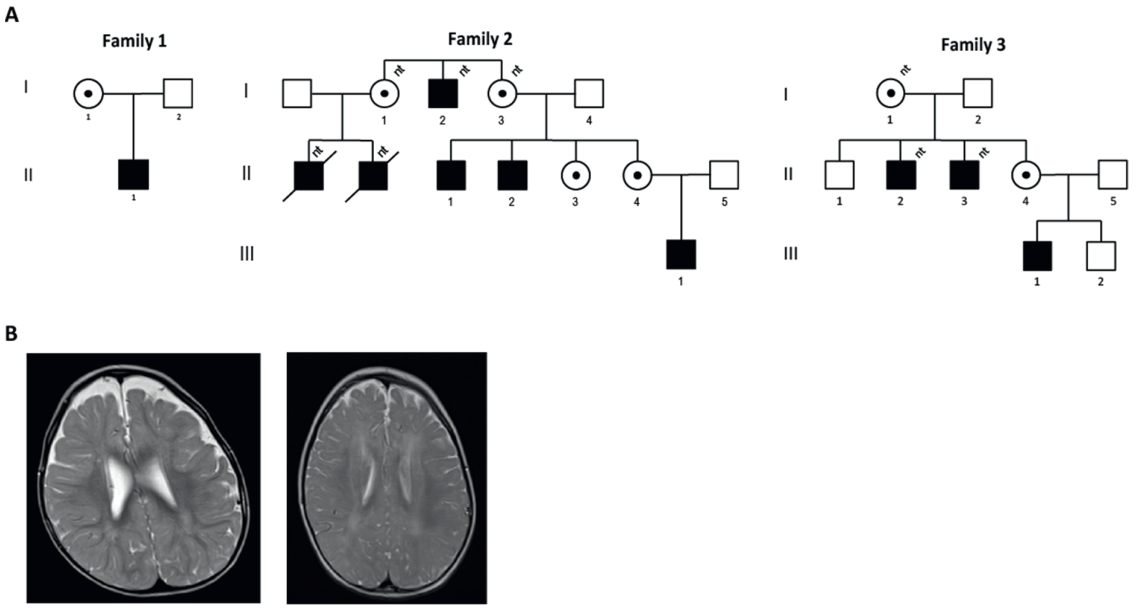

Supplemental Figure S1: Pedigrees of the three families and MRI scans of two probands. (A) In the pedigrees, black squares represent affected males and the circles with a dot represent heterozygous female carriers. Crossed black squares represent the two deceased uncles of proband 2. nt: TFTs not tested. (B) T2 weighted brain MRI images of proband 1 (age 2 years) on the left and proband 2 (age 2 years) on the right. Delayed myelination is visible in both patients.

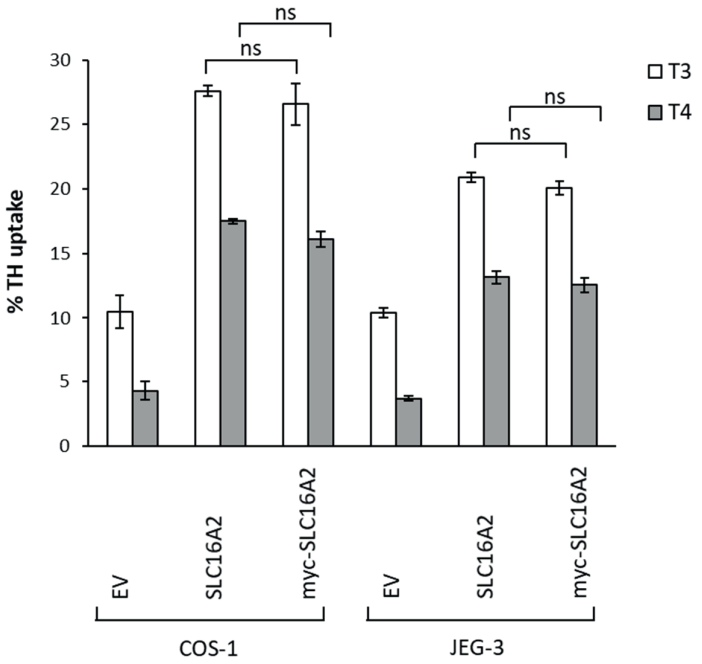

Supplemental Figure S2 TH transport by SLC16A2 and myc- SLC16A2. COS-1 or JEG-3 cells co-transfected with pcDNA3 empty vector (EV), SLC16A2-pcDNA3 or myc-SLC16A2-pcDNA3 plus CRYM-pSG5 were incubated for 30 minutes at 37ºC with 1 nM [^{125}I]T3 or [^{125}I]T4. Uptake is expressed as percentage of added radioactivity and presented as means ± SEM (n=2). One-way ANOVA analysis with a Bonferroni posttest indicated no significant differences between SLC16A2 and myc- SLC16A2.

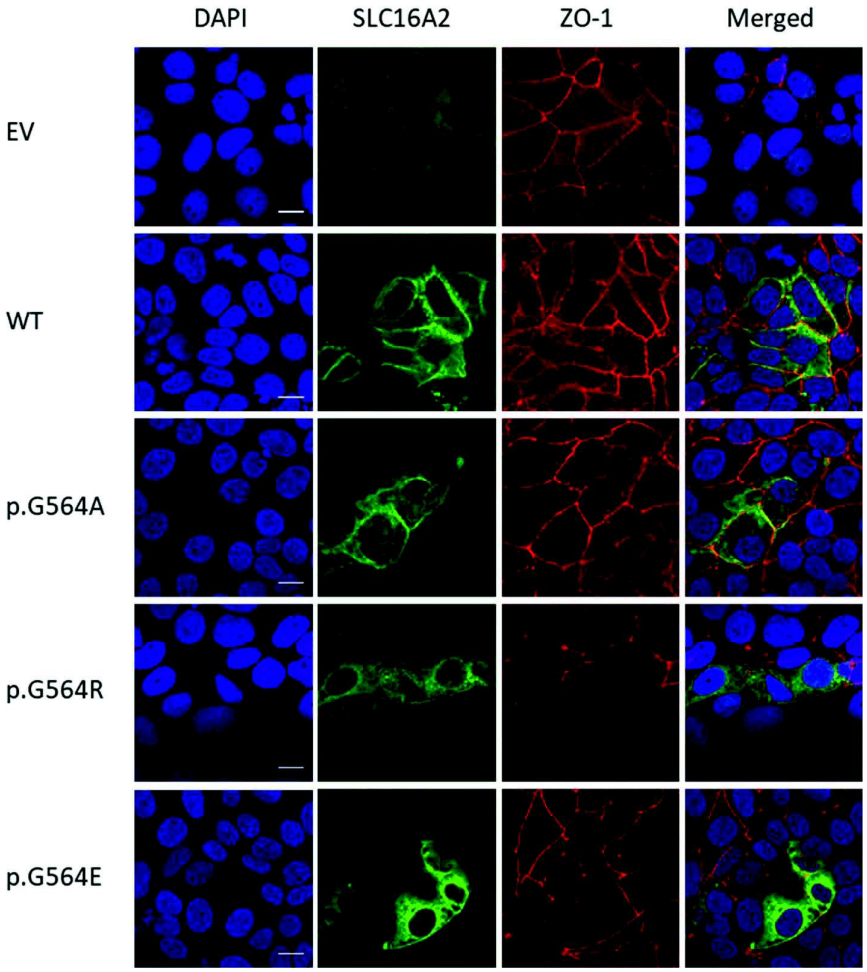

Supplemental Figure S3 Subcellular localization of WT and mutant SLC16A2 in JEG-3 cells. Nuclear staining with 4`,6-diamidino-2-phenylindole (DAPI) is presented in the first panel, SLC16A2 staining in the second panel, and staining of the cell membrane marker ZO-1 in the third panel. The fourth panel shows the merged image of all stainings. Scale bars correspond to 4 µm.

REFERENCES

1. Hennemann G, Docter R, Friesema EC, de Jong M, Krenning EP, Visser TJ. Plasma membrane transport of thyroid hormones and its role in thyroid hormone metabolism and bioavailability. Endocr Rev. 2001;22(4):451-76.
2. Friesema EC, Ganguly S, Abdalla A, Manning Fox JE, Halestrap AP, Visser TJ. Identification of monocarboxylate transporter 8 as a specific thyroid hormone transporter. J Biol Chem. 2003;278(41):40128-35.
3. Ceballos A, Belinchon MM, Sanchez-Mendoza E, Grijota-Martinez C, Dumitrescu AM, Refetoff S, et al. Importance of monocarboxylate transporter 8 for the blood-brain barrier-dependent availability of 3,5,3'-triiodo-L-thyronine. Endocrinology. 2009;150(5):2491-6.
4. Heuer H, Visser TJ. Minireview: Pathophysiological importance of thyroid hormone transporters. Endocrinology. 2009;150(3):1078-83.
5. Wirth EK, Roth S, Blechschmidt C, Holter SM, Becker L, Racz I, et al. Neuronal 3',3,5-triiodothyronine (T3) uptake and behavioral phenotype of mice deficient in Mct8, the neuronal T3 transporter mutated in Allan-Herndon-Dudley syndrome. J Neurosci. 2009;29(30):9439-49.
6. Kinne A, Kleinau G, Hoefig CS, Gruters A, Kohrle J, Krause G, et al. Essential molecular determinants for thyroid hormone transport and first structural implications for monocarboxylate transporter 8. J Biol Chem. 2010;285(36):28054-63.
7. Friesema EC, Grueters A, Biebermann H, Krude H, von Moers A, Reeser M, et al. Association between mutations in a thyroid hormone transporter and severe X-linked psychomotor retardation. Lancet. 2004;364(9443):1435-7.
8. Dumitrescu AM, Liao XH, Best TB, Brockmann K, Refetoff S. A novel syndrome combining thyroid and neurological abnormalities is associated with mutations in a monocarboxylate transporter gene. Am J Hum Genet. 2004;74(1):168-75.
9. Matheus MG, Lehman RK, Bonilha L, Holden KR. Redefining the Pediatric Phenotype of X-Linked Monocarboxylate Transporter 8 (MCT8) Deficiency: Implications for Diagnosis and Therapies. J Child Neurol. 2015.
10. Visser WE, Jansen J, Friesema EC, Kester MH, Mancilla E, Lundgren J, et al. Novel pathogenic mechanism suggested by ex vivo analysis of MCT8 (SLC16A2) mutations. Hum Mutat. 2009;30(1):29-38.
11. Visser TJ. In: LJ Groot, G Chrousos, K Dungan, A Grossman, JM Hershman, C Koch, M Korbonits, R McLachlan, M New, J Purnell, R Rebar, F Singer, A Vinik, editors. Source Endotext [Internet]. South Dartmouth, MA: MDText.com, Inc. 2016.
12. Kinne A, Roth S, Biebermann H, Kohrle J, Gruters A, Schweizer U. Surface translocation and tri-iodothyronine uptake of mutant MCT8 proteins are cell type-dependent. J Mol Endocrinol. 2009;43(6):263-71.
13. Kersseboom S, Kremers GJ, Friesema EC, Visser WE, Klootwijk W, Peeters RP, et al. Mutations in MCT8 in patients with Allan-Herndon-Dudley-syndrome affecting its cellular distribution. Mol Endocrinol. 2013;27(5):801-13.
14. Groeneweg S, Friesema EC, Kersseboom S, Klootwijk W, Visser WE, Peeters RP, et al. The role of Arg445 and Asp498 in the human thyroid hormone transporter MCT8. Endocrinology. 2014;155(2):618-26.
15. Braun D, Lelios I, Krause G, Schweizer U. Histidines in potential substrate recognition sites affect thyroid hormone transport by monocarboxylate transporter 8 (MCT8). Endocrinology. 2013;154(7):2553-61.
16. Armour CM, Kersseboom S, Yoon G, Visser TJ. Further Insights into the Allan-Herndon-Dudley Syndrome: Clinical and Functional Characterization of a Novel MCT8 Mutation. PLoS One. 2015;10(10):e0139343.
17. Jansen J, Friesema EC, Kester MH, Milici C, Reeser M, Gruters A, et al. Functional analysis of monocarboxylate transporter 8 mutations identified in patients with X-linked psychomotor retardation and elevated serum triiodothyronine. J Clin Endocrinol Metab. 2007;92(6):2378-81.
18. Yamamoto T, Takanashi J, Kurosawa K, Deguchi K, Osaka H, Inoue K. Comment on "delayed myelination is not a constant feature of Allan-Herndon-Dudley syndrome: report of a new case and review of the literature" by Azzolini S et al. Brain & Development 2014;36:716-720. Brain Dev. 2015;37(10):988-9.
19. Lopez-Espindola D, Morales-Bastos C, Grijota-Martinez C, Liao XH, Lev D, Sugo E, et al. Mutations of the thyroid hormone transporter MCT8 cause prenatal brain damage and persistent hypomyelination. J Clin Endocrinol Metab. 2014;99(12):E2799-804.
20. Trajkovic-Arsic M, Muller J, Darras VM, Groba C, Lee S, Weih D, et al. Impact of monocarboxylate transporter-8 deficiency on the hypothalamus-pituitary-thyroid axis in mice. Endocrinology. 2010;151(10):5053-62.

21. Liao XH, Di Cosmo C, Dumitrescu AM, Hernandez A, Van Sande J, St Germain DL, et al. Distinct roles of deiodinases on the phenotype of Mct8 defect: a comparison of eight different mouse genotypes. Endocrinology. 2011;152(3):1180-91.
22. Anik A, Kersseboom S, Demir K, Catli G, Yis U, Bober E, et al. Psychomotor retardation caused by a defective thyroid hormone transporter: report of two families with different MCT8 mutations. Horm Res Paediatr. 2014;82(4):261-71.
23. Wemeau JL, Pigeyre M, Proust-Lemoine E, d'Herbomez M, Gottrand F, Jansen J, et al. Beneficial effects of propylthiouracil plus L-thyroxine treatment in a patient with a mutation in MCT8. J Clin Endocrinol Metab. 2008;93(6):2084-8.
24. Verge CF, Konrad D, Cohen M, Di Cosmo C, Dumitrescu AM, Marcinkowski T, et al. Diiodothyropropionic acid (DITPA) in the treatment of MCT8 deficiency. J Clin Endocrinol Metab. 2012;97(12):4515-23.
25. Mol JA, Visser TJ. Synthesis and some properties of sulfate esters and sulfamates of iodothyronines. Endocrinology. 1985;117(1):1-7.
26. Friesema EC, Kuiper GG, Jansen J, Visser TJ, Kester MH. Thyroid hormone transport by the human monocarboxylate transporter 8 and its rate-limiting role in intracellular metabolism. Mol Endocrinol. 2006;20(11):2761-72.
27. Friesema EC, Jansen J, Jachtenberg JW, Visser WE, Kester MH, Visser TJ. Effective cellular uptake and efflux of thyroid hormone by human monocarboxylate transporter 10. Mol Endocrinol. 2008;22(6):1357-69.

Chapter

Novel mutations in SLC16A2 associated with a less severe phenotype of MCT8 deficiency

3.2

Silvia Masnada, Stefan Groeneweg, Veronica Saletti, Luisa Chiapparini, Barbara Castellotti, Ettore Salsano, W. Edward Visser, Davide Tonduti

Metab Brain Dis. 2019;34(6):1565-1575.

ABSTRACT

Mutations in the thyroid hormone transporter MCT8 cause severe intellectual and motor disability and abnormal serum thyroid function tests, a syndrome known as MCT8 deficiency (or: Allan-Herndon-Dudley syndrome, AHDS). Although the majority of patients are unable to sit or walk independently and do not develop any speech, some are able to walk and talk in simple sentences. Here, we report on two cases with such a less severe clinical phenotype and consequent gross delay in diagnosis. Genetic analyses revealed two novel hemizygous mutations in the SLC16A2 gene resulting in a p.Thr239Pro and a p.Leu543Pro substitution in the MCT8 protein. In vitro studies in transiently transfected COS-1 and JEG-3 cells, and ex vivo studies in patient-derived fibroblasts revealed substantial residual uptake capacity of both mutant proteins (Leu543Pro > Thr239Pro), providing an explanation for the less severe clinical phenotype. Both mutations impair MCT8 protein stability and interfere with proper subcellular trafficking. In one of the patients calcifications were observed in the basal ganglia at the age of 29 years; an abnormal neuro-radiological feature at this age that has been linked to untreated (congenital) hypothyroidism and neural cretinism. Our studies extend on previous work by identifying two novel pathogenic mutations in SLC16A2 gene resulting in a mild clinical phenotype.

INTRODUCTION

Thyroid hormone (TH) is crucial for the development of many tissues, in particular the brain, and it regulates energy metabolism throughout life (1). The thyroid gland mainly produces the pro-hormone thyroxine (T4) and a small amount of the active hormone 3,3',5-tri-iodothyronine (T3). Most effects of TH are exerted through binding of T3 to the nuclear thyroid hormone receptors (TRs) (2). The amount of T3 available for receptor action in TH-target tissues is tightly regulated by the de-iodinating enzymes (3). Since TH action and metabolism take place inside the target cells, it needs to cross the cell membrane for which TH transporter proteins are required (4). The most specific TH transporter identified to date is the monocarboxylate transporter (MCT)8 (5). Mutations in the SLC16A2 gene, which encodes MCT8, have been associated with MCT8 deficiency (also known as: Allan-Herndon-Dudley syndrome, AHDS), characterized by severe intellectual and motor disability and abnormal serum thyroid function tests comprising elevated serum T3 concentrations, low serum (free) T4 concentrations and a (high-) normal TSH concentration (6, 7). Compiling evidence suggests that MCT8 is essential for the transport of TH across the blood-brain-barrier and into different cell-types inside the brain (8, 9). Therefore, it has been widely accepted that MCT8 deficiency results in a hypothyroid state in the brain which impairs prenatal and post-natal brain development. In addition, the elevated serum T3 concentrations render tissues that rely on transporters other than MCT8 thyrotoxic (10), contributing to the very low body weight, tachycardia and muscle wasting observed in patients with MCT8 deficiency.

Over the last decades an increasing number of patients harboring different genetic mutations have been reported (summarized in (11)). The majority of patients present severe cognitive impairment, hypotonia, signs of pyramidal and extrapyramidal involvement, together contributing to the poor head control and inability to sit or stand independently. Neuro-imaging usually reveals a severe delay in myelination which is, by definition, mostly pronounced in the first years of life (12, 13). However, a small subset of patients present a relatively mild clinical phenotype and are able to walk and talk in simple words (e.g. (14-18)). Limited clinical and molecular information is available for this subgroup of MCT8 deficiency. Here, we report on two of such patients, harboring two different novel hemizygous missense mutations in MCT8, and extend on the currently available clinical characteristics of MCT8 deficiency.

MATERIALS AND METHODS

Materials

[^{125}I]T_3 and [^{125}I]T_4 were synthesized as described previously (19). Unlabeled iodothyronines, silychristin, bovine serum albumin (BSA), and D-glucose were obtained from Sigma-Aldrich (Zwijndrecht, The Netherlands [NL]); culture dishes from Corning (Schiphol, NL); culture medium from Invitrogen (Bleiswijk, NL); transfection reagent X-tremeGENE 9 from Roche Diagnostics (Almere, NL); 4–20% gradient Mini-PROTEAN TGX Precast Protein Gel from from Bio-Rad (Veenendaal, NL), polyvinylidene difluoride membranes and NuPAGE 4x lithium dodecyl sulfate loading buffer from Thermo Fisher Scientific (Bleiswijk, NL). Rabbit polyclonal antibody HPA003353 against human SLC16A2 amino acids 75 to 155 from Sigma Aldrich (Manufacturer: Atlas Antibodies, Stockholm; RRID AB_1079343); mouse monoclonal glyceraldehyde-3-phosphate dehydrogenase (GAPDH) antibody Mab 374 from Merck Millipore (Amsterdam, NL; RRID AB_2107445); IRDye680-labeled goat anti-rabbit

IgG (RRID AB_621843) and IRDye800-labeled goat anti-mouse IgG antibodies (RRID AB_10706161) from LI-COR (Leusden, NL); mouse monoclonal ZO-1 antibody from Invitrogen (RRID:AB_2533147). Alexa Fluor 488-labeled goat anti-rabbit IgG (RRID AB_143165) and Alexa Fluor 633-labeled goat anti-mouse IgG antibodies (RRID AB_2535718) from Thermo Fisher Scientific; Vectashield H-1200 containing DAPI from Brunschwig (Amsterdam, NL).

Genetic analyses

Genomic DNA was extracted from peripheral blood lymphocytes, according to a standard procedure. Written informed consent for DNA analysis was obtained from all patients and family members. DNA samples were screened for mutations in the *SLC16A2* gene (Xq13.2). Exons and intron–exon boundaries (exons 1–6) were analyzed by direct sequence analysis using an automated sequencing system (ABI 3130 XL). The primers are available on request. Nucleotides and amino acid residues were numbered according to the reference gene sequence of the transcript GenBank (NCBI): *SLC16A2* (*Homo sapiens* NM_006517.3, NP_006508.2). Sequence variations and predicted protein changes were described according to nomenclature recommendations (http://www.hgvs.org/mutnomen/recs.html). Segregation of genetic variants was analyzed through validation in all available family members. Frequencies of novel missense variants were determined by comparison with The Human Gene Mutation Database (http://www.hgmd.cf.ac.uk/ac/index.php), the NCBI dbSNP132ver (http://www.ncbi.nlm.nih.gov/projects/SNP/) and the Exome Variant Server (http://evs.gs.washington.edu/EVS/). In silico analysis of missense variants was performed using the PolyPhen-2 (http://genetics.bwh.harvard.edu/pph2/), and SIFT prediction test (http://sift.jcvi.org/).

Plasmids

The cloning of human MCT8 into pcDNA3 and of human CRYM into pSG5 expression vectors has been previously described (20, 21). CRYM is an intracellular high-affinity TH-binding protein that prevents the efflux of internalized TH. The p.Thr239Ala, p.Thr239Ala, p.Leu543Pro and p.Leu543Ala mutations were introduced using QuikChange site-directed mutagenesis according to manufacturer's protocol (Stratagene, Amsterdam, NL; primer sequences available upon request). The presence of the intended mutations was verified by Sanger sequencing of the complete cDNA insert. We have previously shown the absence of differences in transfection efficacy between wild-type (WT) and mutant MCT8 expression vectors (22). Positions of the mutations are determined using the NM_006517.3 reference sequence, which uses +1 as the A of the ATG translation initiation codon of the long MCT8 translational isoform, with the initiation codon as codon 1.

Cell culture and transfection

JEG-3 human choriocarcinoma (CVCL_0363) and COS-1 African green monkey kidney cells (CVCL_0223), obtained from ECACC (Sigma-Aldrich), were cultured under standard conditions (Groeneweg et al. 2018). For uptake studies, COS-1 or JEG-3 cells were seeded in 24-well plates and transiently transfected with 100 ng empty vector, or wild-type or mutant MCT8 alone, or in combination with 50 ng CRYM. For immunoblotting, cells were seeded in 6-well plates and transfected with 500 ng empty vector control, or WT or mutant MCT8. For immunocytochemistry studies, cells were cultured on 20 mm glass coverslips coated with poly-D-lysine (Sigma-Aldrich) and transfected with 100 ng wild-type or mutant MCT8. X-tremeGENE 9 (Roche Diagnostics, Almere, NL) was used as a transfection reagent according to manufacturer's protocol and all transfections were carried at 70%

cellular confluence. All experiments have been performed 48 h after transfection. Patient-derived fibroblasts were cultured as previously described (Groeneweg et al. 2018).

TH uptake studies

T3 and T4 uptake studies were conducted as previously described (23). Briefly, cells were washed with incubation medium (Dulbecco's phosphate buffered saline with 0.9 mmol/L $MgCl_2$ and 0.5 mmol/L $CaCl_2$ supplemented with 0.1% BSA and 0.1% D-glucose), and subsequently incubated for 30 min at 37 °C with 1 nM (50,000 cpm) [125I]T3 or [125I]T4 in 0.5 ml incubation medium. After incubation, cells were briefly washed with incubation medium and lysed with 0.1 M NaOH. Radioactivity in the cell lysates was measured with a γ-counter. T3 uptake levels in fibroblasts were adjusted for total protein levels measured by Bradford assay according to manufacturer's guideline (Bio-Rad).

Immunoblotting

Two days after transfection, cells were rinsed with D-PBS, collected in 100 mM sodium phosphate, 2 mM EDTA, pH 7.2 (P100E2) containing protease inhibitor cocktail (Roche Diagnostics), and sonicated on ice. After incubation for 10 min at 70 °C in the presence of 1x NuPAGE 1x lithium dodecyl sulfate loading buffer, 15 µg of total lysate was separated on a 4%–20% gradient Mini-PROTEAN TGX Precast Protein Gel, blotted on polyvinylidene difluoride membranes, blocked with 5% milk and probed overnight at 4 °C with N-terminal MCT8 antibody (dilution 1:20 000). GAPDH (antibody dilution 1:20 000) was used as a loading control. MCT8 and GAPDH were visualized as previously described (24). Expression levels of WT and mutant MCT8 proteins were quantified by densitometry using ImageJ and adjusted for GAPDH expression levels.

Immunocytochemistry

Immunocytochemistry was essentially carried out as previously described (23). Briefly, cells were fixed with 4% paraformaldehyde, and permeabilized with 0.2% triton X-100 in PBS. Samples were blocked for 1h at RT in PBS containing 2% BSA, and incubated overnight with rabbit anti-MCT8 (1:1,000) and mouse monoclonal ZO-1 antibody (RRID:AB_2533147; 1:500). After secondary staining with goat antirabbit Alexa Fluor 488 (1:1000) and goat antimouse Alexa 633 (1:1000), cover slips were mounted on glass slides with Prolong Gold containing DAPI (Invitrogen) and examined on a Zeiss Meta 510 microscope, using Zeiss LSM software (Zeiss NL, Sliedrecht, NL).

Ethical considerations

Skin fibroblasts were kindly provided by care-giving physicians and concerned stored samples that were previously collected for diagnostic purposes. Written informed consent was obtained from the parents or legal representatives of the involved patients and controls. This study was conducted in agreement with the Medical Research Involving Human Subjects Act was carried out through routine diagnostic activity; formal ethics review was therefore not requested by our institutional ethical committee.

Statistics

All statistical analyses were performed as indicated in the Figure legends using GraphPad Prism Version 5 software (GraphPad Software Inc., San Diego, USA). Statistically significant differences are indicated as described in the legends of the corresponding Figures.

This study adheres to the principle of the Helsinki Declaretion and was carried out through routine diagnostic activity; all families provided written informed consent for clinical and genetic testing and their publication according to the Italian bioethics laws.

RESULTS

Case reports (Table 1)

Patient 1

A 29-years old man, who had been previously diagnosed with cerebral palsy, presented to our clinic for a second opinion of his neurological condition. He was the third child (two previous healthy sisters) of non-consanguineous healthy Italian parents. His maternal uncle suffered from an undiagnosed early onset encephalopathy with severe intellectual disability, had no speech development, and was wheelchair-dependent. The patient was born after an uneventful pregnancy and delivery. From the first months of life diffuse hypotonia, feeding difficulties and developmental delay became evident. He achieved trunk control at 10 months of age, he was able to stand at 4 years and walk with support since 6 years of age; he pronounced his first words at 5 years of age. During infancy, startle reactions in response to even mild sensory stimuli were reported. The clinical picture had initially remained stable, but from 16 years of age it started to slowly deteriorate. Initially, he only needed a wheelchair to cover long distances, but from the age of 20 years he became wheelchair dependent. Dysarthria also worsened and his speech, which was limited to some words, or short sentences of 2–3 words, became less clear. At 29 years of age, neurological examination revealed diffuse muscular hypotrophy, severe scoliosis, pyramidal (peripheral hypertonia, brisk reflexes, clonus, joint contractures) and extrapyramidal signs (bradykinesia, mild dystonic movements of the limbs and resting and action tremor). He had a moderate cognitive impairment (Wechsler Adult Intelligence Scale- WAIS-R performance quotient <45, other scales not conducted; Raven CPM <5° percentile), but he graduated from secondary school with assistance. His facies was hypomimic and some minor dysmorphisms were observed (bitemporal narrowing, large protruding lower lip, macroglossia, and a high and narrow palate). He had a poor weight gain (45 kg, < -2SD). No dysphagia was reported.

Magnetic Resonance Imaging (MRI) was performed at 29 years of age and revealed no significant white matter abnormalities (**Figure 1**). Pallidal T2 hypo-intensities were observed, which were designated as calcifications by a CT scan. A calcium-phosphorus metabolism check-up only showed a marginal deficit of vitamin D, with calcium and phosphate concentrations in the normal range.

Thyroid function tests had been performed at the age of 28 years as part of a routine evaluation of the global hypotrophy and demonstrated elevated free T3 (4,27 pg/dL, normal values 1,71-3,71), slightly reduced free (F)T4 (0.73 ng/dL, normal values 0,7-1,48), and normal TSH concentrations. Because of the characteristic thyroid hormone profile, direct sequencing of the *SLC16A2* gene was performed and revealed a novel hemizygous c.715A > C missense mutation in exon 2, causing a p.Thr239Pro

substitution in the MCT8 protein. This mutation was predicted to have a (probable) pathogenic effect on the MCT8 protein by PolyPhen-2 and SIFT. The mother was heterozygous for the same mutation.

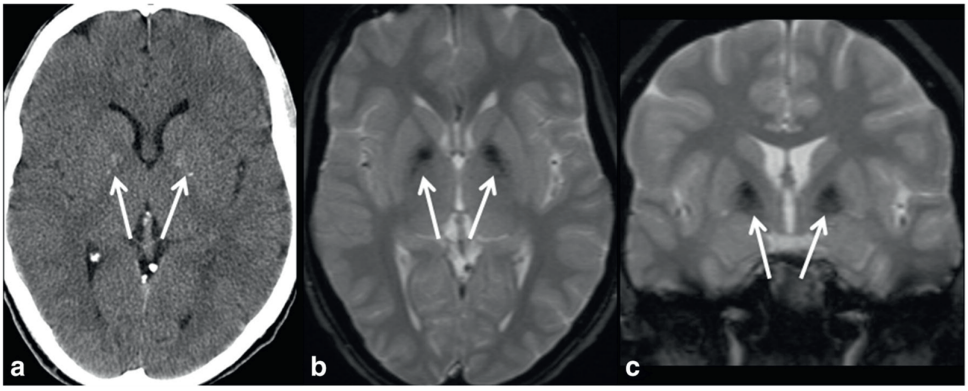

Figure 1 Brain CT (a) and T2 FFE MRI (b, c) of patient 1 at 29 years of age demonstrating calcifications in both globus pallidus (arrow); note the blooming effect on T2FFE.

Patient 2

A 12-years old patient presented to our clinic at the age of 11 months for a diagnostic work-up of developmental delay. He was the second child born from non-consanguineous Italian parents, after an uneventful pregnancy and cesarean section delivery. The mother declared she had received L-thyroxine for hypothyroidism during pregnancy, and later she underwent a right hemi-thyroidectomy. During the first years of life, he presented neuro-developmental delay: head control was achieved at 6 months, trunk control at 16 months, standing position at 20 months, walking without support since 41 months of age, walking up and down the stairs with aid since 4 years, and first words were pronounced before 36 months. The neurological picture was dominated by cognitive impairment. This was accompanied by moderate truncal hypotonia, subtle pyramidal (brisk reflexes, Babinski and bilateral ankle clonus) and mild extrapyramidal signs (slight bradykinesia, hypomimia, but no dystonia). He had moderate intellectual disability (Griffiths Scale performed at 7 years of age: Global Quotient 47), and was able to communicate using short sentences and understand simple tasks.

MRI of the brain demonstrated a-specific delay of myelination at the age of 11.5 months and was normal at the age of 4.5 and 7 years (**Figure 2**).

Since the first exam at the age of 11 months, electroencephalography showed poor and slow background activity. From the age of 4 years, also diffuse high voltage spike-waves (10–40 Hz) were observed during photic stimulation. From the age of 7 years, bilateral temporal epileptiform discharges during drowsiness and sleep were evident. However, he never suffered from clinically evident epileptic seizures. Electroneurography, sensory and visual evoked potential, and electromyography were all unremarkable (last evaluation performed at 7 years).

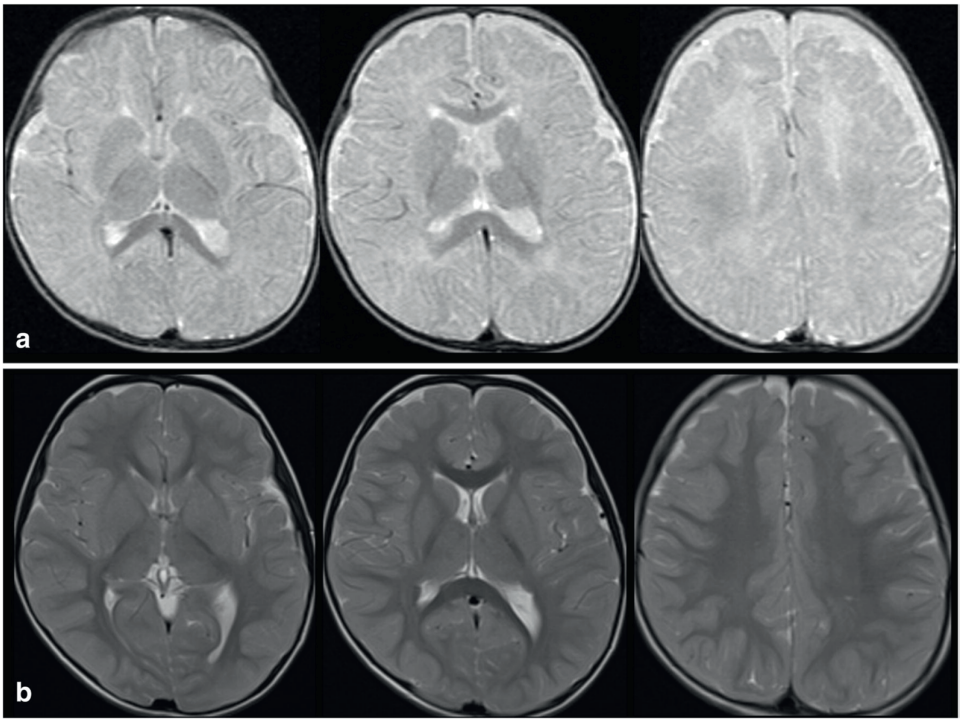

Figure 2 Brain MRI, T2-w.i. at 11,5 months (TOP) and at 4,5 years (BOTTOM) show delayed myelination at 1 years and the myelination progression until normal appearance at 4,5 years

Biochemical investigations, including urine and plasma guanidinoacetic acid and creatine dosage, lactate and pyruvate, urinary orgnic, acids, plasma and urinary aminoacids, urinary mucopolysaccharides, B12 vitamine and folate, Beta-Galactosidase, Beta-N Acetyl Glucosaminidase), and targeted genetic analysis including karyotyping, fish analyses of subtelomeric regions, a CGH array, and the methylation status of 15q11.2 for Angelman Syndrome were all unremarkable. Only thyroid function tests were found abnormal at 7 years of age and revealed elevated serum free T3 concentrations (5,39 pg/dL normal values 1,71-3,71), and low-normal FT4 (0,82 ng/dl, normal values 0,70-1,48) and TSH (1,52 mIU/L normal values 0,45-3,50) concentrations. Direct sequencing of the SLC16A2 gene was therefore performed and revealed a novel hemizygous c.1625 T > C missense mutation in exon 6 which results in a p.Leu543Pro substitution in the MCT8 protein, inherited from the mother. This mutation was predicted to have a (probable) pathogenic effect on the MCT8 protein by PolyPhen-2 and SIFT.

Functional analyses

Since both mutations had not been reported before, functional analyses were conducted to confirm their pathogenicity. First the p.Thr239Pro and p.Leu543Pro mutations were introduced into the MCT8 expression construct. In addition, both residues were substituted by an Ala to evaluate if the original Thr239 and Leu543 residues are critical for MCT8 function. In COS-1 cells co-transfected with the intracellular TH-binding protein mu-Crystallin (CRYM), T3 and T4 uptake by the p.Thr239Pro mutant amounted up to 40% of WT, and the T3 and T4 uptake by the p.Leu543Pro mutant to 50% of WT MCT8 (**Figure 3a**).

Table 1 Clinical characteristics Overview of clinical and developmental characteristics at time the patients came to our attention.

	Patient 1	**Patient 2**
Current age	29 y	12 y
Mutation	c.715A>C , p.Thr239Pro	c.1625T>C, p.Leu543Pro
Age at onset symptoms	first months of life	first months of life
Weight in kg (percentile)	45(<P3, 28y)	21 (P25, 7y)
Head circumference in cm (percentile, age)	na	52 (P25-50, 7y)
Feeding problems	+	-
Muscle wasting	+	-
Signs of peripheral thyrotoxicosis	-	elevated heart rate (127 bpm)
Hypotonia	+	-
Pyramidal signs	+	mild
Extrapyramidal signs	bradykinesia, tremor, dystonic movements of the limbs, hypomimia	slight bradykinesia, hypomimia
Head control (age)	yes (na)	yes (6 m)
Independent sitting (age)	yes (10 m)	yes (16 m)
Ability to walk (age)	yes, with support (6 y)	yes (4 y)
Speech development (age)	first words at 5 y	first words <3 y
Neuromotor Rregression	yes, after the age of 16y	no
Cognitive impairment (IQ)	<45	47
Serum FT3 in pg/ml (normal range)	4.27 pg/mL, (1.71-3.71)	5.39 pg/mL, (1.71-3.71)
Serum FT4 in pg/ml (normal range)	0.73 ng/mL, (0,70-1,48)	0,82 ng/dl (0,70-1,48)
Serum TSH in mU/l (normal range)	normal	1,52 mIU/L (0,45-3,50)
Clinically evident seizures	no	no
EEG	na	4y: high voltage spike-waves during IPS; 7y: bilateral temporal EDs during drowsiness and sleep
MRI (age performed)	29 y: normal myelination, pallidal calcification	delayed myelination at 11.5 m, normal at 4.5 and 7 y

EDs epileptiform discharges, EEG electroencephalogram, IPS intermittent photic stimulation, m months, MRI magnetic resonance imaging, Na not available, p percentile, SD standard deviation, y years

TH uptake by the p.Thr239Ala and p.Leu543Ala mutants was not significantly different from WT. Similar results were obtained in JEG-3 cells, although residual uptake capacity was slightly lower with 10% for the p.Thr239Pro mutant and 20% for the p.Leu543Pro mutant (**Figure 3b**). Saturation experiments in the absence of CRYM revealed an apparent IC_{50} of 18.2 (±1.2) µM for WT MCT8 (**Figure 3c**). A similar IC_{50} was found for the p.Thr239Pro mutant (16.9 ± 1.4), whereas the IC50 for the p.Leu543Pro mutant was slightly reduced (9.3 ± 1.2 µM). Immunoblotting on total lysates of COS-1 cell

transiently transfected with WT or mutant MCT8 revealed that the protein expression levels of the p.Thr239Ala and p.Leu543Ala mutants were similar to WT, whereas those of p.Thr239Pro and p.Leu543Pro were moderately reduced (**Figure 3d**). Similar results were obtained in JEG-3 cells (data not shown). Subcellular localization studies in JEG-3 cells by confocal microscopy showed prominent cell membrane expression of WT (**Figure 3e**), whereas a large fraction of the p.Thr239Pro and p.Leu543Pro mutant protein was localized intracellularly and accumulated around the nucleus (**Figure 3e**). Both Ala substituents showed a similar subcellular distribution pattern as WT (data not shown). Taken together, these data suggest that both mutations reduce MCT8-mediated TH transport, predominantly by reducing protein expression levels and interference with the intracellular trafficking. This was further supported by our structural model of MCT8 in the outward-open conformation (24), in which both residues are located within an a-helical part of transmembrane domain 2 (Thr239) and 11 (Leu543), respectively (**Figure 3f**). The introduction of a Pro at these positions likely results in pronounced structural changes of these domains.

In addition to these in vitro studies in over-expressing cells, we also studied the impact of both mutations on MCT8-mediated T3 transport in patient-derived fibroblasts, a well-established ex vivo model to study MCT8 deficiency. As a control we also included fibroblasts from a patient harboring a frameshift mutation that truncates the MCT8 protein prematurely, resulting in a complete loss of MCT8-mediated T3 uptake (25). In line with the in vitro studies, the p.Thr239Pro and p.Leu543Pro mutant fibroblasts showed a significant reduction in T3 uptake compared to fibroblasts derived from healthy controls at all tested time points, but exceeded those observed in Q97fsX mutant fibroblasts (**Figure 1g**). In addition, MCT8 protein expression levels were clearly lower in the p.Thr239Pro and p.Leu543Pro mutant fibroblasts compared to control fibroblasts (**Figure 3h**). Finally, T3 uptake by patient and control fibroblasts was measured in the absence and presence of the MCT8-specific inhibitor silychristin (26). In the presence of silychristin, T3 uptake levels in control fibroblasts were diminished by about 70%, whereas no reduction was observed in the Q97fsX fibroblasts corresponding to a complete loss of MCT8 function (**Figure 3i**). In contrast, T3 uptake was moderately reduced by silychristin in p.Thr239Pro (~16%) and p.Leu543Pro (~49%) mutant fibroblasts, indicating the presence of some residual MCT8-mediated T3 uptake.

DISCUSSION

Here, we report two novel mutations in the *SLC16A2* gene (p.Thr239Pro and p.Leu543Pro), resulting in a less severe clinical phenotype of MCT8 deficiency. Although both patients were able to walk and developed some speech, neuro-motor development was considerably better in the one harboring the p.Leu543Pro mutation. In vitro and ex vivo studies confirmed that both mutations resulted in a reduction of MCT8 function. In line with the less severe clinical phenotype, a relatively higher residual transport capacity was observed for the p.Leu543Pro mutant.

To date, up to a hundred different genetic mutations in MCT8 have been reported and for the majority of patients with MCT8 deficiency at least some aspects of the clinical phenotype have been described (reviewed in(11)). With the growing number of identified patients, the presence of heterogeneity in the severity of the clinical phenotype has become increasingly clear. The majority of patients reported has severe intellectual disability and are unable to sit or stand without support, but a subset of patients is able to walk and talk in simple words (e.g. (14-18).

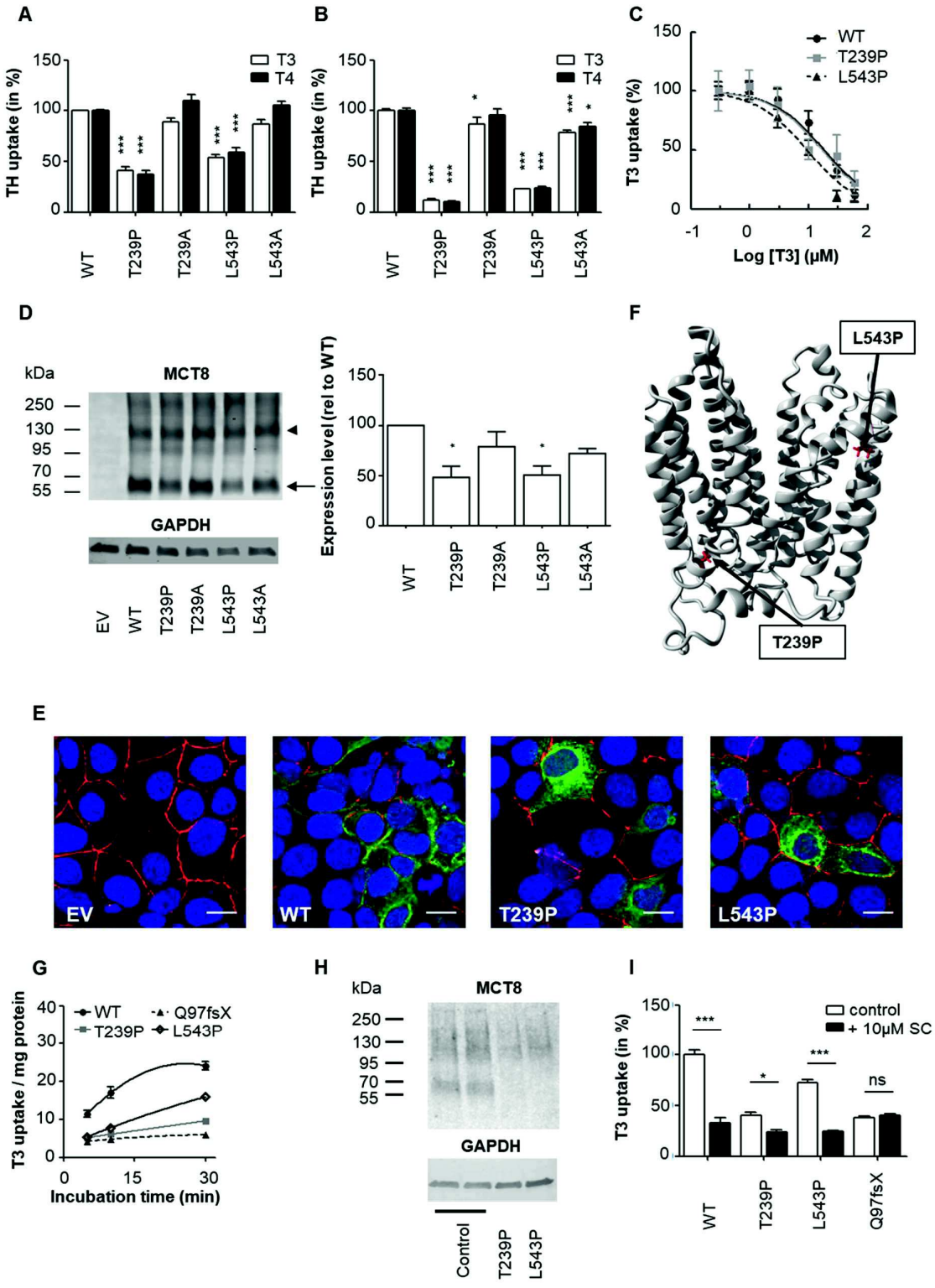
A
TH uptake (in %)
T3
T4
WT
T239P
T239A
L543P
L543A
B
TH uptake (in %)
C
T3 uptake (%)
WT
T239P
L543P
Log [T3] (μM)
D
kDa
MCT8
250
130
95
70
55
GAPDH
EV
WT
T239P
T239A
L543P
L543A
Expression level (rel to WT)
F
L543P
T239P
E
EV
WT
T239P
L543P
G
T3 uptake / mg protein
WT
Q97fsX
T239P
L543P
Incubation time (min)
H
kDa
MCT8
GAPDH
Control
T239P
L543P
I
T3 uptake (in %)
control
+ 10μM SC
ns
WT
T239P
L543P
Q97fsX

Figure 3 Functional analyses of the p.Thr239Pro and p.Leu543Pro mutants in in vivo and ex vivo disease models for MCT8 deficiency. T3 (white bars) and T4 (black bars) uptake in COS-1 (**a**) and JEG-3 (**b**) cells transiently transfected with WT MCT8 or indicated mutants in the presence of the intracellular TH-binding protein CRYM, after 30 min at 37 °C. Uptake levels were corrected for those observed in empty vector (EV) transfected cells and expressed relative to WT (100%; *N* = 3). One-way ANOVA with Bonferroni posthoc tests were used and statistically significant differences to WT are indicated as follows $P < 0.001$, ***, $P < 0.05$, *. **c** Saturation experiments in transiently transfected COS-1 cells in the absence of CRYM, corrected for background uptake levels observed in cell transfected with EV. Non-linear regression was used to plot the saturation curves. IC50 values for WT (18.2, 95% confidence interval [CI] 12.4–26.7 μM), p.Thr239Pro (16.9, 95%CI 8.6–33.1 μM) and p.Leu543Pro (9.3, 95% CI 6.2–14.0 μM) mutant MCT8 were calculated based on the means of N = 3 independent experiments using GraphPad Prism. **d** Immunoblot on total lysates of COS-1 cells transiently transfected with WT or mutant MCT8. MCT8 monomer is indicated with an arrow and MCT8 homo-dimer with an arrowhead. Glyceraldehyde-3-phosphate dehydrogenase (GAPDH) was used as loading control. The expression levels of wildtype and indicated mutant MCT8 proteins has been quantified using ImageJ and adjusted for GAPDH levels. All levels are expressed relative to WT MCT8 and presented as mean ± SEM of 3 independent experiments. One-way ANOVA followed by a Bonferroni multiple-comparison test was used to compare the expression levels of all tested mutants to WT MCT8. * denote statistically significant differences ($p < 0.05$). **e** Confocal microscopy in transiently transfected JEG-3 cells using antibodies against MCT (green), the membrane marker ZO-1 (red) and the nuclear marker DAPI (blue), presented as an overlay image. **f** Structural homology model of MCT8 in the outwardopen configuration (25) in which the position of the affected Thr239 and Leu543 have been indicated. **g** T3 uptake in patient and control fibroblasts after indicated incubation times at 37 °C. T3 uptake levels are presented as mean ± SEM percentage internalized T3 per milligram protein to correct for differences in cell density between different fibroblast lines. T3 uptake in fibroblasts derived from patients with MCT8 deficiency was significantly lower than in those obtained from healthy controls (mean of 2 different control cell lines) at all tested incubation times (One-way ANOVA with Bonferroni post-hoc tests: $P < 0.001$ at all time-points, not indicated in graph). **h** MCT8 expression levels in patient and control fibroblasts. **i** T3 uptake levels in patient and control fibroblasts in the absence (−) or presence (+) of 10 μM silychristin (SC). Silychristin is a potent and, thus far the most specific, inhibitor of MCT8-mediated TH transport (26). The silychristin-induced reduction in T3 uptake in all patient lines was significantly smaller (One-way ANOVA with Bonferroni posthoc tests, $P < 0.05$) than in control fibroblasts.

Regardless the severity of the clinical phenotype, the presence of abnormal thyroid function tests appears to be a consistent finding, with serum T3 concentration being elevated, free and total T4 concentrations reduced and TSH concentrations mostly within normal range.

Early diagnosis of patients with a clinical phenotype in the milder spectrum of MCT8 deficiency is often challenging and complicated by initial misclassification. This was also the case with our two patients who both presented a relatively mild clinical phenotype. The first patient (p.Thr239Pro) presented as a non-progressive encephalopathy with intellectual disability, and pyramidal and extrapyramidal signs. Despite a normal perinatal history, he had been initially diagnosed with cerebral palsy. The second patient (p.Leu543Pro) mainly presented with cognitive delay. A congenital static neurodevelopmental encephalopathy had been considered the most probable diagnostic hypothesis. Although both patients presented classical clinical hallmarks of MCT8 deficiency, including early hypotonia, pyramidal and extrapyramidal signs, intellectual disability and slightly abnormal myelination (only proband 2), these features were so mild to make them considered as a-specific and the diagnosis of MCT8 deficiency was therefore initially not deemed very likely. Moreover, beside the low body weight and muscular hypotrophy in patient 1, and an elevated heart rate in patient 2, both of them did not have

other obvious clinical signs of peripheral hyperthyroidism. The presence of abnormal thyroid function tests finally led to the correct diagnosis.

Although the elevated T3 concentrations are an important clue for the diagnosis of MCT8 deficiency, they are not routinely measured or unavailable in clinical practice. The evaluation of thyroid function tests is often restricted to TSH, sometimes accompanied with FT4, the results of which are regularly misinterpreted as central hypothyroidism. Consequently, some patients are treated with levothyroxine supplementation, which in fact may further deteriorate the thyrotoxicosis in the peripheral tissues and worsen the peripheral phenotype (e.g. (27, 28)). Therefore, the additional measurement of T3 in male subjects with global developmental delay should be routinely considered.

In agreement with the relatively mild clinical presentation, both identified mutations resulted in a mutant MCT8 protein with considerable residual TH transport capacity. In vitro studies in overexpressing COS-1 cells showed residual uptake functions of 40% for the p.Thr239Pro mutant and 50% for the p.Leu543Pro mutant, which is similar to the levels reported for other mutations identified in patients with a less severe phenotype (e.g.(17)). Also, the ex vivo experiments in patient fibroblasts indicated that both mutant proteins have significant residual transport capacity. Our findings are in line with previous studies that have suggested that the severity of the clinical phenotype is related to the residual transport capacity of the mutant MCT8 protein in functional studies (e.g. (18, 29)). Additional in vitro studies, suggested that both mutations reduce the stability of the MCT8 protein, resulting in lower protein expression levels and more pronounced perinuclear subcellular localization compared to wild-type. The latter may indicate an impaired trafficking of both mutant proteins to the cell membrane. Since both residues are predicted to be located within a transmembrane domain with an alpha-helical structure, the helix-breaking properties of a Pro likely result in disorganization of the secondary protein structure. Indeed, substitution of Thr239 or Leu543 by an Ala, which has a small side-chain and backbone properties that allow incorporation in an alpha-helical structure, resulted in mutant proteins with a TH transport activity similar to WT. These findings also suggest that the Thr239 and Leu543 themselves are not strictly essential for MCT8 function and that the introduction of a Pro at these positions likely mediates the pathogenic effects of both identified mutations.

Of interest, the neuroradiological evaluation of patient 1 at 29 years of age showed the presence of bilateral pallidal calcifications. This feature has been mentioned in only two previously described patients (7, 30), but left unattended ever since. In one case, calcium deposits were found during autopsy at the age of 10 years (7), and in another T1 shortening signals considered suggestive for calcification, were detected in the bilateral globus pallidus and dentate nucleus at the age of 21 years (30). Since brain imaging at these relatively advanced ages is not routinely performed in patients with MCT8 deficiency, it is currently not known to what extent calcifications in the basal ganglia are present at the pediatric age. This in particular holds for CT imaging of the brain which is the preferred detection method for cerebral calcifications. Of note, the presence of calcifications of the basal ganglia has been reported in patients with neural cretinism (31) and (congenital) hypothyroidism (32), which may suggest a link between the abnormal TH signaling in the brain and this phenomenon. Nevertheless, it remains unclear if the presence of calcifications in the basal ganglia at a relatively young age is a common feature in patients with MCT8 deficiency, and if it is directly related to the aberrant TH signaling in the brain or to premature (para-) physiological calcification that normally occurs with aging. Alternative causes were excluded in our patient. More detailed neuroradiological studies in patients at different ages are needed to further elucidate the etiology of this finding. Should (premature)

calcifications of the basal ganglia be directly related to the defect in TH signaling, our finding may suggest that besides the developmental defects associated with MCT8 deficiency, additional pathological changes may occur later in life.

Finally it is to note that in both patients extrapyramidal signs manifested as bradykinesia and hypomimia, while dystonia was only mild or even absent. Dystonia has been often reported as the main extrapyramidal feature of MCT8 patients (13), but it has already pointed out that this is not constantly present, as our cases (33).

In conclusion, we reported on two novel mutations in *SLC16A2* which are associated with clinical features at the milder side of the spectrum of MCT8 deficiency. Our cases illustrate that a timely diagnosis of such patients can be challenging and prone to misclassification. We therefore advocate to measure thyroid function tests, including serum T3 concentrations, in the work-up of patients with X-linked intellectual disability, even when the typical neurological and neuro-radiological signs of MCT8 deficiency are only subtle and apparently a-specific.

Acknowledgements

We thank Ramona E.A. van Heerebeek and Selmar Leeuwenburgh for the technical assistance, the Optical Imaging Center (Erasmus Medical Center Rotterdam) for technical support regarding the confocal imaging studies, and the physicians of the involved patients and healthy controls for providing the fibroblasts.

Financial support: This work was supported by a grant from the Netherlands Organisation for Health Research and Development (project number 113303005) (to WEV), from the Sherman Foundation (to WEV).

REFERENCES

1. Yen PM. Physiological and molecular basis of thyroid hormone action. Physiol Rev. 2001;81(3):1097-142.
2. Yen PM, Ando S, Feng X, Liu Y, Maruvada P, Xia X. Thyroid hormone action at the cellular, genomic and target gene levels. Mol Cell Endocrinol. 2006;246(1-2):121-7.
3. Gereben B, Zavacki AM, Ribich S, Kim BW, Huang SA, Simonides WS, et al. Cellular and molecular basis of deiodinase-regulated thyroid hormone signaling. Endocr Rev. 2008;29(7):898-938.
4. Hennemann G, Docter R, Friesema EC, de Jong M, Krenning EP, Visser TJ. Plasma membrane transport of thyroid hormones and its role in thyroid hormone metabolism and bioavailability. Endocr Rev. 2001;22(4):451-76.
5. Friesema EC, Ganguly S, Abdalla A, Manning Fox JE, Halestrap AP, Visser TJ. Identification of monocarboxylate transporter 8 as a specific thyroid hormone transporter. J Biol Chem. 2003;278(41):40128-35.
6. Friesema EC, Grueters A, Biebermann H, Krude H, von Moers A, Reeser M, et al. Association between mutations in a thyroid hormone transporter and severe X-linked psychomotor retardation. Lancet. 2004;364(9443):1435-7.
7. Dumitrescu AM, Liao XH, Best TB, Brockmann K, Refetoff S. A novel syndrome combining thyroid and neurological abnormalities is associated with mutations in a monocarboxylate transporter gene. Am J Hum Genet. 2004;74(1):168-75.
8. Vatine GD, Al-Ahmad A, Barriga BK, Svendsen S, Salim A, Garcia L, et al. Modeling Psychomotor Retardation using iPSCs from MCT8-Deficient Patients Indicates a Prominent Role for the Blood-Brain Barrier. Cell Stem Cell. 2017;20(6):831-43 e5.
9. Mayerl S, Muller J, Bauer R, Richert S, Kassmann CM, Darras VM, et al. Transporters MCT8 and OATP1C1 maintain murine brain thyroid hormone homeostasis. J Clin Invest. 2014;124(5):1987-99.
10. Groeneweg SP, R.P.; Visser, T.J.; Visser, W.E. Diagnostic and Therapeutic Challenges in the Allan–Herndon–Dudley Syndrome. US Endocrinology. 2016;12(2):90-3.
11. Groeneweg S, Visser WE, Visser TJ. Disorder of thyroid hormone transport into the tissues. Best Pract Res Clin Endocrinol Metab. 2017;31(2):241-53.
12. Tonduti D, Vanderver A, Berardinelli A, Schmidt JL, Collins CD, Novara F, et al. MCT8 deficiency: extrapyramidal symptoms and delayed myelination as prominent features. J Child Neurol. 2013;28(6):795-800.
13. Matheus MG, Lehman RK, Bonilha L, Holden KR. Redefining the Pediatric Phenotype of X-Linked Monocarboxylate Transporter 8 (MCT8) Deficiency: Implications for Diagnosis and Therapies. J Child Neurol. 2015.
14. Stevenson RE, Goodman HO, Schwartz CE, Simensen RJ, McLean WT, Jr., Herndon CN. Allan-Herndon syndrome. I. Clinical studies. Am J Hum Genet. 1990;47(3):446-53.
15. Schwartz CE, May MM, Carpenter NJ, Rogers RC, Martin J, Bialer MG, et al. Allan-Herndon-Dudley syndrome and the monocarboxylate transporter 8 (MCT8) gene. Am J Hum Genet. 2005;77(1):41-53.
16. Vaurs-Barriere C, Deville M, Sarret C, Giraud G, Des Portes V, Prats-Vinas JM, et al. Pelizaeus-Merzbacher-Like disease presentation of MCT8 mutated male subjects. Ann Neurol. 2009;65(1):114-8.
17. Visser WE, Jansen J, Friesema EC, Kester MH, Mancilla E, Lundgren J, et al. Novel pathogenic mechanism suggested by ex vivo analysis of MCT8 (SLC16A2) mutations. Hum Mutat. 2009;30(1):29-38.
18. Novara F, Groeneweg S, Freri E, Estienne M, Reho P, Matricardi S, et al. Clinical and Molecular Characteristics of SLC16A2 (MCT8) Mutations in Three Families with the Allan-Herndon-Dudley Syndrome. Hum Mutat. 2017;38(3):260-4.
19. Mol JA, Visser TJ. Synthesis and some properties of sulfate esters and sulfamates of iodothyronines. Endocrinology. 1985;117(1):1-7.
20. Friesema EC, Kuiper GG, Jansen J, Visser TJ, Kester MH. Thyroid hormone transport by the human monocarboxylate transporter 8 and its rate-limiting role in intracellular metabolism. Mol Endocrinol. 2006;20(11):2761-72.
21. Friesema EC, Jansen J, Jachtenberg JW, Visser WE, Kester MH, Visser TJ. Effective cellular uptake and efflux of thyroid hormone by human monocarboxylate transporter 10. Mol Endocrinol. 2008;22(6):1357-69.
22. Jansen J, Friesema EC, Kester MH, Milici C, Reeser M, Gruters A, et al. Functional analysis of monocarboxylate transporter 8 mutations identified in patients with X-linked psychomotor retardation and elevated serum triiodothyronine. J Clin Endocrinol Metab. 2007;92(6):2378-81.
23. Groeneweg S, Friesema EC, Kersseboom S, Klootwijk W, Visser WE, Peeters RP, et al. The role of Arg445 and Asp498 in the human thyroid hormone transporter MCT8. Endocrinology. 2014;155(2):618-26.

24. Groeneweg S, Lima de Souza EC, Meima ME, Peeters RP, Visser WE, Visser TJ. Outward-Open Model of Thyroid Hormone Transporter Monocarboxylate Transporter 8 Provides Novel Structural and Functional Insights. Endocrinology. 2017;158(10):3292-306.
25. Groeneweg S, van den Berge A, Meima ME, Peeters RP, Visser TJ, Visser WE. Effects of Chemical Chaperones on Thyroid Hormone Transport by MCT8 Mutants in Patient-Derived Fibroblasts. Endocrinology. 2018;159(3):1290-302.
26. Johannes J, Jayarama-Naidu R, Meyer F, Wirth EK, Schweizer U, Schomburg L, et al. Silychristin, a Flavonolignan Derived From the Milk Thistle, Is a Potent Inhibitor of the Thyroid Hormone Transporter MCT8. Endocrinology. 2016;157(4):1694-701.
27. de Menezes-Filho HC, Marui S, Manna TD, Brust ES, Radonsky V, Kuperman H, et al. Novel mutation in MCT8 gene in a Brazilian boy with thyroid hormone resistance and severe neurologic abnormalities. Arq Bras Endocrinol Metabol. 2011;55(1):60-6.
28. Kim JH, Kim YM, Yum MS, Choi JH, Lee BH, Kim GH, et al. Clinical and endocrine features of two Allan-Herndon-Dudley syndrome patients with monocarboxylate transporter 8 mutations. Horm Res Paediatr. 2015;83(4):288-92.
29. Capri Y, Friesema EC, Kersseboom S, Touraine R, Monnier A, Eymard-Pierre E, et al. Relevance of different cellular models in determining the effects of mutations on SLC16A2/MCT8 thyroid hormone transporter function and genotype-phenotype correlation. Hum Mutat. 2013;34(7):1018-25.
30. Ono E, Ariga M, Oshima S, Hayakawa M, Imai M, Ochiai Y, et al. Three novel mutations of the MCT8 (SLC16A2) gene: individual and temporal variations of endocrinological and radiological features. Clin Pediatr Endocrinol. 2016;25(2):23-35.
31. Halpern JP, Boyages SC, Maberly GF, Collins JK, Eastman CJ, Morris JG. The neurology of endemic cretinism. A study of two endemias. Brain. 1991;114 (Pt 2):825-41.
32. Arii J, Tanabe Y, Makino M, Sato H, Kohno Y. Children with irreversible brain damage associated with hypothyroidism and multiple intracranial calcifications. J Child Neurol. 2002;17(4):309-13.
33. La Piana R, Vanasse M, Brais B, Bernard G. Myelination Delay and Allan-Herndon-Dudley Syndrome Caused by a Novel Mutation in the SLC16A2 Gene. J Child Neurol. 2015;30(10):1371-4.

Chapter

C-terminal mutations in the thyroid hormone transporter monocarboxylate transporter 8

3.3

Stefan Groeneweg, Ferdy S. van Geest, Kyra Stuurman, Nicole Wolf, Cláudia Fernandes Lorea, Nicola Brunetti, Gerarda Cappuccio, Priyanka Bakthiani, Robin P. Peeters, W. Edward Visser

Manuscript in preparation

ABSTRACT

Context Mutations in the thyroid hormone transporter MCT8 can cause intellectual and motor disability and abnormal serum thyroid function tests, known as MCT8 deficiency. Here, we studied the functional characteristics of five novel mutations within the poorly conserved C-terminal domain of MCT8 and their relation to the clinical phenotypes.

Methods Whole exome sequencing or Sanger sequencing of *SLC16A2* was performed in five families of seven boys with developmental delay. The impact of identified MCT8 mutations was evaluated in transiently transfected cell lines and patient-derived fibroblasts.

Results All affected patients harboured potentially deleterious mutations in exon 6 of *SLC16A2*, encoding the C-terminal domain of MCT8. Two patients with clinical features considered atypical for MCT8 deficiency, had a missense mutation (H575R or N599S) that did not affect MCT8 function in transfected cells or patient-derived fibroblasts, challenging a causal relation. Two brothers with classical MCT8 deficiency had a truncating A565Sfs*1 mutation that completely inactivated MCT8 *in vitro*. The three other patients had relatively less severe features of MCT8 deficiency and harboured frameshift mutations that elongate the MCT8 protein (L602fs*78 and P609fs*68) and retained ~50% residual activity. Additional studies with artificial mutations revealed that truncating mutations within transmembrane domain 12 were fully inactivating, whereas those within the intracellular C-terminal tail were tolerated.

Conclusions Our studies demonstrate that mutations affecting the intracellular C-terminal tail of MCT8 are likely benign unless they result in frameshifts that elongate the MCT8 protein. These findings provide clinical guidance in the assessment of the pathogenicity of variants within the C-terminal domain of MCT8.

INTRODUCTION

Thyroid hormone requires transporter proteins to facilitate its transport across the cell membrane (1). The monocarboxylate transport (MCT)8 is the most specific thyroid hormone transporter identified to date and facilitates the cellular uptake and efflux of T3 and T4 (2, 3). Mutations in MCT8 can result in MCT8 deficiency (Allan-Herndon-Dudley syndrome, AHDS) characterized by severe intellectual and motor disability and abnormal thyroid function tests (increased serum T3, reduced T4 and high-normal TSH concentrations) (4, 5). The profound neurocognitive phenotype has been attributed to impaired transport of thyroid hormone across the blood-brain barrier and into target cells inside the brain (6, 7). Tissues that rely on transporters other than MCT8 are exposed to high serum T3 concentrations, resulting in classical signs of tissue thyrotoxicosis such as impaired weight gain, tachycardia and increased perspiration.

Over the last decade, many patients with MCT8 deficiency have been described harboring different underlying mutations in the *SLC16A2* gene that encodes MCT8 (reviewed in (8, 9)). The majority of patients exhibit severe intellectual disability, have poor head control, are unable to sit independently and do not develop any speech. However, a small subset is able to walk and talk in simple sentences (e.g. (10)). Not all mutations in *SLC16A2* cause MCT8 deficiency which may lead to misinterpretation of causality and diagnostic delay. Therefore, it is of utmost importance to differentiate disease causing mutations from those that have no impact on MCT8 thyroid hormone transport function. This is particularly relevant in the context of next generation sequencing technologies which are steadily incorporated in the diagnostic work-up of many diseases. For this purpose, *in silico* prediction tools, based on genetic conservation, are often used (e.g. (11-14). However, such tools frequently yield inconclusive results, especially when mutations affect poorly conserved regions. This warrants complementary approaches to prove causality. Ideally this entails functional evaluation of the mutation in over-expression models or patient-derived fibroblasts. Although these systems have proven to provide good disease models for MCT8 deficiency (e.g. (15-17)), they are not ubiquitously available. Alternatively, knowledge on protein structure may allow more adequate prediction of the consequences of mutations on protein function. However, at present, crystal structures of MCT8 are not available. Although protein homology models have provided important insights into the structure-function relation of some domains within MCT8 (18-20), their accuracy is low for regions with low structural similarity to the template structures. For this reason, the available models even lack the complete intracellular N- and C-terminal tails. The function of these domains is currently unknown, although they account for ~25% of the protein size. Insights on their functional relevance would be vital to the interpretation of novel mutations in these regions.

Here, we studied the functional characteristics of five novel mutations within the C-terminal domain of MCT8 and examined their relation to the observed phenotype in patients whom were clinically suspected for MCT8 deficiency. We took advantage of these and additional mutations to determine the minimal length of the C-terminal tail required for normal MCT8 function *in vitro*. Together, our findings provide important guidance in the assessment of the pathogenicity of variants within the C-terminal tail of the MCT8 protein.

METHODS

Materials

Nonradioactive iodothyronines were obtained from Henning (Berlin, Germany). [3´-125I]T3 and [3´,5´-125I]T4 were prepared as previously described (21). X-tremeGENE9 transfection reagent was obtained from Roche Diagnostics (Woerden, The Netherlands [NL]). Cell culture flasks and plates were obtained from Corning (Schiphol, NL). An overview of the antibodies is provided in **Supplemental Table 1**. Sulfo-NHS-biotin was obtained from Gentaur (Eersel, NL). Neutravidin agarose was obtained from Thermo Fisher scientific (Bleiswijk, NL).

Genetic analysis

Genetic analyses were carried out using next generation sequencing or target sequencing of the SLC16A2 gene (Xq13.2) according to standard methods. Nucleotides and amino acid residues were numbered according to the reference gene sequence of the transcript GenBank (NCBI) NM_006517.3 (NP_006508.2) with the A of the ATG translation initiation codon of the long MCT8 translational isoform regarded as nucleotide position +1 and the corresponding initiation coding as the first amino acid codon. In silico analysis of pathogenicity was performed using the PolyPhen-2 (http://genetics.bwh.harvard.edu/pph2/), CADD (https://cadd.gs.washington.edu/), PROVEAN (http://provean.jcvi.org/index.php), and SIFT (http://sift.jcvi.org/) prediction tools.

Plasmids

The cloning of wild-type (WT) human MCT8 cDNA into pcDNA3 and human μ-crystallin (CRYM) into pSG5 has been described previously (3, 22). The generation of a WT human MCT8 expression containing a 227-nucleotide extension of the 3'UTR (further referred to as 3'UTR-MCT8) has been described before (23). The indicated mutations were introduced using site-directed mutagenesis according to manufacturer's protocol (Stratagene, Amsterdam, NL), using primers available upon request. The 3'UTR-MCT8 construct was used as a template for all frameshift mutations that resulted in an alternate reading frame that exceeded the natural stop codon of MCT8, whereas the regular MCT8 expression construct was used as a template for all other mutations. All constructs were sequenced to confirm the presence of the intended mutation.

Cell culture and transfection

COS-1 (African green monkey kidney fibroblasts) cells, JEG-3 (human choriocarcinoma) cells were cultured and transiently transfected as previously described (19). For T3 uptake studies, COS-1 or JEG-3 cells were cultured in 24-well plates, and transiently transfected at 70% confluence with 100 ng pcDNA3 empty vector (EV), or 100 ng WT or indicated mutant MCT8 expression construct in the presence or absence of 50 ng CRYM. For surface biotinylation studies, cells were seeded in 6-well plates (6-wells per condition) and transiently transfected with 500 ng pcDNA3 EV, WT or indicated mutant MCT8. For immunocytochemistry, JEG-3 cells were cultured in 24-well dishes on 10-mm glass coverslips coated with poly-D-lysine (Sigma-Aldrich, Zwijndrecht, NL).

Human fibroblasts were cultured as previously described (24). For uptake studies, fibroblasts were seeded in 6-well plates and grown until >95% confluence.

Thyroid hormone uptake studies

Thyroid hormone uptake studies were performed using well-established protocols (e.g. (25)). Cells were washed once with incubation buffer (D-PBS+Ca^{2+}/Mg^{2+} supplemented with 0.1% glucose and 0.1% BSA) and incubated in incubation buffer containing 1 nM (50,000 cpm) [^{125}I]-T3 or [^{125}I]-T4. After indicated incubation times, cells were briefly washed with incubation buffer and lysed in 0.1 M sodium hydroxide. The internalized radioactivity was measured with a gamma-counter. Thyroid hormone uptake levels in human fibroblasts were corrected for total protein concentrations as measured by Bradford assay according to manufacturer's guideline (Bio-Rad, Veenendaal, NL).

Cell surface biotinylation and immunoblotting

Cell surface biotinylation studies were performed according to well-established protocols (19, 24). Cell surface proteins were labeled with Sulfo-NHS-biotin and lysed in IP buffer (50 mM Tris-HCl, 150 mM NaCl, 10 mM EDTA, 1% Triton X-100), containing protease inhibitor cocktail (Roche). After brief sonication, samples were clarified from nuclear debris by centrifugation (15 000 rcf for 10 minutes). A 5% aliquot was used as an input control. Cell surface proteins were isolated using Neutravidin agarose beads (Thermo Fisher Scientific) and eluted in NuPAGE 1x lithium dodecyl sulfate (LDS) loading buffer (Thermo Fisher Scientific) containing 10 mM DTT by incubating the beads for 5 minutes at 90 °C prior to immunoblot analyses. Samples were analyzed by immunoblotting as previously described (19, 24), using antibodies listed in **Supplemental Table S1**.

Immunocytochemistry

Transiently transfected JEG-3 cells were fixed with 4% paraformaldehyde and permeabilized with 0.2% triton X-100 in PBS 48 h after transfection. Samples were blocked for 1 hour at room temperature in PBS containing 2% BSA (Sigma Aldrich), and incubated overnight with rabbit anti-MCT8 (1:1,000) and mouse monoclonal ZO-1 antibody (RRID:AB_2533147; 1:500), which served as a membrane marker. After secondary staining with goat anti-rabbit Alexa Fluor 488 (1:1000) and goat anti-mouse Alexa 633 (1:1000), cover slips were mounted on glass slides with Prolong Gold containing DAPI (Invitrogen) and examined as previously described (25).

Ethical considerations

Skin fibroblasts were kindly provided by care-giving physicians and concerned samples that were collected for diagnostic purposes. Clinical examinations were carried out in the context of routine patient care and were described in this study retrospectively. Written informed consent was obtained from the parents or legal representatives of the involved patients and controls to use their medical data for publication. This study was conducted in agreement with the Medical Research Involving Human Subjects Act and (if applicable) formal ethics approval was obtained from the relevant institutional ethical committee(s).

Statistical analysis

All statistical analyses were performed using GraphPad Prism Version 5 software (GraphPad Software Inc., San Diego, USA). Statistically significant differences are indicated as described in the legends of the Figures.

RESULTS

Clinical features

Patients P1 and P2 are dizygotic twins born to non-consanguineous parents. The initial presentation of both patients comprised severe developmental delay and feeding problems, necessitating percutaneous tube feeding from the first year of life. At time of referral, both boys were 7 years old and did not achieve early developmental milestones (**Table 1**). Severe truncal hypotonia was present, accompanied by dystonic posturing and brisk tendon reflexes in the limbs. Language development was limited to some phonation. Scoliosis and gastric reflux disorder were present in both boys. Body height and weight were low for age (**Table 1**). Resting heart rate was normal. Isolated systolic hypertension and increased perspiration were present in P1. Sequential brain MRI studies showed delayed myelination in both patients. Serum thyroid function tests showed the characteristic pattern of MCT8 deficiency, with high serum T3 concentrations and low (free) T4 concentrations (**Table 1**). In addition, serum sex-hormone binding globulin concentrations were elevated and total cholesterol concentrations were low (**Table 1**).

P3 was born to non-consanguineous parents at term of gestation by caesarean section with a birth weight of 2780 grams (<P5). He presented at the age of 7 years with moderate intellectual disability, microcephaly and a low body weight for age. Motor development was delayed. Independent sitting was achieved by the age of 11 months and he was able to walk independently by the age of 4 years. He was able to speak his first words by the age of 5 years. By the age of 8 years, he developed tonic-clonic seizures with epileptic abnormalities detectable on EEG. At time of last evaluation at the age of 9 years and 4 months, he still exhibited mild clumsiness with difficulties in climbing the stairs and he could only speak 3-4 words. Social interaction was normal. Body weight (-3.23 SD) and height (-1.9 SD) were low for age. He did not present pronounced hypotonia, and spasticity as well as dystonic features were absent. Dysmorphic features included an elongated face, bulbous nose, large ears and convergent exotropia. Auditory brain stem responses and ophthalmology evaluation were normal. Cardiac and abdominal ultrasound examination did not detect any anomalies. Brain MRI scans were performed twice and they were reportedly normal. A metabolic diagnostic work-up, including plasma aminoacids and acylcarnitines, urinary organic acids and glycosaminoglycans (GAGs), urinary oligosaccharides, blood and urine creatine-derived metabolites, was unremarkable. Isoelectric focusing of serum transferrin showed an increase of di- and tri-sialotransferrins. Thyroid function tests at the age of 7 years exhibited serum T3 concentrations within normal range and (free) T4 concentrations at the lower end of the normal range (**Table 1**).

P4 is a 5-year old boy born to non-consanguineous parents. He first presented at the age of 4 years with mild global developmental delay without additional health problems other than recurrent ear-nose-throat infections. Achievement of motor milestones and speech was delayed. He was 5 years at time of referral when he was able to walk and jump and speak in simple sentences. He reportedly had reduced exercise tolerance and was unable to walk for long distances. Mild swallowing difficulties were reported by his parents. Physical examination did not reveal apparent abnormalities. He did not present pronounced hypotonia and dystonic and spastic features were absent, although he reportedly experienced increased muscle tone during emotional distress. Seizures were absent. Body weight and height were normal for age and resting tachycardia and excessive perspiration were absent during

physical examination. Serum T3 concentrations were within normal range, whereas serum rT3 and (free) T4 concentrations were at the lower end of the normal range (**Table 1**).

P5 is a currently 4.5-year-old boy born to non-consanguineous parents, who presented global developmental delay and poor weight gain. He presented generalized hypotonia and delayed motor development for which he was referred to the pediatric neurologist by the age of 14 months. At that time a was able to roll-over and attained head control. Brain MRI was reportedly normal. Electroencephalography revealed a slow background pattern, but no epileptic activity despite the presence of staring spells. At time of last evaluation at the age of 4.5 years, he was able to briefly stand independently and understand verbal commands. He had been able to speak in words, but with poor articulation. This recently regressed to babbling. Despite his ability to maintain body posturing, truncal hypotonia was present. His initial growth was unremarkable, but at present he has difficulty gaining weight. Tachycardia was present in rest. Serum thyroid function tests showed the classical pattern of MCT8 deficiency (**Table 1**).

P6 and his younger half-brother P7 are born to non-consanguineous parents and have the same biological mother. Both boys presented developmental delay with truncal hypotonia, dystonic posturing and spasticity. P7 achieved full head control at the age of 1 year, although independent sitting had never been acquired. Body weight was low for age in both cases, and particularly P7 was severe underweight. Irritability was present in both patients. Measurement of thyroid hormone function tests revealed a marginally increased T3, a low normal free T4 and normal TSH in P6, and a marginally increased T3, low free T4 and normal TSH in P7 (**Table 1**). Notably, also serum sex hormone binding globulin was elevated in P7.

Genetic studies

Based on their clinical and biochemical features, DNA of patients P1, P2, and P5-P7 were tested for mutations in SLC16A2. In P3 and P4, whole exome sequencing was performed in the context of unknown developmental delay. The results of the sequencing analyses are graphically depicted in **Figures 1A-C**. A c.1695delT mutation was found in P1 and P2, resulting in a frameshift mutation and premature truncation of the MCT8 protein at the next codon (p.A565Afs*1, further referred to as A565fsX). In patient P5 a single nucleotide deletion (c.1805delT) was identified in exon 6, resulting in a frameshift and elongation of the MCT8 protein (p.L602Hfs*78, further referred to as L602fsX). In P6 and P7, a deletion of 10 nucleotides (c.del1826-1835) was found in exon 6, causing a frameshift and elongation of the MCT8 protein (p.P609fs*68, further referred to as P609fsX). The unaffected mother was heterozygous for the same mutation. In P3, whole exome sequencing was performed on both affected members of the family and their parents. A hemizygous c.1724A>G variant was identified resulting in substitution of His575 by an Arg (p.H575R). This mutation was inherited through his unaffected mother and has an allele frequency of 0.0057% in ExAC (http://exac.broadinstitute.org/), with 2 hemizygotes reported. Whole exome sequencing in P4 revealed a novel c.1796A>G mutation, which results in the substitution of Asn599 by a Ser (p.N599S). This variant was also found in the healthy mother and maternal grandmother and absent in two healthy brothers of the maternal grandmother. The His575 and Asn599 are both highly conserved among species (**Supplemental Figure S1**). **Table 2** summarizes the predicted pathogenicity of the different mutations based on different *in silico* prediction tools frequently used in clinical practice. Considerable variation was present in the predicted pathogenicity of both missense mutations.

Table 1. Patient characteristics.

Proband	I	II	III	IV	V	VI	VII
Age (years)	7	7	9.9	5	4	15.2	7.5
Mutation	p.A565Afs*1	p.A565Afs*1	p.H575R	p.N599S	p.L602Hfs*78	p.P609Qfs*68	p.P609Qfs*68
Birth weight in percentile (grams)	NA	NA	2780 (<P5)	3895 (p98)		3080	2820
Endocrine features							
Serum total T3 (nmol/L)	6.4 (2.0-3.3)	4.38 (2.0-3.3)	2.44 (2.0-3.3) *	2.26 (2.0-3.3)	3.47 (1.61-3.20) #	3.05 (1.6-3.0)	3.73 (2.0-3.3)
Serum TT4 (nmol/L)	54 (74-151)	41 (74-151)	81 (74-151)*	82 (74-151)	42.5 (57.9-154.5) #	79 (62-136)	57 (74-151)
Serum FT4 (pmol/L)	6.6 (13-26)	6.4 (13-26)	15.6 (13-26)*	17.6 (13-26)	11.6 (11.6-18) #	12.3 (12-24)	9.7 (13-26)
Serum rT3 (nmol/L)	0.11 (0.2-0.5)	0.10 (0.2-0.5)	0.37 (0.2-0.5)*	0.24 (0.2-0.5)	0.08 (0.12-0.38) #	0.19 (0.2-0.5)	0.11 (0.2-0.5)
Serum TSH (mU/L)	4.42 (0.6-5.6)	5.19 (0.6-5.6)	0.94 (0.6-5.6)*	2.47 (0.6-5.6)	3.02 (0.5-4.3) #	1.22 (0.6-5.2)	3.90 (0.6-5.6)
Serum SHBG (nmol/L)	275 (40-140)	282 (40-140)	149.9 (40-140)*	ND	163 (40-140) #	ND	214.6 (40-140)
Serum total cholesterol (mmol/L)	2.1 (2.8-5.4)	2.7 (2.8-5.4)	ND	4.0 (2.8-5.4)	ND	ND	ND
Tachycardia in rest	-	-	-	-	+		
Body weight in kg (SD)	21.2 (-1.47)	22.0 (-1.15)	19.5 (-3.2)	17.8 (0)	14.5	25 (-1.5)	26.5 (-8.5)
Head circumference in cm (SD)	52.5	51	47.5 (-4.2)	50 (0.75)	51	54.5 (1.0)	52 (-2.8)
Body height in cm (SD)	115 (-2.55)	115 (-2.56)	123.4 (-1.9)	107.5 (0.4)	109	133.5 (-0.8)	137 (-4.0)
BMI	16.03 (0.50)	16.64 (0.91)	12.8 (-2.7)		12.28		
Increased perspiration	+	-	-	-	-	+	-
Diarrhea	-	-	-	-	-	-	-
Neurological features							
Dystonia	++	++	-	-	+	+	+
Spasticity	+	+	-	-	+/-	+	+
Hypotonia	++	++	+	-	+	+	+
Speech development	Absent	Absent	No verbal speech	Sentences (delayed)	Some words	No verbal speech	No verbal speech
Head control	-	-	+	+	+	+/-	+
Sitting independently	-	-	+ (11 m)	+	+/-	-	-
Walking independently	-	-	+ (4y6m)	+ (22 m)	-	-	-
Delay in achieving motor milestones	Severe	Severe	Moderate	Mild	Severe	Severe	Severe
GMFM-G88 score (%)[1]	7	8	ND	ND	29.7	ND	ND
IQ score (test)	ND	ND	ND	ND	ND	ND	ND
Psychiatric symptoms	ND	ND	-	-	-	Irritability	Irritability, aggressive
EEG-proven seizures	-	-	+	-	-	+	+
Feeding problems	+	+	+	-	+	+	+
Brain MRI abnormalities	Delayed myelination	Delayed myelination	-	-	-	-	Peirventricular WM hyperintensities, choroid cyst

[1] GMFM-G88 is Gross Motor Function Measure-G88 which assesses the gross motor function. Scores range from 0 to 100%, with higher scores indicating better motor function and where a 100% score is achieved by a normal developing child of 4 years of age. Thyroid function tests are measured at the age of 7 years and 6 months (*) or 3 years (#). WM, white matter; ND, not determined.

Table 2 *In silico* prediction of the pathogenicity of the identified *SLC16A2* mutations

Patient	Mutation	PROVEAN(11)	CADD (12)	PolyPhen2 (13)	SIFT (14)
P1, P2	p.A565Afs*1	Deleterious (-44.7)	NA	NA	NA
P3	p.H575R	Deleterious (-3.4)	Possibly deleterious (21.9)	Benign (0.04)	Tolerated (0.33)
P4	p.N599S	Neutral (-1.8)	Possibly deleterious (23.5)	Possibly deleterious (0.21)	Tolerated (0.12)
P5	p.L602Hfs*78	Deleterious (-16.3)	NA	NA	NA
P6, P7	p.P609Qfs*68	Deleterious (-9.0)	NA	NA	NA

In silico prediction tools were used according to their online instructions. The following cut-offs were recommended. PROVEAN scores <-2.5 are considered deleterious. CADD scores >15 are generally regarded as possibly deleterious. PolyPhen-2 scores between 0.85-1.0 are considered deleterious, whereas scores between 0.15-0.85 are considered possibly deleterious. A SIFT score between 0.0-0.05 is considered deleterious, whereas scores between 0.05-1.0 are considered benign.

Functional analyses of identified mutations

To investigate if the identified mutations in SLC16A2 were causative for the observed clinical phenotype, MCT8 expression constructs harboring these mutations were transiently overexpressed in COS-1 cells. MCT8-mediated T3 and T4 uptake in cells expressing H575R or N599S mutant MCT8 did not significantly differ from cells expressing WT MCT8 (**Figure 2A**). The L602fsX and P609fsX mutations showed a ~50% reduction in T3 and T4 uptake compared to WT MCT8, whereas the A565fsX mutant was completely inactive. Expression levels of the H575R and N599S mutant MCT8 proteins did not differ from WT MCT8, whereas those of all three frameshift mutants were significantly lower than WT in total lysates of transfected COS-1 cells (**Figure 2B**). Similarly, the expression levels of H575R and N599S mutant proteins at the cell membrane were equal to those observed for WT MCT8, whereas those of the frameshift mutants were significantly reduced (**Figure 2C** and **2D**). Kinetic analyses of T3 transport showed that the apparent Km and Vmax of the H575R mutant did not differ from WT, whereas the N599S mutant showed a marginal increase in Vmax (**Figure 2E**). In contrast, the L602fsX and P609fsX mutations significantly reduced the Vmax and Km of T3 transport by MCT8 (**Figure 2E**). The kinetic properties of the A565fsX mutant could not be studied due to the low residual uptake capacity.

In line with the observations in COS-1 cells, the H575R and N599S mutants did not affect T3 or T4 uptake in transiently transfected JEG-3 cells, whereas the A565fsX mutant was completely inactive. The L602fsX and P609fsX mutants showed T3 and T4 uptake levels amounting up to ~20-30% of WT MCT8 (**Figure 3A**). Immunocytochemistry performed in JEG-3 cells showed that the H575R and N599S mutant proteins were predominantly localized at the cell membrane, as was the case for WT MCT8 (**Figure 3B**). In contrast, all three frameshift mutant proteins showed a pronounced perinuclear staining and only little expression at the cell membrane.

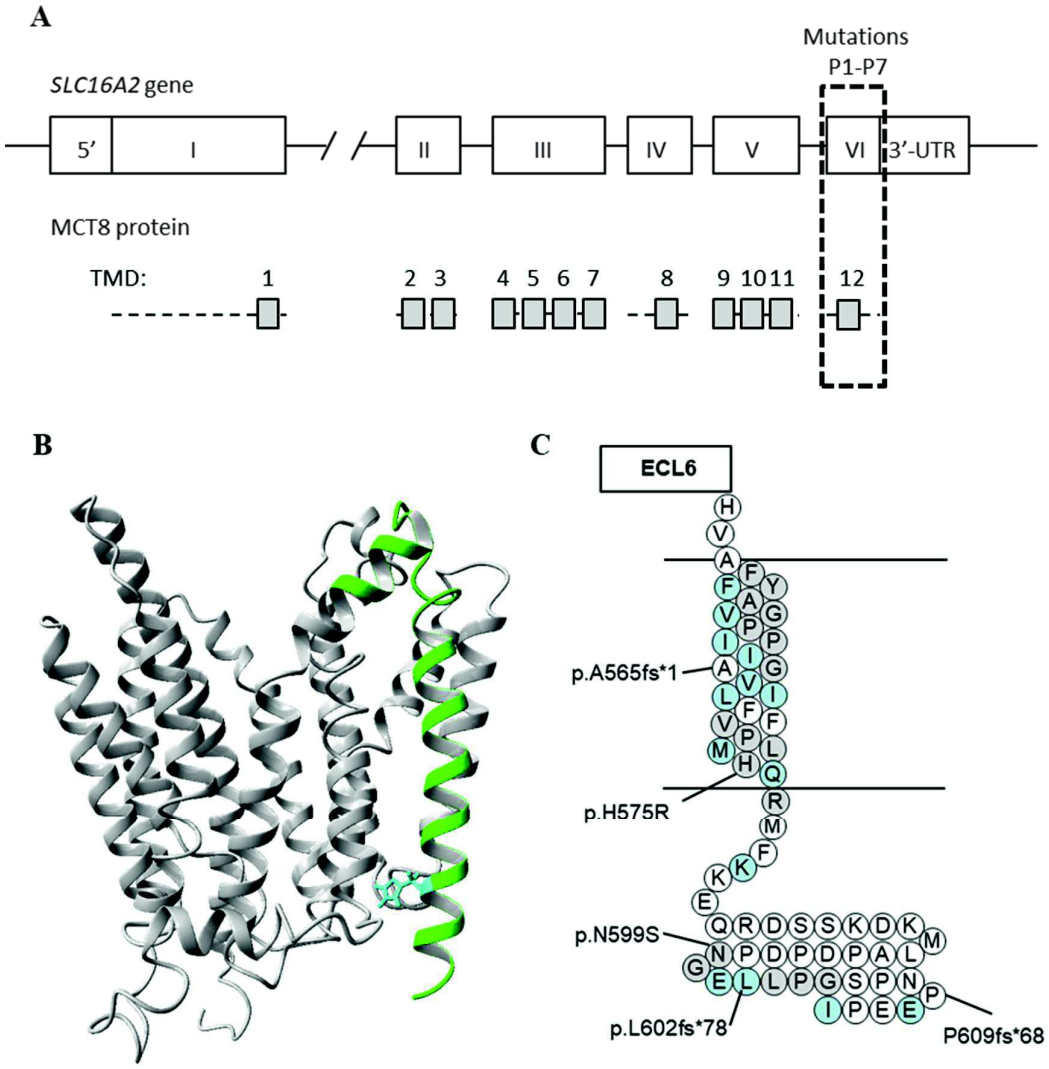

Figure 1 (A) Schematic representation of the *SLC16A2* gene and MCT8 protein. The transmembrane domains (TMDs) are displayed as grey boxes and aligned to their coding exons. All mutations identified in this study locate to exon 6 (boxed with dashed lines). **(B)** MCT8 homology model in which the residues encoded by exon 6 are highlighted in green. The His575 residue is highlighted in blue. **(C)** Schematic representation of TMD12 and the intracellular C-terminal tail. The locations of the identified mutations are indicated. Strongly conserved residues are colored blue, whereas those with strongly similar properties across species are colored grey (see **Supplemental Figure 1** for detailed alignment).

Next, we substituted the His575 and Asn599 by an Ala to confirm that both residues are not crucial for MCT8 function despite their strong evolutionary conservation (**Figure 1C**). Indeed, both, the H575A and N599A mutants, facilitated the uptake of T3 and T4 as efficient as WT MCT8 in COS-1 and JEG-3 cells (**Supplemental Figure S2**).

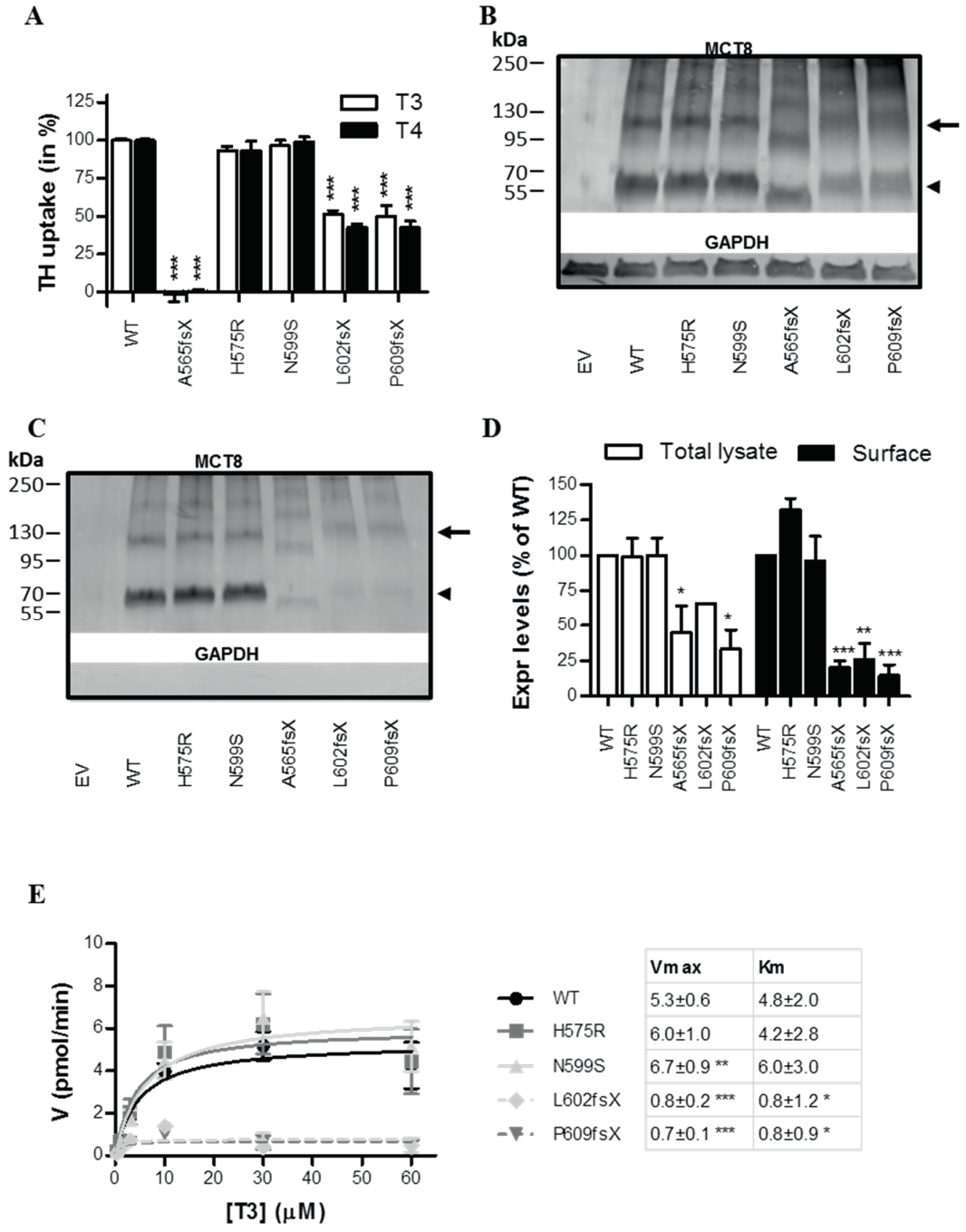

Figure 2 (A) T3 and T4 uptake in transiently transfected COS-1 cells in presence of the intracellular thyroid hormone-binding protein CRYM, after 30 min incubation at 37 °C. Uptake levels are corrected for those observed in pcDNA3 empty vector (EV) transfected control cells and expressed relative to wild-type (WT) MCT8. Two-way ANOVA with Bonferroni post-tests were performed to assess for statistically significant differences between WT and indicated mutant MCT8. Immunoblot of total lysates **(B)** and biotinylated cell surface fraction **(C)** derived from COS-1 cells transiently transfected with WT or indicated mutant MCT8. The total lysate comprised a 5% input samples of the clarified lysate from which the presented surface fraction was derived. MCT8 monomers (arrowhead) and homo-dimers (arrow) are indicated. **(D)** Quantification of the total and cell surface expression levels using densitometry (ImageJ). The means ± SEM from N=3 independent experiments are displayed. Two-

way ANOVA with Bonferroni post-tests were performed to assess for statistically significant differences between WT and indicated mutant MCT8. **(E)** Michaelis-Menten plots showing kinetic properties of WT and mutant MCT8 transiently expressed in COS-1 cells in the absence of CRYM. The uptake in cells transfected with pcDNA3 empty vector was subtracted as background. Incubations were performed for 10 min at 37 °C with increasing concentrations of T3. Data are expressed as means of 3 independent experiments performed in duplo +/- SEM. Apparent Km and Vmax values are summarized and were compared to those obtained for WT using One-way ANOVA with Dunnett's post-tests. All statistically significant differences are indicated as follows: ($p<0.05$, *; $p<0.01$, **, $p<0.005$ ***).

To validate the apparent benign nature of the H575R and N599S mutations in an independent ex vivo model, we also performed T3 uptake studies in patient-derived fibroblasts which have been previously shown to be a good model to study the pathogenicity of MCT8 mutations (15). Also in patient-derived fibroblasts, T3 uptake did not differ between cells harboring the H575R or N599S mutation and healthy controls (**Figure 3C**). In contrast, T3 uptake was greatly diminished in fibroblasts derived from a patient with a Q97Rfs*60 mutation (referred to as Q97fsX) that results in premature truncation of the protein (**Figure 3C**). The MCT8-specific inhibitor silychristin (26) reduced T3 uptake by the H575R and N599S mutant fibroblasts and control fibroblasts by a similar extent, whereas no effect was observed in the Q97fsX mutant fibroblasts (**Figure 3C**). These results indicate that the H575R and N599S mutations have no apparent functional consequences on thyroid hormone transport in this ex vivo model.

Exploring tolerable variation in the C-terminal tail of MCT8

All identified mutations were located in exon 6 which encodes transmembrane domain (TMD)12 and the intracellular C-terminal tail, but had different effects on MCT8 function. To further delineate the relevance of the C-terminal domain for MCT8 function, we generated a series of artificial premature stop mutations that result in successive truncation of the C-terminal tail. Guided by our previously published MCT8 homology model (**Figure 4A**), premature stop codons were introduced at positions Pro560 and Leu568 (both located within TMD12), His575 (located at the transition of TMD12 and C-terminal tail), and Gly600, Pro604 and Glu610 (all within C-terminal tail) (**Figure 4B**). Upon over-expression in COS-1 or JEG-3 cells, the Pro560X and L568X diminished MCT8-mediated T3 and T4 uptake, whereas all other mutations had no or very limited effects (**Figure 4C** and **4D**). Immunoblotting on total lysates from transiently transfected COS-1 cells showed that the protein expression levels of all premature stop mutants were lower than WT MCT8, although the difference only reached statistical significance for the P560X and L568X mutants (**Figure 4E**, **Table 3**). Similarly, the cell surface expression levels of the P560X and L568X mutants were about 50% lower than WT MCT8 (**Figure 4F**, **Table 3**). The fraction of the total cellular MCT8 protein content being expressed at the cell membrane of the P560X and L568X mutants was similar to WT, whereas this fraction showed an increasing trend for all other premature stop mutants tested (**Table 3**). In line with the observed cell surface expression levels in COS-1 cells, immunocytochemistry in JEG-3 cells showed pronounced perinuclear staining of the P560X and L568X mutants, whereas all other tested premature stop mutants were predominantly expressed at the cell membrane (**Figure 4G** and **Supplemental Figure S3**).

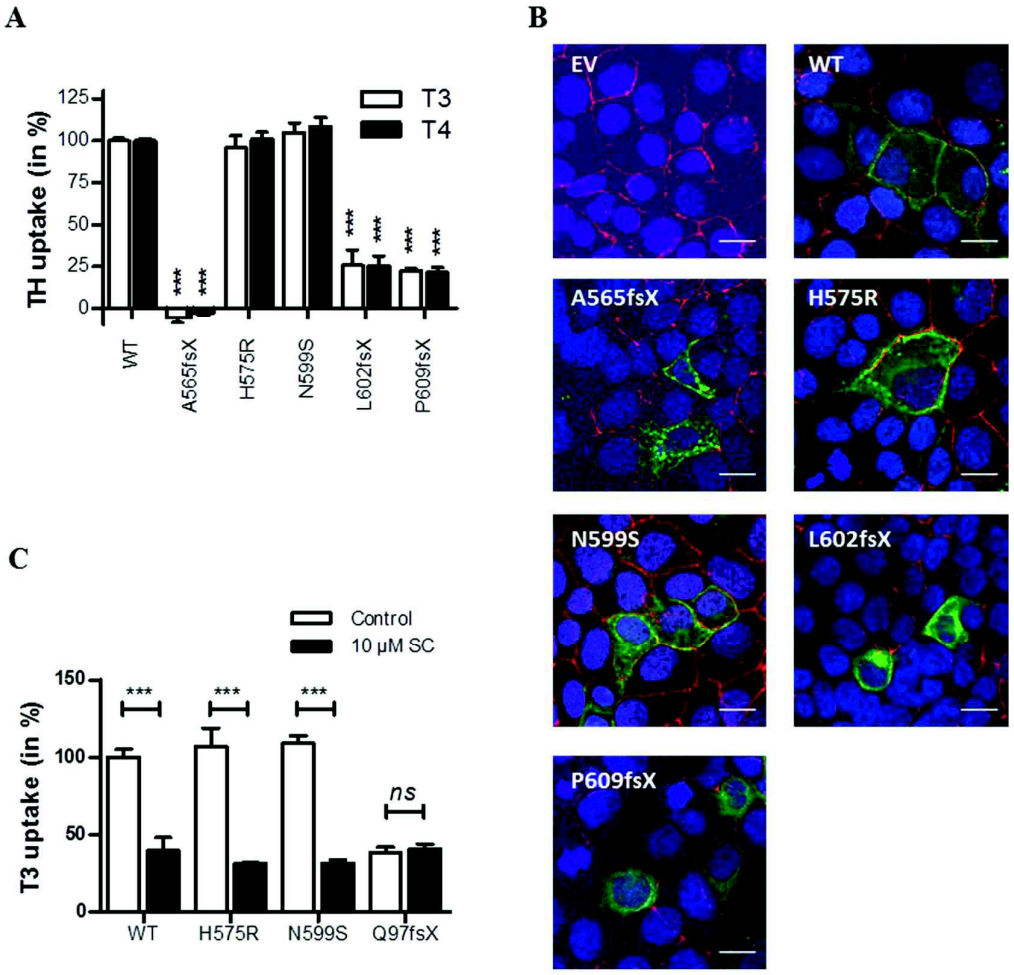

Figure 3 (A) T3 and T4 uptake in transiently transfected JEG-3 cells in presence of CRYM, after 30 min incubation at 37 °C. Uptake levels are corrected for those observed in pcDNA3 empty vector (EV) transfected control cells and expressed relative to wild-type (WT) MCT8. Two-way ANOVA with Bonferroni post-tests were performed to assess for statistically significant differences between WT and indicated mutant MCT8 ($p<0.005$ ***). **(B)** Immunocytochemistry in JEG-3 cells transiently transfected with EV, WT, or indicated mutant MCT8 using antibodies against MCT8 (green) and the membrane marker ZO-1 (red). Cell nuclei were stained with DAPI (blue). Images are presented as an overlay image. The scale bar represents 20µm. **(C)** T3 uptake in patient and control fibroblasts in the absence (-) or presence (+) of 10µM silychristin (SC). Silychristin is a potent and, thus far the most specific, inhibitor of MCT8-mediated TH transport (26). Silychristin significantly reduced T3 uptake in control and H575R and N599S patient fibroblasts (Two-way ANOVA with Bonferroni posttests; $p<0.001$, ***), but not in Q97fsX fibroblasts. The silychristin-induced reduction in T3 uptake did not differ between H575R and N599S *versus* control fibroblasts (One-way ANOVA with Bonferroni posthoc tests, not indicated in the graph).

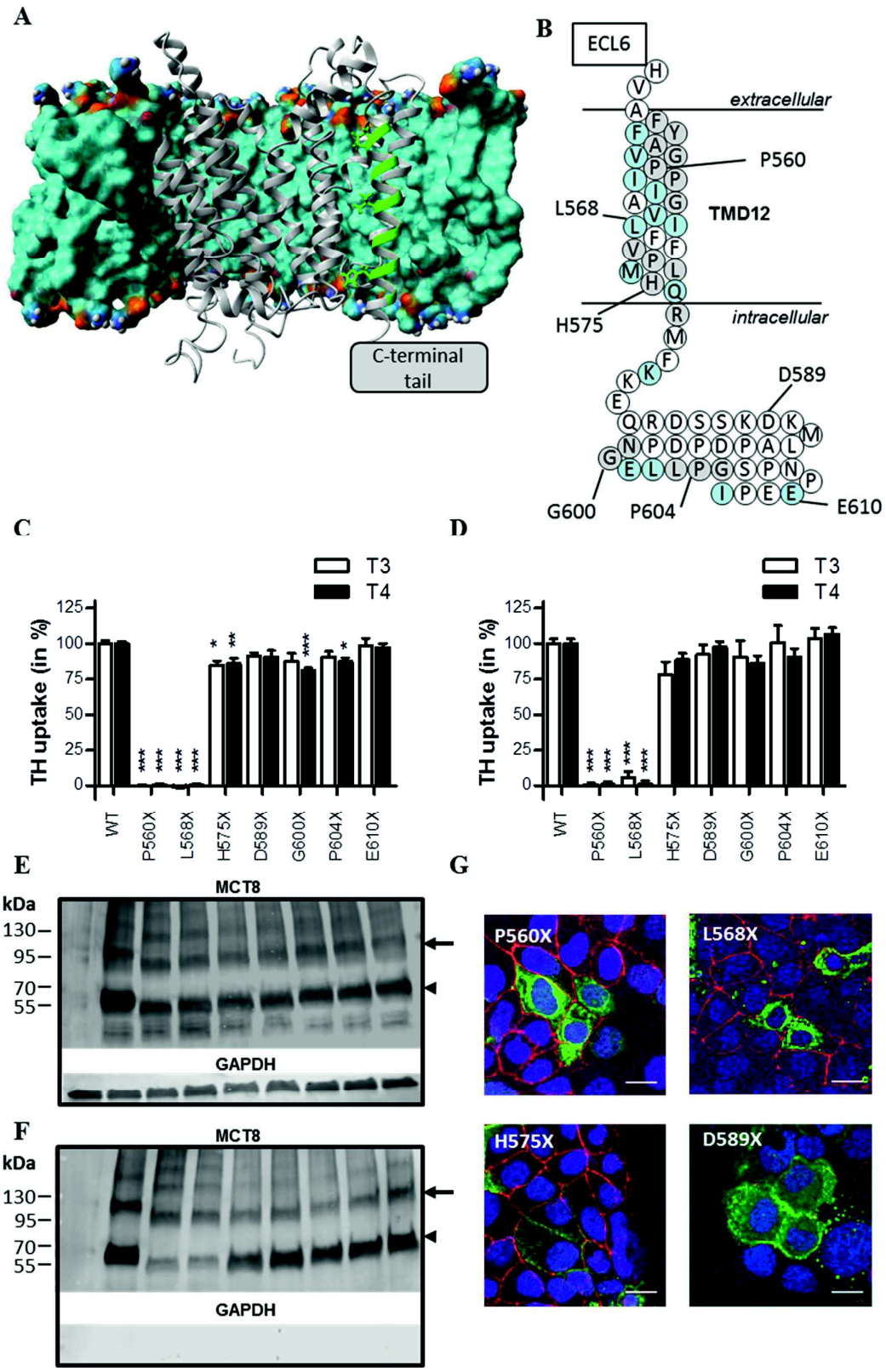
A
C-terminal tail
B
ECL6
extracellular
P560
L568
TMD12
H575
intracellular
D589
G600
P604
E610
C
T3
T4
TH uptake (in %)
WT
P560X
L568X
H575X
D589X
G600X
P604X
E610X
D
E
MCT8
kDa
130
95
70
55
GAPDH
F
G
P560X
L568X
H575X
D589X

Figure 4 (A) MCT8 homology model embedded in a lipid bilayer (displayed as the molecular surface, colored according to atom colors). For clarity, the lipid bilayer in front of the MCT8 protein is hidden. TMD12 is highlighted in green. **(B)** schematic representation of TMD12 and the intracellular C-terminal tail as shown in **Figure 1A**, indicating the position of the truncating mutations that were generated. T3 and T4 uptake in transiently transfected COS-1 **(C)** or JEG-3 **(D)** cells in presence of CRYM, after 30 min incubation at 37 °C. Uptake levels are corrected for those observed in pcDNA3 empty vector (EV) transfected control cells and expressed relative to wild-type (WT) MCT8. Two-way ANOVA with Bonferroni post-tests were performed to assess for statistically significant differences between WT and indicated mutant MCT8 ($p<0.05$, *; $p<0.01$, **, $p<0.005$ ***). Immunoblot of total lysates **(E)** and biotinylated cell surface fraction **(F)** derived from COS-1 cells transiently transfected with WT or indicated mutant MCT8. The total lysate comprised a 5% input samples of the clarified lysate from which the presented surface fraction was derived. MCT8 monomers (arrowhead) and homo-dimers (arrow) are indicated. Expression levels have been quantified in **Table 3**. **(G)** Immunocytochemistry in JEG-3 cells transiently transfected with indicated mutant MCT8 using antibodies against MCT8 (green) and the membrane marker ZO-1 (red). Cell nuclei were stained with DAPI (blue). Images are presented as an overlay image. The scale bar represents 20µm.

Table 3 Quantification of expression levels truncated MCT8 proteins

Construct	Total lysate	Cell surface	Cell surface fraction
WT	1	1	8.6±0.08
P560X	0.56±0.15 **	0.45±0.07 **	7.7±0.32
L568X	0.56±0.06 **	0.46±0.12 **	7.7±2.1
H575X	0.65±0.03	0.83±0.05	11.8±0.31
D589X	0.63±0.04	0.78±0.02	11.8±2.1
G600X	0.72±0.14	0.75±0.13	9.2±1.7
P604X	0.69±0.09	0.87±0.17	11.7±0.3
E610X	0.66±0.02	0.88±0.15	12.4±1.5

Quantification of WT and indicated mutant MCT8 protein in total lysates and the biotinylated cell surface fraction in transiently transfected COS-1 cells (representative blots are shown in **Figure 4E** and **4F**). Expression levels are quantified and presented as mean ± SEM of 3 independent experiments. The cell surface fraction depicts the fraction of total MCT8 protein translocated to the cell membrane (cell surface / 5% input x 20). Expression levels of all mutants were compared to WT using One-way ANOVA followed by Dunnett's posttest. Statistically significant differences are indicated as follows: $p<0.01$, **.

DISCUSSION

Here, we studied the clinical and molecular characteristics associated with a series of mutations that affect the C-terminal domain of the MCT8 protein. We found that missense mutations in two highly conserved residues in this region, H575R and N599S, did not affect MCT8 function *in vitro* and *ex vivo*, despite being predicted as potentially pathogenic. In line with these findings, we observed that successive C-terminal truncations were generally well-tolerated until reaching the transition between the intracellular C-terminal tail and TMD12, suggesting that the intracellular C-terminal tail has no major role in MCT8 function *in vitro*. By contrast, elongation of the C-terminal tail by frameshift mutations was found to reduce MCT8 function by interfering with proper cell membrane trafficking. Such mutations were associated with a relatively less severe clinical phenotype. Taken together, our studies provided important insight into the functional relevance and tolerable variation in the C-

terminal tail of the MCT8 protein which may help predicting the pathogenicity of novel mutations identified in this region.

At present, the pathogenicity of novel mutations in the *SLC16A2* gene are difficult to predict *in silico* approaches. This particularly applies to the less conserved regions of the MCT8 protein including the intracellular C-terminal tail. In such cases, functional evaluation of identified mutations remains critical to prove causality, the importance of which is illustrated by the H575R (patient P3) and N599S (patient P4) mutations described in this study. Both mutations were detected through whole exome sequencing in boys with developmental delay of unknown origin. Typical manifestations of MCT8 deficiency, such as dystonia and delayed myelination on brain MRI, were absent in both patients. Moreover, thyroid function tests showed serum T3 and (free) T4 concentrations within the lower segment of the age-appropriate normal range. This combination casted reasonable doubt on the presence of a causal relation between the identified mutations and the observed phenotype, although thyroid function tests have been previously reported to be within normal range in few MCT8 deficient patients with a relatively less severe clinical phenotype (e.g. (23, 27, 28)). Indeed, both mutations did not affect MCT8-mediated thyroid hormone transport in transiently transfected COS-1 or JEG-3 cells or patient-derived fibroblasts, despite the strong conservation of the affected residues and possible deleterious effects according to some *in silico* prediction tools. This prompted sequencing of additional family members of P3 which revealed the same H575R mutation in a non-affected maternal male cousin. In retrospect, the H575R variant had also been reported in two other apparently healthy hemizygous male individuals (rs140303247, ExAC database, *SLC16A2*). Taken together, these findings support the benign nature of the H575R variant and alternative diagnoses are being considered. No alternative genetic diagnoses have been identified in patient P4. Even though our well-established disease models in transfected mammalian cells and human fibroblasts suggest that the N599S does not cause the observed phenotype, cell-type specific effects of this mutation cannot be fully excluded. Although the clinical features are seemingly aspecific, they could fit with very mild MCT8 deficiency. Further studies in patient-derived induced pluripotent stem cells (IPSc) may provide definitive conclusions on the pathogenicity of this mutation.

To further delineate the role of the intracellular C-terminal tail, we have generated MCT8 constructs with successive C-terminal truncations. We found that the P560X and L568X mutations were fully inactivating, both of which truncating the MCT8 protein within TMD12. Such mutations likely interfere with correct membrane integration and may thereby disturb protein stability and sub-cellular trafficking. In line with these observations, the Ala565Afs*1 mutation, identified in patient P1 and P2, was completely inactive and showed decreased cell membrane expression levels. Accordingly, both patients exhibited classical clinical and biochemical features of MCT8 deficiency (8). In contrast, truncations beyond His575, marking the transition of TMD12 to the intracellular C-terminal tail, did not affect MCT8-mediated thyroid hormone transport. Based on these findings, we postulate that truncating mutations proximal to Leu568 likely result in complete loss of MCT8 function and cause severe clinical features of MCT8 deficiency, whereas truncations beyond His575 are likely to be benign. Interestingly, the most C-terminally located missense mutation reported to be pathogenic also affects the Leu568 residue (L568P) (27), suggesting that missense mutations beyond this point may also be tolerated. The apparent benign nature of the H575R and N599S variants would be in line with this hypothesis.

Although premature truncation of the MCT8 protein beyond His575 was well tolerated *in vitro*, elongation of the MCT8 protein due to frameshift mutations beyond this point (L602Hfs*78 and P609Qfs*68) reduced MCT8 function. In line with their modest residual activity, both mutations were associated with a relatively less severe clinical phenotype. Affected patients acquired several motor skills, including attaining head control and P5 achieved independent standing, and was able to babble. These findings were in line with a previous report describing a family with a c.1834delC frameshift mutation that also elongates the MCT8 protein (P609Qfs*68). The affected males in this family also displayed relatively normal thyroid function tests and had acquired more advanced motor skills, such as sitting without support and eating independently (23). Here, we showed that this type of mutations likely reduce protein stability and interfere with sub-cellular trafficking. We speculate that elongation of the C-terminal tail causes structural constraints with other intracellular domains, may establish novel unfavorable protein-protein interactions, and/or interferes directly with substrate passage.

The function of the C-terminus is unknown. Many membrane proteins require ancillary protein to govern proper cell membrane targeting, some of which have been found to predominantly recognize the C-terminal tail of their targets (29). Although other members of the MCT family require interactions with ancillary proteins for proper cell surface translocation (30), it is unknown if this also holds true for MCT8 (31). Should this be the case, such interactions are not likely to be established through its intracellular C-terminal tail as mutant proteins lacking this domain exhibited surface expression levels similar to WT MCT8. It should however be emphasized that a subset of our studies have been carried out in over-expressing mammalian cell lines. Factors required for optimal MCT8 expression and subcellular targeting may well be different *in vivo* and may, moreover, vary among tissues and different cell populations within the same tissue. Nevertheless, over-expression studies in COS-1 and JEG-3 cells have been shown to correspond well with the *in vivo* MCT8 transport capacity in physiologically relevant tissues. Also, MCT8 function in patient-derived fibroblasts is typically consistent with the findings in over-expression studies (e.g. (10, 15, 24)).

Taken together, we demonstrate that mutations within the intracellular C-terminal tail of MCT8 generally have no impact on MCT8 function *in vitro*, unless they concern frameshift mutations that elongate the MCT8 protein. These findings provide clinical guidance in the assessment of the pathogenicity of variants within the C-terminal tail of the MCT8 protein and underscore the relevance of validating the functional impact of novel variants.

Acknowledgements

We thank Ramona E.A. van Heerebeek and Selmar Leeuwenburgh for the technical assistance, the Optical Imaging Center (Erasmus Medical Center Rotterdam) for technical support regarding the confocal imaging studies, and the physicians of the involved patients and healthy controls for providing the fibroblasts.

Financial support: This work was supported by a grant from the Netherlands Organisation for Health Research and Development (project number 113303005) (to WEV), from the Sherman Foundation (to WEV).

SUPPLEMENTAL MATERIALS

Supplemental Tables

Supplemental Table S1 Antibody Table

Target protein/ antigen	Antigen sequence (if known)	Name of AB	Species raised (P or M)	Manufacturer (and catalog number)	Dilution used for WB	Dilution used for ICH	RRID
hsMCT8	AA 52-155	MCT8	Rabbit (P)	ATLAS (HPA003353)	1:2000	1:1000	AB_1079343
GAPDH		GAPDH	Mouse (M)	Millipore (Mab 374)	1:20000		AB_2107445
ZO1		ZO1	Mouse (M)	Thermo Fisher (33-9100)		1:1000	AB_2533147
Rabbit IgG		IRDye800	Goat	LI-COR (926-32211)	1:20000		AB_621843
Mouse IgG		IRDye680	Goat	LI-COR (926-68020)	1:20000		AB_10706161
Rabbit IgG		Alexa 488	Goat	Thermo Fisher (A11008)		1:1000	AB_143165
Mouse IgG		Alexa 633	Goat	Thermo Fisher (A21050)		1:1000	AB_2535718

AB: antibody; GAPDH: glyceraldehyde-3-phosphate dehydrogenase; ZO-1: zona occludens 1;P: polyclonal antibody; M: monoclonal antibody; WB: Western Blot ; ICH: immunohistochemistry

Supplemental Figures

```
Zebrafish       HVAFYlAGVPPIvGgIVmFFVPLvHQRMqKrrketddpsmdkmlkncsNGdmLPGytdmEthI
Xenopus_tr      dlAFYlAGiPPlIGAmVLlsVPLvHeRdlKKkrqmee-eKekTqDsvvNGELLPGSPvtdEcV
X. Laevis (s)   dlAFYlAGiPPlIGAlVLlsVPLlHeRdlKKkrqmee-eKekTqDsvvNGELLPGSPvtdEcV
X. Laevis (l)   dlAFYlAGiPPlIGAlVLlsVPLiHeRelKKkrqmee-eKekTqDsvvNGELLPGSPvtdEcV
Chicken         HagFYFAGVPPIIGglVLsvVPLvHQRMlqKqrlDSgKDKMLTpeavvNGELLPGcPasEahm
Human (l)       HVAFYFAGVPPIIGAViLFFVPLMHQRMFKKEQRDSSKDKMLapDPdPNGELLPGSPnPEEpI
Human (s)       HVAFYFAGVPPIIGAViLFFVPLMHQRMFKKEQRDSSKDKMLapDPdPNGELLPGSPnPEEpI
Rat             HVAFYFAGVPPIIGAViLFFVPLMHQRMFKKEQRESSKDKMLshDPdPNGELLPGSPtPEEpI
Mouse           HVAFYFAGVPPIIGAViLFFVPLMHQRMFKKEQRDSSKDKMLshDPdPNGELLPGSPtPEEpI
                  .**:**:**::*.:::  ***:*:*  :. .  .  .     .   **::*** .  :  :
                                  TMD12
```

Supplemental Figure S1 Multiple sequence alignment of the C-terminal end of the MCT8 protein. This region includes transmembrane domain (TMD)12 and the intracellular C-terminal tail (see **Figure 1A** and **B**). Amino acid sequences of human, mouse, zebrafish, *Xenopus Tropicalis* (Xenopus tr), the short (s) and long (l) isoforms of *Xenopus laevis* (X. Laevis), chicken, and rat were included. Identical amino acids in all species are indicated with an *. Conservation between amino acids with strongly similar properties (equivalent to scoring > 0.5 in the Gonnet PAM 250 matrix) is indicated with an :, whereas conservation between amino acids with weakly similar properties (equivalent to scoring 0< score <0.5 in the Gonnet PAM 250 matrix) are indicated with a . . Multiple sequence alignments were generated using Clustal Omega.

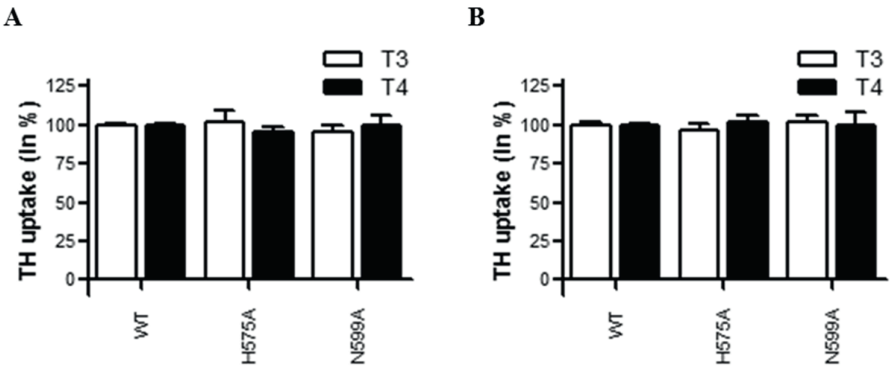

Supplemental Figure S2 T3 and T4 uptake in transiently transfected COS-1 **(A)** or JEG-3 **(B)** cells in presence of CRYM, after 30 min incubation at 37 °C. Uptake levels are corrected for those observed in pcDNA3 empty vector (EV) transfected control cells and expressed relative to wild-type (WT) MCT8. Two-way ANOVA with Bonferroni post-tests were performed to assess for statistically significant differences between WT and indicated mutant MCT8.

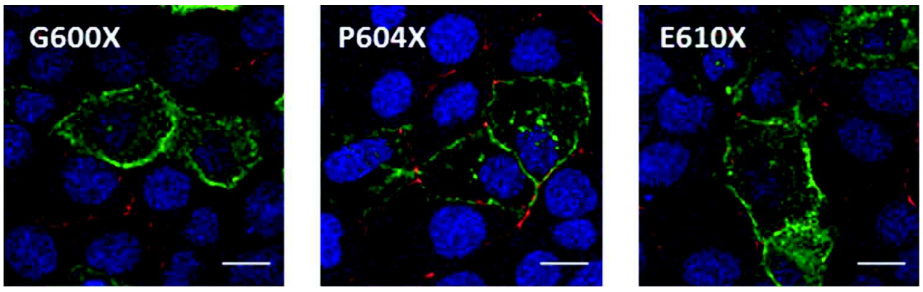

Supplemental Figure S3 Immunocytochemistry in JEG-3 cells transiently transfected with EV, WT, or indicated mutant MCT8 using antibodies against MCT8 (green) and the membrane marker ZO-1 (red). Cell nuclei were stained with DAPI (blue). Images are presented as an overlay image. The scale bar represents 20µm.

REFERENCES

1. Bianco AC, Dumitrescu A, Gereben B, Ribeiro MO, Fonseca TL, Fernandes GW, et al. Paradigms of Dynamic Control of Thyroid Hormone Signaling. Endocr Rev. 2019.
2. Friesema EC, Ganguly S, Abdalla A, Manning Fox JE, Halestrap AP, Visser TJ. Identification of monocarboxylate transporter 8 as a specific thyroid hormone transporter. J Biol Chem. 2003;278(41):40128-35.
3. Friesema EC, Kuiper GG, Jansen J, Visser TJ, Kester MH. Thyroid hormone transport by the human monocarboxylate transporter 8 and its rate-limiting role in intracellular metabolism. Mol Endocrinol. 2006;20(11):2761-72.
4. Friesema EC, Grueters A, Biebermann H, Krude H, von Moers A, Reeser M, et al. Association between mutations in a thyroid hormone transporter and severe X-linked psychomotor retardation. Lancet. 2004;364(9443):1435-7.
5. Dumitrescu AM, Liao XH, Best TB, Brockmann K, Refetoff S. A novel syndrome combining thyroid and neurological abnormalities is associated with mutations in a monocarboxylate transporter gene. Am J Hum Genet. 2004;74(1):168-75.
6. Vatine GD, Al-Ahmad A, Barriga BK, Svendsen S, Salim A, Garcia L, et al. Modeling Psychomotor Retardation using iPSCs from MCT8-Deficient Patients Indicates a Prominent Role for the Blood-Brain Barrier. Cell Stem Cell. 2017;20(6):831-43 e5.
7. Heuer H, Visser TJ. The pathophysiological consequences of thyroid hormone transporter deficiencies: Insights from mouse models. Biochim Biophys Acta. 2013;1830(7):3974-8.
8. Groeneweg S, Visser WE, Visser TJ. Disorder of thyroid hormone transport into the tissues. Best Pract Res Clin Endocrinol Metab. 2017;31(2):241-53.
9. Groeneweg S, van Geest FS, Peeters RP, Heuer H, Visser WE. Thyroid hormone transporters. Endocr Rev. 2019 (accepted).
10. Masnada S, Groenweg S, Saletti V, Chiapparini L, Castellotti B, Salsano E, et al. Novel mutations in SLC16A2 associated with a less severe phenotype of MCT8 deficiency. Metab Brain Dis. 2019 (accepted).
11. Choi Y, Chan AP. PROVEAN web server: a tool to predict the functional effect of amino acid substitutions and indels. Bioinformatics. 2015;31(16):2745-7.
12. Rentzsch P, Witten D, Cooper GM, Shendure J, Kircher M. CADD: predicting the deleteriousness of variants throughout the human genome. Nucleic Acids Res. 2019;47(D1):D886-D94.
13. Adzhubei IA, Schmidt S, Peshkin L, Ramensky VE, Gerasimova A, Bork P, et al. A method and server for predicting damaging missense mutations. Nat Methods. 2010;7(4):248-9.
14. Vaser R, Adusumalli S, Leng SN, Sikic M, Ng PC. SIFT missense predictions for genomes. Nat Protoc. 2016;11(1):1-9.
15. Visser WE, Jansen J, Friesema EC, Kester MH, Mancilla E, Lundgren J, et al. Novel pathogenic mechanism suggested by ex vivo analysis of MCT8 (SLC16A2) mutations. Hum Mutat. 2009;30(1):29-38.
16. Capri Y, Friesema EC, Kersseboom S, Touraine R, Monnier A, Eymard-Pierre E, et al. Relevance of different cellular models in determining the effects of mutations on SLC16A2/MCT8 thyroid hormone transporter function and genotype-phenotype correlation. Hum Mutat. 2013;34(7):1018-25.
17. Kinne A, Roth S, Biebermann H, Kohrle J, Gruters A, Schweizer U. Surface translocation and tri-iodothyronine uptake of mutant MCT8 proteins are cell type-dependent. J Mol Endocrinol. 2009;43(6):263-71.
18. Kinne A, Kleinau G, Hoefig CS, Gruters A, Kohrle J, Krause G, et al. Essential molecular determinants for thyroid hormone transport and first structural implications for monocarboxylate transporter 8. J Biol Chem. 2010;285(36):28054-63.
19. Groeneweg S, Lima de Souza EC, Meima ME, Peeters RP, Visser WE, Visser TJ. Outward-Open Model of Thyroid Hormone Transporter Monocarboxylate Transporter 8 Provides Novel Structural and Functional Insights. Endocrinology. 2017;158(10):3292-306.
20. Protze J, Braun D, Hinz KM, Bayer-Kusch D, Schweizer U, Krause G. Membrane-traversing mechanism of thyroid hormone transport by monocarboxylate transporter 8. Cell Mol Life Sci. 2017;74(12):2299-318.
21. Mol JA, Visser TJ. Synthesis and some properties of sulfate esters and sulfamates of iodothyronines. Endocrinology. 1985;117(1):1-7.
22. Friesema EC, Jansen J, Jachtenberg JW, Visser WE, Kester MH, Visser TJ. Effective cellular uptake and efflux of thyroid hormone by human monocarboxylate transporter 10. Mol Endocrinol. 2008;22(6):1357-69.
23. Maranduba CM, Friesema EC, Kok F, Kester MH, Jansen J, Sertie AL, et al. Decreased cellular uptake and metabolism in Allan-Herndon-Dudley syndrome (AHDS) due to a novel mutation in the MCT8 thyroid hormone transporter. J Med Genet. 2006;43(5):457-60.

24. Groeneweg S, van den Berge A, Meima ME, Peeters RP, Visser TJ, Visser WE. Effects of Chemical Chaperones on Thyroid Hormone Transport by MCT8 Mutants in Patient-Derived Fibroblasts. Endocrinology. 2018;159(3):1290-302.
25. Groeneweg S, Friesema EC, Kersseboom S, Klootwijk W, Visser WE, Peeters RP, et al. The role of Arg445 and Asp498 in the human thyroid hormone transporter MCT8. Endocrinology. 2014;155(2):618-26.
26. Johannes J, Jayarama-Naidu R, Meyer F, Wirth EK, Schweizer U, Schomburg L, et al. Silychristin, a Flavonolignan Derived From the Milk Thistle, Is a Potent Inhibitor of the Thyroid Hormone Transporter MCT8. Endocrinology. 2016;157(4):1694-701.
27. Schwartz CE, May MM, Carpenter NJ, Rogers RC, Martin J, Bialer MG, et al. Allan-Herndon-Dudley syndrome and the monocarboxylate transporter 8 (MCT8) gene. Am J Hum Genet. 2005;77(1):41-53.
28. Boccone L, Dessi V, Meloni A, Loudianos G. Allan-Herndon-Dudley syndrome (AHDS) in two consecutive generations caused by a missense MCT8 gene mutation. Phenotypic variability with the presence of normal serum T3 levels. Eur J Med Genet. 2013;56(4):207-10.
29. Zhang M, Wang W. Organization of signaling complexes by PDZ-domain scaffold proteins. Acc Chem Res. 2003;36(7):530-8.
30. Kirk P, Wilson MC, Heddle C, Brown MH, Barclay AN, Halestrap AP. CD147 is tightly associated with lactate transporters MCT1 and MCT4 and facilitates their cell surface expression. EMBO J. 2000;19(15):3896-904.
31. Visser WE, Philp NJ, van Dijk TB, Klootwijk W, Friesema EC, Jansen J, et al. Evidence for a homodimeric structure of human monocarboxylate transporter 8. Endocrinology. 2009;150(11):5163-70.

Chapter

MCT8 deficiency in females

3.4

Stefan Groeneweg, Ginevra Zanni, Anna Dolcetta, Marieke M. van der Knoop, René F. de Coo, Paolo Alfieri, Heike Biebermann, Kim J. Oostrom, Marta Nardella, Ulrich Schweizer, Robin P. Peeters, Laura Paone, Enrico Bertini, Marco Cappa, Heiko Krude, Paul van Trotsenburg, W. Edward Visser

Manuscript in preparation.

ABSTRACT

Context Thyroid hormones (TH) are essential for brain development and function. Monocarboxylate transporter (MCT)8 facilitates the transport of TH across the blood-brain-barrier and into neuronal cells. Mutations in MCT8 have been associated with Allan-Herndon-Dudley syndrome (MCT8 deficiency), characterized by intellectual disability and abnormal thyroid function tests. MCT8 deficiency typically affects males due to its X-linked inheritance. Here, we report three female carriers of a heterozygous pathogenic mutation in *MCT8* who presented moderate-severe intellectual disability, behavioral problems and the characteristic TH function profile of MCT8 deficiency.

Methods We performed exome sequencing and X-chromosome inactivation studies in order to identify disease causing mutations in *SLC16A2* and studied their effects in a panel of *in vitro* experiments, including TH uptake and surface biotinylation studies, and functional studies in patient-derived fibroblasts.

Results Exome sequencing identified a heterozygous mutation in the *MCT8* gene in all three patients (p.R445C, p.N193I, and p.G276R), which all substantially reduced MCT8-mediated TH uptake in transiently transfected cells. X-chromosome inactivation studies in peripheral blood showed strongly skewed X-inactivation in favor of the mutant allele. Accordingly, MCT8-mediated T3 uptake in patient-derived fibroblasts was impaired to a similar degree as in fibroblasts derived from male patients with MCT8 deficiency.

Conclusions We show that female carriers of a heterozygous pathogenic mutation in *SLC16A2* may present neuro(psycho)logical and endocrine abnormalities in case of unfavorable skewing of X-chromosome inactivation. This work illustrates that MCT8 deficiency should also be considered in female patients presenting intellectual disability and abnormal thyroid function tests.

INTRODUCTION

Thyroid hormone (TH) is essential for growth and development of virtually all tissues including the brain (1). TH mainly exerts its effect through binding of the active hormone 3, 3',5-triiodothyronine (T3) to its nuclear receptors (2). The local availability of T3 is tightly controlled by the intracellular deiodinating enzymes (3) and membrane transporters (4). The most specific TH transporter identified to date is monocarboxylate transporter (MCT)8 (5). Accumulating evidence suggests that MCT8 is crucial for TH transport across the blood-brain-barrier (BBB), thereby ensuring the availability of TH in the human brain (6, 7). Mutations in MCT8 have been associated with Allan-Herndon-Dudley syndrome (AHDS, or MCT8 deficiency) (8, 9). As a consequence of impaired TH entry into the brain, patients with MCT8 deficiency typically present severe intellectual and motor disability, and fail to achieve early developmental milestones. Most patients have severe hypotonia, dystonia and spasticity and do not develop speech. High serum T3 concentrations, low or low-normal (free) T4 concentrations and high or high-normal TSH concentrations comprise the characteristic endocrine fingerprint of MCT8 deficiency. The peripheral tissues that rely on TH transporters other than MCT8 are exposed to the high serum T3 concentrations, resulting in thyrotoxic signs and symptoms.

Since the *MCT8* gene (*SLC16A2*) is located on the X-chromosome (Chr Xq13.2), mutations therein typically result in a clinical phenotype in males. Most female carriers do not present phenotypic abnormalities, since they have a second, unaffected, copy of the *MCT8* gene, resulting in the presence of functional MCT8 in at least a subset of cells (10, 11). However, skewing of the X-chromosome inactivation process could result in a variable phenotype resembling features of MCT8 deficiency in males. Indeed, this may explain mild biochemical abnormalities and variable degree of cognitive dysfunction reported in some carriers (e.g. (9, 12-14)). One female harboring an X-autosome translocation affecting the *MCT8* gene was reported to have a clinical phenotype resembling male MCT8 deficiency due to complete skewing of X-chromosome inactivation resulting in the exclusive expression of the mutant MCT8 allele (15). However, systematic clinical, biochemical and molecular evaluation of females with features reminiscent of MCT8 deficiency is lacking.

Here, we detail three female cases with a heterozygous pathogenic mutation in *MCT8* and skewed X-chromosome inactivation, which was associated with variable neuro(psycho)logical abnormalities, behavioral problems and abnormal thyroid functions tests as well as reduced TH transport in patient-derived cells.

MATERIALS AND METHODS

Patients

We studied three females with unexplained intellectual disability in whom next generation sequencing was carried out to identify the underlying cause. In addition, we describe two newly identified male subjects with MCT8 deficiency.

Ethical considerations

Written informed consent was obtained from the parents or legal representatives of the involved patients and controls. All investigations were clinically indicated and/or ethically approved (Medical

Ethical Committee of the Erasmus Medical Center, Rotterdam, The Netherlands, METC identifier: MEC-2015-362).

Clinical and biochemical evaluations

All patients were clinically evaluated by a trained (paediatric) neurologist and/or paediatric endocrinologist as well as a neuropsychologist. Imaging studies were clinically indicated and as such performed in different centres using local scanning protocols implemented in clinical care. All measurements in serum have been carried out using standard laboratory methods. Skin fibroblasts were kindly provided by care-giving physicians and had been (previously) collected for diagnostic purposes.

Patient sequencing, data analysis and confirmation by sanger sequencing

Detailed methods on the (whole-exome or targeted) sequencing analyses carried out in the female patients are available in the Supplemental Material. The genetic mutation in both male patients had been established elsewhere. All identified mutations in the *MCT8* gene were confirmed by Sanger sequencing on genomic DNA derived from white blood cells and patient-derived fibroblasts using primers that amplify the site of the mutation. Positions of the mutations are determined using the NM_006517.3 reference sequence, which uses +1 as the A of the ATG translation initiation codon of the long MCT8 translational isoform, with the initiation codon as codon 1.

X-chromosome inactivation studies

X-chromosome inactivation studies were carried out on DNA extracted from white blood cells using well-defined techniques used in routine clinical practice.

In vitro characterization of the identified MCT8 mutations

Full technical details on the functional studies are available in the Supplemental Material. Briefly, COS-1 and JEG-3 cells were cultured and transfected as described before (16). Two days after transfection, TH uptake studies, immunocytochemistry, and immunoblotting on total lysates and the surface biotinylated fraction were carried out using well-established protocols (16). T3 uptake studies in the presence and absence of the MCT8-inhibitor silychristin were carried out as previously described (17).

Statistical analysis

All uptake results are expressed as means ± SEM of at least three independent experiments in duplicate. Statistical significance was determined using indicated statistical tests carried out in GraphPad Prism, version 6.

RESULTS

Clinical and biochemical characterization of three female subjects with intellectual disability and abnormal thyroid function tests

Family I

The first female patient (patient P1) was born to non-consanguineous healthy parents with a birth weight of 2,400 g (-1,36 SD) (**Supplemental Figure S1**). She presented at the age of 25 years with a

history of delayed motor development, intellectual disability, and a depressive mood and anxiety disorder. Her older brother and a maternal first cousin reportedly had severe motor dysfunction and cognitive impairment. At time of first presentation, physical examination revealed a body length of 161 cm, a weight of 80 kg (BMI 32.5), and a normal head circumference. Her general clinical condition was good, but speech was limited to simple sentences. At neurological examination, cranial nerve functions were normal, and dystonia, spasticity or hypotonia were absent. MRI studies of the brain at the age of 21 years did not show any signs of white matter involvement, but had moderately increased subarachnoid spaces (**Figure 1A**). Neuropsychological evaluations revealed a low IQ (45) and adaptive skills were poorly developed (**Table 1**). Especially communicative and social skills were greatly impaired. Gross motor function was normal at time of evaluation, but there had been a considerable delay in achieving all developmental motor milestones. Biochemical evaluation demonstrated low-normal serum FT4 (12.0 pmol/L; normal range: 11.5-22.7), slightly elevated FT3 (7.7 pmol/L; normal range: 3.5-6.5) with normal TSH (2.22 mU/L; normal range: 0.41-4.30) concentrations. She did not manifest any clinical features of thyroid dysfunction. Her heart rate (75 beats per minute) and blood pressure 123/84 mmHg (50-75th percentile) were unremarkable and bone age was normal. She used Lamotrigine and Aripiprazole to treat her depressive and anxiety symptoms. Her 30-year old brother (patient 1B) has a history of developmental delay (he sat at 1,5 years, he walked at 3 years), spasticity and intellectual disability (non-verbal IQ=44). His thyroid function tests were characteristic for MCT8 deficiency with high FT3 (7.7 pmol/L; normal range 3.1-6.8), low free T4 (10.3 pmol/L; normal range 12.0-22.0) and normal TSH (1.23 mU/L; normal range 0.27-4.20) concentrations. A recent neurological examination showed mild signs of spasticity in the lower limbs. Nevertheless, he was able to walk long distances without support. Other clinical and neurological examinations did not reveal obvious abnormalities. Besides intellectual disability, he had relational inhibition and anxiety in the interaction with unknown individuals. The brain MRI of the affected brother, performed at the age of 25 years, showed no signs of white matter involvement and only moderately increased subarachnoid spaces (**Figure 1B**).

Family II

The second female patient (patient P2) was born to non-consanguineous parents. She was referred for further evaluation of abnormal thyroid function tests. At time of first presentation the general clinical condition was good, and physical examination revealed no obvious abnormalities. Neurological examination revealed normal cranial nerve functions, and absence of hypotonia, dystonic posturing or spasticity. MRI of the brain showed no abnormalities, in particular no signs of delayed myelination. Neuropsychological evaluation yielded a total IQ of 80, which is classified as low average. Biochemical evaluation demonstrated a low serum FT4 (8.6 nmol/L; normal range 12.6-24.0), a normal FT3 (5.7 pmol/L; normal range 3.5-8.6), normal basal TSH concentrations (6.2 mU/L; normal range 0.4-5.6). She did not manifest any clinical features of thyroid dysfunction (**Table 1**).

Family III

The third female patient (patient P3) was born at term to non-consanguineous parents with a birth weight of 2800 g (-1.85 SD). At the age of three years she migrated with her parents from the Caucasian region to the Netherlands. Although she developed normally during the first years of life and entered regular education at the age of four years (kindergarten), anxious and withdrawn behavior during the following two years made it impossible to follow regular primary education. At age six years she was

transferred to special education for children with serious behavioral problems, but soon thereafter she was relocated to special education for children with intellectual disability. During the entire period, her physical health was excellent. Because of the unexplained intellectual disability, the girl was referred to a psychologist who measured her IQ and found total scores of 74 and 56 at the ages of six and approximately nine years, respectively. At the age of nine years and ten months, she was referred to a general pediatrician for further investigations into the cause of the intellectual disability. Physical examination revealed a shy but healthy-looking girl, without any obvious abnormalities. Her height, weight and BMI were 142 cm (-0,2 SD), 32.9 kg (+0,2 SD) and 16,3 (+0,2 SD), respectively. Puberty had started, the Tanner stage was M2, P3. Brain MRI conducted shortly thereafter showed no abnormalities (non-dilated, symmetrical ventricles, normal sulci, and no areas of in- or decreased signal intensity). Laboratory investigation showed normal kidney and liver function, and normal hematology test results. However, endocrine testing showed repeatedly low FT4 in combination with normal TSH concentrations (7.3 and 7.6 pmol/L; normal 10-23, and 1.1 and 1.4 mIU/L; normal 0.3-4.6, respectively). To corroborate the working diagnosis "central hypothyroidism" TRH, CRH and classic (250 mcg) ACTH tests were conducted. In the TRH test, TSH and FT4 concentrations were 1.2 mIU/L and 8.7 pmol/L at T=0 minutes, respectively. Maximum TSH concentrations were 10 mIU/L at T=15 min, with TSH concentrations of 4.1 and 1.4 mU/L at T=60 and T=180 minutes, respectively. Maximum cortisol concentrations in the CRH and ACTH tests were 377 and 486 nmol/L (normal: >480 and >550 nmol/L, respectively). Based on these results, the girl was diagnosed with central hypothyroidism and central adrenal insufficiency. Treatment with oral hydrocortisone and thyroxine was started, and she was referred to our academic medical center.

The family history revealed no other cases of pituitary disease or intellectual disability. A repeat MRI of the hypothalamus-pituitary region and brain conducted at the age of ten years and seven months showed normal morphology and signal intensity of the hypothalamus, pituitary and pituitary stalk. Treatment with thyroxine and hydrocortisone was continued. Because further growth and pubertal development went perfectly well and prolactin levels were normal, doubt arose about the diagnosis central adrenal insufficiency. At the age of 14 years, repeat adrenal axis testing after hydrocortisone treatment was phased out, showed normal adrenal function (max. cortisol in classic ACTH test: 655 nmol/L. To evaluate the accuracy of the possible diagnosis isolated central hypothyroidism, thyroxine treatment was stopped at the age of 15,5 years, resulting in persistently low FT4 concentrations confirming abnormal thyroid axis functioning (plasma FT4 concentrations 8.2, 7.8 and 8.0 pmol/L (normal 10-23) after six, 10 and 14 weeks of stopping treatment, respectively; 14 weeks after stopping total T4 was 40 nmol/L (normal 70-150), TSH was 2.1 mU/L (normal 0.4-4.0), T3 was 2.55 nmol/L (normal 1.3-2.7) and rT3 0.1 nmol/L (normal 0.11-0.4). Subsequent testing for known genetic (and thus congenital) causes of isolated central hypothyroidism revealed no abnormalities in the TSHB, TRHR and IGSF1 genes (in 2014), and TBL1X and IRS4 genes (in 2015 and 2017).

At time of latest clinical evaluation at the age of 18 years, neurological examination showed normal cranial nerves and motor functioning, normal and symmetrical reflexes, normal sensory functioning, and normal coordination and gait. In particular, there was absence of dystonia, spasticity or hypotonia. Reassessment of the brain MRI's performed around the age of 10 years did not yield any new insights. Neuropsychological examination at the age of 19 years using the Wechsler Intelligence Scale for Children (WISC-III^{NL}), and comparing results to those of 16 years and 8 months to 16 years and 11 months old children, yielded a total IQ of 53 (verbal and performal IQ were 55 and 57, respectively), matching with light intellectual disability. Language – assessed by verbal fluency, category fluency and

appointment task – was weak. However, further neuropsychological examination showed no disturbances in single attention tasks, learning or memory.

Table 1. Patient characteristics.

Patient	I	II	III	IV[1]	V[1]
Gender	Female	Female	Female	Male	Male
Age (years) last evaluation	25		15.5	62	4.6
Mutation	p.R445C (c.1333C>T)	p.N193I (c.A578T)	p.G276R (c.G826A)	p.R445C (c.1333C>T)	p.Q97fsX (c.C289del)
Birth weight (SD)	-1,36	N.A.	N.A.	N.A.	-0.7
Endocrine features					
Serum total T3 (nmol/L)	2.98 (1.4-2.5)	n.a.	2.55 (1.3-2.7)	1.77 (1.4-2.5)	3.43 (2.0-3.3)
Serum TT4 (nmol/L)	74 (58-128)	n.a.	40 (70-150)	43 (58-128)	66 (82-167)
Serum FT4 (pmol/L)	12.0 (11.5-22.7)	8.6 (12.6-24.0)	8.0 (10.0-23.0)	9.9 (11.0-25.0)	15.6 (13.0-26.0)
Serum rT3 (nmol/L)	0.19 (0.22-0.54)	n.a.	0.10 (0.11-0.40)	0.10 (0.22-0.54)	0.07 (0.20-0.50)
Serum TSH (mU/L)	2.22 (0.41-4.30)	6.2 (0.4-5.6)	2.10 (0.4-4.0)	5.05 (0.40-4.30)	2.11 (0.60-5.60)
Serum SHBG (nmol/L)	67.8 (20-120)	n.a.	n.a.	91.6 (10-70)	164 (40-140)
Heart rate (bpm)	75	n.a.	n.a.	78	130
Body weight in kg (SD)	80	n.a.	32.9 (+0.2) [4]	63	15.4 (-1.79)
Body height in cm (SD)	161	n.a.	142 (-0.2) [4]	174	106 (-1.0)
BMI	32.5	n.a.	16.3 (+0.2) [4]	20.8	13.7 (-1.72)
Sweating	No	No	No	No	Yes
Diarrhea	No	No	No	No	No
Neurological features					
Dystonia	No	No	No	Yes (mild)	Yes
Spasticity	No	No	No	Yes	Yes
Hypotonia	No	No	No	Yes (mild)	Yes
Speech development	Simple sentences	normal	Simple sentences	Some words	No
Head control	Yes	Yes	Yes	Yes	No
Sitting independently	Yes	Yes	Yes	Yes	No
Walking independently	Yes	Yes	Yes	No	No
Delay in achieving motor milestones	Yes	no	no	Yes	Yes
GMFM-G88 score (%)[2]	97.6	n.a.	n.a.	83	10
VABS[3] – communication (percentile rank)	<0.1	n.a.	n.a.	<0.1	<0.1
VABS[3] – daily living skills (percentile rank)	<0.1	n.a.	n.a.	<0.1	<0.1
VABS[3]– socialization (percentile rank)	<0.1	n.a.	n.a.	<0.1	<0.1
IQ score (test)	45 (WAIS r)	80	53 (WISC-III)	N.D.	N.D.
Psychiatric symptoms	Depression, anxiety	No	Anxiety	N.D.	N.D.
EEG-proven seizures	No	No	No	Yes	Yes
Feeding problems	No	No	No	No	Yes
Brain MRI abnormalities	Yes	No	No	n.a.	Yes

[1] Patient IV and V are two newly identified male patients which were included into this table as a comparison. A description of the clinical phenotype is provided in the Supplemental Material.

[2] GMFM-G88 stands for Gross Motor Function Measure-G88. The GMFM-G88 assesses the gross motor function in which scores range from 0 to 100%, with higher scores indicating better motor function and where a 100% score is achieved by a normal developing child of 4 years of age.

[3] VABS stands for Vineland Adaptive Behavior II. The VABs II is a survey which assesses different aspects of development. The survey was completed by primary care-givers in presence of a trained neuropsychologist or physician. The level of development on indicated sub-domains of the VABs II is provided as percentile ranks and reflects the percentage of individuals in the patients` normative age group who scored the same or lower than the patient.

[4] The latest available body weight, height and BMI are provided, measured at the age of 9 years and 10 months.

Clinical and biochemical characterization of two newly identified male subjects with MCT8 deficiency

Family IV and V

To allow comparison of the phenotypic characteristics observed in the female cases to those observed in male patients with MCT8 deficiency, we also studied two newly identified male patients with mutations in *SLC16A2* gene. Patient P4 is a 65-year old male with moderate-severe intellectual and motor disability and mildly abnormal thyroid function tests (**Table 1**). By contrast, patient P5 presented at an age of 4 years with severe developmental delay and classical biochemical and clinical features at the severe end of the spectrum of MCT8 deficiency (**Table 1**). Sequential brain MRI studies performed during the first year of life showed delayed myelination and slightly widened ventricles (**Figure 1C**). A detailed clinical description of both patients is provided in the Supplementary Appendix.

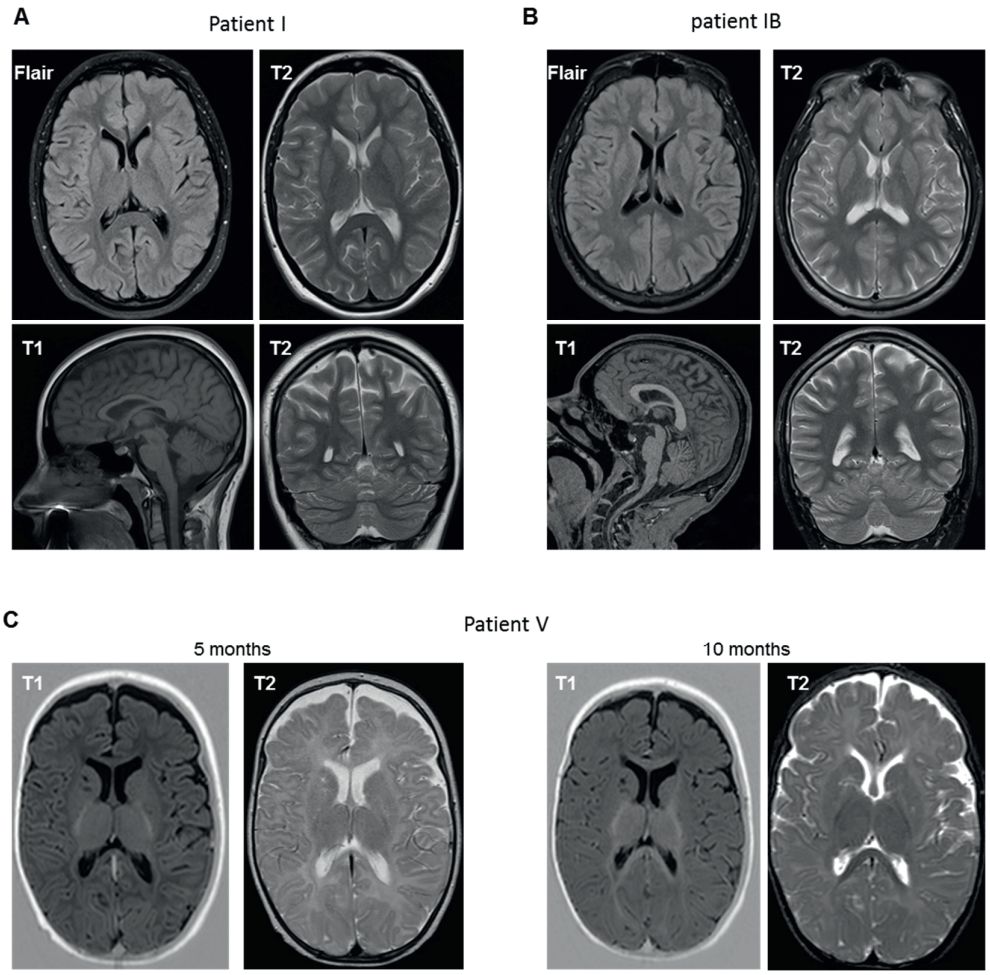

Figure 1 MRI studies in patient P1 (female), her affected brother (patient P1B) and patient P5 (male). (**A**) Flair-, T1- and T2-weighted MRI of the brain of patient P1 performed at the age of 21 years showing mild cortical atrophy without signs of leukodystrophy. (**B**) Flair-, T1- and T2-weighted MRI of the brain of the brother of patient P1 (patient IB) performed at the age of 25 years, showing signs of mild cortical atrophy without obvious signs of leukodystrophy. (**C**) T1- and T2-weighted MRI of the brain of patient P5 at the age of 5 months (left) and 10 months (right) showing a global delay in myelination which is particularly apparent in the frontal white matter, anterior limb of the internal capsule and periventricular white matter. Myelination appears progressive over time. The applied MRI sequences are indicated in each image.

Molecular genetic studies

Since routine diagnostics did not result in the identification of the underlying cause of the observed phenotype in the female patients, next generation sequencing was carried out. A heterozygous c.1333C>T, p.R445C mutation in the *MCT8* gene was identified in patient P1, which has been previously reported in a male subject with MCT8 deficiency (18). Skewing analyses in white blood cells indicated non-random X-inactivation (90:10). The same genetic mutation was identified in her older brother (patient 1B), but not in other family members. In patient P2 a heterozygous c.A578T;p.I193N mutation was found. X-inactivation was clearly skewed (~90:10). In patient P3, a CGH array was performed followed by whole exome sequencing with filters "mental disorder" (1157 genes; IDv10)) and "central hypothyroidism" (154 genes; CH-Cplusv2). The CGH array showed a normal array profile in a woman. However, WES yielded a heterozygous de novo variant c.826G>A; p.(Gly276Arg) in the *SLC16A2* gene, known to result in overt MCT8 deficiency in male subjects (19). This variant was not found in the girl's sister, mother or father. Analyses of the X-chromosome inactivation pattern in this patient also revealed skewing of X-inactivation. A heterozygous c.1333C>T, p.R445C mutation was found in the male patient P4, which was identical to the mutation identified in female patient I. In the male patient P5, a heterozygous c.C289del, p.Q97fsX mutation was found, resulting in a premature truncation of the MCT8 protein. Given the absence of a substantial part of the MCT8 protein, this mutant is prototypic for mutations that completely inactivate the MCT8 protein.

Functional studies

To substantiate the diagnosis of MCT8 deficiency in the female patients, we evaluated the impact of the identified mutations *in vitro*. Upon transient transfection in COS-1 cells, both T3 and T4 uptake by the N193I, G276R, R445C mutant MCT8 proteins were strongly diminished compared to WT (**Figure 2A**). Similar results were obtained in JEG-3 cells (data not shown). Although all mutants could be detected in the cell surface fraction, the total and cell surface expression levels of the R445C and G276R were considerably lower than WT (**Figure 2B**). Accordingly, immunocytochemistry in JEG-3 cells showed the presence of all three mutants at the cell membrane (**Figure 2C**).

Next, we studied T3 uptake in fibroblasts derived from the three female (patient P1-P3), and both male (P4-5) patients and controls. In contrast to control fibroblasts, almost no time-dependent increase of T3 uptake was observed in the Q97fsX fibroblasts, compatible with the severe clinical phenotype of this male patient (**Figure 3A**). T3 uptake levels in the fibroblasts derived from the female patients was significantly lower than in control fibroblasts. Interestingly, the T3 uptake capacity in the R445C mutant fibroblasts derived from the male and female patient were similar. In line with the *in vitro* over-expression studies, the expression levels of the G276R and R445C mutants were strongly reduced compared to WT (**Figure 3B**). To confirm that the impaired T3 accumulation was due to a reduced transport capacity of MCT8, we performed T3 uptake studies in the presence and absence of the MCT8-specific inhibitor silychristin (20). Indeed, T3 uptake was less reduced by silychristin in the patient-derived fibroblasts than in controls, strongly supporting MCT8 dysfunction in cells derived from female patients (**Figure 3C** and **3D**). For female patients, the silychristin-induced reduction of T3 uptake in fibroblasts (i.e. MCT8 function) showed a positive trend with IQ (**Figure 3E**).

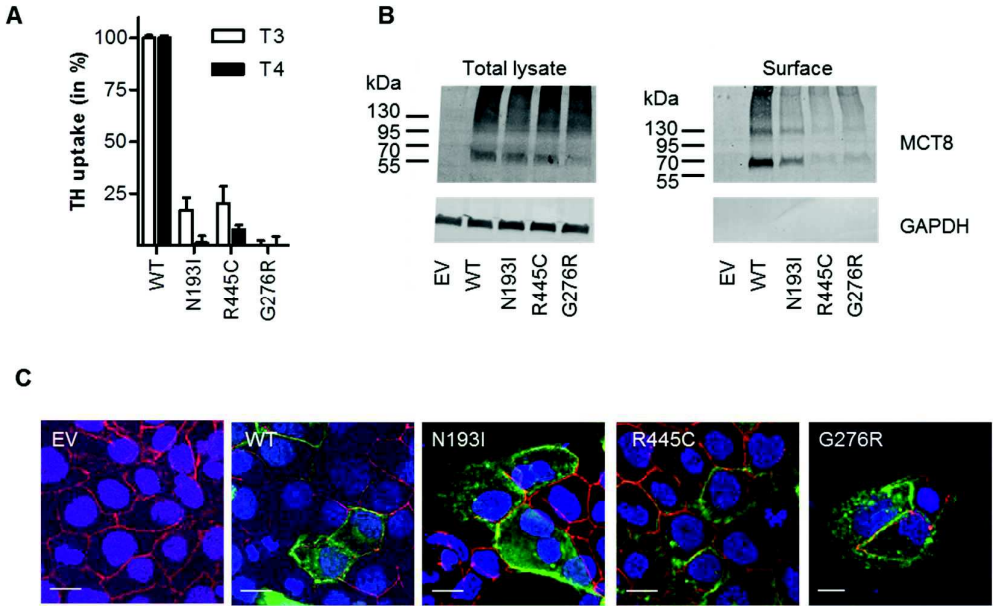

Figure 2 *In vitro* functional studies confirmed pathogenicity of identified mutations. (A) T3 and T4 uptake studies in COS-1 cells transiently transfected with wild-type MCT8 or indicated mutants and the intracellular TH-binding protein CRYM in 30 minutes at 37 °C. Data are expressed relative to wild-type MCT8 and are corrected for background TH uptake in empty vector transfected control cells. Results are presented as means ± SEM (N=4). One-way ANOVA with Dunnett`s post-hoc tests were used to test for statistically significant differences between wild-type and mutant MCT8. Statistically significant differences ($p<0.05$) are indicated with an *. (B) Immunoblot quantification of MCT8 protein in total lysates (left) and the surface biotinylated fraction (right) of COS-1 cells transfected with indicated constructs. GAPDH was used as a loading control. (C) Immunocytochemistry in transfected JEG-3 cells to visualize wild-type and mutant MCT8 (green) subcellular localization. Zona Occludens (ZO-)1 was used as a membrane marker and DAPI as a nuclear marker.

Comparison of female index patients to a-symptomatic carriers and non-carriers

To further substantiate that the observed clinical features are related to the identified mutations in *SLC16A2* and unfavorable skewing of X-chromosome inactivation, we compared the serum thyroid function tests of the female index patients to those available from carriers that were self-reportedly a-symptomatic, and non-carriers. The female patients showed significantly lower serum free T4 concentrations than asymptomatic carriers and non-carriers (**Figure 4A**). In addition, serum T3 concentrations significantly exceeded those observed in asymptomatic carriers (**Figure 4B**). Total rT3 concentrations in the female patients were significantly lower compared to non-carriers and were similar to the lowest quartile of asymptomatic carriers (**Figure 4C**). This resulted in a pronounced increase of total T3/rT3 and total T3/free T4 ratios in the female patients (**Figure 4D** and **4E**), respectively. TSH concentrations did not significantly differ between the three groups (**Figure 4F**). Together, the thyroid function tests in the female patients thus clearly differed from those observed in a-symptomatic carriers and non-carriers. Although somewhat less severe, the pattern closely resembled the pathognomic biochemical signature of MCT8 deficiency reported in affected males (21). No IQ measurements were available for a-symptomatic carriers or non-carriers, hampering a comparison of neurocognitive performance.

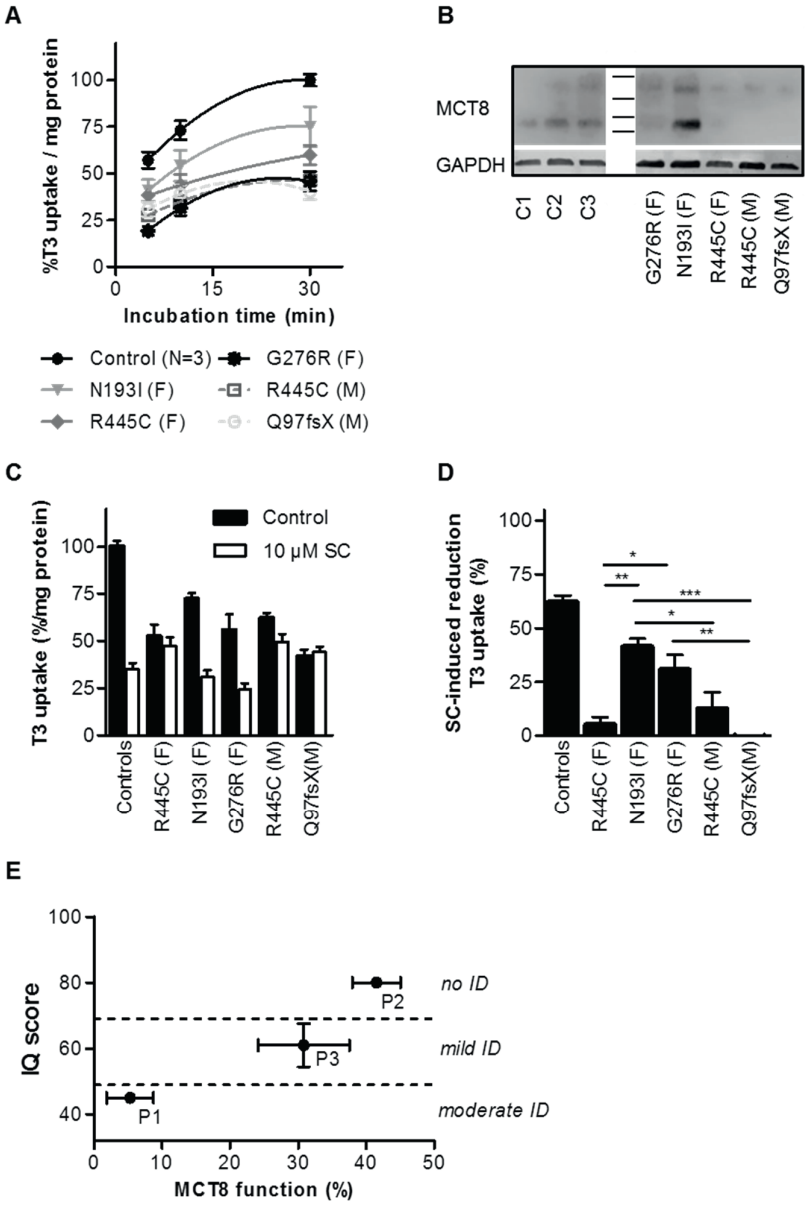

Figure 3 ***Ex vivo*** **analyses of MCT8 function in patient-derived fibroblasts** (A) Time-dependent intracellular accumulation of T3 in fibroblasts derived from indicated female (solid line) and male (dashed lines) fibroblasts and female control fibroblasts. For control fibroblasts the mean of three different control lines is depicted. All data are expressed relative to the amount of intracellular T3 accumulation in control fibroblasts after 30 minutes incubation. Results are presented as means ± SEM (N=4). T3 accumulation was significantly ($p<0.05$) lower in all patient cell lines compared to controls. (B) Immunoblot on total lysates derived from indicated patient and control fibroblasts. GAPDH was used as a loading control. (C) T3 uptake in patient and control fibroblasts in the absence (black) and presence (white) of 10 µM silychristin (SC), a specific inhibitor of MCT8. Data are expressed relative to the amount of T3 accumulation in control cells in the absence of SC. (D) Silychristin-induced reduction in T3 uptake in control and patient fibroblasts. Data are derived from (C). One-way ANOVA with Tukey`s posttest were used to assess for statistically significant differences ($p<0.05$, *; $p<0.01$, **; $p<0.001$, ***). (E) Correlation plot of patient`s IQ *versus* MCT8 function, defined as percentage silychristin-induced reduction in T3 uptake shown in (E). In case of multiple available measurements, the mean ± SEM are displayed.

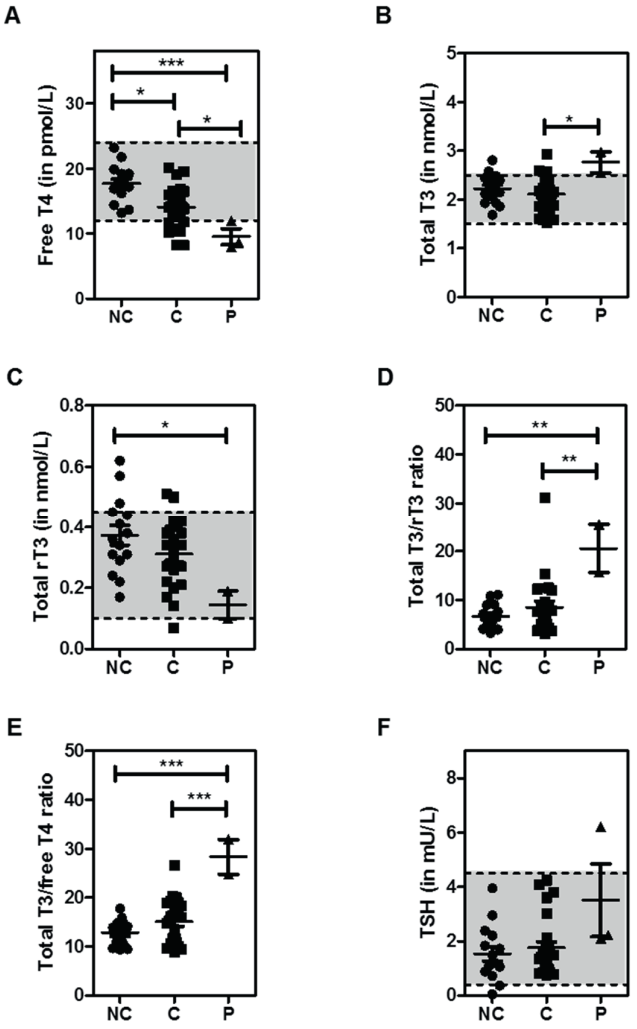

Figure 4 Serum thyroid function tests in female patients in comparison to a-symptomatic carriers and non-carriers. (**A**) serum free T4, (**B**) total T3, and (**C**) total rT3 concentrations, as well as (**D**) total T3/rT3 and (**E**) total T3/ free T4 ratios, and (**F**) serum TSH concentrations in female patients (P), female carriers (C) that were self-reportedly a-symptomatic and non-carriers (NC). Data were derived from historical control families available in the Erasmus MC. One-way ANOVA with Tuckey`s post-hoc tests were used to test for statistically significant differences between groups ($p<0.05$, *; $p<0.01$, **; $p<0.001$, ***).

DISCUSSION

Here, we report on the clinical and biochemical phenotype associated with heterozygous pathogenic mutations in the *MCT8* gene and unfavorable skewing of X-chromosome inactivation in three female patients. The major presenting features were variable degree of neuropsychological abnormalities, behavioral symptoms and mildly abnormal serum thyroid function tests. The causality of these variants to the phenotype was supported by functional studies in patient-derived fibroblasts which showed a reduction in MCT8-mediated T3 uptake.

In comparison to a male patient with typical MCT8 deficiency, the clinical presentation was considerably milder in these female patients. Especially motor function and development were hardly affected and key neurological features such as hypotonia, dystonia and spasticity, typically present in affected males, were either absent or present at a very mild degree compared to affected males. In two out of three female patients (P1 and P3), domains of cognitive functioning were clearly affected. In these patients, total IQ scores were <60, indicative for mild-moderate intellectual disability. Their speech development was restricted to simple sentences and social skills were poorly developed. In addition, both patients exhibited behavioral problems such as anxiety and withdrawn behavior. Patient P1 (p.R445C) whose neurocognitive dysfunction was most outspoken also has depressive mood disorder and reportedly had delayed development of motor skills. Together, these features hampered participation in daily life activities and attendance to regular education systems. The third patient (P2) has an IQ of 80 which clearly exceeded the IQ of both other female index patients and is considered to be within the normal range. Nevertheless, the thyroid hormone profile of all three female index patients clearly differed from asymptomatic carriers and non-carriers and in particular the total T3/rT3 and total T3/free T4 ratios were clearly elevated. This signature is similar to the abnormal thyroid function tests observed in males with MCT8 deficiency, but in the mild spectrum of severity. In part, this may explain the absence of evident thyrotoxicity in peripheral tissues in the affected female cases. Together, these observations are compatible with abnormal MCT8 function.

Indeed, in line with previous studies (18, 19, 22), the p.R445C and p.G276R mutations decreased MCT8-mediated T3 transport in over-expressing cells and in patient-derived fibroblasts. Also the newly identified p.N193I mutation clearly reduced MCT8 function. The functional reduction in T3 uptake by fibroblasts derived from the female index patients was of a similar magnitude as observed in fibroblasts derived from male patients with MCT8 deficiency, confirming MCT8 dysfunction in these cells.

The strong effects observed in our functional studies contrast the milder motor and intellectual disability in female *versus* male patients. This suggests that at least a proportion of cells in the blood-brain-barrier and neural cells express the wild-type allele which can substantially modify the phenotype. Compiling evidence suggests that X-chromosome inactivation in humans is random and is initiated during early development (approximately day 5.5 after fertilization) (23). Therefore, it is not surprising that recent studies have indicated that the level of skewing in X-chromosome inactivation is usually relatively homogenous across tissues (24). However, subjects with the highest degree of skewing generally also show the highest variability across tissues. In addition, some genes reportedly escape X-chromosome inactivation, some of which in a tissue-specific way (24, 25). Although the available literature is undecided, this may also apply to the *MCT8* gene in at least some individuals (25). Therefore, it is conceivable that some tissues or even cell populations in our female patients express the wild-type MCT8 allele, and hence ensure adequate intracellular TH availability.

Although proving causality in case of X-linked disorders in females is challenging, we believe a causal relation between the genotype and phenotype in our cases is plausible given the presence of a pathogenic mutation in *SLC16A2* and skewed X-chromosome inactivation, characteristic thyroid function tests, and defective MCT8-mediated T3 transport in patient cells. Yet, the three female patients have a variable degree of intellectual disability and behavioral problems. Therefore, alternative (epi-)genetic causes or modifier genes for the observed phenotype cannot be completely excluded. However, the absence of exonic mutations in any other known candidate genes associated

with intellectual disability (or thyroid dysfunction) argues against this possibility. Moreover, the silychristin-induced reduction of T3 uptake in fibroblasts of the female patients corresponded with their intellectual performance, with most severe intellectual disability observed in patient P1 (p.R445C) whose fibroblasts showed the least silychristin-induced reduction in T3 uptake.

Limited information is known about female MCT8 mutant carriers. Most of the female carriers in whom X-inactivation patterns have been analyzed showed no evidence for a skewed inactivation and did not present intellectual disability or endocrine abnormalities (11). So far, only one female case with the full-blown phenotype of MCT8 deficiency has been described (15). This was attributed to the presence of a balanced X-autosome translocation (t(X;9)(q13.2;p24)) with the breakpoint on the X-chromosome located within the *MCT8* gene. Such mutations result in completely skewed X-inactivation in favor of the mutant allele and, thus, the exclusive expression of mutant MCT8. In addition, a few female family members of reported MCT8 deficient males have been mentioned to have a variable degree of intellectual disability (e.g. (11)). Moreover, low-normal serum (free) T4 and relatively high serum T3 concentrations have been reported in some female carriers (9, 12). The implications of such isolated endocrine abnormalities are currently unknown. Although detailed clinical and genetic information is often not available, it is conceivable that these clinical and biochemical features arise from skewed X-chromosome inactivation. Extending on these reports, our *ex vivo* studies in fibroblasts derived from female carriers strongly indicate that unfavorable skewing of X-chromosome inactivation (ratio>20:80 in peripheral white blood cells) may indeed result in MCT8 dysfunction at the cellular level. In our three cases, this was associated with clinical and biochemical manifestations compatible with MCT8 deficiency. We therefore postulate that disease penetrance in female carriers is importantly determined by the degree of skewing in X-chromosome inactivation and, thus, the amount of cells expressing the mutant MCT8 allele.

Given the advanced age of the female patients and the absence of clinical signs of overt hyperthyroidism, it is unclear if female subjects would benefit from treatment with TH analogues such as Triac (26), levothyroxine as a mono-therapy, or in combination with anti-thyroid drugs.

In conclusion, the present work demonstrates that heterozygous mutations in *MCT8* in female carriers with skewed X-chromosome inactivation resemble the biochemical features and to some extent the neurocognitive abnormalities seen in MCT8-deficient males. Our findings indicate that MCT8 deficiency should be considered in females presenting mild-moderate intellectual disability with or without psychiatric symptoms and abnormal thyroid function tests (low T4, high T3). Future studies in larger cohorts that pursue more thorough phenotypic evaluation will help to identify any potential adverse medical effects associated with heterozygous *MCT8* mutations in females.

Acknowledgements

We are grateful to the families for taking part in this study. We thank Dr Fabiana Fattori (Unit of Neuromuscular and Neurodegenerative Disorders, B.Gesù Children's Hospital) for expert technical advice and Dr Marco Zazza (Unit of Functional Rehabilitation, B. Gesù Children's Hospital).

SUPPLEMENTARY MATERIALS

Supplemental Methods

Genome sequencing

In patient P1, targeted parallel sequencing was performed on the index case using the Nextera Custom Enrichment panel (Illumina, San Diego, Ca) for 140 previously described XLID genes according to manufacturers' protocols. Variants were detected by the HaplotypeCaller tool of GATK version 4.3 (Cambridge, MA, USA), and were annotated with ANNOVAR. Variants were filtered out to exclude those located in intronic regions and synonymous variants not predicted to affect splice sites, as well as non-synonymous variants with reported minor allele frequency (MAF) ≥ 0.01 in publicly available human variation resources (dbSNP146, 1000 Genomes, Exome Aggregation Consortium (ExAC), NHLBI Exome Sequencing Project Exome Variant Server). Pathogenicity of the retained variants was investigated by *in silico* prediction tools, including PolyPhen-2 (http://genetics.bwh.harvard.edu/pph2/), SIFT (http://sift.jcvi.org/), Mutation Taster (http://www.mutationtaster.org/), and Alamut (http://www.interactive-biosoftware.com/). Sanger sequencing was used to confirm the annotated variants of interest and perform segregation analysis.

In patient P2 and P3, whole-exome sequencing was performed. In patient P3, whole-exome sequencing (HiSeq2500 Illumina platform) was used and the analyses (RoDa4 pipeline and Cartagenia 4.2) was focused on genes linked to intellectual disability (1157 genes, IDv10) and central hypothyroidism (154 genes, CH-Cplusv2). Only *de novo* variants (dominant model) and hemi-/homozygote or compound heterozygote variants (recessive model) were selected and cross-checked with the Genome Aggregation controle Database (gnomAD, http://gnomad.broadinstitute.org). Pathogenicity of the retained variants was investigated by *in silico* prediction tools, including PolyPhen-2, and Alamut and cross-checked with available literature.

Patient P4 and P5 had been diagnosed elsewhere using next generation sequencing (patient P4) or Sanger sequencing of a familial mutation (patient P5).

Materials

[^{125}I]T_3 and [^{125}I]T_4 were synthesized as described previously (27). Unlabeled iodothyronines, Silychristin, bovine serum albumin (BSA), and D-glucose were obtained from Sigma-Aldrich (Zwijndrecht, The Netherlands [NL]); culture dishes from Corning (Schiphol, NL); culture medium from Invitrogen (Bleiswijk, NL); transfection reagent X-tremeGENE 9 from Roche Diagnostics (Almere, NL); 4-20% gradient Mini-PROTEAN TGX Precast Protein Gel from from Bio-Rad (Veenendaal, NL), polyvinylidene difluoride membranes and NuPAGE 4x lithium dodecyl sulfate loading buffer from Thermo Fisher Scientific (Bleiswijk, NL). An overview of the antibodies is provided in **Supplementary Table 1**. Vectashield H-1200 containing DAPI from Brunschwig (Amsterdam, NL).

Plasmids

Cloning of wild-type (WT) human MCT8 in pcDNA3 and of human μ-crystallin (CRYM) in pSG5 has been previously described (28, 29). The p.N193I, p.G276R, and p.R445C mutations were introduced in the WT MCT8 expression construct according to previously described methods (22). The presence of the desired mutations was verified by sanger sequencing. Positions of the mutations are determined using

the NM_006517.3 reference sequence which uses +1 as the A of the ATG translation initiation codon of the long MCT8 translational isoform, with the initiation codon as codon 1.

Cell culture and transfection

COS-1 and JEG-3 cells were cultured in DMEM/F-12 medium (Life Technologies, Bleiswijk, NL) supplemented with 9% heat-inactivated fetal calf serum (FCS; Invitrogen, Breda, NL) and 2% penicillin/streptomycin (Pen/Strep; Roche Diagnostics). COS-1 or JEG-3 cells were cultured in 24-well plates (uptake assays), 6-well plates (immunoblotting), or 10 cm dishes (surface biotinylation assays) and transiently transfected at 70% confluence with 50 ng (uptake), 500 ng (immunoblotting) or 2000 ng (surface biotinylation assays) of WT or mutant MCT8 using X-tremeGENE9 as a transfection reagent (Roche Diagnostics,Woerden, NL).

Human fibroblasts were derived from skin biopsies and were cultured in 6-well plates (for uptake assays) or 10 cm dishes (for immunoblotting) in DMEM/F-12 medium supplemented with 9% heat-inactivated FCS and 2% Pen/Strep.

TH uptake studies

Cells were washed with incubation medium (Dulbecco`s phosphate buffered saline containing 0.1% bovine serum albumin and 0.1% glucose) and incubated for 30 minutes at 37°C in incubation medium containing 1 nM unlabeled T3 and 50,000 cpm [^{125}I]T3. After incubation, cells were briefly washed with incubation medium and lysed in 0.1 M NaOH. The amount of internalized radioactivity was measured with a γ-counter. T3 uptake levels in human fibroblasts were corrected for total protein levels measured with Bradford assay according to manufacturers` protocol (Bio-Rad).

Cell surface biotinylation and immunoblotting

Cell surface biotinylation was carried out in transiently transfected COS-1 cells as previously described (16). Immunoblotting on total lysates and the cell surface biotinylated fraction were carried out using standards methods as described before (17). Membranes were probed with MCT8 and Glyceraldehyde-3-phosphate dehydrogenase (GAPDH) antibodies (as a loading control) which were visualized by Odyssey using IRDye680 goat anti-rabbit and IRDye800 goat anti-mouse (LI-COR, Leusden, NL) secondary antibodies, respectively.

Immunocytochemistry

Immunocytochemistry was carried out in JEG-3 cells using previously described techniques (22). Samples were fixed and permeabilized prior to blocking with 1% BSA. Samples were incubated overnight at 4°C with MCT8 (AB-3353) antibody. Zona Occludens (ZO)-1 was used as a cell membrane marker. Primary antibodies were visualized with goat anti-rabbit Alexa Fluor 488 and goat anti-mouse Alexa 633 (**Supplemental Table 1**). Coverslips were mounted on glass slides using Vectashield H-1200 containing DAPI (Brunschwig) and analyzed as before on a Zeiss Meta 510 microscope using Zeiss LSM software (Zeiss NL, Sliedrecht, NL).

Supplemental results

Clinical and biochemical characteristics of two novel male subjects with MCT8 deficiency

Family IV

Patient P4 presented at an age of 65 year with moderate to severe intellectual disability and was referred to our hospital after he had been diagnosed with MCT8 deficiency. He was born to non-consanguineous parents, and presented clear developmental delay, spastic diplegia and frequent tonic-clonic seizures in early childhood. In adulthood, he was diagnosed with central hypothyroidism (low T4 and normal TSH and inadequate TRH response) and treatment with levothyroxine was initiated. At time of referral, he showed typical symptoms of MCT8 deficiency, although relatively mild in severity, and treatment with levothyroxine had just been stopped. Gross motor function was relatively well developed and he had full head control, was able to sit independently and could walk a few steps with support (**Table 1**). Dystonic features were relatively mild, but tendon reflexes were clearly elevated and contractions had progressively reduced his physical abilities. Communicative skills were relatively well developed and he could engage in simple conversations by using “yes” and “no”. Thyroid functions tests were mildly abnormal showing serum T3 concentrations within the normal range, reverse T3 and (free) T4 concentrations slightly below the normal range, and TSH was marginally elevated. He had no overt signs of peripheral hyperthyroidism, although the serum SHBG concentration was slightly elevated and body weight somewhat low (**Table 1**). A DXA scan of the total body revealed moderate osteopenia (T-score -1.4 SD), with marked osteoporosis of the hips (T-score -2.9 SD). Cardiac monitoring was normal (**Table 1**).

Family V

Patient P5 presented at an age of 4 years and showed the classical phenotype associated with MCT8 deficiency. Head control was absent and he was unable to sit independently. Dystonic movements were pronounced and spastic features, including elevated deep tendon reflexes and mild contractions, were present. He failed to achieve early motor milestones and did not develop any speech (**Table 1**). Brain MRI studies at the age of 5 and 10 months showed a global delay in myelination and a relatively thin corpus callosum (**Figure 1C**). Serum thyroid function tests showed elevated serum T3 levels and markedly decreased serum (free) T4 and rT3 concentrations with a normal TSH (**Table 1**). Serum sex hormone binding globulin concentrations were elevated and the heart rate was relatively high for age (**Table 1**). In addition, increased perspiration was reported. A gradual decline in body weight and swallowing difficulties required percutaneous tube feeding.

Supplemental Tables

Supplementary Table S1. Antibody overview.

Protein target	Antigen sequence (if known)	Antibody name	Manufacturer (catalog #)	Species raised in; (M) or (P)	Dilution	RRID
hMCT8	AA 52-155	MCT8	ATLAS (HPA003353)	Rabbit (P)	1:20000 (IB) and 1:1000 (ICC)	AB_1079343
GAPDH		GAPDH	Merck Millipore (Mab374)	Mouse (M)	1:20000 (IB)	AB_2107445
ZO1		ZO1	Thermo Fisher (33-9100)	Mouse (M)	1:1000 (ICC)	AB_2533147
Rabbit IgG		IRDye680	LI-COR (926-68020)	Goat	1:20000 (IB)	AB_10706161
Mouse IgG		IRDye800	LI-COR (926-32211)	Goat	1:20000 (IB)	AB_621843
Rabbit IgG		Alexa 488	Thermo Fisher (A11008)	Goat	1:1000 (ICC)	AB_143165
mouse IgG		Alexa 633	Thermo Fisher (A21050)	Goat	1:1000 (ICC)	AB_2535718

Abbreviations: RRID, research resource identifiers; M, mono-clonal; P, poly-clonal; WB, immunoblots; ICC, immunocytochemistry.

Supplemental Figures

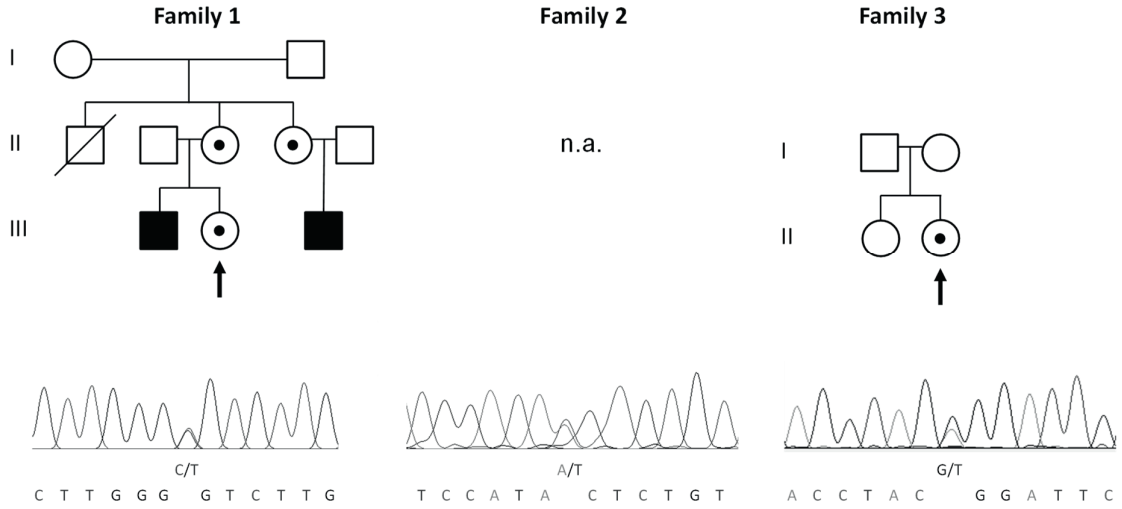

Figure S1 Pedigrees of the three female patients and results of molecular genetic studies. Pedigree and mutational analysis of patient P1 (A), patient P2 (B) and patient P3 (C).

REFERENCES

1. Yen PM. Physiological and molecular basis of thyroid hormone action. Physiol Rev. 2001;81(3):1097-142.
2. Yen PM, Ando S, Feng X, Liu Y, Maruvada P, Xia X. Thyroid hormone action at the cellular, genomic and target gene levels. Mol Cell Endocrinol. 2006;246(1-2):121-7.
3. Gereben B, Zavacki AM, Ribich S, Kim BW, Huang SA, Simonides WS, et al. Cellular and molecular basis of deiodinase-regulated thyroid hormone signaling. Endocr Rev. 2008;29(7):898-938.
4. Hennemann G, Docter R, Friesema EC, de Jong M, Krenning EP, Visser TJ. Plasma membrane transport of thyroid hormones and its role in thyroid hormone metabolism and bioavailability. Endocr Rev. 2001;22(4):451-76.
5. Friesema EC, Ganguly S, Abdalla A, Manning Fox JE, Halestrap AP, Visser TJ. Identification of monocarboxylate transporter 8 as a specific thyroid hormone transporter. J Biol Chem. 2003;278(41):40128-35.
6. Mayerl S, Muller J, Bauer R, Richert S, Kassmann CM, Darras VM, et al. Transporters MCT8 and OATP1C1 maintain murine brain thyroid hormone homeostasis. J Clin Invest. 2014;124(5):1987-99.
7. Vatine GD, Al-Ahmad A, Barriga BK, Svendsen S, Salim A, Garcia L, et al. Modeling Psychomotor Retardation using iPSCs from MCT8-Deficient Patients Indicates a Prominent Role for the Blood-Brain Barrier. Cell Stem Cell. 2017;20(6):831-43 e5.
8. Friesema EC, Grueters A, Biebermann H, Krude H, von Moers A, Reeser M, et al. Association between mutations in a thyroid hormone transporter and severe X-linked psychomotor retardation. Lancet. 2004;364(9443):1435-7.
9. Dumitrescu AM, Liao XH, Best TB, Brockmann K, Refetoff S. A novel syndrome combining thyroid and neurological abnormalities is associated with mutations in a monocarboxylate transporter gene. Am J Hum Genet. 2004;74(1):168-75.
10. Friesema EC, Jansen J, Heuer H, Trajkovic M, Bauer K, Visser TJ. Mechanisms of disease: psychomotor retardation and high T3 levels caused by mutations in monocarboxylate transporter 8. Nat Clin Pract Endocrinol Metab. 2006;2(9):512-23.
11. Schwartz CE, Stevenson RE. The MCT8 thyroid hormone transporter and Allan-Herndon-Dudley syndrome. Best Pract Res Clin Endocrinol Metab. 2007;21(2):307-21.
12. Schwartz CE, May MM, Carpenter NJ, Rogers RC, Martin J, Bialer MG, et al. Allan-Herndon-Dudley syndrome and the monocarboxylate transporter 8 (MCT8) gene. Am J Hum Genet. 2005;77(1):41-53.
13. Herzovich V, Vaiani E, Marino R, Dratler G, Lazzati JM, Tilitzky S, et al. Unexpected peripheral markers of thyroid function in a patient with a novel mutation of the MCT8 thyroid hormone transporter gene. Horm Res. 2007;67(1):1-6.
14. Ramos HE, Morandini M, Carre A, Tron E, Floch C, Mandelbrot L, et al. Pregnancy in women heterozygous for MCT8 mutations: risk of maternal hypothyroxinemia and fetal care. Eur J Endocrinol. 2011;164(2):309-14.
15. Frints SG, Lenzner S, Bauters M, Jensen LR, Van Esch H, des Portes V, et al. MCT8 mutation analysis and identification of the first female with Allan-Herndon-Dudley syndrome due to loss of MCT8 expression. Eur J Hum Genet. 2008;16(9):1029-37.
16. Groeneweg S, Lima de Souza EC, Meima ME, Peeters RP, Visser WE, Visser TJ. Outward-Open Model of Thyroid Hormone Transporter Monocarboxylate Transporter 8 Provides Novel Structural and Functional Insights. Endocrinology. 2017;158(10):3292-306.
17. Groeneweg S, van den Berge A, Meima ME, Peeters RP, Visser TJ, Visser WE. Effects of Chemical Chaperones on Thyroid Hormone Transport by MCT8 Mutants in Patient-Derived Fibroblasts. Endocrinology. 2018;159(3):1290-302.
18. Vaurs-Barriere C, Deville M, Sarret C, Giraud G, Des Portes V, Prats-Vinas JM, et al. Pelizaeus-Merzbacher-Like disease presentation of MCT8 mutated male subjects. Ann Neurol. 2009;65(1):114-8.
19. Dateki S, Haraguchi K, Sato T, Nakatomi A, Fujiwara M, Sakurai M, et al. A novel MCT8 mutation in a Japanese patient with Allan-Herndon-Dudley syndrome. Horm Res. 2013;80(Suppl 1):360.
20. Johannes J, Jayarama-Naidu R, Meyer F, Wirth EK, Schweizer U, Schomburg L, et al. Silychristin, a Flavonolignan Derived From the Milk Thistle, Is a Potent Inhibitor of the Thyroid Hormone Transporter MCT8. Endocrinology. 2016;157(4):1694-701.
21. Groeneweg S, Visser WE, Visser TJ. Disorder of thyroid hormone transport into the tissues. Best Pract Res Clin Endocrinol Metab. 2017;31(2):241-53.
22. Groeneweg S, Friesema EC, Kersseboom S, Klootwijk W, Visser WE, Peeters RP, et al. The role of Arg445 and Asp498 in the human thyroid hormone transporter MCT8. Endocrinology. 2014;155(2):618-26.
23. Maduro C, de Hoon B, Gribnau J. Fitting the Puzzle Pieces: the Bigger Picture of XCI. Trends Biochem Sci. 2016;41(2):138-47.

24. Tukiainen T, Villani AC, Yen A, Rivas MA, Marshall JL, Satija R, et al. Landscape of X chromosome inactivation across human tissues. Nature. 2017;550(7675):244-8.
25. Cotton AM, Ge B, Light N, Adoue V, Pastinen T, Brown CJ. Analysis of expressed SNPs identifies variable extents of expression from the human inactive X chromosome. Genome Biol. 2013;14(11):R122.
26. Groeneweg S, Peeters RP, Moran C, Stoupa A, Auriol F, Tonduti D, et al. Effectiveness and safety of the tri-iodothyronine analogue Triac in children and adults with MCT8 deficiency: an international, single-arm, open-label, phase 2 trial. Lancet Diabetes Endocrinol. 2019;7(9):695-706.
27. Mol JA, Visser TJ. Synthesis and some properties of sulfate esters and sulfamates of iodothyronines. Endocrinology. 1985;117(1):1-7.
28. Friesema EC, Jansen J, Jachtenberg JW, Visser WE, Kester MH, Visser TJ. Effective cellular uptake and efflux of thyroid hormone by human monocarboxylate transporter 10. Mol Endocrinol. 2008;22(6):1357-69.
29. Friesema EC, Kuiper GG, Jansen J, Visser TJ, Kester MH. Thyroid hormone transport by the human monocarboxylate transporter 8 and its rate-limiting role in intracellular metabolism. Mol Endocrinol. 2006;20(11):2761-72.

Chapter 4

Identification of novel patients with MCT8 deficiency

Chapter

Disease characteristics of MCT8 deficiency: an international, retrospective, multicenter cohort study

4.1

Stefan Groeneweg, Milou Stals, Anna Dolcetta, Ferdy S. van Geest, Marieke M. van der Knoop, Femke K. Aarsen, Ingrid van Beynum, Robin P. Peeters, Marjolein Dremmen, Ireneus F.M. de Coo, W. Edward Visser, on behalf of the MCT8 deficiency Working Group.

Manuscript in preparation.

ABSTRACT

Background - Deficiency of the thyroid hormone transporter monocarboxylate transporter 8 (MCT8) causes severe intellectual disability and abnormal thyroid function tests. The neurocognitive phenotype has been attributed to the hypothyroid state in the MCT8-dependent brain, whereas the elevated serum T3 concentrations lead to chronic thyrotoxicosis in tissues that do not rely on MCT8 (peripheral phenotype). Data are scarce on the natural history of this rare disorder. We aimed to analyze the phenotypic characteristics in an international cohort of patients with MCT8 deficiency.

Methods - This study was a retrospective, multicenter, international study in male patients with genetically confirmed mutations in the *MCT8* gene with no age restrictions. The study was done using data from 22 centers. Data from patients followed-up from 2003 to 2018 were retrieved from October, 2014, to January 1, 2019. Patients were not to receive any thyroid hormone (analogue) therapy at time of evaluation. Our primary objectives were to determine overall survival and the level of neurocognitive development throughout life. We also assessed clinical measures including body weight and heart rate, biochemical markers of thyroid function and neuro(radio)logical features.

Results - 138 subjects with 69 different underlying mutations in the *MCT8* gene were included. 26 (19.5%) patients of the cohort died at a median age of 10.5 years (range 1.6-71.0). Survival curves significantly differed between individuals that attained head control and those who did not (comparison of survival curves by log-rank test: p=0.002; hazard ratio 5.87, 95% CI 2.05-12.83). Main causes of death were pulmonary infections (19.2%), sudden (cardiac) death (15.4%), and aspiration pneumonia (7.7%). Median motor function and cognitive abilities did not significantly differ between patients aged <4 years, 4-18 years, or >18 years. Thyroid function tests showed elevated T3 concentrations in 87 (93.6%) of patients and reduced total T4 concentrations in 84 (89.3%) patients. Seven out of 8 patients with available data (87.5%) displayed T4 concentrations below -1 SD during neonatal screening. 42 of 65 (64.6%) of patients with available data were underweight (<-2 SD). Cardiovascular abnormalities were observed in the majority of patients with available data, with 11 of 39 (28.2%) patients having systolic hypertension, 20 of 51 (39.2%) patients having tachycardia in rest, and 35 of 45 (77.8%) having premature atrial contractions.

Interpretation - This international cohort study is the first to report in detail core neurological and peripheral characteristics, including clinical relevant sequelae in patients with MCT8 deficiency. These data can help to improve clinical management and may serve as historical control for the assessment of current and future therapies.

INTRODUCTION

Thyroid hormone is crucial for normal development, particularly neurodevelopment, and regulates basal metabolism throughout life (1, 2). Intracellular thyroid hormone action requires membrane transporter proteins that facilitate the cellular entry of thyroid hormones (3). MCT8 (monocarboxylate transporter 8) deficiency (also known as Allan-Herndon-Dudley syndrome (AHDS)) is a debilitating disorder comprising a severe neurodevelopmental delay and various negative clinical sequelae of chronic peripheral thyrotoxicosis (4-6).

MCT8 deficiency is caused by mutations in the gene encoding MCT8 (*SLC16A2*, located on Chr Xq13.2, and has an estimated prevalence of 1:70 000 males (7). Intracellular thyroid hormone bioavailability is dictated by thyroid hormone transporters in the cell membrane of target cells, of which MCT8 is the most specific transporter identified to date (8, 9). MCT8 is critical for the transport of thyroid hormone across the blood-brain barrier and into neuronal cells (10-12). Until 2019, when a clinical trial demonstrated that treatment with triiodothyroacetic acid (Triac) ameliorates key features of the peripheral thyrotoxicosis and might benefit brain development once treatment is commenced early in life, only supportive therapy was available for patients with MCT8 deficiency (13).

The number of patients with MCT8 deficiency is steadily increasing. To date, phenotypic description of MCT8 deficiency has been published as case reports or case series of (related) patients (e.g. (14, 15)). These reports have focused on the neurological phenotype but with variable tools precluding consistent assessments, while the peripheral clinical features of this disorder have been largely neglected (15, 16). The lack of a consistent quantitative description of the natural history of the full spectrum of MCT8 deficiency hampers early diagnosis and uniform clinical care. The development of therapeutics requires a detailed understanding of the clinical course and its variability across patients.

Given the sparsity of published data, and by taking advantage of a large international network, we aimed to provide a comprehensive and structured phenotypic characterization of MCT8 deficiency using clinical, radiological and biochemical data.

METHODS

Study design and participants

This international study was initiated on 1 October 2014 by founding a consortium of centres where patients with MCT8 deficiency were followed from all over the world (see **appendix**) to centralize all available data in order to detail the clinical course of MCT8 deficiency.

The key inclusion criterion was genetically confirmed pathogenic mutation in the *SLC16A2* gene. Additionally, data on first-degree and second-degree male relatives with clinical MCT8 deficiency (when genetic testing was not available at that time) were included. Patients of all ages were included. Our cohort consisted of patients that had been enrolled in the international, multi-centre Triac Trial (NTC NCT02060474, (13)), patients who participated in the named-patient program for Triac treatment, patients who were enrolled in the international MCT8 deficiency patient registry and patients in whom the Erasmus MC fulfilled a consultancy role. Some (n=45) of the patients were previously reported with incomplete data. For such patients, updated and exhaustive data were collected (13). There were no exclusion criteria.

Ethical considerations

This study conforms to the Declaration of Helsinki, Good Clinical Practice guidelines and was evaluated and granted by the appropriate local institutional review boards or ethics committees (leading Center Erasmus Medical Center Rotterdam, METC identifier MEC-2014-199, and MEC-2015-362). However, for the retrospective analysis of existing data obtained in the context of routine patient care, the majority of the centers did not require additional specific institutional review board approval. Written informed consent was obtained from the parents or legal representatives of all enrolled patients.

Procedures

A general outline of the study procedures is provided in **figure s1**. In this retrospective study, we included the available, routinely collected data on the genetic diagnosis, the clinical phenotype and biochemical features of MCT8 deficiency based on availability. The genetic mutation was documented for all patients enrolled in the cohort. For patients with available medical information, we retrieved the following general features from their medical files based on availability: pregnancy duration, birth weight and height, age of onset of symptoms, age of genetic diagnosis, ability to maintain head control, the age last known alive, and, if applicable, cause of death. We also included the available results of thyroid function measurements during neonatal screening programs. In the analyses of thyroid hormone function, we included all patients of whom thyroid function had been measured in the central laboratory of the Erasmus Medical Center, Rotterdam, The Netherlands.

Patients who had been evaluated according to standard operating procedures during the baseline visit of the Triac Trial (NCT02060474, (13)) or Triac named-patient programs were included in the deep-phenotyping analyses. This restriction was made to ascertain that all measures had been captured by well-trained investigators using uniform procedures and definitions, prior to the start of potential disease-modifying therapy. The following data were collected regarding the neurocognitive disease features: neurological clinical examination (i.e. reflexes, muscle tone, extra-pyramidal signs), and the results of neurodevelopmental assessments (i.e. Gross Motor Function Measure [GMFM]-G88 (17), Vineland Adaptive Behavior scales [VABs] II (18) and Bayley Scales of Infant Development [BSID] III (19)). In addition to these standardized assessments, we re-evaluated available historical results of neurophysiological examinations (including electro-encephalograms, and evoked potentials) and historical brain imaging studies. Historical brain imaging studies had all been conducted as part of routine care and were therefore not captured using uniform acquisition protocols. Scans were re-analyzed to identify key characteristics of MCT8 deficiency. The following data were collected regarding the peripheral disease features: clinical examination (including blood pressure, body weight and height, signs of tissue thyrotoxicosis), results on 24h cardiac monitoring, electrocardiography, transthoracic cardiac ultrasounds, DXA-imaging studies, growth curves, and the presence of co-morbidities (including gastroesophageal reflux disease, feeding problems, recurrent infections, pulmonary problems, scoliosis, hip luxation). Data on biochemical analyses included serum markers that reflect thyroid hormone action in peripheral organs (including serum sex hormone binding globulin, creatinine, total cholesterol and creatine kinase concentrations), endocrine parameters (including serum markers for bone metabolism and sex hormones). All biochemical analyses had been carried out in a centralized laboratory (Erasmus MC, Rotterdam, The Netherlands). Data from patients followed up from January 2003 until January 2018 were retrieved from October 2014 to January 2019. The principle investigators (SG and WEV) analyzed the data. To minimize the confounding effect of

missing data in the medical files of each patient, the presence or absence of a specific sign was recorded only when it was specifically mentioned as absent of present in the medical file.

Outcomes

Our primary objective was to analyze the overall survival of patients with MCT8 deficiency. We also compared the survival among patients that did not attain full head control and those that achieve this early motor milestone.

Other main objectives were to characterize the natural history of MCT8 deficiency and establish the occurrence of neurological and extra-neurological features and the progression thereof. The presence or absence of specific features was noted only when it was specifically reported in the data file of the patients. Finally, we aimed to provide a detailed mutational landscape of MCT8 deficiency.

Statistical analysis

We summarized continuous variables as mean and SD, or median and range. We established overall survival and compared patients with and without full head control with log-rank analysis. Survival was defined as the age at last date known alive. All statistical tests were two-sided, and p values of less than 0.05 were considered statistically significant. Statistical analyses were performed using GraphPad Prism, version 6 (GraphPad, La Jolla, CA, USA).

RESULTS

In 22 centers, 138 patients were enrolled between October 14th 2014 and January 1st 2019. The cohort contained patients with 23 different nationalities, and 133 patients had available medical information (**figure s1**). Serum thyroid function tests had been measured in the central laboratory in 95 cases, of which 67 had been assessed according to standardized protocols for deep phenotyping purposes at a median age of 5.0 years (IQR 2.3-10.5, range 0.75-66) (**figure s1**). The demographics and basic characteristics of the enrolled patients are summarized in **table s1**.

Among the 138 enrolled cases, 69 different underlying genetic mutations were identified, of which 34 had not been reported before (**figure s2**). A total of 15 mutations were identified in at least two unrelated families. Twelve (9.8%) cases with available data on the inheritance of the mutation were *de novo* cases (non-familial). The 34 missense mutations all locate to the transmembrane helices (**figure 1A**).

Based on the patients with available medical information (n=133), the median age at diagnosis was 24.0 months (range: 0.0-744.0) (**figure 1B**). By contrast, the median age at onset of first symptoms was 4.0 months (range: 0.0-13.0) (**figure 1B**). The median time to diagnosis was 20 months (IQR 6.0-82.0, range 0.0-738). Gross developmental delay (85.5%), hypotonia (42.0%), feeding problems (11.6%), and poor weight gain (10.1%) were the most frequently reported initial concerns that prompted medical evaluation (**figure 1C**).

At a median age at last follow-up of 9.2 years (IQR 4.9-13.8, range 0.7-71), 26 (19.5%) patients had died. Median age of death was 10.5 years (IQR 5.8-18.3, range 1.6-71). The main causes of death were pulmonary infections (19.2%), sudden (cardiac) death (15.4%), and aspiration pneumonia (7.7%). For 13 (50.0%) deceased subjects the cause of death was unclear and postmortem examination had not

been performed. 53 (86.7%) of 61 patients were alive by age 10, 12 (66.7%) of 18 by age 20 and 4 (50.0%) of 8 by age 60 years. The overall survival is shown in **figure 1D**. The survival curves were significantly different for patients who achieved full head control *versus* no full head control (**figure 1E**, comparison of survival curves by log-rank test: p= 0.0021; hazard ratio 5.87, 95% CI 2.05-12.83).

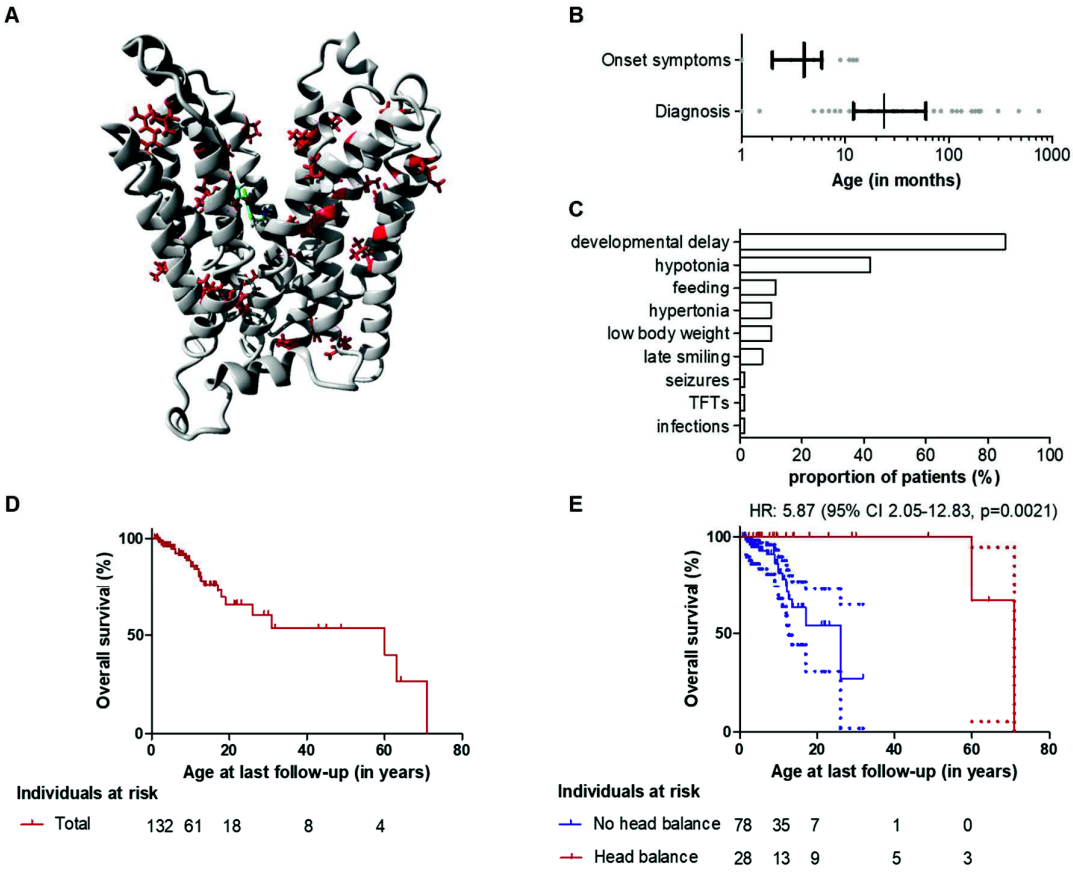

Figure 1 – Panel **A** indicates the localization of the identified missense mutations in a three-dimensional model of the MCT8 structure (32). Mutations cluster within the transmembrane helices. Panel **B** graphically presents the mean ± SEM (black lines) age at onset of symptoms and panel **C** the age at time of diagnosis. Grey dots represent measurements in individual patients. Panel **D** shows the overall survival based on age at last follow-up (Kaplan-Meier estimates). Panel **E** shows the Kaplan-Meier estimates of MCT8-specific survival in patients who attained head control (red line) versus those who did not (blue line). HR: hazard ratio.

The prevalence of specific neurological features among patients included in the deep-phenotyping cohort (N=67, median age 5.0 years, IQR 2.3-10.5, range 0.8-66.0) is reported in **table 1** and **figure 2**, and the neurological sequelae are summarized in **figure s3**. Pregnancy and delivery were unremarkable in the majority of cases, with most children having good APGAR scores, and a normal term birth weight and head circumference (**table 1**). At first presentation, most patients had global hypotonia with a pronounced head-lag and slipping through. Typically, by the end of the first year, dystonic posturing of the limbs and neck became evident. Exaggerated deep tendon reflexes were present in 50 (82.0 %) cases, and 54 (91.5%) patients developed hypertonia in wrists, knees or heels upon aging. Primitive reflexes remained present in 45 (90.0%) of 50 cases, with a positive tonic neck reflex (85.0%) and

glabellar sign (78.0%) being most abundant, irrespective of patient age. The overall prevalence of electro encephalogram (EEG)-confirmed seizures was 24.6% and mostly concerned generalized, absence-like episodes without clear motor component.

Table 1. Deep phenotyping neuro-developmental features

Characteristic	**N =67**
Age at assessment (years)	5.0 (0.75-66.8)
Perinatal features	
Pregnancy duration (weeks)	40.0 (32.0-42.0)
APGAR score >9 after 5 min	11 (92.0)
Term birth weight (grams)	3472 (±548)
Microcephalic (P<5) at birth (n=11)	1 (9.1)
Neurological examination	
Hypotonia (n=59)	59 (100%)
Dystonia (n=59)	54 (92%)
Primitive reflexes (>1 present) (n=50)	45 (90%)
Tonic neck reflex (n=20)	17 (85%)
Glabellar sign (n=50)	39 (78%)
Startle response (n=24)	17 (71%)
Scoliosis (>8 years) (n=17)	15 (88%)
Muscular hypoplasia (n=44)	37 (84%)
Spasticity (n=50)	50 (82%)
Urinary / faecal incontinence (n=51)	42 (82%)
Hip dislocation (>8 years, n=11)	8 (73%)
Plantar extension response (babinski sign, n=53)	37 (70%)
Feeding problems (n=62)	43 (69%)
Extrapyramidal signs (other) (n=25)	10 (40%)
Tube feeding (n=60)	24 (40%)
Delayed evoked potentials (<6 months, n=5)	2 (40%)
Sleep problems (n=44)	17 (39%)
Strabismus (n=45)	17 (38%)
Nystagmus (n=45)	13 (29%)
Seizures (EEG proven) (n=57)	14 (25%)
Apneusis (n=30)	7 (23%)
Abnormal hearing (n=40)	1 (3%)
Delayed evoked potentials (>1 year, n=2)	0 (0%)
Development	
Head control (n=63)	18 (29%)
Speech (at least 1 word) (n=60)	5 (8%)
Independent sitting (n=64)	5 (8%)
Independent walking (n=63)	3 (5%)
MRI/MRS characteristics*	
Normal global anatomy (n=14)	14 (100%)
Delayed myelination (n=14)	14 (100%)
Reduced cerebral white matter volume (n=14)	13 (93%)
Prominent supratentorial ventricular system (n=14)	13 (93%)
Prominent peripheral liquor spaces (n=14)	13 (93%)
Low NAA peak (n=8)	7 (88%)
High choline peak (n=8)	7 (88%)

Data are median (range), n (%), or mean (±SD). Systematic deep phenotyping of neurological phenotype in 67 eligible patients. Most parameters were not available for all patients.

* MRI images were available for 14 patients (median age at last available MRI scan: 23.5 months, range 8.8-74.3); MRS was available in 8 cases. All images were centrally re-evaluated. Details are provided in **table s2**.

14 patients had available MRI scans of the brain, acquired at a median age of 8 months (range: 5-69), with 9 patients having at least 1 repetitive scan available (**table 1**, **figure s3**, **table s2**).

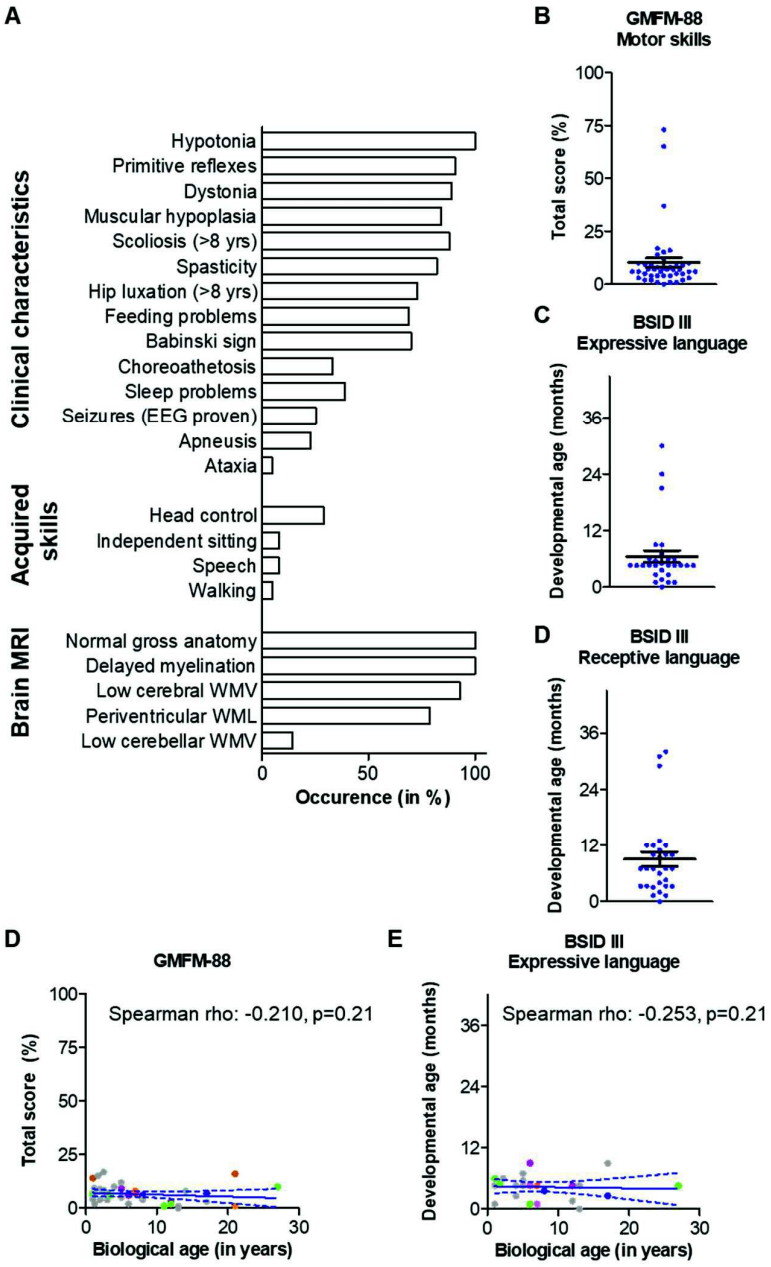

Figure 2 – Panel **A** shows the prevalence of clinical, radiological and developmental key features in MCT8 deficiency. Bars indicate the proportion of patients presenting the indicated feature. Panel **B** represents the gross motor function development in patients with MCT8 deficiency measured by the Gross Motor Function Measure (GMFM) 88 (17). A 100% score indicates the level of development that is normally achieved by a 4-year old child. Panel **C** shows the development of expressive language and panel **D** the development of receptive language, measured by the respective sub-domains of the Bayley Scales of Infant Development (BSID) III (19). Scores are expressed as developmental age in months. Blue dots indicate measurements in individual patients and black lines indicate the mean ± SEM score. Panel **E** shows the GMFM 88 score by age and panel **F** the developmental age on the sub-domain expressive language of the BSID III *versus* the biological age. Only severely affected patients were considered in panel **E** and **F**. Linear regression was used to plot the trend and the 95% confidence intervals (blue lines). Spearman rho values and corresponding p values are indicated in the graph. Patients harboring the same genetic mutation are displayed in the same color: p.F230del (green), c.651-652+20del (blue), G564R (purple), p.A565fs566X (pink), and R271H (orange). Unique mutations are colored in grey.

The most pronounced and consistent abnormality was a global decrease in myelination, evidenced by diffuse white matter hyper-intensities on T2-weighted images. Myelination improved with aging, but had not fully normalized in the oldest patient (15 years) with available data. Most cases showed diffuse cortical and subcortical atrophy with dilatation of the ventricular spaces, widening of the subarachnoid spaces, and prominence of the supra- and infra-tentorial sulci. Magnetic resonance spectroscopy (MRS) showed an increased choline peak and a decreased N-acetyl aspartate (NAA) peak in 7 out of 8 (87.5%) patients with available investigations which is compatible with aberrant myelination and general atrophy. These neuro-radiological findings were supported by post-mortem examination of the brain of a deceased 8-year old patient showing a reduction of global brain volume and a diffuse reduction in myelin (see **supplementary results**).

All patients had moderate-severe intellectual disability with a severe delay in motor and language development (**table s3**). Only 5 (7.8%) patients achieved independent sitting and were clearly less severely affected than the other patients with available data (**figure 2A** and **B**). The median scores on the Gross Motor Function Measure 88 did not exceed 10% of the total score that should be obtained by healthy 4-year old children (**figure 2B**, **table s3**). 29 subjects had been evaluated with the Bayley Scales of Infant Development III at a median biological age of 5.0 years (range 1.0-66.0), which revealed median developmental ages well-below 12 months on all tested sub-domains (**figure 2C** and **D**, **figure s4A-C**, **table s3**). When only considering severely affected patients, scores on none of the developmental domains improved with age, whereas fine motor skills even showed significant regression (**figure 2E** and **F**, **figure s4D-G**).

Serum thyroid function tests were available in 95 treatment-naive patients at a median age of 6.0 years (IQR 2.2-10.4, range 0.8-66.0). TSH concentrations were within normal range in 87% of patients (**figure 3A**). Free and total T4 levels were below the age-specific lower limit in 84 (88.4%) and 84 (89.4%) patients, respectively (**figure 3B** and **figure s5A** and **s5B**). Mean T3 concentrations were 4.64±1.38 nmol/L and exceeded the age-specific upper limit in 87 (93.6%) patients (**figure 3C**), which resulted in a pronounced increase in the T3/T4 ratio (**figure s5C**). Reverse T3 (rT3) concentrations were decreased in 90.7% of patients (**figure s5D**), resulting in a pronounced increase in the T3/rT3 ratio (**figure s5E**). In 3 out of 7 subjects TRH-stimulation tests showed an inadequately low response. In 7 out of 8 (87.5%) subjects with available T4-based neonatal screening results, total T4 concentrations were below the 20th percentile (**figure 3D**). Although this prompted additional measurement of TSH, none of the patients was diagnosed with MCT8 deficiency. Serum total T4 concentrations were significantly less reduced in patients with less severe compared to those with severe developmental delay (**figure s5F**). Serum T3 concentrations were not significantly different between both groups (**figure s5G**). Consequently, the T3/T4 ratio, a measure for peripheral thyroid hormone metabolism, was significantly lower in patients with a less severe phenotype (**figure s5G**).

Deep phenotyping of the peripheral phenotype was carried out in 67 patients (median age 5.0 years, IQR 2.3-10.5, range 0.8-66.0) and the main findings are summarized in **table 2** and **table s4**. Body weight for age showed progressive deterioration over time, with 64.6% (42 out 65) patients being severe underweight (< -2SD) (**figure 3E**, **table 2**). Twenty-four (40.0%) patients had tube feeding, although impaired swallowing function was reported in up to 43 (69.4%) of these patients. Body height for age also deteriorated with age (**figure 3F**). Delayed progression of puberty was present 4 (22.2%) patients (**figure s6A-D**). In patients above 8 years of age, bone mineral density (BMD) was below the p5, but bone turn-over markers were generally within the low-normal range (**figure s7A-D**).

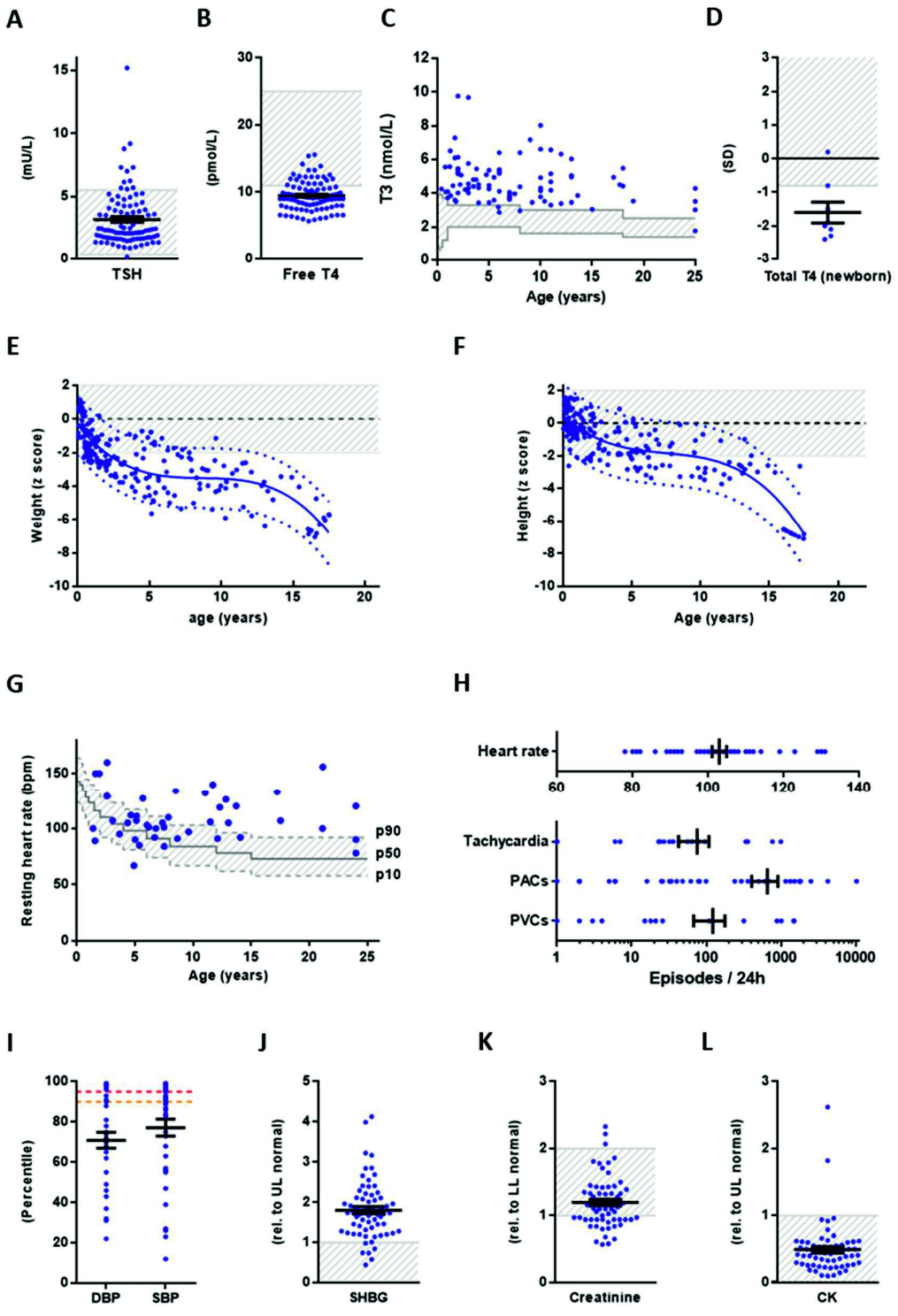

Figure 3 –Mean ± SEM (black lines) serum concentrations of thyroid stimulating hormone (panel **A**) and free T4 (panel **B**). Panel **C** presents the serum total T3 concentrations *versus* age. Panel **D** shows the available results on total T4 measurements during neonatal screening expressed in SDs. Blue dots represent measurements in individual patients and grey areas the normal range. Panel **E** shows the natural course of bodyweight change in patients with MCT8 deficiency. Blue dots represent available historical bodyweight measurements in Triac-naive patients. Although these measurements were not carried out under standardized conditions, these

measurements have been carried out in the context of regular medical care in patients that had different co-morbidities, co-medication, and socio-economic backgrounds and are, as such, likely to constitute a representative set of clinical observations. Non-linear (third order) polynomial regression was used to plot the trend with its 95% error band. Similarly, panel **F** shows the natural course of body height. Panel **G** shows the resting heart rate by age. Normal range in healthy children is derived from studies of Fleming and colleagues (20). Panel **H** shows the mean ± SEM (black lines) occurrence of indicated features during 24h cardiac monitoring in 45 individuals. Panel **I** shows the mean ± SEM diastolic and systolic blood pressure. The orange line represents the threshold for classification as elevated blood pressure and the red line the threshold of hypertension, as defined by the guidelines from the American Academy of Pediatrics (21) and the American College of Cardiology and American Heart Association (22). Serum concentration of serum sex hormone binding globulin (SHBG) (panel **J**), creatinine (panel **K**), and creatine kinase (panel **L**) are expressed relative to the age-specific lower (panel **K**) or upper (panel **J** and **L**) limit of the normal range. Abbreviations: TSH, thyroid stimulating hormone; T4, thyroxine, T3, triiodothyronine, PACs, premature atrial contractions; PVCs premature ventricular contractions; CK, creatine kinase, SHBG, sex hormone binding globulin. The absolute mean values of all parameters are summarized in **table s4**.

Extensive cardiovascular screening was available in 45 cases. At time of evaluation, 44 out of 45 (98%) patients reportedly had no cardiovascular abnormalities. The mean resting heart rate measured by electrocardiography was 110 beats per minute (±20), with 20 (39.2%) patients exceeding the p90 for age (**figure 3G**) (20). Four out of 52 patients (7.6%) had a second degree atrioventricular block and 6 out of 52 patients (11.5%) had an (incomplete) right bundle branch block. In addition, corrected QT intervals (QTc) were above the 98th percentile in three (5.8%) patients (**table 2**, **figure s8A**). Even though most patients were fully immobilized, 24h ambulatory cardiac monitoring showed a high resting heart rate (103±13 beats per minute), with frequent tachycardic episodes, and premature atrial or ventricular contractions (**figure 3H**, **table s4**). One pediatric patient had an episode of atrial fibrillation and another patient a short episode of (non-sustained) ventricular tachycardia.

The results of detailed cardiac echocardiography (n=16) are reported in **figure s8B** and revealed, amongst others, the presence of dilated aortic root (>+2SD) in 5 (33.3%) patients (range 2.0-2.74 SD). Systolic blood pressure exceeded the p90 in 54 percent of evaluated cases (21 out of 39), whereas the diastolic blood pressure exceeded the p90 in 11 out 39 cases (28.2%) (**figure 3I**). Fourteen (35.9%) patients were classified as hypertensive (21, 22).

Serum concentrations of sex hormone binding globulin (SHBG), a well-established marker for thyroid hormone action in the liver, were elevated in 56 (86.2%) patients (**figure 3J**), whereas total cholesterol concentrations were in the lower part of the normal range (**Figure s9A**). Serum alanine aminotransferase (ALT), aspartate aminotransferase (AST), and gamma glutamyl transferase (GGT) were mildly elevated in a substantial proportion of patients (**table 2**, **figure s9B**). Of note, 2 patients have had an episode of hepatic insufficiency following a (viral) infection. Serum glucose and ammonia were unremarkable.

37 (84.1%) patients had muscular hypotrophy. Creatinine concentrations in serum were within the low-normal range for age (**figure 3K**). Creatine kinase concentrations were mostly low-normal (**figure 3L**), with some exceptions attributable to recent seizures or severe dystonic episodes. Serum lactate concentrations were slightly increased in 3 (27.3%) patients (**Figure s9C**). Electron microscopic evaluation of muscle biopsies (n=2) revealed an increased number of mitochondria with normal morphology.

Gastro-oesophageal reflux disease (GORD) was present in 30 (78.9%) patients, and alleviation often required pharmacological interventions. Spontaneous gastro-intestinal bleeding was reported in 2 patients and was the cause of death in one of them. Constipation was present in 33 (62.3%) patients. Twenty-five (69.4%) patients had recurrent pulmonary infections (**table 2**).

Table 2. Deep phenotyping peripheral features

Characteristic	**N =95**
Thyroid function	
Age at measurement (years)	6.0 (2.2-10.4)
Elevated T3 (n=93)	87 (94%)
Reduced free T4 (n=95)	84 (88%)
Deep phenotyping	
Age at assessment (years)	5.0 (2.3-10.5)
Biochemical features *	
Elevated sex hormone binding globulin (n=60)	53 (88%)
Elevated alanine aminotransferase (n=61)	28 (46%)
Reduced creatinine (n=62)	21 (34%)
Elevated lactate (n=11)	3 (27%)
Reduced total cholesterol (n=62)	12 (19%)
Elevated aspartate aminotransferase (n=53)	10 (19%)
Elevated creatine kinase (n=62)	2 (3%)
Clinical features	
Low bone mineral density (>8 years, n=5)	5 (100%)
Hypotrohic musculature (n=44)	37 (84%)
Gastro-esophageal reflux disease (n=38)	30 (79%)
Premature atrial complexes (n=45)	35 (73%)
Recurrent (pulmonary) infections (n=36)	25 (69%)
Underweight (<-2 SD, n=65)	42 (65%)
Constipation (n=53)	33 (62%)
Elevated systolic blood pressure ** (n=39)	21 (54%)
Increased perspiration (n=51)	26 (51%)
Short stature (<-2 SD, n=57)	24 (42%)
Premature ventricular complexes (n=44)	19 (43%)
Tachycardia in rest † (n=51)	20 (39%)
Aortic root dilatation (n=15)	5 (33%)
Elevated diastolic blood pressure ¶ (n=39)	11 (28%)
Delayed puberty (>8 years, n=18)	4 (22%)
Cardiac conduction abnormalities ‡ (n=52)	10 (19%)
Cryptorchidism (n=46)	10 (19%)

Data are median (range), or n (%). Systematic deep phenotyping of the peripheral phenotype. Please note that most parameters have not been captured in all patients. All absolute and relative values are provided in **table s4**.

* Reduced and elevated indicated concentrations below or above the normal range (2.5-97.5 centile in the healthy population).

† Tachycardia was defined as a resting heart rate above the 90th percentile for the corresponding age, with cut-offs described by Fleming and colleagues (20).

‡Four out of 52 patients (7.6%) had a second degree atrioventricular block and 6 out of 52 patients (11.5%) had an (incomplete) right bundle branch block and 1 patient (1.9%) had a left posterior hemiblock.

¶ Elevated systolic and diastolic blood pressure were defined using the guidelines from the American Academy of Pediatrics (21) and the American College of Cardiology and American Heart Association (22).

DISCUSSION

This international, multi-centre, retrospective study is, to our knowledge, the largest study of quantitative natural history data and provides a detailed description of the clinical key features and outcomes of MCT8 deficiency. We characterized important disease features, which may aid accurate diagnosis, guide management and serve as context for any therapeutic intervention trials.

A principal finding is that overall survival of patients with MCT8 deficiency is greatly diminished, with an overall median life expectancy of only 30 years. Stratification of the analyses for head control revealed that patients who attain full head control are more likely to have a better survival than those who do not. Therefore, attaining full head control, as a marker for overall development, could be a relevant objective for future therapeutic trials in MCT8 deficiency.

The most common cause of death was pneumonia, either caused by aspiration or by infections. Aspiration is a frequent occurrence in MCT8 deficiency due to the impaired swallowing function, which could be, at least partially, ameliorated by tube feeding. Surprisingly, a substantial number of patients that exhibit swallowing problems reportedly had no feeding tube and thus remained at risk for aspiration. Tube feeding may also be an effective measure to prevent underweight and concomitant adverse clinical sequelae (23). Therefore, tube feeding should be considered in all patients with swallowing difficulties to reduce the risk for aspiration and prevent underweight.

A second major cause of death comprised sudden death. Although sudden death may have several etiologies, the presence of several features that have been linked to sudden cardiac death may suggest a cardiovascular origin. These features include the high abundance of premature atrial and ventricular contractions in a subset of patients, which are uncommon in healthy individuals, especially in young children (24-28). We also observed non-sustained ventricular tachycardia and QTc elongation in some patients, both also well known risk factors for sudden cardiac death. Moreover, a substantial proportion of patients exhibited systolic hypertension and/or tachycardia and had several structural and electrophysiological cardiac changes that have been linked to these traits. Importantly, 98 percent of patients reportedly had no history of cardiac abnormalities, illustrating that these cardiovascular features currently remain undetected in this population. Therefore, a more thorough cardiac screening is recommended to facilitate timely detection and treatment of cardiac risk factors.

Underweight and most of the cardiovascular features have been associated with hyperthyroidism and, thus, reduction of circulating T3 concentrations could offer a causative treatment. Indeed, in a recent clinical trial, treatment with the thyroid hormone analogue Triac efficiently reduced serum T3 concentrations and improved key clinical features such as body weight and cardiovascular parameters in MCT8 deficiency (13).

The study also identified several other clinical features that require treatment or close follow-up, of which gastro-esophageal reflux disease, scoliosis, hip luxation and constipation have the highest prevalence. The presence of mildly elevated aminotransferases in treatment-naïve patients may also be of clinical relevance given the frequent use of medication with hepatotoxic side-effects and the occurrence of transient hepatic failure in at least three reported cases following a viral infection (this report and (5)). The exhaustive clinical and biochemical analyses carried out in this study will also help clinicians to interpret laboratory findings in the context of MCT8 deficiency. Well-established markers

for thyroid hormone action in peripheral tissues suggest that especially the liver, kidney, muscle and heart are in a hyperthyroid state, whereas bone remains relatively euthyroid.

The detailed delineation of the neurological sequelae of MCT8 deficiency provided by this study will help to better discriminate MCT8 deficiency on clinical grounds from other neurodevelopmental disorders, with the combination of global hypotonia and the presence of primitive reflexes and delayed myelination on the MRI being important diagnostic clues. These findings were in agreement with other studies to the neuro-radiological phenotype in MCT8 deficiency (15, 29, 30).

An important finding in this study is the large diagnostic delay, with a median time to diagnosis of 20 months. Only 14 (16.5%) patients were diagnosed in the first year of life. This is in part attributable to the high proportion of *de novo* mutations and the aspecific symptoms (i.e. failure to thrive, developmental delay, feeding problems) at first presentation. Nevertheless, T3 concentrations were already elevated in patients as young as 9 months of age. Therefore, measurement of serum T3 concentrations may constitute a key biochemical clue for early diagnosis, and should thus be routinely performed in all infants with developmental delay. Future studies should confirm if T3 concentrations are already abnormal in early post-natal life. Should this be the case, implementation of T3 measurement in a T4-based screening algorithm may pose an opportunity for early detection.

The importance of early diagnosis is supported by preclinical studies in animal models for MCT8 deficiency. Importantly, Triac completely normalized neuro-development in *Mct8/Oatp1c1* double knock-out mice once administrated at birth (31). Should Triac also be able to modulate neuro-development in human, it is conceivable that maximal therapeutic benefits will be obtained once treatment is initiated shortly after birth. A further phase 2 clinical trial will investigate the effects of Triac neuro-development once treatment is commenced at very young age (NTC02396459).

This study has limitations inherent to its retrospective design. However, MCT8 deficiency is a rare disorder with patients living scattered throughout the world and thus the most suitable method to expand our understanding of this disorder was to retrospectively analyze the available clinical data. In general, such a design is prone to the collection of incomplete data, subjective data extraction and heterogeneous follow-up. However, in this study, data of the majority of cases had been uniformly collected during baseline screenings as part of the Triac Trial and the named-patient programs, offering a unique opportunity for systematic cross-sectional evaluation of key clinical outcomes. Although selection bias cannot be excluded, our study included a substantial proportion of currently diagnosed patients.

In summary, this study provides a comprehensive and structured phenotypic characterization of MCT8 deficiency and illustrates the complexity of this disorder with involvement of multiple extra-neurological tissues. Our data underscore the need for a multi-disciplinary approach in the treatment and follow-up, as both neurological and extra-neurological features may predispose to life-limiting co-morbidity. In addition, our study provides unique (semi-)quantitative natural history data that may function as historical control in future interventional studies in this rare disorder, for which a biological control group is often deemed not feasible. This collaborative effort will moreover fuel further initiatives to centralize natural history data on patients with MCT8 deficiency and other rare thyroid hormone signaling disorders. Therefore, our study improves understanding on the clinical sequalae and long-term outcomes of MCT8 deficiency and will help to improve the diagnostics and clinical care for patients with MCT8 deficiency.

Contributors

SG, WEV, IFMC, and MD designed the study, acquired and analyzed the results and drafted and approved the manuscript. All other authors equally contributed to the acquisition, analysis, and interpretation of data; and drafted and approved the manuscript.

Declaration of Interest

The Erasmus Medical Centre (Rotterdam, Netherlands), which employs SG, RPP, IMvB, MMvdK, CAU, MCZ, MCYdW, YBdR, MMe, and WEV, might receive royalties from Rare Thyroid Therapeutics (the manufacturer of Triac) in the future, dependent on any future commercialisation. None of the authors will benefit personally from any royalties. Rare Thyroid Therapeutics had no influence on the conduct or analysis of this study. All other authors declare no competing interests.

Acknowledgements

We thank the parents and families of our patients and the clinicians looking after them. Our study was funded by the Netherlands Organisation for Health Research and Development (project number 113303005; to WEV), and the Sherman Foundation (to WEV). The centres in Rotterdam, Berlin, Paris, and Toulouse are part of the European Reference Network on rare endocrine conditions (Endo-ERN).

SUPPLEMENTARY MATERIALS

Supplementary results

Histopathological evaluation of brain tissue

Post-mortem examination of the brain of a deceased 8-year old patient showed a reduction of global brain volume and a diffuse reduction in myelin, which was most pronounced in the cortico-spinal tract, transverse tracts in the pons and subcortical white matter in the cerebellum, with positive staining for myelin basic protein. The micro-architecture of the cortex was normal without loss of neurons. Minimal subpial gliosis was present. The basal ganglia and hippocampus had a normal microscopic appearance. The substantia nigra had a normal cell count, but showed hypopigmentation without signs of pigment-incontinence, neuronal inclusion or reactive gliosis. The cerebellar architecture was normal, with normal neuronal migration patterns. An apparent decrease in neuronal cells was observed in the dentate nucleus which moreover showed focal overexpression of p22 phosphorylated neurofilaments. Concomitantly, the number of neuronal cells in the inferior olivary nucleus was reduced. Together, these neuro-anatomical findings support the involvement of brain areas responsible for motor function control in MCT8 deficiency.

Neuropsychological evaluation

29 subjects had been evaluated with the Bayley Scales of Infant Development (BSID) III at a median biological age of 5.0 years (range 1.0-66.0) which revealed a median developmental ages well-below 12 months on all tested sub-domains (**table s3**). Fine and gross motor skills equaled a median developmental age of 3.0 (IQR 1.5-4.7) and 1.0 (0.5-3.0) months, respectively, and were limited by the severe hypotonia, dystonic posturing and poor coordination (**figure s4B** and **C**). Accordingly, median scores on the Gross Motor Function Measure 88 did not exceed 10% of the total score that should be

obtained by healthy 4-year old children (**figure 2B, table s3**). Importantly, 90% of patient did not receive any points on scale B (sitting and crawling), whereas 95% of the tested patients did not receive any points on scale C-E (standing, walking, jumping). Those individuals that were able to walk (with some assistence) had an atactic gait pattern. Motor function scores did not show statistically significant differences between different age-groups, indicating that major developmental progression is not to be expected in the majority of cases (**table s3**). Expressive language was restricted to some phonation without production of any meaningful words (developmental age: 4.6 (IQR 3.1-6.0) (**figure 2C**). Individuals who acquired some speech (N=5, 7.8%) were clearly dysarthric, but were able to express themselves in simple words, 2 to 3-word sentences, or computer-aided communication. Receptive language was slightly better with a median developmental age of 7.0 (3.3-11.5) (**figure 2D**). Cognitive abilities were limited with a median developmental age of 3.6 months (2.5-4.8) (**figure s4A**). The developmental age on the sub-domains cognition, expressive and receptive language and gross motor skills did not increase upon aging, whereas a significant inverse correlation was observed between fine motor skills and age on the fine motor skills sub-domain of the BSID III (**figure 2G**, **figure s4 D-G**).

Supplementary Figures

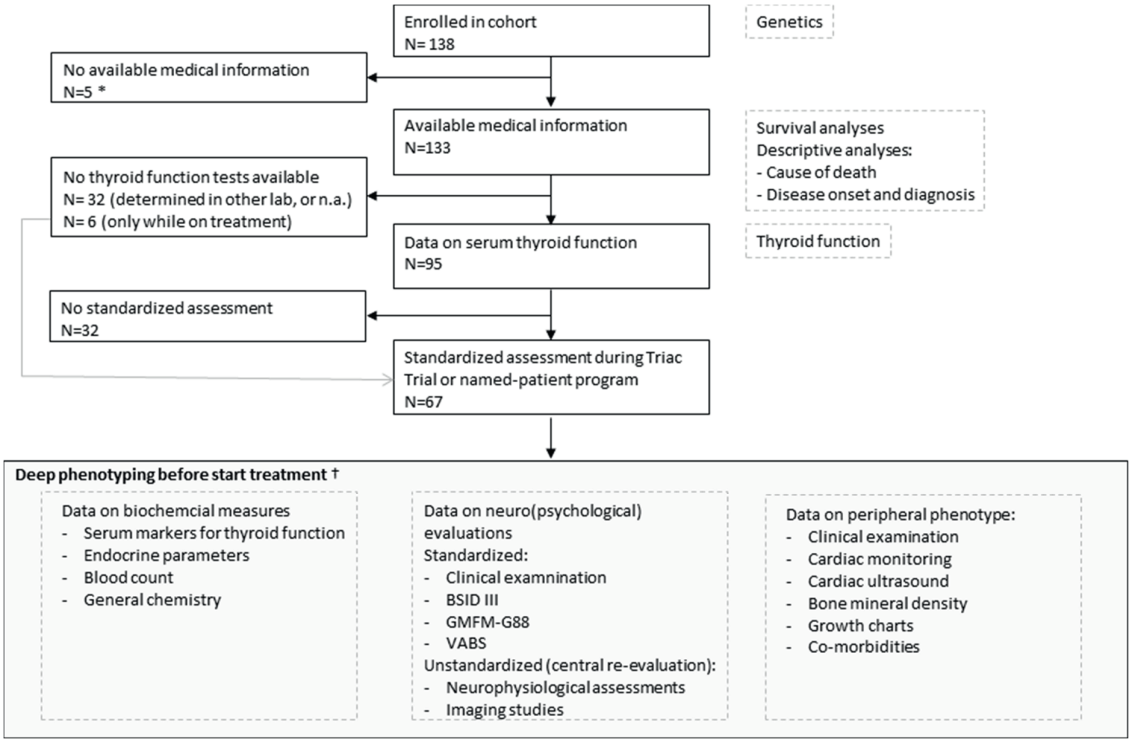

Figure s1 – Flow diagram of the study. Indicated is the number of eligible patients (N) for each of the parameter sets (boxed in grey dashed lines). * Subjects were deceased family members. † Most assessments could not be carried out in all eligible patients, resulting in missing data. Missing data can be attributed to the poor clinical condition of patients, their inability to follow instructions and common manifestations of MCT8 deficiency such as scoliosis and dystonic posturing that hamper investigations for which patients needed proper positioning. Neuropsychological evaluations were carried out according to local availability of the testing method and expertise.

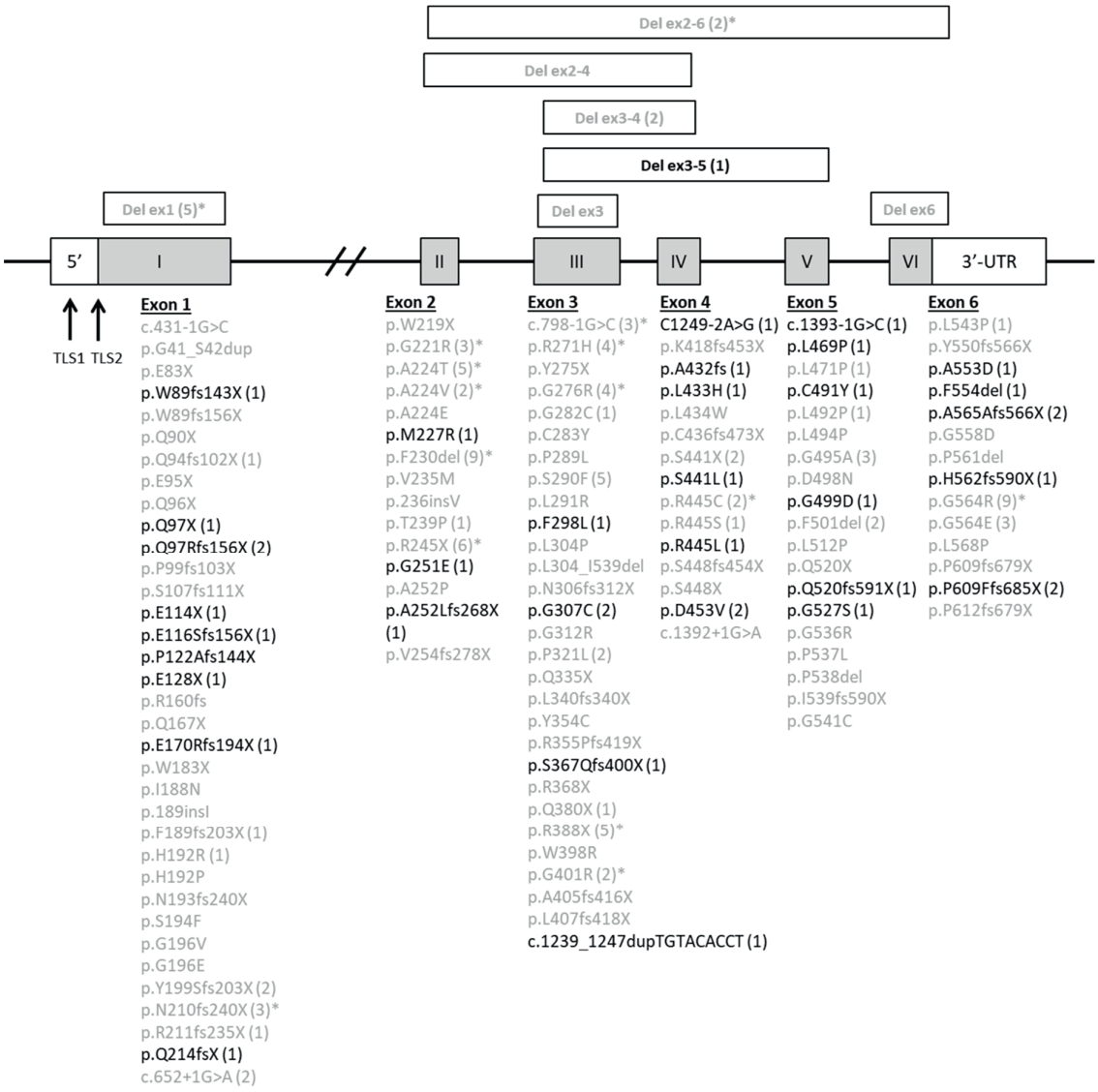

Figure s2 - Overview of all genetic mutations identified in the *SLC16A2* gene encoding MCT8 that have been reported in literature thus far (6). The mutations that were identified in patients in this study are indicated with a frequency indicated between brackets. Mutations that had not been reported before are indicated in light grey. * denotes mutations that occurred in more than 1 unrelated families.

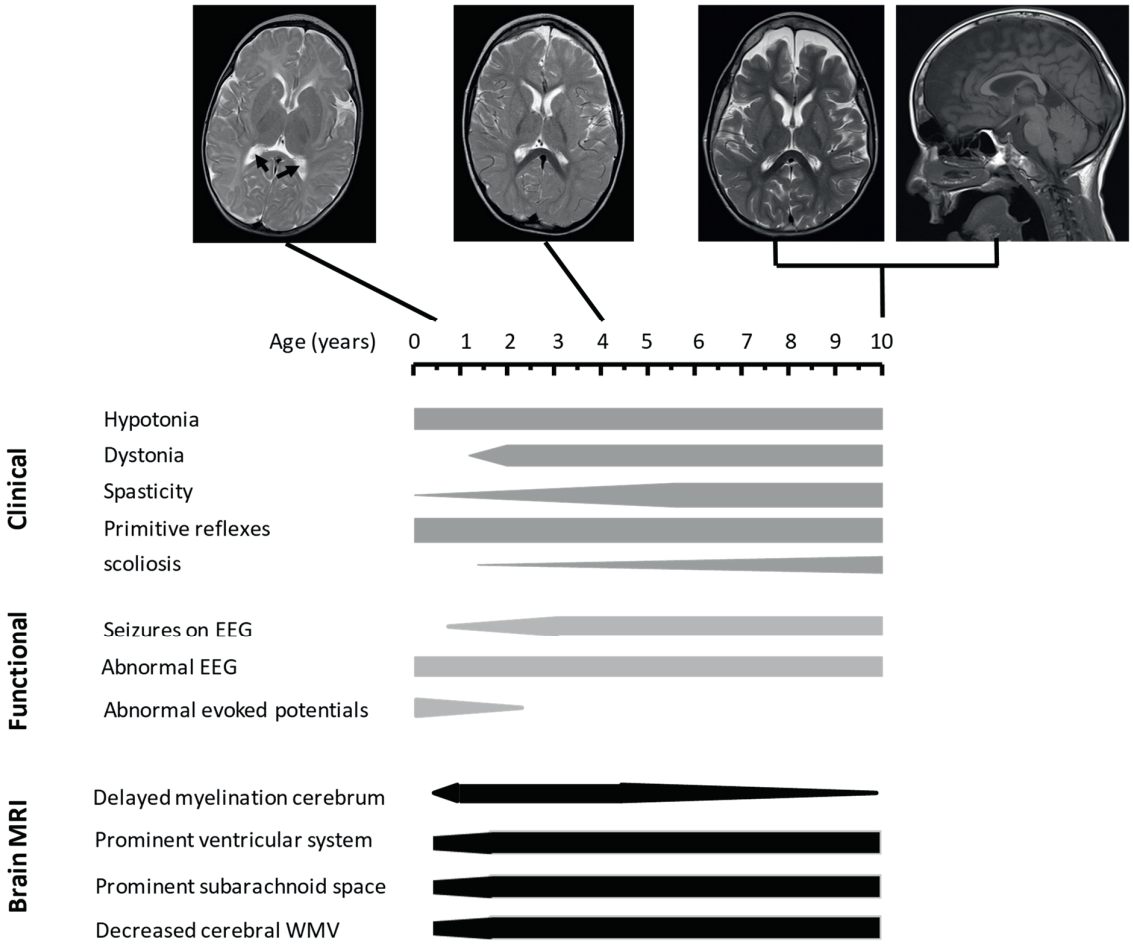

Figure s3 – Representative MRI scans at indicated ages and schematic representation of the neurological sequelae in patients with MCT8 deficiency, based on a cross-sectional analysis of the cohort eligible for deep phenotyping (N=66). Abbreviations: EEG, electroencephalography; WMV, white matter volume.

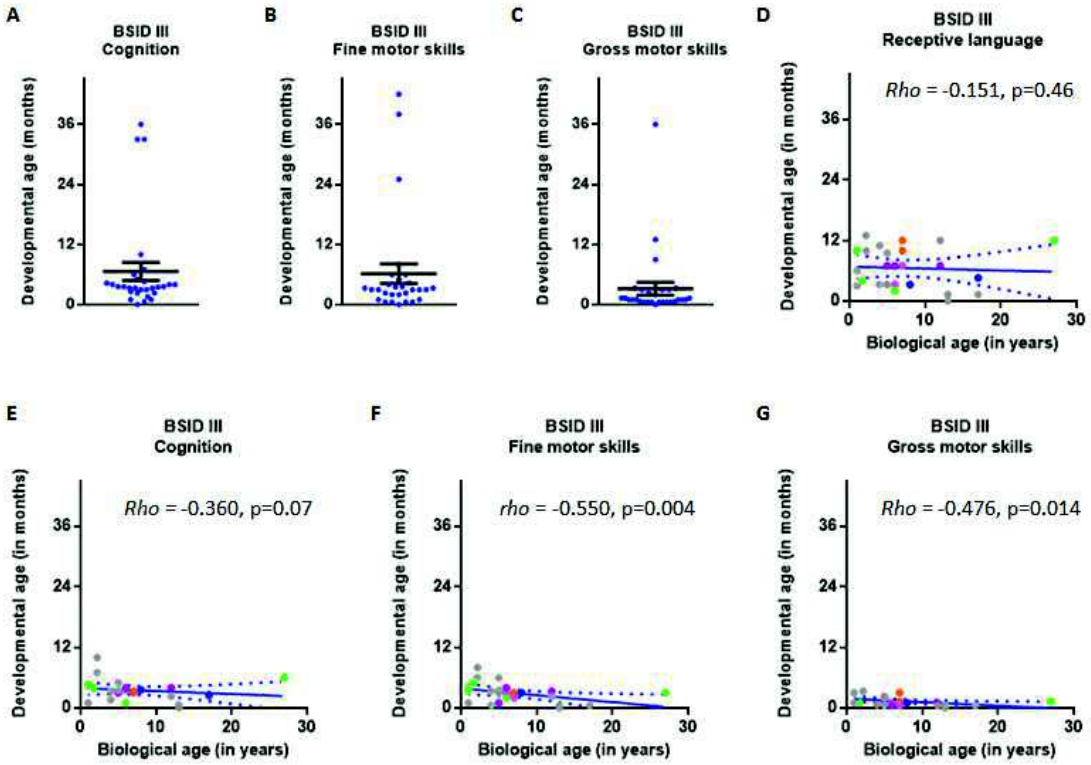

Figure s4 - Neuropsychological evaluations in patients with MCT8 deficiency using the cognition (**A**), fine (**B**) and gross (**C**) motor skills of the Bayley scales of Infant Development III (19). Blue dots represent measurements in individual patients, expressed as the developmental age in months. Black lines indicate the mean±SEM score. Developmental age in months on the sub-domains receptive language (**D**), cognition (**E**), fine motor (**F**), and gross motor (**G**) skills of the BSID III (y-axis) *versus* the biological age in years (x-axis) of patients with a severe neurocognitive phenotype. Dots represent measurements in individual patients. Patients harboring the same genetic mutation are displayed in the same color: p.F230del (green), c.651-652+20del (blue), G564R (purple), p.A565fs566X (pink), and R271H (orange). Unique mutations are colored in grey. Linear regression was used to plot the trend and the 95% confidence intervals (blue lines). Spearman rho values and corresponding p values are indicated in the graph.

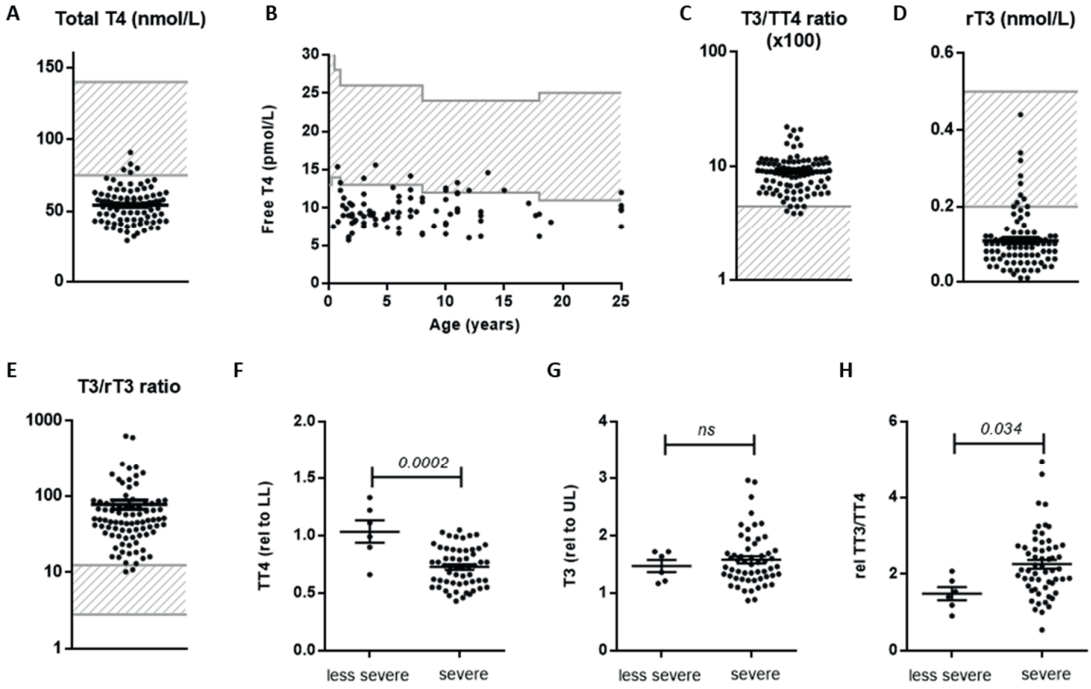

Figure s5 – (**A)** Mean ± SEM (black lines) serum concentrations of total T4. (**B**) Serum free T4 concentrations by age. Mean ± SEM (black lines) serum total T3/T4 ratio x 100 (**C**), reverse T3 (**D**) and T3/rT3 ratio (**E**). Black dots represent measurements in individual patients. Grey areas mark the normal ranges in adults (**A, C-E**), or the age-specific normal range (**B**). (**F**) Mean ± SEM (black lines) total T4 and **(G)** total T3 concentrations in patients with a less severe *versus* severe neurocognitive phenotype. Patients with a less severe phenotype were defined as those individuals that achieved at least 2 of the following abilities: talk in simple words, attain head control, independent sitting, and/or walking with assistance. T4 and T3 concentrations are expressed relative to the age-specific lower and upper limit of the normal range, respectively. (**H**) The ratio between total T3 and T4 concentrations (when expressed relative to the age-specific normal range). Dots represent measurements in individual patients. T-tests were deployed to assess for statistically significant differences between groups. Serum T4 concentrations were significantly more reduced in patients with a severe neurocognitive phenotype (0.73 (±0.24) times the lower limit of normal) than in those with more advanced neurocognitive abilities (1.04 (±0.17) times the age-specific lower limit of normal) (mean difference 0.31, 95% CI 0.16-0.46, P=0.0002) (**figure s5F**). T3 concentrations were slightly, but not significantly less increased in patients with a less severe neurocognitive phenotype than in those with a severe neurocognitive phenotype (mean difference -0.11, 95% CI -0.5-0.27, P=0.56) (**figure s5G**). The T3/T4 ratio was significantly lower in patients with a less severe phenotype *versus* those with a severe neurocognitive phenotype (mean difference -0.76, 95% CI -1.48- -0.06, P=0.034) (**figure s5H**).

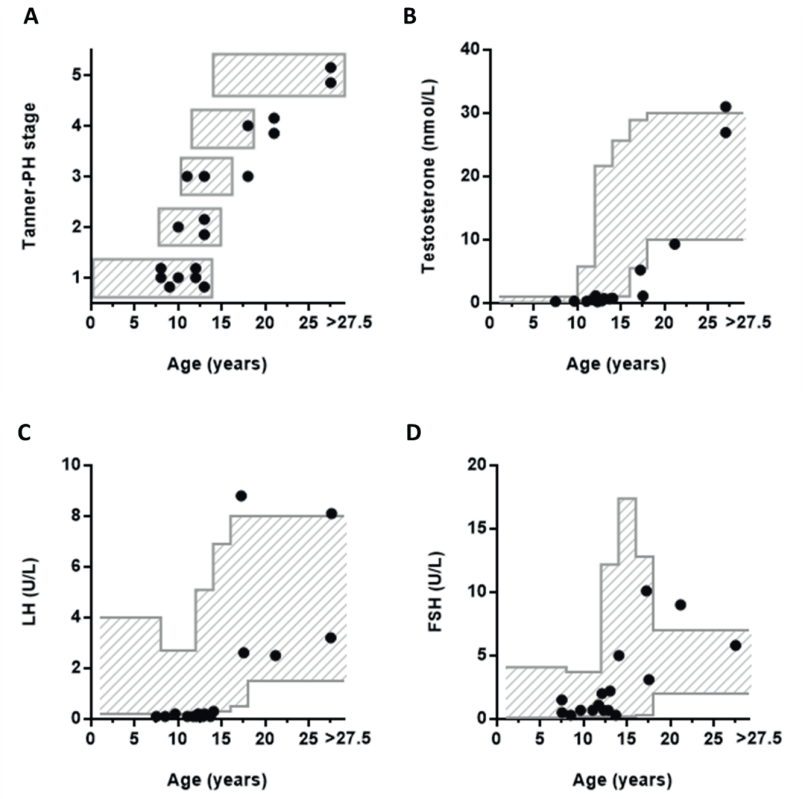

Figure s6 – **(A)** Tanner stage of the patients aged above 8 years. The grey boxes indicate normal development in boys (33). Black dots represent measurements in individual patients. Similarly, serum testosterone (**B**), luteinizing hormone (**C**), and follicle stimulating hormone (**D**) concentrations expressed against biological age. Abbreviations: PH, pubic hair; LH, luteinizing hormone; FSH, follicle stimulating hormone.

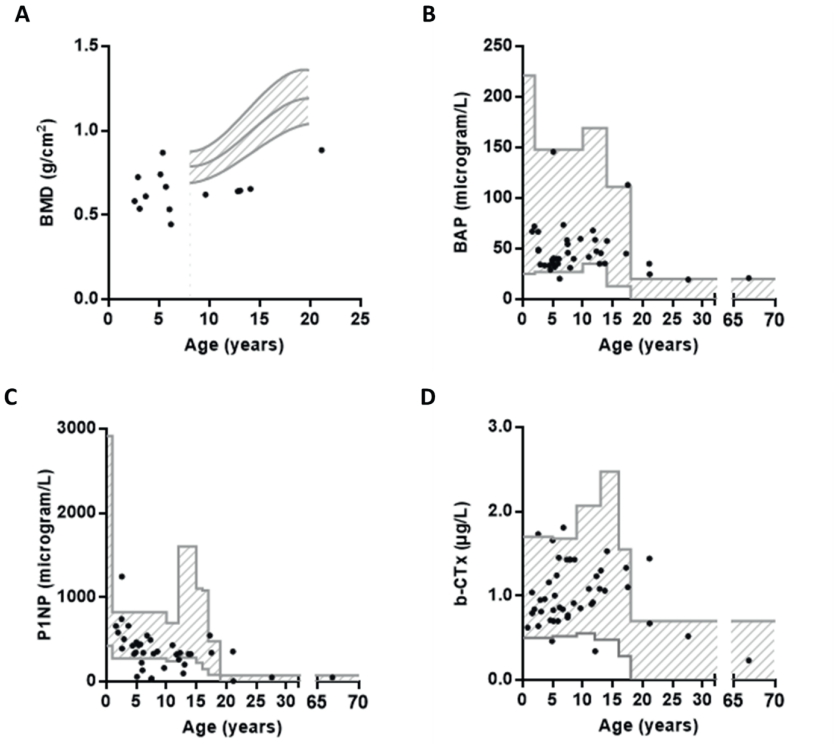

Figure s7 – (A) Cross-sectional evaluation of total body bone mineral density. Reference range is derived from (34). **(B)** Cross-sectional overview of serum bone alkaline phosphatase concentrations by age (normal ranges derived from (35)), (**C**) procollagen type I propeptides (PINP) concentrations by age (36), and (**D**) plasma C-terminal collagen crosslinks by age. Indicated are the measurements in individual patients (black dots) and the age-specific normal ranges (grey shaded areas).

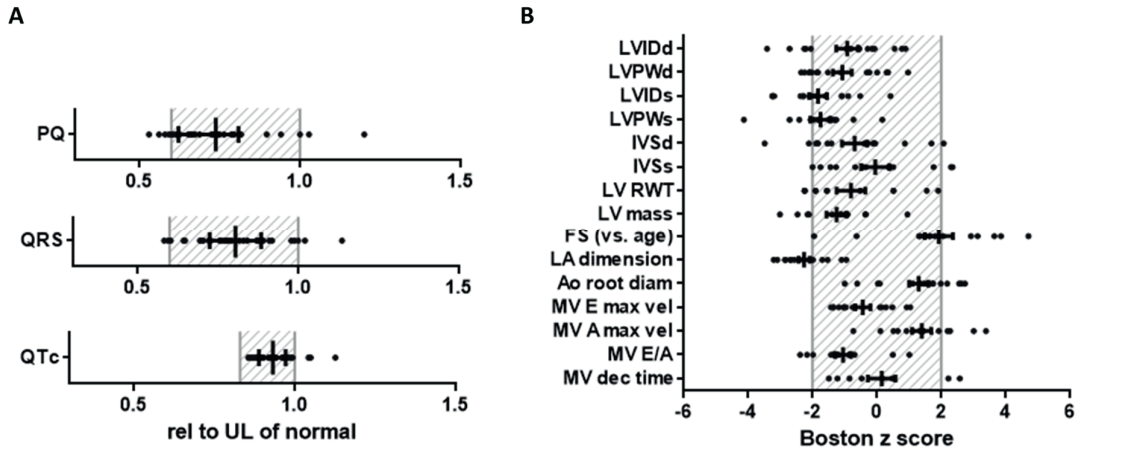

Figure s8 – (**A**) PQ interval, QRS interval, and QTc interval derived from resting electrocardiography. Data of individual patients are presented as black dots, and are expressed relative the age-specific 98th percentile (=1.0). Grey shaded areas indicated the normal range (2nd -98th percentile). (**B**) Detailed cardiac ultrasound evaluations in 16 patients. The means ± SEM of indicated parameters are displayed in black lines and individual measurements as black dots. Measurements are expressed as Boston z scores and are adjusted for age and body surface area. Abbreviations: LVIDd, diameter left ventricle in systole; LVPWd, diameter left ventricle posterior wall in diastole; LVIDs, diameter left ventricle in systole; LVPWs diameter left ventricle posterior wall in systole; IVSd, diameter interventricular septum in diastole; IVSs, diameter interventricular septum in systole; LV RWT, left ventricular relative wall thickness; LV mass, left ventricular mass; FS, fractional shortening; LA dimension, left atrium diameter; Ae root diam, aortic root diameter; MV E max vel, maximal early filling wave velocity (peak E-wave); MV A max vel, maximal late filling wave velocity (peak A-wave); MV E/A, ratio maximal early / late filling wave velocity; MV dec time, early filling wave deceleration time.

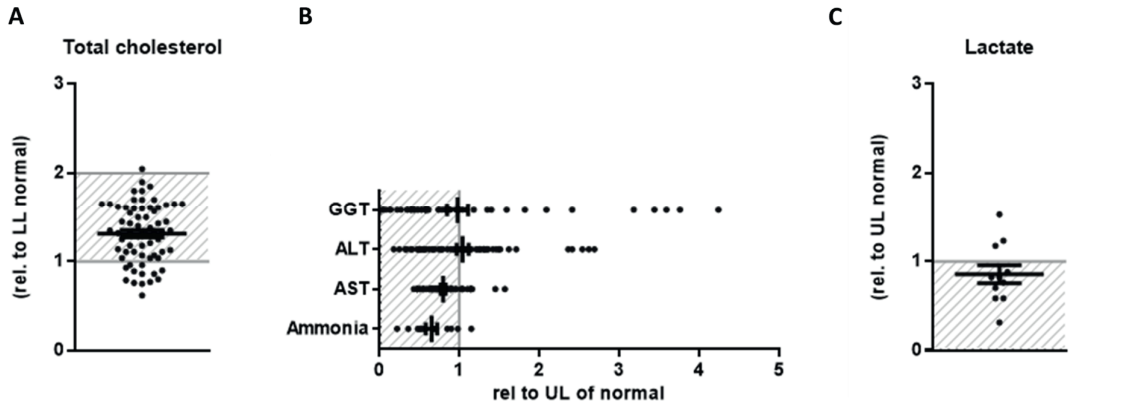

Figure s9 – (**A**) Serum total cholesterol concentrations, (**B**) liver parameters, and (**C**) lactate concentrations. Data of individual patients are presented as black dots, and are expressed relative the age-specific lower (**A**) or upper (**B** and **C**) limit of the normal range (=1.0). Black lines indicate the mean ± SEM. ALT concentrations were mildly elevated in 31 (47.0%) patients, whereas serum AST concentrations were mildly elevated in only 10 (17.5%) patients. In none of the cases, AST or ALT concentrations exceeded the upper limit more than 4 times. GGT was elevated in 16 (28.1%) patients, of whom 12 patients also had elevated aminotransferase concentrations. Abbreviations: GGT, gamma glutamyl transferase; ALT, alanine transaminase, AST, asparagine transaminase.

Supplementary tables

Table s1. Demographical and clinical characteristics

Characteristic	**N =138**
Age (years)	9.2 (0.7 to 66.8)
Age composition	
<4 years	25 (18.1%)
4-10 years	55 (39.9%)
11-18 years	35 (25.4%)
Adults (>18 years)	23 (16.7%)
Sex	
Female	0
Male	138 (100%)
Alive *	107 (80.5%)
Ethnic origin	
European	93 (67.4%)
Middle-Eastern	14 (10.1%)
North-Africa	7 (5.1%)
Latino	9 (6.5%)
Asian	7 (5.1%)
Other	8 (5.8%)
Patients per country	
Australia	3 (2.2%)
Belgium	3 (2.2%)
Brazil	6 (4.3%)
Canada	7 (5.1%)
Chile	2 (1.4%)
Czech Republic	1 (0.7%)
France	10 (7.2%)
Germany	7 (5.1%)
Hungary	3 (2.2%)
India	5 (3.6%)
Israel	4 (2.9%)
Italy	17 (12.3%)
Netherlands	22 (15.9%)
Poland	5 (3.6%)
Romania	5 (3.6%)
Russia	1 (0.7%)
South-Africa	1 (0.7%)
Spain	1 (0.7%)
Sweden	3 (2.2%)
Swiss	3 (2.2%)
Turkey	5 (3.6%)
UK	18 (13.0%)
USA	3 (2.2%)
Unknown	3 (2.2%)
Cases that have been previously reported	45 (32.6%)
Age onset of symptoms (months) *	4.0 (0.0-13.0)
Age diagnosis (months) *	24.0 (0.0-744.0)

Data are median (range), or n (%). Demographic information and basic characteristics of patients at time they were enrolled in the cohort. * Data based on the 133 cases with available medical record information.

Table s2. MRI characteristics

Characteristic	**N =14**
No of scans	2 (1-4)
Age at latest MRI scan (months)	23.5 (8.8-74.3)
Abnormal global anatomy	
Hemispheres	0 (0.0%)
Corpus callosum	0 (0.0%)
Vermis, pons, brainstem	0 (0.0%)
Other midline structures	0 (0.0%)
Abnormal volume	
Cerebral white matter	13 (92.9%)
Cerebellar white matter	2 (14.3%)
Corpus callosum	9 (64.3%)
Abnormal migration features	
Gyration pattern	0 (0.0%)
Cortical disposition	0 (0.0%)
Myelination	
Delayed myelination	14 (100%)
Myelination stage (months) – median (range)	6.0 (1-42)
Δ with biological age (months) – median (range)	13.0 (4.0-145.0)
Periventricular WML	11 (78.6%)
Progression of myelination on succeeding MRI scans	8 (88.9%)
CSF	
Prominent supratentorial ventricular system	13 (92.9%)
Prominent peripheral liquor spaces	13 (92.9%)
Abnormal vasculature	
Large cranial vessels	0 (0.0%)
MRS	
Low NAA peak	7 (87.5%)
High choline peak	7 (87.5%)

Data are median (range) or n (%). Characteristics of brain MRI scans derived from 14 patients. Data of the last available MRI scan are summarized in this table.

Table s3. Neuropsychological evaluations

Characteristic	<4 yr	4-10 yr	>10 yr	Overall
GMFM-G88* - percentage of total score				
N	15	12	12	39
Total score (%) – Median (IQR)	7.0 (4.0-9.4)	7.0 (5.0-9.8)	5.0 (1.3-14.5)	7.0 (4.0-10.0)
BSID III† - developmental age in months				
N	6	14	9	29
Cognition	4.4 (3.3-7.8)	3.4 (3.0-3.7)	2.6 (1.5-19.5)	3.6 (2.5-4.8)
Receptive language	8.0 (3.8-10.8)	7.0 (3.3-10.3)	7.0 (1.3-20.5)	7.0 (3.3-11.5)
Expressive language	5.5 (3.7-6.0)	4.6 (3.4-6.0)	4.6 (2.1-16.5)	4.6 (3.1-6.0)
Fine motor function	4.7 (3.0-6.5)	3.0 (2.0-3.6)	2.3 (0.5-14.2)	3.0 (1.5-4.7)
Gross motor function	3.0 (1.0-3.3)	1.0 (0.5-2.1)	0.6 (0.5-5.2)	1.0 (0.5-3.0)
VABS II ‡ - raw scores				
N	8	13	13	34
Communication				
Receptive	10.0 (6.5-12.0)	12.0 (9.0-12.5)	11.0 (9.0-13.0)	11.0 (8.8-12.3)
Expressive	11.5 (8.8-13.0)	12.0 (11.5-13.5)	10.0 (8.0-18.0)	12 (8.8-13.3)
Written	0.0 (0.0-0.0)	0.0 (0.0-0.0)	0.0 (0.0-0.0)	0.0 (0.0-0.0)
Daily living skills				
Personal	5.5 (2.0-6.0)	6.0 (4.5-9.5)	7.0 (5.0-9.0)	6.0 (4.0-8.0)
Domestic	0.0 (0.0-0.0)	0.0 (0.0-0.0)	0.0 (0.0-0.0)	0.0 (0.0-0.0)
Community	0.0 (0.0-0.0)	0.0 (0.0-0.0)	0.0 (0.0-0.0)	0.0 (0.0-0.0)
Socialization				
Interpersonal relationships	18.0 (17.0-19.8)	18.0 (16.0-22.5)	17.0 (13.0-22.5)	18.0 (15.0-20.25)
Play and leisure time	4.5 (3.3-6.0)	8.0 (6.0-11.5)	4.0 (2.5-5.5)	5.5 (3.8-9.3)
Coping skills	0.0 (0.0-0.0)	0.0 (0.0-3.0)	0.0 (0.0-3.5)	0.0 (0.0-2.3)
Motor skills				
Gross motor skills	4.0 (2.0-4.8)	2.0 (0.0-4.0)	1.0 (0.0-5.0)	2.5 (0.0-4.0)
Fine motor skills	4.0 (1.5-5.5)	1.0 (0.0-2.0)	1.0 (0.0-4.5)	1.0 (0.0-4.0)

Neuropsychological evaluations stratified by age.

* The GMFM-G88 **(17)** assesses the gross motor function in which scores range from 0 to 100%, with higher scores indicating better motor function and where a 100% score is achieved by a normal developing child of 4 years of age.

† The BSID III **(19)** is a multi-scale battery that assesses different aspects of child development. In the study the subscales cognition, expressive language, receptive language, fine motor skills and gross motor skills have been conducted. The BSID III measures the developmental age ranging from 16 days to 42 months and 15 days. Scores on the subscales are presented as age equivalent scores representing the developmental age in months.

‡ The VABs II **(37)** is a survey which assesses different aspects of development. In the study the subdomains receptive language, expressive language, writing, personal, domestic, community, interpersonal relationships, playing, coping, gross motor and fine motor skills have been assessed. The survey was completed by primary care-givers in presence of a trained neuropsychologist or physician. The VABs II measures the developmental age ranging from birth to 90 years of age. Scores on the VABS II are presented as raw scores.

Table s4. Deep phenotpying peripheral features

Characteristic	Absolute mean	Relative to	
		Lower limit	Upper limit
Thyroid function			
Age at measurement (yrs)	6.0 (2.2-10.4)		
TSH (mU/L, n=95)	3.16 (±2.19)		0.59 (0.51 to 0.67)
Free T4 (pmol/L, n=95)	9.5 (±2.2)	0.76 (0.72 to 0.79)	
Total T3(nmol/L, n=93)	4.7 (±1.4)		1.48 (1.39 to 1.57)
Total T4 (nmol/L, n=94)	54 (±12)	0.74 (0.70 to 0.78)	
rT3 (nmol/L, n=86)	0.11 (±0.07)	0.48 (0.41 to 0.55)	
Deep phenotyping			
Age at assessment (yrs)	5.0 (2.3 to 10.5)		
Biochemical features			
Sex hormone binding globulin (nmol/L, n=60)	229 (±95)		1.77 (1.59 to 1.95)
Total cholesterol (mmol/L, n=62)	3.2 (±0.7)	1.31 (1.23 to 1.40)	
HDL cholesterol (mmol/L, n=56)	1.22 (±0.29)	1.91 (1.69 to 2.13)	
LDL cholesterol (mmol/L, n=56)	1.80 (±0.51)	2.00 (1.71 to 2.30)	
Triglycerides (mmol/L, n=56)	0.77 (±0.41)	2.50 (2.14 to 2.87)	
Aspartate aminotransferase (U/L, n=53)	42 (±15)		0.78 (0.72 to 0.85)
Alanine aminotransferase (U/L, n=61)	39 (±21)		1.01 (0.86 to 1.15)
Gamma glutamyl transferase (U/L, n=53)	25 (±25)		1.00 (0.73 to 1.27)
Alkaline phosphatase (U/L, n=61)	189 (±57)		0.57 (0.46 to 0.67)
Albumin (g/L, n=55)	46.3 (±2.6)		0.93 (0.91 to 0.93)
Amonium (µmol/L, n=13)	27.4 (±9.5)		0.65 (0.49 to 0.81)
Lactate (mmol/L, n=11	1.47 (±0.56)		0.86 (0.63 to 1.09)
Glucose (mmol/L, n=33)	5.0 (±1.0)		0.78 (0.72 to 0.84)
Creatinine (µmol/L, n=62)	31.4 (±11.0)	1.22 (1.13 to 1.32)	
Urea (mmol/L, n=54)	4.44 (±1.63)	1.60 (1.40 to 1.79)	
Creatine kinase (U/L, n=62)	110 (±87)		0.48 (0.38 to 0.58)
Bone-specific alkaline phosphatase (µg/L, n=52) *	49 (±24)		0.42 (0.33 to 0.50)
Procollagen type I propeptides (µg/L, n=54) †	366 (±225)		0.55 (0.36 to 0.73)
C-terminal collagen crosslinks (µg/L, n=55)	0.96 (±0.35)		0.61 (0.20 to 0.69)
Testosterone (nmol/L, n=16)	0.69 (0.32 to 4.20)	3.92 (2.45 to 5.40)	
Luteinizing hormone (U/L, n=16)	0.20 (0.10 to 2.58)	0.67 (0.50 to 1.72)	
Follicle stimulating hormone (U/L, n=16)	1.75 (0.70 to 5.60)	4.75 (3.50 to 10.75)	
Ferritine (µg/L, n=60)	45 (±35)	1.50 (1.20 to 1.80)	
Hemoglobin (mmol/L, n=35) ‡	7.91 (±0.92)	1.16 (1.12 to 1.19)	
Clinical features			
Weight-for-age Z score (n=65)	-2.97 (±1.94)		
Height-for-age Z score (n=57)	-1.76 (±1.60)		
BMI-for-age Z score (n=57)	-2.36 (±2.37)		
Fat percentage-for-age Z score (n=9) §	-0.56 (±1.53)		
Lean body mass-for age Z score (n=7) §	-1.37 (-2.91to -0.20)		
Resting heart rate (bpm, n=51) ¶	110 (±20)		
Mean heart rate 24 h (bpm, n=46)	103 (±13)		
Premature atrial complexes (n=45) **	32 (1-554)		
Premature ventricular complexes (n=44) **	0 (0 to 4)		
Blood pressure (n=39) ††			
Systolic (mm Hg)	106 (±10)		
Systolic (percentile)	89 (56 to 96)		
Diastolic (mm Hg)	63 (±10)		
Diastolic (percentile)	74 (49 to 93)		
Tachycardia episodes (n=39) **	0 (0 to 36)		
Aortic root diameter (Z score, n=15) ‡‡	1.30 (±1.17)		

Systematic deep phenotyping of the peripheral phenotype. Please note that not most parameters have been captured in all patients. Reported are the means±SD or median (IQR) values as well as the mean (95% CI) values relative to the age-specific lower or upper limit normal range.

* normal ranges for serum bone-specific alkaline phosphatase are derived from **(35).** † normal ranges for serum Procollagen type I propeptides are derived from **(36).** ‡ Hemoglobin values were measured in local hospitals using routine diagnostic procedures. § normal values were derived from Kelly and colleagues (34). ¶ Percentile scores were derived from Fleming and colleagues (20). ** Provided are the number of episodes per 24 hours. **††** Percentile scores were based on guidelines from the American Academy of Pediatrics (21) and the American College of Cardiology and American Heart Association (22). ‡‡ Z scores were calculated using the Boston Z-score calculator and were corrected for body surface area and age.

REFERENCES

1. Mullur R, Liu YY, Brent GA. Thyroid hormone regulation of metabolism. Physiol Rev. 2014;94(2):355-82.
2. Yen PM. Physiological and molecular basis of thyroid hormone action. Physiol Rev. 2001;81(3):1097-142.
3. Hennemann G, Docter R, Friesema EC, de Jong M, Krenning EP, Visser TJ. Plasma membrane transport of thyroid hormones and its role in thyroid hormone metabolism and bioavailability. Endocr Rev. 2001;22(4):451-76.
4. Friesema EC, Grueters A, Biebermann H, Krude H, von Moers A, Reeser M, et al. Association between mutations in a thyroid hormone transporter and severe X-linked psychomotor retardation. Lancet. 2004;364(9443):1435-7.
5. Dumitrescu AM, Liao XH, Best TB, Brockmann K, Refetoff S. A novel syndrome combining thyroid and neurological abnormalities is associated with mutations in a monocarboxylate transporter gene. Am J Hum Genet. 2004;74(1):168-75.
6. Groeneweg S, Visser WE, Visser TJ. Disorder of thyroid hormone transport into the tissues. Best Pract Res Clin Endocrinol Metab. 2017;31(2):241-53.
7. Visser WE, Vrijmoeth P, Visser FE, Arts WF, van Toor H, Visser TJ. Identification, functional analysis, prevalence and treatment of monocarboxylate transporter 8 (MCT8) mutations in a cohort of adult patients with mental retardation. Clin Endocrinol (Oxf). 2013;78(2):310-5.
8. Friesema EC, Ganguly S, Abdalla A, Manning Fox JE, Halestrap AP, Visser TJ. Identification of monocarboxylate transporter 8 as a specific thyroid hormone transporter. J Biol Chem. 2003;278(41):40128-35.
9. Friesema EC, Kuiper GG, Jansen J, Visser TJ, Kester MH. Thyroid hormone transport by the human monocarboxylate transporter 8 and its rate-limiting role in intracellular metabolism. Mol Endocrinol. 2006;20(11):2761-72.
10. Heuer H, Maier MK, Iden S, Mittag J, Friesema EC, Visser TJ, et al. The monocarboxylate transporter 8 linked to human psychomotor retardation is highly expressed in thyroid hormone-sensitive neuron populations. Endocrinology. 2005;146(4):1701-6.
11. Ceballos A, Belinchon MM, Sanchez-Mendoza E, Grijota-Martinez C, Dumitrescu AM, Refetoff S, et al. Importance of monocarboxylate transporter 8 for the blood-brain barrier-dependent availability of 3,5,3'-triiodo-L-thyronine. Endocrinology. 2009;150(5):2491-6.
12. Vatine GD, Al-Ahmad A, Barriga BK, Svendsen S, Salim A, Garcia L, et al. Modeling Psychomotor Retardation using iPSCs from MCT8-Deficient Patients Indicates a Prominent Role for the Blood-Brain Barrier. Cell Stem Cell. 2017;20(6):831-43 e5.
13. Groeneweg S, Peeters RP, Moran C, Stoupa A, Auriol F, Tonduti D, et al. Effectiveness and safety of the tri-iodothyronine analogue Triac in children and adults with MCT8 deficiency: an international, single-arm, open-label, phase 2 trial. Lancet Diabetes Endocrinol. 2019;7(9):695-706.
14. Schwartz CE, May MM, Carpenter NJ, Rogers RC, Martin J, Bialer MG, et al. Allan-Herndon-Dudley syndrome and the monocarboxylate transporter 8 (MCT8) gene. Am J Hum Genet. 2005;77(1):41-53.
15. Remerand G, Boespflug-Tanguy O, Tonduti D, Touraine R, Rodriguez D, Curie A, et al. Expanding the phenotypic spectrum of Allan-Herndon-Dudley syndrome in patients with SLC16A2 mutations. Dev Med Child Neurol. 2019.
16. Groeneweg SvG, F.S.; Peeters, R.P.; Heuer, H.; Visser, W.E. Thyroid hormone transporters. Endocr Rev. 2019.
17. Russell DJ, Rosenbaum PL, Cadman DT, Gowland C, Hardy S, Jarvis S. The gross motor function measure: a means to evaluate the effects of physical therapy. Dev Med Child Neurol. 1989;31(3):341-52.
18. Sparrow SC, D.; Balla, D.A. Vineland-II Adaptive Behavior Scales: Survey Forms Manual. Circle Pines, MN, US: AGS Publishing; 2005.
19. Bayley N. Bayley scales of infant and toddler development–Third edition. San Antonio, TX: Pearson Education, Inc.; 2006.
20. Fleming S, Thompson M, Stevens R, Heneghan C, Pluddemann A, Maconochie I, et al. Normal ranges of heart rate and respiratory rate in children from birth to 18 years of age: a systematic review of observational studies. Lancet. 2011;377(9770):1011-8.
21. Flynn JT, Kaelber DC, Baker-Smith CM, Blowey D, Carroll AE, Daniels SR, et al. Clinical Practice Guideline for Screening and Management of High Blood Pressure in Children and Adolescents. Pediatrics. 2017;140(3):pii: e20171904.
22. Whelton PK, Carey RM, Aronow WS, Casey DE, Jr., Collins KJ, Dennison Himmelfarb C, et al. 2017 ACC/AHA/AAPA/ABC/ACPM/AGS/APhA/ASH/ASPC/NMA/PCNA Guideline for the Prevention, Detection, Evaluation, and Management of High Blood Pressure in Adults: A Report of the American College of

Cardiology/American Heart Association Task Force on Clinical Practice Guidelines. Hypertension. 2018;71(6):e13-e115.
23. Falagas ME, Athanasoulia AP, Peppas G, Karageorgopoulos DE. Effect of body mass index on the outcome of infections: a systematic review. Obes Rev. 2009;10(3):280-9.
24. von Olshausen K, Bischoff S, Kahaly G, Mohr-Kahaly S, Erbel R, Beyer J, et al. Cardiac arrhythmias and heart rate in hyperthyroidism. Am J Cardiol. 1989;63(13):930-3.
25. Scott O, Williams GJ, Fiddler GI. Results of 24 hour ambulatory monitoring of electrocardiogram in 131 healthy boys aged 10 to 13 years. Br Heart J. 1980;44(3):304-8.
26. Binici Z, Intzilakis T, Nielsen OW, Kober L, Sajadieh A. Excessive supraventricular ectopic activity and increased risk of atrial fibrillation and stroke. Circulation. 2010;121(17):1904-11.
27. Healey JS, Connolly SJ, Gold MR, Israel CW, Van Gelder IC, Capucci A, et al. Subclinical atrial fibrillation and the risk of stroke. N Engl J Med. 2012;366(2):120-9.
28. Perez MV, Dewey FE, Marcus R, Ashley EA, Al-Ahmad AA, Wang PJ, et al. Electrocardiographic predictors of atrial fibrillation. Am Heart J. 2009;158(4):622-8.
29. Matheus MG, Lehman RK, Bonilha L, Holden KR. Redefining the Pediatric Phenotype of X-Linked Monocarboxylate Transporter 8 (MCT8) Deficiency: Implications for Diagnosis and Therapies. J Child Neurol. 2015.
30. Sijens PE, Rodiger LA, Meiners LC, Lunsing RJ. 1H magnetic resonance spectroscopy in monocarboxylate transporter 8 gene deficiency. J Clin Endocrinol Metab. 2008;93(5):1854-9.
31. Kersseboom S, Horn S, Visser WE, Chen J, Friesema EC, Vaurs-Barriere C, et al. In vitro and mouse studies supporting therapeutic utility of triiodothyroacetic acid in MCT8 deficiency. Mol Endocrinol. 2014;28(12):1961-70.
32. Groeneweg S, Lima de Souza EC, Meima ME, Peeters RP, Visser WE, Visser TJ. Outward-Open Model of Thyroid Hormone Transporter Monocarboxylate Transporter 8 Provides Novel Structural and Functional Insights. Endocrinology. 2017;158(10):3292-306.
33. Herman-Giddens ME, Steffes J, Harris D, Slora E, Hussey M, Dowshen SA, et al. Secondary sexual characteristics in boys: data from the Pediatric Research in Office Settings Network. Pediatrics. 2012;130(5):e1058-68.
34. Kelly TL, Wilson KE, Heymsfield SB. Dual energy X-Ray absorptiometry body composition reference values from NHANES. PLoS One. 2009;4(9):e7038.
35. Bone Alkaline Phosphatase, serum. Mayo Clinic Laboratories, https://www.mayomedicallaboratories.com/test-catalog/Clinical+and+Interpretive/82985.
36. Crofton PM, Evans N, Taylor MR, Holland CV. Procollagen type I amino-terminal propeptide: pediatric reference data and relationship with procollagen type I carboxyl-terminal propeptide. Clin Chem. 2004;50(11):2173-6.
37. Sparrow SC, D.; Balla, D.A. Vineland-II Adaptive Behavior Scales: Survey Forms Manual. Circle Pines, MN, US: AGS Publishing; 2005.

Chapter 5

Therapies in MCT8 deficiency

Chapter

Effects of Chemical Chaperones on Thyroid Hormone Transport by MCT8 Mutants in Patient-Derived Fibroblasts.

5.1

Stefan Groeneweg, Amanda van den Berge, Marcel E. Meima, Robin P. Peeters, Theo J. Visser, W. Edward Visser

Endocrinology. 2018 May;159(3):1290-1302.

ABSTRACT

Mutations in the thyroid hormone (TH) transporter monocarboxylate transporter 8 (MCT8) result in severe intellectual and motor disability. At present, no effective therapy is available to restore TH signaling in MCT8-dependent tissues. Recent in vitro studies in stable overexpression cell models suggested that the function of certain mutant MCT8 proteins, specifically those that affect protein stability and intracellular trafficking (e.g., p.F501del), could be partially recovered by chemical chaperones. However, the effects of chaperones have not been demonstrated in other commonly used models for MCT8 deficiency, including transient overexpression models and patient-derived fibroblasts. Here, we demonstrate that the chemical chaperone 4-phenylbutyric acid (PBA) similarly potentiates the T3 transport function of wild-type and p.F501del mutant MCT8 in transiently transfected COS-1 cells by increasing MCT8 messenger RNA, total protein, and cell surface expression levels. Although PBA also increased the cell surface expression levels of the p.R445L mutant, no functional improvement was observed, which is in line with the proposed important role of Arg445 in substrate translocation. In contrast, PBA showed only minimal effects in ex vivo studies using control or p.F501del patient-derived fibroblasts. Moreover, the MCT8-specific inhibitor silychristin did not change these minimal effects, suggesting that the underlying mechanism is unrelated to the rescue of functional MCT8. Together, these findings indicate that the potency of chaperones to rescue mutant MCT8 function strongly depends on the cellular model and stress the need for further preclinical studies before clinically available chaperones should be considered as a treatment option in patients with MCT8 deficiency.

INTRODUCTION

Monocarboxylate transporter 8 (MCT8; SLC16A2) facilitates the transport of thyroid hormone (TH) across the cell membrane and is crucial for TH transport across the blood-brain barrier (BBB) and into neuronal cells (1, 2). Given the important role of TH during brain development, functional MCT8 is vital for normal neurocognitive development. Mutations in MCT8 result in the Allan-Herndon-Dudley syndrome (or MCT8 deficiency), characterized by severe intellectual and motor disability and abnormal serum thyroid function tests comprising a high T3, low T4 and rT3, and high-normal to high thyroid-stimulating hormone (3, 4).

Many different mutations in MCT8 have been identified (reviewed in (5)). Different pathogenic mechanisms may underlie MCT8 inactivation, *e.g.*, deletions or nonsense mutations that prevent the production of full-length MCT8 protein or missense mutations that specifically interfere with substrate translocation (*e.g.*, p.R445C or p.D498N) or with protein expression and subcellular localization (*e.g.*, p.G564R and p.G282C) (6-8). Although most mutations result in (near-) complete inactivation of MCT8 transport function, some mutant proteins retain considerable residual transport function. Different *in vitro* models are used to determine the impact of mutations on MCT8 function, including transient and stable overexpression systems and patient-derived fibroblasts. Patient-derived fibroblasts especially allow the study of mutations in MCT8 under endogenous conditions and generally show a good correlation with the severity of clinical disease (9, 10). Recently, induced pluripotent stem cells derived from MCT8-deficient patients have been successfully differentiated toward different cell lineages, providing unique opportunities for *ex vivo* analyses of MCT8 deficiency (11).

Currently, there is no established therapy for MCT8 deficiency, although preclinical studies on TH analog therapy have shown promising results (12). Another therapeutic approach that has been recently explored *in vitro* is the use of chemical and pharmacological chaperones (13, 14). Being key players in the protein quality control system, endogenous chaperones govern the correct folding of proteins and their assembly in complexes, thereby preventing their degradation and aggregation. This ensures proper subcellular trafficking and protein function (reviewed in (15, 16)). Exogenous administration of chaperones has been explored as therapeutic approach in neurodegenerative disorders that involve protein folding defects, such as Alzheimer's disease, Parkinson disease, and Huntington disease (reviewed in (15, 16)). In addition, chaperones have been shown to rescue misfolded mutant transporter proteins, including different members of the ABC transporter family such as cystic fibrosis transmembrane conductance regulator (reviewed in (17)). In the latter, different chemical chaperones were found to enhance the translocation of the most commonly encountered p.F508del mutant to the cell membrane and potentiate its function (17). Likewise, the chemical chaperones 4-phenylbutyric acid (PBA), its salt sodium phenylbutyrate (NaPB), and dimethyl sulfoxide (DMSO) were recently shown to stabilize and potentiate the cell membrane expression of the p.F501del mutant MCT8 protein in stably transfected Madin-Darby canine kidney cells, thereby increasing its TH transport capacity (13). Several other MCT8 mutants were recently reported that could also be potentially rescued upon chaperone treatment (14). Interestingly, these mutations have all been associated with milder forms in the clinical spectrum of MCT8 deficiency and retain at least some residual transporter activity in experimental studies (9, 18-20). Importantly, previous studies in transiently transfected cells could not demonstrate such beneficial effects (21). The therapeutic potency of chaperones has not been evaluated in patient-derived fibroblasts so far.

For these reasons, we here explored the therapeutic potential of chaperones in transiently transfected COS-1 cells and patient-derived fibroblasts, which are established and frequently used cellular models for MCT8 deficiency. Chaperone treatment modestly potentiated p.F501del mutant MCT8 function in transiently transfected COS-1 cells. However, chaperones showed minimal effects in patient-derived fibroblasts, unrelated to the rescue of MCT8 function. These findings indicate that the potency of chaperones to rescue mutant MCT8 function strongly depends on the cellular model. Further preclinical studies are warranted before clinically available chaperones should be considered as a treatment option in patients with MCT8 deficiency.

MATERIALS AND METHODS

Materials

X-tremeGENE9 transfection reagent was obtained from Roche Diagnostics (Woerden, Netherlands). DMSO, PBA, NaPB, and 3-(4,5-dimethylthiazol-2-yl)-2,5-diphenyltetrazolium bromide (MTT) were purchased from Sigma-Aldrich (Zwijndrecht, Netherlands). Nonradioactive iodothyronines were obtained from Henning (Berlin, Germany). (3'-^{125}I)T_3 and (3',5'-^{125}I)T_4 were prepared as previously described (22). All cell culture flasks and plates were obtained from Corning (Schiphol, Netherlands).

Plasmids

Cloning of wild-type (WT) human MCT8 in pcDNA3 and of human μ-crystallin (CRYM) in pSG5 has been previously described (23, 24), as well as the generation of the p.F501del mutant MCT8 construct (9). CRYM is a cytosolic TH-binding protein, which greatly reduces TH efflux and thereby increases the net cellular TH accumulation. The p.R445L and p.Q97fsX mutations were introduced into the WT MCT8 complementary DNA (cDNA) construct as described previously (25), using primers listed in **Supplemental Table 1**. DNA sequencing was performed to confirm the presence of the introduced mutations. Positions of the mutations are determined using the NM_006517.3 reference sequence, which uses +1 as the A of the ATG translation initiation codon of the long MCT8 translational isoform, with the initiation codon as codon 1.

Cell culture, transfection, and chaperone treatment in transient expression models

COS-1 and JEG-3 cells were cultured in DMEM/F-12 medium (Life Technologies, Bleiswijk, Netherlands) supplemented with 9% heat-inactivated fetal calf serum (Invitrogen, Breda, Netherlands) and 2% penicillin/streptomycin (Roche Diagnostics). For T3 uptake assays, COS-1 or JEG-3 cells were cultured in 24-well plates (uptake assays), 6-well plates (immunoblotting), or 10-cm dishes (surface biotinylation assays) and transiently transfected at 70% confluence with the indicated concentrations of WT or mutant MCT8. Standard conversion factors were used to convert plasmid concentrations between different well formats and confirmed by analysis of plasmid dose-dependent T3 uptake in 24- and 6-well plates. For uptake assays, cells were cotransfected with 100 ng (24-well format) or 250 ng (6-well format) CRYM. We have previously demonstrated the absence of differences in transfection efficiency between WT and mutant MCT8 constructs (26). In case of chaperone treatment, incubation medium was substituted 1 day after transfection by incubation medium containing the indicated concentrations of DMSO, PBA, or NaPB. Next, cells were cultured for 48 hours in the presence or absence of chaperones with refreshment of medium after 24 hours, in line with previously reported studies (13, 14).

Cell culture and chaperone treatment of human fibroblasts

Human fibroblasts were derived from skin biopsies and were cultured in six-well plates (for uptake assays and RNA isolation) or 10-cm dishes (for immunoblotting) in DMEM/F-12 medium (Life Technologies) supplemented with 9% heat-inactivated fetal calf serum (Invitrogen) and 2% penicillin/streptomycin (Roche Diagnostics). Chaperone treatment was initiated at indicated concentrations of DMSO, PBA, or NaPB at 90% confluence for indicated time frames, and medium was refreshed daily.

Toxicity assays

Toxicity was assessed by determination of total protein levels using a Bradford assay according to manufacturer's protocol (Bio-Rad, Veenendaal, Netherlands) and cell viability using an MTT (Sigma-Aldrich) assay in cells exposed to indicated chaperone concentrations for 48 hours as described previously. Assays were performed in parallel to the T3 transport studies. Measurement of total protein levels was carried out in cells cultured in 24-well plates similarly transfected as for T3 uptake assays. MTT assays were carried out as previously described (25) using untransfected cells cultured on a 96-wells plate.

TH uptake studies

Cells were washed with incubation medium [Dulbecco's phosphate-buffered saline containing 0.1% bovine serum albumin (Sigma-Aldrich) and 0.1% glucose] and incubated for 30 minutes at 37°C in incubation medium containing 1 nM unlabeled T3 (Sigma-Aldrich) and 50,000 cpm (^{125}I)T3. After incubation, cells were briefly washed with incubation medium and lysed in 0.1 M NaOH. The amount of internalized radioactivity was measured with a *γ*-counter.

Surface biotinylation assays

Cell surface biotinylation assays were performed as previously described (25). Briefly, cell surface proteins were labeled with EZ-link Sulfo-NHS-biotin (Thermo Fisher Scientific, Bleiswijk, Netherlands), and cells were subsequently lysed with immunoprecipitation buffer [50 mM tris(hydroxymethyl)aminomethane-HCl, 150 mM NaCl, 10 mM EDTA, 1% Triton X-100], containing protease inhibitor cocktail (Roche Diagnostics). An aliquot (5% of the total volume) of the clarified lysate was saved as an input control. The biotinylated cell surface proteins were isolated using Neutravidin agarose beads (Thermo Fisher Scientific) and eluted by incubating the beads for 10 minutes at 70°C with NuPAGE 1× lithium dodecyl sulfate loading buffer (Thermo Fisher Scientific) prior to immunoblot analyses as described later.

Immunoblotting

Immunoblotting was performed as previously described (25). After incubation for 10 minutes at 70°C in presence of NuPAGE 1× lithium dodecyl sulfate loading buffer (Thermo Fisher Scientific), 15 μg of total lysate was separated on a 4% to 20% gradient Mini-PROTEAN TGX Precast Protein Gel (Bio-Rad), blotted to polyvinylidene difluoride membranes (Thermo Fisher Scientific), blocked with 5% milk, and probed overnight at 4°C with rabbit anti-MCT8 antibody. Glyceraldehyde-3-phosphate dehydrogenase (GAPDH) was used as loading control. MCT8 and GAPDH were visualized as previously described (25).

Quantitative polymerase chain reaction

Total RNA was extracted from fibroblasts and transfected COS-1 cells cultured in six-well plates using the High Pure RNA Isolation Kit (Roche Diagnostics), and cDNA was produced from 1 µg messenger RNA (mRNA) using the Transcriptor High Fidelity cDNA Synthesis Kit (Roche Diagnostics) according to the manufacturer`s protocol. Quantitative polymerase chain reaction was performed as previously described, using a probe-based assay for the detection of MCT8 and cyclophilin A (12) and the qPCR Core Kit for SYBR Green (Eurogentec, Maastricht, Netherlands) and primers listed in **Supplemental Table 2** for the detection of African green monkey–specific GAPDH. Expression levels are presented as fold difference compared with untreated cells.

Statistical analysis

All uptake results are expressed as means ± standard error of the mean (SEM) of at least three independent experiments in duplicate. Statistical significance was determined using indicated statistical tests carried out in GraphPad Prism version 6 (GraphPad, La Jolla, CA).

Ethical considerations

Skin fibroblasts were kindly provided by care-giving physicians and concerned stored samples that were previously collected for diagnostic purposes. Written informed consent was obtained from the parents or legal representatives of the involved patients and controls. This study was conducted in agreement with the Medical Research Involving Human Subjects Act and was evaluated and granted by the Medical Ethical Committee of the Erasmus Medical Center, Rotterdam, Netherlands (Medical Ethical Committee identifier: MEC-2015-362).

RESULTS

Because the proposed mechanism of chaperone action entails the stabilization and improvement of cell membrane expression of (mutant) MCT8 protein, we postulated that the effect size of chaperone therapy depends on the production rate of (mutant) MCT8 protein in untreated cells. For this reason, we first performed a plasmid dose titration curve by transiently cotransfecting COS-1 cells with increasing amounts of WT MCT8 plasmid and a fixed amount of CRYM plasmid (100 ng) using 24-well plates. Maximum T3 uptake was observed at 25 to 100 ng WT MCT8 (**Figure 1(a)**). To determine the optimal amount of CRYM plasmid, we also transiently cotransfected COS-1 cells with a fixed amount of WT MCT8 plasmid (50 ng) and increasing amounts of CRYM plasmid, yielding maximum T3 uptake at ≥50 ng CRYM plasmid (**Supplemental Figure 1A**). To verify the standard conversion factors between different well formats, a similar dose-response curve was analyzed in a six-well plate format showing maximum induction of T3 uptake at 100 ng MCT8 plasmid (**Supplemental Figure 1B**). Parallel immunoblot analyses of lysates of COS-1 cells cultured in six-well plates revealed that MCT8 protein expression was hardly detectable using up to 100 ng plasmid (**Figure 1(b)**). At plasmid amounts above 100 ng, a dose-dependent increase in MCT8 monomers and homodimers was observed (**Figure 1(b)**). Similar results were obtained in JEG-3 cells (data not shown). Together, these findings indicate plasmid dose-dependent increases in MCT8 protein expression and TH uptake, although the uptake plateaus at a relatively lower plasmid dose.

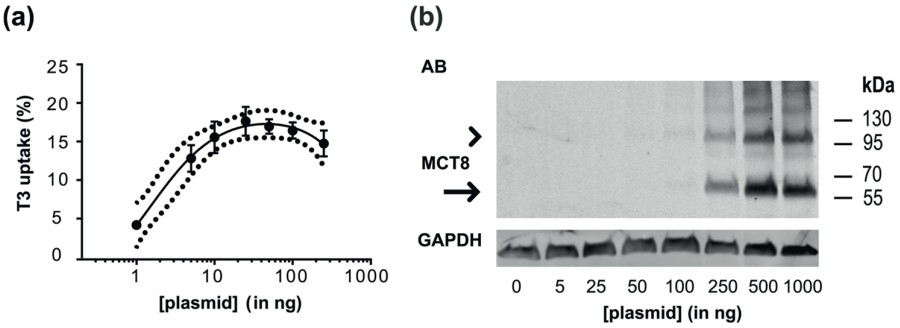

Figure 1 (**a**) Intracellular T3 accumulation in COS-1 cells transiently transfected with indicated concentration of WT MCT8 plasmid and 100 ng CRYM after 30 minutes incubation at 37°C. All uptake values are corrected for background TH uptake levels observed in COS-1 cells transfected with pcDNA3 empty vector. Experiments were carried out in a 24-well format. Data are presented as individual data points representing the mean of three separate experiments (± SEM) in duplicate, and standard nonlinear regression methods were used to plot a trend line with a 95% confidence interval. (**b**) Representative immunoblot on total lysates derived from COS-1 cells transiently transfected with indicated concentration of WT MCT8 expression construct. MCT8 detection was performed with the N-terminal MCT8 antibody (3353) and visualized with IRDye680 goat anti-rabbit secondary antibody. GAPDH was used as loading control. Bands of approximately 55 kDa, representing the MCT8 monomer (arrow), and a second band around 110 kDa, representing the MCT8 homodimer (arrowhead), were observed.

To evaluate the effect of chaperone treatment, we selected three different MCT8 mutations that have been identified in patients with MCT8 deficiency: (1) p.F501del, which has been previously reported to respond to chaperones (13), (2) p.R445L, a recently newly identified mutation that affects the presumed substrate-interacting residue Arg445 (6, 25, 27), and (3) p.Q97fsX, which results in a frameshift and premature truncation of the protein, precluding a response to chaperone treatment. Upon transient expression in COS-1 cells, the p.F501del mutant showed considerable residual T3 uptake capacity, whereas the p.R445L and p.Q97fsX mutants were functionally inactive (**Figure 2(a)**). Total expression levels of the p.R445L mutant were not significantly different from WT, whereas those of the p.F501del mutant were slightly reduced (**Figure 2(b)**). The cell surface expression levels of both mutants were significantly reduced (**Figure 5** (see below)). As expected, the p.Q97fsX mutant could not be detected at the protein level due to loss of the epitope for antibody recognition. Similar results were obtained in JEG-3 cells (**Supplemental Figure 2A–2C**).

Toxicology studies in transfected and untransfected COS-1 cells revealed that the chemical chaperones PBA and NaPB strongly affected cell viability and total protein content at concentrations above 1 mM, whereas a concentration of 1% DMSO was well tolerated (**Supplemental Figure 3A–3D**). Because JEG-3 cells already showed an increased cell death at the lowest chaperone concentrations (data not shown), COS-1 cells were selected for further experiments.

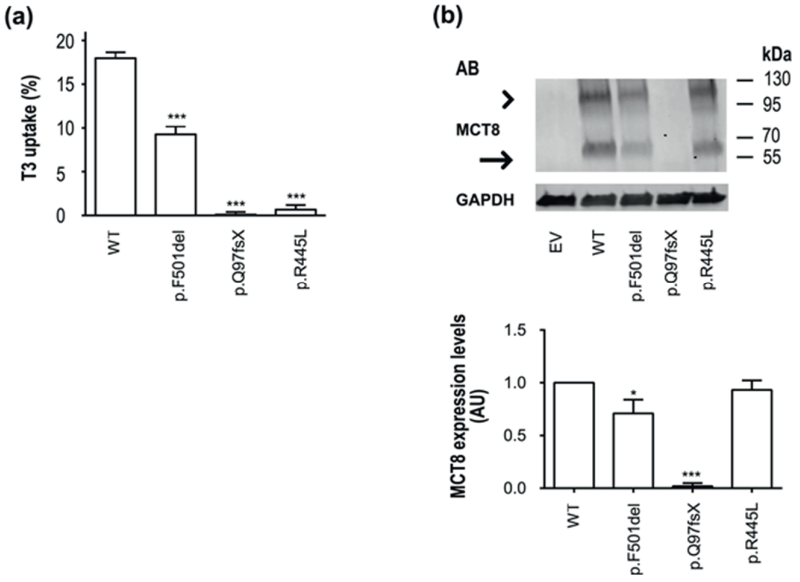

Figure 2 (**a**) T3 uptake by COS-1 cells transiently cotransfected with 50 ng WT or indicated mutant MCT8 and 100 ng CRYM in 30 minutes at 37°C (24-well format). All uptake values are corrected for background TH uptake levels observed in COS-1 cells transfected with pcDNA3 empty vector. Results are presented as means ± SEM (n = 4). (**b**) Immunoblot on total lysates derived from COS-1 cells transfected with 250 ng WT or indicated mutant MCT8 (six-well format). MCT8 protein was detected as described in the legend of Fig. 1. MCT8 and GADPH expression levels were quantified by densitometry using ImageJ. WT and mutant MCT8 expression levels are expressed as MCT8/GADPH ratio relative to WT MCT8 (100%) and presented as mean ± SEM of three independent experiments. Statistical significance was tested using one-way analysis of variance followed by Dunnett multiple-comparison test. Statistically significant differences are indicated as follows: **P* < 0.05; ****P* < 0.005. AB, antibody; AU, arbitrary unit; EV, empty vector.

We next evaluated the effects of the highest tolerable concentrations of different chaperones on WT or mutant MCT8-mediated T3 uptake in COS-1 cells. For this purpose, COS-1 cells were transiently cotransfected with nonsaturating (1 or 10 ng) or saturating (50 ng) amounts of WT or mutant MCT8 plasmid and CRYM. Preincubation for 48 hours with 1% DMSO did not potentiate T3 uptake by WT or mutant MCT8 at any plasmid dose (**Figure 3(a)–3(c)**, left panels). In contrast, preincubation for 48 hours with 1 mM PBA significantly increased T3 uptake by both WT MCT8 and the p.F501del mutant in COS-1 cells transfected with 1 or 10 ng plasmid. The fold increase was the same for WT MCT8 and the p.F501del mutant (**Figure 3(a)** and **3(b)**, left panels). No effects were observed for the p.R445L or p.Q97fsX mutant at any plasmid dose (**Figure 3(a)–3(c)**). T3 uptake by either WT MCT8 or the p.F501del mutant was not increased by chaperone treatment after transfection with 50 ng cDNA (**Figure 3(c)**). Please note that under these conditions a slight decrease of total protein levels was observed (**Supplemental Figure 3**), which may indicate cellular toxicity. As expected, similar results were obtained with NaPB, which provides the same chemical composition in solution as PBA (**Figure 3(a)–3(c)**). Higher concentrations of PBA (10 mM), NaPB (10 mM), or DMSO (2%) decreased intracellular T3 accumulation, likely due to the reduced cellular viability, whereas no effects on T3 transport levels were observed after preincubation with lower concentrations of PBA (0.1 mM), NaPB (0.1 mM), or DMSO (0.5%) (data not shown). Together, these findings suggest that PBA does not specifically rescue the function of the p.F501del mutant, but rather potentiates T3 uptake by cells overexpressing WT MCT8 or mutants with significant residual activity.

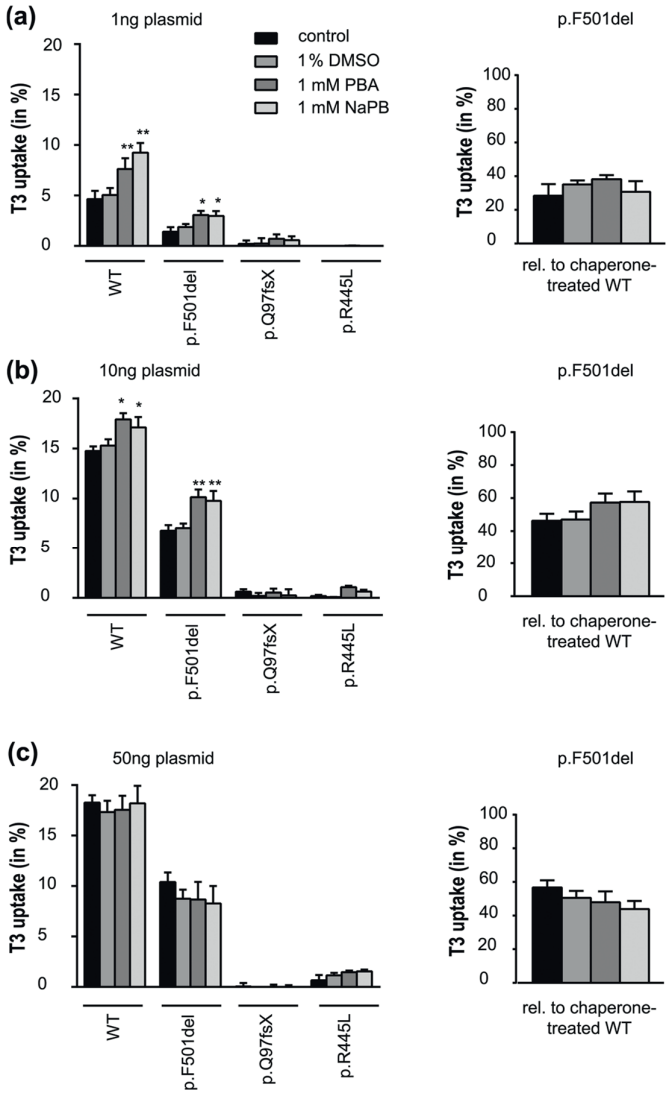

Figure 3 T3 uptake levels in COS-1 cells transiently transfected with either (a) 1, (b) 10, or (c) 50 ng plasmid encoding WT or indicated mutant MCT8 and 100 ng CRYM after preincubation in absence (control) or presence of indicated concentrations of DMSO, PBA, or NaPB (24-well format). All uptake values are corrected for background TH uptake levels observed in COS-1 cells transfected with pcDNA3 empty vector preincubated under the corresponding conditions. Data of WT and indicated mutants is provided as mean ± SEM absolute T3 uptake values (left panels; n = 3). p.F501del mutant MCT8–mediated T3 uptake capacity after the different preincubation conditions is also expressed relative to WT MCT8–expressing cells treated with the corresponding chaperone (right panels). Statistical significance was tested using two-way analysis of variance followed by Bonferroni multiple-comparison test. Statistically significant differences are indicated as follows: *$P < 0.05$; **$P < 0.01$. AB, antibody; AU, arbitrary units; EV, empty vector.

To further elucidate the mode of action of PBA, parallel immunoblot analyses were performed that showed an increase in protein expression levels of WT MCT8 and the p.F501del and p.R445L mutants upon preincubation with 1 mM PBA, but not 1% DMSO as compared with cells cultured in control medium (**Figure 4**). A similar increase in MCT8 protein expression levels was observed using NaPB (data not shown). In addition, preincubation with 1 mM PBA increased the abundance of WT MCT8 and both p.F501del and p.R445L mutants at the cell membrane (**Figure 5**). The proportion of the total amount

of WT MCT8 or the p.R445L mutant protein expressed at the cell membrane did not change (10% and 5%, respectively). However, in case of the p.delF501 mutant, the proportion of the total amount of p.F501del protein expressed at the cell membrane showed a modest increase after PBA treatment (from ~7% to ~10%), indicating more efficient cell membrane trafficking in the presence of PBA (derived from **Figure 5**). Together, these findings are in agreement with previous studies (13) and indicate that PBA potentiates the function of WT MCT8 and the p.F501del mutant by increasing MCT8 protein expression levels at the cell membrane. Despite the increase in cell membrane expression levels, the p.R445L mutant showed no functional increase upon treatment with PBA.

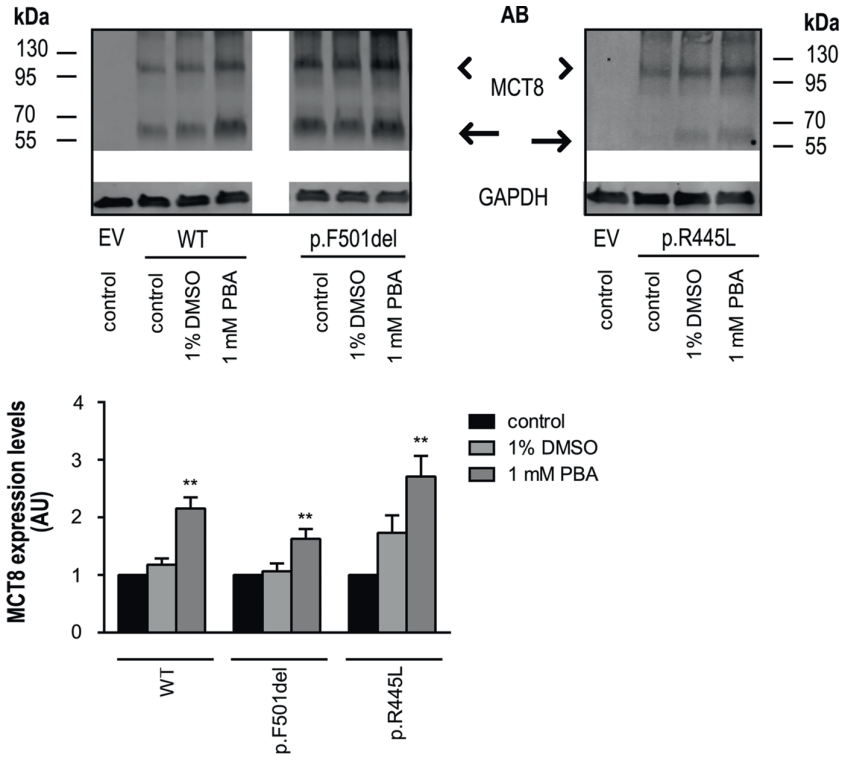

Figure 4 Representative immunoblots on total lysates derived from COS-1 cells transfected with 100 ng WT or indicated mutant MCT8 (six-well format) preincubated for 48 hours in absence or presence of indicated concentrations of PBA or DMSO. MCT8 protein was detected as described in the legend of Fig. 1. Please note that a higher scanning intensity was used compared with Figs. 1 and 2 to obtain appropriate signal intensities. MCT8 and GADPH expression levels were quantified by densitometry using ImageJ. WT and mutant MCT8 expression levels are expressed as MCT8/GADPH ratio relative to untreated control cells expressing either WT or corresponding mutant MCT8 (100%) and presented as mean ± SEM of three independent experiments. Statistical significance was tested using one-way analysis of variance followed by Dunnett multiple-comparison test. Statistically significant differences are indicated as follows: *$P < 0.05$; **$P < 0.01$. AB, antibody; AU, arbitrary units; EV, empty vector.

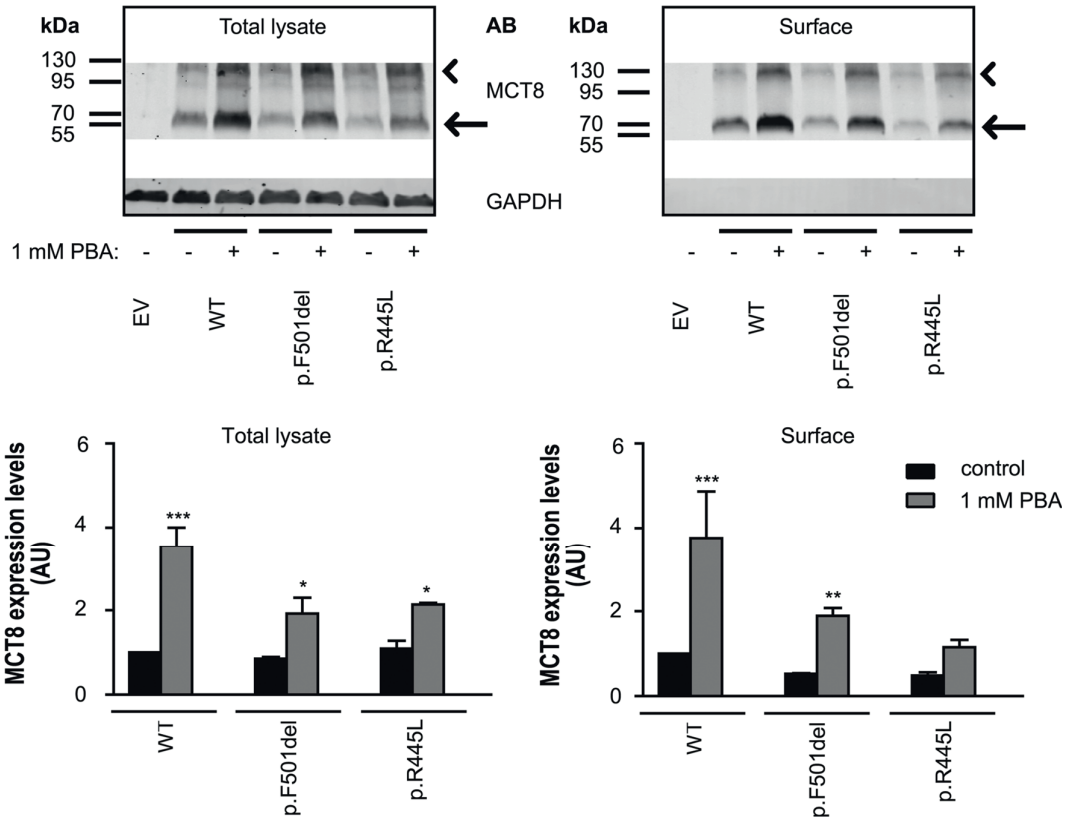

Figure 5 Representative immunoblot analyses on total lysates and the cell surface fraction derived from COS-1 cells transfected with 750 ng pcDNA3 EV, WT, or indicated mutant MCT8. Cells were preincubated in the absence (–) or presence (+) of 1 mM PBA for 48 hours prior to sample preparation. The input sample comprises 5% of the clarified lysate from which the presented surface fraction was derived. MCT8 detection was performed with the N-terminal MCT8 antibody (3353) and visualized with IRDye680 goat anti-rabbit secondary antibody. GAPDH was used as loading control. Note the absence of GAPDH in the cell surface samples, demonstrating the purity of the cell surface fraction. MCT8 and GADPH expression levels were quantified by densitometry using ImageJ. WT and mutant MCT8 expression levels in the input sample (total lysate) are expressed as MCT8/GADPH ratio relative to untreated control cells expressing either WT or corresponding mutant MCT8 (100%), and WT and mutant MCT8 cell surface expression levels are expressed as MCT8 (surface)/GADPH (input) ratio relative to untreated control cells expressing either WT or corresponding mutant MCT8 (100%). All data are presented as mean ± SEM of two to three independent experiments. Statistical significance was tested using two-way analysis of variance analyses followed by Bonferroni multiple-comparison test. Statistically significant differences are indicated as follows: *$P < 0.05$; **$P < 0.01$; ***$P < 0.005$.

Because PBA may act as a chemical chaperone and as a histone deacetylase inhibitor (28), we next explored to what extent an increase in MCT8 mRNA expression levels may underlie the observed increase in MCT8 protein expression levels. Indeed, MCT8 mRNA expression levels increased significantly by approximately threefold in transiently transfected COS-1 cells after incubation with 1 mM PBA compared with untreated control cells and cells exposed to 1% DMSO (**Figure 6(a)**). In contrast, mRNA expression levels of GAPDH showed an approximately twofold decrease in the PBA-treated cells, which is in line with previous studies (**Figure 6(b)**) (29). These findings suggest that at least part of the stimulatory effect of PBA occurs at the transcriptional level for both WT MCT8 and the p.F501del mutant.

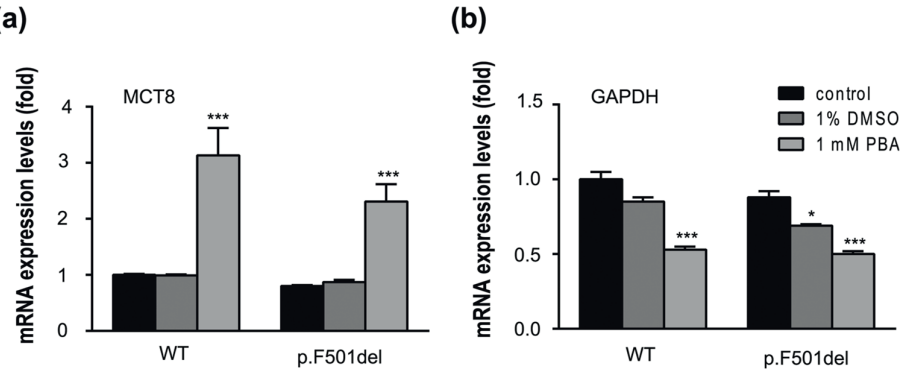

Figure 6 WT or p.F501del mutant (**a**) MCT8 and (**b**) GADPH mRNA expression levels in COS-1 cells transiently transfected with 100 ng WT or p.F501del mutant MCT8, preincubated in the absence (control) or presence of 1% DMSO or 1 mM PBA for 48 hours (six-well format). The MCT8 primer/probe combination was designed in a way that endogenously expressed csMCT8 could not be detected. Data are presented as means ± SEM of two independent experiments performed in triplicate and expressed as fold difference compared with untreated COS-1 cells expressing WT MCT8. Statistical significance was tested using two-way analysis of variance analyses followed by Bonferroni multiple-comparison test. Statistically significant differences are indicated as follows: *P < 0.05; ***P < 0.005.

Importantly, in both transient and stable overexpression systems, the expression of MCT8 is not controlled by its native promoter. Hence, we aimed to study the efficiency of chaperone treatment in patient-derived (p.F501del, p.Q97fsX, or p.R445L) and control fibroblasts. Previous studies have shown that TH uptake is severely impaired in fibroblasts from patients with MCT8 deficiency, suggesting that MCT8 importantly mediates the uptake of TH in these cells (10). Indeed, T3 uptake capacity of the p.Q97fsX and p.R445L mutant fibroblasts amounted to ∼30% of control fibroblasts, whereas T3 uptake by the p.F501del mutant fibroblasts was less affected, amounting to ∼50% of control fibroblasts (**Figure 7**). This is in accordance with the relatively mild clinical phenotype of the patient harboring this mutation (9). To further demonstrate the important contribution of MCT8 to the cellular T3 uptake in human fibroblasts, we next performed T3 uptake assays in the presence or absence of 10 μM silychristin, the most specific MCT8 inhibitor identified to date (30). T3 uptake by the control and p.F501del patient fibroblasts decreased to similar levels as p.Q97fsX mutant fibroblasts (**Figure 7**).

Finally, the effects of 48-hour preincubation with increasing concentrations of DMSO and PBA on T3 uptake levels in fibroblasts were evaluated. Concentrations of 10 mM PBA and 2% DMSO were generally well tolerated and only resulted in a minor reduction of cellular viability or total protein content (**Figure 8(a)** and **8(b)**, middle and right panels). Preincubation with 2% DMSO significantly increased T3 uptake in control and p.F501del mutant fibroblasts but had no effect on p.Q97fsX and p.R445L mutant fibroblasts (**Figure 8(a)**). Preincubation with 10 mM PBA resulted in a small but significant increase in T3 uptake in p.F501del mutant fibroblasts, which was not observed at lower concentrations. No effects were observed in control or p.R445L mutant fibroblasts (**Figure 8(a)** and **8(b)**).

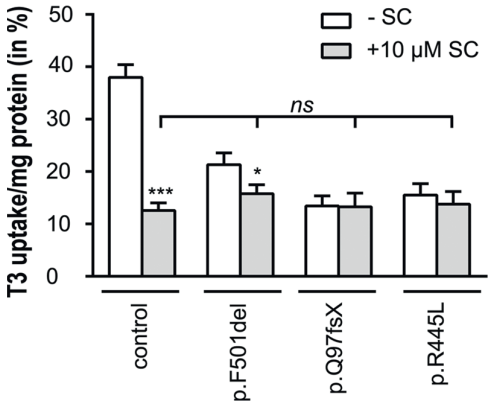

Figure 7 T3 uptake levels in skin fibroblasts derived from MCT8-deficient patients harboring the indicated MCT8 mutation or two sex-matched control subjects (the average of both control lines is provided) after 30 minutes incubation at 37°C in the absence (–) or presence (+) of 10 µM silychristin (SC). Silychristin is a potent and, thus far the most specific, inhibitor of MCT8-mediated TH transport (30). Ten micromolars was found to be the lowest SC concentration resulting in maximal MCT8 inhibition, without affecting cell viability (MTT assay) or total protein content (Bradford assay) (data not shown). T3 uptake levels are presented as mean (± SEM) percentage internalized T3 per milligram protein to correct for differences in cell density between different fibroblast lines (n = 4 to 6). Experiments were performed between P2 and P8, and fibroblasts of the different subjects had the same passage number at time of the experiments. In the absence of silychristin, all three patient-derived fibroblasts lines showed a significantly lower T3 uptake capacity as compared with control cells ($P < 0.001$; not indicated in the graph). Residual T3 uptake by the p.F501del mutant fibroblasts was significantly higher compared with the p.Q97fsX and p.R445L mutant fibroblasts ($P < 0.05$; not indicated in the graph), as assessed by repeated-measures two-way analysis of variance with Bonferroni *post hoc* tests. T3 uptake levels in control and p.F501del mutant fibroblasts were significantly reduced to p.Q97fsX and p.R445L mutant levels in presence of 10 µM silychristin, as assessed by two-way analysis of variance with Bonferroni *post hoc* tests (*$P < 0.05$; ***$P < 0.005$).

Unexpectedly, a small and insignificant increase in T3 uptake was also observed in p.Q97fsX mutant fibroblasts after preincubation with 10 mM PBA (**Figure 8(b)**), which suggests that the observed increase in T3 uptake is not solely the result of the rescue of mutant MCT8 function. Similar results were obtained using NaPB (data not shown). Lower chaperone concentrations did not affect T3 uptake in any of the fibroblast lines (**Figure 8(a)** and **8(b)**). In contrast to the transient overexpression system, the absolute endogenous MCT8 mRNA expression levels in control or p.F501del mutant fibroblasts did not significantly increase in response to 48-hour incubations with 10 mM PBA (**Figure 9(a)**). In agreement with previous studies, mRNA expression levels of the housekeeping gene cyclophilin were found to be reduced by PBA (**Figure 9(b)**) (31).

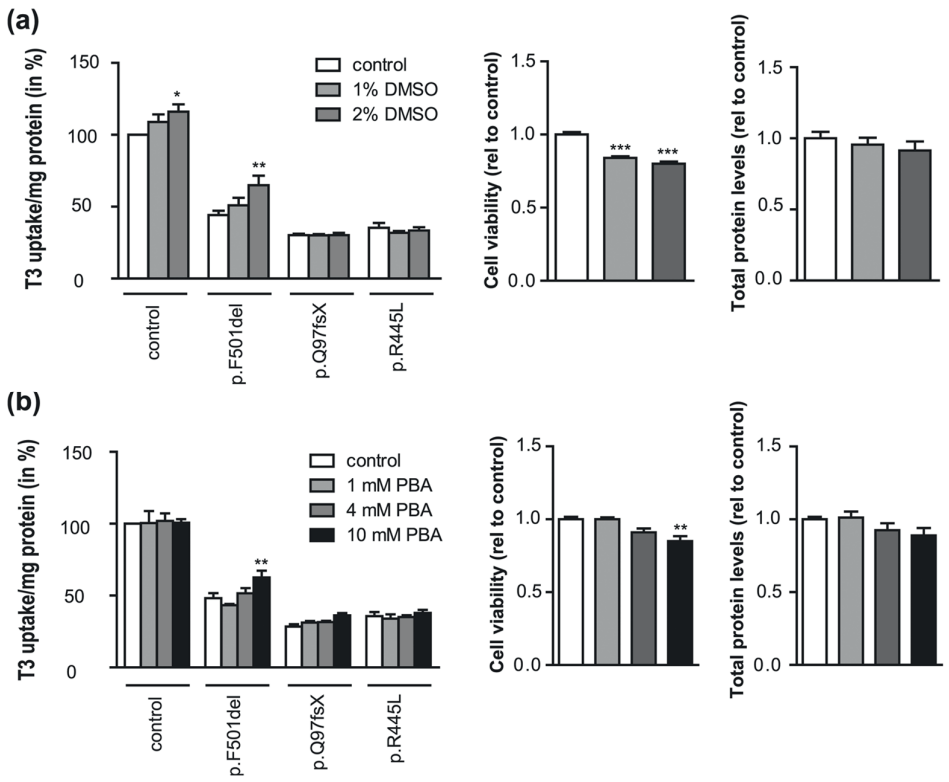

Figure 8 T3 uptake levels in patient-derived or control fibroblasts in 30 minutes at 37°C. Cells were preincubated in the absence (control) or presence of (**a**, left panel) 1% to 2% DMSO or (**b**, left panel) 1 to 10 mM PBA for 48 hours. In parallel, (**a** and **b**, middle panel) cell viability and (a and b, right panel) total protein levels were measured using MTT and Bradford assays, respectively. T3 uptake levels are presented as mean (± SEM) percentage internalized T3 per milligram protein (n = 4). Statistical significance was tested using two-way analysis of variance analyses followed by Bonferroni multiple-comparison test. Statistically significant differences are indicated as follows: **P* < 0.05; ***P* < 0.01.

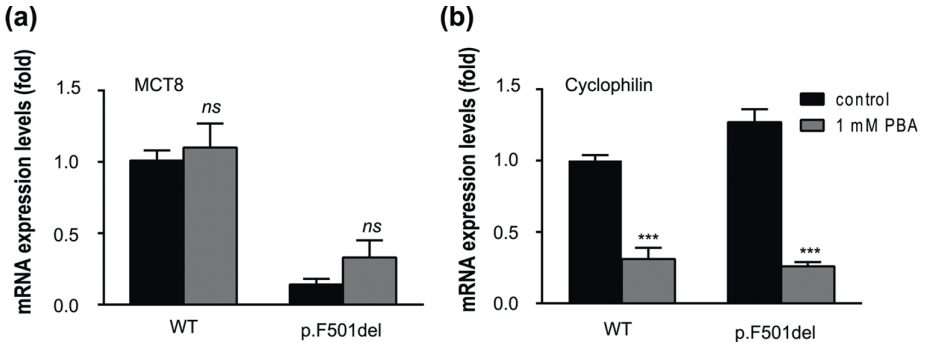

Figure 9 (**a**) MCT8 and (**b**) cyclophilin A mRNA expression levels in control (presented as mean of two different control lines) or p.F501del mutant MCT8 fibroblasts, preincubated in the absence (control) or presence of 10 mM PBA for 48 hours. Data are presented as means ± SEM of two independent experiments in triplicate and expressed as fold difference vs untreated control fibroblasts. Statistical significance was tested using two-way analysis of variance analyses followed by Bonferroni multiple-comparison test. Statistically significant differences are indicated as follows: ****P* < 0.005.

Finally, we reasoned that if PBA specifically improves MCT8 mutant function, addition of the MCT8-specific inhibitor silychristin would prevent this increase. We observed that the increase in T3 uptake in p.F501del cells preincubated with 10 mM PBA was not reduced in the presence of 10 µM silychristin during the uptake experiment (**Figure 10**). Indeed, silychristin-sensitive T3 uptake did not differ between cells preincubated without (17% ± 3%) or with (17% ± 4%) 10 mM PBA [Fig. 9; $t(6) = 0.10$, $P = 0.92$]. Together, this suggests that the increase in T3 uptake in PBA-treated p.F501del cells is mediated through other T3 transporters than MCT8.

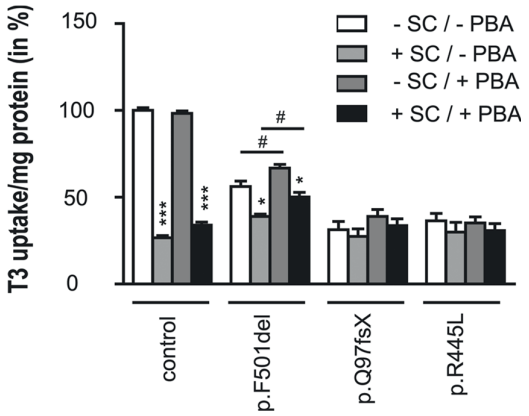

Figure 10 T3 uptake levels in patient-derived or control fibroblasts in 30 minutes at 37°C in the absence (–) or presence of 10 µM silychristin (SC) after preincubation in the absence (control) or presence of 10 mM PBA for 48 hours. T3 uptake levels are presented as mean (± SEM) percentage internalized T3 per milligram protein (n = 4). Please note that preincubation of the p.F501del mutant fibroblasts with 10 mM PBA resulted in a significant increase in intracellular T3 accumulation as compared with untreated cells. However, at least part of this gain in T3 uptake function was not sensitive to silychristin, because a significant difference was observed between both conditions once silychristin was added during the uptake experiment (horizontal bar). Statistical significance was tested using two-way analysis of variance analyses followed by Bonferroni multiple-comparison test. Statistically significant effects of PBA are indicated as follows: $^{\#}P < 0.05$. Statistically significant effects of silychristin are indicated as follows: $^{*}P < 0.05$; $^{***}P < 0.005$.

DISCUSSION

MCT8 deficiency results in a severe neurocognitive phenotype, urging the development of an effective treatment. At present, different therapeutic strategies are being explored in a clinical (T3 analogs) and preclinical (gene therapy and chaperone therapy) setting. In the current study, we provide unique insights into the use of chaperones in the treatment of MCT8 deficiency. We here extend and complement previous studies, by demonstrating that the chemical chaperone PBA may also effectively potentiate the function of WT MCT8 and the p.F501del mutant in a transient overexpression model. In addition, we further delineate the underlying molecular mechanism of PBA action, by demonstrating substantial effects on WT and p.F501del mutant MCT8 mRNA levels in our *in vitro* overexpression model. Importantly, only minor effects of PBA on cellular T3 uptake were observed in control and patient-derived fibroblasts in which the expression of MCT8 is under the control of its native promoter. Moreover, the effects of PBA in fibroblasts were unchanged in the presence of the MCT8-specific inhibitor silychristin, suggesting that the underlying mechanism is unrelated to the rescue of functional MCT8.

Functional MCT8 is crucial for the maintenance of appropriate intracellular TH levels in different tissues and cell types. In particular, it has a critical role in the transport of TH across the BBB (11). MCT8 deficiency results in a relatively hypothyroid state in cells that highly depend on functional MCT8. Hence, effective therapies should, among others, aim to restore local TH signaling in these cells. In addition to therapeutic approaches using TH analog therapy (32-37) and gene therapy (38), the use of chemical and pharmacological chaperones has recently been explored *in vitro* (13, 14).

The use of chaperone therapy was prompted by the observation that several mutations showed varying impact in different cell types (21, 39). These observations suggested that some mutations do not (completely) abolish intrinsic transport activity but reduce the abundance of the transporter at the cell membrane by disturbing subcellular trafficking or protein stability in a cell type–dependent way. Based on the beneficial effects observed for chaperone therapy on mutant cystic fibrosis transmembrane conductance regulator (associated with cystic fibrosis) (40-42), it was postulated that such mutant proteins may also benefit from chaperone therapy. Indeed, previous studies in stably transfected Madin-Darby canine kidney cells demonstrated that PBA, NaPB, DMSO and, to a lesser extent, genistein increased TH uptake by the p.F501del mutant (13) and several other mutants, most of which were associated with a relatively mild clinical phenotype (14). In line with these studies, we found that T3 uptake by the p.F501del mutant was stimulated by the chemical chaperone PBA in transiently transfected COS-1 cells. Importantly, we demonstrated that the magnitude of the effect of chaperone therapy is strongly related to the plasmid dose, and thus presumably to the amount of MCT8 protein being synthesized. The strongest effects of PBA were observed at low plasmid concentrations, at which T3 uptake by the p.F501del mutant could be restored to levels observed in untreated WT MCT8–expressing cells. No further gain in T3 transport capacity was observed in cells transfected with higher plasmid levels, suggesting that under these conditions, the maximum transport capacity has already been reached. Hence, the use of relatively high plasmid concentrations may explain the lack of efficacy of chaperone treatment in previous studies using transient overexpression systems (21).

As expected, neither PBA nor DMSO improved T3 uptake by the Q97fsX mutant, because this mutation prevents the production of full-length MCT8. Although PBA effectively increased the total and surface expression levels of p.R445L mutant protein, no corresponding increase in T3 uptake capacity was observed. This suggests, that the pR445L mutation most likely directly affects the substrate translocation mechanism, which is in line with previous studies demonstrating an important role for Arg445 in substrate interactions (6, 25, 27).

In contrast to previous studies claiming that PBA increases TH transport by MCT8 mutants but not by WT MCT8, the current study shows similar effect sizes of 1 mM PBA on the T3 uptake function of WT MCT8 and the p.F501del mutant in transiently transfected COS-1 cells. Because WT MCT8 is less susceptible to protein misfolding than the p.F501del mutant, the stimulatory effects of PBA cannot be solely attributed to its chaperone function. Although the molecular mechanisms underlying the therapeutic action of PBA are not yet fully understood, they include histone deacetylase inhibition and, consequently, effects on gene expression (28). Therefore, we here also evaluated the effects of PBA on MCT8 mRNA expression, which has not been addressed in previous studies. Indeed, profound stimulatory effects on MCT8 mRNA expression were found, which suggests that at least part of the beneficial effects of PBA occur at the transcriptional level.

Because the expression of MCT8 in stable and transient overexpression systems is under the control of an artificial promoter, it was imperative to also evaluate the effects of PBA in cells in which MCT8 expression is controlled by its native promoter. For this reason, we here evaluated the effects of chaperones on skin fibroblasts, which have been previously shown to be a suitable *ex vivo* model for MCT8 deficiency (9, 10). Our current studies using the MCT8-specific inhibitor silychristin (30) further underscore the importance of MCT8 for TH transport into fibroblasts and the relevance of this model. Importantly, fibroblasts have been previously used to demonstrate the efficacy of chaperone treatment, including PBA, in other diseases (43-45). In contrast to the effects observed in overexpression models, only small, but significant, beneficial effects of high concentrations of PBA were observed in the p.F501del fibroblasts. Although it is intuitive to speculate that an increase in p.F501del mutant function accounts for this observation, the increase in T3 uptake levels observed in PBA-treated fibroblasts was not suppressed by silychristin. In line with this, MCT8 mRNA expression levels did not significantly change upon incubation with PBA, suggesting that PBA also exerts stimulatory effects on other T3 transporters expressed in skin fibroblasts. The exact mechanism underlying this observation and the endogenous transporter(s) involved remain to be elucidated. Thus, the effect of PBA on T3 uptake in fibroblasts does not appear to be specific for WT MCT8 or for the p.F501del mutant.

Regardless of its exact underlying mechanism, the observed increase in T3 uptake in PBA-treated p.F501del fibroblasts might be of clinical significance, because the magnitude of this increase corresponds to the difference in T3 uptake of untreated fibroblasts with the mild p.F501del mutation and cells with the severe p.R445L and p.Q97fsX mutations. As the MCT8-independent response to PBA was less pronounced in the control and p.R445L and p.Q97fsX mutant fibroblasts, the effect of PBA on other transporters than MCT8 may differ per individual. Also, it remains to be elucidated to what extent similar effects can be obtained in other MCT8-dependent cell types, most importantly the endothelial cells of the BBB in which, at least in humans, the redundancy of other TH transporters appears to be limited. Thus, it is yet unclear to what extent the results of the present and previous *in vitro* studies can be extrapolated to the *in vivo* situation. Nonetheless, PBA has been shown to cross the BBB and exert effects inside the brain. It should be noted that PBA is also a well-known nitrogen scavenger capable of inducing the urinary excretion of 2 mol of nitrogen per mole of PBA through reaction of its active metabolite phenylacetate with glutamine. Although this mechanism underlies the therapeutic potency of PBA in the treatment of urea cycle defects, it may pose a concern when PBA is applied to patients with a very low body weight and a compromised nitrogen balance due to impaired food intake, as is the case in MCT8 deficiency (46).

In contrast to previous studies (13, 14), we did not find any effects of DMSO in transiently transfected COS-1 cells. A potential explanation is that we were unable to apply similar DMSO concentrations in our model due to toxic effects. DMSO was less toxic in fibroblasts, and consequently, higher concentrations could be tested. We found that 2% DMSO potentiated T3 uptake in p.F501del and WT fibroblasts, but not in p.Q97fsX and p.R445L fibroblasts. Because DMSO cannot be applied in clinical practice, we did not further follow-up on this finding.

In general, the magnitude of the effect of chaperone treatment may depend on (1) the underlying pathogenic mechanism of the mutation and (2) the cell model, but most likely also on (3) cell type–specific factors. Because chaperones such as PBA may also affect mRNA expression, the effects of such compounds should be preferably studied in the native genomic context. Although easily accessible,

the role of MCT8 in skin fibroblasts is yet unclear but appears to be of less physiological relevance compared with its role in the BBB and in neuronal cells. Therefore, it would be highly interesting to study the impact of chaperone treatment in disease models representing these cell types.

Taken together, we here demonstrate that PBA effectively potentiates T3 uptake by WT MCT8 and the p.F501del mutant in transiently transfected COS-1 cells. In contrast, only minor effects were observed in p.F501del fibroblasts. The latter effects seem MCT8 independent and are likely mediated through other transporters. Because the magnitude of the effect of chaperone therapy strongly depends on the disease model, more extensive preclinical studies are warranted before clinically available chaperones should be considered as a treatment option in patients with MCT8 deficiency.

Acknowledgements

We thank Ramona E. van Heerebeek and Selmar Leeuwenburgh for technical assistance, the Optical Imaging Center (Erasmus Medical Center Rotterdam) for technical support regarding the confocal imaging studies, and the physicians of the involved patients for providing the fibroblasts.

Financial Support: This work was supported by a grant from the Netherlands Organisation for Health Research and Development (project 113303005; to W.E.V.) and the Sherman Foundation (to W.E.V.).

Disclosure Summary: The authors have nothing to disclose.

SUPPLEMENTARY MATERIALS

Supplemental Tables

Supplemental Table 1 Antibody Table

Target protein/ antigen	Antigen Sequence (if known)	Name of Antibody	Species Raised (polyclonal or monoclonal)	Manufacturer (and catalog number)	Dilution used for WB	Dilution used for ICH
hMCT8	AA 52-155	MCT8	Rabbit (P)	ATLAS (HPA003353)	1:20000	1:1000
GAPDH		GAPDH	Mouse (M)	Millipore (Mab 374)	1:20000	
ZO1		ZO1	Mouse (M)	Thermo Fisher (33-9100)		1:1000
Rabbit IgG		IRDye680	Goat	LI-COR	1:20000	
Mouse IgG		IRDye800	Goat	LI-COR	1:20000	
Rabbit IgG		Alexa 488	Goat	Invitrogen		1:1000
Mouse IgG		Alexa 633	Goat	Invitrogen		1:1000

GAPDH: glyceraldehyde-3-phosphate dehydrogenase; ZO-1: zona occludens 1;P: polyclonal antibody; M: monoclonal antibody; WB: Western Blot ; ICH: immunohistochemistry

Supplemental Table 2 Overview of primers	
Name	sequence from 5' to 3'
Q97fsX_Fw	agaccaggaacagaggagccggtggg
Q97fsX_Rev	cccaccggctcctctgttcctggtct
MCT8_R445L_Fw	ctcaggccttgggcttcttgtgtcaggcc
MCT8_R445L_Rev	ggcctgacacaagaagcccaaggcctgag
csGAPDH_Fw_qPCR	aatgacccctttattgac
csGAPDH_Rev_qPCR	tccacgacgtactcagcgc
GAPDH: glyceraldehyde-3-phosphate dehydrogenase	

Supplemental Figures

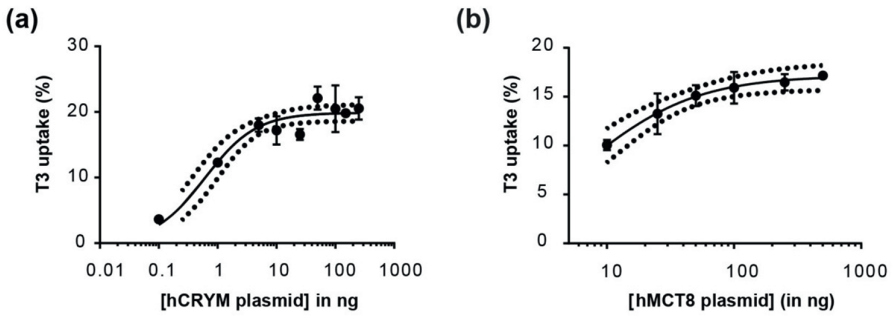

Supplemental Figure 1 (A) Intracellular T3 accumulation in COS-1 cells transiently transfected with a fixed amount of WT MCT8 expression construct (50 ng) and indicated concentration of the expression construct encoding the intracellular TH-binding protein CRYM after 30 minutes incubation at 37°C. Experiments were carried out in a 24-well format. Data are presented as individual data points representing the main of 3 separate experiments (± SEM) in duplo and standard non-linear regression methods were used to plot a trend line with 95% confidence interval. **(B)** Intracellular T3 accumulation in COS-1 cells transiently transfected with indicated concentration of WT MCT8 expression construct and a fixed amount of CRYM plasmid (250 ng) after 30 minutes incubation at 37°C after subtraction of background T3 uptake mediated by endogenous T3-transporters. Experiments were carried out in a 6-well format. Data are presented as individual data points representing the main of 3 separate experiments (± SEM) in duplo and standard non-linear regression methods were used to plot a trend line with 95% confidence interval.

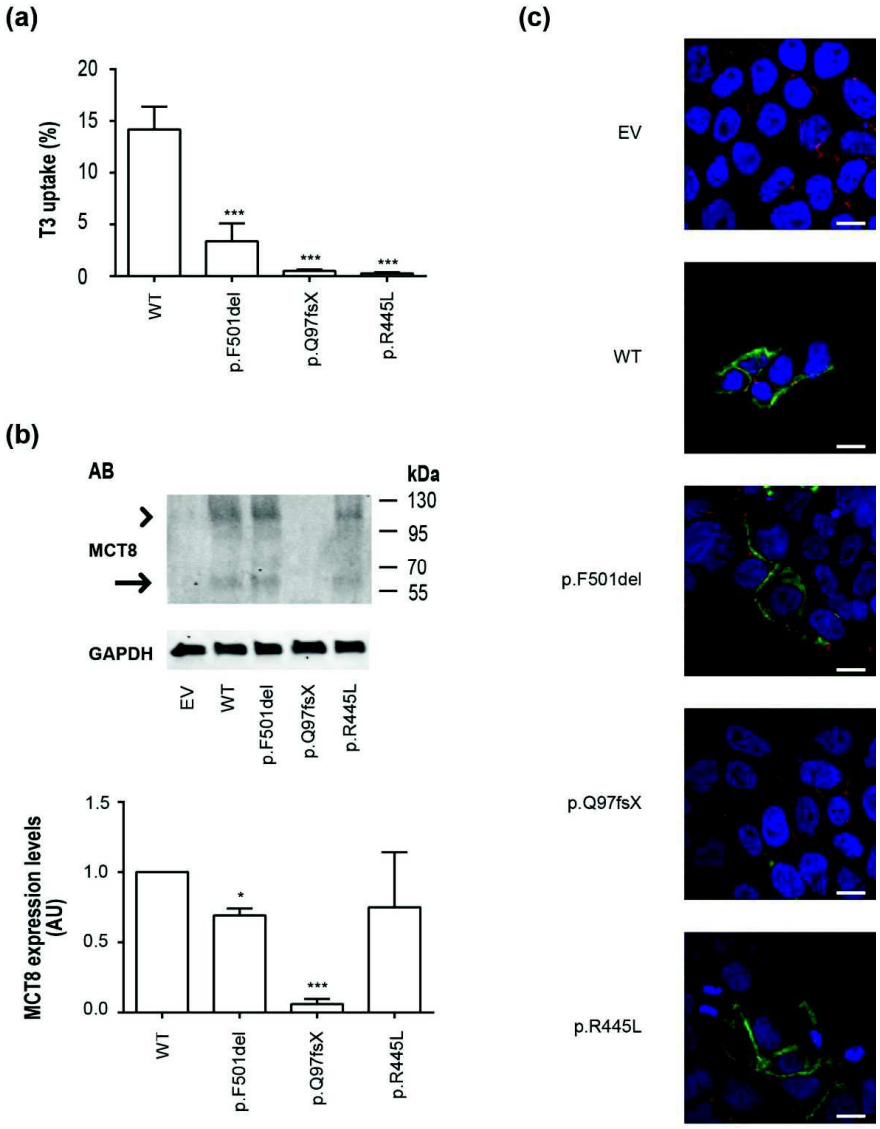

Supplemental figure 2 T3 uptake by JEG-3 cells transiently co-transfected with 50 ng WT or indicated mutant MCT8 and 100 ng CRYM in 30 minutes at 37°C (24-well format). All uptake values are corrected for background TH uptake levels observed in JEG-3 cells transfected with pcDNA3 empty vector. Results are presented as means ± SEM (n = 4). **(B)** Immunoblot on total lysates derived from JEG-3 cells transfected with 250 ng WT or indicated mutant MCT8 (6-well format). MCT8 protein was detected as described in the legend of **Figure 1**. MCT8 and GADPH expression levels were quantified by densitometry using ImageJ. WT and mutant MCT8 expression levels are expressed as MCT8/GADPH ratio relative to WT MCT8 (100%) and presented as mean ± SEM of 3 independent experiments. Statistical significance was tested using 1-way ANOVA followed by Dunnett's multiple-comparison test. Statistically significant differences are indicated as follows: $P<0.05$, *; $P<0.005$, ***. **(C)** Subcellular localization of WT and mutant MCT8 in transiently transfected JEG-3 cells assessed by confocal microscopy. Fixated cells were stained for the cell membrane marker ZO-1 (red) and MCT8 (green). DAPI was used as a nuclear staining (blue). A composite image is shown for WT MCT8 and the indicated mutants. The WT, p.F501del and p.R445L mutant MCT8 proteins showed intact localization at the cell membrane in the majority of cells, whereas the p.Q97fsX mutant could not be detected at all due to loss of the epitope for the MCT8 antibody. All images were generated using ImageJ software. The scale bar represents 4 µm.

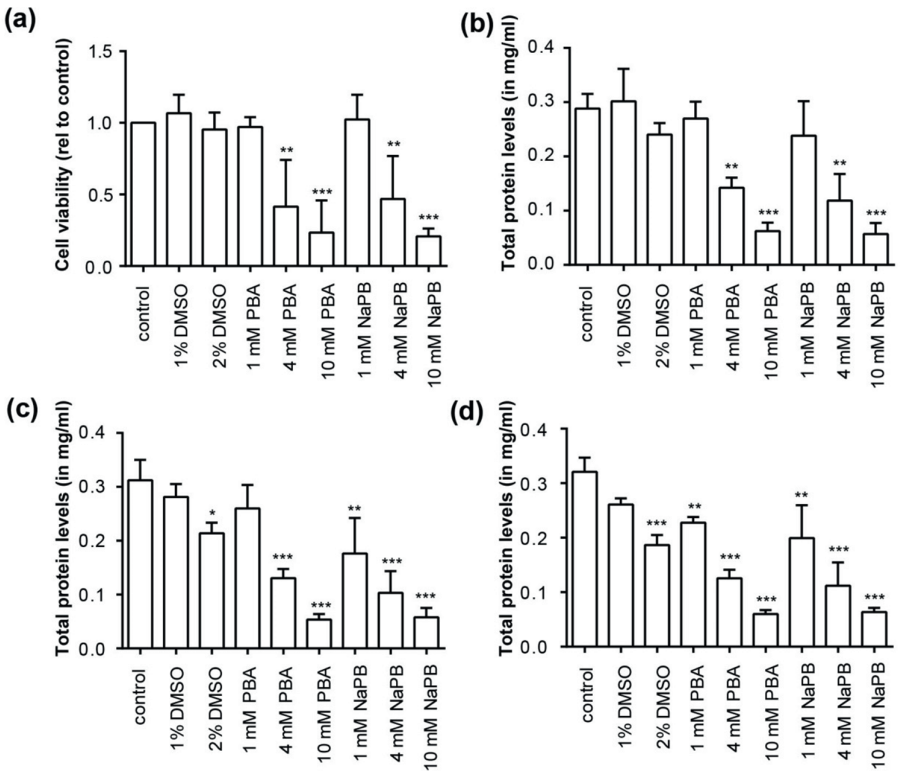

Supplemental Figure 3 (A) Cell viability in untransfected COS-1 cells (96-well format) and total protein concentrations of COS-1 cells transiently transfected with 1 (**B**), 10 (**C**) or 50 (**D**) ng WT MCT8 and 100 ng CRYM (24-well format), pre-incubated with indicated concentrations of DMSO, PBA or NaPB for 48h in parallel to the cells used for T3 uptake analyses presented in **Figure 3**. Cell viability was measured with an MTT assay and is expressed relatively to the cell viability of cells pre-incubated in control medium (first column, 1.0). Total protein levels were determined with a Bradford assay and are presented in mg/ml. Data are presented as mean ± SEM of 3 independent experiments. Statistical significance was tested using 1-way ANOVA followed by Dunnett's multiple-comparison test. Statistically significant differences are indicated as follows: $P<0.05$, *; $P<0.01$, **, $P<0.005$, ***.

REFERENCES

1. Ceballos A, Belinchon MM, Sanchez-Mendoza E, Grijota-Martinez C, Dumitrescu AM, Refetoff S, et al. Importance of monocarboxylate transporter 8 for the blood-brain barrier-dependent availability of 3,5,3'-triiodo-L-thyronine. Endocrinology. 2009;150(5):2491-6.
2. Heuer H, Visser TJ. Minireview: Pathophysiological importance of thyroid hormone transporters. Endocrinology. 2009;150(3):1078-83.
3. Friesema EC, Grueters A, Biebermann H, Krude H, von Moers A, Reeser M, et al. Association between mutations in a thyroid hormone transporter and severe X-linked psychomotor retardation. Lancet. 2004;364(9443):1435-7.
4. Dumitrescu AM, Liao XH, Best TB, Brockmann K, Refetoff S. A novel syndrome combining thyroid and neurological abnormalities is associated with mutations in a monocarboxylate transporter gene. Am J Hum Genet. 2004;74(1):168-75.
5. Groeneweg S, Visser WE, Visser TJ. Disorder of thyroid hormone transport into the tissues. Best Pract Res Clin Endocrinol Metab. 2017;31(2):241-53.
6. Groeneweg S, Friesema EC, Kersseboom S, Klootwijk W, Visser WE, Peeters RP, et al. The role of Arg445 and Asp498 in the human thyroid hormone transporter MCT8. Endocrinology. 2014;155(2):618-26.
7. Kersseboom S, Kremers GJ, Friesema EC, Visser WE, Klootwijk W, Peeters RP, et al. Mutations in MCT8 in patients with Allan-Herndon-Dudley-syndrome affecting its cellular distribution. Mol Endocrinol. 2013;27(5):801-13.
8. Novara F, Groeneweg S, Freri E, Estienne M, Reho P, Matricardi S, et al. Clinical and Molecular Characteristics of SLC16A2 (MCT8) Mutations in Three Families with the Allan-Herndon-Dudley Syndrome. Hum Mutat. 2017;38(3):260-4.
9. Visser WE, Jansen J, Friesema EC, Kester MH, Mancilla E, Lundgren J, et al. Novel pathogenic mechanism suggested by ex vivo analysis of MCT8 (SLC16A2) mutations. Hum Mutat. 2009;30(1):29-38.
10. Capri Y, Friesema EC, Kersseboom S, Touraine R, Monnier A, Eymard-Pierre E, et al. Relevance of different cellular models in determining the effects of mutations on SLC16A2/MCT8 thyroid hormone transporter function and genotype-phenotype correlation. Hum Mutat. 2013;34(7):1018-25.
11. Vatine GD, Al-Ahmad A, Barriga BK, Svendsen S, Salim A, Garcia L, et al. Modeling Psychomotor Retardation using iPSCs from MCT8-Deficient Patients Indicates a Prominent Role for the Blood-Brain Barrier. Cell Stem Cell. 2017;20(6):831-43 e5.
12. Kersseboom S, Horn S, Visser WE, Chen J, Friesema EC, Vaurs-Barriere C, et al. In vitro and mouse studies supporting therapeutic utility of triiodothyroacetic acid in MCT8 deficiency. Mol Endocrinol. 2014;28(12):1961-70.
13. Braun D, Schweizer U. Efficient Activation of Pathogenic DeltaPhe501 Mutation in Monocarboxylate Transporter 8 by Chemical and Pharmacological Chaperones. Endocrinology. 2015;156(12):4720-30.
14. Braun D, Schweizer U. The Chemical Chaperone Phenylbutyrate Rescues MCT8 Mutations Associated With Milder Phenotypes in Patients With Allan-Herndon-Dudley Syndrome. Endocrinology. 2017;158(3):678-91.
15. Ciechanover A, Kwon YT. Protein Quality Control by Molecular Chaperones in Neurodegeneration. Front Neurosci. 2017;11:185.
16. Cortez L, Sim V. The therapeutic potential of chemical chaperones in protein folding diseases. Prion. 2014;8(2).
17. Vauthier V, Housset C, Falguieres T. Targeted pharmacotherapies for defective ABC transporters. Biochem Pharmacol. 2017;136:1-11.
18. Schwartz CE, May MM, Carpenter NJ, Rogers RC, Martin J, Bialer MG, et al. Allan-Herndon-Dudley syndrome and the monocarboxylate transporter 8 (MCT8) gene. Am J Hum Genet. 2005;77(1):41-53.
19. Jansen J, Friesema EC, Kester MH, Schwartz CE, Visser TJ. Genotype-phenotype relationship in patients with mutations in thyroid hormone transporter MCT8. Endocrinology. 2008;149(5):2184-90.
20. Bialer MG, Lawrence L, Stevenson RE, Silverberg G, Williams MK, Arena JF, et al. Allan-Herndon-Dudley syndrome: clinical and linkage studies on a second family. Am J Med Genet. 1992;43(1-2):491-7.
21. Kinne A, Roth S, Biebermann H, Kohrle J, Gruters A, Schweizer U. Surface translocation and tri-iodothyronine uptake of mutant MCT8 proteins are cell type-dependent. J Mol Endocrinol. 2009;43(6):263-71.
22. Mol JA, Visser TJ. Synthesis and some properties of sulfate esters and sulfamates of iodothyronines. Endocrinology. 1985;117(1):1-7.
23. Friesema EC, Kuiper GG, Jansen J, Visser TJ, Kester MH. Thyroid hormone transport by the human monocarboxylate transporter 8 and its rate-limiting role in intracellular metabolism. Mol Endocrinol. 2006;20(11):2761-72.

24. Friesema EC, Jansen J, Jachtenberg JW, Visser WE, Kester MH, Visser TJ. Effective cellular uptake and efflux of thyroid hormone by human monocarboxylate transporter 10. Mol Endocrinol. 2008;22(6):1357-69.
25. Groeneweg S, Lima de Souza EC, Meima ME, Peeters RP, Visser WE, Visser TJ. Outward-Open Model of Thyroid Hormone Transporter Monocarboxylate Transporter 8 Provides Novel Structural and Functional Insights. Endocrinology. 2017;158(10):3292-306.
26. Jansen J, Friesema EC, Kester MH, Milici C, Reeser M, Gruters A, et al. Functional analysis of monocarboxylate transporter 8 mutations identified in patients with X-linked psychomotor retardation and elevated serum triiodothyronine. J Clin Endocrinol Metab. 2007;92(6):2378-81.
27. Protze J, Braun D, Hinz KM, Bayer-Kusch D, Schweizer U, Krause G. Membrane-traversing mechanism of thyroid hormone transport by monocarboxylate transporter 8. Cell Mol Life Sci. 2017;74(12):2299-318.
28. Lea MA, Tulsyan N. Discordant effects of butyrate analogues on erythroleukemia cell proliferation, differentiation and histone deacetylase. Anticancer Res. 1995;15(3):879-83.
29. Ranganna K, Yatsu FM. Inhibition of platelet-derived growth factor BB-induced expression of glyceraldehyde-3-phosphate dehydrogenase by sodium butyrate in rat vascular smooth muscle cells. Arterioscler Thromb Vasc Biol. 1997;17(12):3420-7.
30. Johannes J, Jayarama-Naidu R, Meyer F, Wirth EK, Schweizer U, Schomburg L, et al. Silychristin, a Flavonolignan Derived From the Milk Thistle, Is a Potent Inhibitor of the Thyroid Hormone Transporter MCT8. Endocrinology. 2016;157(4):1694-701.
31. Orchel A, Molin I, Dzierzewicz Z, Latocha M, Weglarz L, Wilczok T. Quantification of p21 gene expression in Caco-2 cells treated with sodium butyrate using real-time reverse transcription-PCR (RT-PCR) assay. Acta Pol Pharm. 2003;60(2):103-5.
32. Ferrara AM, Liao XH, Ye H, Weiss RE, Dumitrescu AM, Refetoff S. The Thyroid Hormone Analog DITPA Ameliorates Metabolic Parameters of Male Mice With Mct8 Deficiency. Endocrinology. 2015;156(11):3889-94.
33. Di Cosmo C, Liao XH, Dumitrescu AM, Weiss RE, Refetoff S. A thyroid hormone analog with reduced dependence on the monocarboxylate transporter 8 for tissue transport. Endocrinology. 2009;150(9):4450-8.
34. Verge CF, Konrad D, Cohen M, Di Cosmo C, Dumitrescu AM, Marcinkowski T, et al. Diiodothyropropionic acid (DITPA) in the treatment of MCT8 deficiency. J Clin Endocrinol Metab. 2012;97(12):4515-23.
35. Horn S, Kersseboom S, Mayerl S, Muller J, Groba C, Trajkovic-Arsic M, et al. Tetrac can replace thyroid hormone during brain development in mouse mutants deficient in the thyroid hormone transporter mct8. Endocrinology. 2013;154(2):968-79.
36. Delbaere J, Vancamp P, Van Herck SL, Bourgeois NM, Green MJ, Wingate RJ, et al. MCT8 deficiency in Purkinje cells disrupts embryonic chicken cerebellar development. J Endocrinol. 2017;232(2):259-72.
37. Zada D, Tovin A, Lerer-Goldshtein T, Appelbaum L. Pharmacological treatment and BBB-targeted genetic therapy for MCT8-dependent hypomyelination in zebrafish. Dis Model Mech. 2016;9(11):1339-48.
38. Iwayama H, Liao XH, Braun L, Barez-Lopez S, Kaspar B, Weiss RE, et al. Adeno Associated Virus 9-Based Gene Therapy Delivers a Functional Monocarboxylate Transporter 8, Improving Thyroid Hormone Availability to the Brain of Mct8-Deficient Mice. Thyroid. 2016;26(9):1311-9.
39. Anik A, Kersseboom S, Demir K, Catli G, Yis U, Bober E, et al. Psychomotor retardation caused by a defective thyroid hormone transporter: report of two families with different MCT8 mutations. Horm Res Paediatr. 2014;82(4):261-71.
40. Rubenstein RC, Egan ME, Zeitlin PL. In vitro pharmacologic restoration of CFTR-mediated chloride transport with sodium 4-phenylbutyrate in cystic fibrosis epithelial cells containing delta F508-CFTR. J Clin Invest. 1997;100(10):2457-65.
41. Iannitti T, Palmieri B. Clinical and experimental applications of sodium phenylbutyrate. Drugs R D. 2011;11(3):227-49.
42. Wainwright CE, Elborn JS, Ramsey BW. Lumacaftor-Ivacaftor in Patients with Cystic Fibrosis Homozygous for Phe508del CFTR. N Engl J Med. 2015;373(18):1783-4.
43. Sorrenson B, Suetani RJ, Williams MJ, Bickley VM, George PM, Jones GT, et al. Functional rescue of mutant ABCA1 proteins by sodium 4-phenylbutyrate. J Lipid Res. 2013;54(1):55-62.
44. Ferriero R, Boutron A, Brivet M, Kerr D, Morava E, Rodenburg RJ, et al. Phenylbutyrate increases pyruvate dehydrogenase complex activity in cells harboring a variety of defects. Ann Clin Transl Neurol. 2014;1(7):462-70.
45. Sanchez-Martinez A, Beavan M, Gegg ME, Chau KY, Whitworth AJ, Schapira AH. Parkinson disease-linked GBA mutation effects reversed by molecular chaperones in human cell and fly models. Sci Rep. 2016;6:31380.
46. Darmaun D, Welch S, Rini A, Sager BK, Altomare A, Haymond MW. Phenylbutyrate-induced glutamine depletion in humans: effect on leucine metabolism. The American journal of physiology. 1998;274(5):E801-7.

Chapter

Effectiveness and safety of the tri-iodothyronine analogue Triac in children and adults with MCT8 deficiency: an international, single-arm, open-label, phase 2 trial

5.2

Groeneweg S, Peeters RP, Moran C, Stoupa A, Auriol F, Tonduti D, Dica A, Paone L, Rozenkova K, Malikova J, van der Walt A, de Coo IFM, McGowan A, Lyons G, Aarsen FK, Barca D, van Beynum IM, van der Knoop MM, Jansen J, Manshande M, Lunsing RJ, Nowak S, den Uil CA, Zillikens MC, Visser FE, Vrijmoeth P, de Wit MCY, Wolf NI, Zandstra A, Ambegaonkar G, Singh Y, de Rijke YB, Medici M, Bertini ES, Depoorter S, Lebl J, Cappa M, De Meirleir L, Krude H, Craiu D, Zibordi F, Oliver Petit I, Polak M, Chatterjee K, Visser TJ, Visser WE.

Lancet Diabetes Endocrinol. 2019 Sep 7(9) 695-706.

ABSTRACT

Background Deficiency of the thyroid hormone transporter monocarboxylate transporter 8 (MCT8) causes severe intellectual and motor disability and high serum tri-iodothyronine (T3) concentrations (Allan–Herndon–Dudley syndrome). This chronic thyrotoxicosis leads to progressive deterioration in bodyweight, tachycardia, and muscle wasting, predisposing affected individuals to substantial morbidity and mortality. Treatment that safely alleviates peripheral thyrotoxicosis and reverses cerebral hypothyroidism is not yet available. We aimed to investigate the effects of treatment with the T3 analogue Triac (3,3',5-tri-iodothyroacetic acid, or tiratricol), in patients with MCT8 deficiency.

Methods In this investigator-initiated, multicentre, open-label, single-arm, phase 2, pragmatic trial, we investigated the effectiveness and safety of oral Triac in male paediatric and adult patients with MCT8 deficiency in eight countries in Europe and one site in South Africa. Triac was administered in a predefined escalating dose schedule—after the initial dose of once-daily 350 µg Triac, the daily dose was increased progressively in 350 µg increments, with the goal of attaining serum total T3 concentrations within the target range of 1·4–2·5 nmol/L. We assessed changes in several clinical and biochemical signs of hyperthyroidism between baseline and 12 months of treatment. The prespecified primary endpoint was the change in serum T3 concentrations from baseline to month 12. The co-primary endpoints were changes in concentrations of serum thyroid-stimulating hormone (TSH), free and total thyroxine (T4), and total reverse T3 from baseline to month 12. These analyses were done in patients who received at least one dose of Triac and had at least one post-baseline evaluation of serum throid function. This trial is registered with ClinicalTrials.gov, number NCT02060474.

Findings Between Oct 15, 2014, and June 1, 2017, we screened 50 patients, all of whom were eligible. Of these patients, four (8%) patients decided not to participate because of travel commitments. 46 (92%) patients were therefore enrolled in the trial to receive Triac (median age 7·1 years [range 0·8–66·8]). 45 (98%) participants received Triac and had at least one follow-up measurement of thyroid function and thus were included in the analyses of the primary endpoints. Of these 45 patients, five did not complete the trial (two patients withdrew [travel burden, severe pre-existing comorbidity], one was lost to follow-up, one developed of Graves' disease, and one died of sepsis). Patients required a mean dose of 38.3 µg/kg of bodyweight (range 6·4–84·3) to attain T3 concentrations within the target range. Serum T3 concentration decreased from 4·97 nmol/L (SD 1·55) at baseline to 1·82 nmol/L (0·69) at month 12 (mean decrease 3·15 nmol/L, 95% CI 2·68–3·62; p<0·0001), while serum TSH concentrations decreased from 2·91 mU/L (SD 1·68) to 1·02 mU/L (1·14; mean decrease 1·89 mU/L, 1·39–2·39; p<0·0001) and serum free T4 concentrations decreased from 9·5 pmol/L (SD 2·5) to 3·4 (1·6; mean decrease 6·1 pmol/L (5·4–6·8; p<0·0001). Additionally, serum total T4 concentrations decreased by 31·6 nmol/L (28·0–35·2; p<0·0001) and reverse T3 by 0·08 nmol/L (0·05–0·10; p<0·0001). Seven treatment-related adverse events (transiently increased perspiration or irritability) occurred in six (13%) patients. 26 serious adverse events that were considered unrelated to treatment occurred in 18 (39%) patients (mostly hospital admissions because of infections). One patient died from pulmonary sepsis leading to multi-organ failure, which was unrelated to Triac treatment.

Interpretation Key features of peripheral thyrotoxicosis were alleviated in paediatric and adult patients with MCT8 deficiency who were treated with Triac. Triac seems a reasonable treatment strategy to ameliorate the consequences of untreated peripheral thyrotoxicosis in patients with MCT8 deficiency.

INTRODUCTION

Intracellular action of thyroid hormones requires membrane transporter proteins to facilitate their cellular entry. Monocarboxylate transporter 8 (MCT8) is a specific thyroid hormone transporter that is crucial for transport of tri-iodothyronine (T_3) and thyroxine (T_4) in several tissues, including the brain (1). The *SLC16A2* gene (which is located on the X-chromosome) encodes MCT8, and mutations in this gene cause MCT8 deficiency (or Allan–Herndon–Dudley syndrome), a rare disorder with an estimated prevalence of one in 70 000 male individuals (2-4). Because thyroid hormone entry into the brain is impaired, individuals with MCT8 deficiency have severe intellectual and motor disability and generally do not achieve early developmental milestones.

The endocrine hallmark of MCT8 deficiency is increased serum T_3 concentrations, reduced free T_4, and normal thyroid-stimulating hormone (TSH) concentrations. Peripheral tissues that rely on transporters other than MCT8 are exposed to high serum T_3 concentrations (5). This chronic tissue thyrotoxicosis in patients with MCT8 deficiency leads to tachycardia, muscle wasting, hypermetabolism, and progressive reduction in bodyweight for age, causing substantial morbidity and mortality (5). It is therefore imperative to treat the permanent hyperthyroidism present in this disorder. However, standard antithyroid drug therapy with thiamazole (also known as methimazole) has been shown to be ineffective (4). The alternative antithyroid drug propylthiouracil has the potential to reduce serum T_3 concentrations through its inhibitory effect on type 1 deiodinase, but this treatment received a black box warning (the strongest drug safety warning) by the US Food and Drug Administration because of an associated risk of severe hepatotoxicity (6). Accordingly, propylthiouracil is not recommended as therapy for hyperthyroidism and its use, particularly in children, is strongly discouraged by current guidelines (7, 8). The unfavourable safety profile of propylthiouracil is particularly relevant in the context of the frequent need to use other drugs with hepatotoxic side-effects (eg, anticonvulsants) in patients with MCT8 deficiency. An optimal therapy for MCT8 deficiency would safely alleviate peripheral thyrotoxicosis and restore euthyroidism in the brain, but, as yet, no such treatment is available. As a result, the majority of patients with MCT8 deficiency are currently left untreated.

Triac (3,3',5-tri-iodothyroacetic acid; also known as tiratricol) is a thyroid hormone analogue the cellular entry of which is not dependent on MCT8 (9-11). Triac can inhibit TSH secretion in human beings, thereby lowering endogenous thyroid hormone production, but it has fairly weak thyromimetic activity in peripheral tissues (12, 13). Data from preclinical studies suggest that Triac restores abnormal neuronal development and myelination in animal models of MCT8 deficiency if given in early postnatal life (9, 14). We therefore aimed to evaluate the effectiveness and safety of Triac treatment for peripheral thyrotoxicosis in paediatric and adult patients with MCT8 deficiency. In view of the wide spectrum of patient age in our study, neurocognitive changes were assessed in an exploratory way only.

METHODS

Study design and participants

In this investigator-initiated, multicentre, open-label, single-arm, phase 2, pragmatic trial, we investigated the effectiveness and safety of Triac in male patients with MCT8 deficiency. We enrolled patients at 11 sites (ten hospitals and one outpatient facility) in eight countries in Europe (Belgium, Czech Republic, France, Germany, Italy, the Netherlands, Romania, and the UK) and one site in South

Africa (f**igure s1**). All patients were assigned to receive Triac for 12 months. The trial was originally intended to be a national study in the Netherlands, but it was amended to allow additional enrolment of patients in other countries. To ascertain long-term effectiveness and safety, the patients enrolled in the Netherlands could enter an open-label treatment extension period, the endpoint of which was defined as the completion date of the last patient in other countries.

Patients with MCT8 deficiency (confirmed by the presence of a mutation in the *SLC16A2* gene) were eligible to participate, irrespective of their age and comorbidities. Patients were either known to the investigators through direct care or were enrolled in the trial after their doctors or parents became aware of the trial through its ClinicalTrials.gov registration. Exclusion criteria were major illness or major surgery within the past 4 weeks, enrolment in other randomised controlled trials, allergy to components in Triac tablets, and the presence of any contraindications to Triac treatment (**table s1**). Patients could be withdrawn from the trial at the request of the parents or guardians, if continued participation was considered to be harmful to participants' health by the investigators because of dose-limiting toxicities, or because of non-adherence to the trial protocol, premature termination of the trial, or loss to follow-up (**table s1**).

Parents or guardians provided written informed consent for individuals they legally represent. The institutional review board at each participating site approved the study protocol and all amendments (see **online appendix** for the full study protocol and statistical analysis plan, available through https://www.thelancet.com/journals/landia/article/PIIS2213-8587(19)30155-X/fulltext).

Procedures

All participants discontinued treatment with antithyroid drugs, levothyroxine, or both (if applicable) before commencing treatment with the study drug. After a washout period of at least 4 weeks, baseline measurements were recorded. We treated all patients with Triac (Téatrois tablets [350 µg], taken orally; Rare Thyroid Therapeutics, Stockholm, Sweden) with individualised dose-escalation that followed a predefined dose-escalation protocol: after the initial dose of 350 µg Triac (one tablet) once per day was given and no predefined dose-limiting toxic effects were identified, the daily dose was increased progressively in 350 µg increments (one tablet) with no maximum dose defined, with a goal of attaining serum total T_3 concentrations within the target range of 1·4–2·5 nmol/L. The maintenance Triac dose was continued for the rest of the study period (**figure s2**), but it could be further adjusted according to the dose-escalation protocol if T_3 concentrations were outside the target range during control visits (**figure s2**).

Patients were assessed for study outcomes at baseline and 12 months after starting Triac treatment. Between these times, we screened patients for clinical and biochemical signs of hyperthyroidism, we recorded adverse events, and we assessed adherence to therapy (**table s2**). All study procedures were specified in standard operating procedures, and they were performed by trained investigators. We did neuropsychological tests (Bailey Scales of Infant Development III, Gross Motor Function Measure 88, and Vineland Adaptive Behaviour II) according to their manuals (**table s2**). We measured all blood components in a central laboratory (Erasmus Medical Centre, Rotterdam, The Netherlands), except for the blood count and serum glucose, which were measured locally in the participating centers at the baseline and month 12 visit. To account for any interference of Triac in the measurement of serum T_3 concentrations, we used an algorithm based on the different levels of cross-reactivity of Triac in two T_3 assays (**supplemental methods**). Bone mineral density was measured by total body or forearm dual-

energy X-ray absorptiometry. Cardiac evaluations consisted of a routine electrocardiogram, transthoracic cardiac ultrasound, and 24 h ambulatory cardiac monitoring.

Outcomes

The prespecified main primary endpoint was the change in the serum T_3 concentrations between baseline and month 12. The prespecified co-primary endpoints were the change in serum TSH, free and total T_4, and total reverse T_3 concentrations between baseline and month 12.

The prespecified secondary endpoints were the change between baseline and month 12 in bodyweight (expressed as bodyweight-for-age *Z* score, to account for natural development in children); mean heart rate, measured by 24 h ambulatory cardiac monitoring, and resting heart rate, measured by electrocardiography, both in bpm; blood pressure (in mm Hg and percentiles, based on reference ranges in healthy people (15, 16); mean of two measurements); and established biochemical parameters that reflect thyroid hormone activity in the liver (sex hormone-binding globulin and total cholesterol) and muscle (creatine kinase). Bodyweight was assessed instead of BMI, because accurate height measurements can be hampered by scoliosis and contractures.

An overview of prespecified exploratory measures, including neuropsychological tests and for which the endpoint was the change from baseline to month 12, is shown in **table s2** and the statistical analysis plan (see **online appendix**).

The prespecified assessments were the documentation of adverse events; echocardiography and 24-h monitoring of heart rhythm; bone mineral density measurement; and biochemical evaluations, including renal and liver function tests and bone turnover markers (see **online appendix**).

Post hoc, we also assessed the change in all available primary and secondary endpoints between baseline and the end of the treatment extension period in the participants treated for this time. Other post-hoc endpoints that we assessed between baseline and month 12 were the changes in total fat mass and percentage and lean body mass by dual-energy X-ray absorptiometry; the number of premature atrial contractions per 24 h; the ratio of HDL to LDL cholesterol; and the change in bodyweight (in kg). We also examined changes in neuropsychological test results after post-hoc stratification by age.

Although the measurement of energy expenditure (secondary endpoint) and hair cortisol concentrations (exploratory endpoint) were prespecified endpoints, their acquisition was compromised by technical difficulties and are, therefore, not reported.

Statistical analysis

We did a power calculation based on a one-sample *t* test to estimate the difference in serum T_3 concentrations after 12 months of treatment, by use of a mean serum T_3 concentration of 4·3 nmol/L (SD 1·2), which we derived from a historical group of 31 patients with MCT8 deficiency (unpublished data). With ten patients we would have 80% power (at a significance level of 0·05) to detect a mean decrease in serum T_3 concentrations from 4·3 nmol/L to 3·3 nmol/L. We thereby ensured sufficient power to detect a decrease in T_3 concentrations to the upper limit of the intended target range (1·4–2·5 nmol/L). This range was based on the reference range for healthy individuals in the Erasmus Medical Center at time of design of the trial protocol. After approval by all relevant ethical

committees, we recruited additional patients to ascertain uniform documentation of the effects of Triac in this rare disorder and to provide more meaningful data on secondary outcomes and safety measures. Since, to our knowledge, this study represents the first clinical trial in patients with MCT8 deficiency, the number of withdrawals and effect sizes were difficult to predict beforehand.

Analyses of the prespecified primary endpoints were based on the full analysis dataset, which included all patients who received at least one dose of Triac and who had at least one control visit after the baseline assessment (**figure s2**). As such, patients who withdrew were included in the analyses, with their last available measurement used. The main analyses of the prespecified secondary endpoints were done in all patients who completed 12 months of treatment. In post-hoc analyses, the prespecified secondary endpoints were also done on the full analysis dataset, which included all patients who received at least one dose of Triac and who had at least one control visit after the baseline assessment. The analyses of prespecified exploratory endpoints and the post-hoc analyses were done in all patients who completed 12 months of treatment and for whom relevant data were available. Analyses of safety endpoints were done in the safety population, which included all patients exposed to at least one dose of the study drug.

For all prespecified primary and secondary endpoints, p values and 95% CIs were calculated for the mean change between baseline and month 12 by use of paired Student's *t* tests. Serum TSH and creatine kinase concentrations were first log-transformed to normalise the distribution. For all prespecified exploratory and safety measures, 95% CIs were calculated for the mean change between baseline and 12 months of Triac treatment. Post-hoc analyses of neurocognitive endpoints after stratification by age are descriptive only. Longitudinal analyses of the primary and secondary endpoints in the treatment extension period were done in all patients who received at least one dose of Triac after enrolment into the long-term treatment extension period, done with paired *t* tests, and they compared baseline versus the end of the treatment extension period.

Missing data can mainly be attributed to the poor clinical condition of patients, poor adherence to trial instructions, and common manifestations of MCT8 deficiency, such as scoliosis and dystonic posturing that hamper investigations for which patients needed proper positioning. With the assumption that omission of data occurred randomly, and given the broad age range of the participants and small group size, pairwise deletion was used to adjust for missing data that were only captured at baseline and 12 months; for missing data that were captured throughout the study, the last available measurement was used.

We used GraphPad Prism (version 6) for all statistical analyses. Two-sided p values of less than 0·05 were considered to denote statistical significance.

An independent data safety monitoring board monitored patient safety. This trial is registered with ClinicalTrials.gov, number NCT02060474.

Role of the funding source

The funders of the study had no role in study design, data collection, data analysis, data interpretation, or writing of the report. The corresponding author had full access to all the data and had final responsibility for the decision to submit for publication.

RESULTS

Between Oct 15, 2014, and June 1, 2017, we screened 50 patients for eligibility for the trial, all of whom were eligible. Of these 50 patients, four declined to participate; 46 patients were therefore enrolled and assigned to receive Triac (**figure s3**), but one (2%) patient was withdrawn before the first control visit because of non-compliance to study procedures. This patient was included in safety analyses, but not primary efficacy analyses. 45 (98%) participants received Triac and had at least one follow-up measurement of thyroid function and thus were included in the analyses of the primary endpoints and in the post-hoc analyses of the secondary endpoints (**table s3**). Five of these patients did not complete the study intervention: two were withdrawn due to parental choice (one because of travel time to the study centre, one because of severe comorbidity [severe epileptic seizures and hydrocephalus]), one was lost to follow-up, one developed Graves' disease, and one patient died from sepsis. 40 (87%) patients completed the 12-month intervention period and thus were included in the analyses of secondary and exploratory endpoints. Ten (22%) patients who completed the follow-up were also included in the long-term (median 40·4 months, IQR 38·1–41·3) treatment extension period (**figure s3**).

At baseline, the median age of the overall study population (n=46) was 7·1 years (range 0·8–66·8) and the mean serum T_3 concentration was 4·91 nmol/L (SD 1·57), which was more than 1·6-times the upper limit of the normal range for age (**table 1**). The mean weight-for-age *Z* score was −2·84 (1·88) and 30 (65%) of the 46 enrolled patients were underweight (*Z* score less than −2). All patients had severe intellectual and motor disability: 41 (89%) of 46 patients were wheelchair-bound and had not reached early developmental milestones such as independent sitting. Resting heart rate was very high (>90th percentile)[17] in 19 (43%) of 44 patients with data available and systolic hypertension was present in 12 (34%) of 35 patients with baseline blood pressure measurements. The median daily Triac dose remained stable after the dose-escalation phase, although seven (16%) of 45 patients required further dose adjustments to maintain T_3 concentrations within the target range (**figure s4**). The median daily Triac dose during the final study visit, either at month 12 or at time of withdrawal, was 37·0 µg/kg bodyweight (IQR 28·9–47·2).

In the 45 patients assessed for the primary endpoint, serum T_3 concentrations had significantly decreased by month 12 (median 13·1 months [IQR 12·4–13·9]), with a mean decrease of 3·15 nmol/L (95% CI 2·68–3·62; p<0·0001; **figure 1**; **table 2**), equivalent to 61% (56–66) from baseline. We also identified significant reductions in serum free T_4 concentrations (mean decrease 6·1 pmol/L, 5·4–6·8; p<0·0001) and serum TSH concentrations (mean decrease 1·89 mU/L, 1·39–2·39; p<0·0001). Additionally, serum total T_4 concentrations decreased by 31·6 nmol/L (28·0–35·2; p<0·0001) and reverse T_3 by 0·08 nmol/L (0·05–0·10; p<0·0001; (**figure s5**).

We assessed the secondary endpoints in the 40 patients who completed the 12-month treatment. We identified a significant increase in weight-for-age *Z* score at month 12 (0·27 SDs, 95% CI 0·03–0·50; p=0·0253; **figure 1**; **table 2**; **figure s6**), equating to a mean increase in bodyweight of 2·7 kg (1·9–3·5; p<0·0001); by contrast, in untreated patients, the bodyweight-for-age *Z* score has been shown to progressively reduce over time (**figure s6**). Between baseline and month 12, resting heart rate, as measured by electrocardiography, decreased by 9 bpm (95% CI 2–16; p=0·010), and mean heart rate, as measured by 24-h cardiac monitoring, decreased by 5 bpm (1–9; p=0·012; **figure s7**).

Table 1 Demographical and clinical characteristics at baseline

Characteristic	**N =46**
Age (years)	7·1 (0·8-66·8)
Age group	
<4 years	11 (24%)
4-10 years	19 (41%)
11-18 years	11 (24%)
Adults (>18 years)	5 (11%)
Sex	
Female	0
Male	46 (100%)
Race	
White	44 (96%)
Other	2 (4%)
Ethnic origin	
European	39 (85%)
North-Africa	3 (7%)
Middle-Eastern	2 (4%)
Asian	1 (2%)
Other	1 (2%)
Country	
Netherlands	14 (30%)
South Africa	1 (2%)
Czech Republic	1 (2%)
Romania	3 (7%)
Belgium	2 (4%)
France	7 (15%)
Germany	3 (7%)
Italy	5 (11%)
United Kingdom	10 (22%)
Living location	
At home	34 (74%)
Institution	5 (11%)
Home and institution	7 (15%)
Developmental stage reached	
Wheelchair-bound	41 (89%)
No or poor head control	32 (70%)
Able to sit independently	5 (11%)
T3 concentration (nmol/L)	4·91 (±1·58)
Weight-for-age Z score	-2·84 (±1·88)
Underweight*	30 (65%)
Feeding tube	20 (43%)
Tachycardia at rest†	19 (43%)
Systolic hypertension‡	12 (34%)

Data are median (range), n (%), or mean (SD). T3=triiodothyronine. *Underweight was based on WHO criteria (*Z* score <–2). Tachycardia was defined as a resting heart rate above the 90th percentile for the corresponding age, with cut-offs described by Fleming and colleagues (17); resting heart rate data were available for 44 patients (denominator for percentage calculation). ‡Systolic hypertension was based on guidelines from the American Academy of Pediatrics (15) and the American College of Cardiology and American Heart Association (16); baseline blood pressure was measured in 35 patients (denominator for percentage calculation).

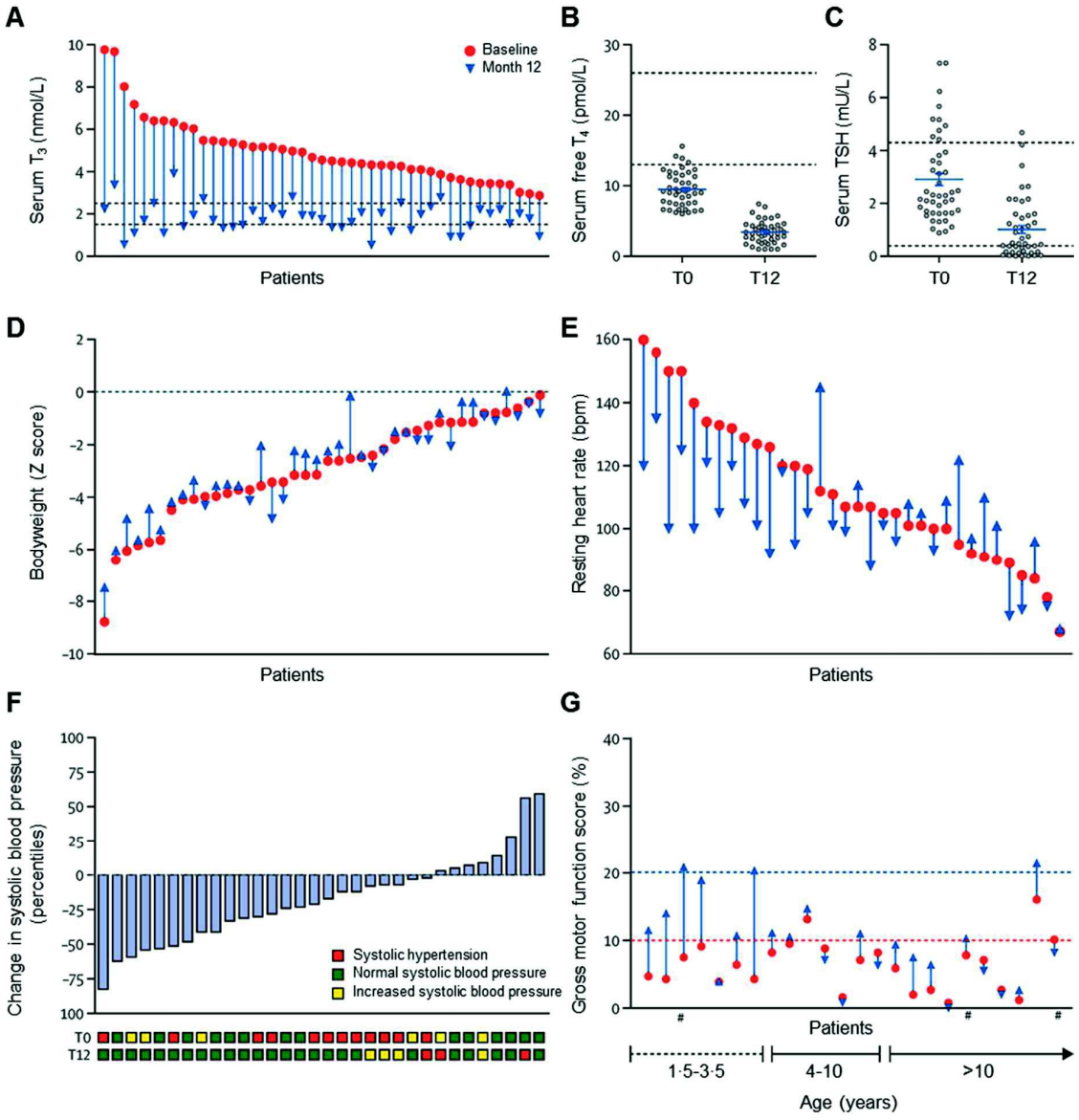

Figure 1. Change from baseline to month 12 in prespecified primary and secondary and exploratory outcome measures. Data are changes between baseline (T0) and month 12 (T12) of treatment with tri-iodothyroacetic acid in serum concentrations of T_3 (by patient; **A**), free T_4 (**B**), and TSH (**C**); bodyweight, as bodyweight-for-age *Z* scores (**D**); resting heart rate (by patient), determined by electrocardiogram (**E**); mean systolic blood pressure (by patient), expressed in percentiles after correction for age and height (**F**); and gross motor function (by patient), determined with the Gross Motor Function Measure 88. Gross motor function scores of 10% are indicated by the red dotted line, and 20% by the blue dotted line. Patients with the same inactivating F230del mutation are indicated with #. Data and p values are indicated in **table 2**. T_3=tri-iodothyronine. T_4=thyroxine. TSH=thyroid-stimulating hormone.

Table 2 Effects of Triac on prespecified and post-hoc outcome measures

Assessment	Baseline Mean (±SD)	12 months Mean (±SD)	Difference Mean (95% CI)	P value
Primary efficacy measures (n=45)				
T3 (nmol/L)	4·97 (±1·55)	1·82 (±0·69)	-3·15 (-3·62--2·68)	<0.0001
TSH (mU/L)*	2·91 (±1·68)	1·02 (±1·14)	-1·89 (-2·39--1·39)	<0·0001
Free T4 (pmol/L)	9·5 (±2·5)	3·4 (±1·6)	-6·1 (-6·8 - -5·4)	<0·0001
Total T4 (nmol/L)	56·0 (±13·0)	24·4 (±9·4)	-31·6 (-35·2--28·0)	<0·0001
Reverse T3 (nmol/L)	0·12 (±0·10)	0·04 (±0·04)	-0·08 (-0·10--0·05)	<0·0001
Secondary efficacy measures				
Weight-for-age Z score (n=40)	-2·98 (±1·93)	-2·71 (±1·79)	0·27 (0·03 - 0·50)	0·025
Resting heart rate (bpm; n=34)	112 (±23)	104 (±17)	-9 (-16 - -2)	0·010
Mean heart rate 24 h (bpm; n=31)	102 (±14)	97 (±9)	-5 (-9 - -1)	0·012
Blood pressure (n=32)				
Systolic (mm Hg)	108 (±8)	102 (±10)	-5 (-9 - -1)	0·0086
Systolic (Percentile) †	78 (±24)	61 (±29)	-18 (- 29- -6)	0·0037
Diastolic (mm Hg)	64 (±9)	62 (±9)	-2 (-6 – 2)	0·35
Diastolic (Percentile) †	74 (±22)	67 (±22)	-6 (-17 – 4)	0·24
Sex hormone-binding globulin (nmol/L; n=39)	212 (±91)	178 (±76)	-35 (-55 - -15)	0·0013
Total cholesterol (mmol/L; n=40)	3·2 (±0·7)	3·4 (±0·7)	0·2 (0·0-0·3)	0·056
CK (U/L; n=40) *	108 (±90)	161 (±117)	53 (27-78)	<0·0001
Exploratory measures (n=40) ‡				
Height (m)	1·20 (±0·23)	1·26 (±0·22)	0·06 (0·04-0·07)	
Height for age Z score	-1·96 (±1·5)	-1·98 (±1·5)	-0·02 (-0·19– 0·16)	
BMI (kg/m^2)	14·2 (±2·7)	14·6 (±2·9)	0·3 (-0·09 - 0·77)	
BMI-for-age Z score	-2·56 (±2·56)	-2·24 (±2·60)	0·32 (-0·14 – 0·77)	
Thyroxine-binding globulin (mg/L)	18·2 (±3·3)	19·7 (±4·6)	1·5 (0·3-2·8)	
Albumin (g/L)	46 (±2·2)	46·8 (±2·1)	0·9 (-0·1-1·9)	
Creatinine (µmol/L)	33 (±12)	38 (±14)	5 (3-7)	
LDL cholesterol (mmol/L)	1·80 (±0·53)	1·85 (±0·53)	0·06 (-0·07-0·19)	
HDL cholesterol (mmol/L)	1·20 (±0·30)	1·37 (±0·31)	0·18 (0·10-0·26)	
Triglycerides (mmol/L)	0·69 (±0·34)	0·72 (±0·35)	0·02 (-0·14– 0·09)	
Ferritin (µg/L)	45 (±40)	29 (±19)	-16 (-27 – -4)	
Thyroglobulin (µg/L) ‡	11·7 (7·1-28·9)	4·1 (1·5-6·8)	-9·2 (-23·6- -2·7)	
Post-hoc measures				
Weight (kg; n=40)	21·8 (±12·2)	24·5 (±12·6)	2·7 (1·9-3·5)	
Body fat (kg; n=15)	5·1 (±3·9)	6·2 (±4·2)	1·1 (0·2-2·1)	
Body fat (%; n=15)	22·8 (±9·8)	25·1 (±10·0)	2·3 (-1·0 – 5·6)	
Lean body mass (kg; n=15)	15·7 (±6·9)	16·9 (±6·8)	1·2 (0·8-1·7)	
Ratio of HDL to LDL cholesterol (n=40)	0·70 (±0·19)	0·78 (±0·22)	0·08 (0·02-0·14)	
Premature atrial complexes (n=31) ‡	48 (1-1322)	0 (0-12)	-22 (-1150- 0)	

Primary outcomes were assessed in all patients who received Triac and had at least one follow-up measurement of thyroid function, including five patients who withdrew (in whom the last available measurement was used in place of the 12-month measurement). Secondary, exploratory, and post-hoc outcomes were assessed in all patients who completed the 12-month intervention period and for whom relevant data were available. If 12-month measurements were not available, the last available observation in the same patient was used (<3% of included datapoints). CIs for exploratory measures have not been adjusted for multiplicity and these data should not be used to infer definitive treatment effects. T3=tri-iodothyronine. TSH=thyroid-stimulating hormone. T4=thyroxine. * TSH and creatine kinase concentrations were log-transformed to ensure a normal distribution before paired t tests were done (non-transformed means [SDs] and mean changes [95% Cis] are presented for the sake of interpretability).† Percentile scores were based on age and height (15, 16).‡ Data for thyroglobulin and premature atrial complexes are median (IQR) instead of mean (SD) because of violation of normality assumptions.

Mean systolic blood pressure decreased over the 12-month study from the 78th percentile to the 61th percentile, equating to a change of 18 percentile points (95% CI 6–29; p=0·0037; **table 2**). The proportion of patients with systolic hypertension decreased from 34% (n=12/35) at baseline to 9% (n=3/32 at month 12). The serum concentrations of sex hormone-binding globulin decreased by 35 nmol/L (15–55; p=0·0013). However, mean serum total cholesterol concentration did not significantly change between baseline and month 12 (difference 0·2, 95% CI 0·0–0·3; p=0·056). Finally, serum creatine kinase concentrations increased by 53 U/L (27–78; p<0·0001) by month 12 (**table 2**; **figure s8**).

The greatest increase in gross motor function was in patients in whom Triac treatment was started before age 4 years (**figure 1**). At baseline, none of the 24 patients with a completely inactivating MCT8 mutation and available data had a score of more than 20% on the Gross Motor Function Measure 88 scale (18), which would roughly reflect the ability to sit independently and achieve full head control in different postural positions. From the seven patients with a completely inactivating mutation who had started with Triac treatment before the age of 4 years, two reached this developmental stage by month 12 of treatment. One of these two patients has the completely inactivating F230del mutation. Other neurological and neuropsychological findings are reported in the **appendix (table s4 and table s5)**.

In the post-hoc analyses to assess only the patients who completed 12 months of treatment, we found that 34 (85%) of 40 patients had attained serum T_3 concentrations within the target range by month 12, and the remaining patients had concentrations just above the target range, but that their T_3 measurements had been within the target range during the previous study assessment visit. All withdrawals had T_3 concentrations within target range at the time of the last available measurement (median follow-up time 7·0 months [IQR 3·9–9·3]). The median time to achieve serum T_3 concentrations within the target range was 2·5 months (IQR 1·5–3·7), which required a mean daily Triac dose of 38·3 µg/kg of bodyweight (SD 15·3; range 6·4–84·3), administered as a median of three doses per day (IQR 2–3; **figure s4**). By month 4, 35 (78%) of 45 patients had attained T_3 concentrations within the target range (**figure s4**). Serum free T_4 concentrations decreased during the dose-escalation phase and were maintained throughout the rest of the study (**figure s4**).

All 46 patients who received at least one dose of Triac were included in drug safety analyses. 43 (93%) patients had at least one adverse event (**table 3; table s7**). Triac treatment was continued during hospital admission in all but one patient. All seven adverse events that were suspected to be related to Triac treatment, which occurred in six (13%) patients, were mild: three patients had a transient increase in perspiration and three patients reported transient irritability. The onset of these events coincided with the start of Triac treatment or modification in Triac dose and resolved spontaneously after a few days. No patients required a dose reduction or discontinued participation because of drug-related toxicity. Most adverse events that occurred during the study period were classified as mild and required symptom relief or no treatment, and resolved while the patients continued to receive Triac. Of the safety measures prespecified in the protocol (**table s2**), no clinically relevant changes in cardiac structure or function were identified.

Table 3 Summary of adverse events by system organ class and preferred term

	Patients with at least one event (n=46)	Number of events
Adverse events	43 (93%)	150
Adverse events occurring in >10% of patients		
Gastrointestinal disorders		
Diarrhoea	5 (11%)	5
Gastroenteritis	11 (24%)	12
Vomiting	5 (11%)	5
General disorders and administration-site conditions		
Influenza or influenza-like illness	9 (20%)	12
Infections and infestations		
Bronchitis	6 (13%)	6
Otitis media	5 (11%)	5
Respiratory, thoracic and mediastinal disorders		
Nasopharyngitis	11 (24%)	14
Upper respiratory tract infection	9 (20%)	9
Serious adverse events *	18 (39%)	26
Gastrointestinal disorders		
Gastroenteritis	2 (3%)	3
Enterocolitis	1 (2%)	1
General disorders and administration-site conditions		
Multiple organ dysfunction syndrome	1 (2%)	1
Hepatobiliary disorders		
Hepatic failure	1 (2%)	1
Infections and infestations		
Bronchitis	2 (3%)	2
Pneumonia	2 (3%)	2
Clostridium difficile infection	1 (2%)	1
Investigations		
Gastroscopy	1 (2%)	1
Nervous system disorders		
Increased seizures	2 (3%)	2
Product issues		
Device malfunction †	2 (3%)	2
Renal and urinary tract disorders		
Urinary tract infection	1 (2%)	1
Respiratory, thoracic and mediastinal disorders		
Bronchiolitis	3 (7%)	3
Respiratory distress	1 (2%)	2
Upper respiratory tract infection	1 (2%)	1
Surgical and medical procedures		
Hip surgery	1 (2%)	1
Drug therapy (bisphosphonates)	1 (2%)	2
Fatal adverse events ‡	1 (2%)	1
Adverse events leading to premature treatment discontinuation	1 (2%)	1
Immune system disorders		
Autoimmune thyroid disorder	1 (2%)	1
Grade of events		
Severe	4 (9%)	4
Moderate	4 (9%)	5
Mild	40 (87%)	141
Relationship to the product		
Probable **	6 (13%)	7
Unlikely	43 (93%)	143

Data are n or n (%). Adverse events were classified according system organ class and preferred term with the Medical Dictionary for Regulatory Activities and were defined as those occurring between the administration of the first dose and 30 days after administration of the final dose of study drug. At baseline, seizures were present in 15 (37%) of 41 patients with available data. *A serious adverse event was defined one that resulted in death, was life-threatening, resulted in hospital admission or prolonged hospital treatment, resulted in persistent or clinically significant disability or incapacity other than might be expected by the effects of the disease-specific mutation, or was otherwise considered medically significant by the investigators. †Device malfunctions were hospital admissions for a dysfunctional ventriculoperitoneal drain or percutaneous enteral feeding tube. ‡One patient died from pulmonary sepsis leading to multi-organ failure; post-mortem examination confirmed the clinical diagnosis and other causes were excluded. **Adverse events with a probable relation to the study drug as deemed by the investigators (adverse reactions) were those for which a causal relation with Triac could not be excluded.

Serum β-carboxy-terminal collagen crosslinks increased by 0·14 µg/L (95% CI 0·03–0·25) and bone-specific alkaline phosphatase concentrations increased by 8·4 µg/L (2·7–14·1), without affecting bone mineral density (**table s7**), consistent with the physiological increase of bone turnover markers in paediatric patients during development. We identified no notable changes in serum electrolytes, serum urea, or random plasma glucose concentrations (**table s7**). Hematopoietic parameters did not differ except in three patients, in whom mild anaemia, which was ascribed to nutritional deficiency, was detected at month 12 (not linked to the intervention). 25 (54%) of 46 patients showed mildly increased serum concentrations of alanine aminotransferase, aspartate aminotransferase, or γ-glutamyl transferase at baseline, which was attributed to the concomitant use of hepatotoxic medications, and these concentrations did not increase further during the study. Two (4%) patients showed an increase in aminotransferase concentrations that were attributed to commencement or dose adjustment of anticonvulsant drugs with known hepatotoxicity (levetiracetam and lamotrigine).

Most serious adverse events were intermittent infections that were treated with antibiotics and supportive care. All serious adverse events were considered to be secondary to MCT8 deficiency and, thus, unrelated to Triac (**table 3**). In three patients with pre-existing seizures, an increase in seizure frequency was reported. In one patient, this increase coincided with a gastrointestinal infection; and the other two patients had a history of seizures that were difficult to control. Hospital admission was required in two patients with pre-existing seizures to treat prolonged seizure or to optimise anticonvulsant therapy. In the patient with a history of seizures in whom Triac treatment was stopped, hepatic insufficiency resulted in hospital admission, during which time Triac treatment was temporarily withheld; this hepatic insufficiency resolved with reduction in anticonvulsant drug dose and supportive measures. One patient died from pulmonary sepsis leading to multi-organ failure; post-mortem examination confirmed the clinical diagnosis, and other causes were excluded.

Post-hoc analyses showed that premature atrial contractions largely subsided in most patients in whom these were present at baseline (**figure s7**). The effects of Triac treatment on secondary outcomes were maintained when the post-hoc analyses were done with the full analysis set population, including patients who did not complete the 12 months of treatment (**table s3**). Post-hoc analyses of the treatment extension endpoints included ten patients. During the long-term treatment extension period, the reductions in T_3 concentrations persisted in all patients (**figure 2**; **table s6**) and reductions in TSH and free T_4 concentrations were maintained (**figure s9** and **table s6**). The reduction in mean heart rate was sustained (**figure 2**) and premature atrial contractions were reduced to fewer than 100 per 24 h (**figure 2**) in all patients enrolled in the treatment extension period; the premature atrial contractions completely subsided in three (43%) of seven children assessed over the treatment extension period. Atrial fibrillation was present in one child at baseline, but not at months 12 or 36. The improvement in bodyweight-for-age *Z* score was maintained, with a mean increase of 0·52 SDs (95% CI 0·02–1·02) at month 12 and 0·62 (0·12–1·12) at month 32, relative to baseline. Bodyweight (**figure 2**), height, and BMI trajectories improved relative to their anticipated natural course in seven (88%) of the eight paediatric patients (**figure s10**). Improvements on circulating tissue markers of thyroid hormone action were maintained in the long-term treatment extension period.

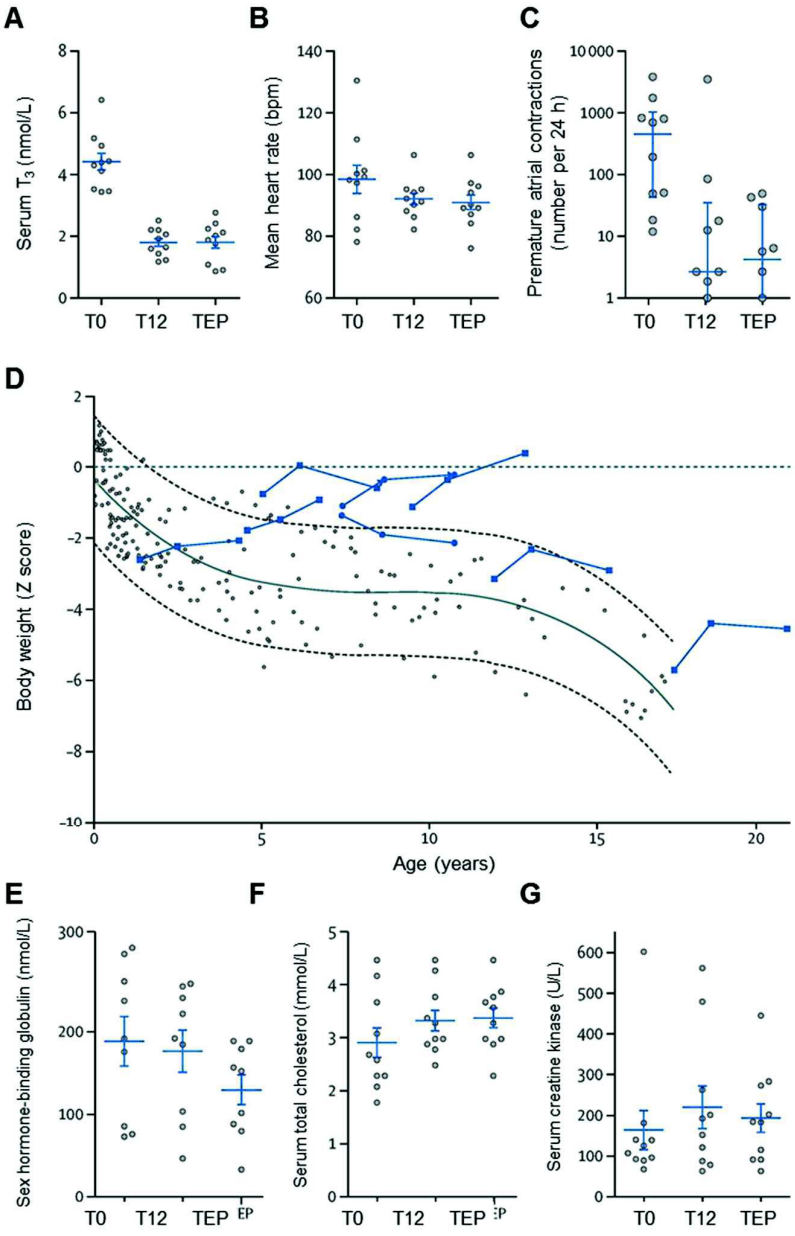

Figure 2. Change from baseline to month 12 and to the end of the treatment extension period in post-hoc outcome measures. Data are changes in serum T_3 concentration (**A**); mean heart rate, determined by 24-h cardiac monitoring (**B**); premature atrial contractions (**C**); bodyweight, as bodyweight-for-age *Z* scores, relative to the natural course of bodyweight development in MCT8 deficiency (represented by a trend line with 95% error band and grey dots of individual historical measurements) and based on historical measurements from growth charts and medical records of the enrolled patients before starting treatment. The trend line (blue) consists of baseline, month 12, and TEP values. (**D**); sex-hormone binding globulin concentrations (**E**); serum total cholesterol (**F**); and creatine kinase concentrations, all across T0, T12, and the TEP following treatment with tri-iodothyroacetic acid. Grey dots represent individual patient measurements, and the mean and SE (**A**, **E**, **F**) and the median and IQR (**B**,**C**,**G**) are shown in blue. The TEP ranged from 26 to 42 months (median length 40·4 months [38·1–41·3]). Data and p values are shown in **table 2**. T_3=tri-iodothyronine. T0=baseline. T12=month 12. TEP=treatment extension period.

DISCUSSION

In this investigator-initiated, international, multicentre trial in patients with MCT8 deficiency, Triac treatment resulted in effective reduction in serum T_3 concentrations, as well as improvements in clinically relevant outcome measures, including bodyweight, heart rate and rhythm, blood pressure, and biochemical markers of thyroid hormone action in different tissues.

During treatment with Triac, serum T_3 concentrations decreased, with 78% of patients achieving serum T_3 concentrations within the normal range by 4 months of treatment, requiring a mean dose of 38·3 µg/kg per day. This effect was maintained in those patients enrolled in the treatment extension period.

Many key clinical outcomes improved during the 12 months of Triac treatment, of which 8 months was at a maintenance dose. Bodyweight-for-age *Z* score increased and patients enrolled in the treatment extension period showed a reversal of the natural course of the disorder, which is typically accompanied by progressive deterioration of bodyweight and often necessitates enteral tube feeding. In this vulnerable population, being severely underweight is associated with adverse clinical outcomes, including an increased risk of infections (19). Heart rate decreased predominantly in patients who had an increased heart rate at baseline, in whom such a reduction is the most clinically relevant. Systolic blood pressure decreased, and hypertension was resolved in most patients receiving Triac treatment. Premature atrial complexes, which are more prevalent in patients with hyperthyroidism (20), also subsided in most participants. The high frequency of premature atrial complexes that is present in untreated patients is uncommon in healthy individuals, particularly in children (21), and premature atrial complexes predispose individuals to other arrhythmias and cardiac death (22-24). Indeed, sudden death is a frequent cause of death in patients with MCT8 deficiency and, in one patient in our study, an episode of atrial fibrillation was recorded during baseline assessment. Thus, improving bodyweight and cardiovascular status could ameliorate important risk factors for premature death in MCT8 deficiency.

Triac treatment was associated with reversal of the hypermetabolic state in different tissues (liver, kidney, and muscle), reflected by a reduction in serum sex hormone-binding globulin concentrations and an increase in serum creatinine and creatine kinase concentrations. The positive clinical and biochemical outcomes were sustained in the subgroup of patients in the long-term treatment extension period. Apart from a decrease in serum T_3 concentrations, consistent positive clinical and biochemical outcomes were not seen in an observational study (25) in which four patients were treated with di-iodothyropropionic acid (DITPA); with this treatment, free T_4 and reverse T_3 concentrations increased and TSH concentrations remained unchanged, whereas, with Triac treatment, TSH concentrations decreased with a concomitant reduction in free T_4, T_3, and total reverse T_3 concentrations. These differential changes in thyroid function tests might point to a different mode of action of DITPA versus Triac.

The consistent reduction in serum T_3 concentrations coincided with improvements in bodyweight, cardiovascular status, and markers of thyroid hormone action in different tissues. Although our study design, including the absence of a control group and open-label design, does not enable us to prove causality, the observed unidirectional changes in serum T_3 concentrations can likely be attributed to Triac treatment, given the substantial evidence from preclinical and clinical studies on the effects of Triac (11).

The mean Triac dose used in our trial was within the range used in previous clinical studies to restore euthyroidism in patients (23–48 μg/kg per day) (11, 26, 27). Therefore, the thyromimetic effects of Triac in peripheral organs probably compensate adequately for the observed reduction in serum T_4 concentrations. This suggestion is supported by the absence of clinical and biochemical signs of hypothyroidism, which was actively monitored for throughout the study.

It is unknown whether the further reduction in circulating T_4 concentrations under Triac treatment aggravates the hypothyroid state in the brain in people with MCT8 deficiency (28, 29). Although MCT8 is believed to be the primary transporter that facilitates both T_3 and T_4 transport across the human blood–brain barrier, we cannot exclude a contribution of other factors (30). In several animal models that recapitulate the neuromotor phenotype of human MCT8 deficiency, Triac has resolved brain hypothyroidism and enabled brain development to progress as normal (9, 14). Our trial was not designed to detect whether Triac also modulates neurodevelopment in human MCT8 deficiency, since the study did not include specific neurodevelopmental outcomes and enrolled patients of all ages. Therefore, most patients studied would have passed the small window of opportunity to modulate brain development. A phase 2 trial (NCT02396459; not yet recruiting) will investigate the effects of Triac on neurodevelopmental outcomes in very young children.

The most commonly reported adverse events were all deemed to be consequences of MCT8 deficiency and unrelated to the intervention. Triac treatment only transiently increased signs of mild hyperthyroidism (perspiration and irritability) after commencement or dose adjustment of treatment in a few patients. Although data from some previous studies (27, 31) have suggested that Triac could increase bone resorption, we identified only marginal increases in bone turnover markers that followed the physiological changes observed during development in children and were not accompanied by noticeable changes in bone mineral density. Although our findings suggest that Triac treatment is generally well tolerated, the acquisition of additional safety data in consecutive trials is warranted to extend knowledge of drug safety in this population.

Since we did not select for patient characteristics, the study population comprises a heterogeneous sample that constitutes a large proportion of identified patients with the condition—as such, the study population is representative of routine clinical practice. Inherent to studies in such a heterogeneous population, the effect size of outcomes varied within the study cohort, suggesting inter-individual variation in degree of benefit between patients. The small sample size did not allow identification or statistical control for factors other than the intervention that might modulate treatment effects. Another limitation was the small number of adult patients enrolled in the study, as a consequence of high mortality during childhood. Moreover, the low physical and cognitive abilities of the participants, a feature that is inherent to the disorder, precluded recording some study parameters in all patients. Together with study withdrawals, this issue might have, unavoidably, caused selection bias in the data used for statistical analyses.

Severe underweight and cardiovascular dysfunction are important clinical sequelae of chronic peripheral thyrotoxicosis, causing significant morbidity and mortality in patients with MCT8 deficiency. The results of our study suggest that several key features related to the peripheral phenotype of MCT8 deficiency are alleviated under Triac treatment in paediatric and adult patients.

Acknowledgements

Our study was funded by the Netherlands Organisation for Health Research and Development (project number 113303005; to WEV), the Sherman Foundation (to WEV), the NeMO Foundation (to IFMdC), the Wellcome Trust (210755/Z/18/Z; to KC) the UK National Institute for Health Research Cambridge Biomedical Centre (to CM and KC), Toulouse University Hospital (to IOP), and the Italian MCT8 family association Una Vita Rara ONLUS (to DT). The centres in Rotterdam, Berlin, Paris, and Toulouse are part of the European Reference Network on rare endocrine conditions (Endo-ERN). We thank Laboratoires Théranol-Deglaude and Rare Thyroid Therapeutics for providing the study drug. Teun van Gelder and Wouter W de Herder (both from the Erasmus Medical Center, Rotterdam, Netherlands) served on the data safety monitoring board, alongside WEV (who had no voting rights in formal decisions or recommendations). We thank Arjanne Aleman (Erasmus Medical Centre) for logistical support for the trial, John Bekhuis and René Grijsen (Saxenburg Groep, Hardenberg, The Netherlands), and Selmar Leeuwenburgh, Monique de Waart, Ronald van der Wal, Hans van Toor, and all members of the trial laboratory and endocrinology diagnostic laboratory of the Erasmus Medical Centre for their dedicated assistance in the coordination and execution of all laboratory procedures. We also thank Petra de Haan (Erasmus Medical Centre) for the analyses of the 24-h cardiac monitoring, Sandra Smits and Els van Zaanen (Erasmus Medical Centre) for performing and interpreting dual-energy X-ray absorptiometry scans, the Erasmus Medical Centre trial pharmacy for logistical support in the distribution of the trial medication, and the trial information technology facility of the Erasmus Medical Centre for their technical support in the use of the trial information technology facilities. We also thank the Nuclear Medicine Unit of Fondazione IRCCS Istituto Nazionale dei Tumorifor (Milan, Italy) for the performance of and interpretation of dual-energy X-ray absorptiometry scans and the Italian MCT8 family association Una Vita Rara ONLUS for the financial support for shipments, cardiac evaluations, and dual-energy X-ray absorptiometry scans. Finally, we thank the patients and their families and caregivers who participated in this trial.

SUPPLEMENTARY MATERIAL

See next page.

Supplementary methods

It is well known that Triac interferes in all immuno-based assays employed in clinical practice. To account for this interference, an algorithm was employed based on the differential level of cross-reactivity of Triac in two widely used T3 assays (Vitros and Immulite). By spiking stripped serum with known concentrations of T3 and Triac, or their combination, correction factors were established which were used in the formulas below.

Formula 1

$T3_{method1} = a*[T3]+b*[Triac]$

Formula 2

$T3_{method2} = c*[T3]+d*[Triac]$

Based on formula 1 and 2, formula 3 and 4 can be deduced to calculate unknown T3 and Triac concentrations based on the results of two independent T3 assay.

$T3 = (d* T3_{method1} – b* T3_{method2})/(da-bc)$

$Triac = (a* T3_{method2} – c* T3_{method1})/(ad-cb)$

To minimise the interference of Triac in the T3 assays, blood samples were collected in the morning before the administration of the morning Triac dose (which was administrated afterwards). This procedure resulted in a minimum washout time of ~8h. With a half-life time of 6.5h, Triac concentrations in the blood are expected at their lowest levels (32). We did not measure the (peak) levels of Triac achieved in the blood due to the absence of commercially available assays.

Supplemental tables

Table S1 Overview of inclusion, exclusion, and withdrawal criteria	
Inclusion criteria:	1. A clinically relevant mutation in the *MCT8* (*SLC16A2*) gene.
Exclusion criteria:	1. Major illness or recent major surgery (within 4 weeks) unrelated to MCT8 deficiency; 2. Participation in ongoing RCTs of therapeutic interventions (including clinical trials of investigational medicinal products); 3. Known allergy to components in Triac tablets; 4. Patients that have any contraindication for Triac treatment.
Withdrawal criteria	1. At wish of parent or guardians 2. Continued participation in the study could be harmful to the subject's health, due to occurrence of DLTs 3. The subject does not take, or is unable to take, the study medication as instructed, does not keep appointments, or otherwise does not adhere to protocol requirements. 4. The study is terminated prematurely by the investigator, research institution, sponsor, IRB. 5. Loss to follow-up.

RCT=randomised controlled trial. DLT=dose-limiting toxicity. IRB=institutional review board.

Table S2 Overview of predefined study parameters and timing of measurement

Visit type	**Baseline**	**Dose-escalation**	**Treatment period**	**End-study**	**Extended End-study**
Name Measure or event \ Months	**M0**	**~M0-M3**	**~M4-M12**	**M12**	**Mx [12]**
Medical History and demographics	x				
Triac dose		x	x	x	x
Patient characteristics (age, sex, race, feeding tube)	x				
Concomitant medications [1]	x	x	x	x	x
Primary efficacy measures					
Total Triiodothyronine (T3)	x	x	x	x	x
Co-primary outcome					
Free Thyroxine fraction (FT4)	x	x	x	x	x
Total thyroxine (TT4)	x	x	x	x	x
Thyroid Stimulating Hormone (TSH)	x	x	x	x	x
Reverse triiodothyronine (rT3)	x	x	x	x	x
Secondary Efficacy Endpoints					
Bodyweight	x	(x)	(x)	x	x
Heart rate at rest (by ECG)	x			x	x
Mean heart rate (by 24h cardiac monitoring)	x			x	x
Systolic blood pressure [2]	x	(x)	(x)	x	
Diastolic blood pressure [2]	x	(x)	(x)	x	
Serum total cholesterol	x	x	x	x	x
Serum sex hormone binding globulin (SHBG)	x	x	x	x	x
Serum creatine kinase (CK)	x	x	x	x	x
Energy expenditure (by DLW) [3]	x			x	
Visit type	Baseline	Dose-escalation	Treatment period	End-study	Extended End-study
Name Measure \ months	M0	M0-M3	M4-M12	M12	Mx 12
Exploratory Measures					
Body height	x	(x)	(x)	x	x
BMI	x	(x)	(x)	x	x
Chemistry and endocrine laboratory measures 4	x			x	x
Gross motor function (by GMFM-88) 5	x			x	x
Cognition (by BSID III) 5	x			x	x
Gross motor function (by BSID III) 5	x			x	x
Fine motor function (by BSID III) 5	x			x	x
Expressive language (by BSID III) 5	x			x	x
Receptive language (by BSID III) 5	x			x	x
Adaptive behaviour (by VABs II) 5	x			x	x
Physical exam 6	x			x	x
General Safety Measures					
Adverse events	x	x	x	x	x

Table S2 Overview of predefined study parameters and timing of measurement (continued)

Serious adverse events	x	x	x	x	x
Treatment related adverse events 7	x	x	x	x	x
Treatment related serious adverse events 7	x	x	x	x	x
Chemistry and haematology laboratory measures 8	x	(x)	(x)	x	x
Treatment-specific Safety Measures					
Bone markers: B-ALP, b-CTx 9	x	x	x	x	x
Bone mineral density (total body, UDR and/or UDU by DXA) 10	x			x	(x)
Cardiac dimension and function (by TTE, ECG) 11	x			x	x
Ventricular arrhythmias (by 24h cardiac monitoring, and ECG)	x			x	(x)
Post-hoc measures					
Total fat mass (by DXA)	x			x	
Fat percentage (by DXA)	x			x	
Total lean body mass (by DXA)	x			x	
Number of premature atrial contractions (by 24h cardiac monitoring)	x			x	x
Bodyweight in kilogram	x			x	

Overview of study measures including timing of assessment (indicated by an x). Assessments that were optional are indicated with an (x).
[1] Concomitant medication was listed at baseline and changes therein at each control visit.
[2]Blood pressure was measured according to standard operating procedures. Effort was taken to measure the blood pressure when the participant was as comfortable as possible. The mean of two independent measurements has been documented to consider natural variability.
[3] Energy expenditure was measured with the doubly labelled water (DLW) technique in a subset of patients in whom the collection of urine was deemed feasible. However, practical limitations in the acquisition of the samples compromised the quality of the assessment. Therefore, results are not reported.
[4] The complete list of pre-defined exploratory chemical and endocrine laboratory measures is provided in the final statistical analysis plan (version 3).
[5] Neuropsychological evaluations were carried out in a subset of study centres based on availability of the test and trained personnel. All tests were performed and scored according to their manual.
[6] The exploratory measures assessed during physical exam were general and neurological parameters and consisted of the assessment of tendon reflexes, the presence of primitive reflexes, and muscle tone.
[7] During each visit specific screening for hypothyroid and hyperthyroid signs and symptoms was applied through general history taking with the primary caregiver of the participant. These signs and symptoms included the presence of diarrhoea, vomiting, excessive perspiration, palpitation, anxiety, and other signs and symptoms attributed to Triac administration by the primary caregiver, and physical examination included heart rate (by palpation of the radial arteria, or by auscultation), the presence of excessive perspiration, general impression of anxiety. Any abnormal findings were recorded as such and no quantitative (descriptive) analyses will be performed.
[8] The complete list of safety chemical and haematology laboratory measures is provided in the final statistical analysis plan (version 3).
[9] At control visits only alkaline phosphatase and b-CTx were determined. Serum was stored to allow analysing P1NP and B-ALP retrospectively if deemed necessary to complement the baseline vs end-study comparison.
[10] DXA scans were performed in a subset of study centres based on local availability of equipment and expertise. Moreover, the acquisition of reliable scans and the type of scans (forearm or total body) was greatly determined by the level of cooperation of the participant. No sedatives were to be used during the procedure. A DXA scan was only repeated in those subjects having a baseline DXA scan of sufficient quality.
[11] Routine transthoracic cardiac ultrasounds (TTE) were performed to assess cardiac structure, dimensions and function at baseline and after Triac treatment.
[12] During the treatment extension period, bi-annual control visits were scheduled to monitor the thyroid function tests and indicated other parameters.
ECG=electrocardiography. DLW=doubly labelled water. GMFM-88=Gross Motor Function Measure-88 [4]. BSID III=Bayley Scales of Infant Development III [5]. VABs II=Vineland Adaptive Behaviour scales II [6]. B-ALP=bone-specific alkaline phosphatase. b-CTx=β-carboxy-terminal collagen crosslinks. UDR=ultra-distal radius. UDU=ultra-distal ulna. DXA=dual-energy X-ray. TTE=trans-thoracic echocardiography.

Table S3 Post-hoc analysis of changes from baseline to month 12 in secondary outcome measures in the full analysis data set

Assessment	N*	Baseline Mean (±SD)*	12-month Mean (±SD)	Difference Mean (95% CI)	P value
Weight for age (z score)	45	-2·85 (±1·90)	-2·63 (±1·74)	0·22 (-0·01- 0·44)	0·061 †
Resting heart rate (bpm)	34	112 (±23)	104 (±17)	-9 (-16 - -2)	0·010
Mean heart rate 24 h (bpm)	31	102 (±14)	97 (±9)	-5 (-9 - -1)	0·012
Blood pressure					
Systolic (mmHg)	35	107 (±9)	103 (±10)	4 (-8 - -1)	0·028
Systolic (Percentile) ‡	35	76 (±26)	61 (±29)	-16 (- 28- -3)	0·013
Diastolic (mmHg)	35	64 (±9)	63 (±10)	-1 (-5 – 3)	0·68
Diastolic (Percentile) ‡	35	71 (±24)	67 (±22)	-4 (-15 – 7)	0·49
SHBG (nmol/L)	44	209 (±88)	177 (±73)	-32 (-50 - -14)	0·0011
Total cholesterol (mmol/l)	45	3·3 (±0·8)	3·4 (±0·7)	0·1 (0·0-0·3)	0·083
CK (U/L) §	45	112 (±98)	168 (±141)	56 (31-82)	<0·0001

*****Pair-wise deletion was used to adjust for missing data that were only captured at baseline and month 12, and the last available measurement was used to adjust for missing data that were captured throughout the study, as outlined in the statistical analysis plan. The number of subjects included in each analysis is specified in the column.

† The full analysis data set includes one subject with intended weight loss (overweight at baseline), post-hoc sensitivity analyses without this subject yields a mean increase in bodyweight-to-age Z score of 0·25 (95% CI 0·03- 0·47), p = 0·03

‡ Percentile scores based on age and body height.

§ Serum CK concentrations were log-transformed to ensure normal distributions before paired T-tests were conducted. Non-transformed means (±SD) and mean changes (95% CI) are presented to increase interpretability.

Table S4 Changes from baseline to month 12 in exploratory neurological and neuropsychological outcome measures

Assessment	Baseline Mean (±SD)	12-month Mean (±SD)	Difference Mean (95% CI)
Clinical – no (%)			
Hyperreflexia	31 (88)	31 (88)	
Hypertonia	27 (77)	29 (83)	
Primitive reflexes	32 (89)	31 (86)	
GMFM-88 (18)- percentage of total score (n=26) *			
Total score (%)	7·1 (3·6-9·2) §	10·4 (6·1-15·7) §	3·3 (1·4-5·2)
BSID III (33)– developmental age in months (n=16) †			
Cognition	3·3 (±1·3)	4·2 (±1·7)	0·9 (0-1·9)
Expressive language	4·6 (±2·2)	6·1 (±2·8)	1·5 (0·2-2·9)
Receptive language	6·6 (±3·7)	8·6 (±2·3)	2·1 (0·2-3·9)
Fine motor	2·5 (±1·6)	3·5 (±2·0)	0·9 (0·1-1·8)
Gross motor	1·0 (±0·7)	2·2 (±1·5)	1·2 (0·7-1·8)
VABs II (34)– raw score (n=26) ‡			
Communication			
Receptive	11·5 (9·8-13·0) §	12·0 (9·8-14·0) §	1·1 (0·2-2·0)
Expressive	11·5 (9·0-13·0) §	12·00 (9-14·5) §	0·1 (-1·5-1·7)
Written	0·0 (0·0-0·0) §	0·0 (0·0-0·0) §	0·0 (0·0-0·0) §
Daily living skills			
Personal	6·0 (5·0-8·0) §	7·5 (5·0-9·0) §	0·8 (-0·3-2·0)
Domestic	0·0 (0·0-0·0) §	0·0 (0·0-0·0) §	0·0 (0·0-0·0) §
Community	0·0 (0·0-0·0) §	0·0 (0·0-2·0) §	0·0 (0·0-0·3) §
Socialisation			
Interpersonal relationships	18·0 (15·0-21·0) §	19·5 (16·0-24·0) §	1·3 (-0·4-2·9)
Play and leisure time	5·0 (3·8-10·0) §	7·0 (4·0-8·5) §	0·5 (-1·2·25) §
Coping skills	0·0 (0·0-3·3) §	0·0 (0·0-2·0) §	0·0 (-2·0-0·0) §
Motor skills			
Gross motor	2·5 (0·0-4·0) §	4·0 (0·8-4·0) §	0·0 (0·0-1·0) §
Fine motor	1·0 (0·0-4·0) §	2·5 (0·8-4·5) §	1·0 (-0·3-2·0) §

Predefined exploratory analysis of the neurological and neuropsychological outcome measures. Reported confidence intervals have not been adjusted for multiplicity, and the intervals should not be used to infer definitive treatment effects·

GMFM-88=Gross Motor Function Measure 88. BSID III=Bayley Scales of Infant Development III. VABs II=Vineland Adaptive Behaviour scales II.

* The GMFM-88 **(18)** assesses the gross motor function in which scores range from 0 to 100%, with higher scores indicating better motor function and where a 100% score is achieved by a normal developing child of 4 years of age.

† The BSID III **(33)** is a multi-scale battery that assesses different aspects of child development. In the study the subscales cognition, expressive language, receptive language, fine motor skills and gross motor skills have been conducted according to the manual. The BSID III measures the developmental age ranging from 16 days to 42 months and 15 days. Scores on the subscales are presented as age equivalent scores representing the developmental age in months.

‡The VABs II **(34)** is a survey which assesses different aspects of development. In the study the subdomains receptive language, expressive language, writing, personal, domestic, community, interpersonal relationships, playing, coping, gross motor and fine motor skills have been assessed. The survey was completed by primary care-givers in presence of a trained neuropsychologist or physician. The VABs II measures the developmental age ranging from birth to 90 years of age. Scores on the VABs II are presented as raw scores.

§ The median and interquartile range is presented due to violation of the normality assumptions for measurements at baseline and month 12 or the change (delta) from baseline to month 12.

Table S5 Post-hoc sensitivity analyses on exploratory neurological and neuropsychological outcome measures stratified by age

	<4 years			4-10 years			11+ years		
	T0	**T12**	**delta**	**T0**	**T12**	**delta**	**T0**	**T12**	**delta**
Clinical – no (%)									
Hyperreflexia	6 (75)	8 (100)	2 (25)	15 (94)	13 (81)	-2 (13)	10 (91)	10 (91)	-
Hypertonia	8 (100)	7 (88)	-1 (12)	12 (75)	14 (88)	2 (13)	7 (64)	8 (73)	1 (9)
Primitive reflexes	7 (100)	7 (100)	-	13 (77)	12 (71)	1 (6)	12 (100)	12 (100)	-
GMFM-88 (18)*- percentage of total score									
N		7			8			9	
Total score (%)	5·7 (±2·0)	14·3 (±6·2)	8·6 (3·6-13·6)	7·8 (±3·3)	8·9 (±4·2)	1·1 (-0·9 – 3·0)	5·6 (±5·1)	7·1 (±6·3)	1·5 (-0·7-3·8)
BSID III (33)† – developmental age in months									
N		2			8			6	
Cognition	3·0 (±1·9)	5·0 (±0·0)	2·1 (0·7-3·4) §	3·6 (±0·7)	4·8 (±1·9)	1·2 (-0·3-2·7)	3·0 (±1·9)	3·2 (±1·1)	0·2 (-1·6–1·9)
Expressive language	3·6 (±1·4)	5·8 (±1·7)	2·2 (2·0-2·4) §	4·9 (±2·3)	7·2 (±3·5)	2·4 (0·2-4·5)	4·5 (±2·5)	4·7 (±1·1)	0·2 (-2·3-2·8)
Receptive language	4·7 (± 1·9)	7·5 (±0·7)	2·9 (2·0-3·7) §	7·2 (±3·1)	10·1 (±4·1)	2·9 (0·0 - 5·8)	6·4 (±4·9)	8·3 (±2·2)	1·9 (-3·1-6·9)
Fine motor	2·4 (± 2·7)	3·7 (±0·9)	1·3 (0·0-2·5) §	3·2 (±1·5)	4·3 (±2·4)	1·1 (-0·1-2·3)	1·7 (±1·3)	2·3 (±1·3)	0·7 (-1·3-2·6)
Gross motor	1·8 (± 1·8)	4·2 (±2·6)	2·4 (1·8-3·0) §	1·0 (±0·6)	2·5 (1·1)	1·5 (0·8-2·3)	0·7 (±0·3)	1·1 (±1·0)	0·4 (-0·3-1·1)
VABS II (34)‡ – raw score									
N		5			10			9	
Communication									
Receptive	11 (± 3·7)	12·4 (±5·2)	1·0 (-1·5-4·5) §	11·1 (±2·5)	11·9 (±3·1)	0·8 (-0·8-2·4)	10·2 (±2·5)	11·3 (±3·6)	1·1 (-0·5-2·7)
Expressive	10·8 (±6·9)	11·6 (±4·5)	2·0 (-3·5-4·5) §	12·1 (±1·4)	12·5 (±4·2)	0·4 (-2·5-3·3)	10·2 (±4·4)	10·9 (±4·1)	0·7 (-0·7-2·0)
Written	0·0 (±0·0)	0·0 (±0·0)	-	0·0 (±0·0)	0·0 (±0·0)	-	0·0 (±0·0)	0·0 (±0·0)	-
Daily living skills									
Personal	4·6 (±2·6)	5·0 (±3·0)	0·0 (-3·0-4·0) §	6·9 (±3·8)	7·9 (±3·4)	1·0 (-0·3-2·3)	6·4 (±2·4)	7·6 (±4·4)	1·1 (-1·5-3·7)
Domestic	0·0 (±0·0)	0·0 (±0·0)	-	0·0 (±0·0)	0·0 (±0·0)	-	0·0 (±0·0)	0·0 (±0·0)	-
Community	0·0 (±0·0)	0·8 (±1·1)	0·0 (0·0-2·0) §	0·4 (±0·8)	0·9 (±1·5)	0·5 (-0·4-1·4)	0·0 (±0·0)	0·2 (±0·7)	0·2 (-0·3-0·7)
Socialisation									
Interpersonal relationships	19·0 (±1·0)	18·6 (±2·4)	0·0 (-2·0-1·0) §	19·5 (±5·3)	20·1 (±5·2)	0·6 (-1·7-1·4)	16·4 (±4·1)	19·1 (±4·3)	2·7 (0·0-5·3)
Play and leisure time	4·0 (±1·6)	6·6 (±1·7)	2·0 (1·0-4·5) §	8·7 (±4·1)	8·1 (±3·5)	-0·6 (-2·4-1·2)	3·6 (±1·7)	5·0 (±2·9)	1·4 (-0·2-3·1)
Coping skills	0·4 (±0·9)	1·8 (±3·0)	0·0 (0·0-3·5) §	1·8 (±2·4)	1·2 (±2·1)	-0·6 (-1·7-0·5)	1·1 (±1·5)	0·1 (±0·3)	-1·0 (-2·0-0·0)
Motor skills									
Gross motor	3·4 (±1·9)	3·8 (±2·6)	1·0 (-1·5-2·0) §	2·3 (1·9)	3·1 (±1·5)	0·8 (-0·5-2·1)	1·6 (±2·2)	1·9 (±2·4)	0·3 (-0·3-1·0)
Fine motor	2·6 (±1·5)	3·8 (±1·5)	2·0 (-1·0-3·0) §	1·6 (±2·1)	3·4 (±3·6)	1·8 (0·3-2·1)	1·3 (±2·0)	2·7 (±4·8)	1·3 (-1·0-3·6)

Post-hoc sensitivity analyses on the exploratory neurological and neuropsychological outcomes in different age groups. These additional analyses were required due to the broad age range of included participants (0·8-66·8 years) to explore if the changes in neurological and neuropsychological outcomes differ with age. These post-hoc analyses were restricted to patients with a severe inactivating mutation and hence two patients with a proven mild mutation (p.F501del and p.L492P) were excluded. Reported confidence intervals have not been adjusted for multiplicity, and the intervals should not be used to infer definitive treatment effects.

GMFM-88=Gross Motor Function Measure 88. BSID III=Bayley Scales of Infant Development III. VABs II=Vineland Adaptive Behaviour scales II (see legend of **table s4** for a brief description of these neuropsychological assessments).

§ The median and interquartile range is presented due to violation of the normality assumptions for measurements at baseline and month 12 or the change (delta) from baseline to month 12. T0=baseline. T12=12-month.

Table S6 Changes from baseline to TEP in primary and secondary outcome measures in patients enrolled in the long-term treatment extension period

Assessment	Baseline Mean (±SD)*	12-month Mean (±SD)	Mean change from baseline (95% CI)	TEP Mean (±SD)	Mean change from baseline (95% CI)	P value †
Primary efficacy measures						
T3 (nmol/l)	4·41 (±0·92)	1·80 (±0·45)	-2·61 (-3·24 – -1·97)	1·81 (±0·65)	-2·59 (-3·35- -1·84)	<0.0001
TSH (mU/l) ‡	3·25 (±1·9)	1·06 (±0·88)	-2·19 (-3·31- -1·08)	1·32 (±1·04)	-1·93 (-3·13 - -0·73)	<0.0001
Free T4 (pmol/l)	8·48 (±3·09)	3·34 (±1·79)	-5·14 (-6·61- -3·67)	4·01 (±1·71)	-4·47 (-6·04 – -2·90)	<0.0001
Total T4 (nmol/l)	54·0 (±11·3)	25·0 (±8·1)	-29·0 (-35·6- -22·4)	24·8 (±8·1)	-29·2 (-37·1 – -21·3)	<0.0001
Reverse T3 (nmol/l)	0·13 (±0·06)	0·05 (±0·04)	--0·08 (-11- -0·05)	0·05 (±0·03)	-0·08 (-0·11 – -0·04)	<0.0001
Secondary efficacy measures						
Weight to age (z score)	-2·18 (±1·54)	-1·62 (±1·31)	0·56 (0·19- 0·92)	-1·52 (±1·39)	0·66 (0·08- 1·24)	0.029
Mean heart rate 24 h (bpm) §	98 (±15)	92 (±6)	-6 (-14-1)	91 (±8)	-7 (-16-1)	0.072
SHBG (nmol/L)	176 (±86)	165 (±74)	-12 (-37-14)	121 (±52)	-55 (-98 - -12)	0.018
Total cholesterol (mmol/l)	2·9 (±0·9)	3·4 (±0·7)	0·4 (0·1-0·8)	3·4 (±0·6)	0·5 (0·0 – 0·9)	0.053
CK (U/L) ‡	165 (±157)	221 (±171)	56 (-19-131)	194 (±116)	29 (-36-94)	0.14

***** Provided data at baseline and month 12 is restricted to those subjects (n=10) enrolled in the long-term treatment extension period (TEP). The median [IQR] treatment time was 40·4 [38·1-41·3] month.

† Paired T-tests were used to detect significant changes from baseline to the end of the treatment extension period (TEP).

‡Serum TSH and CK concentrations were log-transformed to ensure a normal distributions before paired T-tests were conducted. Non-transformed means (±SD) and mean changes (95% CI) are presented to increase interpretability.

§ Measured by 24h ambulatory cardiac monitoring.

Table S7 Overview of adverse events by system organ class and preferred term

	Number	**(%)**	**E**
Total number of subjects	46	(100)	
All adverse events	43	(93)	150
Blood and lymphatic system disorders			
Anaemia	3	(7)	3
Gastrointestinal disorders			
Diarrhoea	5	(11)	5
Gastroenteritis	11	(24)	12
Obstipation	2	(4)	4
Vomiting	5	(11)	5
Gastro-oesophageal reflux disease (aggravation)	1	(2)	1
Enterocolitis	1	(2)	1
General disorders and administration site conditions			
Influenza (like illness)	9	(20)	12
Hyperthermia	1	(2)	1
Sweating	3	(7)	4
Multiple organ dysfunction syndrome	1	(2)	1
Hepatobiliary disorders			
Hepatic failure	1	(2)	1
Immune system disorders			
Allergic rhinitis	1	(2)	1
Bronchospasm	1	(2)	1
Dermatitis atopic	1	(2)	1
Autoimmune thyroid disorder	1	(2)	1
Infections and infestations			
Bronchitis	6	(13)	6
Chickenpox	1	(2)	1
Otitis media	5	(11)	5
Pneumonia	2	(4)	3
Otitis media chronic	1	(2)	2
Clostridium difficile infection	1	(2)	2
Injury, poisoning and procedural complications			
Hip dislocation	2	(4)	2
Hip fracture	1	(2)	1
Bone fracture (not spontaneous)	1	(2)	1
Accidental injury	1	(2)	1
Investigations			
Gastroscopy	1	(2)	1
Nervous system disorders			
Seizures (increase)	4	(9)	5
Dystonia aggravated	2	(4)	2
Procedural related injuries and complications NEC			
Stoma site erythema	2	(4)	3
Product issues			
Device malfunction *	2	(4)	2
Psychiatric disorders			
Anxiety	1	(2)	1
Nightmare	1	(2)	1
Irritability	2	(4)	2
Renal and urinary tract disorders			
Urinary tract infection	3	(7)	3
Respiratory, thoracic and mediastinal disorders			
Nasopharyngitis	11	(24)	14
Cough	3	(7)	3

Table S7 Overview of adverse events by system organ class and preferred term (continued)			
Hypoventilation	2	(4)	2
Pharyngitis	3	(7)	3
Respiratory distress	1	(2)	2
Upper respiratory tract Infection	9	(20)	9
Rhinitis	1	(2)	1
Bronchiolitis	4	(9)	4
Scoliosis (progression)	3	(7)	4
Skin and subcutaneous disorders			
Dermatitis	1	(2)	1
Rash	1	(2)	1
Impetigo	2	(4)	2
Viral rash	2	(4)	2
Surgical and medical procedures			
Endodontic procedure	1	(2)	1
Hip surgery	1	(2)	1
Drug therapy	1	(2)	2

Adverse events were classified according system organ class and preferred term using the Medical Dictionary for Regulatory Activities (MedDRA). * ventriculoperitoneal shunt malfunction and ruptured PEG tube.

Table S8 Changes from baseline to month 12 in predefined safety measures

Assessment	Baseline Mean ±SD	N out of range / total N	12-month Mean ±SD	N out of range / total N	Difference Mean (95% CI)
Abnormal cardiac dimension and function *	-	1/46	-	0/37	-
Ventricular arrhythmias	-	0/45	-	0/39	-
BMD forearm UDR (g/cm^2) †	0·263 (±0·23)	n·a·	0·292 (±0·041)	n·a·	0·029 (-0·010 -0·068)
BMD forearm UDU (g/cm^2) †	0·220 (±0·039)	n·a·	0·241 (±0·051)	n·a·	0·021 (-0·011 -0·054)
BMD total body (g/cm^2) †	0·654 (± 0·12)	n·a·	0·662 (±0·12)	n·a·	0·008 (-0·034 – 0·050)
β-CTx (µg/l)	0·98 (±0·38)	4/43	1·12 (±0·38)	5/43	0·14 (0·03-0·25)
B-ALP (µg/l) ‡	48·0 (±24·5)	5/38	56·4 (±23·1)	6/38	8·4 (2·7-14·1)
PINP (µg/l) §	347 (±235)	11/37	522 (±290)	7/37	175 (110-241)
ALT (U/l)	40 (±230	21/45	34 (±17)	16/45	-6 (-11 - -1)
AST (U/l)	39 (±15)	5/39	38 (±11)	4/39	-1 (-5 -2)
Gamma-GT (U/l)	27 (±28)	13/38	24 (±24)	11/38	-4 (-6 - -1)
Haemoglobin mmol/l ¶	7·95 (±0·95)	0/28	7·73 (±1·07)	3/28	-0·22 (-0·48 – 0·03)
Leukocytes ($x10^9/l$)**	7·5 (±2·0)	1/21	5·8 (±1·8)	3/21	-1·8 (-2·9 - -0·6)
Thrombocytes ($x10^9/l$) ††	268 (±87)	6/26	250 (±73)	3/26	18 (-45 – 10)
Glucose (mmol/l)	4·9 (±1·0)	2/27	4·9 (±0·9)	0/27	0·0 (-0·5 – 0·4)
Urea (mmol/l)	4·5 (±1·7)	6/45	4·1 (±1·1)	2/45	-0·4 (-0·9 – 0·1)
Potassium (mmol/l)‡‡	4·3 (±0·2)	0/45	4·4 (±0·4)	2/45	0·0 (-0·1 – 0·1)
Sodium (mmol/l)	142 (±3)	4/45	141 (±3)	2/45	0 (-1 – 1)
Calcium (mmol/l)	2·45 (±0·09)	3/39	2·43 (±0·06)	0/39	-0·02 (-0·05 – 0·01)

Except for cardiac safety parameters, the means (±SD) of pre-specified safety parameters are presented for those patients in the safety population with data available at baseline and at least one subsequent measurement. Reported confidence intervals have not been adjusted for multiplicity, and the intervals should not be used to infer definitive treatment effects.

* One patient presented a clinically relevant persistent ductus Botalli requiring closure before treatment with Triac was initiated.

† Reference ranges for children of these ages were not available.

‡ Available reference ranges from the Mayo Clinic Laboratories [7] were used for the paediatric patients. B-ALP exceeded the reference range in 4 adolescent patients at baseline and were below the reference range in 1 paediatric patient. At month 12, B-ALP concentrations were below the reference range in 1 paediatric patient and (marginally) increased in 5 adolescent patients.

§ Available references ranges from Crofton et al. [8] were used for the paediatric patients. P1NP levels were below the normal range for age in 9 patients (all children) and above normal range for age in 2 patients at baseline; 5 patients had P1NP levels exceeding the normal range for age at month 12 of whom 2 had a delayed onset of puberty, and 2 patients had P1NP levels below the normal range for age (both children) at month 12.

¶ Two out of three patients who had a mild anaemia (0-5% under lower limit) at month 12, had hemoglobulin concentrations just above the lower limit of normal at baseline which decreased by only 0.2-0.3 mmol/L. There was no clear relationship between Triac dose and change in Hb concentrations or between changes in T3 concentrations versus change in Hb concentrations.

** One patient had mild leucopenia at baseline and 3 patients had mild leucopenia at month 12 (maximal 0-10% below the lower limit of the normal range).

†† One patient had thrombocytosis and five had thrombocytopenia at baseline, one of these patients still had thrombocytopenia at month 12. One patient with borderline normal thrombocyte levels developed mild thrombocytopenia at month 12. In addition, one patient developed mild thrombocytosis.

‡‡ Both patients had a mild and isolated hyperkalaemia (0.1 mmol/L above reference range) at month 12 and had been normal in previous and subsequent measurements.

BMD=bone mineral density. UDR=ultra-distal radius. UDU=ultra-distal ulna. β-CTx=β-C-terminal telopeptide. B-ALP=bone-specific alkaline phosphatase. PINP=Procollagen I Intact N-Terminal. ALT=alanine aminotransferase. AST=aspartate aminotransferase. Gamma-GT=gamma-glutamyl transferase.

Supplemental figures

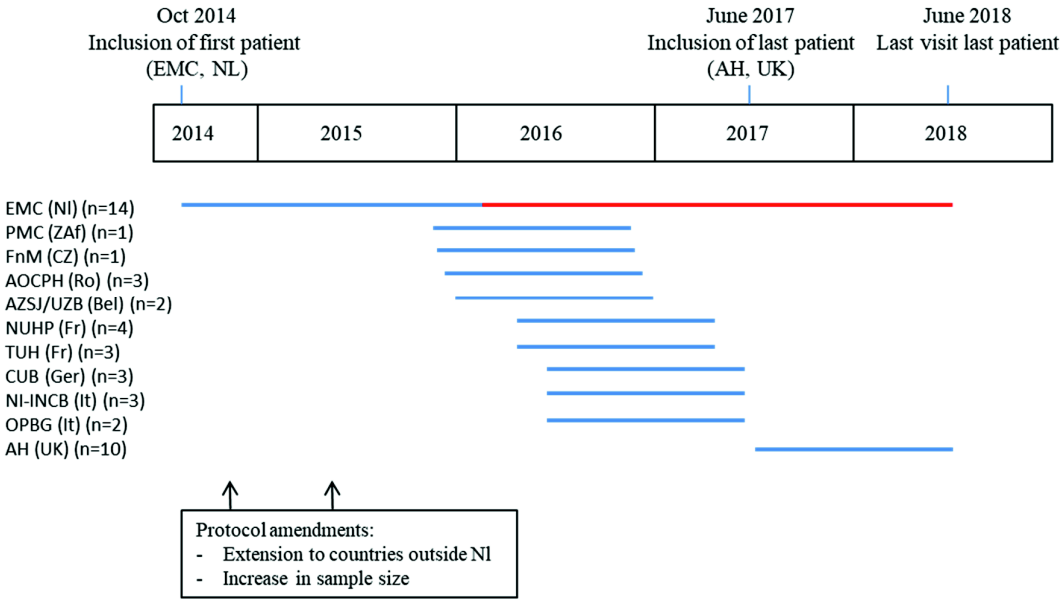

Figure s1. Overview of number and timing of inclusions per study centre

Overview of number and timing of inclusions per study centre. Blue lines denote the time span in which patients have been enrolled and treated in the context of the Triac Trial study protocol (T0 to T12) in the indicated study centres. The red line denotes the treatment extension period offered to patients erolled in the EMC (Nl). The timing and the main content of the protocol amendments has been indicated. EMC=Erasmus Medical Centre. Nl=Netherlands. PMC=Panorama Medical Centre. ZAf=Republic of South Africa. M=Fakultní nemocnice v Motole. CZ=Czech Republic. AOCPH=Alexandy Obregia Clinical Psychiatric Hospital. Ro=Romania. AZSJ=AZ Sint-Jan. UZB=UZ Brussel. Bel=Belgium. NI=Necker University Hospital Paris. Fr=France. TUH=Toulouse University Hospital. Char=Charite-Universitätsmedizin Berlin. Ger=Germany. INCB=U.O. Neuropsichiatria Infantile–Instituto Neurologica Carlo Besta. It=Italy. OPBG=Ospedale Pediatrico Bambino Gesù. AH=Addenbrooke`s Hospital, Cambridge. UK=United Kingdom.

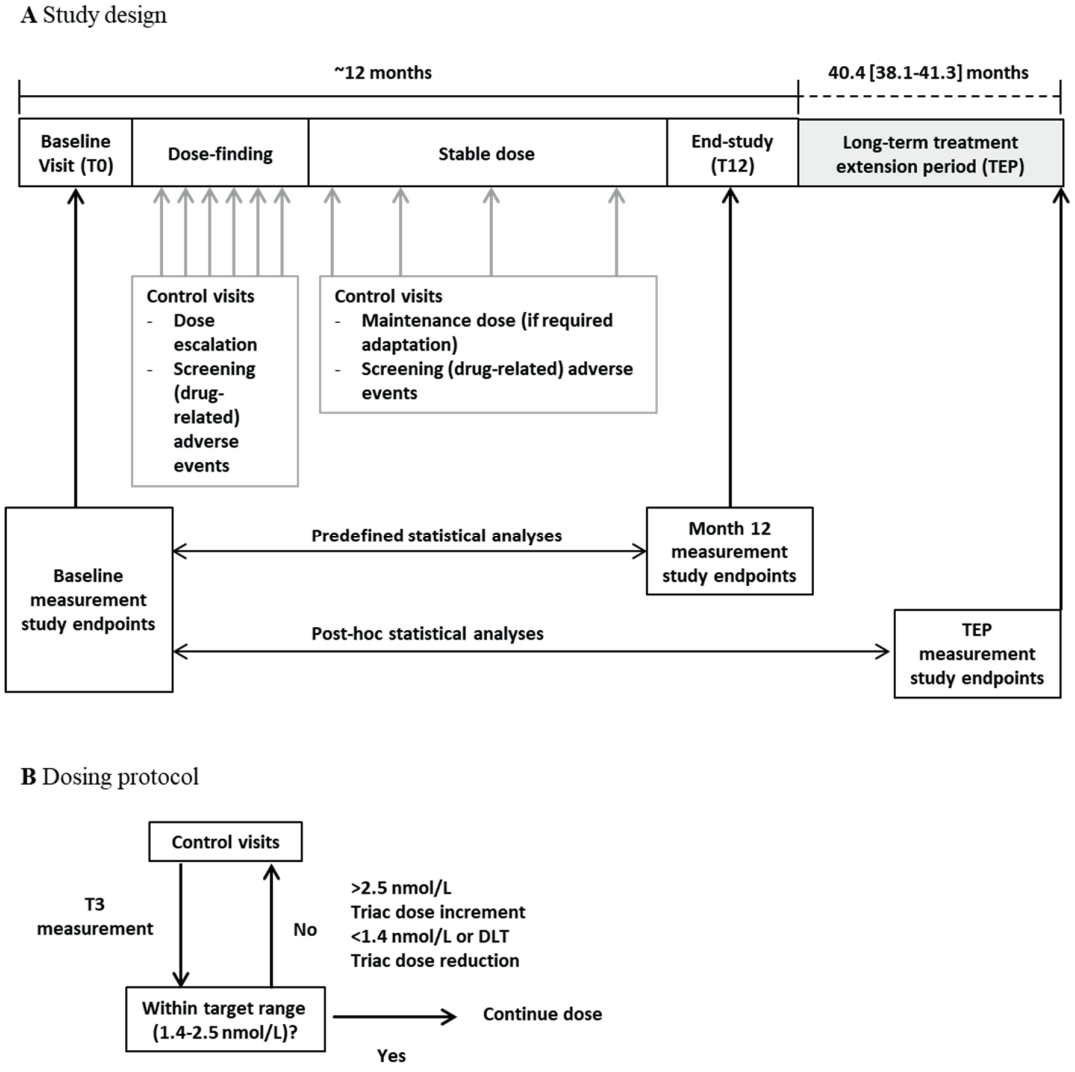

Figure s2. Triac Trial study design and dosing protocol

Panel **A** provides a chart of the study design. Panel **B** shows the predefined dosing protocol that has been used during the trial. DLT=dose-limiting toxicity.

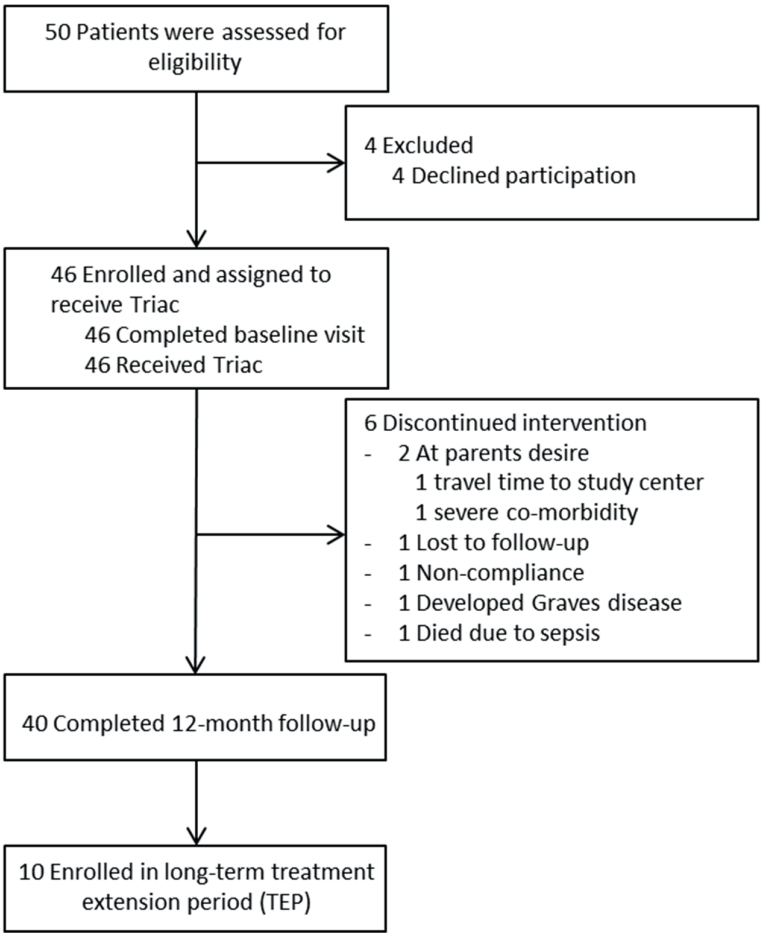

Figure s3. Triac Trial study flow chart

The flow chart shows the screening, enrolment, treatment and follow-up of patients.

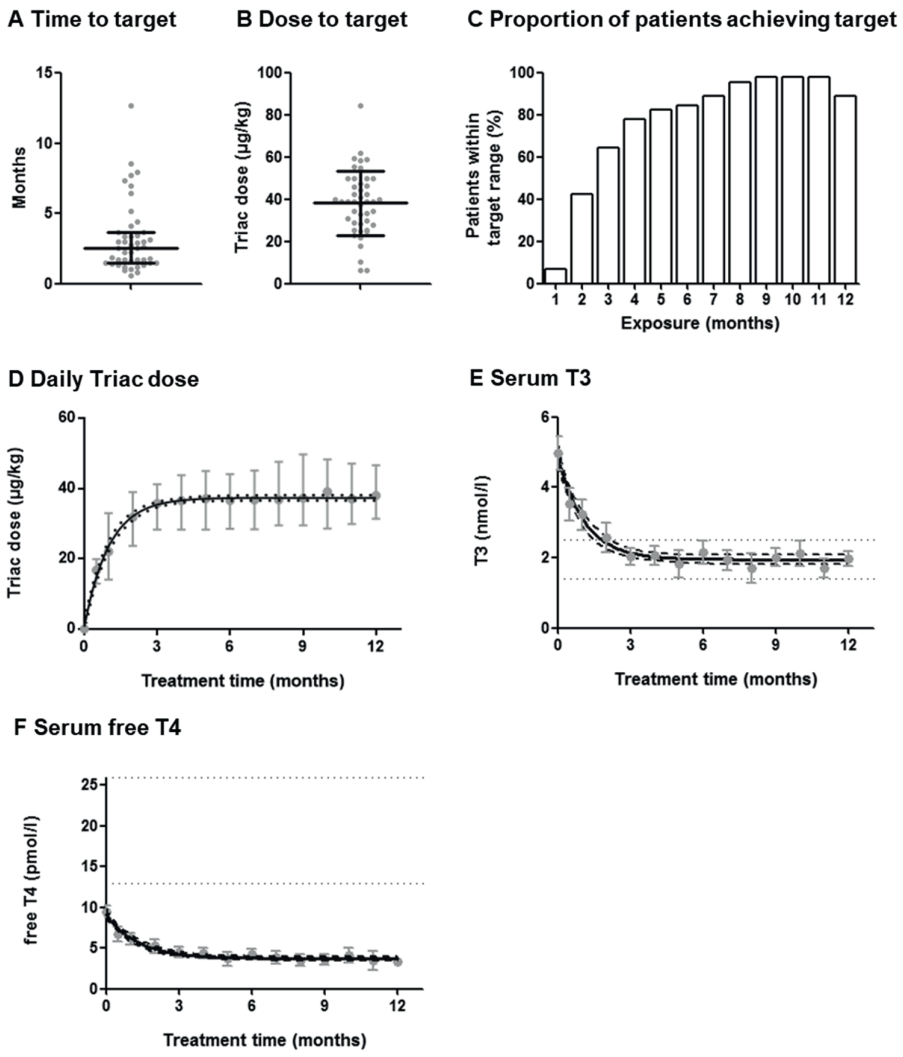

Figure s4. Triac dosages and longitudinal effects of Triac on serum T3 and free T4 concentrations

Panel **A** shows the time of Triac treatment required to attain T3 concentrations within the target range. Black lines display the median and interquartile range (IQR), and grey dots represent individual patients. Panel **B** shows the daily Triac dose in µg per kilogram bodyweight used at time serum T3 concentrations first reached the target range. Black lines display the mean and SD, and grey dots represent individual patients. Note that the dose in 7 patients required further adjustment in the remainder of the study in order to attain serum T3 concentrations within the normal range. Panel **C** shows the proportion of patients having serum T3 concentrations within the target range at indicated time points. Panel **D** shows the median Triac dose in microgram per kilogram bodyweight per day with the IQR at indicated time points during the study. The exposure time at each control visit was calculated and rounded to the nearest full number of months. In case of more than 1 measurement per month, the highest Triac dose was plotted. Non-linear regression was used to plot a regression line with 95% confidence interval (CI). Similarly, panel **E** shows the mean total T3 concentration and 95% CI and panel **F** the mean serum free T4 concentration at indicated time points with the corresponding 95% CI. Data from all patients who received Triac and had at least one follow-up measurement of thyroid function (N=45) are depicted and considered in the analyses, including five patients who dropped-out for whom the last available measurement was considered.

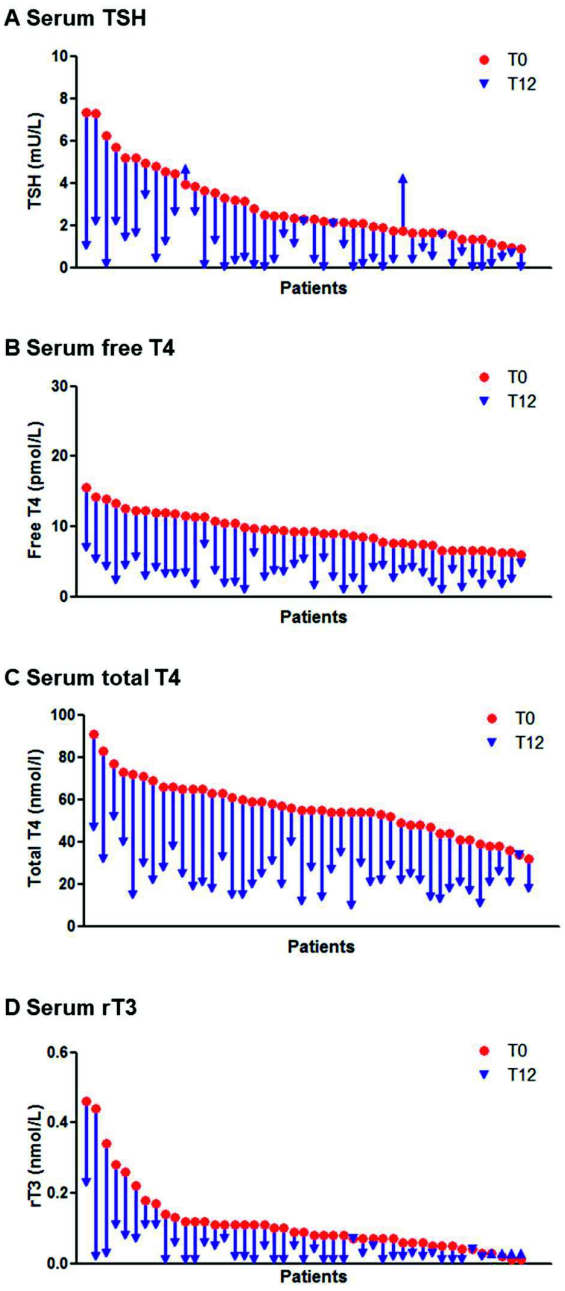

Figure s5. Changes from baseline to month 12 in serum TSH, free T4, total T4 and reverse T3 concentrations during Triac treatment

The change in serum TSH (panel **A**), free T4 (panel **B**), total T4 (panel **C**) and reverse (r)T3 (panel **D**) concentrations per patient from baseline (red dot) to month 12 (blue arrowhead), which all showed a significant reduction (P<0·0001) (see **Table 2** for details). All patients who received Triac and had at least one follow-up measurement of thyroid function (N=45) are depicted and included in the analyses, including five patients who dropped-out for whom the last available measurement was considered.

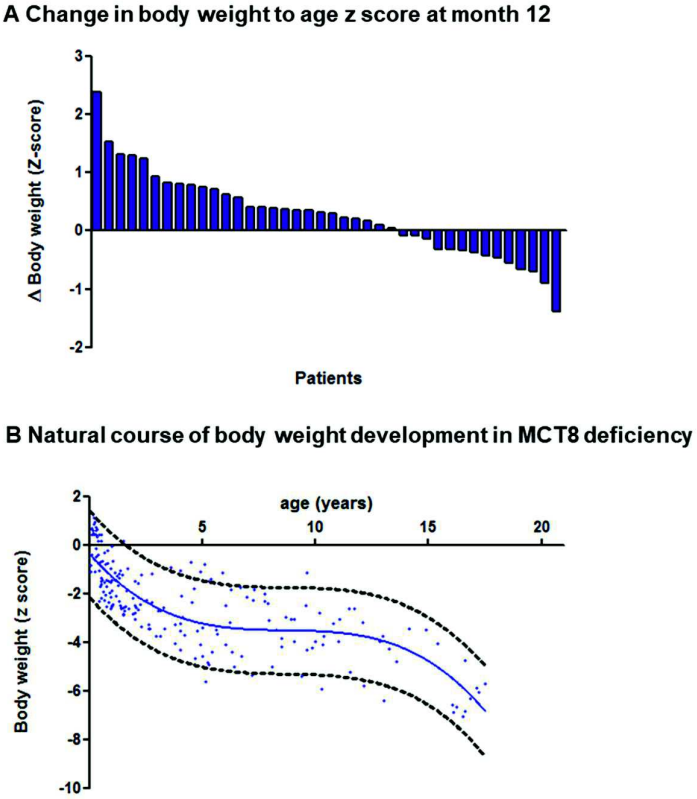

Figure s6. Changes from baseline to month 12 in bodyweight during Triac treatment

Panel **A** shows a waterfall plot depicting the change in bodyweight–for-age Z score from baseline to month 12 (P=0.025). Data from all patients who completed the 12–month intervention period (n=40) are displayed. Panel **B** shows the natural course of bodyweight change in patients with MCT8 deficiency. Blue dots represent available historical bodyweight measurements in Triac-naive patients enrolled in the Triac Trial. The natural course is based on historical measurements from the growth charts and medical records of the patients enrolled in the study. All measurements were captured before Triac treatment was commenced. Although not carried out under standardised conditions, these measurements have been carried out in the context of regular medical care in patients that had different co-morbidities, co-medication, and socio-economic backgrounds and are, as such, likely to constitute a representative set of clinical observations. Non-linear (third order) polynomial regression was used to plot the trend with its 95% error band. The increase in bodyweight-for-age Z score from baseline to month 12 (panel A) in the majority of Triac-treated patients is in contrast to the deterioration in bodyweight-for-age Z score over time observed in the natural course (panel **B**).

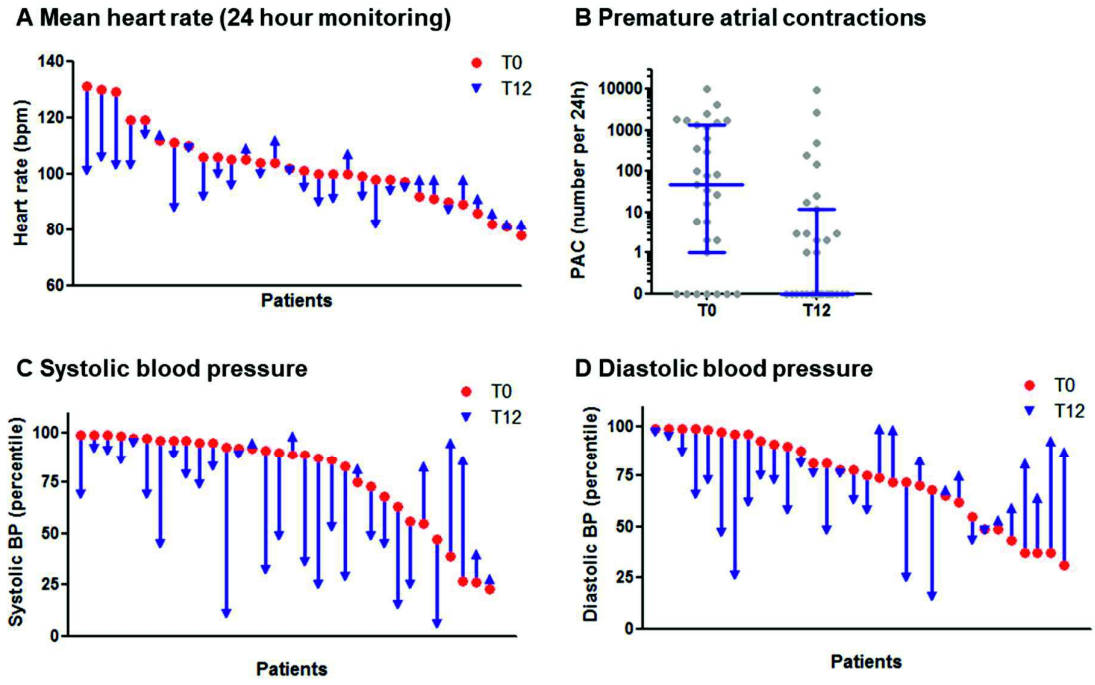

Figure s7. Changes from baseline to month 12 in cardiovascular endpoints during Triac treatment

Panel **A** represents the mean heart rate during 24 h, determined by ambulatory cardiac monitoring, per patient at baseline (red dot) and at month 12 (blue arrowhead), indicating a reduction in mean heart rate in the majority of the patients (P=0.012). Panel **B** shows post-hoc exploratory analyses of the occurrence of premature atrial contractions which are a recognised feature in patients with overt hyperthyroidism (20). Although such premature atrial contractions are uncommon in healthy individuals, especially in children (21), premature atrial contractions at high frequency were observed in up to 75% patients with MCT8 deficiency at the time of enrolment in this trial. The changes from baseline (red dot) to month 12 (blue arrowhead) in systolic blood pressure are displayed in panel **C** and in diastolic blood pressure in panel **D**. Both systolic and diastolic blood pressure are expressed in age and height adjusted percentiles. The change in systolic blood pressure reached statistical significance (P=0·0037), whereas the change in diastolic blood pressure was non-significant. All patients who completed the 12–month intervention period and had paired-observation (baseline and month 12) are displayed (for A and B, n=31; for C and D, n=32).

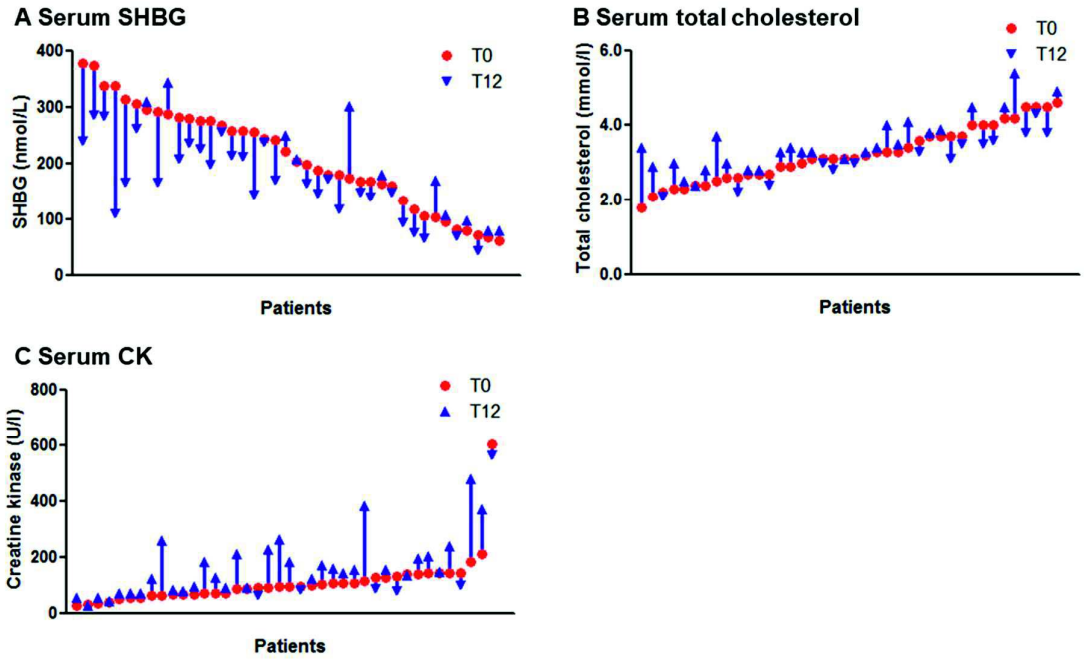

Figure s8. Changes from baseline to month 12 in biochemical secondary endpoints during Triac treatment

Panel **A** represents the change in serum sex hormone binding globulin (SHBG) concentrations per patient from baseline (red dot) and at month 12 (blue arrowhead), indicating a reduction in serum SHBG in the majority of the patients (P=0·0013). Similarly, panel **B** shows the change in serum total cholesterol concentrations, which did not reach statistical significance (p=0·056). Panel **C** shows the change in serum creatine kinase (CK) concentrations, which increased significantly (P<0·0001). Data from all patients who completed the 12–month intervention period (n=40) are displayed.

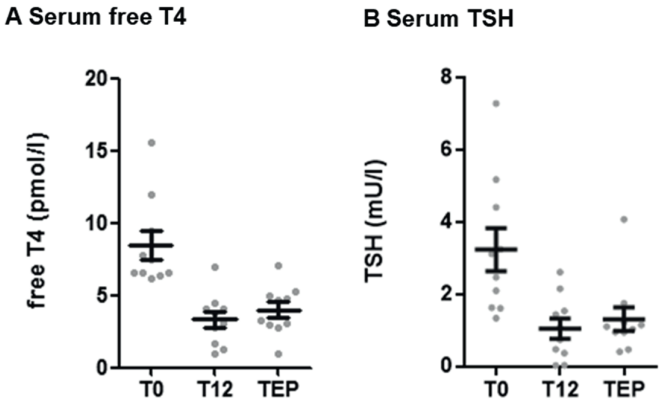

Figure S9. Changes from baseline to TEP in serum free T4 and TSH concentrations in patients enrolled in the treatment extension period

Panel **A** shows the change in serum free T4 concentrations from baseline (T0) to month 12 (T12) and end of the treatment extension period (TEP) (median [IQR] treatment time, 40·4 [38·1-41·3] month). Panel **B** shows the change in serum TSH concentrations from baseline (T0) to month 12 (T12) and end of the treatment extension period (TEP). Grey dots represent measurements in the individual patients; means and SEM are displayed in black. Means and mean changes with their corresponding 95% CI are presented in **Table S6**.

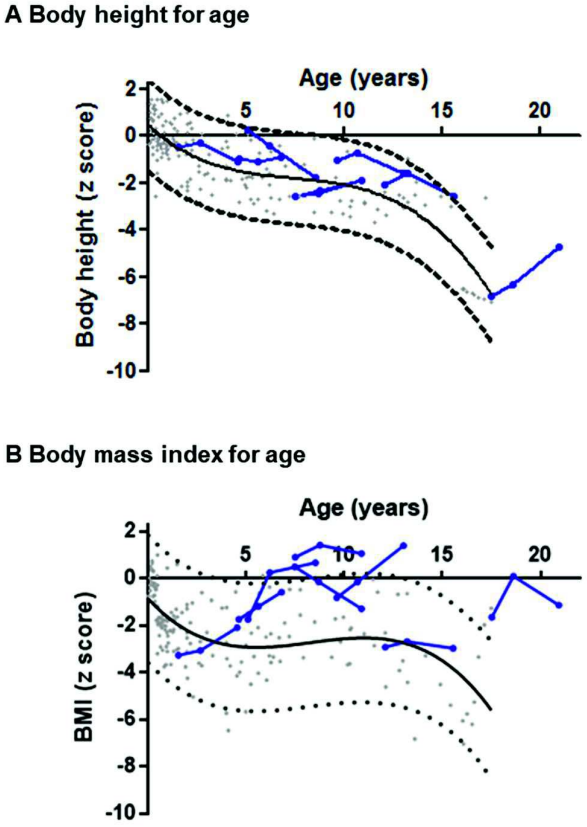

Figure S10. Changes from baseline to TEP in body height and BMI in patients enrolled in the treatment extension period

Panel **A** shows the change in body height and panel **B** change in body mass index (BMI) of each of the paediatric patients enrolled in the treatment extension period (black dots and connecting lines; median [IQR] treatment time, 40·4 [38·1-41·3] month) during Triac treatment in comparison to the natural trajectory of change in body height and BMI in MCT8 deficiency. The natural course of change in body height and BMI are denoted by a trend line (black solid line) with its 95% error band (black dotted line). Both natural courses are based on historical measurements from the growth charts and medical records of the patients enrolled in the study. All measurements were captured before Triac treatment was commenced. Although not carried out under standardised conditions, these measurements have been carried out in the context of regular medical care in patients that had different co-morbidities, co-medication, and socio-economic backgrounds and are, as such, likely to constitute a representative set of clinical observations. Trend lines were established by using non-linear (third order) polynomial regression. Body height for age stabilised or showed a moderate catch-up. In contrast to the natural course, BMI for age showed a clear increasing trend in most Triac-treated patients.

REFERENCES

1. Friesema EC, Ganguly S, Abdalla A, Manning Fox JE, Halestrap AP, Visser TJ. Identification of monocarboxylate transporter 8 as a specific thyroid hormone transporter. J Biol Chem. 2003;278(41):40128-35.
2. Friesema EC, Grueters A, Biebermann H, Krude H, von Moers A, Reeser M, et al. Association between mutations in a thyroid hormone transporter and severe X-linked psychomotor retardation. Lancet. 2004;364(9443):1435-7.
3. Dumitrescu AM, Liao XH, Best TB, Brockmann K, Refetoff S. A novel syndrome combining thyroid and neurological abnormalities is associated with mutations in a monocarboxylate transporter gene. Am J Hum Genet. 2004;74(1):168-75.
4. Visser WE, Vrijmoeth P, Visser FE, Arts WF, van Toor H, Visser TJ. Identification, functional analysis, prevalence and treatment of monocarboxylate transporter 8 (MCT8) mutations in a cohort of adult patients with mental retardation. Clin Endocrinol (Oxf). 2013;78(2):310-5.
5. Groeneweg S, Visser WE, Visser TJ. Disorder of thyroid hormone transport into the tissues. Best Pract Res Clin Endocrinol Metab. 2017;31(2):241-53.
6. (FDA) UFaDA. FDA drug safety communication: new boxed warning on severe liver injury with propylthiouracil. https://wwwfdagov/drugs/postmarket-drug-safety-information-patients-and-providers/fda-drug-safety-communication-new-boxed-warning-severe-liver-injury-propylthiouracil. 2010;Accessed 29th Jul 2019.
7. Rivkees SA, Mattison DR. Ending propylthiouracil-induced liver failure in children. N Engl J Med. 2009;360(15):1574-5.
8. Ross DS, Burch HB, Cooper DS, Greenlee MC, Laurberg P, Maia AL, et al. 2016 American Thyroid Association Guidelines for Diagnosis and Management of Hyperthyroidism and Other Causes of Thyrotoxicosis. Thyroid. 2016;26(10):1343-421.
9. Kersseboom S, Horn S, Visser WE, Chen J, Friesema EC, Vaurs-Barriere C, et al. In vitro and mouse studies supporting therapeutic utility of triiodothyroacetic acid in MCT8 deficiency. Mol Endocrinol. 2014;28(12):1961-70.
10. Messier N, Langlois MF. Triac regulation of transcription is T(3) receptor isoform- and response element-specific. Mol Cell Endocrinol. 2000;165(1-2):57-66.
11. Groeneweg S, Peeters RP, Visser TJ, Visser WE. Triiodothyroacetic acid in health and disease. J Endocrinol. 2017;234(2):R99-R121.
12. Bracco D, Morin O, Schutz Y, Liang H, Jequier E, Burger AG. Comparison of the metabolic and endocrine effects of 3,5,3'-triiodothyroacetic acid and thyroxine. J Clin Endocrinol Metab. 1993;77(1):221-8.
13. Burger AG, Engler D, Sakoloff C, Staeheli V. The effects of tetraiodothyroacetic and triiodothyroacetic acids on thyroid function in euthyroid and hyperthyroid subjects. Acta Endocrinol (Copenh). 1979;92(3):455-67.
14. Zada D, Tovin A, Lerer-Goldshtein T, Appelbaum L. Pharmacological treatment and BBB-targeted genetic therapy for MCT8-dependent hypomyelination in zebrafish. Dis Model Mech. 2016;9(11):1339-48.
15. Flynn JT, Kaelber DC, Baker-Smith CM, Blowey D, Carroll AE, Daniels SR, et al. Clinical Practice Guideline for Screening and Management of High Blood Pressure in Children and Adolescents. Pediatrics. 2017;140(3):pii: e20171904.
16. Whelton PK, Carey RM, Aronow WS, Casey DE, Jr., Collins KJ, Dennison Himmelfarb C, et al. 2017 ACC/AHA/AAPA/ABC/ACPM/AGS/APhA/ASH/ASPC/NMA/PCNA Guideline for the Prevention, Detection, Evaluation, and Management of High Blood Pressure in Adults: A Report of the American College of Cardiology/American Heart Association Task Force on Clinical Practice Guidelines. Hypertension. 2018;71(6):e13-e115.
17. Fleming S, Thompson M, Stevens R, Heneghan C, Pluddemann A, Maconochie I, et al. Normal ranges of heart rate and respiratory rate in children from birth to 18 years of age: a systematic review of observational studies. Lancet. 2011;377(9770):1011-8.
18. Russell DJ, Rosenbaum PL, Cadman DT, Gowland C, Hardy S, Jarvis S. The gross motor function measure: a means to evaluate the effects of physical therapy. Dev Med Child Neurol. 1989;31(3):341-52.
19. Falagas ME, Athanasoulia AP, Peppas G, Karageorgopoulos DE. Effect of body mass index on the outcome of infections: a systematic review. Obes Rev. 2009;10(3):280-9.
20. von Olshausen K, Bischoff S, Kahaly G, Mohr-Kahaly S, Erbel R, Beyer J, et al. Cardiac arrhythmias and heart rate in hyperthyroidism. Am J Cardiol. 1989;63(13):930-3.
21. Scott O, Williams GJ, Fiddler GI. Results of 24 hour ambulatory monitoring of electrocardiogram in 131 healthy boys aged 10 to 13 years. Br Heart J. 1980;44(3):304-8.

22. Binici Z, Intzilakis T, Nielsen OW, Kober L, Sajadieh A. Excessive supraventricular ectopic activity and increased risk of atrial fibrillation and stroke. Circulation. 2010;121(17):1904-11.
23. Healey JS, Connolly SJ, Gold MR, Israel CW, Van Gelder IC, Capucci A, et al. Subclinical atrial fibrillation and the risk of stroke. N Engl J Med. 2012;366(2):120-9.
24. Perez MV, Dewey FE, Marcus R, Ashley EA, Al-Ahmad AA, Wang PJ, et al. Electrocardiographic predictors of atrial fibrillation. Am Heart J. 2009;158(4):622-8.
25. Verge CF, Konrad D, Cohen M, Di Cosmo C, Dumitrescu AM, Marcinkowski T, et al. Diiodothyropropionic acid (DITPA) in the treatment of MCT8 deficiency. J Clin Endocrinol Metab. 2012;97(12):4515-23.
26. Mechelany C, Schlumberger M, Challeton C, Comoy E, Parmentier C. TRIAC (3,5,3'-triiodothyroacetic acid) has parallel effects at the pituitary and peripheral tissue levels in thyroid cancer patients treated with L-thyroxine. Clin Endocrinol (Oxf). 1991;35(2):123-8.
27. Sherman SI, Ringel MD, Smith MJ, Kopelen HA, Zoghbi WA, Ladenson PW. Augmented hepatic and skeletal thyromimetic effects of tiratricol in comparison with levothyroxine. J Clin Endocrinol Metab. 1997;82(7):2153-8.
28. Barez-Lopez S, Obregon MJ, Martinez-de-Mena R, Bernal J, Guadano-Ferraz A, Morte B. Effect of Triiodothyroacetic Acid Treatment in Mct8 Deficiency: A Word of Caution. Thyroid. 2016;26(5):618-26.
29. Visser WE, Heuer H, Visser TJ. Triiodothyroacetic Acid Treatment in MCT8 Deficiency: A Word of Nuance. Thyroid. 2016;26(5):615-7.
30. Bernal J, Guadano-Ferraz A, Morte B. Thyroid hormone transporters--functions and clinical implications. Nat Rev Endocrinol. 2015;11(7):406-17.
31. Brenta G, Schnitman M, Fretes O, Facco E, Gurfinkel M, Damilano S, et al. Comparative efficacy and side effects of the treatment of euthyroid goiter with levo-thyroxine or triiodothyroacetic acid. J Clin Endocrinol Metab. 2003;88(11):5287-92.
32. Menegay C, Juge C, Burger AG. Pharmacokinetics of 3,5,3'-triiodothyroacetic acid and its effects on serum TSH levels. Acta Endocrinol (Copenh). 1989;121(5):651-8.
33. Bayley N. Bayley scales of infant and toddler development–Third edition. San Antonio, TX: Pearson Education, Inc.; 2006.
34. Sparrow SC, D.; Balla, D.A. Vineland-II Adaptive Behavior Scales: Survey Forms Manual. Circle Pines, MN, US: AGS Publishing; 2005.

Chapter 6

Identification of a novel TH transporter and syndromes of TH resistance

Chapter

6.1

Genome-wide analyses identify a role for SLC17A4 and AADAT in thyroid hormone regulation

Alexander Teumer*, Layal Chaker*, **Stefan Groeneweg***, Yong Li*, Celia Di Munno*, Caterina Barbieri* et al.

Nat Commun. 2018 Oct;9(1):4455.

ABSTRACT

Thyroid dysfunction is an important public health problem, which affects 10% of the general population and increases the risk of cardiovascular morbidity and mortality. Many aspects of thyroid hormone regulation have only partly been elucidated, including its transport, metabolism, and genetic determinants. Here we report a large meta-analysis of genome-wide association studies for thyroid function and dysfunction, testing 8 million genetic variants in up to 72,167 individuals. One-hundred-and-nine independent genetic variants are associated with these traits. A genetic risk score, calculated to assess their combined effects on clinical end points, shows significant associations with increased risk of both overt (Graves' disease) and subclinical thyroid disease, as well as clinical complications. By functional follow-up on selected signals, we identify a novel thyroid hormone transporter (SLC17A4) and a metabolizing enzyme (AADAT). Together, these results provide new knowledge about thyroid hormone physiology and disease, opening new possibilities for therapeutic targets.

INTRODUCTION

Thyroid dysfunction is a common clinical condition, affecting ~10% of the general adult population (1). Adequate thyroid hormone levels are essential for normal growth and differentiation, regulation of energy metabolism, and physiological function of virtually all human tissues. Thyroxine (T4) is the prohormone produced by the thyroid, which is largely converted into the active hormone 3,3',5-triiodothyronine (T3) in peripheral tissues. Circulating T4 levels are regulated by the hypothalamus–pituitary–thyroid (HPT) axis, in which pituitary thyroid-stimulating hormone (TSH) stimulates T4 production. In turn, T4 and T3 negatively regulate TSH synthesis via a negative feedback loop.

To exert their actions, T4 and T3 cross the membranes of target cells via specific transporters. Once intracellular, they are metabolized, including the conversion of T4 to T3, followed by binding of T3 to its nuclear receptor to regulate transcription of target genes. Both T4 and T3 transport and metabolism are therefore key determinants of thyroid hormone action.

In daily clinical practice, thyroid function is assessed by measuring circulating TSH and free T4 (FT4) levels, with increased TSH indicating hypothyroidism and decreased TSH indicating hyperthyroidism. FT4 levels are decreased in overt hypothyroidism, increased in overt hyperthyroidism and in the reference range in subclinical hypo and hyperthyroidism. In the last decade, it has become clear that not only overt but also subclinical hypo and hyperthyroidism are associated with several pathological conditions, such as atrial fibrillation, coronary heart disease, stroke, depression, as well as cardiovascular and overall mortality (2-7). More recently, studies have shown that even variation in thyroid function within the normal range is associated with many of these complications (4, 8-10). Despite the physiological significance of thyroid hormones, as well as the prevalence and clinical importance of thyroid dysfunction, many key players in the regulation of thyroid hormone bioavailability and action, including its transport and metabolism, still need to be elucidated.

Genome-wide association studies (GWAS) performed so far have revealed genetic variants in about 30 loci robustly associated with thyroid function (11-13). However, these variants explain only <9% of the heritability of TSH and FT4 variation (14), while in total, it has been estimated at 65 and 39–80% for TSH and FT4, respectively (15, 16), suggesting that many loci still await discovery.

Here, we report the results of a large meta-analysis of GWAS for circulating TSH and FT4 levels, as well as for hypo and hyperthyroidism, followed by independent replication and functional studies. Results are complemented with genetic risk score (GRS) analyses, gene expression, co-localization analyses, and associations with various clinical phenotypes (**Supplementary Figure 1**) to discover new pathways underlying thyroid function and disease. We identify 109 significant independent genetic associations with these traits. The GRS shows a significant association with increased risk of both Graves' disease and subclinical thyroid disease, as well as clinical complications. Finally, we identify a novel thyroid hormone transporter and a metabolizing enzyme. Together, these results enhance our knowledge about thyroid hormone physiology and disease.

RESULTS

New loci affecting thyroid hormone levels

Our GWAS meta-analyses and replication in up to 72,167 subjects of European ancestry with TSH levels within the reference range (**Supplementary Data 1**) discovered 19 novel loci for circulating TSH levels and 16 novel loci for circulating FT4 levels (**Tables 1 and 2**, **Supplementary Figures 2–5**), leading to a total of 42 and 21 known and novel associated loci for these two traits. As illustrated in **Figure 1**, TSH and FT4 capture distinct and complementary genetic underpinnings of thyroid function.

Some of the novel loci include genes that have been previously implicated in thyroid development (*GLIS3*), thyroid hormone action and transport (*NCOR1*, *TTR*, *SLCO1B1)*, thyroid hormone metabolism (*DIO2*, *DIO3OS*), and thyroid cancer (e.g., *HES1*, *SPATA13*, *DIRC3*, *ID4*) by various candidate gene studies of monogenic diseases and animal models. Multiple independent variants were found for *PDE8B*, *DIO1*, *DIO2*, *TSHR*, and *CAPZB*.

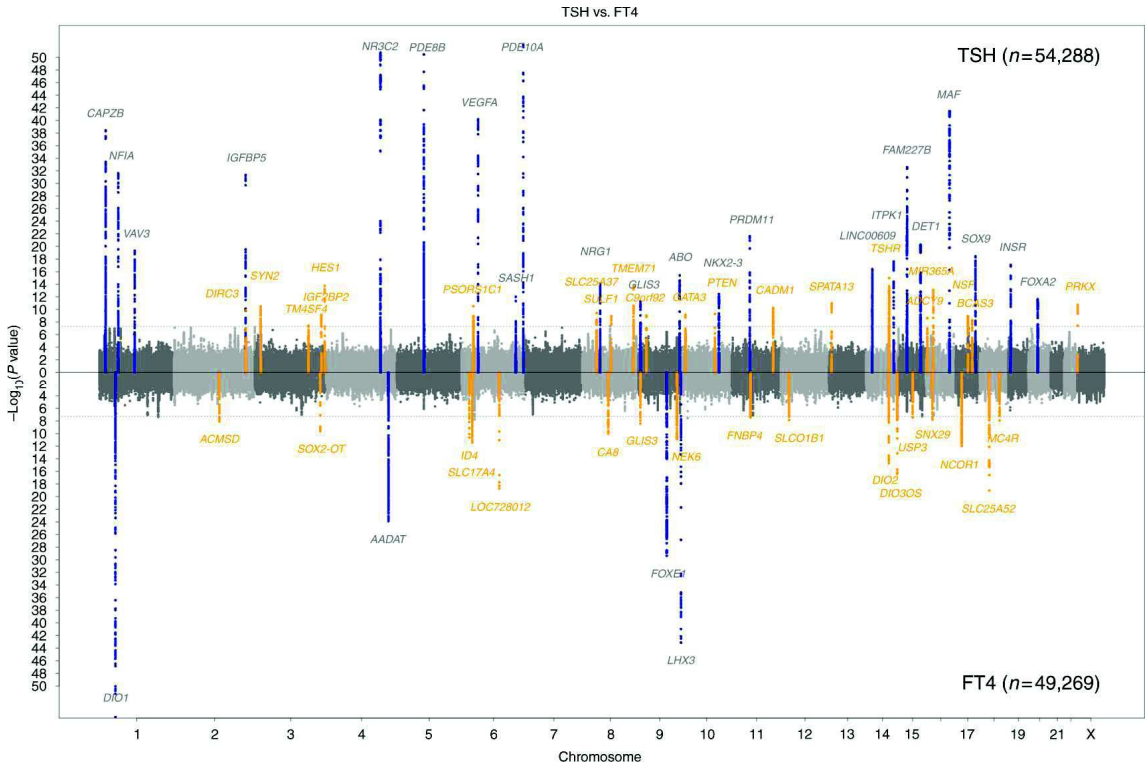

Figure 1 Manhattan plots for GWAS meta-analyses of thyroid function. Manhattan plots of the GWAS meta-analysis results for TSH and FT4 contrasted with each other. SNPs are plotted on the *x* axis according to their position on each chromosome with $-\log_{10}$(*p*-value) of the association test on the *y* axis. The upper solid horizontal line indicates the threshold for genome-wide significance, i.e., 5×10^{-8}. Genomic loci previously known to contain trait-associated variants are colored in blue, new loci in orange.

Table 1 Novel GWAS loci associated with TSH

SNP	Chr	Position	Locus	A1	A2	AF1	Effect	SE	P	I^2	P_{het}	N	SNP Function	P hyper-thyroidism	P hypo-thyroidism
rs6724073	2	218,236,786	*DIRC3*	t	c	0.74	0.045	0.007	3.1E-10	29.4	0.041	61058	intron	1.10E-01	6.30E-02
rs28502438	3	149,220,109	*TM4SF4*	t	c	0.57	0.035	0.006	7.3E-10	0.0	0.853	63299	intron	7.60E-01	7.20E-02
rs13100823	3	185,514,088	*IGF2BP2*	t	c	0.30	-0.042	0.006	4.1E-12	2.1	0.432	63299	intron	8.50E-04	**1.70E-04**
rs59381142	3	193,916,181	*HES1*	a	g	0.24	-0.054	0.007	3.6E-15	0.0	0.801	61059	unknown	1.80E-03	2.40E-02
rs1265091	6	31,108,129	*PSORS1C1*	t	c	0.19	0.058	0.007	5.0E-15	40.4	0.005	64423	near-gene-3	3.00E-01	3.00E-02
rs56009477	8	23,356,964	*SLC25A37*	a	g	0.84	0.050	0.008	1.1E-10	0.0	0.955	63299	unknown	9.20E-03	3.50E-02
rs10957494	8	70,365,025	*SULF1*	a	g	0.69	-0.036	0.006	3.6E-09	21.4	0.111	63299	unknown	3.50E-02	2.50E-01
rs118039499	8	133,771,635	*TG*	a	c	0.97	0.185	0.020	2.9E-21	28.6	0.042	66615	intron	**1.80E-12**	4.00E-01
rs2739067*	8	133,951,991	*TG*	a	g	0.60	-0.042	0.006	2.4E-11	0.0	0.540	54288	intron	1.20E-01	1.30E-01
rs9298749	9	16,214,340	*C9orf92*	a	c	0.59	-0.038	0.006	1.6E-10	10.4	0.280	63299	unknown	9.00E-01	6.90E-03
rs11255790	10	8,682,180	*GATA3*	t	c	0.30	-0.039	0.006	2.5E-10	0.0	0.738	63299	unknown	1.30E-02	7.90E-01
rs4933466	10	89,849,519	*PTEN*	a	g	0.60	0.037	0.006	2.2E-10	24.3	0.079	63299	unknown	2.60E-01	6.60E-03
rs4445669	11	115,045,237	*CADM1*	t	c	0.45	-0.039	0.006	3.6E-12	0.0	0.854	63299	untranslated-3	5.10E-02	9.40E-02
rs7329958	13	24,782,080	*SPATA13*	t	c	0.35	-0.044	0.006	7.1E-14	0.0	0.913	63299	intron	6.10E-01	4.50E-03
rs11159482*	14	81,490,842	*TSHR*	t	c	0.09	0.085	0.013	6.3E-11	0.0	0.727	54288	intron	1.90E-01	**1.80E-04**
rs59334515*	14	81,594,143	*TSHR*	t	c	0.22	-0.054	0.007	1.1E-13	25.7	0.080	54288	intron	1.40E-02	3.10E-03
rs12893151	14	81,619,945	*TSHR*	a	c	0.21	-0.057	0.007	2.3E-15	27.4	0.052	63299	unknown	**3.20E-04**	**1.90E-04**
rs1045476	16	4,015,313	*ADCY9*	a	g	0.17	0.047	0.007	3.2E-11	0.0	0.979	72167	untranslated-3	1.70E-01	4.60E-03
rs30227	16	14,405,428	*MIR365A*	t	c	0.61	-0.046	0.005	2.3E-17	3.0	0.415	72167	intron	2.60E-02	1.10E-01
rs77819282	17	44,762,589	*NSF*	a	g	0.24	0.043	0.007	4.3E-10	0.0	0.653	62192	intron	5.20E-01	7.10E-03
rs1157994	17	59,338,574	*BCAS3*	a	g	0.05	-0.083	0.014	4.0E-09	21.0	0.120	59243	intron	1.80E-01	4.10E-01
rs12390237[a]	23	3,612,081	*PRKX*	a	g	0.62	-0.046	0.007	1.7E-11	0.0	0.760	36501	intron	1.00E-02	6.60E-01

The table contains the list of the index SNPs and additional independent associations of replicated TSH susceptibility loci. The values are provided for the combined discovery and replication sample, for additional independent hits (*) for the discovery stage only

Bold values of the hyper and hypothyroidism p-values indicate significance after Bonferroni correction for the 61 independent TSH-associated SNPs tested ($p < 8.2E{-}4$)

A1 effect allele, AF1 allele frequency of A1, SE standard error of the effect, P association p-value, I^2 percentage of total variation across studies that is due to heterogeneity, N sample size

Table 2 Novel GWAS loci associated with FT4

SNP	Chr	Position	Locus	A1	A2	AF1	Effect	SE	P	I^2	P_{het}	N	SNP Function
rs4954192	2	135,632,98	*ACMSD*	t	c	0.43	-0.033	0.006	9.3E-09	2.6	0.424	62680	intron
rs6785807	3	181,718,601	*SOX2-OT*	a	g	0.15	-0.057	0.009	6.9E-11	7.4	0.340	55096	intron
rs10946313	6	19,381,386	*ID4*	t	c	0.63	0.044	0.006	6.2E-12	0.0	0.907	55096	unknown
rs9356988	6	25,777,481	*SLC17A4*	a	g	0.27	-0.052	0.007	5.7E-14	0.0	0.745	55096	intron
rs137964359*	6	26,001,742	*SLC17A4*	t	c	0.99	-0.200	0.032	2.1E-10	0.0	0.479	49269	unknown
rs17185536	6	100,620,931	*LOC728012*	t	c	0.24	0.071	0.008	2.7E-20	0.0	0.973	53801	unknown
rs67583169	8	61,212,179	*CA8*	c	g	0.86	0.062	0.009	7.1E-12	0.0	0.936	53801	unknown
rs10119187	9	4,223,660	*GLIS3*	t	c	0.81	0.048	0.008	8.0E-10	6.4	0.357	56936	intron
rs10818937	9	127,015,440	*NEK6*	t	c	0.32	-0.039	0.006	4.9E-11	15.8	0.196	63971	unknown
rs11039355	11	47,737,501	*FNBP4*	t	c	0.34	-0.039	0.006	7.9E-11	12.2	0.258	62677	near-gene-5
rs4149056	12	21,331,549	*SLCO1B1*	t	c	0.84	-0.048	0.007	6.3E-11	0.0	0.636	67091	missense
rs150816132*	14	80,464,293	*DIO2*	a	g	0.01	-0.220	0.040	3.5E-08	24.1	0.122	38640	unknown
rs978055*	14	80,534,869	*DIO2*	a	t	0.38	0.038	0.007	1.1E-08	10.5	0.296	49269	unknown
rs225014	14	80,669,580	*DIO2*	t	c	0.64	0.047	0.006	4.6E-17	0.0	0.702	63971	missense
rs12323871*	14	101,852,075	*DIO3OS*	t	c	0.82	-0.047	0.008	1.4E-08	25.7	0.091	49269	unknown
rs11626434	14	101,998,443	*DIO3OS*	c	g	0.36	0.053	0.007	1.7E-16	40.2	0.006	55095	unknown
rs12907106	15	63,873,658	*USP3*	c	g	0.27	-0.039	0.007	3.7E-08	0.0	0.529	53801	intron
rs8063103	16	12,703,395	*SNX29*	c	g	0.85	-0.051	0.009	7.8E-09	7.9	0.335	53801	unknown
rs11078333	17	16,049,626	*NCOR1*	a	t	0.51	0.042	0.006	2.0E-12	0.0	0.513	62677	intron
rs56069042	18	57,914,644	*MC4R*	a	g	0.95	0.099	0.017	3.6E-09	0.0	0.735	58197	unknown

The table contains the list of the index SNPs and additional independent associations of replicated FT4 susceptibility loci. The values are provided for the combined discovery and replication sample, for additional independent hits (*) for the discovery stage only.
A1 effect allele, *AF1* allele frequency of A1, *SE* standard error of the effect, *P* association *p*-value, I^2 percentage of total variation across studies that is due to heterogeneity, *N* sample size

Across the 42 TSH and 21 FT4 loci, allelic heterogeneity (i.e., independently associated single-nucleotide polymorphisms (SNPs) at the same locus) was detected at 11 and 7 loci, respectively, by using linkage structure information and summary statistics-based conditional analyses (**Supplementary Tables 1** and **2**). All significant associations together accounted for 33% and 21% of the genetic variance of TSH and FT4, respectively, explained by all common and low-frequency variants with a minor allele frequency (MAF) >1%.

Since TSH and FT4 regulation are inversely correlated through the HPT axis, we investigated the association of the TSH-associated loci with FT4 levels, and vice versa. As shown in **Figure 1** and in **Supplementary Tables 1** and **2**, we observed overlapping associations (Bonferroni-corrected threshold $p < 8.2 \times 10^{-4}$) at various loci (TSH: *FGF7*, *PDE8B*, *DET1*, *ITPK1*, *VEGFA*, *GLIS3*, *NFIA*, and *MBIP*, and FT4: *FOXE1* and *GLIS3*), although only *GLIS3* showed genome-wide significance for both traits. All alleles associated with higher TSH were associated with lower FT4, with the exception of *MBIP* and *FOXE1*.

Hypo and hyperthyroidism are more prevalent in women than in men. However, sex-stratified GWAS meta-analyses for TSH and FT4 did not show any significant gene-by-sex interaction in our samples (**Supplementary Figure 6**, **Supplementary Tables 1** and **2**).

Given the high degree of functional homology between the mouse and human genome, we selected from The International Mouse Phenotyping Consortium database (17) genes that when manipulated in mice cause abnormal thyroid physiology (i.e., hormone levels, $n = 26$) or morphology ($n = 51$), and assessed whether their human homologs contained SNPs significantly ($p < 2.5 \times 10^{-5}$ for physiology and $p < 1.9 \times 10^{-5}$ for morphology, see Methods) associated in our FT4 and TSH GWAS (**Supplementary Data 2**). Of these candidate genes, SNPs in *CGA* (rs6924373) and *TPO* (rs9678281) contained significant associations that did not reach genome-wide significance in our GWAS for TSH. These associations were tested for replication in 9011 independent samples and achieved genome-wide significance for TSH ($p < 5 \times 10^{-8}$) in the combined dataset (**Supplementary Figure 7A**). Overall, these results highlight the potential of nested candidate gene approaches in GWAS summary results and emphasize the functional conservation of genes regulating thyroid function between mice and humans.

Relation to hypo and hyperthyroidism

Genetic variants that determine variation in circulating TSH and FT4 levels within the reference range (i.e., the individual HPT-axis setpoint) are expected to differ from variants that underlie thyroid dysfunction (hypo or hyperthyroidism). To clarify this, we also conducted a case–control GWAS meta-analysis of increased TSH levels (i.e., hypothyroidism), including cases with TSH levels above the cohort-specific reference range ($n = 3340$) and controls with TSH levels within the reference range ($n = 49{,}983$). The decreased TSH level (i.e., hyperthyroidism) GWAS meta-analysis included cases with TSH below the reference range ($n = 1840$ cases) and the same controls as in the increased TSH GWAS. The distribution of sex and age groups of these subjects is provided in **Supplementary Table 3**. Since in both GWAS analyses, cases were defined on the basis of a TSH level above or below the reference range, these groups included subjects with overt but also mild subclinical forms of hypothyroidism and hyperthyroidism, respectively.

We detected seven loci for hypothyroidism and eight loci for hyperthyroidism (**Supplementary Figure 8**, **Supplementary Table 4**). At some of the loci, the variant was significantly associated with

both hypo and hyperthyroidism, with effects in opposing directions. For example, a variant at *PDE10A* (rs2983514) was associated with both higher risk of hypothyroidism and lower risk of hyperthyroidism. Some of the hypothyroidism loci had already previously been implicated in hypothyroidism through GWAS, including *TPO*, *FOXE1*, *VAV3*, and a variant in *ATXN2* (rs597808) in high linkage disequilibrium (LD) with the R262W polymorphism in *SH2B3* (18). However, we did not detect variants in a number of well-known autoimmune thyroid disease genes (e.g., *CTLA4*, *HLA class I* and *II*). This may be due to the fact that, in these population-based cohorts, patients receiving medication for autoimmune thyroiditis were excluded. Thus, thyroid autoimmunity caused by auto-antibodies may have a different set of predisposing variants. All variants associated with hyperthyroidism have not been previously found in association with hyperthyroidism, except for *FOXE1* (19). However, all of these variants were in high LD with variants associated with TSH or FT4 levels within the reference range in the current or previous GWAS (11, 13). The same holds true for variants associated with hypothyroidism, suggesting that the effects of many genetic variants on thyroid function extend beyond the physiological range, thus affecting the risk of thyroid dysfunction.

As complementary analyses to investigate whether the TSH loci are also related to autoimmune thyroid diseases, we tested all variants or their proxies for association with thyroid peroxidase antibody (TPOAb) positivity of a former GWAS (20) as an early marker of autoimmune hypothyroidism, as well as in patients with Graves' disease (i.e., autoimmune hyperthyroidism) from the BioBank Japan Project. For TPOAb positivity, significant associations were found for *MAF*, *SPATA13*, and *VAV3* (**Supplementary Table 5**). *SPATA13* and *VAV3* have previously been linked to self-reported diagnosed hypothyroidism (18, 21), while no studies have investigated their potential autoimmune origin. The observed associations of these gene variants with variation in TSH levels within the normal range could therefore be due to a mild early stage of thyroid autoimmunity, instead of reflecting physiological differences in the HPT-axis setpoint.

For Graves' disease, only the psoriasis (22) *PSORS1C1* locus showed a significant association, consistent with shared genetic determinants between these two autoimmune diseases (23).

Detailed results of the mouse candidate analysis, results of pathway analyses, and look-ups for pleiotropy of the TSH, FT4, hypo and hyperthyroidism loci are described in **Supplementary Note 1–3**.

Gene expression analyses

To obtain insights into gene expression patterns and potential effector transcripts at the identified loci, we assessed whether the 94 independent index variants from the TSH, FT4, hypo and hyperthyroidism GWAS were correlated with transcript levels of nearby (*cis*-) or distant (*trans*-) genes. The results of 22 published expression quantitative trait loci (eQTL) studies were interrogated (Methods), assessing the relation between the genetic variants and gene expression patterns in a total of 127 different tissues and cell types. First, we evaluated the presence of eQTLs in at least one tissue or cell type: 38 variants showed eQTL effects (**Figure 2a** and **Supplementary Data 3**). While many variants were associated with transcript expression in only one or few (≤8) tissues, two variants located on chromosome 17 showed ubiquitous associations with gene expression: the FT4-associated variant rs11078333 at *NCOR1* locus and the TSH-associated variant rs199461 at the *NSF* locus. The FT4-increasing allele at rs11078333 was associated with higher expression levels of *NCOR1* in blood and brain, but also affected the expression of *ADORA2B* (increased) and *ZSWIM7* and *TTC19* (decreased) in many other tissues (including thyroid for *TTC19*). *NCOR1* is an essential nuclear co-repressor that is recruited by

thyroid hormone receptors in the absence of thyroid hormone to mediate transcriptional repression. At the *NSF* locus, the TSH increasing allele at rs199461 increased expression of *KANSL1* and *LRRC37A2* and decreased expression of *WNT3* in several tissues, including thyroid. Consistent with known thyroid physiology, the majority of TSH-associated variants acted as eQTLs in thyroid tissue (**Figure 2a**), with 45% of the variants being thyroid-specific eQTLs. In contrast, none of the nine FT4 eQTLs acted exclusively on the thyroid but were also associated with transcript expression changes in multiple known thyroid hormone effector organs, including liver, muscle, and adipose tissue.

Second, we used a summary-based Mendelian randomization (SMR) method coupled with testing for heterogeneity of effects (HEIDI) to assess co-localization, i.e., to investigate whether the overlap between eQTLs and GWAS hits could be attributable to the same underlying causative variant (24). In thyroid tissue, we found evidence for co-localization with differential gene expression at 13 different GWASloci: *PD8EB*, *PRDM11*, *MBIP* (with *RP11-116N8.1* expression), *NKX2-3* , NSF (with *WNT3* expression), *IGFBP2, FOXA2, SLC25A37, and C9orf92 for TSH*; *AADAT*, *NEK6* (with both *NEK6* and *PSMB7* expressions) for FT4; and *TPO*, *PDE8B*, and *PDE10A* for hypothyroidism (**Supplementary Data 4**). At these loci, our findings implicate the causal gene among the many genes present in the locus.

For example, the FT4-associated variant rs6854291-influenced transcript levels of *AADAT* in thyroid while there were no effects on transcript levels of the neighboring *MFAP3L* gene, implicating *AADAT* as the causal gene underlying the FT4 association at this locus (**Figure 2b**, **Supplementary Data 4**). We also observed that independent variants at the same locus were associated with gene expression in different tissues. For example, while the index variant rs6885099 at *PDE8B* co-localized with changes in *PDE8B* expression in thyroid, the independent variant rs1119208 was associated with *PDE8B* expression in pancreas (**Supplementary Data 4).** Notably, also the variants at *AADAT* and *SLC17A4* co-localized with gene expression in pancreas (**Figure 2c**), which is of interest given the close interrelations between thyroid hormone signaling, insulin regulation, and glucose metabolism (25, 26).

***In vitro* studies**

Thyroid hormone action in target tissues is importantly determined by the amount of T3 available for receptor binding inside the cell. Therefore, the transport of thyroid hormone across the cell membrane and its metabolism inside the cell represent crucial regulatory layers in thyroid hormone signaling. Although several key players in thyroid hormone signaling have been described over the last decades, including deiodinases and several thyroid hormone transporters, many others remain to be identified. Based on their associations with circulating FT4 levels and the co-localization studies, *SLC17A4* and *AADAT* were further studied in vitro to explore a direct role in thyroid hormone signaling.

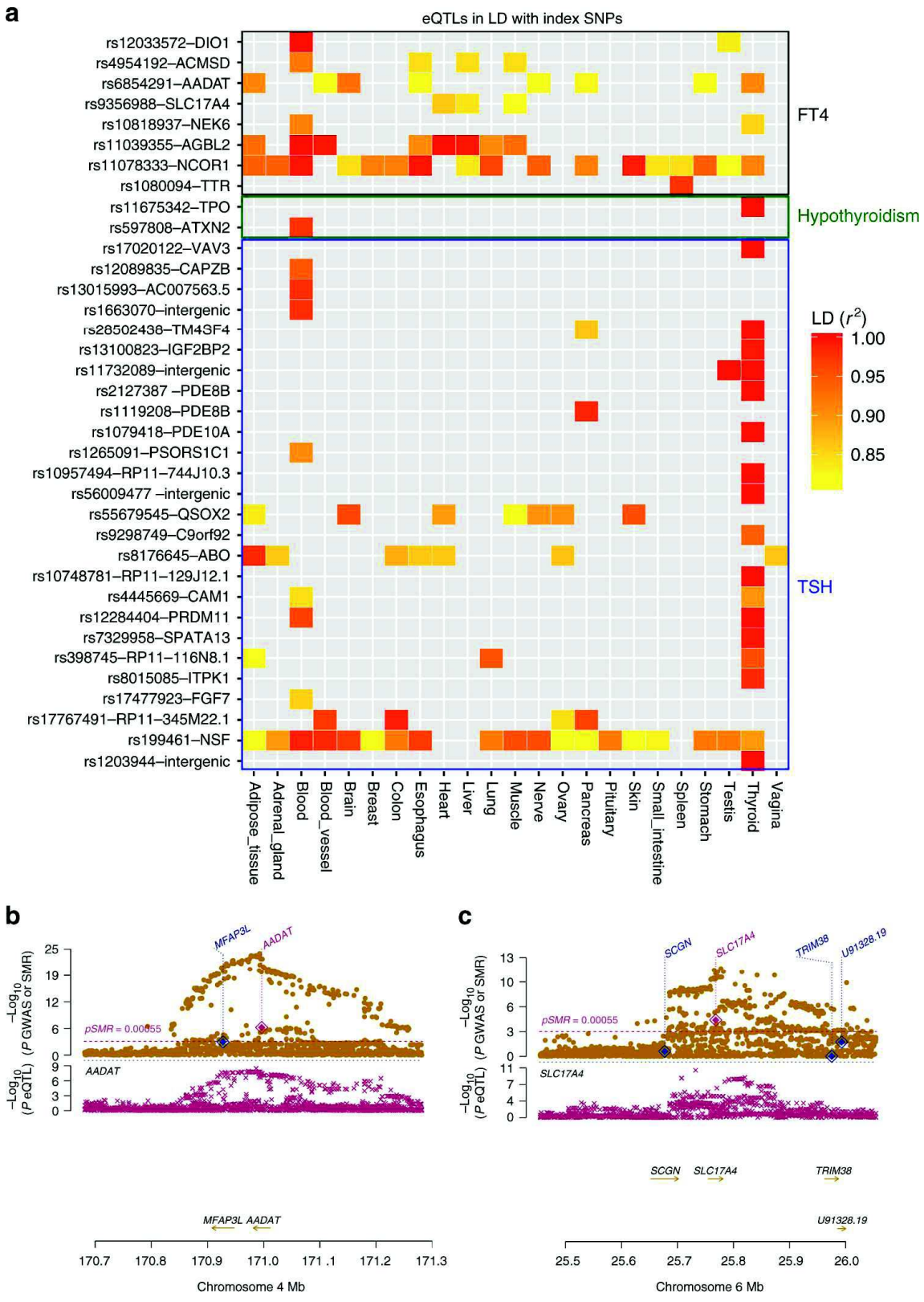
a
eQTLs in LD with index SNPs
rs12033572–DIO1
rs4954192–ACMSD
rs6854291–AADAT
rs9356988–SLC17A4
rs10818937–NEK6
rs11039355–AGBL2
rs11078333–NCOR1
rs1080094–TTR
rs11675342–TPO
rs597808–ATXN2
rs17020122–VAV3
rs12089835–CAPZB
rs13015993–AC007563.5
rs1663070–intergenic
rs28502438–TM4SF4
rs13100823–IGF2BP2
rs11732089–intergenic
rs2127387 –PDE8B
rs1119208–PDE8B
rs1079418–PDE10A
rs1265091–PSORS1C1
rs10957494–RP11–744J10.3
rs56009477 –intergenic
rs55679545–QSOX2
rs9298749–C9orf92
rs8176645–ABO
rs10748781–RP11–129J12.1
rs4445669–CAM1
rs12284404–PRDM11
rs7329958–SPATA13
rs398745–RP11–116N8.1
rs8015085–ITPK1
rs17477923–FGF7
rs17767491–RP11–345M22.1
rs199461–NSF
rs1203944–intergenic
FT4
Hypothyroidism
TSH
LD (r^2)
1.00
0.95
0.90
0.85
Adipose_tissue
Adrenal_gland
Blood
Blood_vessel
Brain
Breast
Colon
Esophagus
Heart
Liver
Lung
Muscle
Nerve
Ovary
Pancreas
Pituitary
Skin
Small_intestine
Spleen
Stomach
Testis
Thyroid
Vagina
b
MFAP3L
AADAT
pSMR = 0.00055
−Log10 (P GWAS or SMR)
−Log10 (P eQTL)
AADAT
MFAP3L AADAT
170.7
170.8
170.9
171.0
171 .1
171.2
171.3
Chromosome 4 Mb
c
SCGN
SLC17A4
TRIM38
U91328.19
pSMR = 0.00055
SLC17A4
SCGN SLC17A4
TRIM38
U91328.19
25.5
25.6
25.7
25.8
25.9
26.0
Chromosome 6 Mb

Figure 2 Impact on gene expression of index SNP. **a** shows tissues in which an expression QTL (eQTL) was found in LD ($r^2 > 0.8$) with FT4, hypothyroidism, and TSH index SNPs. SNPs are ordered according to trait they are associated with and then by genomic position; squares are colored according to the LD between the eQTL and the index variant, as depicted in the legend. When multiple eQTLs were detected in the same tissue, the eQTL with the highest LD is shown. **b** and **c** illustrate results of the summary-based Mendelian randomization (SMR) test for FT4 levels and expression QTLs at *AADAT* and *SLC17A4* loci, respectively. The upper box shows the regional association curve with FT4 levels, with level of significance of the SMR test (*y* axis) for each transcript in the locus indicated by a diamond positioned at the center of the transcript. A significant SMR test indicates an association of the transcript level of the respective genes with the trait. The lower box shows the regional association distribution with changes in expression of the highlighted transcript in pancreas. In both boxes, *x* axis refers to GRCh37/hg19 genomic coordinates

SLC17A4 is an organic anion transporter that is particularly expressed in the liver, kidney, and gastrointestinal tract (27). We transiently over-expressed human *SLC17A4* (hSLC17A4) in COS-1 cells and observed increased cellular T3 (**Figure 3a**) and T4 (**Figure 3b**) accumulation compared to empty-vector transfected control cells. These effects were even stronger upon co-transfection with the intracellular thyroid hormone-binding protein mu-crystallin (CRYM) (**Figure 3a, b**) and were similar in magnitude to those obtained by the monocarboxylate transporter (MCT) 8 (**Supplementary Figure 9**), the most specific thyroid hormone transporter identified to date. Saturation experiments in the absence of CRYM showed a dose-dependent decrease in the uptake of T3 (**Figure 3c**) and T4 (**Figure 3d**). The estimated IC_{50} values for T3 (0.35 ± 0.13 µM, $n = 4$) and T4 (0.06 ± 0.01 µM, $n = 4$) transport by SLC17A4 are considerably lower than those of MCT8 (T3: 20.61 ± 1.26 µM and T4: 23.22 ± 1.22 µM, $n = 3$, **Supplementary Figure 9**), and other currently known thyroid hormone transporters (28-33), and indicate a high substrate affinity. Together, these findings strongly indicate that *SLC17A4* encodes a high-affinity T3 and T4 transporter.

AADAT encodes a mitochondrial aminotransferase with broad substrate specificity, which acts on kynurenic acid and α-aminoadipate, important intermediates in tryptophan, and lysine metabolism (34, 35). The association of circulating FT4 with the *AADAT* locus suggested that AADAT may also be involved in thyroid hormone metabolism. In that case, it could facilitate the oxidative deamination of the alanine side-chain of thyroid hormone, yielding a pyruvic acid moiety (36). Therefore, lysates of AADAT over-expressing COS-1 cells were incubated with T4 and T3 in the presence of the co-factor pyridoxal phosphate and the co-substrate α-ketoglutaric acid, and the reaction mixtures were analyzed by ultra-performance liquid chromatography (UPLC). The results demonstrated effective time- and AADAT concentration-dependent conversion of T4 and T3 to their pyruvic acid metabolites TK3 and TK4 (**Figure 4**), with saturation occurring at substrate concentrations between 10 and 100 µM. Importantly, this is well below the reported Km values of AADAT for α-aminoadipate (0.9 mM) and kynurenine (4.7 mM) (34).

Given the observed effects of *SLC17A4* and *AADAT* on T3 and T4 transport and metabolism, we additionally tested the associations of the identified genetic variants in *SLC17A4* and *AADAT* with T3 levels and the T3/T4 ratio (**Supplementary Table 6).** *SLC17A4*-rs9356988 was associated with the T3/T4 ratio, while *AADAT*-rs6854291 was associated with both the T3/T4 ratio and T3 levels.

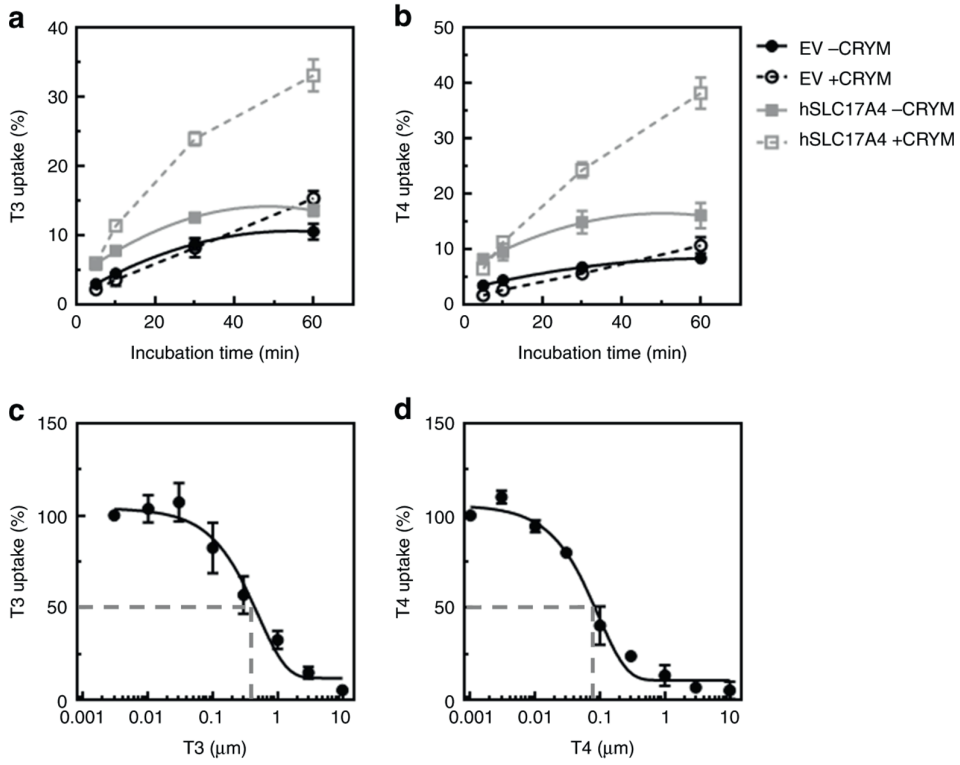

Figure 3 Thyroid hormone transport by hSLC17A4. Cellular T3 (**a**) and T4 (**b**) accumulation in COS-1 cells, transiently transfected with empty vector (EV), or wild-type hSLC17A4 in the absence (solid lines) or presence (dashed lines) of the intracellular thyroid hormone-binding protein CRYM, after indicated incubation times at 37 °C. All uptake levels are expressed relative to the amount of radio-labeled T3 or T4 added to the cells at the start of the incubation (1 nM (5 × 10*E*4 c.p.m.) [^{125}I]-T3 or [^{125}I]-T4). All results are presented as means ± SEM (n = 4). In the presence and absence of CRYM, T3 and T4 accumulation in hSLC17A4 transfected cells was significantly higher compared to empty-vector control cells at all time points (one-way ANOVA with a Bonferroni-corrected post hoc test, $p < 0.001$). T3 (**c**) and T4 (**d**) saturation curves in COS-1 cells transiently transfected with hSLC17A4 in the absence of CRYM. All data points are corrected for background thyroid hormone uptake in control cells and presented relatively to the amount of internalized thyroid hormone in the presence of the lowest substrate concentration (0.003 µM for T3 and 0.001 µM for T4, respectively). Apparent IC_{50} values were determined by standard second order polynomial regression analyses implemented in GraphPad Prism (La Jolla, USA).

Genetic TSH and FT4 risk score associations

To assess the cumulative clinical impact of our GWAS findings, we calculated a weighted GRS for TSH and FT4 levels, which included all independent TSH- and FT4-associated variants, respectively. Next, these GRSs were tested for association with the risk of hypothyroidism and hyperthyroidism in up to 21,287 individuals. **Figure 5** shows substantial differences in the risk of thyroid dysfunction across the range of GRS scores. Individuals with a TSH-based GRS in the highest quartile compared to individuals with a GRS in the lowest quartile had an odds ratio of 2.53 ($p = 6.8 \times 10^{-32}$) for hypothyroidism and 0.19 ($p = 9.8 \times 10^{-31}$) for hyperthyroidism, respectively. Conversely, the FT4-based GRS did not show any significant associations with either hypo or hyperthyroidism (**Supplementary Table 7**), which is consistent with the limited overlap observed between TSH and FT4 loci.

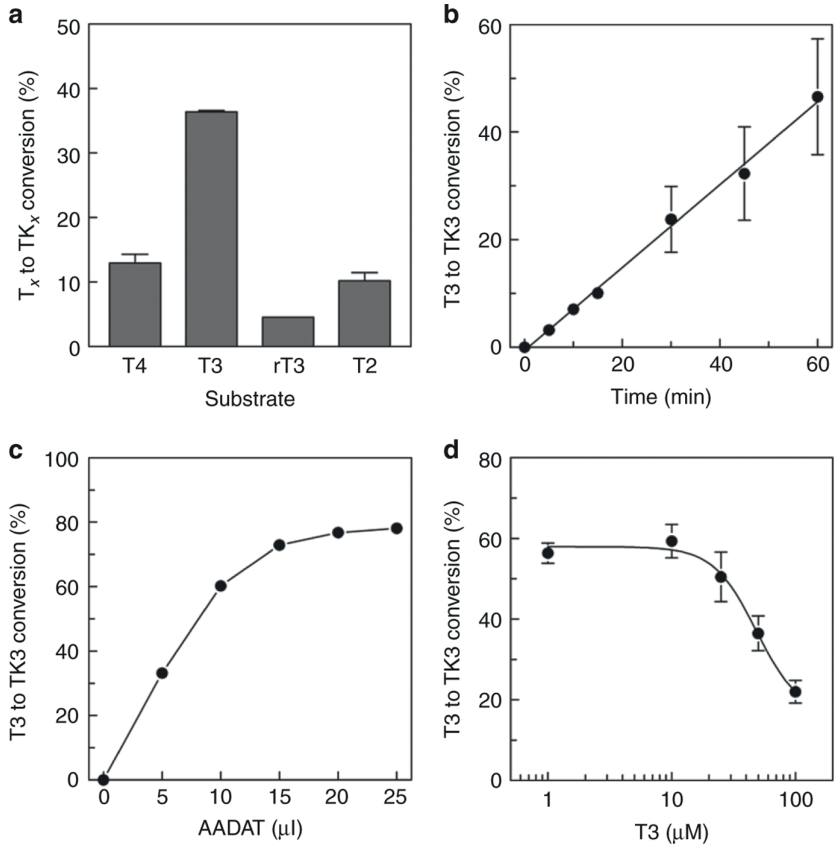

Figure 4 AADAT converts T3 and T4 to their respective pyruvic acid metabolites. **a** shows the conversion of T3 and T4 to their pyruvic acid metabolites TK3 and TK4 in cell lysates of hAADAT over-expressing COS-1 cells. Cell lysates were incubated with [I^{125}]-T3 or [I^{125}]-T4 (2×10^5 c.p.m.) in the presence of 0.1 mM pyridoxal 5′-phosphate and 1 mM α-ketoglutaric acid for 30 min and the resulting radio-labeled metabolites were separated by UPLC. The conversion of T3 to TK3 depends on the incubation time (**b**) and amount of cell lysate added to the incubation reaction (**c**) and is saturated at substrate concentrations between 10 and 100 µM (**d**). The percentage conversion reflects the amount of TK3 as a percentage of the total radioactivity eluted from the UPLC column and is corrected for the TK3 production in lysates derived from empty-vector-transfected control cells (which was nearly absent). All data are presented as means ± SEM ($n = 3$).

A GRS using all TSH-associated variants showed a significant association with Graves' disease ($p = 2.9 \times 10^{-5}$) that remained significant after excluding the *PSORS1C1* variant ($p = 2.5 \times 10^{-4}$), indicating a polygenic contribution of TSH-associated variants detected in the general population to Graves' disease.

As normal thyroid function is essential for the physiological function of virtually all human tissues, we tested if the TSH and FT4 GRSs were associated with a broader range of phenotypes by using available GWAS results of these phenotypes. These results are shown in **Supplementary Table 8** with effects provided per increase in standard deviation of either TSH or FT4. A higher TSH GRS was associated with both a lower risk of Graves' disease (odds ratio (OR) = 0.64, $p = 2.0 \times 10^{-5}$) and goiter (OR = 0.30, $p = 3.9 \times 10^{-27}$), and lower thyroid volume (Δvol = −23%, $p = 1.3 \times 10^{-37}$), whereas a higher

FT4 GRS was associated with a higher risk of goiter (OR = 1.52, $p = 7.9 \times 10^{-3}$) and higher thyroid volume (Δvol = 9%, $p = 3.8 \times 10^{-3}$). In addition, a higher TSH GRS was associated with a lower risk of schizophrenia (OR = 0.94, $p = 0.01$), shorter height (sd[height]:beta = −0.05, $p = 2.0 \times 10^{-11}$), and reduced kidney function (ΔeGFR = −1%, $p = 1.4 \times 10^{-5}$), as well as higher LDL (sd[LDL]:beta = 0.04, $p = 4.9 \times 10^{-3}$) and total cholesterol levels (sd[chol]:beta = 0.05, $p = 1.1 \times 10^{-5}$). A higher FT4 GRS was additionally associated with taller height (sd[height]:beta = 0.04, $p = 2.9 \times 10^{-4}$), lower BMI (sd[BMI]:beta = −0.04, $p = 2.7 \times 10^{-3}$), and lower LDL (sd[LDL]:beta = −0.06, $p = 3.1 \times 10^{-4}$) and total cholesterol levels (sd[chol]:beta = −0.05, $p = 6.1 \times 10^{-3}$) (**Supplementary Table 9**). These associations match clinical and epidemiological observations.

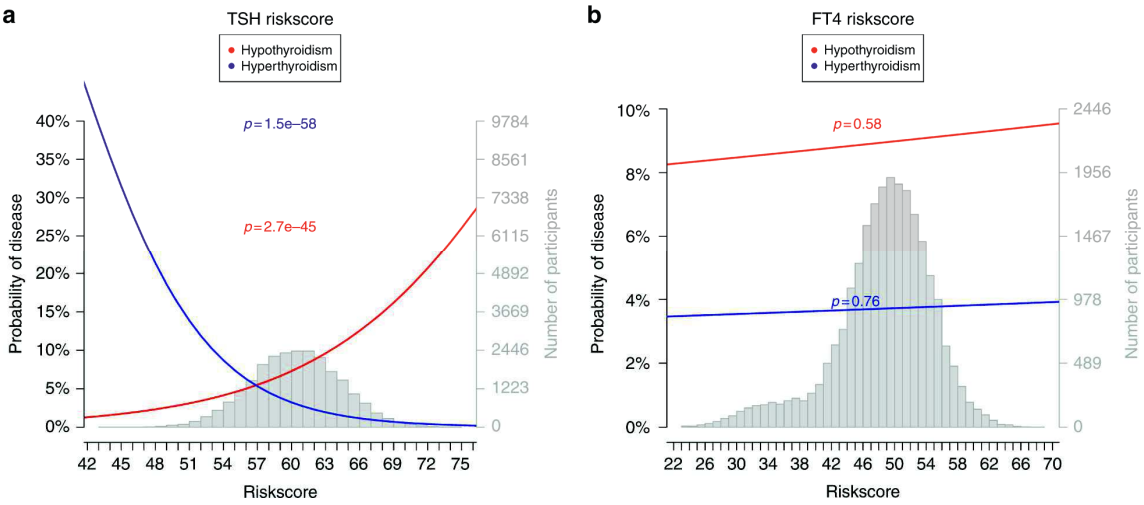

Figure 5 Associations of genetic risk scores with hypothyroidism and hyperthyroidism. The *y* axis shows the probability of hypothyroidism (red) or hyperthyroidism (blue) with the *p*-value of the association test of the trait on the risk score. The *x* axis shows the percentage of risk alleles carried based on a weighted genetic risk score (GRS) built using the 61 TSH-associated (**a**) and 31 FT4-associated GWAS SNPs (**b**). The gray histogram shows the distribution of the GRS in the study sample

DISCUSSION

With 8 million genetic variants tested in up to 72,167 individuals, we present results of the largest GWAS on thyroid function and dysfunction performed so far. We identified 109 significantly and independently associated genetic variants, doubling the number of loci known to regulate thyroid function, which explain a substantial part of the variation in these traits. Importantly, we detected associations between these variants and thyroid diseases as well as various clinical end points, and functionally characterized a new thyroid hormone transporter as well as a new thyroid hormone metabolizing enzyme.

Almost all previously identified TSH and FT4-associated SNPs were also genome-wide significantly associated with the respective trait in our analyses: the 20 TSH and 4 FT4 associations of the sex-combined GWAS of Porcu et al.(11), the two additional TSH SNPs as well as the FT4 association revealed

in Taylor et al.(12), and 17 of the 21 genome-wide significantly TSH-associated SNPs identified by Gudmundsson et al.(13). The remaining loci of the latter study were discovered in our study via the mouse candidate analysis and were also associated with hypothyroidism (*TPO*), associated with FT4, hypo and hyperthyroidism (*FOXE1*), or had a $p < 1 \times 10^{-6}$ (*FOXE1*, *ELK3*, *SIVA1*). Only two FT4-associated loci, *LPCAT2/CAPNS2* and *NETO1/FBXO15*, identified in the sex-stratified analysis of Porcu et al. did not replicate in our sex-specific GWAS ($p \geq 0.01$). While all but 2 of the 18 cohorts (the Old Order Amish and the Baltimore longitudinal study on Aging) of Porcu et al. as well as four of the seven cohorts (TwinsUK GWAS, SardiNIA, Val Borbera and BHS) of Taylor et al. were also included in our GWAS, we more than doubled the sample size for both traits, thereby significantly increasing our power to detect new loci.

Consistent with HPT-axis physiology, most TSH-associated variants acted on gene expression levels in thyroid tissue, while the FT4-associated variants had more widespread effects on multiple known thyroid hormone target tissues. In addition, four of the newly identified variants were either associated with the risk of TPOAb positivity or Graves' disease, suggesting an underlying autoimmune-related pathophysiology. All of these findings confirm that GWAS in the general population provides a valuable method to identify genes implicated in thyroid physiology and/or thyroid disease. Moreover, these insights can be successfully translated into experimental evidence, as illustrated by our in vitro studies on S*LC17A4* and *AADAT*.

To investigate the combined effect of the thyroid hormone associated risk variants, we calculated a GRS. The GRS of TSH-associated variants was significantly associated with the risk of hypothyroidism and hyperthyroidism. For some FT4-associated hits, the lack of association with TSH levels can be explained on physiological grounds. For example, the identified SNP in *DIO1* decreases the enzymatic activity of the protein, leading to less T4 to T3 conversion, resulting in higher T4 levels, but lower T3 levels, resulting in no net effect on feedback to the pituitary and therefore no effect on TSH levels. Similar hypotheses could be postulated for other loci involved in thyroid hormone metabolism, such as *DIO3OS* and *AADAT*. To assess whether these genetically estimated TSH levels are clinically relevant or merely reflect physiological inter-individual differences in TSH levels (i.e., HPT-axis setpoint), we tested the GRS against various clinical end points. These analyses showed significant associations with thyroid diseases, and also with altered lipid levels (total and LDL cholesterol) and height, which are both known to be affected by hypo and hyperthyroidism. For example, short stature is one of the key characteristics of patients suffering from congenital hypothyroidism. Interestingly, associations were also found with kidney function and schizophrenia, for which the causal relationships are less apparent. Thyroid hormone has been shown to influence kidney development and filtration function (37, 38). Likewise, rodent and human studies have shown that both hypo and hyperthyroidism lead to disrupted prenatal glial cell development, which is an important step in the development of schizophrenia (39), while various psychiatric diseases including schizophrenia are also thought to influence thyroid function via central effects on the HPT axis (40). Future studies are needed to clarify the mechanisms underlying these associations, as it is not possible to solve these potential inverse causal relationships solely with GWAS results. Irrespective of the direction of the effects, our results suggest that the presence of kidney dysfunction and psychiatric symptoms in patients with thyroid disease deserve attention. Given the substantial increase in number of TSH and FT4-associated variants, which explain a substantial part of the variation in these traits, future studies should start exploring the use of these markers to predict the individual HPT-axis setpoint. This predicted setpoint could be used to guide

treatment of thyroid diseases, which is important as despite normalized TSH and FT4 levels, a substantial part of treated patients still have persistent hypo or hyperthyroid complaints, leading to a lower quality of life (41). This could be due to the fact that the TSH and FT4 levels are normalized to within the population-based reference ranges, but still deviate from the patient's individual setpoint. For this purpose, a GWAS on the TSH/FT4 ratio could prove to be a more sensitive method to identify more variants, which specifically affect the HPT-axis setpoint.

When interpreting the results of our GWAS studies on increased and decreased TSH levels, it is important to realize that these studies were performed in population-based cohorts, and not in dedicated thyroid disease patient cohorts. Individuals on thyroid medication or a history of thyroid surgery were excluded, resulting in a relative overrepresentation of individuals with subclinical forms of thyroid dysfunction. The identified variants are therefore expected to be a mix of variants, which have been previously associated with hypo or hyperthyroidism (e.g., *TPO*, *FOXE1*, and *ATXN2*) and variants that lead to a TSH level, which is slightly above or below the population-based reference ranges. These latter effects can either reflect true mild thyroid dysfunction with increased risk of clinical consequences or merely reflect a deviation from the individual HPT-axis setpoint with no clinical consequences. While our GRS analyses suggest that carrying multiple risk alleles leads to an increased risk of overt thyroid dysfunction and related clinical consequences, the exact contribution of each individual variant needs to be clarified in future studies.

Thyroid hormone is importantly metabolized through enzymatic deiodination by DIO1-3, but also undergoes alternative metabolic reactions, including conjugation with sulfate or glucuronic acid and modification of the alanine side-chain. The latter includes the conversion of T3 and T4 to their respective pyruvic acid metabolites TK3 and TK4, which requires the oxidative deamination of their alanine side-chain (36). TK3 and TK4 have been detected in urine and bile of rat injected with radio-labeled T3 and T4 (42). Although these and other studies suggested an important role for the liver and kidney in the formation of these pyruvic acid metabolites, the involved enzyme(s) had not been identified. Our functional analyses demonstrated that AADAT effectively catalyzes the transamination of T4 and in particular T3 to TK4 and TK3, respectively. Moreover, AADAT is highly expressed in the liver, gastrointestinal tract, and kidney in human (43). Taken together, AADAT activity may thus be critical for the rate of thyroid hormone metabolism, which likely underlies the association of *AADAT* with circulating FT4. Although the specific impact of the associated variant on *AADAT* expression has not been assessed yet, our eQTL co-localization studies indicate that the index SNP decreases *AADAT* transcript levels in the thyroid, and this in turn leads to increased circulating FT4 levels.

The functional analyses further demonstrate that human SLC17A4 is able to transport both T4 and T3. The protein belongs to the solute carrier 17 family, whose members transport various organic anions, such as *p*-aminohippuric acid. Genetic variation in the *SLC17A4* locus has been associated with the progression of elevated serum urate levels to gout (27, 44). According to the GTEx data resource and previously reported studies (27), *SLC17A4* is predominantly expressed in human small intestinal and colonic epithelial cells, pancreas, liver, and kidney cortex, which could imply a role for this transporter in the metabolic clearance and entero-hepatic cycle of thyroid hormone. Future studies should investigate the pharmacokinetic properties of SLC17A4, its relative contributions to thyroid hormone transport in various individual tissues, as well as the effects of the identified *SLC17A4* variants on thyroid hormone transport.

The findings from our functional studies do not only provide new insights into thyroid hormone physiology, but may also have important clinical implications. Hypothyroidism is treated with levothyroxine (LT4), which is inexpensive and administered orally. In recent decades, various factors have been identified which help to determine LT4 dose, such as weight, gastrointestinal diseases, and interfering drugs (45, 46). Despite this knowledge, ineffective LT4 supplementation is still a major clinical problem, as 30–50% of patients are either under- or over-treated and therefore remain at risk for the symptoms and complications associated with thyroid dysfunction (45, 46). Therefore, the identification of SLC17A4 as a thyroid hormone transporter and AADAT as a thyroid hormone metabolizing enzyme provides new insights into thyroid hormone physiology and opens up a potential avenue for novel therapeutic targets or optimization of existing ones to improve the care of patients suffering from thyroid dysfunction. All genetic findings in our study were limited to common or low-frequency SNPs, whereas rare SNPs or structural variants may also contribute to the yet unexplained variance of thyroid function. Large whole-exome or -genome sequencing studies are required to reveal these rare variant associations (47). Furthermore, additional GWAS with increased sample size will help to reveal the yet undiscovered associations of common and low-frequency SNPs. Our ThyroidOmics Consortium (http://www.thyroidomics.com) provides a well-established infrastructure to address these knowledge gaps in future projects.

METHODS

Included studies

Discovery meta-analyses included data from 22 independent cohorts with 54,288 subjects for the TSH analyses, and from 19 cohorts with 49,269 subjects for FT4, 53,423 subjects (3440 cases) for hypothyroidism, and 51,823 subjects (1840 cases) for hyperthyroidism (**Supplementary Data 1**). Selected SNPs from the TSH or FT4 analyses were carried forward for replication with in silico GWAS data from 5 cohorts (9053 subjects) and de novo genotyping in additional 5 cohorts (13,330 subjects). All subjects gave informed consent and studies were approved by the cohort-specific ethics committees.

We used the results of the GWAS of TPOAb positivity that included 18,297 subjects (20) for a look-up of all the 53 TSH-associated loci or their HapMapII proxies ($r^2 > 0.8$ in a 1 Mb window) that were available in that dataset to assess their relation to autoimmune hypothyroidism. A complementary look-up was performed for the 52 SNPs that were available in a GWAS on Graves' disease diagnosed by clinical examinations, circulating thyroid hormone and TSH concentrations, serum levels of antibodies against thyroglobulin, thyroid microsomes, and TSH receptors, ultrasonography, $^{[99m]}TCO_4^-$ (technetium-99m pertechnetate) (or [^{123}I] (radioactive iodine)) uptake and thyroid scintigraphy using the data of the BioBank Japan Project (BBJ) including 1747 patients and 6420 controls (**Supplementary Data 1**).

Trait definition

In each study, only subjects with TSH levels within the cohort-specific reference range were included for the TSH and FT4 analyses. TSH and FT4 were analyzed as continuous variables after inverse normal transformation. Increased TSH was defined by a TSH level above the upper limit of the cohort-specific TSH reference range, while decreased TSH was defined by a level below the lower limit of the reference range. For both increased and decreased TSH analyses, the comparison group consisted of subject with a TSH level within the cohort-specific reference range. Exclusion criteria for all analyses were non-European ancestry, use of thyroid medication (defined as ATC (Anatomical Therapeutic Chemical) code H03), or previous thyroid surgery.

GWAS in individual studies

In each study of the discovery GWAS, genotyping was performed on genome-wide arrays. Genome-wide data were imputed to the 1000 Genomes, phase 1 version 3 (March 2012) ALL populations reference panel, including the X chromosome. Quality control before imputation was applied in each study separately. Details on study-specific genotyping and imputation information are provided in the **Supplementary Data 1**.

In the individual study GWAS, the association of the SNPs was analyzed using linear regression for TSH and FT4, and logistic regression for decreased and increased TSH. The genotype–phenotype association was conducted using an additive genetic model on SNP dosages, thus taking genotype uncertainties of imputed SNPs into account. The analyses for TSH and FT4 were initially sex-stratified and meta-analyzed as a second step. The analyses were adjusted for age, age-squared (to account for non-linear effects), and relevant study-specific covariates such as principal components for population stratification, study center, and family structure (e.g., by inclusion of the kinship matrix as a random effect), if applicable. The family-based cohorts GARP, SardiNIA, ValBorbera, MICROS, TwinsUK, LLS, and FHS conducted additional analyses on the men and women-combined sample, with additional adjustment for sex, to properly account for their family relatedness.

Statistical methods for meta-analysis

Result files from individual studies included in this analysis underwent extensive quality control before meta-analysis: file format checks as well as plausibility and distributions of association results including effects, standard errors, allele frequencies, and imputation quality of the SNPs were obtained by using the gwasqc() function of the GWAtoolbox package v2.2.4 (48). Additionally, the known associations of rs6885099 in *PDE8B* with TSH and rs2235544 in *DIO1* with FT4 were checked for consistent effect direction and size in each study. All cohort-specific genomic control values (λ_{GC}) ranged from 0.94 to 1.14 (median 1.00) for the continuous trait and from 0.68 to 1.04 (median 0.91) for the dichotomous trait GWAS.

All meta-analyses were carried out in duplicate by three independent analysts. We conducted a fixed-effect meta-analysis applying inverse-variance weighting as implemented in Metal (49). SNPs with MAF ≤0.005 or an imputation quality score ≤0.4 were excluded prior to the meta-analyses resulting in a median of 9,653,808 SNPs per cohort (IQR: 9,302,604–10,705,092). During the meta-analysis, the study-specific results were corrected by their specific λ_{GC} if >1. Results were checked for possible errors like use of incorrect unit, trait transformation, or association model by plotting the association *p*-values

of the analyses against those from a *z*-score-based meta-analysis for verifying overall concordance. SNPs that were present in <75% of the total sample size contributing to the respective meta-analysis (separately for autosomal and X-chromosomal SNPs) or with a MAF ≤0.01 (hypo and hyperthyroidism MAF ≤0.05 because of the low number of cases in the analysis) were excluded from subsequent analyses. Finally, data for up to 8,048,941 genotyped or imputed autosomal and X-chromosomal SNPs were available after the discovery stage meta-analysis of TSH, FT4, and up to 5,965,951 SNPs after hypo and hyperthyroidism.

Quantile–quantile plots of the meta-analysis results are provided in **Supplementary Figures 10** and **11**. To assess whether there was an inflation of *p*-values in the meta-analysis results attributed to reasons other than polygenicity, we performed LD score regression (50). The LD score-corrected λ_{GC} values of the meta-analysis results ranged from 1.00 to 1.04, supporting the absence of unaccounted population stratification. Genome-wide significance was defined as a *p*-value of $<5 \times 10^{-8}$, corresponding to a Bonferroni correction of one million independent tests. Unless stated otherwise, all reported *p*-values are two-sided. The I^2 statistic was used to evaluate between-study heterogeneity (51).

Gene-by-sex interaction on the circulating TSH and FT4 levels were obtained for each SNP by comparing the discovery meta-analysis results from men (TSH: $n = 24{,}618$; FT4 $n = 22{,}315$) and women using a *t*-test. Test statistics were calculated using the formula $t = (\beta_{men} - \beta_{women})/\text{sqrt}(SE_{men}^2 + SE_{women}^2)$, assuming independent effect sizes between men and women.

To evaluate the presence of independent SNPs within each locus, SNPs were clustered based on their correlation with the SNP showing the lowest *p*-value at that locus (index SNP) using the software PLINK(52) and the genotypes of the combined individuals of the 1000Genomes phase1v3 all ethnicities reference panel (linkage disequilibrium pruning using $r^2 \leq 0.01$ within windows of ±1 Mb). The loci were named according to the nearest gene of the index SNP. Genomic positions correspond to build 37 (GRCh37).

Replication analysis

The genome-wide significant index SNPs of newly identified loci from the sex-combined TSH ($n = 22$) and FT4 meta-analyses ($n = 19$) were taken forward to the replication stage (**Supplementary Table 10**). When SNPs were not available in the in silico replication datasets, a proxy SNP in LD with $r^2 > 0.8$ was selected.

Of the ten studies that contributed to replication, five studies used 1000Genomes imputed dosages, three studies performed de novo genotyping, and two studies were genotyped on both the Illumina ExomeChip and CardiometaboChip. No SNP or proxy for the X-chromosomal locus was available in any replication dataset. The results from the discovery meta-analysis and the results of replication studies were meta-analyzed to obtain the overall *p*-values of the selected SNPs. SNPs with *p*-values below genome-wide significance in this combined analysis and with concordant effect directions in both stages were considered as replicated (53).

Integration of information from genetically manipulated mice

We tested whether information about thyroid function or disease from genetically manipulated mice could facilitate the detection of additional human thyroid loci that did not reach genome-wide significance in the GWAS (nested candidate gene approach). To this end, all genes that when manipulated cause abnormal thyroid physiology (MP:0002876; 26 genes) or abnormal thyroid gland morphology (MP:0000681; 51 genes) were selected from the comprehensive Mouse Genome Informatics resource in October of 2016 (http://www.informatics.jax.org/mp/). Next, genes were translated to their human homologs, followed by the calculation of the number of independent SNPs in these genes with MAF > 0.01 in the 1000 Genomes EUR populations (PLINK option—indep-pairwise 50 5 0.2) to obtain multiple testing corrected significance thresholds ($p < 2.5 \times 10^{-5}$ for physiology and $p < 1.9 \times 10^{-5}$ for morphology). The genes in the respective mouse lists were then queried for the presence of SNPs that showed association with TSH and/or FT4 below the significance threshold. To test whether the number of genes with significant associations was higher than expected by chance, results were compared to those from 2000 iterations of random gene lists of equal length. A *p*-value for enrichment was computed from a complementary cumulative binomial distribution as described in detail previously (54). Lastly, novel loci that were not identified at genome-wide significance in the GWAS of TSH or FT4 were tested for replication in up to 9011 and 4532 independent samples for TSH and FT4, respectively. Successful replication was defined as direction-consistent association and genome-wide significance in a meta-analysis of the discovery and replication samples.

eQTL look-up

To assess the possible effect of our lead signals on transcriptional activity, we queried expression QTL (eQTL) results from 22 publicly available studies (specific reference listed in **Supplementary Data 3**). These studies were carried out from 2007 to February 2017 on 127 different tissues and cell types, and used either micro-array or sequencing-based assessment of gene expression. For each study, we derived the list of top eQTLs by LD clumping, and searched top eQTLs in high LD ($r^2 > 0.8$ in 1000Genomes EUR samples) with the 94 thyroid function-associated index or independent SNPs (TSH, FT4, and *ATXN2* and *TPO* as additional GWAS loci from hypothyroidism) (**Supplementary Tables 1**, **2**, and **4**).

To evaluate the evidence of co-localization between the index GWAS and eQTL SNPs, we used the SMR method (24), coupled with the test for heterogeneity of effects (HEIDI) (24). The first tests whether the effect on expression seen at a SNP or at its proxies correlates with the signal observed in the GWAS (SMR test), while the second evaluates if the eQTL and GWAS associations can be attributable to the same causative variant (HEIDI test). Because direction of effects has to be taken into account, we focused this analysis only on GTEx data for which full summary results were available. For SMR, we considered the experiment-wise *p*-value of 2×10^{-4} (corresponding to a Bonferroni correction for 242 gene-thyroid trait-tissue combinations assessed). Specifically, we tested all genes with an eQTL *p*-value $<1 \times 10^{-7}$ and for which the top eQTL showed genome-wide significant association with any thyroid hormone traits, regardless of LD between the top eQTL and the thyroid hormone index SNP. For the HEIDI test, we used the suggested *p*-value >0.05 cutoff to declare co-localization, and further required that at least five SNPs were available for the test (24).

Materials for *in vitro* studies

[^{125}I]T3 and [^{125}I]T4 were synthesized using the standard chloramine-T method (55). Unlabeled iodothyronines, pyridoxal 5'-phosphate (PLP), 4-(2-hydroxyethyl)-1-piperazineethanesulfonic acid (HEPES), bovine serum albumin, D-glucose, and Na_2SeO_3 were obtained from Sigma-Aldrich (Zwijndrecht, The Netherlands); and α-ketoglutaric acid (KG) from Merck Millipore (Amsterdam, NL).

Expression constructs and cloning

The cDNA of MCT8 and CRYM was cloned into pcDNA3 and pSG5 expression vectors, respectively, using standard cloning techniques (56, 57). A pCMV6-Entry_SLC17A4 expression vector containing a C-terminal Myc and Flag tag was obtained from OriGene Technologies (Rockville, USA). A pbluescript AADAT cDNA construct was obtained from Thermo Scientific (Bleiswijk, NL) and subcloned into pcDNA3 with addition of a C-terminal Flag-tag using standard cloning techniques. Any variants were substituted in agreement with the NM_001286683.1 reference sequence using Quikchange site-directed mutagenesis according to manufacturer's protocol (Stratagene, Amsterdam, The Netherlands). All primers are available upon request. Correctness of all expression constructs was confirmed by sequencing of the inserts.

Cell culture and transfection

COS-1 African green monkey kidney cells were obtained from ECACC (Sigma-Aldrich, Zwijndrecht, NL) and cultured in DMEM/F12 (Life Technologies, Bleiswijk, NL) containing 9% heat-inactivated fetal bovine serum (Sigma-Aldrich) and 0.2 mg mL^{-1} penicillin/streptomycin (Life Technologies). Cell culture flasks and dishes were obtained from Corning (Schiphol, NL).

For T3 and T4 uptake studies, COS-1 cells were seeded in 24-well dishes (1×10^5 cells per well) and transiently transfected at 70% confluence with 250 ng empty vector (EV), SLC17A4, or MCT8, with or without the addition of 100 ng CRYM. CRYM is a cytoplasmic high-affinity thyroid hormone-binding protein, which prevents efflux of internalized thyroid hormones. For thyroid hormone metabolism assays, COS-1 cells were seeded on 10 cm dishes (5×10^5 cells per well) and transiently transfected with 2000 ng EV or AADAT at 70% confluence. Xtreme-Gene 9 was used as a transfection reagent according to manufacturer's protocol (Roche Diagnostics, Almere, NL).

Thyroid hormone uptake studies

Thyroid hormone uptake studies were performed according to well-established protocols (58, 59). Cells were washed with incubation medium (Dulbecco's PBS (D-PBS) and 0.1% D-glucose) and incubated for 10 min with 1 nM (5×10^4 c.p.m.) [^{125}I]T_3 or [^{125}I]T_4 in 375 µl incubation medium at 37 °C. Finally, cells were washed once with incubation medium and lysed with 0.1 M NaOH. Radioactivity in the lysates was measured with a γ-counter. For saturation experiments, the indicated concentrations of unlabeled T3 or T4 were added to the incubation medium.

Thyroid hormone metabolism studies

Two days after transfection, cells were harvested in 20 mM HEPES buffer (pH 7.5) and lysed by vortexing the sample for 30 s. Samples were clarified by centrifugation at 20,000×*g* for 30 min at 4 °C. Thyroid hormone aminotransferase activity was measured in duplicate by incubating 0.1-100 µM of T3

or T4 in the presence of 2×10^5 c.p.m. ^{125}I-labled hormone for 5–60 min at 37 °C with 5–25 µl clarified lysate, 1 mM KG and 0.1 mM PLP in a total volume of 100 µl HEPES buffer. Reactions were quenched by addition of 125 µl ice-cold 0.1% acetic acid in acetonitrile, followed by 1 h of incubation on ice to precipitate proteins. After centrifugation (20,000×*g*, 15 min, 4 °C), 125 µl of the supernatant was mixed with 125 µl ammonium acetate buffer (20 mM, pH 4.0), and 100 µl was analyzed by UPLC (Waters, Etten-Leur, NL) using a BEH C18 reversed phase column (130 Å, 2.1 × 100 mm, 1.7 µm). Ammonium acetate buffer (20 mM, pH 4.0, solvent A) and 0.1% acetic acid in acetonitrile (solvent B) were used as mobile phase. Flow rate was 0.35 mL min^{-1}, and column temperature 30 °C. The gradient used was: 0–1 min (30% B), 1–7 min (30–42% B), 7–23 min (42–58% B), 25–27 min (58–100% B), and 27–32 min (100–30% B). The radioactivity in the eluate was monitored using a Radiomatic A-500 flow scintillation detector (Packard Instruments, Meriden, CT).

Genetic risk score analysis

Two separate GWAS effect size-weighted GRS were generated to evaluate the combined effect of the TSH- and FT4-increasing alleles, respectively, on the risk of hypo and hyperthyroidism using individual level data from four of our largest GWAS studies: ARIC, CHS, Rotterdam Study, and SHIP (hypothyroidism cases: $n = 1613$; hyperthyroidism cases: $n = 662$; controls: $n = 19{,}674$). The GRS were based on the 61 and 31 replicated GWAS SNPs for TSH and FT4, respectively (**Supplementary Tables 1** and **2**), normalized to a range of 0 to 100, associated in each cohort separately using a logistic regression adjusted for sex and age, and combined afterwards by a fixed-effect inverse-variance meta-analysis using R (60). The probability of disease was calculated using the formula $1/(1 + \exp(-(\beta_0 + \beta_1 * x)))$, where β_0 and β_1 correspond to the intercept and GRS-related effect in the regression model, respectively.

To test the combined effect of the replicated TSH and FT4 SNPs on various traits (**Supplementary Tables 8** and **9**), a GRS-based association on meta-analyses results was performed as described in reference (61) using the function grs.summary() of the R-package gtx. If a specific SNP was not available in the look-up GWAS dataset, a proxy SNP in LD with $r^2 > 0.8$ was included where possible. The association effects correspond to a change in the look-up GWAS trait (or natural logarithm of the odds ratio in the case of a binary trait) per standard deviation unit of TSH and FT4, respectively. In case the trait was logarithm-transformed in the GWAS, $(e^{beta}-1) \times 100$ corresponds to a 1% change of this trait.

Pathway analyses

We performed Data-Driven Expression Prioritized Integration for Complex Traits (DEPICT) (62) analyses to prioritize the most likely causal genes at the associated loci and identify enriched pathways and tissues. We used DEPICT version 1 rel194 and included variants with GC-corrected *p*-value $<1 \times 10^{-5}$ from discovery GWAS as input. The following parameters were applied in the DEPICT analyses: 50 repetitions used to compute the false discovery rate, 500 permutations used to adjust for biases such as gene length, and 500 null GWAS used to run repetitions and permutations.

Genes for network analysis were selected using the associated genes from DEPICT using the lead SNPs from the analyses of the discovery GWAS. The Ingenuity Pathway Analysis Software Tool (IPA; Ingenuity® Systems, CA, USA) Network was used in order to perform pathway analysis (core analysis). Molecules and/or relationships considered were the ones available in the IPA Knowledge Base for mammals. Confidence filters considered only relationships, direct and indirect, where the confidence

is experimentally observed or high (predicted). Networks were generated with a maximum size of 35 genes and allowing up to 25 networks per analysis. We did not restrict for tissue and cell lines or mutations. The networks are constructed using the IPA algorithm with the Ingenuity Knowledge Base as a reference set generating a score as well as a *p*-value. IPA computes a score for each network according to the fit of that network to the user-defined set of focus genes. The score indicates the likelihood of the focus genes in a network being found together due to random chance. The significance of *p*-value is calculated using the right-tailed fisher exact test.

Look-up of pleiotropy

The look-up of additional traits associated with the replicated GWAS findings were performed using the PhenoScanner (63) database with the default search options, whereas the independent SNPs of the replicated TSH, FT4, hypo, and hyperthyroidism-associated loci or their proxies ($r^2 > 0.8$) obtained by SNiPa (64) were used as input. Look-up results with genome-wide significant *p*-value (5×10^{-8}) were reported.

Data availability

Summary genetic association results are available for full download or visualization on the CHARGE dbGaP website under accession phs000930 (https://www.ncbi.nlm.nih.gov/gap) and in the locuszoom web page: http://locuszoom.sph.umich.edu/genform.php.

SUPPLEMENTAL MATERIAL

Full author list and affiliations

Teumer A, Chaker L, Groeneweg S, Li Y, Di Munno C, Barbieri C, Schultheiss UT, Traglia M, Ahluwalia TS, Akiyama M, Appel EVR, Arking DE, Arnold A, Astrup A, Beekman M, Beilby JP, Bekaert S, Boerwinkle E, Brown SJ, De Buyzere M, Campbell PJ, Ceresini G, Cerqueira C, Cucca F, Deary IJ, Deelen J, Eckardt KU, Ekici AB, Eriksson JG, Ferrrucci L, Fiers T, Fiorillo E, Ford I, Fox CS, Fuchsberger C, Galesloot TE, Gieger C, Gögele M, De Grandi A, Grarup N, Greiser KH, Haljas K, Hansen T, Harris SE, van Heemst D, den Heijer M, Hicks AA, den Hollander W, Homuth G, Hui J, Ikram MA, Ittermann T, Jensen RA, Jing J, Jukema JW, Kajantie E, Kamatani Y, Kasbohm E, Kaufman JM, Kiemeney LA, Kloppenburg M, Kronenberg F, Kubo M, Lahti J, Lapauw B, Li S, Liewald DCM; Lifelines Cohort Study, Lim EM, Linneberg A, Marina M, Mascalzoni D, Matsuda K, Medenwald D, Meisinger C, Meulenbelt I, De Meyer T, Meyer Zu Schwabedissen HE, Mikolajczyk R, Moed M, Netea-Maier RT, Nolte IM, Okada Y, Pala M, Pattaro C, Pedersen O, Petersmann A, Porcu E, Postmus I, Pramstaller PP, Psaty BM, Ramos YFM, Rawal R, Redmond P, Richards JB, Rietzschel ER, Rivadeneira F, Roef G, Rotter JI, Sala CF, Schlessinger D, Selvin E, Slagboom PE, Soranzo N, Sørensen TIA, Spector TD, Starr JM, Stott DJ, Taes Y, Taliun D, Tanaka T, Thuesen B, Tiller D, Toniolo D, Uitterlinden AG, Visser WE, Walsh JP, Wilson SG, Wolffenbuttel BHR, Yang Q, Zheng HF, Cappola A, Peeters RP, Naitza S, Völzke H, Sanna S, Köttgen A, Visser TJ, Medici M.

Supplementary information

All supplementary information, supplementary figures and supplementary tables are available online through https://www.nature.com/articles/s41467-018-06356-1#Bib1.

REFERENCES

1. Cooper DS, Biondi B. Subclinical thyroid disease. Lancet. 2012;379(9821):1142-54.
2. Chaker L, Baumgartner C, den Elzen WP, Ikram MA, Blum MR, Collet TH, et al. Subclinical Hypothyroidism and the Risk of Stroke Events and Fatal Stroke: An Individual Participant Data Analysis. J Clin Endocrinol Metab. 2015;100(6):2181-91.
3. Collet TH, Gussekloo J, Bauer DC, den Elzen WP, Cappola AR, Balmer P, et al. Subclinical hyperthyroidism and the risk of coronary heart disease and mortality. Arch Intern Med. 2012;172(10):799-809.
4. Medici M, Direk N, Visser WE, Korevaar TI, Hofman A, Visser TJ, et al. Thyroid function within the normal range and the risk of depression: a population-based cohort study. J Clin Endocrinol Metab. 2014;99(4):1213-9.
5. Cappola AR, Arnold AM, Wulczyn K, Carlson M, Robbins J, Psaty BM. Thyroid function in the euthyroid range and adverse outcomes in older adults. J Clin Endocrinol Metab. 2015;100(3):1088-96.
6. Roef GL, Taes YE, Kaufman JM, Van Daele CM, De Buyzere ML, Gillebert TC, et al. Thyroid hormone levels within reference range are associated with heart rate, cardiac structure, and function in middle-aged men and women. Thyroid. 2013;23(8):947-54.
7. Chaker L, Heeringa J, Dehghan A, Medici M, Visser WE, Baumgartner C, et al. Normal Thyroid Function and the Risk of Atrial Fibrillation: the Rotterdam Study. J Clin Endocrinol Metab. 2015;100(10):3718-24.
8. Baumgartner C, da Costa BR, Collet TH, Feller M, Floriani C, Bauer DC, et al. Thyroid Function Within the Normal Range, Subclinical Hypothyroidism, and the Risk of Atrial Fibrillation. Circulation. 2017;136(22):2100-16.
9. Bano A, Dhana K, Chaker L, Kavousi M, Ikram MA, Mattace-Raso FUS, et al. Association of Thyroid Function With Life Expectancy With and Without Cardiovascular Disease: The Rotterdam Study. JAMA Intern Med. 2017;177(11):1650-7.
10. Chaker L, Baumgartner C, den Elzen WP, Collet TH, Ikram MA, Blum MR, et al. Thyroid Function Within the Reference Range and the Risk of Stroke: An Individual Participant Data Analysis. J Clin Endocrinol Metab. 2016;101(11):4270-82.
11. Porcu E, Medici M, Pistis G, Volpato CB, Wilson SG, Cappola AR, et al. A meta-analysis of thyroid-related traits reveals novel loci and gender-specific differences in the regulation of thyroid function. PLoS Genet. 2013;9(2):e1003266.
12. Taylor PN, Porcu E, Chew S, Campbell PJ, Traglia M, Brown SJ, et al. Whole-genome sequence-based analysis of thyroid function. Nat Commun. 2015;6:5681.
13. Gudmundsson J, Sulem P, Gudbjartsson DF, Jonasson JG, Masson G, He H, et al. Discovery of common variants associated with low TSH levels and thyroid cancer risk. Nat Genet. 2012;44(3):319-22.
14. Medici M, Visser WE, Visser TJ, Peeters RP. Genetic determination of the hypothalamic-pituitary-thyroid axis: where do we stand? Endocr Rev. 2015;36(2):214-44.
15. Panicker V, Wilson SG, Spector TD, Brown SJ, Falchi M, Richards JB, et al. Heritability of serum TSH, free T4 and free T3 concentrations: a study of a large UK twin cohort. Clin Endocrinol (Oxf). 2008;68(4):652-9.
16. Roef G, Taes Y, Toye K, Goemaere S, Fiers T, Verstraete A, et al. Heredity and lifestyle in the determination of between-subject variation in thyroid hormone levels in euthyroid men. Eur J Endocrinol. 2013;169(6):835-44.
17. Brown SD, Moore MW. The International Mouse Phenotyping Consortium: past and future perspectives on mouse phenotyping. Mamm Genome. 2012;23(9-10):632-40.
18. Eriksson N, Tung JY, Kiefer AK, Hinds DA, Francke U, Mountain JL, et al. Novel associations for hypothyroidism include known autoimmune risk loci. PLoS One. 2012;7(4):e34442.
19. Denny JC, Crawford DC, Ritchie MD, Bielinski SJ, Basford MA, Bradford Y, et al. Variants near FOXE1 are associated with hypothyroidism and other thyroid conditions: using electronic medical records for genome- and phenome-wide studies. Am J Hum Genet. 2011;89(4):529-42.
20. Medici M, Porcu E, Pistis G, Teumer A, Brown SJ, Jensen RA, et al. Identification of novel genetic Loci associated with thyroid peroxidase antibodies and clinical thyroid disease. PLoS Genet. 2014;10(2):e1004123.
21. Pickrell JK, Berisa T, Liu JZ, Segurel L, Tung JY, Hinds DA. Detection and interpretation of shared genetic influences on 42 human traits. Nat Genet. 2016;48(7):709-17.
22. Holm SJ, Carlen LM, Mallbris L, Stahle-Backdahl M, O'Brien KP. Polymorphisms in the SEEK1 and SPR1 genes on 6p21.3 associate with psoriasis in the Swedish population. Exp Dermatol. 2003;12(4):435-44.
23. Zhernakova A, Withoff S, Wijmenga C. Clinical implications of shared genetics and pathogenesis in autoimmune diseases. Nat Rev Endocrinol. 2013;9(11):646-59.
24. Zhu Z, Zhang F, Hu H, Bakshi A, Robinson MR, Powell JE, et al. Integration of summary data from GWAS and eQTL studies predicts complex trait gene targets. Nat Genet. 2016;48(5):481-7.

25. Somogyi V, Gyorffy A, Scalise TJ, Kiss DS, Goszleth G, Bartha T, et al. Endocrine factors in the hypothalamic regulation of food intake in females: a review of the physiological roles and interactions of ghrelin, leptin, thyroid hormones, oestrogen and insulin. Nutr Res Rev. 2011;24(1):132-54.
26. Medina MC, Fonesca TL, Molina J, Fachado A, Castillo M, Dong L, et al. Maternal inheritance of an inactive type III deiodinase gene allele affects mouse pancreatic beta-cells and disrupts glucose homeostasis. Endocrinology. 2014;155(8):3160-71.
27. Togawa N, Miyaji T, Izawa S, Omote H, Moriyama Y. A Na+-phosphate cotransporter homologue (SLC17A4 protein) is an intestinal organic anion exporter. American journal of physiology Cell physiology. 2012;302(11):C1652-60.
28. Friesema EC, Ganguly S, Abdalla A, Manning Fox JE, Halestrap AP, Visser TJ. Identification of monocarboxylate transporter 8 as a specific thyroid hormone transporter. J Biol Chem. 2003;278(41):40128-35.
29. Johannes J, Braun D, Kinne A, Rathmann D, Kohrle J, Schweizer U. Few Amino Acid Exchanges Expand the Substrate Spectrum of Monocarboxylate Transporter 10. Mol Endocrinol. 2016;30(7):796-808.
30. Pizzagalli F, Hagenbuch B, Stieger B, Klenk U, Folkers G, Meier PJ. Identification of a novel human organic anion transporting polypeptide as a high affinity thyroxine transporter. Mol Endocrinol. 2002;16(10):2283-96.
31. Fujiwara K, Adachi H, Nishio T, Unno M, Tokui T, Okabe M, et al. Identification of thyroid hormone transporters in humans: different molecules are involved in a tissue-specific manner. Endocrinology. 2001;142(5):2005-12.
32. Abe T, Kakyo M, Tokui T, Nakagomi R, Nishio T, Nakai D, et al. Identification of a novel gene family encoding human liver-specific organic anion transporter LST-1. J Biol Chem. 1999;274(24):17159-63.
33. Friesema EC, Docter R, Moerings EP, Verrey F, Krenning EP, Hennemann G, et al. Thyroid hormone transport by the heterodimeric human system L amino acid transporter. Endocrinology. 2001;142(10):4339-48.
34. Han Q, Cai T, Tagle DA, Li J. Structure, expression, and function of kynurenine aminotransferases in human and rodent brains. Cell Mol Life Sci. 2010;67(3):353-68.
35. Hallen A, Cooper AJ. Reciprocal Control of Thyroid Binding and the Pipecolate Pathway in the Brain. Neurochem Res. 2017;42(1):217-43.
36. Wilkinson JH. Recent work on thyroid hormones. Postgraduate medical journal. 1957;33(381):333-7.
37. Iglesias P, Diez JJ. Thyroid dysfunction and kidney disease. Eur J Endocrinol. 2009;160(4):503-15.
38. Asvold BO, Bjoro T, Vatten LJ. Association of thyroid function with estimated glomerular filtration rate in a population-based study: the HUNT study. Eur J Endocrinol. 2011;164(1):101-5.
39. Noda M. Possible role of glial cells in the relationship between thyroid dysfunction and mental disorders. Front Cell Neurosci. 2015;9:194.
40. Dickerman AL, Barnhill JW. Abnormal thyroid function tests in psychiatric patients: a red herring? Am J Psychiatry. 2012;169(2):127-33.
41. Wiersinga WM. Paradigm shifts in thyroid hormone replacement therapies for hypothyroidism. Nat Rev Endocrinol. 2014;10(3):164-74.
42. Roche J, Michel R, Tata J. [The nature of iodinated compounds excreted by liver and kidneys after administration of L-thyroxin and L-3,5,3'-triiodothyronine]

Sur la nature des combinaisons iodees excretees par le foie et le rein apres administration de L-thyroxine et de L-3:5:3'-triiodothyronine. Biochim Biophys Acta. 1954;15(4):500-7.
43. Thul PJ, Akesson L, Wiking M, Mahdessian D, Geladaki A, Ait Blal H, et al. A subcellular map of the human proteome. Science. 2017;356(6340).
44. Dong Z, Zhou J, Jiang S, Li Y, Zhao D, Yang C, et al. Effects of multiple genetic loci on the pathogenesis from serum urate to gout. Sci Rep. 2017;7:43614.
45. Biondi B, Cooper DS. The clinical significance of subclinical thyroid dysfunction. Endocr Rev. 2008;29(1):76-131.
46. Chaker L, Bianco AC, Jonklaas J, Peeters RP. Hypothyroidism. Lancet. 2017;390(10101):1550-62.
47. Zuk O, Schaffner SF, Samocha K, Do R, Hechter E, Kathiresan S, et al. Searching for missing heritability: designing rare variant association studies. Proc Natl Acad Sci U S A. 2014;111(4):E455-64.
48. Fuchsberger C, Taliun D, Pramstaller PP, Pattaro C, consortium CK. GWAtoolbox: an R package for fast quality control and handling of genome-wide association studies meta-analysis data. Bioinformatics. 2012;28(3):444-5.
49. Willer CJ, Li Y, Abecasis GR. METAL: fast and efficient meta-analysis of genomewide association scans. Bioinformatics. 2010;26(17):2190-1.

50. Bulik-Sullivan BK, Loh PR, Finucane HK, Ripke S, Yang J, Schizophrenia Working Group of the Psychiatric Genomics C, et al. LD Score regression distinguishes confounding from polygenicity in genome-wide association studies. Nat Genet. 2015;47(3):291-5.
51. Higgins JP, Thompson SG, Deeks JJ, Altman DG. Measuring inconsistency in meta-analyses. BMJ. 2003;327(7414):557-60.
52. Purcell S, Neale B, Todd-Brown K, Thomas L, Ferreira MA, Bender D, et al. PLINK: a tool set for whole-genome association and population-based linkage analyses. Am J Hum Genet. 2007;81(3):559-75.
53. Skol AD, Scott LJ, Abecasis GR, Boehnke M. Joint analysis is more efficient than replication-based analysis for two-stage genome-wide association studies. Nat Genet. 2006;38(2):209-13.
54. Hoppmann AS, Schlosser P, Backofen R, Lausch E, Kottgen A. GenToS: Use of Orthologous Gene Information to Prioritize Signals from Human GWAS. PLoS One. 2016;11(9):e0162466.
55. Mol JA, Visser TJ. Synthesis and some properties of sulfate esters and sulfamates of iodothyronines. Endocrinology. 1985;117(1):1-7.
56. Friesema EC, Jansen J, Jachtenberg JW, Visser WE, Kester MH, Visser TJ. Effective cellular uptake and efflux of thyroid hormone by human monocarboxylate transporter 10. Mol Endocrinol. 2008;22(6):1357-69.
57. Friesema EC, Kuiper GG, Jansen J, Visser TJ, Kester MH. Thyroid hormone transport by the human monocarboxylate transporter 8 and its rate-limiting role in intracellular metabolism. Mol Endocrinol. 2006;20(11):2761-72.
58. Groeneweg S, Lima de Souza EC, Meima ME, Peeters RP, Visser WE, Visser TJ. Outward-Open Model of Thyroid Hormone Transporter Monocarboxylate Transporter 8 Provides Novel Structural and Functional Insights. Endocrinology. 2017;158(10):3292-306.
59. Groeneweg S, Lima de Souza EC, Visser WE, Peeters RP, Visser TJ. Importance of His192 in the human thyroid hormone transporter MCT8 for substrate recognition. Endocrinology. 2013;154(7):2525-32.
60. Team RC. R: A Language and Environment for Statistical Computing. https://wwwr-projectorg 2016.
61. International Consortium for Blood Pressure Genome-Wide Association S, Ehret GB, Munroe PB, Rice KM, Bochud M, Johnson AD, et al. Genetic variants in novel pathways influence blood pressure and cardiovascular disease risk. Nature. 2011;478(7367):103-9.
62. Pers TH, Karjalainen JM, Chan Y, Westra HJ, Wood AR, Yang J, et al. Biological interpretation of genome-wide association studies using predicted gene functions. Nat Commun. 2015;6:5890.
63. Staley JR, Blackshaw J, Kamat MA, Ellis S, Surendran P, Sun BB, et al. PhenoScanner: a database of human genotype-phenotype associations. Bioinformatics. 2016;32(20):3207-9.
64. Arnold M, Raffler J, Pfeufer A, Suhre K, Kastenmuller G. SNiPA: an interactive, genetic variant-centered annotation browser. Bioinformatics. 2015;31(8):1334-6.

Chapter

Functional characterization of the novel thyroid hormone transporter SLC17A4

6.2

Stefan Groeneweg, Ferdy S. van Geest, Zhongli Chen, Stefania Farina, Ramona E.A. van Heerebeek, Marcel E. Meima, Robin P. Peeters, Heike Heuer, Marco Medici, and W. Edward Visser

Manuscript in preparation

ABSTRACT

Introduction A recent genome-wide association study identified the *SLC17A4* locus associated with circulating free T4 concentrations. Subsequently, SLC17A4, being widely expressed in the gastro-intestinal tract, was characterized as a novel T3 and T4 transporter. However, many basic transporter characteristics such as substrate specificity and transport direction are still unknown. Here, we delineated these key characteristics.

Methods We performed a broad range of well-established thyroid hormone (TH) transport studies in COS-1 cells transiently over-expressing SLC17A4. We studied cellular TH uptake in various incubation buffers, TH efflux, and the inhibitory effects of different TH metabolites and known inhibitors of other TH transporters on SLC17A4-mediated TH transport. Finally, we determined the effect of tunicamycin, a pharmacological inhibitor of N-linked glycosylation, and targeted mutations in Asn residues on SLC17A4 function.

Results SLC17A4 induced the cellular uptake of T3 and T4 by ~4-times, and of reverse (r)T3 by only 1.5-times over control cells. The uptake of T4 by SLC17A4 was Na^+- and Cl^--independent, stimulated by low extracellular pH, and reduced by various iodothyronines and metabolites thereof, particularly those that contain at least 3 iodine moieties irrespective of the presence of modification at the alanine side-chain. None of the classical TH transporter inhibitors studied attenuated SLC17A4-mediated TH transport. SLC17A4 enhanced the intracellular metabolism of T3 and T4 by the type 3 deiodinase. Immunoblot studies on lysates of transfected cells cultured in absence or presence of tunicamycin indicated that SLC17A4 is subject to N-linked glycosylation. Complementary mutational studies identified Asn66, Asn75 and Asn90, which are located in extracellular loop 1, as primary targets.

Discussion Our studies show that SLC17A4 efficiently facilitates the uptake and efflux of T3, T4 >> rT3 > 3,3'-T2. Future studies should reveal the physiological role of SLC17A4 in thyroid hormone regulation.

INTRODUCTION

Transporter proteins are a prerequisite for transfer of thyroid hormones across the plasma membrane (1). Over the last decade, several TH transporters have been identified including several members of the OATP family, LAT1 and LAT2, NTCP, MCT8 and MCT10 (2, 3). Each of these transporters has its own substrate specificity and tissue distribution, with the majority of transporters also accepting a broad variety of other substrates. The most specific thyroid hormone transporter identified to date is MCT8 which facilitates the cellular uptake and efflux of triiodothyronine (T3) and T4, and to a lesser extent reverse (r)T3 and diiodothyronine (T2) (4, 5). Mutations in MCT8 have been associated with MCT8 deficiency, which is characterized by severe intellectual and motor disability (6, 7). Mutations in the brain-specific T4 transporter OATP1C1 have been recently linked to a neuro-degenerative phenotype (8). These and other studies have proven the physiological relevance of TH transporters.

In a recent genome-wide association study, we demonstrated that genetic variation in SLC17A4 was associated with serum free thyroxine (T4) concentrations (9). Subsequent functional studies indicated that SLC17A4 facilitates the uptake of T3 and T4 as efficient as MCT8 (9). The SLC17 family consists of nine structurally related proteins that have been identified as organic anion transporters (10). Based on their homology and following the characterization of SLC17A1 as a Na^+-dependent phosphate transporter, the first four members (SLC17A1-4) had been initially classified as Na^+-dependent inorganic phosphate transporters. Over the years, it turned out that SLC17A1-3 accept a broad range of organic anions (10). However, SLC17A4 has long been designated as an orphan transporter (10). The few available studies indicated that SLC17A4 is predominantly expressed at mRNA level in liver, kidney, small intestine, colon and pancreas in human and rat (11, 12). Its function has only been studied in proteoliposomal systems, in which it induced the uptake of uric acid (11).

The transporter characteristics of this novel thyroid hormone transporter, beyond the cellular uptake of T3 and T4, are currently unknown. It is unknown if SLC17A4 also accepts other iodothyronines and metabolites thereof as a substrate. To understand its role in cellular thyroid hormone homeostasis and unravel its physiological role, it is imperative to establish if SLC17A4 also facilitates the cellular efflux of T3 and T4. Moreover, it is important to evaluate the sensitivity of SLC17A4 towards frequently applied pharmacological inhibitors of other thyroid hormone transporters such as silychristin and 2-Aminobicyclo[2.2.1]heptane-2-carboxylic acid (BCH). Knowledge on these key features will allow positioning SLC17A4 among the currently known thyroid hormone transporters.

To close this gap in current knowledge, we here delineated the basic functional characteristics of the human SLC17A4 protein. Our studies indicate that SLC17A4 efficiently facilitates the cellular uptake and efflux of T3 and T4 with great specificity. Together, these studies are a crucial step in determining the role of SLC17A4 in TH homeostasis.

MATERIALS AND METHODS

Materials

Nonradioactive iodothyronines, amino acids, bovine serum albumin (BSA), and D-glucose were obtained from Sigma Aldrich (Zwijndrecht, The Netherlands [NL]). [^{125}I]-T3, [^{125}I]-rT3, [^{125}I]-T4, [^{125}I]-3,3',5-triiodothyroacetic acid (Triac; TA3), and [^{125}I]-3,3',5,5'-tetraiodothyroacetic acid (Tetrac; TA4) were produced as previously described (16, 17). [^{125}I]-3,3'-T2 was generated accordingly using 3-T1.

[^{14}C] uric acid was obtained from American radiolabeled chemicals (St. Louis, USA). The monoclonal M2 mouse anti-Flag antibody was obtained from Sigma Aldrich (RRID: AB_262044), and the mouse anti-Glyceraldehyde-3-phosphate dehydrogenase (GAPDH) antibody (Mab374; RRID: AB_2107445) was obtained from Merck Millipore (Amsterdam, NL). All cell culture flasks and plates were obtained from Corning (Schiphol, NL). X-tremeGENE9 transfection reagent was obtained from Roche Diagnostics (Woerden, NL).

Constructs

The generation of expression constructs encoding human type 3 deiodinase (pClneo-hD3) and human μ-crystallin (pSG5-hCRYM) has been previously described (5, 13). hCRYM is a cytoplasmic high affinity TH-binding protein, which greatly reduces the cellular TH efflux, thereby increasing the net cellular TH uptake. A pCMV6-Entry_human SLC17A4 expression vector containing a C-terminal Myc and Flag tag was obtained from OriGene Technologies (Rockville, USA). The N66A, N75A, N90A mutations were introduced using site-directed mutagenesis according to manufacturers` protocol (Agilent, Middelburg, NL). A mutant construct containing a combination of all three substitutions was generated by sequential reactions. The coding sequence was fully sequenced to verify correctness of the resulting construct.

Cell culture and transfection

COS-1 African green monkey kidney cells were obtained from ECACC (Sigma-Aldrich) and cultured under standard conditions (e.g. (14)). For uptake studies cells were seeded on 24-well dishes and transiently transfected with 125 ng empty vector or wild-type hSLC17A4 expression construct with or without 50 ng of pSG5-hCRYM at ~70% confluence using X-tremeGENE9 transfection reagent according to manufacturers` protocol, unless otherwise indicated. For T3 and T4 metabolism studies, cells were seeded on 24 well plates and transfected with 100 ng empty vector or wild-type hSLC17A4 expression construct with or without 100 ng of pClneo-hD3. For immunoblotting, cells were cultured in 6-well plates and transfected with indicated amounts of empty vector or Flag-tagged SLC17A4. All experiments were carried out 48 h after transfection.

Uptake studies

All uptake studies were carried out as previously described according to well-established protocols (e.g. (14)). Cells were washed with D-PBS buffer (Dulbecco`s phosphate buffered saline + Ca^{2+}/Mg^{2+} with 0.1% BSA and 0.1% glucose, unless otherwise indicated) and incubated in D-PBS buffer containing 1 nM (50 000 cpm) [^{125}I]-3,3'-T2, [^{125}I]-T3, [^{125}I]-rT3, [^{125}I]-T4, [^{125}I]-TA3, [^{125}I]-TA4, or 100 μM [^{14}C] uric acid for indicated incubation times at 37°C. After a brief wash, the amount of internalized radioactivity was measured in cell lysates as previously described (4, 14). Uptake studies with TA3 and TA4 and all cis-inhibition and inhibitor studies were performed in incubation buffer without BSA, as previously described (e.g. (15)).

A similar protocol was used to study the Na^+-dependence of SLC17A4-mediated TH uptake. Cells were washed twice with choline chloride buffer (142.9 mM choline chloride, 4.7 mM KCl, 1.8 mM $CaCl_2$, 1.2 mM $MgSO_4$, 20 mM HEPES, 0.1% glucose, pH 7.3) for 5 minutes and were then incubated with choline chloride buffer containing 1 nM (50 000 cpm) [^{125}I]T4 or a corresponding buffer in which choline chloride was substituted by an equimolar amount of NaCl. Using the same incubation protocol, the Cl^-

dependence was studied by using a sodium gluconate buffer in which Cl^- was replaced by an equimolar amount of gluconate.

Efflux studies

Efflux studies were carried out according to previously described methods (20). Cells were pre-loaded with 1 nM (50,000 cpm) [^{125}I]-3,3'-T2, [^{125}I]-T3, [^{125}I]-rT3 or [^{125}I]-T4 for 120 minutes in incubation medium. After a brief wash with incubation medium, cells were incubated in efflux medium (incubation medium containing 1% BSA) for indicated incubation times at 37°C. After termination of the incubation, cells were briefly washed in incubation medium and lysed in 0.1 M NaOH. The amount of radioactivity was measured in cell lysates.

TH metabolism studies

Metabolism assays were performed according to well-established protocols (5, 13). Briefly, cells were washed once with 0.5 ml incubation buffer (D-PBS containing Ca^{2+}/Mg^{2+}, 0.1% BSA and 0.1% glucose,) and incubated in 500 µl incubation medium containing 1 nM (250 000 cpm) [^{125}I]-T3 or [^{125}I]-T4. An aliquot of 100 µl incubation medium was collected at indicated time points and mixed with 100 µl ice-cold 0.1% acetic acid in acetonitrile. After centrifugation, 125 µl of the supernatant was added to 100 µl 0.02 M amonium acetate pH 4.0 and analyzed by UPLC as described previously (5).

Immunoblotting

Immunoblotting of total lysates was carried out as previously described (16). Monoclonal mouse anti-Flag antibody was used to detect the Flag-tagged SLC17A4 protein. Glyceraldehyde-3-phosphate dehydrogenase (GAPDH) was used as loading control. To study if SLC17A4 is subject to N-linked glycosylation, cells were incubated in presence of 1 µg/ml tunicamycin (Sigma Aldrich) for 48 h before lysates were collected.

Structural modeling and prediction of glycosylation sites

Structural modeling was performed in YASARA Structure using the same approach as we previously applied to model the protein structure of MCT8 (16) and OATP1C1 (8). All images were created using YASARA Structure (24) and Pov-Ray v3.6 software (www.povray.org). The NetNGlyc 1.0 Server (http://www.cbs.dtu.dk/services/NetNGlyc/) was used to predict target sites for N-linked glycosylation.

Statistics

All statistical analyses were carried out using GraphPad Prism version 6 (GraphPad Software, San Diego California, USA). The applied statistical tests and levels of significance are mentioned in the legend of the corresponding figure.

RESULTS

To establish the optimal conditions for studying the functional characteristics of SLC17A4, we first performed a plasmid dose titration curve by transiently transfecting COS-1 cells in 24-well dishes with increasing amounts of SLC17A4 plasmid, alone or in combination with a fixed amount of CRYM plasmid (50 ng). In the absence of CRYM, a dose-dependent increase of T4 uptake was observed with an

apparent optimum at 250 ng of SLC17A4 plasmid (**Figure 1A**). In line with previous studies, the intracellular accumulation of T4 was enhanced in the presence of CRYM, with a plateau starting at a SLC17A4 plasmid dose of ~50 ng (**Figure 1A**). Based on these results, we selected the 250 ng dose for all further experiments in the absence of CRYM and the 125 ng dose for all further transport studies in presence of CRYM. In six-well dishes, transient transfection of COS-1 cells with increasing concentrations of SLC17A4 expression construct also resulted in a dose-dependent increase in T4 uptake (data not shown) and SLC17A4 protein expression levels (**Figure 1B**). Immuno-reactive bands were detected at ~47 and ~55 kDa, which are close to the predicted size of the SLC17A4 monomer (~54 kDa). The most prominent band was observed at ~90-100 kDa, which may correspond with SLC17A4 (hetero-)dimer (**Figure 1B**). In further expression studies, a plasmid dose of 500 ng was used.

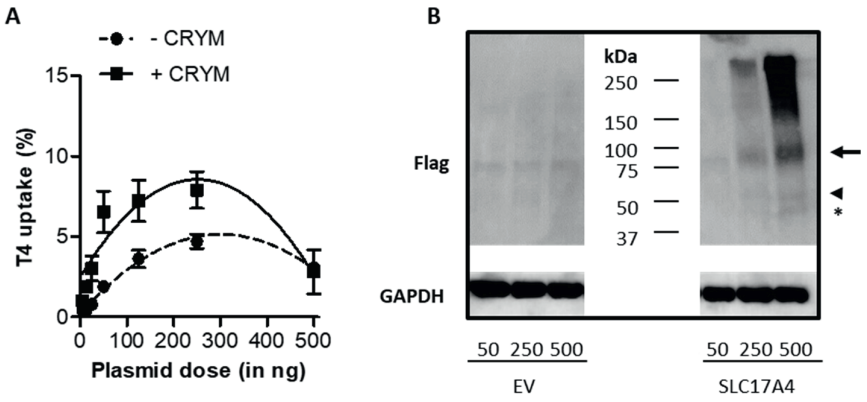

Figure 1 (A) Intracellular T4 accumulation in COS-1 cells transiently transfected with indicated amounts of SLC17A4 plasmid in the absence (dashed line) and presence (solid line) of 50 ng CRYM after 30 minutes incubation at 37 °C. All uptake values are corrected for background TH uptake levels observed in COS-1 cells transfected with empty vector. Experiments were carried out in a 24-well format. Data are presented as means (± SEM) of 3 separate experiments in duplicate. **(B)** Representative immunoblot on total lysates derived from COS-1 cells transiently transfected with indicated amounts of Flag-SLC17A4 expression construct. Glyceraldehyde-3-phosphate dehydrogenase (GAPDH) was used as loading control. Bands that may represent the SLC17A4 monomer (predicted size ~54 kDa) are indicated with an arrowhead and asterix, whereas a putative (hetereo-)dimer is indicated with an arrow.

SLC17A1-4 members have been previously defined as Na^+-dependent inorganic phosphate transporters (10). To study the Na^+-dependence of SLC17A4-mediated T4 transport in transfected COS-1 cells, T4 uptake was measured in NaCl uptake buffer and in Na^+-free uptake buffer in which NaCl was replaced by an equimolar amount of choline chloride. Elimination of extracellular Na^+ did not affect T4 uptake by SLC17A4, indicating that the transport of T4 is Na^+-independent (**Figure 2A**). The transport of T4 was also not sensitive to alterations in membrane potential because the elevation of extracellular K^+ (which depolarizes the cell membrane) did not change T4 uptake rate (**Figure 2B**). Previous studies in proteoliposomes showed that Cl^- is indispensable for the transport of at least some substrates by various members of the SLC17 family (11, 17, 18). However, creating an outward gradient of Cl^- by replacing the extracellular Cl^- by gluconate did not change the T4 uptake rate (**Figure 2C**), indicating that SLC17A4 is not a Cl^-/T4 exchanger. To study if SLC17A4 also transports T4 in presence of (near-) physiological concentrations of vitamins and nutrients, T4 uptake was measured in DMEM incubation medium and compared to levels observed in D-PBS uptake buffer.

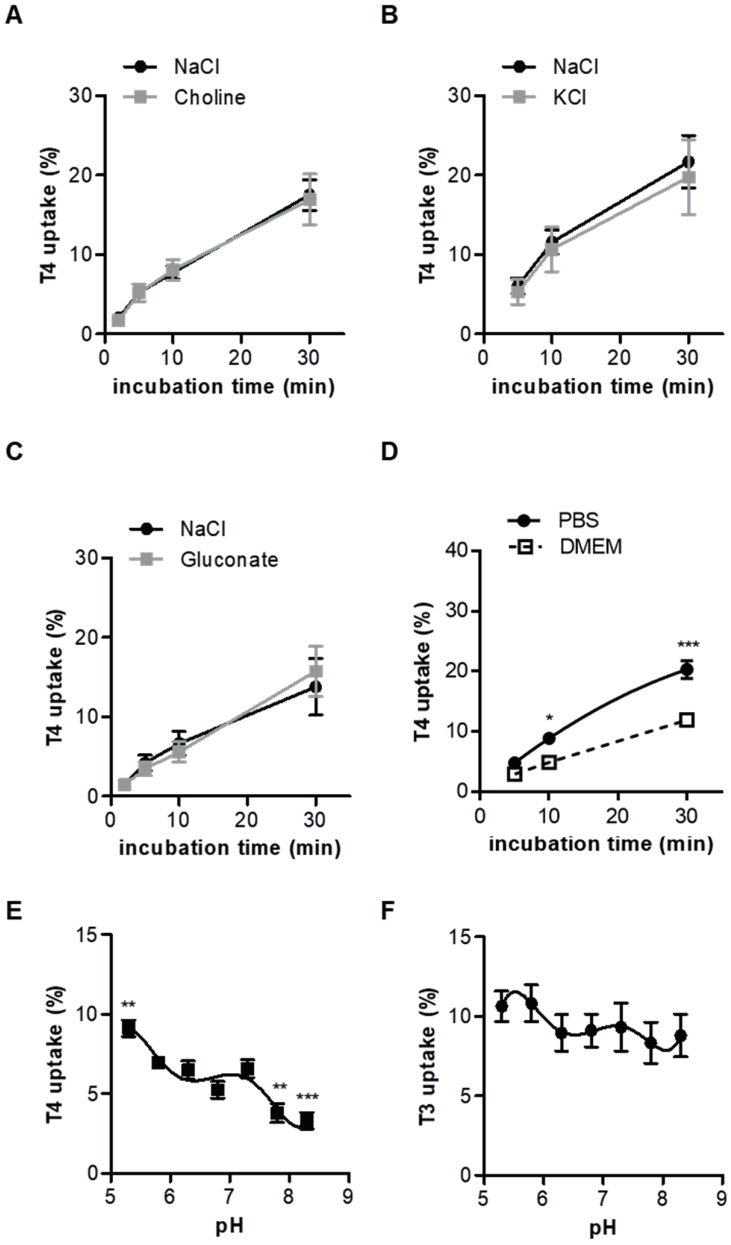

Figure 2 (A) SLC17A4-mediated T4 uptake in NaCl buffer or a Na^+-free choline chloride buffer after indicated incubation times at 37 °C. **(B)** T4 uptake in NaCl buffer and a high K^+ buffer in which NaCl was replaced by an equimolar amount of KCl. **(C)** Cl^--dependence of T4 uptake. T4 uptake was measured after indicated time points. All Cl_2 was replaced by gluconate. **(D)** SLC17A4-mediated T4 uptake in D-PBS and DMEM uptake medium. The pH dependence of T4 **(E)** and T3 **(F)** uptake. T4 and T3 uptake were measured in D-PBS uptake buffer at indicated pH. Data are presented as percentage uptake relative to the amount of [^{125}I]-T4 that was added to the cells at t=0 and corrected for background T4 uptake in empty vector control cells. All data are presented as means (± SEM) of 3 separate experiments in duplicate. Two-way ANOVA followed by Bonferroni posttests (**A-D**) and One-way ANOVA followed by Dunnett`s posttests (**(E** and **F)**) were applied to assess for statistically significant differences between the tested conditions and pH 7.3 ($p<0.05$, *; $p<0.01$, **, $p<0.001$, ***).

T4 uptake was strongly induced by SLC17A4 in DMEM incubation medium, although the observed uptake levels after 10 and 30 minutes incubation were lower than in D-PBS (**Figure 2D**). SLC17A4-mediated T4 uptake was pH-sensitive, with T4 uptake levels at pH 5.3 significantly exceeding those observed at neutral pH (7.3). By contrast, T4 uptake was reduced at (slightly) basic pH (7.8 and 8.3) (**Figure 2E**). A similar pattern was observed for SLC17A4-mediated T3 uptake, although the differences between the conditions did not reach statistical significance (**Figure 2F**). The uptake of T4, but not T3, was also enhanced at pH <6.3 in empty vector control cells (data not shown).

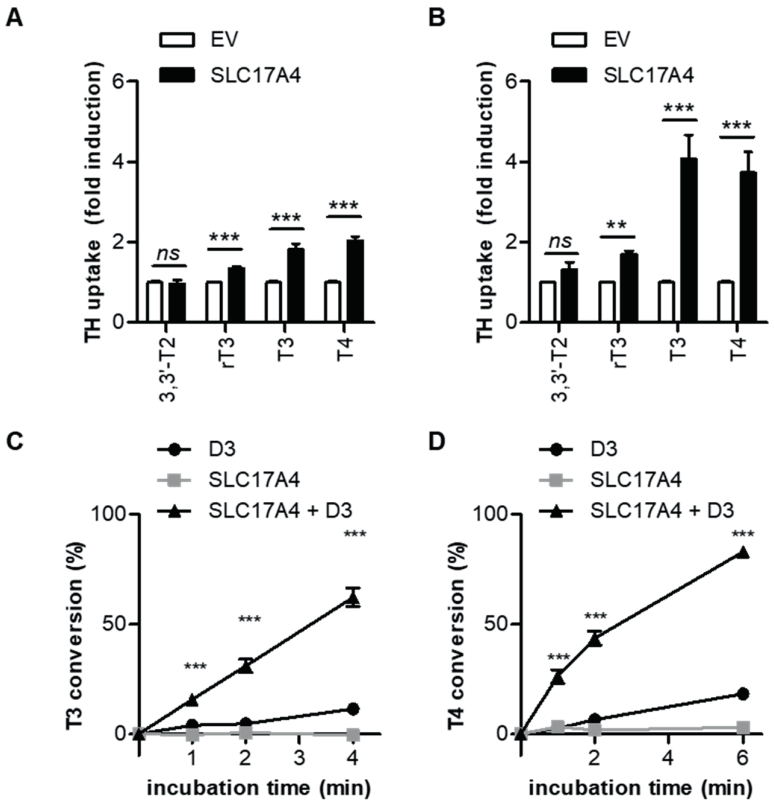

Figure 3 Substrate specificity of SLC17A4. **(A)** and **(B)** uptake of indicated iodothyronines in transiently transfected COS-1 cells after 10 minutes incubation at 37 °C in the absence **(A)** or presence **(B)** of CRYM. The uptake of various iodothyronines is expressed as fold induction over uptake levels observed in empty vector transfected cells (n=4). **(C)** T3 and **(D)** T4 metabolism in COS-1 cells transiently transfected with type 3 deiodinase (D3) and empty vector or in combination with SLC17A4. T3 and T4 metabolism is presented as the percentage of T2 and rT3 that was formed due to de-iodination of T3 and T4, respectively, and expressed relatively to the amount of T3 and T4 that was added to the cells at t=0. All data are presented as means (± SEM) of 2-3 separate experiments in duplicate. Two-way ANOVA followed by Bonferroni posttests were applied to assess for statistically significant differences between the tested conditions ($p<0.05$, *; $p<0.01$, **, $p<0.001$, ***).

Next, we delineated the substrate specificity of SLC17A4. COS-1 cells transfected with SLC17A4 alone or in combination with CRYM were incubated for 10 minutes with 1 nM of 3,3'-T2, rT3, T3 and T4. In the absence of CRYM, cells transfected with SLC17A4 showed a ~2-times induction of T3 and T4 uptake and a ~1.8-times induction of rT3 uptake over control cells, whereas SLC17A4 did not increase the uptake of 3,3'-T2 (**Figure 3A**). In presence of CRYM, a similar substrate preference was observed, with

the induction of T3 and T4 uptake (~4-times) exceeding the induction of rT3 uptake (1.8-times) and 3,3'-T2 (1.3-times) (**Figure 3B**). However, putative differences in binding affinity of CRYM for the different iodothyronines should also be taken into account. Co-expression of SLC17A4 and type 3 deiodinase (D3) greatly increased the intracellular deiodination of T3 **(Figure 3C**) and T4 (**Figure 3D**) compared to cells transfected with SLC17A4 or D3 alone. This observation confirms that SLC17A4 translocates T3 and T4 across the cell membrane and increases their availability for intracellular deiodination.

Since the uptake levels in presence of CRYM exceeded those observed in the absence of CRYM, we next studied if SLC17A4 also facilitates the cellular efflux of iodothyronines. After pre-loading transfected COS-1 cells with radio-labeled iodothyronines for 2 h, the amount of intracellular 3,3'-T2, rT3, T3, and T4 was measured after different incubation times in efflux medium. The decline in cellular 3,3'-T2 and rT3 content did not differ between COS-1 cells expressing SLC17A4 *versus* control cells, except for a minimal difference in cellular 3,3'-T2 levels after 5 minutes in favor of SLC17A4 expressing cells (**Figure 4A** and **4B**). In contrast, T3 and T4 efflux was markedly faster from cells transfected with SLC17A4 than from control cells (**Figure 4C** and **4D**). Together, these data indicate that SLC17A4 facilitates the cellular uptake and efflux of iodothyronines.

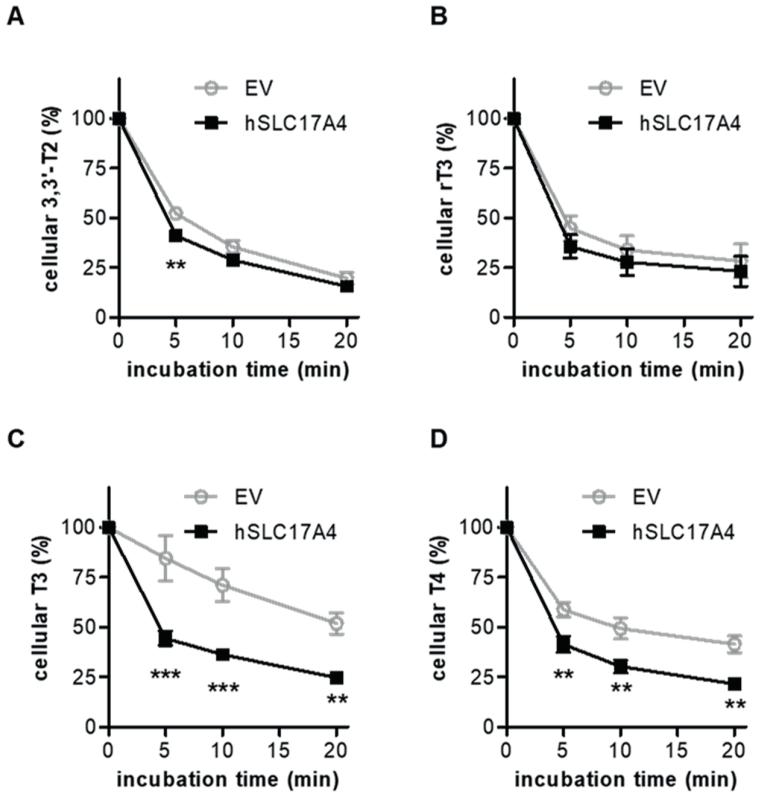

Figure 4 (A-D) cellular efflux of 3,3'-T2 **(A)**, rT3 **(B)**, T3 **(C)** and T4 **(D)** efflux by empty vector or SLC17A4 transfected COS-1 cells in 2-20 minutes. Cells were incubated for 120 min with 1 nM (50 000 cpm) of the indicated substrates (pre-loading), before efflux was measured. The amount of radio-activity that remained within the cell after 2-20 minutes incubation in efflux medium is displayed relatively to the amount of radio-activity that was present after pre-loading (t=0). All results are presented as means ± SEM (n=3). Two-way ANOVA followed by Bonferroni posttests were applied to assess for statistically significant differences between the tested conditions ($p<0.05$, *; $p<0.01$, **, $p<0.001$, ***).

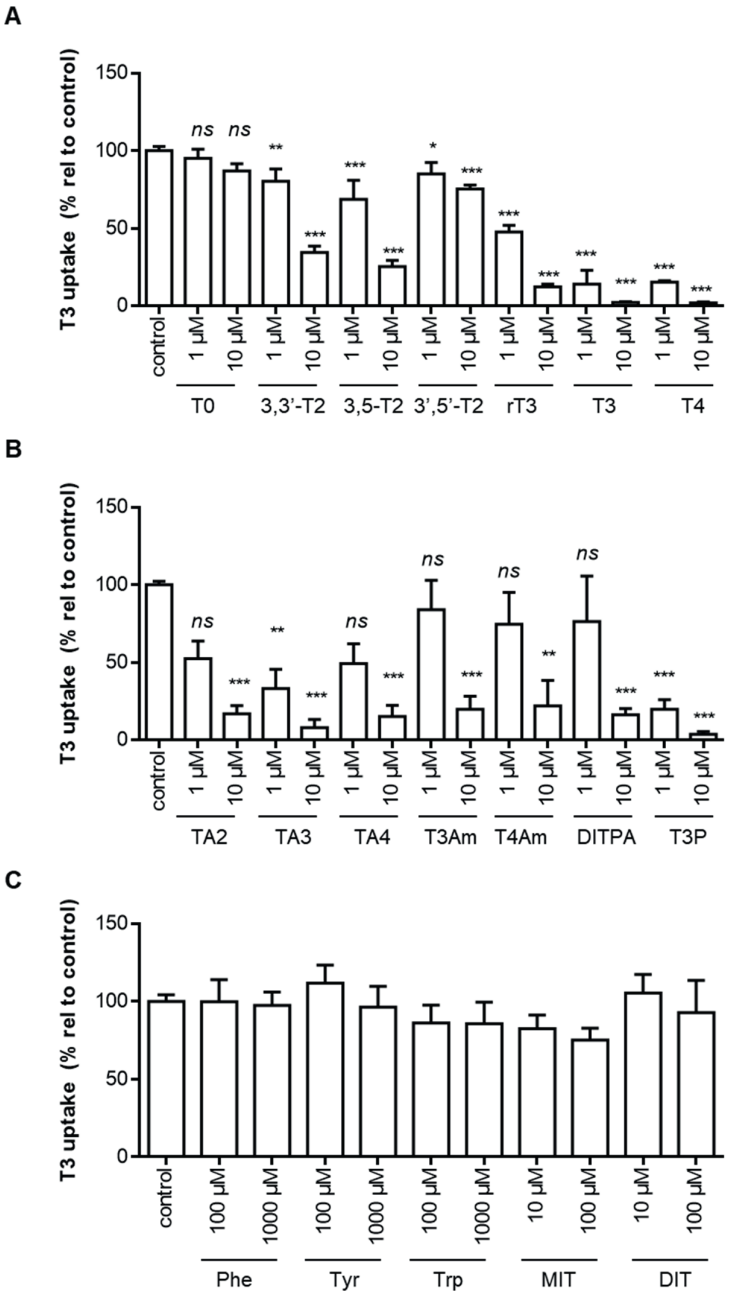

Figure 5 (A) SLC17A4-mediated T3 uptake after 30 minutes incubation in presence of 1 or 10 µM of the indicated iodothyronines. **(B)** SLC17A4-mediated T3 uptake in presence of 1 or 10 µM of the indicated alanine side-chain metabolites of iodothyronines and **(C)** 100 or 1000 µM of the indicated aromatic amino acids and 10 or 100 µM of the indicated iodotyrosines. All uptake levels are corrected for background T3 uptake in empty vector transfected control cells incubated in the presence of the same competitor. T3 uptake levels are displayed relative to the amount of intracellular [^{125}I]-T3 in cells incubated in the absence of any competitors (100%) and presented as means ± SEM (n=3). All experiments were carried out in COS-1 cells co-transfected with CRYM. A One-way ANOVA was carried out followed by Dunnett's posttests to asses for significant differences between the T3 uptake levels in the absence or presence of the tested competitors ($p<0.05$, *; $p<0.01$, **, $p<0.001$, ***). Abbreviations: TA2, diiodothyroacetic acid; TA3, triiodothyroacetic acid; TA4, tetraiodothyroacetic acid; T3Am, triiodothyronamine; T4Am, tetraiodothyronamine; DITPA, diiodothyroproprionic acid; TP3, triiodothyroproprionic acid; MIT, monoiodotyrosine; DIT, diiodotyrosine.

The substrate preference of SLC17A4 was addressed further by investigating the uptake of [^{125}I]-T3 in the presence or absence of various structurally related compounds. The first group of compounds constituted various iodothyronines that differ from T3 in number and position of the iodine moieties. At 1 µM concentrations, T3 uptake was slightly, but significantly, reduced by 3,3'-T2, 3,5-T2 and 3',5'-T2, but not T0. By contrast, T3 uptake was largely diminished in presence of 1 µM T3 or T4, which is in line with previously reported IC_{50} values of <1 µM for these substrates (9). At a higher concentration (10 µM), 3,3'-T2, 3,5-T2 and to a lesser extent by 3',5'-T2 also reduced SLC17A4-mediated T3 uptake, whereas T0 had still no effect (**Figure 5A**). T3 uptake was (near-) completely blocked in presence of 10 µM rT3, T3 and T4 (**Figure 5A**). The second group of compounds constituted various alanine side-chain metabolites, including iodothyroacetic (TA_x) and -proprionic (TP_x) acid derivatives as well as thyronamines (T_xAm). In particular TA3 and T3P reduced SLC17A4-mediated T3 uptake at 1µM concentrations, whereas all compounds largely diminished T3 uptake at 10 µM concentrations (**Figure 5B**). The third group of compounds constituted the aromatic amino acids and the iodotyrosines mono-iodotyrosine (MIT) and di-iodotyrosine (DIT). These compounds differ from T3 due to the absence of the phenolic outer ring and/or the inner ring iodine moieties. SLC17A4-mediated T3 uptake was not affected by either 100 or 1000 µM Tyr, Phe or Trp, or the iodotyrosines MIT or DIT (**Figure 5C**). These findings were confirmed by similar experiments conducted with [^{125}I]-T4 in the absence of CRYM (data not shown). For these experiments [^{125}I]-T4 was used instead of [^{125}I]-T3 because of the slightly higher induction of T4 uptake in absence of CRYM. Together, these data show that SLC17A4-mediated TH uptake is reduced by compounds that retained the two phenolic rings, in particular those that contain three or four iodine moieties. The composition of the alanine side-chain had only little impact on cis-inhibition potency.

To study if compounds that potently inhibited SLC17A4-mediated TH uptake are also genuine substrates for SLC17A4, we assessed the uptake of [^{125}I]-TA3 and [^{125}I]-TA4 in COS-1 cells transfected with SLC17A4 or empty vector control. Indeed, the uptake of [^{125}I]-TA3 was slightly, but significantly induced by SLC17A4, whereas it did not enhance [^{125}I]-TA4 uptake (**Figure 6A** and **6B**). Since SLC17A4 was found to induce uric acid uptake in proteoliposomes (11), we also studied if SLC17A4 facilitates the cellular uptake of uric acid in COS-1 cells. Uric acid uptake in SLC17A4-transfected COS-1 cells was increased by ~1.4 times over control cells in which uric acid uptake rate varied between 3-15 pmol/min (**Figure 6C**). However, even at a concentration of 1000 µM, which is well-above the reported reference ranges in serum (e.g. (19)), uric acid had no effect on SLC17A4-mediated T3 uptake (**Figure 6D**).

In addition to the various structurally related compounds, we studied the impact of well-established inhibitors of other TH transporters on SLC17A4-mediated T3 uptake. For these studies we selected narangin (OATP inhibitor), BCH (LAT inhibitor), sulfobromophthalein (BSP) and verapamil (inhibitors of multiple transporters), silychristin (MCT8 inhibitor) and estrone sulfate (E3S; substrate for NTCP and OATPs). However, none of these compounds reduced SLC17A4-mediated T3 uptake when applied at concentrations known to reduce the function of other TH transporters (**Figure 7**).

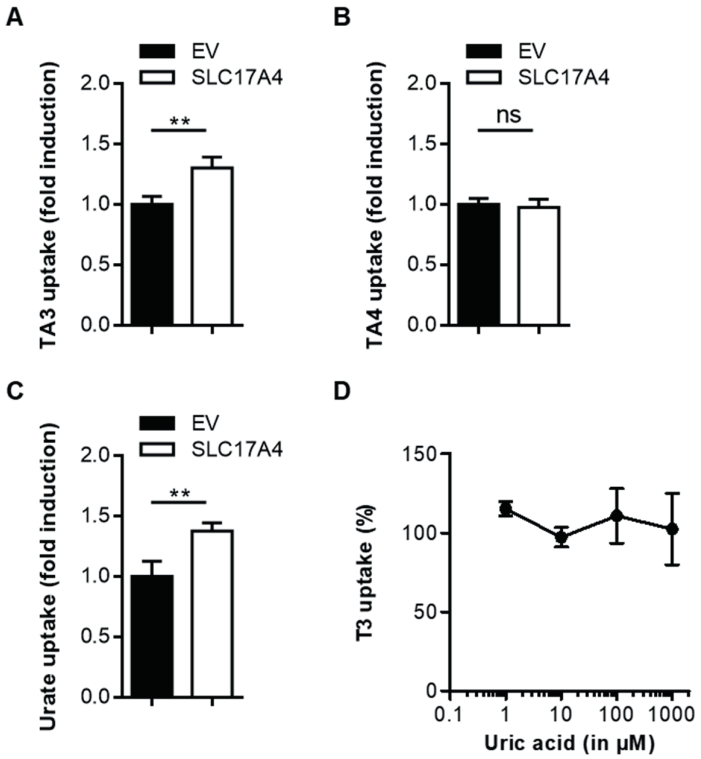

Figure 6 (A) [^{125}I]-TA3, **(B)** [^{125}I]-TA4, **(C)** [^{14}C]-uric acid uptake in COS-1 cells transfected with empty vector (EV) or SLC17A4 in the presence of CRYM after 10 min incubation at 37 ºC. Uptake is expressed as times-induction over empty-vector transfected control cells. Paired t-test have been applied to assess for statistically significant differences ($p<0.01$, **). **(C)** SLC17A4-mediated T3 uptake in the presence of indicated concentrations uric acid. T3 uptake levels are displayed relative to the amount of intracellular [^{125}I]-T3 in cells incubated in the absence of any inhibitor (100%) and presented as means ± SEM (n=3). A two-way ANOVA with Bonferroni post-hoc tests was carried out to asses for significant differences between the T3 uptake levels in the absence or presence of the tested inhibitors ($P<0.05$, *).

Finally, we studied if SLC17A4 is subject to glycosylation which may help elucidating the nature of the 47 kDa and 54 kDa bands observed on immunoblots of SLC17A4 over-expressing COS-1 cells (**Figure 1B**). Since the migration of transmembrane proteins may differ from their calculated molecular weights due to detergent binding (20), both bands could theoretically represent the SLC17A4 monomer. In contrast to transfected cells cultured in normal culturing medium, which showed immune-reactive bands at 47 kDa and 54 kDa, SLC17A4 over-expressing COS-1 cells cultured in the presence of the N-linked glycosylation blocker tunicamycin only showed an immuno-reactive band at 47 kDa (**Figure 8A**). Parallel uptake studies showed a strong reduction of SLC17A4-mediated T4 uptake in presence of tunicamycin (**Figure 8B**). To identify the putative target residues for N-linked glycosylation, we first used N-linked glycosylation prediction tools based on the presence of Asn-Xaa-Ser/Thr sequons and topology predictions. These tools identified Asn47, Asn56, Asn66, Asn75, and Asn90 as putative target sites for N-linked glycosylation. To further refine the accuracy of these predictions, we next generated an SLC17A4 protein homology model based on the crystal structure of the D-galactonate/proton symporter in inward open conformation (PDB ID: 6E9N, (21)) with some refinements based on the structure of multidrug transporter MdfA (PDB ID: 6EUQ, (22)) (**Figure 8C**).

According to this three-dimensional model and additional hydropathy plots, the SLC17A4 protein is predicted to consist of 12 transmembrane domains (TMDs) organized in two near-symmetrical bundles of 6 TMDs with an intracellular N-terminal and C-terminal domain. The TMDs are interconnected by intra- and extracellular loops, of which in particular the first extracellular loop (ECL1) and third intracellular loop (ICL3) are relatively large. This SLC17A4 homology model was then used to locate the predicted N-glycosylation sites. We found that only Asn66, Asn75 and Asn90 were located at accessible positions in ECL1, whereas Asn47 and Asn56 were located within TMD1 (**Figure 8C**). To validate that these three Asn residue are indeed the prime target sites for N-linked glycosylation, we generated SLC17A4 expression constructs in which each of these Asn residues was substituted by an Ala individually (N66A, N75A, N90A), as well as a combined mutant construct in which all three Asn residues were substituted by an Ala (further referred to as triple mutant). The ~54 kDa band migrated slightly lower in all three single mutants, whereas the triple mutant only showed a prominent band at ~47 kDa, corresponding to the band observed after treatment with tunicamycin (**Figure 8D**). Parallel T4 uptake studies showed that the N60A and N75A single mutants did not affect SLC17A4-mediated T4 uptake, whereas the N90A single mutant showed a modest reduction of ~30% (**Figure 8E**). By contrast, the triple mutant exhibited a functional reduction of ~70% compared to WT SLC17A4 (**Figure 8E**). Thus, glycosylation of Asn residues in ECL1 appears to be crucial for proper SLC17A4 function.

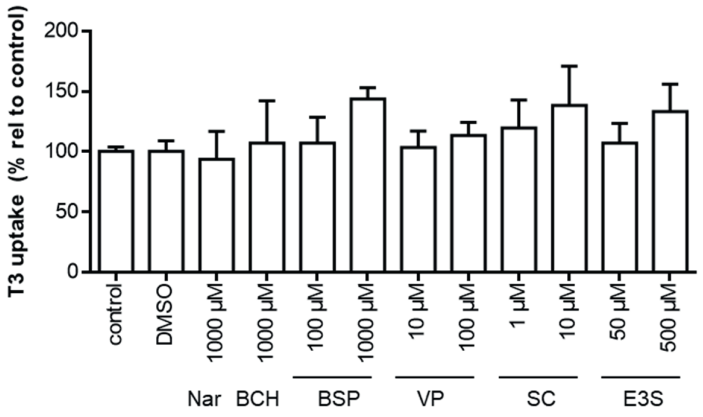

Figure 7 T3 uptake in the presence or absence of the indicated known inhibitors of other well-established TH transporters after 30 minutes incubation at 37 ºC. All uptake levels are corrected for background T3 uptake in empty vector transfected control cells incubated in the presence of the same inhibitor. All uptake levels are corrected for background T3 uptake in empty vector transfected control cells incubated in the presence of the same inhibitor. T3 uptake levels are displayed relative to the amount of intracellular [^{125}I]-T3 in cells incubated in the absence of any competitors (100%) and presented as means ± SEM (n=3). All experiments were carried out in COS-1 cells co-transfected with CRYM. A One-way ANOVA was carried followed by Dunnett's posttests to asses for significant differences between the T3 uptake levels in the absence or presence of the tested inhibitors. Abbreviations: nar, narangin; BCH, 2-Aminobicyclo[2.2.1]heptane-2-carboxylic acid; BSP, sulfobromophthalein; VP, verapamil; SC, silychristin; E3S, estrone sulfate.

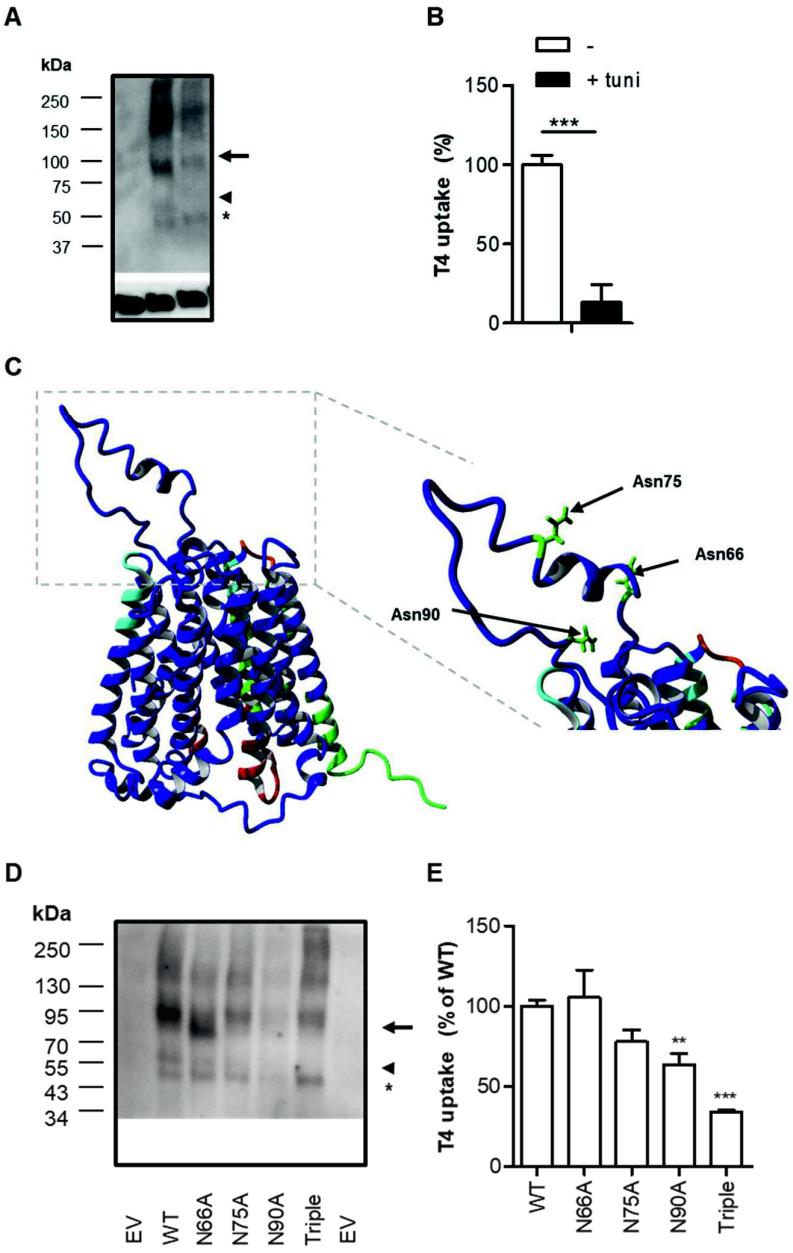

Figure 8 (A) Representative immunoblot of lysates derived from COS-1 cells transfected with empty vector or Flag-SLC17A4 cultured in the presence (+) or absence (-) of 1 µg/ml tunicamycin. **(B)** Parallel T4 uptake studies in presence of CRYM. **(C)** Protein homology model of SLC17A4 based on the crystal structure of the the D-galactonate/proton symporter (PDB ID: 6E9N). The first extracellular loop (ECL1) is magnified and the accessible Asn residues that were predicted as putative targets for N-linked glycosylation are highlighted in green. **(D)** Representative immunoblot of lysates derived from COS-1 cells transfected with empty vector, wild-type (WT) or indicated mutant Flag-SLC17A4. **(E)** Parallel T4 uptake studies in COS-1 cells transfected with wild-type (WT) or indicated mutant constructs. All uptake levels are corrected for background T4 uptake in empty vector transfected control cells under the same culturing and incubation conditions. T4 uptake is expressed relative to the levels observed in COS-1 cells transfected with SLC17A4 cultured in presence of vehicle (1% DMSO) for **(B)** or wild-type SLC17A4 for **(E)**. Unpaired t-tests and One-way ANOVA followed by Dunnett`s posttests were performed to assess for statistically significant differences between the conditions in **(B)** and **(E)**, respectively.

DISCUSSION

The orphan transporter SLC17A4 has been recently shown to facilitate the cellular uptake of T3 and T4 (9), but data on its basic functional characteristics, including substrate selectivity, transport directionality, and sensitivity to known thyroid hormone transporter-inhibitors, are still unknown. . Here, we further detailed the functional characteristics of this novel TH transporter. Using transfected mammalian COS-1 cells, we demonstrated that SLC17A4 efficiently facilitates the cellular uptake and efflux of T3 and T4 and to a lesser extent rT3, but not 3,3'-T2. The cellular uptake of T4 was Na^+- and Cl^--independent, and was stimulated at low extracellular pH. SLC17A4-mediated TH uptake was diminished by a wide range of iodothyronines and alternate alanine side-chain metabolites, but not by iodotyrosines, aromatic amino acids, or classical TH transporter inhibitors. Finally, we showed that SLC17A4 is subject to N-linked glycosylation, which likely targets Asn-residues in the first extracellular loop. The results of our study thus yield key insights into the functional characteristics of SLC17A4 and enable defining its contribution to cellular TH homeostasis as well as comparing SLC17A4 to the well-established TH transporters.

Among the thyroid hormone transporters identified over the last decades (reviewed in e.g. (2, 3)), MCT8 is generally considered as the most specific and efficient iodothyronine transporter. In contrast to MCT8 which accepts T3 and T4, as well as rT3 and 3,3'-T2 as a substrate (4, 23), SLC17A4 particularly transports T3 and T4 and to a lesser extent rT3, but not 3,3'-T2. Like MCT8 (23), SLC17A4 increases the intracellular availability of T3 and T4 for deiodination which confirms that SLC17A4 controls intracellular TH homeostasis by regulating the transport of TH across the cell membrane. The apparent Km values of SLC17A4 for T3 (0.41±0.14 µM) and T4 (0.18±0.17 µM) transport (9) are moreover about 10-20-times lower than those reported for MCT8 as well as most other known TH transporters (24).

Cis-inhibition studies suggested that SLC17A4 may also recognize other iodothyronines and alanine side-chain metabolites thereof, including the iodothyroproprionic acid and –acetic acid derivatives as well as the thyronamines. The most effective cis-inhibitory compounds contained two phenolic rings with two inner-ring iodine and at least one outer-ring iodine moiety, whereas the presence of any modifications to the alanine side-chain made no apparent differences and might not be critical for initial substrate recognition. By contrast, direct uptake studies indicated that TA3 is a less suitable substrate for SLC17A4 than T3, whereas TA4 was not directly transported by SLC17A4 at all. Therefore, we speculate that the composition of the alanine side-chain is critical to induce conformational changes that lead to the actual transport of the substrate. In light of these findings, it should be emphasized that other compounds that exhibited pronounced cis-inhibitory effects in our studies are not necessarily genuine substrates for SLC17A4. None of the classical TH transporter inhibitors reduced SLC17A4-mediated TH uptake. Therefore, there was no need to reconsider their specificities towards the well-established TH transporter systems.

SLC17A4 has been previously shown to exhibit membrane potential ($\Delta\psi$) and Cl^--dependent transport of urate and p-aminohippuric acid (PAH) in proteoliposomes (11). However, our functional studies in transiently transfected mammalian COS-1 cells indicated that SLC17A4 does not require Cl^- to transport T4. Moreover, T4 transport was not attenuated by changes in membrane potential secondary to high extracellular K^+ concentrations. T4 transport was moreover Na^+-independent and was stimulated at low extracellular pH. It is yet unclear if the transport of TH is proton-coupled, given the pronounced residual T4 uptake at basic pH and the limited impact of extracellular pH on T3 transport. Alternatively,

changes in extracellular pH may also affect the protonation state of the substrate and/or amino acid side-chains at the substrate binding pocket of the transporter. Further structural and mutational studies may help to elucidate the underlying mechanism. Nonetheless, our studies indicate that the mechanism by which SLC17A4 transports T4 differs from those described for its other putative substrates.

Although we also observed a marginal induction of uric acid uptake in SLC17A4-expressing COS-1 cells, uric acid concentrations up to 1000 µM did not inhibit SLC17A4-mediated TH transport. As these levels are well above the reported normal range of uric acid in serum (19), it is not to be expected that SLC17A4-mediated TH transport is modulated by circulating uric acid concentrations *in vivo*. Importantly, the observed 1.3-times induction of uric acid transport in transfected COS-1 cells was less pronounced compared to the reported ~3-times induction of uric acid uptake in proteoliposomes (11) and may suggest that SLC17A4 is not an efficient uric acid transporter in living cells. These differences may be inherent to the different expression systems, applied buffers, established ion gradients, and differential abundance of redundant transporters in COS-1 cells that may influence the flux of uric acid across the cell membrane.

Our studies also indicated that SLC17A4 is subject to N-linked glycosylation which may contribute to the appearance of different immune-reactive bands around the predicted size of the SLC17A4 monomere. A similar phenomenon was observed on immunoblots for SLC17A3 on the membrane fraction of rat kidney (25). We demonstrated that the inhibition of N-linked glycosylation diminished the 54 kDa band and reduced T4 uptake, suggesting that the ~54 kDa protein represents the glycosylated active form of SLC17A4. Our studies suggest that three Asn residues within ECL1 are the most likely targets for N-linked glycosylation, substitution of which by an alanine resulted in a pronounced functional reduction and exclusive appearance of the ~47 kDa band, but not ~54 kDa band. Together, these findings support that the ~47 kDa band represents immature, non-glycosylated SLC17A4. In addition, we also observed a prominent band migrating at ~90-100 kDa. The nature of this band remains to be elucidated.

Although the association of the *SLC17A4* locus with serum free T4 concentrations implies that SLC17A4 is involved in the regulation of thyroid function (9), further studies in *Slc17a4* knock-out animals or humans carrying pathogenic mutations in SLC17A4 are needed to delineate the physiological role of SLC17A4 in TH homeostasis. Given its predominant expression at mRNA level along the gastro-intestinal tract (11), SLC17A4 may be crucial for the absorption of TH from the gut, which comprises a critical step in the enterohepatic cycle of TH (26) and drug-delivery in patients treated with levothyroxine (LT4). Further studies will detail in which gastro-intestinal cells SLC17A4 is expressed and define its subcellular distribution. Since our study showed that SLC17A4 facilitates the cellular uptake and efflux of TH, it may contribute to the transcellular transport of TH at the apical and basolateral membrane. Should SLC17A4 indeed be responsible for the gastro-intestinal absorption of TH, drugs that interfere with SLC17A4 function may importantly impair the absorption of TH and increase its metabolic clearance.

Taken together, SLC17A4 facilitates the cellular uptake and efflux of T3 and T4 with great specificity and is among the most efficient TH transporters identified to date.

Acknowledgements

This work was supported by a grant from the European Thyroid Association (to SG) and the Netherlands Organisation for Health Research and Development (project number 113303005) (to WEV).

REFERENCES

1. Hennemann G, Docter R, Friesema EC, de Jong M, Krenning EP, Visser TJ. Plasma membrane transport of thyroid hormones and its role in thyroid hormone metabolism and bioavailability. Endocr Rev. 2001;22(4):451-76.
2. Visser WE, Friesema EC, Visser TJ. Minireview: thyroid hormone transporters: the knowns and the unknowns. Mol Endocrinol. 2011;25(1):1-14.
3. Schweizer U, Johannes J, Bayer D, Braun D. Structure and function of thyroid hormone plasma membrane transporters. Eur Thyroid J. 2014;3(3):143-53.
4. Friesema EC, Ganguly S, Abdalla A, Manning Fox JE, Halestrap AP, Visser TJ. Identification of monocarboxylate transporter 8 as a specific thyroid hormone transporter. J Biol Chem. 2003;278(41):40128-35.
5. Friesema EC, Kuiper GG, Jansen J, Visser TJ, Kester MH. Thyroid hormone transport by the human monocarboxylate transporter 8 and its rate-limiting role in intracellular metabolism. Mol Endocrinol. 2006;20(11):2761-72.
6. Friesema EC, Grueters A, Biebermann H, Krude H, von Moers A, Reeser M, et al. Association between mutations in a thyroid hormone transporter and severe X-linked psychomotor retardation. Lancet. 2004;364(9443):1435-7.
7. Dumitrescu AM, Liao XH, Best TB, Brockmann K, Refetoff S. A novel syndrome combining thyroid and neurological abnormalities is associated with mutations in a monocarboxylate transporter gene. Am J Hum Genet. 2004;74(1):168-75.
8. Stromme P, Groeneweg S, Lima de Souza EC, Zevenbergen C, Torgersbraten A, Holmgren A, et al. Mutated thyroid hormone transporter OATP1C1 associates with severe brain hypometabolism and juvenile neurodegeneration. Thyroid. 2018.
9. Teumer A, Chaker L, Groeneweg S, Li Y, Di Munno C, Barbieri C, et al. Genome-wide analyses identify a role for SLC17A4 and AADAT in thyroid hormone regulation. Nat Commun. 2018;9(1):4455.
10. Reimer RJ. SLC17: a functionally diverse family of organic anion transporters. Molecular aspects of medicine. 2013;34(2-3):350-9.
11. Togawa N, Miyaji T, Izawa S, Omote H, Moriyama Y. A Na+-phosphate cotransporter homologue (SLC17A4 protein) is an intestinal organic anion exporter. American journal of physiology Cell physiology. 2012;302(11):C1652-60.
12. Shibui A, Tsunoda T, Seki N, Suzuki Y, Sugane K, Sugano S. Isolation and chromosomal mapping of a novel human gene showing homology to Na+/PO4 cotransporter. J Hum Genet. 1999;44(3):190-2.
13. Friesema EC, Jansen J, Jachtenberg JW, Visser WE, Kester MH, Visser TJ. Effective cellular uptake and efflux of thyroid hormone by human monocarboxylate transporter 10. Mol Endocrinol. 2008;22(6):1357-69.
14. Groeneweg S, Friesema EC, Kersseboom S, Klootwijk W, Visser WE, Peeters RP, et al. The role of Arg445 and Asp498 in the human thyroid hormone transporter MCT8. Endocrinology. 2014;155(2):618-26.
15. Groeneweg S, Kersseboom S, van den Berge A, Dolcetta-Capuzzo A, van Geest FS, van Heerebeek REA, et al. In vitro characterization of human, mouse and zebrafish MCT8 orthologues. Thyroid. 2019.
16. Groeneweg S, Lima de Souza EC, Meima ME, Peeters RP, Visser WE, Visser TJ. Outward-Open Model of Thyroid Hormone Transporter Monocarboxylate Transporter 8 Provides Novel Structural and Functional Insights. Endocrinology. 2017;158(10):3292-306.
17. Iharada M, Miyaji T, Fujimoto T, Hiasa M, Anzai N, Omote H, et al. Type 1 sodium-dependent phosphate transporter (SLC17A1 Protein) is a Cl(-)-dependent urate exporter. J Biol Chem. 2010;285(34):26107-13.
18. Togawa N, Juge N, Miyaji T, Hiasa M, Omote H, Moriyama Y. Wide expression of type I Na+-phosphate cotransporter 3 (NPT3/SLC17A2), a membrane potential-driven organic anion transporter. American journal of physiology Cell physiology. 2015;309(2):C71-80.
19. Desideri G, Castaldo G, Lombardi A, Mussap M, Testa A, Pontremoli R, et al. Is it time to revise the normal range of serum uric acid levels? European review for medical and pharmacological sciences. 2014;18(9):1295-306.
20. Rath A, Glibowicka M, Nadeau VG, Chen G, Deber CM. Detergent binding explains anomalous SDS-PAGE migration of membrane proteins. Proc Natl Acad Sci U S A. 2009;106(6):1760-5.
21. Leano JB, Batarni S, Eriksen J, Juge N, Pak JE, Kimura-Someya T, et al. Structures suggest a mechanism for energy coupling by a family of organic anion transporters. PLoS Biol. 2019;17(5):e3000260.
22. Zomot E, Yardeni EH, Vargiu AV, Tam HK, Malloci G, Ramaswamy VK, et al. A New Critical Conformational Determinant of Multidrug Efflux by an MFS Transporter. Journal of molecular biology. 2018;430(9):1368-85.

23. Friesema EC, Jansen J, Heuer H, Trajkovic M, Bauer K, Visser TJ. Mechanisms of disease: psychomotor retardation and high T3 levels caused by mutations in monocarboxylate transporter 8. Nat Clin Pract Endocrinol Metab. 2006;2(9):512-23.
24. Bernal J, Guadano-Ferraz A, Morte B. Thyroid hormone transporters--functions and clinical implications. Nat Rev Endocrinol. 2015;11(7):406-17.
25. Ishibashi K, Matsuzaki T, Takata K, Imai M. Identification of a new member of type I Na/phosphate co-transporter in the rat kidney. Nephron Physiol. 2003;94(1):p10-8.
26. Hazenberg MP, de Herder WW, Visser TJ. Hydrolysis of iodothyronine conjugates by intestinal bacteria. FEMS microbiology reviews. 1988;4(1):9-16.

Chapter

Characterization of the mouse orthologue of the thyroid hormone transporter SLC17A4

6.3

Stefan Groeneweg, Ferdy S. van Geest, Marcel E. Meima, Robin P. Peeters, Heike Heuer, Marco Medici, and W. Edward Visser

Manuscript in preparation

ABSTRACT

Introduction Recently, the *SLC17A4* locus has been associated with circulating free T4 concentrations. Subsequent studies characterized SLC17A4 as a novel T3 and T4 transporter. However, little is known about the role of SLC17A4 in thyroid hormone (TH) homeostasis *in vivo*. Here, we characterized the mouse orthologue of SLC17A4 as a first step to establish if mice may provide a suitable model to study human SLC17A4 function *in vivo*.

Methods We performed a broad range of TH transport studies in COS-1 cells transiently overexpressing mouse (mm)SLC17A4, including uptake and efflux studies of various [^{125}I]-labelled iodothyronines, transport kinetics and cis-inhibition studies. Moreover, we assessed the mouse orthologues of SLC17A1-3 for TH uptake capacity.

Results Upon over-expression in mammalian COS-1 cells, mmSLC17A4 effectively induced the cellular uptake of T3, T4 and rT3 by ~4-times and the uptake of 3,3'-T2 by 2.3-times. The induction of rT3 and T4 uptake did not greatly differ in the presence or absence of CRYM. The apparent Km of T3 uptake was 0.75 µM and of T4 uptake 47 nM. The mouse SLC17A4 orthologue also facilitated the cellular efflux of in particular 3,3'-T2 and T3. The uptake of T3 and T4 was reduced by various iodothyronines and metabolites thereof, particularly those that contain at least 3 iodine moieties irrespective of the presence of modification at the alanine side-chain. Overexpression of mmSLC17A4 effectively induced the uptake of triiodothyroacetic acid (TA3). None of the classical TH transporter inhibitors studied attenuated mmSLC17A4-mediated TH transport. The mouse orthologues of SLC17A1-3, which are the only other cell membrane transporters within the SLC17 family, did not facilitate uptake of iodothyronines, although SLC17A3 induced the uptake of TA3 by ~1.5-times.

Discussion Our studies demonstrated that mouse SLC17A4 is an efficient T3 and T4 transporter with grossly similar functional characteristics as its human orthologue. Together, these observations pave the way to further detail SLC17A4 function *in vivo*.

INTRODUCTION

Transporter proteins are indispensable for the cellular uptake and efflux of thyroid hormone (TH) (1). Over the last decades multiple TH transporter protein families have been identified (2, 3). The most specific TH transporter identified to date is monocarboxylate transporter (MCT)8, which efficiently facilitates the cellular uptake and efflux of 3,3',5-tri-iodothyronine (T3), thyroxine (T4), and to a lesser extent 3,3',5'-reverse T3 (rT3) and 3,3'-di-iodothyronine (3,3'-T2) (4, 5). Recently we identified SLC17A4 as a novel TH transporter with a particular substrate preference for T3 and T4. Genetic variation within the *SLC17A4* locus is associated with circulating free T4 concentrations (6), suggesting an important role of this transporter in the regulation of thyroid function.

The SLC17 family consists of nine structurally related proteins that have been identified as organic anion transporters (7). The first 4 members of the SLC17 are considered as cell membrane transporters and are encoded by the *SLC17A1-4* genes that cluster on Chr6p22.2. SLC17A1-4 appear to be the most recent members of this family, and are only present as such in mammals (8). SLC17A1-4 had been initially classified as Na^+-dependent inorganic phosphate transporters, but over the years it has become clear that SLC17A1-3 accept a broad range of organic anions (7). By contrast, the function of SLC17A4 has long been largely unknown (7). One study showed that SLC17A4, also known as NPT4-homologue, induced the membrane potential ($\Delta\psi$) and Cl^--dependent transport of urate and p-aminohippuric acid (PAH) in proteoliposomes (9). However, functional studies in cell-based models demonstrated that SLC17A4 is actually a much more proficient TH transporter (**chapter 6.2**).

Although it has been established that human SLC17A4 facilitates the cellular uptake and efflux of T3 and T4, little is known about the role of SLC17A4 in TH homeostasis *in vivo*. To address this need, the establishment of a *Slc17A4* knock-out (ko) animal model will yield valuable information. Since the *SLC17A4* gene is only conserved in mammals, mouse may pose the most suitable model to study SLC17A4 function *in vivo*. However, it is currently unknown if mouse SLC17A4 has similar functional characteristics as its human orthologue. Together with species-specific tissue distribution of SLC17A4 expression and the presence of alternative TH transporters at sites where SLC17A4 is expressed, the basic functional characteristics of the mouse SLC17A4 orthologue importantly determine if mice provide a suitable *in vivo* model to study SLC17A4 function.

Here, we functionally characterized the mouse orthologue of SLC17A4 and, moreover, assessed the mouse SLC17A1-3 members for TH transport capacity. We demonstrate that the mouse SLC17A4 orthologue is an efficient T3 and T4 transporter and likely, at least in mice, the only member of the SLC17 that effectively transports TH across the cell membrane. Together, our studies pave the way to further detail SLC17A4 function *in vivo*.

METHODS

Materials

Nonradioactive iodothyronines, amino acids, D-glucose, fetal bovine serum, and bovine serum albumin (BSA) were obtained from Sigma Aldrich (Zwijndrecht, The Netherlands [NL]). [^{125}I]-3,3'-T2 [^{125}I]-T3, [^{125}I]-rT3, [^{125}I]-T4, [^{125}I]-3,3',5-triiodothyroacetic acid (Triac; TA3), and [^{125}I]-3,3',5,5'-tetraiodothyroacetic acid (Tetrac; TA4) were produced as previously described (16, 17). [^{14}C] uric acid was obtained from American radiolabeled chemicals (St. Louis, USA). The monoclonal M2 mouse anti-

Flag antibody was obtained from Sigma Aldrich (RRID: AB_262044), and the mouse anti-Glyceraldehyde-3-phosphate dehydrogenase (GAPDH) antibody (Mab374; RRID: AB_2107445) was obtained from Merck Millipore (Amsterdam, NL). All cell culture flasks and plates were obtained from Corning (Schiphol, NL). X-tremeGENE9 transfection reagent was obtained from Roche Diagnostics (Woerden, NL). DMEM/F12 and penicillin/streptomycin were obtained from Life Technologies (Bleiswijk, NL)

Constructs

The generation of the expression construct encoding human µ-crystallin (pSG5-hCRYM) has been previously described (5, 10). hCRYM is a high affinity intracellular TH-binding protein that greatly reduces the cellular TH efflux and thereby increases the net cellular TH uptake. A pCMV6-Entry_ human (hs) SLC17A4, mouse (mm) SLC17A1, mmSLC17A42, mmSLC17A3, and mmSLC17A4 expression vectors containing a C-terminal Myc and Flag tag were obtained from OriGene Technologies (Rockville, USA). The coding sequence was fully sequenced to verify correctness of all constructs. Unintended mutations were corrected to the reference sequences using site-directed mutagenesis according to manufacturers` protocol (Agilent, Middelburg, NL).

Cell culture and transfection

COS-1 African green monkey kidney cells were obtained from ECACC (Sigma-Aldrich) and cultured under standard conditions (e.g. (11)). For uptake studies cells were seeded on 24-well dishes and transiently transfected with 150 ng empty vector, hsSLC17A4 or mmSLC17A1-4 expression construct with or without 50 ng of pSG5-hCRYM at ~70% confluence using X-tremeGENE9 transfection reagent according to manufacturers` protocol, unless otherwise indicated. For immunoblotting, cells were cultured in 6-well dishes and transfected with 500 ng empty vector or Flag-tagged SLC17A1-4 constructs. All experiments were carried out 48 h after transfection.

TH transport studies

Uptake studies were carried out as previously described (e.g. (11)). Cells were first briefly washed with incubation buffer (Dulbecco`s phosphate buffered saline with Ca^{2+}/Mg^{2+}, 0.1% BSA and 0.1% glucose, unless otherwise indicated) and incubated in incubation buffer containing 1 nM (50 000 cpm) of indicated [^{125}I]-labelled [^{125}I]-3,3'-T2, [^{125}I]-T3, [^{125}I]-rT3, [^{125}I]-T4, [^{125}I]-TA3, [^{125}I]-TA4, or 100 µM [^{14}C] uric acid for indicated incubation times at 37°C. After a brief wash, internalized radioactivity was measured as previously described (4). TA3 and TA4 uptake, cis-inhibition and inhibitor studies were performed in incubation medium without BSA as described before (12).

Efflux studies were essentially performed according to well-established protocols (e.g. (10)). Cells were washed with incubation medium and pre-loaded in incubation medium containing 1 nM (50 000 cpm) [^{125}I]-labelled iodothyronines for 2 h. After a brief wash with incubation medium, cells were incubated in efflux medium (D-PBS with Ca^{2+}/Mg^{2+}, 1.0% BSA and 0.1% glucose). After indicated incubation times at 37 °C, cells were briefly washed in incubation medium and lysed in 0.1 M sodiumhydroxide. The amount of radioactivity that remained inside the cells was measured with a γ-counter.

Immunoblotting

Immunoblotting of total lysates was carried out using routine techniques (13). Monoclonal M2 mouse anti-Flag antibody was used to detect the Flag-tagged SLC17A1-4 proteins. Glyceraldehyde-3-phosphate dehydrogenase (GAPDH) was used as loading control. Primary antibodies were visualized with Odyssey techniques as previously described (e.g. (13)).

Statistics

All statistical analyses were carried out using GraphPad Prism version 6 (GraphPad Software, San Diego California, USA). Apparent IC_{50} and Km values were calculated using the log[inhibitor] vs normalized response function and Michaelis-Menten equations, respectively, which are both embedded in GraphPad Prism. The applied statistical tests and levels of significance are explained in the legend of the corresponding figure.

RESULTS

The putative mouse *Slc17A4* mRNA transcript is 2483 base pairs in length (NM_177016.3; ENSMUST00000021769.15) and contains 12 exons of which the first 11 exons are coding for a protein of 492 amino acids long. Another mRNA transcript has been detected which results from the use of alternative splice sites in exon 11 (ENSMUST00000110407.3). This transcript encodes a protein of 452 amino acids, due to the introduction of a frameshift and premature stop signal (ENSMUST00000110407.3). The long mouse *Slc17A4* transcript (NM_177016.3) is most reminiscent to the human SLC17A4 isoform (NM_005495.3) that we recently characterized as a TH transporter (6). The human and mouse orthologue have 78.3% amino acid sequence identity and 95.4% sequence similarity using a PAM250 scoring matrix (**Figure 1**).

Transfection of mammalian COS-1 cells with increasing amounts of mmSLC17A4 plasmid induced a dose-dependent increase of T4 uptake compared to control cells (**Figure 2A**). T4 uptake was not clearly further potentiated in presence of the intra-cellular TH-binding protein CRYM (**Figure 2A**). Transfection of COS-1 cells with 150 ng mmSLC17A4 resulted in a time-dependent increase of T4 uptake which did not differ in the absence or presence of CRYM (**Figure 2B**). In contrast, T4 uptake by hsSLC17A4 was significantly higher in the presence of CRYM than in the absence of CRYM at all tested time-points (**Figure 2B**).

Transfection of COS-1 cells with an increasing dose of SLC17A4 plasmid resulted in a dose-dependent increase in mmSLC17A4 protein expression levels. The most prominent immune-reactive band was observed around ~75 kDa, whereas a second band was observed around ~54 kDa (**Figure 2C**). The 54 kDa band corresponds to the calculated size of the mmSLC17A4 protein, whereas the immune-reactive band at ~75 kDa corresponds with the size at which previous studies also detected immune-reactive band for other SLC17A family members (14). As for hsSLC17A4, treatment of mmSLC17A4-transfected COS-1 cells with the N-linked glycocylation inhibitor tunicamycin resulted in the appearance of a band just below the 50 kDa. Both the ~54 kDa and ~75 kDa bands disappeared, suggesting that these bands represent glycosylated mmSLC17A4 protein or complexes that contain glycosylated mmSLC17A4 protein (**Figure 2D**).

Figure 1 Amino acid sequence alignment of the mouse and human SLC17A4 orthologues. Identical residues are indicated with :, whereas similar residues are indicated with a . using a PAM250 scoring matrix.

Next, we delineated the substrate specificity of mmSLC17A4 in greater detail. COS-1 cells transfected with mmSLC17A4 alone or in combination with CRYM were incubated for 10 minutes with 1 nM of 3,3'-T2, rT3, T3 and T4. In the absence of CRYM, cells transfected with mmSLC17A4 showed a ~4-times induction of T3 and T4 uptake and a ~3.5-times induction of rT3 uptake over control cells, whereas mmSLC17A4 increased the uptake of 3,3'-T2 by only 1.4 times (**Figure 3A**). In presence of CRYM, a similar substrate preference was observed, with the induction of T3 (~5-times), T4 and rT3 uptake (~4-times) exceeding the induction of 3,3'-T2 (2.3-times) (**Figure 3B**). Thus, in particular the uptake of 3,3'-T2 and T3 was stimulated in presence of CRYM. Kinetic analysis of T3 transport revealed an apparent Km of 0.75 µM (95% confidence interval [CI] 0.34-1.16) and a Vmax of 2.7 pmol/min (95% CI 2.3-3.1) (**Figure 3C**). The apparent Km was well in line with the apparent IC_{50} value of 0.47 µM (95% CI 0.32-0.71) (**Figure 3D**). The apparent Km for T4 transport was 37.6 nM (95% CI 0.0-77.7) with a Vmax of 15.8 pmol/min (95% CI 11.1-20.6), which was again in line with the apparent IC_{50} value of 47 nM (95% CI 35.2-62.8) (**Figure 3E** and **3F**). Together, these data indicate that mmSLC17A4 facilitates the cellular uptake of iodothyronines (T3, T4 > rT3 >>3,3'-T2), with high affinity for T3 and T4.

We also studied if mmSLC17A4 facilitates the cellular efflux of iodothyronines. After pre-loading transfected COS-1 cells with radio-labeled iodothyronines for 2 h, the amount of intracellular 3,3'-T2, rT3, T3, and T4 was measured after indicated incubation times in efflux medium (**Figure 4A-D**). When expressed relative to the amount of internalized radio-labeled iodothyronines after pre-loading, the decline in cellular 3,3'-T2 and T3 was significantly faster from cells expressing mmSLC17A4 than from control cells (**Figure 4A** and **4C**). The efflux of rT3 and T4 did not significantly differ between COS-1 cells

expressing mmSLC17A4 *versus* control cells, except for a minimal difference in cellular rT3 levels after 5 minutes in favor of mmSLC17A4 expressing cells (**Figure 4B** and **4D**). It should however be noted that the absolute decline in cellular rT3 and in particular T4 content in cells expressing mmSLC17A4 greatly exceeded that of control cells in the first 5 minutes (**Supplemental Figure S1**).

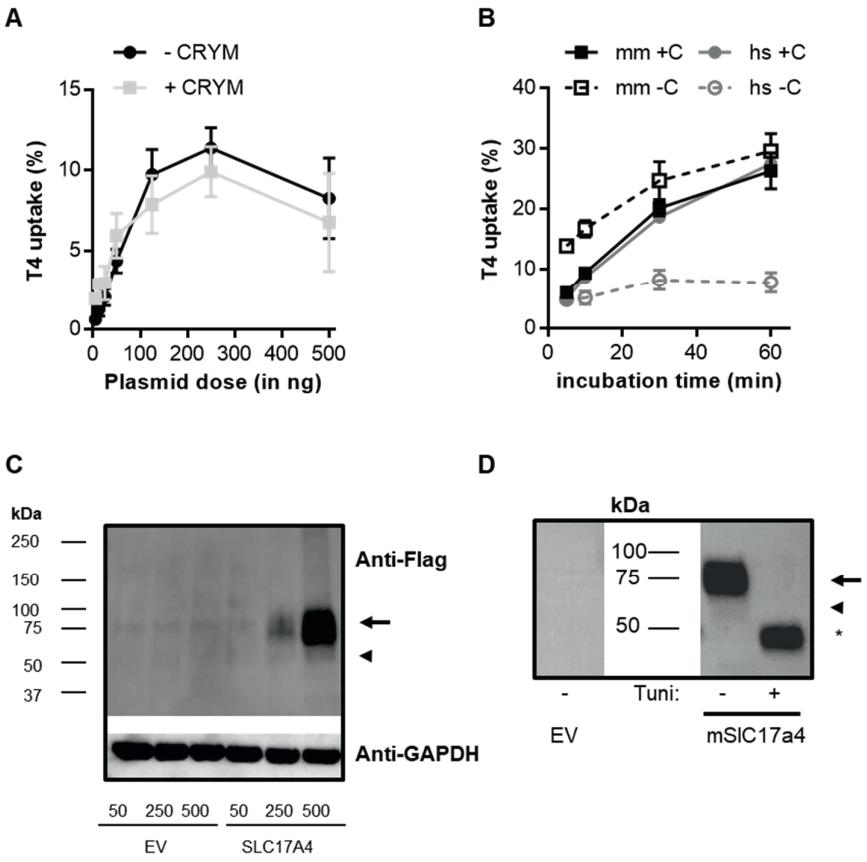

Figure 2 (A) T4 uptake in COS-1 cells transiently transfected with indicated amounts of mmSLC17A4 plasmid in the absence (dashed line) and presence (solid line) of 50 ng CRYM after 30 minutes incubation at 37 °C. **(B)** Time-dependent uptake of T4 in COS-1 cells transfected with human (hs, grey lines) or mouse (mm, black lines) SLC17A4 in the absence (dashed lines) or presence (solid lines) of CRYM. All uptake values are corrected for background TH uptake levels observed in COS-1 cells transfected with empty vector and presented as means (± SEM) of 3 separate experiments in duplicate. **(C)** Representative immunoblot on total lysates derived from COS-1 cells transiently transfected with indicated amounts of Flag-mmSLC17A4 expression construct. Glyceraldehyde-3-phosphate dehydrogenase (GAPDH) was used as loading control. **(D)** Representative immunoblot of lysates derived from COS-1 cells transfected with empty vector or Flag-mmSLC17A4 cultured in the presence (+) or absence (-) of 1 µg/ml tunicamycin. Bands that may represent the mmSLC17A4 monomer (predicted size ~54 kDa) are indicated with an arrowhead, whereas a putative (hetereo-)dimer is indicated with an arrow. The putative de-glycosylated mmSLC17A4 monomer (~47 kDa) is indicated with an *.

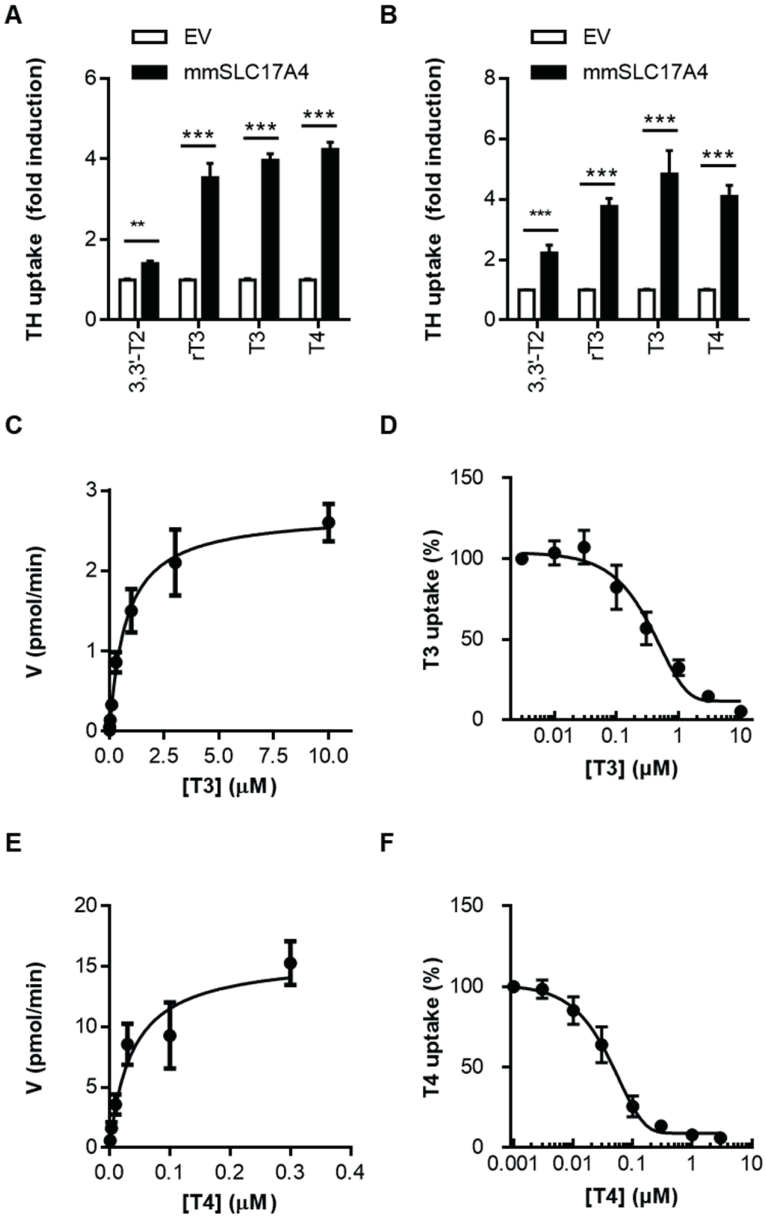

Figure 3 Substrate specificity of SLC17A4. **(A)** and **(B)** uptake of indicated iodothyronines in transiently transfected COS-1 cells after 10 minutes incubation at 37 °C in the absence **(A)** or presence **(B)** of CRYM. The uptake of various iodothyronines is expressed as fold induction over uptake levels observed in empty vector transfected cells (n=4). Two-way ANOVA followed by Bonferroni posttests were applied to assess for statistically significant differences between empty vector control and mmSLC17A4 transfected COS-1 cells ($p<0.01$, **, $p<0.001$, ***). **(C)** Kinetic analysis of T3 using Michaelis-Menten equation and **(D)** data of the same experiments presented as a saturation curve. Km values were calculated using a standard Michaelis-Menten equation **(C)** and the IC_{50} using log[inhibitor] *versus* normalized response curves **(D)**, both implemented in GraphPad Prism. Similarly, **(E)** and **(F)** present the kinetic analysis and saturation curve of T4 uptake.

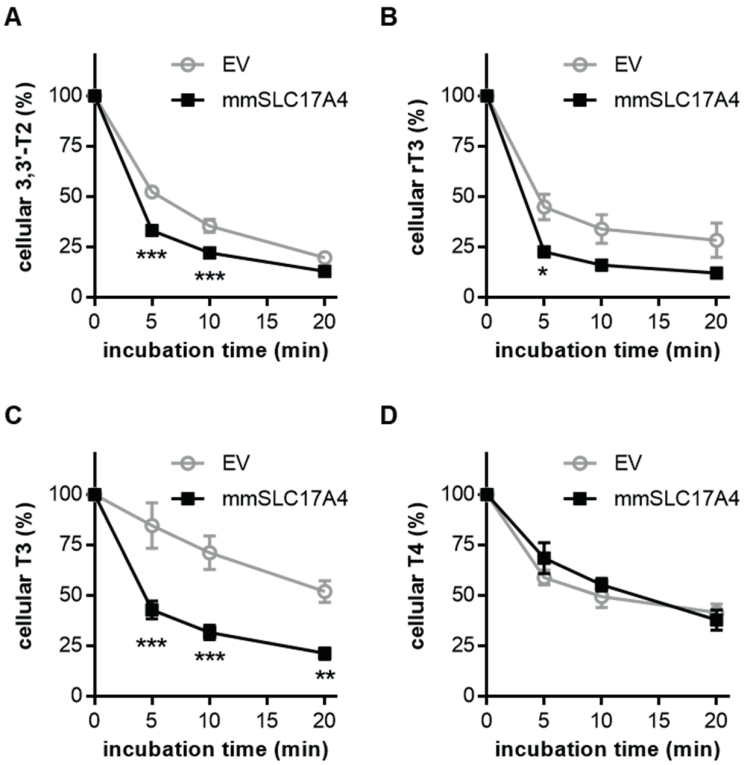

Figure 4 (A-D) cellular efflux of 3,3'-T2 **(A)**, rT3 **(B)**, T3 **(C)** and T4 **(D)** efflux by empty vector or mmSLC17A4 transfected COS-1 cells in 2-20 minutes. Cells were incubated for 120 min with 1 nM (50 000 cpm) of the indicated substrates (pre-loading), before efflux was measured. The amount of radio-activity that remained within the cell after 2-20 minutes incubation in efflux medium is displayed relatively to the amount of radio-activity that was present after pre-loading (t=0). All results are presented as means ± SEM (n=3-4). Two-way ANOVA followed by Bonferroni posttests were applied to assess for statistically significant differences between the tested conditions ($p<0.05$, *; $p<0.01$, **, $p<0.001$, ***).

To further study the substrate specificity of mmSLC17A4, we also performed cis-inhibition studies with iodothyronines and structurally related compounds. First, we studied the cis-inhibitory effect of different iodothyronines on mmSLC17A4-mediated [^{125}I]-T3 uptake in the presence of CRYM. At 1 µM concentrations, the uptake of T3 was greatly diminished by T4, T3 and rT3, whereas T0 and various T2 derivatives had no or only little effect (**Figure 5A**). At 10 µM concentrations, 3,3'-T2 and 3,5-T2 also decreased mmSLC17A4-mediated T3 uptake, whereas T0 and 3',5'-T2 still had no effect (**Figure 5A**). Second, we evaluated the effects of various alanine side-chain metabolites, including iodothyroacetic (TA_x) and -proprionic (TP_x) acid derivatives as well as thyronamines (T_xAm). In particular TA2, TA3, TA4 and T3P reduced mmSLC17A4-mediated T3 uptake at 1 µM concentrations, whereas the other compounds that were tested had no effect at this concentration (**Figure 5B**). At a concentration of 10 µM, significant cis-inhibitory effects were observed for alanine side-chain metabolites, with greatest effects for TA3 and T3P (**Figure 5B**).

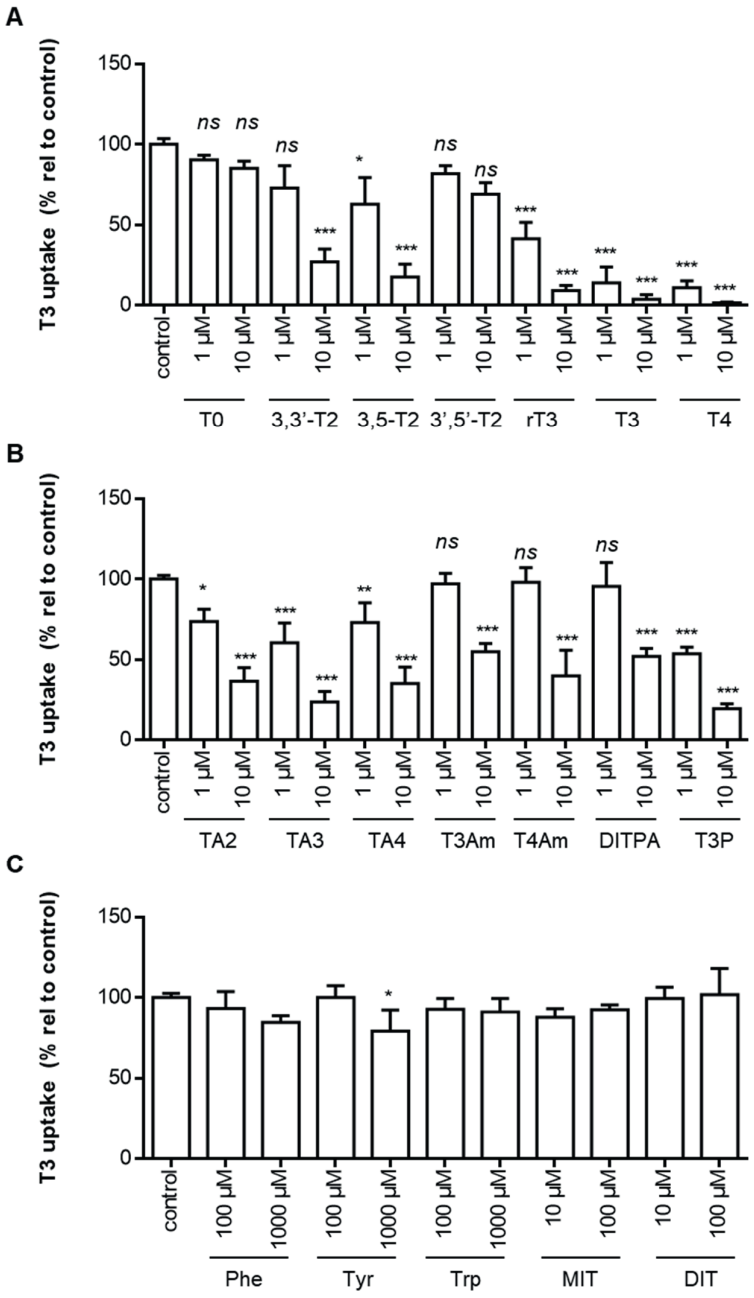

Figure 5 (A) mmSLC17A4-mediated T3 uptake after 30 minutes incubation in presence of 1 or 10 µM of the indicated iodothyronines in COS-1 cells co-transfected with CRYM. **(B)** mmSLC17A4-mediated T3 uptake in presence of 1 or 10 µM of the indicated alanine side-chain metabolites of iodothyronines or **(C)** 100 or 1000 µM of the indicated aromatic amino acids and 10 or 100 µM of the indicated iodotyrosines. All uptake levels are corrected for background T3 uptake in empty vector transfected control cells incubated in the presence of the same competitor. T3 uptake levels are displayed relative to the amount of intracellular [^{125}I]-T3 in cells incubated in the absence of any competitors (100%) and presented as means ± SEM (n=3). A One-way ANOVA was carried followed by Dunnett's posttests to asses for significant differences between the T3 uptake levels in the absence or presence of the tested competitors ($p<0.05$, *; $p<0.01$, **, $p<0.001$, ***). Abbreviations: TA2, diiodothyroacetic acid; TA3, triiodothyroacetic acid; TA4, tetraiodothyroacetic acid; T3Am, triiodothyronamine; T4Am, tetraiodothyronamine; DITPA, diiodothyropropionic acid; TP3, triiodothyropropionic acid; MIT, monoiodotyrosine; DIT, diiodotyrosine.

Finally, mmSLC17A4-mediated T3 uptake was measured in presence of aromatic amino acids and the iodotyrosines mono-iodotyrosine (MIT) and di-iodotyrosine (DIT). These compounds did not exert significant cis-inhibitory effects, except for tyrosine which slightly, but significantly, reduced T3 uptake when present in the supra-physiological concentration of 1000 µM (**Figure 5C**). These findings were confirmed by similar experiments conducted with [^{125}I]-T4 in the absence of CRYM (data not shown).

In addition to the various structurally related compounds, we studied the impact of well-established inhibitors of other TH transporters on mmSLC17A4-mediated T3 uptake. For these studies we selected narangin (OATP inhibitor), 2-Aminobicyclo[2.2.1]heptane-2-carboxylic acid (BCH; LAT inhibitor), sulfobromophthalein (BSP) and verapamil (inhibitors of multiple transporters), silychristin (MCT8 inhibitor) and estrone sulfate (E3S; substrate for NTCP and OATPs). However, none of these compounds reduced SLC17A4-mediated T3 uptake when applied at concentrations known to reduce the function of other TH transporters (**Figure 6**).

Finally, we studied if other members of the SLC17 family may also transport iodothyronines. Phylogenetic analysis revealed that SLC17A4 has greatest sequence homology to the cell membrane transporters SLC17A1-3 which had been initially classified as sodium-dependent phosphate transporters (NPTs) (7). The vesicular transporters including the vesicular excitatory amino acid transporters (VEAT, SLC17A5), vesicular glutamate transporters (VGLUTs, SLC17A6-8), and vesicular nucleotide transporters (VNUT, SLC17A9) compose a separate branch in the phylogenetic tree (**Figure 7A**). Therefore, we focused our analyses on mmSLC17A1-3. Upon over-expression of C-terminally Myc-Flag-tagged SLC17A1-4 in COS-1 cells, immune-reactive bands were detected for mmSLC17A2 at ~66 kDa which is in agreement with previous observations (15) and for mmSLC17A3 at ~70 kDa, which is in line with the observed size of the most prominent band of mmSLC17A4 (**Figure 7B**).

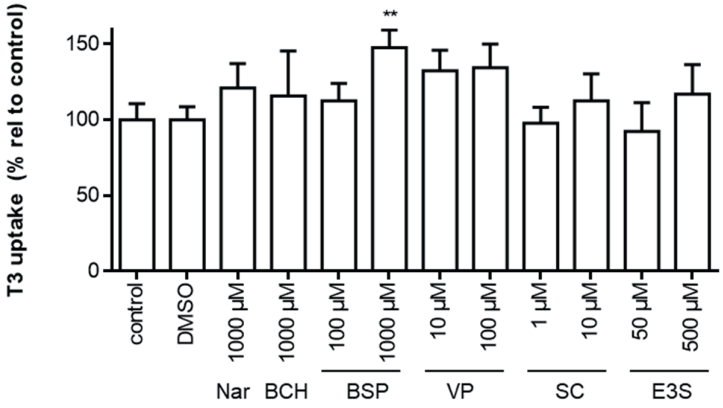

Figure 6 T3 uptake after 30 minutes incubation in the presence or absence of the indicated known inhibitors of other TH transporters in COS-1 cells co-transfected with CRYM. All uptake levels are corrected for background T3 uptake in empty vector transfected control cells incubated in the presence of the same inhibitor. All uptake levels are corrected for background T3 uptake in empty vector transfected control cells incubated in the presence of the same inhibitor. T3 uptake levels are displayed relative to the amount of intracellular [^{125}I]-T3 in cells incubated in the absence of any competitors (100%) and presented as means ± SEM (n=3). A One-way ANOVA was carried followed by Dunnett's posttests to asses for significant differences between the T3 uptake levels in the absence or presence of the tested inhibitors. Abbreviations: nar, narangin; BCH, 2-Aminobicyclo[2.2.1]heptane-2-carboxylic acid; BSP, sulfobromophthalein; VP, verapamil; SC, silychristin; E3S, estrone sulfate.

Although the mmSLC17A1 contained the correct cDNA sequence, we were unable to detect the mmSLC17A1 protein using either anti-Flag or anti-Myc antibodies, suggesting that it is not effectively expressed at protein level in our cell-based model. In line with previous studies that evaluated their human orthologues in proteoliposomes or *Xenopus* oocytes (9, 16, 17), over-expression of mmSLC17A3 and mmSLC17A4 induced the uptake of uric acid in COS-1 cells (**Figure 7C**). No induction of uric acid was observed in cells transfected with mmSLC17A1 and mmSLC17A2 (**Figure 7C**). In contrast to mmSLC17A4, none of the tested family members induced the uptake of 3,3'-T2 (**Figure 7D**), rT3 (**Figure 7E**), T3 (**Figure 7F**), or T4 (**Figure 7G**). Providing its strong cis-inhibitory effects on SLC17A4-mediated TH uptake, we also evaluated direct TA3 uptake. Both mmSLC17A3 and mmSLC17A4 induced the uptake of TA3 by 1.5- and 2.2-times, respectively (**Figure 7H**).

DISCUSSION

Human SLC17A4 has been recently characterized as a novel TH transporter with great substrate specificity towards T3 and T4 (6) and **chapter 6.2**. Moreover, the SLC17A4 locus has been associated with circulating free T4 concentrations, suggesting a physiological relevant role for this transporter in the regulation of thyroid function. Yet, the precise mechanism via which SLC17A4 controls thyroid function is unknown. Here, we studied if the mouse orthologue of SLC17A4 has similar functional characteristics as its human orthologue which importantly determines if mice provide a suitable *in vivo* model to study SLC17A4 function. We demonstrate that mmSLC17A4 is a very efficient T3 and T4 transporter with even higher affinity for these substrates than its human orthologue. Moreover, the inhibitory effects of structurally related compounds and TH transporter inhibitors completely overlapped between mouse and human SLC17A4, suggesting a common mechanism for substrate recognition. Although mmSLC17A4 effectively facilitates the cellular efflux of 3,3'-T2 and T3, the efflux of T4 appeared less effective compared to its human orthologue (**chapter 6.2**). Taken together, our studies showed that mmSLC17A4 is a very efficient T3 and T4 transporter with grossly similar functional characteristics as its human orthologue, supporting the use of mice as an *in vivo* model to study human SLC17A4 function.

Similar to hsSLC17A4, T3 and T4 were the most suitable substrates for its mouse orthologue. With an apparent Km of 0.75 µM for T3 and 47 nM for T4, the apparent affinity of mmSLC17A4 for these substrates is even higher than those reported for hsSLC17A4 and any of the other TH transporters known to date (2). Although hsSLC17A4 only slightly induced the cellular uptake of rT3 and 3,3'-T2, these substrates were transported more effectively by the mouse orthologue. Interestingly, the uptake of in particular rT3 and T4 by mmSLC17A4 was not potentiated in presence of CRYM, which was clearly the case for hsSLC17A4. These observations suggested that mmSLC17A4 does not effectively facilitate the cellular efflux of rT3 and T4, which was confirmed by cellular efflux studies. It should however be realized that cells expressing mmSLC17A4 contained much higher amounts of rT3 and in particular T4 after the required pre-loading step, which poses a limitation for direct comparison of cellular efflux rate between mmSLC17A4 and empty vector transfected cells. Should factors other than the substrate concentration gradient across the cell membrane determine efflux efficacy, the mouse SLC17A4 orthologue may thus still significantly contribute to the decline in cellular rT3 and T4 content. Further studies in systems that allow studying transcellular transport may yield additional information to address the question if mmSLC17A4 also facilitates the efflux of T4.

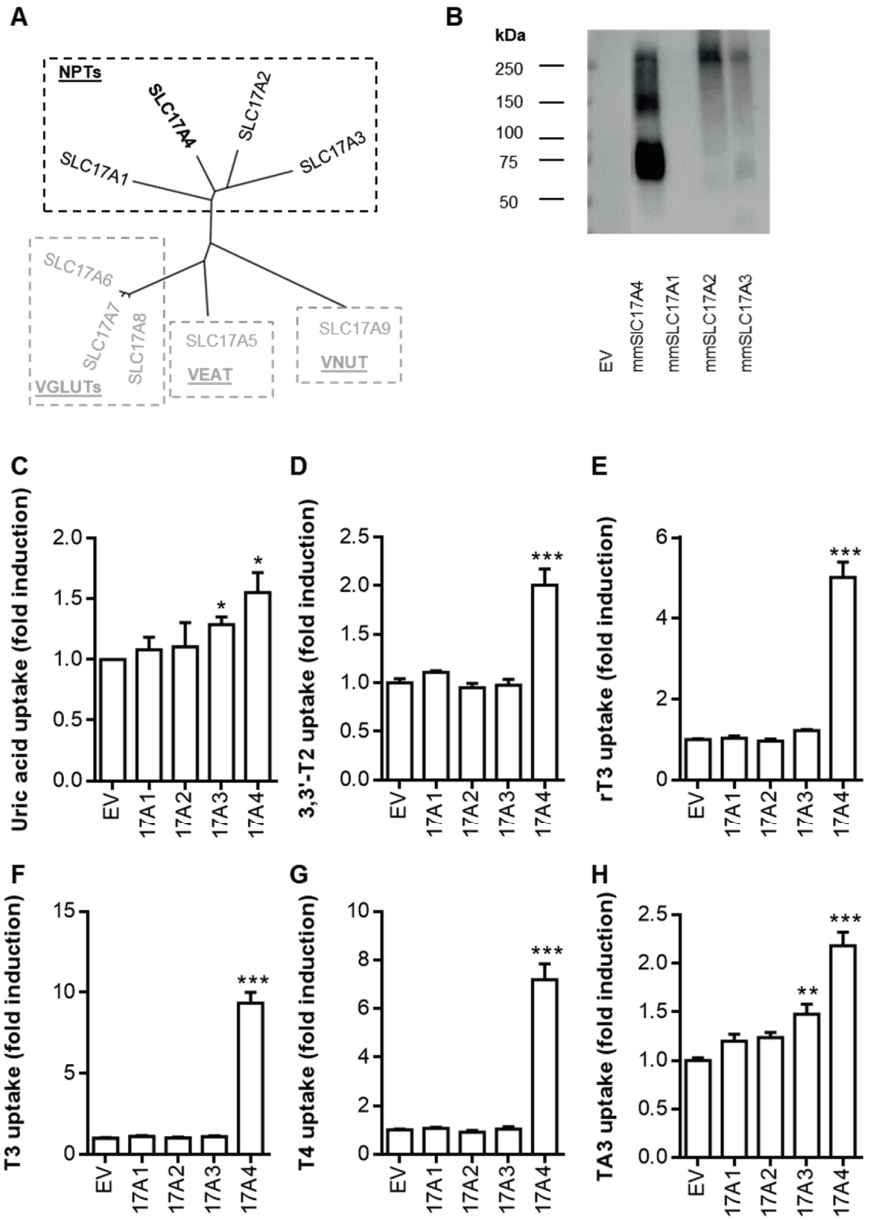

Figure 7 (A) Phylogenetic tree of the SLC17 members. Boxes indicate members that have been previously shown to share similar functional characteristics. **(B)** representative immunoblot on total lysates of COS-1 cells transfected with the indicated mmSLC17 family members. Monoclonal mouse M2 anti-Flag antibody was used for immune detection. **(C)** Uptake of [^{14}C] radio-labeled uric acid in transfected COS-1 cells after 10 minutes incubation at 37 °C. **(D)** 3,3'-T2, **(E)** rT3, **(F)** T3, **(G)** T4 uptake after 30 minutes incubation in COS-1 cells co-transfected with indicated mmSLC17 family members and CRYM. **(H)** TA3 uptake after 10 minutes incubation in COS-1 cells co-transfected with indicated mmSLC17 family members and CRYM. All uptake values are presented as times-induction over empty vector control cells and expressed as means (±SEM) of at least n=3 independent experiments. One-way ANOVAs were carried out followed by Dunnett's posttests to asses for significant differences between empty vector control cells and cell transfected with the indicated mmSLC17 family members ($p<0.05$, *; $p<0.01$, **, $p<0.001$, ***).

Similar to hsSLC17A4, T3 uptake by mmSLC17A4 was reduced in presence of various iodothyronines, in particular those that contained three or four iodine moieties. In contrast to 3,3'-T2 and 3,5-T2, 3',5'-T2 which lacks iodine moieties in the inner ring did not reduce T3 uptake, suggesting that the presence of at least one inner ring iodine moiety might be essential for substrate recognition. Based on the cis-inhibition studies, the composition of the alanine side-chain is, at least for inhibitory effects, not of major importance as the thryoproprionic acid and -acetic acid derivatives as well as thyronamines exerted pronounced inhibitory effects. In line with these findings, we found that mmSLC17A4 effectively transports TA3 and doubled the amount of internalized TA3 after 10 minutes incubation in transfected COS-1 cells. Although previous studies with the human SLC17A4 orthologue already demonstrated induction of TA3 uptake (**chapter 6.2**), this was even more pronounced for its mouse orthologue. The transporter(s) responsible for the cellular uptake of iodothyroacetic acid derivatives, in particular TA3, are currently unknown and none of the mouse or human orthologues of other currently known TH transporters reportedly transport TA3 (18). Recently, the use of TA3 regained interest in the context of treatment of MCT8 deficiency, since it exerts T3-like effects at transcriptional level but does not rely on MCT8 for its cellular entry (11, 18, 19). Absence of functional MCT8 results in profound neuro-developmental abnormalities, which are restored by early post-natal treatment with TA3 in various animal models for MCT8 deficiency (19-21). In human, TA3 effectively reduced the strongly elevated circulating T3 concentrations and ameliorated signs of peripheral thyrotoxicity in patients with MCT8 deficiency (22). Gaining insight into factors that govern (tissue) availability of TA3 are thus of direct clinical importance. Although exploratory tissue expression studies indicated that SLC17A4 is not expressed in brain, it was highly abundant in the gastro-intestinal tract where it may be involved in the absorption of TA3 from the gut.

In addition to the basic transporter properties, the putative presence of species-specific tissue distribution and the presence of alternative TH transporters at sites where SLC17A4 is expressed may importantly determine if mice provide a suitable *in vivo* model to study SLC17A4 function. Further studies should therefore detail and compare the tissue expression and subcellular distribution of SLC17A4 in mice and human. The results of such studies will importantly direct the assessment of *Slc17a4* ko animals.

In the present study, we also showed that mmSLC17A1-3, which are the only other cell membrane transporters within the SLC17 family, do not facilitate the cellular transport iodothyronines effectively. It should however be taken into account that we could not confirm effective expression of mmSLC17A1 at protein or functional level. Unlike previous reports, we did not find induction of uric acid uptake in cells transfected with mmSLC17A1 (23). Therefore, the absence of iodothyronine transport by mmSLC17A1 should be interpreted with caution. In agreement with previous studies in over-expressing oocytes (16), SLC17A3 induced the uptake of uric acid in mammalian COS-1 cells. Nonetheless, in contrast to mmSLC17A4, it did not accept any of the tested iodothyronines as a substrate. Like mouse and human SLC17A4, mmSLC17A3 slightly induced the cellular uptake of TA3. Studies in preteoliposomes suggested that the orphan transporter SLC17A2 also transports organic anions, including uric acid (15). Despite the presence of immune-reactive bands at the same molecular weight as previously reported (15), our studies did not confirm that SLC17A2 facilitates the uptake of uric acid in a cell-based model. Alternative substrates for SLC17A2 are currently unknown (7) and therefore it was not possible to further prove functional expression of SLC17A2 in our cellular model.

Taken together, we demonstrated that the mouse SLC17A4 orthologue is an efficient T3 and T4 transporter and likely, at least in mice, the only member of the SLC17 that effectively transports TH across the cell membrane. Our studies pave the way to further detail SLC17A4 function *in vivo*.

Acknowledgements

We thank Ramona E.A. van Heerebeek and Selmar Leeuwenburgh for the technical assistance.

Financial support: This work was supported by a grant from the Netherlands Organisation for Health Research and Development (project number 113303005) (to WEV), from the Sherman Foundation (to WEV).

Disclosure Summary: The authors have nothing to declare.

SUPPLEMENTAL MATERIAL

Supplemental Figures

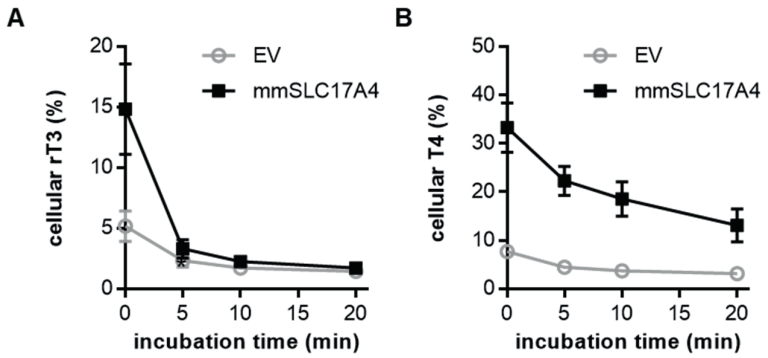

Supplemental Figure S1 Cellular efflux of rT3 **(A)** and T4 **(B)** by empty vector or mmSLC17A4 transfected COS-1 cells in 2-20 minutes. Cells were incubated for 120 min with 1 nM (50 000 cpm) of the indicated substrates (pre-loading), before efflux was measured. The amount of radio-activity that remained within the cell after 2-20 minutes incubation in efflux medium is displayed as a percentage of the amount of radio-activity that was added to the cells at the start of the pre-loading phase. Please note the steeper decline in intracellular rT3 and T4 content in mmSLC17A4-transfected cells during the first 5 minutes of incubation in efflux medium.

REFERENCES

1. Hennemann G, Docter R, Friesema EC, de Jong M, Krenning EP, Visser TJ. Plasma membrane transport of thyroid hormones and its role in thyroid hormone metabolism and bioavailability. Endocr Rev. 2001;22(4):451-76.
2. Bernal J, Guadano-Ferraz A, Morte B. Thyroid hormone transporters--functions and clinical implications. Nat Rev Endocrinol. 2015;11(7):406-17.
3. Visser WE, Friesema EC, Visser TJ. Minireview: thyroid hormone transporters: the knowns and the unknowns. Mol Endocrinol. 2011;25(1):1-14.
4. Friesema EC, Ganguly S, Abdalla A, Manning Fox JE, Halestrap AP, Visser TJ. Identification of monocarboxylate transporter 8 as a specific thyroid hormone transporter. J Biol Chem. 2003;278(41):40128-35.
5. Friesema EC, Kuiper GG, Jansen J, Visser TJ, Kester MH. Thyroid hormone transport by the human monocarboxylate transporter 8 and its rate-limiting role in intracellular metabolism. Mol Endocrinol. 2006;20(11):2761-72.
6. Teumer A, Chaker L, Groeneweg S, Li Y, Di Munno C, Barbieri C, et al. Genome-wide analyses identify a role for SLC17A4 and AADAT in thyroid hormone regulation. Nat Commun. 2018;9(1):4455.
7. Reimer RJ. SLC17: a functionally diverse family of organic anion transporters. Molecular aspects of medicine. 2013;34(2-3):350-9.
8. Sreedharan S, Shaik JH, Olszewski PK, Levine AS, Schioth HB, Fredriksson R. Glutamate, aspartate and nucleotide transporters in the SLC17 family form four main phylogenetic clusters: evolution and tissue expression. BMC Genomics. 2010;11:17.
9. Togawa N, Miyaji T, Izawa S, Omote H, Moriyama Y. A Na+-phosphate cotransporter homologue (SLC17A4 protein) is an intestinal organic anion exporter. American journal of physiology Cell physiology. 2012;302(11):C1652-60.
10. Friesema EC, Jansen J, Jachtenberg JW, Visser WE, Kester MH, Visser TJ. Effective cellular uptake and efflux of thyroid hormone by human monocarboxylate transporter 10. Mol Endocrinol. 2008;22(6):1357-69.
11. Groeneweg S, Friesema EC, Kersseboom S, Klootwijk W, Visser WE, Peeters RP, et al. The role of Arg445 and Asp498 in the human thyroid hormone transporter MCT8. Endocrinology. 2014;155(2):618-26.
12. Groeneweg S, Kersseboom S, van den Berge A, Dolcetta-Capuzzo A, van Geest FS, van Heerebeek REA, et al. In vitro characterization of human, mouse and zebrafish MCT8 orthologues. Thyroid. 2019.
13. Groeneweg S, Lima de Souza EC, Meima ME, Peeters RP, Visser WE, Visser TJ. Outward-Open Model of Thyroid Hormone Transporter Monocarboxylate Transporter 8 Provides Novel Structural and Functional Insights. Endocrinology. 2017;158(10):3292-306.
14. Ishibashi K, Matsuzaki T, Takata K, Imai M. Identification of a new member of type I Na/phosphate co-transporter in the rat kidney. Nephron Physiol. 2003;94(1):p10-8.
15. Togawa N, Juge N, Miyaji T, Hiasa M, Omote H, Moriyama Y. Wide expression of type I Na+-phosphate cotransporter 3 (NPT3/SLC17A2), a membrane potential-driven organic anion transporter. American journal of physiology Cell physiology. 2015;309(2):C71-80.
16. Jutabha P, Anzai N, Kimura T, Taniguchi A, Urano W, Yamanaka H, et al. Functional analysis of human sodium-phosphate transporter 4 (NPT4/SLC17A3) polymorphisms. J Pharmacol Sci. 2011;115(2):249-53.
17. Jutabha P, Anzai N, Kitamura K, Taniguchi A, Kaneko S, Yan K, et al. Human sodium phosphate transporter 4 (hNPT4/SLC17A3) as a common renal secretory pathway for drugs and urate. J Biol Chem. 2010;285(45):35123-32.
18. Groeneweg S, Peeters RP, Visser TJ, Visser WE. Triiodothyroacetic acid in health and disease. J Endocrinol. 2017;234(2):R99-R121.
19. Kersseboom S, Horn S, Visser WE, Chen J, Friesema EC, Vaurs-Barriere C, et al. In vitro and mouse studies supporting therapeutic utility of triiodothyroacetic acid in MCT8 deficiency. Mol Endocrinol. 2014;28(12):1961-70.
20. Zada D, Tovin A, Lerer-Goldshtein T, Appelbaum L. Pharmacological treatment and BBB-targeted genetic therapy for MCT8-dependent hypomyelination in zebrafish. Dis Model Mech. 2016;9(11):1339-48.
21. Delbaere J, Vancamp P, Van Herck SL, Bourgeois NM, Green MJ, Wingate RJ, et al. MCT8 deficiency in Purkinje cells disrupts embryonic chicken cerebellar development. J Endocrinol. 2017;232(2):259-72.
22. Groeneweg S, Peeters RP, Moran C, Stoupa A, Auriol F, Tonduti D, et al. Effectiveness and safety of the tri-iodothyronine analogue Triac in children and adults with MCT8 deficiency: an international, single-arm, open-label, phase 2 trial. Lancet Diabetes Endocrinol. 2019;7(9):695-706.
23. Iharada M, Miyaji T, Fujimoto T, Hiasa M, Anzai N, Omote H, et al. Type 1 sodium-dependent phosphate transporter (SLC17A1 Protein) is a Cl(-)-dependent urate exporter. J Biol Chem. 2010;285(34):26107-13.

Chapter

Mutated Thyroid Hormone Transporter OATP1C1 Associates with Severe Brain Hypometabolism and Juvenile Neurodegeneration

6.4

Petter Strømme*, **Stefan Groeneweg***, Elaine Lima de Souza, Chantal Zevenbergen, Anette Torgersbråten, Asbjørn Holmgren, Ebrar Gurcan, Marcel E. Meima, Robin P. Peeters, W. Edward Visser, Linda Høneren Johansson, Almira Babovic, Henrik Zetterberg, Heike Heuer, Eirik Frengen, Doriana Misceo, Theo J. Visser

Thyroid. 2018 Nov;28(11):1406-1415.

ABSTRACT

Background: Thyroid hormones (TH) are essential for brain development and function. The TH transporters monocarboxylate transporter 8 (MCT8) and organic anion transporter1 C1 (OATP1C1) facilitate the transport of TH across the blood–brain barrier and into glia and neuronal cells in the brain. Loss of MCT8 function causes Allan–Herndon–Dudley syndrome (AHDS, OMIM 300523) characterized by severe intellectual and motor disability due to cerebral hypothyroidism. Here, the first patient with loss of OATP1C1 function is described. The patient is a 15.5-year-old girl with normal development in the first year of life, who gradually developed dementia with spasticity and intolerance to cold. Brain imaging demonstrated gray and white matter degeneration and severe glucose hypometabolism.

Methods: Exome sequencing of the patient and parents was performed to identify the disease-causing mutation, and the effect of the mutation was studied through a panel of *in vitro* experiments, including thyroxine uptake studies, immunoblotting, and immunocytochemistry. Furthermore, the clinical effects of treatment with the triiodothyronine analogue triiodothyroacetic acid (Triac) are described.

Results: Exome sequencing identified a homozygous missense mutation in OATP1C1, changing the highly conserved aspartic acid 252 to asparagine (D252N). *In vitro*, the mutated OATP1C1 displays impaired plasma membrane localization and decreased cellular thyroxine uptake. After treatment with Triac, the clinical condition improved in several domains.

Conclusions: This is the first report of human OATP1C1 deficiency compatible with brain-specific hypothyroidism and neurodegeneration.

INTRODUCTION

Thyroid hormones (TH), the pro-hormone thyroxine (T4) and its active form triiodothyronine (T3), are critical for brain development and functioning, as illustrated by the devastating consequences of congenital hypothyroidism (1). Important steps leading to TH action in the brain include transport of T4 across the blood–brain barrier, uptake of T4 by astrocytes, conversion to T3 by type 2 deiodinase (DIO2), and supply of T3 to target cells such as oligodendrocytes and neurons (2-4). By binding to nuclear T3 receptors in these cells, T3 initiates powerful genetic regulation of myelination (5) and neuronal differentiation in various brain regions (6). In the human brain, T4 transport across the blood–brain barrier is predominantly mediated by monocarboxylate transporter 8 (MCT8, encoded by *SLC16A2*; OMIM 300095), while T4 uptake by astrocytes is facilitated by organic anion transporting polypeptide 1C1 (OATP1C1 encoded by *SLCO1C1*; OMIM 613389) (7). MCT8 deficiency in humans causes intellectual disability, dystonia, spasticity, and delayed myelination due to a hypothyroid state in the brain (Allan–Herndon–Dudley syndrome; OMIM 300523), and is associated with low serum T4 and high T3 levels, resulting in a hyperthyroid state in peripheral tissues (8, 9). Until now, patients with OATP1C1 defects have not been reported. Here, such a patient showing features of brain hypothyroidism is described.

METHODS

Patient

The patient is a 15.5-year-old girl, born to healthy parents in a rural area in Norway. Her two younger sisters are healthy. Birth measurements were normal. Eye contact was achieved at an early age, and development was unremarkable in the first months. Although she walked independently at 10 months, her mother had the impression that "something was wrong." As a toddler, movements were clumsy, and vocal sounds and language seemed to develop unexpectedly slow. Between two and three years, she appeared aggressive with stereotypic behaviour and was considered to be autistic. Intellectual disability was suspected by the local health service at four years of age. Psychomotor functioning was best between five and six years, when she spoke in two- or three-word sentences, ate independently, was continent, could walk, and jumped on a trampoline. Due to suspected loss of skills, she was then referred to our hospital at nine-and-a-half years of age. Despite extensive workup, no diagnosis was made. She started to lose expressive verbal language and gradually lost cognitive and motor functioning (**Table 1** and **Figure 1A**). In addition, body weight and height development stunted and declined to the 2.5th percentile, prompting the placement of a percutaneous gastrointestinal feeding tube at 11 years of age. At 13 years, she was demented and incontinent for bowel and bladder functioning. Later, urinary retention required daily bladder catheterization. She had no expressive verbal language, and walking was impaired due to gait apraxia, cerebellar ataxia, scoliosis, and spasticity of the lower limbs. At 14 years, she lost the ability to use her hands. There was no clinical suspicion of epilepsy. Startle response episodes became easily provoked accompanied by apnea of 30 seconds duration and cyanosis. She had myoclonic-like movements in the hands. Electroencephalographic examination showed intermittent slow frequency of 6 Hz without epileptic discharges. Electromyography and nerve conduction studies did not indicate peripheral nerve pathology. Cerebral magnetic resonance imaging (MRI) examinations at 7 and 13 years showed progressive atrophy starting in the cerebral cortex, continuing into subcortical white matter and cerebellum (**Figure 1B**). Cerebral magnetic resonance spectroscopy with the voxels in the left basal

ganglia and subcortical area at 9.5 and 11 years did not show abnormal metabolic peaks. Positron emission tomography–computed tomography (PET-CT) examination using 18F-fluorodeoxyglucose (18F-FDG) demonstrated severely decreased glucose metabolism in nearly all areas of the brain at the age of 14 years (**Figure 1C**). PET-CT with 18F-flutemetamol showed no amyloid-β aggregation (Fig. 1C), consistent with normal concentrations of amyloid-*β* (712 ng/L, normal range >550 ng/L) and tau (155 ng/L, normal range <250 ng/L) in the cerebrospinal fluid. Neurofilament light protein concentration in the cerebrospinal fluid was markedly elevated (2600 ng/L at 11 years and 1400 ng/L at 14 years, reference value <380 ng/L), indicating rapid degeneration of the cytoskeleton of axonal fibers in the cerebrum, consistent with degeneration of central white matter observed on MRI. Glial fibrillary acidic protein was mildly elevated (280 ng/L at 11 years and 180 ng/L at 14 years, reference value <175 ng/L), indicating that astrocytes were also involved in the degenerative process. She suffered inexplicable intolerance to cold and had cold hands and feet and frequent shivering and preferred to dress warmly even on hot days. In accordance, body temperature was generally low (**Figure 1D**, left), and she once needed full-body warming blankets for hypothermia during general anesthesia. Hypothyroidism was considered. However, serum thyroid function tests were normal (thyrotropin 1.96 [0.5–4.9] mIU/L, free T4 15.3 [10.0–18.0] pmol/L, and free T3 6.2 [3.6–8.3] pmol/L at 11 years and also at 14 years of age). At almost 12 years of age, whole exome sequencing of the patient and her healthy parents was carried out to unravel the underlying cause of the phenotype.

Ethical considerations

The current study was formally approved by the Regional Committees for Medical Research Ethics—South-East Norway (REK 2010/1152a and REK 2016/1227). Written informed consent was obtained from the parents to treat the patient with Triac and use the medical information, videos, and pictures of the patient for scientific and educational purposes.

Brain PET-CT scan and biochemical analyses

Brain PET-CT (Siemens Biograph; Siemens Healthcare, Oslo, Norway) with 18F-FDG and 18F-flutemetamol was performed with time-of-flight system and 46-slice computed tomography and carried out following a well defined protocol in pediatric patients (10, 11). All measurements in cerebrospinal fluid and serum were carried out using standard laboratory methods. Technical details are described in the Supplementary Appendix (Supplementary Data are available online at www.liebertpub.com/thy).

Exome sequencing, data analysis, and confirmation by Sanger sequencing

Exome libraries from DNA of the patient and healthy parents were prepared using standard methods and subjected to routine quality checks and sequenced on a HiSeq2000 (Illumina, San Diego, CA) with 100 bp paired-end reads. Reads that did not pass Illumina's chastity filter were removed prior to alignment to the reference human genome (hg19). Variant calling was performed using GATK HaplotypeCaller and analysed using FILTUS program (12). All variants with allelic frequency >0.01 or with a predicted benign impact on protein function (Combined Annotation Dependent Depletion [CADD] score <15) (13) were excluded, and the focus was on missense, nonsense, frameshift, and small insertion/deletion variants. Sanger sequencing on DNA from the patient, parents, and two healthy younger sisters was used to confirm the presence of a homozygous missense mutation in *SLCO1C1* in the patient. Full technical details are provided in the Supplementary Appendix.

Expression constructs, cell culture, and transfection

The cloning of human OATP1C1 cDNA into pcDNA3.1 and human CRYM cDNA into pSG5 has been previously described (14, 15). OATP1C1 cDNA was subcloned into pSG5 with addition of a C-terminal V5 tag (further referred to as wild-type OATP1C1-V5), which did not affect T4 transport function (data available upon request). The D252N and D252A variants were introduced into wild-type OATP1C1-V5 using QuikChange site-directed mutagenesis according to manufacturer`s protocol (Stratagene, Amsterdam, The Netherlands). All primers are available upon request. Correctness of the constructs was confirmed by complete sequencing of the inserts. JEG-3 human choriocarcinoma (CVCL_0363) and COS-1 African green monkey kidney cells (CVCL_0223) were obtained from ECACC (Sigma–Aldrich, Zwijndrecht, The Netherlands) and cultured and transfected under standard conditions (16, 17). Technical details are provided in the **Supplementary Appendix**.

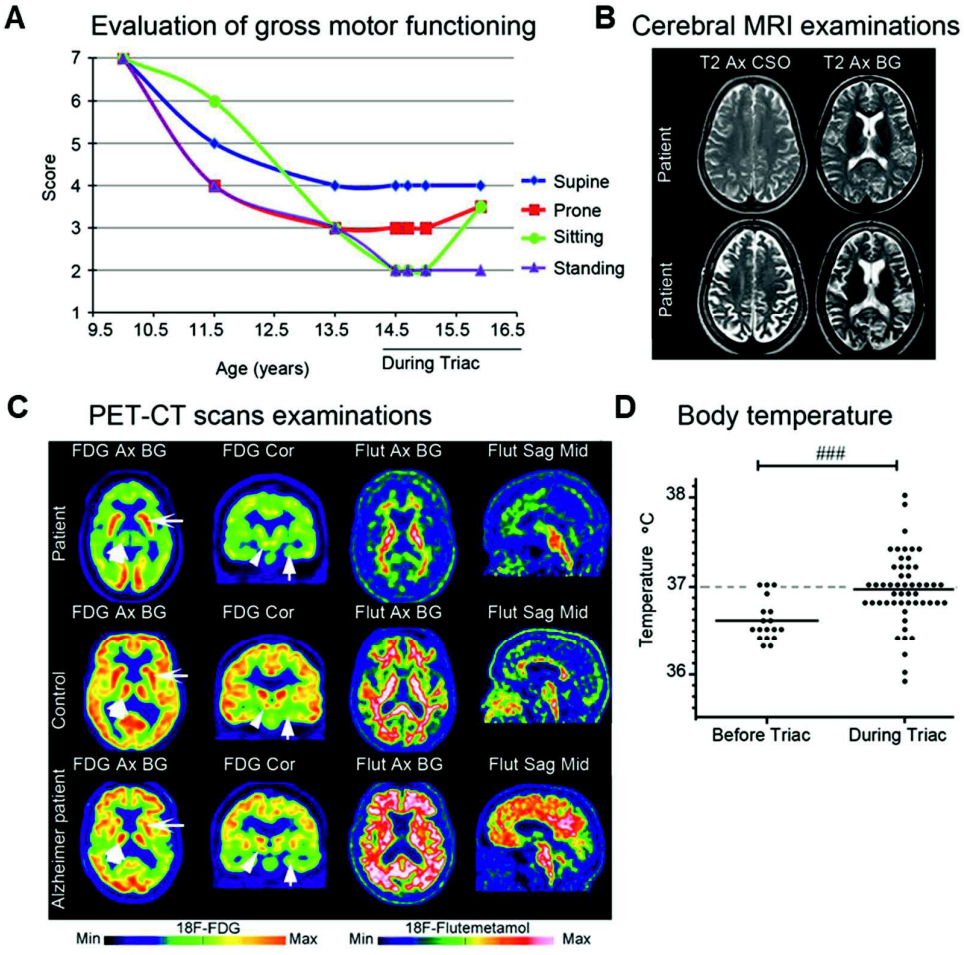

Figure 1 Clinical and neuroimaging data. (**A**) Postural ability, a part of gross motor functioning, evaluated with PPAS at different ages (38). A score of 7 indicates performance at the highest level of postural ability and 1 at the lowest. Levels 1 and 2 indicate no ability to maintain a postural position, and levels 3–7 indicate varying degrees of postural control, to either maintain or change position without assistance. The scores decreased markedly in all four postural positions (supine, prone, sitting, and standing) between the ages of 10 and 13.5 years. During treatment with Triac, which started at 14.5 years, the scores either remained at the same level (supine and standing positions) or increased (prone and sitting positions). The most noticeable improvement was in the sitting position, which went from level 2 (placed in an aligned sitting posture but needs support) to between 3 and 4 (able to maintain sitting position when placed, and able to move the trunk forwards/backwards). Scores were obtained in retrospect from relevant data in the patient's chart by the local physiotherapist or pediatrician in the hospital. (**B**) Series of T2- and T1-weighted cerebral magnetic resonance imaging (MRI) examinations at the age of 7 years (top panel) and 13 years (bottom panel). Axial views through the centrum semiovale (T2 Ax CSO) show increased widening of the subarachnoid spaces, indicating progressive cortical atrophy. Axial views at the level of the basal ganglia (T2 Ax BG) show progression from mild to marked cortical atrophy, accompanied by widening of the lateral ventricles due to loss of central white matter. (**C**) PET-CT scan images of the brain of the patient at 14 years compared to a healthy control and to a patient with Alzheimer's disease using 18F-fludeoxyglucose (FDG; left) or 18F-flutemetamol (Flut) as tracer. In the patient, the axial basal ganglia (Ax BG) view showed severely decreased 18F-FDG uptake, in the frontal, temporal, and parietal lobes and in the thalami (thick arrow), and normal uptake in the occipital cortex and the basal ganglia (thin arrow). The coronal (Cor) view also demonstrate decreased 18F-FDG uptake in the hypothalamus (arrow head) and hippocampus. As expected, the Alzheimer's patient showed reduced 18F-FDG uptake compared to the control. However, glucose metabolism in the patient, as indicated by these examinations, was also markedly diminished compared to the Alzheimer's patient. In the patient, Flut uptake was almost undetectable in the gray matter, implying absence of amyloid-β deposition in this part of the cortex. The overall Flut uptake seen on axial basal ganglia (Ax BG) and sagittal midline (Sag Mid) views in the patient was less than in the control, corresponding with loss of white matter shown on MRI. To illustrate the contrast, extensive Flut uptake was documented in the cerebral cortex in the patient with Alzheimer's disease, reflecting typical aggregation of amyloid-β in this disease. The examinations were performed as positron emission tomography–computed tomography (PET-CT), but only PET images are shown. The uptake intensity scale for each tracer is shown at the bottom of the panel. (**D**) Home rectal temperature measurements of the patient before and during treatment with Triac (1050 mg/day). Before treatment, the mean temperature was 36.65°C (number of measurements = 18); during treatment, the mean temperature increased to 36.95°C (number of measurements = 52; ###$p < 0.001$). PPAS, Posture and Postural Ability Scale.

Functional studies

T4 uptake, cell surface biotinylation, immunoblotting, and immunocytochemistry studies were essentially performed as recently described (16, 17). Full technical details are available in the **Supplementary Appendix**.

OATP1C1 homology modeling

An OATP1C1 homology model was constructed similarly as has recently been done for MCT8 using YASARA Structure Software (www.yasara.org) (17-19). The *Escherichia coli* multidrug transporter MdfA (PDB#4ZP0) in inward-open conformation was selected as the most suitable template. The KAZAL-like sequence motif present in extracellular loop (ECL) 5, spanning R470 to C523, was modeled separately based on the KAZAL-type inhibitor infestin 4 (PDB#2ERW) and integrated into the OATP1C1 model. Full details are available in the **Supplementary Appendix** and the final alignment between target and template in **Supplementary Figure S1**.

Table 1. Patient characteristics.

Proband	I	II	III	IV	V	VI	VII
Age (years)	7	7	9.9	5	4	15.2	7.5
Mutation	p.A565Afs*1	p.A565Afs*1	p.H575R	p.N599S	p.L602Hfs*78	p.P609Qfs*68	p.P609Qfs*68
Birth weight in percentile (grams)	NA	NA	2780 (<P5)	3895 (p98)		3080	2820
Endocrine features							
Serum total T3 (nmol/L)	6.4 (2.0-3.3)	4.38 (2.0-3.3)	2.44 (2.0-3.3) *	2.26 (2.0-3.3)	3.47 (1.61-3.20) #	3.05 (1.6-3.0)	3.73 (2.0-3.3)
Serum TT4 (nmol/L)	54 (74-151)	41 (74-151)	81 (74-151)*	82 (74-151)	42.5 (57.9-154.5) #	79 (62-136)	57 (74-151)
Serum FT4 (pmol/L)	6.6 (13-26)	6.4 (13-26)	15.6 (13-26)*	17.6 (13-26)	11.6 (11.6-18) #	12.3 (12-24)	9.7 (13-26)
Serum rT3 (nmol/L)	0.11 (0.2-0.5)	0.10 (0.2-0.5)	0.37 (0.2-0.5)*	0.24 (0.2-0.5)	0.08 (0.12-0.38) #	0.19 (0.2-0.5)	0.11 (0.2-0.5)
Serum TSH (mU/L)	4.42 (0.6-5.6)	5.19 (0.6-5.6)	0.94 (0.6-5.6)*	2.47 (0.6-5.6)	3.02 (0.5-4.3) #	1.22 (0.6-5.2)	3.90 (0.6-5.6)
Serum SHBG (nmol/L)	275 (40-140)	282 (40-140)	149.9 (40-140)*	ND	163 (40-140) #	ND	214.6 (40-140)
Serum total cholesterol (mmol/L)	2.1 (2.8-5.4)	2.7 (2.8-5.4)	ND	4.0 (2.8-5.4)	ND	ND	ND
Tachycardia in rest	-	-	-	-	+		
Body weight in kg (SD)	21.2 (-1.47)	22.0 (-1.15)	19.5 (-3.2)	17.8 (0)	14.5	25 (-1.5)	26.5 (-8.5)
Head circumference in cm (SD)	52.5	51	47.5 (-4.2)	50 (0.75)	51	54.5 (1.0)	52 (-2.8)
Body height in cm (SD)	115 (-2.55)	115 (-2.56)	123.4 (-1.9)	107.5 (0.4)	109	133.5 (-0.8)	137 (-4.0)
BMI	16.03 (0.50)	16.64 (0.91)	12.8 (-2.7)		12.28		
Increased perspiration	+	-	-	-	-	+	-
Diarrhea	-	-	-	-	-	-	-
Neurological features							
Dystonia	++	++	-	-	+	+	+
Spasticity	+	+	-	-	+/-	+	+
Hypotonia	++	++	+	-	+	+	+
Speech development	Absent	Absent	No verbal speech	Sentences (delayed)	Some words	No verbal speech	No verbal speech
Head control	-	-	+	+	+	+/-	+
Sitting independently	-	-	+ (11 m)	+	+/-	-	-
Walking independently	-	-	+ (4y6m)	+ (22 m)	-	-	-
Delay in achieving motor milestones	Severe	Severe	Moderate	Mild	Severe	Severe	Severe
GMFM-G88 score (%)[1]	7	8	ND	ND	29.7	ND	ND
IQ score (test)	ND	ND	ND	ND	ND	ND	ND
Psychiatric symptoms	ND	ND	-	-	-	Irritability	Irritability, aggressive
EEG-proven seizures	-	-	+	-	-	+	+
Feeding problems	+	+	+	-	+	+	+
Brain MRI abnormalities	Delayed myelination	Delayed myelination	-	-	-	-	Peirventricular WM hyperintensities, choroid cyst

[1] GMFM-G88 is Gross Motor Function Measure-G88 which assesses the gross motor function. Scores range from 0 to 100%, with higher scores indicating better motor function and where a 100% score is achieved by a normal developing child of 4 years of age. Thyroid function tests are measured at the age of 7 years and 6 months (*) or 3 years (#). WM, white matter; ND, not determined.

Statistical analysis for functional studies

All statistical analyses were performed as indicated in the figure legends using GraphPad Prism v5 (GraphPad Software, Inc., San Diego, CA). Statistically significant differences are indicated as described in the legends of the corresponding figures.

RESULTS

A homozygous variant identified in the TH transporter SLCO1C1 (OATP1C1)

Exome sequencing of the family trio identified in the patient a homozygous variant in *SLCO1C1* Chr12(GRCh37):g.20870143G>A; NM_001145946.1:c.754G>A; p.(D252N); **Supplementary Figure S2A** and **B**), changing a highly conserved aspartic acid at position 252 to asparagine (D252N) in the OATP1C1 protein (**Supplementary Figure S2C**) and predicted to be damaging to the protein function (CADD 34). The parents and one sister were heterozygous for the variant (**Supplementary Figure S2A** and **B**). In the patient, the variant was part of a region of autozygosity of estimated minimum size of 4.38 Mb, and the total fraction of autozygosity in the patient was compatible with the parents being second cousins (data not shown). The variant was not reported in the public database of sequence variants Genome Aggregation database (gnomad.broadinstitute.org).

Functional studies confirm loss of T4 transport function in mutated OATP1C1

In order to study if the identified mutation impairs OATP1C1 function, complementary *in vitro* studies were performed. To allow immunochemical detection, expression constructs were made of wild-type OATP1C1 and the D252N mutant equipped with a C-terminal V5 epitope. Since asparagine residues may undergo hydrolysis to aspartic acid (20), the native residue in OATP1C1, the D252A mutation was also introduced. The effect of both mutations on T4 transport by OATP1C1 was evaluated in transiently transfected JEG-3 cells. Compared to wild-type OATP1C1, T4 uptake was diminished by 70% by the patient mutation (D252N) and nearly completely inhibited by the artificial alanine (D252A) mutation (**Figure 2A**). The impact of both mutations on OATP1C1 protein expression levels was evaluated by immunoblotting on total lysates of JEG-3 cells transfected with wild-type or mutant OATP1C1. For wild-type OATP1C1-V5, bands were detected at ~75 kDa, representing the mature, glycosylated protein (21), and at ~50 kDa, most likely representing its immature form (**Figure 2B**), as has been described for OATP2B1 (22). The D252N mutation predominantly reduced the abundance of the mature protein, whereas the D252A mutation resulted in a marked reduction of both proteins (**Figure 2B**). Cell surface protein expression determined by surface biotinylation analyses showed that both OATP1C1 mutants were markedly reduced in the cell membrane fraction compared to mature wild-type OATP1C1 (**Figure 2C**). This corresponded with the predominant peri-nuclear localization of both mutants, as revealed by immunocytochemistry (**Figure 2D**). Similar results were obtained in COS-1 cells (data not shown). These findings suggest that both mutations affect OATP1C1 protein maturation, stability, and intracellular trafficking. To substantiate this hypothesis, an OATP1C1 structure homology model was generated based on the crystal structure of the *E. coli* multidrug transporter MdfA (PDB#4ZP0; **Figure 2E**). Molecular dynamic simulations suggested that D252 forms hydrogen bonds with K248, both predicted to be located at the extracellular end of transmembrane domain 5, and S389 at the extra-cellular end of transmembrane domain 8 (**Figure 2F**). Such an inter-helical interaction is likely important for proper protein folding and stability.

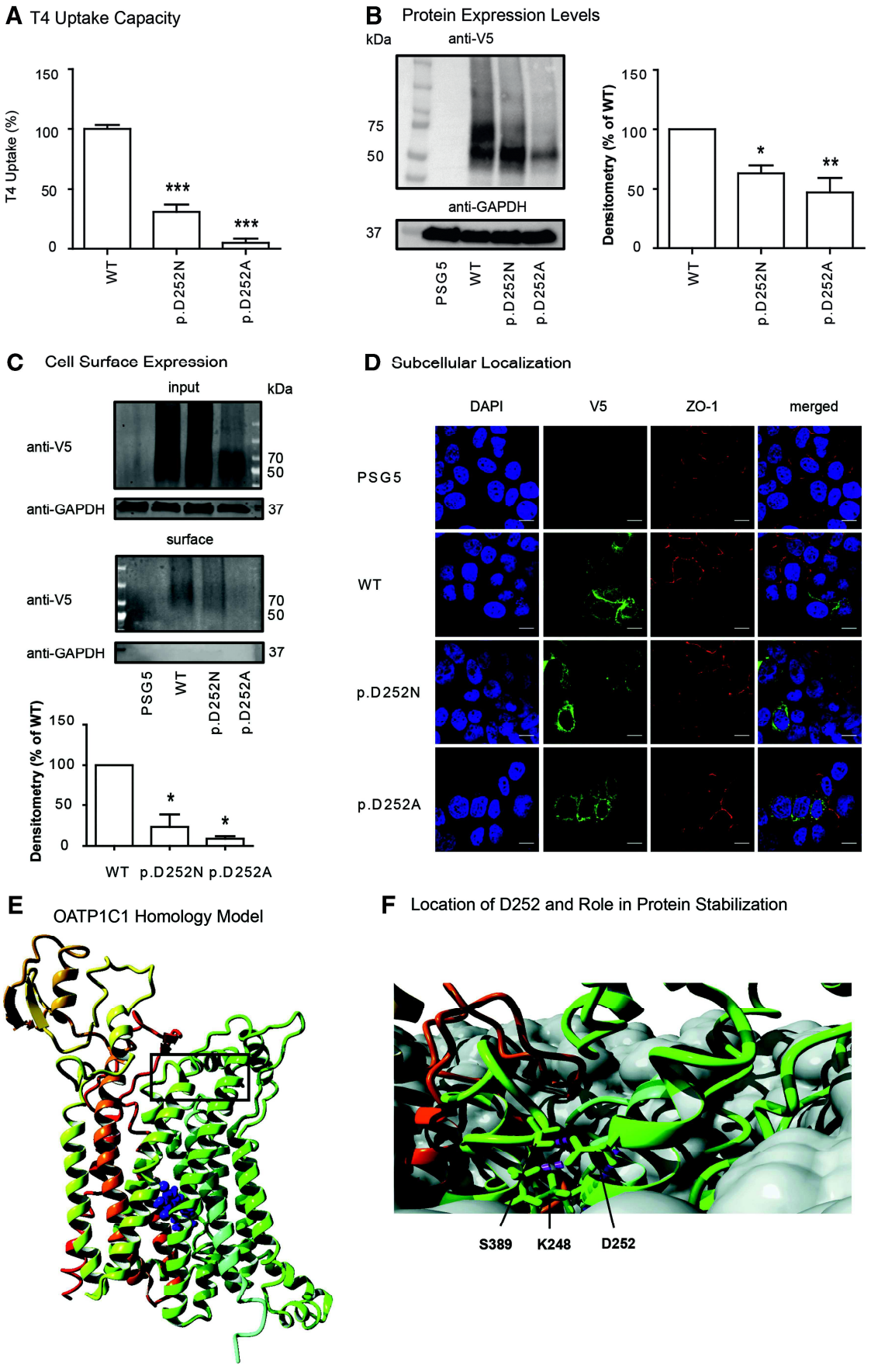
A T4 Uptake Capacity
T4 Uptake (%)
150
100
50
0
***
***
WT
p.D252N
p.D252A
B Protein Expression Levels
kDa
anti-V5
75
50
anti-GAPDH
37
PSG5
WT
p.D252N
p.D252A
Densitometry (% of WT)
150
100
50
0
*
**
WT
p.D252N
p.D252A
C Cell Surface Expression
input
kDa
anti-V5
70
50
anti-GAPDH
37
surface
anti-V5
70
50
anti-GAPDH
37
PSG5
WT
p.D252N
p.D252A
Densitometry (% of WT)
150
100
50
0
*
*
WT
p.D252N
p.D252A
D Subcellular Localization
DAPI
V5
ZO-1
merged
PSG5
WT
p.D252N
p.D252A
E OATP1C1 Homology Model
F Location of D252 and Role in Protein Stabilization
S389
K248
D252

Figure 2 Functional *in vitro* analyses of the patient's mutation (D252N). (**A**) Organic anion transporter1 C1 (OATP1C1)-mediated thyroxine (T4) transport in transiently transfected JEG-3 cells. The D252N mutation identified in the patient and the D252A artificial mutation both display markedly reduced T4 transport by OATP1C1. Some residual activity of the D252N mutant may be due to partial hydrolysis of asparagine 252 to the native aspartic residue (20). The results are presented as means ± standard error of the mean (SEM) of three experiments, each performed in triplicate. T4 transport levels are corrected for background T4 uptake in empty vector transfected cells and expressed relative to wild-type. Statistical significance of the differences was determined by one-way analysis of variance (ANOVA) with Bonferroni post test (***$p < 0.001$ vs. wild type). (**B**) Representative immunoblot of total lysates of JEG-3 cells transfected with wild-type or mutant OATP1C1-V5 construct. The band at 75 kDa represents mature, glycosylated OATP1C1, and the band at 50 kDa supposedly represents an immature, non-glycosylated form. The quantity of the 75 kDa band is significantly reduced by the D252N and D252A mutations. Quantification of the 75 kDa band was performed using imaging software and levels are shown relative to wild type (100%) after normalization for GAPDH (presented as means ± SEM of three experiments). One-way ANOVA with Dunnett's post test was used to test for statistically significant differences between wild-type and mutant protein expression levels (*$p < 0.05$; **$p < 0.01$). (**C**) Representative surface biotinylation assay in transfected JEG-3 cells, indicating the reduced abundance of the D252N and D252A mutants at the plasma membrane. Cell surface OATP1C1 protein expression levels are expressed as OATP1C1 (surface)/GADPH (total lysate) ratio relative to wild-type OATP1C1 (100%) and presented as the mean ± SEM of two independent experiments. One-way ANOVA with Dunnett's post test was used to test for statistically significant differences between wild-type and mutant surface expression levels (*$p < 0.05$). (**D**) Subcellular distribution of wild-type and mutant OATP1C1-V5 protein (in green) in transfected JEG-3 cells. Plasma membrane localization is indicated by co-localization with tight junction protein ZO-1 (in red). Nuclear DNA is stained with DAPI (in blue). Wild-type OATP1C1 co-localized with ZO-1 at the plasma membrane, while both mutants show a predominant perinuclear staining, suggesting abnormal protein trafficking. (**E**) OATP1C1 homology model in inward-open conformation, based on the crystal structures of the *Escherichia coli* multidrug transporter MdfA (PDB# 4ZP0) and KAZAL-type inhibitor infestin 4 (PDB#2ERW). A T4 molecule (blue) is docked in the substrate channel. The black box indicates the region magnified in (**F**). (**F**) Molecular dynamic simulations (Methods in the Supplementary Appendix) indicating hydrogen bond formation (purple dots) of D252 with K248 and S389, which may be important for proper protein folding and exposure of glycosylation sites. The lipid bilayer is depicted in gray.

Condition of the patient stabilized with Triac treatment

Treatment with Triac was started at 14.5 years of age, with co-administration of low-dose levothyroxine to maintain serum T4 and T3 concentrations in the low-normal range. After six weeks, she resumed eye contact and became more alert (**Table 1**). Her general condition and quality of life improved. Importantly, the startle response episodes were markedly reduced in number and severity. Painful muscle spasms almost disappeared, she could swallow her own tablets and much of her own food, and urinary retention causing the need for bladder catheterization became rare. After the treatment with Triac was started, there was no further decrease in postural ability; in fact, in two postural positions the level of ability increased (**Figure 1A**). However, scoliosis continued to progress. Rectal temperature increased to normal values (**Figure 1D**, right). A slight increase in heart rate during Triac treatment was considered tolerable (median heart rate during treatment = 87 beats per minute taken at home by a nurse.

DISCUSSION

This study reports for the first time a human disease associated with mutation of the brain specific T4 transporter protein OATP1C1. It manifested in childhood, at first with developmental impairments and later evolving as a neurodegenerative disease with a distinct intolerance to cold and severely reduced brain glucose metabolism. The progressive course appeared to be halted by treatment with the T3 analogue Triac. *In vitro* evaluation of the D252N mutation identified in the patient demonstrated a marked decrease in OATP1C1-mediated T4 transport caused by intracellular retention of the transporter. Further, *in silico* modeling suggested that the highly conserved D252 residue stabilizes the transporter by hydrogen bond formation with K248 and S389. Moreover, the D252 residue is located close to the most evolutionary conserved domain in OATPs ("signature sequence" 267–279) (23), where single amino acid changes have been found to cause cytoplasmic protein retention (24). Thus, both *in vitro* and *in silico* analyses support a damaging effect of the mutation identified in the patient.

In the brain, impaired OATP1C1 function likely reduces T4 uptake in astrocytes and its subsequent conversion to T3. Thus, the reduced availability of T3 to target cells within the central nervous system appears to be the critical consequence of the OATP1C1 mutation in this disorder (**Figure 3**) to which the observed developmental delay, abnormal energy metabolism, and subsequent neurodegeneration can be attributed. The causality between defective OATP1C1 and the observed phenotype is strengthened by the following aspects. First, the compromised brain glucose metabolism is compatible with a hypothyroid state of the brain (25). Importantly, a high glycolytic rate is typically observed in astrocytes, the main site of OATP1C1 expression. Second, cerebellar ataxia, present in the patient, is a known consequence of hypothyroidism in the brain (e.g., Cremer *et al*.) (26). The presence of transient autism may also be attributed to the hypothyroid state, since T3 also exerts a regulatory effect on cortical interneurons (27), found reduced in numbers in children with autism (28). Third, the single nucleotide polymorphism rs73069071, located downstream of *SLC01C1* and affecting its expression, has been associated with increased risk for hippocampal sclerosis in elderly patients (29), which supports the link between defective OATP1C1 and neurodegeneration. Fourth, the most notable cerebrospinal fluid abnormality was a vast increase in neurofilament light protein concentration, indicating cytoskeletal decay of myelinated axonal fibers compatible with subcortical white matter atrophy and shrinkage of the corpus callosum. Key factors in the formation and maintenance of myelin in the brain include Krüppel-like factor 9 and myelin basic protein, which are T3-dependent genes (6, 30). Finally, progression of the clinical course in the patient appeared to be halted or even improved by treatment with the T3 analogue Triac.

Despite the severe phenotypes associated with human MCT8 and OATP1C1 deficiency, neither Oatp1c1- (31) nor Mct8- (32) deficient mice exhibit a neurological phenotype due to functional overlap of the two transporters in the mouse brain. However, deletion of both *Mct8* and *Oatp1c1* leads to brain hypothyroidism and neurological deficits (33). In these animals, the therapeutic effect of the T3-analogue Triac, which enters the cell independent of Mct8 and Oatp1c1, was evident by restoring impaired neural differentiation caused by T3 deprivation (34). In the current patient, there was a rapid reduction in the number of exaggerated startle response episodes, which are pathological and involve glycine inhibitory circuits in the brain stem and are potentially lethal (35).

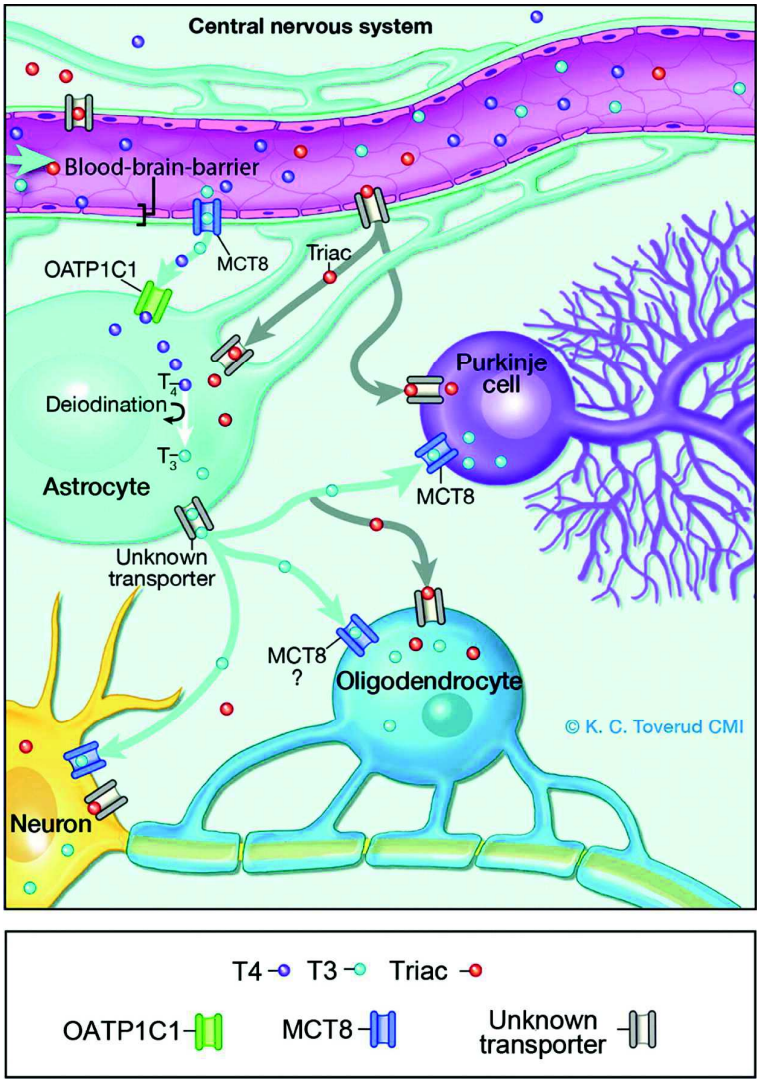

Figure 3 Thyroid hormone physiology in the brain. The thyroid gland produces the prohormone T4 and to a lesser extent its active hormone triiodothyronine (T3). In the body, the majority of T3 is produced locally by deiodination of T4. The main access of thyroid hormone to the brain is across the blood–brain barrier, where MCT8 transports both T4 and T3. T4 uptake in astrocytes is mediated mainly by OATP1C1. T4 in astrocytes is converted by the DIO2 deiodinase to T3, which is released into the brain parenchyma by an unknown transporter. By this mechanism, astrocytes supply neurons and oligodendrocytes with sufficient amounts of T3 for proper neural differentiation and functioning. A defective OATP1C1 results in impaired uptake of T4 in astrocytes and therefore insufficient availability of T3 in neural cells. Triac, a T3 analogue with T3-like biological effect, normally excreted at very low concentration, passes the blood–brain barrier and enters brain cells through an unknown transporter.

Body temperature normalization with Triac may have been mediated by hypothalamic regulatory mechanisms (36), although a direct thermogenic effect of Triac on brown adipose tissue is not excluded (37). At present, it cannot be excluded that deficiency of additional substrates for OATP1C1 contribute to the neurological phenotype, but the positive effects of Triac on key features suggest that brain hypothyroidism is an important hallmark of this disease. Moreover, a direct impact of OATP1C1 deficiency on the TH status in tissues other than brain cannot be excluded, although its expression levels are generally low in the peripheral tissues. The normal serum TH concentrations observed in the

patient suggest that inactivation of OATP1C1 does not have a major impact on the hypothalamic–pituitary–thyroid axis, which is in line with the normal serum TH concentration in the *Oatp1c1* knockout mouse model (31). Future studies and identification of new patients will help to advance the mechanisms of disease underlying OATP1C1 deficiency.

The field of TH transport has impressively expanded in the last 15 years. After decades of belief that cellular entry of TH occurs via passive diffusion, the identification of MCT8 as a specific transporter for TH and the subsequent identification of mutations therein in patients revealed the physiological relevance of TH transporters. In recent years, it has become clear that OATP1C1 is a specific T4 transporter, which is importantly expressed in human astrocytes. It is hoped that this study, describing a novel neurodegenerative disease associated with a mutation in the T4 transporter OATP1C1, will fuel further research in the field of TH transporters.

Acknowledgements

We are grateful to the family for taking part in this study. The sequencing service was provided by the Norwegian Sequencing Centre, a national technology platform supported by the "Functional Genomics" and "Infrastructure" programs of the Research Council of Norway and the Southeastern Regional Health Authorities. **Figure 3** was made by Kari C. Toverud, MS, Certified Medical Illustrator.

This work was funded by the Division of Pediatric and Adolescent Medicine, Oslo University Hospital, Oslo, Norway, and Netherlands Organisation for Health Research and Development (project number 113303005, 2014, to W.E.V.).

Disclosure Summary: The Erasmus Medical Center receives royalties from Medical Need. For all authors, no competing financial interests exist.

SUPPLEMENTAL APPENDIX

Supplemental methods

Measurements in the cerebrospinal fluid and serum

Total tau and the 42 amino acid form of amyloid-β (Aβ1–42) were measured using INNOTEST ELISAs (Fujirebio, Ghent, Belgium). Neurofilament light (NFL) protein was analysed using the NF-light ELISA kit (UmanDiagnostics AB, Umeå, Sweden). Glial fibrillary acidic protein (GFAP) was measured using an in house ELISA based on polyclonal antibodies as previously described in detail (39). Serum concentrations of TSH, free T4, and free T3 were measured according to standard laboratory procedures at our hospital.

Brain positron emission tomography–computed tomography (PET-CT) with 18F-FDG and 18F-flutemetamol

The examination was performed using a PET-CT scanner (Siemens Biograph, Siemens Healthcare, Oslo, Norway) with time of flight system and 46-slice computed tomography. PET-CT was essentially carried out following a well-defined protocol in paediatric patients (10, 11). Briefly, the patient fasted over 6 hours before the examination (water was allowed). Blood glucose concentration was normal (4.9

mmol/L). The patient lay in a quiet room with eyes covered for 10 minutes before intravenous injection of 108 MBq 18F-FDG via a cannula. She was lightly sedated for the whole procedure with 12.5 mg midazolam (a benzodiazepine). The PET-CT scan was done 30 minutes after 18F-FDG injection, performing low dose CT first, then PET. During scanning, the head was placed in a head holder to prevent movement artefacts and to make the examination more comfortable. PET imaging from vertex to brain stem in one bed position lasted 6 minutes.

On a separate occasion, 135 MBq Vizamyl (18F-flutemetamol, GE Healthcare, Oslo Norway) was injected 94 minutes before scanning from vertex to the lower edge of the cerebellum, using one bed position for 20 minutes. Low dose CT over the same area was done as a first step. No sedation was necessary. An experienced nuclear medicine physician assessed the 18F-FDG examination by viewing uptake intensity using PET rainbow colour scale. We used cerebellum as a reference region. The 18F-flutemetamol examination was also assessed visually and interpreted as amyloid- negative (no pathology), according to the EANM Practice Guideline for Amyloid PET Imaging of the Brain 1.0 (40).

Exome sequencing, data analysis, and Sanger sequencing

DNA from the patient and parents was sheared using a Covaris sonicator (Covaris, Woburn, MA) to produce fragments with an average size of 200 bp. Paired-end adapters were ligated to the fragments and exome capture was performed with the Illumina TruSeq Exome Enrichment kit (Illumina, San Diego, CA) according to the manufacturer's recommendations. The final amplified exome captured library was quantified using a Qubit Fluorometer (Life Technologies, Carlsbad, CA) and qPCR using primers annealing to the adapter sequences and Power SYBR Green PCR Master Mix (Life Technologies). Illumina PhiX control kit v2.0 DNA was used for standard curve generation. Fragment size distribution of the input library was measured using a 2100 Bioanalyzer and Agilent High Sensitivity DNA Chip (Agilent Technologies, Santa Clara, CA). The exome captured library was sequenced on an Illumina HiSeq2000 with 100 bp paired-end reads. A total of more than 50 million reads were generated. Reads that did not pass Illumina's chastity filter were removed prior to alignment. The remaining reads were aligned to the reference human genome (hg19) using Burrows-Wheeler Alignment tool (41). The alignment was refined by the Genome Analysis Toolkit (GATK) (42) and PCR duplicates were marked by Picard (picard.sourceforge.net). Variant calling was performed using GATK HaplotypeCaller. Variants were annotated by SnpEff v2.0.5 (43). The three variant calling files (VCFs) generated were simultaneously analyzed using the FILTUS program (44). We discarded variants with allelic frequency >0.01. We also discarded variants in silico predicted benign/tolerated for protein function according to the Combined Annotation Dependent Depletion (CADD) (CADD score <15) (45). We focused on missense, nonsense, frameshift, and small insertion/deletion variants. Exome data were analyzed with autosomal recessive (homozygous and compound heterozygous) and autosomal dominant mode of inheritance. Regions of homozygosity in the patient were estimated from the exome data using the autozygosity function in FILTUS. Only high quality variants were considered in the analysis (confidence of genotype assigned being accurate (GQ)>29; MQ= mapping quality of reads supporting variant call (MQ)>45; depth (number of reads) (DP) >50), and only homozygosity regions longer than 1 centi Morgan (cM) and containing more than 15 variants or regions of any size containing >100 variants were included in the output.

The presence of the missense mutation in SLCO1C1 was verified using sanger sequencing on genomic DNA derived from the patient and her healthy parents and two younger sisters using the following

primers: Fwd 5'-CTGACTGGATCACACATTTCTTG-3' and Rev 5'-TTTGATAATTTCCACACTGTTCC-3'. PCR products were purified and Sanger sequenced using an ABI 3730xl DNA analyzer and ABI BigDye dye terminator cycle-sequencing kits v3.1 (Life Technologies). Sequences were aligned using EMBL-EBI Emboss Needle pairwise alignment tool for nucleotides (ebi.ac.uk/Tools/psa/emboss_needle/nucleotide.html).

Cell culture and transfection

For T4 uptake studies, cells were seeded in 24-well dishes and transiently co-transfected with 80 ng pSG5 empty vector, 20 ng wild-type or mutant OATP1C1-V5, and 100 ng CRYM. For immunoblot analyses on total lysates, cells were seeded in 6-well dishes and transiently transfected with 200 ng wild-type or mutant OATP1C1-V5. For cell surface biotinylation assays, cells were seeded on 10 cm dishes and transiently transfected with 2000 ng wild-type or mutant OATP1C1-V5. For immunocytochemistry studies, cells were cultured on 20 mm glass coverslips coated with poly-D-lysine (Sigma-Aldrich) and transfected with 100 ng wild-type or mutant OATP1C1-V5. X-tremeGENE 9 (Roche Diagnostics, Almere, NL) was used as a transfection reagent according to manufacturer`s protocol and all transfections were carried at 70% cellular confluence. Optimal plasmid concentrations were obtained from plasmid dose titration curves (data not shown). All experiments have been performed 48 h after transfection.

T4 uptake studies

Cells were washed with Dulbecco's phosphate buffered saline with 0.9 mmol/L $MgCl_2$ and 0.5 mmol/L $CaCl_2$ (DPBS-CM) supplemented with 0.1% bovine serum albumin and 0.1% D-glucose (Sigma-Aldrich), and subsequently incubated for 60 min at 37 °C with 1 nM (50,000 cpm) [125I]T4 in 0.5 ml DMEM/F12 with 0.1% BSA. After incubation, cells were briefly washed with DPBS-CM containing 0.1% BSA and lysed with 0.1 M NaOH. Radioactivity in the cell lysates was measured with a y-counter.

Cell surface biotinylation assays

Cell surface biotinylation assays were performed as recently described (17). Briefly, surface proteins were labeled with 1 mg/mL EZ-Link Sulfo-NHS-Biotin (Thermo Fisher, Bleiswijk, NL) in DPBS-CM. After quenching of free biotin, cells were lysed with IP buffer (50 mM Tris-HCl, 150 mM NaCl, 10 mM EDTA, 1% Triton-X-100), containing protease inhibitor cocktail (Roche Diagnostics). An aliquot (5% of the total volume) of the clarified lysate was stored as input control. Biotin-labeled surface proteins were isolated by incubating clarified lysates overnight with 50 µL pre-washed NeutrAvidin agarose beads (Thermo Fisher). Extracted proteins were eluted by incubating the beads for 10 min at 70°C with 20 µL 4× NuPAGE lithium dodecyl sulfate loading buffer (Thermo Fisher). The complete eluates and input samples were used for immunoblot analyses as described below.

Immunoblot analyses

Cells were lysed in radioimmunoprecipitation (RIPA) buffer (50 mM Tris.HCl, 150 mM NaCl, 1% NP-40, 0.5% deoxycholate, 0.1% SDS) containing protease inhibitor cocktail (Roche Diagnostics), sonicated and clarified by centrifugation. Protein concentrations were measured using BCA protein quantification (Thermo Fisher) and 25 µg protein was used for immunoblots as previously described (16). OATP1C1 was visualized with rabbit anti-V5 (Cell Signaling Technology, Leiden, NL; mAB #13202;

RRID:AB_2687461; 1:1,000). GAPDH was used as a loading control and detected with mouse anti-GAPDH (Millipore, Amsterdam, NL; mAB #374; RRID: AB_2107445; 1:10,000) antibody. For immunoblots on total lysates, membranes were incubated for 1 hour with goat anti-rabbit or goat anti-mouse IgG antibody labelled with horse-radish peroxidase (#172-1011; RRID: AB_11125936, Bio-Rad, Veenendaal, NL; 1:3,000) in TBS-T containing 5% milk, washed, and developed using enhanced chemiluminescence reagent (Bio-Rad) using the Alliance 4.0 Uvitec platform (Uvitec Limited, Cambridge, UK). For cell surface biotinylation assays, OATP1C1-V5 and GAPDH were visualized by Odyssey detection systems as previously described (16). Expression levels were quantified by densitometry analyses using ImageJ software (46).

Immunocytochemistry

Immunocytochemistry (ICC) was carried out as previously described (17). Briefly, cells were fixed with 4% paraformaldehyde, and permeabilized with 0.2% triton X-100 in PBS. Samples were blocked for 1 hour at RT in PBS containing 2% BSA, and incubated overnight with rabbit anti-V5 antibody (1:1,000) and mouse monoclonal ZO-1 antibody (Invitrogen, Breda, NL, #61-7300, RRID:AB_2533147; 1:500). After secondary staining with goat anti-rabbit Alexa Fluor 488 (Thermo Fisher, #A11008, RRID: AB_143165, 1:1,000) and goat anti-mouse Alexa 633 (Thermo Fisher, #A21050, RRID:AB_2535718, 1:1,000), cover slips were mounted on glass slides with Prolong Gold containing DAPI (Invitrogen) and examined on a Zeiss Meta 510 microscope, using Zeiss LSM software (Zeiss NL, Sliedrecht, NL) as previously described (17).

OATP1C1 homology modelling

An OATP1C1 homology model was constructed similarly as we have recently described for MCT8 using YASARA Structure Software (www.yasara.org) (17, 18, 19). Based on sequence similarity, percentage coverage and model quality score, the crystal structure of the *E.coli* multidrug transporter MdfA (PDB#4ZP0) in inward-open conformation was selected as the most suitable template. The models based on the top ten putative structural alignments were checked against the available in vitro data and compared to previously published homology models of rat OATP1C1 (24). In line with these studies, we selected the model in which previously identified mutation sensitive residues (Asp85, Glu89, Asn92, Arg597) were located along the substrate pore. The KAZAL-like sequence motif present in extracellular loop (ECL) 5, spanning Arg470 to Cys523, was modelled separately based on the KAZAL-type inhibitor Infestin 4 (PDB#2ERW) and integrated into the OATP1C1 model. The final alignment is presented in **Figure S1**. The resulting model was subjected to energy minimization and validated with WHAT_CHECK (47), yielding a protein structure quality (Z)-score of -1.29 (range: <-5, terrible to >0, optimal). A T4 molecule was docked into the substrate pore using the substrate docking algorithm of YASARA Structure and the OATP1C1 protein model was embedded into a lipid bilayer as previously described (17). Despite the good resolution of the original template crystals (4ZP0, 2.00 Å; 2ERW, 1.40 Å), the relatively low similarity score between target and template (33% to MdfA and 51% to infestin 4 based on a BLOSUM62 score>0) limits the prediction of the exact orientation of amino acid side-chains, especially in those regions that contain differences in the (predicted) secondary structure of target and template(s) proteins. All images were created using YASARA Structure and Pov-Ray v3.6 software (www.povray.org).

Supplemental Figures

Figure S1 Sequence alignment of hOATP1C1 and the E. coli multidrug transporter MdfA (4ZP0) and Infestin 4 (2ERW). Final alignment between OATP1C1 and the *E. coli* multidrug transporter MdfA (PDB# 4ZP0) using multiple sequence alignments and position-specific scoring matrices (PSSM) implemented in YASARA Structure as described previously. Here, the sequences of OATP1C1 (target in black) and MdfA (PDB# 4ZP0; template. In dark grey) are shown and OATP1C1 residue numbers are indicated. Only template residues that keep their position in the model are displayed. All other residues (gaps in the template) are assumed to occupy a different position in the target model and are thus placed via loop modelling. The transmembrane domains of OATP1C1 predicted based on the membrane embedded OATP1C1 structural model are underlined. The KAZAL-like sequence motif present in extracellular loop (ECL) 5 spanning from Arg470-Cys523 was modelled separately based on the highly homologues sequence of the KAZAL-type inhibitor infestin 4 (PDB#2ERW highlighted in light grey). When only taking into account the aligned residues, the sequence similarity between target and template(s) was found to be 33% for MdfA and 51% for infestin 4 (similarity was defined by a BLOSUM62 score>0. calculated by YASARA Structure). The positions of the K248, D252 and S389 residues are highlighted in black and the most evolutionary conserved domain in OATPs (“signature sequence” 267-279) is highlighted in grey.

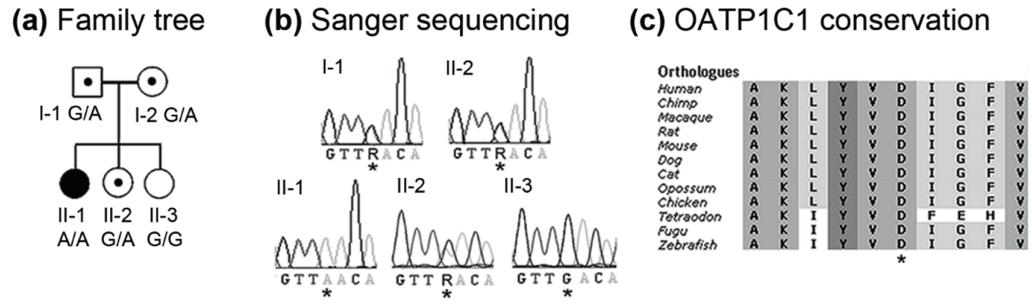

Figure S2. Pedigree of the family, Sanger sequencing of the *SLCO1C1* homozygous variant Chr12(GRCh37):g.20870143G>A; NM_001145946.1:c.754G>A; p.(D252N) and its evolutionary conservation. (**a**) Family pedigree and segregation of the *SLCO1C1* mutation. The patient (filled circle) was homozygous for the mutant allele (A/A) while her parents (I-1 and I-2) and one sister (II-2) were heterozygous (G/A). The youngest sister (II-3) was homozygous for the wild-type allele (G/G). (**b**) Nucleotide profile obtained by Sanger sequencing of *SLCO1C1* with the missense mutation (indicated with an asterisk) in the family (R indicates G or A).(**c**) Evolutionary conservation of the Asp residue (D), mutated in the patient, in a cross-species alignment of the OATP1C1 protein (only part of the protein is shown). The asterisk indicates the amino acid mutated in the patient.

REFERENCES

1. Gruters A, Krude H. Detection and treatment of congenital hypothyroidism. Nat Rev Endocrinol. 2011;8(2):104-13.
2. Bernal J. Thyroid hormone regulated genes in cerebral cortex development. J Endocrinol. 2017;232(2):R83-R97.
3. Bianco AC, Salvatore D, Gereben B, Berry MJ, Larsen PR. Biochemistry, cellular and molecular biology, and physiological roles of the iodothyronine selenodeiodinases. Endocr Rev. 2002;23(1):38-89.
4. Groeneweg S, Visser WE, Visser TJ. Disorder of thyroid hormone transport into the tissues. Best Pract Res Clin Endocrinol Metab. 2017;31(2):241-53.
5. Lee JY, Petratos S. Thyroid Hormone Signaling in Oligodendrocytes: from Extracellular Transport to Intracellular Signal. Mol Neurobiol. 2016;53(9):6568-83.
6. Bernal J. Thyroid hormones and brain development. Vitam Horm. 2005;71:95-122.
7. Alkemade A, Friesema EC, Kalsbeek A, Swaab DF, Visser TJ, Fliers E. Expression of thyroid hormone transporters in the human hypothalamus. J Clin Endocrinol Metab. 2011;96(6):E967-71.
8. Friesema EC, Grueters A, Biebermann H, Krude H, von Moers A, Reeser M, et al. Association between mutations in a thyroid hormone transporter and severe X-linked psychomotor retardation. Lancet. 2004;364(9443):1435-7.
9. Dumitrescu AM, Liao XH, Best TB, Brockmann K, Refetoff S. A novel syndrome combining thyroid and neurological abnormalities is associated with mutations in a monocarboxylate transporter gene. Am J Hum Genet. 2004;74(1):168-75.
10. Fahey FH, Bom HH, Chiti A, Choi YY, Huang G, Lassmann M, et al. Standardization of Administered Activities in Pediatric Nuclear Medicine: A Report of the First Nuclear Medicine Global Initiative Project, Part 2-Current Standards and the Path Toward Global Standardization. J Nucl Med. 2016;57(7):1148-57.
11. Varrone A, Asenbaum S, Vander Borght T, Booij J, Nobili F, Nagren K, et al. EANM procedure guidelines for PET brain imaging using [18F]FDG, version 2. Eur J Nucl Med Mol Imaging. 2009;36(12):2103-10.
12. Vigeland MD, Gjotterud KS, Selmer KK. FILTUS: a desktop GUI for fast and efficient detection of disease-causing variants, including a novel autozygosity detector. Bioinformatics. 2016;32(10):1592-4.
13. Kircher M, Witten DM, Jain P, O'Roak BJ, Cooper GM, Shendure J. A general framework for estimating the relative pathogenicity of human genetic variants. Nat Genet. 2014;46(3):310-5.
14. Friesema EC, Jansen J, Jachtenberg JW, Visser WE, Kester MH, Visser TJ. Effective cellular uptake and efflux of thyroid hormone by human monocarboxylate transporter 10. Mol Endocrinol. 2008;22(6):1357-69.
15. van der Deure WM, Hansen PS, Peeters RP, Kyvik KO, Friesema EC, Hegedus L, et al. Thyroid hormone transport and metabolism by organic anion transporter 1C1 and consequences of genetic variation. Endocrinology. 2008;149(10):5307-14.
16. Groeneweg S, Friesema EC, Kersseboom S, Klootwijk W, Visser WE, Peeters RP, et al. The role of Arg445 and Asp498 in the human thyroid hormone transporter MCT8. Endocrinology. 2014;155(2):618-26.
17. Groeneweg S, Lima de Souza EC, Meima ME, Peeters RP, Visser WE, Visser TJ. Outward-Open Model of Thyroid Hormone Transporter Monocarboxylate Transporter 8 Provides Novel Structural and Functional Insights. Endocrinology. 2017;158(10):3292-306.
18. Krieger E, Joo K, Lee J, Lee J, Raman S, Thompson J, et al. Improving physical realism, stereochemistry, and side-chain accuracy in homology modeling: Four approaches that performed well in CASP8. Proteins. 2009;77 Suppl 9:114-22.
19. Krieger E, Vriend G. YASARA View - molecular graphics for all devices - from smartphones to workstations. Bioinformatics. 2014;30(20):2981-2.
20. Yang H, Zubarev RA. Mass spectrometric analysis of asparagine deamidation and aspartate isomerization in polypeptides. Electrophoresis. 2010;31(11):1764-72.
21. Roth M, Obaidat A, Hagenbuch B. OATPs, OATs and OCTs: the organic anion and cation transporters of the SLCO and SLC22A gene superfamilies. British journal of pharmacology. 2012;165(5):1260-87.
22. Hanggi E, Grundschober AF, Leuthold S, Meier PJ, St-Pierre MV. Functional analysis of the extracellular cysteine residues in the human organic anion transporting polypeptide, OATP2B1. Mol Pharmacol. 2006;70(3):806-17.
23. Taylor-Wells JC, Meredith S, Kelly S. Structural determination of OATP transporters utilising homology models and cell based assays. FASEB J. 2012;26(1).
24. Westholm DE, Marold JD, Viken KJ, Duerst AH, Anderson GW, Rumbley JN. Evidence of evolutionary conservation of function between the thyroxine transporter Oatp1c1 and major facilitator superfamily members. Endocrinology. 2010;151(12):5941-51.

25. Constant EL, de Volder AG, Ivanoiu A, Bol A, Labar D, Seghers A, et al. Cerebral blood flow and glucose metabolism in hypothyroidism: a positron emission tomography study. J Clin Endocrinol Metab. 2001;86(8):3864-70.
26. Cremer GM, Goldstein NP, Paris J. Myxedema and ataxia. Neurology. 1969;19(1):37-46.
27. Westerholz S, de Lima AD, Voigt T. Regulation of early spontaneous network activity and GABAergic neurons development by thyroid hormone. Neuroscience. 2010;168(2):573-89.
28. Hashemi E, Ariza J, Rogers H, Noctor SC, Martinez-Cerdeno V. The Number of Parvalbumin-Expressing Interneurons Is Decreased in the Prefrontal Cortex in Autism. Cerebral cortex. 2017;27(3):1931-43.
29. Nelson PT, Katsumata Y, Nho K, Artiushin SC, Jicha GA, Wang WX, et al. Genomics and CSF analyses implicate thyroid hormone in hippocampal sclerosis of aging. Acta Neuropathol. 2016;132(6):841-58.
30. Dugas JC, Ibrahim A, Barres BA. The T3-induced gene KLF9 regulates oligodendrocyte differentiation and myelin regeneration. Mol Cell Neurosci. 2012;50(1):45-57.
31. Mayerl S, Visser TJ, Darras VM, Horn S, Heuer H. Impact of Oatp1c1 deficiency on thyroid hormone metabolism and action in the mouse brain. Endocrinology. 2012;153(3):1528-37.
32. Wirth EK, Roth S, Blechschmidt C, Holter SM, Becker L, Racz I, et al. Neuronal 3',3,5-triiodothyronine (T3) uptake and behavioral phenotype of mice deficient in Mct8, the neuronal T3 transporter mutated in Allan-Herndon-Dudley syndrome. J Neurosci. 2009;29(30):9439-49.
33. Mayerl S, Muller J, Bauer R, Richert S, Kassmann CM, Darras VM, et al. Transporters MCT8 and OATP1C1 maintain murine brain thyroid hormone homeostasis. J Clin Invest. 2014;124(5):1987-99.
34. Kersseboom S, Horn S, Visser WE, Chen J, Friesema EC, Vaurs-Barriere C, et al. In vitro and mouse studies supporting therapeutic utility of triiodothyroacetic acid in MCT8 deficiency. Mol Endocrinol. 2014;28(12):1961-70.
35. Wilkins ME, Caley A, Gielen MC, Harvey RJ, Smart TG. Murine startle mutant Nmf11 affects the structural stability of the glycine receptor and increases deactivation. J Physiol. 2016;594(13):3589-607.
36. Alvarez-Crespo M, Csikasz RI, Martinez-Sanchez N, Dieguez C, Cannon B, Nedergaard J, et al. Essential role of UCP1 modulating the central effects of thyroid hormones on energy balance. Mol Metab. 2016;5(4):271-82.
37. Medina-Gomez G, Calvo RM, Obregon MJ. Thermogenic effect of triiodothyroacetic acid at low doses in rat adipose tissue without adverse side effects in the thyroid axis. Am J Physiol Endocrinol Metab. 2008;294(4):E688-97.
38. Rodby-Bousquet E, Agustsson A, Jonsdottir G, Czuba T, Johansson AC, Hagglund G. Interrater reliability and construct validity of the Posture and Postural Ability Scale in adults with cerebral palsy in supine, prone, sitting and standing positions. Clin Rehabil. 2014;28(1):82-90.
39. Rosengren LE, Wikkelso C, Hagberg L 1994 A Sensitive Elisa for Glial Fibrillary Acidic Protein - Application in Csf of Adults. J Neurosci Meth 51:197-204.
40. Minoshima S, Drzezga AE, Barthel H, Bohnen N, Djekidel M, Lewis DH, Mathis CA, McConathy J, Nordberg A, Sabri O, Seibyl JP, Stokes MK, Van Laere K 2016 SNMMI Procedure Standard/EANM Practice Guideline for Amyloid PET Imaging of the Brain 1.0. J Nucl Med 57:1316-1322.
41. Li H, Durbin R 2009 Fast and accurate short read alignment with Burrows-Wheeler transform. Bioinformatics 25:1754-1760.
42. McKenna A, Hanna M, Banks E, Sivachenko A, Cibulskis K, Kernytsky A, Garimella K, Altshuler D, Gabriel S, Daly M, DePristo MA 2010 The Genome Analysis Toolkit: A MapReduce framework for analyzing next-generation DNA sequencing data. Genome Res 20:1297-1303.
43. Cingolani P, Platts A, Wang LL, Coon M, Nguyen T, Wang L, Land SJ, Lu XY, Ruden DM 2012 A program for annotating and predicting the effects of single nucleotide polymorphisms, SnpEff: SNPs in the genome of Drosophila melanogaster strain w(1118); iso-2; iso-3. Fly 6:80-92.
44. Vigeland MD, Gjotterud KS, Selmer KK 2016 FILTUS: a desktop GUI for fast and efficient detection of disease-causing variants, including a novel autozygosity detector. Bioinformatics 32:1592-1594.
45. Kircher M, Witten DM, Jain P, O'Roak BJ, Cooper GM, Shendure J 2014 A general framework for estimating the relative pathogenicity of human genetic variants. Nat Genet 46:310-+.
46. Schneider CA, Rasband WS, Eliceiri KW 2012 NIH Image to ImageJ: 25 years of image analysis. Nat Methods 9:671-675.
47. Hooft RWW, Vriend G, Sander C, Abola EE 1996 Errors in protein structures. Nature 381:272-272.

Chapter

General discussion

Parts of this chapter are based on

Thyroid hormone transporters
Stefan Groeneweg, Ferdy S. van Geest, Robin P. Peeters, Heike Heuer, W. Edward Visser. Endocrine Rev 2019 (accepted for publication)

Diagnostic and therapeutic challenges in the Allan-Herndon-Dudley Syndrome.
Stefan Groeneweg, Robin P. Peeters, Theo J. Visser, W. Edward Visser. US Endocrinology 2016;12 (02):90.

7

It has long been thought that thyroid hormone enters the cell through passive diffusion due to its lipophilic nature. But if it likes the cell membrane so much, why would it ever come out again? Seminal work in the late 70s provided first proof that the transport of thyroid hormone across the cell membrane is a saturable process and likely relies on carrier-mediated mechanisms (1, 2). In the subsequent decades characteristics of these transporter systems started to be elucidated, although the molecular basis remained unknown until the late 90s when the first transporter proteins were identified at the molecular level. The ultimate proof for the (patho-) physiological relevance of transporter-mediated thyroid hormone passage across cell membranes was provided by the identification of a clinical phenotype associated with genetic mutations in MCT8 (3, 4). Numerous patients have been described in literature and many studies sought to delineate the pathogenesis of MCT8 deficiency ever since. The first part of the work presented in this thesis aimed to further elucidate the transport mechanism by which MCT8 transports iodothyronines and how this is affected by mutations encountered in patients with MCT8 deficiency. The second part aimed to delineate the clinical phenotype of MCT8 in greater detail taking advantage of several case series, but most importantly, also of a large international cohort of patients with MCT8 deficiency we established over the last decade. The third part aimed to explore therapeutic options for patients with MCT8 deficiency for which no effective therapy had been available. The final chapters include studies employed to identify novel transporters and describe a novel syndrome of resistance to thyroid hormone associated with defective OATP1C1. In this chapter the main findings of these studies will be integrated and their implications for the field of thyroidology will be discussed.

MOLECULAR CHARACTERISTICS OF MCT8

Unraveling the transport mechanism of MCT8

In order to understand the pathophysiological mechanism of mutation identified in patients with MCT8 deficiency at the molecular level, it was imperative to unravel the protein structure-function relationship of the wild-type transporter. As structural features are likely to determine the functional properties of MCT8, research over the last decade focused on the identification of amino acid residues that participate in substrate recognition and in the maintenance of protein stability. An optimal strategy to identify such residues would be to solve the crystal structure of the MCT8 protein. However, crystallization of integral membrane proteins is a challenging procedure and only few transporter proteins have been successfully crystallized so far. As an alternative, we combined several chemical modification studies with targeted mutational studies and protein homology modeling (described in **chapters 2.1-2.5**). Protein homology modelling is a procedure by which the structure of the protein of interest is predicted based on its similarities with a protein, or combination of proteins with available crystal structures. These crystals may function as a template on which the MCT8 protein could be modelled. Obviously, the reliability of the resulting models improves if the template bears more similarity to the protein of interest. Therefore, templates should be carefully selected in order to obtain meaningful homology models.

Because the MCT family is classified as a member of the MFS, it likely shares a common topology with 12 transmembrane domains (TMDs) and intracellular C- and N-termini and transports its substrates according to the rocker-switch model (5, 6). Despite considerable variation in amino acid sequences among the members of the MFS family, their structure and transport mechanism appears to be relatively reminiscent. Therefore, Kinne et al generated a three-dimensional homology model of the

MCT8 protein based on the crystal structure of the bacterial glycerol-3-phosphate transporter GlpT in the inward-open conformation (PDB ID: 1pw4) (7, 8). This model revealed a critical role of the positively charged Arg445 (TMD8) and negatively charged Asp498 (TMD10) in T3 transport due to their location within the membrane plane and side-chains that direct towards the substrate pore. The importance of these residues was supported by the deleterious effect of their respective alanine substitutions carried out in different experimental models (**chapter 2.3** and (7)). The model also predicted a salt-bridge between both residues (7), of which the presence was supported experimentally by a charge reversal mutant (R445D/D498R) that regained activity compared to both single mutants (**chapter 2.3**). Additional studies using the R445K and D498E mutants as well as their combined substitution indicated that not only the charge, but also the exact distance between both residues might be of importance. By extrapolating the effects of these mutations on the wild-type transporter, we postulated that the presence of substrate molecules may also impact on the strength of this bond and therewith elicit conformational changes of the MCT8 protein during the transport cycle.

In analogy to the binding mode of T3 to the T3 receptors and the catalytic side of D3 (9, 10), it was postulated that MCT8 contains a so-called His-Arg clamp (11). Three of such His-Arg pairs were identified in the inward-open model of MCT8, comprising residue pairs His192/Arg445, His192/Arg301 and His415/Arg301 (7, 11). Indeed, substitution of His192 by Ala or Phe altered the transporter kinetics (12). In parallel to these studies by the Schweizer group, we identified the His192 residue as a target for the His-reactive chemical reagent diethylpyrocarbonate (DEPC) (**chapter 2.2**), indeed supporting that this residue is located at an accessible position in the protein. The modification by DEPC was fully prevented in presence of substrate, suggesting that the imine side-chain of His192 faces the substrate pore (**chapter 2.2).** This observation also indicated that His192 is the only target for DEPC-modification and questions the involvement of His415 in substrate recognition by forming a His/Arg clamp with Arg301 as predicted by the inward-open MCT8 homology model. Although substitution of His415 by Phe or Ala reduced thyroid hormone transport efficiency (12), substitution of Arg301 by Ala greatly impaired protein stability. This finding suggests a role for this residue in the maintenance of protein stability rather than in substrate recognition (12). For these reasons, the existence of His/Arg clamps other than the His192/Arg445 is currently not well supported by *in vitro* studies.

Additional structure-function information has been derived from studies using the membrane-impermeable cysteine-specific modifying reagents P-Chloromercuribenzenesulfonate and mercury(II) chloride, which identified Cys481 (extracellular loop [ECL] 5) and Cys497 (TMD10) as accessible target residues (**chapter 2.1**). Again, the effect of these compounds was partially ameliorated in presence of substrate, suggesting that at least one of these residues is located along the substrate channel. Although not ultimately proven experimentally, Cys497 is the most likely candidate given its predicted location in the middle of TMD10 (13). This finding provided important information on the putative configuration of TMD10 and its orientation relative to TMD8, since the side-chain of its neighboring residue Asp498 is likely to direct towards Arg445 in TMD8.

For a long time, the generation of homology models in transporter conformations other than the inward-open conformation had been limited by the paucity of available crystal structure templates with sufficient homology to MCT8 (14). The generation of homology models in different configurations is indispensable to better understand the full transport cycle (see **Figure 12** in **chapter 1**). By combining different template structures, Protze et al established homology models of the MCT8 protein in different structural conformations (15). These studies again suggested critical roles for Arg445, Asp498

and His192 in the transit of substrate through the substrate channel. All three residues were found at the substrate binding pocket in the inward-open and outward-open conformation. Also other charged residues were implied in the recruitment of substrate such as Glu422 and Glu423. In contrast to the precise charge (and size) restriction that apply to the position of Arg445 and Asp498, the exact charge at the position of these Glu residues did not seem to be important, as oppositely charged residues were also well-tolerated. Therefore, these residues are not likely to be located within the narrow substrate channel as this would have put more restraints to their side-chain properties to secure precise configuration of the substrate. By contrast, they may exert a role during substrate recruitment at the outside of the transporter by interacting with the zwitterionic alanine side-chain of thyroid hormone. Based on the series of models, several other residues were suggested to have an important function in maintaining protein stability (Lys418, Tyr419, Ser313, Ser314, Tyr503).

In parallel to these studies, we generated an alternative homology model in the outward-open conformation based on the E. Coli fucose:proton symporter (FucP) (16) (**chapter 2.4**). This model replicated several features of the models proposed by Kinne et al and Protze et al. Importantly, the model complied to all *in vitro* data that had been published thus far, including the results of mutational screens and chemical modification studies. In line with the other available models, it supported an important role for His192, Arg445 and Asp498 in substrate docking. *In vitro* chemical modification studies supported the involvement of Arg445 in substrate docking by identifying Arg445 as an accessible target for the Arg-reactive compound phenylglyoxal, which was prevented in presence of substrate. The model was also in agreement with our earlier hypotheses that the interaction between Arg445 and Asp498 is modulated in presence of substrate (**chapter 2.3**). Model-based mutagenesis studies furthermore pointed to a putative role for Phe189, Phe279 and Phe287 in substrate docking through the formation of pi-pi interactions with the phenolic rings of TH (17). Interestingly, the position of His415 in our model diverged from its position in the other available models, arguing against its involvement in a His-Arg clamp with Arg301.

Together, these studies identified relevant residues for substrate recognition at different stages during the transport cycle. Yet, none of these studies explored the involvement of the iodine moieties in substrate-transporter interactions. It is beyond doubt that these moieties are involved in the recognition of iodothyronines by their target proteins, as these proteins exhibit distinct affinities, transactivation, conversion, or transport rates for the different iodothyronines. Although this might be due to differences in size, structural flexibility or net charge of these molecules, the involvement of the iodine moieties in direct interactions with the target proteins through the formation of halogen bonds poses a tempting alternative. Indeed, halogenation of molecules, including iodination, has been shown to potentiate the affinity of multiple molecules known in biology and often forms the basis for therapeutic approaches (18-20). In addition to the amino acid backbone, several amino acids side-chains may engage in the formation of halogen-bonds including Glu, Asp, Gln and Asn. Based on our homology model, we predicted that the Asn193 residue might be a good candidate to be involved in such an interaction given its location near the substrate binding pocket (**chapter 2.5**). Indeed, docking studies predicted that its side-chain is ideally located to establish halogen-bonds with the 3 and 3' iodine moieties of T4 and with the 3 iodine moiety of T3. A series of *in vitro* experiments confirmed that the loss of Asn193 by means of an N193A mutant decreased affinity for T3, but in particular also for T4. Especially the transport rate of T4 was affected by the loss of Asn193, pointing to a role of this residue in the exact orientation of the outer-ring of T4 though the establishment of a halogen-bond.

Although our model proved to comply with the different available *in vitro* data and was useful in the prediction of functionally relevant residues, this may also be the case for other models based on different templates or target-template alignments. It is therefore important to realize that homology models are only an approximation of the real structure of the transporter. In the end, discrepancies between the existing models (e.g. the position of His415) will be resolved only when crystal structures of MCT8 or one of its MCT family members have been elucidated. Alternatively, crystallization of other MFS members with a higher sequence similarity to MCT8 and a higher resolution than those that currently exist would offer more suitable templates for MCT8 modeling. For now, it remains imperative to consider details on side-chain orientation with some reservation. This precludes the use of the current models for *in silico* drug screening and as a tool to unambiguously determine the pathogenicity of mutations identified in MCT8 deficient patients. With respect to the latter, functional studies in over-expression systems or patient-derived fibroblasts are therefore still indispensable.

Broadening the substrate spectrum of MCT8

Seminal studies of Friesema et al demonstrated that MCT8 effectively transports T4, T3 and to a lesser extent rT3 and 3,3'-T2, but not aromatic amino acids (21, 22). Also MCT10 was found to transport T3, rT3 and 3,3'-T2, but not T4 (23). Although the amino acid sequence of MCT8 and MCT10 are very similar (80% sequence similarity), both transporters have a remarkable difference in substrate specificity. In contrast to MCT8, MCT10 also effectively transports aromatic amino acids and amino acid metabolites such as L-3,4-dihydroxyphenylalanine (L-dopa) (24, 25). These findings suggest that the presence of the phenolic outer ring, nor the iodine moieties is critical for substrate recognition by MCT10. Yet, it was unknown if MCT8 also accepts other substrates than iodothyronines. The few available studies on the substrate specificity of MCT8 have only evaluated the direct transport of a limited number of potential substrates in MCT8-overexpressing *Xenopus* oocytes or mammalian cell lines, or applied cis-inhibition approaches which provide no definitive prove for direct transport (7, 21-23). As an alternative for these targeted approaches we performed metabolome analyses in MCT8 over-expressing *Xenopus* oocytes (**chapter 2.8**).

Through these studies we identified mono-iodotyrosine (MIT) and di-iodotyrosine (DIT) as novel substrates for MCT8. Complementary studies in transiently transfected mammalian cell lines and human fibroblasts suggested that MCT8 predominantly facilitates the cellular efflux of MIT and DIT and that the role of MCT8 in the cellular uptake of these compounds is limited. MIT and DIT were both found to compete with MCT8-mediated efflux of T3 and T4, although the apparent affinities for T3 and T4 appear to exceed those for MIT and DIT. Should MCT8 also transport MIT and DIT *in vivo*, our observations may be of particular relevance to thyroid hormone transport in the thyroid gland. MIT and DIT are both intermediates of thyroid hormone synthesis (26) and are also released to some extent into the blood stream (27-29). As animal studies suggested that MCT8 is involved in the cellular efflux of T3 and T4 from the thyrocytes (30, 31), the high intracellular concentrations of MIT and DIT in these cells may modulate the release of T3 and T4 from the thyroid gland. Further studies should unravel if MCT8 would indeed facilitate the transport of MIT and DIT *in vivo*. In this context, it might be of interest to measure circulating DIT and MIT concentrations in patients with MCT8 deficiency. It would also be of interest to study if MCT10 also accepts iodotyrosines as a substrate. Should this be the case, the iodotyrosines would be the missing link between aromatic amino acids and iodothyronines as substrates for MCT10.

Based on the currently available studies, it is tempting to speculate that the substrate range of MCT10 includes smaller molecules than that of MCT8. This is supported by recent findings of Johannes et al, who showed that enlarging the substrate pocket of MCT10 by changing a series of residues to their corresponding residue in MCT8, allows MCT10 to transport T4 (32). Interestingly, one of these residues concerned Tyr184, which corresponds to Phe287 in MCT8 which we identified as an important substrate interacting residue in **chapter 2.4**. By contrast, the substrate range of MCT8 appears to be shifted to larger molecules and the presence of at least a mono-iodinated tyrosyl group seems critical for substrate recognition.

Further studies should elucidate how MIT and DIT are recognized by MCT8. Based on the transport direction, a high-quality homology model of MCT8 in the inward-open conformation would be a pre-requisite to this purpose. Given their differential substrate preference, establishment of comparative homology models of MCT10, which are currently lacking, may importantly help to identify the substrate-interacting residues. Moreover, such studies may reveal why MCT10 accepts aromatic amino acids as substrates and MCT8 not. In this context, it should be stressed that differences in substrate selectively may importantly determine the contribution of both transporters to thyroid hormone transport in tissues *in vivo*, as thyroid hormone transport by MCT10, but not MCT8, may be importantly inhibited by aromatic amino acids. Indeed, *Mct10* ko mice showed altered amino acid concentrations in plasma and a variety of tissue, but rather normal thyroid hormone concentrations (33).

Although metabolome analyses also identified other candidate substrates, complementary uptake studies in MCT8 over-expressing cell lines and (patient-derived) human fibroblasts did not confirm direct MCT8-mediated transport of some compounds we were able to test. This may have several reasons as outlined in **chapter 2.8**. Most importantly, MCT8 may transport upstream or downstream metabolites of the identified candidate metabolites. Another explanation could be that the absence of MCT8 in control oocytes already altered the expression of T3-sensitive genes during routine culture preceding the metabolome experiment. Nonetheless, the identification of differentially abundant metabolites in oocytes expressing MCT8 *versus* controls may point to novel metabolic pathways that are altered in patients with MCT8 deficiency, including cellular glutamine/glutamate metabolism. The cellular uptake of glutamate was indeed different between MCT8 deficient and control fibroblasts. Since this difference was not affected by the MCT8-specific inhibitor silychristin, this is presumably caused by, T3-responsive, factors other than MCT8. Indeed, several key players in glutamine/glutamate metabolism have been shown to be responsive to thyroid state with lower cellular glutamate uptake and utilization documented during hypothyroidism (34, 35). Since our *in vitro* and *ex vivo* studies focused on individual cell types, it is challenging to extrapolate these observations to the *in vivo* situation in which intermediate metabolism is regulated through a complex interplay of different organs. Metabolome studies in patients with MCT8 deficiency may help further elucidating the metabolic pathways that are affected in MCT8 deficiency. Obviously, such studies would be limited to metabolites in blood, urine or cerebral spinal fluid (CSF), which do not necessarily reflect changes in the metabolome in tissues.

Taken together, defective MCT8 may directly and/or indirectly alter cellular transport and metabolism of compounds other than iodothyronines. It is currently unclear if and how these alterations contribute to the clinical features observed in patients with MCT8 deficiency.

Assessing tolerable variability in MCT8

Apart from delineating the substrate specificity and transport mechanism, we also aimed to advance understanding of the tolerable variability in the MCT8 protein. Although the introduction of a huge series of different mutations would be the only way to provide ultimate proof, we decided to take advantage of evolution and compared the functional properties of the MCT8 orthologues in mouse and zebrafish to those of the human protein (**chapter 2.6**). The natural variance in amino acid sequence among species may provide important guidance in identifying relevant domains within the protein structure and those that are seemingly less important. Another important purpose of detailing the transport characteristics of mouse (mm) and zebrafish (dr) MCT8 was to ascertain the absence of important differences in substrate selectivity and efficacy between these orthologues and human (hs) MCT8. Together with the species-specific tissue distribution of MCT8 expression and the presence of redundant transporters at sites where MCT8 is expressed, the intrinsic properties of the MCT8 protein may importantly determine the suitability of these animals to model human MCT8 deficiency. Despite their frequent use in modeling human MCT8 deficiency, these properties had not been compared in detail.

DrMCT8 shares only 57% sequence identity and 77% sequence similarity with hsMCT8. Previous studies have shown that drMct8 transports T3 and T4 as effectively as hsMCT8, but did not include the transport of substrates other than T3 and T4 or any cis-inhibition studies to screen for potential alternative substrates. In **chapter 2.6** we therefore made a full *in vitro* comparison between hsMCT8, mmMCT8 and drMct8. Surprisingly, many features of drMct8 closely resemble those of hsMCT8, suggesting that the major functions of MCT8 (i.e. the transport of T3 and T4) have been preserved during evolution, despite the considerable differences in amino acid sequence. Therefore, it is tempting to speculate that residues that are not conserved, predominantly those located in the predicted extracellular and intracellular loops, might be less critical for MCT8 function. Indeed, most mutations encountered in MCT8 patients map into the relatively well-conserved TMDs and only one mutation has been mapped to an extracellular loop (L512P in ECL5 (4)). Nevertheless, subtle differences in transport kinetics and substrate specificity were observed between hsMCT8 and mmMCT8 *versus* drMct8. The T3 transport by the zebrafish orthologue was inhibited by a broader range of iodothyronines and metabolites thereof, including Triac and Tetrac. Direct uptake studies indicated that drMct8 is indeed capable of transporting Triac, whereas hsMCT8 and mmMCT8 are not. These observations may further support recent studies demonstrating that Triac has an important biological role in evolutionary more distant species. For example, in amphioxus Triac and not T3 was found to be the main receptor-active TH metabolite (36), and substrate for its deiodinating enzyme (37).

Together, these studies have filled important gaps in the field by demonstrating that the main functional properties of the MCT8 orthologues of mouse and zebrafish are similar to those of human MCT8, supporting the use of these animal species in modelling human MCT8 deficiency. Despite the large variation between drMCT8 and hsMCT8 in the composition of in particular the intracellular and extracellular domains, both orthologues transport T3 and T4 equally proficient. Nonetheless, the non-conserved residues in drMct8 allowed the acceptance of a broader set of substrates that potentially include iodothyroacetic acid derivatives such as Triac. Such differences in intrinsic transporter properties should be considered when comparing studies in different species. It is unknown, if mutations in hsMCT8 affecting less well-conserved domains result in similar subtle changes in

transport characteristics and to which extent these are clinically meaningful. Should variants in these regions be identified in patients with delayed neurodevelopment, functional evaluation would be essential to establish causality (see also **chapter 3.3**, and paragraph **Genotype-phenotype relation** in this chapter).

Regulation of MCT8 expression and activity

At present, little is known about the regulation of MCT8 expression and activity. As highlighted in the **chapter 1**, the only factor that has been shown to regulate MCT8 expression in the mouse genome is retinoic acid (38). Since the identified response element is not conserved in human, it is unclear if retinoic acid also regulates the human *MCT8* gene. Additional studies have suggested that the expression of MCT8 may be sensitive to thyroid hormone state in some cell-types, but not in others (39-41). Yet, the factors and conditions that modulate the expression of MCT8 in tissues in which it is probably most relevant (i.e. in the brain and at brain-barriers) are currently unknown. Tissue expression studies have revealed that the expression of MCT8 shows high spatiotemporal variation throughout development (e.g. (42, 43)), suggesting that tight regulation of its expression is critical. Further studies should aim to identify such regulating factors to better understand the developmental sequelae in which MCT8 is involved. Combined with in depth tissue expression studies for MCT8, and possible alternative thyroid hormone transporters, this information will help establishing in which cell types and at what time during development MCT8 is indispensable.

Also at protein level, little is known about factors that may regulate MCT8 activity and expression levels at the cell membrane. One of the involved factors might be the formation of oligomeric complexes between MCT8 proteins. Early studies already revealed that MCT8 is detected as a monomer, homo-dimer and possibly also as a homo-oligomer, in lysates of transient and stable overexpression systems (44, 45). More recent work using bimolecular fluorescent complementation techniques showed that MCT8 dimers were also formed in a cellular context. For many proteins it has been shown that dimerization modulates protein stability, and/or may even be crucial to establish functional complexes. In an attempt to study if the formation of such oligomeric complexes also modulates MCT8 activity, we aimed to disentangle the mechanism of MCT8 oligomerization and identify the protein domains involved in such interactions. In **chapter 2.7**, we showed that MCT8 oligomerization involves non-covalent interactions which could be disrupted by lithium dodecyl sulphate (LDS). Moreover, by co-immunoprecipation techniques we demonstrated that the formation of MCT8 dimers/oligomers requires a cellular context and is not a procedural artefact. Extensive C-terminal and N-terminal truncations of the protein did not abrogate oligomerization capacity, suggesting that MCT8-MCT8 interactions involve multiple domains in the protein. For this reason, we were unable to abrogate MCT8 dimerization by targeted mutational studies, preventing studies on its functional relevance. These findings were in line with the observation that none of the many missense mutations that have been tested for oligomerization capacity abrogated MCT8 oligomerization (e.g. (46)). Although our studies provided important complementary insights into the mechanism of MCT8 oligomerization, its functional relevance remains unknown.

Many membrane proteins require ancillary protein to govern proper cell membrane targeting, some of which have been found to predominantly recognize the C-terminal tail of their targets (47). Interactions with such proteins may form another mechanism by which the expression levels of transporters at the cell membrane are regulated. Other members of the MCT family indeed require

interactions with ancillary proteins for proper cell surface translocation (48). However, it is unknown if this also holds true for MCT8 (44), and if so, these factors likely differ from those required by other MCTs. Should this be the case, such interactions are not likely to be established through its intracellular C-terminal tail as mutant proteins lacking this domain exhibited surface expression levels similar to WT MCT8 (**chapter 3.3**). Recent studies showed that interaction of MCT8 with Pituitary tumor-transforming gene-binding factor (PBF; PTTG1IP) impeded cell membrane expression of MCT8 in tumor cells overexpressing this factor (49), demonstrating that interactions with other proteins may indeed regulate cell membrane expression of MCT8. *Vice versa*, MCT8 may also modulate the activity of other protein through direct interactions, as has been shown for the TSH-receptor (50). The relevance of these interactions in physiology remains to be explored. Further proteomic studies may identify additional interacting factors.

The mechanisms that regulate the degradation of the MCT8 protein are currently unknown. Recent work showed that the Lys56 residue in the extended N-terminal domain, unique to the long MCT8 isoform, makes the long MCT8 protein more susceptible to degradation through the ubiquitin-proteasome system (51). It is yet unclear if other Lys residues, particularly those that are shared among the long and short isoform of MCT8, are also targets for ubiquitination.

In summary, little is known about the regulation of MCT8 at transcriptional and post-translational level. Further studies are warranted to better understand how the timing and dosing of MCT8 expression is regulated in different tissues.

CLINICAL PHENOTYPE OF MCT8 DEFICIENCY

Following the landmark studies of Friesema et al. and Dumitrescu et al. in 2004 (3, 4), many patients with MCT8 deficiency have been identified and reported. Through these case descriptions published over the last 15 years, it became increasingly clear that the clinical phenotype of MCT8 deficiency comprises two major entities: 1) a neurocognitive phenotype and 2) signs of thyrotoxicosis in peripheral tissues, also termed the peripheral phenotype. Although each of these studies contributed to a better understanding of MCT8 deficiency, precise data for the phenotypic characteristics and natural history of MCT8 deficiency remained scarce. The available studies are mostly case reports or small case series of (related) patients and predominantly focused on the neurological phenotype, but with variable tools precluding consistent assessments. Moreover, the features of the peripheral phenotype have been largely neglected. The lack of a consistent quantitative description of the natural history of MCT8 deficiency hampers early diagnosis and uniform clinical care. Given the sparsity of published data, and by taking advantage of a large international network, we sought to provide a comprehensive and structured phenotypic characterization of MCT8 deficiency using clinical, radiological and biochemical data (**chapter 4.1**).

Deep phenotyping of the neurocognitive phenotype identified hypotonia, dystonic posturing and the presence of primitive reflexes as core clinical features present in most of the evaluated patients. The incidence rate of hypotonia and dystonia were grossly in line with a recent neuro-phenotypic description of 24 patients with MCT8 deficiency (52). The presence of peripheral hypertonia in combination with elevated tendon reflexes and contractures had long been referred to as spastic tetraplegia. However, in depth neurological phenotyping studies by Matheus et al. (2015) have

attributed the peripheral hypertonia to dystonia rather than spasticity (53). Although signs of spasticity were detected, the authors stated that dystonic features prevailed early in life. In retrospect, in some of the earlier studies the presence of dystonia and other dyskinetic movements have been mentioned, including athetosis, ataxia, and paroxysmal dyskinesia (e.g. (54)), whereas in others hypertonia reportedly varied and could be triggered by environmental cues, which better fits the definition of dyskinisia. Indeed, in the studies described in **chapter 4.1** we also observed that dystonic posturing preceded the development of prominent spastic features, in particular contractures. These clinical observations are substantiated by brain imaging studies (53), as diffusion tensor imaging revealed poor definition of especially the anteroposteriorly directed white matter association tracks, which is consistent with the presence of dystonia (53). Based on these observations, MCT8 deficiency is increasingly regarded as a movement disorder. In addition to hypotonia and dystonia, our study now adds the presence of primitive reflexes as a third clinical hallmark. Together with the presence of pronounced delay in myelination and absence of noticeable disease progression, these features may help to discriminate MCT8 deficiency from other neurodevelopmental disorders, such as Pelizaeus-Merzbacher disease, on clinical characteristics.

Complementary to the existing literature, our study quantitatively assessed neurocognitive development of a substantial group of patients using well-established neuropsychological tests such as the Bayley Scales of Infant Development III and the Gross Motor Function Measure-G88. The results of these studies showed that most patients with MCT8 deficiency exhibit profound neurocognitive and motor disability and do not reach a developmental age beyond 6-12 months. The developmental level was very homogenous irrespective of age, with few patients (<~10%) that could walk and talk in simple sentences being notable exceptions. Therefore, it may be concluded that the level of neurocognitive development is not expected to substantially improve nor decline with aging.

The neurological features are accompanied by abnormal thyroid function tests. In most patients total T4 and FT4 concentrations are below the reference range, whereas the T3 concentrations are elevated. Like T4, also rT3 concentrations are decreased in most patients. Therefore, T3/(F)T4 and T3/rT3 ratios are strongly elevated. TSH concentrations were mostly within normal range. This pattern is characteristic for MCT8 deficiency and may provide a key to improve early diagnosis (see paragraph “Diagnostic challenges” in this **chapter**). The elevated serum T3 concentrations may result in signs of hyperthyroidism in peripheral organs that rely on transporters other than MCT8. Detailed documentation of these proxy-parameters allowed determining thyroid hormone state in different tissues and compare these findings with *in vivo* models for MCT8 deficiency (see section **Mechanism of disease** of this chapter).

In line with previous reports (45, 55-57), we found a progressive decline in body weight for age in most patients with longitudinal data. About 60% of patients had underweight (age-adjusted z score < -2SD), which may predispose to significant co-morbidity including recurrent infections.

Although cardiovascular abnormalities have only been documented in some patients (56, 58-61), we found that about 50 percent of the patients manifest cardiovascular features that have been associated with overt hyperthyroidism. Elevated systolic blood pressure and tachycardia were present in up to 30-40 percent of patients. In addition, premature atrial complexes were highly abundant in a subset of patients. The high abundance of premature atrial complexes is uncommon, in particular in healthy children, and has been previously shown to predispose other cardiac arrhythmias and sudden

cardiac death (62-66). In addition, non-sustained ventricular tachycardia and QTc elongation were observed in some patients, which are both well known risk factors for sudden cardiac death. These findings thus justify a more thorough cardiac screening in patients with MCT8 deficiency and may require treatment in a subset of patients.

The presence of elevated serum sex hormone globulin concentrations and/or low-normal total cholesterol concentrations may indicate a hyperthyroid state in liver and were in line with previous observations in some reported patients with MCT8 deficiency (45, 56-58, 60, 67-70). Apart from these typical markers for liver thyroid hormone state, we also observed a mild increase in serum transaminases. Although this might be linked to the medication use, it was also observed in young patient that did not use any medication. This observation may be of clinical relevance given the frequent use of medication with hepatotoxic side-effects and the occurrence of transient hepatic failure in at least three reported cases following a trivial infection (**chapter 4.1** and (4)).

Also skeletal muscle appears to be in a hyperthyroid state, as most patients have a pronounced dystrophic appearance. Muscular dystrophy is a classical consequence of T3 toxicity. Excess T3 has been linked to defects in muscle development and regeneration, as well as enhanced uncoupling of ATP synthesis and decreased metabolic efficacy, which all amplify manifestations of the dystrophic phenotype (71-73). Nevertheless, the low muscle mass can also be, at least in part, ascribed to the immobility of most patients. Yet, electron microscopy on muscle tissue derived from a patient with a severe neurocognitive and motor phenotype revealed an increased number of mitochondria with normal morphology, which is compatible with a hyperthyroid state in skeletal muscle (74). Indeed, the increased serum lactate concentrations found in some patients may be indicative for skeletal muscle catabolism due to tissue hyperthyroidism, although the poor feedings status of these patients should also be taken into account.

Proxy-parameters that reflect thyroid hormone state in kidney are limited and only serum creatinine concentrations have been reported (**chapter 4.1**). The low serum creatinine concentrations may be indicative for an increased glomerular filtration rate, which is well-known to be modulated by thyroid hormone state (e.g. (75, 76)). However, it is unclear to which extent alterations in creatinine metabolism in skeletal muscle account for this observation. Nevertheless, changes in serum creatinine concentrations paralleled those observed in thyroid hormone concentrations in MCT8 deficient patients treated with Triac (**chapter 5.2**), and preceded noticeable changes in body weight and muscle appearance. Although not ultimately proven, this may point to a renal origin.

The thyroid status in bone is notoriously difficult to interpret due to the paucity of normal values for bone markers and bone mineral density in developing children. Moreover, it is largely unknown to what extent these parameters differ from the normal population in immobilized children. Although bone mineral density was low for age, serum bone turnover markers in pediatric patients were typically within the low normal range. Also in some adult patients that acquired more advanced motor skills, including walking, bone turnover markers did not indicate enhanced bone-turnover, although bone mineral density was low. Therefore, it appears that bone is relatively euthyroid.

Another objective of the studies in **chapter 4.1** was to determine overall survival and identify the main causes of death in patients with MCT8 deficiency. The available data on life expectancy in literature are highly variable and in most cases the exact cause of death has not been reported or was unknown. This precluded the identification of the major causes of death and thus the implementation of targeted

strategies that may improve survival in these patients. We showed that patients with MCT8 deficiency have a reduced life expectancy, with 40% of patients not reaching adolescence. Stratification of these analyses for head control revealed that patients who attained full head control are more likely to have a better survival than those that fail to attain full head control. For this reason, attaining full head control could be a very relevant objective in therapeutic trials in MCT8 deficiency. This observation may also explain why life expectancy had been previously reported to be normal in some individuals with a relatively less severe neurocognitive phenotype (77). It should be noted that survival data have been collected over the past 20 years during which general health and supportive care for patients with intellectual and motor disability have substantially improved. However, these measures have only partly –if any- resolved the putative underlying risk factor for premature death (i.e. the poor motor function, feeding problems and thyrotoxicity in peripheral tissues).

In addition, we retrieved the cause of death of a substantial number of patients, which allowed identification of major risk factors for premature death. The most common cause of death was pneumonia, either caused by aspiration or by infections. Aspiration is a frequent occurrence in MCT8 deficiency due to the impaired swallowing function, which could be, at least partially, ameliorated by tube feeding. Surprisingly, a substantial number of patients that exhibit swallowing problems reportedly had no feeding tube and thus remained at risk for aspiration. Tube feeding may be an effective measure to prevent underweight and concomitant adverse clinical sequelae. Therefore, tube feeding should be considered in all patients with swallowing difficulties to reduce the risk for aspiration and prevent underweight. A second major cause of death comprises sudden death. Although sudden death may have several etiologies, the presence of several cardiovascular symptoms that have been linked to sudden cardiac death may suggest a cardiovascular origin.

Together with recent other reports (52, 53), the studies described in **chapter 4.1** extended on previous work by describing novel details of MCT8 deficiency and providing a comprehensive and structured phenotypic characterization of MCT8 deficiency. This study illustrates the complexity of this disorder and highlights the involvement of multiple extra-neurological tissues. Our data underscore the need for a multi-disciplinary approach in the treatment and follow-up of patients with MCT8 deficiency, as both neurological and extra-neurological features may predispose to life-limiting co-morbidity. In addition, the unique (semi-)quantitative natural history data may function as historical control in future interventional studies in this rare disorder, for which a biological control group is often deemed not feasible. In order to further substantiate these findings and obtain longitudinal data, we have recently established an MCT8 deficiency patient registry. This will allow localizing MCT8 patients throughout the world and collect essential data on disease characteristics and their progression over time, including additional data on survival. Centralization of knowledge is of utmost importance to gain novel insights into rare disorders. In turn, a patient registry may also serve to directly feedback novel insights to doctors and patients all over the world and localize patients eligible to participate in clinical trials.

GENOTYPE-PHENOTYPE RELATION

One of the striking conclusions of our phenotyping studies was the pronounced difference in clinical severity associated with different genetic mutations. Previous studies already suggested the presence of a genotype-phenotype relation by showing that patients with a relatively less severe clinical phenotype harbored mutations with modest residual transport capacity *in vitro* and *ex vivo* in patient-

derived skin fibroblasts (78-80). Indeed, it is conceivable that various mutations may have a differential impact on MCT8 function. Single amino acid substitutions may reduce MCT8 function not only due to loss of the critical properties of the mutated residue, but also due to the unfavorable properties of the acquired residue. Therefore, the functional consequences of a mutation are determined by its location in the protein and the properties of the acquired residue. The relevance of the latter is illustrated in **chapter 3.1** where we described, amongst others, two patients with different mutations affecting the same Gly564 residue. Interestingly, the patient harboring the G564E mutation exhibited a relatively less severe clinical phenotype, whereas the patient harboring a G564R mutation exhibited a classical severe form of MCT8 deficiency. The severity of the phenotype correlated with the differential impact of both mutations in our *in vitro* studies. In **chapter 3.2** we could also demonstrate significant residual MCT8-mediated T3 uptake in fibroblasts of two patients with a relatively less severe clinical phenotype harboring a T239P and L543P mutation, respectively. In all cases, substitution of the affected residue by an Ala resulted in a fully functional protein, supporting that the unfavorable properties of the acquired residue comprise the pathogenic mechanism of the mutation at molecular level. Indeed, we observed that all four patient mutations reduced MCT8 protein stability and interfered with plasma membrane localization.

Although **chapter 3.1** and **3.2** further substantiate the presence of a relation between the genotype and the severity of the phenotype, large scale studies are currently lacking. With the detailed phenotypic characterization of an extensive cohort of patients with MCT8 deficiency (**chapter 5.1**), extensive functional evaluation of the mutations identified in these patients would allow for such studies. Prediction of the severity of the clinical phenotype based on *in vitro* or *ex vivo* residual function of mutant MCT8 proteins may allow optimization of patient care and improve counseling of parents of newly diagnosed patients. Importantly, should the residual function of MCT8 mutants reliably reflect the severity of the clinical phenotype, such assays may importantly help to confirm the pathogenicity of novel mutations. This is particularly relevant in the context of next generation sequencing technologies which are steadily incorporated in the diagnostic work-up of many diseases. As illustrated by our studies in **chapter 3.3**, not all mutations in SLC16A2 cause MCT8 deficiency which may lead to misinterpretation of causality and diagnostic delay. In this chapter, we demonstrated that pathogenicity of novel mutations in MCT8 cannot always be reliably predicted by *in silico* prediction tools. These tools are widely used in clinical practice and often predominantly rely on genetic conservation (e.g. (81-84). However, such tools frequently yield inconclusive or contradicting results, especially when mutations affect poorly conserved regions. Although predicted to be potentially inactivating, the H575R and N599S variants in the C-terminus of MCT8 exhibited functional properties undistinguishable from wild-type MCT8 *in vitro* and *ex vivo* in patient-derived fibroblasts, suggesting a benign nature for both variants. In retrospect, the H575R variant was also present in an unaffected family member, supporting this conclusion. It is not ultimately excluded that the N599S may exert cell-type specific effects *in vivo*, resulting in altered MCT8 function in some, but not in other cells. Further studies using patient-derived iPSCs may help addressing this question.

In the context of genotype-phenotype studies it should be realized that the impact of mutations may be cell-type specific. Careful selection of the experimental model thus seems imperative. This is illustrated by the pronounced differences in residual activity of MCT8 mutants in different over-expressing cell-lines (e.g. (85) and this thesis). Hence, residual activities found in functional studies may not be identical to those present in relevant MCT8-expressing tissues *in vivo*. Such cell-type specific differences may be related to several factors. First, the accuracy of protein quality control and

degradation systems may differ among cell-types. Second, factors that influence MCT8 function (i.e. interacting proteins, post-translational modification) may differ among tissues. Third, the role of MCT8 in cellular thyroid hormone homeostasis and its contribution to cellular thyroid hormone uptake and efflux likely depends on the presence of other transporters and may, as such, differ between cell-types. In case of over-expression studies, transfection efficacy may also importantly determine the occupancy of the cell membrane (as discussed in **chapter 5.1**). For these reasons it might be appropriate to study MCT8 mutations in vascular endothelial or neuronal cell lines, which are presumably the most relevant cell-types that express MCT8 *in vivo*. However, such studies are limited by the poor transfection efficacy (in case of over-expression models), or feasibility (in case of re-differentiated patient-derived iPSCs). Since several small scale studies in transiently transfected COS-1 and JEG-3 cells have indicated that the residual activity of mutant MCT8 proteins in these cell lines reflects the degree of intellectual disability in patients with MCT8 deficiency (78, 80, 86), these models apparently represent MCT8 function at critical sites in the human body.

In summary, the thyroid hormone transport capacity of mutant MCT8 can be quantified reasonably by *in vitro* over-expression systems as well as patient-derived fibroblasts. Large-scale genotype-phenotype studies should reveal if these models can serve to predict disease-specific outcomes.

CLINICAL AND BIOCHEMICAL PHENOTYPE IN FEMALE CARRIERS

Since the SLC16A2 gene is located on the X-chromosome, mutations therein mainly result in a clinical phenotype in males. Female carriers typically do not present with phenotypic characteristics of MCT8 deficiency because they have a second, unaffected, copy of the *SLC16A2* gene (87, 88). This results in the presence of functional MCT8 in at least a subset of cells. However, some female carriers reportedly have mild biochemical abnormalities that resemble those observed in affected male patients. Moreover, some of these carriers exhibited various degree of cognitive dysfunction (4, 57, 77, 86, 89, 90). This may be attributable to the presence of skewing in X-chromosome inactivation. In one extreme example, the inactivation of the X-chromosome was completely skewed due to the presence of an X-autosome translocation which affected the *SLC16A2* gene (91). Consequently, this patient manifested characteristic features of MCT8 deficiency observed in male patients with full inactivation of MCT8. However, it is unknown to what extent clinical features may arise if skewing is less severe. In **chapter 3.4** we extent on these previous reports and show that three female carriers of a pathogenic MCT8 mutation and skewing of X-chromosome inactivation in favor of the affected allele present typical endocrine features of MCT8 deficiency as well as neurocognitive and psychiatric features of variable severity. We demonstrated that MCT8 function was reduced in fibroblasts derived from these patients, and that residual MCT8 function in these cells was associated with the severity of intellectual disability. In addition, we found significant differences in serum thyroid function tests between these three female patients and other carriers who were self-reportedly a-symptomatic and non-carriers. In particular, the elevated total T3/rT3 and T3/free T4 ratios were clearly higher, which resembles the abnormal thyroid hormone profile observed in male patients with MCT8 deficiency. Although proving causality is always challenging in case of X-linked recessive disorders in female carriers, we believe these findings make a causal relationship very plausible. This is further supported by the absence of potentially pathogenic mutations in the coding regions of other genes that may explain the observed clinical features. For this reason, it would be recommended to screen thyroid function in female

patients with intellectual disability of unknown origin. As MCT8 deficiency is now not routinely considered in such cases, we speculate that this diagnosis might be otherwise missed.

The consequences of isolated endocrine features in female carriers remain to be determined. This would require further studies in a larger cohort of female carriers using standardized methodologies to measure thyroid hormone-related outcomes. The relatively low number of known female carriers and the many confounding factors that need to be addressed may pose major challenges in retrieving meaningful answers from such a study. It is yet unknown if treatment with thyroxine or thyroid hormone analogues is of potential benefit for symptomatic female carriers.

MECHANISMS OF DISEASE - MCT8 DEFICIENCY IN HUMAN AND ANIMAL MODELS

At time of the identification of the first patients (3, 4), the exact mechanisms by which MCT8 deficiency evokes the characteristic changes in serum thyroid hormone parameters and causes the severe neurological impairments were unclear. Tissue expression profiling in mice and humans as well as different animal models for human MCT8 deficiency have enhanced our understanding of the role of MCT8 in tissue thyroid hormone homeostasis and have provided insights regarding the pathogenesis of MCT8 deficiency. The principle findings of these studies will now be integrated with the clinical features described in **chapter 4.1**. For a full review on models for human MCT8 deficiency, the reader is referred to (92) and (93).

The role of MCT8 within the HPT axis and peripheral organs

Following the abundant expression of MCT8 in the hypothalamus, pituitary and thyroid gland, *Mct8* ko mice showed pronounced changes at all levels of the HPT-axis (30, 94-98). In these mice, serum thyroid function tests exhibit elevated serum T3, low T4 and low rT3 concentrations while TSH concentrations are in the normal range or even slightly elevated (98, 99). These features are in line with the characteristic thyroid hormone profile observed in patients with MCT8 deficiency (**chapter 4.1** and summarized in (100)). Supported by molecular studies and abnormal TSH suppression tests in mice and human MCT8 deficiency, the hypothalamus and pituitary are relatively insensitive towards thyroid hormones (98, 99, 101). Consequently, serum TSH concentrations are not a valid read-out parameter for assessing the general thyroid hormone status in MCT8 deficient patients. By contrast, the thyroid hormone content of the thyroid gland was highly elevated pointing to tissue-specific thyroid hormone excess suggesting an impaired thyroid hormone secretion (30, 31, 98).

It is still unknown what mechanism causes the increased serum T3/T4 ratio in MCT8 deficiency. It has been postulated that MCT8 may be of differential importance for thyroidal T4 and T3 secretion. Although T4 secretion is indeed reduced in *Mct8* ko mice, it is still unknown if the secretion of T3 is increased in these animals, as conflicting data have been published (30, 31). In athyroid MCT8 deficient mice as well as in one patient, the high T3 concentrations persisted during T4 replacement therapy, suggesting that another mechanism independent of the thyroid gland, at least partly, accounts for the altered T3/T4 ratios (31, 101). This may well be an increase in T4 to T3 conversion, as *Mct8* ko mice show strongly increased D1 activities in liver and kidneys, as well as increased D2 activities in brain, pituitary and skeletal muscle (98, 99, 102). The increased D1 activities in kidney, but not liver (103), appear primarily responsible for the altered T3/T4 ratio (104). Taken into account the increased

accumulation of peripherally injected radio-labeled T3 and T4 in kidney but not in liver homogenates of *Mct8* ko mice, it is tempting to speculate that renal efflux of T4 is compromised, resulting in a progressive built up of T4 in kidney. Together with the steep increase in renal D1 activity, this may represent the key event for generating the abnormal serum thyroid hormone parameters. Also in human MCT8 deficiency, kidney (and liver) appears to be in hyperthyroid state (**chapter 4.1**), which could be compatible with this hypothetical mechanism.

In line with the proxy parameters for muscular thyroid hormone status in patients, *Mct8* ko mice showed increased muscle T3 content along with anticipated changes in T3-regulated gene expression patterns of myosin heavy chains. Furthermore, analysis of muscle fiber composition in different skeletal muscle subtypes indicate a shift from slow-twitch to fast-twitch fibers as expected from a hyperthyroid muscle tissue (102, 105). Although thyroid hormone status in bone of patients is difficult to interpret in the context of their immobility, postnatal skeletal development and bone maintenance is compromised in *Mct8* ko mice (106). In particular the decreased bone mass and mineralization together with reduced bone strength observed in adult MCT8 deficient mice are typical changes linked to hyperthyroidism and may warrant more thorough evaluation of bone status in ambulatory patients with MCT8 deficiency.

Role of MCT8 in the brain

MCT8 is abundantly expressed in different cell-types in the brain and at different brain barriers in mice and human. In contrast to the human situation, brain development in *Mct8* ko mice was surprisingly normal, due to the presence of the T4-transporter OATP1C1 at the rodent, but not human BBB (as detailed in **chapter 1** and (92)). Mice deficient for both transporters have pronounced thyroid hormone deficiency in the central nervous system (CNS) and display similar neuropathological abnormalities as seen in MCT8 deficient patients ((107, 108) and **chapter 4.1**). In particular the presence of abnormal myelination and impaired axonal maturation in these mice is consistent with key features in the human MCT8 deficient brain (**chapter 4.1** and (107)), and indicates the involvement of both neurons and glia cells. These features may result from reduced T3 and T4 transport across the brain barriers, or from deficient uptake into target cells (**Figure 1**).

Role of MCT8 in neurons

The seemingly lack of overt neuronal damage in *Mct8* ko mice and normal response of cerebellar Purkinje cells to T3 treatment *in vitro* indicated that MCT8 is not critical for neuronal T3 uptake in mice (98, 109) and suggested the involvement of other, yet unknown, T3 transporters. The role of MCT8 in human neurons is currently unclear. Recent immunohistochemistry studies on human tissues demonstrated that MCT8 expression in cortical neurons particularly increases beyond gestational week (GW)32, which may support a minor role for MCT8 in earlier stages of neuronal development in human (43). MCT8 is also present in radial glia cells and Cajal Retzius cells, suggesting its involvement in neuronal specification, migration and/or differentiation (43). However, the absence of clear migration abnormalities on MRI scans of patients with MCT8 deficiency may argue against a critical role for MCT8 in these early neuro-developmental events (**chapter 4.1**). This may provide an important clue on the window of opportunity for interventions that restore thyroid hormone signaling in the brain. The minor role for MCT8 in neuronal specification and differentiation is supported by recent studies in re-differentiated patient-derived induced pluri-potent stem cells (iPSCs). These studies

showed that despite a decreased T3 uptake, the differentiation potential of these cells towards neuronal progenitors and beta III-tubulin expressing neurons was not greatly compromised, suggesting that sufficient amounts of T3 were imported even in the absence of MCT8 under the conditions tested (110). Further studies are thus needed to elucidate the role of MCT8 in neurons, which may well differ among neuronal populations and throughout development.

Role of MCT8 at Brain Barriers

The presence of MCT8 in vascular endothelial cells and choroid plexus structures strongly suggested a role of MCT8 at the BBB and the blood cerebrospinal fluid barrier (BCSFB) (see **chapter 1**). Recent protein expression studies in human tissues detected MCT8 in ependymocytes, leptomeningeal cells, and blood vessels in the subarachnoid space, as well as radial glia cells, suggesting that MCT8 may also facilitate the transfer of thyroid hormone across the inner and outer cerebrospinal fluid brain barriers (CSFBB) (43). It is unknown if the transfer of thyroid hormone across these barriers is physiologically relevant. Currently available evidence points to the BBB as the main entrance route for thyroid hormone into the brain, since D2 and D3 expression in the BBB is relatively low compared to other barriers (43) and only peripherally administered thyroid hormones reach all brain regions (111). Proof of functional relevance of MCT8 in human endothelial cells was ultimately provided by *in vitro* studies using iPSC-derived BMECs. Indeed, MCT8 deficient BMECs cultured in specialized wells to induce BBB-like features exhibited a reduced T3 uptake and transported significantly lower levels of T3 from the blood to the brain compartment of the BBB model system (110).

Role of MCT8 in glia cells

The role of MCT8 in glia cells has not been extensively investigated so far. Although MCT8 is expressed in several astrocyte population in fetal and adult human brain, it is unclear o which extent MCT8 contributes to the cellular uptake of thyroid hormone in these cells (43, 95, 112, 113).

It is well established that thyroid hormone plays a major role in myelination by controlling oligodendrocyte differentiation and maturation and the production of main myelin proteins (114). In agreement with the critical role of thyroid hormone in myelination, delayed myelination is a hallmark on brain MRI in patients with MCT8 deficiency (52, 53, 115, 116) and pronounced microscopic changes in myelin content are observed in the MCT8 deficient mouse and human brain ((107) and **chapter 4.1**). These alterations might well be direct consequences of reduced brain thyroid hormone content, but also of deficient T3 uptake into oligodendrocytes and/or its precursor cells (117). However, reduced myelination secondary to poor neuronal development cannot be completely excluded.

Taken together, MCT8 appears to be predominantly important at the BBB, although a pivotal role in other cells during distinct developmental stages is certainly not excluded.

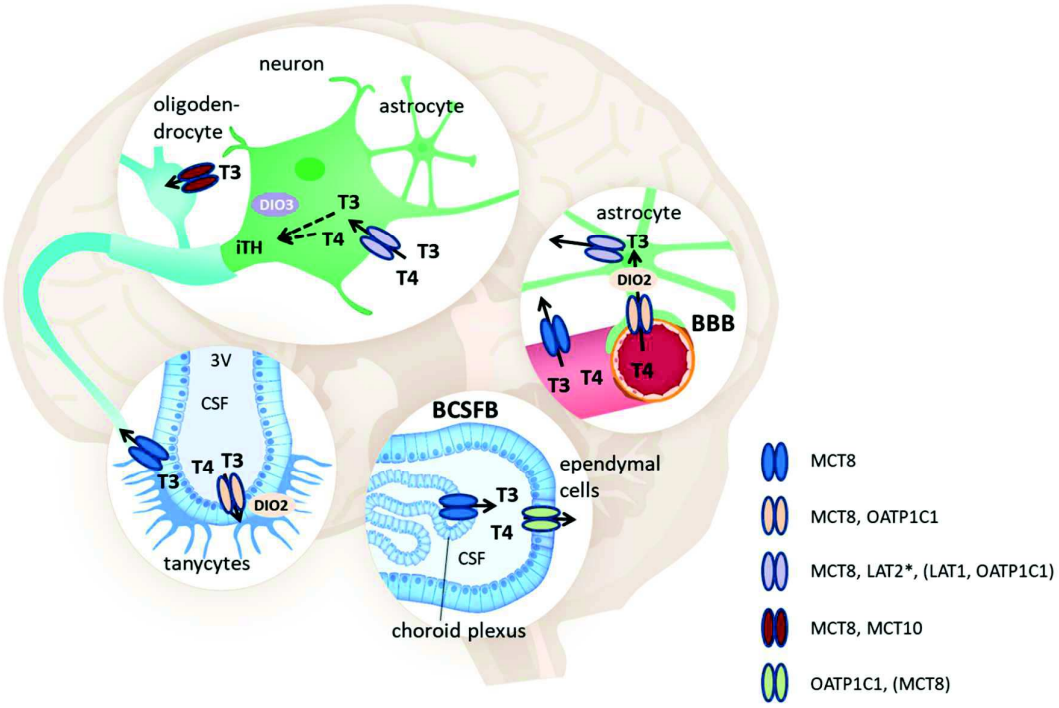

Figure 1 A putative model of thyroid hormone signaling in the human brain based on the available studies. In order to exert its effects inside the brain, thyroid hormone needs to cross multiple barriers. This cartoon provides a schematic overview of the different barriers in human brain where MCT8 and OATP1C1, and possibly additional transporters, might be involved in the transport of thyroid hormone. It should be noted that in most cases definite proof of functional contribution to thyroid hormone transport is lacking. Moreover, it should be emphasized that the expression and contribution of the various thyroid hormone transporters likely depends on the developmental stage and vary between different cell populations of the same tissue. It is also unclear to what extent transporters other than those displayed in this cartoon are expressed at protein level at the different sites and contribute to thyroid hormone transport in the human brain. * LAT2 is localized to adult neurons and microglia, but is absent in fetal neurons. Recently proposed novel routes by which thyroid hormone may enter the brain through the inner and outer cerebrospinal fluid brain barrier are not depicted. Abbreviations: iTH, inactivated thyroid hormones; BBB, blood-brain barrier; BCSFB, blood-cerebrospinal fluid barrier; CSF, cerebrospinal fluid; 3V, third ventricle. Adapted from Groeneweg et al., Endocr Rev., 2019 (92).

Thus, in light of the currently available evidence, the current paradigm of MCT8 deficiency still holds that tissues that importantly rely on functional MCT8, especially the brain, reside in a hypothyroid state, whereas tissues that mostly rely on transporters other than MCT8 are exposed to the elevated serum T3 concentrations which results in symptoms of tissue thyrotoxicosis (**Figure 2**). However, this paradigm might need expansion, as it does not accommodate tissues that rely on MCT8 for cellular thyroid hormone efflux. These tissues, including the kidney and thyroid gland, may also reside in a hyperthyroid state due to progressive intracellular accumulation of T4 and T3. Thus, the impact of MCT8 deletion on cellular thyroid hormone homeostasis is ultimately determined by the presence of redundant thyroid hormone transporters and the role of MCT8 in the cellular system.

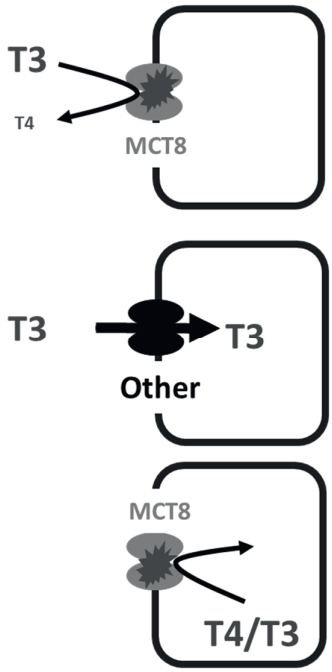

Hypothyroid

CNS – developmental delay, intellectual disability
Pituitary – dysproportional TSH

Hyperthyroid

General – low body weight, increased perspiration, increased metabolism
Cardiovascular – tachycardia, PACS, hypertension
Liver – increased SHBG, low cholesterol, (high TH content)
Muscle – muscle wasting, low creatinine
Kidney – low creatinine, (high TH content)
Thyroid – (high TH content)

Figure 2 Schematic representation of the pathophysiology of MCT8 deficiency based on the available human and mouse data. Features that were specifically observed in mice are indicated between brackets. The current paradigm of MCT8 deficiency holds that tissues that largely rely on MCT8 for cellular thyroid hormone uptake, including the brain, reside in a hypothyroid state; whereas tissues that rely on transporters other than MCT8 reside in a hyperthyroid state due to exposure to the elevated serum T3 concentrations. In addition, tissues that mainly rely on MCT8 for cellular efflux may also reside in a hyperthyroid state (indicated in bold).

THERAPEUTIC APPROACHES IN MCT8 DEFICIENCY

It is beyond doubt that development of effective treatment for MCT8 deficiency has high priority. Effective therapy for MCT8 deficiency entails 1) restoring thyroid hormone signaling in the brain and 2) alleviating the thyrotoxic state in peripheral tissues. The therapeutic approaches that have been investigated over the last decade are summarized and discussed in this section. **Table 1** provides a summary of the effects of those treatments applied in patients.

Classical (anti-)thyroid drugs

Based on the low serum FT4 concentrations and modestly increased TSH concentrations, many patients have been suspected for mild (central) hypothyroidism and 25 of them have been commenced on levothyroxine (L-T4) (3, 4, 45, 57, 60, 70, 86, 118-131) (**Table 1**). However, LT4 treatment had no obvious beneficial effects on neurodevelopment. Instead, in at least four cases serum T3 concentrations further increased and aggravated the peripheral thyrotoxicosis.

Five patients have been reportedly treated with antithyroid drugs, alone or in combination with L-T4 (56, 69, 132-134). Administration of methimazol had no effects on the serum thyroid function tests (134). Alternatively, the administration of propylthiouracil (PTU), which not only blocks thyroid hormone production but also inhibits the T4 to T3 conversion, combined with L-T4 has shown some

clinical benefits in several patients (56, 69, 134). After 10-24 weeks of treatment with PTU, (F)T3 concentrations normalized, (F)T4 concentrations decreased and TSH concentrations increased. When L-T4 was added, serum thyroid function tests largely normalized and the thyrotoxic state in peripheral tissues was alleviated as evidenced by improvement of body weight, heart rate, and serum markers of tissue thyroid hormone state (56, 134). No beneficial effect was observed on neurodevelopment, although treatment had been initiated at relatively advanced age (69) (**Table 1**). Importantly, the treatment with PTU was stopped in one patient due to the occurrence of hypogranulocytosis (69). Due to this and other potential side-effects of PTU, including hepatotoxicity, the use of PTU for treatment of hyperthyroidism is discouraged, in particular in children (135).

Thyroid hormone analogues

The lack of beneficial effects of L-T4 treatment on neurodevelopment has been attributed to the impaired transport of L-T4 across the BBB and into the ultimate target cells in the brain. This prompted studies to the application of thyroid hormone analogues, which enter the cell independent from MCT8, but exert similar effects as T3 once inside the cell. The general hypothesis underlying the potential therapeutic mechanism of these analogues consists of the simultaneous inhibition of TSH secretion and hence endogenous thyroid hormone production, while providing adequate thyromimetic effects in all body tissues, including the brain (136). Following promising results in preclinical studies (summarized in **chapter 1**), two thyroid hormone analogues diiodothyropropionic acid (DITPA) and Triac, have been applied in patients with MCT8 deficiency so far.

Four patients with MCT8 deficiency have been reportedly treated with DITPA (**Table 1**), which normalized the high serum T3 concentrations in all four patients and improved several markers of peripheral thyroid hormone action, including serum SHBG concentrations. Heart rate and body weight were unchanged in two patients (69). No improvements were observed in neurodevelopment. Interestingly, TSH concentrations did not drastically decrease, whereas T4 concentrations even increased under DITPA treatment. This may suggest that DITPA is not inhibiting TSH secretion in human, but rather reduces D1 and D2-mediated conversion of T4 to T3. Indeed, studies in mice showed a pronounced reduction of D1 and D2 activity in mice treated with DITPA.

In 2014, we launched a clinical trial that primarily evaluated the potency of Triac to alleviate the thyrotoxicosis in peripheral tissues (**chapter 5.2**). In this international, multicenter, open-label, single arm, phase 2 trial, 46 patients with MCT8 deficiency were enrolled and treated with Triac. The Triac dose was increased according to a predefined dose-escalation protocol until serum T3 concentrations were within the target range of 1.4-2.5 nmol per liter. Forty patients finished the 12 months of treatment, of whom ten entered an open-label treatment extension period. Triac treatment effectively lowered serum T3 concentrations in all patients and was associated with improvements in heart rate and blood pressure. The occurrence of premature atrial complexes largely subsided in the majority of patients. Moreover, under Triac treatment, body weight to age z scores increased and clearly deviated from the natural history in those subjects enrolled in the treatment extension period. In addition, serum markers for tissue thyroid hormone state including SHBG concentrations improved. Together, these observations indicated that several key features related to the peripheral phenotype of MCT8 deficiency are alleviated under Triac treatment in pediatric and adult patients. Although the study design and lack of control for confounding factors precludes proving causality between these effects and the intervention, based on its known biological action, which is supported by high quality evidence

in animal models, as well as previously reported preclinical and clinical studies, it is plausible that Triac decreases T3 concentrations through the central inhibitory effect of Triac on pituitary TSH synthesis and secretion resulting in alleviation of well-known consequences of tissue thyrotoxicosis.

Explorative analysis showed an improvement in motor function in patients who commenced on Triac before 4 years of age. Since this trial was not designed to detect changes in neurodevelopment, a second phase 2 trial (NTC02396459) with a focus on neurodevelopment and specific neuro-developmental endpoints is currently being designed to provide a more definitive answer if Triac administration results in modulation of neurocognitive development. At this stage, the observed changes in neurocognitive and motor endpoints do at least not suggest a further decline in neurocognitive function, justifying the conduction of a consecutive trial. This trial will specifically enroll very young infants in an attempt to start treatment as close as possible to the putative window of opportunity to modulate brain development. Being very efficient in rescuing the neurodevelopmental phenotype observed in *Mct8/Oatp1c1* ko mice once administrated from post-natal day 1, the outcome of this trial will provide important guidance on the required timing of treatment in human. In this context it should be emphasized that important processes of fetal brain development in human occur in the early postnatal period in mice – an important difference that may determine the effectiveness in human. With this in mind, it would be of interest to study the impact of Triac on neurodevelopmental features in *Mct8/Oatp1c1* ko mice once treatment is commenced somewhat later in life. It also remains largely elusive how Triac enters its target cells and if these processes differ between species. This will importantly determine the cellular availability of Triac in target tissues. Further studies should aim identifying these transporter(s), in particular in brain cells.

In addition to DITPA and Triac, also other thyroid hormone analogues are currently being studied in a preclinical setting, including sobetirome and its prodrug Sob-AM2 (137, 138). Both compounds accumulated in brain of *Mct8/Dio2* dko mice, with Sob-AM2 yielding higher final sobetirome concentrations in the brain. In the cerebral cortex of these animals, both compounds restored the expression levels of some, predominantly, neuronal TH-target genes, whereas TH-target genes in astrocytes and oligodendrocytes showed only minor changes (137). Although both compounds lowered the strongly elevated serum T3 concentrations in *Mct8/Dio2* dko mice, the expression levels of several thyroid hormone target genes in heart and liver did not restore to levels observed in wild-type animals (137). In fact, some markers in liver even further deteriorated, indicating worsening of the thyrotoxic state in at least some peripheral tissues. Future studies should investigate the effects of these and other thyromimetic drugs in additional animal models for human MCT8 deficiency and compare their effects and safety profile to the clinically available thyroid hormone analogue Triac. In contrast to Triac, DITPA is no longer clinically available. For this reason treatment with Triac is the only therapeutic option currently available that may modulate the symptoms of MCT8 deficiency.

Gene therapy

Since MCT8 deficiency is a monogenetic disorder, gene therapy theoretically poses an attractive treatment to restore MCT8 function in tissues where it is of most physiological relevance. The first pilot studies in *Mct8* ko mice indicated that intravenously administrated AAV9-MCT8 increased the expression of functional MCT8 at the BBB and brain T3 concentrations (140). It is however unclear if the moderate increase in MCT8 expression is sufficient to adequately restore thyroid hormone signaling in the brain.

Table 1 Overview of treatment effects in MCT8 deficient patients

	LT4	**LT4+PTU**	**DITPA***	**TRIAC**
Type of study	Case reports/series	Case reports	Case series	Phase II clinical trial
Refs	(3, 4, 45, 57, 60, 70, 86, 118-131)	(56, 69, 132-134)	(69)	(139)
N	25	5	4	46
Dose ranges	2.5-15 µg/kg/day (~25-150 µg/day)	2.5-10 µg/kg/day (~25-100 µg/day) + 200-400 mg/day	1~2 mg/kg/day	13-88 µg/kg/day
Age at start in months - M (range)	20 (0.5-36)	20 (19-456)	25 (8.5-25)	85 (10-800)
Duration in months - M (range)	Variable (often n.d.)	~8.5 (1-16)	~37 (26-40)	13 (0.5-42)
Effects				
T3	=/↑	↓	↓	↓
(F)T4	=/↑	↑	↑	↓
TSH	↓	↓	=	↓
SHBG	n.a.	↓	↓	↓
Body weight	↓	↑	~	↑
Heart rate	n.a.	↓	↓	↓
Development	=	=	=	~/=
Drug-related adverse outcomes	Increase in peripheral thyrotoxicity	Hypogranulocytosis	Not observed	Transient mild signs of hyperthyroidism during initiation of treatment
Recommendation	Avoid: Not effective Side-effects	Avoid: Side-effects	Consider	Recommended

Treatment effects have been scores as follows: for case reports and series the direction of the response observed in the majority (>50%) of cases with available data is provided; for clinical trial the direction of the response at group level is provided (where = is used for responses that were not statistically significant at group level). *DITPA is not available for purchase.

It also remains to be investigated whether re-expression of MCT8 at BBB is sufficient to restore thyroid hormone action in the CNS since at least during development, MCT8 is expressed in a broad variety of other cell types in the brain, including neurons and glial cells. In this context, it would be relevant to study the effects of gene therapy in other (mouse) models for human MCT8 deficiency, as the *Mct8* ko mice used in the only available study do not exhibit clear brain abnormalities. As outlined in the **Introduction** and **this chapter**, expression of MCT8 in different tissues follow distinct spatiotemporal patterns. Therefore, expression of MCT8 under control of a constitutively active promoter may pose a risk to expose cells during certain developmental stages to excessive amounts of thyroid hormone, the consequences of which are unknown. Ideally, such vectors should contain the native MCT8 promoter to mimic the dynamics of MCT8 expression as closely as possible. Further studies are thus warranted to optimize the gene delivery strategy and assess its safety. Should gene therapy be effective and safe, it would have obvious practical advantages over life-long medicinal treatments.

Other types of gene therapy, such as gene editing by CRISPR-Cas methodologies, are currently not pursued as a treatment for MCT8 deficiency. In particular the wide-spread distribution of MCT8 in brain poses a limitation for this approach. Yet, this technique already proved to be a valuable tool in fundamental research (e.g. (110)).

Chemical chaperones

For a subset of mutations the application of chemical or pharmacological chaperones could restore MCT8 function by improving the folding and trafficking of misfolded mutant MCT8 proteins. Several studies of Braun et al in stably transfected MDCK-1 cells suggested that the function of certain mutant MCT8 proteins can be enhanced by treatment with phenylbutyrate or dimethylsulfoxide, and to a lesser extent with genistein (141, 142). Especially those mutations that have been associated with a relatively less severe clinical phenotype, such as the p.F501del mutation, appear to respond to this intervention *in vitro*. Complementary studies in transiently transfected COS-1 cells revealed that treatment with phenylbutyrate pronouncedly increased *MCT8* expression levels of wild-type and mutant MCT8 transfected cells, suggesting that this intervention has pronounced effects at transcriptional level (**chapter 5.1**). Since the transcriptional control of MCT8 is under control of an artificial promoter in both the transiently and stably transfected cell lines it can be questioned if phenylbutyrate also exerts a stimulatory effect on MCT8 expression in the context of its native promotor. However, this appeared not to be the case in *ex vivo* studies in fibroblasts derived from a patient with this p.F501del mutation (**chapter 5.1**). Further studies are required to assess the effectiveness of chaperones in other models for human MCT8 deficiency, including iPSC-derived vascular endothelial cells and neurons, as well as *in vivo* models for MCT8 deficiency. The latter would require the knock-in of a mutant *Mct8* gene. It should be considered that chaperone treatment is an unspecific approach that may also have significant off-target effects, including unfavorable effects on the body nitrogen pool.

Supportive care

Since therapeutic interventions that effectively restore euthyroidism in all tissues are currently lacking, symptomatic treatment is often necessitated to treat key clinical features such as dystonia and spasticity and seizures. Moreover, a substantial number of patients reportedly required tube feeding to safeguard sufficient dietary intake and/or prevent aspiration. However, many studies did not report in detail on the use of co-medication and the occurrence of co-morbidities, which hampers proper identification of common medical concerns in MCT8 deficiency and the assessment of the effectiveness of symptomatic interventions. The MCT8 patient registry aims to collect detailed data on the use of and experiences with symptomatic treatment and supportive measures. This will guide future studies to maximize effectiveness of such interventions and unravel putative etiologies.

Considerations for treatment development

The conduction of clinical trials in rare disorders is often very challenging due to the limited number of eligible patients, often located in different countries, and the relatively high ethical and financial burden. In case of MCT8 deficiency, the low prevalence, the severe clinical phenotype and absence of effective therapies to modulate brain development preclude placebo-controlled trials from an ethical perspective. Also other (quasi)controlled designs are generally not well-suited or desirable to assess the impact of any intervention on neurodevelopment. One of the few remaining alternatives to prove

effectiveness is a strong natural history that may serve as a historical control group, which underscores the relevance of our studies presented in **chapter 4.1**. Although this potentially allows future single-arm studies, an international collaborative effort is nonetheless needed to streamline preclinical and clinical research on different therapeutic approaches with the ultimate goal to safeguard that at least one of the interventions obtains formal registration and will be clinically available for patients outside clinical trials.

The ultimate question which remains to be addressed concerns the timing of treatment onset. It is unclear at what stage of brain development therapeutic interventions should be initiated to have a reasonable chance to modulate brain development. MCT8 is already highly expressed in some cell-types during early fetal brain development, which at that stage depends on adequate thyroid hormone concentrations (143-146). Although the level of dependence of these cells on functional MCT8 is largely unknown, the presence of neuropathological changes in the brain of an MCT8 deficient fetus ((107) and **introduction**) suggests that MCT8 may indeed be critical in at least some cells during early developmental stages. It is yet the question to which extent the observed changes are still modifiable during later stages of development should thyroid hormone signaling be restored. Importantly, in some cell-types, including neuronal cells in the cerebral cortex, MCT8 expression only starts to increase from GW32 onwards (43), suggesting that the window of opportunity may differ between cells and may extend to late-embryonic stages. This is seemingly supported by the lack of obvious neurological abnormalities in the early postnatal period in MCT8 deficient neonates, evidenced by a good APGAR score and, thus, absence of hypotonia. Therefore, it seems plausible that initiation of therapeutic interventions prenatally would yield highest benefit, although early postnatal initiation may still have significant beneficial effects. Obviously this dilemma applies to all interventions. Nonetheless, early initiation of treatment would be key to maximize therapeutic benefit, not only to modulate the neurocognitive phenotype, but also to alleviate the thyrotoxic state of peripheral organs and thus improve the physical condition and growth. Efforts should thus be made to improve early diagnosis of MCT8 defciency (see **this chapter: diagnostics challenges**).

Diagnostic challenges

Diagnosing MCT8 deficiency can be challenging, as is evidenced by the large diagnostic delay in many patients, with a median time to diagnosis of 2 years, range 0-744 months (**chapter 4.1**). This is most likely attributable to the observation that affected children typically present with unspecific signs and symptoms including failure to thrive and feeding problems in the first months of life. Therefore, the link with aberrant thyroid hormone action can be easily missed. Aside from (next-generation) sequencing approaches, measurement of serum thyroid function tests would yield an important clue to properly diagnose MCT8 early in life. Measurement of thyroid function should therefore be considered in all individuals with (severe) developmental delay. For this purpose, it is important to include the measurement of (F)T3 concentrations in addition to the routinely performed (F)T4 and TSH measurements to avoid misdiagnosis. The combination of low or low-normal (F)T4 concentrations and normal (to slightly elevated) TSH concentrations is often misinterpreted for secondary hypothyroidism, further delaying the diagnostic process and in some occasions unnecessary side-effects of treatment with L-T4.

For similar reasons, MCT8 deficiency is unlikely to be detected with the currently employed neonatal screening programs for congenital hypothyroidism. In most countries, these programs are based on

measurement of TSH concentrations alone, while in a small number of countries the measurement of T4 concentrations is the first step of the screening procedure. With either approach, the presence of normal TSH concentrations precludes affected children from being diagnosed with congenital hypothyroidism despite serum T4 concentrations being low in affected neonates (**chapter 4.1** and (79)). It remains to be studied if newborns with MCT8 deficiency already display the characteristic thyroid hormone profile and to what extent measurement of additional thyroid function tests during neonatal screening is technically and economically feasible. Although the pattern of the abnormal thyroid function tests is rather specific for MCT8 deficiency, a similar profile can be observed in patients with resistance to thyroid hormone (RTH) α due to mutations in *THRA,* encoding thyroid hormone receptor α (147).

The increasing availability of next-generation sequencing in clinical practice will undoubtedly increase the number of patients diagnosed at a relatively younger age. However, the results of next-generation sequencing should always be interpreted in the context of the clinical presentation, serum thyroid function tests and, if available, *in vitro* or *ex vivo* confirmation of reduced thyroid hormone transport by the mutant transporter. As illustrated in **chapter 3.3** it is of utmost importance to conduct these functional studies to establish the pathogenicity of novel variants as some of these variants can be benign. This may lead to misdiagnosis and further delay in installment of proper treatment.

THE PHYSIOLOGICAL RELEVANCE OF OTHER THYROID HORMONE TRANSPORTERS

The relevance of transporters other than MCT8 in maintaining cellular thyroid hormone homeostasis is evident from the residual thyroid hormone uptake in many tissues in absence of MCT8. Yet, it has been poorly defined to what extent the transporters that have been currently shown to transport thyroid hormone *in vitro* also contribute to thyroid hormone homeostasis *in vivo*. In fact, it is even questionable whether they function as thyroid hormone transporters *in vivo* at all, as most of these transporters also accept a broad variety of substrates other than iodothyronines. To address this important issue, several ko animal models have been studied over the years. Moreover, patients with genetic defects in several of these transporters have been recently identified, of which the description of the first patient with OATP1C1 deficiency is described in **chapter 6.4**. This section will summarize the knowns and unknowns of these transporters in thyroid hormone signaling.

OATP1C1

In rodents, OATP1C1 is highly expressed in the brain where it was detected in capillary endothelial cells, choroid plexus structures and astrocytes (see **chapter 1**). Given its very restricted expression pattern, it is not surprising that *Oatp1c1* ko mice do not show any alterations in serum thyroid hormone profile nor any signs for an altered thyroid hormone content in peripheral tissues (148). However, brain T4 content of *Oatp1c1* ko mice was decreased to around 60 % compared to healthy littermates, which is likely attributable to a reduction in blood-brain T4 transport (108, 148). Notably, D2 activities in brain were threefold elevated indicating that D2-expressing cells (e.g. astrocytes (146)) are in a T4 deficient state. As a consequence, brain T3 signaling was only slightly reduced in *Oatp1c1* ko mice, presumably due to increased local T3 production and the presence of MCT8 which ensures normal T3 transport across brain barriers in these animals.

OATP1C1 is also expressed in the human CNS, where its expression pattern and timing shows a remarkable overlap with MCT8 (43), with at least one noticeable exception. In contrast to the situation in rodents, OATP1C1 is not expressed at the human BBB. Assuming that the BBB is the main route by which thyroid hormone enters the brain, the human CNS is thus probably most dependent on MCT8. Nevertheless, it is not excluded that OATP1C1 may contribute to the transport of thyroid hormone across the inner and outer CSFBB and the BCSFB (43). Importantly, OATP1C1 is also expressed in astrocytes populations, including those surrounding the vascular endothelial cells of the BBB, which may point to a distinct role of OATP1C1 in these cells.

In **chapter 6.4** we described the first case of OATP1C1 deficiency, which first proved its relevance for normal CNS function. This concerned a 15.5 year-old girl with apparent normal development in the first two years of life, who gradually developed autistic features and presented with progressive deterioration of cognitive and motor functions. In addition, she developed intolerance for cold. These clinical features were accompanied by gray and white matter degeneration and severe cerebral glucose hypometabolism. As in *Oatp1c1* ko mice, Serum free T4, free T3 and TSH concentrations were repeatedly within normal range. Exome sequencing identified a homozygous c.754G>A; p.D252N mutation that was shown to considerably diminish OATP1C1 transporter function *in vitro*.

The exact mechanisms underlying the clinical features observed in the patient are currently not known. However, several observations support the assumption that at least part of the phenotype can be ascribed to insufficient T4 uptake in OATP1C1-expressing astrocytes, which would lead to reduced availability of T3 to target cells within the CNS. At first, the presence of a strong reduction of brain glucose metabolism is compatible with a hypothyroid state of the brain (149). The presence of cerebellar ataxia and autistic features have both been linked to a hypothyroid state in brain (150-152). In addition, the presence of subcortical white matter atrophy may indicate deficiency of thyroid hormone in oligodendrocytes (153). Finally, treatment with the T3-analogue Triac appeared to halt the progression of the clinical course in the patient. The identification of additional cases will further advance the understanding of the mechanism of disease underlying OATP1C1 deficiency.

Other OATPs

Details on thyroid hormone homeostasis in animal models deficient in other OATPs are currently lacking. It should however be realized that many of these OATPs show a relatively low affinity towards iodothyronines and transport a multitude of other substrates. In addition, the organization of some of the OATP(sub)families is very different in humans than in mice and rats since some members have not been conserved among species (154, 155). For these reasons, it is currently unclear if all OATPs that were found to transport thyroid hormone *in vitro*, also exert meaningful contributions to cellular thyroid hormone homeostasis *in vivo*. Analyses on the association of common genetic variants with serum thyroid hormone concentrations indicated that common variants in ubiquitously expressed OATP1A2 and the liver-specific OATP1B1 are associated with serum T3 and T4(S) concentrations in healthy blood bank donors, respectively (13, 156). Only in case of the OATP1B1 variant, diminished transport of T4S was observed, suggesting a role for OATP1B1 in the uptake of T4S and possibly other sulfo-conjugated iodothyronines in liver (13, 156). Interestingly, this variant was also found to be significantly associated with serum free T4 concentrations in our recent genome-wide association study (**chapter 6.1**).

MCT10

In rodents, *Mct10* is particularly expressed at small intestinal epithelial cells, renal proximal tubule cells, follicular epithelial cells of the thyroid, and in perivenous hepatocytes, where its expression in brain appears limited. *Mct10* ko mice exhibit increased plasma, muscle and kidney aromatic amino acids, but no alterations in thyroid hormone homeostasis or brain development (33). Nevertheless, studies in *Mct8/Mct10* dko mice suggested that MCT10 and MCT8 cooperatively regulate tissue thyroid hormone homeostasis in liver, kidney and thyroid (157). In these animals, thyroid hormone content in liver, kidney and thyroid was even further elevated than in *Mct8* single ko animals, suggesting that MCT10 significantly contributes to T3 efflux in these tissues if MCT8 is missing. Also in the cochlea, skeletal muscle and in bone, MCT8 and MCT10 appear to collaboratively contribute to tissue thyroid hormone homeostasis (102, 158-160). Yet, MCT10 cannot fully compensate for loss of functional MCT8, presumably due to differences in basic transporter properties and spatiotemporal expression, particularly in brain.

In human, some common genetic variants in the MCT10 locus were found to modulate serum FT4 concentrations (161) or, in conjunction with D2 polymorphisms, the preference for L-T4+L-T3 *versus* L-T4 replacement treatment in hypothyroid patients (162). No patients with MCT10 deficiency have been reported thus far. It is unknown if such patients would manifest abnormal serum thyroid function tests, or rather display alterations in serum (or urinary) amino acids as main biochemical finding. The increasing application of next generation sequencing may help identifying such mutations and resolving the role of MCT10 in thyroid hormone signaling in human.

SLC17A4

Through a meta-analysis of available genome-wide association studies on FT4 and TSH concentrations, we identified the orphan transporter SLC17A4 to be associated with serum FT4 concentrations (**chapter 6.1**). Subsequent *in vitro* studies in a mammalian over-expression system showed that SLC17A4 potently induced the intracellular accumulation of T3 and T4. Its affinities for T3 and T4 are in the sub-micromolar range and therefore among the highest of all thyroid hormone transporters identified to date. In **chapter 6.2**, we further detailed the functional characteristics of SLC17A4 and demonstrated that it preferentially facilitates the uptake and, also, the efflux of T3 and T4. SLC17A4-mediated T3 uptake was effectively inhibited by different iodothyronines and metabolites thereof, including Triac and Tetrac, suggesting that these compounds might also be suitable substrates. Indeed, SLC17A4 also increased the cellular uptake of Triac. The uptake of T4 was found to be Na^+-independent and pH-sensitive, with highest uptake efficiency at low extracellular pH.

The SLC17 family consists of nine structurally related proteins that have been identified as organic anion transporters (163). From an evolutionary perspective it is important to realize that SLC17A1-4 appear to be the most recent members of the SLC17 family, and are only present in mammals (164). As such, frequently used animal models in thyroid research other than mice, such as zebrafish, chicken and *Xenopus*, will be of limited use for determining SLC17A4 function *in vivo*. To assess the eligibility of mice as a model to study human SLC17A4 function, we also characterized the functional properties of the mouse SLC17A4 orthologue in **chapter 6.3**, which turned out to be very similar.

The physiological role of SLC17A4 is currently unclear. Previous studies showed that SLC17A4 is predominantly expressed in liver, small intestine, colon and pancreas (165). Although further studies

should detail the exact sub-cellular distribution of SLC17A4 in these cells, it is tempting to speculate that SLC17A4 is important for the gastro-intestinal absorption of thyroid hormones. This would be a crucial step in the entero-hepatic cycle of thyroid hormone, but also for the absorption of L-T4 in patients with hypothyroidism. Further studies in *Slc17a4* ko mice will reveal the relevance of SLC17A4 for cellular thyroid hormone transport in the intestinal tract and will help elucidating the mechanism by which it regulates serum T4 concentrations.

LATs

Though several members of the L-type amino acid transporter family were shown to transport iodothyronine *in vitro*, most importantly LAT1 and LAT2, mouse mutants have largely failed to provide solid evidence for such a function *in vivo* thus far. The phenotype of the respective global ko mouse can be dominated by an impaired amino acid transport that can lead to malnutrition and premature death as observed in LAT4 (SLC43A2) deficient animals (166).

Homozygous inactivation of the catalytic subunit LAT1 (SLC7A5) in mice causes embryonic lethality while heterozygous *Lat1* animals are viable, fertile and phenotypically similar to wild-type littermates (167). Most importantly, several patients diagnosed with autism spectrum disorder and motor problems were shown to harbor inactivating mutations in LAT1 (168). Though the neurobehavioral phenotypes of BBB-specific *Lat1* mouse mutants and the symptoms of LAT1 patients may be largely explained by reduced concentrations of branched chain amino acids in brain, it still needs to be unraveled to which extent LAT1 contributes to passage of thyroid hormones into and within the mouse and human CNS.

Global *Lat2* ko mice are viable and fertile and exhibit normal (169), or slightly decreased (170) thyroid hormone parameters in serum, brain, liver and kidney. In line, concomitant deletion of LAT2 and MCT8 had only subtle transient effects on brain thyroid hormone concentrations compared to *Mct8* ko mice (171, 172). Therefore, the role of LAT2 in thyroid hormone transport *in vivo* appears to be limited. *Lat2* ko mice rather display a moderate neutral aminoaciduria and vestibular damage (169, 173). In line, mutations in LAT2 were found in patients with age-related hearing impairment (173). It remains to be determined whether a disturbed local thyroid hormone homeostasis represents a major pathogenic mechanism underlying this phenotype.

NTCP

Genetic defects in the liver-specific NTCP have been identified in several patients with conjugated hypercholanemia (174-178). In at least one of these patients, serum thyroid function tests have been conducted which were reported to be normal (174). However, since NTCP predominantly transports sulfo-conjugated iodothyronines, more extensive biochemical studies will provide additional insights into the effects of such mutations on thyroid hormone homeostasis, particularly in liver. The thyroid hormone status in *Ntcp* ko mice is not known. Given its broad substrate specificity and high affinity for alternative substrates, it is tempting to speculate that NTCP functions as a general hepatic anion transporter in liver rather than a specific thyroid hormone transporter.

FUTURE PERSPECTIVES ON THYROID HORMONE TRANSPORTERS

The number of transporter proteins found to transport thyroid hormones or metabolites thereof is continuously growing, with about 16 transporters identified to date. One of the challenges remains to elucidate the contribution of each individual transporter to the complex regulation of tissue thyroid hormone homeostasis. Some thyroid hormone transporters also accept a wide range of alternative substrates, which concentrations in plasma or urine are much closer to the apparent transporter Km values than it is the case for thyroid hormone, which only has free plasma concentrations in the picomolar range. Although the presence of a multitude of thyroid hormone transporters may provide a sophisticated system to secure adequate thyroid hormone supply in every tissue, some transporters may be more relevant than others. This is illustrated by the devastating effects on brain development of defects in MCT8, which is considered the most crucial thyroid hormone transporter. Yet, the recent identification of a patient with apparent OATP1C1 deficiency illustrates that defects in transporters other than MCT8 may also result in novel syndromes of resistance to thyroid hormone with tissue-specific alterations in thyroid hormone state. The increasing availability of next-generation sequencing in clinical practice and the establishment of global data repositories will help identifying individuals with (pathogenic) variants in thyroid hormone transporters and establish their clinical and biochemical effects.

At the same time, effort should be made to improve knowledge of known disorders associated with thyroid hormone transporter defects. For MCT8 deficiency, it is imperative to further expand the systematic description of the various dimensions of the phenotype and detail their progress over time. Such a natural history is crucial to recognize common features of the disorder which allows optimization of patient care, and to establish a historical control cohort that can be used in the efficacy and safety assessments of any potential novel therapies that reach the clinical stage. The recently established patient registry will certainly contribute to achieving this goal. For OATP1C1 deficiency, identification of additional patients will be of great value to better establish the features of this novel disorder and gain insights into its exact pathophysiology. To this end, the establishment of suitable animal models that mimic human features as well as cell-based models will be needed to disentangle the underlying molecular alterations.

It is beyond doubt that establishing an effective therapy for MCT8 deficiency will be one of the major tasks of the field. Research over the last years predominantly focused on the use of thyroid hormone analogues of which DITPA and in particular Triac showed promising results in preclinical studies (105, 179, 180). In **chapter 5.2**, we showed that Triac effectively ameliorates the peripheral phenotype of MCT8 deficiency, which has long been an unmet medical need for patients with this disorder. Further clinical studies will reveal if and to which extent Triac can positively modulate neurodevelopment. Additional lines of ongoing research focus on alternative approaches to restore or circumvent defective MCT8, including gene therapy and application of other thyroid hormone analogues or chaperone molecules in selected patients.

Another major remaining challenge is to elucidate the contribution of individual thyroid hormone transporters to cellular thyroid hormone homeostasis under physiological and pathophysiological conditions. Although the profound phenotypes of patients with specific transporter defects have provided an answer to some questions, many others remain to be addressed through studies in animals and advanced cellular models. It should certainly be acknowledged that global ko animals may

not always pose the most optimal model to study the respective thyroid hormone transporter function in selected organs as it may be masked by systemic effects. Even within the same tissue, different cell populations may require different transporters to ascertain adequate thyroid hormone signaling. Consequently, generating and studying cell- specific transporter ko mice appears to be an attractive approach that is expected to disclose further distinct thyroid hormone transporter functions. Complementary, the application of iPSCs will also allow studying the impact of transporter defects in a cell-specific way.

For a long time, a major gap in the field had been the absence of crystal structures of thyroid hormone transporters or any homologous proteins. Although structural homology models have broadened our understanding of the mechanism by which thyroid hormone transporters translocate the various iodothyronine substrates ((7, 15, 181, 182) and **chapter 2.4)**, the sequence similarity to template structures is generally low preventing accurate molecular predictions. In this context, thorough functional characterization of the wild-type and mutant thyroid hormone transporters will be a pre-requisite to interpret the impact of any genetic variant and prove pathogenicity in case of *MCT8* mutations. The recent elucidation of the LAT1 protein structure (183) will undoubtedly provide more detailed insights into the mechanism by which it transports iodothyronines. As LAT1 has a different protein fold than the thyroid hormone transporters that belong to other protein families, it most likely cannot serve as a template to model the structure of other thyroid hormone transporters. It is thus still needed to resolve the molecular structure of additional thyroid hormone transporters, or homologous proteins, in order to advance the application of *in silico* approaches in substrate discovery, design of transporter specific inhibitors and prediction of the pathogenicity of amino acid substitutions.

So far, most research focused on the transport of the classical thyroid hormones T3 and T4, with some studying 3,3'-T2 and rT3. However, compiling evidence suggests that also other metabolites are being formed *in vivo* that very likely also require transporter proteins to cross the plasma membrane. Such transporters remain to be identified.

Moreover, the renal and hepatic transport of sulfo-conjugated and glucuronide-conjugated iodothyronines that represent major thyroid hormone metabolites in bile and urine is still poorly understood. In a field in which studies have long been dependent on the availability of [^{125}I]-radio-labelled iodothyronines (184, 185), the establishment of nonradioactive assays based on Sandell-Kolthoff reactions (186, 187) or liquid chromatography-mass spectrometry techniques (7, 188) for determining iodothyronine concentrations has already significantly improved thyroid hormone research and is expected to greatly amplify the number of potential transporter substrates that can be studied.

The application of these novel technologies are of particular interest to further explore to role of alpha-aminoadipate aminotransferase (AADAT) in thyroid hormone metabolism. In **chapter 6.**1 we identified AADAT as a novel thyroid hormone metabolizing enzyme that apparently controls thyroid hormone function by converting iodothyronines to their respective iodothyropyruvic acid metabolites. This observation may shed new light on the physiological relevance of alternate side-chain metabolism in thyroid hormone homeostasis, discussion of which falls beyond the scope of this thesis.

Although major advancements have been made in the field of thyroid hormone transport during the last 15 years, many unknowns still need to be resolved. With the recent identification of a novel thyroid hormone transporter, metabolizing enzyme and a second disorder associated with a thyroid hormone transporter defect, as well as the implementation of more sophisticated models and experimental techniques, the field is ready to take the next step forwards in unraveling the complex mechanisms involved in the regulation of tissue thyroid hormone state.

REFERENCES

1. Krenning EP, Docter R, Bernard HF, Visser TJ, Hennemann G. Active transport of triiodothyronine (T3) into isolated rat liver cells. FEBS Lett. 1978;91(1):113-6.
2. Hennemann G, Docter R, Friesema EC, de Jong M, Krenning EP, Visser TJ. Plasma membrane transport of thyroid hormones and its role in thyroid hormone metabolism and bioavailability. Endocr Rev. 2001;22(4):451-76.
3. Friesema EC, Grueters A, Biebermann H, Krude H, von Moers A, Reeser M, et al. Association between mutations in a thyroid hormone transporter and severe X-linked psychomotor retardation. Lancet. 2004;364(9443):1435-7.
4. Dumitrescu AM, Liao XH, Best TB, Brockmann K, Refetoff S. A novel syndrome combining thyroid and neurological abnormalities is associated with mutations in a monocarboxylate transporter gene. Am J Hum Genet. 2004;74(1):168-75.
5. Poole RC, Sansom CE, Halestrap AP. Studies of the membrane topology of the rat erythrocyte H+/lactate cotransporter (MCT1). Biochem J. 1996;320 (Pt 3):817-24.
6. Forrest LR, Kramer R, Ziegler C. The structural basis of secondary active transport mechanisms. Biochim Biophys Acta. 2011;1807(2):167-88.
7. Kinne A, Kleinau G, Hoefig CS, Gruters A, Kohrle J, Krause G, et al. Essential molecular determinants for thyroid hormone transport and first structural implications for monocarboxylate transporter 8. J Biol Chem. 2010;285(36):28054-63.
8. Huang Y, Lemieux MJ, Song J, Auer M, Wang DN. Structure and mechanism of the glycerol-3-phosphate transporter from Escherichia coli. Science. 2003;301(5633):616-20.
9. Nascimento AS, Dias SM, Nunes FM, Aparicio R, Ambrosio AL, Bleicher L, et al. Structural rearrangements in the thyroid hormone receptor hinge domain and their putative role in the receptor function. Journal of molecular biology. 2006;360(3):586-98.
10. Schweizer U, Schlicker C, Braun D, Kohrle J, Steegborn C. Crystal structure of mammalian selenocysteine-dependent iodothyronine deiodinase suggests a peroxiredoxin-like catalytic mechanism. Proc Natl Acad Sci U S A. 2014;111(29):10526-31.
11. Kleinau G, Schweizer U, Kinne A, Kohrle J, Gruters A, Krude H, et al. Insights into molecular properties of the human monocarboxylate transporter 8 by combining functional with structural information. Thyroid Res. 2011;4 Suppl 1:S4.
12. Braun D, Lelios I, Krause G, Schweizer U. Histidines in potential substrate recognition sites affect thyroid hormone transport by monocarboxylate transporter 8 (MCT8). Endocrinology. 2013;154(7):2553-61.
13. van der Deure WM, Peeters RP, Visser TJ. Molecular aspects of thyroid hormone transporters, including MCT8, MCT10, and OATPs, and the effects of genetic variation in these transporters. J Mol Endocrinol. 2010;44(1):1-11.
14. Schweizer U, Johannes J, Bayer D, Braun D. Structure and function of thyroid hormone plasma membrane transporters. Eur Thyroid J. 2014;3(3):143-53.
15. Protze J, Braun D, Hinz KM, Bayer-Kusch D, Schweizer U, Krause G. Membrane-traversing mechanism of thyroid hormone transport by monocarboxylate transporter 8. Cell Mol Life Sci. 2017;74(12):2299-318.
16. Dang S, Sun L, Huang Y, Lu F, Liu Y, Gong H, et al. Structure of a fucose transporter in an outward-open conformation. Nature. 2010;467(7316):734-8.
17. Groeneweg S, Lima de Souza EC, Meima ME, Peeters RP, Visser WE, Visser TJ. Outward-Open Model of Thyroid Hormone Transporter Monocarboxylate Transporter 8 Provides Novel Structural and Functional Insights. Endocrinology. 2017;158(10):3292-306.
18. Gonzalez V, Pal R, Narayan M. The oxidoreductase behavior of protein disulfide isomerase impedes fold maturation of endoplasmic reticulum-processed proteins in the pivotal structure-coupled step of oxidative folding: implications for subcellular protein trafficking. Biochemistry. 2010;49(29):6282-9.
19. Zimmermann MO, Lange A, Zahn S, Exner TE, Boeckler FM. Using Surface Scans for the Evaluation of Halogen Bonds toward the Side Chains of Aspartate, Asparagine, Glutamate, and Glutamine. Journal of chemical information and modeling. 2016;56(7):1373-83.
20. Gruber CW, Cemazar M, Heras B, Martin JL, Craik DJ. Protein disulfide isomerase: the structure of oxidative folding. Trends Biochem Sci. 2006;31(8):455-64.
21. Friesema EC, Ganguly S, Abdalla A, Manning Fox JE, Halestrap AP, Visser TJ. Identification of monocarboxylate transporter 8 as a specific thyroid hormone transporter. J Biol Chem. 2003;278(41):40128-35.

22. Friesema EC, Kuiper GG, Jansen J, Visser TJ, Kester MH. Thyroid hormone transport by the human monocarboxylate transporter 8 and its rate-limiting role in intracellular metabolism. Mol Endocrinol. 2006;20(11):2761-72.
23. Friesema EC, Jansen J, Jachtenberg JW, Visser WE, Kester MH, Visser TJ. Effective cellular uptake and efflux of thyroid hormone by human monocarboxylate transporter 10. Mol Endocrinol. 2008;22(6):1357-69.
24. Kim DK, Kanai Y, Chairoungdua A, Matsuo H, Cha SH, Endou H. Expression cloning of a Na+-independent aromatic amino acid transporter with structural similarity to H+/monocarboxylate transporters. J Biol Chem. 2001;276(20):17221-8.
25. Kim DK, Kanai Y, Matsuo H, Kim JY, Chairoungdua A, Kobayashi Y, et al. The human T-type amino acid transporter-1: characterization, gene organization, and chromosomal location. Genomics. 2002;79(1):95-103.
26. Tietze F, Kohn LD, Kohn AD, Bernardini I, Andersson HC, Adamson MD, et al. Carrier-mediated transport of monoiodotyrosine out of thyroid cell lysosomes. The Journal of biological chemistry. 1989;264(9):4762-5.
27. Meinhold H, Beckert A, Wenzel KW. Circulating diiodotyrosine: studies of its serum concentration, source, and turnover using radioimmunoassay after immunoextraction. J Clin Endocrinol Metab. 1981;53(6):1171-8.
28. Faber J, Kirkegaard C, Meinhold H, Bregengaard C. Metabolic clearance and production of diiodotyrosine in healthy man. Scand J Clin Lab Invest. 1988;48(8):747-50.
29. Tan SA, Lewis JE, Berk LS, Wilcox RB. Extrathyroidal physiology of monoiodotyrosine in humans. Clin Physiol Biochem. 1990;8(3):109-15.
30. Di Cosmo C, Liao XH, Dumitrescu AM, Philp NJ, Weiss RE, Refetoff S. Mice deficient in MCT8 reveal a mechanism regulating thyroid hormone secretion. J Clin Invest. 2010;120(9):3377-88.
31. Trajkovic-Arsic M, Muller J, Darras VM, Groba C, Lee S, Weih D, et al. Impact of monocarboxylate transporter-8 deficiency on the hypothalamus-pituitary-thyroid axis in mice. Endocrinology. 2010;151(10):5053-62.
32. Johannes J, Braun D, Kinne A, Rathmann D, Kohrle J, Schweizer U. Few Amino Acid Exchanges Expand the Substrate Spectrum of Monocarboxylate Transporter 10. Mol Endocrinol. 2016;30(7):796-808.
33. Mariotta L, Ramadan T, Singer D, Guetg A, Herzog B, Stoeger C, et al. T-type amino acid transporter TAT1 (Slc16a10) is essential for extracellular aromatic amino acid homeostasis control. J Physiol. 2012;590(24):6413-24.
34. Mendes-de-Aguiar CB, Alchini R, Decker H, Alvarez-Silva M, Tasca CI, Trentin AG. Thyroid hormone increases astrocytic glutamate uptake and protects astrocytes and neurons against glutamate toxicity. J Neurosci Res. 2008;86(14):3117-25.
35. Ardawi MS, Jalalah SM. Effects of hypothyroidism on glucose and glutamine metabolism by the gut of the rat. Clin Sci (Lond). 1991;81(3):347-55.
36. Paris M, Escriva H, Schubert M, Brunet F, Brtko J, Ciesielski F, et al. Amphioxus postembryonic development reveals the homology of chordate metamorphosis. Curr Biol. 2008;18(11):825-30.
37. Klootwijk W, Friesema EC, Visser TJ. A nonselenoprotein from amphioxus deiodinates triac but not T3: is triac the primordial bioactive thyroid hormone? Endocrinology. 2011;152(8):3259-67.
38. Kogai T, Liu YY, Richter LL, Mody K, Kagechika H, Brent GA. Retinoic acid induces expression of the thyroid hormone transporter, monocarboxylate transporter 8 (Mct8). J Biol Chem. 2010;285(35):27279-88.
39. Walter KM, Miller GW, Chen X, Yaghoobi B, Puschner B, Lein PJ. Effects of thyroid hormone disruption on the ontogenetic expression of thyroid hormone signaling genes in developing zebrafish (Danio rerio). Gen Comp Endocrinol. 2019;272:20-32.
40. Herwig A, Campbell G, Mayer CD, Boelen A, Anderson RA, Ross AW, et al. A thyroid hormone challenge in hypothyroid rats identifies T3 regulated genes in the hypothalamus and in models with altered energy balance and glucose homeostasis. Thyroid. 2014;24(11):1575-93.
41. Romano RM, Gomes SN, Cardoso NC, Schiessl L, Romano MA, Oliveira CA. New insights for male infertility revealed by alterations in spermatic function and differential testicular expression of thyroid-related genes. Endocrine. 2017;55(2):607-17.
42. Friesema EC, Visser TJ, Borgers AJ, Kalsbeek A, Swaab DF, Fliers E, et al. Thyroid hormone transporters and deiodinases in the developing human hypothalamus. Eur J Endocrinol. 2012;167(3):379-86.
43. Lopez-Espindola D, Garcia-Aldea A, Gomez de la Riva I, Rodriguez-Garcia AM, Salvatore D, Visser TJ, et al. Thyroid hormone availability in the human fetal brain: novel entry pathways and role of radial glia. Brain Struct Funct. 2019;224(6):2103-19.
44. Visser WE, Philp NJ, van Dijk TB, Klootwijk W, Friesema EC, Jansen J, et al. Evidence for a homodimeric structure of human monocarboxylate transporter 8. Endocrinology. 2009;150(11):5163-70.

45. Biebermann H, Ambrugger P, Tarnow P, von Moers A, Schweizer U, Grueters A. Extended clinical phenotype, endocrine investigations and functional studies of a loss-of-function mutation A150V in the thyroid hormone specific transporter MCT8. Eur J Endocrinol. 2005;153(3):359-66.
46. Fischer J, Kleinau G, Muller A, Kuhnen P, Zwanziger D, Kinne A, et al. Modulation of monocarboxylate transporter 8 oligomerization by specific pathogenic mutations. J Mol Endocrinol. 2015;54(1):39-50.
47. Zhang M, Wang W. Organization of signaling complexes by PDZ-domain scaffold proteins. Acc Chem Res. 2003;36(7):530-8.
48. Kirk P, Wilson MC, Heddle C, Brown MH, Barclay AN, Halestrap AP. CD147 is tightly associated with lactate transporters MCT1 and MCT4 and facilitates their cell surface expression. EMBO J. 2000;19(15):3896-904.
49. Smith VE, Read ML, Turnell AS, Sharma N, Lewy GD, Fong JC, et al. PTTG-binding factor (PBF) is a novel regulator of the thyroid hormone transporter MCT8. Endocrinology. 2012;153(7):3526-36.
50. Fischer J, Kleinau G, Rutz C, Zwanziger D, Khajavi N, Muller A, et al. Evidence of G-protein-coupled receptor and substrate transporter heteromerization at a single molecule level. Cell Mol Life Sci. 2018;75(12):2227-39.
51. Zwanziger D, Schmidt M, Fischer J, Kleinau G, Braun D, Schweizer U, et al. The long N-terminus of the human monocarboxylate transporter 8 is a target of ubiquitin-dependent proteasomal degradation which regulates protein expression and oligomerization capacity. Mol Cell Endocrinol. 2016;434:278-87.
52. Remerand G, Boespflug-Tanguy O, Tonduti D, Touraine R, Rodriguez D, Curie A, et al. Expanding the phenotypic spectrum of Allan-Herndon-Dudley syndrome in patients with SLC16A2 mutations. Dev Med Child Neurol. 2019.
53. Matheus MG, Lehman RK, Bonilha L, Holden KR. Redefining the Pediatric Phenotype of X-Linked Monocarboxylate Transporter 8 (MCT8) Deficiency: Implications for Diagnosis and Therapies. J Child Neurol. 2015.
54. Brockmann K, Dumitrescu AM, Best TT, Hanefeld F, Refetoff S. X-linked paroxysmal dyskinesia and severe global retardation caused by defective MCT8 gene. J Neurol. 2005;252(6):663-6.
55. Boccone L, Mariotti S, Dessi V, Pruna D, Meloni A, Loudianos G. Allan-Herndon-Dudley syndrome (AHDS) caused by a novel SLC16A2 gene mutation showing severe neurologic features and unexpectedly low TRH-stimulated serum TSH. Eur J Med Genet. 2010;53(6):392-5.
56. Wemeau JL, Pigeyre M, Proust-Lemoine E, d'Herbomez M, Gottrand F, Jansen J, et al. Beneficial effects of propylthiouracil plus L-thyroxine treatment in a patient with a mutation in MCT8. J Clin Endocrinol Metab. 2008;93(6):2084-8.
57. Herzovich V, Vaiani E, Marino R, Dratler G, Lazzati JM, Tilitzky S, et al. Unexpected peripheral markers of thyroid function in a patient with a novel mutation of the MCT8 thyroid hormone transporter gene. Horm Res. 2007;67(1):1-6.
58. Rego T, Lado CG, Rodriguez PC, Santos FS, Angueira FB, Castro-Feijoo L, et al. Severe neurological abnormalities in a young boy with impaired thyroid hormone sensitivity due to a novel mutation in the MCT8 gene. Hormones (Athens). 2017;16(2):194-9.
59. Vaurs-Barriere C, Deville M, Sarret C, Giraud G, Des Portes V, Prats-Vinas JM, et al. Pelizaeus-Merzbacher-Like disease presentation of MCT8 mutated male subjects. Ann Neurol. 2009;65(1):114-8.
60. Zung A, Visser TJ, Uitterlinden AG, Rivadeneira F, Friesema EC. A child with a deletion in the monocarboxylate transporter 8 gene: 7-year follow-up and effects of thyroid hormone treatment. Eur J Endocrinol. 2011;165(5):823-30.
61. Wang J, Zhang Q, Bao X, Chen Y, Yu S. [Clinical and genetic features of five patients with Allan-Herndon-Dudley syndrome]. Zhonghua yi xue yi chuan xue za zhi = Zhonghua yixue yichuanxue zazhi = Chinese journal of medical genetics. 2018;35(4):484-8.
62. von Olshausen K, Bischoff S, Kahaly G, Mohr-Kahaly S, Erbel R, Beyer J, et al. Cardiac arrhythmias and heart rate in hyperthyroidism. Am J Cardiol. 1989;63(13):930-3.
63. Scott O, Williams GJ, Fiddler GI. Results of 24 hour ambulatory monitoring of electrocardiogram in 131 healthy boys aged 10 to 13 years. Br Heart J. 1980;44(3):304-8.
64. Binici Z, Intzilakis T, Nielsen OW, Kober L, Sajadieh A. Excessive supraventricular ectopic activity and increased risk of atrial fibrillation and stroke. Circulation. 2010;121(17):1904-11.
65. Healey JS, Connolly SJ, Gold MR, Israel CW, Van Gelder IC, Capucci A, et al. Subclinical atrial fibrillation and the risk of stroke. N Engl J Med. 2012;366(2):120-9.
66. Perez MV, Dewey FE, Marcus R, Ashley EA, Al-Ahmad AA, Wang PJ, et al. Electrocardiographic predictors of atrial fibrillation. Am Heart J. 2009;158(4):622-8.

67. Boccone L, Dessi V, Meloni A, Loudianos G. Allan-Herndon-Dudley syndrome (AHDS) in two consecutive generations caused by a missense MCT8 gene mutation. Phenotypic variability with the presence of normal serum T3 levels. Eur J Med Genet. 2013;56(4):207-10.
68. Faruk Aydin O, Kara C, Jones J, Wood TC, May MM, Friez MJ, et al. Allan-Herndon-Dudley syndrome caused by a novel MCT8/SLC16A2 mutation in a Turkish family. Horm Res. 2013;80(Suppl 1):352-3.
69. Verge CF, Konrad D, Cohen M, Di Cosmo C, Dumitrescu AM, Marcinkowski T, et al. Diiodothyropropionic acid (DITPA) in the treatment of MCT8 deficiency. J Clin Endocrinol Metab. 2012;97(12):4515-23.
70. Anik A, Kersseboom S, Demir K, Catli G, Yis U, Bober E, et al. Psychomotor retardation caused by a defective thyroid hormone transporter: report of two families with different MCT8 mutations. Horm Res Paediatr. 2014;82(4):261-71.
71. Doi J, Ohtsubo A, Ohtsuka A, Hayashi K. Triiodothyronine but not thyroxine accelerates myofibrillar proteolysis via ATP production in cultured muscle cells. Biosci Biotechnol Biochem. 2003;67(11):2451-4.
72. Salvatore D, Simonides WS, Dentice M, Zavacki AM, Larsen PR. Thyroid hormones and skeletal muscle--new insights and potential implications. Nat Rev Endocrinol. 2014;10(4):206-14.
73. Brown JG, Millward DJ. Dose response of protein turnover in rat skeletal muscle to triiodothyronine treatment. Biochim Biophys Acta. 1983;757(2):182-90.
74. Sinha RA, Singh BK, Zhou J, Wu Y, Farah BL, Ohba K, et al. Thyroid hormone induction of mitochondrial activity is coupled to mitophagy via ROS-AMPK-ULK1 signaling. Autophagy. 2015;11(8):1341-57.
75. Chaker L, Sedaghat S, Hoorn EJ, Elzen WP, Gussekloo J, Hofman A, et al. The association of thyroid function and the risk of kidney function decline: a population-based cohort study. Eur J Endocrinol. 2016;175(6):653-60.
76. Mariani LH, Berns JS. The renal manifestations of thyroid disease. J Am Soc Nephrol. 2012;23(1):22-6.
77. Schwartz CE, May MM, Carpenter NJ, Rogers RC, Martin J, Bialer MG, et al. Allan-Herndon-Dudley syndrome and the monocarboxylate transporter 8 (MCT8) gene. Am J Hum Genet. 2005;77(1):41-53.
78. Capri Y, Friesema EC, Kersseboom S, Touraine R, Monnier A, Eymard-Pierre E, et al. Relevance of different cellular models in determining the effects of mutations on SLC16A2/MCT8 thyroid hormone transporter function and genotype-phenotype correlation. Hum Mutat. 2013;34(7):1018-25.
79. Visser WE, Jansen J, Friesema EC, Kester MH, Mancilla E, Lundgren J, et al. Novel pathogenic mechanism suggested by ex vivo analysis of MCT8 (SLC16A2) mutations. Hum Mutat. 2009;30(1):29-38.
80. Jansen J, Friesema EC, Kester MH, Schwartz CE, Visser TJ. Genotype-phenotype relationship in patients with mutations in thyroid hormone transporter MCT8. Endocrinology. 2008;149(5):2184-90.
81. Choi Y, Chan AP. PROVEAN web server: a tool to predict the functional effect of amino acid substitutions and indels. Bioinformatics. 2015;31(16):2745-7.
82. Rentzsch P, Witten D, Cooper GM, Shendure J, Kircher M. CADD: predicting the deleteriousness of variants throughout the human genome. Nucleic Acids Res. 2019;47(D1):D886-D94.
83. Adzhubei IA, Schmidt S, Peshkin L, Ramensky VE, Gerasimova A, Bork P, et al. A method and server for predicting damaging missense mutations. Nat Methods. 2010;7(4):248-9.
84. Vaser R, Adusumalli S, Leng SN, Sikic M, Ng PC. SIFT missense predictions for genomes. Nat Protoc. 2016;11(1):1-9.
85. Kinne A, Roth S, Biebermann H, Kohrle J, Gruters A, Schweizer U. Surface translocation and tri-iodothyronine uptake of mutant MCT8 proteins are cell type-dependent. J Mol Endocrinol. 2009;43(6):263-71.
86. Novara F, Groeneweg S, Freri E, Estienne M, Reho P, Matricardi S, et al. Clinical and Molecular Characteristics of SLC16A2 (MCT8) Mutations in Three Families with the Allan-Herndon-Dudley Syndrome. Hum Mutat. 2017;38(3):260-4.
87. Friesema EC, Jansen J, Heuer H, Trajkovic M, Bauer K, Visser TJ. Mechanisms of disease: psychomotor retardation and high T3 levels caused by mutations in monocarboxylate transporter 8. Nat Clin Pract Endocrinol Metab. 2006;2(9):512-23.
88. Schwartz CE, Stevenson RE. The MCT8 thyroid hormone transporter and Allan-Herndon-Dudley syndrome. Best Pract Res Clin Endocrinol Metab. 2007;21(2):307-21.
89. Ramos HE, Morandini M, Carre A, Tron E, Floch C, Mandelbrot L, et al. Pregnancy in women heterozygous for MCT8 mutations: risk of maternal hypothyroxinemia and fetal care. Eur J Endocrinol. 2011;164(2):309-14.
90. Dateki S, Haraguchi K, Sato T, Nakatomi A, Fujiwara M, Sakurai M, et al. A novel MCT8 mutation in a Japanese patient with Allan-Herndon-Dudley syndrome. Horm Res. 2013;80(Suppl 1):360.
91. Frints SG, Lenzner S, Bauters M, Jensen LR, Van Esch H, des Portes V, et al. MCT8 mutation analysis and identification of the first female with Allan-Herndon-Dudley syndrome due to loss of MCT8 expression. Eur J Hum Genet. 2008;16(9):1029-37.

92. Groeneweg SvG, F.S.; Peeters, R.P.; Heuer, H.;Visser, W.E. Thyroid hormone transporters. Endocr Rev. 2019;(accepted for publication).
93. Vancamp P, Darras VM. From zebrafish to human: A comparative approach to elucidate the role of the thyroid hormone transporter MCT8 during brain development. Gen Comp Endocrinol. 2018;265:219-29.
94. Alkemade A, Friesema EC, Unmehopa UA, Fabriek BO, Kuiper GG, Leonard JL, et al. Neuroanatomical pathways for thyroid hormone feedback in the human hypothalamus. J Clin Endocrinol Metab. 2005;90(7):4322-34.
95. Heuer H, Maier MK, Iden S, Mittag J, Friesema EC, Visser TJ, et al. The monocarboxylate transporter 8 linked to human psychomotor retardation is highly expressed in thyroid hormone-sensitive neuron populations. Endocrinology. 2005;146(4):1701-6.
96. Kallo I, Mohacsik P, Vida B, Zeold A, Bardoczi Z, Zavacki AM, et al. A novel pathway regulates thyroid hormone availability in rat and human hypothalamic neurosecretory neurons. PLoS One. 2012;7(6):e37860.
97. Fliers E, Unmehopa UA, Alkemade A. Functional neuroanatomy of thyroid hormone feedback in the human hypothalamus and pituitary gland. Mol Cell Endocrinol. 2006;251(1-2):1-8.
98. Trajkovic M, Visser TJ, Mittag J, Horn S, Lukas J, Darras VM, et al. Abnormal thyroid hormone metabolism in mice lacking the monocarboxylate transporter 8. J Clin Invest. 2007;117(3):627-35.
99. Dumitrescu AM, Liao XH, Weiss RE, Millen K, Refetoff S. Tissue-specific thyroid hormone deprivation and excess in monocarboxylate transporter (mct) 8-deficient mice. Endocrinology. 2006;147(9):4036-43.
100. Groeneweg S, Visser WE, Visser TJ. Disorder of thyroid hormone transport into the tissues. Best Pract Res Clin Endocrinol Metab. 2017;31(2):241-53.
101. Wirth EK, Sheu SY, Chiu-Ugalde J, Sapin R, Klein MO, Mossbrugger I, et al. Monocarboxylate transporter 8 deficiency: altered thyroid morphology and persistent high triiodothyronine/thyroxine ratio after thyroidectomy. Eur J Endocrinol. 2011;165(4):555-61.
102. Mayerl S, Schmidt M, Doycheva D, Darras VM, Huttner SS, Boelen A, et al. Thyroid Hormone Transporters MCT8 and OATP1C1 Control Skeletal Muscle Regeneration. Stem Cell Reports. 2018;10(6):1959-74.
103. Wirth EK, Rijntjes E, Meyer F, Kohrle J, Schweizer U. High T3, Low T4 Serum Levels in Mct8 Deficiency Are Not Caused by Increased Hepatic Conversion through Type I Deiodinase. Eur Thyroid J. 2015;4(Suppl 1):87-91.
104. Liao XH, Di Cosmo C, Dumitrescu AM, Hernandez A, Van Sande J, St Germain DL, et al. Distinct roles of deiodinases on the phenotype of Mct8 defect: a comparison of eight different mouse genotypes. Endocrinology. 2011;152(3):1180-91.
105. Di Cosmo C, Liao XH, Ye H, Ferrara AM, Weiss RE, Refetoff S, et al. Mct8-deficient mice have increased energy expenditure and reduced fat mass that is abrogated by normalization of serum T3 levels. Endocrinology. 2013;154(12):4885-95.
106. Leitch VD, Di Cosmo C, Liao XH, O'Boy S, Galliford TM, Evans H, et al. An Essential Physiological Role for MCT8 in Bone in Male Mice. Endocrinology. 2017;158(9):3055-66.
107. Lopez-Espindola D, Morales-Bastos C, Grijota-Martinez C, Liao XH, Lev D, Sugo E, et al. Mutations of the thyroid hormone transporter MCT8 cause prenatal brain damage and persistent hypomyelination. J Clin Endocrinol Metab. 2014;99(12):E2799-804.
108. Mayerl S, Muller J, Bauer R, Richert S, Kassmann CM, Darras VM, et al. Transporters MCT8 and OATP1C1 maintain murine brain thyroid hormone homeostasis. J Clin Invest. 2014;124(5):1987-99.
109. Wirth EK, Roth S, Blechschmidt C, Holter SM, Becker L, Racz I, et al. Neuronal 3',3,5-triiodothyronine (T3) uptake and behavioral phenotype of mice deficient in Mct8, the neuronal T3 transporter mutated in Allan-Herndon-Dudley syndrome. J Neurosci. 2009;29(30):9439-49.
110. Vatine GD, Al-Ahmad A, Barriga BK, Svendsen S, Salim A, Garcia L, et al. Modeling Psychomotor Retardation using iPSCs from MCT8-Deficient Patients Indicates a Prominent Role for the Blood-Brain Barrier. Cell Stem Cell. 2017;20(6):831-43 e5.
111. Dratman MB, Crutchfield FL, Schoenhoff MB. Transport of iodothyronines from bloodstream to brain: contributions by blood:brain and choroid plexus:cerebrospinal fluid barriers. Brain Res. 1991;554(1-2):229-36.
112. Zhang Y, Chen K, Sloan SA, Bennett ML, Scholze AR, O'Keeffe S, et al. An RNA-sequencing transcriptome and splicing database of glia, neurons, and vascular cells of the cerebral cortex. J Neurosci. 2014;34(36):11929-47.
113. Zhang Y, Sloan SA, Clarke LE, Caneda C, Plaza CA, Blumenthal PD, et al. Purification and Characterization of Progenitor and Mature Human Astrocytes Reveals Transcriptional and Functional Differences with Mouse. Neuron. 2016;89(1):37-53.

114. Calza L, Baldassarro VA, Fernandez M, Giuliani A, Lorenzini L, Giardino L. Thyroid Hormone and the White Matter of the Central Nervous System: From Development to Repair. Vitam Horm. 2018;106:253-81.
115. Sijens PE, Rodiger LA, Meiners LC, Lunsing RJ. 1H magnetic resonance spectroscopy in monocarboxylate transporter 8 gene deficiency. J Clin Endocrinol Metab. 2008;93(5):1854-9.
116. Tonduti D, Vanderver A, Berardinelli A, Schmidt JL, Collins CD, Novara F, et al. MCT8 deficiency: extrapyramidal symptoms and delayed myelination as prominent features. J Child Neurol. 2013;28(6):795-800.
117. Lee JY, Kim MJ, Deliyanti D, Azari MF, Rossello F, Costin A, et al. Overcoming Monocarboxylate Transporter 8 (MCT8)-Deficiency to Promote Human Oligodendrocyte Differentiation and Myelination. EBioMedicine. 2017;25:122-35.
118. Fuchs O, Pfarr N, Pohlenz J, Schmidt H. Elevated serum triiodothyronine and intellectual and motor disability with paroxysmal dyskinesia caused by a monocarboxylate transporter 8 gene mutation. Dev Med Child Neurol. 2009;51(3):240-4.
119. Papadimitriou A, Dumitrescu AM, Papavasiliou A, Fretzayas A, Nicolaidou P, Refetoff S. A novel monocarboxylate transporter 8 gene mutation as a cause of severe neonatal hypotonia and developmental delay. Pediatrics. 2008;121(1):e199-202.
120. Crushell E, Reardon W. Elevated TSH levels in a mentally retarded boy. Eur J Pediatr. 2010;169(5):573-5.
121. Ugrasbul F, H.H. A. A patient presenting with central hypothyroidism, developmental delay and poor head control. Should we be checking T3 levels? Horm Res. 2009;72(Suppl 1):458-9.
122. de Menezes-Filho HC, Marui S, Manna TD, Brust ES, Radonsky V, Kuperman H, et al. Novel mutation in MCT8 gene in a Brazilian boy with thyroid hormone resistance and severe neurologic abnormalities. Arq Bras Endocrinol Metabol. 2011;55(1):60-6.
123. Garcia-de Teresa B, Gonzalez-Del Angel A, Reyna-Fabian ME, Ruiz-Reyes Mde L, Calzada-Leon R, Perez-Enriquez B, et al. Deletion of exon 1 of the SLC16A2 gene: a common occurrence in patients with Allan-Herndon-Dudley syndrome. Thyroid. 2015;25(3):361-7.
124. Kakinuma H, Itoh M, Takahashi H. A novel mutation in the monocarboxylate transporter 8 gene in a boy with putamen lesions and low free T4 levels in cerebrospinal fluid. J Pediatr. 2005;147(4):552-4.
125. Philips AK, Siren A, Avela K, Somer M, Peippo M, Ahvenainen M, et al. X-exome sequencing in Finnish families with intellectual disability--four novel mutations and two novel syndromic phenotypes. Orphanet J Rare Dis. 2014;9:49.
126. Shimojima K, Maruyama K, Kikuchi M, Imai A, Inoue K, Yamamoto T. Novel SLC16A2 mutations in patients with Allan-Herndon-Dudley syndrome. Intractable Rare Dis Res. 2016;5(3):214-7.
127. Kim JH, Kim YM, Yum MS, Choi JH, Lee BH, Kim GH, et al. Clinical and endocrine features of two Allan-Herndon-Dudley syndrome patients with monocarboxylate transporter 8 mutations. Horm Res Paediatr. 2015;83(4):288-92.
128. Choi JH, Cho JH, Kim JH, Yoo EG, Kim GH, Yoo HW. Variable Clinical Characteristics and Molecular Spectrum of Patients with Syndromes of Reduced Sensitivity to Thyroid Hormone: Genetic Defects in the THRB and SLC16A2 Genes. Horm Res Paediatr. 2018;90(5):283-90.
129. Namba N, Etani Y, Kitaoka T, Nakamoto Y, Nakacho M, Bessho K, et al. Clinical phenotype and endocrinological investigations in a patient with a mutation in the MCT8 thyroid hormone transporter. Eur J Pediatr. 2008;167(7):785-91.
130. Levenson A, Tan WH, Huang SA. Diagnostic Dilemma: A 3-Year Old Boy with Global Developmental Delay, Truncal Hypotonia, Peripheral Hypertonia, and Central Hypothyroidism. 95th Annual Meeting of The Endocrine Society; San Francisco2013. p. SUN-430.
131. Ngu LH. Developmental delay and abnormal thyroid function test in two siblings caused by a novel mutation in SLC16A2 gene affecting a thyroid hormone specific transporter (MCT8): first report from Malaysia. Conference abstract: 35th Malaysian Paediatrics Association Congress. 2013.
132. Fu J, Refetoff S, Dumitrescu AM. Inherited defects of thyroid hormone-cell-membrane transport: review of recent findings. Curr Opin Endocrinol Diabetes Obes. 2013;20(5):434-40.
133. Gika AD, Siddiqui A, Hulse AJ, Edward S, Fallon P, McEntagart ME, et al. White matter abnormalities and dystonic motor disorder associated with mutations in the SLC16A2 gene. Dev Med Child Neurol. 2010;52(5):475-82.
134. Visser WE, Vrijmoeth P, Visser FE, Arts WF, van Toor H, Visser TJ. Identification, functional analysis, prevalence and treatment of monocarboxylate transporter 8 (MCT8) mutations in a cohort of adult patients with mental retardation. Clin Endocrinol (Oxf). 2013;78(2):310-5.
135. Rivkees SA, Mattison DR. Ending propylthiouracil-induced liver failure in children. N Engl J Med. 2009;360(15):1574-5.

136. Groeneweg S, Peeters RP, Visser TJ, Visser WE. Therapeutic applications of thyroid hormone analogues in resistance to thyroid hormone (RTH) syndromes. Mol Cell Endocrinol. 2017;458:82-90.
137. Barez-Lopez S, Hartley MD, Grijota-Martinez C, Scanlan TS, Guadano-Ferraz A. Sobetirome and its Amide Prodrug Sob-AM2 Exert Thyromimetic Actions in Mct8-Deficient Brain. Thyroid. 2018;28(9):1211-20.
138. Hartley MD, Banerji T, Tagge IJ, Kirkemo LL, Chaudhary P, Calkins E, et al. Myelin repair stimulated by CNS-selective thyroid hormone action. JCI insight. 2019;4(8).
139. Groeneweg SP, R.P.; Moran, C.; Stoupa, A.; Auriol, F.; Tonduti, D.; Dica, A.; Paone, L.; Rozenkova, K.; Malikova, J.; van der Walt, A.; de Coo, IFM; McGowan, A.; Lyons, G.; Aarsen, F.K.; Barca, D.; van Beynum, I.M.; van der Knoop, M.M.; Jansen, J.; Manshande, M.; Lunsing, R.J.; Nowak, S.; den Uil, A.; Zillikens, M.C.; Visser, F.E.; Ambegaonkar, G.; Singh, Y.; de Rijke, Y.B.; Medici, M.; Bertini, E.S.; Depoorter, S.; Lebl, J.; Cappa, M.; de Meirleir, L.; Krude, H.; Craiu, D.; Zibordi, F.; Oliver Petit, I.; Polak, M.; Chatterjee, K.; Visser, T.J.; Visser, W.E. Effectiveness and safety of Triac in children and adults with MCT8 deficiency: an international, multicentre, single group, open-label, phase 2 trial. Lancet Diabetes Endocrinol. 2019;accepted.
140. Iwayama H, Liao XH, Braun L, Barez-Lopez S, Kaspar B, Weiss RE, et al. Adeno Associated Virus 9-Based Gene Therapy Delivers a Functional Monocarboxylate Transporter 8, Improving Thyroid Hormone Availability to the Brain of Mct8-Deficient Mice. Thyroid. 2016;26(9):1311-9.
141. Braun D, Schweizer U. The Chemical Chaperone Phenylbutyrate Rescues MCT8 Mutations Associated With Milder Phenotypes in Patients With Allan-Herndon-Dudley Syndrome. Endocrinology. 2017;158(3):678-91.
142. Braun D, Schweizer U. Efficient Activation of Pathogenic DeltaPhe501 Mutation in Monocarboxylate Transporter 8 by Chemical and Pharmacological Chaperones. Endocrinology. 2015;156(12):4720-30.
143. Kang HJ, Kawasawa YI, Cheng F, Zhu Y, Xu X, Li M, et al. Spatio-temporal transcriptome of the human brain. Nature. 2011;478(7370):483-9.
144. Bernal J. Thyroid hormone transport in developing brain. Curr Opin Endocrinol Diabetes Obes. 2011;18(5):295-9.
145. Bernal J. Thyroid hormone receptors in brain development and function. Nat Clin Pract Endocrinol Metab. 2007;3(3):249-59.
146. Bernal J, Guadano-Ferraz A, Morte B. Thyroid hormone transporters--functions and clinical implications. Nat Rev Endocrinol. 2015;11(7):406-17.
147. Moran C, Chatterjee K. Resistance to Thyroid Hormone alpha-Emerging Definition of a Disorder of Thyroid Hormone Action. J Clin Endocrinol Metab. 2016;101(7):2636-9.
148. Mayerl S, Visser TJ, Darras VM, Horn S, Heuer H. Impact of Oatp1c1 deficiency on thyroid hormone metabolism and action in the mouse brain. Endocrinology. 2012;153(3):1528-37.
149. Constant EL, de Volder AG, Ivanoiu A, Bol A, Labar D, Seghers A, et al. Cerebral blood flow and glucose metabolism in hypothyroidism: a positron emission tomography study. J Clin Endocrinol Metab. 2001;86(8):3864-70.
150. Cremer GM, Goldstein NP, Paris J. Myxedema and ataxia. Neurology. 1969;19(1):37-46.
151. Westerholz S, de Lima AD, Voigt T. Regulation of early spontaneous network activity and GABAergic neurons development by thyroid hormone. Neuroscience. 2010;168(2):573-89.
152. Hashemi E, Ariza J, Rogers H, Noctor SC, Martinez-Cerdeno V. The Number of Parvalbumin-Expressing Interneurons Is Decreased in the Prefrontal Cortex in Autism. Cerebral cortex. 2017;27(3):1931-43.
153. Bernal J. Thyroid hormones and brain development. Vitam Horm. 2005;71:95-122.
154. Hagenbuch B, Meier PJ. Organic anion transporting polypeptides of the OATP/ SLC21 family: phylogenetic classification as OATP/ SLCO superfamily, new nomenclature and molecular/functional properties. Pflugers Arch. 2004;447(5):653-65.
155. Hagenbuch B, Stieger B. The SLCO (former SLC21) superfamily of transporters. Molecular aspects of medicine. 2013;34(2-3):396-412.
156. van der Deure WM, Friesema EC, de Jong FJ, de Rijke YB, de Jong FH, Uitterlinden AG, et al. Organic anion transporter 1B1: an important factor in hepatic thyroid hormone and estrogen transport and metabolism. Endocrinology. 2008;149(9):4695-701.
157. Muller J, Mayerl S, Visser TJ, Darras VM, Boelen A, Frappart L, et al. Tissue-specific alterations in thyroid hormone homeostasis in combined Mct10 and Mct8 deficiency. Endocrinology. 2014;155(1):315-25.
158. Sharlin DS, Ng L, Verrey F, Visser TJ, Liu Y, Olszewski RT, et al. Deafness and loss of cochlear hair cells in the absence of thyroid hormone transporters Slc16a2 (Mct8) and Slc16a10 (Mct10). Sci Rep. 2018;8(1):4403.
159. Sharlin DS, Visser TJ, Forrest D. Developmental and cell-specific expression of thyroid hormone transporters in the mouse cochlea. Endocrinology. 2011;152(12):5053-64.

160. Abe S, Namba N, Abe M, Fujiwara M, Aikawa T, Kogo M, et al. Monocarboxylate transporter 10 functions as a thyroid hormone transporter in chondrocytes. Endocrinology. 2012;153(8):4049-58.
161. Medici M, van der Deure WM, Verbiest M, Vermeulen SH, Hansen PS, Kiemeney LA, et al. A large-scale association analysis of 68 thyroid hormone pathway genes with serum TSH and FT4 levels. Eur J Endocrinol. 2011;164(5):781-8.
162. Carle A, Faber J, Steffensen R, Laurberg P, Nygaard B. Hypothyroid Patients Encoding Combined MCT10 and DIO2 Gene Polymorphisms May Prefer L-T3 + L-T4 Combination Treatment - Data Using a Blind, Randomized, Clinical Study. Eur Thyroid J. 2017;6(3):143-51.
163. Reimer RJ. SLC17: a functionally diverse family of organic anion transporters. Molecular aspects of medicine. 2013;34(2-3):350-9.
164. Sreedharan S, Shaik JH, Olszewski PK, Levine AS, Schioth HB, Fredriksson R. Glutamate, aspartate and nucleotide transporters in the SLC17 family form four main phylogenetic clusters: evolution and tissue expression. BMC Genomics. 2010;11:17.
165. Togawa N, Miyaji T, Izawa S, Omote H, Moriyama Y. A Na+-phosphate cotransporter homologue (SLC17A4 protein) is an intestinal organic anion exporter. American journal of physiology Cell physiology. 2012;302(11):C1652-60.
166. Guetg A, Mariotta L, Bock L, Herzog B, Fingerhut R, Camargo SM, et al. Essential amino acid transporter Lat4 (Slc43a2) is required for mouse development. J Physiol. 2015;593(5):1273-89.
167. Poncet N, Mitchell FE, Ibrahim AF, McGuire VA, English G, Arthur JS, et al. The catalytic subunit of the system L1 amino acid transporter (slc7a5) facilitates nutrient signalling in mouse skeletal muscle. PLoS One. 2014;9(2):e89547.
168. Tarlungeanu DC, Deliu E, Dotter CP, Kara M, Janiesch PC, Scalise M, et al. Impaired Amino Acid Transport at the Blood Brain Barrier Is a Cause of Autism Spectrum Disorder. Cell. 2016;167(6):1481-94 e18.
169. Braun D, Wirth EK, Wohlgemuth F, Reix N, Klein MO, Gruters A, et al. Aminoaciduria, but normal thyroid hormone levels and signalling, in mice lacking the amino acid and thyroid hormone transporter Slc7a8. Biochem J. 2011;439(2):249-55.
170. Nunez B, Martinez de Mena R, Obregon MJ, Font-Llitjos M, Nunes V, Palacin M, et al. Cerebral cortex hyperthyroidism of newborn mct8-deficient mice transiently suppressed by lat2 inactivation. PLoS One. 2014;9(5):e96915.
171. Barez-Lopez S, Obregon MJ, Bernal J, Guadano-Ferraz A. Thyroid Hormone Economy in the Perinatal Mouse Brain: Implications for Cerebral Cortex Development. Cerebral cortex. 2018;28(5):1783-93.
172. Ferrara AM, Liao XH, Gil-Ibanez P, Marcinkowski T, Bernal J, Weiss RE, et al. Changes in thyroid status during perinatal development of MCT8-deficient male mice. Endocrinology. 2013;154(7):2533-41.
173. Espino Guarch M, Font-Llitjos M, Murillo-Cuesta S, Errasti-Murugarren E, Celaya AM, Girotto G, et al. Mutations in L-type amino acid transporter-2 support SLC7A8 as a novel gene involved in age-related hearing loss. eLife. 2018;7.
174. Vaz FM, Paulusma CC, Huidekoper H, de Ru M, Lim C, Koster J, et al. Sodium taurocholate cotransporting polypeptide (SLC10A1) deficiency: conjugated hypercholanemia without a clear clinical phenotype. Hepatology. 2015;61(1):260-7.
175. Tan HJ, Deng M, Qiu JW, Wu JF, Song YZ. Monozygotic Twins Suffering From Sodium Taurocholate Cotransporting Polypeptide Deficiency: A Case Report. Front Pediatr. 2018;6:354.
176. Deng M, Mao M, Guo L, Chen FP, Wen WR, Song YZ. Clinical and molecular study of a pediatric patient with sodium taurocholate cotransporting polypeptide deficiency. Exp Ther Med. 2016;12(5):3294-300.
177. Liu R, Chen C, Xia X, Liao Q, Wang Q, Newcombe PJ, et al. Homozygous p.Ser267Phe in SLC10A1 is associated with a new type of hypercholanemia and implications for personalized medicine. Sci Rep. 2017;7(1):9214.
178. Qiu JW, Deng M, Cheng Y, Atif RM, Lin WX, Guo L, et al. Sodium taurocholate cotransporting polypeptide (NTCP) deficiency: Identification of a novel SLC10A1 mutation in two unrelated infants presenting with neonatal indirect hyperbilirubinemia and remarkable hypercholanemia. Oncotarget. 2017;8(63):106598-607.
179. Kersseboom S, Horn S, Visser WE, Chen J, Friesema EC, Vaurs-Barriere C, et al. In vitro and mouse studies supporting therapeutic utility of triiodothyroacetic acid in MCT8 deficiency. Mol Endocrinol. 2014;28(12):1961-70.
180. Di Cosmo C, Liao XH, Dumitrescu AM, Weiss RE, Refetoff S. A thyroid hormone analog with reduced dependence on the monocarboxylate transporter 8 for tissue transport. Endocrinology. 2009;150(9):4450-8.
181. Hinz KM, Meyer K, Kinne A, Schulein R, Kohrle J, Krause G. Structural insights into thyroid hormone transport mechanisms of the L-type amino acid transporter 2. Mol Endocrinol. 2015;29(6):933-42.

182. Hinz KM, Neef D, Rutz C, Furkert J, Kohrle J, Schulein R, et al. Molecular features of the L-type amino acid transporter 2 determine different import and export profiles for thyroid hormones and amino acids. Mol Cell Endocrinol. 2017;443:163-74.
183. Yan R, Zhao X, Lei J, Zhou Q. Structure of the human LAT1-4F2hc heteromeric amino acid transporter complex. Nature. 2019;568(7750):127-30.
184. Mol JA, Visser TJ. Synthesis and some properties of sulfate esters and sulfamates of iodothyronines. Endocrinology. 1985;117(1):1-7.
185. Rooda SJ, Otten MH, van Loon MA, Kaptein E, Visser TJ. Metabolism of triiodothyronine in rat hepatocytes. Endocrinology. 1989;125(4):2187-97.
186. Jayarama-Naidu R, Johannes J, Meyer F, Wirth EK, Schomburg L, Kohrle J, et al. A Nonradioactive Uptake Assay for Rapid Analysis of Thyroid Hormone Transporter Function. Endocrinology. 2015;156(7):2739-45.
187. Dong H, Wade MG. Application of a nonradioactive assay for high throughput screening for inhibition of thyroid hormone uptake via the transmembrane transporter MCT8. Toxicol In Vitro. 2017;40:234-42.
188. Rathmann D, Rijntjes E, Lietzow J, Kohrle J. Quantitative Analysis of Thyroid Hormone Metabolites in Cell Culture Samples Using LC-MS/MS. Eur Thyroid J. 2015;4(Suppl 1):51-8.

Chapter

Summary

Samenvatting

Author affiliations

List of publications

Curriculum Vitae

PhD Portfolio

Dankwoord

8

SUMMARY

Thyroid hormone is indispensable for normal development of tissues and control of energy metabolism throughout life. The thyroid gland mainly produces the inactive prohormone thyroxine (T4) and to a lesser extent the bioactive hormone triiodothyronine (T3). Diseases of the thyroid gland affect the amount of thyroid hormone that is produced. In hypothyroidism, reduced thyroid hormone production may result in weight gain, cold intolerance, a slow heart rate and depression. Opposite clinical features can be observed in patients with hyperthyroidism.

Thyroid hormone exerts its effects at the cellular level. These effects are regulated in the cell at different levels: 1) the thyroid hormone transporters that govern the passage of thyroid hormone across the plasma membrane, 2) the deiodinating enzymes that activate T4 to T3 or inactivate these hormones to receptor inactive metabolites, and 3) the T3-receptors that regulate the expression of T3-responsive genes upon binding or release of T3. Together these factors comprise the thyroid hormone signalling cascade which ensures that the amount of T3 action meets the needs of the cell, tissue and body throughout life. Under physiological conditions, modulation of any of these factors allows cells to adapt to changes in their environment and governs their growth and differentiation. Alterations in the thyroid hormone signalling cascade may disturb thyroid hormone homeostasis in the cell and cause disease. Inborn defects in T3-receptors and transporter proteins have been associated with clinical syndromes of resistance to thyroid hormone, a common name for conditions in which cells do not properly “sense” the amount of thyroid hormone in the blood.

This thesis particularly focusses on MCT8 deficiency which is an inherited defect in one of the thyroid hormone transporter proteins. Given its important role in brain development, mutations in MCT8 result in severe intellectual and motor disability. In addition, affected patients have increased T3 concentrations in the blood which are harmful for tissues that use other transporters than MCT8. This thesis covers the full spectrum from studies on MCT8 function at the molecular level to the first therapeutic clinical trial in patients with MCT8 deficiency.

Chapter 1 provides a general background of thyroid hormone physiology and summarizes the knowns and unknowns of thyroid hormone signalling at the cellular level, with a particular focus on the thyroid hormone transporter proteins. In addition, the general aims and outline of this thesis are summarized.

The studies in **chapter 2** aimed to elucidate how the MCT8 protein recognizes thyroid hormone molecules and how these molecules move through the substrate channel of MCT8 into the cell. The MCT8 protein is organized in 12 helical bundles that cross the plasma membrane – hence termed transmembrane domains (TMD) – linked through extracellular (ECL) and intracellular (ICL) loop regions. Together, these bundles form a pore (or substrate channel) through which thyroid hormones can enter or exit the cell. We reasoned that identification of accessible and functionally important amino acid residues could guide the generation of a three-dimensional model of the MCT8 protein structure. In turn, such a structural model may help unravelling the mechanism by which MCT8 recognizes and transports thyroid hormones. **Chapter 2.1** demonstrates that amino acid residues Cys481 (ECL5) and Cys497 (in TMD10) are target for chemical reactions with compounds that specifically react with the side-chains of cysteine residues (p-chloromercuribenzene sulfonate and HgCl2). These reactions were substantially prevented in presence of thyroid hormone, suggesting that at least one of both residues

is protected from modification once thyroid hormone is present in the substrate pore. Therefore, we reasoned that at least one Cys side-chain should face the substrate channel, most likely being Cys497.

Using a similar approach, the His192 residue in TMD1 was identified as a target for chemical modification with histidine-specific reagent diethyl pyrocarbonate (DEPC) in **chapter 2.2**. Again, this reaction was largely prevented in presence of substrate, supporting a location of His192 within the substrate channel. The studies presented in **chapter 2.3** support the presence of an electrostatic interaction between the positively charged side-chain of Arg445 in TMD8 and the negatively charged side-chain of Asp498 in TMD10. We demonstrated that mutations in these residues are detrimental for MCT8 function, unless their local charges are maintained or swapped from position. Both charged residues are usually not located within TMDs, which suggested a functional role for these residues and their interaction. In **chapter 2.4**, we performed additional chemical modification studies targeting residues other than cysteine and histidine which substantiated that Arg445 is located along the substrate channel. Next, we translated the results obtained in **chapters 2.1-2.4** into a predictive three-dimensional protein homology model of MCT8. This model supported a role for His192 and Arg445 in substrate transport through the formation of transient interactions with the phenolic-hydroxyl and carboxyl-group of thyroid hormone, respectively. Also the substitution of some other residues that were predicted to be located along the substrate channel reduced MCT8 function. One of these residues, Asn193 in TMD1, was further studied in **chapter 2.5**. Substitution of this residue by an alanine predominantly reduced the capacity of MCT8 to transport of T4, but not so much of T3. Computerized simulations of the passage of T4 through the substrate channel suggested that Asn193 forms interactions with the iodine moieties of T4, also termed halogen bonds, which may particularly govern the exact orientation of the T4 molecule during passage through the substrate channel.

In **chapter 2.6**, we have compared the functional characteristics of human MCT8 to its orthologues in mouse and zebrafish, which are the most frequently used animals to model human MCT8 deficiency. The MCT8 orthologues of both species efficiently transport T3 and T4, further supporting their wide application in the field. These findings also indicated that poorly conserved residues are probably less important for MCT8 function. Therefore, mutations in these residues are less likely to cause MCT8 deficiency in human. Subtle differences were present between human and mouse *versus* zebrafish MCT8, in particular the ability to transport the T3 metabolite triiodothyroacetic acid (Triac) which is lost in human and mouse, but retained in zebrafish. The MCT8 protein exists as a monomer, homo-dimer (complex of two MCT8 proteins) and oligomer (complexes of multiple MCT8 proteins). In **chapter 2.7** we further studied how such complexes are formed and aimed to delineate the function of this phenomenon. We found that these interactions likely depend on extensive hydrophobic and/or electrostatic contacts between multiple domains within the first 6 TMDs of the MCT8 protein. The formation of these complexes could not be disrupted by mutations, unless a substantial part of the protein was removed. This precluded studies on the physiological relevance of this process. As many other thyroid hormone transporters also accept a variety of alternative substrates, we questioned in **chapter 2.8** if MCT8 also accepts other substrates. By using metabolome analyses in transfected *Xenopus* oocytes and subsequent confirmatory studies in mammalian cell lines, we identified monoiodotyrosine (MIT) and diiodotyrosine (DIT) as novel substrates for MCT8. MIT and DIT are the building blocks of thyroid hormone synthesis and are highly abundant in the thyroid gland where MCT8 is highly expressed. In high concentrations, MIT and DIT reduced T3 and T4 transport *in vitro*, the consequences of which on thyroid hormone secretion by the thyroid gland *in vivo* are yet unknown.

The second part aimed to delineate the clinical phenotype of MCT8 in greater detail. For some mutations, we also explored the possible link between the impact of the mutation on MCT8 transport function in cells *versus* the severity of symptoms in the patient. In **chapter 3.1** we describe two patients with different mutations affecting the same Gly564 residue associated with a differential severity of the clinical phenotype. In line with the functional studies, the patient harboring the G564E mutation exhibited relatively less severe clinical features, whereas the G564R was associated with severe clinical features. These observations illustrate that the impact of a mutations on MCT8 function is not only determined by the loss of the properties of the mutated residue, but also by the (unfavorable) properties of the acquired residue. Although the majority of patients with MCT8 deficiency manifest severe developmental delay and intellectual disability, a small subset is able to walk and talk in simple sentences. In **chapter 3.2** we described two of such patients. Both mutations (T239P and L543P) had relatively high residual T3 uptake capacity in our cell models and in skin fibroblasts obtained from both patients. Since T3 uptake in skin fibroblasts mainly relies on MCT8, these cells comprise an easily accessible model to study the impact of mutation in patient cells. In **chapter 3.3** we describe 5 families with mutations affecting the C-terminal end of the MCT8 protein. In these studies we identified His575, located at the end of TMD12, as the pivotal point beyond which missense mutations and truncations of the MCT8 protein had no or minimal effects on MCT8 function *in vitro*, with a notable exception of frameshift mutations that elongate the MCT8 protein. Importantly, the novel H575R variant identified in a boy with unexplained intellectual disability by next-generation sequencing was found to have no impact on MCT8 function in transfected cells or in skin fibroblasts derived from the patient. Remarkably, this mutation had been classified as potentially pathogenic by computerized prediction tools that are frequently used in clinical practice. This study illustrates that functional evaluation of novel mutations in MCT8 is imperative to determine their pathogenicity and establish the correct diagnosis. In **chapter 3.4** we described 3 female carriers of mutations in the *MCT8* gene and unfavorable skewing of the X-chromosome. The altered serum thyroid hormone profile and presence of mild-moderate intellectual disability in 2 out of 3 cases were reminiscent to features observed in male patients with MCT8 deficiency, but much less pronounced clinical phenotype. The residual T3 uptake in fibroblasts of these patients correlated with the severity of the intellectual disability, which further supported causality. These findings indicate that MCT8 deficiency should also be considered in females with unexplained mild-moderate intellectual disability and abnormal thyroid function tests.

Since the clinical phenotype of MCT8 has only been described in case reports and small case series, a uniform description of the core clinical features of MCT8 deficiency and their natural progression over time is lacking. **Chapter 4.1** focuses on establishing a better description of the phenotype associated with mutations in MCT8 and establish a natural history, by taking advantage of a large international cohort of patients with MCT8 deficiency we established over the last decade. We showed that the overall life-expectancy in MCT8 deficiency is reduced, but that survival rates are significantly better in those subjects that attained head control. We identified (aspiration) pneumonia and sudden death as the principle causes of death in this population, both potentially modifiable by timely treatment. By conducting deep-phenotyping studies, we identified several novel features of MCT8 deficiency, including a broad spectrum of cardiovascular features, and established natural history data for key parameters that can be used as a reference in the assessment of efficacy of therapeutic interventions.

The third part of this thesis, **Chapter 5,** focuses on the therapeutic strategies for patients with MCT8 deficiency. Preclinical studies in mammalian cell lines had suggested that a subset of mutant MCT8

proteins, including the Phe501del mutant, may benefit from treatment with chemical chaperones such as phenylbutyrate. These chaperones may improve folding and modify the protein quality control system. In **chapter 5.1** we replicated these findings reported by others, but found that phenylbutyrate had also pronounced stimulatory effects at transcriptional level, which is regulated by an artificial promoter sequence in the applied models. Complementary studies in patient-derived fibroblasts showed that the stimulatory effects of phenylbutyrate were minimal, suggesting that the effects of phenylbutyrate on transcriptional regulation are much less pronounced in the context of the native MCT8 promoter. Further preclinical studies to the efficacy of phenylbutyrate are thus needed before it should be applied in patients with MCT8 deficiency. Given the promising results in preclinical studies, we evaluated the effectiveness and safety of the T3 analogue Triac in patients with MCT8 deficiency in **chapter 5.2.** This international clinical trial showed that Triac reduces serum T3 concentrations in all patients and concomitantly resulted in a significant increase of body weight, reduction in heart rate and alleviation of cardiac arrhythmia's as well as systolic hypertension. These clinical improvements were supported by changes in serum parameters that reflect tissue thyroid hormone state in the liver, kidney and muscle. Some patients experienced transient side-effects of Triac treatment, comprising signs of hyperthyroidism such agitation and increased perspiration, which spontaneously resolved within weeks. Therefore, Triac can be considered as the first therapeutic intervention that alleviates important clinical sequelae of MCT8 deficiency.

The final chapters describe studies employed to identify novel key-players in thyroid hormone signaling as well as the first report on a patient with a novel syndrome of resistance to thyroid hormone associated with deficiency of the T4-transporter OATP1C1. In **chapter 6.1**, we described a meta-analysis of genome-wide association studies on serum free T4 and thyroid hormone stimulating hormone (TSH) concentrations in up to 70 000 individuals with normal thyroid function. Through these studies, we identified SLC17A4 to be associated with serum free T4 concentrations. Subsequent functional studies showed that SLC17A4, like MCT8, is an efficient T3 and T4 transporter. We also identified AADAT as a novel thyroid hormone metabolizing enzyme, the further analysis of which falls beyond the scope of this thesis. In **chapter 6.2**, we further delineated the basic transporter characteristics of SLC17A4 and demonstrate that it particularly transports T3 and T4, in an Na^+- and Cl^--independent and pH-sensitive fashion. Importantly, SLC17A4 also facilitated the cellular efflux of T3 and T4. Glycosylation appears to be critical for SLC17A4 function. As the first step towards an *in vivo* mouse model to study SLC17A4 function, we compared the functional characteristics of the human and mouse SLC17A4 orthologues in **chapter 6.3**. Overall these characteristics are very similar, although the efflux capacity of mouse SLC17A4 appears to be somewhat lower than that of its human counterpart. Interestingly, both human and mouse SLC17A4 facilitated the uptake of Triac into the cell. Finally, we described the first patient with a homozygous inactivating mutation in the brain-specific T4 transporter OATP1C1 which was associated with a profound neurodegenerative phenotype (**chapter 6.4**). She presented progressive deterioration of cognitive and motor functions, accompanied by gray and white matter degeneration and severe cerebral glucose hypometabolism.

A general discussion of the findings described in this thesis as well as their implication on the field of thyroidology is presented in **chapter 7**. The gaps in current understanding of cellular thyroid hormone transporters, in particular MCT8, are discussed and future directions for research are presented.

SAMENVATTING

Schildklierhormoon is onmisbaar voor een normale ontwikkeling en is een belangrijke regulator van de energiehuishouding gedurende het leven. De schildklier, gelegen in de hals, maakt vooral het inactieve "voorloperhormoon" T4 en een kleine hoeveelheid "actief" hormoon T3. Ziekten aan de schildklier kunnen de productie van schildklierhormoon beïnvloeden en kunnen leiden tot een tekort aan schildklierhormoon (hypothyroïdie) of een overschot aan schildklierhormoon in het bloed (hyperthyreoïdie). Hypothyreoïdie kan leiden tot gewichtstoename, intolerantie voor koude, een trage hartslag en depressie. De tegenovergestelde symptomen kunnen voorkomen bij mensen met hyperthyreoïdie: gewichtsverlies, snelle hartslag, gejaagdheid en zweten.

De effecten van schildklierhormoon komen uiteindelijk tot stand door haar werking op de cel. De hoeveelheid en werking van schildklierhormoon in de cel wordt gereguleerd op verschillende niveaus: 1) schildklierhormoontransporters, te vergelijken met een soort "poortje" in de celwand (plasmamembraan) waardoor schildklierhormoon de cel in en uit kan, 2) verschillende enzymen (dejodases) die schildklierhormoon "activeren" door T4 om te zetten in T3, of juist af te breken en 3) receptoren voor schildklierhormoon in de celkern (schildklierhormoonreceptoren) die de expressie van T3-gevoelige genen beïnvloeden wanneer T3 aan hen bindt. Genen vormen de blauwdruk van het menselijk lichaam en worden gekopieerd naar messenger RNA (mRNA). Dit mRNA wordt vervolgens gebruikt door de cel om eiwitten te maken. Eiwitten zijn grote moleculen die verschillende functies kunnen hebben in de cel, zoals het maken van energie, het transporteren van stoffen over de plasmamembraan en het communiceren met andere cellen in de omgeving. Elk eiwit bestaat uit een keten van verschillende aminozuren. De verschillende aminozuren hebben een gemeenschappelijk gedeelte waarmee ze aan elkaar geschakeld kunnen worden en een uniek gedeelte, ook wel zijketen genoemd, die de eigenschappen van het aminozuur bepaald. De volgorde waarin de aminozuren aan elkaar geschakeld zitten bepaald de functie van het eiwit, vergelijk het met de manier waarop de volgorde van letters de inhoud van het woord bepaalt.

Schildklierhormoontransporters en dejodases bepalen hoeveel schildklierhormoon beschikbaar is in de cel om te binden aan haar receptoren. Tezamen zorgen deze 3 factoren ervoor dat de hoeveelheid en werking van schildklierhormoon in de cel nauwkeurig is afgestemd op haar behoefte, bijvoorbeeld tijdens haar groei en uitrijping (ook wel differentiatie genoemd), of tijdens het doormaken van een ontsteking. Ook wanneer de hoeveelheid schildklierhormoon in het bloed daalt, zullen deze factoren ervoor zorgen dat de hoeveelheid en werking van schildklierhormoon in de cel niet afnemen. Veranderingen of defecten in transporters, dejodases of receptoren kunnen leiden tot ziekte. Aangeboren defecten in receptoren en sommige transporters kunnen ertoe leiden tot cellen ongevoeligheid worden voor schildklierhormoon. Dit wordt schildklierhormoonresistentie genoemd. Bij deze aandoeningen is de cel niet in staat om schildklierhormoon goed waar te nemen.

Dit proefschrift richt zich vooral op MCT8 deficiëntie wat veroorzaakt wordt door een aangeboren defect (mutatie) in de schildklierhormoontransporter MCT8. MCT8 transporteert zowel T3 als T4 en is vooral belangrijk voor de opname van schildklierhormoon in de hersenen. Wanneer MCT8 niet goed werkt, komt er onvoldoende schildklierhormoon terecht in de hersenen. Dit leidt tot verstoring van de hersenontwikkeling en zeer ernstig verstandelijke en meervoudige beperkingen. Daarnaast zijn er sterk verhoogde hoeveelheden T3 aanwezig in het bloed. Cellen die gebruik maken van andere transporters dan MCT8 (bijvoorbeeld levercellen en spiercellen) worden hieraan blootgesteld, wat kan

leiden tot symptomen van hyperthyreoïdie. Het *MCT8* gen ligt op het vrouwelijke geslachtschromosoom (het X-chromosoom). Normaal gesproken heeft iedere vrouw twee kopieën van het X-chromosoom en daarmee van het *MCT8* gen. Het hebben van een mutatie in 1 kopie van het *MCT8* gen leidt bij vrouwen daarom meestal niet tot ziekte. Mannen hebben echter maar 1 X-chromosoom en daardoor maar 1 kopie van het *MCT8* gen. Wanneer dit éne exemplaar een mutatie bevat, gaat de werking van MCT8 verloren. Daarom komt MCT8 deficiëntie vooral voor bij mannen. Dit proefschrift bevat zowel basaal onderzoek naar de functie van MCT8 op moleculair niveau, als klinische studies bij patiënten met MCT8 deficiëntie.

Hoofdstuk 1 geeft een algemene inleiding op de werking en regulatie van schildklierhormoon. In het bijzonder wordt hier aandacht besteedt aan de schildklierhormoontransporters. Lange tijd werd aangenomen dat schildklierhormoon vanzelf het plasmamembraan kan passeren, omdat het goed zou kunnen oplossen in de vettige substantie waaruit het plasmamembraan bestaat. Eind vorige eeuw werd echter in toenemende mate duidelijk dat dit niet het geval is en dat schildklierhormoontransport eiwitten onmisbaar zijn voor dit proces. Uiteindelijk duurde het tot het begin van deze eeuw voordat de eerste schildklierhormoontransport eiwitten werden ontdekt. De belangrijkste eigenschappen van deze transporters zijn samengevat in dit hoofdstuk. Het belang van deze transporters werd pas onomstreden toen er mutaties werden gevonden in het *MCT8* gen bij mensen met ernstige verstandelijke en motorische beperkingen. Het eerste hoofdstuk eindigt met een beschrijving van de doelstellingen en de hoofdlijnen van het proefschrift.

Het eerste gedeelte van het proefschrift richt zich vooral op het beantwoorden van de vragen hoe schildklierhormoon door MCT8 wordt herkent en hoe het vervolgens de cel in getransporteerd wordt. Het MCT8 eiwit bestaat uit een keten van aminozuren die zijn georganiseerd in 12 bundels die door de plasmamembraan heen steken – daarom ook wel transmembraan domeinen (TMDs) genoemd. Deze bundels hebben de vorm van een helix, wat er voor zorgt dat het eiwit een stabiele vorm behoudt. De vrij rigide TMDs worden aan de binnenkant en de buitenkant van de cel aan elkaar verbonden door tussenliggende domeinen met een flexibele structuur, respectievelijk de intracellulaire loops (ICLs) en extracellulaire loops (ECLs). De 12 bundels liggen min of meer in een cirkel en vormen daardoor samen een gat, wat we het substraatkanaal noemen. De eigenschappen van de aminozuren die grenzen aan het substraatkanaal zorgen ervoor dat MCT8 alleen schildklierhormoon doorlaat en alle andere stoffen niet, dit noemt men substraat-selectiviteit. Om de werking van MCT8 te begrijpen is het dus belangrijk om te weten welke aminozuren dit precies zijn. Op basis van deze kennis is het mogelijk een model te maken van de structuur van het MCT8 eiwit en verder te ontrafelen hoe MCT8 precies werkt.

In **hoofdstuk 2.1** vonden we dat de zijketens van twee cysteïne aminozuren, Cys481 in ECL5 en Cys497 in TMD10, kunnen reageren met chemische verbindingen die specifiek cysteïnes herkennen (p-chloromercuribenzeen sulfonaat and $HgCl_2$). Deze reacties vinden alleen plaats als de cysteïne zijketen op een bereikbare plek zit in het MCT8 eiwit, bijvoorbeeld in het substraatkanaal of een van de extracellulaire loops. De effecten van de verbindingen waren minder groot in de aanwezigheid van schildklierhormoon, wat suggereert dat op zijn minst een van de beide cysteïnes (waarschijnlijk Cys497 in TMD10) wordt afgeschermt wanneer er schildklierhormoon in het substraatkanaal aanwezig is. Op eenzelfde manier vonden we in **hoofdstuk 2.2** dat een histidine residu in TMD1 (His192) kan reageren met een chemische verbinding die specifiek toegankelijke histidines herkend (diethyl pyrocarbonaat). Dit kon geheel worden voorkomen door de aanwezigheid van schildklierhormoon, wat suggereert dat ook His192 grenst aan het substraatkanaal. In **hoofdstuk 2.3** vonden we dat een arginine (Arg445) in

TMD8 en een asparaginezuur in TMD10 (Asp498) belangrijk zijn voor de functie van MCT8. De zijketen van arginine heeft een positieve lading en die van asparaginezuur een negatieve lading. Daarom is hun positie in een TMD opmerkelijk. In verschillende experimentele cel-modellen, vonden we dat MCT8 zijn transport functie verliest wanneer een van beide aminozuren vervangen wordt door een aminozuur zonder lading. Daarentegen, bleef de functie van MCT8 (grotendeels) behouden wanneer we beide aminozuren vervingen door een aminozuur met eenzelfde lading, of wanneer we de arginine en asparaginezuur van plek verwisselden. Dit suggereert dat de lading van deze aminozuren op deze posities erg belangrijk is en dat beide residuen zich mogelijk tot elkaar aangetrokken voelen en een zoutbrug vormen (een type moleculaire verbinding). In **hoofdstuk 2.4** laten we bovendien zien dat de zijketen van Arg445 kan reageren met een chemische verbinding die toegankelijke arginine zijketens herkent. Ook dit kon voorkomen worden door de aanwezigheid van schildklierhormoon, wat bevestigd dat Arg445 op een belangrijke locatie in het substraatkanaal zit. Op basis van de bevindingen in **hoofdstukken 2.1-2.4** hebben we de driedimensionale structuur van het MCT8 voorspeld met behulp van geavanceerde computer software. Dit MCT8 model liet zien dat His192 en Arg445 een tijdelijke verbinding vormen met schildklierhormoon wanneer dit zich in het substraatkanaal bevindt. Dit leidt er onder meer toe dat de verbinding tussen Arg445 en Asp498 verbroken wordt, wat een belangrijke stap kan zijn in het transport proces. Aan de hand van het model hebben we ook enkele andere aminozuren veranderd en de gevolgen hiervan op MCT8 functie getest in het laboratorium. Een van deze aminozuren betrof een asparagine in TMD1 (Asn193). In **hoofdstuk 2.5** vonden we dat het inkorten van deze zijketen het transport van T4 sterk verminderde, maar weinig effect had op dat van T3. Door de passage van T4 door het substraatkanaal te simuleren in het MCT8 model zagen we dat Asn193 verbindingen maakt met de jodiumgroepen van schildklierhormoon – zogenaamde halogeen-verbindingen. Deze verbindingen lijken vooral belangrijk om T4 met grote precisie door het substraatkanaal te loodsen. Deze precisie is waarschijnlijk minder noodzakelijk voor T3, omdat het wat kleiner is.

Ook de meeste diersoorten hebben een *MCT8* gen. Door genetische variatie ziet het MCT8 eiwit er in de meeste dieren net iets anders uit dan in de mens. Deze variatie kan er soms voor zorgen dat de functie van een eiwit verschilt tussen mens en dier. Toch worden dieren vaak gebruikt om te bestuderen hoe bepaalde ziektebeelden in de mens werken. Voor MCT8 deficiëntie worden vooral de muis en de zebravis gebruikt. In **hoofdstuk 2.6** hebben we de transport eigenschappen van muis en zebravis MCT8 vergeleken met die van de mens. Dit is cruciaal om te weten of deze dieren wel gebruikt kunnen worden als model voor MCT8 deficiëntie. Het bleek dat de meest belangrijke eigenschap, namelijk het transporteren van T3 en T4, niet veel verschilt tussen het MCT8 van de muis en zebravis en dat van de mens. Het lijkt er dus op dat de aminozuren die verschillen tussen mens, muis en zebravis MCT8 waarschijnlijk niet cruciaal zijn voor de functie van MCT8. Daarom leiden mutaties in deze aminozuren in de mens waarschijnlijk niet tot MCT8 deficiëntie.

Voorgaande studies hadden laten zien dat het MCT8 eiwit een verbinding kan maken met een tweede MCT8 eiwit. Deze complexen noemen we homodimeren. Wanneer MCT8 verbindingen maakt met meerdere andere MCT8 eiwitten, spreken we van homo-oligomeren. In **hoofdstuk 2.7** hebben we bestudeerd hoe deze verbindingen worden gemaakt en welke domeinen van het MCT8 eiwit hierbij betrokken zijn. We toonden aan dat deze verbindingen erg sterk zijn en dat meerdere gedeeltes van de eerste 6 TMDs hierbij betrokken zijn. MCT8 vormt dan ook alleen geen complexen meer wanneer

grote gedeeltes van het MCT8 verwijderd zijn. Daarom hebben we niet kunnen achterhalen wat de precieze functie is van dit fenomeen.

In **hoofdstuk 2.8** hebben we gekeken of MCT8 naast schildklierhormoon ook nog andere substraten kan transporteren. Dit hebben we gedaan door een groot aantal metabolieten te meten in eicellen van kikkers (oocyten) waaraan we MCT8 hebben toegevoegd en deze te vergelijken met eicellen zonder MCT8. Hieruit bleek dat MCT8 ook MIT en DIT kan transporteren. MIT en DIT zijn de bouwstenen van schildklierhormoon en zijn in hoge concentraties aanwezig in de schildklier. In de schildklier speelt MCT8 een belangrijke rol bij de afgifte van schildklierhormonen aan het bloed. In onze cel modellen vonden we dat hoge concentraties MIT en DIT het transport van schildklierhormonen door MCT8 kan verminderen. We weten nog niet of MCT8 ook in de mens MIT en DIT transporteert en in hoeverre dit het transport van schildklierhormoon kan beïnvloeden.

Het voornaamste doel van het tweede gedeelte van dit proefschrift was het in kaart brengen van de symptomen van patiënten met MCT8 deficiëntie. Hiertoe hebben we eerst naar een aantal patiënten met bijzondere mutaties in MCT8 gekeken en later, in samenwerkingen met vele dokters in het buitenland, ook naar een hele grote groep patiënten met MCT8 deficiëntie. Voor sommige mutaties hebben we ook onderzocht of de ernst van de symptomen samenhangt met de rest-capaciteit van het foutieve MCT8 eiwit. In **hoofdstuk 3.1** beschrijven we twee patiënten bij wie de mutatie hetzelfde glycine (Gly564) residu veranderd. De patiënt bij wie het Gly564 is vervangen door een glutaminezuur (G564E) had relatief minder ernstige symptomen dan de patiënt bij wie de Gly564 vervangen is door een arginine (G564R). Dit correspondeerde sterk met de gemeten transport functie van beide mutant eiwitten in onze cel modellen. Deze studies tonen aan dat niet alleen het verlies van een belangrijk aminozuur, maar ook de (ongunstige) eigenschappen van het verworven aminozuur in belangrijke mate het effect van de mutatie bepalen. Hoewel veel patiënten met MCT8 deficiëntie een ernstige ontwikkelingsachterstand hebben, is een klein gedeelte in staat om te lopen en te praten. In **hoofdstuk 3.2** beschrijven twee patiënten met een relatief minder ernstige uitingsvorm (fenotype) van MCT8 deficiëntie. Beide MCT8 mutaties hadden ten opzichten van andere patiëntmutaties nog een relatief hoge opnamecapaciteit in onze cel modellen en in huidfibroblasten van de patiënten. Huidfibroblasten zijn grotendeels afhankelijk van MCT8 en vormen daardoor een goed model om de effecten van mutaties in MCT8 te meten in lichaamscellen van de patiënt zelf. In **hoofdstuk 3.3** beschrijven we een aantal patiënten met mutaties in de zogenaamde C-terminale staart. Deze staart steekt aan de binnenkant van de cel uit het plasmamembraan. We vonden dat verschillende mutaties in deze staart of het geheel ontbreken ervan (met His575 als beginpunt) geen invloed heeft op de functie van MCT8 in onze cel modellen. Dit gold ook voor een His575Arg mutatie die we vonden in een patiënt met ontwikkelingsachterstand. Dit was opmerkelijk, omdat enkele veelgebruikte computerprogramma`s hadden voorspeld dat deze verandering het MCT8 eiwit inactief maakt. Het testen van de invloed van MCT8 mutaties in cel modellen blijft daarom erg belangrijk om aan te tonen dat deze ook echt de ontwikkelingsachterstand veroorzaken. In **hoofdstuk 3.4** rapporteren we drie vrouwelijke patiënten met verschillende maten van ontwikkelingsachterstand en milde schildklierhormoonafwijkingen in het bloed. Deze combinatie had gelijkenissen met de symptomen van mannelijke patiënten met MCT8 deficiëntie, maar waren wel milder. We vonden dat deze patiëntes inderdaad een mutatie in één kopie van het *MCT8* gen hadden. Normaal ontwikkelen vrouwen hierbij geen symptomen, omdat ze nog een tweede, gezonde kopie hebben; maar bij deze patiëntes stond ook deze (deels) uit. Inderdaad vonden we dat de MCT8 functie in de huid fibroblasten van deze patiëntes verlaagd was. Op basis van deze bevindingen concluderen we dat MCT8 deficiëntie soms ook bij vrouwen kan voorkomen en kan leiden

tot een milde tot matige ontwikkelingsachterstand en afwijkende schildklierhormoonwaardes in het bloed.

Tot voorkort waren de symptomen en het beloop van MCT8 deficiëntie alleen beschreven in studies waarin naar afzonderlijke patiënten of kleine aantallen patiënten werd gekeken. Deze studies hadden veelal verschillende invalshoeken waardoor steeds andere symptomen werden belicht en op verschillende wijze zijn gemeten. Een systematische vergelijking van patiënten was hierdoor onmogelijk. In **hoofdstuk 4.1** hebben we gekeken naar een grote groep patiënten met MCT8 deficiëntie en de symptomen die optreden op een eenduidige wijze vastgelegd. Ook hebben we gekeken naar het verloop van deze symptomen en naar de meest voorkomende doodsoorzaken. We vonden dat de levensverwachting van patiënten met MCT8 deficiëntie over het algemeen verlaagd is en dat de levensverwachting van patiënten met een goede hoofdbalans beter is dan die van patiënten zonder hoofdbalans. Longontstekingen, verslikking en plotse dood zijn de meest voorkomende doodsoorzaken, welke mogelijk te voorkomen zijn door tijdige preventieve maatregelen. Ook vonden we een aantal, tot dusver onderbelichte, symptomen regelmatig terug, zoals een snelle hartslag, hoge bloeddruk en een afwijkend hartritme, en hebben we de ontwikkeling en het tijdsbeloop van veel voorkomende symptomen in kaart gebracht. Deze gegevens kunnen we in de toekomst gebruiken om te kijken of nieuwe behandelingen het ziektebeloop gunstig beïnvloeden.

In het derde gedeelte van dit proefschrift kijken we naar verschillende behandelstrategieën. Voorgaand laboratoriumonderzoek suggereerde dat de nadelige effecten van sommige MCT8 mutaties afnemen door behandeling met chemische “helper” verbindingen (chaperons), zoals fenylbutyraat. Deze chaperons verbeteren mogelijk de structuur en daarmee de functie van het gemuteerde MCT8 eiwit. In **hoofdstuk 5.1** hebben we deze bevindingen kunnen bevestigen in onze cel modellen, maar vonden we dat de positieve effecten niet alleen toe te schrijven zijn aan het verbeteren van de eiwit structuur, maar ook aan het opschroeven van de hoeveelheid mRNA en MCT8 eiwit dat wordt gemaakt in de cel. Dit laatste effect kan sterk worden bepaald door de manier waarop we (foutieve) MCT8 eiwitten maken in onze cel modellen. Daarom hebben we ook gekeken naar het effect van fenylbutyraat in huidcellen van een patiënt met een mutatie die gevoelig was voor deze behandeling in onze cel modellen. In deze huidcellen, waarin MCT8 op natuurlijke wijze wordt aangemaakt, bleek het effect van fenylbutyraat veel minder te zijn. Verder onderzoek naar de effectiviteit van fenylbutyraat is dus nodig, voordat het kan worden toegepast bij patiënten met MCT8 deficiëntie. Naar aanleiding van gunstige effecten in diermodellen voor MCT8 deficiëntie, hebben we in **hoofdstuk 5.2** de effectiviteit en veiligheid van Triac onderzocht bij patiënten met MCT8 deficiëntie. Triac lijkt erg op het actieve schildklierhormoon T3, maar heeft geen MCT8 nodig om de cel binnen te komen. In deze geneesmiddelen studie, vonden we dat Triac de hoge T3 concentraties in het bloed bij alle patiënten verlaagde. Dit ging gemiddeld gezien gepaard met een verbetering van het lichaamsgewicht, een daling van de hartslagfrequentie en systolische bloeddruk en een verbetering van het hartritme. Ook in het bloed zagen we veranderingen die passen bij een verbeterde schildklierhormoonwerking in de lever, nier en spier. Sommige patiënten hadden last van tijdelijke bijwerkingen, zoals overmatig zweten en onrust, maar die verdwenen spontaan binnen een aantal weken. Op basis van dit onderzoek, lijkt Triac het eerste medicijn te zijn dat het ziektebeloop van MCT8 deficiëntie gunstig kan beïnvloeden.

Het laatste gedeelte van dit proefschrift beschrijft de studies die erop gericht waren om nieuwe genen te vinden die betrokken zijn bij het regelen van de hoeveelheid schildklierhormoon in het bloed. In

hoofdstuk 6.1 hebben we gekeken naar de relatie tussen veelvoorkomende varianten in genen en de hoeveelheid vrij T4 (het voorloperhormoon) en TSH (de stof die de schildklier aanzet tot het maken van hormoon) in ruim 70 000 mensen met een gezonde schildklierfunctie. We vonden onder anderen dat variaties in het *SLC17A4* gen van invloed zijn op de hoeveelheid vrij T4 in het bloed. In het laboratorium vonden we dat SLC17A4, net als MCT8, een erg efficiënte schildklierhormoontransporter is. In **hoofdstuk 6.2** hebben we de transporteigenschappen van SLC17A4 verder in kaart gebracht en vonden we dat voornamelijk T3 en T4 via deze transporter de cel in, maar ook uit kunnen. Om precies te weten te komen wat SLC17A4 doet in ons lichaam en hoe het de hoeveelheid T4 in het bloed beïnvloed is het in de toekomst nodig om verder onderzoek te doen in muizen. Daarom hebben we in **hoofdstuk 6.3** gekeken of de eigenschappen van het SLC17A4 eiwit van de muis hetzelfde zijn als die van de mens. Dit bleek het geval, hoewel de muis variant schildklierhormoon iets minder goed de cel uit laat gaan.

In **hoofdstuk 6.4** beschrijven we de eerste patiënte met een nieuw schildklierhormoonresistentie syndroom, veroorzaakt door een mutatie in het schildklierhormoontransporteiwit OATP1C1. De belangrijkste kenmerken van dit syndroom zijn progressieve achteruitgang van verschillende hersenfuncties, zoals het verliezen van motorische vaardigheden, taal en spraak. Deze symptomen gingen gepaard met verschillende afwijkingen op de hersenscan, zoals een sterk verlaagde stofwisseling. Dit is een proces dat sterk wordt beïnvloed door de hoeveelheid schildklierhormoon in de hersenen.

Hoofdstuk 7 bevat een algemene discussie van alle bevindingen en beschrijft de impact hiervan op het onderzoeksgebied. Hier worden ook een aantal punten genoemd op het gebied van schildklierhormoontransporters die we nu nog onvoldoende begrijpen en verder onderzocht moeten worden.

AUTHOR AFFILIATIONS

Department of Internal Medicine, section Endocrinology and Academic Center for Thyroid Diseases, Erasmus University Medical Center, Rotterdam, The Netherlands.
Stefan Groeneweg, Ferdy S. van Geest, Elaine C. Lima de Souza, Edith C.H. Friesema, Simone Kersseboom, Wim Klootwijk, Anna Dolcetta-Capuzzo, Amanda van den Berge, Ramona E.A. van Heerebeek, Chantal Zevenbergen, Stefania Farina, Milou Stals, Ebrar Gurcan, Zhongli Chen, Celia Di Munno, Layal Chaker, Marco Medici, Marcel E. Meima, Theo J. Visser, W. Edward Visser, Robin P. Peeters

Sophia Children's Hospital, Department of Pediatric Neurology, Erasmus Medical Center, University Medical Center Rotterdam, Rotterdam, The Netherlands.
Marieke M. van der Knoop, Femke K. Aarsen, René F.M. de Coo, Marie-Claire Y. de Wit

Sophia Children's Hospital, Division of Paediatric Cardiology, Erasmus Medical Centre, Rotterdam, The Netherlands.
Ingrid M. van Beynum

Department of Cardiology and Intensive Care Medicine, Erasmus Medical Centre, Rotterdam, The Netherlands.
Corstiaan A. den Uil

Department of Internal Medicine, Erasmus Medical Centre, Rotterdam, The Netherlands.
M. Carola Zillikens

Department of Clinical Chemistry, Erasmus Medical Centre, Rotterdam, The Netherlands.
Yolanda B. de Rijke

Department of Pediatric Radiology, Erasmus University Medical Center Sophia Children's Hospital, Rotterdam, The Netherlands.
Marjolein H.G. Dremmen

Department of Clinical Genetics, Erasmus Medical Center, University Medical Center Rotterdam, Rotterdam, The Netherlands.
Kyra Stuurman

Department of Pediatric Neurology, Emma Children's Hospital, Amsterdam University Medical Centre, Amsterdam, The Netherlands.
Nicole I. Wolf

Department of Paediatrics, Meander Medical Center, Amersfoort, The Netherlands.
Jurgen Jansen

's Heeren Loo, Julianadorp, The Netherlands.
Martien Manshande

's Heeren Loo, Ermelo, The Netherlands.
Frank E. Visser

Baalderborg, Hardenberg, The Netherlands.
Paul Vrijmoeth

Latyrus, Dedemsvaart, The Netherlands.
Angelique Zandstra

Department of Child Neurology, University Medical Center Groningen, University of Groningen, Groningen, The Netherlands.
Ineke J. Lunsing

Department of Paediatrics, Refaja Hospital, Stadskanaal, The Netherlands.
Stan Nowak

Psychosocial Department, Emma Children's Hospital, Amsterdam UMC, University of Amsterdam, The Netherlands.
Kim J. Oostrom

Department of Pediatric Endocrinology, Emma Children's Hospital, Amsterdam UMC, University of Amsterdam, The Netherlands.
Paul van Trotsenburg

Department of Animal Ecology and Physiology, Institute for Water and Wetland Research, Faculty of Science, Radboud University Nijmegen, Nijmegen, The Netherlands.
Francisco J. Arjona

Wellcome Trust-Medical Research Council Institute of Metabolic Science, University of Cambridge, Cambridge, UK.
Carla Moran, Greta Lyons, Anne McGowan, Krish Chatterjee

Department of Paediatric Neurology, Addenbrooke's Hospital, Cambridge University Hospitals NHS Foundation Trust, Cambridge, UK.
Gautem Ambegaonkar

Department of Paediatric Cardiology, Addenbrooke's Hospital, Cambridge University Hospitals NHS Foundation Trust, Cambridge, UK.
Yogen Singh

Paediatric Endocrinology, Diabetology and Gynaecology Department, Necker Children's University Hospital, Imagine Institute, Paris, France.
Athanasia Stoupa, Michel Polak

Department of Paediatric Endocrinology and Genetics, Children's Hospital, Toulouse University Hospital, Toulouse, France.
Françoise Auriol, Isabelle Oliver Petit

Paediatric Neurology Clinic, Alexandru Obregia Hospital, Bucharest, Romania.
Alice Dica, Diana Barca, Dana Craiu

Department of Paediatrics, Second Faculty of Medicine, Charles University, University Hospital Motol, Prague, Czech Republic.
Klara Rozenkova, Jana Malikova, Jan Lebl

Panorama Medical Centre, Cape Town, South Africa.
Adri van der Walt

Department of Paediatrics, Algemeen Ziekenhuis Sint-Jan, Bruges, Belgium.
Sylvia Depoorter

Paediatric Neurology Unit, Department of Paediatrics, Universitair Ziekenhuis Brussel, Brussels, Belgium.
Linda De Meirleir

Department of Endocrinology, Diabetes and Metabolism, University Hospital Essen, University Duisburg-Essen; Essen, Germany.
Heike Heuer

Department of Paediatric Endocrinology and Diabetology, Charité-Universitätsmedizin Berlin, Berlin, Germany.
Heiko Krude

Institute for Community Medicine, University Medicine Greifswald, Greifswald, Germany.
Alexander Teumer

Department of Biometry, Epidemiology and Medical Bioinformatics, Institute of Genetic Epidemiology, Faculty of Medicine and Medical Center-University of Freiburg, Freiburg, Germany.
Yong Li

Institut für Experimentelle Pädiatrische Endokrinologie, Charité—Universitätsmedizin Berlin, Germany.
Heike Biebermann

Institut für Biochemie und Molekularbiologie, Rheinische Friedrich-Wilhelms-Universität Bonn, Bonn, Germany.
Ulrich Schweizer

Unit of Neuromuscular and Neurodegenerative diseases, Department of Neurosciences, Bambino Gesù Research Hospital, Rome, Italy.
Ginevra Zanni, Marta Nardella, Laura Paone, Enrico Bertini, Marco Cappa

Unit of Child Neuropsychiatry, Department of Neurosciences, Bambino Gesù Research Hospital, Rome, Italy.
Paolo Alfieri

Department of Child Neurology, IRCCS Foundation C. Besta Neurological Institute, Milan, Italy.
Veronica Saletti, Davide Tonduti, Federica Zibordi

Department of Pediatric Neuroscience, IRCCS Foundation C. Besta Neurological Institute, Milan, Italy.
Elena Freri, Margherita Estienne, Sara Matricardi

Unit of Genetics of Neurodegenerative and Metabolic Diseases, IRCCS Foundation C. Besta Neurological Institute, Milan, Italy.
Barbara Castellotti, Ettore Salsano

Neuroradiology Unit, IRCCS Foundation C. Besta Neurological Institute, Milan, Italy.
Luisa Chiapparini

Division of Genetics and Cell Biology, San Raffaele Scientific Institute, Milan, Italy.
Caterina Barbieri

Department of Endocrinology and Internal Medicine, San Raffaele Scientific Institute, Milan, Italy.
Anna Dolcetta-Capuzzo

Department of Molecular Medicine, University of Pavia, Pavia, Italy.
Francesca Novara, Paolo Reho, Orseta Zuffardi

Department of Pediatric Neurology, V. Buzzi Children's Hospital, Milan, Italy.
Silvia Masnada, Davide Tonduti

Department of Translational Medicine, Federico II University, Naples, Italy.
Nicola Brunetti, Gerarda Cappuccio

Department of Clinical Genetics, Hospital de Clínicas de Porto Alegre, Porto Alegre, Brazil.
Cláudia Fernandes Lorea

Division of Endocrinology, University of Louisville, School of Medicine, Louisville, USA.
Priyanka Bakthiani

Division of Pediatric and Adolescent Medicine; Oslo University Hospital , Oslo, Norway.
Petter Strømme, Linda Høneren Johansson

Department of Medical Genetics, Oslo University Hospital and University of Oslo , Oslo, Norway.
Anette Torgersbråten, Asbjørn Holmgren, Eirik Frengen, Doriana Misceo

Department of Nuclear Medicine; Oslo University Hospital , Oslo, Norway.
Almira Babovic

Clinical Neurochemistry Laboratory, Sahlgrenska University Hospital , Mölndal, Sweden.
Henrik Zetterberg

Institute of Medical Molecular Genetics, University of Zurich, Switzerland.
Barbara Kloeckener-Gruissem

Functional Genomics Center, University and ETH Zurich, Zurich, Switzerland.
Endre Laczko

Institute of Physiology and Zurich Center for Integrative Human Physiology, University of Zurich, Zurich, Switzerland.
François Verrey, Simone M.R. Camargo

LIST OF PUBLICATIONS

Groeneweg S, van Geest FS, Peeters RP, Heuer H, Visser WE. 2019 Thyroid hormone transporters. Endocr Rev, accepted for publication.

Wejaphikul K, van Gucht A, **Groeneweg S**, Visser WE, Visser TJ, Peeters R, Meima M. 2019 The *in vitro* functional impairment of thyroid hormone receptor alpha 1 isoform mutants is mainly dictated by reduced ligand-sensitivity. Thyroid, accepted for publication.

Groeneweg S*, Kersseboom S*, van den Berge A, Dolcetta-Capuzzo A, van Geest FS, van Heerebeek REA, Arjona FJ, Meima M, Peeters R, Visser WE, Visser TJ. 2019 *In vitro* characterization of human, mouse and zebrafish MCT8 orthologues. Thyroid, 29(10):1499-1510.

Masnada S, **Groeneweg S**, Saletti V, Chiapparini L, Castellotti B, Salsano E, Visser WE, Tonduti D. 2019 Novel mutations in SLC16A2 associated with a less severe phenotype of MCT8 deficiency. Metab Brain Dis, 34(6):1565-1575.

Groeneweg S, Peeters RP, Moran C, Stoupa A, Auriol F, Tonduti D, et al. 2019 Effectiveness and safety of Triac in children and adults with MCT8 deficiency: an international, multicentre, single group, open-label, phase 2 trial. Lancet Diabetes Endocrinol, 7(9):695-706.

Wejaphikul K, **Groeneweg S**, Hilhorst-Hofstee Y, Chatterjee VK, Peeters RP, Meima ME, Visser WE. 2019 Insight into molecular determinants of T3 vs. T4 recognition from mutations in thyroid hormone receptor alpha and beta. J Clin Endocrinol Metab, pii: jc.2018-02794.

Zevenbergen C, **Groeneweg S**, Swagemakers SMA, de Jong A, Medici-Van den Herik E, Rispens M, et al. 2019 Functional Analysis of Genetic Variation in the SECIS Element of Thyroid Hormone Activating Type 2 Deiodinase. J Clin Endocrinol Metab, 104(5):1369-1377.

Stromme P*, **Groeneweg S***, Lima de Souza EC, Zevenbergen C, Torgersbraten A, Holmgren A, et al. 2018 Mutated thyroid hormone transporter OATP1C1 associates with severe brain hypometabolism and juvenile neurodegeneration. Thyroid, 28(11):1406-1415.

Wejaphikul K, **Groeneweg S**, Dejkhamron P, Unachak K, Visser WE, Chatterjee VK, et al. 2018 Role of leucine 341 in thyroid hormone receptor beta revealed by a novel mutation causing thyroid hormone resistance. Thyroid, 28(12).

Teumer A*, Chaker L*, **Groeneweg S***, Li Y*, Di Munno C*, Barbieri C*, Schultheiss U* et al. 2018 Genome-wide analyses identify a role for SLC17A4 and AADAT in thyroid hormone regulation. Nat Commun, 9(1):4455.

Groeneweg S, van den Berge A, Meima ME, Peeters RP, Visser TJ, Visser WE. 2018 Effects of chemical chaperones on thyroid hormone transport by MCT8 mutants in patient-derived fibroblasts. Endocrinology, 159(3):1290-1302.

Groeneweg S, Lima de Souza EC, Meima ME, Peeters RP, Visser WE, Visser TJ. 2017 Outward-Open Model of Thyroid Hormone Transporter Monocarboxylate Transporter 8 Provides Novel Structural and Functional Insights. Endocrinology, 158(10):3292-3306.

Groeneweg S, Visser WE, Visser TJ. 2017 Disorder of thyroid hormone transport into the tissues. Best Pract Res Clin Endocrinol Metab, 31(2):241-253.

Groeneweg S, Peeters RP, Visser TJ, Visser WE. 2017 Triiodothyroacetic acid in health and disease. J Endocrinol, 234(2):R99-R121.

Groeneweg S, Peeters RP, Visser TJ, Visser WE. 2017 Therapeutic applications of thyroid hormone analogues in resistance to thyroid hormone (RTH) syndromes. Mol Cell Endocrinol, S0303-7207(17)30116-8.

Novara F*, **Groeneweg S***, Freri E, Estienne M, Reho P, Matricardi S, Castellotti B, Visser WE, Zuffardi O, Visser TJ. 2017 Clinical and Molecular Characteristics of SLC16A2 (MCT8) Mutations in Three Families with the Allan-Herndon-Dudley Syndrome. Hum Mutat, 38(3):260-264.

Groeneweg S, Peeters RP, Visser TJ, Visser WE. 2016 Diagnostic and therapeutic challenges in the Allan-Herndon-Dudley Syndrome. US Endocrinology, 12 (02):90.

Groeneweg S, Friesema ECH, Kersseboom S, Klootwijk W, Visser WE, Peeters RP, Visser TJ. 2013 The role of Arg445 and Asp498 in the human thyroid hormone transporter MCT8. Endocrinology, 155(2):618-26.

Groeneweg S, Lima de Souza EC, Visser WE, Peeters RP, Visser TJ. 2013 Importance of His192 in the human thyroid hormone transporter MCT8 for substrate recognition. Endocrinology, 154(7):2525-32.

Lima de Souza EC, **Groeneweg S**, Visser WE, Peeters RP, Visser TJ. 2013 Importance of Cysteine residues in the thyroid hormone transporter MCT8. Endocrinology, 154(5):1948-55.

CURRICULUM VITAE

Stefan Groeneweg was born on February 28th, 1989 in Rotterdam. After completing secondary school at the Krimpenerwaard College in Krimpen aan den IJssel, he started his study of Medicine at the Erasmus University Medical Centre in Rotterdam. After successful completion of the first and second year, he also started the Molecular Medicine research master at the Erasmus Medical Centre. In September 2012 he obtained his Master degree in Molecular Medicine and in January 2016 he obtained his medical degree. During his studies, he entered the field of thyroid research at the laboratory of the thyroid expert prof. dr. ir. Theo Visser, where he performed his internship of the Molecular Medicine research master program. Following this exciting and inspiring collaboration, he started as a PhD candidate in 2014 and meanwhile continued his medical training. The results of this fruitful collaboration are presented in this thesis. For his studies on thyroid hormone signalling, in particular thyroid hormone transporters, he obtained three travel grants from the European Thyroid Association (2016, Colorado Springs, USA; 2018, Newcastle, UK; and 2019, Budapest, Hungary), and two travel grants from the American Thyroid Association (2015, Orlando, USA; and 2016, Denver, USA). In addition, he was awarded the NVE-Ipsen prize for the best endocrinology paper in 2018. In 2019, he received his first personal research grant from the European Thyroid Association. Moreover, he is co-founder of the MCT8 deficiency patient registry and member of the working group “Thyroid disease” of the European Registries for Rare Endocrine Conditions (EuRRECa), part of the ERN-Endo. He married Marieke van der Knoop and they have three beautiful children Elin, Hidde and Jurre.

Name PhD Student	Stefan Groeneweg
Erasmus MC Department	Internal Medicine – Academic Center for thyroid disease
Research school	Molecular Medicine
PhD period	May 2014-December 2019
Promotor	Prof. dr. R.P. Peeters

Courses	Year	Workload
Radiation course 5B, Erasmus MC, Rotterdam	2009	5 days
Molecular Imaging course, Erasmus MC, Rotterdam	2013	5 days
Introduction to confocal microscopy, Erasmus MC, Rotterdam	2013	2 days
The course Biomedical Research Techniques, Erasmus MC, Rotterdam	2013	5 days
Drugs and the brain, Caltech, USA	2013	5 days
Health Informatics in the Cloud, Georgia Institute of Technology, USA	2013	5 days
Basic course on Regulation and Organisation for clinical investigators (NFU BROK), Erasmus MC, Rotterdam	2014	5 days
Course on the use of Open Clinica, Erasmus MC, Rotterdam	2014	2 days
International Thyroid Conference basic research track, Orlando, USA	2015	2 days
American Thyroid Association basic research track	2016	2 days
Endnote workshop, Erasmus MC, Rotterdam	2017	1 day
Course on the use of Limesurvey and Gemstracker, Erasmus MC, Rotterdam	2018	2 days
Biomedical English writing and communication, Erasmus MC, Rotterdam	2018	10 weeks
European Thyroid Association, basic research track, Newcastle, UK	2018	1 day
The Ensemble workshop, Erasmus MC, Rotterdam	2018	2 days
Research integrity course, Erasmus MC, Rotterdam	2018	1 day
European Thyroid Association, basic research track, Budapest, Hungary	2019	1 day

Recurrent internal meetings	Year	Workload
Work discussion thyroid laboratory (weekly)	2014-2019	0.25 day
Focus meeting on thyroid hormone transporters (bi-weekly)	2016-2019	0.25 day
Focus meeting on thyroid hormone receptors and metabolism (bi-weekly)	2016-2019	0.25 day
Endocrine lectures	2014-2016	0.25 day

Conferences	Year	Workload
Internal Medicine Science days, Antwerp, Belgium	2012	2 days
Voorjaarsvergadering Nederlandse Vereniging voor Kinderneurologie, Heemsteede, The Netherlands	2015	1 day
MCT8 deficiency conference, Los Angeles, USA	2015	3 days
Internal Medicine Science days, Antwerp, Belgium	2015	2 days
International Thyroid Congress, Orlando, USA	2015	5 days
MCT8 deficiency conference, Los Angeles, USA	2016	3 days
Internal Medicine Science days, Antwerp, Belgium	2016	2 days
Stichting Schildklieronderzoek Nederland, Groningen, The Netherlands	2016	1 day
European Thyroid Association, Copenhagen, Denmark	2016	4 days
International workshop on Resistance to Thyroid Hormone, Colorado Springs, USA	2016	4 days
American Thyroid Association, Denver, USA	2016	5 days

Conferences (continued)	**Year**	**Workload**
European Pediatric Neurology Society, Aachen, Germany	2016	1 day
MCT8 deficiency conference, Los Angeles, USA	2017	3 days
European Congress of Endocrinology, Lisbon, Portugal	2017	4 days
Annual symposium of the Dutch Thyroid Research Foundation, Amsterdam, The Netherlands	2017	1 day
Dutch Endocrine Meeting, Noordwijkerhout, The Netherlands	2018	1 day
Internal Medicine Science days, Antwerp, Belgium	2018	1 day
European Congress of Endocrinology, Barcelona, Spain	2018	4 days
Stichting Schildklieronderzoek Nederland, Rotterdam, The Netherlands	2018	1 day
Annual symposium of the Dutch Thyroid Research Foundation, Amsterdam, The Netherlands	2018	1 day
MCT8 deficiency conference, Doorn, The Netherlands	2018	2 days
International workshop on Resistance to Thyroid Hormone, Doorn, The Netherlands	2018	3 days
European Thyroid Association, Newcastle, UK	2018	4 days
European Society for Pediatric Endocrinology, Athens, Greece	2018	4 days
Dutch Endocrine Meeting, Noordwijkerhout, The Netherlands	2019	1 day
European Thyroid Association, Budapest, Hungary	2019	4 days

Presentations	**Year**	**Type**
Characterization of the dimerization domain of MCT8 and its role in MCT8 plasma membrane localization Internal Medicine Science days, Antwerp, Belgium	2012	Poster
Triac Trial in patients with MCT8 deficiency Voorjaarsvergadering Nederlandse Vereniging voor Kinderneurologie, Heemsteede, The Netherlands	2015	Oral
Thyroid Hormone Analog Therapy in Patients with the Allan-Herndon-Dudley Syndrome: The Triac Trial Internal Medicine Science days, Antwerp, Belgium	2015	Poster
Thyroid Hormone Analog Therapy in Patients with the Allan-Herndon-Dudley Syndrome (AHDS): the Triac Trial International Thyroid Conference, Orlando, USA (topic highlight)	2015	Oral
Thyroid Hormone Analog Therapy in Patients with the Allan-Herndon-Dudley Syndrome (AHDS): the Triac Trial Internal Medicine Science days, Antwerp, Belgium	2016	Oral
Thyroid Hormone Analog Therapy in Patients with the Allan-Herndon-Dudley Syndrome (AHDS): the Triac Trial Stichting Schildklieronderzoek Nederland, Groningen, The Netherlands	2016	Oral
Thyroid Hormone Analog Therapy in Patients with the Allan-Herndon-Dudley Syndrome (AHDS): the Triac Trial European Thyroid Association, Copenhagen, Denmark	2016	Oral
Thyroid Hormone Analog Therapy in Patients with the Allan-Herndon-Dudley Syndrome (AHDS): the Triac Trial International workshop on Resistance to Thyroid Hormone, Colorado Springs, USA	2016	Oral
Outward-Open Model Of Thyroid Hormone Transporter MCT8 Provides Novel Structural And Functional Insights American Thyroid Association, Denver, USA	2016	Oral

Presentations (continued)	Year	Type
Thyroid hormone analog therapy in patients with the Allan-Herndon-Dudley Syndrome (AHDS): The Triac Trial Internal Medicine Research Meeting, Rotterdam, The Netherlands	2016	Oral
Allan-Herndon-Dudley syndrome: diagnosis and treatment European Pediatric Neurology Society, Aachen, Germany	2016	Oral
Triac Trial in patients with MCT8 deficiency MCT8 deficiency conference, Los Angeles, USA	2017	Oral
Restoring TH action in patients with transporter defects: the Triac Trial European Congress of Endocrinology, Lisbon, Portugal	2017	Oral
Clinical, genetic and functional studies in mct8 deficiency Internal Medicine Science days, Antwerp, Belgium	2018	Poster
TRIAC Trial in Allan-Herndon-Dudley-Syndrome (MCT8) European Congress of Endocrinology, Barcelona, Spain	2018	Oral
Genotype-phenotype relation in patients with MCT8 deficiency Stichting Schildklieronderzoek Nederland, Rotterdam, The Netherlands	2018	Oral
The TRIAC Trial Annual symposium of the Dutch Thyroid Research Foundation, Amsterdam, The Netherlands	2018	Oral
Thyroid hormone analog therapy in patients with the Allan-Herndon-Dudley Syndrome (AHDS): The Triac Trial MCT8 deficiency conference, Doorn, The Netherlands	2018	Oral
MCT8 deficiency patient registry introduction & pilot results MCT8 deficiency conference, Doorn, The Netherlands	2018	Oral
Thyroid hormone analog therapy in patients with MCT8 deficiency: the Triac Trial International workshop on Resistance to Thyroid Hormone, Doorn, The Netherlands	2018	Oral
Thyroid hormone analog therapy in patients with MCT8 deficiency: the Triac Trial European Thyroid Association, Newcastle, UK (topic highlight)	2018	Oral
Thyroid hormone analog therapy in patients with MCT8 deficiency: the Triac Trial European Society for Pediatric Endocrinology, Athens, Greece	2018	Oral
Translational research in thyroid hormone regulation Annual Course on Molecular Medicine, Rotterdam, The Netherlands	2019	oral
Functional characterization of SLC17A4, a novel player in the thyroid hormone transport field European Thyroid Association (Young Investigators session), Budapest, Hungary	2019	oral

Teaching activities	Year	Workload
Vaardigheidsonderwijs first year medical students	2014	2 days
Vaardigheidsonderwijs first year medical students	2015	2 days
Vaardigheidsonderwijs first year medical students	2016	2 days
Vaardigheidsonderwijs first year medical students	2017	2 days
Journal Club first year medical students	2018	2 days
Vaardigheidsonderwijs first year medical students	2019	2 days
MolMed Course Basic and Translational Endocrinology	2019	1 day

Supervision	Year	Workload
Amanda van den Berge, Life sciences (Master thesis) *Genotype-phenotype association MCT8 deficiency*	2016	12 months
Ferdy van Geest, Medicine (Master thesis) *Physiology and pathophysiology of MCT8 and MCT10*	2016	6 months
Pascal Julia, Technische geneeskunde (Lab rotation) *Regulation of MCT8 mRNA expression*	2016	3 months
Milou Stals, Medicine (Master thesis) *development of an international MCT8 deficiency patient registry*	2017	12 months
Anna Dolcetta, Medicine, San Raffaele Scientific Institute, Milano, Italy (Research during residence training) *Genotype-phenotype association MCT8 deficiency*	2017	8 months

Awards and prizes	Year
American Thyroid Association Traineeship, Orlando, USA	2015
European Thyroid Association Travel grant, Colorado Springs, USA	2016
American Thyroid Association Traineeship, Denver, USA	2016
European Thyroid Association travel grant, Newcastle, UK	2016
NVE-Ipsen prize for the best endocrinology paper 2018	2018
European Thyroid Association travel grant, Budapest, Hungary	2019

Grant applications	Year
Sherman Family Trust Research Grant, Triac Trial goes global, EUR 126,320 (co-applicant)	2015-2018
Sherman Family Trust Research Grant, AHDS patient registry, EUR 30,552 (co-applicant)	2016-2018
Sherman Family Trust Research Grant, Triac Trial II, EUR 180,000 (co-applicant)	2018
ETA translational research grant, Functional characterization of SLC17A4, EUR 20,000 (applicant)	2019-2021

Reviewer experiences	# articles
Molecular Cellular Endocrinology	2
Clinical Endocrinology	1
Endocrine Related Cancer	1
Frontiers in Endocrinology	1
Thyroid	2
Endocrinology	1
Journal of Clinical Research in Pediatric Endocrinology	1

Other research experiences	Year
EMA procedure for registration Triac	2018-present
Medical advisor off-label programs on Triac treatment in patients with MCT8 deficiency	2015-present
Organizer of the National MCT8 deficiency day	2016
Co-founder of the International MCT8 deficiency patient registry	2018
Member of Expert Working Group “Thyroid disease” of the European Registries for Rare Endocrine Conditions (EuRRECa) , ERN-Endo	2018-present

“How I wish, how I wish you were here”

- Roger Waters & David Gilmour -

In *memoriam* Prof. dr. Ir. Theo J. Visser

“Wauw moet je eens kijken”… Een uitspraak die ik niet snel zal vergeten. Het moment is daar dat ik mag beginnen aan het schrijven van mijn dankwoord. Voor velen wellicht een verademing en een relatief gemakkelijke opgave; voor mij een brok in mijn keel en tranen in de ogen. Wat had ik dit graag met jou samen afgerond, Theo. Tijdens het schrijven van dit boekje zijn mijn gedachten talloze keren afgedwaald naar de bijzonder plezierige en talrijke discussies die we samen gevoerd hebben, de papers die we samen hebben geschreven en de mooie momenten die we samen hebben beleefd op het lab en daarbuiten. Een van de hoogtepunten was het vieren van je verjaardag – samen met de jongens- ergens op een parkeerplaats tussen Denver en Colorado Springs met een aantal bij de plaatselijke slijter gekochte flesjes IPA. Ook herinner ik me nog goed dat je me mee nam op mijn eerste “congres” in Los Angeles, een onvergetelijke ervaring.

Jouw inspirerende Lectio Magistralis over schildklierhormoontransporters tijdens mijn studie geneeskunde vormde het startsein voor onze samenwerking en heeft mijn passie voor de schildklier doen aanwakkeren. Nog in dezelfde week stuurde ik een e-mail naar Prof. Dr. Ir. T.J. Visser met de vraag of ik een keer langs mocht komen om te praten over onderzoek. “Je bent van harte welkom. Groet, Theo”. Deze woorden staan symbool voor hoe ik je als mens heb leren kennen. Samen met Edith stuurde je me op pad en liet je me ervaren wat onderzoek doen is. Ik was verbaasd over de mate van vrijheid die je me hierin altijd gaf – jaren later zou ik begrijpen waarom. Al gauw werd me duidelijk hoever je kennis van de schildklier en wetenschap in algemene zin reikte en was het glashelder dat ik ontzettend veel van je kon leren.

Je liet je ogenschijnlijk maar zelden gek maken. Zelfs niet toen ik aan het ploeteren was op mijn eerste manuscript en een andere groep ons net voor was met het publiceren van vergelijkbare bevindingen. Je wist wel weer een nieuwe insteek te vinden en, met het voor jouw kenmerkende lijstje met additionele experimenten, is het toch nog helemaal goed gekomen. De kortste route naar de oplossing van ieder academisch probleem leidde vaak naar Ee502, waar de deur van jouw kamer altijd openstond voor constructieve discussies en de nodige kennisoverdracht; maar ook voor een luisterend oor bij tegenslagen buiten het werk. Dit gaf enorm veel rust en vertrouwen.

Tegelijkertijd kon jouw bevlogenheid ook zorgen voor de nodige hoeveelheid werk: het ene idee was nog niet uitgewerkt, of het volgende werd al op tafel gelegd. Vaak was dit het begin van een nieuwe serie interessante en relevante bevindingen. Van nieuwe inzichten in de werking van MCT8 en de pathogenese van MCT8 deficiëntie, tot aan de toepassing van Triac als behandeling voor MCT8 deficiëntie en transporters en dejodases in exotische diersoorten. Veel van de studies in dit proefschrift zijn op deze manier tot stand gekomen. Kenmerkend voor jou waren de out-of-the-box ideeën en het zien van verbanden die voor anderen grotendeels onopgemerkt bleven. Ik herinner me nog goed hoe groot de vreugde was toen SLC17A4 inderdaad een nieuwe schildklierhormoon-transporter bleek te zijn. Het feest werd nog groter toen we in dezelfde week vonden dat AADAT schildklierhormoon metaboliseerde. Twee hoogtepunten die we gelukkig nog op traditionele wijze hebben kunnen vieren met een IPA bij het Westerpaviljoen.

Het bericht van jouw plotselinge overlijden kwam aan als een mokerslag, toen Edward me op woensdagmorgen 21 maart 2018 belde met het droevige nieuws. Het gemis van jouw aanwezigheid is nog altijd intens en dagelijks voelbaar. Tegelijkertijd ben ik zo ontzettend dankbaar en trots dat ik zoveel van je heb mogen leren. Een uitrusting voor de rest van mijn wetenschappelijke carrière. Een betere mentor had ik me niet kunnen wensen. Theo, bedankt voor alles.

Het was een lange en zware, maar ook mooie en onvergetelijke tocht richting de laatste “punt” achter de zin van dit hoofdstuk. Als ik één ding geleerd heb de afgelopen jaren is het wel dat wetenschap echte topsport is. Het vraagt om toewijding, volharding, incasseringsvermogen en een nauwe samenwerking met anderen. Daarom wil ik dit moment aangrijpen om mijn dank uit te spreken tot de vele mensen die op welke wijze dan ook hebben bijgedragen aan de totstandkoming van dit proefschrift. Samen hebben we de finish gehaald.

Als allereerst wil ik mijn promotor Prof.dr. R.P. Peeters bedanken. Beste Robin, het is een bijzonder grote eer dat ik je als promotor gehad heb. Ik vind het ontzettend knap hoe je weet te excelleren in de wetenschap en dit combineert met het werk in de kliniek. Een schoolvoorbeeld voor menig dokter met wetenschappelijke ambities in de academie. Jouw bevlogenheid en mondiaal-erkende expertise worden wellicht het best geïllustreerd door de veelvuldig aanstaande afwezigheidsmelding in Outlook. Ondanks je overvolle agenda, stel je vaak dé cruciale vraag op het juiste moment en weet je duidelijk richting te geven aan de onderzoekslijnen binnen de groep. Ook buiten het wetenschappelijk inhoudelijke gebied heb ik veel van je kunnen leren. Zo weet je als geen ander belangrijke bevindingen op een pakkende en voor iedereen begrijpelijke manier te brengen en blink je uit in het vinden van politieke compromissen. Dit heeft me in mijn ontwikkeling als wetenschapper enorm geholpen. Ik hoop dat we nog lange tijd mogen samenwerken en nog vaak een biertje zullen drinken tijdens congressen of bij jou in de achtertuin.

Dr. W.E. Visser, mijn copromotor. Beste Edward, wat is het een avontuur geweest de afgelopen jaren. Ik weet nog goed dat we begonnen als twee jongens achter een laptop met het opstellen van studieprotocollen, ABR-formulieren, en de nodige SOPs en SAPs, maar we hebben ons er doorheen geslagen en zelfs nog wat tijd gehad om basaal onderzoek te verrichten. Mijn dank voor alles wat je de afgelopen jaren voor me hebt gedaan en betekend is in geen woorden uit te drukken. Ik heb genoten van onze wetenschappelijke discussies, de congressen waar we zijn geweest, het bezoek aan de EMA en nog vele andere hoogtepunten. Ik waardeer je eerlijkheid, openheid en steun op wetenschappelijk en persoonlijk vlak ten zeerste en mag me gelukkig prijzen met jou als copromotor. Je kritische en nieuwsgierige houding tezamen met een grote hoeveelheid kennis en creativiteit maken je een uitmuntende wetenschapper, met recht een echte “Visser”. Ik hoop dat we nog heel lang onze passie voor schildklierhormoontransporters mogen delen. Ik kijk er naar uit met een glas whisky te toasten op het afronden van dit proefschrift. Bedankt, ouwe reus.

Mijn hartelijke dank gaat uit naar de leden van de kleine commissie. Prof. dr. Heuer, dear Heike, I am honored to have you as a member of the small committee. Your knowledge on thyroidology and passion for research are of great inspiration. It was a great honor writing a review on thyroid hormone transporters in memory of Theo together with you, being one of his long-standing and highly appreciated collaborators. I am looking forward to our ongoing collaboration, in particular with regard to MCT8 and the further characterization of SLC17A4. Prof. dr. A van der Ploeg, ontzettend bedankt voor het plaatsnemen in de kleine commissie en voor de bijzonder leerzame en inspirerende tijd bij de metabole kinderziekten tijdens mijn oudste coschap. Prof. dr. E. Fliers, bijzonder veel dank voor het beoordelen van het proefschrift als lid van de kleine commissie.

Overige leden van de commissie. Prof. dr. Chatterjee, dear Krish, it is an honor to have you as a member of the committee. It was a great pleasure collaborating with you and the colleagues from Cambridge

in the Triac Trial. In particular, many thanks for the linguistic editing of the final report. Prof. dr. A.J. van der Lely en Dr. E. van den Akker, enorm bedankt voor het plaatsnemen in de commissie.

Onderzoek doe je nooit alleen; sterker nog, goede wetenschap komt vaak pas tot stand wanneer je met elkaar van gedachten wisselt, discussieert, elkaar verder wil helpen, uitdaagt en bevraagt, complimenteert, maar soms ook bekritiseert. Door de jaren heen heb ik altijd het voorrecht gehad te mogen samenwerken met een groep fantastische collega's die een enorm stimulerende omgeving hebben gecreëerd voor wetenschap. Enorm bedankt hiervoor! Zonder jullie was dit proefschrift waarschijnlijk niets meer dan een ongeorganiseerde stapel ideeën.

Toen ik in 2009 voor het eerst op het lab kwam, vertelde Theo dat ik maar met Edith mee moest kijken, van jou kon ik wel leren hoe het reilt en zeilt in het lab en hoe ik een pipet moest vasthouden. Nou dat heb je gedaan. Nog altijd maak ik dankbaar gebruik van je trucjes om verdunningen uit te rekenen en om tijdens experimenten systematiek aan te houden. Enorm bedankt! Ellen en Wim, twee rotsen in de branding tijdens mijn eerste jaren op het lab. Jullie zijn altijd bereid geweest om belangeloos te helpen, Wim zelfs tot diep in zijn pensioen. De fijne kneepjes van de HPLC ben ik inmiddels vergeten, maar misschien ben je nog eens in de buurt? Beste Selmar en Ramona, bedankt allebei voor het vlugge en soms vele bestellen de afgelopen jaren. Selmar, als IT expert heb je meerdere onderdelen van dit proefschrift gereanimeerd wanneer mijn pc voor de zoveelste keer op hol sloeg (of had ik hier zelf debet aan?). Jouw nieuwsgierigheid en tomeloze inzet zijn bewonderingswaardig. Zelfs op de late vrijdagavond mocht ik je bellen toen de UPLC vastliep. Ook al heb ik ook soms genoten van de rust als je eens een dagje vrij had, jouw gepraat en humor hebben kleur gegeven aan menig dag die ik op het lab gespendeerd heb. Beste Ramona, mijn vraagbaak voor chemische structuren en reacties, regelgeving omtrent lab-procedures, cellijnen in het stikstofvat, en zo kan ik nog wel even doorgaan - tot aan veel voorkomende baby- en kinderproblemen. Bij jou kon ik altijd terecht voor raad en soms ook om mijn frustraties over het een en ander te uiten. Ik ben je hiervoor erg dankbaar. Linda, ik heb veel bewondering voor je grote mate van zelfstandigheid, assertiviteit en doortastendheid. Ik hoop dat je nog een tijd verbonden zal blijven aan onze groep. Ik heb vaak gekscherend geroepen dat ik een analist van het jaar award zou toekennen aan het einde van het jaar - nou, jullie verdienen hem alle drie!

Beste Marcel, ontzettend bedankt voor de belangrijke rol die je de afgelopen jaren op je heb genomen. Jouw kennis en inzichten zijn van onschatbare waarde geweest voor vele studies in dit proefschrift en daarbuiten. Ook jouw deur stond altijd voor me open. Soms struikelde ik wel over de fossielen of spookmaskers, maar een nuttig antwoord op mijn vragen kreeg ik altijd wel. Jouw bereidwilligheid om anderen te helpen is bewonderingswaardig en maakt je een ontzettend fijne collega om mee samen te werken. Ik ga het sparren over wetenschappelijke ideeën, je humor en gezelligheid ontzettend missen. Wellicht dan maar onder het genot van een biertje na diensttijd?

Dear Nilhan, although you have just started as a post-doc in our group, I am impressed by the novel research dimensions you brought along with you to the lab. The use of induced pluripotent stem cells in thyroid hormone research is a very exciting new step! I wish you all the best!

Beste Marco, in het begin kon ik je altijd maar moeilijk onderscheiden van Edward – zelfde kamer, dezelfde spijkerbroek en dezelfde blauw-wit gestreepte overhemden. Al snel werd me echter duidelijk dat jij alleen sporadisch op het lab kwam voor je “corvee-taken” en dat je je verder bezig hield met epidemiologie. Al ben ik lang wat sarcastisch geweest over GWAS, ik ben het gaandeweg steeds meer

gaan waarderen en ben er nu zelfs van overtuigd dat het (nog altijd) zeer nuttige informatie kan opleveren op het moment dat het gecombineerd wordt met basale wetenschap. Het was een genoegen om de afgelopen jaren op dit vlak met je te mogen samenwerken en ik hoop dat we dit de komende jaren een succesvol vervolg kunnen geven. Het ga je goed in Nijmegen! Beste Simone, wat gaat de tijd snel. Ik herinner me nog altijd de mooie microscopieplaatjes en filmpjes tijdens de werkbespreking, indrukwekkend! Beste Alies, ook jij kon er wat van met al die luciferase-experimenten! Vond het altijd gezellig om het over onze toenmalige, gemeenschappelijke woonplaats te hebben – en af en toe te kunnen profiteren van een lift. Beste Chantal, met je humor zorgde je altijd voor een goede sfeer op het lab - wat hebben we wat afgelachen! Dear Elaine, I am very grateful for the time we have worked together in the lab – it certainly was one of the most enjoyable and productive periods while I have been in the lab. Beste Anja, wat heb ik gelachen toen je vertelde dat je tijdens een congresdiner tussen de “oude mannetjes” werd gedirigeerd! Succes in de kliniek! Beste Tim en Layal, statistiek kent voor jullie geen geheimen. Fijn om zo nu en dan op jullie expertise te kunnen terugvallen! Beste Elske, ik hoop dat je het ontzettend naar je zin hebt in Dordrecht en dat je de stapels quality of life vragenlijsten en microRNA studies niet al te veel mist! Beste Evert, het was een genoegen om met je samen te werken. Hopelijk heb ik je niet al te veel van je werk gehouden als ik weer eens wat aan Marcel kwam vragen. Ik wens je het allerbeste toe in de kliniek en met je jonge gezin! Dear Karn, it has been a pleasure working with you! I will always remember your calmness, critic look on results, and tidiness. Your well-organized way of working is an example for every person working in a lab. I`m very grateful for the many times I could ask for your opinion on a wide variety of topics, including the skin rash of our children. I wish you all the best for your further career in Thailand. Dear Celia, it has been a pleasure working with you on the alternate side-chain metabolism of thyroid hormone. I`m looking forward extending this collaboration! The best of luck in Italy! Dear Zhongli, you’re an excellent and hardworking basic scientist, ingredients required to identify the thyroid hormone transporters involved in placental thyroid hormone transport. Many thanks for the times you have helped me out with taking care for the cell cultures or taking along some samples in your experiments. I wish you all the best! Beste Ferdy, wat ben ik blij dat we jou tijdens je master-onderzoek ervan hebben kunnen overtuigen dat het schildklieronderzoek ontzettend leuk is en dat je nu het stokje gaat overnemen. Wat hebben we veel platen weggewerkt, soms wel tegen de 100 stuks in de week (of hebben we de magische grens toch stiekem al een keer overschreden?). Ik ben je ontzettend dankbaar voor je tomeloze inzet, hulp in alle facetten en bovenal de ontzettend gezellig periode. Ik hoop nog lange tijd met je te mogen samenwerken! Beste Wouter, ontzettend veel succes met het opzetten van nieuwe methodes om schildklierhormoonmetabolieten te meten! Beste Mathé en Anna, heel veel succes met jullie onderzoek!

Beste Amanda en Milou, het was ontzettend leuk om jullie begeleider te mogen zijn tijdens jullie onderzoeksstages. Ik heb ontzettend veel van jullie geleerd, ik hoop ook andersom! Dear Anna, it was a huge pleasure to work together with you on a project with, seemingly, no end. We have characterized so many MCT8 mutants together that this chapter was not even near the finish at time of finalizing this thesis. I regret that I had no opportunity to join your defense in Milano! Beste Merel, ook al was ik niet je begeleider, toch heb ik met veel plezier mijn kamer met je gedeeld. Bedankt voor je hulp bij statistische vragen. Beste, Caroline, Arash, Oscar en Tessa, het was leuk om samen een bed&breakfast te delen in Budapest! Beste Betule, Ebrar, Melitza, Giulia, Stefania, Carolien, Mirjana, Arjola, Deborah, Alexander, Rutchanna and Wesley, many thanks for your contributions during work discussions, help

in the lab and/or enjoyable evenings during conferences! Beste Arjanne, bedankt voor al je hulp bij de uitvoering van de Triac Trial!

Alle andere collega`s van de 5de verdieping ben ik ook erg dankbaar. Mijn bijzondere dank gaat uit naar Bas. Door de jaren heen heb je dozen vol celkweek platen besteld, door de gang gezeuld en weer opnieuw kunnen bestellen, omdat ze dezelfde week alweer op waren. Anke en Jeroen, bedankt voor het helpen herinneren wanneer ik wat veel oude LB platen in de koelkast van het VMT lab had liggen. Iris en Marijke, bedankt voor de bestellingen voor het Chemicaliënhok, Peter bedankt voor je technische ondersteuning en mooie verhalen over vroeger, Leo, Annelies, Eline, Fadime, Rosanna, Bram, Patrick, Keng, Cobie, Jenny, Michael, André, Fernando en zo kan ik nog wel even doorgaan met de lange lijst collegae die op enige manier hebben bijgedragen aan de leuke werksfeer, de studies in dit proefschrift en mijn ontwikkeling als wetenschapper en mens. Beste Anneke en Karin, ontzettend bedankt voor jullie uitmuntende secretariële ondersteuning!

Onderzoek betekent vaak ook samenwerken met andere disciplines binnen het ziekenhuis. Mijn bijzondere dank gaat uit naar Ronald, Hans, Yolanda, en alle collega`s van het diagnostisch laboratorium endocrinologie (DLE) voor de talloze buisjes serum die jullie hebben geanalyseerd de voorbijgaande jaren. Ronald, mijn bewondering is zeer groot voor de manier waarop je alle monsters van de Triac Trial hebt georganiseerd en opgeslagen en altijd feilloos wist waar nog spijtmateriaal gevonden kon worden. Beste Monique en collega`s van het trial-lab, wat begon als een kleine nationale studie, is toch behoorlijk uitgedijd! Vanuit alle windrichtingen krijgen jullie dagelijks samples binnen van patiënten die met Triac behandeld worden. Jullie zijn een kei in het ontcijferen van onleesbare handschriften en oplappen van verkeerd verstuurde monsters. Ontzettend bedankt! Beste Sonja, Rianne, Rachida en collega`s van de trial-apotheek, bedankt voor jullie hulp tijdens de trial! Beste Aldert en collega`s van de trial-IT, bedankt voor je hulp bij het gebruik van Open Clinica! Hopelijk zijn jullie niet gek geworden van de vele mailtjes met de vraag om gebruikers toe te voegen! Liesbeth, Menno, Selda en collega`s van de IT, ontzettend veel dank voor de hulp bij het opzetten van een registry voor patiënten met MCT8 deficiëntie. Beste Ingrid, ik bewonder je enorme betrokkenheid en kunde op het gebied van de kindercardiologie. Het was een genoegen om met je te mogen samenwerken op wetenschappelijk gebied; hopelijk komen we elkaar in de toekomst weer tegen in de kliniek. Beste Corstiaan, Petra, en collega`s van de afdeling cardiologie, bedankt voor jullie onschatbare bijdrage aan de Triac Trial! Beste Carola, Sandra en Els, geen uitdaging was jullie te veel de afgelopen jaren – gelukkig hebben we uiteindelijk nog aardig wat bruikbare DEXA-scans kunnen maken! Beste René, Marie-Claire en Femke, ontzettend veel dank voor het bijspijkeren van mijn neuro(psycho)logie-kennis. Beste Kyra, laten we hopen dat we handen in de toekomst nog vaker in een kunnen slaan wat betreft onderzoek naar schildklierhormoon signaling defecten. Wilfred en Rutger, hopelijk gaan we nog eens achterhalen waar de translocatie nou echt zit.

Veel samenwerkingen reikten echter verder dan de muren van het Erasmus MC. Een zeer groot woord van dank komt toe aan iedereen die betrokken is geweest bij de Triac Trial in binnen- en buitenland. In de eerste plaats natuurlijk alle ouders/wettelijk vertegenwoordigers die ons het vertrouwen hebben gegeven om deze studie uit te voeren en dag in dag uit vol toewijding het studieprotocol hebben opgevolgd. Daarnaast alle (persoonlijk) begeleiders die in veel gevallen een belangrijke praktische bijdrage hebben geleverd aan de studie(s). Vervolgens alle Raden van Bestuur en directies van ziekenhuizen en zorginstellingen die toestemming hebben gegeven voor deelname aan het onderzoek: Vrije Universiteit Amsterdam, Universitair Medisch Centrum Groningen, Meander Ziekenhuis te

Amersfoort, Refaja Ziekenhuis te Stadskanaal, `s Heerenloo (locaties Julianadorp en Ermelo), de Baalderborg Groep (Hardenberg), en Huisartsenpraktijk de Latyrus (Dedemsvaart). De grote inspanningen van de vele betrokken artsen hebben veel indruk gemaakt. Enorm bedankt voor jullie grote bijdrage: Nicole Wolf, Ineke Lunsing, Jurgen Jansen, Stan Nowak, Frank Visser, Paul Vrijmoeth en Angelique Zandstra. Mijn gedachten gaan in het bijzonder uit naar Martien Manshande, die zich met hart en ziel heeft ingespannen voor de trial, maar tot ons verdriet de afronding niet heeft mogen meemaken. Uiteraard gaat ook veel dank uit naar alle betrokken doktersassistenten, medewerkers van de bloedafname en laboranten. Fantastisch om te zien dat er zoveel mensen zijn die zich belangeloos en vol passie hebben ingezet voor hun patiënten en cliënten de afgelopen jaren. A special thanks to all our collaborators abroad: Krish Chatterjee, Carla Moran, Greta Lyons, Anne McGowan, Yogen Singh, Gautam Ambegaonkar, Michel Polak, Athanasia Stoupa, Isabelle Oliver Petit, Françoise Auriol, Enrico Bertini, Marco Cappa, Laura Paone, Heiko Krude, Federica Zibordi, Davide Tonduti, Dana Craiu, Diana Barca, Alice Dica, Jan Lebl, Klara Rozenkova, Jana Malikova, Sylvia Depoorter, Adri van der Walt, and many of their colleagues that made valuable contributions to the Triac Trial. Mijn gedachten gaan ook uit naar Linda de Meirleir, die tot onze grote ontsteltenis vlak voor het einde van de trial overleden is.

Also a special thanks to all other collaborators in and outside The Netherlands, some of whom have co-authored on the studies of this thesis, in particular Alexander Teumer, Francisco Arjona, Doriana Miceo, Petter StrØmme, Sylvia Masnada, Francesca Novara, Zanni Zinevra, and Paul van Trotsenburg.

Beste Monique, Hidde, Esmee en Hannerieke, ontzettend bedankt voor de leerzame tijd bij de metabole kinderziekten. Monique, met je enthousiasme, kennis en ervaring heb je me in zeer korte tijd kennis laten maken met veel aspecten van het vak. Ik kom snel weer een kop thee bij je drinken!

Familieleden en vrienden, ook al hebben jullie inhoudelijk niet bijgedragen aan dit proefschrift, jullie zijn door de jaren heen wel van onschatbare waarde geweest daarbuiten. In het bijzonder mijn schoonouders die mij vanaf het eerste moment enorm hartelijk hebben ontvangen binnen de familie. Ontzettend bedankt voor het vele oppassen en de liefdevolle zorg voor de kinderen. Hopelijk eten we snel weer eens een biefstuk om te vieren dat dit hoofdstuk afgesloten is!

Lieve pa en ma, ontzettend bedankt voor jullie onvoorwaardelijke steun en alles wat jullie me hebben meegegeven in het leven. Het is een groot voorrecht dat jullie altijd voor ons en de kinderen klaarstaan. Bedankt dat jullie ook af en toe aan de rem getrokken hebben wanneer mijn werkgedrag buitensporige vormen aannam – maar hier is het proefschrift dan. Laten we het snel gaan vieren met een midweek weg!

Lieve Elin, Hidde en Jurre, wat zou het toch ontzettend stil zijn in huis zonder jullie! Het is ontzettend mooi om te zien hoe jullie groeien, leren en alles in en buiten het huis aan het onderzoeken zijn. Soms gaat de tijd wat dat betreft veel te snel. Papa is eindelijk klaar met het schrijven van zijn boek Elin – hopelijk laten jullie hem heel tot het moment dat jullie hem zelf kunnen lezen, hoewel een paar extra tekeningen nog wat meer kleur zouden kunnen aanbrengen. Nu eerst weer lekker samen boekjes lezen, met de auto`s spelen, stoeien, zwemmen en naar Bollo gaan!

Lieve Marieke, wat had ik zonder jou gemoeten. Je bent al jaren mijn steun en toeverlaat, door dik en dun en door weer en wind. Ik ben ontzettend gelukkig dat ik zoveel mooie momenten met je heb kunnen delen en ik ben er zeker van dat er nog velen zullen volgen. Tegelijkertijd realiseer ik me, dat je je jarenlang in allerlei bochten hebt gewrongen om het mogelijk te maken dat ik elke ochtend weer

vroeg op pad kon naar het Erasmus, je ontfermd hebt over een groot gedeelte van het huishouden en de doordeweekse zorg voor de kinderen – wat met schoolgaande kinderen echt een enorme uitdaging is. Zelfs op dagen dat ik tot diep in de nacht op het lab werkte, zorgde je er altijd voor dat er avondeten in m`n tas zat. Ik vind het ontzettend bewonderingswaardig dat je dit alles hebt gedaan naast je eigen opleiding(en) en werk als psycholoog. Uiteindelijk begon die schildklier ook bij jou te kriebelen en besloot je mee te doen aan het familiebedrijf en in de houdanigheid van neuro-psychologe je steentje bij te dragen aan de Triac Trial – ontzettend leuk dat we ook dit hebben kunnen delen! Hoewel ik al jaren roep dat er een rustigere periode aan gaat komen, denk ik dat het nu dan eindelijk zover is. Met alle verhuizingen, verbouwingen, opleidingen, slapeloze nachten en zorgen om de kinderen (grotendeels) achter de rug, hoop ik dat we binnenkort weer volop samen kunnen genieten van de dingen die echt belangrijk zijn in het leven. Ik hou van je.